
Notes in

Fracture Mechanics

Victor E. Saouma

saouma@colorado.edu

University of Colorado, Boulder

2022

This work is licensed under a [Creative Commons “Attribution-NonCommercial-ShareAlike 4.0 International”](https://creativecommons.org/licenses/by-nc-sa/4.0/) license.



Dedication

To my grandfather



whom I never met.

Notice

Intentionally, this document cannot be printed.

It is best read on a computer to easily follow the multiple hyperlinks and bookmarks.

Contents

I Syllabus

II Lecture Notes

III Homeworks

IV Exam

V Mathematica Solutions

VI Early (partially outdated) Manuscript

PREFACE

Philosophy

I have been teaching fracture mechanics on and off¹ at the University of Colorado for over 40 years.

My focus was to cover in sufficient details fundamental aspects of fracture mechanics, numerical methods that could be (or are) implemented in finite element codes, and finally properly address fracture of cementitious materials (fancy word for concrete really).

As many (good) Professors, I was never pleased with any particular textbook that could cover the three topics. So, I wrote my own set of notes over the years, and kept on refining them over the years².

Unfortunately, it is very challenging to sufficiently motivate (even graduate) students to embark in such a course.

Let us face it the fracture mechanics tools that many practicing (specially forensic) engineers can be taught in less than a week: Stress concentrations/stress intensity factors concepts, Paris law for fatigue, and rudimentary concepts of plastic zones (metals) or fracture process zones (concrete).

However, I always felt that a good graduate student in structural engineering/Mechanics should also be exposed to the complexity and beauty of some of the fundamental equations in fracture mechanics³. This will not only provide a library of analytical “tricks” that could be adapted to other disciplines, but it will also instill an added respect for theory and the endurance it takes to solve a complex problem.

Of course, most modern finite element codes can compute stress intensity factors, J integrals, and have cohesive crack models. It is regretful that many students rush to those codes without a basic understanding of the underlying method.

As to concrete fracture (topic of my Ph.D. dissertation in 1980 under the supervision of Tony Ingraffea), it has attracted some of the brightest researchers in academia. Yet, it is nevertheless an ever-ending search for a solution which can capture the localization of a crack (unless you use a discrete crack model that is) without making compromises numerical “tricks” along the way.

Yet, I have been amazed to see many students refer to cohesive cracks, yet they have never heard of Hillerborg. Clearly different “tribes” who seldom talk to each others.

Notes not a Book

It has never been my intention to publish yet another book covering Fracture Mechanics (though I flirted with the thought about 10 years ago when I started merging notes in what may look like a book)

Beside, with my experience in publishing [Aging, Shaking, and Cracking of Infrastructures; From Mechanics to Concrete Dams and Nuclear Structures](#) and a few others, I concluded that: a) publishing a book nowadays with a “major” publisher reaps very little benefit; b) except a handful few (who may have watered-down content to please a large audience), no ones makes enough money to spend a night in NY; and as to “fame”, no serious author needs to get it through a book which would be readily accepted by even some of the “big” publisher.

¹Though it was not always easy to find sufficient students interested in such an advanced course, and then to retain them after a few weeks.

²Likewise, I am proud to have never used a commercial code (i.e. Abaqus) with its multitude of their features, instead I relied on Merlin that was developed by two of my former students (It would be nearly impossible today to find a graduate student who can develop from scratch a decent nonlinear finite element code.

³Consider the derivation of $\sigma = \sigma_0 \left(1 + 2\sqrt{\frac{a}{\rho}}\right)$, to derive such a simple and beautiful equation, one has to use elliptical coordinate system, complex potentials and Airy stress functions!!

As a University Professor, our responsibility is to acquire and share knowledge. We are semi-decently paid by our institution, and the crumbs given to us by publisher are not worth it.

Accordingly, these notes are to be freely distributed.

Formatting

For over 35 years, I have been a big fan of L^AT_EX and felt pity for those who insisted in writing technical documents in a tool originally meant for lawyers (Word). As such, with a decent command of L^AT_EX; countless *packages* developed by others, and few macros I wrote myself I always tried to make sure that any manuscript I author is not only rigorous, complete, but also “looks nice”⁴

So, I have paid great attention to the layout, and as much as possible prepared all drawings myself with Visio or Matlab.

Oh “my English” is far from perfect, evidently is is not my native language, tried my best, so be kind not to be too critical.

Contents

This document is composed of the following parts

1. Syllabus
2. Lecture Notes (Beamer based files)
3. Assigned homework with their solutions
4. Mathematica Solutions
5. Exams
6. Early version of the manuscript I assembled based on my notes

The respective pdfs have been collated.

Books consulted

The preparation of these notes greatly benefited from a multitude of papers⁵, and a few books:

1. Anderson, T.L., *Fracture Mechanics; Fundamentals and Applications*, CRC Press, 1995.
2. Atkins, A.G., and Mai, Y.W., *Elastic & Plastic Fracture*, John Wiley, 1985.
3. Broek D., *The Practical Use of Fracture Mechanics*, Kluwer Academic Publishers, 1989.
4. Broek D., *Elementary Engineering Fracture Mechanics*, 4th Revised Edition, Martinus Nijhoff Publishers, 1986.
5. Cherepanov G.P., *Mechanics of Brittle Fracture*, McGraw Hill, 1979.
6. Gdoutos, E.E., *Fracture Mechanics; An Introduction*, Kluwer Academic Press, 1993

⁴I have been fortunate to collaborate for nine years with the Tokyo Electric Power Company (TEPCO) on the nonlinear seismic analysis of tall arch dams. After about six years, I thought that we had accomplished all the work. *No! no! Prof. Saouma, in Japan, a program has not only to work properly but it must look beautiful.* This simple comment, along with my many visits/stays in Switzerland (where a great value is placed on sobriety), and a certain taste for architecture, influenced me.

⁵Which unfortunately have not been cited inside Beamer (L^AT_EX based program used for the notes), but are within the “manuscript”.

7. Hertzberg, *Deformation and Fracture Mechanics of Engineering Materials*, Fifth Ed., J. Wiley.
8. Hudson, C.M. and Rich, T.P. (Eds.) *Case Histories Involving Fatigue and Fracture Mechanics*, ASTM STP918, American Society for Testing and Materials, Philadelphia, 1986.
9. Kanninen, M.F., and Popelar, C.H., *Advanced Fracture Mechanics*, Oxford Engineering Science, Series 15, 1985.
10. Knott, J.F., *Fundamentals of Fracture Mechanics*, Halsted Press/John Wiley & sons 1973.
11. Liebowitz (Ed.), *Fracture -An Advanced Treatise*, Academic Press, 1968.
12. Owen, D.R., and Fawkes, A.J., *Engineering Fracture Mechanics Numerical Methods and Applications*, Pineridge Press, 1983.
13. Rolfe, S., and Barsom, J., *Fracture and Fatigue Control in Structures: Applications of Fracture Mechanics*, Prentice-Hall Inc., 1977.
14. Suresh, S., *Fatigue of Materials*, Cambridge University Press, 1991.
15. Tada and Irwin, *Stress Analysis of Cracks*, Del Research Corp.

Part I

Syllabus

Spring 2020
FRACTURE MECHANICS

CVEN-6831/7161

T-Th 2:00-3:15 ECCE-1B47

Victor E. Saouma

saouma@colorado.edu

ECOT450; 2-1622

Dept. of Civil, Environmental and Architectural Engineering

University of Colorado, Boulder, CO

Jan. 8, 2020

Target This course addresses the need of students interested in: a) Fundamental understanding of fracture mechanics starting from continuum mechanics; b) Understanding failure and size effects; c) role of fracture mechanics in understanding design and analysis of flawed or potentially flawed components; d) forensic engineering.

Open to M.S. and PhD students.

Course description: In most structures (Civil, Mechanical, Aerospace), failure is directly or indirectly related to fracture. This course will blend theoretical (50%) computational (20%), and material (30%) aspects into a course geared for students interested in exploring the analysis of fracture based failures. Very heavy emphasis will be placed on independent work/project/presentations.

Meeting prerequisites: Mechanics of Materials, Finite element. The course will start with a brief review of continuum mechanics and elasticity. Mathematica will be extensively used throughout the course.

Schedule: T-Th: 3:30-4:45

Textbooks: None required. Occasionally, selected pages from Instructor's notes will be provided.

Assignments: There will be approximately 5 homework assignments, a term paper, a term project and one exam. The term paper and project may be related to a student research interest or industrial application.

Instructor: Has been involved in theoretical, numerical and experimental fracture mechanics for over 30 years. His research has been applied to dams, nuclear reactors, solid-rocket propellants, and metal fatigue. He is past President of the international Association of Fracture Mechanics of Concrete [FraMCoS](#). This course has been offered in Boulder, Milan, Barcelona, Lausanne and Paris.

Enrollment: Only students registered for the course could attend the lectures

Outcome After completion of this course, you would have strengthened your basic understanding in Mechanics (and Mathematica), acquired the knowledge to conduct forensic studies in the investigation of failures/accidents and to understand the true strength of many materials.

Tentative Course Outline (not necessarily in this order)

Following is the *tentative* course outline. Coverage may vary depending on student interests.

I Introduction

1. Historical Overview
2. Stress based failure theories
3. Design Philosophies

II Review of Mechanics (\sim 1-2 weeks) Review of the fundamental relations in Mechanics using tensor (indicial) notation: Strain, Strain, Equilibrium, Compatibility, Hooke's Law, Airy Stress Function, Complex Functions using Mathematica.

III Linear Elastic Fracture Mechanics: (\sim 2 weeks)

1. Elastic Crack Tip Stress Field: Stress around an Elliptical Hole (Inglis, 1913), Complex Stress Functions (Westergaard, 1939), Bi-Material (Williams, 1959).
2. Stress Intensity Factors (Irwin, 1957): Elliptical Cracks, Design Philosophy (Example)
3. Energy Principles (Griffith, 1921): Ideal Fracture Strength (?), Griffith's Theory (Griffith, 1924), Energy Release Rate, G_c and R Curves, Compliance Calibration Method (Mostovoy, 1967).
4. Fracture of Anisotropic Bodies: Basic Equations of Anisotropic Elasticity (Lekhnitskii), Stress Analysis (Sih, Paris, and Irwin, 1965).
5. Mixed Mode Crack Propagation: Maximum Circumferential Tensile Stress (Erdogan, 1963), Maximum Strain Energy Release Rate (Hussain et al. 1974), Minimum Strain Energy Density (Sih, 1974), Anisotropic Materials (Saouma, Ayari, Leavell, 1986).

IV Elasto-Plastic Fracture Mechanics: (\sim 1 Week)

1. The Crack Tip Plastic Zone: First and second Order Approximation (Irwin), Dugdale and Barenblat's models, Multiaxial Stress Based (Von-Mises, Tresca); Plane Stress versus Plane Strain.
2. Crack Tip Opening Displacements (Wells)
3. Energy Methods: J Integral Derivation (Rice); Variations on Original J Formulation, J-R Concept, EPRI method.

V Fracture Toughness Testing: (\sim 1 week)

1. Fracture toughness (ASTM E399)
2. Fracture Energy (RILEM, ISRM)

VI Subcritical Crack Growth: (\sim 1 week)

1. Fatigue Models: Paris Law (Paris, 1963), Forman Law (Forman, 1967), Walker's Law, Table Look-Up.
2. Other: Mixed Mode Fatigue Crack Growth, Fatigue Life Prediction, Variable Amplitude Loading,
3. Load Interaction, Retardation Model: Wheeler, Generalized Willenborg
4. Corrosion

VII Numerical Methods: (\sim 2 weeks)

1. Isoparametric singular element: Original Formulation (Barsoum), Subsequent Extensions, Assessment of Singular Isoparametric Elements (Fawkes et al.).
2. Extraction of SIF: Nodal Displacement Based: Without Singular Elements (Displacement Extrapolation) With Singular Elements (Displacement Correlation Method), Energy Based Methods: Energy Release Rate, Virtual Crack Extension (Park), Virtual Crack Extension (Sha), J_1 and J_2 Integrals (Hellen and Blackburn), Mutual Potentials (Stern & Becker), Surface Integral (Babuska)

3. Elasto-Plastic Analysis, J Integral
4. Fracture of cementitious materials: Fictitious Crack Model, (Hillerborg 1976), Size Effect Law (Bazant, 1984), ICM (Červenka and Saouma, 1994), Crack Band Model (Bazant, LEFM and NLFM (Fictitious Crack Model), (Reich 1992)
5. Lattice Model.

VIII Applications And Case Studies: (~ 4 weeks)

1. Concrete: Applications to nuclear power containment vessels: Creep fracture, Transport (gas and liquid) in porous media, permeability, hydro-mechanical behavior.
2. Rock: Blasting; Hydro-fracturing.
3. Metals (connections under seismic excitation).
4. Solid rocket propellants (polymers).

Past Term Projects

- Analysis Of Butt Welded Joints
- Cohesive Crack Models
- Cohesive Cracks For Interfaces
- Concrete Under High Temperatures
- Concrete Fracture
- Crack Between 2 Dissimilar Materials
- Crack Detection Location With White Noise Vibration
- Crack Propagation In Draw Cylinder
- Crack Propagation In Aluminium Panels
- Dynamic Fracture Mechanics
- Fatigue Crack Propagation With Retardation
- Fatigue Crack Propagation
- Fracture Mechanics Based Simulation Of Anchors
- Fracture And Fractals
- Fracture In Solid Rocket Propellants
- Fracture Mechanics Of Bond In reinforced concrete
- Fracture Mechanics Partition Unity Method
- Fracture Steel Connection Under Earthquake Load
- Fracture Testing Of Concrete
- Indentation Of Rock; Numerical Simulation
- Numerical Fracture Simulation Of Porous Sintered Steels
- Size Effects On Shear Strength
- Slope Stability
- Fracture and flow (liquid and/or gas).
- Numerical analysis of brittle fracture; Exploration of the Phase Field Method in the Framework of Finite Elements.
- Fracture Mechanics of a Pressure Vessel
- Compliance Change in Linear Elastic Solids due to Microcracking
- Stress Corrosion Cracking
- Finite element Analysis of fracture mechanics in plane problems using a Cohesive Surface Element (CSE)
- Fracture of Steel Building's Welded Connections When Subjected to Seismic Ground Motions
- Cohesive constitutive law; Review of Puntel's model and Matlab implementation
- Probabilistic Fracture Mechanics
- Dynamic Crack Propagation

Part II

Lecture Notes

Following are the lecture notes I used in class. Typically, I would redact key concepts/definitions, parts of equations, of axis labels. Make the redacted files available to the students, who would then have to complete the redacted parts.

This part is the most up-to-date one of my course, however it is not as detailed as the part that includes an early version of the manuscript.

Fracture Mechanics

Introduction

Victor E. Saouma
saouma@colorado.edu

University of Colorado, Boulder

Spring 2022

Table of Contents I

- 1 Mechanics Landscape
- 2 Models
- 3 Motivation
- 4 Examples of Failure
- 5 Cost and Consequences
- 6 MOM vs FM
- 7 Major Historical Developments
- 8 Coverage
- 9 Approach
 - Term Projects

Courses (not disciplines)

Statics Rigid bodies, forces and moments, basic equilibrium, no stress or strain.

Mechanics of Materials beams, deformable bodies, stress, strain, engineering notation (σ_x , ϵ_y), temperature, deformation, elastic/plastic solutions, simple structural elements.

Structural Analysis idealized structures (trusses, frames, cables), force-displacements, determinate and indeterminate structures; no stress-strain.

Continuum Mechanics Strain (small, large), Stress (Cauchy, Piola-Kirchoff), Fundamental laws (conservation of mass, momentum and energy); Constitutive equations.

Solid Mechanics

Elasticity Mathematical solution of simple problems using fundamental equations, polynomial/Fourier solutions, Airy stress functions; Cartesian or polar coordinates; Real or Complex solutions.

Plasticity continuum, structural component, or structural level.

Fracture Mechanics Analysis of structures subjected to presence/propagation of cracks. Crack formation is studied by Metallurgists of Material Scientists.

Fluid Mechanics Non listing sub-categories

Computational Mechanics To be addressed once one or more of the above well understood

- Fracture Mechanics could really be called **Failure Mechanics**.
- Models for material failure
 - Yield Theory plastic deformation, **stress based failure theory**.
 - Damage Theory gradual **degradation** of properties, decrease in E , large deformation.
 - Fracture Theory brittle behavior, leads to **material rupture**.

The fundamental requirement of any structure is that it should be designed to resist mechanical failure through any (or a combination of) the following modes:

- 1 Elastic instability (buckling)
- 2 Large elastic deformation (jamming)
- 3 Gross plastic deformation (yielding)
- 4 Tensile instability (necking)
- 5 **Fracture**

Some well-known, and classical, examples of fracture failures include:

- Mechanical, aeronautical, or marine
 - Fracture of train wheels, axles, and rails
 - Fracture of the Liberty ships during and after World War II
 - Fracture of airplanes, such as the Comet airliners, which exploded in mid-air during the fifties, or more recently fatigue fracture of bulkhead in a Japan Air Line Boeing 747
 - Fatigue fractures found in the Grumman buses in New York City, which resulted in the recall of 637 of them
 - Fatigue crack that triggered the sudden loss of the upper cockpit in the Air Aloha plane in Hawaii in 1988.
 - Fracture of solid rocket propellants.
- Civil engineering
 - Compressive failure of cementitious materials (concrete, ceramic, rock).
 - Fractures of bridge girders (Silver bridge in Ohio)
 - Fracture of Statfjord A platform concrete off-shore structure
 - Cracks in nuclear reactor piping systems
 - Fractures found in dams (usually unpublicized)

- Delamination in a Nuclear reactor containment vessel (Crystal River).

Despite the usually well-known detrimental effects of fractures, in many cases fractures are man-made and induced for beneficial purposes Examples include:

- Rock cutting in mining
- Hydro-fracturing for oil, gas, and geothermal energy recovery
- “Biting” of candies (!)

Fracture environmental interactions:

- Fatigue crack propagation.
- Corrosion assisted crack propagation.
- Fracture-Fluid interaction (Fracking).
- Fracture gas interaction (gas leakage through concrete in nuclear containment structures).

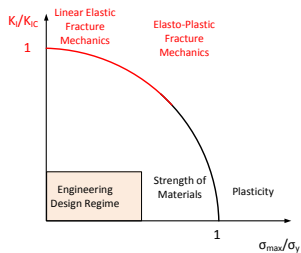
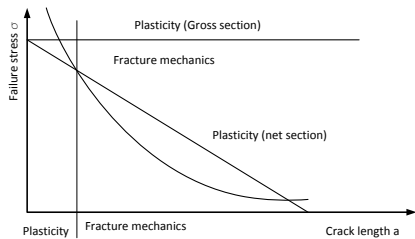
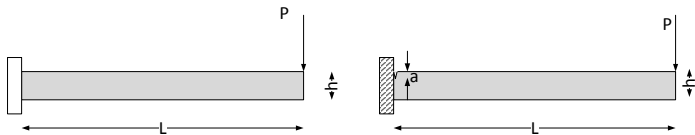
Even under all-around compressive loads, brittle materials tend to fail by the formation of tensile microcracks at microdefects such as cavities, grain boundaries, inclusions, and other inhomogeneities

Cost

[The] cost of material fracture to the US [is] \$ 119 billion per year, about 4 percent of the gross national product. The costs could be reduced by an estimated missing 35 billion per year if technology transfer were employed to assure the use of best practice. Costs could be further reduced by as much as \$ 28 billion per year through fracture-related research.

In light of the variety, and complexity of problems associated with fracture mechanics, it has become a field of research interest to mathematicians, scientists, and engineers (metallurgical, mechanical, aerospace, and civil).

MOM vs FM



- 1 1898, Kirsch **Stress concentration around circular hole**
- 2 1913, Inglis **Stress concentration around ellipse**
- 3 1930's Griffith, **Theoretical Strength**
- 4 1930's Griffith **Thermodynamical criterion for fracture**
- 5 1939 Westergaard, **stress field near a sharp crack tip**
- 6 1940's Irwin **Plastic zone size**
- 7 1940's, Irwin **Energy Release rate**
- 8 1961, Paris **empirical equation relating the range of the stress intensity factor to the rate of crack growth**
- 9 1963, Rice, **J Integral**
- 10 1960's, Erdogan and Sih, **first model for mixed-mode crack propagation.**
- 11 In 1976, Hillerborg: **fictitious crack model**
- 12 In 1979 Bažant and Cedolin **Requirements for an "objective" analysis**

I Introduction

II Review of Mechanics (~ 1-2 weeks) Review of the fundamental relations in Mechanics using tensor (indicial) notation: Strain, Strain, Equilibrium, Compatibility, Hooke's Law, Airy Stress Function, Complex Functions using Mathematica.

III Linear Elastic Fracture Mechanics: (~ 2 weeks)

- 1 Elastic Crack Tip Stress Field: Stress around an Elliptical Hole (Inglis, 1913), Complex Stress Functions (Westergaard, 1939), Bi-Material (Williams, 1959).
- 2 Stress Intensity Factors (Irwin, 1957): Elliptical Cracks, Design Philosophy (Example)
- 3 Energy Principles (Griffith, 1921): Ideal Fracture Strength (?), Griffith's Theory (Griffith, 1924), Energy Release Rate, G_c and R Curves, Compliance Calibration Method (Mostovoy, 1967).

- ④ Fracture of Anisotropic Bodies: Basic Equations of Anisotropic Elasticity (Lekhnitskii), Stress Analysis (Sih, Paris, and Irwin, 1965).
- ⑤ Mixed Mode Crack Propagation: Maximum Circumferential Tensile Stress (Erdogan, 1963), Maximum Strain Energy Release Rate (Hussain et al. 1974), Minimum Strain Energy Density (Sih, 1974), Anisotropic Materials (Saouma, Ayari, Leavell, 1986).

IV Elasto-Plastic Fracture Mechanics: (~ 1 Week)

- ① The Crack Tip Plastic Zone: First and second Order Approximation (Irwin), Dugdale and Barenblat's models, Multiaxial Stress Based (Von-Mises, Tresca); Plane Stress versus Plane Strain.
- ② Crack Tip Opening Displacements (Wells)
- ③ Energy Methods: J Integral Derivation (Rice); Variations on Original J Formulation, J-R Concept, EPRI method.

V Fracture Toughness Testing: (~ 1 week)

- 1 Fracture toughness (ASTM E399)
- 2 Fracture Energy (RILEM, ISRM)

VI Subcritical Crack Growth: (~ 1 week)

- 1 Fatigue Models: Paris Law (Paris, 1963), Forman Law (Forman, 1967), Walker's Law, Table Look-Up.
- 2 Other: Mixed Mode Fatigue Crack Growth, Fatigue Life Prediction, Variable Amplitude Loading,
- 3 Load Interaction, Retardation Model: Wheeler, Generalized Willenborg
- 4 Corrosion

VII Numerical Methods: (~ 2 weeks)

- 1 Isoparametric singular element: Original Formulation (Barsoum), Subsequent Extensions, Assessment of Singular Isoparametric Elements (Fawkes et al.).

- ② Extraction of SIF: Nodal Displacement Based: Without Singular Elements (Displacement Extrapolation) With Singular Elements (Displacement Correlation Method), Energy Based Methods: Energy Release Rate, Virtual Crack Extension (Park), Virtual Crack Extension (Sha), J_1 and J_2 Integrals (Hellen and Blackburn), Mutual Potentials (Stern & Becker), Surface Integral (Babuska)
- ③ Elasto-Plastic Analysis, J Integral
- ④ Fracture of cementitious materials: Fictitious Crack Model, (Hillerborg 1976), Size Effect Law (Bazant, 1984), ICM (Červenka and Saouma, 1994), Crack Band Model (Bažant, LEFM and NLFM (Fictitious Crack Model), (Reich 1992)
- ⑤ Lattice Model.

VIII Applications And Case Studies: (~ 4 weeks)

- 1 Concrete: Applications to nuclear power containment vessels: Creep fracture, Transport (gas and liquid) in porous media, permeability, hydro-mechanical behavior.
- 2 Rock: Blasting; Hydro-fracturing.
- 3 Metals (connections under seismic excitation).
- 4 Solid rocket propellants (polymers).

- Emphasis will be on **Problem formulation** and outline of solution (skipping details) and **final solution**
- Coverage will not be exclusively mechanics, theory, application, but rather a **delicate (and dynamically varying) mix**.
- Heavy emphasis on term paper and term project which could hopefully be tied to your research interest.
- Occasional presentation of your work throughout the semester.

A very important component of the course. **Past Term Projects** Can be viewed [here](#).

- Cohesive Crack Models
- Cohesive Cracks For Interfaces
- Concrete Under High Temperatures
- Concrete Fracture
- Crack Between 2 Dissimilar Materials
- Crack Propagation In Aluminium Panels
- Dynamic Fracture Mechanics
- Fatigue Crack Propagation With Retardation
- Fatigue Crack Propagation
- Fracture Mechanics Based Simulation Of Anchors
- Fracture And Fractals
- Analysis Of Butt Welded Joints
- Cohesive Crack Models
- Cohesive Cracks For Interfaces
- Concrete Under High Temperatures
- Fracture and flow (liquid and/or gas).
- Concrete Fracture
- Crack Between 2 Dissimilar Materials
- Crack Detection Location With White Noise Vibration
- Crack Propagation In Draw Cylinder
- Crack Propagation In Aluminium Panels
- Fracture In Solid Rocket Propellants
- Fracture Mechanics Of Bond In reinforced concrete
- Fracture Mechanics Partition Unity Method
- Fracture Steel Connection Under Earthquake Load
- Fracture Testing Of Concrete
- Indentation Of Rock; Numerical Simulation
- Numerical Fracture Simulation Of Porous Sintered Steels
- Size Effects On Shear Strength
- Slope Stability
- Steel Fiber Reinforced Concrete

Elements of Solid Mechanics

for Fracture Mechanics

Victor E. Saouma
saouma@colorado.edu

University of Colorado, Boulder

Spring 2022

1 Tensors

- Tensors: Definition
- Tensors: Indicjal Notation
- Tensor Operations
- Rotation of Axes
- Tensor Transformation
- Trace and Inverse
- Principal Values of Symmetric Second Order Tensors

2 Calculus Review

3 Kinetics

- Force, Traction and Body Forces
- Cauchy's Stress Tensor
 - Example
- Spherical and Deviatoric Stress Tensors

4 Kinematic

- Position and Displacement
- Strains

- Compatibility Equation

5 Fundamental Laws of Continuum Mechanics

- Conservation Laws
- Conservation of Momentum
- Conservation of Energy; First Principle of Thermodynamics

6 Intermission

7 Constitutive Equations

- Hooke
- Lamé's Constants
- Expanded

8 Airy Stress Functions

- Real Variables; Cartesian
- Complex Variables; Cartesian
- Complex variables; Elliptical Coordinates

9 Basic Equations of Anisotropic Elasticity

- Plane Stress-Strain Compliance Transformation

Table of Contents III

- Stress Functions
- Stresses and Displacements

- Generalize the concept of a vector by introducing the **tensor** (\mathbb{T}).
- A tensor is an operator which **operates on tensors to produce other tensors**.
- Designate this operation as $\mathbb{T} \cdot \mathbf{v}$ or simply $\mathbb{T}\mathbf{v}$.
- A tensor is also a physical quantity, **independent of any particular coordinate system** yet specified most conveniently by referring to an appropriate system of coordinates.
- A tensor is classified by the **rank or order**. A Tensor of order zero is specified in any coordinate system by one coordinate and is a scalar (such as temperature). A tensor of order one has three coordinate components in space, hence it is a vector (such as force). In general 3-D space the number of components of a tensor is 3^n where n is the order of the tensor.
- A force and a stress are tensors of order 1 and 2 respectively.

- Engineering notation may be the simplest and most intuitive one, it often leads to long and repetitive equations. Alternatively, tensor or the dyadic form will lead to shorter and more compact forms.
- The following rules define indicial notation:

- If there is one letter index (**free index**), that index goes from i to n (range of the tensor). For instance:

$$a_i = a^j = [a_1 \quad a_2 \quad a_3] = \left\{ \begin{array}{c} a_1 \\ a_2 \\ a_3 \end{array} \right\} \quad i = 1, 3$$

assuming that $n = 3$.

- A **repeated** index or (**dummy index**) will take on all the values of its range, and the resulting tensors summed. In general no index occurs more than twice in a properly written expression. For instance:

$$a_{1i}x_i = a_{11}x_1 + a_{12}x_2 + a_{13}x_3$$

- Tensor's order:

- **First order** tensor (such as force) has only one free index:

$$a_i = a^i = [a_1 \quad a_2 \quad a_3]$$

other first order tensors $a_j b_j = a_{j1} b_1 + a_{j2} b_2 + a_{j3} b_3$, F_{ikk} , $\varepsilon_{ijk} u_j v_k$
(note that there is only one free index).

- **Second order** tensor (such as stress or strain) will have two free indices.

$$T_{ij} = \begin{bmatrix} T_{11} & T_{12} & T_{13} \\ T_{21} & T_{22} & T_{23} \\ T_{31} & T_{32} & T_{33} \end{bmatrix}$$

other examples A_{jip} , $\delta_{ij} u_k v_k$.

- A **fourth order** tensor (such as Elastic constants) will have four free indices: $\sigma_{ij} = D_{ijkl} \varepsilon_{kl}$

- ④ **Derivatives** of tensor with respect to x_i is written as $_{,i}$. For example:

$$\frac{\partial \phi}{\partial x_i} = \phi_{,i} \quad \frac{\partial v_j}{\partial x_i} = v_{i,j} \quad \frac{\partial v_i}{\partial x_j} = v_{i,j} \quad \frac{\partial T_{i,j}}{\partial x_k} = T_{i,j,k}$$

- Usefulness of the indicial notation is in presenting systems of equations in **compact form**. For instance:

$$x_i = c_{ij}z_j$$

this simple compacted equation, when expanded would yield:

$$x_1 = c_{11}z_1 + c_{12}z_2 + c_{13}z_3$$

$$x_2 = c_{21}z_1 + c_{22}z_2 + c_{23}z_3$$

$$x_3 = c_{31}z_1 + c_{32}z_2 + c_{33}z_3$$

Similarly:

$$A_{ij} = B_{ip}c_{jq}d_{pq}$$

$$A_{11} = B_{11}c_{11}d_{11} + B_{11}c_{12}d_{12} + B_{12}c_{11}d_{21} + B_{12}c_{12}d_{22}$$

$$A_{12} = B_{11}c_{21}d_{11} + B_{11}c_{22}d_{12} + B_{12}c_{21}d_{21} + B_{12}c_{22}d_{22}$$

$$A_{21} = B_{21}c_{11}d_{11} + B_{21}c_{12}d_{12} + B_{22}c_{11}d_{21} + B_{22}c_{12}d_{22}$$

$$A_{22} = B_{21}c_{21}d_{11} + B_{21}c_{22}d_{12} + B_{22}c_{21}d_{21} + B_{22}c_{22}d_{22}$$

- Using indicial notation, we may rewrite the definition of the **dot product**

$$\mathbf{a} \cdot \mathbf{b} = a_i b_i = (a_x \mathbf{i} + a_y \mathbf{j} + a_z \mathbf{k}) \cdot (b_x \mathbf{i} + b_y \mathbf{j} + b_z \mathbf{k}) = a_x b_x + a_y b_y + a_z b_z$$

- Note that one can adopt the **dyadic** instead of the **indicial** notation for tensors as **linear vector operators** $\mathbf{u} = \mathbf{T} \cdot \mathbf{v}$ or $u_i = T_{ij} v_j$

- The **sum** of two tensors (must be of the same order) is simply defined as:

$$S_{ij} = T_{ij} + U_{ij}$$

- The **scalar multiplication** of a (second order) tensor is defined by:

$$S_{ij} = \lambda T_{ij}$$

- The **outer product** of two tensors is the tensor whose components are formed by multiplying each component of one of the tensors by every component of the other. This produces a tensor with an order equal to the sum of the orders of the factor tensors.

$$\begin{aligned}
 a_i b_j &= T_{ij} & \text{or } \left\{ \begin{array}{l} \\ \end{array} \right\}_{nx1} \left[\begin{array}{l} \\ \end{array} \right]_{1xm} &= \left[\begin{array}{l} \\ \end{array} \right]_{nxm} \\
 v_i F_{jk} &= b_{ijk} \\
 D_{ij} T_{km} &= \Phi_{ijklm}
 \end{aligned}$$

- The **inner product** of two tensors: **contraction** of one index from each tensor

$$\begin{aligned}
 & a_i b_i \\
 a_i E_{ik} &= f_k \quad \text{or} \quad \left[\begin{array}{c}]_{1xm} \\ \end{array} \right] \left[\begin{array}{c} \\ \end{array} \right]^{mxn} = \left[\begin{array}{c}]_{1xn} \\ \end{array} \right] \\
 E_{ij} F_{jm} &= G_{im} \quad \text{or} \quad \left[\begin{array}{c} \\ \end{array} \right]_{nxp} \left[\begin{array}{c} \\ \end{array} \right]^{pxm} = \left[\begin{array}{c} \\ \end{array} \right]_{nxm}
 \end{aligned}$$

- The **cross product** can be defined

$$\mathbf{a} \times \mathbf{b} = \varepsilon_{pqr} a_q b_r \mathbf{e}_p = (a_y b_z - a_z b_y) \mathbf{i} + (a_z b_x - a_x b_z) \mathbf{j} + (a_x b_y - a_y b_x) \mathbf{k}$$

In the second equation, there is one free index p thus there are three equations, there are two repeated (dummy) indices q and r , thus each equation has nine terms. ε_{pqr} is called the **permutation symbol** and is defined as

$$\varepsilon_{pqr} = \begin{cases} 1 & \text{If the value of } i, j, k \text{ are an } \mathbf{even permutation} \text{ of } 1,2,3 \\ & \text{(i.e. if they appear as } 1\ 2\ 3\ 1\ 2) \\ -1 & \text{If the value of } i, j, k \text{ are an } \mathbf{odd permutation} \text{ of } 1,2,3 \\ & \text{(i.e. if they appear as } 3\ 2\ 1\ 3\ 2) \\ 0 & \text{If the value of } i, j, k \text{ are } \mathbf{not permutation} \text{ of } 1,2,3 \\ & \text{(i.e. if two or more indices have the same value)} \end{cases}$$

- The **scalar product** of two tensors is defined as

$$\mathbf{T} : \mathbf{U} = T_{ij} U_{ij}$$

in any rectangular system.

- The following **inner-product** axioms are satisfied:

$$\begin{aligned} \mathbf{T} : \mathbf{U} &= \mathbf{U} : \mathbf{T} \\ \mathbf{T} : (\mathbf{U} + \mathbf{V}) &= \mathbf{T} : \mathbf{U} + \mathbf{T} : \mathbf{V} \\ \alpha(\mathbf{T} : \mathbf{U}) &= (\alpha\mathbf{T}) : \mathbf{U} = \mathbf{T} : (\alpha\mathbf{U}) \\ \mathbf{T} : \mathbf{T} &> 0 \text{ unless } \mathbf{T} = 0 \end{aligned}$$

- Consider two different sets of cartesian orthonormal coordinate systems $\{e_1, e_2, e_3\}$ and $\{\bar{e}_1, \bar{e}_2, \bar{e}_3\}$, any vector \mathbf{v} can be expressed in one system or the other

$$\mathbf{v} = v_j \mathbf{e}_j = \bar{v}_j \bar{\mathbf{e}}_j$$

- To determine the relationship between the two sets of components, we consider the dot product of \mathbf{v} with one (any) of the base vectors

$$\bar{\mathbf{e}}_i \cdot \mathbf{v} = \bar{v}_i = v_j (\bar{\mathbf{e}}_i \cdot \mathbf{e}_j)$$

- We can thus define the nine scalar values

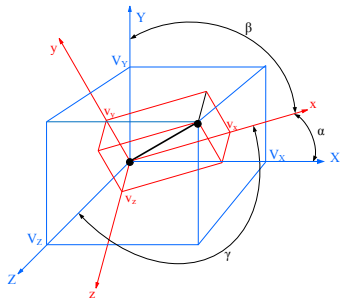
$$a_j^i \equiv \bar{\mathbf{e}}_i \cdot \mathbf{e}_j = \cos(\bar{X}_i, X_j)$$

which are the **direction cosines** between the nine pairing of base vectors.

- A **covariant transformation** will transform a tensor from one basis to another:

$$\bar{v}_j = a_j^p v_p \quad (1)$$

note that the free index in the first and second equations appear on the upper and lower index respectively.



- Consider the transformation of a vector V from (X, Y, Z) coordinate system to (x, y, z)
- From Eq. 1

$$V_j = a_j^p \bar{V}_p \text{ or } \begin{cases} V_1 &= a_1^1 \bar{V}_1 + a_1^2 \bar{V}_2 + a_1^3 \bar{V}_3 \\ V_2 &= a_2^1 \bar{V}_1 + a_2^2 \bar{V}_2 + a_2^3 \bar{V}_3 \\ V_3 &= a_3^1 \bar{V}_1 + a_3^2 \bar{V}_2 + a_3^3 \bar{V}_3 \end{cases}$$

or

$$\begin{Bmatrix} V_x \\ V_y \\ V_z \end{Bmatrix} = \underbrace{\begin{bmatrix} a_x^X & a_x^Y & a_x^Z \\ a_y^X & a_y^Y & a_y^Z \\ a_z^X & a_z^Y & a_z^Z \end{bmatrix}}_{a_j^k} \begin{Bmatrix} V_X \\ V_Y \\ V_Z \end{Bmatrix}$$

- a_j^i is the direction cosine of axis i with respect to axis j
 - $a_x^j = (a_x^X, a_x^Y, a_x^Z)$ direction cosines of x with respect to X, Y and Z

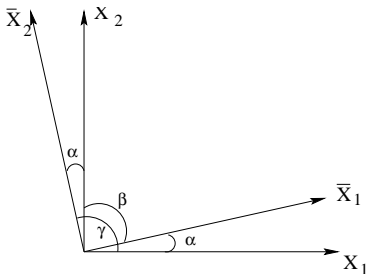
- $a_y^j = (a_y^X, a_y^Y, a_y^Z)$ direction cosines of y with respect to X, Y and Z
- $a_z^j = (a_z^X, a_z^Y, a_z^Z)$ direction cosines of z with respect to X, Y and Z

For the 2D case, the transformation matrix is written as

$$T = \begin{bmatrix} a_1^1 & a_1^2 \\ a_2^1 & a_2^2 \end{bmatrix} = \begin{bmatrix} \cos \alpha & \cos \beta \\ \cos \gamma & \cos \alpha \end{bmatrix}$$

but since $\gamma = \frac{\pi}{2} + \alpha$, and $\beta = \frac{\pi}{2} - \alpha$, then $\cos \gamma = -\sin \alpha$ and $\cos \beta = \sin \alpha$, thus the transformation matrix becomes

$$T = \begin{bmatrix} \cos \alpha & \sin \alpha \\ -\sin \alpha & \cos \alpha \end{bmatrix}$$



- Rotation of a second order tensor T_{jq} :

$$\begin{aligned}\bar{u}_j &= T_{jq}\bar{v}_q \\ \bar{u}_i &= a_i^j u_j \\ &= a_i^j T_{jq} v_q \\ &= a_i^j T_{jq} a_p^q \bar{v}_p\end{aligned}$$

But we also have $\bar{u}_i = \bar{T}_{ip}\bar{v}_p$ in the barred system, equating these two expressions we obtain

$$\bar{T}_{ip} = a_i^j a_p^q T_{jq}$$

hence

$$\bar{T}_{ip} = a_i^j a_p^q T_{jq} \text{ in Matrix Form } [\bar{T}] = [A]^T [T] [A] \quad (2)$$

$$T_{jq} = a_j^i a_q^p \bar{T}_{ip} \text{ in Matrix Form } [T] = [A] [\bar{T}] [A]^T \quad (3)$$

- If we consider the 2D case, From Eq. 13

$$A = \begin{bmatrix} \cos \alpha & \sin \alpha & 0 \\ -\sin \alpha & \cos \alpha & 0 \\ 0 & 0 & 1 \end{bmatrix}$$

$$T = \begin{bmatrix} T_{xx} & T_{xy} & 0 \\ T_{xy} & T_{yy} & 0 \\ 0 & 0 & 0 \end{bmatrix}$$

$$\bar{T} = \begin{bmatrix} \bar{T}_{xx} & \bar{T}_{xy} & 0 \\ \bar{T}_{xy} & \bar{T}_{yy} & 0 \\ 0 & 0 & 0 \end{bmatrix} = A^T T A$$

Substituting

$$\bar{T} = \begin{bmatrix} \cos^2 \alpha T_{xx} + \sin^2 \alpha T_{yy} + \sin 2\alpha T_{xy} & \frac{1}{2}(-\sin 2\alpha T_{xx} + \sin 2\alpha T_{yy} + 2 \cos 2\alpha T_{xy}) & 0 \\ \frac{1}{2}(-\sin 2\alpha T_{xx} + \sin 2\alpha T_{yy} + 2 \cos 2\alpha T_{xy}) & \sin^2 \alpha T_{xx} + \cos^2 \alpha T_{yy} - 2 \sin \alpha \cos \alpha T_{xy} & 0 \\ 0 & 0 & 0 \end{bmatrix}$$

alternatively, using $\sin 2\alpha = 2 \sin \alpha \cos \alpha$ and $\cos 2\alpha = \cos^2 \alpha - \sin^2 \alpha$, this last equation can be rewritten as

$$\begin{Bmatrix} \bar{T}_{xx} \\ \bar{T}_{yy} \\ \bar{T}_{xy} \end{Bmatrix} = \begin{bmatrix} \cos^2 \theta & \sin^2 \theta & 2 \sin \theta \cos \theta \\ \sin^2 \theta & \cos^2 \theta & -2 \sin \theta \cos \theta \\ -\sin \theta \cos \theta & \cos \theta \sin \theta & \cos^2 \theta - \sin^2 \theta \end{bmatrix} \begin{Bmatrix} T_{xx} \\ T_{yy} \\ T_{xy} \end{Bmatrix}$$

- The **trace** of a second-order tensor, denoted $\text{tr } \mathbf{T}$ is a scalar invariant function of the tensor and is defined as

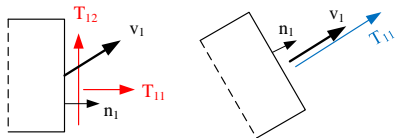
$$\text{tr } \mathbf{T} \equiv T_{ii}$$

Thus it is equal to the sum of the diagonal elements in a matrix.

- An **inverse tensor** is simply defined as follows

$$\mathbf{T}^{-1}(\mathbf{T}\mathbf{v}) = \mathbf{v} \quad \text{and} \quad \mathbf{T}(\mathbf{T}^{-1}\mathbf{v}) = \mathbf{v}$$

alternatively $\mathbf{T}^{-1}\mathbf{T} = \mathbf{T}\mathbf{T}^{-1} = \mathbf{I}$, or $T_{ik}^{-1}T_{kj} = \delta_{ij}$ and $T_{ik}T_{kj}^{-1} = \delta_{ij}$



- Two fundamental tensors in continuum mechanics are **second order and symmetric** (stress and strain), we examine some important properties of these tensors.

- For every symmetric tensor T_{ij} defined at some point in space, there is associated with each direction (specified by unit normal n_j) at that point, a vector given by the inner product

$$v_i = T_{ij}n_j$$

It will be later shown that this is the relationship between stress (T) and traction (v)

- If the direction is one for which v_i is **parallel** to n_i , the inner product is

$$T_{ij}n_j = \lambda n_i$$

and the direction n_i is called **principal direction** of T_{ij} . Since $n_i = \delta_{ij}n_j$, this can be rewritten as

$$(T_{ij} - \lambda\delta_{ij})n_j = 0$$

- This is an **Eigenvalue problem** in which the Eigenvalues correspond to the principal stresses and the **Eigenvectors** correspond to the principal stress directions. Hence, we can easily compute principal stresses for any Cauchy stress tensor by simply computing the Eigenvalues of the stress tensor.
- To have a non-trivial solution ($n_i \neq 0$) the determinant of the coefficients must be zero,

$$|T_{ij} - \lambda\delta_{ij}| = 0$$

- Expansion of this determinant leads to the following **characteristic equation**

$$\lambda^3 - I_T\lambda^2 + II_T\lambda - III_T = 0$$

the roots are called the **principal values** of T_{ij} and

$$\begin{aligned} I_T &= T_{ii} = \text{tr } T_{ij} \\ II_T &= \frac{1}{2}(T_{ii}T_{jj} - T_{ij}T_{ji}) \\ III_T &= |T_{ij}| = \det T_{ij} \end{aligned}$$

are called the first, second and third **invariants** respectively of T_{ij} .

- It is customary to order those roots as $\lambda_{(1)} > \lambda_{(2)} > \lambda_{(3)}$
- In terms of the principal stresses, those invariants can be simplified into

$$\begin{aligned}I_T &= T_{(1)} + T_{(2)} + T_{(3)} \\II_T &= -(T_{(1)} T_{(2)} + T_{(2)} T_{(3)} + T_{(3)} T_{(1)}) \\III_T &= T_{(1)} T_{(2)} T_{(3)}\end{aligned}$$

- For a symmetric tensor with real components, the principal values are also real. If those values are distinct, the three principal directions are **mutually orthogonal**.

$$A + B = B + A$$

$$A \times B = -B \times A$$

$$A = A_x i + A_y j + A_z k$$

$$\begin{aligned} A \cdot B &= |A||B|\cos(A, B) \\ &= A_x B_x + A_y B_y + A_z B_z \end{aligned}$$

$$A \otimes B = \begin{vmatrix} i & j & k \\ A_x & A_y & A_z \\ B_x & B_y & B_z \end{vmatrix}$$

$$\text{grad } A = \nabla A = i \frac{\partial A}{\partial x} + j \frac{\partial A}{\partial y} + k \frac{\partial A}{\partial z}$$

$$\begin{aligned} \text{div } A = \nabla \cdot A &= \left(i \frac{\partial}{\partial x} + j \frac{\partial}{\partial y} + k \frac{\partial}{\partial z} \right) \\ &\quad \cdot (iA_x + jA_y + kA_z) \\ &= \frac{\partial A_x}{\partial x} + \frac{\partial A_y}{\partial y} + \frac{\partial A_z}{\partial z} \end{aligned}$$

$$\begin{aligned} \text{Laplacian } \nabla^2 &= \nabla \cdot \nabla \\ &= \frac{\partial^2 A}{\partial x^2} + \frac{\partial^2 A}{\partial y^2} + \frac{\partial^2 A}{\partial z^2} \end{aligned}$$

Integration by part

$$\int_a^b u(x)v'(x)dx = u(x)v(x)|_a^b - \int_a^b v(x)u'(x)dx$$

$$\int_a^b u dv = uv|_a^b - \int_a^b v du$$

Green-Gradient Theorem

$$\oint (Rdx + Sdy) = \int_{\Gamma} \left(\frac{\partial S}{\partial x} - \frac{\partial R}{\partial y} \right) dx dy$$

Gauss-Divergence Theorem

$$\int_{\Gamma} v \cdot n d\Gamma = \int_{\Omega} \text{div } v d\Omega$$

$$\int_{\Gamma} v_i n_i d\Gamma = \int_{\Omega} v_{i,i} d\Omega$$

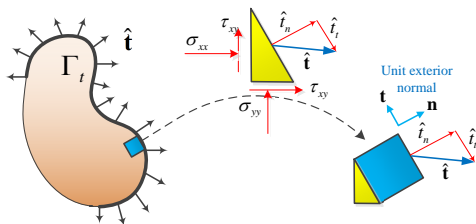
$$\int_{\Omega} \text{div } q d\Omega = \int_{\Gamma} q^T \cdot n d\Gamma$$

$$\int_{\Omega} v_{i,i} d\Omega = \int_{\Gamma} v_i n_i d\Gamma$$

- There are two kinds of **forces** in continuum mechanics

body forces: act on the elements of volume or mass inside the body, e.g. gravity, electromagnetic fields. $d\mathbf{F} = \rho \mathbf{b} dVol$.

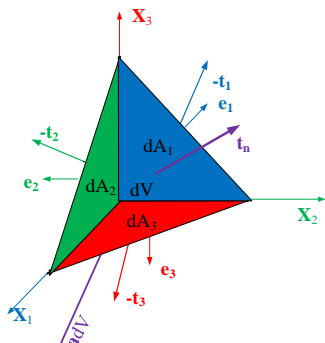
Surface forces (or **traction**) are contact forces acting on the free body at its bounding surface. Those will be defined in terms of **force per unit area**.



$$\int_{\Gamma} \mathbf{t} d\Gamma = i \int_{\Gamma} t_x d\Gamma + j \int_{\Gamma} t_y d\Gamma + k \int_{\Gamma} t_z d\Gamma$$

- Usually limit the term traction to an actual bounding surface of a body, and use the term **stress vector** (\mathbf{t}) (not yet defined, see below) for an imaginary interior surface.

- The concept of force was at first abstract, Aristotelian physics referred to **impetus**. Galileo and Newton (1687) formalized it.
- The concept of **stress** was not firmly understood until Cauchy
- In 1822, Cauchy presented the idea of traction vector that contains both the normal and tangential components $t = t_n e_n + t_t e_t$
- His “genius” was to consider what became known as the **Cauchy tetrahedron** and applied Newton's second law (or more precisely its extension to particles by Euler: Euler's first law of motion)



- Equilibrium of the Cauchy tetrahedron:

$$t dA - t_1 dA_1 - t_2 dA_2 - t_3 dA_3 = \rho dV a \quad (4)$$

a is the acceleration and ρ the mass density.

- The areas of the faces are given by

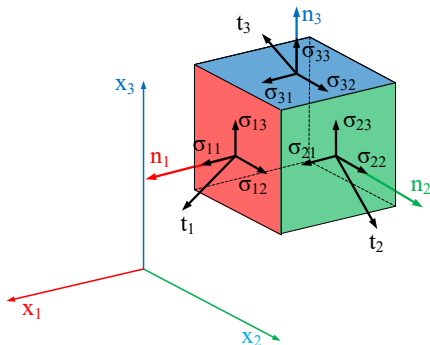
$$dA_1 = n \cdot e_1 dA = n_1 dA$$

$$dA_2 = n \cdot e_2 dA = n_2 dA$$

$$dA_3 = n \cdot e_3 dA = n_3 dA$$

- Substituting in the equilibrium equation, and considering the limiting case where $dV \rightarrow 0$

$$\mathbf{t} = t_1 \mathbf{n}_1 + t_2 \mathbf{n}_2 + t_3 \mathbf{n}_3 \quad (5)$$



- The traction vectors must have components

$$\begin{aligned} t_1 &= \sigma_{11} \mathbf{e}_1 + \sigma_{12} \mathbf{e}_2 + \sigma_{13} \mathbf{e}_3 \\ t_2 &= \sigma_{21} \mathbf{e}_1 + \sigma_{22} \mathbf{e}_2 + \sigma_{23} \mathbf{e}_3 \\ t_3 &= \sigma_{31} \mathbf{e}_1 + \sigma_{32} \mathbf{e}_2 + \sigma_{33} \mathbf{e}_3 \end{aligned} \quad (6)$$

- Note that historically and traditionally in continuum mechanics the stress is denoted by \mathbb{T} . This was replaced by σ (I believe through the Voigt notation).

- Substituting into Eq. 5

$$\begin{aligned} \mathbf{t} &= n_1(\sigma_{11} \mathbf{e}_1 + \sigma_{12} \mathbf{e}_2 + \sigma_{13} \mathbf{e}_3) + n_2(\sigma_{21} \mathbf{e}_1 + \sigma_{22} \mathbf{e}_2 + \sigma_{23} \mathbf{e}_3) + n_3(\sigma_{31} \mathbf{e}_1 + \sigma_{32} \mathbf{e}_2 + \sigma_{33} \mathbf{e}_3) \\ &= (n_1 \sigma_{11} + n_2 \sigma_{21} + n_3 \sigma_{31}) \mathbf{e}_1 + (n_1 \sigma_{12} + n_2 \sigma_{22} + n_3 \sigma_{32}) \mathbf{e}_2 + (n_1 \sigma_{13} + n_2 \sigma_{23} + n_3 \sigma_{33}) \mathbf{e}_3 \end{aligned} \quad (7)$$

or

$$\mathbf{t}_n = \mathbf{n} \cdot \boldsymbol{\sigma} \quad (8)$$

- Hence, there is a second order tensor called **Cauchy stress tensor** where the 1st subscript (i) refers to the direction of outward facing normal, and the second one (j) to the direction of component force.

$$\left\{ \begin{array}{c} t_1 \\ t_2 \\ t_3 \end{array} \right\} = \underbrace{\begin{bmatrix} \sigma_{11} & \sigma_{12} & \sigma_{13} \\ \sigma_{21} & \sigma_{22} & \sigma_{23} \\ \sigma_{31} & \sigma_{32} & \sigma_{33} \end{bmatrix}}_{\boldsymbol{\sigma}} \quad (9)$$

- The preceding equations played a major role in the foundation of **Continuum mechanics**.
- Voigt Notation (commonly used in engineering) is a way to represent the symmetric tensor by reducing its order.

$$\boldsymbol{\sigma} = \begin{bmatrix} \sigma_{xx} & \sigma_{xy} & \sigma_{xz} \\ \sigma_{yx} & \sigma_{yy} & \sigma_{yz} \\ \sigma_{zx} & \sigma_{zy} & \sigma_{zz} \end{bmatrix} \rightarrow [\sigma_{xx} \quad \sigma_{yy} \quad \sigma_{zz} \quad \sigma_{xy} \quad \sigma_{xz} \quad \sigma_{yz}] \quad (10)$$

- Note: we have not yet introduced the equation of equilibrium (momentum equation).

- For a stress tensor at point P given by

$$\sigma = \begin{bmatrix} 7 & -5 & 0 \\ -5 & 3 & 1 \\ 0 & 1 & 2 \end{bmatrix} = \begin{Bmatrix} t_1 \\ t_2 \\ t_3 \end{Bmatrix}$$

We seek to determine the traction (or stress vector) t passing through P and parallel to the plane ABC where $A(4, 0, 0)$, $B(0, 2, 0)$ and $C(0, 0, 6)$.

- The vector normal to the plane can be found by taking the cross products of vectors AB and AC :

$$\begin{aligned} N &= AB \times AC = \begin{vmatrix} e_1 & e_2 & e_3 \\ -4 & 2 & 0 \\ -4 & 0 & 6 \end{vmatrix} \\ &= 12e_1 + 24e_2 + 8e_3 \end{aligned}$$

- The unit normal of N is given by

$$\mathbf{n} = \frac{3}{7}\mathbf{e}_1 + \frac{6}{7}\mathbf{e}_2 + \frac{2}{7}\mathbf{e}_3$$

Hence the stress vector (traction) will be

$$\begin{bmatrix} \frac{3}{7} & \frac{6}{7} & \frac{2}{7} \end{bmatrix} \begin{bmatrix} 7 & -5 & 0 \\ -5 & 3 & 1 \\ 0 & 1 & 2 \end{bmatrix} = \begin{bmatrix} -\frac{9}{7} & \frac{5}{7} & \frac{10}{7} \end{bmatrix}$$

and thus $\mathbf{t} = -\frac{9}{7}\mathbf{e}_1 + \frac{5}{7}\mathbf{e}_2 + \frac{10}{7}\mathbf{e}_3$

- let σ denote the **mean normal stress** p

$$\sigma = -p = \frac{1}{3}(\sigma_{11} + \sigma_{22} + \sigma_{33}) = \frac{1}{3}\sigma_{ii} = \frac{1}{3}\text{tr } \sigma$$

then the **stress tensor can be written as the sum of two tensors:**

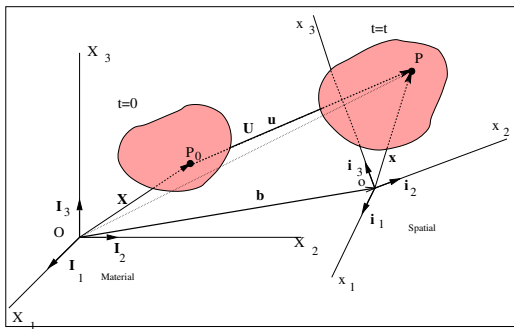
Hydrostatic stress in which **each normal stress is equal to $-p$ and the shear stresses are zero.** The hydrostatic stress produces **volume change without change in shape in an isotropic medium.**

$$\sigma_{hyd} = -p\mathbf{I} = \begin{bmatrix} -p & 0 & 0 \\ 0 & -p & 0 \\ 0 & 0 & -p \end{bmatrix}$$

Deviatoric Stress: which **causes the change in shape.**

$$\sigma_{dev} = \begin{bmatrix} \sigma_{11} - \sigma & \sigma_{12} & \sigma_{13} \\ \sigma_{21} & \sigma_{22} - \sigma & \sigma_{23} \\ \sigma_{31} & \sigma_{32} & \sigma_{33} - \sigma \end{bmatrix}$$

- The undeformed configuration of a material continuum at time $t = 0$ together with the deformed configuration at $t = t$.



- In the initial configuration P_0 has the **position vector**

$$\mathbf{X} = X_1 \mathbf{I}_1 + X_2 \mathbf{I}_2 + X_3 \mathbf{I}_3$$

which is here expressed in terms of the **material coordinates** (X_1, X_2, X_3) .

- In the deformed configuration, the particle P_0 has now moved to the new position P and has the following position vector

$$\mathbf{x} = x_1 \mathbf{i}_1 + x_2 \mathbf{i}_2 + x_3 \mathbf{i}_3$$

which is expressed in terms of the **spatial coordinates**.

- The displacement vector \mathbf{u} connecting P_0 and P is the **displacement vector** which can be expressed in both the material or spatial coordinates

$$\mathbf{U} = U_K \mathbf{I}_K$$

$$\mathbf{u} = u_k \mathbf{i}_k$$

- From the preceding figure we can express motion as

$$x_i = x_i(X_1, X_2, X_3, t) \quad \text{Lagrangian formulation}$$

$$X_i = X_i(x_1, x_2, x_3, t) \quad \text{Eulerian formulation}$$

- Ignoring a detailed analysis of large deformation, it is determined that

		Displacement gradient	
		Small	Large
Displacement	Small	Lagrangian small strain (Cauchy)	Lagrangian large strain (Green-Lagrange)
	Large	Eulerian small strain	Eulerian finite strain (Eulerian-Almansi)

- The **Lagrangian finite strain tensor** can be written as

$$\varepsilon_{ij} = \frac{1}{2} (u_{i,j} + u_{j,i} + u_{k,i}u_{k,j})$$

- Alternatively these equations may be expanded as

$$\varepsilon_{xx} = \frac{\partial u}{\partial x} + \frac{1}{2} \left[\left(\frac{\partial u}{\partial x} \right)^2 + \left(\frac{\partial v}{\partial x} \right)^2 + \left(\frac{\partial w}{\partial x} \right)^2 \right]$$

$$\varepsilon_{yy} = \frac{\partial v}{\partial y} + \frac{1}{2} \left[\left(\frac{\partial u}{\partial y} \right)^2 + \left(\frac{\partial v}{\partial y} \right)^2 + \left(\frac{\partial w}{\partial y} \right)^2 \right]$$

$$\varepsilon_{zz} = \frac{\partial w}{\partial z} + \frac{1}{2} \left[\left(\frac{\partial u}{\partial z} \right)^2 + \left(\frac{\partial v}{\partial z} \right)^2 + \left(\frac{\partial w}{\partial z} \right)^2 \right]$$

$$\varepsilon_{xy} = \frac{1}{2} \left(\frac{\partial v}{\partial x} + \frac{\partial u}{\partial y} + \frac{\partial u}{\partial x} \frac{\partial u}{\partial y} + \frac{\partial v}{\partial x} \frac{\partial v}{\partial y} + \frac{\partial w}{\partial x} \frac{\partial w}{\partial y} \right)$$

$$\varepsilon_{xz} = \frac{1}{2} \left(\frac{\partial w}{\partial x} + \frac{\partial u}{\partial z} + \frac{\partial u}{\partial x} \frac{\partial u}{\partial z} + \frac{\partial v}{\partial x} \frac{\partial v}{\partial z} + \frac{\partial w}{\partial x} \frac{\partial w}{\partial z} \right)$$

$$\varepsilon_{yz} = \frac{1}{2} \left(\frac{\partial w}{\partial y} + \frac{\partial v}{\partial z} + \frac{\partial u}{\partial y} \frac{\partial u}{\partial z} + \frac{\partial v}{\partial y} \frac{\partial v}{\partial z} + \frac{\partial w}{\partial y} \frac{\partial w}{\partial z} \right)$$

- We define the **engineering shear strain** as

$$\gamma_{ij} = 2\varepsilon_{ij} \quad (i \neq j)$$

- Note that for small displacements, the strains can be expressed as

$$\underbrace{\begin{Bmatrix} \varepsilon_{xx} \\ \varepsilon_{yy} \\ \varepsilon_{zz} \\ \varepsilon_{xy} \\ \varepsilon_{xz} \\ \varepsilon_{yz} \end{Bmatrix}}_{\boldsymbol{\varepsilon}} = \underbrace{\begin{bmatrix} \frac{\partial}{\partial x} & 0 & 0 \\ 0 & \frac{\partial}{\partial y} & 0 \\ 0 & 0 & \frac{\partial}{\partial z} \\ \frac{\partial}{\partial y} & \frac{\partial}{\partial x} & 0 \\ \frac{\partial}{\partial z} & 0 & \frac{\partial}{\partial x} \\ 0 & \frac{\partial}{\partial z} & \frac{\partial}{\partial y} \end{bmatrix}}_{\mathbf{L}} \underbrace{\begin{Bmatrix} u_x \\ u_y \\ u_z \end{Bmatrix}}_u \quad (11)$$

- If $\varepsilon_{ij} = \frac{1}{2} (u_{i,j} + u_{j,i})$ then we have six differential equations (in 3D the strain tensor has a total of 9 terms, but due to symmetry, there are 6 independent ones) for determining (upon integration) three unknowns displacements u_i . Hence the system is overdetermined, and there must be some linear relations between the strains or **compatibility equations**
- It can be shown (through appropriate successive differentiation) that the compatibility relation for strain reduces to:

$$\frac{\partial^2 \varepsilon_{ik}}{\partial x_j \partial x_j} + \frac{\partial^2 \varepsilon_{jj}}{\partial x_i \partial x_k} - \frac{\partial^2 \varepsilon_{jk}}{\partial x_i \partial x_j} - \frac{\partial^2 \varepsilon_{ij}}{\partial x_j \partial x_k} = 0.$$

In 3D, this would yield 9 equations in total, however only six are distinct.

- In 2D, this results in (by setting $i = 2, j = 1$ and $k = 2$):

$$\frac{\partial^2 \varepsilon_{11}}{\partial x_2^2} + \frac{\partial^2 \varepsilon_{22}}{\partial x_1^2} = \frac{\partial^2 \gamma_{12}}{\partial x_1 \partial x_2} \quad (12)$$

(recall that $2\varepsilon_{12} = \gamma_{12}$).

- We have thus far studied **tensor fields** (stress and strain).
- We have also obtained only one differential equation, that was the compatibility equation.
- Next we still derive **additional differential equations** governing the way stress and deformation vary at a point and with time. They will apply to any continuous medium, and yet we will **not have enough equations** to determine unknown tensor field. For that we need to wait for constitutive laws relating stress and strain will be introduced.
- A conservation law states that a particular measurable property of an **isolated physical system** does not change as the system evolves over time.
- The fundamental equations are:
 - 1 Conservation of mass (continuity equation)
 - 2 **Conservation of momentum** (Equation of motion; Equilibrium)
 - 3 **Conservation of Energy.**

- A conservation law establishes a balance of a scalar or tensorial quantity in volume V bounded by a surface S (inside a control surface). In its most general form, such a law may be expressed as

$$\underbrace{\frac{d}{dt} \int_V A dV}_{\text{Rate of variation}} - \underbrace{\int_S \alpha dS}_{\text{Exchange by Diffusion}} = \underbrace{\int_V A dV}_{\text{Source}}$$

- The preceding equation reads: *rate of increase of A inside a control volume plus the rate of outward flux of A through the surface of the control volume is equal to the rate of increase of A inside the control volume*
- The dimensions of various quantities are given by

$$\dim(\alpha) = \dim(\mathcal{A}Lt^{-1})$$

$$\dim(A) = \dim(\mathcal{A}t^{-1})$$

rightfully all expressed in terms of \mathcal{A} .

- the time rate of change of the total momentum of a given set of particles equals the vector sum of all external forces acting on the particles of the set, provided Newton's Third Law applies.
- The continuum form of this principle is a **basic postulate of continuum mechanics** (postulate: a statement, also known as an axiom, which is taken to be true without proof).
- Starting with

$$\frac{d}{dt} \int_V \underbrace{\rho \mathbf{v}}_{\mathcal{A}} dV - \int_S \underbrace{\mathbf{t}}_{\alpha} dS = \int_V \underbrace{\rho \mathbf{b}}_{\mathcal{A}} dV$$

and noting that

$$\begin{aligned} \dim(\mathcal{A}) &= \rho \mathbf{v} = \frac{m}{L^2 t} \\ \dim(\alpha) &= \mathbf{t} = \frac{m \mathbf{a}}{L^2} = \frac{m}{L t^2} \\ \dim(\mathcal{A}) &= \rho \mathbf{b} = \frac{m}{L^3} \frac{L}{t^2} = \frac{m}{L^2 t^2} \end{aligned}$$

\mathbf{v} : velocity; \mathbf{t} : traction; \mathbf{b} body force

- Recall **Divergence Theorem**

$$\int_V v_{i,j} dV = \int_S \underbrace{v_i n_j}_{\text{flux}} dS$$

The flux of a vector function through some closed surface equals the integral of the divergence of that function over the volume enclosed by the surface.

- we substitute $t_i = T_{ij}n_j$ and apply the divergence theorem to obtain

$$\begin{aligned} \int_V \left(\frac{\partial T_{ij}}{\partial x_j} + \rho b_i \right) dV &= \int_V \rho \frac{dv_i}{dt} dV \\ \int_V \left[\frac{\partial T_{ij}}{\partial x_j} + \rho b_i - \rho \frac{dv_i}{dt} \right] dV &= 0 \end{aligned}$$

or for an arbitrary volume

$$\frac{\partial T_{ij}}{\partial x_j} + \rho b_i = \rho \frac{dv_i}{dt}$$

which is **Cauchy's (first) equation of motion**, or **the linear momentum principle**, or more simply **equilibrium equation**.

- When expanded in 3D, and for static problems, this equation yields:

$$\frac{\partial T_{11}}{\partial x_1} + \frac{\partial T_{12}}{\partial x_2} + \frac{\partial T_{13}}{\partial x_3} + \rho b_1 = 0$$

$$\frac{\partial T_{21}}{\partial x_1} + \frac{\partial T_{22}}{\partial x_2} + \frac{\partial T_{23}}{\partial x_3} + \rho b_2 = 0$$

$$\frac{\partial T_{31}}{\partial x_1} + \frac{\partial T_{32}}{\partial x_2} + \frac{\partial T_{33}}{\partial x_3} + \rho b_3 = 0$$

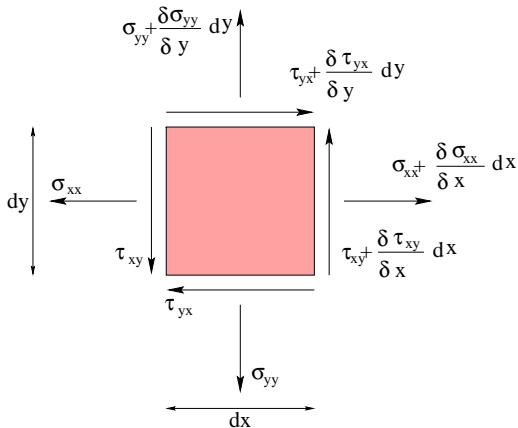
$$\underbrace{\begin{bmatrix} \frac{\partial}{\partial x_1} & 0 & 0 & \frac{\partial}{\partial x_2} & \frac{\partial}{\partial x_3} & 0 \\ 0 & \frac{\partial}{\partial x_2} & 0 & \frac{\partial}{\partial x_1} & \frac{\partial}{\partial x_3} & \frac{\partial}{\partial x_2} \\ 0 & 0 & \frac{\partial}{\partial x_3} & 0 & \frac{\partial}{\partial x_1} & \frac{\partial}{\partial x_2} \end{bmatrix}}_{\mathbf{L}} \underbrace{\begin{Bmatrix} T_{11} \\ T_{22} \\ T_{33} \\ T_{12} \\ T_{13} \\ T_{23} \end{Bmatrix}}_{\mathbf{T}} + \rho \underbrace{\begin{Bmatrix} b_1 \\ b_2 \\ b_3 \end{Bmatrix}}_{\mathbf{T}} = \begin{Bmatrix} 0 \\ 0 \\ 0 \end{Bmatrix} \quad (13)$$

Compare with Eq. 11.

- Divergence of the stress tensor is zero** (in the absence of body force and static).

$$\nabla \cdot \mathbf{T} = 0$$

- We note that these equations could also have been derived from the free body diagram with the **assumption of equilibrium** (via Newton's second law) considering an infinitesimal element of dimensions $dx_1 \times dx_2 \times dx_3$.



- If mechanical quantities only are considered, the **principle of conservation of energy** for the continuum may be derived directly from the equation of motion by taking the integral over the volume V of the scalar product and the **velocity v_i** .

$$\int_V v_i T_{ji,j} dV + \int_V v_i \rho b_i dV = \int_V v_i \rho \frac{dv_i}{dt} dV$$

Applying the divergence theorem, and skipping details of the derivation, we obtain:

$$\frac{dK}{dt} + \frac{dU}{dt} = \frac{dW}{dt} + Q$$

this equation relates the time rate of change of total mechanical energy of the continuum on the left side to the rate of work done by the surface and body forces on the right hand side.

- If both mechanical and non mechanical energies are to be considered, the first principle states that **the time rate of change of the kinetic plus the internal energy is equal to the sum of the rate of work plus all other energies supplied to, or removed from the continuum per unit time (heat, chemical, electromagnetic, etc.)**.

- For a thermomechanical continuum, it is customary to express the time rate of change of internal energy by the integral expression

$$\frac{dU}{dt} = \frac{d}{dt} \int_V \rho u dV$$

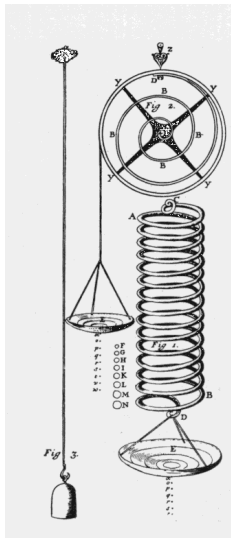
where u is the internal energy per unit mass or **specific internal energy**.

- The dimension of U is one of energy $\dim U = ML^2T^{-2}$, and the SI unit is the Joule, similarly $\dim u = L^2T^{-2}$ with the SI unit of Joule/Kg.

- If we define the tensor

$$\mathbb{T} = \begin{bmatrix} xy & x^2y \\ x^2y & 2x^2y \end{bmatrix}$$

- if $\mathbb{T} = \boldsymbol{\sigma}$, then it would have to satisfy the equation of equilibrium. If it fails, then we could add a body force vector to enforce equilibrium
- if $\mathbb{T} = \boldsymbol{\varepsilon}$, then it would have to satisfy the compatibility equation.



Hooke

ceiinossstuu

Hooke, 1676

Ut tensio sic vis

Hooke, 1678

- The Generalized Hooke's Law can be written as:

$$\sigma_{ij} = D_{ijkl} \varepsilon_{kl} \quad i, j, k, l = 1, 2, 3$$

- The (fourth order) tensor of elastic constants D_{ijkl} has 81 (3^4) components however, due to the symmetry of both σ and ε , there are at most 36 $\left(\frac{9(9-1)}{2}\right)$ distinct elastic terms.

- In terms of **Lame's constants** (which are naturally derived from continuum mechanics consideration, but can not be both experimentally measured), Hooke's Law for an isotropic body is written as

$$T_{ij} = \lambda \delta_{ij} E_{kk} + 2\mu E_{ij}; \quad E_{ij} = \frac{1}{2\mu} \left(T_{ij} - \frac{\lambda}{3\lambda + 2\mu} \delta_{ij} T_{kk} \right)$$

- In terms of engineering constants (which can be measured in the laboratory)

$$\begin{aligned} \frac{1}{E} &= \frac{\lambda + \mu}{\mu(3\lambda + 2\mu)}; & \nu &= \frac{\lambda}{2(\lambda + \mu)} \\ \lambda &= \frac{\nu E}{(1 + \nu)(1 - 2\nu)}; & \mu &= G = \frac{E}{2(1 + \nu)} \end{aligned}$$

- Hooke's law for isotropic material in terms of engineering constants becomes

$$\sigma_{ij} = \frac{E}{1 + \nu} \left(\varepsilon_{ij} + \frac{\nu}{1 - 2\nu} \delta_{ij} \varepsilon_{kk} \right); \quad \varepsilon_{ij} = \frac{1 + \nu}{E} \sigma_{ij} - \frac{\nu}{E} \delta_{ij} \sigma_{kk}$$

- When the strain equation is expanded in 3D cartesian coordinates it would yield:

$$\begin{Bmatrix} \varepsilon_{xx} \\ \varepsilon_{yy} \\ \varepsilon_{zz} \\ \gamma_{xy}(2\varepsilon_{xy}) \\ \gamma_{yz}(2\varepsilon_{yz}) \\ \gamma_{zx}(2\varepsilon_{zx}) \end{Bmatrix} = \frac{1}{E} \begin{bmatrix} 1 & -\nu & -\nu & 0 & 0 & 0 \\ -\nu & 1 & -\nu & 0 & 0 & 0 \\ -\nu & -\nu & 1 & 0 & 0 & 0 \\ 0 & 0 & 0 & 1+\nu & 0 & 0 \\ 0 & 0 & 0 & 0 & 1+\nu & 0 \\ 0 & 0 & 0 & 0 & 0 & 1+\nu \end{bmatrix} \begin{Bmatrix} \sigma_{xx} \\ \sigma_{yy} \\ \sigma_{zz} \\ \tau_{xy} \\ \tau_{yz} \\ \tau_{zx} \end{Bmatrix}$$

- Plane Strain

$$\begin{Bmatrix} \sigma_{xx} \\ \sigma_{yy} \\ \sigma_{zz} \\ \tau_{xy} \end{Bmatrix} = \frac{E}{(1+\nu)(1-2\nu)} \begin{bmatrix} (1-\nu) & \nu & 0 \\ \nu & (1-\nu) & 0 \\ \nu & \nu & 0 \\ 0 & 0 & \frac{1-2\nu}{2} \end{bmatrix} \begin{Bmatrix} \varepsilon_{xx} \\ \varepsilon_{yy} \\ \gamma_{xy} \end{Bmatrix}$$

- Axisymmetry

$$\begin{aligned}\varepsilon_{rr} &= \frac{\partial u}{\partial r}; & \varepsilon_{\theta\theta} &= \frac{u}{r} \\ \varepsilon_{zz} &= \frac{\partial w}{\partial z}; & \varepsilon_{rz} &= \frac{\partial u}{\partial z} + \frac{\partial w}{\partial r}\end{aligned}$$

The constitutive relation is again analogous to 3D/plane strain

$$\begin{Bmatrix} \sigma_{rr} \\ \sigma_{zz} \\ \sigma_{\theta\theta} \\ \tau_{rz} \end{Bmatrix} = \frac{E}{(1+\nu)(1-2\nu)} \begin{bmatrix} 1-\nu & \nu & \nu & 0 \\ \nu & 1-\nu & \nu & 0 \\ \nu & \nu & 1-\nu & 0 \\ \nu & \nu & 1-\nu & 0 \\ 0 & 0 & 0 & \frac{1-2\nu}{2} \end{bmatrix} \begin{Bmatrix} \varepsilon_{rr} \\ \varepsilon_{zz} \\ \varepsilon_{\theta\theta} \\ \gamma_{rz} \end{Bmatrix}$$

- Plane Stress

$$\begin{Bmatrix} \sigma_{xx} \\ \sigma_{yy} \\ \tau_{xy} \end{Bmatrix} = \frac{1}{1-\nu^2} \begin{bmatrix} 1 & \nu & 0 \\ \nu & 1 & 0 \\ 0 & 0 & \frac{1-\nu}{2} \end{bmatrix} \begin{Bmatrix} \varepsilon_{xx} \\ \varepsilon_{yy} \\ \gamma_{xy} \end{Bmatrix}$$

$$\varepsilon_{zz} = -\frac{1}{1-\nu} \nu (\varepsilon_{xx} + \varepsilon_{yy})$$

- The solution of a **boundary value problem** must satisfy
 - 1 Equilibrium
 - 2 constitutive relation (if compatibility was expressed solely in terms of strains)
 - 3 Compatibility (of strains or stresses)
 - 4 Boundary conditions
- We enforced this in the solution of statically indeterminate structures, and in the derivation of an element stiffness matrix.
- Q: Can we define a general solution which automatically satisfies the first three conditions (e.g. “Grand Unifying theory”) within a **continuum**?
 - In some **simple problems**: yes
 - In general: no; unless we use **Airy stress functions**
- Airy has shown that we can define a **potential function** $\Phi(\mathbf{x})$ in terms of the stresses as:

$$\sigma_{11} = \frac{\partial^2 \Phi}{\partial x_2^2}; \quad \sigma_{22} = \frac{\partial^2 \Phi}{\partial x_1^2}; \quad \sigma_{12} = -\frac{\partial^2 \Phi}{\partial x_1 \partial x_2}; \quad (14)$$

- Based on this definition, **equilibrium**

$$\frac{\partial \sigma_{ij}}{\partial x_j} = 0$$

$$\frac{\partial \sigma_{11}}{\partial x_1} + \frac{\partial \sigma_{12}}{\partial x_2} = 0$$

is automatically satisfied.

- In polar coordinates:

$$\sigma_{rr} = \frac{1}{r} \frac{\partial \Phi}{\partial r} + \frac{1}{r^2} \frac{\partial^2 \Phi}{\partial \theta^2} \quad \sigma_{\theta\theta} = \frac{\partial^2 \Phi}{\partial r^2} \quad \sigma_{r\theta} = -\frac{\partial}{\partial r} \left(\frac{1}{r} \frac{\partial \Phi}{\partial \theta} \right)$$

- We must satisfy constitutive relation. Substituting with the constitutive relations, we express the strains components in terms of Φ from Hooke's law,

$$\varepsilon_{11} = \frac{1}{E} \left[(1 - \nu^2)\sigma_{11} - \nu(1 + \nu)\sigma_{22} \right] = \frac{1}{E} \left[(1 - \nu^2) \frac{\partial^2 \Phi}{\partial x_2^2} - \nu(1 + \nu) \frac{\partial^2 \Phi}{\partial x_1^2} \right]$$

$$\varepsilon_{22} = \frac{1}{E} \left[(1 - \nu^2)\sigma_{22} - \nu(1 + \nu)\sigma_{11} \right] = \frac{1}{E} \left[(1 - \nu^2) \frac{\partial^2 \Phi}{\partial x_1^2} - \nu(1 + \nu) \frac{\partial^2 \Phi}{\partial x_2^2} \right]$$

$$\varepsilon_{12} = \frac{1}{E}(1 + \nu)\sigma_{12} = -\frac{1}{E}(1 + \nu) \frac{\partial^2 \Phi}{\partial x_1 \partial x_2}$$

- What is still missing: compatibility equation is (Eq.12)

$$\frac{\partial^2 \varepsilon_{11}}{\partial x_2^2} + \frac{\partial^2 \varepsilon_{22}}{\partial x_1^2} = 2 \frac{\partial^2 \varepsilon_{12}}{\partial x_1 \partial x_2} \quad (15)$$

- Substituting, and simplifying:

$$(1 - \nu) \left(\frac{\partial^4 \Phi}{\partial x_1^4} + 2 \frac{\partial^4 \Phi}{\partial x_1^2 \partial x_2^2} + \frac{\partial^4 \Phi}{\partial x_2^4} \right) = 0 \quad (16)$$

or

$$\nabla^4 \Phi = \nabla^2 (\nabla^2 \Phi) = 0 \quad (17)$$

$$\frac{\partial^4 \Phi}{\partial x_1^4} + 2 \frac{\partial^4 \Phi}{\partial x_1^2 \partial x_2^2} + \frac{\partial^4 \Phi}{\partial x_2^4} = 0 \quad (18)$$

note that the Lapacian (∇^2) is simply:

$$\nabla^2 = \frac{\partial^2 \Phi}{\partial x_1^2} + \frac{\partial^2 \Phi}{\partial x_2^2} \quad (19)$$

- Hence, any function which satisfies the preceding equation will satisfy all three requirements: equilibrium, kinematic, stress-strain (albeit plane strain) and is thus an **acceptable elasticity solution**.

- In polar coordinates

$$\nabla^2 (\nabla^2 \Phi) = \underbrace{\left(\frac{\partial^2}{\partial r^2} + \frac{1}{r} \frac{\partial}{\partial r} + \frac{1}{r^2} \frac{\partial^2}{\partial \theta^2} \right)}_{\nabla^2} \underbrace{\left(\frac{\partial^2 \Phi}{\partial r^2} + \frac{1}{r} \frac{\partial \Phi}{\partial r} + \frac{1}{r^2} \frac{\partial^2 \Phi}{\partial \theta^2} \right)}_{\nabla^2 \Phi}$$

- ∇^2 (or $\nabla \cdot \nabla$) is the **Laplacian operator**; $\nabla^2 \Phi = 0$ is **Laplace equation**; A solution to Laplace's equation is referred to as a **harmonic function**. ∇^4 is the **biharmonic** or bi-Laplacian operator,
- Back to the boundary value problem formulation from above,
 - Φ must satisfy the **bi-harmonic equation** however, there is an infinite number of such equations!
 - For Φ to satisfy a specific problem, the solution **must satisfy its boundary conditions** which may be expressed in terms of displacements or stresses.
- The **trick is to guess** Φ which satisfies a given set of boundary conditions.
- Only approach, come up with Φ and find out which set of B.C. are satisfied (i.e we have **a solution in search of a problem**). Hopefully it corresponds to a real physical problem (if one is **lucky**)

- Airy stress function with real variables enable us to determine the stress field around a circular hole (Kirsch)
- Need to extend Airy stress functions to complex variables in order to analyze stresses around:
 - Elliptical hole (Inglis),
 - Sharp crack (Westergaard).
- We define complex number z as:

$$z = x_1 + ix_2 = re^{i\theta}$$

where $i = \sqrt{-1}$, x_1 and x_2 are the cartesian coordinates, and r and θ are the polar coordinates.

- We define an **analytic function**, $f(z)$ one which derivatives depend only on z . Applying the chain rule

$$\frac{\partial}{\partial x_1} f(z) = \frac{\partial}{\partial z} f(z) \frac{\partial z}{\partial x_1} = f'(z) \frac{\partial z}{\partial x_1} = f'(z) \quad (20)$$

$$\frac{\partial}{\partial x_2} f(z) = \frac{\partial}{\partial z} f(z) \frac{\partial z}{\partial x_2} = f'(z) \frac{\partial z}{\partial x_2} = if'(z) \quad (21)$$

- If $f(z) = \alpha + i\beta$ where α and β are real functions of x_1 and x_2 , and $f(z)$ is analytic, then from Eq. 20 and 21 we have:

$$\left. \begin{aligned} \frac{\partial f(z)}{\partial x_1} &= \frac{\partial \alpha}{\partial x_1} + i \frac{\partial \beta}{\partial x_1} = f'(z) \\ \frac{\partial f(z)}{\partial x_2} &= \frac{\partial \alpha}{\partial x_2} + i \frac{\partial \beta}{\partial x_2} = if'(z) \end{aligned} \right\} i \underbrace{\left(\frac{\partial \alpha}{\partial x_1} + i \frac{\partial \beta}{\partial x_1} \right)}_{i1^{st} \text{ Equation}} = \underbrace{\frac{\partial \alpha}{\partial x_2} + i \frac{\partial \beta}{\partial x_2}}_{2^{nd} \text{ Equation}}$$

- Equating the real and imaginary parts yields the **Cauchy-Riemann** equations:

$$\frac{\partial \alpha}{\partial x_1} = \frac{\partial \beta}{\partial x_2}; \quad \frac{\partial \alpha}{\partial x_2} = -\frac{\partial \beta}{\partial x_1}$$

- Differentiate the first equation with respect to x_1 , the second wrt x_2 and sum

$$\frac{\partial^2 \alpha}{\partial x_1^2} + \frac{\partial^2 \alpha}{\partial x_2^2} = 0 \quad \text{or} \quad \nabla^2 (\alpha) = 0$$

which is **Laplace's equation**.

- Similarly we can have:

$$\nabla^2 (\beta) = 0$$

- Thus the real (α) and the imaginary part (β) of an **analytic function** will **separately** provide solution to Laplace's equation.
- α and β are **conjugate harmonic functions**.
- It can be shown that any stress function can be expressed as

$$\Phi = \Re[(x_1 - ix_2)\psi(z) + \chi(z)] \quad (22)$$

provided that both $\psi(z)$ (psi) and $\chi(z)$ (chi) are harmonic (i.e. $\nabla^2(\psi) = \nabla^2(\chi) = 0$) analytic functions of x_1 and x_2 .

- ψ and χ are often referred to as the **Kolonov-Muskhelishvili complex potentials**.
- If $f(z) = \alpha + i\beta$ and both α and β are real, then we define its **conjugate function**:

$$\bar{f}(\bar{z}) = \alpha - i\beta$$

- Conjugate functions should not be confused with conjugate harmonic functions.

- Rewrite Eq. 22 as:

$$\Phi = \Re[\bar{z}\psi(z) + \chi(z)] \quad (23)$$

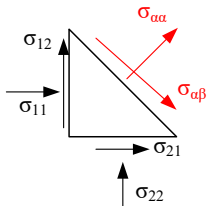
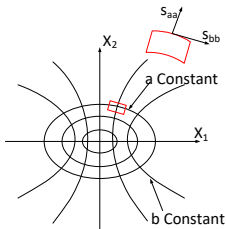
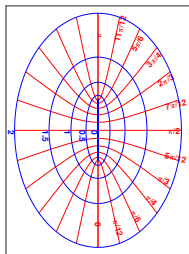
- Substituting Eq. 23 into Eq. 14, we can determine the stresses

$$\sigma_{11} + \sigma_{22} = 4\Re\psi'(z) \quad (24)$$

$$\sigma_{22} - \sigma_{11} + 2i\sigma_{12} = 2[\bar{z}\psi''(z) + \chi''(z)] \quad (25)$$

- By separation of real and imaginary parts we can then solve for $\sigma_{22} - \sigma_{11}$ & σ_{12} . Displacements can be similarly obtained.

- There is a multitude of orthogonal co-ordinate systems: cartesian, polar, spherical, and **elliptical**.
- An elliptical co-ordinate system is a two-dimensional orthogonal coordinate system in which the coordinate lines are **confocal ellipses and hyperbolae**.



- The two foci F_1 and F_2 are generally taken to be fixed at $-a$ and $+a$, respectively, on the x -axis of the Cartesian co-ordinate system.
- Rather than using cartesian or polar ($x - y, r - \theta$) coordinate system, we use an elliptical one ($\alpha - \beta$) where $p = \alpha + i\beta$. α and β are the **co-ordinates in the elliptical system**.

- We seek to solve for x_1 and x_2 in terms of α and β .
- The relationship between $p = \alpha + i\beta$ and $z = x_1 + ix_2$ in a cartesian coordinate system is given by

$$z = x_1 + ix_2 = c \cosh p = c \cosh(\alpha + i\beta) \quad (26)$$

where c is a constant. This is the definition of elliptical coordinates α and β .

- Recalling that

$$\cosh \alpha = \frac{1}{2}(e^\alpha + e^{-\alpha})$$

$$\sinh \alpha = \frac{1}{2}(e^\alpha - e^{-\alpha})$$

$$e^{i\beta} = \cos \beta + i \sin \beta$$

- we substitute those equations into Eq. 26

$$\begin{aligned}
 x_1 + ix_2 &= \frac{c}{2} \left(e^{\alpha+i\beta} + e^{-\alpha-i\beta} \right) \\
 &= \frac{c}{2} \left(\underbrace{e^{\alpha} \cos \beta + ie^{\alpha} \sin \beta}_{\cos \beta (e^{\alpha} + e^{-\alpha})} + \underbrace{e^{-\alpha} \cos \beta - ie^{-\alpha} \sin \beta}_{i \sin \beta (e^{\alpha} - e^{-\alpha})} \right) \\
 &= \frac{c}{2} \left(\cos \beta \underbrace{(e^{\alpha} + e^{-\alpha})}_{2 \cosh \alpha} + i \sin \beta \underbrace{(e^{\alpha} - e^{-\alpha})}_{2 \sinh \alpha} \right) \\
 &= c(\cosh \alpha \cos \beta + i \sinh \alpha \sin \beta)
 \end{aligned}$$

- Separating reals from imaginary parts we obtain

$$x_1 = c \cosh \alpha \cos \beta$$

$$x_2 = c \sinh \alpha \sin \beta$$

- If we eliminate β from those equation, we obtain

$$\frac{x_1^2}{\cosh^2 \alpha} + \frac{x_2^2}{\sinh^2 \alpha} = c^2$$

- Constant value of α represents the equation of an **ellipse in the $x_1 - x_2$ plane**.
- Constant β represent **confocal hyperebolae** which intersect the ellipse at right angle.
- In terms of complex potentials, it can be shown that the stresses are given in an analogous way as in Eq. 24:

$$\begin{aligned}\sigma_{\alpha\alpha} + \sigma_{\beta\beta} &= 2[\psi'(z) + \bar{\psi}'(\bar{z})] = 4\Re\psi'(z) \\ \sigma_{\beta\beta} - \sigma_{\alpha\alpha} + 2i\sigma_{\alpha\beta} &= 2e^{2i\theta}[\bar{z}\psi''(z) + \psi''(z)]\end{aligned}$$

- Note that what we have here is a set of three equations in terms of three unknowns. Individual stresses are obtained by separating the real from the imaginary components.

- An alternate form of Eq. 47 is

$$\varepsilon_i = a_{ij}\sigma_j \quad (27)$$

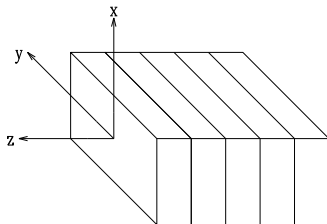
where the indices i and j go from 1 to 6.

- In the most general case this would yield **36 independent constants** a_{ij} however by virtue of symmetry ($a_{ij} = a_{ji}$) this reduces to $21 \left(\frac{(7)(6)}{2} \right)$.
- If the the material has one plane of elastic symmetry, then there would 13 independent constants;
- If it has three mutually orthogonal planes of elastic symmetry, then we would say that it is **orthogonally anisotropic** or **orthotropic**, and we will have $a_{16} = a_{26} = a_{36} = a_{45} = 0$, thus there will be 9 independent constants.

$$\begin{Bmatrix} \varepsilon_1 \\ \varepsilon_2 \\ \varepsilon_3 \\ \varepsilon_4 \\ \varepsilon_5 \\ \varepsilon_6 \end{Bmatrix} = \begin{bmatrix} a_{11} & a_{12} & a_{13} & & & \\ & a_{22} & a_{23} & & & \\ & & a_{33} & & & \\ & & & a_{44} & & \\ & & & & a_{55} & \\ & & & & & a_{66} \end{bmatrix} \begin{Bmatrix} \sigma_1 \\ \sigma_2 \\ \sigma_3 \\ \sigma_4 \\ \sigma_5 \\ \sigma_6 \end{Bmatrix} \quad (28)$$

- If the material is **transversally isotropic** then it will have 5 independent constants,

$$\begin{Bmatrix} \varepsilon_1 \\ \varepsilon_2 \\ \varepsilon_3 \\ \varepsilon_4 \\ \varepsilon_5 \\ \varepsilon_6 \end{Bmatrix} = \begin{bmatrix} a_{11} & a_{12} & a_{13} & & & \\ & a_{11} & a_{13} & & & \\ & & a_{33} & & & \\ & & & 2(a_{11} - a_{12}) & & \\ & & & & a_{44} & \\ & & & & & a_{44} \end{bmatrix} \begin{Bmatrix} \sigma_1 \\ \sigma_2 \\ \sigma_3 \\ \sigma_4 \\ \sigma_5 \\ \sigma_6 \end{Bmatrix} \quad (29)$$



- The total number of coefficients for different materials is

Class of Material	Number of Non Zero Coeff.		Number of Indep. Coeff.	
	3D	2D	3D	2D
General Anisotropy	36	9	21	6
One plane of Symmetry	20	9	13	6
Orthotropic	12	5	9	4
Transversely Isotropic	12	5	5	4
Isotropic	12	5	2	2

- In terms of **engineering constants** for an **orthotropic solid** we would have

$$\varepsilon_x = \frac{1}{E_1} \sigma_x - \frac{\nu_{21}}{E_2} \sigma_y - \frac{\nu_{31}}{E_3} \sigma_z \quad (30)$$

$$\varepsilon_y = -\frac{\nu_{12}}{E_1} \sigma_x + \frac{1}{E_2} \sigma_y - \frac{\nu_{32}}{E_3} \sigma_z \quad (31)$$

$$\varepsilon_z = -\frac{\nu_{13}}{E_1} \sigma_x - \frac{\nu_{23}}{E_2} \sigma_y + \frac{1}{E_3} \sigma_z \quad (32)$$

$$\gamma_{yz} = \frac{1}{\mu_{23}} \tau_{yz} \quad (33)$$

$$\gamma_{xz} = \frac{1}{\mu_{13}} \tau_{xz} \quad (34)$$

$$\gamma_{xy} = \frac{1}{\mu_{12}} \tau_{xy} \quad (35)$$

however, of the 12 elastic constants, only 9 are independent because the following: relations

$$E_1 \nu_{21} = E_2 \nu_{12} \quad (36)$$

$$E_2 \nu_{32} = E_3 \nu_{23} \quad (37)$$

$$E_3 \nu_{13} = E_1 \nu_{31} \quad (38)$$

- Preceding equations are written for the principal directions of elasticity, x , y , and z in terms of the **principal elastic constants** (as opposed to constants in equations for an arbitrary system of coordinates).
- Whereas very few natural or man-made materials are truly orthotropic (certain crystals as topaz are), a number of others are **transversely isotropic**. They have through every point a plane in which all directions are equivalent with respect to elastic properties (such as in laminates, shist, quartz, roller compacted concrete, etc...).

- For **transversely isotropic** solids in 3D, we have

$$\varepsilon_x = a_{11}\sigma_x + a_{12}\sigma_y + a_{13}\sigma_z \quad (39)$$

$$\varepsilon_y = a_{12}\sigma_x + a_{11}\sigma_y + a_{13}\sigma_z \quad (40)$$

$$\varepsilon_z = a_{13}(\sigma_x + \sigma_y) + a_{33}\sigma_z \quad (41)$$

$$\gamma_{xy} = 2(a_{11} - a_{12})\tau_{xy} \quad (42)$$

$$\gamma_{yz} = a_{44}\tau_{xy} \quad (43)$$

$$\gamma_{xz} = a_{44}\tau_{xz} \quad (44)$$

and

$$a_{11} = \frac{1}{E}; \quad a_{12} = -\frac{\nu}{E}; \quad a_{13} = -\frac{\nu'}{E'}; \quad a_{33} = -\frac{1}{E'}; \quad a_{44} = -\frac{1}{\mu'} \quad (45)$$

- Thus we have five elastic constants.

- E the Young's modulus in the plane of isotropy and E' the one in the plane normal to it, we would have ν corresponds to the transverse contraction in the plane of isotropy when tension is applied in the plane; ν' corresponding to the transverse contraction in the plane of isotropy when tension is applied normal to the plane; μ' corresponding to the shear moduli for the plane of isotropy and any plane normal to it, and μ is shear moduli for the plane of isotropy.

- If we consider $\varepsilon_i = a_{ij}\sigma_j$ for plane strain and $\varepsilon_i = b_{ij}\sigma_j$ for plane stress then it can be shown that

$$b_{ij} = a_{ij} - \frac{a_{i3}a_{j3}}{a_{33}} \quad (46)$$

- The stress function $\Phi(x, y)$ can be written as

$$\Phi(x, y) = 2\text{Re}[\Phi_1(z_1) + \Phi_2(z_2)] \quad (47)$$

where $\Phi_1(z_1)$ is an arbitrary function of $z_1 = x + s_1y$ and $\Phi_2(z_2)$ is an arbitrary function of $z_2 = x + s_2y$

- Note the analogy with $\phi = \text{Re}[(x_1 - ix_2)\psi(z) + \chi(z)]$ derived earlier for isotropic cases, Eq. 22, where ψ and χ were the Muskhelishvili complex potentials.
- It can be shown that using the Airy stress function defined in Eq. 14 and combined with the compatibility Equation (Eq. 12) for anisotropic solids we obtain (neglecting body forces)

$$a_{22} \frac{\partial^4 \Phi}{\partial x^4} - 2a_{26} \frac{\partial^4 \Phi}{\partial x \partial y} + (2a_{12} + a_{66}) \frac{\partial^4 \Phi}{\partial x^2 \partial y^2} - 2a_{16} \frac{\partial^4 \Phi}{\partial x \partial y^3} + a_{11} \frac{\partial^4 \Phi}{\partial y^4} = 0 \quad (48)$$

- For isotropic material this equation reduces to:

$$\frac{\partial^4 \Phi}{\partial x^4} + 2 \frac{\partial^4 \Phi}{\partial x^2 \partial y^2} + \frac{\partial^4 \Phi}{\partial y^4} = 0 \quad (49)$$

- The characteristic equation of this homogeneous partial differential equation is

$$a_{11}s^4 - 2a_{16}s^3 + (2a_{12} + a_{66})s^2 - 2a_{26}s + a_{22} = 0 \quad (50)$$

- By energy considerations, Leknitskii, has shown that:

- All roots are complex or purely imaginary for an ideally elastic body with $a_{11} \neq 0$, $2a_{12} + a_{66} \neq 0$, & $a_{22} \neq 0$
- Only exceptions are:
 - $a_{22} = a_{26} = 0 \Rightarrow 2$ roots equal to zero
 - $a_{22} = a_{26} = 2a_{12} + a_{66} = a_{16} = 0 \Rightarrow$ all four roots are zero
 - $a_{11} = a_{16} = 0 \Rightarrow 2$ roots are infinite
 - $a_{11} = a_{16} = 2a_{12} + a_{66} = a_{26} = 0 \Rightarrow 4$ roots are infinite.
- Two of the roots are conjugates of the two others: if we let

$$s_1 = \alpha_1 + i\beta_1 \quad s_2 = \alpha_2 + i\beta_2 \quad (51)$$

then

$$s_3 = \bar{s}_1 \quad s_4 = \bar{s}_2 \quad (52)$$

then β_1 & β_2 are both positive and $\beta_1 \neq \beta_2$

- Two cases are possible:

- 1 Roots are all different
 - 2 Roots are pairwise equal
- 5 For isotropic material

$$\alpha = 0 \quad (53)$$

$$\beta = 1 \quad (54)$$

$$s_1 = s_2 = i \quad (55)$$

$$\bar{s}_1 = \bar{s}_2 = -i \quad (56)$$

So s_1 and s_2 are complex parameters of first order of plane stress (or strain). They characterize the degree of anisotropy for plane problems. From it we can judge how much a body differs from isotropy.

- 6 If a material is orthotropic and x and y coincide with 1 and 2, then $a_{16} = a_{26} = 0$ and we have

$$s^4 + \left(\frac{E_1}{\mu} - 2\nu_1\right)s^2 + \frac{E_1}{E_2} = 0 \quad (57)$$

and

- 1 $s_1 = \beta i$ & $s_2 = \delta i$; purely imaginary and unequal roots
- 2 $s_1 = s_2 = \beta i$; complex and equal roots

$$\textcircled{3} \quad s_1 = \alpha + \beta i; s_2 = -\alpha + \beta i$$

$\textcircled{7}$ In addition we have

$$s'_1 = \frac{s_2 \cos \psi - \sin \psi}{\cos \psi + s_1 \sin \psi} \quad (58)$$

$$s'_2 = \frac{s_1 \cos \psi - \sin \psi}{\cos \psi + s_2 \sin \psi} \quad (59)$$

$\textcircled{8}$ Invariants for orthotropic bodies are

$$I_1 = a_{11} + a_{22} + 2a_{12} = \frac{1}{E_1} + \frac{1}{E_2} - \frac{2\nu_{12}}{E_1} \quad (60)$$

$$I_2 = a_{66} - 4a_{12} = \frac{1}{\mu_{12}} + \frac{4\nu_{12}}{E_1} \quad (61)$$

$$I_3 = a_{44} + a_{55} = \frac{1}{\mu_{13}} + \frac{1}{\mu_{23}} \quad (62)$$

$$I_4 = a_{13} + a_{23} = -\left(\frac{\nu_{13}}{E_1} + \frac{\nu_{23}}{E_2}\right) = -\frac{\nu_{31} + \nu_{32}}{E_2} \quad (63)$$

- If we define:

$$\phi_1(z_1) = \frac{d\Phi_1}{dz_1} \quad \text{and} \quad \phi_2(z_2) = \frac{d\Phi_2}{dz_2} \quad (64)$$

and using the definition of stress functions, the stresses are

$$\sigma_x = 2\text{Re}[s_1^2 \phi_1'(z_1) + s_2^2 \phi_2'(z_2)] \quad (65)$$

$$\sigma_y = 2\text{Re}[\phi_1'(z_1) + \phi_2'(z_2)] \quad (66)$$

$$\tau_{xy} = -2\text{Re}[s_1 \phi_1'(z_1) + s_2 \phi_2'(z_2)] \quad (67)$$

and the displacements are

$$u = 2\text{Re}[p_1 \phi_1(z_1) + p_2 \phi_2(z_2)] \quad (68)$$

$$v = 2\text{Re}[q_1 \phi_1(z_1) + q_2 \phi_2(z_2)] \quad (69)$$

where

$$\begin{cases} p_i &= a_{11}s_i^2 + a_{12} - a_{16}s_i, \quad (i = 1, 2) \\ q_i &= a_{12}s_i + \frac{a_{22}}{s_i} - a_{26} \end{cases} \quad (70)$$

Elasticity Based Solutions

for SCF or SIF

Victor E. Saouma
saouma@colorado.edu

University of Colorado, Boulder

Spring 2022

Table of Contents I

- 1 Introduction
- 2 Circular Hole
 - Fermi's Solution
 - Formulation
- 3 Circular Hole, (Kirsch, 1898)
 - Solution
- 4 Elliptical hole
 - Formulation
 - Boundary Conditions
 - Solution
- 5 Crack; Westergaard
 - Formulation
 - Solution
- 6 Williams Solution
 - Formulation
 - Solution

7 Interface between Two Dissimilar Materials

- General Function
- Boundary Conditions
- Homogeneous Equations
- Homogeneous Equations
- Solve for λ
- Near Crack Tip Stresses

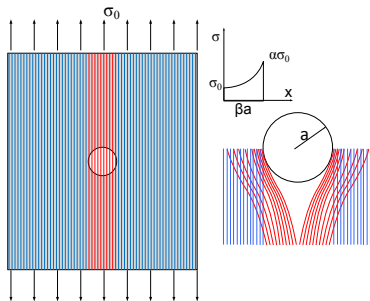
8 Homogeneous Anisotropic Material (Sih and Paris)

9 Stress Intensity Factors (Irwin)

- Near Crack Tip Stresses and Displacements in Isotropic Cracked Solids

Introduction

Problem	Coordinate System	Real/Complex	Solution	Date
Circular Hole	Polar	Real	Kirsh	1898
Elliptical Hole	Elliptical	Complex	Inglis	1913
Crack	Cartesian	Complex	Westergaard	1939
V Notch	Polar	Complex	Williams	1952
Dissimilar Materials	Polar	Complex	Williams	1959
Anisotropic Materials	Cartesian	Complex	Sih	1965



- **Fermi's** problem, is an **estimation** based on a back-of-the-envelope solution to a complex problem. It involves making **guesses** about quantities and does not seek an exact solution.
- A simple approximate solution should always be sought before a more complex (and “exact” one is searched, typically finite element). Fermi's solution is simple, easy to follow, and less prone to error than the exact one.

- To examine the problem of stress concentration around a circular hole, let us consider a pictorial representation of two rigid plates subjected to σ_0 connected by an infinite number of elastic strings. The stress trajectory is pretty simple.
- If the strings are perturbed by inserting through them a circular tube, then strings are to be displaced.
- Initial internal uniform stress is σ_0 , total force which would have been transmitted through the opening (considering symmetry) $\Delta F^- = \int_0^a \sigma_0 dx = \sigma_0 a$. This force has to be redirected over a segment βa .
- Assume a quadratic stress redistribution

$$\sigma^+ = \frac{\alpha \sigma_0}{\beta^2 a^2} x^2$$

$$\Delta F^+ = \int_0^{\beta a} \frac{\alpha \sigma_0}{\beta^2 a^2} x^2 dx = \frac{\alpha \sigma_0 \beta a}{3}$$

- Equating ΔF^- to ΔF^+ we obtain

$$\alpha = \frac{\beta}{3}$$

- Hence at $x = \beta a$,

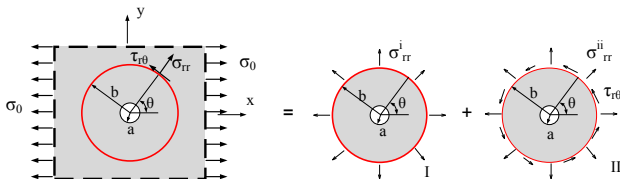
$$\begin{aligned}\sigma^T &= \sigma_0 + \sigma^+ \\ &= \sigma_0(1 + \alpha) = \sigma_0 \left(\frac{3 + \beta}{\beta} \right)\end{aligned}$$

The stress concentration factor is σ^T/σ_0 or

$$\text{SCF} = \frac{3 + \beta}{\beta}$$

As $\beta \rightarrow 0$ **SCF=3**, and correspondingly $\beta = 1$ (consistent with St Venant Principle).

- Of course, a different SCF would have been obtained had a different stress distribution been assumed.



- Far-field boundary conditions are better expressed in cartesian coordinates, whereas the ones around the hole should be written in polar coordinate system.
- Solve by replacing plate with a thick tube subjected to **two different set of loads**.
 - I: Thick cylinder subjected to **uniform radial pressure** (solution of which is well known from *Strength of Materials*)
 - II: Thick cylinder subjected to **both radial and shear stresses** which must be compatible with the traction applied on the rectangular plate.
- Stress function must satisfies biharmonic Equation $\nabla^2 (\nabla^2 \Phi)$ and the far-field boundary conditions.

- From St Venant principle, away from the hole, the boundary conditions are given by:

$$\sigma_{xx} = \sigma_0; \quad \sigma_{yy} = \tau_{xy} = 0$$

- Recalling that $\sigma_{xx} = \frac{\partial^2 \Phi}{\partial y^2}$, this would suggest a stress function Φ of the form $\Phi = \sigma_0 y^2$.
- Alternatively, the presence of the circular hole would suggest a **polar representation** of Φ .
- Substituting $y = r \sin \theta$ would result in $\Phi = \sigma_0 r^2 \sin^2 \theta$.
- Since $\sin^2 \theta = \frac{1}{2}(1 - \cos 2\theta)$, we could simplify the stress function into

$$\Phi = f(r) \cos 2\theta$$

- This function must also satisfy the biharmonic equation

$$\left(\frac{\partial^2}{\partial r^2} + \frac{1}{r} \frac{\partial}{\partial r} + \frac{1}{r^2} \frac{\partial^2}{\partial \theta^2} \right) \left(\frac{\partial^2 \Phi}{\partial r^2} + \frac{1}{r} \frac{\partial \Phi}{\partial r} + \frac{1}{r^2} \frac{\partial^2 \Phi}{\partial \theta^2} \right) = 0$$

or

$$\left(\frac{d^2}{dr^2} + \frac{1}{r} \frac{d}{dr} - \frac{4}{r^2} \right) \left(\frac{d^2 f}{dr^2} + \frac{1}{r} \frac{df}{dr} - \frac{4f}{r^2} \right) = 0$$

(note that the $\cos 2\theta$ term is dropped since f does not depend on θ)

- The general solution of this ordinary linear fourth order differential equation is

$$f(r) = Ar^2 + Br^4 + C\frac{1}{r^2} + D$$

- Stress function becomes

$$\Phi = \left(Ar^2 + Br^4 + C\frac{1}{r^2} + D \right) \cos 2\theta \quad (1)$$

- The stresses are given by:

$$\sigma_{rr} = \frac{1}{r} \frac{\partial \Phi}{\partial r} + \frac{1}{r^2} \frac{\partial^2 \Phi}{\partial \theta^2} \quad \sigma_{\theta\theta} = \frac{\partial^2 \Phi}{\partial r^2} \quad \sigma_{r\theta} = -\frac{\partial}{\partial r} \left(\frac{1}{r} \frac{\partial \Phi}{\partial \theta} \right) \quad (2)$$

- Substituting into Eq. 1

$$\begin{aligned} \sigma_{rr} &= \frac{1}{r} \frac{\partial \Phi}{\partial r} + \frac{1}{r^2} \frac{\partial^2 \Phi}{\partial \theta^2} = -\left(2A + \frac{6C}{r^4} + \frac{4D}{r^2} \right) \cos 2\theta \\ \sigma_{\theta\theta} &= \frac{\partial^2 \Phi}{\partial r^2} = \left(2A + 12Br^2 + \frac{6C}{r^4} \right) \cos 2\theta \\ \tau_{r\theta} &= -\frac{\partial}{\partial r} \left(\frac{1}{r} \frac{\partial \Phi}{\partial \theta} \right) = \left(2A + 6Br^2 - \frac{6C}{r^4} - \frac{2D}{r^2} \right) \sin 2\theta \end{aligned} \quad (3)$$

- We still need to solve for $A \rightarrow D$ through enforcement of the boundary conditions.
- Solve for the four constants of integration by applying the boundary conditions.
- But first we must transform the cartesian stress $\sigma_{xx} = \sigma_0$ away from the hole into polar stresses (inner around $r = b$). The stress transformation from cartesian to polar is given by

$$\begin{bmatrix} \sigma_{rr} & \sigma_{r\theta} \\ \sigma_{r\theta} & \sigma_{\theta\theta} \end{bmatrix} = \begin{bmatrix} \cos \theta & -\sin \theta \\ \sin \theta & \cos \theta \end{bmatrix} \begin{bmatrix} \sigma_0 & 0 \\ 0 & 0 \end{bmatrix} \begin{bmatrix} \cos \theta & -\sin \theta \\ \sin \theta & \cos \theta \end{bmatrix}^T$$

- Recall that $\sin^2 \theta = \frac{1 - \cos 2\theta}{2}$, and $\cos^2 \theta = \frac{1 + \cos 2\theta}{2}$.
- Substituting, we obtain

$$(\sigma_{rr})_{r=b} = \sigma_0 \cos^2 \theta = \frac{1}{2} \sigma_0 \left(\underbrace{1}_I + \underbrace{\cos 2\theta}_{II} \right) \quad (4)$$

$$(\sigma_{r\theta})_{r=b} = \underbrace{\frac{1}{2} \sigma_0 \sin 2\theta}_{II} \quad (5)$$

$$(\sigma_{\theta\theta})_{r=b} = \frac{\sigma_0}{2} (1 - \cos 2\theta) \quad (6)$$

- The **trick** now is to decompose the state of stress given by Eq. 4 and 5, into two states I and II (see figure)

- State I**

$$(\sigma_{rr})'_{r=b} = \frac{1}{2}\sigma_0 \quad (7)$$

$$(\sigma_{r\theta})'_{r=b} = 0 \quad (8)$$

which actually corresponds to a thick cylinder with external pressure applied on $r = b$ and of magnitude $\sigma_0/2$. We know how to solve this from

Strength of Materials

- State II**

$$(\sigma_{rr})''_{r=b} = \frac{1}{2}\sigma_0 \cos 2\theta \quad \text{BC \# 1} \quad (9)$$

$$(\sigma_{r\theta})''_{r=b} = \frac{1}{2}\sigma_0 \sin 2\theta \quad \text{BC \# 2} \quad (10)$$

We have 2 boundary conditions at $r = b$, we need 2 more. **Around the inner hole**: the stresses should be equal to zero:

$$(\sigma_{rr})_{r=a} = 0 \quad \text{BC \# 3} \quad (11)$$

$$(\sigma_{r\theta})_{r=a} = 0 \quad \text{BC \# 4} \quad (12)$$

- Note that we could not have obtained a closed form solution by simply adding stat I and II solutions as the \cos term will not cancel out.
- Upon substitution in Eq. 3 the four boundary conditions (Eq. 9, 10, 11, and 12)

$$-\left(2A + \frac{6C}{b^4} + \frac{4D}{b^2}\right) = \frac{1}{2}\sigma_0 \quad (13)$$

$$\left(2A + 6Bb^2 - \frac{6C}{b^4} - \frac{2D}{b^2}\right) = \frac{1}{2}\sigma_0 \quad (14)$$

$$-\left(2A + \frac{6C}{a^4} + \frac{4D}{a^2}\right) = 0 \quad (15)$$

$$\left(2A + 6Ba^2 - \frac{6C}{a^4} - \frac{2D}{a^2}\right) = 0 \quad (16)$$

- Solve for the four unknowns, and taking $\frac{a}{b} = 0$ (i.e. an infinite plate), we obtain:

$$A = -\frac{\sigma_0}{4}; \quad B = 0; \quad C = -\frac{a^4}{4}\sigma_0; \quad D = \frac{a^2}{2}\sigma_0$$

- To this solution, we must superimpose the one of a thick cylinder subjected to a uniform radial traction $\sigma_0/2$ on the outer surface (solution I), and with b much greater than a (Eq. 7 and 8).
- Stresses are obtained from *Strength of Materials* yielding for this problem (careful about the sign)

$$\sigma_{rr} = \frac{\sigma_0}{2} \left(1 - \frac{a^2}{r^2} \right) \quad (17)$$

$$\sigma_{\theta\theta} = \frac{\sigma_0}{2} \left(1 + \frac{a^2}{r^2} \right) \quad (18)$$

- Substituting Eq. 13-16, and 17-18 into Eq. 3, we obtain

$$\sigma_{rr} = \underbrace{\frac{\sigma_0}{2} \left(1 - \frac{a^2}{r^2}\right)}_I + \underbrace{\left(1 + 3\frac{a^4}{r^4} - \frac{4a^2}{r^2}\right) \frac{1}{2}\sigma_0 \cos 2\theta}_II \quad (19)$$

$$\sigma_{\theta\theta} = \underbrace{\frac{\sigma_0}{2} \left(1 + \frac{a^2}{r^2}\right)}_I - \underbrace{\left(1 + \frac{3a^4}{r^4}\right) \frac{1}{2}\sigma_0 \cos 2\theta}_II \quad (20)$$

$$\sigma_{r\theta} = - \underbrace{\left(1 - \frac{3a^4}{r^4} + \frac{2a^2}{r^2}\right) \frac{1}{2}\sigma_0 \sin 2\theta}_II \quad (21)$$

- Observe that as $r \rightarrow \infty$, both σ_{rr} and $\sigma_{r\theta}$ are equal to the values given in Eq. 4 and 5 respectively.

- Alternatively, at the edge of the hole when $r = a$ we obtain

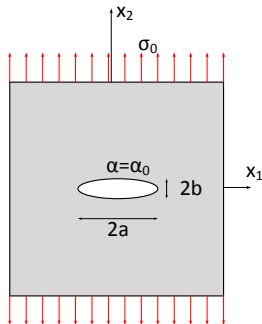
$$\sigma_{rr} = 0$$

$$\sigma_{r\theta} = 0$$

$$\sigma_{\theta\theta}|_{r=a} = \sigma_0(1 - 2\cos 2\theta)$$

which gives the following stress concentration factors

θ	SCF
$\pi/2, 3\pi/2$ (Normal to load)	3
$0, \pi$ (Along load)	-1



- a and b are the major and minor semi-axes.
- Elliptical hole defined along $\alpha = \alpha_0$, and as we go around the ellipse $0 \leq \beta \leq 2\pi$.
- Note that for infinite boundary conditions we will use cartesian, and around the ellipse curvilinear coordinate system equations.

- In order to properly apply the boundary condition around the elliptical hole, we need to relate a and b to α and β . Substitute $\beta = 0$ and $\beta = \frac{\pi}{2}$ in

$$x_1 = c \cosh \alpha \cos \beta = \frac{c}{2} \cos \beta (e^\alpha + e^{-\alpha}) \quad (22)$$

$$x_2 = c \sinh \alpha \sin \beta = \frac{c}{2} \sin \beta (e^\alpha - e^{-\alpha}) \quad (23)$$

$$x_1|_{\beta=0; \alpha=\alpha_0} \Rightarrow a = c \cosh \alpha \cos \beta = c \cosh \alpha_0 \Rightarrow \cosh \alpha_0 = \frac{a}{c} \quad (24)$$

$$x_2|_{\beta=\pi/2; \alpha=\alpha_0} \Rightarrow b = c \sinh \alpha \sin \beta = c \sinh \alpha_0 \Rightarrow \sinh \alpha_0 = \frac{b}{c} \quad (25)$$

- Boundary conditions:

- 1 At infinity we have $\sigma_{22} = \sigma_0$ and $\sigma_{11} = \sigma_{12} = 0$. Substituting,

$$\sigma_{11} + \sigma_{22} = 4\Re\psi'(z) = \sigma_0 \quad (26)$$

$$\sigma_{22} - \sigma_{11} + 2i\sigma_{12} = 2[\bar{z}\psi''(z) + \chi''(z)] = \sigma_0 \quad (27)$$

- 2 Around the elliptical hole ($\alpha = \alpha_0$): $\sigma_{\alpha\alpha} = \sigma_{\alpha\beta} = 0$

- Inglis found that the following complex potentials satisfy those boundary conditions:

$$4\psi(z) = \sigma_0 c \left[(1 + e^{2\alpha_0}) \sinh p - e^{2\alpha_0} \cosh p \right]$$

$$4\chi(z) = -\sigma_0 c^2 \left[(\cosh 2\alpha_0 - \cosh \pi) p + \frac{1}{2} e^{2\alpha_0} - \cosh 2 \left(p - \alpha_0 - i \frac{\pi}{2} \right) \right]$$

Note that they are periodic in β (period of 2π) and that $p = \alpha + i\beta$

- Since $\sigma_{\alpha\alpha} = 0$ for $\alpha = \alpha_0$, we can solve for $\sigma_{\beta\beta}$ from

$$\underbrace{\sigma_{\alpha\alpha}}_0 + \sigma_{\beta\beta} = 2[\psi'(z) + \bar{\psi}'(\bar{z})]$$

thus differentiating $\psi(z)$ and $\bar{\psi}'(\bar{z})$ and substituting

$$(\sigma_{\beta\beta})_{\alpha=\alpha_0} = \frac{\sinh 2\alpha_0 - 1 + e^{2\alpha_0} \cos 2\beta}{\cosh 2\alpha_0 - \cos 2\beta} \sigma_0$$

- The **maximum value of $\sigma_{\beta\beta}$** occurs at the end of the ellipse where $\beta = 0$ or π . For those points we have $\cos 2\beta = 1$, and since the tangent to the ellipse is now parallel to x_2 we have:

$$(\sigma_{\beta\beta})_{\alpha=\alpha_0}^{\beta=0,\pi} = \sigma_{22} = \frac{\sinh 2\alpha_0 - 1 + e^{2\alpha_0}}{\cosh 2\alpha_0 - 1} \sigma_0 \quad (28)$$

- We now have a solution for the stress at the tip of the ellipse. However it is expressed in curvilinear coordinates. We seek a solution **in terms of a and b** . This will be achieved through $\sinh(2\alpha_0)$ and $\cosh(2\alpha_0)$
- We can exploit these relationships

$$\begin{aligned} \cosh 2\alpha_0 &= 2 \cosh^2 \alpha_0 - 1 \\ \sinh 2\alpha_0 &= 2 \sinh \alpha_0 \cosh \alpha_0 \end{aligned}$$

and from Eq. 24 and 25 we have $\cosh \alpha_0 = \frac{a}{c}$ and $\sinh \alpha_0 = \frac{b}{c}$. Substituting

$$\begin{aligned} \sinh 2\alpha_0 &= \frac{2ab}{c^2} \\ \cosh 2\alpha_0 &= \frac{a^2 + b^2}{c^2} \end{aligned}$$

- Finally, substituting those two equations into Eq. 28

$$(\sigma_{\beta\beta})_{\alpha=\alpha_0}^{\beta=0,\pi} = \sigma_0 \left(1 + 2\frac{a}{b} \right) \quad (29)$$

We observe that for $a = b$, we recover the stress concentration factor of 3 of a circular hole, and that for a degenerated ellipse, i.e a crack there is an infinite stress.

- Alternatively, let ρ be the radius of curvature of a parametric curve. From analytical geometry,

$$\rho^2 = \frac{(x'^2 + y'^2)^3}{(x'y'' - y'x'')^2}$$

derivatives taken with respect to a parameter t .

- Define $x_1 = a \cos t$ and $x_2 = b \sin t$; substituting

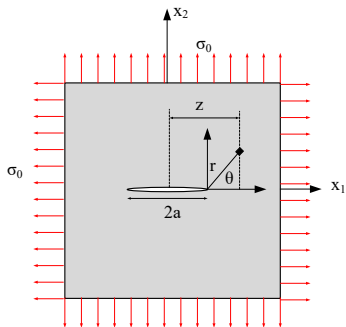
$$\rho^2 = \frac{1}{a^2 b^2} (a^2 \sin^2 t + b^2 \cos^2 t)^3$$

- At the tip of the ellipse $x_2 = 0$ and $x_1 = \pm a$. Thus, $\sin t = 0$ and $\cos t = 1$, and ρ becomes equal to $\rho = \frac{b^2}{a}$.

- Substituting into Eq. 29

$$(\sigma_{\beta\beta})_{\alpha=\alpha_0}^{\beta=0,\pi} = \sigma_0 \left(1 + 2\sqrt{\frac{a}{\rho}} \right) \quad (30)$$

- Note that the stress concentration factor is inversely proportional to the radius of curvature of an opening.



- Consider an infinite plate subjected to uniform biaxial stress σ_0 with a central crack of length $2a$,
- From Inglis solution, we know that there would be a theoretically infinite stress at the tip of the crack, however **neither the nature of the singularity nor the stress field can be derived from it.**

- Let $\phi'(z)$ and $\phi''(z)$ the first and second derivatives respectively, and $\bar{\phi}(z)$ and $\bar{\bar{\phi}}(z)$ its first and second integrals respectively of the function $\phi(z)$.
- Westergaard's solution**, starts by assuming $\Phi(z)$ as a harmonic function (thus satisfying Laplace's equation $\nabla^2(\Phi) = 0$) and **postulates** that

$$\Phi = \Re \bar{\bar{\phi}}(z) + x_2 \Im \bar{\phi}(z)$$

is a solution to the crack problem. Must determine ϕ such that **the boundary conditions are satisfied**.

- For reasons which will become apparent later, we generalize our problem to one in which we have a biaxial state of stress applied on the plate. Hence:
 - Along the crack: at $x_2 = 0$ and $-a < x_1 < a$ we have $\sigma_{22} = 0$ (traction free crack).**
 - At infinity: at $x_2 = \pm\infty$, $\sigma_{22} = \sigma_0$**

- The function is **analytic**

$$\frac{\partial}{\partial x_1} = \frac{d}{dz}$$

and from **Cauchy-Riemann**

$$\frac{\partial \Re e}{\partial x_1} = \frac{\partial \Im m}{\partial x_2};$$

- The stress σ_{22} will then be given by

$$\sigma_{22} = \frac{\partial^2 \Phi}{\partial x_1^2} = \frac{\partial}{\partial z} \left(\frac{\partial \Phi}{\partial z} \right) = \Re \phi(z) + x_2 \Im \phi'(z) \quad (31)$$

thus at $x_2 = 0$, σ_{22} reduces to

$$(\sigma_{22})_{x_2=0} = \Re \phi(z) \quad (32)$$

- Furthermore, we expect $\sigma_{22} \rightarrow \sigma_0$ as $x_1 \rightarrow \infty$, and σ_{22} to be greater than σ_0 when $|x_1 - a| > \epsilon$ (due to anticipated singularity predicted by Inglis), thus a possible choice for σ_{22} would be $\sigma_{22} = \frac{\sigma_0}{1 - \frac{a}{x_1}}$, for symmetry, this is extended to $\sigma_{22} = \frac{\sigma_0}{\left(1 - \frac{a^2}{x_1^2}\right)}$. However, we also need to have $\sigma_{22} = 0$ when $x_2 = 0$ and $-a < x_1 < a$, thus the function $\phi(z)$ should become imaginary along the crack, and

$$\sigma_{22} = \Re \left(\frac{\sigma_0}{\sqrt{1 - \frac{a^2}{z^2}}} \right)$$

- Thus from Eq. 32 we have (note the transition from x_1 to z).

$$\phi(z) = \frac{\sigma_0}{\sqrt{1 - \frac{a^2}{z^2}}}$$

- we first consider the first term of Eq. 31 ($\Re\phi(z)$):
 - Perform a change of variable and define $\eta = z - a = re^{i\theta}$

- Assume $\frac{\eta}{a} \ll 1$
- Recall that $e^{i\theta} = \cos \theta + i \sin \theta$,

then $\Re\phi(z)$ can be rewritten as

$$\begin{aligned}\Re\phi(z) &= \Re \frac{\sigma_0}{\sqrt{\frac{\eta^2+2a\eta}{\eta^2+a^2+2a\eta}}} \approx \Re \frac{\sigma_0}{\sqrt{\frac{2a\eta}{a^2}}} \\ &\approx \Re \sigma_0 \sqrt{\frac{a}{2\eta}} \approx \Re \sigma_0 \sqrt{\frac{a}{2re^{i\theta}}} \approx \Re \sigma_0 \sqrt{\frac{a}{2r}} e^{-i\frac{\theta}{2}} \approx \sigma_0 \sqrt{\frac{a}{2r}} \cos \frac{\theta}{2}\end{aligned}$$

- We then consider the second term of Eq. 31 ($x_2 \Im \phi'(z)$) (and recall that $\sin 2\theta = 2 \sin \theta \cos \theta$; $e^{-i\theta} = \cos \theta - i \sin \theta$), substitute $x_2 = r \sin \theta$ into the second term to obtain

$$x_2 \Im \phi' = r \sin \theta \Im \frac{\sigma_0}{2} \sqrt{\frac{a}{2(re^{i\theta})^3}} = \sigma_0 \sqrt{\frac{a}{2r}} \sin \frac{\theta}{2} \cos \frac{\theta}{2} \sin \frac{3\theta}{2}$$

- We thus obtain

$$\sigma_{22} = \sigma_0 \sqrt{\frac{a}{2r}} \cos \frac{\theta}{2} \left(1 + \sin \frac{\theta}{2} \sin \frac{3\theta}{2} \right) + \dots \quad (33)$$

$$\sigma_{11} = \sigma_0 \sqrt{\frac{a}{2r}} \cos \frac{\theta}{2} \left(1 - \sin \frac{\theta}{2} \sin \frac{3\theta}{2} \right) + \dots \quad (34)$$

$$\sigma_{12} = \sigma_0 \sqrt{\frac{a}{2r}} \sin \frac{\theta}{2} \cos \frac{\theta}{2} \cos \frac{3\theta}{2} + \dots \quad (35)$$

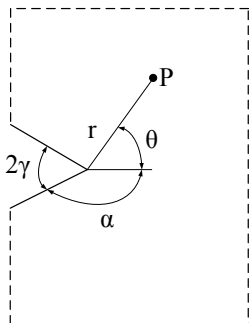
- Recall that this was the biaxial case, the uniaxial case may be reproduced by superimposing a traction in the x_1 direction equal to $-\sigma_0$, however this should not affect the stress field close to the crack tip.

- Using a similar approach, we can derive expressions for the stress field around a crack tip in a plate subjected to **far field shear stresses** (mode II as defined later) using the following expression of ϕ

$$\Phi_{II}(z) = -\kappa_2 \Re \bar{\phi}_{II}(z) \Rightarrow \phi_{II} = \frac{\tau}{\sqrt{1 - \frac{a^2}{z^2}}}$$

and for the same crack but subjected to **antiplane shear stresses** (mode III)

$$\Phi'_{III}(z) = \frac{\sigma_{13}}{\sqrt{1 - \frac{a^2}{z^2}}}$$



- Using the method of **separation of variables** in 1952, Williams proposed the following solution

$$\Phi(r, \theta) \equiv r^{\lambda+1} F(\theta, \lambda) \quad (36)$$

where $F(\theta, \lambda) = e^{m(\lambda)\theta}$ is a real function, and $m(\lambda)$ is **yet to be determined**, by satisfying the bi-harmonic equation.

$$\nabla^2 (\nabla^2 \Phi) = \left(\frac{\partial^2}{\partial r^2} + \frac{1}{r} \frac{\partial}{\partial r} + \frac{1}{r^2} \frac{\partial^2}{\partial \theta^2} \right) \left(\frac{\partial^2 \Phi}{\partial r^2} + \frac{1}{r} \frac{\partial \Phi}{\partial r} + \frac{1}{r^2} \frac{\partial^2 \Phi}{\partial \theta^2} \right) = 0 \quad (37)$$

- Considered problem is not a crack, but rather a plate under tension with **angular corners** making an angle 2γ (for $\gamma = 0$ we recover the crack problem of Westergaard).

- Substituting Eq. 36 into the biharmonic equation (Eq. 37) gives

$$\frac{\partial^4 F(\theta, \lambda)}{\partial \theta^4} + 2(\lambda^2 + 1) \frac{\partial^2 F(\theta, \lambda)}{\partial \theta^2} + (\lambda^2 - 1)^2 F(\theta, \lambda) = 0$$

- Substituting $F(\theta, \lambda)$ with $e^{m(\lambda)\theta}$, this equation reduces to

$$e^{m(\lambda)\theta} [(\lambda - 1)^2 + m(\lambda)^2] [(1 + \lambda)^2 + m(\lambda)^2] = 0$$

- The roots of this equation are

$$m(\lambda) = \pm i(\lambda - 1)$$

$$m(\lambda) = \pm i(\lambda + 1)$$

- Since $F(\theta, \lambda) = e^{m(\lambda)\theta} = e^{\pm i(\lambda \pm 1)\theta}$ is a real function then the solutions of the differential equation 37 are also real functions. Recalling that

$$e^{im(\lambda)\theta} = \cos m(\lambda)\theta + i \sin m(\lambda)\theta$$

we select as solution

$$F_1(\theta, \lambda) = \cos(\lambda - 1)\theta$$

$$F_2(\theta, \lambda) = \cos(\lambda + 1)\theta$$

$$F_3(\theta, \lambda) = \sin(\lambda - 1)\theta$$

$$F_4(\theta, \lambda) = \sin(\lambda + 1)\theta$$

and finally $F(\theta, \lambda)$ will be a linear combination of F_1 , F_2 , F_3 and F_4 , thus

$$\Phi(r, \theta) = r^{\lambda+1} \left[\underbrace{A \cos(\lambda - 1)\theta + B \cos(\lambda + 1)\theta}_{\text{Symmetric}} + \underbrace{C \sin(\lambda - 1)\theta + D \sin(\lambda + 1)\theta}_{\text{Unsymmetric}} \right]_{F(\theta, \lambda)} \quad (38)$$

- We seek to determine the stresses in **polar coordinates** in order to apply the boundary conditions. Substituting Eq. 36 into Eq. 2

$$\sigma_{\theta\theta} = \frac{\partial^2 \Phi}{\partial r^2}$$

$$\sigma_{r\theta} = -\frac{\partial}{\partial r} \left(\frac{1}{r} \frac{\partial \Phi}{\partial \theta} \right)$$

we obtain:

$$\sigma_{\theta\theta} = r^{\lambda-1} \lambda(\lambda+1) F(\theta, \lambda) \quad (39)$$

$$\sigma_{r\theta} = r^{\lambda-1} [-\lambda F'(\theta, \lambda)] \quad (40)$$

Substituting

$$\sigma_{\theta\theta} = r^{\lambda-1} \lambda(\lambda+1) [A \cos(\lambda-1)\theta + B \cos(\lambda+1)\theta + C \sin(\lambda-1)\theta + D \sin(\lambda+1)\theta]$$

$$\sigma_{r\theta} = -\lambda r^{\lambda-1} [-A(\lambda-1) \sin(\lambda-1)\theta - B(\lambda+1) \sin(\lambda+1)\theta + C(\lambda-1) \cos(\lambda-1)\theta + D(\lambda+1) \cos(\lambda+1)\theta]$$

- The **boundary conditions** are next applied by considering a plate with a central crack, applying the following 4 boundary conditions along the crack edges

$$\sigma_{\theta\theta} |_{\theta=\pm\alpha} = 0$$

$$\sigma_{r\theta} |_{\theta=\pm\alpha} = 0$$

where $\alpha + \gamma = \pi$, which implies that

$$F(\alpha) = F(-\alpha) = F'(\alpha) = F'(-\alpha) = 0$$

$$\begin{bmatrix} \cos(\lambda - 1)\alpha & \cos(\lambda + 1)\alpha & 0 & 0 \\ \omega \sin(\lambda - 1)\alpha & \sin(\lambda + 1)\alpha & 0 & 0 \\ 0 & 0 & \sin(\lambda - 1)\alpha & \sin(\lambda + 1)\alpha \\ 0 & 0 & \omega \cos(\lambda - 1)\alpha & \cos(\lambda + 1)\alpha \end{bmatrix} \begin{Bmatrix} A \\ B \\ C \\ D \end{Bmatrix} = 0$$

where $\omega = \frac{\lambda-1}{\lambda+1}$.

- Note that whereas Eq. 39 and 40 are expressed in terms of the four constants (A , B , C , and D), the above equation is **written in terms of the summation and the differences of the stress equations**, thus yielding a block diagonal matrix.

- It can readily be seen that A and B are independent of C and D , and that for this homogeneous equation a nontrivial solution would exist if and only if the **determinant of the system of linear equations vanishes to zero**. This would lead (after some simplifications) to:

$$\sin 2\lambda\alpha \pm \lambda \sin 2\alpha = 0 \quad (41)$$

- We observe from Eq. 38 that the coefficients A and B correspond to symmetric loadings (mode I), and C and D to unsymmetric loading (mode II).
- Let us denote by λ_n the eigenvalues of λ which are solution of Eq. 41 for the symmetrical loading, and ξ_n solutions for the antisymmetric loading:

$$\sin 2\lambda_n\alpha + \lambda_n \sin 2\alpha = 0$$

$$\sin 2\xi_n\alpha - \xi_n \sin 2\alpha = 0$$

- For the case of a crack, i.e $\alpha = \pi$ solution of the characteristic equation¹ is

$$\sin(2\pi\lambda_n) = 0$$

$$\sin(2\pi\xi_n) = 0$$

which has solutions $\lambda_n = \frac{n}{2}$ with $n = 1, 3, 4, \dots$ (it can be shown that $n = 2$ gives rise to a rigid body motion contribution). Substituting into Eq. 38

$$F(\theta, \lambda) = A_n \cos\left(\frac{n}{2} - 1\right)\theta + B_n \cos\left(\frac{n}{2} + 1\right)\theta \\ + C_n \sin\left(\frac{n}{2} - 1\right)\theta + D_n \sin\left(\frac{n}{2} + 1\right)\theta$$

- We observe that the previous expression can be simplified by noting that for each eigenvalue λ_n and ξ_n there is a relationship between A and B , and between C and D in Eq. 32. For symmetrical loading we have

$$A_n \cos(\lambda_n - 1)\alpha + B_n \cos(\lambda_n + 1)\alpha = 0$$

$$A_n \omega \sin(\lambda_n - 1)\alpha + B_n \sin(\lambda_n + 1)\alpha = 0$$

and for antisymmetric loading we have

$$\begin{aligned} C_n \sin(\xi_n - 1)\alpha + D_n \sin(\xi_n + 1)\alpha &= 0 \\ C_n \omega \cos(\xi_n - 1)\alpha + D_n \cos(\xi_n + 1)\alpha &= 0 \end{aligned}$$

- Thus we can define

$$\begin{aligned} a_n &= \frac{A_n}{B_n} = -\frac{\cos(\lambda_n - 1)\alpha}{\cos(\lambda_n + 1)\alpha} = -\frac{\omega \sin(\lambda_n - 1)\alpha}{\sin(\lambda_n + 1)\alpha} \\ b_n &= \frac{C_n}{D_n} = -\frac{\sin(\lambda_n - 1)\alpha}{\sin(\lambda_n + 1)\alpha} = -\frac{\omega \cos(\lambda_n - 1)\alpha}{\cos(\lambda_n + 1)\alpha} \end{aligned}$$

these ratios are equal to $1/3$ and -1 respectively for $\alpha = \pi$ and $\lambda = 1/2$. and

$$F(\theta) = \sum \left[a_n \left(\sin \frac{3}{2}\theta + \sin \frac{1}{2}\theta \right) + b_n \left(\frac{1}{3} \cos \frac{3}{2}\theta + \cos \frac{1}{2}\theta \right) \right]$$

- The stresses are obtained by substituting

$$\begin{aligned}\sigma_{rr} &= \sum \left[\frac{b_n}{\sqrt{r}} \left(\frac{5}{4} \cos \frac{\theta}{2} - \frac{1}{4} \cos \frac{3\theta}{2} \right) + \frac{a_n}{\sqrt{r}} \left(-\frac{5}{4} \sin \frac{\theta}{2} + \frac{3}{4} \sin \frac{3\theta}{2} \right) \right] \\ \sigma_{\theta\theta} &= \sum \left[\frac{b_n}{\sqrt{r}} \left(\frac{3}{4} \cos \frac{\theta}{2} + \frac{1}{4} \cos \frac{3\theta}{2} \right) + \frac{a_n}{\sqrt{r}} \left(-\frac{3}{4} \sin \frac{\theta}{2} - \frac{3}{4} \sin \frac{3\theta}{2} \right) \right] \\ \sigma_{r\theta} &= \sum \left[\frac{b_n}{\sqrt{r}} \left(\frac{1}{4} \sin \frac{\theta}{2} + \frac{1}{4} \sin \frac{3\theta}{2} \right) + \frac{a_n}{\sqrt{r}} \left(\frac{1}{4} \cos \frac{\theta}{2} + \frac{3}{4} \cos \frac{3\theta}{2} \right) \right]\end{aligned}$$

- These equations can be further simplified into

$$\begin{aligned}\sigma_{rr} &= \sum \left[\frac{b_n}{\sqrt{r}} \cos \frac{\theta}{2} \left(1 + \sin^2 \frac{\theta}{2} \right) + \frac{a_n}{\sqrt{r}} \left(-\frac{5}{4} \sin \frac{\theta}{2} + \frac{3}{4} \sin \frac{3\theta}{2} \right) \right] \\ \sigma_{\theta\theta} &= \sum \left[\frac{b_n}{\sqrt{r}} \cos \frac{\theta}{2} \left(1 - \sin^2 \frac{\theta}{2} \right) + \frac{a_n}{\sqrt{r}} \left(-\frac{3}{4} \sin \frac{\theta}{2} - \frac{3}{4} \sin \frac{3\theta}{2} \right) \right] \\ \sigma_{r\theta} &= \sum \left[\frac{b_n}{\sqrt{r}} \sin \frac{\theta}{2} \cos^2 \frac{\theta}{2} + \frac{a_n}{\sqrt{r}} \left(\frac{1}{4} \cos \frac{\theta}{2} + \frac{3}{4} \cos \frac{3\theta}{2} \right) \right]\end{aligned}$$

- It can be shown that the displacements will be given by

$$u = \frac{1}{2\mu} \sum \operatorname{Re} \left\{ a_n r^{\lambda_n} [(\kappa + \lambda_n \cos 2\alpha + \cos 2\lambda_n \alpha) \cos \lambda_n \theta - \lambda_n \cos(\lambda_n - 2)\theta] - b_n r^{\xi_n} [(\kappa + \xi_n \cos 2\alpha - \cos 2\xi_n \alpha) \sin \xi_n \theta - \xi_n \sin(\xi_n - 2)\theta] \right\}$$

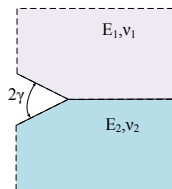
$$v = \frac{1}{2\mu} \sum \operatorname{Re} \left\{ a_n r^{\lambda_n} [(\kappa - \lambda_n \cos 2\alpha - \cos 2\lambda_n \alpha) \sin \lambda_n \theta + \lambda_n \sin(\lambda_n - 2)\theta] + b_n r^{\xi_n} [(\kappa - \xi_n \cos 2\alpha + \cos 2\xi_n \alpha) \cos \xi_n \theta + \xi_n \cos(\xi_n - 2)\theta] \right\}$$

- This solution can be compared with Westergaard's solution by comparing Equations 137 and 137 with Eq. 42; Eq. 137 and 137 with Eq. 42; and Eq. 137 and 137 with Eq. 42 for $n = 1$. From this we observe that

$$b_1 = \frac{K_I}{\sqrt{2\pi}}$$

$$a_1 = \frac{K_{II}}{\sqrt{2\pi}}$$

¹Note that the solution for λ_n and ξ_n for other angles can not be obtained algebraically, a numerical technique must be used.



- Problem of a crack at the interface between two dissimilar isotropic materials, rewrite Eq. 36 as

$$\Phi_i(r, \theta) \equiv r^{\lambda+1} F_i(\theta, \lambda) \quad (42)$$

where the subscript i refers to material 1 and 2

- Hence:

$$F_i(\theta, \lambda) = A_i \cos(\lambda - 1)\theta + B_i \cos(\lambda + 1)\theta + C_i \sin(\lambda - 1)\theta + D_i \sin(\lambda + 1)\theta \quad (43)$$

Boundary conditions:

- 1 **Zero stresses**, $\sigma_{\theta\theta}$, on the free edges (at $\theta = \pm\pi$). From Eq. 39

$$\sigma_{\theta\theta}|_{\theta=\pi} = r^{\lambda-1}\lambda(\lambda+1)[A_1 \cos(\lambda-1)\pi + B_1 \cos(\lambda+1)\pi + C_1 \sin(\lambda-1)\pi + D_1 \sin(\lambda+1)\pi] = 0 \quad (44)$$

$$\sigma_{\theta\theta}|_{\theta=-\pi} = r^{\lambda-1}\lambda(\lambda+1)[A_2 \cos(\lambda-1)\pi + B_2 \cos(\lambda+1)\pi - C_2 \sin(\lambda-1)\pi - D_2 \sin(\lambda+1)\pi] = 0 \quad (45)$$

$$\text{or } F_1(\pi) = F_2(-\pi) = 0$$

- 2 **Zero stresses**, $\sigma_{r\theta}$, on the free edges (at $\theta = \pm\pi$); From Eq. 40

$$\sigma_{r\theta}|_{\theta=\pi} = -\lambda r^{\lambda-1}[-A_1(\lambda-1) \sin(\lambda-1)\theta - B_1(\lambda+1) \sin(\lambda+1)\theta + C_1(\lambda-1) \cos(\lambda-1)\theta + D_1(\lambda+1) \cos(\lambda+1)\theta] = 0 \quad (46)$$

$$\sigma_{r\theta}|_{\theta=-\pi} = -\lambda r^{\lambda-1} F'(\theta) \quad (47)$$

$$= -\lambda r^{\lambda-1}[+A_2(\lambda-1) \sin(\lambda-1)\theta + B_2(\lambda+1) \sin(\lambda+1)\theta - C_2(\lambda-1) \cos(\lambda-1)\theta - D_2(\lambda+1) \cos(\lambda+1)\theta] = 0 \quad (48)$$

$$\text{or } F_1'(\pi) = F_2'(-\pi) = 0$$

- 3 **Continuity** of $\sigma_{\theta\theta}$ at the interface, $\theta = 0$

$$A_1 + B_1 = A_2 + B_2 \quad (49)$$

- 4 **Continuity** of $\sigma_{r\theta}$ at $\theta = 0$ along the interface

$$(\lambda - 1)C_1 + (\lambda + 1)D_1 = -(\lambda - 1)C_2 - (\lambda + 1)D_2 \quad (50)$$

- 5 **Continuity** of displacements (u_r, u_θ) at the interface. Using the polar expression of the displacements

$$u_r^i = \frac{1}{2\mu_i} r^\lambda \{ -(\lambda + 1)F_i(\theta) + 4(1 - \alpha_i)[C_i \sin(\lambda - 1)\theta + A_i \cos(\lambda - 1)\theta] \} \quad (51)$$

$$u_\theta^i = \frac{1}{2\mu_i} r^\lambda \{ -F_i'(\theta) - 4(1 - \alpha_i)[C_i \cos(\lambda - 1)\theta - A_i \sin(\lambda - 1)\theta] \} \quad (52)$$

where μ is the shear modulus, and $\alpha_i \equiv \frac{\nu_i}{1 + \nu_i}$
we obtain

$$\frac{1}{2\mu_1} [-(\lambda + 1)F_1(0) + 4A_1(1 - \alpha_1)] = \frac{1}{2\mu_2} [-(\lambda + 1)F_2(0) + 4A_2(1 - \alpha_2)] \quad (53)$$

$$\frac{1}{2\mu_1} [-F_1'(0) - 4C_1(1 - \alpha_1)] = \frac{1}{2\mu_2} [-F_2'(0) - 4C_2(1 - \alpha_2)] \quad (54)$$

- Applying those boundary conditions, will lead to 8 homogeneous linear equations (Eq. 44, 45, 47, 48, 49, 50, 53, 54) in terms of the 8 unknowns $A_1, B_1, C_1, D_1, A_2, B_2, C_2$ and D_2 .
- A nontrivial solution exists if the determinant of the 8 equations is equal to zero. This determinant² is equal to

$$\cot^2 \lambda \pi + \left[\frac{2k(1 - \alpha_2) - 2(1 - \alpha_1) - (k - 1)}{2k(1 - \alpha_2) + 2(1 - \alpha_1)} \right]^2 = 0 \quad (55)$$

where $k = \frac{\mu_1}{\mu_2}$.

²The original paper states: ... *After some algebraic simplification...*

- For the homogeneous case $\alpha_1 = \alpha_2$ and $k = 1$, the previous equation reduces to $\cot^2 \lambda\pi = 0$ or $\sin^2 \lambda\pi = 0$ thus we recover the same solution as the one of Eq. 42 for a crack in one material:

$$\lambda = \frac{n}{2} \quad n = 1, 2, 3, \dots \quad (56)$$

Note that we exclude negative values of n to ensure finite displacements as the origin is approached, and the lowest eigenvalue controls.

- Noting that there can not be a real solution to Eq. 55, we define

$$\beta = \frac{2k(1 - \alpha_2) - 2(1 - \alpha_1) - (k - 1)}{2k(1 - \alpha_2) + 2(1 - \alpha_1)} \quad (57)$$

and thus, Eq. 55 leads to $\cot^2 \lambda\pi = -\beta^2$, or

$$\cot \lambda\pi = \pm i\beta \quad (58)$$

- To solve this equation, we use the following trigonometric relations

$$\cot z = \frac{\sin 2x - i \sinh 2y}{\cosh 2y - \cos 2x} \quad (59)$$

$$\sin 2\theta\pi = \frac{2u}{1 + u^2} \quad (60)$$

$$\cos 2\theta\pi = \frac{1 - u^2}{1 + u^2} \quad (61)$$

$$\sinh 2\theta\pi = \frac{2v}{1 - v^2} \quad (62)$$

$$\cosh 2\theta\pi = \frac{1 + v^2}{1 - v^2} \quad (63)$$

where

$$u = \tan \lambda_r \pi \quad (64)$$

$$v = \tanh \lambda_j \pi \quad (65)$$

where we have assumed a complex value for λ

$$\lambda = \lambda_r + i\lambda_j \quad (66)$$

Then, we obtain

$$\sin 2\lambda_r\pi = \frac{2u}{1+u^2} \quad (67)$$

$$\cos 2\lambda_r\pi = \frac{1-u^2}{1+u^2} \quad (68)$$

$$\sinh 2\lambda_j\pi = \frac{2v}{1-v^2} \quad (69)$$

$$\cosh 2\lambda_j\pi = \frac{1+v^2}{1-v^2} \quad (70)$$

- Substituting in Eq. 59 lead to

$$\cot \lambda\pi = \frac{u(1-v^2) - iv(1+u^2)}{u^2 + v^2} \quad (71)$$

$$= \underbrace{\frac{\tan \lambda_r\pi(1 - \tanh^2 \lambda_j\pi)}{\tan^2 \lambda_r\pi + \tanh^2 \lambda_j\pi}}_{\Re(\cot \lambda\pi)=0} - i \underbrace{\frac{(\tan^2 \lambda_r\pi + 1) \tanh \lambda_j\pi}{\tan^2 \lambda_r\pi + \tanh^2 \lambda_j\pi}}_{\Im(\cot \lambda\pi)=\pm\beta} \quad (72)$$

- Thus, Eq. 55 finally leads to

$$\Re(\cot \lambda\pi) = 0 \quad (73)$$

$$\Im(\cot \lambda\pi) = \pm\beta \quad (74)$$

we thus have two equations with two unknowns.

Let us solve those two equations. Two sets of solutions are possible:

- ① If from 72 $\tan \lambda_r \pi = 0$ then

$$\lambda_r = n = 0, 1, 2, 3, \dots \quad (75)$$

and accordingly from Eq. 74

$$\lambda_j = \pm \frac{1}{\pi} \coth^{-1} \beta \quad (76)$$

- ② Alternatively, from Eq. 73 $\cot \lambda_r \pi = 0 \Rightarrow \tan \lambda_r \pi = \infty$ and³:

$$\lambda_r = \frac{2n+1}{2} \quad n = 0, 1, 2, 3, \dots \quad (77)$$

$$\lambda_j = \pm \frac{1}{\pi} \tanh^{-1} \beta \quad (78)$$

$$= \frac{1}{2\pi} \log \left[\frac{\beta + 1}{\beta - 1} \right] \quad (79)$$

We note that for this case, $\lambda_j \rightarrow 0$ as $\alpha_1 \rightarrow \alpha_2$ and $k \rightarrow 1$ in β .

³Recall that $\tanh^{-1} x = \frac{1}{2} \log \frac{1+x}{1-x}$

- Now that we have solved for λ , we need to derive expressions for the near crack tip stress field. We rewrite Eq. 42 as

$$\Phi(r) = \underbrace{r^{\lambda+1}}_{G(r)} F(\theta, \lambda) \quad (80)$$

we note that we no longer have two sets of functions, as the effect of dissimilar materials has been accounted for and is embedded in λ .

- The stresses will be given by Eq. 2

$$\sigma_{rr} = \frac{1}{r^2} \frac{\partial^2 \Phi}{\partial \theta^2} + \frac{1}{r} \frac{\partial \Phi}{\partial r} = r^{-2} G(r) F''(\theta) + r^{-1} G'(r) F(\theta) \quad (81)$$

$$\sigma_{\theta\theta} = \frac{\partial^2 \Phi}{\partial r^2} = G''(r) F(\theta) \quad (82)$$

$$\sigma_{r\theta} = \frac{1}{r^2} \frac{\partial \Phi}{\partial \theta} - \frac{1}{r} \frac{\partial^2 \Phi}{\partial r \partial \theta} = r^{-2} G(r) F'(\theta) - r^{-1} G'(r) F'(\theta) \quad (83)$$

Therefore, we must solve for $F'(\theta)$, $F''(\theta)$, $G'(r)$ and $G''(r)$ in terms of $\lambda = \lambda_r + i\lambda_j$.

- First we note that

$$G(r) = r^{\lambda+1} = r^{\lambda r+1+i\lambda_j} \quad (84)$$

$$r^{i\lambda_j} = e^{i\lambda_j \log(r)} \quad (85)$$

recalling that $\log(z) = \log|z| + i \arg z$, and since $|z| = \sqrt{x^2 + y^2} = \sqrt{r^2 + 0} = r$, we have $\arg z = 2k\pi$, and $k = 0, \pm 1, \pm 2, \dots$. Hence,

$$\log(r) = \log|r| + i2k\pi \quad (86)$$

and Eq. 85 becomes

$$r^{i\lambda_j} = e^{i\lambda_j \log(r)} \quad (87)$$

$$= e^{i\lambda_j [\log(r) + i2k\pi]} \quad (88)$$

$$= e^{i\lambda_j \log(r) - 2k\pi \lambda_j} \quad (89)$$

$$= e^{-2k\pi \lambda_j} e^{i\lambda_j \log(r)} \quad (90)$$

$$= e^{-2k\pi \lambda_j} \left[\cos(\lambda_j \log(r)) + i \sin(\lambda_j \log(r)) \right] \quad (91)$$

- Now, for $k = 0$, $r^{i\lambda_j}$ becomes

$$r^{i\lambda_j} = \cos(\lambda_j \log(r)) + i \sin(\lambda_j \log(r)) \quad (92)$$

and accordingly, Eq. 84 becomes

$$G(r) = r^{\lambda+1} = r^{\lambda_r+1} r^{i\lambda_j} \quad (93)$$

$$= r^{\lambda_r+1} [\cos(\lambda_j \log(r)) + i \sin(\lambda_j \log(r))] \quad (94)$$

and for $\lambda_r = 1/2$

$$G(r) = r^{\frac{3}{2}} [\cos(\lambda_j \log(r)) + i \sin(\lambda_j \log(r))] \quad (95)$$

$$\Re G(r) = r^{\frac{3}{2}} \cos(\lambda_j \log(r)) \quad (96)$$

$$G'(r) = r^{\frac{1}{2}} \left[\frac{3}{2} \cos(\lambda_j \log(r)) + \lambda_j \sin(\lambda_j \log(r)) \right] \quad (97)$$

$$G''(r) = r^{-\frac{1}{2}} \left[\left(\frac{3}{4} - \lambda_j^2 \right) \cos(\lambda_j \log(r)) + \left(\frac{3}{2} + \frac{\lambda_j}{2} \right) \sin(\lambda_j \log(r)) \right] \quad (98)$$

- Back to $F(\theta)$, which was defined in Eq. 43

$$F(\theta, \lambda) = A \cos(\lambda - 1)\theta + B \cos(\lambda + 1)\theta + C \sin(\lambda - 1)\theta + D \sin(\lambda + 1)\theta \quad (99)$$

we need to replace λ by $\lambda_r + i\lambda_j$. However, first we recall the following relations

$$\sin(x + iy) = \sin(x) \cosh(y) - i \cos(x) \sinh(y) \quad (100)$$

$$\cos(x + iy) = \cos(x) \cosh(y) + i \sin(x) \sinh(y) \quad (101)$$

thus,

$$\Re \left\{ \sin [(\lambda_r \pm 1) + i\lambda_j] \theta \right\} = \sin(\lambda_r \pm 1) \cos(\theta) \cosh \lambda_j \theta \quad (102)$$

$$\Re \left\{ \cos [(\lambda_r \pm 1) + i\lambda_j] \theta \right\} = \cos(\lambda_r \pm 1) \cos(\theta) \cosh \lambda_j \theta \quad (103)$$

- Substituting those relations in Eq. 99

$$\Re [F(\theta)] = \underbrace{\cosh \lambda_j \theta}_{f(\theta)} \quad (104)$$

$$\underbrace{[A \cos(\lambda_r - 1)\theta + B \cos(\lambda_r + 1)\theta + C \sin(\lambda_r - 1)\theta + D \sin(\lambda_r + 1)\theta]}_{g(\theta)} \quad (105)$$

$$\Re [\Phi(r, \theta)] = r^{\lambda_r + 1} \cos(\lambda_j \log(r)) \cosh \lambda_j \theta \\ [A \cos(\lambda_r - 1)\theta + B \cos(\lambda_r + 1)\theta \\ + C \sin(\lambda_r - 1)\theta + D \sin(\lambda_r + 1)\theta] \quad (106)$$

- For $\lambda_r = \frac{1}{2}$

$$g(\theta) = A \cos \frac{\theta}{2} + B \cos \frac{3\theta}{2} - C \sin \frac{\theta}{2} + D \sin \frac{3\theta}{2} \quad (107)$$

- Applying the boundary conditions at $\theta = \pm\pi$, $\sigma_{\theta\theta} = 0$, Eq. 82 $F(\theta) = 0$, that is $g_1(-\pi) = g_2(\pi)$ or

$$C = -D = -a \quad (108)$$

- Similarly at $\theta = \pm\pi$, $\sigma_{r\theta} = 0$. Thus, from Eq. 83 $F'(\theta) = 0$, or $g_1'(-\pi) = g_2'(\pi)$ or

$$A = 3B = b \quad (109)$$

- From those two equations we rewrite Eq. 107

$$g(\theta) = a \left(\sin \frac{\theta}{2} + \sin \frac{3\theta}{2} \right) + b \left(3 \cos \frac{\theta}{2} + \cos \frac{3\theta}{2} \right) \quad (110)$$

- We now determine the derivatives

$$f'(\theta) = \lambda_j \sinh \lambda_j \theta \quad (111)$$

$$g'(\theta) = a \left(\frac{3}{2} \cos \frac{3\theta}{2} + \frac{1}{2} \cos \frac{\theta}{2} \right) + b \left(-\frac{3}{2} \sin \frac{3\theta}{2} - \frac{3}{2} \sin \frac{\theta}{2} \right) \quad (112)$$

- Thus, we now can determine

$$F'(\theta) = f'(\theta)g(\theta) + f(\theta)g'(\theta) \quad (113)$$

$$= a \left\{ \cosh \lambda_j \theta \left[\frac{3}{2} \cos \frac{3\theta}{2} + \frac{1}{2} \cos \frac{\theta}{2} \right] + \lambda_j \sinh \lambda_j \theta \left[\sin \frac{3\theta}{2} + \sin \frac{\theta}{2} \right] \right\} \\ + b \left\{ \cosh \lambda_j \theta \left[-\frac{3}{2} \sin \frac{3\theta}{2} - \frac{3}{2} \sin \frac{\theta}{2} \right] + \lambda_j \sinh \lambda_j \theta \left[\cos \frac{3\theta}{2} + 3 \cos \frac{\theta}{2} \right] \right\} \quad (114)$$

- Similarly, the second derivative $F''(\theta)$ is determined

$$F''(\theta) = f''(\theta)g(\theta) + 2f'(\theta)g'(\theta) + f(\theta)g''(\theta) \quad (115)$$

$$= a \left\{ \cosh \lambda_j \theta \left[-\frac{9}{4} \sin \frac{3\theta}{2} - \frac{1}{4} \sin \frac{\theta}{2} \right] + 2\lambda_j \sinh \lambda_j \theta \left[\frac{3}{2} \cos \frac{3\theta}{2} + \frac{1}{2} \cos \frac{\theta}{2} \right] \right. \\ \left. + \lambda_j^2 \cosh^2 \lambda_j \theta \left[\sin \frac{3\theta}{2} + \sin \frac{\theta}{2} \right] \right\} + \\ b \left\{ \cosh \lambda_j \theta \left[-\frac{9}{4} \cos \frac{3\theta}{2} - \frac{3}{4} \cos \frac{\theta}{2} \right] + 2\lambda_j \sinh \lambda_j \theta \left[-\frac{3}{2} \sin \frac{3\theta}{2} - \frac{3}{2} \sin \frac{\theta}{2} \right] \right. \\ \left. + \lambda_j^2 \cosh^2 \lambda_j \theta \left[\cos \frac{3\theta}{2} + 3 \cos \frac{\theta}{2} \right] \right\} \quad (116)$$

- We can now substitute in Eq. 82, 83 and 81 to determine the stresses

$$\sigma_{rr} = r^{-\frac{1}{2}} \cos(\lambda_j \log(r)) F''(\theta) + r^{-\frac{1}{2}} \left[\frac{3}{2} \cos(\lambda_j \log(r)) + \lambda_j \sin(\lambda_j \log(r)) \right] F(\theta) \quad (117)$$

$$\sigma_{\theta\theta} = r^{-\frac{1}{2}} \left[\left(\frac{3}{4} - \lambda_j^2 \right) \cos(\lambda_j \log(r)) + \left(\frac{3}{2} + \frac{\lambda_j}{2} \right) \sin(\lambda_j \log(r)) \right] F(\theta) \quad (118)$$

$$\sigma_{r\theta} = r^{-\frac{1}{2}} \left\{ \cos(\lambda_j \log(r)) F'(\theta) + \left[\frac{3}{2} \cos(\lambda_j \log(r)) + \lambda_j \sin(\lambda_j \log(r)) \right] F'(\theta) \right\} \quad (119)$$

- To analyze an anisotropic body with with a crack, we need to derive the two stress functions Φ_1 and Φ_2 in Eq. ?? such that they satisfy the boundary conditions of the problem under consideration.
- For an infinite plate with a central crack in an anisotropic body the derivation for the stress functions was undertaken by Sih, Paris and Irwin This solution is the

“counterpart” or generalization of Westergaard’s solutions.

$$u_1 = K_I \sqrt{\frac{2r}{\pi}} \operatorname{Re} \left\{ \frac{1}{s_1 - s_2} \left[s_1 p_2 (\cos \theta + s_2 \sin \theta)^{\frac{1}{2}} - s_2 p_1 (\cos \theta + s_1 \sin \theta)^{\frac{1}{2}} \right] \right\} \quad (120)$$

$$v_1 = K_I \sqrt{\frac{2r}{\pi}} \operatorname{Re} \left\{ \frac{1}{s_1 - s_2} \left[s_1 q_2 (\cos \theta + s_2 \sin \theta)^{\frac{1}{2}} - s_2 q_1 (\cos \theta + s_1 \sin \theta)^{\frac{1}{2}} \right] \right\} \quad (121)$$

$$w_1 = 0 \quad (122)$$

$$u_2 = K_{II} \sqrt{\frac{2r}{\pi}} \operatorname{Re} \left\{ \frac{1}{s_1 - s_2} \left[p_2 (\cos \theta + s_2 \sin \theta)^{\frac{1}{2}} - p_1 (\cos \theta + s_1 \sin \theta)^{\frac{1}{2}} \right] \right\} \quad (123)$$

$$v_2 = K_{II} \sqrt{\frac{2r}{\pi}} \operatorname{Re} \left\{ \frac{1}{s_1 - s_2} \left[q_2 (\cos \theta + s_2 \sin \theta)^{\frac{1}{2}} - q_1 (\cos \theta + s_1 \sin \theta)^{\frac{1}{2}} \right] \right\} \quad (124)$$

$$w_2 = 0 \quad (125)$$

$$u_3 = 0 \quad (126)$$

$$v_3 = 0 \quad (127)$$

$$w_3 = K_{III} \sqrt{\frac{2r}{\pi}} \left(c_{44} c_{55} - c_{45}^2 \right)^{-\frac{1}{2}} \operatorname{Im} \left[(\cos \theta + s_3 \sin \theta)^{\frac{1}{2}} \right] \quad (128)$$

- where s_1 and s_2 are roots, in general complex, of Eq. ?? where $s_j = \alpha_j + i\beta_j$ for $j = 1, 2$, and the roots of interests are taken such that $\beta_j > 0$, and

$$p_j = a_{11}s_j^2 + a_{12} - a_{16}s_j \quad (129)$$

$$q_j = a_{12}s_j + \frac{a_{22}}{s_j} - a_{26} \quad (130)$$

- After appropriate substitution, it can be shown that the cartesian stresses at the tip of the crack for symmetric loading are

$$\sigma_x = \frac{K_I}{\sqrt{2\pi r}} \operatorname{Re} \left[\frac{s_1 s_2}{s_1 - s_2} \left(\frac{s_2}{(\cos \theta + s_2 \sin \theta)^{\frac{1}{2}}} - \frac{s_1}{(\cos \theta + s_1 \sin \theta)^{\frac{1}{2}}} \right) \right] \quad (131)$$

$$\sigma_y = \frac{K_I}{\sqrt{2\pi r}} \operatorname{Re} \left[\frac{1}{s_1 - s_2} \left(\frac{s_1}{(\cos \theta + s_2 \sin \theta)^{\frac{1}{2}}} - \frac{s_2}{(\cos \theta + s_1 \sin \theta)^{\frac{1}{2}}} \right) \right] \quad (132)$$

$$\sigma_{xy} = \frac{K_I}{\sqrt{2\pi r}} \operatorname{Re} \left[\frac{s_1 s_2}{s_1 - s_2} \left(\frac{1}{(\cos \theta + s_1 \sin \theta)^{\frac{1}{2}}} - \frac{s_1}{(\cos \theta + s_2 \sin \theta)^{\frac{1}{2}}} \right) \right] \quad (133)$$

- and, for plane skew-symmetric loading:

$$\sigma_x = \frac{K_{II}}{\sqrt{2\pi r}} \operatorname{Re} \left[\frac{1}{s_1 - s_2} \left(\frac{s_2^2}{(\cos \theta + s_2 \sin \theta)^{\frac{1}{2}}} - \frac{s_1^2}{(\cos \theta + s_1 \sin \theta)^{\frac{1}{2}}} \right) \right] \quad (134)$$

$$\sigma_y = \frac{K_{II}}{\sqrt{2\pi r}} \operatorname{Re} \left[\frac{1}{s_1 - s_2} \left(\frac{1}{(\cos \theta + s_2 \sin \theta)^{\frac{1}{2}}} - \frac{1}{(\cos \theta + s_1 \sin \theta)^{\frac{1}{2}}} \right) \right] \quad (135)$$

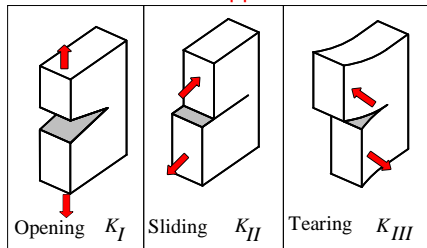
$$\sigma_{xy} = \frac{K_{II}}{\sqrt{2\pi r}} \operatorname{Re} \left[\frac{1}{s_1 - s_2} \left(\frac{s_1}{(\cos \theta + s_1 \sin \theta)^{\frac{1}{2}}} - \frac{s_2}{(\cos \theta + s_2 \sin \theta)^{\frac{1}{2}}} \right) \right] \quad (136)$$

- For in-plane loadings, these stresses can be summed to give the stresses at a distance r and an angle θ from the crack tip.
- An important observation to be made is that the form of the stress singularity $r^{-1/2}$ is identical to the one found in isotropic solids.
- It should be noted that contrarily to the isotropic case where both the stress magnitude and its spatial distribution are controlled by the stress intensity factor only, in the anisotropic case they will also depend on the material elastic properties and the orientation of the crack with respect to the principal planes of elastic symmetry (through s_1 and s_2).

- 1 Irwin introduced the concept of *stress intensity factor* defined as:

$$\begin{Bmatrix} K_I \\ K_{II} \\ K_{III} \end{Bmatrix} = \lim_{r \rightarrow 0, \theta = 0} \sqrt{2\pi r} \begin{Bmatrix} \sigma_{22} \\ \sigma_{12} \\ \sigma_{23} \end{Bmatrix}$$

where σ_{ij} are the near crack tip stresses, and K_i are associated with **three independent kinematic movements of the upper and lower crack surfaces with**



respect to each other

- **Opening Mode, I:** The two crack surfaces are pulled apart in the y direction, but the deformations are symmetric about the $x - z$ and $x - y$ planes.

- **Shearing Mode, II:** The two crack surfaces slide over each other in the x -direction, but the deformations are symmetric about the $x - y$ plane and skew symmetric about the $x - z$ plane.
- **Tearing Mode, III:** The crack surfaces slide over each other in the z -direction, but the deformations are skew symmetric about the $x - y$ and $x - z$ planes.

② From Eq. 33, 34 and 35 with $\theta = 0$, we have

$$\begin{aligned}
 K_I &= \sqrt{2\pi r}\sigma_{22} \\
 &= \sqrt{2\pi r}\sigma_0\sqrt{\frac{a}{2r}} \\
 &= \sigma_0\sqrt{\pi a}
 \end{aligned}$$

where r is the length of a small vector extending directly forward from the crack tip.

- ③ Thus stresses and displacements can all be rewritten in terms of the SIF

$$\begin{Bmatrix} \sigma_{22} \\ \sigma_{12} \\ \sigma_{23} \end{Bmatrix} = \frac{1}{\sqrt{2\pi r}} \begin{bmatrix} f_{11}'(\theta) & f_{11}''(\theta) & f_{11}'''(\theta) \\ f_{22}'(\theta) & f_{22}''(\theta) & f_{22}'''(\theta) \\ f_{12}'(\theta) & f_{12}''(\theta) & f_{12}'''(\theta) \end{bmatrix} \begin{Bmatrix} K_I \\ K_{II} \\ K_{III} \end{Bmatrix}$$

i.e.

$$\sigma_{12} = \frac{K_{II}}{\sqrt{2\pi r}} \underbrace{\sin \frac{\theta}{2} \cos \frac{\theta}{2} \cos \frac{3\theta}{2}}_{f_{12}''}$$

- ① Since higher order terms in r were neglected, previous equations are **exact in the limit as $r \rightarrow 0$**
- ② Distribution of elastic stress field at tip can be described by K_I , K_{II} and K_{III} .
- ③ SIF are additives.
- ④ The SIF is the measure of the strength of the singularity (analogous to SCF)
- ⑤ $K = \beta \sigma \sqrt{\pi a}$ where β is a parameter that **depends on the specimen, crack geometry, and loading.**

- ⑥ One of the underlying principles of FM is that **unstable fracture occurs when the SIF reaches a critical value K_{Ic} . K_{Ic} or fracture toughness represents the inherent ability of a material to withstand a given stress field intensity at the tip of a crack and to resist progressive tensile crack extensions.**

- 1 Using Irwin's concept of the stress intensity factors, which characterize the strength of the singularity at a crack tip, the near crack tip ($r \ll a$) stresses and displacements are always expressed as:

Pure mode I loading:

$$\sigma_{xx} = \frac{K_I}{(2\pi r)^{\frac{1}{2}}} \cos \frac{\theta}{2} \left[1 - \sin \frac{\theta}{2} \sin \frac{3\theta}{2} \right] + \dots$$

$$\sigma_{yy} = \frac{K_I}{(2\pi r)^{\frac{1}{2}}} \cos \frac{\theta}{2} \left[1 + \sin \frac{\theta}{2} \sin \frac{3\theta}{2} \right] + \dots$$

$$\tau_{xy} = \frac{K_I}{(2\pi r)^{\frac{1}{2}}} \sin \frac{\theta}{2} \cos \frac{\theta}{2} \cos \frac{3\theta}{2} + \dots$$

$$\sigma_{zz} = \nu(\sigma_x + \sigma_y) + \dots$$

$$\tau_{xz} = \tau_{yz} = 0$$

$$u = \frac{K_I}{2\mu} \left[\frac{r}{2\pi} \right]^{\frac{1}{2}} \cos \frac{\theta}{2} \left[\kappa - 1 + 2 \sin^2 \frac{\theta}{2} \right] + \dots$$

$$v = \frac{K_I}{2\mu} \left[\frac{r}{2\pi} \right]^{\frac{1}{2}} \sin \frac{\theta}{2} \left[\kappa + 1 - 2 \cos^2 \frac{\theta}{2} \right] + \dots$$

$$w = 0$$

Pure mode II loading:

$$\sigma_{xx} = -\frac{K_{II}}{(2\pi r)^{\frac{1}{2}}} \sin \frac{\theta}{2} \left[2 + \cos \frac{\theta}{2} \cos \frac{3\theta}{2} \right] + \dots$$

$$\sigma_{yy} = \frac{K_{II}}{(2\pi r)^{\frac{1}{2}}} \sin \frac{\theta}{2} \cos \frac{\theta}{2} \cos \frac{3\theta}{2} + \dots$$

$$\tau_{xy} = \frac{K_{II}}{(2\pi r)^{\frac{1}{2}}} \cos \frac{\theta}{2} \left[1 - \sin \frac{\theta}{2} \sin \frac{3\theta}{2} \right] + \dots$$

$$\sigma_{zz} = \nu(\sigma_x + \sigma_y)$$

$$\tau_{xz} = \tau_{yz} = 0$$

$$u = \frac{K_{II}}{2\mu} \left[\frac{r}{2\pi} \right]^{\frac{1}{2}} \sin \frac{\theta}{2} \left[\kappa + 1 + 2 \cos^2 \frac{\theta}{2} \right] + \dots$$

$$v = -\frac{K_{II}}{2\mu} \left[\frac{r}{2\pi} \right]^{\frac{1}{2}} \cos \frac{\theta}{2} \left[\kappa - 1 - 2 \sin^2 \frac{\theta}{2} \right] + \dots$$

$$w = 0$$

Pure mode III loading:

$$\tau_{xz} = -\frac{K_{III}}{(2\pi r)^{\frac{1}{2}}} \sin \frac{\theta}{2} + \dots$$

$$\tau_{yz} = \frac{K_{III}}{(2\pi r)^{\frac{1}{2}}} \cos \frac{\theta}{2} + \dots$$

$$\sigma_{xx} = \sigma_y = \sigma_z = \tau_{xy} = 0$$

$$w = \frac{K_{III}}{\mu} \left[\frac{2r}{\pi} \right]^{\frac{1}{2}} \sin \frac{\theta}{2} + \dots$$

$$u = v = 0$$

where $\kappa = 3 - 4\nu$ for plane strain, and $\kappa = \frac{3-\nu}{1+\nu}$ for plane stress.

2 we can write the stresses in **polar coordinates**

Pure mode I loading:

$$\begin{aligned}\sigma_{rr} &= \frac{K_I}{\sqrt{2\pi r}} \cos \frac{\theta}{2} \left(1 + \sin^2 \frac{\theta}{2} \right) + \dots \\ \sigma_{\theta\theta} &= \frac{K_I}{\sqrt{2\pi r}} \cos \frac{\theta}{2} \left(1 - \sin^2 \frac{\theta}{2} \right) + \dots \\ \tau_{r\theta} &= \frac{K_I}{\sqrt{2\pi r}} \sin \frac{\theta}{2} \cos^2 \frac{\theta}{2} + \dots\end{aligned}$$

Pure mode II loading:

$$\begin{aligned}\sigma_{rr} &= \frac{K_{II}}{\sqrt{2\pi r}} \left(-\frac{5}{4} \sin \frac{\theta}{2} + \frac{3}{4} \sin \frac{3\theta}{2} \right) + \dots \\ \sigma_{\theta\theta} &= \frac{K_{II}}{\sqrt{2\pi r}} \left(-\frac{3}{4} \sin \frac{\theta}{2} - \frac{3}{4} \sin \frac{3\theta}{2} \right) + \dots \\ \tau_{r\theta} &= \frac{K_{II}}{\sqrt{2\pi r}} \left(\frac{1}{4} \cos \frac{\theta}{2} + \frac{3}{4} \cos \frac{3\theta}{2} \right) + \dots\end{aligned}$$

Applications of LEFM

Victor E. Saouma
saouma@colorado.edu

University of Colorado, Boulder

Spring 2022

- 1 Stress Intensity Factors
 - Middle Tension Panel; MT
 - Single Edge Notch Tension Panel; SENT
 - Double Edge Notch Tension Panel; DENT
 - Three Point Bend; TPB
 - Compact tension Specimen; CTS
 - Circular Holes; Approximate
 - Point Load on Crack Surface
 - Point Load Acting on Crack Surfaces of an Edge Crack
 - Embedded Elliptical Crack
 - Surface Crack
- 2 Indicative Fracture Toughness Values
- 3 Examples
 - Material Selection
 - Forensic Study
- 4 Leak Before Break (LBB)
- 5 Inspection

Table of Contents II

- Techniques
- Inspection Rate
- Example

Fundamental Relation

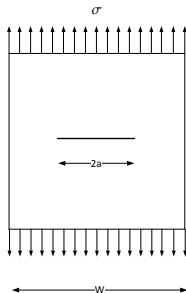
$$K_{Ic} = \beta \sigma \sqrt{\pi a}$$

- Three design variables are:
 - 1 **Material properties:** (such as special steel to resist corrosive liquid) $\Rightarrow K_c$ is fixed.
 - 2 **Design stress level:** (which may be governed by weight considerations) $\Rightarrow \sigma$ is fixed.
 - 3 **Flaw size:** a refers to half the total crack length, $\Rightarrow a$.

	Known	Unknown	Determine
K_{Ic}	a_c	σ_c	Maximum load that can be carried
K_{Ic}	σ_c	a_c	Maximum crack (should be detectable)
a_c	σ_c	K_{Ic}	Material with sufficient toughness

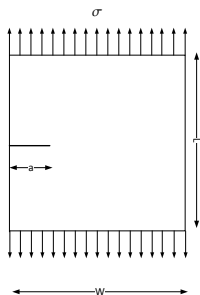
- Even if we do not “see” a crack, a **crack equal to the smallest detectable one should always be assumed to be present.**

- If a is known, it must be least equal to the **smallest flaw size which can be detected**.
- Simple inspection, “large” a , expensive nondestructive techniques, “small” a .
- Once two parameters are specified, **the third one is fixed**.
- In most cases the geometry is fixed (hence β), occasionally, there is the possibility to alter it in such a way to reduce (or maximize).
- Stress Intensity Factor handbooks.
 - 1 Tada, H., P. Paris, and G. R. Irwin. *The Stress Analysis Handbook*, Del Research Corporation, St. Louis, USA (1973). <http://www.ltas-cm3.ulg.ac.be/MECA0058-1/TheHandbookExcerpts.pdf>
 - 2 Murakami, Y. *Stress Intensity Factors Handbook*, Elsevier (1987).
 - 3 Rooke, D.P. and Cartwright, D.J., 1976. *Compendium of stress intensity factors. Procurement Executive*, Ministry of Defence. H. M. S. O. 1976, 330 p(Book).



$$\begin{aligned}
 K_I &= \underbrace{\sqrt{\sec \frac{\pi a}{W}}}_{\beta} \sigma \sqrt{\pi a} \\
 &= \underbrace{\left[1 + 0.256 \left(\frac{a}{W} \right) - 1.152 \left(\frac{a}{W} \right)^2 + 12.2 \left(\frac{a}{W} \right)^3 \right]}_{\beta} \sigma \sqrt{\pi a}
 \end{aligned}$$

We note that for W very large with respect to a , $\sqrt{\pi \sec \frac{\pi a}{W}} = 1$ as anticipated.

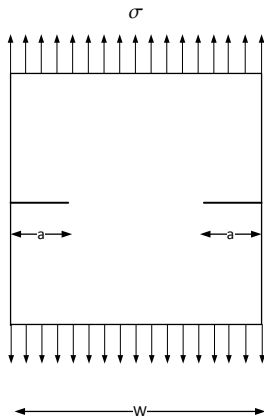


For $\frac{L}{W} \geq 2$ and $a/W \leq 0.6$

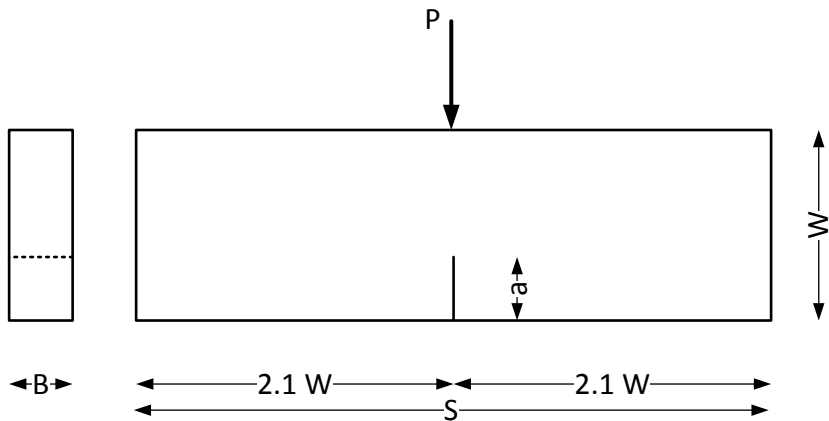
$$K_I = \underbrace{\left[1.12 - 0.23 \left(\frac{a}{W} \right) + 10.56 \left(\frac{a}{W} \right)^2 - 21.74 \left(\frac{a}{W} \right)^3 + 30.42 \left(\frac{a}{W} \right)^4 \right]}_{\beta} \sigma \sqrt{\pi a} \quad (1)$$

We observe that here the β factor for small crack ($\frac{a}{W} \ll 1$) is greater than one and is approximately 1.12.

$$\text{For } \frac{L}{W} \geq 2 \text{ and } a/W \geq 0.3 \quad K_I = \sigma \sqrt{\pi a} \left[\frac{1 + 3 \frac{a}{b}}{2 \sqrt{\pi \frac{a}{b} \left(1 - \frac{a}{b} \right)^{3/2}}} \right]$$

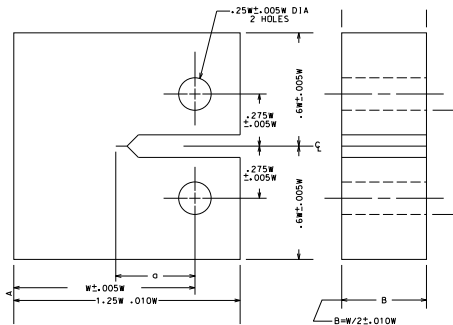


$$K_I = \underbrace{\left[1.12 + 0.43 \left(\frac{a}{W} \right) - 4.79 \left(\frac{a}{W} \right)^2 + 15.46 \left(\frac{a}{W} \right)^3 \right]}_{\beta} \sigma \sqrt{\pi a} \quad (2)$$



$$K_I = \frac{PS}{BW^{3/2}} \left[2.9 \left(\frac{a}{W} \right)^{1/2} - 4.6 \left(\frac{a}{W} \right)^{3/2} + 21.8 \left(\frac{a}{W} \right)^{5/2} - 37.6 \left(\frac{a}{W} \right)^{7/2} + 38.7 \left(\frac{a}{W} \right)^{9/2} \right] \quad (3)$$

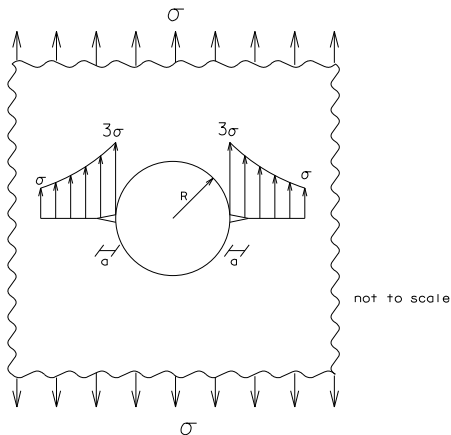
Used in ASTM E-399 Standard Test Method for Plane-Strain Fracture Toughness of Metallic Materials



$$K_I = \underbrace{\left[16.7 - 104.6 \left(\frac{a}{W} \right) + 370 \left(\frac{a}{W} \right)^2 - 574 \left(\frac{a}{W} \right)^3 + 361 \left(\frac{a}{W} \right)^4 \right]}_{\beta} \underbrace{\frac{P}{BW}}_{\sigma} \sqrt{\pi a} \quad (4)$$

We note that this is not exactly the equation found in the ASTM standard, but rather an equivalent one written in the standard form.

For a plate with a far field uniform stress σ , we know that there is a stress concentration factor of 3.



for a crack radiating from this hole, we consider two cases

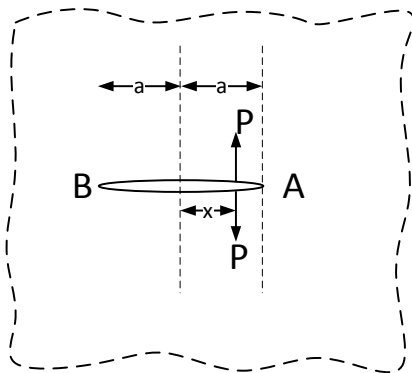
- 1 **Short Crack:** $\frac{a}{D} \rightarrow 0$, and thus we have an approximate far field stress of 3σ , and for an edge crack $\beta = 1.12$

$$\begin{aligned} K_I &= 1.12(3\sigma)\sqrt{\pi a} \\ &= 3.36\sigma\sqrt{\pi a} \end{aligned}$$

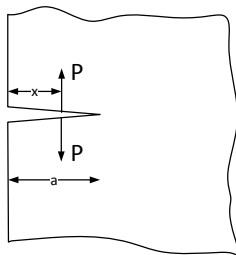
- 2 **Long Crack** $D \ll 2a + D$, in this case, we can for all practical purposes ignore the presence of the hole, and assume that we have a central crack with an effective length $a_{eff} = \frac{2a+D}{2}$, thus

$$\begin{aligned} K_I &= \sigma\sqrt{\pi\frac{2a+D}{2}} \\ &= \underbrace{\sqrt{1 + \frac{D}{2a}}}_{\beta} \sigma\sqrt{\pi a} \end{aligned}$$

The solution of this problem, is of great practical importance, as it provides the Green's function for numerous other ones.



$$K_I^A = \frac{P}{\pi a} \sqrt{\frac{a+x}{a-x}} \quad K_I^B = \frac{P}{\pi a} \sqrt{\frac{a-x}{a+x}} \quad (5)$$

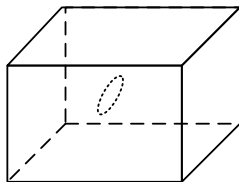


$$K_I = \frac{2P}{\pi a} \frac{C}{\sqrt{1 + \left(\frac{x}{a}\right)^2}} \left[-0.4 \left(\frac{x}{a}\right)^2 + 1.3 \right] \quad (6)$$

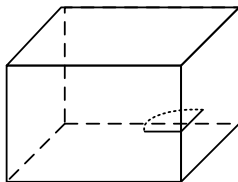
where C is given by

$\frac{x}{a}$	C
< 0.6	1
0.6-0.7	1.01
0.7-0.8	1.03
0.8-0.9	1.07
> 0.9	1.11

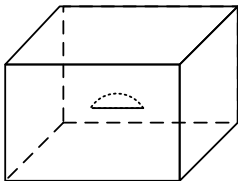
A large number of naturally occurring defects are present as embedded, surface or corner cracks (such as fillet welding)



Embedded Crack



Corner Crack



Surface Crack

- Irwin proposed the following solution for the elliptical crack, with $x = a \cos \theta$ and $y = b \sin \theta$:

$$K_I(\theta) = \frac{1}{\Phi_0} \left(\sin^2 \theta + \frac{b^2}{a^2} \cos^2 \theta \right)^{\frac{1}{4}} \sigma \sqrt{\pi b} \quad (7)$$

where Φ_0 is a complete elliptical integral of the second kind

$$\begin{aligned} \Phi_0 &= \int_0^{\frac{\pi}{2}} \sqrt{1 - \frac{a^2 - b^2}{a^2} \sin^2 \theta} d\theta \\ &= \sqrt{Q} \end{aligned}$$

- An approximation to Eq. 7 was given by Cherepanov

$$K_I(\theta) = \left[\sin^2 \theta + \left(\frac{b}{a} \right)^2 \cos^2 \theta \right]^{\frac{1}{4}} \sigma \sqrt{\pi b} \quad (8)$$

for $0 \leq \frac{b}{a} \leq 1$.

- Observations:

- 1 If $a = b$ then we have a “penny-shape’ circular crack and Eq. 7 reduces to

$$K_I = \frac{2}{\pi} \sigma \sqrt{\pi a} \quad (9)$$

- 2 If $a = \infty$ & $\theta = \frac{\pi}{2}$ then we retrieve the solution $K_I = \sigma \sqrt{\pi a}$ of a through crack.

- 3 At the end of the minor axes, $\theta = \frac{\pi}{2}$ the stress intensity factor is **maximum**:

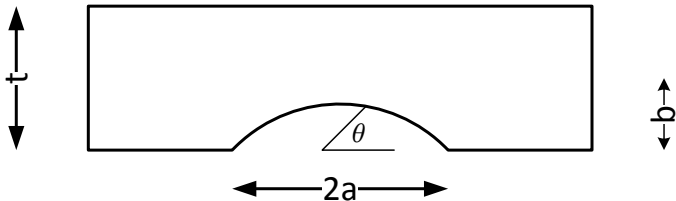
$$(K_I)_{\theta=\frac{\pi}{2}} = \frac{\sigma \sqrt{\pi b}}{\Phi_0} = \sigma \sqrt{\frac{\pi b}{Q}} \quad (10)$$

- 4 At the end of the major axes, $\theta = 0$ the stress intensity factor is **minimum**

$$(K_I)_{\theta=0} = \frac{\sigma \sqrt{\pi \frac{b^2}{a}}}{\Phi_0} \quad (11)$$

Thus an embedded elliptical crack will **propagate into a circular one** “penny-shaped”.

- Irwin's original solution has been **extended** to semi-elliptical surface flaws, quarter elliptical corner cracks, and to surface cracks emanating from circular holes.
- Using the results of **three dimensional finite element analysis**, Newman and Raju developed an empirical SIF equation for semi-elliptical surface cracks,
- This is perhaps the **most accurate solution and is almost universally used**:



$$K = \sigma\sqrt{\pi b} \left[M_1 + M_2 \left(\frac{b}{t}\right)^2 + M_3 \left(\frac{b}{t}\right)^4 \right] \left[1 + 1.464 \left(\frac{b}{a}\right)^{1.65} \right]^{-\frac{1}{2}} \\ \left[\left(\frac{b}{a}\right)^2 \cos^2 \theta + \sin^2 \theta \right]^{\frac{1}{4}} \left\{ 1 + \left[0.1 + 0.35 \left(\frac{b}{t}\right)^2 \right] (1 - \sin \theta)^2 \right\} \quad (12)$$

$$M_1 = 1.13 - 0.09 \left(\frac{b}{a}\right)$$

$$M_2 = 0.89 \left[0.2 + \left(\frac{b}{a}\right) \right]^{-1} - 0.54$$

$$M_3 = 0.5 - \left[0.65 + \left(\frac{b}{a}\right) \right]^{-1} + 14 \left[1 - \left(\frac{b}{a}\right) \right]^{24}$$

- This equation is accurate within ± 5 percent, provided $0 < \frac{b}{a} \leq 1.0$ and $\frac{b}{t} \leq 0.8$. For $\frac{b}{a}$ approximately equal to 0.25, K is roughly independent of θ .

- For shallow cracks $\frac{b}{t} \ll 1$, Equation 12 reduces to

$$K = 1.13\sigma\sqrt{\pi b} \left[1 - .08 \left(\frac{b}{a} \right) \right] \left[1 + 1.464 \left(\frac{b}{a} \right)^{1.65} \right]^{-\frac{1}{2}} \quad (13)$$

- For very long cracks $\frac{b}{a} \ll 1$, Equation 12 reduces to

$$K = 1.13\sigma\sqrt{\pi b} \left[1 + 3.46 \left(\frac{b}{t} \right)^2 + 11.5 \left(\frac{b}{t} \right)^4 \right] \quad (14)$$

Material Type	K_{Ic} ksi $\sqrt{\text{in}}$
Steel, Medium Carbon	49
Steel, Pressure Vessel	190
Hardened Steel	20
Aluminum	20-30
Titanium	70
Copper	100
Lead	18
Glass	0.7
Westerly Granite	16
Cement Paste	0.5
Concrete	1
Nylon	3

Material Type	K_{Ic} MPa $\sqrt{\text{m}}$
Metal	
Aluminum alloy (7075)	24
Steel alloy (4340)	50
Titanium alloy	44-66
Aluminum	14-28
Ceramic	
Aluminum oxide	3-5
Silicon carbide	3-5
Soda-lime glass	0.7-0.8
Concrete	0.2-1.4
Polymer	
Polymethyl methacrylate	0.7-1.6
Polystyrene	0.7-1.1

Note that stress intensity factors in metric units are commonly expressed in $\text{Mpa}\sqrt{\text{m}}$, and that

$$1\text{ksi}\sqrt{\text{in}} = 1.099\text{Mpa}\sqrt{\text{m}} \quad (15)$$

Assume that a component in the shape of a large sheet is to be fabricated from .45C – Ni – Cr – Mo steel, with a decreasing fracture toughness with increase in yield stress

Yield Stress Ksi	K_{Ic} ksi $\sqrt{\text{in}}$
210	65
220	60
230	40
240	38
290	35
300	30

The smallest crack size ($2a$) which can be detected is approximately .12 in. The specified design stress is $\frac{\sigma_y}{2}$. To save weight, an increase of tensile strength from 220 ksi to 300 ksi is suggested. $\beta = 1$. Is this reasonable?

- ① At 220 ksi $K_{Ic} = 60 \text{ ksi}\sqrt{\text{in}}$, and at 300 ksi $K_{Ic} = 30 \text{ ksi}\sqrt{\text{in}}$. Thus, the design stress will be given by $\sigma_d = \frac{\sigma_y}{2}$ and from $K_{Ic} = \sigma_d \sqrt{\pi a_{cr}} \Rightarrow a_{cr} = \frac{1}{\pi} \left(\frac{K_{Ic}}{\frac{\sigma_y}{2}} \right)^2$

2 Thus,

Yield Stress σ_y	Design Stress σ_d	Fracture Tough. K_{Ic}	Critical Crack a_{cr}	Total Crack $2a_{cr}$
220	110	60	.0947	.189
300	150	30	.0127	.0255

- 3 We observe that for the first case, the total crack length is larger than the smallest one which can be detected (which is O.K.);
- 4 Alternatively, for the second case the total critical crack size is approximately five times smaller than the minimum flaw size required and approximately eight times smaller than the flaw size tolerated at the 220 ksi level.
- 5 Hence, σ_y should not be raised to 300 ksi.

- 6 if we wanted to use the flaw size found with the 300 ksi alloy, we should have a **decrease in design stress** (since K_{Ic} and a_{cr} are now set)

$$K_{Ic} = \sigma_d \sqrt{\pi a_{vis}} \Rightarrow \sigma_d = \frac{K_{Ic}}{\sqrt{\pi a_{vis}}} = \frac{30 \text{ksi} \sqrt{\text{in}}}{\sqrt{0.06\pi}} = 69 \text{ksi}$$
, with a potential factor of safety of one against cracking (we can not be sure 100% that there is no crack of that size or smaller as we can not detect it). We observe that since the design stress level is approximately half of that of the weaker alloy, there will be a two fold increase in weight.

A small beer barrel of diameter 15" and wall thickness of .126" made of aluminum alloy exploded when a pressure reduction valve malfunctioned and the barrel experienced the 610 psi full pressure of the CO₂ cylinder supplying it with gas. Afterwards, cracks approximately 4.0 inch long by (probably) .07 inch deep were discovered on the inside of the salvaged pieces of the barrel (it was impossible to measure their depth). Independent tests gave 40. ksi√in for K_{Ic} of the aluminum alloy. The **question is whether the cracks were critical for the 610 psi pressure?**

- 1 For a cylinder under internal pressure, the hoop stress is

$$\sigma = \frac{pD}{2t} = \frac{610 \text{ lb}}{\text{in}^2} \frac{15 \text{ in}}{2(.126) \text{ in}} = 36,310 \text{ psi} = 36.3 \text{ ksi. This can be used as the far field stress (neglecting curvature).}$$

- 2 First we use the exact solution as given in Eq. 12, with $a = 2$. in, $b = .07$ in, and $t = .126$ in. upon substitution we obtain:

$$M_1 = 1.13 - 0.09 \left(\frac{.07}{2.} \right)$$

$$= 1.127$$

$$M_2 = 0.89 \left[0.2 + \left(\frac{.07}{2.} \right) \right]^{-1} - 0.54$$

$$= 3.247$$

$$M_3 = 0.5 - \left[0.65 + \left(\frac{.07}{2} \right) \right]^{-1} + 14 \left[1. - \left(\frac{.07}{2} \right) \right]^{24}$$

$$= 4.994$$

3 Substituting

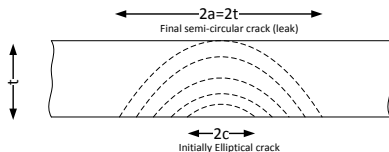
$$\begin{aligned}
 K &= 36.3\sqrt{\pi(.07)} \left[1.127 + 3.247 \left(\frac{.07}{.126} \right)^2 + 4.994 \left(\frac{.07}{.126} \right)^4 \right] \left[1 + 1.464 \left(\frac{.07}{2} \right) \right. \\
 &\quad \left. \left[\left(\frac{.07}{2} \right)^2 + 1 \right]^{\frac{1}{4}} \left\{ 1 + \left[0.1 + 0.35 \left(\frac{.07}{.126} \right)^2 \right] (1 - 1)^2 \right\} \right] \\
 &= 44.2\text{ksi}\sqrt{\text{in}}
 \end{aligned}$$

This is about equal to the fracture toughness.

- 4 Note that if we were to use the approximate equation, for long cracks we would have obtained:

$$\begin{aligned}
 K &= (1.13)(36.3)\sqrt{\pi(.07)} \left[1 + 3.46 \left(\frac{.07}{.126} \right)^2 + 11.5 \left(\frac{.07}{.126} \right)^4 \right] \\
 &= 60.85 \\
 &> K_{Ic}
 \end{aligned}$$

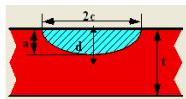
- As observed from the preceding example, many pressurized vessels are subject to crack growth if internal flaws are present. Two scenarios may happen,



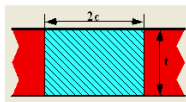
- Break-through:** In this case critical crack configuration is reached before the crack has “daylighted”, and there is a sudden and unstable crack growth.
- Leak Before Fail:** In this case, crack growth occur, and the crack “pierces” through the thickness of the vessel before unstable crack growth occurs. This in turn will result in a sudden depressurization, and this will stop any further crack growth.

Pressurized vessels should be designed to ensure a **leak before fail failure scenario**, as this would usually be immediately noticed and corrected (assuming that there is no leak of flammable gas!).

Leak before break - better



Crack

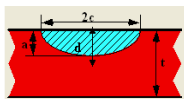


Leak but stable crack serves as a warning

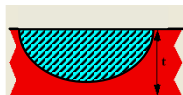


Hypothetical rupture at much larger crack

Break before leak - worse



Crack



Crack becomes unstable before breaking through



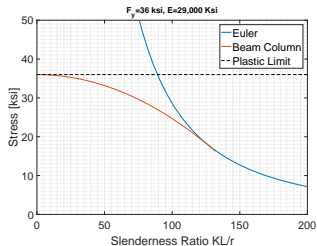
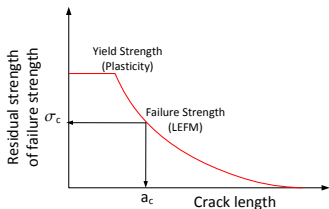
Catastrophic rupture without warning

Courtesy Dr. Brian Rose

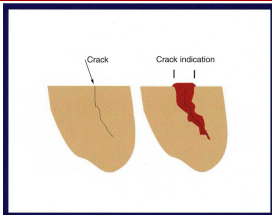
©

- Leak before break assessment should be made on the basis of a complete residual strength diagram for both the part through and the through crack. Various ratios should be considered

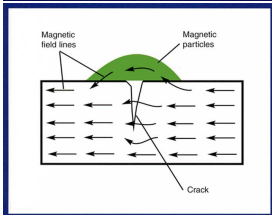
- Fracture mechanics is not limited to determining the critical crack size, load, or stress combination. It can also be applied to establish a fracture control plan, or **damage tolerance analysis** with the following objectives:
 - Determine the effect of cracks on strength. This will result in a plot of crack size versus residual strength, or **Residual Strength Diagram**



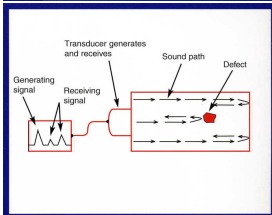
- Note analogy with column curve.
- Determine crack growth with time, resulting in **Crack Growth Curve**.



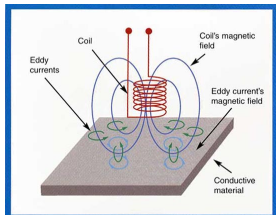
Penetrant Testing: Penetrant solution is applied to the surface of a precleaned component. The liquid is pulled into surface-breaking defects by capillary action. Excess penetrant material is carefully cleaned from the surface. A developer is applied to pull the trapped penetrant back to the surface where it is spread out and forms an indication. The indication is much easier to see than the actual defect.



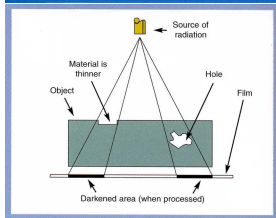
Magnetic Particle Testing: A magnetic field is established in a component made from ferromagnetic material. The magnetic lines of force travel through the material, and exit and reenter the material at the poles. Defects such as crack or voids cannot support as much flux, and force some of the flux outside of the part. Magnetic particles distributed over the component will be attracted to areas of flux leakage and produce a visible indication.



Ultrasonic Testing: High frequency sound waves are sent into a material by use of a transducer. The sound waves travel through the material and are received by the same transducer or a second transducer. The amount of energy transmitted or received and the time the energy is received are analyzed to determine the presence of flaws. Changes in material thickness, and changes in material properties can also be measured.



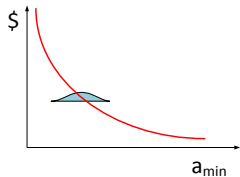
Eddy Current Testing: Alternating electrical current is passed through a coil producing a magnetic field. When the coil is placed near a conductive material, the changing magnetic field induces current flow in the material. These currents travel in closed loops and are called eddy currents. Eddy currents produce their own magnetic field that can be measured and used to find flaws and characterize conductivity, permeability, and dimensional features.



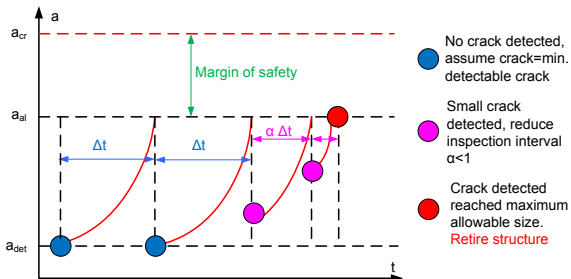
Radiographic Testing: X-rays are used to produce images of objects using film or other detector that is sensitive to radiation. The test object is placed between the radiation source and detector. The thickness and the density of the material that X-rays must penetrate affects the amount of radiation reaching the detector. This variation in radiation produces an image on the detector that often shows internal features of the test object

<https://www.nde-ed.org>

⚠ Always assume the existence of a crack equal to the smallest detectable one.



- **Cost** is inversely proportional to the minimum crack size to be detected
- Increasing cost of detection equipment, **reduces** the frequency of inspection



A cylindrical pressure vessel, with $R = 1$ m, $t=50$ mm, is subjected to an internal pressure p .

- 1 Draw the residual strength diagram.
- 2 What is the maximum permissible crack a_c for $p = 20$ MPa.

$$\sigma_{\theta} = \frac{pR}{t}$$

$$\sigma_z = \frac{pR}{2t}$$

von Mises yield criteria

$$\sigma_{\theta}^2 - \sigma_z \sigma_{\theta} + \sigma_z^2 = \left(\frac{\sigma_y}{2}\right)^2$$

$$p_y = \frac{\sigma_y t}{\sqrt{3}R}$$

- 3 What is p_c for a maximum detectable crack $a_c = 2$ mm

Use

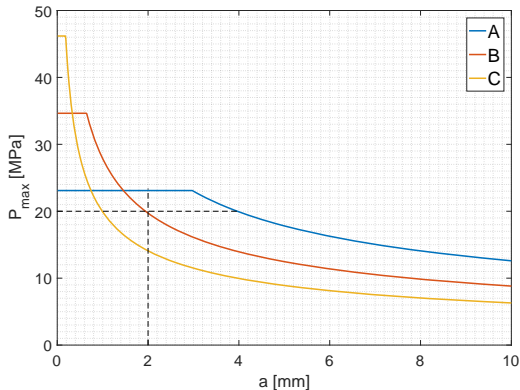
Steel	σ_y [MPa]	K_{Ic} [MPa $\sqrt{\text{m}}$]
A	800	100
B	1,200	70
C	1,600	50

p_c [MPa]		
A	B	C
23.1	34.6	46.2

For long axial surface crack of depth a , can use $K_I = 1.12\sigma_{\theta}\sqrt{\pi a}$

$$p_c = \frac{tK_{Ic}}{2.24R\sqrt{\pi a}}$$

1 Residual strength diagram



2 $a_c = 1, 2$ and 4.2 mm for A, B, and C respectively.

3 $p_c = 14, 20, 23$ MPa for A, B and C respectively

Theoretical Strength

Victor E. Saouma

`saouma@colorado.edu`

University of Colorado, Boulder

Spring 2022

1 Objective

2 Derivation

- Energy of Interaction

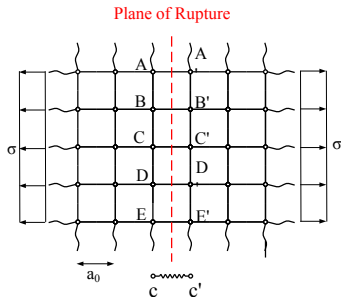
3 Tensile Strength

- In Terms of Physical Parameters
- Example
- In Terms of Engineering Parameters

4 Griffith's Theory

- Introduction
- Derivation
- Example

- Griffith tried to explain the increase in strength with the decrease in diameter of glass fibers.
- He postulated that this can be explained by the presence of internal flaws (idealized as elliptical) and then used Inglis solution to explain this discrepancy.
- We shall derive an expression for the theoretical strength of perfect crystals (theoretically the strongest form of solid). This derivation starts at the atomic level.



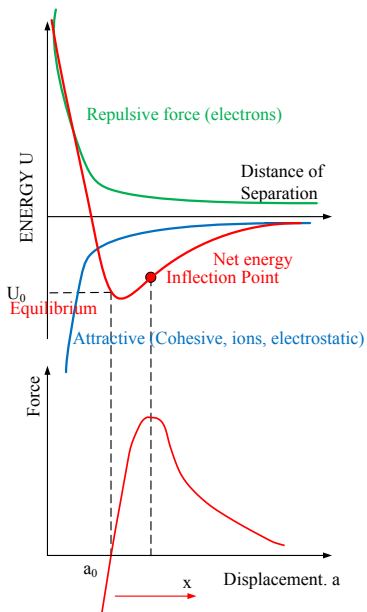
- Total energy which must be supplied to **separate atom C from C'** at equilibrium separated by a distance a_0 is

$$U_0 = 2\gamma \quad (1)$$

where γ is the **surface energy**

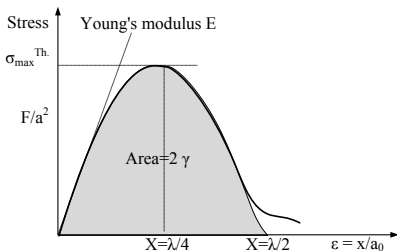
- Factor of 2 is due to the fact that upon separation, we have **two distinct surfaces**.
- Surface energy γ is expressed in J/m^2 and the surface energies of water, most solids, and diamonds are approximately .077, 1.0, and 5.14 respectively.

Solution I, Forces/Newtonian:



- 1 Consider **interatomic forces** (from Physics) or rather the potential energies. Two components:
 - 1 **Attractive** (or cohesive) forces between two ions (of opposite charges)
 - 2 **Repulsive** due to the electrons interacting as the ions get too close.
- 2 Net potential energy is the sum of the two.
- 3 Force being the derivative of energy, we have $F = \frac{dU}{da}$, thus $F = 0$ at $a = a_0$ and is maximum at the inflection point of the $U_0 - a$ curve.

- 4 Slope of the force displacement curve is the stiffness of the atomic spring and should be related to E .
- 5 If we let $x = a - a_0$, then the strain would be equal to $\varepsilon = \frac{x}{a_0}$. Furthermore, if we define the stress as $\sigma = \frac{F}{a^2}$, then the $\sigma - \varepsilon$ curve can be approximated by a sine curve.



- 6 From this diagram, it would appear that the sine curve would be an adequate approximation to this relationship. Hence,

$$\sigma = \sigma_{max}^{theor} \sin 2\pi \frac{x}{\lambda} \quad (2)$$

and the maximum stress σ_{max}^{theor} would occur at $x = \frac{\lambda}{4}$.

- 7 The energy required to separate two atoms is thus given by the area under the sine curve, and from Eq. 1, we would have

$$2\gamma = U_0 = \int_0^{\frac{\lambda}{2}} \sigma_{max}^{theor} \sin\left(2\pi\frac{x}{\lambda}\right) dx \quad (3)$$

$$= \frac{\lambda}{2\pi} \sigma_{max}^{theor} \left[-\cos\left(\frac{2\pi x}{\lambda}\right) \right] \Big|_0^{\frac{\lambda}{2}} \quad (4)$$

$$= \frac{\lambda}{2\pi} \sigma_{max}^{theor} \left[-\overbrace{\cos\left(\frac{2\pi\lambda}{2\lambda}\right)}^{-1} + \overbrace{\cos(0)}^1 \right] \quad (5)$$

$$\Rightarrow \lambda = \frac{2\gamma\pi}{\sigma_{max}^{theor}} \quad (6)$$

- 8 For very small displacements (small x) $\sin x \approx x$, thus Eq. 2 reduces to

$$\sigma \approx \sigma_{max}^{theor} \frac{2\pi x}{\lambda} \stackrel{\text{def}}{=} E \frac{x}{a_0}$$

eliminating x ,

$$\sigma_{max}^{theor} \approx \frac{E}{a_0} \frac{\lambda}{2\pi} \quad (7)$$

- 9 Substituting for λ from Eq. 6, we get

$$\sigma_{max}^{theor} \approx \sqrt{\frac{E\gamma}{a_0}} \quad (8)$$

Solution II, Energy/Lagrangian:

- 1 For two layers of atoms a_0 apart, the **strain energy per unit area due to σ** (for linear elastic systems) is

$$\left. \begin{aligned} U &= \frac{1}{2} \sigma \varepsilon a_0 \\ \sigma &= \frac{E \varepsilon} \end{aligned} \right\} U = \frac{\sigma^2 a_0}{2E}$$

- 2 Assume that there is a **transfer** from strain energy to surface energy where **γ is the surface energy of the solid per unit area**, then the total surface energy of two new fracture surfaces is 2γ .

3 For our theoretical strength, $U = 2\gamma \Rightarrow \frac{(\sigma_{max}^{theor})^2 a_0}{2E} = 2\gamma$ or $\sigma_{max}^{theor} = 2\sqrt{\frac{E\gamma}{a_0}}$

Note that here we have assumed that the material obeys Hooke's Law up to failure, since this is seldom the case, we can simplify this approximation to:

$$\sigma_{max}^{theor} = \sqrt{\frac{E\gamma}{a_0}}$$

which is the same as Equation 8

As an example, let us consider steel which has the following properties: $\gamma = 1 \frac{\text{J}}{\text{m}^2}$; $E = 2 \times 10^{11} \frac{\text{N}}{\text{m}^2}$; and $a_0 \approx 2 \times 10^{-10} \text{ m}$. Thus from Eq. 8 we would have:

$$\begin{aligned}\sigma_{max}^{theor} &\approx \sqrt{\frac{(2 \times 10^{11})(1)}{2 \times 10^{-10}}} \\ &\approx 3.16 \times 10^{10} \frac{\text{N}}{\text{m}^2} \\ &\approx \frac{E}{6}\end{aligned}$$

Thus this would be the ideal theoretical strength of steel.

- 1 The **force to separate two atoms** drops to zero when the distance between them is $a_0 + a$ where a_0 corresponds to the origin and a to $\frac{\lambda}{2}$.
- 2 If we take $a = \frac{\lambda}{2}$ or $\lambda = 2a$, combined with Eq. 7 would yield $\sigma_{max}^{theor} \approx \frac{E}{a_0} \frac{a}{\pi}$
- 3 Alternatively combining Eq. 6 with $\lambda = 2a$ gives $a \approx \frac{\gamma\pi}{\sigma_{max}^{theor}}$
- 4 Combining those two equations $\gamma \approx \frac{E}{a_0} \left(\frac{a}{\pi}\right)^2$
- 5 However, since as a first order approximation $a \approx a_0$ then the surface energy will be $\gamma \approx \frac{Ea_0}{10}$
- 6 This equation, combined with Eq. 8 will finally give

$$\sigma_{max}^{theor} \approx \frac{E}{\sqrt{10}}$$

which is an approximate expression for the theoretical maximum strength in terms of E .

- Around 1920, Griffith was exploring the **theoretical strength of solids by performing a series of experiments on glass rods** of various diameters.
- He observed that the **tensile strength (σ_t) of glass decreased with an increase in diameter**, and that for a diameter $\phi \approx \frac{1}{10,000}$ in., $\sigma_t = 500,000$ psi; furthermore, by extrapolation to “zero” diameter he obtained a theoretical maximum strength of approximately 1,600,000 psi, and on the other hand for very large diameters the asymptotic values was around 25,000 psi.
- Griffith had thus demonstrated that the theoretical strength could be experimentally approached, he now **needed to show why the great majority of solids fell so far below it.**

- In his quest for an explanation, he came across Inglis's paper, and his "strike of genius" was to **assume that strength is reduced due to the presence of internal flaws**.
- Griffith postulated that the **theoretical strength can only be reached at the point of highest stress concentration, and accordingly the far-field applied stress will be much smaller**.
- Hence, **assuming an elliptical imperfection**, and from $(\sigma_{\beta\beta})_{\alpha=0, \pi}^{\beta=0, \pi} = \sigma_0 \left(1 + 2\sqrt{\frac{a}{\rho}}\right)$ determined $\sigma_{max}^{theor} = \sigma_{cr}^{act} \left(1 + 2\sqrt{\frac{a}{\rho}}\right)$ where σ is the stress at the tip of the ellipse which is caused by a (lower) far field stress σ_{cr}^{act} .
- Assuming $\rho \approx a_0$ and since $2\sqrt{\frac{a}{a_0}} \gg 1$, for an ideal plate under tension with only one single elliptical flaw the strength may be obtained from

$$\underbrace{\sigma_{max}^{theor}}_{\text{micro}} = \underbrace{2\sigma_{cr}^{act} \sqrt{\frac{a}{a_0}}}_{\text{macro}}$$

hence, equating with Eq. 8, we obtain

$$\sigma_{max}^{theor} = \underbrace{2\sigma_{cr}^{act}}_{\text{Macro}} \sqrt{\frac{a}{a_0}} = \underbrace{\sqrt{\frac{E\gamma}{a_0}}}_{\text{Micro}}$$

- From this very important equation, we observe that
 - The left hand side is based on a linear elastic solution of a **macroscopic problem** solved by Inglis.
 - The right hand side is based on the theoretical strength derived from the sinusoidal stress-strain assumption of the **interatomic forces**, and finds its roots in micro-physics.
- Equating both sides of the preceding equations yields (at fracture)

$$\sigma_{cr}^{act} = \sqrt{\frac{E\gamma}{4a}}$$

- Consider a flaw with a size of $2a = 5,000a_0$

$$\left. \begin{aligned} \sigma_{cr}^{act} &= \sqrt{\frac{E\gamma}{4a}} \\ \gamma &= \frac{Ea_0}{10} \end{aligned} \right\} \left. \begin{aligned} \sigma_{cr}^{act} &= \sqrt{\frac{E^2 a_0}{40 a}} \\ \frac{a}{a_0} &= 2,500 \end{aligned} \right\} \sigma_{cr}^{act} = \sqrt{\frac{E^2}{100,000}} = \frac{E}{100\sqrt{10}}$$

- Thus if we set a flaw size of $2a = 5,000a_0$ in $\gamma \approx \frac{Ea_0}{10}$ this is **enough to lower the theoretical fracture strength from $\frac{E}{\sqrt{10}}$ to a critical value of magnitude $\frac{E}{100\sqrt{10}}$, or a factor of 100.**
- Also

$$\left. \begin{aligned} \sigma_{max}^{theor} &= 2\sigma_{cr}^{act} \sqrt{\frac{a}{a_0}} \\ a &= 10^{-6} m = 1 \mu m \\ a_0 &= 1 = \rho = 10^{-10} m \end{aligned} \right\} \sigma_{max}^{theor} = 2\sigma_{cr}^{act} \sqrt{\frac{10^{-6}}{10^{-10}}} = 200\sigma_{cr}^{act}$$

- At failure

$$\left. \begin{aligned} \sigma_{cr}^{act} &= \frac{\sigma_{max}^{theor}}{200} \\ \sigma_{max}^{theor} &= \frac{E}{10} \end{aligned} \right\} \sigma_{cr}^{act} \approx \frac{E}{2,000}$$

which can be attained. For instance for steel $\frac{E}{2,000} = \frac{30,000}{2,000} = 15$ ksi

Thermodynamics of Crack Growth

Victor E. Saouma
saouma@colorado.edu

University of Colorado, Boulder

Spring 2022

1 Introduction

- Thermodynamics
- Brittle Material, Griffith's Model

2 Energy Release Rate; Global; Compliance

- Derivation
- Example

3 Energy Release Rate; Local

- Derivation of G
- Derivation of $R (G_{cr})$

4 Crack Stability

- Impact of Geometry
- Plane Strain
- Plane Stress
- Observations

- **First Law of Thermodynamics** can be expressed as

$$\dot{W} = \dot{U} + \dot{K} + \dot{\Gamma}$$

W work, K kinetic energy, U internal energy (elastic and plastic), Γ **surface energy** (energy needed to increase the crack area). Derivative is with respect to time.

- Since all changes with respect to time are caused by changes in crack size, we can write

$$\frac{\partial}{\partial t} = \frac{\partial A}{\partial t} \frac{\partial}{\partial A}$$

In **adiabatic** system (no heat exchange), loads are applied in a **quasi static** manner (no kinetic energy), then Q and K are zero.

- For unit thickness replace A by a

$$\underbrace{\frac{\partial W}{\partial a}}_{\text{External}} = \underbrace{\left(\frac{\partial U^e}{\partial a} + \frac{\partial U^p}{\partial a} \right)}_{\text{Internal}} + \frac{\partial \Gamma}{\partial a}$$

- We can rewrite it as

$$\underbrace{\frac{\partial W}{\partial a} - \frac{\partial U^e}{\partial a}}_G = \underbrace{\frac{\partial U^p}{\partial a} + \frac{\partial \Gamma}{\partial a}}_R$$

R is the rate of energy dissipation during stable crack growth = plastic deformation + energy consumed during crack propagation.

- In terms of Potential Energy Π :

$$\begin{aligned}\Pi &\equiv U^e - W \\ -\frac{\partial \Pi}{\partial a} &= -\frac{\partial U^e}{\partial a} + \frac{\partial W}{\partial a} \\ &= \frac{\partial U^p}{\partial a} + \frac{\partial \Gamma}{\partial a}\end{aligned}$$

- Crack stability can be assessed from

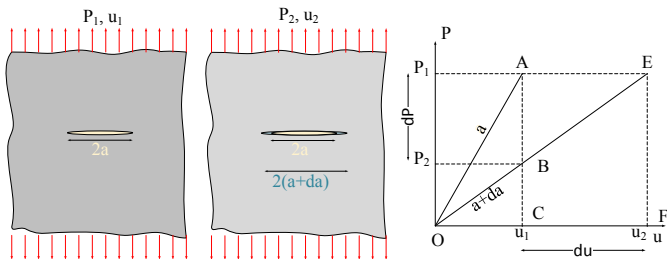
$$-\frac{\partial \Pi}{\partial a} \begin{cases} < \frac{\partial U^p}{\partial a} + \frac{\partial \Gamma}{\partial a} & \text{No crack growth} \\ = \frac{\partial U^p}{\partial a} + \frac{\partial \Gamma}{\partial a} & \text{Quasi static crack growth} \\ > \frac{\partial U^p}{\partial a} + \frac{\partial \Gamma}{\partial a} & \text{Dynamic crack growth} \end{cases}$$

- For quasi-static crack growth: Rate of potential energy decrease during crack growth is equal to the rate of energy dissipated in plastic deformation and crack growth.
- For brittle material ($U^p = 0$) potential energy is released from a volume ($\propto L^3$) whereas surface energy is consumed over a surface ($\propto L^2$), thus we have a size discrepancy or a size effect (which will be studied later).

- For a perfectly brittle material, **potential energy is released to create surface energy**

$$G \stackrel{\text{def}}{=} \underbrace{\frac{\partial W}{\partial a} - \frac{\partial U^e}{\partial a}}_{-\frac{\partial \Pi}{\partial a}} = \frac{\partial \Gamma}{\partial a} = 2\gamma \quad (1)$$

- Griffith assumed that it was possible to produce a macroscopical load displacement ($P - u$) curve for two different crack lengths a and $a + da$.
- Consider two limiting cases for the **propagation of a crack from a to $a + da$** :



- ① **Fixed Grip:** Displacement constant ($u_2 = u_1$), but load drops from P_1 to P_2 ,
Work: None as there is no displacement.
Internal Strain Energy: **decreases**, (OBC-OAC=-OAB):

$$\begin{aligned}\Delta U &= \frac{1}{2}P_2u_1 - \frac{1}{2}P_1u_1 \\ &= \frac{1}{2}(P_2 - P_1)u_1 \\ &< 0\end{aligned}$$

Change in potential energy: **decrease** is the same as the decrease in stored internal strain energy:

$$\begin{aligned}\Pi_2 - \Pi_1 &= \Delta W - \Delta U \\ &= -\frac{1}{2}(P_2 - P_1)u_1 = \frac{1}{2}(P_1 - P_2)u_1\end{aligned}$$

- ② **Fixed Load:** $P_2 = P_1$, there is an increase in displacement from u_1 to u_2 .
External Work (AEFC):

$$\Delta W = P_1(u_2 - u_1)$$

Internal Strain Energy: increases from OAC to OEF, or OAE. Increase caused by the load $\frac{1}{2}P_1 (u_2 - u_1)$

Change in potential energy: is thus

$$\begin{aligned}\Pi_2 - \Pi_1 &= \Delta W - \Delta U \\ &= P_1 (u_2 - u_1) - \frac{1}{2}P_1 (u_2 - u_1) \\ &= \frac{1}{2}P_1 (u_2 - u_1)\end{aligned}$$

Since AEFC is twice OAE, the net is OAE

- Fixed grip: decrease in strain energy of magnitude $\frac{1}{2}u_1(P_1 - P_2)$ as the crack extends from a to $(a + \Delta a)$, under constant load, there is a net decrease in potential energy of magnitude $\frac{1}{2}P_1(u_2 - u_1)$.
- Neglecting AEB ($dp \times du/2$), in the limit: OAB=OAE or energy available for crack growth is the same in both extreme cases.
- Mathematically, as $\Delta a \rightarrow da$, then $dP = P_2 - P_1$ and $du = u_2 - u_1$.
- As $da \rightarrow 0$,

Fixed Grip: **Decrease** in strain energy (and potential energy in this case),
and $d\Pi = \frac{1}{2}udP$.

Constant Load: **Increase** in strain energy and decrease in potential energy with
 $d\Pi = \frac{1}{2}Pdu$

- **Compliance** (inverse of the stiffness) is

$$u = CP \Rightarrow du = CdP$$

Then **decrease in potential energy** for both cases

$$d\Pi = \frac{1}{2}CP dP$$

- In summary, **As the crack extends there is a release of excess energy. The energy released is consumed to form surface energy.**
- A criteria for crack propagation would be

$$d\Pi \geq 2\gamma da$$

The difference between the two sides of the inequality will appear as **kinetic energy at a real crack propagation.**

- Under constant load, energy to extend crack by da was $\frac{1}{2}Pdu$, G the energy release rate, B thickness, and $u = CP$, (where u , C and P are the point load displacement, compliance and the load respectively)

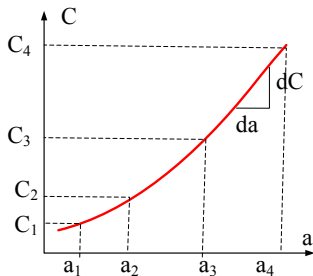
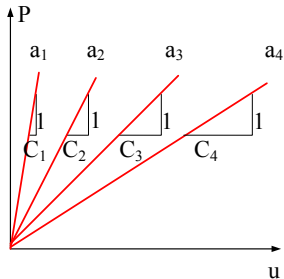
$$GBda = \frac{1}{2}Pd(CP) = \frac{1}{2}P^2dC$$

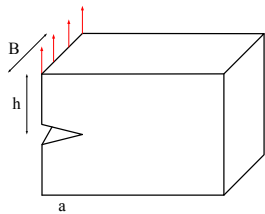
at the limit as $da \rightarrow 0$:

$$G = \frac{1}{2} \frac{P^2}{B} \left(\frac{dC}{da} \right) \quad (2)$$

i.e. energy release rate is proportional to the rate of change of the compliance.

- Thus can use numerical or experimental techniques to obtain G and from $G = \frac{K_I^2}{E'}$ (to be derived later) get K_I ,





- From strength of materials:

$$C = \underbrace{\frac{24}{EB} \int_0^a \frac{x^2}{h^3} dx}_{\text{flexural}} + \underbrace{\frac{6(1+\nu)}{EB} \int_0^a \frac{1}{h} dx}_{\text{shear}}$$

- Taking $\nu = \frac{1}{3}$ we obtain

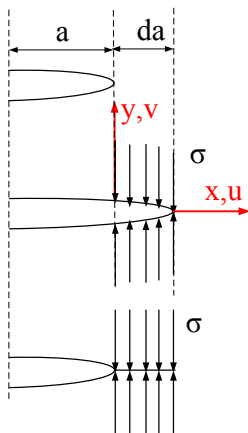
$$C = \frac{8}{EB} \int_0^a \left(\frac{3x^2}{h^3} + \frac{1}{h} \right) dx \Rightarrow \frac{dC}{da} = \frac{8}{EB} \left(\frac{3a^2}{h^3} + \frac{1}{h} \right) \quad (3)$$

- Substituting in Eq. 2

$$G = \frac{1}{2} \frac{P^2}{B} \left(\frac{dc}{da} \right) = \frac{1}{2} \frac{P^2 8}{EB^2} \left(\frac{3a^2}{h^3} + \frac{1}{h} \right) = \frac{4P^2}{EB^2 h^3} (3a^2 + h^2)$$

- Thus, the stress intensity factor will be

$$K = \sqrt{GE} = \frac{2P}{B} \left(\frac{3a^2}{h^3} + \frac{1}{h} \right)^{\frac{1}{2}} \quad (4)$$



- Need to **relate energy release rate G to the SIF K** . Both previously derived but not tied together.
- Energy change is given by:

$$G = \frac{2}{\Delta a} \int_a^{a+\Delta a} \frac{1}{2} \sigma_{yy}(x) v(x - da) dx$$

2 in the numerator: two crack surfaces (upper and lower); 2 in the denominator due to the linear elastic assumption.

- Substitution for σ_{yy} and v (with $\theta = \pi$) from the Westergaard equations

$$\sigma_{yy} = \frac{K_I}{\sqrt{2\pi r}} \cos \frac{\theta}{2} \left[1 + \sin \frac{\theta}{2} \sin \frac{3\theta}{2} \right]$$

$$v = \frac{K_I}{2\mu} \sqrt{\frac{r}{2\pi}} \sin \frac{\theta}{2} \left[\kappa + 1 - 2 \cos^2 \frac{\theta}{2} \right]$$

(μ is shear modulus); Setting $\theta = \pi$, and after simplification:

$$G = \frac{K_I^2}{E'}$$

where $E' = E$ for plane stress, and $E' = \frac{E}{1-\nu^2}$ for plane strain.

- For the simple case $K = \sigma\sqrt{\pi a}$ we obtain the energy release rate in terms of the far field stress

$$G = \frac{\sigma^2 \pi a}{E'}$$

- Total energy consumed over the crack extension will be:

$$d\Pi = \int_0^{da} G dx = \int_0^{da} \frac{\sigma^2 \pi a}{E'} dx = \frac{\sigma^2 \pi a da}{E'} = 2\gamma da \quad (5)$$

- Crack instability will occur when for an infinitesimal crack extension da , the rate of energy released is just equal to surface energy absorbed.

$$\underbrace{\frac{\sigma_{cr}^2 \pi a da}{E'}}_{d\Pi} = 2\gamma da$$

or

$$\sigma_{cr} = \sqrt{\frac{2E'\gamma}{\pi a}}$$

originally derived by Griffith.

- This equation can be rewritten as

$$\underbrace{\frac{\sigma_{cr}^2 \pi a}{E'}}_{G_{cr}} \equiv \underbrace{R}_{2\gamma}$$

and as

$$\sigma_{cr} \sqrt{\pi a} = \sqrt{2E'\gamma} = K_{Ic}$$

thus

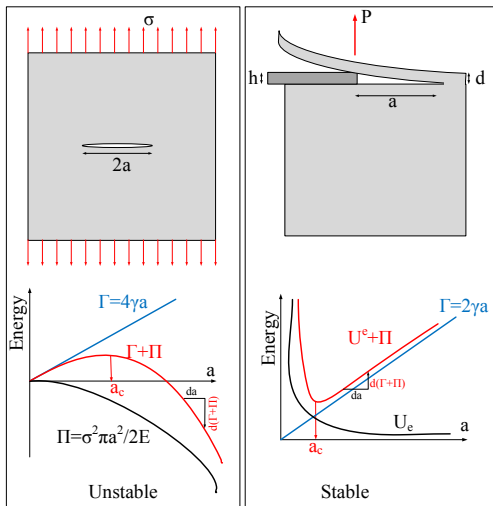
$$R = G_{cr} = \frac{d\Pi}{da} = 2\gamma = \frac{K_{Ic}^2}{E'}$$

- R (for Resistance) is only equal to a **constant (G_{cr})** under **plane strain conditions**.
- R is **material dependent** and Π is **problem dependent**.
- Critical energy release rate for plane stress is **not a constant**, thus K_{Ic} is not constant, and we will instead use **K_{Ic} and G_{Ic}** .
- Alternatively, K_{Ic} , and G_{Ic} correspond to plane strain in mode I which is constant.

- Shape of the R-curve depends on the plate thickness, where plane strain is approached for thick plates, and is constant; and for thin plates we do not have constant R due to plane stress conditions.
- As with the Westergaard/Irwin criteria (where we zoomed on the crack tip), a global energy change can also predict a local event (crack growth).
- The duality between energy and stress approach $G > G_{cr} = R$, or $K > K_{Ic}$, should also be noted.

- Criteria for crack growth can best be understood through a graphical representation of those curves under plane strain and plane stress conditions.
- Crack stability depends on both the geometry, and on the material resistance.
- From Eq. 1, crack growth is considered unstable when the energy at equilibrium is a maximum, and stable when it is a minimum. Hence, a sufficient condition for crack stability is

$$\frac{\partial^2(\Pi + \Gamma)}{\partial A^2} \begin{cases} < 0 & \text{unstable fracture} \\ > 0 & \text{stable fracture} \\ = 0 & \text{neutral equilibrium} \end{cases} \quad \&G > R \quad (6)$$



- Line crack in an infinite plate subjected to uniform stress, potential energy of the system is $\Pi = U^e$ where Eq. 1 yields

$$K_I = \sigma \sqrt{\pi a}$$

$$G = \frac{K_I^2}{E'} = \frac{\sigma^2 \pi a}{E'}$$

$$\Pi = \int G da = -\frac{1}{2} \frac{\sigma^2 \pi a^2}{E'}$$

and $\Gamma = 4\gamma a$ (crack length is $2a$). Note that U^e is negative because there is a decrease in strain energy during crack propagation.

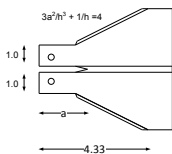
If we plot Γ , Π and $\Gamma + \Pi$, then we observe that the total potential energy of the system ($\Pi + \Gamma$) is maximum at the critical crack length which corresponds to unstable equilibrium.

- A wedge of thickness h is inserted under a flake of mica which is detached from a mica block along a length a . Energy is determined by considering the mica flake as a cantilever beam with depth d .
- From beam theory

$$U^e = \frac{Ed^3h^2}{8a^3}$$

U^e is positive because there is an increase in strain energy as a increases

- Surface energy is $\Gamma = 2\gamma a$ (crack length is a).
- Substituting in Eq. 6, the equilibrium crack is $a_c = \left(\frac{3Ed^3h^2}{16\gamma}\right)^{1/4}$
- Total potential energy of the system at a_c is a minimum, which corresponds to stable equilibrium.

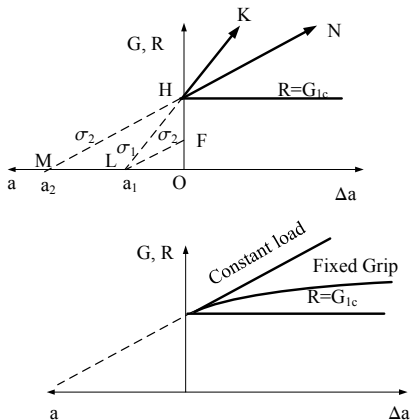
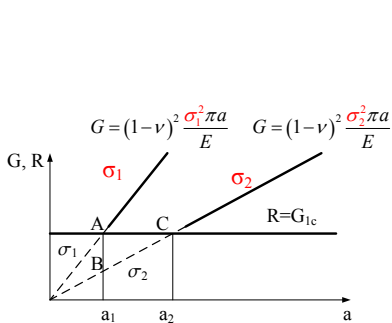


Revisiting Eq. 4 K increases with a , hence unstable crack growth. If B increases with a , such that $\frac{3a^2}{h^3} + \frac{1}{h} = m = \text{Cst}$, then

$$K = \frac{2P}{B} m^{1/2} \quad (7)$$

K is now independent of a (Mostovoy's test).

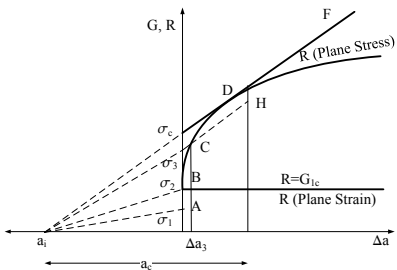
- Plane strain conditions, the R curve is constant and is equal to G_{Ic} .



- $G = \frac{\sigma^2 \pi a}{E'}$, thus G is always a linear function of a , and is a **straight line**.

- For a_1 , and stress σ_2 , energy release rate is point B .
- Increase stress from σ_2 to σ_1 , will raise G from B to A where the crack will extend. Had we had a longer crack a_2 , it would have extended at σ_2 .
- Shift the plot, a_i on the left, Δa to the right.
- At σ_2 , G line is LF (really only point F).
- Loading the crack from 0 to σ_2 , G increases from O to F, further increase of the stress to σ_1 raises G from F to H, and then fracture occurs, and the crack goes from H to K.
- For a_2 loaded from 0 to σ_2 , G increases from O to H (note that LF and MH are parallel). At H crack extension occurs along HN.
- Depending on the boundary conditions, G may increase linearly (constant load) or as a polynomial (fixed grips).

- Plane Stress condition.



- R is found to be an **increasing function of a** . Examining a_i :
- under σ_1 at A, $G < R$, thus **no crack extension**.
- Increase σ_1 to σ_2 , point B, then $G = R$ **crack propagates** by an infinitesimal increment Δa and **will immediately stop** as G becomes smaller than R .

- Increase σ_1 to σ_3 , (point C) then $G > R$ crack extends to $a + \Delta a_3$. G increases to H , however, this increase is at a **lower rate than the increase in R**

$$\frac{dG}{da} < \frac{dR}{da}$$

thus the crack stabilizes: **stable crack growth**.

- Increase σ_1 to σ_c , not only is G equal to R , but it grows faster than R : **unstable crack growth**.

- From this simple illustrative example:

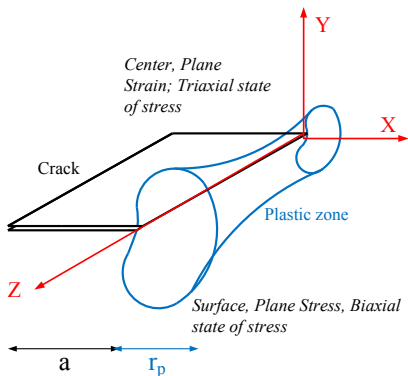
$$\text{Stable Crack Growth: } G > R \quad \frac{dG}{da} < \frac{dR}{da}$$

$$\text{Unstable Crack Growth: } G > R \quad \frac{dG}{da} > \frac{dR}{da}$$

For unstable crack growth, **excess energy is transformed into kinetic energy.**

- Analogous to to Eq. 6 where the potential energy has been expressed in terms of G , and the surface energy expressed in terms of R .
- Some materials exhibit a flat R curve, while other have an ascending one. **The shape of the R curve is a material property.**
- For ideally brittle material, R is flat since the surface energy γ is constant.
- Nonlinear material would have a **small plastic zone** at the tip of the crack. The driving force in this case must increase. If the plastic zone is small compared to the crack (as would be eventually the case for sufficiently long crack in a large body), then R would approach a constant value.

- The **thickness** of the cracked body can also play an important role. For thin sheets, the load is predominantly plane stress



- Alternatively, for a thick plate it would be predominantly plane strain. Hence a plane stress configuration would have a steeper R curve.

Mixed Mode Crack Propagation

Victor E. Saouma
saouma@colorado.edu

University of Colorado, Boulder

Spring 2022

1 Introduction

2 Models

- Maximum Circumferential Tensile Stress
- Maximum Energy Release Rate
- Minimum Strain Energy Density Criteria

3 Observations

- Practical engineering cracked structures are subjected to **mixed mode loading**, thus in general K_I and K_{II} are both nonzero, yet we usually measure only mode I fracture toughness
- So far the only fracture propagation criterion we have is for mode I only (K_I vs K_{Ic} , and G_I vs R)
- Under pure mode I in homogeneous isotropic material, **crack propagation is collinear**, in all other cases the propagation will be **curvilinear and at an angle θ_0 with respect to the crack axis**. Thus, for the general mixed mode case, we seek to formulate a criterion that will determine:
 - 1 The **angle of incipient propagation**, θ_0 , with respect to the crack axis.
 - 2 If the stress intensity factors are in such a **critical combination as to render the crack locally unstable** and force it to propagate.

(in that order)

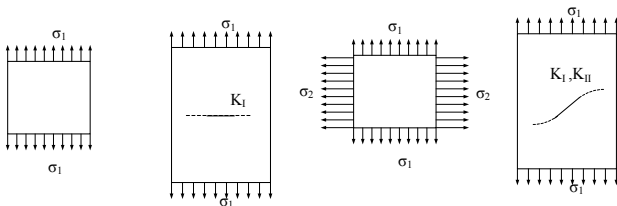
- The determination of a fracture initiation criterion for an existing crack in mode I and II would require a relationship between K_I , K_{II} , and K_{Ic} of the form

$$F(K_I, K_{II}, K_{Ic}) = 1$$

and would be analogous to the one between the two principal stresses and a yield stress such as von-Mises

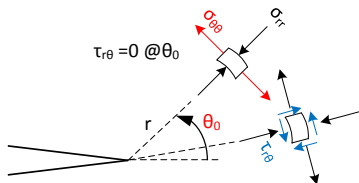
$$F(J_2) = J_2 - k^2 = \frac{(\sigma_{(1)} - \sigma_{(2)})^2 + (\sigma_{(2)} - \sigma_{(3)})^2 + (\sigma_{(1)} - \sigma_{(3)})^2}{2} - \sigma_y^2 = 0$$

- Model could be based on SIFs (K_I , K_{II}), energy release rate (G), or strain energy density (S).



- The maximum circumferential stress theory states that the crack extension starts:

- At its tip in a radial direction
- In the plane perpendicular to the direction of greatest tension, i.e at an angle θ_0 such that $\tau_{r\theta} = 0$
- When $\sigma_{\theta\theta}$ reaches a critical material constant



- $\sigma_{\theta\theta}$ reaches its maximum value when $\tau_{r\theta} = 0$. Replacing $\tau_{r\theta}$ for mode I and II by their expressions

$$\tau_{r\theta} = \frac{K_I}{\sqrt{2\pi r}} \sin \frac{\theta}{2} \cos^2 \frac{\theta}{2} + \frac{K_{II}}{\sqrt{2\pi r}} \left(\frac{1}{4} \cos \frac{\theta}{2} + \frac{3}{4} \cos \frac{3\theta}{2} \right) = 0$$

$$\Rightarrow \cos \frac{\theta_0}{2} [K_I \sin \theta_0 + K_{II} (3 \cos \theta_0 - 1)] = 0$$

this equation has two solutions:

$$\theta_0 = \pm\pi \quad \text{trivial}$$

$$K_I \sin \theta_0 + K_{II} (3 \cos \theta_0 - 1) = 0$$

Solution of the second equation yields the angle of crack extension θ_0

$$\tan \frac{\theta_0}{2} = \frac{1}{4} \frac{K_I}{K_{II}} \pm \frac{1}{4} \sqrt{\left(\frac{K_I}{K_{II}}\right)^2 + 8}$$

- For the crack to extend, the maximum circumferential tensile stress, σ_θ

$$\sigma_{\theta\theta} = \frac{K_I}{\sqrt{2\pi r}} \cos \frac{\theta_0}{2} \left(1 - \sin^2 \frac{\theta_0}{2}\right) + \frac{K_{II}}{\sqrt{2\pi r}} \left(-\frac{3}{4} \sin \frac{\theta_0}{2} - \frac{3}{4} \sin \frac{3\theta_0}{2}\right)$$

must reach a critical value which is obtained by rearranging the previous equation

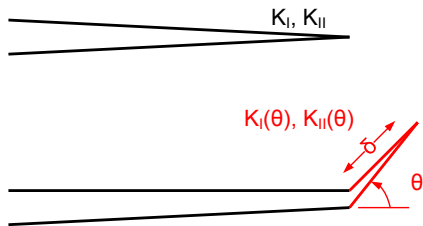
$$\sigma_{\theta\max} \sqrt{2\pi r} = K_{Ic} = \cos \frac{\theta_0}{2} \left[K_I \cos^2 \frac{\theta_0}{2} - \frac{3}{2} K_{II} \sin \theta_0 \right]$$

which can be normalized as

$$\frac{K_I}{K_{Ic}} \cos^3 \frac{\theta_0}{2} - \frac{3}{2} \frac{K_{II}}{K_{Ic}} \cos \frac{\theta_0}{2} \sin \theta_0 = 1$$

- If we accept Griffith (energy) theory, then the crack will **grow in the direction along which the elastic energy release per unit crack extension will be maximum** and the crack will start to grow when this energy reaches a critical value (or $G = G(\delta, \theta)$).

- The stress intensity factor of a major crack with an infinitesimal "kink" at an angle θ , are $K_I(\theta)$ and $K_{II}(\theta)$ (in terms of the stress intensity factors of the original crack K_I and K_{II} and θ).



- This was an extremely (mathematically) complex problem, which was solved by Hussain, Pu and Underwood:

$$\begin{Bmatrix} K_I(\theta) \\ K_{II}(\theta) \end{Bmatrix} = \left(\frac{4}{3 + \cos^2 \theta} \right) \begin{pmatrix} 1 - \frac{\theta}{\pi} \\ 1 + \frac{\theta}{\pi} \end{pmatrix}^{\frac{\theta}{2\pi}} \begin{Bmatrix} K_I \cos \theta + \frac{3}{2} K_{II} \sin \theta \\ K_{II} \cos \theta - \frac{1}{2} K_I \sin \theta \end{Bmatrix}$$

- $K_I(\theta)$ and $K_{II}(\theta)$ are then substituted into Irwin's generalized expression for the energy release rate (assuming collinear crack growth)

$$G(\theta) = \frac{1}{E'} \left(K_I^2(\theta) + K_{II}^2(\theta) \right)$$

yielding

$$G(\theta) = \frac{4}{E'} \left(\frac{1}{3 + \cos^2 \theta} \right)^2 \left(\frac{1 - \frac{\theta}{\pi}}{1 + \frac{\theta}{\pi}} \right)^{\frac{\theta}{\pi}}$$

$$[(1 + 3 \cos^2 \theta)K_I^2 + 8 \sin \theta \cos \theta K_I K_{II} + (9 - 5 \cos^2 \theta)K_{II}^2]$$

- The angle of crack propagation θ_0 is found by **maximizing** $G(\theta)$;

$$\frac{\partial G(\theta)}{\partial \theta} = 0$$

$$\frac{\partial^2 G(\theta)}{\partial \theta^2} < 0$$

For pure mode II ($K_I = 0$), it is found that $\theta_0 = 75.2^\circ$

- Crack extension occurs when G reaches a critical value (same scalar quantity for all cases), that can be determined by setting $K_{II} = 0$ and $G_{cr} = \frac{K_{Icr}^2}{E}$; thus

$$4 \left(\frac{1}{3 + \cos^2 \theta_0} \right)^2 \left(\frac{1 - \frac{\theta_0}{\pi}}{1 + \frac{\theta_0}{\pi}} \right)^{\frac{\theta_0}{\pi}} \left[\left(1 + 3 \cos^2 \theta_0 \right) \left(\frac{K_I}{K_{Ic}} \right)^2 + 8 \sin \theta_0 \cos \theta_0 \left(\frac{K_I K_{II}}{K_{Ic}^2} \right) + \left(9 - 5 \cos^2 \theta_0 \right) \left(\frac{K_{II}}{K_{Ic}} \right)^2 \right] = 1$$

- Minimum strain energy density theory postulates that a fracture initiates from the crack tip in a direction θ_0 , along which the strain energy density at a critical distance is a minimum (i.e. crack propagates along path of minimum resistance), when this minimum reaches a critical value.
- The strain energy density dU per unit volume dV is

$$S = \frac{dU}{dV} = \frac{1}{2E}(\sigma_{xx}^2 + \sigma_{yy}^2 + \sigma_{zz}^2) - \frac{\nu}{E}(\sigma_{xx}\sigma_{yy} + \sigma_{yy}\sigma_{zz} + \sigma_{zz}\sigma_{xx}) + \frac{1}{2\mu}(\tau_{xy}^2 + \tau_{yz}^2 + \tau_{zx}^2)$$

where μ is the shear modulus (often referred to as G).

- In two dimensional problems, this equation reduces to:

$$S = \frac{dU}{dV} = \frac{1}{4\mu} \left[\frac{\kappa + 1}{4} (\sigma_{xx} + \sigma_{yy})^2 - 2(\sigma_{xx}\sigma_{yy} - \tau_{xy}^2) \right] \quad (1)$$

where $\kappa = 3 - 4\nu$ plane strain, and $\kappa = \frac{3-\nu}{1+\nu}$ for plane stress.

- Using Westergaard's solution for a cracked infinite plate and substituting the stress into Eq. 1, $\frac{dU}{dV}$, we obtain

$$S = \frac{\partial U}{\partial V} = \frac{1}{r_0 \pi} \left(a_{11} K_I^2 + 2a_{12} K_I K_{II} + a_{22} K_{II}^2 \right) = \frac{S(\theta)}{r_0}$$

where

$$a_{11} = \frac{1}{16\mu} [(1 + \cos \theta) (\kappa - \cos \theta)]$$

$$a_{12} = \frac{\sin \theta}{16\mu} [2 \cos \theta - (\kappa - 1)]$$

$$a_{22} = \frac{1}{16\mu} [(\kappa + 1) (1 - \cos \theta) + (1 + \cos \theta) (3 \cos \theta - 1)]$$

where

$$\kappa = \frac{3-\nu}{1+\nu} \quad (\text{plane stress})$$

$$\kappa = 3 - 4\nu \quad (\text{plane strain})$$

and μ is the shear modulus.

- This model is based on the following assumptions:
 - 1 Direction of fracture initiation (in 3-D) is toward the point of minimum strain energy density factor S_{min} as compared to other points on the same spherical surface surrounding that point

$$\frac{\partial S}{\partial \theta} = 0$$

$$\frac{\partial^2 S}{\partial \theta^2} > 0$$

- 2 Fracture initiation is assumed to occur when $S_{\theta min}$ reaches the maximum critical value S_{cr} .
- If we set $K_{II} = 0$, thus $\theta_0 = 0$ and $S_{cr} = (S(\theta))_{min} = S(\theta = 0) = a_{11} K_{Ic}$

$$S_{cr} = \frac{2(\kappa - 1)K_{Ic}^2}{16\mu\pi}$$

$$= \frac{(\kappa - 1)}{8\pi\mu} K_{Ic}^2$$

- Thus, the fracture locus predicted by this theory is given by:

$$\frac{8\mu}{(\kappa - 1)} \left[a_{11} \left(\frac{K_I}{K_{Ic}} \right)^2 + 2a_{12} \left(\frac{K_I K_{II}}{K_{Ic}^2} \right) + a_{22} \left(\frac{K_{II}}{K_{Ic}} \right)^2 \right] = 1$$

- Note: decompose strain energy density into two components a **volumetric one** and a **deviatoric one**:

$$S = \frac{dU}{dV} = \left(\frac{dU}{dV} \right)_D + \left(\frac{dU}{dV} \right)_V$$

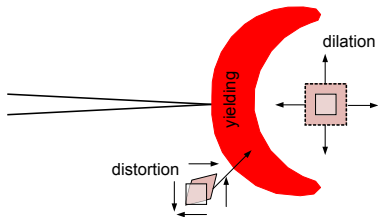
where the **deviatoric** part is given by

$$\left(\frac{dU}{dV} \right)_D = \frac{1 + \nu}{6E} \left[(\sigma_{xx} - \sigma_{yy})^2 + (\sigma_{yy} - \sigma_{zz})^2 + (\sigma_{zz} - \sigma_{xx})^2 + 6(\tau_{xy}^2 + \tau_{yz}^2 + \tau_{xz}^2) \right]$$

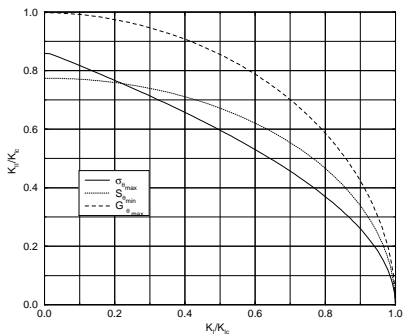
and the **volumetric** one by

$$\left(\frac{dU}{dV} \right)_V = \frac{1 - 2\nu}{6E} (\sigma_{xx} + \sigma_{yy} + \sigma_{zz})^2$$

- S_{min} is associated with brittle fracture, S_{max} with yielding. Its direction coincides with the direction of maximum distortion while S_{min} coincides with maximum dilation.



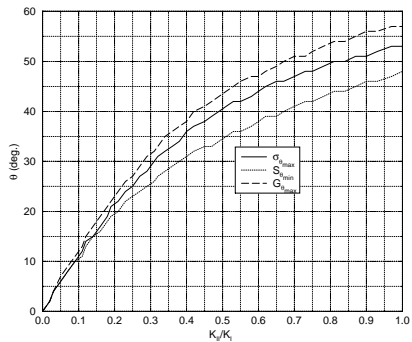
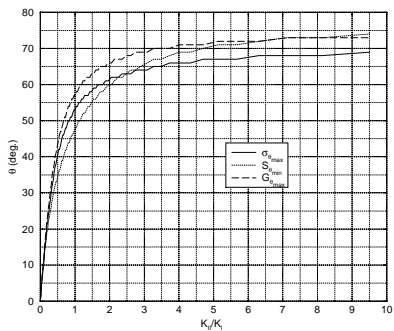
Check for corrections in Chapter 5 of book by Sun and Jin (in this folder) for maximum energy release rate. I also do have the matlab



code

- 1 Algorithmically, the **angle of crack propagation θ_0** is first obtained and then the criteria are assessed for local fracture stability.
- 2 Near the crack tip we have a near **state of biaxial stress**

- 3 All models can be represented by a **normalized fracture locus**.
- 4 For all practical purposes, **all three theories give identical results for small ratios of $\frac{K_{II}}{K_I}$** and diverge slightly as this ratio increases.
- 5 A crack will always extend in the **direction which minimizes $\frac{K_{II}}{K_I}$** .
- 6 For mixed-mode loading crack will **reorient itself so that K_{II} is minimized**. During its trajectory a crack will most often be in that portion of the normalized $\frac{K_I}{K_{Ic}} - \frac{K_{II}}{K_{IIc}}$ space where the three theories are in close agreement.
- 7 If the pair of SIF is inside the fracture loci, then that crack cannot propagate without sufficient increase in stress intensity factors. If outside, then the crack is locally unstable and will continue to propagate in either of the following ways:
 - 1 With an increase in the SIF (and the energy release rate G), thus resulting in a **global instability**, failure of the structure (crack reaching a free surface) will occur.
 - 2 With a decrease in the SIF (and the energy release rate G), due to a **stress redistribution**, the SIF pair will return to within the locus.



Plastic Zone Size

Victor E. Saouma
saouma@colorado.edu

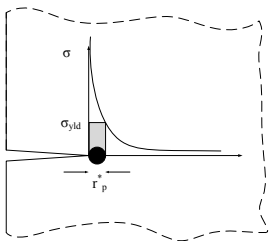
University of Colorado, Boulder

Spring 2022

- 1 Introduction
- 2 Uniaxial Stress Criteria
 - First Order Approximation
 - Second Order Approximation
 - Example
 - Dugdale's Model
 - Barenblatt's Model
- 3 Multiaxial Yield Criteria
 - Shape of Plastic Zone
- 4 Plane Strain vs. Plane Stress
- 5 Nice Pictures

- LEFM: stress at crack tip theoretically infinite. All materials have a finite strength, there will always be a **small plastified zone around the crack tip**.
- If this zone is small compared to the crack size, then LEFM assumptions are correct; **if not, LEFM is not applicable** and a nonlinear model must be used. This “damaged” zone is referred to as a **plastic zone** for metals, and a **fracture process zone** for cementitious materials and ceramics.
- There are two important issues associated with nonlinear fracture:
 - 1 What is the **relative size** of the plastic or process zone (with respect to the crack length a)?
 - 2 If the relative size is “large”, what would be the **criteria** for crack growth?
- The **evaluation of the plastic zone** for plastified materials can be determined through various levels of approximations:
 - 1 Uniaxial stress criteria
 - 1 first order approximation
 - 2 second order approximation (Irwin)
 - 3 Dugdale’s model
 - 2 Multiaxial yield criteria

Simplest and most straightforward model:



- Solve

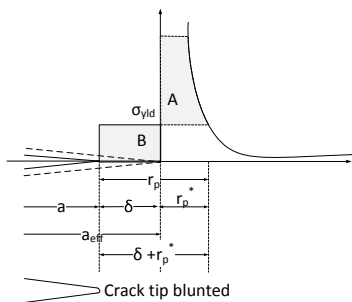
- Equate σ_{yy} to σ_{yld}

$$\sigma_{yy} = \frac{K_I}{(2\pi r)^{\frac{1}{2}}} \cos \frac{\theta}{2} \left[1 + \sin \frac{\theta}{2} \sin \frac{3\theta}{2} \right]$$

- set $\theta = 0$, $r = r_p^*$, $\sigma_{yy} = \sigma_{yld}$

$$\sigma_{yld} = \frac{K_I}{\sqrt{2\pi r_p^*}}$$

$$r_p^* = \frac{1}{2\pi} \frac{K_I^2}{\sigma_{yld}^2} = \frac{a}{2} \left(\frac{\sigma}{\sigma_{yld}} \right)^2 \quad (1)$$



Equilibrium must be maintained through
stress redistribution

$$B = \sigma_{\text{yld}} \delta$$

$$A = \int_0^{r_p^*} \sigma dr - \sigma_{\text{yld}} r_p^* = \int_0^{r_p^*} \frac{K}{\sqrt{2\pi r}} dr - \sigma_{\text{yld}} r_p^*$$

$$= \int_0^{r_p^*} \frac{\sigma \sqrt{\pi a}}{\sqrt{2\pi r}} dr - \sigma_{\text{yld}} r_p^* = \sigma \sqrt{2ar_p^*} - \sigma_{\text{yld}} r_p^*$$

Equating A to B we obtain:

$$\sigma \sqrt{2ar_p^*} - \sigma_{\text{yld}} r_p^* = \sigma_{\text{yld}} \delta; \quad \sigma_{\text{yld}} (\delta + r_p^*) = \sigma \sqrt{2ar_p^*}; \quad (\delta + r_p^*)^2 = \frac{2a\sigma^2}{\sigma_{\text{yld}}^2} r_p^*$$

From Eq. 1, $r_p^* = \frac{a}{2} \left(\frac{\sigma}{\sigma_{\text{yld}}} \right)^2$, thus this simplifies into

$$\delta + r_p^* = 2r_p^* \Rightarrow \delta = r_p^*; \quad r_p = 2r_p^*; \quad \text{or} \quad r_p = \frac{1}{\pi} \frac{K_I^2}{\sigma_{\text{yld}}^2} = \left(\frac{\sigma}{\sigma_{\text{yld}}} \right)^2 a$$

- Note that $r_p = 2r_p^*$ and that we can still use r_p^* but with $a_{eff} = a + r_p^*$; thus we can consider an **effective crack length of $a + r_p^*$** which would result in:

$$K_{eff} = f(g)\sigma\sqrt{\pi(a + r_p^*)} = f(g)\sigma\sqrt{\pi\left(a + \frac{K^2}{2\pi\sigma_{yld}^2}\right)}$$

- For linear elastic fracture mechanics to be applicable, we must have:

$$\text{LEFM} \Leftrightarrow K \approx K_{eff}$$

Considering an infinite with central crack of size $2a = 16$ mm, a far field applied stress $\sigma_{app} = 350$ MPa, and the plate has a yield stress $\sigma_{yld} = 1,400$ MPa.

- ① Using the 1st order approximation:

$$r_p^* = \frac{\sigma^2 a}{2\sigma_{yld}^2} = \frac{(350)^2 (.008)}{2(1,400)^2} \approx .00025 \text{ m} = .25 \text{ mm}$$

Since $\frac{r_p}{a}$ is very small, $K_{eff} \approx K_{applied}$

- ② The effective SIF are then given by

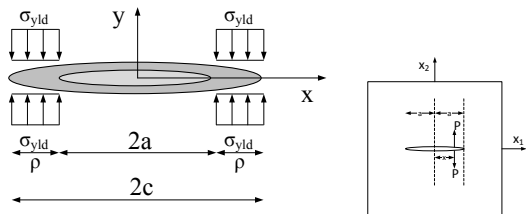
$$K_{eff} = \sigma \sqrt{\pi(a + r_p^*)} = 350 \sqrt{\pi(.008 + .00025)} = 56.4 \text{ MPa}\sqrt{m}$$

$$K_{app} = \sigma \sqrt{\pi a} = 350 \sqrt{\pi(.008)} = 55.5 \text{ MPa}\sqrt{m}$$

- ③ We note that there is only 2 percent difference between those two solutions, hence LEFM is applicable.
- ④ If yield stress was decreased by heat treatment to 385 MPa, then

$$r_p^* = \frac{(350)^2 (.008)}{2(385)^2} = 3.3 \text{ mm.}; \text{ and } K_{eff} = 350 \sqrt{\pi(.008 + .0033)} = 66 \text{ MPa}\sqrt{m}$$

and in this case **LEFM may no longer be applicable.**



- Dugdale assumed that the actual physical crack of length $2a$ is **replaced by a total effective crack of length $2c$** , where $c = a + \rho$ such that: a **constant stress σ_{yld}** is applied over ρ where $a < x < c$ causing (a negative) K_ρ and c is selected in such a manner that $\sum K = 0$ or $K_{remote} = -K_\rho$.

- Considering first

$$K_A = \frac{P}{\sqrt{\pi a}} \sqrt{\frac{a+x}{a-x}}; \quad K_B = \frac{P}{\sqrt{\pi a}} \sqrt{\frac{a-x}{a+x}}$$

and assuming $dP = \sigma_{yld} dx$, and replacing in the above equations, we obtain:

$$K_p = \frac{\sigma_{yld}}{\sqrt{\pi a}} \int_a^c \left\{ \sqrt{\frac{a+x}{a-x}} + \sqrt{\frac{a-x}{a+x}} \right\} dx$$

- Integration of this equation results in

$$K_p = 2\sigma_y \sqrt{\frac{c}{\pi}} \arccos \frac{a}{c}$$

SIF caused by the remote far field stress is given by: $K_{remote} = \sigma \sqrt{\pi c}$

- Equating, we obtain:

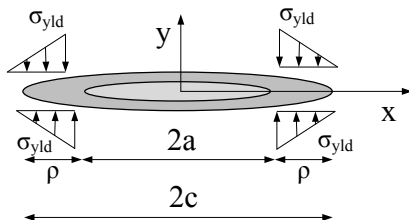
$$\frac{a}{c} = \cos \left(\frac{\pi \sigma}{2 \sigma_{yld}} \right)$$

- It can be shown that

$$\rho = \frac{\pi^2}{8} \left(\frac{\sigma}{\sigma_{yld}} \right)^2 \quad a = \frac{\pi}{8} \frac{K_I^2}{\sigma_{yld}^2}$$

This should be compared with Eq. 5 $r_p = \left(\frac{\sigma}{\sigma_{yld}} \right)^2 a$ previously obtained.

A variation of Dugdale's model was suggested by **Barenblatt** where linear stress distribution replaces the constant one



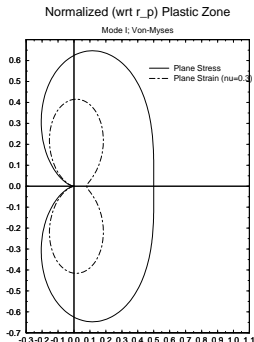
- All the previous models have restricted themselves to $\theta = 0$ and have used **uniaxial yield criteria**, but the size of the plastic zone can be similarly derived from a multi-axial yield criterion.
- The crack tip stress field equations in terms of principal stresses are:

$$\begin{aligned}\sigma_{(1)} &= \frac{K_I}{\sqrt{2\pi r}} \cos \frac{\theta}{2} \left[1 + \sin \frac{\theta}{2} \right] \\ \sigma_{(2)} &= \frac{K_I}{\sqrt{2\pi r}} \cos \frac{\theta}{2} \left[1 - \sin \frac{\theta}{2} \right] \\ \sigma_{(3)} &= \nu(\sigma_1 + \sigma_2) \text{ plane strain} \\ &= 0 \text{ Plane stress}\end{aligned}$$

- Using the **von Mises criteria**

$$\sigma_e = \frac{1}{\sqrt{2}} \left[(\sigma_{(1)} - \sigma_{(2)})^2 + (\sigma_{(2)} - \sigma_{(3)})^2 + (\sigma_{(3)} - \sigma_{(1)})^2 \right]^{\frac{1}{2}}$$

and yielding would occur when σ_e reaches σ_{yld} .



- Substituting the principal stresses (with $r = r_p$) into this equation and solving for r_p yields

- Plane strain:

$$\frac{K_I^2}{2\pi r} \left[\frac{3}{2} \sin^2 \theta + (1 - 2\nu)^2 (1 + \cos \theta) \right] = 2\sigma_{yld}^2$$

$$r_p(\theta) = \frac{1}{4\pi} \frac{K_I^2}{\sigma_{yld}^2} \left[\frac{3}{2} \sin^2 \theta + (1 - 2\nu)^2 (1 + \cos \theta) \right]$$

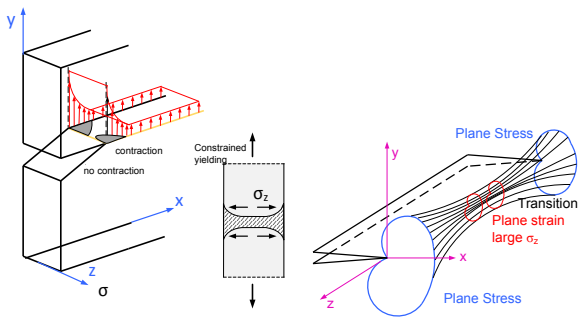
- plane stress:

$$\frac{K_I^2}{2\pi r} \left[1 + \frac{3}{2} \sin^2 \theta + \cos \theta \right] = 2\sigma_{yld}^2$$

$$r_p(\theta) = \frac{1}{4\pi} \frac{K_I^2}{\sigma_{yld}^2} \left[1 + \frac{3}{2} \sin^2 \theta + \cos \theta \right]$$

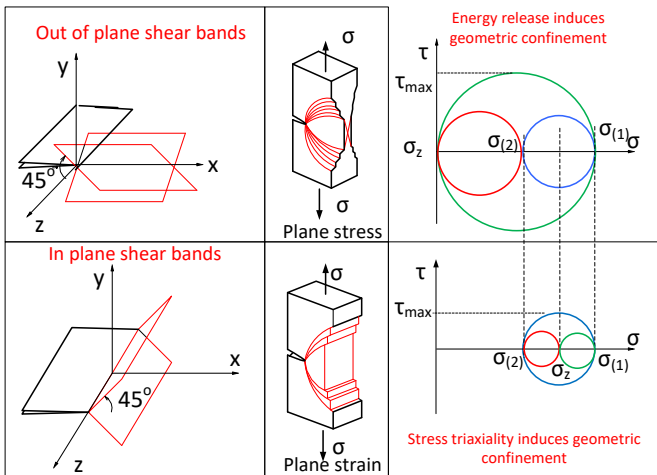
- For the **Drucker-Prager model**, and for different mixed mode ratios, the expected plastic (or more appropriately **process**) zones.
- The **plastic zone size for plane strain is much smaller than the one for plane stress** (by a factor of $(1 - 2\nu)^2$).
- Which is why all **fracture tests should be conducted under plane strain conditions**.

- Irrespective of a plate thickness, there is a **gradual decrease in size of the plastic zone** from the plate surface (plane stress) to the interior (plane strain).



- The ratio of the plastic zone size to the plate thickness $\frac{r_p}{B}$ must be much smaller than unity for plane strain to prevail. It has been experimentally shown that this ratio should be less than 0.025.
- For **Plane Strain** $K_{Ic} \Leftrightarrow r_p < .025B$

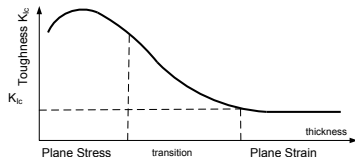
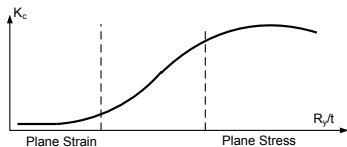
- We also observe that since r_p is proportional to $\left(\frac{K_I}{\sigma_{yld}}\right)^2$, the plate **thickness should increase** as either the SIF increase or the yield stress decrease.
- Furthermore, the different stress fields present at the tip of the crack under plane stress and plane strain will result in **different deformation patterns**. This is best explained in terms of the **orientation of the planes of maximum shear stress** for both cases.

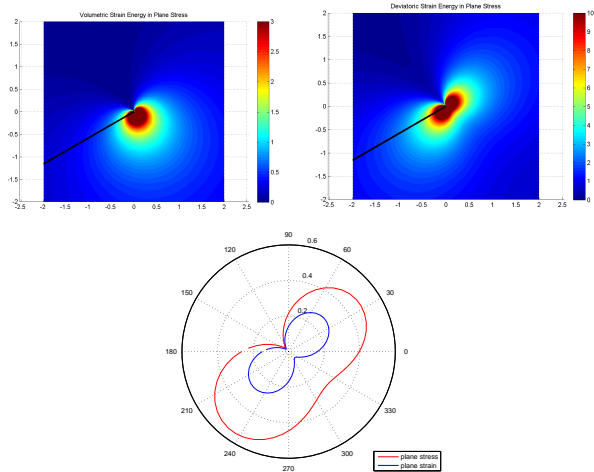


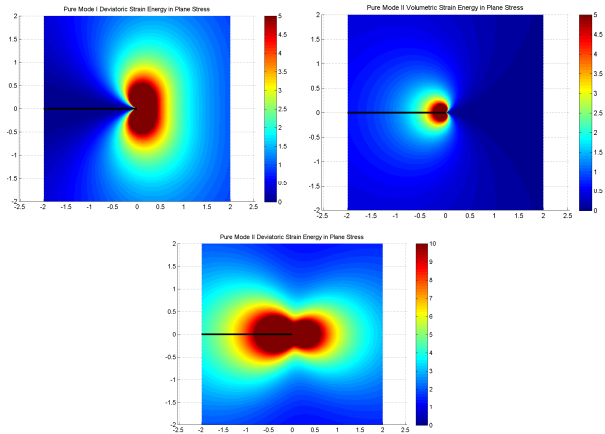
Plane Stress: $\sigma_z = 0$, and the maximum shear stress τ_{max} is at planes rotated 45° from the directions of $\sigma_{(1)}$ and $\sigma_{(3)}$. If $\sigma_{(1)} = \sigma_{y/d}$ and $\sigma_{(3)} = 0$, then crack will be at 45° with the X-Z plane

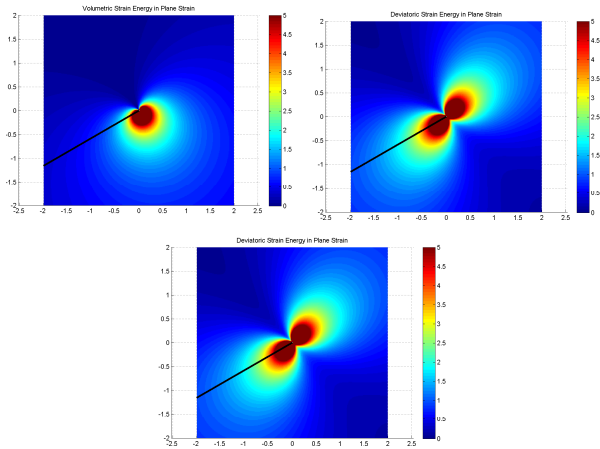
Plane Strain: In this case we have $\sigma_{(1)}$ and $\sigma_{(2)}$ that have same magnitude, as in plane stress, the third principal stress is $\sigma_{(3)} = \nu(\sigma_{(1)} + \sigma_{(2)})$. For plastic deformation $\nu = 1/2$, thus $\sigma_{(3)} = \frac{1}{2}(\sigma_{(1)} + \sigma_{(2)})$, τ_{max} is much smaller than in plane stress, and is on a different plane, rotated 45° from the directions of $\sigma_{(2)}$ and $\sigma_{(1)}$.

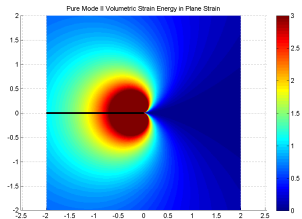
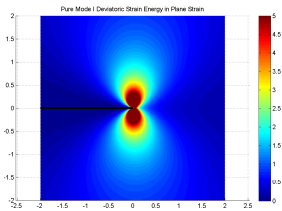
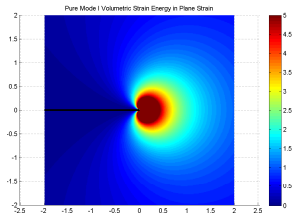
- Finally, it should be noted, once again, that fracture toughness K_{Ic} can only be measured under plane strain conditions.

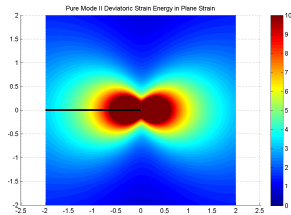












Elasto-Plastic Fracture Mechanics

Victor E. Saouma
saouma@colorado.edu

University of Colorado, Boulder

Spring 2022

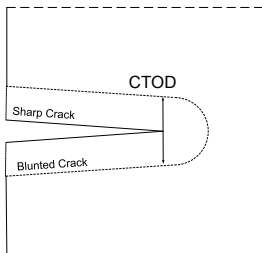
1 Introduction

2 CTOD; Irwin

3 J Integral

- Definition
- Proof $J = 0$ in closed path
- Proof Path Independence
- Physical Meaning: Nonlinear Elastic Energy Release Rate
- Plastic Crack Tip Fields
- Nonlinear Energy Release Rate
- J Testing
- Engineering Approach to Fracture
- Example of EPRI'Solutions
- Numerical Example
- J_1 and J_2 Generalization

Note the various stages of ductile fracture:



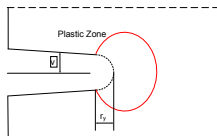
- 1 **Blunting:** Under LEFM assumptions, the crack tip opening displacement (CTOD) is zero, however in elasto-plastic material due to blunting it is different from zero.
- 2 Crack initiation
- 3 Slow (stable) crack growth
- 4 Unstable crack growth

- LEFM can be either: **too conservative and expensive** (does not account for plastification at the crack tip), and/or **invalid** based on calculations of r_p^* .
- When LEFM is not applicable, an **alternative criteria for crack growth** in Elasto Plastic Fracture Mechanics (EPFM) is sought.
- Two approaches are currently in use
 - 1 a **local** criterion based on the crack tip opening displacement (**CTOD**).
 - 2 a **global** criterion based on the quasi-strain energy release rate (J integral), J_{IC} .

- As usual, we have a Newtonian (stress based) or Lagrangian (energy based) approach.

	Local Vector	Global Scalar
LEFM	$K (K_I, K_{II})$	G
EPFM	<i>CTOD, CSOD, CTOD</i>	<i>J</i>

- CTOD: Crack Tip Opening Displacement (0 in LEFM, $\neq 0$ in NLFM)



- The vertical displacement of a point next to the crack tip due to mode I loading is given by

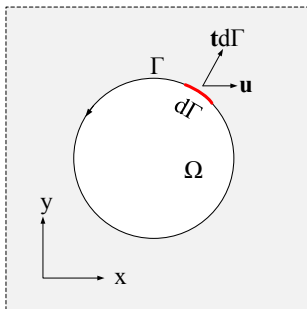
$$v = \frac{K_I}{2\mu} \left[\frac{r}{2\pi} \right]^{\frac{1}{2}} \sin \frac{\theta}{2} \left[\kappa + 1 - 2 \cos^2 \frac{\theta}{2} \right]$$

- If we substitute $\theta = \pm\pi$ we obtain the upper and lower displacements of the crack face, and due to symmetry their sum corresponds to the crack opening displacement. Hence the crack opening is given by

$$\text{COD} = 2v = \frac{\kappa + 1}{\mu} K_I \sqrt{\frac{r}{2\pi}}$$

- If we substitute the crack tip opening displacement a distance r_p^* away from the crack tip using Irwin's plastic zone correction $r_p^* = \frac{1}{2\pi} \frac{K_I^2}{\sigma_{\text{yld}}^2}$ and using $\kappa = \frac{3-\nu}{1+\nu}$ for plane stress, and recall that $\mu = E/2(1 + \nu)$, we obtain

$$\text{CTOD} = \frac{4}{\pi} \frac{K_I^2}{E \sigma_{\text{yld}}}$$



Eshelby defined a number of **contour integrals that are path independent** by virtue of the theorem of energy conservation. The two-dimensional form of one of these integrals can be written as:

$$J = \oint_{\Gamma} \left(w dy - t \frac{\partial u}{\partial x} d\Gamma \right) = 0 \quad (1)$$

with

$$w = \int_0^{\epsilon} \sigma_{ij} d\epsilon_{ij}$$

- Where w is the strain energy density; Γ is a closed contour followed counter-clockwise; t is the traction vector on a plane defined by the outward drawn normal \mathbf{n} and $t = \sigma \mathbf{n}$; u the displacement vector, and $d\Gamma$ is the element of the arc along the path Γ .
- Whereas Eshelby had defined a number of similar path independent contour integrals, **he had not assigned them with a particular physical meaning.**

- Given $J = \oint_{\Gamma} \left(w dy - t_i \frac{\partial u_i}{\partial x} d\Gamma \right)$ and assuming Γ to be defined counterclockwise, then $dx = -n_y d\Gamma$, and $dy = n_x d\Gamma$ and $t_i = n_j \sigma_{ij}$ where n_x , n_y and n_j are direction cosines.
- Substituting

$$J = \oint_{\Gamma} \left(w n_x - n_j \sigma_{ij} \frac{\partial u_i}{\partial x} \right) d\Gamma$$

- Invoking **Divergence theorem** ($\oint_{\Gamma} v_i n_i d\Gamma = \int_{\Omega} v_{i,i} d\Omega$) we obtain

$$J = \int_{\Omega} \left[\underbrace{\frac{\partial w}{\partial x}}_A - \underbrace{\frac{\partial}{\partial x_j} \left(\sigma_{ij} \frac{\partial u_i}{\partial x} \right)}_B \right] dx dy \quad (2)$$

- Applying the chain rule, the first term A in the square bracket becomes

$$\frac{\partial w}{\partial x} = \frac{\partial w}{\partial \varepsilon_{ij}} \frac{\partial \varepsilon_{ij}}{\partial x} = \sigma_{ij} \frac{\partial \varepsilon_{ij}}{\partial x} \quad (3)$$

where the strain is given by

$$\varepsilon_{ij} = \frac{1}{2} (u_{i,j} + u_{j,i})$$

- Substituting for the first term A

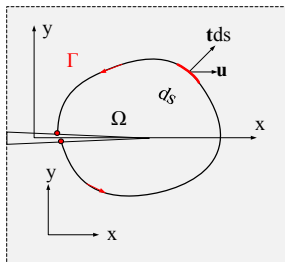
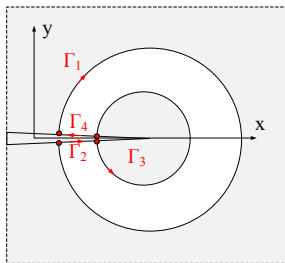
$$A = \frac{\partial w}{\partial x} = \frac{1}{2} \sigma_{ij} \left[\frac{\partial}{\partial x} \left(\frac{\partial u_i}{\partial x_j} \right) + \frac{\partial}{\partial x} \left(\frac{\partial u_j}{\partial x_i} \right) \right] = \sigma_{ij} \frac{\partial}{\partial x_j} \left(\frac{\partial u_i}{\partial x} \right) \quad (4)$$

- On the other hand, we have for the second term B

$$B = \frac{\partial}{\partial x_j} \left(\sigma_{ij} \frac{\partial u_i}{\partial x} \right) = \underbrace{\sigma_{ij} \frac{\partial}{\partial x_j} \left(\frac{\partial u_i}{\partial x} \right)}_0 + \frac{\partial \sigma_{ij}}{\partial x_j} \frac{\partial u_i}{\partial x}$$

which is identical to A . Thus, the integrand in Eq. 2 vanishes and $J = 0$ for any closed contour.

- second term is zero (divergence of stress tensor is zero $\nabla \cdot \mathbf{T} = 0$)



- Proved $J = 0$ along closed path. Need to prove that J is non-zero and constant around an arbitrary path.
- Consider the closed path $\Gamma = \Gamma_1 + \Gamma_2 + \Gamma_3 + \Gamma_4$ in which Γ_1 and Γ_3 are arbitrarily chosen contours.
- $J = 0$ over Γ .
- Along Γ_2 and Γ_4 , the traction vector $t_i = 0$, $dy = 0$. Consequently, the contributions to J from Γ_2 and Γ_4 vanish.
- Considering the difference sense of integration along Γ_1 and Γ_3 we conclude that the values of J integrated over paths Γ_1 and Γ_3 are identical and opposite.
- The two paths were arbitrarily chosen, hence, the path independence of J is assured

- When J is applied along a contour around a crack tip, it represents the **change in potential energy for a virtual crack extension da** .
- Consider a two-dimensional crack surrounded by a line Γ which encompasses an area Ω .
- Under quasi-static conditions, and in the absence of body forces, the potential energy is given by

$$\Pi = \underbrace{\int_{\Omega} w d\Omega}_U - \underbrace{\oint_{\Gamma} t_i u_i d\Gamma}_W \quad (5)$$

- For a virtual crack extension, the change in potential energy is

$$\begin{aligned} \frac{d\Pi}{da} &= \int_{\Omega} \frac{dw}{da} d\Omega - \oint_{\Gamma} \left[t_i \frac{du_i}{da} + u_i \frac{dt_i}{da} \right] d\Gamma \\ &= \int_{\Omega} \frac{dw}{da} d\Omega - \underbrace{\oint_{\Gamma_U} \left[t_i \frac{du_i}{da} + u_i \frac{dt_i}{da} \right] d\Gamma}_0 - \oint_{\Gamma_t} \left[t_i \frac{du_i}{da} + \underbrace{u_i \frac{dt_i}{da}}_0 \right] d\Gamma \quad (6) \end{aligned}$$

- Contour path was decomposed into two parts, **one with prescribed displacement (Γ_u)** and the other **with prescribed traction (Γ_t)**.
- Γ_u is zero along the path, we maintain a closed contour integral along Γ_t .
- The second term inside the square bracket will be zero along Γ_t because the **traction is constant during crack growth**.
- Thus we can write

$$\frac{d}{da} = \frac{\partial}{\partial a} + \frac{\partial}{\partial x} \frac{\partial x}{\partial a} = \frac{\partial}{\partial a} - \frac{\partial}{\partial x}$$

for a crack extension along a ($\frac{\partial x}{\partial a} = -1$) with respect to the new coordinate system.

- Substituting into Eq. 6

$$\frac{d\Pi}{da} = \int_{\Omega} \left[\frac{\partial w}{\partial a} - \frac{\partial w}{\partial x} \right] d\Omega - \oint_{\Gamma_t} t_i \left(\frac{\partial u_i}{\partial a} - \frac{\partial u_i}{\partial x} \right) d\Gamma \quad (7)$$

But from the **divergence theorem** (and $t_i = n_j \sigma_{ij}$)

$$\oint_{\Gamma_t} t_i \frac{\partial u_i}{\partial a} d\Gamma = \int_{\Omega} \sigma_{ij} \frac{\partial}{\partial x_j} \left(\frac{\partial u_i}{\partial a} \right) d\Omega = \int_{\Omega} \frac{\partial w}{\partial a} d\Omega$$

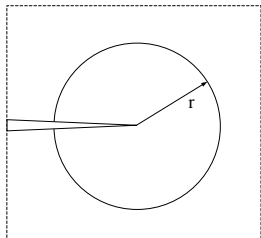
- Hence, the first terms in each of the two integrals in Eq. 7 cancel out, and we are left with

$$\frac{d\Pi}{da} = \oint_{\Gamma_t} t_i \frac{\partial u_i}{\partial x} d\Gamma - \int_{\Omega} \frac{\partial w}{\partial x} d\Omega$$

- Apply the **divergence theorem** again, multiply both sides by -1 and recalling that $n_x d\Gamma = dy$

$$-\frac{d\Pi}{da} = \oint_{\Gamma_t} \left(wn_x - t_i \frac{\partial u_i}{\partial x} \right) d\Gamma = \oint_{\Gamma_t} \left(wdy - t_i \frac{\partial u_i}{\partial x} d\Gamma \right)$$

which is the same as Eq. 1. Henceforth, the **J integral is equal to the energy release rate for linear and nonlinear elastic material under quasi-static conditions.**



- Under LEFM assumptions, we had a $\frac{1}{\sqrt{r}}$ stress and strain singularity, we now seek to determine the corresponding one, for EPFM.
- Starting with

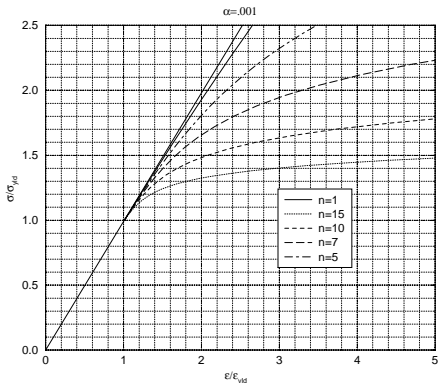
$$J = \oint_{\Gamma} \left(w dy - t \frac{\partial u}{\partial x} d\Gamma \right)$$

- Taking the contour around a circle of radius r we substitute $d\Gamma = r d\theta$; $y = r \sin \theta$; and $dy = r \cos \theta d\theta$

$$J = \oint_{-\pi}^{\pi} \left(w \cos \theta - t \frac{\partial u}{\partial x} \right) r d\theta \quad (8)$$

but J should be independent of r by virtue of path independence hence both $w \cos \theta$ and $t \frac{\partial u}{\partial x}$ should be proportional to $\frac{1}{r}$.

Ramberg–Osgood Stress–Strain Relation



- Consider a material with a (uniaxial) power law hardening model (Ramberg-Osgood) (often used to curve-fit stress-strain data):

$$\frac{\epsilon}{\epsilon_{yld}} = \frac{\sigma}{\sigma_{yld}} + \alpha \left(\frac{\sigma}{\sigma_{yld}} \right)^n \quad (9)$$

n is the strain hardening exponent, and for $n = 1$ we have a linear elastic response, for $n = \infty$ we would have an elastic perfectly plastic one. α is a dimensionless constant.

- In the vicinity of the crack tip, plastic strain is dominant (the elastic one is negligible) and

$$\frac{\epsilon}{\epsilon_{yld}} = \alpha \left(\frac{\sigma}{\sigma_{yld}} \right)^n \quad (10)$$

- Let x and y be the order of the stress and strain singularities:

$$\sigma = \frac{C_1}{r^x}; \quad \varepsilon = \frac{C_2}{r^y}$$

- From Eq. 8, energy w must be proportional to $\frac{1}{r}$, so

$$\sigma\varepsilon \propto \frac{1}{r} \Rightarrow x + y = 1 \quad (11)$$

- Furthermore, from Eq. 9 and 10

$$\frac{C_2}{r^y \varepsilon_{yld}} = \alpha \left(\frac{C_1}{r^x \sigma_{yld}} \right)^n \Rightarrow \frac{C_3}{r^y} = C_4 \frac{1}{r^{nx}} \Rightarrow y = nx \quad (12)$$

- Solving Eq. 11 and 12, we obtain

$$x = \frac{1}{1+n}; \quad y = \frac{n}{1+n}$$

- Thus the singularities are:

$$\varepsilon(r) = \frac{C}{r^{\frac{n}{1+n}}}; \quad \sigma(r) = \frac{D}{r^{\frac{1}{1+n}}}$$

- For linear elastic solids $n = 1$ and these equations reduce to the familiar

$$\varepsilon(r) = \frac{C}{r^{\frac{1}{2}}}; \quad \sigma = \frac{D}{r^{\frac{1}{2}}}$$

- For elastic perfectly plastic material $n = \infty$ (elasto-plastic), the stress field is non-singular (as expected) while the strain field has a **singularity of the form r^{-1}** .
- Those singularities $\frac{n}{1+n}$ and $\frac{1}{1+n}$ are often referred to as the **HRR singularities after Hutchinson, Rice, and Rosengren**.

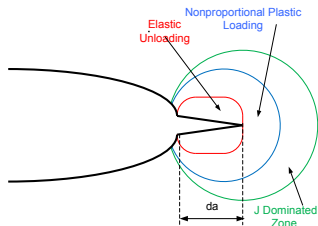
- It can be shown that there is a **relationship between J and the crack tip $\sigma - \varepsilon$ field**:

$$\sigma_{ij} = \sigma_{\text{yld}} \left(\frac{EJ}{\alpha \sigma_{\text{yld}}^2 I_n r} \right)^{\frac{1}{1+n}} \check{\sigma}_{ij}(\theta, n)$$

$$\varepsilon_{ij} = \frac{\alpha \sigma_{\text{yld}}}{E} \left(\frac{EJ}{\alpha \sigma_{\text{yld}}^2 I_n r} \right)^{\frac{n}{1+n}} \check{\varepsilon}_{ij}(\theta, n)$$

where I_n is an integration constant which depends on the $\sigma - \varepsilon$ curve, and $\check{\sigma}$ & $\check{\varepsilon}$ are dimensionless functions of n and θ (analogous to $f_{ij}(\theta)^l$ in LEFM which also depend on the stress state (plane stress/strain))

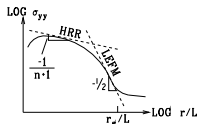
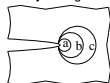
- Thus, **J also characterizes the σ and ε singularities in EPFM** just as K did in LEFM ($\sigma_{ij} = \frac{K}{\sqrt{2\pi r}}$).
- Finally, we should note that at the crack tip we have **two stress singularities**, the first one $\frac{1}{\sqrt{r}}$ **in the elastic region**, and the later $\frac{1}{r^{\frac{1}{1+n}}}$.



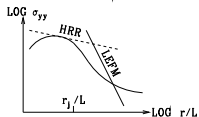
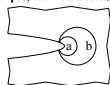
- We observe that material **behind a propagating crack unload elastically** (as opposed to nonlinear elastic). Note **analogy with cohesive crack model** to be discussed later.

a Large Strain Region b: J-dominated zone; c: K-dominated zone

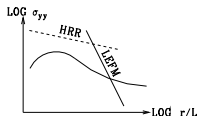
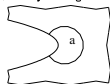
(a) Small scale yielding



(b) Elastic-plastic conditions



(c) Large scale yielding

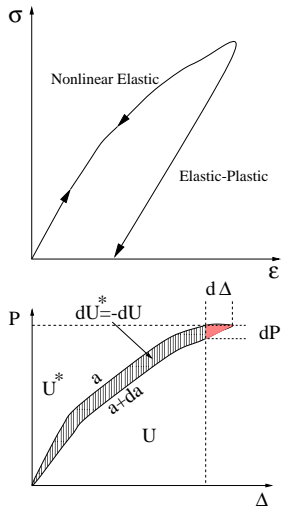


	Large Strain	J Dominated	K Dominated
Small scale yielding	Y	Y	Y
Elastic Plastic Conditions	Y	Y	N
Large Scale Yielding	Y	N	N

Small Scale Yielding: both K and J characterize this zone. At a short distance from the crack tip (relative to a), the stress is proportional to $\frac{1}{\sqrt{r}}$ this area is K -dominated region. If we have monotonic loading, a J dominated region occurs in the plastic zone where the elastic singularity is no longer valid. Inside the plastic zone, the HRR is approximately valid. **Finite strain** region occurs within approximately 2δ from the crack tip where the large deformation invalidates HRR.

Elastic-Plastic: J is still valid, but K no longer.

Large Scale Yielding: here the **size of the finite strain zone becomes significant relative to a** and there is no longer a region uniquely characterized by J . J becomes **size and geometry dependent**.



- Whereas **LEFM is restricted to linear elastic materials**, most **metals have a nonlinear stress-strain curve**.
- **Loading** behavior of both materials is identical, differ at **unloaded**.
- If no unloading, we can assume a nonlinear elastic behavior, and the deformation theory of plasticity, which relates the total strains to stresses, is applicable.
- Recall that for nonlinear **elastic material J is the energy release rate in nonlinear elastic materials**:

$$J = -\frac{d\Pi}{da} \quad (13)$$

for a unit thickness crack extension.

- Following a similar approach, we consider the load displacement curves curve of a notched specimen made of nonlinear elastic material for two different conditions, **during crack extension from a to $a + da$** :

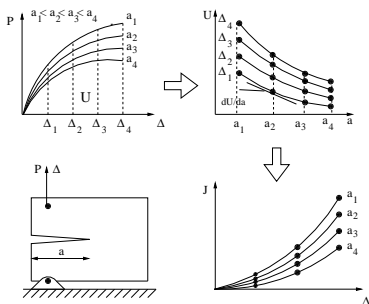
Load control we have $d\Delta = 0$ and $\Pi = U - W = U - P\Delta = -U^*$ where

$$U^* \stackrel{\text{def}}{=} \int_0^P \Delta dP \text{ is the complimentary strain energy. Thus for constant}$$

$$\text{load } J_P = \left(\frac{dU^*}{da} \right)_P$$

Constant Displacement, $dP = 0$, and $J_\Delta = - \left(\frac{dU}{da} \right)_\Delta$

- The difference between J_P and J_Δ is $\frac{1}{2}dPd\Delta$ (shown in red in the previous figure) which is vanishingly small compared to dU .
- Therefore J is the same for load control and displacement control.
- For linear elastic materials $J = G = \frac{K^2}{E'}$.



- For **nonlinear material**, the principle of superposition does not apply, and can not have a simple relation between J , the load, and the crack length.
- Test a number of identical specimens, but with slightly different crack lengths.
- Recall that $J = -\frac{1}{B} \left(\frac{\partial U}{\partial a} \right)_{\Delta}$

- 1 Test specimens with different crack lengths a_i .
- 2 Record load displacement curves.
- 3 Compute the strain energy U (The area under each $P - \Delta$ curve) at different displacements Δ_j for each a_i
- 4 plot U in terms of a , at various fixed displacements.
- 5 Since $J = -\frac{1}{B} \left. \frac{\partial U}{\partial a} \right|_{\Delta}$, J could be determined from the slope of the tangent to the curves.

- 6 Determine a **calibration curve applicable to the material, specimen size, specimen geometry, and temperature** from which it was obtained. This can be a very expensive test.

- The solution of a plastic problem involves the determination of the J integral. This usually involves a finite element analysis.
- If such a capability is not available, and a first order approximation of J is required, then a **simplified engineering approach** can be followed.
- **General Solution:** For **Ramberg-Osgood material**, we can write

$$\begin{aligned}
 J &= J_e(a_e) + J_P(a, n) \\
 \delta &= \delta_e(a_e) + \delta_P(a, n) \\
 \Delta_c &= \Delta_{ec}(a_e) + \Delta_{Pc}(a, n)
 \end{aligned}$$

where: J , δ , and Δ are the J integral, the crack tip opening displacement, and point load displacement respectively, and

$$\begin{aligned}
 a_e &= a + \phi r_y \\
 r_y &= \frac{1}{\beta\pi} \frac{n-1}{n+1} \left(\frac{K_I}{\sigma_y} \right)^2 \\
 \phi &= \frac{1}{1 + (P/P_o)^2}
 \end{aligned}$$

for plane stress $\beta = 2$ and for plane strain $\beta = 6$. $J_p(a, n)$, $\delta_p(a, n)$, and $\Delta_{pc}(a, n)$ are the plastic contributions based on the material hardening exponent n . P_0 is the limit load based on σ_y

We note that P is the generalized load per unit thickness, Δ is the load-point displacement, and that δ is the crack opening displacement.

- **Elastic Solution:** The elastic solution can be written as

$$J_e = f_1 \left(\frac{a}{W} \right) \frac{P^2}{E'} = \frac{K_I^2}{E'}$$

$$\delta_e = f_2 \left(\frac{a}{W} \right) \frac{P}{E'}$$

$$\Delta_{ce} = f_3 \left(\frac{a}{W} \right) \frac{P}{E'}$$

- **Fully Plastic Solution:** where $\varepsilon^e \ll \varepsilon^p$ if the plastic deformation can be described by J_2 , deformation plasticity theory with power law and isotropic hardening,

- The **small strain constitutive relation** is given by

$$\frac{\varepsilon_{ij}}{\varepsilon_{yld}} = \frac{3}{2} \alpha \left(\frac{\bar{\sigma}}{\sigma_{yld}} \right)^{n-1} \frac{S_{ij}}{\sigma_{yld}}$$

where S_{ij} and $\sigma_e = \frac{3}{2} \sqrt{S_{ij} S_{ij}}$ are the stress deviator and the von-Mises effective stress, respectively.

- For such a material Ilyushin has shown that the solution of the boundary value problems based on the above equation, and involving a single load or displacement parameter which is increasing monotonically has two important properties:
 - Field quantities increase in direct proportion to the load or displacement** parameter raised to some power dependent on n . For example if the traction is $T_i = PT'_i$ and P is a loading parameter, then

$$\sigma_{ij} = P \sigma'_{ij}(x_i, n)$$

$$\varepsilon_{ij} = \alpha \varepsilon_y \left(\frac{P}{\sigma_y} \right)^n \varepsilon'_{ij}(x_i, n)$$

$$u_i = \alpha \varepsilon_y \left(\frac{P}{\sigma_y} \right)^n u'_i(x_i, n)$$

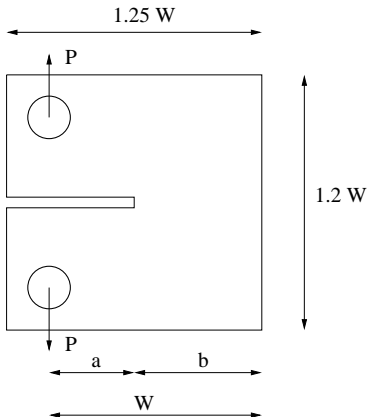
where $\sigma'_{ij}(x_i, n)$, $\varepsilon'_{ij}(x_i, n)$ and $u'_i(x_i, n)$ are functions of x_i and n and are independent of P .

- Since σ and ε increase in the same proportion, **fully plastic solution based on deformation plasticity is also the exact solution to the same problem posed for incremental or flow theory.**
- Since the integrand of J involves the product of σ and u gradients, then the **fully plastic J will be proportional to P^{n+1}** and we can write:

$$\begin{aligned}
 J_p &= \alpha \varepsilon_y \sigma_y b g_1(a/W) h_1(a/W, n) (P/P_0)^{n+1} \\
 \delta_p &= \alpha \varepsilon_y a g_2(a/W) h_2(a/W, n) (P/P_0)^n \\
 \Delta_{cp} &= \alpha \varepsilon_y a g_3(a/W) h_3(a/W, n) (P/P_0)^n \\
 \delta_{tp} &= \alpha \varepsilon_y b g_4(a/W) h_4(a/W, n) (P/P_0)^{n+1}
 \end{aligned} \tag{14}$$

b is the ligament length ($W - a$). α is from Eq. 10 $\varepsilon/\varepsilon_{yld} = \alpha(\sigma/\sigma_{yld})^n$.

- The dimensionless functions ($h_1 - h_4$) depend upon a/W and n and possibly other geometric parameters, but are independent of P . Those functions can be obtained from F.E. analysis and are **tabulated ($\pm 5\%$) in an EPRI report.**



Considering the **Compact Tension Specimen**

$$P_0 = 1.455\beta b\sigma_y \quad \text{Plane Strain}$$

$$P_0 = 1.071\beta b\sigma_y \quad \text{Plane Stress}$$

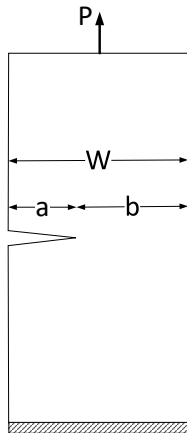
$$\beta = \sqrt{\left(2\frac{a}{b}\right)^2 + 4\frac{a}{b} + 2} - 2\frac{a}{b} - 1$$

$$g_i = 1$$

Δ crack opening displacement at the load line; δ is the crack mouth opening displacement.

		$n = 1$	$n = 2$	$n = 3$	$n = 5$	$n = 7$	$n = 10$	$n = 13$	$n = 16$	$n = 20$
		Plane Strain								
$\frac{a}{W} = \frac{1}{4}$	h1	2.23	2.05	1.78	1.48	1.33	1.26	1.25	1.32	1.57
	h2	17.9	12.5	11.7	10.9	10.5	10.7	11.5	12.6	14.6
	h3	9.85	8.51	8.17	7.77	7.71	7.92	8.52	9.31	10.9
$\frac{a}{W} = \frac{3}{8}$	h1	2.15	1.72	1.39	0.97	0.69	0.443	0.28	0.176	0.098
	h2	12.60	8.18	6.52	4.32	2.97	1.79	1.10	0.686	0.370
	h3	7.94	5.76	4.64	3.10	2.14	1.29	0.793	0.494	0.266

Consider a **single edge notched panel** with $W = 1$ m, $a = 125$ mm. Determine J in terms of the applied load assuming plane stress conditions, neglect plastic zone correction.



- Assume: $\sigma_{yld} = 414$ MPa, $n = 10$, $\alpha = 1.0$, $E = 207,000$ MPa, $\varepsilon_{yld} = \sigma_{yld}/E = 0.002$.
- From the EPRI report

$$b = W - a = 1000 - 125 = 875 \text{ mm}$$

$$\frac{a}{b} = \frac{125}{875} = 0.143$$

$$\beta = \sqrt{1 + \left(\frac{a}{b}\right)^2} - \frac{a}{b}$$

$$= \sqrt{1 + (0.143)^2} - 0.143 = 0.867$$

$$\begin{aligned} P_0 &= 1.072\beta b\sigma_y \\ &= (1.072)(0.867)(414) \text{ MPa}(875) \text{ mm}(25) \text{ mm} \\ &= 8.42 \text{ MN} \end{aligned}$$

		n = 1	n = 2	n = 3	n = 5	n = 7	n = 10	n = 13	n = 16	n = 20
Plane Strain										
$\frac{\sigma}{W} = \frac{1}{8}$	h1	4.95	6.93	8.57	11.50	13.5	16.1	18.1	19.9	21.2
	h2	5.250	6.47	7.56	9.46	11.1	12.9	14.4	15.7	16.8
	h3	26.60	25.80	25.20	24.20	23.6	23.2	23.2	23.5	23.7
$\frac{\sigma}{W} = \frac{1}{4}$	h1	4.34	4.77	4.64	3.82	3.06	2.170	1.55	1.11	0.712
	h2	4.760	4.56	4.28	3.39	2.64	1.910	1.25	0.875	0.552
	h3	10.30	7.64	5.87	3.70	2.48	1.500	0.97	0.654	0.404
$\frac{\sigma}{W} = \frac{3}{8}$	h1	3.88	3.25	2.63	1.68	1.06	0.539	0.276	0.142	0.060
	h2	4.540	3.49	2.67	1.57	0.94	0.458	0.229	0.116	0.048
	h3	5.14	2.99	1.90	0.923	0.51	0.240	0.119	0.060	0.025
$\frac{\sigma}{W} = \frac{1}{2}$	h1	3.40	2.30	1.69	0.928	0.51	0.213	0.090	0.039	0.012
	h2	4.450	2.77	1.89	0.954	0.50	0.204	0.085	0.036	0.011
	h3	3.15	1.54	0.91	0.417	0.21	0.085	0.036	0.015	0.004
$\frac{\sigma}{W} = \frac{5}{8}$	h1	2.86	1.80	1.30	0.697	0.37	0.153	0.064	0.026	0.008
	h2	4.370	2.44	1.62	0.081	0.42	0.167	0.067	0.027	0.008
	h3	2.31	1.08	0.68	0.329	0.17	0.067	0.027	0.011	0.003
$\frac{\sigma}{W} = \frac{3}{4}$	h1	2.34	1.61	1.25	0.769	0.47	0.233	0.116	0.059	0.022
	h2	4.320	2.52	1.79	1.03	0.69	0.296	0.146	0.074	0.027
	h3	2.02	1.10	0.765	0.435	0.26	0.125	0.062	0.031	0.011
$\frac{\sigma}{W} = \frac{7}{8}$	h1	1.91	1.57	1.37	1.10	0.92	0.702			
	h2	4.29	2.75	2.14	1.55	1.23	0.921			
	h3	2.01	1.27	0.988	0.713	0.56	0.424			
Plane Stress										
$\frac{\sigma}{W} = \frac{1}{8}$	h1	3.58	4.55	5.06	5.30	4.96	4.14	3.29	2.60	1.92
	h2	5.15	5.43	6.05	6.01	5.47	4.46	3.48	2.74	2.02
	h3	26.10	21.60	18.00	12.70	9.24	5.98	3.94	2.72	2.00
$\frac{\sigma}{W} = \frac{1}{4}$	h1	3.14	3.26	2.920	2.120	1.53	0.96	0.615	0.40	0.23
	h2	4.67	4.30	3.700	2.530	1.76	1.05	0.656	0.419	0.237
	h3	10.10	6.49	4.360	2.190	1.24	0.63	0.362	0.224	0.123
$\frac{\sigma}{W} = \frac{3}{8}$	h1	2.81	2.37	1.940	1.370	1.01	0.677	0.474	0.324	0.226
	h2	4.47	3.43	2.630	1.690	1.18	0.762	0.524	0.372	0.244
	h3	5.05	2.65	1.600	0.812	0.525	0.328	0.223	0.157	0.102
$\frac{\sigma}{W} = \frac{1}{2}$	h1	2.46	1.67	1.250	0.776	0.510	0.286	0.164	0.0956	0.0469
	h2	4.37	2.73	1.91	1.09	0.694	0.380	0.216	0.124	0.0607
	h3	3.10	1.43	0.871	0.461	0.286	0.155	0.088	0.0506	0.0247
$\frac{\sigma}{W} = \frac{5}{8}$	h1	2.07	1.41	1.105	0.755	0.551	0.363	0.248	0.172	0.107
	h2	4.30	2.55	1.840	1.160	0.816	0.523	0.353	0.242	0.150
	h3	2.27	1.13	0.771	0.478	0.336	0.215	0.146	0.100	0.062
$\frac{\sigma}{W} = \frac{3}{4}$	h1	1.70	1.14	0.910	0.624	0.447	0.280	0.181	0.118	0.067
	h2	4.24	2.47	1.81	1.150	0.798	0.490	0.314	0.203	0.115
	h3	1.98	1.09	0.784	0.494	0.344	0.211	0.136	0.0581	0.0496
$\frac{\sigma}{W} = \frac{7}{8}$	h1	1.38	1.11	0.962	0.792	0.677	0.574			
	h2	4.22	2.68	2.08	1.54	1.27	1.04			
	h3	1.97	1.25	0.969	0.716	0.592	0.483			

- From EPRI report, for $a/W = 0.125$, and $n = 10$, $h_1 = 0.96$ Thus the fully plastic J is given by Eq. 14

$$\begin{aligned}
 J_p &= \alpha \varepsilon_y \sigma_y b g_1(a/W) h_1(a/W, n) (P/P_0)^{n+1} \\
 &= (1.0)(0.002)(414,000) \text{ kPa}(0.875) \text{ m} \frac{125}{1000} (0.96) \left(\frac{P}{8.42 \text{ MN}} \right)^{10+1} \\
 &= 5.76 \times 10^{-9} P^{11}
 \end{aligned}$$

where P in in MN, and J_{pl} in in kJ/m^2 .

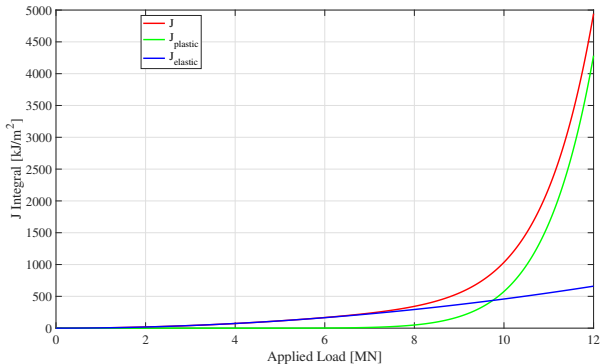
- K_I and the Elastic J are given by

$$\begin{aligned}
 K_I &= \left[1.12 - 0.23 \left(\frac{a}{W} \right) + 10.56 \left(\frac{a}{W} \right)^2 \right. \\
 &\quad \left. - 21.74 \left(\frac{a}{W} \right)^3 + 30.42 \left(\frac{a}{W} \right)^4 \right] \sigma \sqrt{\pi a} \\
 J_{el} &= \frac{K_I^2}{E} = G = \frac{1,000 P^2 (0.770)^2}{(0.025)^2 \text{ m}^2 (1.0) \text{ m} (207,000) \text{ MPa}} = 4.584 P^2
 \end{aligned}$$

where P in in MN, and J_{el} in in kJ/m^2 .

- The total J is

$$J = J_{el} + J_{pl} = 4.584P^2 + 5.76 \times 10^{-9}P^{11}$$



- Knowles and Stenberg have extended the definition of Rice's J integral to

$$J_k = \int \left\{ w n_k - t_i \frac{\partial u_i}{\partial x_k} \right\} d\Gamma$$

which is also path independent.

- When written in vector form, this gives

$$J_1 = \int_{\Gamma} \left(w dy - t \frac{\partial u}{\partial x} d\Gamma \right)$$

$$J_2 = \int_{\Gamma} \left(w dx - t \frac{\partial u}{\partial y} d\Gamma \right)$$

- Heller and Blackburn showed that

$$J = J_1 - iJ_2 = \frac{(1 + \nu)(1 + \kappa)}{4E} (K_I^2 + K_{II}^2 + 2iK_I K_{II})$$

- Thus the values of energy release rates (J₁ and J₂) for crack extensions parallel and perpendicular to the crack, respectively, will be given by:

$$J_1 = \frac{K_I^2 + K_{II}^2}{H}$$
$$J_2 = \frac{-2K_I K_{II}}{H}$$

where

$$H = E \text{ plane strain;}$$

$$H = \frac{E}{1 - \nu^2} \text{ plane stress}$$

- Convenient set of integrals to numerically determine the SIF's.

Compact Tension Specimen: Table 11.2, Fig. 11.14.

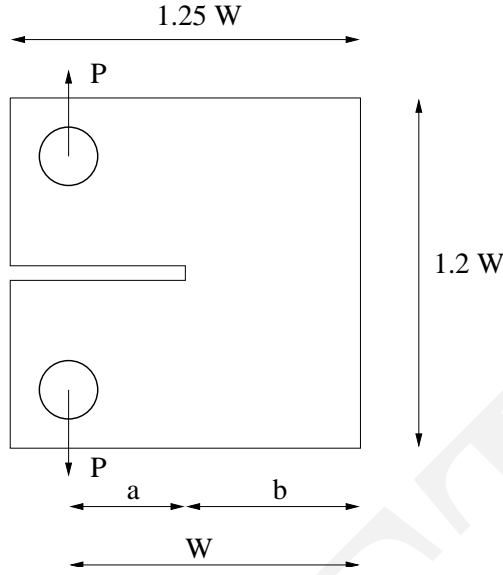


Figure 11.14: Compact tension Specimen

$$\text{Plane Strain } P_0 = 1.455\beta b\sigma_y \quad (11.70)$$

$$\text{Plane Stress } P_0 = 1.071\beta b\sigma_y \quad (11.71)$$

$$\beta = \sqrt{\left(2\frac{a}{b}\right)^2 + 4\frac{a}{b} + 2 - 2\frac{a}{b} - 1} \quad (11.72)$$

$$g_i = 1 \quad (11.73)$$

Δ corresponds to the crack opening displacement at the load line and δ is the crack mouth opening displacement.

Center Cracked Panel: Table 11.3, Fig. 11.15

$$\text{Plane Strain } P_0 = 4b\sigma_y/\sqrt{3} \quad (11.74)$$

$$\text{Plane Stress } P_0 = 2b\sigma_y \quad (11.75)$$

$$g_1 = g_4 = a/W \quad (11.76)$$

$$g_2 = g_3 = 1 \quad (11.77)$$

Δ corresponds to the average load-point displacement defined by

$$\Delta = \frac{1}{2W} \int_W^W [u_2(x_1, L) - u_2(x_1, L)] dx_1 \quad (11.78)$$

δ is the crack opening displacement at the center of the crack.

Single Edge Notched Specimen: Table 11.4, Fig. 11.16.

$$\text{Plane Strain } P_0 = 1.455\beta b\sigma_y \quad (11.79)$$

$$\text{Plane Stress } P_0 = 1.072\beta b\sigma_y \quad (11.80)$$

$$\beta = \sqrt{1 + \left(\frac{a}{b}\right)^2} - \frac{a}{b} \quad (11.81)$$

$$g_1 = g_4 = a/W \quad (11.82)$$

$$g_2 = g_3 = 1 \quad (11.83)$$

		$n = 1$	$n = 2$	$n = 3$	$n = 5$	$n = 7$	$n = 10$	$n = 13$	$n = 16$	$n = 20$
Plane Strain										
$\frac{a}{W} = \frac{1}{4}$	h1	2.23	2.05	1.78	1.48	1.33	1.26	1.25	1.32	1.57
	h2	17.9	12.5	11.7	10.9	10.5	10.7	11.5	12.6	14.6
	h3	9.85	8.51	8.17	7.77	7.71	7.92	8.52	9.31	10.9
$\frac{a}{W} = \frac{3}{8}$	h1	2.15	1.72	1.39	0.97	0.69	0.443	0.28	0.176	0.098
	h2	12.60	8.18	6.52	4.32	2.97	1.79	1.10	0.686	0.370
	h3	7.94	5.76	4.64	3.10	2.14	1.29	0.793	0.494	0.266
$\frac{a}{W} = \frac{1}{2}$	h1	1.94	1.51	1.24	0.919	0.68	0.461	0.314	0.216	0.132
	h2	9.33	5.85	4.30	2.75	1.91	1.20	0.788	0.530	0.370
	h3	6.41	4.27	3.16	2.02	1.41	0.998	0.585	0.393	0.236
$\frac{a}{W} = \frac{3}{4}$	h1	1.76	1.45	1.24	0.97	0.75	0.602	0.459	0.347	0.248
	h2	7.61	4.57	3.42	2.36	1.51	1.32	0.983	0.749	0.485
	h3	5.52	3.43	2.58	1.79	1.37	1.00	0.746	0.568	0.368
$\frac{a}{W} = \frac{3}{4}$	h1	1.71	1.42	1.26	1.03	0.86	0.717	0.575	0.448	0.345
	h2	6.37	3.95	3.18	2.34	1.89	1.440	1.120	0.887	0.665
	h3	4.86	3.05	2.46	1.81	1.45	1.110	0.869	0.686	0.514
$\frac{a}{W} \approx 1$	h1	1.57	1.45	1.35	1.18	1.08	0.95	0.85	0.73	0.63
	h2	5.39	3.74	3.09	2.43	2.12	1.80	1.57	1.33	1.14
	h3	4.31	2.99	2.47	1.95	1.79	1.44	1.26	1.07	0.909
Plane Stress										
$\frac{a}{W} = \frac{1}{4}$	h1	1.61	1.460	1.28	1.06	0.90	0.729	0.601	0.511	0.395
	h2	17.60	12.00	10.70	8.74	7.32	5.74	4.63	3.75	2.92
	h3	9.67	8.00	7.21	5.94	5.00	3.95	3.19	2.59	2.023
$\frac{a}{W} = \frac{3}{8}$	h1	1.55	1.25	1.050	0.801	0.64	0.484	0.377	0.284	0.22
	h2	12.40	8.20	6.540	4.56	3.45	2.44	1.83	1.36	1.02
	h3	7.80	5.73	4.620	3.250	2.48	1.77	1.33	0.99	0.746
$\frac{a}{W} = \frac{1}{2}$	h1	1.40	1.08	0.901	0.686	0.55	0.436	0.356	0.298	0.238
	h2	9.16	5.67	4.21	2.80	2.12	1.57	1.25	1.03	0.814
	h3	6.29	4.15	3.11	2.09	1.59	1.18	0.938	0.774	0.614
$\frac{a}{W} = \frac{3}{4}$	h1	1.27	1.03	0.875	0.695	0.59	0.494	0.423	0.37	0.310
	h2	7.470	4.48	3.35	2.37	1.92	1.540	1.29	1.12	0.928
	h3	5.42	3.38	2.54	1.80	1.47	1.180	0.988	0.853	0.710
$\frac{a}{W} = \frac{3}{4}$	h1	1.23	0.977	0.833	0.683	0.59	0.506	0.431	0.373	0.314
	h2	6.25	3.78	2.89	2.14	1.78	1.440	1.20	1.03	0.857
	h3	4.77	2.92	2.24	1.66	1.38	1.120	0.936	0.80	0.666
$\frac{a}{W} \approx 1$	h1	1.130	1.01	0.775	0.68	0.65	0.620	0.490	0.47	0.42
	h2	5.29	3.54	2.41	1.91	1.73	1.59	1.23	1.17	1.03
	h3	4.23	2.83	1.93	1.52	1.39	1.270	0.985	0.933	0.824

Table 11.2: h -Functions for Standard ASTM Compact Tension Specimen, (Kumar et al., 1981)

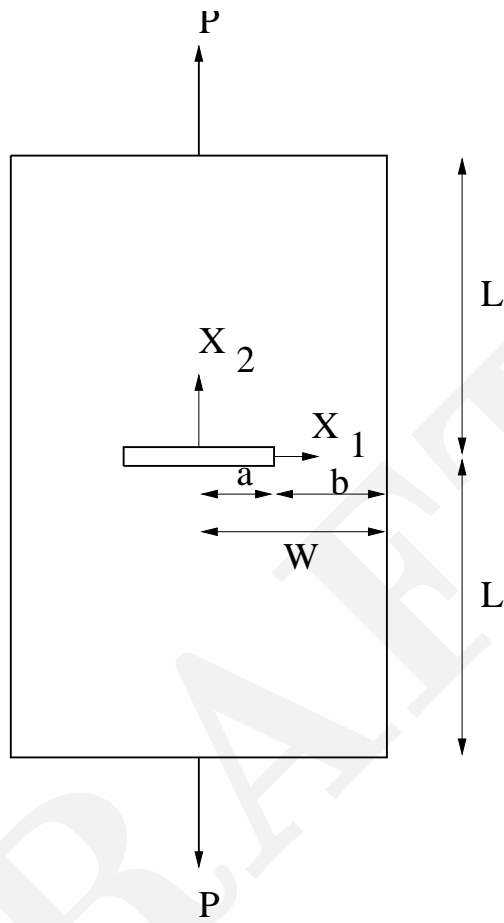


Figure 11.15: Center Cracked Panel

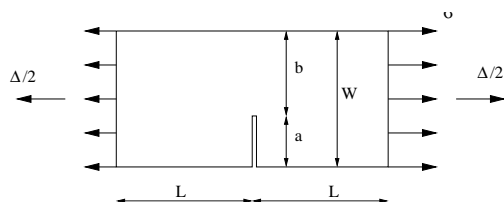


Figure 11.16: Single Edge Notched Specimen

		$n = 1$	$n = 2$	$n = 3$	$n = 5$	$n = 7$	$n = 10$	$n = 13$	$n = 16$	$n = 20$
Plane Strain										
$\frac{a}{W} = \frac{1}{8}$	h1	2.80	3.61	4.06	4.35	4.33	4.02	3.56	3.06	2.46
	h2	3.05	3.62	3.91	4.06	3.93	3.54	3.07	2.60	2.06
	h3	0.303	0.574	0.84	1.30	1.63	1.95	2.03	1.96	1.77
$\frac{a}{W} = \frac{1}{4}$	h1	2.54	3.01	3.21	3.29	3.18	2.92	2.63	2.34	2.03
	h2	2.68	2.99	3.01	2.85	2.61	2.30	1.00	1.71	1.45
	h3	0.536	0.911	1.22	1.64	1.84	1.85	1.80	1.64	1.43
$\frac{a}{W} = \frac{3}{8}$	h1	2.340	2.62	2.65	2.51	2.28	1.97	1.71	1.46	1.19
	h2	2.350	2.39	2.23	1.88	1.58	1.28	1.07	0.89	0.715
	h3	0.699	1.06	1.28	1.44	1.40	1.23	1.05	0.888	0.719
$\frac{a}{W} = \frac{1}{2}$	h1	2.21	2.29	2.20	1.97	1.76	1.52	1.32	1.16	0.978
	h2	2.030	1.860	1.60	1.23	1.00	0.799	0.664	0.564	0.466
	h3	0.803	1.07	1.16	1.10	0.96	0.796	0.665	0.565	0.469
$\frac{a}{W} = \frac{3}{4}$	h1	2.12	1.96	1.76	1.43	1.17	0.863	0.628	0.458	0.300
	h2	1.71	1.320	1.04	0.707	0.52	0.358	0.250	0.178	0.114
	h3	0.844	0.937	0.879	0.701	0.52	0.361	0.251	0.178	0.115
$\frac{a}{W} = \frac{3}{4}$	h1	2.070	1.73	1.47	1.11	0.89	0.642	0.461	0.337	0.216
	h2	1.350	0.857	0.596	0.361	0.25	0.167	0.114	0.081	0.0511
	h3	805	0.70	0.555	0.359	0.25	0.168	0.114	0.081	0.052
$\frac{a}{W} = \frac{7}{8}$	h1	2.08	1.64	1.40	1.14	0.98	0.814	0.688	0.573	0.461
	h2	0.889	0.428	0.287	0.181	0.13	0.105	0.084	0.068	0.0533
	h3	0.632	0.400	0.291	0.182	0.14	0.106	0.084	0.068	0.054
Plane Stress										
$\frac{a}{W} = \frac{1}{8}$	h1	2.80	3.57	4.01	4.47	4.65	4.62	4.41	4.13	3.72
	h2	3.530	4.09	4.43	4.74	4.79	4.63	4.33	4.00	3.55
	h3	0.350	0.661	1.00	1.55	2.05	2.56	2.83	2.95	2.92
$\frac{a}{W} = \frac{1}{4}$	h1	2.54	2.97	3.14	3.20	3.11	2.86	2.65	2.47	2.20
	h2	3.100	3.29	3.30	3.15	2.93	2.56	2.29	2.08	1.81
	h3	0.619	1.01	1.35	1.83	2.08	2.19	2.12	2.01	1.79
$\frac{a}{W} = \frac{3}{8}$	h1	2.340	2.53	2.52	2.35	2.17	1.95	1.77	1.61	1.43
	h2	2.710	2.62	2.41	2.03	1.75	1.47	1.28	1.13	0.988
	h3	0.807	1.20	1.43	1.59	1.57	1.43	1.27	1.13	0.994
$\frac{a}{W} = \frac{1}{2}$	h1	2.210	2.20	2.06	1.81	1.63	1.43	1.30	1.17	1.00
	h2	2.340	2.01	1.70	1.30	1.07	0.871	0.757	0.666	0.557
	h3	0.927	1.19	1.26	1.18	1.04	0.867	0.758	0.668	0.560
$\frac{a}{W} = \frac{3}{4}$	h1	2.12	1.91	1.69	1.41	1.22	1.01	0.853	0.712	0.573
	h2	1.970	1.46	1.13	0.785	0.61	0.474	0.383	0.313	0.256
	h3	0.975	1.05	0.97	0.763	0.62	0.478	0.386	0.318	0.273
$\frac{a}{W} = \frac{3}{4}$	h1	2.07	1.71	1.46	1.21	1.08	0.867	0.745	0.646	0.532
	h2	1.550	0.97	0.685	0.452	0.36	0.262	0.216	0.183	0.148
	h3	0.929	0.802	0.642	0.45	0.36	0.263	0.216	0.183	0.149
$\frac{a}{W} = \frac{7}{8}$	h1	2.08	1.57	1.31	1.08	0.97	0.862	0.778	0.715	0.630
	h2	1.030	0.485	0.31	0.196	0.15	0.127	0.109	0.0971	0.0842
	h3	0.730	0.452	0.313	0.198	0.15	0.127	0.109	0.0973	0.0842

Table 11.3: Plane Stress h -Functions for a Center-Cracked Panel, (Kumar et al., 1981)

Δ is the load-point displacement at the centerline of the specimen, and δ is the crack mouth opening displacement.

		$n = 1$	$n = 2$	$n = 3$	$n = 5$	$n = 7$	$n = 10$	$n = 13$	$n = 16$	$n = 20$
Plane Strain										
$\frac{a}{W} = \frac{1}{8}$	h1	4.95	6.93	8.57	11.50	13.5	16.1	18.1	19.9	21.2
	h2	5.250	6.47	7.56	9.46	11.1	12.9	14.4	15.7	16.8
	h3	26.60	25.80	25.20	24.20	23.6	23.2	23.2	23.5	23.7
$\frac{a}{W} = \frac{1}{4}$	h1	4.34	4.77	4.64	3.82	3.06	2.170	1.55	1.11	0.712
	h2	4.760	4.56	4.28	3.39	2.64	1.910	1.25	0.875	0.552
	h3	10.30	7.64	5.87	3.70	2.48	1.500	0.97	0.654	0.404
$\frac{a}{W} = \frac{3}{8}$	h1	3.88	3.25	2.63	1.68	1.06	0.539	0.276	0.142	0.060
	h2	4.540	3.49	2.67	1.57	0.94	0.458	0.229	0.116	0.048
	h3	5.14	2.99	1.90	0.923	0.51	0.240	0.119	0.060	0.025
$\frac{a}{W} = \frac{1}{2}$	h1	3.40	2.30	1.69	0.928	0.51	0.213	0.090	0.039	0.012
	h2	4.450	2.77	1.89	0.954	0.50	0.204	0.085	0.036	0.011
	h3	3.15	1.54	0.91	0.417	0.21	0.085	0.036	0.015	0.004
$\frac{a}{W} = \frac{5}{8}$	h1	2.86	1.80	1.30	0.697	0.37	0.153	0.064	0.026	0.008
	h2	4.370	2.44	1.62	0.681	0.42	0.167	0.067	0.027	0.008
	h3	2.31	1.08	0.68	0.329	0.17	0.067	0.027	0.011	0.003
$\frac{a}{W} = \frac{3}{4}$	h1	2.34	1.61	1.25	0.769	0.47	0.233	0.116	0.059	0.022
	h2	4.320	2.52	1.79	1.03	0.69	0.296	0.146	0.074	0.027
	h3	2.02	1.10	0.765	0.435	0.26	0.125	0.062	0.031	0.011
$\frac{a}{W} = \frac{7}{8}$	h1	1.91	1.57	1.37	1.10	0.92	0.702			
	h2	4.29	2.75	2.14	1.55	1.23	0.921			
	h3	2.01	1.27	0.988	0.713	0.56	0.424			
Plane Stress										
$\frac{a}{W} = \frac{1}{8}$	h1	3.58	4.55	5.06	5.30	4.96	4.14	3.29	2.60	1.92
	h2	5.15	5.43	6.05	6.01	5.47	4.46	3.48	2.74	2.02
	h3	26.10	21.60	18.00	12.70	9.24	5.98	3.94	2.72	2.00
$\frac{a}{W} = \frac{1}{4}$	h1	3.14	3.26	2.920	2.120	1.53	0.96	0.615	0.40	0.23
	h2	4.67	4.30	3.700	2.530	1.76	1.05	0.656	0.419	0.237
	h3	10.10	6.49	4.360	2.190	1.24	0.63	0.362	0.224	0.123
$\frac{a}{W} = \frac{3}{8}$	h1	2.81	2.37	1.940	1.370	1.01	0.677	0.474	0.342	0.226
	h2	4.47	3.43	2.630	1.690	1.18	0.762	0.524	0.372	0.244
	h3	5.05	2.65	1.600	0.812	0.525	0.328	0.223	0.157	0.102
$\frac{a}{W} = \frac{1}{2}$	h1	2.46	1.67	1.250	0.776	0.510	0.286	0.164	0.0956	0.0469
	h2	4.37	2.73	1.91	1.09	0.694	0.380	0.216	0.124	0.0607
	h3	3.10	1.43	0.871	0.461	0.286	0.155	0.088	0.0506	0.0247
$\frac{a}{W} = \frac{5}{8}$	h1	2.07	1.41	1.105	0.755	0.551	0.363	0.248	0.172	0.107
	h2	4.30	2.55	1.840	1.160	0.816	0.523	0.353	0.242	0.150
	h3	2.27	1.13	0.771	0.478	0.336	0.215	0.146	0.100	0.062
$\frac{a}{W} = \frac{3}{4}$	h1	1.70	1.14	0.910	0.624	0.447	0.280	0.181	0.118	0.067
	h2	4.24	2.47	1.81	1.150	0.798	0.490	0.314	0.203	0.115
	h3	1.98	1.09	0.784	0.494	0.344	0.211	0.136	0.0581	0.0496
$\frac{a}{W} = \frac{7}{8}$	h1	1.38	1.11	0.962	0.792	0.677	0.574			
	h2	4.22	2.68	2.08	1.54	1.27	1.04			
	h3	1.97	1.25	0.969	0.716	0.592	0.483			

Table 11.4: h -Functions for Single Edge Notched Specimen, (Kumar et al., 1981)

Double Edge Notched Specimen: Table 11.5, Fig. 11.17.

$$\text{Plane Strain } P_0 = (0.72W + 1.82b)\sigma_y \tag{11.84}$$

$$\text{Plane Stress } P_0 = 4b\sigma_y/\sqrt{3} \tag{11.85}$$

$$\beta = \sqrt{1 + \left(\frac{a}{b}\right)^2} - \frac{a}{b} \tag{11.86}$$

$$g_1 = g_4 = 1 \tag{11.87}$$

$$g_2 = g_3 = W/a - 1 \tag{11.88}$$

Δ is the load-point displacement at the centerline of the specimen, and δ is the crack mouth opening displacement.

Axially Cracked Pressurized Cylinder: Table ??, Fig. 11.18.

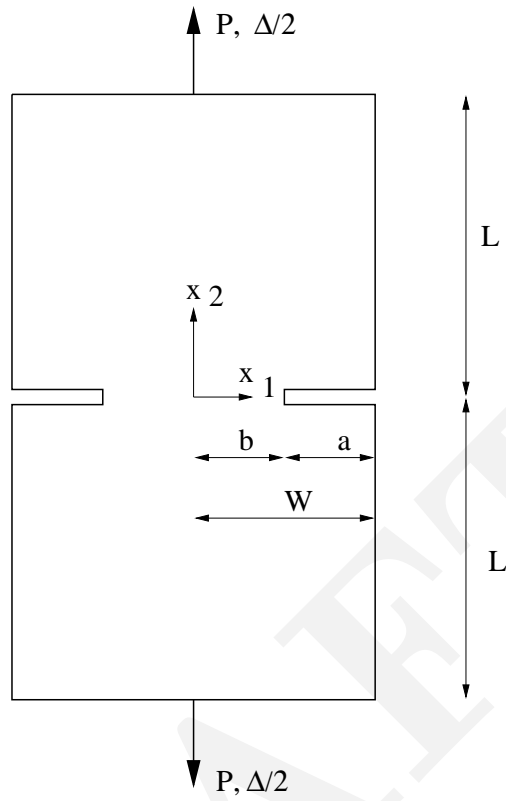


Figure 11.17: Double Edge Notched Specimen

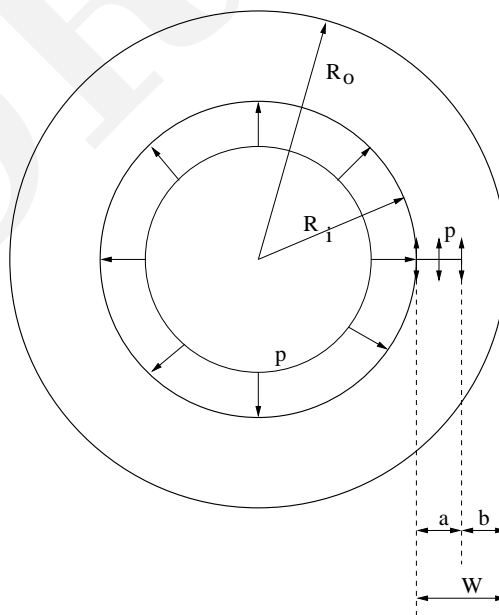


Figure 11.18: Axially Cracked Pressurized Cylinder

		$n = 1$	$n = 2$	$n = 3$	$n = 5$	$n = 7$	$n = 10$	$n = 13$	$n = 16$	$n = 20$
Plane Strain										
$\frac{a}{W} = \frac{1}{8}$	h1	0.572	0.772	0.922	1.13	1.35	1.61	1.86	2.09	2.44
	h2	0.732	0.852	0.961	1.14	1.29	1.50	1.70	1.94	2.17
	h3	0.063	0.126	0.200	0.372	0.57	0.911	1.30	1.74	2.29
$\frac{a}{W} = \frac{1}{4}$	h1	1.10	1.320	1.38	1.65	1.75	1.82	1.86	1.89	1.92
	h2	1.56	1.63	1.70	1.79	1.80	1.81	1.79	1.78	1.76
	h3	0.267	0.479	0.698	1.11	1.47	1.92	2.25	2.49	2.73
$\frac{a}{W} = \frac{3}{8}$	h1	1.61	1.83	1.92	1.92	1.84	1.68	1.49	1.32	1.12
	h2	2.51	2.41	2.35	2.15	1.94	1.68	1.44	1.25	1.05
	h3	0.637	1.05	1.40	1.87	2.11	2.20	2.09	1.92	1.67
$\frac{a}{W} = \frac{1}{2}$	h1	2.22	2.43	2.49	2.43	2.32	2.12	1.91	1.60	1.51
	h2	3.73	3.40	3.15	2.70	2.37	2.01	1.72	1.40	1.38
	h3	1.26	1.92	2.37	2.79	2.85	2.68	2.40	1.99	1.94
$\frac{a}{W} = \frac{5}{8}$	h1	3.16	3.38	3.45	3.42	3.28	3.00	2.54	2.36	2.27
	h2	5.57	4.76	4.23	3.46	2.97	2.48	2.02	1.82	1.66
	h3	2.36	3.29	3.74	3.90	3.68	3.23	2.66	2.40	2.19
$\frac{a}{W} = \frac{3}{4}$	h1	5.24	6.29	7.17	8.44	9.46	10.90	119.0	11.3	17.4
	h2	9.10	7.76	7.14	6.64	6.83	7.48	7.790	7.14	11.0
	h3	4.73	6.26	7.03	7.63	8.14	9.04	9.4	8.58	13.5
$\frac{a}{W} = \frac{7}{8}$	h1	14.2	24.8	39.0	78.4	140.	341.0	777.0	1570.0	3820.0
	h2	20.1	19.4	22.7	36.1	58.9	133.0	294.0	585.0	1400.0
	h3	12.7	18.2	24.1	40.4	65.9	149.0	327.0	650.0	1560.0
Plane Stress										
$\frac{a}{W} = \frac{1}{8}$	h1	0.583	0.825	1.02	1.37	1.71	2.24	2.84	3.54	4.62
	h2	0.853	1.050	1.23	1.55	1.87	2.38	2.96	3.65	4.70
	h3	0.0729	0.159	0.26	0.504	0.82	1.41	2.18	3.16	4.73
$\frac{a}{W} = \frac{1}{4}$	h1	1.01	1.23	1.36	1.48	1.54	1.58	1.59	1.59	1.59
	h2	1.73	1.82	1.89	1.92	1.91	1.85	1.80	1.75	1.70
	h3	0.296	0.537	0.77	1.17	1.49	1.82	2.02	2.12	2.20
$\frac{a}{W} = \frac{3}{8}$	h1	1.29	1.42	1.43	1.34	1.24	1.09	0.97	0.873	0.674
	h2	2.59	2.39	2.22	1.86	1.59	1.28	1.07	0.922	0.709
	h3	658	1.04	1.30	1.52	1.55	1.41	1.23	1.07	0.830
$\frac{a}{W} = \frac{1}{2}$	h1	1.48	1.47	1.38	1.17	1.01	0.845	0.732	0.625	0.208
	h2	3.51	2.82	2.34	1.67	1.28	0.944	0.762	0.630	0.232
	h3	1.18	1.58	1.69	1.56	1.32	1.01	0.809	0.662	0.266
$\frac{a}{W} = \frac{5}{8}$	h1	1.59	1.45	1.29	1.04	0.88	0.737	0.649	0.466	0.020
	h2	4.56	3.15	2.32	1.45	1.06	0.790	0.657	0.473	0.028
	h3	1.93	2.14	1.95	1.44	1.09	0.809	0.665	0.487	0.032
$\frac{a}{W} = \frac{3}{4}$	h1	1.65	1.43	1.22	0.979	0.83	0.701	0.630	0.297	
	h2	5.90	3.37	2.22	1.30	0.96	0.741	0.636	0.312	
	h3	3.06	2.67	2.06	1.31	0.97	0.747	0.638	0.318	
$\frac{a}{W} = \frac{7}{8}$	h1	1.69	1.43	1.22	0.979	0.84	0.738	0.664	0.614	0.562
	h2	8.02	3.51	2.14	1.27	0.97	0.775	0.663	0.596	0.535
	h3	5.07	3.180	2.16	1.30	0.98	0.779	0.665	0.597	0.538

Table 11.5: h -Functions for Double Edge Notched Specimen, (Kumar et al., 1981)

$$p_0 = \frac{2b\sigma_y}{\sqrt{3}R_c} \tag{11.89}$$

$$R_c = R_i + a \tag{11.90}$$

$$g_1 = \frac{a}{W} \tag{11.91}$$

$$g_2 = 1 \tag{11.92}$$

δ is the crack mouth opening displacement. Note that in the elastic range:

$$K_I = \frac{2pR_0^2\sqrt{\pi a}}{R_0^2 - R_i^2} F\left(\frac{a}{W}, \frac{R_i}{R_0}\right) \tag{11.93}$$

$$\delta_e = \frac{8pR_0^2 a}{(R_0^2 - R_i^2)E'} V\left(\frac{a}{W}, \frac{R_i}{R_0}\right) \tag{11.94}$$

where the dimensionless functions F and V are tabulated in Table 11.7.

		$n = 1$	$n = 2$	$n = 3$	$n = 5$	$n = 7$	$n = 10$
$\frac{W}{R_i} = \frac{1}{5}$							
$\frac{a}{W} = \frac{1}{8}$	h1	6.32	7.93	9.32	11.50	13.1	14.94
	h2	5.83	7.01	7.96	9.49	10.6	11.96
$\frac{a}{W} = \frac{1}{4}$	h1	7.00	9.34	9.03	9.59	9.71	9.45
	h2	5.92	8.72	7.07	7.26	7.14	6.71
$\frac{a}{W} = \frac{1}{2}$	h1	9.79	10.37	9.07	5.61	3.52	2.11
	h2	7.05	6.97	6.01	3.70	2.28	1.25
$\frac{a}{W} = \frac{3}{4}$	h1	11.00	5.54	2.84	1.24	0.83	0.493
	h2	7.35	3.86	1.86	0.56	0.26	0.129
$\frac{W}{R_i} = \frac{1}{10}$							
$\frac{a}{W} = \frac{1}{8}$	h1	5.22	6.64	7.59	8.76	9.34	9.55
	h2	5.31	6.25	6.88	7.65	8.02	8.09
$\frac{a}{W} = \frac{1}{4}$	h1	6.16	7.49	7.96	8.08	7.78	6.98
	h2	5.56	6.31	6.52	6.40	6.01	5.27
$\frac{a}{W} = \frac{1}{2}$	h1	10.5	11.6	10.7	6.47	3.95	2.27
	h2	7.48	7.72	7.01	4.29	2.58	1.37
$\frac{a}{W} = \frac{3}{4}$	h1	16.10	8.19	3.87	1.46	1.05	0.787
	h2	9.57	5.40	2.57	0.71	0.37	0.232
$\frac{W}{R_i} = \frac{1}{20}$							
$\frac{a}{W} = \frac{1}{8}$	h1	4.50	5.79	6.62	7.65	8.07	7.75
	h2	4.96	5.71	6.20	6.82	7.02	6.66
$\frac{a}{W} = \frac{1}{4}$	h1	5.57	6.91	7.37	7.47	7.21	6.53
	h2	5.29	5.98	6.16	6.01	5.63	4.93
$\frac{a}{W} = \frac{1}{2}$	h1	10.80	12.80	12.80	8.16	4.88	2.62
	h2	7.66	8.33	8.13	5.33	3.20	1.65
$\frac{a}{W} = \frac{3}{4}$	h1	23.10	13.10	5.87	1.90	1.23	0.883
	h2	12.10	7.88	3.84	1.01	0.45	0.24

Table 11.6: h -Functions for an Internally Pressurized, Axially Cracked Cylinder, (Kumar et al., 1981)

		$\frac{a}{W} = \frac{1}{8}$	$\frac{a}{W} = \frac{1}{4}$	$\frac{a}{W} = \frac{1}{2}$	$\frac{a}{W} = \frac{3}{4}$
$\frac{W}{R_I} = \frac{1}{5}$	F	1.19	1.38	2.10	3.30
	V_1	1.51	1.83	3.44	7.50
$\frac{W}{R_I} = \frac{1}{10}$	F	1.20	1.44	2.36	4.23
	V_1	1.54	1.91	3.96	10.40
$\frac{W}{R_I} = \frac{1}{20}$	F	1.20	1.45	2.51	5.25
	V_1	1.54	1.92	4.23	13.50

Table 11.7: F and V_1 for Internally Pressurized, Axially Cracked Cylinder, (Kumar et al., 1981)

Circumferentially Cracked Cylinder: Table 11.8, Fig. 11.19.

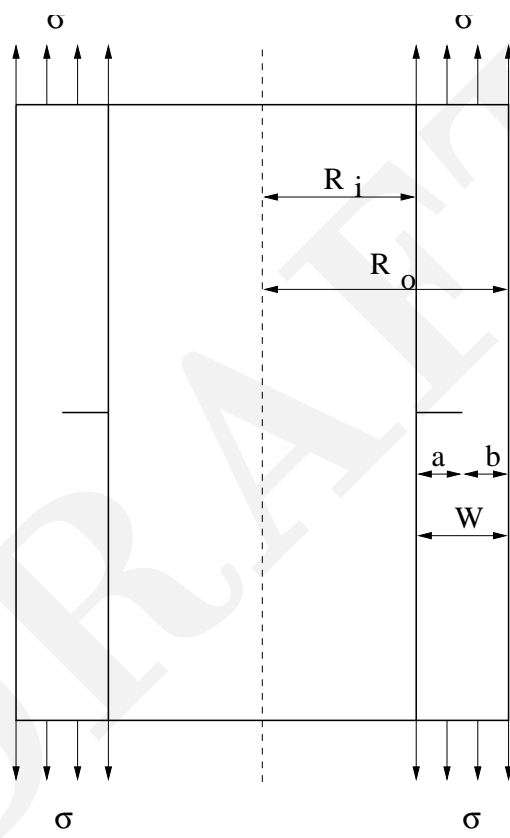


Figure 11.19: Circumferentially Cracked Cylinder

$$P_0 = \frac{2\pi\sigma_y(R_0^2 - R_i^2)}{\sqrt{3}} \tag{11.95}$$

$$R_c = R_i + a \tag{11.96}$$

$$g_1 = g_4 = \frac{a}{W} \tag{11.97}$$

$$g_2 = g_3 = 1 \tag{11.98}$$

δ is the crack mouth opening displacement.

In the elastic range

$$K_I = \sigma\sqrt{\pi a}F\left(\frac{a}{W}, \frac{R_i}{R_0}\right) \tag{11.99}$$

$$\delta_e = \frac{4\sigma a V_1\left(\frac{a}{W}, \frac{R_i}{R_0}\right)}{E'} \tag{11.100}$$

$$\Delta_{ce} = \frac{4\sigma a V_2\left(\frac{a}{W}, \frac{R_i}{R_0}\right)}{E'} \tag{11.101}$$

where the functions F , V_1 , and V_2 are tabulated in Table 11.9.

		$n = 1$	$n = 2$	$n = 3$	$n = 5$	$n = 7$	$n = 10$
		$\frac{W}{R_i} = \frac{1}{5}$					
$\frac{a}{W} = \frac{1}{8}$	h1	3.78	5.00	5.94	7.54	8.99	11.1
	h2	4.560	5.55	6.37	7.79	9.10	11.0
	h3	0.369	0.70	1.07	1.96	3.04	4.94
$\frac{a}{W} = \frac{1}{4}$	h1	3.88	4.95	5.64	6.49	6.94	7.22
	h2	4.40	5.12	5.57	6.07	6.28	6.30
	h3	0.673	1.25	1.79	2.79	3.61	4.52
$\frac{a}{W} = \frac{1}{2}$	h1	4.40	4.78	4.59	3.79	3.07	2.34
	h2	4.36	4.30	3.91	3.00	2.26	1.55
	h3	1.33	1.93	2.21	2.23	1.94	1.46
$\frac{a}{W} = \frac{3}{4}$	h1	4.12	3.03	2.23	1.546	1.30	1.110
	h2	3.46	2.19	1.36	0.638	0.43	0.325
	h3	1.54	1.39	1.04	0.686	0.50	0.366
		$\frac{W}{R_i} = \frac{1}{10}$					
$\frac{a}{W} = \frac{1}{8}$	h1	4.00	5.13	6.09	7.69	9.09	11.1
	h2	4.71	5.63	6.45	7.85	9.09	10.9
	h3	0.548	0.733	1.13	2.07	3.16	5.07
$\frac{a}{W} = \frac{1}{4}$	h1	4.17	5.35	6.09	6.93	7.30	7.41
	h2	4.58	5.36	5.84	6.31	6.44	6.31
	h3	757	1.35	1.93	2.96	3.78	4.60
$\frac{a}{W} = \frac{1}{2}$	h1	5.40	5.90	5.63	4.51	3.49	2.47
	h2	4.99	5.01	4.59	3.48	2.56	1.67
	h3	1.555	2.26	2.59	2.57	2.18	1.56
$\frac{a}{W} = \frac{3}{4}$	h1	5.18	3.78	2.57	1.59	1.31	1.10
	h2	4.22	2.79	1.67	0.725	0.48	0.30
	h3	1.86	1.73	1.26	0.775	0.56	0.36
		$\frac{W}{R_i} = \frac{1}{20}$					
$\frac{a}{W} = \frac{1}{8}$	h1	4.04	5.23	6.22	7.82	9.19	11.1
	h2	4.82	5.69	6.52	7.90	9.11	10.8
	h3	0.68	0.76	1.17	2.13	3.23	5.12
$\frac{a}{W} = \frac{1}{4}$	h1	4.39	5.68	6.45	7.29	7.62	7.65
	h2	4.71	5.56	6.05	6.51	6.59	6.39
	h3	0.82	1.43	2.03	3.10	3.91	4.69
$\frac{a}{W} = \frac{1}{2}$	h1	6.55	7.17	6.89	5.46	4.13	2.77
	h2	5.67	5.77	5.36	4.08	2.97	1.88
	h3	1.80	2.59	2.99	2.98	2.50	1.74
$\frac{a}{W} = \frac{3}{4}$	h1	6.64	4.87	3.08	1.68	1.30	1.07
	h2	5.18	3.57	2.07	0.808	0.47	0.316
	h3	2.36	2.18	1.53	0.772	0.49	0.330

Table 11.8: h -Functions for a Circumferentially Cracked Cylinder in Tension, (Kumar et al., 1981)

11.9.2 Numerical Example

From (Anderson, 1995), Consider a single edge notched panel with $W = 1$ m, $a = 125$ mm. Determine J in terms of the applied load assuming plane stress conditions, neglect plastic zone correction.

Fatigue Crack propagation

Victor E. Saouma

`saouma@colorado.edu`

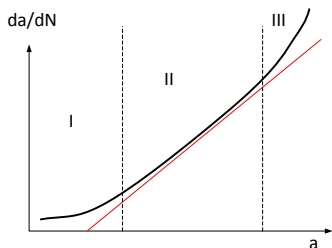
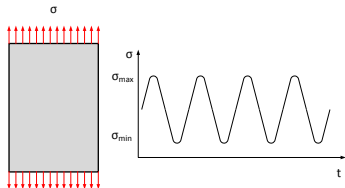
University of Colorado, Boulder

Spring 2022

- 1 Introduction
- 2 Experimental Observation
- 3 Fatigue Laws Under Constant Amplitude Loading
 - Paris Law
 - Forman; Walker Laws
- 4 Examples
 - Example 1
 - Example 2
- 5 Effective Stress Intensity Factor Range
- 6 Variable Amplitude Loading with Load Interaction
 - No Load Interactions
 - Load Interactions; Retardation Models
 - Wheeler's Model
 - Generalized Willenborg's Model

Introduction

- Crack propagation occurs for critical crack lengths a_{cr} .
- **Subcritical crack growth** may occur for $a < a_{cr}$ under two conditions: Crack subjected to either **fatigue** (i.e. cyclic) loading or **corrosive** environment.
- Thus an important question that arises is **how long (i.e. how many cycles) would it be before this subcritical crack of length a_i grows to reach a critical size a_{cr} and thus trigger failure?** in order to predict the minimum fatigue life and to establish safe inspection intervals.



- A plate that has no crack subjected to a series of repeated loading, three distinct stages:
 - 1 Stage 1 : **Micro coalescence of voids** and formation of microcracks. Difficult to capture, realm of **metallurgists** or material scientists, compared to stage II and III by far the longest.
 - 2 Stage II: Micro crack of finite size was formed, its SIF well below K_{Ic} , ($K \ll K_{Ic}$), and **crack growth occurs after each cycle of loading**.
 - 3 Stage III: Crack has reached a size a such that $a = a_c$, thus **rapid unstable crack growth** occurs.
- Primarily be **concerned by stage II**.

- First (and most widely used) fracture mechanics-based model for fatigue crack growth: **Paris Law** early '60s.
- **Empirical law** based on experimental observations. Most other empirical laws are direct extensions, or refinements.

$$\frac{da}{dN} = C (\Delta K)^n$$

Straight line on a log-log plot of $\frac{da}{dN}$ vs ΔK , and

$$\Delta K = K_{max} - K_{min} = (\sigma_{max} - \sigma_{min})f(g)\sqrt{\pi a}$$

a a crack length; N the number of load cycles; C the intercept of line along $\frac{da}{dN}$ (of the order of 10^{-6}) units of $m/cycle/(MPa\sqrt{m})^n$; n is the slope of the line and ranges from 2 to 10. **C and n are experimentally determined.** Very expensive test.

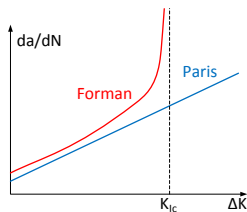
- Paris law can be rewritten as :

$$\Delta N = \frac{\Delta a}{C [\Delta K(a)]^n}$$

or

$$N = \int dN = \int_{a_i}^{a_f} \frac{da}{C [\Delta K(a)]^n}$$

- Small error in the SIF calculations would be magnified greatly as n ranges from 2 to 6.
- Analytical solutions for SIF often do not exist resulting in large approximation errors. More reliable numerical solutions should be used.



- When compared with experimental data, it is evident that Paris law does not account for:

- Increase in crack growth rate as K_{max} approaches K_{Ic}
- Slow increase in crack growth at $K_{min} \approx K_{th}$

thus it was **modified by Forman**

$$\frac{da}{dN} = \frac{C(\Delta K)^n}{(1-R)K_c - \Delta K}$$

- Walker's model** is yet another variation of Paris Law which accounts for the **stress ratio** $R = \frac{K_{min}}{K_{max}} = \frac{\sigma_{min}}{\sigma_{max}}$

$$\frac{da}{dN} = C \left[\frac{\Delta K}{(1-R)^{(1-m)}} \right]^n$$

An aircraft flight produces 10 gusts per flight (between take-off and landing). It has two flights per day. Each gust has a $\sigma_{max} = 200$ MPa and $\sigma_{min} = 50$ MPa. The aircraft is made up of aluminum which has $R = 15$ kJ/m² $E = 70$ GPa $C = 5 \times 10^{-11}$ m/cycle, and $n = 3$. The smallest detectable flaw is 4 mm. **How long would it be before the crack will propagate to its critical length?**

- Assuming $K = \sigma\sqrt{\pi a}$ and $K_{Ic} = \sqrt{ER}$, then $a_c = \frac{K_c^2}{\sigma_{max}^2 \pi} = \frac{ER}{\sigma_{max}^2 \pi}$ or

$$a_c = \frac{(70 \times 10^9)(15 \times 10^3)}{(200 \times 10^6)^2 \pi} = 0.0084 \text{ m} = \mathbf{8.4 \text{ mm}}$$

$$\begin{aligned} \Rightarrow N &= \int_{a_i}^{a_f} \frac{da}{C[\Delta K(a)]^n} = \int_{a_i}^{a_f} \frac{da}{C \underbrace{(\sigma_{max} - \sigma_{min})^n}_{(\Delta \sigma)^n} ((\pi a)^{\frac{1}{2}})^n} \\ &= \int_{4 \times 10^{-3}}^{8.4 \times 10^{-3}} \frac{da}{\underbrace{(5 \times 10^{-11})}_C \underbrace{(200 - 50)^3}_{(\Delta \sigma)^3} \underbrace{(\pi a)^{1.5}}_{((\pi a)^{\cdot 5})^3}} = 1064 \int_{.004}^{.0084} a^{-1.5} da \\ &= -2128 a^{-.5} \Big|_{.004}^{.0084} = 2128 \left[-\frac{1}{\sqrt{.0084}} + \frac{1}{\sqrt{.004}} \right] \\ &= \mathbf{10,428 \text{ cycles}} \end{aligned}$$

thus the time t will be: $t = (10,428) \text{ cycles} \times \frac{1}{10} \frac{\text{flight}}{\text{cycle}} \times \frac{1}{2} \frac{\text{day}}{\text{flight}} \times \frac{1}{30} \frac{\text{month}}{\text{day}}$
 $\approx 17.38 \text{ month} \approx 1.5 \text{ years.}$

- If a longer lifetime is desired, then we can:
 - Employ a **different material with higher K_{Ic}** , so as to increase the critical crack length a_c at instability;
 - **reduce the maximum value of the stress σ_{max} .**
 - **reduce the stress range $\Delta\sigma$;**
 - **improve the inspection** so as to reduce the assumed initial crack length a_{min} .

Repeat the previous problem except that more sophisticated (and expensive) NDT equipment is available with a resolution of .1 mm thus $a_i = .1\text{mm}$

- $t = 2128 \left[-\frac{1}{\sqrt{.0084}} + \frac{1}{\sqrt{.0001}} \right] = 184,583$ cycles
- $t = \frac{1738}{10,428} (189,583) = 316$ months ≈ 26 years!

- Paris Law in terms of ΔK_I ; Must consider fatigue crack growth under mixed mode conditions.
- Using the **maximum circumferential stress theory**, use

$$\Delta K_{I_{eff}} = \Delta K_I \cos^3 \frac{\theta_0}{2} - \frac{3}{2} \Delta K_{II} \cos \frac{\theta_0}{2} \sin \theta_0$$

- Root Mean Square Model (Barsoum)

$$\frac{da}{dN} = C(\Delta K_{rms})^n$$

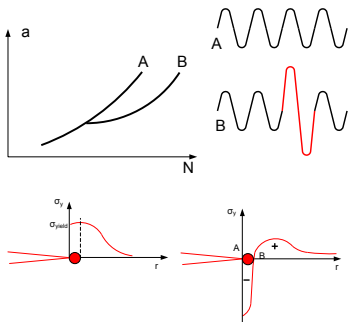
$$\Delta K_{rms} = \sqrt{\frac{\sum_{i=1}^n \Delta K_i^2}{n}}$$

where ΔK_{rms} is the square root of the mean of the squares of the individual stress intensity factors cycles in a spectrum.

- Accurate “block by block” numerical integration of the fatigue law

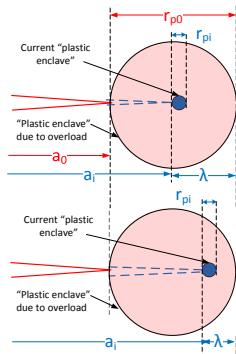
$$\Delta a = C(\Delta K)^n \Delta N$$

solve for a instead of N .



- Load **spike** in a sequence of low amplitude cycles significantly **reduces the rate of crack growth** during the cycles applied subsequent to the overload. This phenomena is called **Retardation**.
- The crack front to **plastically deform** and a **tensile plastic zone** is formed.
- When load is released, the surrounding material is **elastically unloaded** and a part of the plastic zone experiences **compressive stresses**.

- If the the load history contains a mix of constant amplitude loads and discretely applied higher level loads, the **patterns of residual stress and plastic deformation are perturbed**.
- As the crack propagates through this perturbed zone under the constant amplitude loading cycles, it **grows slower** (the crack is **retarded**).
- Once it **emerges** from the previously formed large plastic zone, then the crack growth rate returns to its typical steady-state level.



- The presence of a **plastic zone at the tip of the crack will constrain** (due to volumetric expansion) its expansion, thus it will retard its growth.
- Wheeler defined a **crack-growth retardation factor C_p** :

$$\frac{da}{dN}_{retarded} = C_p \left(\frac{da}{dN} \right)_{linear}$$

$$C_p = \left(\frac{r_{pi}}{\lambda} \right)^m = \left(\frac{r_{pi}}{a_o + r_{po} - a_i} \right)^m$$

as long as $a_i + r_{pi} < a_o + r_{po}$

in which r_{pi} is the current plastic zone size in the i^{th} cycle under consideration, a_i is the current crack size, r_{poL} is the **plastic size generated by a previous higher load excursion**, a_{oL} is the crack size at which the higher load excursion occurred, and m is an empirical constant.

- Thus there is **retardation as long as the current plastic zone is contained within the previously generated one.**

- In the generalized Willenborg model, the stress intensity factor K_I is replaced by an effective one in which K_R that senses the differences in compressive residual stress state caused by difference in load levels and is given by:

$$K_I^{eff} = K_I - K_R$$

$$K_R = \phi K_R^w$$

$$\phi = \frac{1 - \frac{K_{max,th}}{K_{max,i}}}{S^{oL} - 1}$$

$$K_R^w = K_{max}^{oL} \sqrt{1 - \frac{a_i - a_{oL}}{r_{poL}}} - K_{max,i}$$

a_i is the current crack size, a_{oL} the crack size at the occurrence of the overload, r_{poL} the yield zone produced by the overload, K_{max}^{oL} the maximum stress intensity of the overload, and $K_{max,i}$ the maximum stress intensity for the current cycle.

- There are **two empirical constants**: $K_{max,th}$ is the threshold SIF level associated with zero fatigue crack growth rates, and S^{oL} is the overload (shut-off) ratio required to cause crack arrest for the given material.

- Hence, retardation will occur until the crack has generated a plastic zone size that reaches the boundary of the overload yield zone. At that time, $a_i - a_{oL} = r_{poL}$ and the reduction becomes zero.
- Maximum and minimum levels ($K_{max,i}$ and $K_{min,i}$), are reduced by the same amount (K_R).
- Retardation effect is sensed by the change in the effective stress ratio calculated from:

$$R_{eff} = \frac{K_{min,i}^{eff}}{K_{max,i}^{eff}} = \frac{K_{min,i} - K_R}{K_{max,i} - K_R}$$

because the range in stress intensity factor is unchanged by the uniform reduction.

- For the i^{th} load cycle, the crack growth increment Δa_i is:

$$\Delta a_i = \frac{da}{dN} = f(\Delta K, R_{eff})$$

- Then this is used in conjunction with Forman's law. thus it was **modified by Foreman**

$$\frac{da}{dN} = \frac{C(\Delta K)^n}{(1 - R)K_c - \Delta K}$$

Numerical Methods

Victor E. Saouma
saouma@colorado.edu

University of Colorado, Boulder

Spring 2022

Table of Contents I

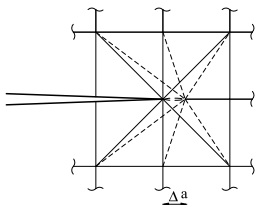
- 1 Introduction
- 2 Energy Release Rate
 - Mode I
 - Virtual Crack Extension.
- 3 Mixed Mode Cases
 - Two Analyses
- 4 Mixed Mode Cases
 - Single Analysis
- 5 Singular Elements
 - Introduction
 - Review of Isoparametric Elements
 - How to Distort the Element to Model the Singularity
 - Order of Singularity
 - Stress Intensity Factors Extraction
 - 3D
- 6 J Integral

Table of Contents II

- Line Integral
- Equivalent Domain Integral; Theoretical Background
- Equivalent Domain Integral; FEA Implementation

7 Reciprocal Work Integrals

- Often times one is confronted with a fracture problem for which there is no readily available analytical solution.
- Should resort to **numerical methods** for analysis.
- This chapter will focus on
 - **SIF**
 - **J Integral**
- EPFM of metals will not be covered.
- **NLFM of concrete** will be separately addressed.



- Recalling that strain energy release rate G is:

$$G = -\frac{\partial \Pi}{\partial a} = \frac{K_I^2}{E'} \simeq \frac{\Delta U}{\Delta a}$$

a simple algorithm for the SIF calculation emerges:

- For an **initial crack length** a , determine the total strain energy:
 - $U = \mathbf{u}^t \mathbf{K} \mathbf{u}$ over Ω where \mathbf{u} nodal displacement, \mathbf{K} structural stiffness matrix.
 - $U = \mathbf{u}^t \mathbf{P}$ along Γ where \mathbf{P} and \mathbf{u} are the externally applied nodal load and displacement, respectively.
- Increase the crack length **from a to $a + \Delta a$** , and reanalyze.
- Determine G from $G \simeq \frac{(U + \Delta U) - U}{(a + \Delta a) - a} = \frac{\Delta U}{\Delta a} = \frac{K_I^2}{E'}$
- Note that:
 - This procedure requires two **complete separate analyses**.
 - The **stress singularity need not be modeled**.

- ③ This technique is **restricted to mode I only**.
- ④ Can be **extended to mixed mode** (would require three complete analysis).

- The stiffness matrix is only **slightly perturbed** in the second analysis (associated with $a + \Delta a$), so take **derivative**
- The potential energy Π is given by:

$$\Pi = \frac{1}{2} [u] [K] \{u\} - [u] \{p\}$$

and

$$\begin{aligned} -G &= \frac{\partial \Pi}{\partial a} = \frac{\partial [u]}{\partial a} [K] \{u\} + \frac{1}{2} [u] \frac{\partial [K]}{\partial a} \{u\} - \frac{\partial [u]}{\partial a} \{P\} - [u] \frac{\partial \{P\}}{\partial a} \\ &= -\frac{\partial [u]}{\partial a} \underbrace{([K] \{u\} - \{P\})}_0 + \frac{1}{2} [u] \frac{\partial [K]}{\partial a} \{u\} - [u] \frac{\partial \{P\}}{\partial a} \end{aligned}$$

- Noting that the first term in the last equation is zero, we obtain:

$$G = -\frac{1}{2} [u] \frac{\partial [K]}{\partial a} \{u\} + [u] \frac{\partial \{P\}}{\partial a}$$

- Thus if the load is unaltered during the crack extension, than the **energy release rate is directly related to the derivative of the stiffness**.

- Note that:
 - 1 Only the portion of the stiffness matrix associated with the elements surrounding the crack tip needs to be perturbed.
 - 2 Better results are obtained if singular elements are used.
 - 3 The method can easily be generalized to three-dimensional problems.
 - 4 It can be shown that this technique is equivalent to the determination of the J integral.
 - 5 This method is restricted to mode I loading only.

- Previous model **did not distinguish the mode I from the mode II components in the energy release rate.**
- Use

$$J_1 = G_1 = \frac{K_I^2 + K_{II}^2}{E'} + \frac{K_{III}^2}{2\mu}$$

$$J_2 = G_2 = \frac{-2K_I K_{II}}{E'}$$

where $E' = E$ for plane stress, and $E' = \frac{E}{1-\nu^2}$ for plane strain. G_1 and G_2 are associated with virtual crack extensions at $\theta = 0$ and $\theta = \frac{\pi}{2}$ respectively.

- Algorithm
 - 1 For an initial crack length a , determine the total strain energy U .
 - 2 Extend the crack length from a to $a + \Delta a$:
 - 1 Along $\theta = 0$, and determine G_1 .
 - 2 Along $\theta = \frac{\pi}{2}$, and determine G_2 .

- 3 Solve for the two SIF from:

$$K_I = \frac{s \pm \sqrt{s^2 + \frac{8G_2}{\alpha}}}{2}$$

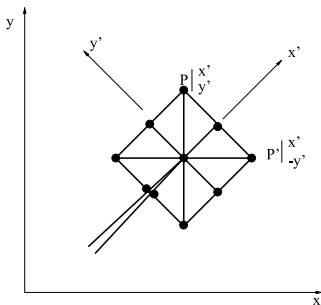
$$K_{II} = \frac{s \mp \sqrt{s^2 + \frac{8G_2}{\alpha}}}{2}$$

where $s = 2\sqrt{\frac{G_1 - G_2}{\alpha}}$ and $\alpha = \frac{(1+\nu)(1+\kappa)}{E}$

- An alternative to this technique is to use $G(\theta) = G_1 \cos(\theta) + G_2 \sin(\theta)$, and use two distinct values of θ , which are not necessarily 0 or $\frac{\pi}{2}$.
- This method **required least one complete finite element analysis, followed by either two separate ones or two virtual crack extensions.**

- This method requires **only one analysis is needed**
- We can decompose the nodal displacements into two local components:

$$\Delta = \Delta^1 + \Delta^2$$



where

$$\{\Delta^1\} = \begin{Bmatrix} u^1 \\ v^1 \end{Bmatrix} = \frac{1}{2} \begin{Bmatrix} u + u' \\ v - v' \end{Bmatrix}$$

$$\{\Delta^2\} = \begin{Bmatrix} u^2 \\ v^2 \end{Bmatrix} = \frac{1}{2} \begin{Bmatrix} u - u' \\ v + v' \end{Bmatrix}$$

- Better results are achieved if singular elements are used around the crack tip, we can determine (following one single analysis):

$$G_1 = -\frac{1}{2} [\Delta^1] \frac{\partial [K]}{\partial a} \{\Delta^1\} + [\Delta^1] \frac{\partial \{P^1\}}{\partial a}$$

$$G_2 = -\frac{1}{2} [\Delta^2] \frac{\partial [K]}{\partial a} \{\Delta^2\} + [\Delta^2] \frac{\partial \{P^2\}}{\partial a}$$

- Because propagation is now assumed to be colinear, we can determine the two stress intensity factors from

$$K_I = \sqrt{E' G_1}$$

$$K_{II} = \sqrt{E' G_{II}}$$

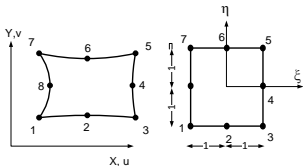
- Saving of one analysis (or virtual crack extension) is **made possible through the constraint of having a symmetrical local mesh** around the crack tip.
- Note this consideration was at one time very important given the limited computer power.

The End for Energy Based Methods

Singular isoparametric elements are the **simplest singular elements** which can be implemented. This sections will

- 1 Cover a brief **review of isoparametric** element formulation
- 2 Show how the element can be **distorted in order to achieve a stress singularity**
- 3 Determine **order of the stress singularity**
- 4 How to **compute SIF**

- In isoparametric finite element representation, **both the internal displacement and coordinates are related to their nodal values through the shape functions:**



$$\begin{Bmatrix} x \\ y \end{Bmatrix} = \sum_{i=1}^8 \begin{bmatrix} N_i & 0 \\ 0 & N_i \end{bmatrix} \begin{Bmatrix} \bar{x}_i \\ \bar{y}_i \end{Bmatrix}$$

$$\{d\} = \begin{Bmatrix} u \\ v \end{Bmatrix} = \sum_{i=1}^8 \begin{bmatrix} N_i & 0 \\ 0 & N_i \end{bmatrix} \begin{Bmatrix} \bar{u}_i \\ \bar{v}_i \end{Bmatrix}$$

where the N_i are the assumed **shape functions**.

- 1 The shape functions are obtained by mere inspection (i.e. **serendipitously**),

$$\begin{aligned} N_i &= \frac{1}{4} (1 + \xi\xi_i) (1 + \eta\eta_i) (\xi\xi_i + \eta\eta_i - 1) & i = 1, 2, 3, 4 \\ N_i &= \frac{1}{2} (1 - \xi^2) (1 + \eta\eta_i) & i = 5, 7 \\ N_i &= \frac{1}{2} (1 + \xi\xi_i) (1 + \eta^2) & i = 6, 8 \end{aligned} \quad (1)$$

Note that we can also use the Lagrangian element (9 nodes).

i	N_i	$N_{i,\xi}$	$N_{i,\eta}$
1	$\frac{1}{4}(1-\xi)(1-\eta)(-\xi-\eta-1)$	$\frac{1}{4}(2\xi+\eta)(1-\eta)$	$\frac{1}{4}(1-\xi)(2\eta+\xi)$
2	$\frac{1}{4}(1+\xi)(1-\eta)(\xi-\eta-1)$	$\frac{1}{4}(2\xi-\eta)(1-\eta)$	$\frac{1}{4}(1+\xi)(2\eta-\xi)$
3	$\frac{1}{4}(1+\xi)(1+\eta)(\xi+\eta-1)$	$\frac{1}{4}(2\xi+\eta)(1+\eta)$	$\frac{1}{4}(1+\xi)(2\eta+\xi)$
4	$\frac{1}{4}(1-\xi)(1+\eta)(-\xi-\eta-1)$	$\frac{1}{4}(2\xi-\eta)(1+\eta)$	$\frac{1}{4}(1-\xi)(2\eta-\xi)$
5	$\frac{1}{2}(1-\xi^2)(1-\eta)$	$-\xi(1-\eta)$	$-\frac{1}{2}(1-\xi^2)$
6	$\frac{1}{2}(1+\xi)(1-\eta^2)$	$\frac{1}{2}(1-\eta^2)$	$-(1+\xi)\eta$
7	$\frac{1}{2}(1-\xi^2)(1+\eta)$	$-\xi(1+\eta)$	$\frac{1}{2}(1-\xi^2)$
8	$\frac{1}{2}(1-\xi)(1-\eta^2)$	$-\frac{1}{2}(1-\eta^2)$	$-(1-\xi)\eta$

- 2 Strain is the derivative of the displacement, we will need later to define $\frac{\partial N}{\partial x}$ and $\frac{\partial N}{\partial y}$. N has been defined in Eq. 1 in terms of the natural coordinates ξ and η . Thus the chain rule will have to be invoked and the inverse of the jacobian will be needed.

- 3 The **strain displacement** relationship is:

$$\{\epsilon\} = \sum_{i=1}^8 [B_i] [\bar{d}_i]$$

where $[B_i]$ is the strain matrix given by:

$$[B_i] = \begin{bmatrix} \frac{\partial N_i}{\partial x} & 0 \\ 0 & \frac{\partial N_i}{\partial y} \\ \frac{\partial N_i}{\partial y} & \frac{\partial N_i}{\partial x} \end{bmatrix}$$

where the following chain rule is invoked to determine the coefficients of $[B]$:

$$\begin{Bmatrix} \frac{\partial N}{\partial x} \\ \frac{\partial N}{\partial y} \end{Bmatrix} = \underbrace{\begin{bmatrix} \frac{\partial \xi}{\partial x} & \frac{\partial \eta}{\partial x} \\ \frac{\partial \xi}{\partial y} & \frac{\partial \eta}{\partial y} \end{bmatrix}}_{[J]^{-1}} \begin{Bmatrix} \frac{\partial N}{\partial \xi} \\ \frac{\partial N}{\partial \eta} \end{Bmatrix}$$

- 4 Recall that given a point in (x, y, z) coordinates, it can be transformed to a general coordinate system (ξ, η) through a **transformation function**, all the first-order partial derivatives of which define the **Jacobian**.

$$\begin{aligned}
 [J] &= \begin{bmatrix} \frac{\partial x}{\partial \xi} & \frac{\partial y}{\partial \xi} \\ \frac{\partial x}{\partial \eta} & \frac{\partial y}{\partial \eta} \end{bmatrix} \\
 &= \begin{bmatrix} \sum_{i=1}^8 \frac{\partial N_i}{\partial \xi} x_i & \sum_{i=1}^8 \frac{\partial N_i}{\partial \xi} y_i \\ \sum_{i=1}^8 \frac{\partial N_i}{\partial \eta} x_i & \sum_{i=1}^8 \frac{\partial N_i}{\partial \eta} y_i \end{bmatrix}
 \end{aligned} \tag{2}$$

- 5 The **inverse jacobian** is then evaluated from the preceding equation

$$\begin{aligned}
 [J]^{-1} &= \begin{bmatrix} \frac{\partial \xi}{\partial x} & \frac{\partial \eta}{\partial x} \\ \frac{\partial \xi}{\partial y} & \frac{\partial \eta}{\partial y} \end{bmatrix} = \begin{bmatrix} \sum_{i=1}^8 \frac{\partial N_i}{\partial \xi} x_i & \sum_{i=1}^8 \frac{\partial N_i}{\partial \xi} y_i \\ \sum_{i=1}^8 \frac{\partial N_i}{\partial \eta} x_i & \sum_{i=1}^8 \frac{\partial N_i}{\partial \eta} y_i \end{bmatrix}^{-1} \\
 &= \frac{1}{\text{Det}J} \begin{bmatrix} \frac{\partial y}{\partial \eta} & -\frac{\partial y}{\partial \xi} \\ -\frac{\partial x}{\partial \eta} & \frac{\partial x}{\partial \xi} \end{bmatrix}
 \end{aligned}$$

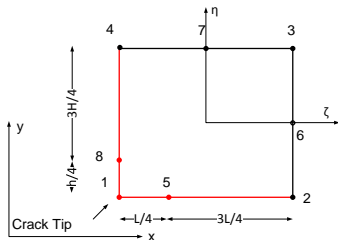
- 6 Finally, the **element stiffness matrix of an element** is given by

$$[K] = \int_{-1}^1 \int_{-1}^1 [B(\xi, \eta)]^T [D] [B(\xi, \eta)] \underbrace{\det J d\xi d\eta}_{dA}$$

where $[D]$ is the stress-strain or constitutive matrix.

- 7 The **stress** is given by:

$$\{\sigma\} = [D] [B] \left\{ \begin{array}{c} \bar{u}_i \\ \bar{v}_i \end{array} \right\} \quad (3)$$



- In Eq. 3 $\{\sigma\} = [D][B] \left\{ \begin{matrix} \bar{u}_i \\ \bar{v}_i \end{matrix} \right\}$ if the stresses are to be singular, then $[B]$ has to be singular as the two other components are constants.
- Consequently, if $[B]$ is to be singular then the determinant of J must vanish to zero (Eq. 2);

$$[J] = \begin{bmatrix} \frac{\partial x}{\partial \xi} & \frac{\partial y}{\partial \xi} \\ \frac{\partial x}{\partial \eta} & \frac{\partial y}{\partial \eta} \end{bmatrix} \text{ at the crack tip.}$$

- A rectangular element of length L along its first side (1-5-2). both off-diagonal terms ($\frac{\partial y}{\partial \xi}$ and $\frac{\partial x}{\partial \eta}$) in J are zero
- Thus, for the determinant of the jacobian to be zero we must have either one of the diagonal terms equal to zero.

- 3 It will suffice to force $\frac{\partial x}{\partial \xi}$ to be zero. Substituting for $\frac{\partial x}{\partial \xi}$ at $\eta = -1$

$$\begin{aligned} \left. \frac{\partial x}{\partial \xi} \right|_{\eta=-1} &= \sum_{i=1}^8 \frac{\partial N_i}{\partial \xi} \bar{x}_i = \frac{1}{4} [-1 + 2\xi + 2\xi - 1] (0) + \frac{1}{4} [1 + 2\xi + 2\xi + 1] (L) \\ &\quad + \frac{1}{4} [-1 + 2\xi - 2\xi + 1] (L) + \frac{1}{4} [1 - 2\xi + 2\xi - 1] (0) - 2\xi (x_5) \\ &\quad + \frac{1}{2} (1 - 1)L + \frac{1}{2} (1 - 1) (L) + \frac{1}{2} (1 - 1) \left(\frac{L}{2} \right) \\ &= \frac{1}{4} (2 + 4\xi) L - 2\xi x_5 \end{aligned}$$

- 4 We set $\frac{\partial x}{\partial \xi} = 0$ at the first corner where $\eta = \xi = -1$:

$$\left. \frac{\partial x}{\partial \xi} \right|_{\substack{\xi=-1 \\ \eta=-1}} = 0 \Rightarrow \frac{1}{4} (2 - 4)L + 2x_5 = 0$$

$$\Rightarrow x_5 = \frac{L}{4} \quad (4)$$

- 5 Thus all the terms in the jacobian vanish if and only if the second node is located at $\frac{L}{4}$ instead of $\frac{L}{2}$, and subsequently both the stresses and strains at the first node will become singular.
- 6 Singularity at the crack tip is achieved by shifting the mid-side node to its quarter-point position
- Note the 9 noded Lagrangian element could similarly be distorted.

What is the degree of singularity?

- 1 Solve for ξ in terms of x and L at $\eta = -1$ (that is, alongside 1-5-2):

$$\begin{aligned}
 x &= \sum_{i=1}^8 N_i \bar{x}_i = \frac{1}{2} (1 - \xi^2) (1 + 1) \frac{L}{4} + \frac{1}{4} (1 + \xi) (1 + 1) (\xi) L \\
 &= \frac{1}{2} \xi (1 + \xi) L + (1 - \xi^2) \frac{L}{4} \\
 \Rightarrow \xi &= -1 + 2\sqrt{\frac{x}{L}}
 \end{aligned} \tag{5}$$

- 2 Recalling that in isoparametric elements the displacement field along $\eta = -1$ is given by:

$$u = -\frac{1}{2} \xi (1 - \xi) \bar{u}_1 + \frac{1}{2} \xi (1 + \xi) \bar{u}_5 + (1 - \xi^2) \bar{u}_2 \tag{6}$$

- 3 we can rewrite Eq. 6 by replacing ξ , with the previously derived expression, Eq. 5):

$$u = -\frac{1}{2} \left(-1 + 2\sqrt{\frac{x}{L}} \right) \left(2 - 2\sqrt{\frac{x}{L}} \right) \bar{u}_1 + \frac{1}{2} \left(-1 + 2\sqrt{\frac{x}{L}} \right) \left(2\sqrt{\frac{x}{L}} \right) \bar{u}_5 + \left(4\sqrt{\frac{x}{L}} - 4\frac{x}{L} \right) \bar{u}_2 \quad (7)$$

This equation can be factorized as:

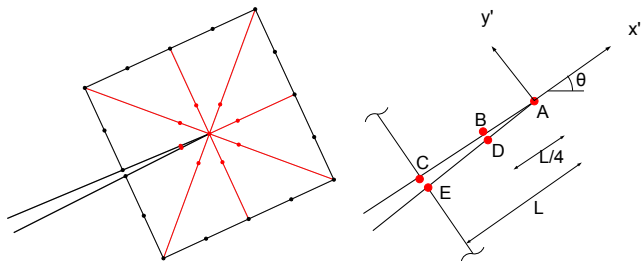
$$u = A + Bx + C\sqrt{\frac{x}{L}} \quad (8)$$

Note that the displacement field has had its quadratic term replaced by $x^{\frac{1}{2}}$.

- 4 Differentiating Eq. 7 we obtain the strain in the x direction

$$\epsilon_x = -\frac{1}{2} \left(\frac{3}{\sqrt{xL}} - \frac{4}{L} \right) \bar{u}_1 + \frac{1}{2} \left(\frac{-1}{\sqrt{xL}} + \frac{4}{L} \right) \bar{u}_5 + \left(\frac{2}{\sqrt{xL}} - \frac{4}{L} \right) \bar{u}_2 \quad (9)$$

- 5 **Strength of the singularity is of order $\frac{1}{2}$** , just as we wanted it to be for linear elastic fracture mechanics !



- Numerical expression of displacement field is obtained from Eq. 7:

$$u' = \bar{u}'_A + (-3\bar{u}'_A + 4\bar{u}'_B - \bar{u}'_C) \sqrt{\frac{r}{L}} + (2\bar{u}'_A + 2\bar{u}'_C - 4\bar{u}'_B) \frac{r}{L}$$

$$v' = \bar{v}'_A + (-3\bar{v}'_A + 4\bar{v}'_B - \bar{v}'_C) \sqrt{\frac{r}{L}} + (2\bar{v}'_A + 2\bar{v}'_C - 4\bar{v}'_B) \frac{r}{L}$$

where \bar{u}' and \bar{v}' are the local displacements (with x' aligned with the crack axis) of the nodes along the crack in the singular elements.

- Analytical expression for v is given by Westergaard with $\theta = 180$, yielding:

$$v = K_I \frac{\kappa + 1}{2G} \sqrt{\frac{r}{2\pi}}$$

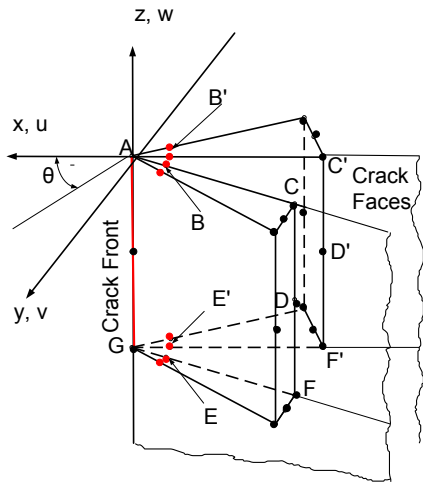
- Equating the terms of equal power ($\frac{1}{2}$) in the preceding two equations, the \sqrt{r} term vanishes, and we obtain:

$$K_I = \frac{2G}{\kappa + 1} \sqrt{\frac{2\pi}{L}} \left(-3\bar{v}'_A + 4\bar{v}'_B - \bar{v}'_C \right)$$

- If this approach is generalized to mixed mode problems, then the two stress intensity factors are given by:

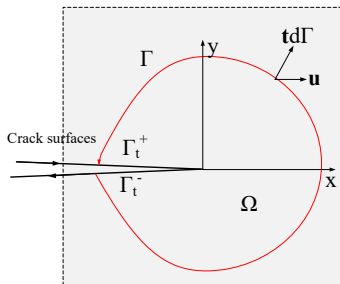
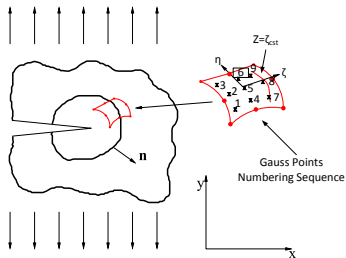
$$\begin{Bmatrix} K_I \\ K_{II} \end{Bmatrix} = \frac{1}{2} \frac{2G}{\kappa + 1} \sqrt{\frac{2\pi}{L}} \begin{bmatrix} 0 & 1 \\ 1 & 0 \end{bmatrix} \begin{bmatrix} -3\bar{u}'_A + 4(\bar{u}'_B - \bar{u}'_D) - (\bar{u}'_C - \bar{u}'_E) \\ -3\bar{v}'_A + 4(\bar{v}'_B - \bar{v}'_D) - (\bar{v}'_C - \bar{v}'_E) \end{bmatrix}$$

- Extraction of the SIF can be accomplished through a “post-processing” routine following a conventional finite element analysis in which the quarter-point elements have been used.



- Method easily extended to 3D
- Meshing around crack front can be problematic

The End for Singular Element



- We seek a finite element based solution to the J integral

$$J = -\frac{\partial \Pi}{\partial a} = \int_r (w dy - t \cdot \frac{\partial d}{\partial x} ds)$$

- Usually, nodal stresses are poorly evaluated, we will rely in **Gauss Points stresses**.
- Assume that **isoparametric elements** are used and that the path can be conveniently chosen to **coincide with $\xi = \xi_{cst}$** .
- For corner elements the integration will have to be performed twice along the two directions.

- Now let us start from the basic definition of J :

$$J = \int_{\Gamma} w dy - \mathbf{t} \cdot \frac{\partial \mathbf{d}}{\partial x} ds \quad (10)$$

where \mathbf{t} is the traction vector along \mathbf{n} , which is normal to the path; \mathbf{d} is the displacement vector; ds is the element of arc along path Γ ; and w is the strain energy density.

- Now, we will be going from an analytical equation to a numerical solution rooted in the finite element method.
- Crack is assumed to be along the x axis. If it is not, stresses and displacements would first have to be rotated.
- First, **expand the terms** in Eq. 10 into their basic constituents:

- Traction vector**

$$t_i = \sigma_{ij} n_j \Rightarrow \mathbf{t} = \left\{ \begin{array}{l} \sigma_{xx} n_1 + \tau_{xy} n_2 \\ \tau_{xy} n_1 + \sigma_{yy} n_2 \end{array} \right\}$$

- Displacement vector:**

$$\mathbf{d} = \left\{ \begin{array}{l} u \\ v \end{array} \right\}$$

- Strain energy density w :

$$\begin{aligned} w &= \frac{1}{2}(\sigma_{xx}\varepsilon_{xx} + 2\tau_{xy}\gamma_{xy} + \sigma_{yy}\varepsilon_{yy}) \\ &= \frac{1}{2}\left[\sigma_{xx}\frac{\partial u}{\partial x} + \tau_{xy}\left(\frac{\partial u}{\partial y} + \frac{\partial v}{\partial x}\right) + \sigma_{yy}\frac{\partial v}{\partial y}\right] \end{aligned}$$

- arc length ds and dy :

$$\begin{aligned} ds &= \sqrt{dx^2 + dy^2} = \sqrt{\left(\frac{\partial x}{\partial \eta}\right)^2 + \left(\frac{\partial y}{\partial \eta}\right)^2} d\eta \\ &= \frac{\partial y}{\partial \eta} d\eta \end{aligned}$$

- Substitution phase:

- 1 Evaluate part of the **second term** of $J = \int_{\Gamma} w dy - t \cdot \frac{\partial d}{\partial x} ds$:

$$t \cdot \frac{\partial d}{\partial x} = (\sigma_{xx}n_1 + \tau_{xy}n_2)\frac{\partial u}{\partial x} + (\tau_{xy}n_1 + \sigma_{yy}n_2)\frac{\partial v}{\partial x}$$

where n_1 and n_2 are the components of \mathbf{n} , which is a unit vector normal to the contour line at the Gauss point under consideration.

- 2 Ready to substitute in $J = \int_{\Gamma} w dy - t \cdot \frac{\partial J}{\partial x} ds$ to obtain the contribution to J from a particular Gauss point within an element.

$$\begin{aligned}
 J^e &= \int_{-1}^1 \left\{ \underbrace{\frac{1}{2} \left[\sigma_{xx} \frac{\partial u}{\partial x} + \tau_{xy} \left(\frac{\partial u}{\partial y} + \frac{\partial v}{\partial x} \right) + \sigma_{yy} \frac{\partial v}{\partial y} \right]}_w \underbrace{\frac{\partial y}{\partial \eta}}_{dy} \right. \\
 &\quad \left. - \underbrace{\left[(\sigma_{xx} n_1 + \tau_{xy} n_2) \frac{\partial u}{\partial x} + (\tau_{xy} n_1 + \sigma_{yy} n_2) \frac{\partial v}{\partial x} \right]}_{t \cdot \frac{\partial J}{\partial x}} \underbrace{\sqrt{\left(\frac{\partial x}{\partial \eta} \right)^2 + \left(\frac{\partial y}{\partial \eta} \right)^2}}_{ds} \right\} d\eta \quad (11) \\
 &= \int_{-1}^1 I d\eta
 \end{aligned}$$

- **Integration** is to be carried out numerically along the path (using the same integration points used for the element stiffness matrix), we have:

$$J^e = \sum_{q=1}^{NGAUS} I(\xi_p, \eta_q) W_q$$

where W_q is the **weighting factor corresponding to η_q** and $NGAUS$ is the order of integration (2 or 3).

- **Where from?** for each term
 - Stresses σ_{xx} , σ_{yy} , τ_{xy} are readily available at the Gauss points.
 - $\frac{\partial u}{\partial x}$, $\frac{\partial u}{\partial y}$, $\frac{\partial v}{\partial x}$, and $\frac{\partial v}{\partial y}$ are **obtained through the shape function**. For instance $\frac{\partial u}{\partial x} = \left[\frac{\partial N_i}{\partial x} \right] \{ \bar{u}_i \}$ where \bar{u}_i are the nodal displacements and $\frac{\partial N_i}{\partial x}$ is the Cartesian derivative of the shape function stored in the $[B]$ matrix:

$$[B] = \begin{bmatrix} \frac{\partial N_i}{\partial x} & 0 \\ 0 & \frac{\partial N_i}{\partial y} \\ \frac{\partial N_i}{\partial y} & \frac{\partial N_i}{\partial x} \end{bmatrix}$$

where i ranges from 1 to 8 for quadrilateral elements.

- Another term not yet defined in Eq. 11 is $\frac{\partial y}{\partial \eta}$. This term is actually stored already in the Gauss point Jacobian matrix:

$$[\mathcal{J}] = \begin{bmatrix} \frac{\partial x}{\partial \xi} & \frac{\partial y}{\partial \xi} \\ \frac{\partial x}{\partial \eta} & \frac{\partial y}{\partial \eta} \end{bmatrix}$$

- Determine n_1 and n_2 (components of \mathbf{n}). Infinite number of vectors normal to ξ , and we want the one which is **in the $\xi - \eta$ plane**. It should be noted that if we had a rectangular element, then η is orthogonal to ξ in the physical space, but in general we have a **distorted element**, and thus η and ξ are not necessarily orthogonal to each others in the physical space.

Hence, we determine the normal as follows:

- Define **two arbitrary vectors**: A along $\xi = \xi_{cst}$ and B along $\eta = \eta_{cst}$ such that:

$$A^t = \left[\frac{\partial x}{\partial \eta}, \quad \frac{\partial y}{\partial \eta}, \quad 0 \right]$$

$$B^t = \left[\frac{\partial x}{\partial \xi}, \quad \frac{\partial y}{\partial \xi}, \quad 0 \right]$$

as **three-dimensional components** of those two vectors.

- Define a third vector, which is normal to the plane defined by the preceding two: $C = A \times B$, (cross product of two vectors) or:

$$\begin{bmatrix} i & j & k \\ \frac{\partial x}{\partial \eta} & \frac{\partial y}{\partial \eta} & 0 \\ \frac{\partial x}{\partial \xi} & \frac{\partial y}{\partial \xi} & 0 \end{bmatrix}$$

This leads to:

$$C = \left[0, 0, \frac{\partial x}{\partial \eta} \frac{\partial y}{\partial \xi} - \frac{\partial y}{\partial \eta} \frac{\partial x}{\partial \xi} \right]$$

- With C defined, we can now return to the original plane and define

$$\begin{aligned} D &= C \times A \\ &= \left[\underbrace{\frac{\partial y}{\partial \eta} \left(\frac{\partial y}{\partial \eta} \frac{\partial x}{\partial \xi} - \frac{\partial x}{\partial \eta} \frac{\partial y}{\partial \xi} \right)}_{D_1}, \underbrace{\frac{\partial x}{\partial \eta} \left(\frac{\partial x}{\partial \eta} \frac{\partial y}{\partial \xi} - \frac{\partial y}{\partial \eta} \frac{\partial x}{\partial \xi} \right)}_{D_2}, 0 \right] \end{aligned}$$

Note that the first term inside the parenthesis corresponds to the **determinant of the Jacobian**, whereas the second term corresponds to the negative of the determinant.

- The unit normal vector is now given by:

$$\mathbf{n} = \begin{Bmatrix} n_1 \\ n_2 \\ 0 \end{Bmatrix} = \begin{Bmatrix} \frac{D_1}{N} \\ \frac{D_2}{N} \\ 0 \end{Bmatrix}$$

where $N = \sqrt{D_1^2 + D_2^2}$ and all terms are taken from the Jacobian matrix.

The End for J

- The **Equivalent Domain Integral** is an **extension of the J integral** as it is to replace line/surface integral by surface/volume integral (through Green's theorem).
- It can be shown (Anderson pg. 256) that the **generalized energy release rate** can be expressed by

$$J = \lim_{\Gamma^0 \rightarrow 0} \int_{\Gamma^0} \left[(w + T) \delta_{1i} - \sigma_{ij} \frac{\partial u_j}{\partial x_1} \right] n_i d\Gamma \quad (12)$$

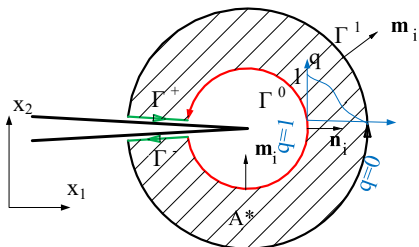
where w is the strain energy density, T is the kinetic energy

$$T = \frac{1}{2} \rho \frac{\partial u_i}{\partial t} \frac{\partial u_i}{\partial t}$$

and δ the Kronecker delta.

- The essence of the method: **replace contour integral, by a closed integral (outer and inner) while multiplying the expression of J by a function q equal to zero on the outer surface and unity on the inner one.**
- Unlike the conventional J integral, **contour path for this equation can not be arbitrarily selected.**

- This equation is **path independent only within an elastic zone**.
- This **equation is not suited for numerical evaluation** as the path would have to be along a vanishingly small one where the stresses and strains could not be determined.



- For quasi-static cases ($T = 0$).
- Consider a closed contour by connecting inner and outer ones. The outer one Γ^1 is finite, while the inner one Γ^0 is **vanishingly small**.

- For linear (or nonlinear) elastic material J can be evaluated along either one of those two contours, **but only the inner one gives the exact solution in the general case**.

- Rewrite Eq. 12 around the following closed contour

$$\Gamma^* = \Gamma^1 + \Gamma^+ + \Gamma^- - \Gamma^0$$

yielding

$$J = \int_{\Gamma^*} \left[\sigma_{ij} \frac{\partial u_j}{\partial x_1} - w \delta_{1i} \right] q m_i d\Gamma - \int_{\Gamma^+ \cup \Gamma^-} \sigma_{2j} \frac{\partial u_j}{\partial x_1} q d\Gamma \quad (13)$$

m_i is the outward normal to Γ^* (thus $m_i = n_i$ on Γ^1 , and $m_i = -n_i$ on Γ^0 , $m_1 = 0$ and $m_2 = \pm 1$ on Γ^+ and Γ^-), and q is an arbitrary but smooth function which is equal to unity on Γ^0 and zero on Γ^1 .

- Since the integral is taken along the contours, by explicitly specifying $q = 0$ on the outer one, and $q = 1$ on the inner one, Eq. 12 and 13 are identical. Furthermore, in the absence of crack surface tractions, the second term is equal to zero.

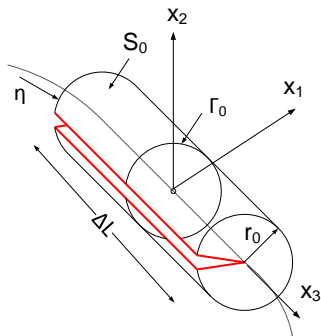
- Apply **divergence theorem** to Eq. 13 $\oint_{\Gamma} \mathbf{v} \cdot \mathbf{n} = \int_A \left(\frac{\partial v_x}{\partial x} + \frac{\partial v_y}{\partial y} \right) dx dy$ we obtain

$$\begin{aligned} J &= \int_{A^*} \frac{\partial}{\partial x_i} \left\{ \left[\sigma_{ij} \frac{\partial u_j}{\partial x_1} - w \delta_{1i} \right] q \right\} dA \\ &= \int_{A^*} \left[\left(\sigma_{ij} \frac{\partial u_j}{\partial x_1} - w \delta_{1i} \right) \frac{\partial q}{\partial x_i} + \left(\frac{\partial}{\partial x_i} \left(\sigma_{ij} \frac{\partial u_j}{\partial x_1} \right) - \frac{\partial w}{\partial x_1} \right) q \right] dA \quad (14) \end{aligned}$$

where A^* is the area enclosed by Γ^* .

- It can be shown (refer to the derivation of J) that the second term in Eq. 14 is equal to zero and we are left with

$$J = \int_{A^*} \left[\sigma_{ij} \frac{\partial u_j}{\partial x_1} - w \delta_{1i} \right] \frac{\partial q}{\partial x_i} dA \quad (15)$$

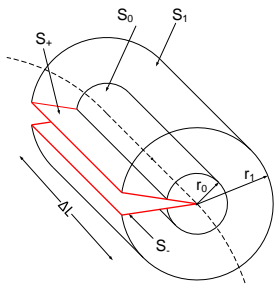


- Let us now **generalize to 3D our previous derivation**
- We define a local coordinate system such that x_1 is normal to the crack front, x_2 normal to the crack plane, and x_3 tangent to the crack front.
- For an arbitrary point, the J integral is given by Eq. 12.

- Consider a tube of length ΔL and radius r_0 that surrounds the segment of the crack front under consideration. We now define a **weighted average J over the crack front segment of length ΔL** as

$$\begin{aligned} \bar{J}\Delta L &= \int_{\Delta L} J(\eta)q d\eta \\ &= \lim_{r_0 \rightarrow 0} \int_{S_0} \left[w\delta_{1i} - \sigma_{ij} \frac{\partial u_j}{\partial x_1} \right] q n_i ds \end{aligned}$$

where $J(\eta)$ is the point-wise value of J , S_0 is the vanishingly small surface area of the tube, q is the weight function previously introduced.



- q can be interpreted as a **virtual crack** advance

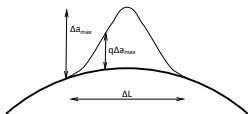
$$\Delta a(\eta) = q(\eta)\Delta a_{max} \quad (16)$$

and the corresponding incremental area of the virtual crack is

$$\Delta A_c = \Delta a_{max} \int_{\Delta L} q(\eta)d\eta \quad (17)$$

- As before, J can not be numerically determined for a vanishingly small radius r_0 , as such and as in the previous 2D case, we define a second tube of radius r_1 around the crack front

$$\bar{J}\Delta L = \oint_{S^*} \left[\sigma_{ij} \frac{\partial u_j}{\partial x_1} - w\delta_{1i} \right] qm_i dS - \oint_{S_- \cup S_+} \sigma_{2j} \frac{\partial u_j}{\partial x_1} q ds$$



where

$$S^* = S_1 + S_+ + S_- - S_0$$

and S_+ and S_- are the upper and lower crack surfaces respectively, S_0 and S_1 the inner and outer tube surfaces. Note that this equation is the 3D counterpart of Eq. 13 which was written in 2D.

- Applying the divergence theorem, this equation reduces to a volume integral

$$\bar{J}\Delta L = \int_{V^*} \left\{ \left[\sigma_{ij} \frac{\partial u_j}{\partial x_1} - w \delta_{1i} \right] \frac{\partial q}{\partial x_i} + \left[-\frac{\partial w}{\partial x_1} + \sigma_{ij} \frac{\partial \varepsilon_{ij}}{\partial x_1} \right] q \right\} dV - \int_{S_+ \cup S_-} \sigma_{2j} \frac{\partial u_j}{\partial x_1} q dS$$

and q must be equal to zero at either end of ΔL that is on A_1 and A_2 .

- It has been shown that in the absence of non-elastic (thermal and plastic) deformations the second term would be equal to zero. The third term will also be equal to zero because q is arbitrarily selected to be zero at each end.
- From Eq. 40 it is impossible to extract the 3 distinct stress intensity factors.

- We now can **generalize** this equation and write it as (ignoring the second and third terms)

$$\bar{J}_k \Delta L = \int_{V^*} \left(\sigma_{ij} \frac{\partial u_i}{\partial x_k} \frac{\partial q}{\partial x_j} - w \frac{\partial q}{\partial x_k} \right) dV$$

- Note that $k = 1, 2$ only thus defining $G_1 = J_1$ and $G_2 = J_2$. However, it has been shown that G_3 has a similar form and is equal to

$$G_{III} = \int_{V^*} \left(\sigma_{3j} \frac{\partial u_3}{\partial x_1} \frac{\partial q}{\partial x_j} - w^{III} \frac{\partial q}{\partial x_1} \right) dV$$

- With G_1 , G_2 and G_3 known we need to extract the three stress intensity factors K_I , K_{II} and K_{III} .

$$\begin{aligned} K_I &= \frac{1}{2} \sqrt{E^*} \left(\sqrt{(J_1 - J_2 - G_3)} + \sqrt{(J_1 + J_2 - G_3)} \right) \\ K_{II} &= \frac{1}{2} \sqrt{E^*} \left(\sqrt{(J_1 - J_2 - G_3)} - \sqrt{(J_1 + J_2 - G_3)} \right) \\ K_{III} &= \sqrt{2\mu G_3} \end{aligned}$$

where

$$E^* = E \left[\frac{1}{1-\nu^2} + \left(\frac{\nu}{1+\nu} \right) \frac{\varepsilon_{33}}{\varepsilon_{11} + \varepsilon_{22}} \right]$$

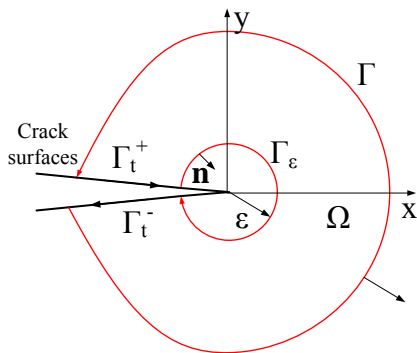
which is a weighted value of E such that we retrieve $E^* = \frac{E}{1-\nu^2}$ for plane strain and $E^* = E$ for plane stress.

The End for Domain Integral

- Betti's reciprocal work theorem defines the **relationship between two equilibrium states for a solid**. In the absence of body forces and initial strains and stresses

$$\oint_{\Gamma} \hat{t}_i \hat{u}_i d\Gamma = \oint_{\Gamma} \hat{t}_i u_i d\Gamma$$

where u_i and t_i are the solution of **any particular equilibrium problem** along the boundary Γ bounding Ω ; \hat{u}_i and \hat{t}_i correspond to another such problem (**complementary/auxiliary state**).



- Ω must be defined such that the **singularity at the crack tip is avoided**, this is done by deleting the body points within a circle of radius ϵ centered at the crack tip. **singularity at the crack tip is thus excluded**.

- Assuming that Γ_t^+ and Γ_t^- are **traction free**

$$\int_{\Gamma} t_j \hat{u}_i d\Gamma + \int_{\Gamma_\epsilon} t_j \hat{u}_i d\Gamma = \int_{\Gamma} \hat{t}_j u_i d\Gamma + \int_{\Gamma_\epsilon} \hat{t}_j u_i d\Gamma$$

contributions from Γ and Γ_ϵ are clearly separated.

- Expanded expression is then rewritten in the form of a **Somigliana's identity**

$$I_\epsilon = \underbrace{-\lim_{\epsilon \rightarrow 0} \int_{\Gamma_\epsilon} (t_j^s \hat{u}_i - \hat{t}_j u_i^s) d\Gamma}_{I_\epsilon = c_1 K_I - c_2 K_{II}} = \int_{\Gamma} (t_j \hat{u}_i - \hat{t}_j u_i) d\Gamma \quad (18)$$

- Approach:

- Determine a suitable auxiliary solution in terms of \hat{u}_i and \hat{t}_j (that are functions of c_1 and c_2).
- Convolute it with the singular tractions and displacements (Westergaard) t_j^s and u_i^s (in terms of K_I and K_{II}) and obtain an equation of the form $I_\epsilon = c_1 K_I - c_2 K_{II}$
- Perform a finite element analysis, and determine u_i and t_j
- Convolute \hat{u}_i and \hat{t}_j with u_i and t_j .

- 5 Integrate over \int_{Γ} and obtain a numerical expression in terms of c_1 and c_2 .
 - 6 Equate factors premultiplying c_1 and c_2 from both sides of the equation, and solve for K_I and K_{II} .
- Major advantage over J integral: single contour integral can determine both K_I and K_{II}
 - For the isotropic case, in the neighborhood of the crack tip, the displacements and the stresses, in polar coordinate system, are given by Westergaard as:

$$\begin{aligned}
 u_r - u_r^0 &= \frac{1}{4\mu} \left(\frac{r}{2\pi}\right)^{\frac{1}{2}} \left\{ \left[(2\kappa - 1) \cos \frac{\theta}{2} - \cos \frac{3\theta}{2} \right] K_I \right. \\
 &\quad \left. - \left[(2\kappa - 1) \sin \frac{\theta}{2} - 3 \sin \frac{3\theta}{2} \right] K_{II} \right\} + O\left(r^{\frac{1}{2}}\right) \\
 u_\theta - u_\theta^0 &= \frac{1}{4\mu} \left(\frac{r}{2\pi}\right)^{\frac{1}{2}} \left\{ \left[-(2\kappa + 1) \sin \frac{\theta}{2} + \sin \frac{3\theta}{2} \right] K_I \right. \\
 &\quad \left. - \left[(2\kappa + 1) \cos \frac{\theta}{2} - 3 \cos \frac{3\theta}{2} \right] K_{II} \right\} + O\left(r^{\frac{1}{2}}\right) \\
 \sigma_r &= \frac{1}{4(2\pi r)^{\frac{1}{2}}} \left\{ \left(5 \cos \frac{\theta}{2} - \cos \frac{3\theta}{2} \right) K_I - \left(5 \sin \frac{\theta}{2} - 3 \sin \frac{3\theta}{2} \right) K_{II} \right\} + O\left(r^{-\frac{1}{2}}\right) \\
 \sigma_\theta &= \frac{1}{4(2\pi r)^{\frac{1}{2}}} \left\{ \left(3 \cos \frac{\theta}{2} + \cos \frac{3\theta}{2} \right) K_I - \left(3 \sin \frac{\theta}{2} + 3 \sin \frac{3\theta}{2} \right) K_{II} \right\} + O\left(r^{-\frac{1}{2}}\right) \\
 \sigma_{r\theta} &= \frac{1}{4(2\pi r)^{\frac{1}{2}}} \left\{ \left(\sin \frac{\theta}{2} + \sin \frac{3\theta}{2} \right) K_I + \left(\cos \frac{\theta}{2} + 3 \cos \frac{3\theta}{2} \right) K_{II} \right\} + O\left(r^{-\frac{1}{2}}\right)
 \end{aligned} \tag{19}$$

where u_r^0 and u_θ^0 are the radial and tangential components, respectively, of the displacements u^0 of the crack tip, and

$$\begin{aligned} K_I &= \lim_{r \rightarrow 0} (2\pi r)^{\frac{1}{2}} \sigma_\theta|_{\theta=0} \\ K_{II} &= \lim_{r \rightarrow 0} (2\pi r)^{\frac{1}{2}} \sigma_{r\theta}|_{\theta=0} \end{aligned} \quad (20)$$

are the usual stress intensity factors.

- Stern (1976) derived the the **Auxiliary solution** based on Williams solution:

$$\begin{aligned} \hat{u}_r &= \frac{1}{2(2\pi r)^{\frac{1}{2}}(1+\kappa)} \left\{ [(2\kappa+1) \cos \frac{3\theta}{2} - 3 \cos \frac{\theta}{2}] c_1 + [(2\kappa+1) \sin \frac{3\theta}{2} - \sin \frac{\theta}{2}] c_2 \right\} \\ \hat{u}_\theta &= \frac{1}{2(2\pi r)^{\frac{1}{2}}(1+\kappa)} \left\{ [-(2\kappa-1) \sin \frac{3\theta}{2} + 3 \sin \frac{\theta}{2}] c_1 + [(2\kappa-1) \cos \frac{3\theta}{2} - \cos \frac{\theta}{2}] c_2 \right\} \\ \hat{\sigma}_r &= -\frac{\mu}{2(2\pi r^3)^{\frac{1}{2}}(1+\kappa)} \left\{ [7 \cos \frac{3\theta}{2} - 3 \cos \frac{\theta}{2}] c_1 + [7 \sin \frac{3\theta}{2} - \sin \frac{\theta}{2}] c_2 \right\} \\ \hat{\sigma}_\theta &= -\frac{\mu}{2(2\pi r^3)^{\frac{1}{2}}(1+\kappa)} \left\{ [\cos \frac{3\theta}{2} + 3 \cos \frac{\theta}{2}] c_1 + [\sin \frac{3\theta}{2} + \sin \frac{\theta}{2}] c_2 \right\} \\ \hat{\sigma}_{r\theta} &= -\frac{\mu}{2(2\pi r^3)^{\frac{1}{2}}(1+\kappa)} \left\{ 3 [\sin \frac{3\theta}{2} + \sin \frac{\theta}{2}] c_1 - [3 \cos \frac{3\theta}{2} - \cos \frac{\theta}{2}] c_2 \right\} \end{aligned} \quad (21)$$

where c_1 and c_2 are arbitrary constants.

- Now, on the inner circular boundary, the evaluation of the contour integral in terms of traction and displacement takes the form:

$$\begin{aligned}
 I_\epsilon &= - \int_{\Gamma^\epsilon} [(\mathbf{u} - \mathbf{u}^0) \cdot \hat{\mathbf{t}} - \hat{\mathbf{u}} \cdot \mathbf{t}] ds \\
 &= \int_{-\pi}^{\pi} [\hat{\sigma}_r (u_r - u_r^0) - \hat{\sigma}_{r\theta} (u_\theta - u_\theta^0) - \sigma_r \hat{u}_r + \sigma_{r\theta} \hat{u}_\theta] r d\theta
 \end{aligned} \tag{22}$$

- Substituting Eq. 19 and 21 we obtain:

$$I_\epsilon = c_1 K_I - c_2 K_{II} \tag{23}$$

- Thus, for arbitrarily small ϵ , Eq. 18 produces

$$c_1 K_I - c_2 K_{II} = \int_{\Gamma} [(\mathbf{u} - \mathbf{u}^0) \cdot \hat{\mathbf{t}}(c_1, c_2) - \hat{\mathbf{u}}(c_1, c_2) \cdot \mathbf{t}] ds \tag{24}$$

Note that the integral is taken along the outer boundary Γ only.

Fracture Mechanics of Softening Material

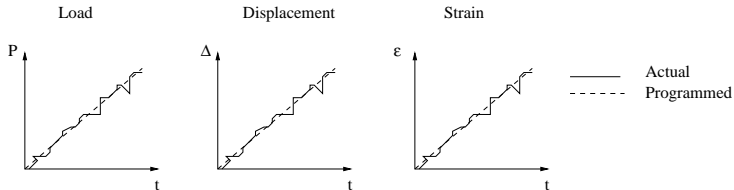
Victor E. Saouma
saouma@colorado.edu

University of Colorado, Boulder

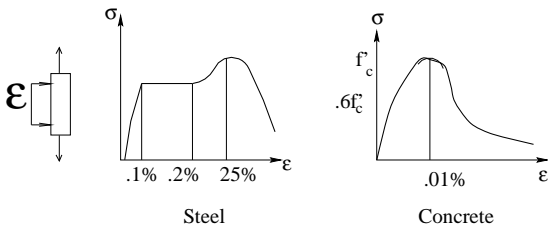
Spring 2022

Table of Contents I

- 1 Introduction
 - Test Controls
 - Pre-Post-Peak Responses
- 2 Experimental Evidence
- 3 σ -COD Diagram, Hillerborg's Model
- 4 Implication
 - Size Effect; Preliminary
 - Example
- 5 Graphical Illustration
- 6 Micro Cracks
 - Theoretical Considerations
- 7 Micro Cracks in Concrete
 - Conjectures
 - Physical Evidences
- 8 Creep Fracture
- 9 Coalescence of Micro-Cracks



- 1 **Load Control:** Cross-head applies an increasing load irrespective of the specimen deformation or response. When peak load is reached, sudden and abrupt brittle failure. The **strain energy accumulated in the specimen** is suddenly released once the ultimate load of the specimen is reached, thus the sudden failure can be **explosive**.
- 2 **Displacement/Stroke Control:** Cross-head applies an increasing displacement to the specimen. For softening material there will be a **post-peak response with a gradual decrease in stress accompanying an increase in displacement**. In this case, there is a **gradual release of strain energy** which is then transferred to surface energy during crack formation.
- 3 **Strain Control:** is analogous to displacement control, except that the feedback is provided by (“strategically positioned”) strain gage or a clip gage or an arbitrary specimen deformation (not necessarily corresponding to the loading direction).

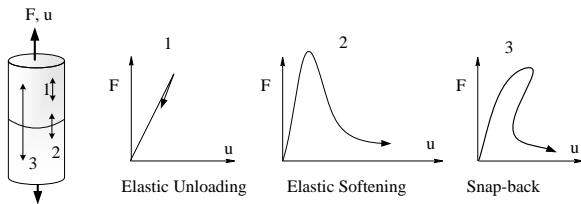


- **Pre-peak:**

- 1 **Metal** Linear elastic response up to the yield stress σ_{yld} ,
- 2 **Cementitious material** Linear response up to $\simeq 0.6f'_t \Rightarrow$ internal microcracking induces a nonlinear response up to a peak stress f'_t

- **Post-peak:**

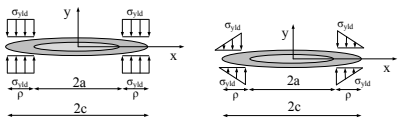
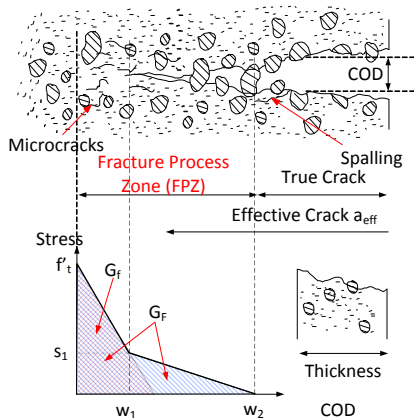
- 1 **Metals** Not yet well understood, not of practical usefulness, largely overshadowed by necking.
- 2 **Cementitious material** Descending branch of the concrete response is an **idealization** of the average material response. A more accurate description should account for the **localization of the induced cracks**.
 - Away from the localized crack there is an elastic unloading
 - At the crack, since a strain cannot be properly defined, a stress-crack opening displacement is a more appropriate model.



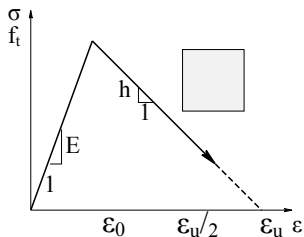
- Once the peak load is reached, and cracking is initiated, Transducers:
 - 1: elastic unloading
 - 2: strain softening
 - 3: snap-back
- If we were to **homogenize** by taking $\sigma = F/A$, and $\varepsilon = u/L$, it is clear that we **can not provide a unique definition of the strain across the crack.**
- At this location, the **strain can no longer be defined**, and instead we should **characterize the crack by its crack opening displacement COD** which will then be plotted along with the stress (σ -COD).

- Capability of **transmitting stresses across a crack** under controlled displacement is a characteristic of **softening materials**.

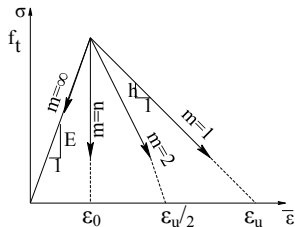
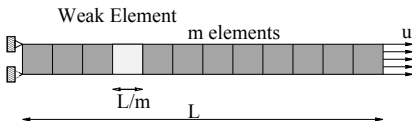
- It is now clear that **Cementitious material softening is characterized by a stress-crack opening width curve** (and not stress-strain).
- The exact characterization of the softening response should ideally be obtained from a **uniaxial test of an uncracked** specimen.
- This is extremely difficult, hence, softening curve is often indirectly determined by **testing notched specimens**.
- **Hillerborg** presented in 1976 a very simple and elegant model (inspired by Barenblatt and Dugdale). In this model, the crack is composed of two parts
 - **True or physical crack** across which no stresses can be transmitted. Along this zone we have both displacement and stress discontinuities.
 - **Fictitious crack, or Fracture Process Zone (FPZ)** ahead of the previous one, characterized by:
 - Peak stress at its tip equal to the tensile strength of Cementitious material
 - decreasing stress distribution from f_t' at the tip of the fictitious crack to zero at the tip of the physical crack
- Along FPZ, we have **displacement discontinuity** and stress continuity.



- There is an **inflection point** in the descending branch.
 - The first part has been associated with **(unconnected) microcracking** ahead of the stress-free crack
 - The second part with **bridging of the crack by aggregates**
- The area under the curve is the **fracture energy G_F** (not to be confused with G_c or critical energy release rate), is a **measure of the energy that needs to be spent to generate a unit surface of crack**.
- Contrast with Dugdale and Barenblat models where the stresses are constant and independent of the COD.



- Consider the response a concrete element subjected to a **uniform displacement** (not load)
 - Prior to reaching the peak stress f_t , we have a **linear stress strain** relationship $\sigma = E\varepsilon$.
 - Once peak load is reached, the **concrete softens** and the peak strain is ε_u . At that point the load carrying capacity of the bar is exhausted.
- Post-peak stress is given by $\sigma = f_t + h(\varepsilon - \varepsilon_0)$ for degrading (softening) material, h is the softening modulus and is less than zero, and for linear softening $h = -\frac{f_t}{\varepsilon_u - \varepsilon_0}$ where $\varepsilon_0 = f_t/E$.
 - Consider next an assemblage of “elements”,



- Assume that one of the elements is weaker than the other $m - 1$ ones. Thus, when this element reaches its own tensile strength (lower than f_t), it fails.
- Upon failure of this element, the other ones will have to unload elastically.

- Thus, in the post-peak zone the displacement will be

$$\begin{aligned}
 u &= \frac{L}{m} \varepsilon_f + (m-1) \frac{L}{m} \varepsilon_e \\
 \varepsilon_f &= \frac{f_t}{E} + \frac{\sigma - f_t}{h} \\
 \varepsilon_e &= \frac{\sigma}{E} \\
 \bar{\varepsilon} &= \frac{u}{L} \\
 \Rightarrow \bar{\varepsilon} &= \frac{\sigma}{E} + \frac{E - h}{Eh} \frac{\sigma - f_t}{m}
 \end{aligned} \tag{1}$$

- If we define $n = \frac{\varepsilon_u}{\varepsilon_0}$ then $h = -E/(n-1)$ the last equation reduces to

$$\bar{\varepsilon} = \frac{\sigma}{E} + \frac{n(f_t - \sigma)}{mE}$$

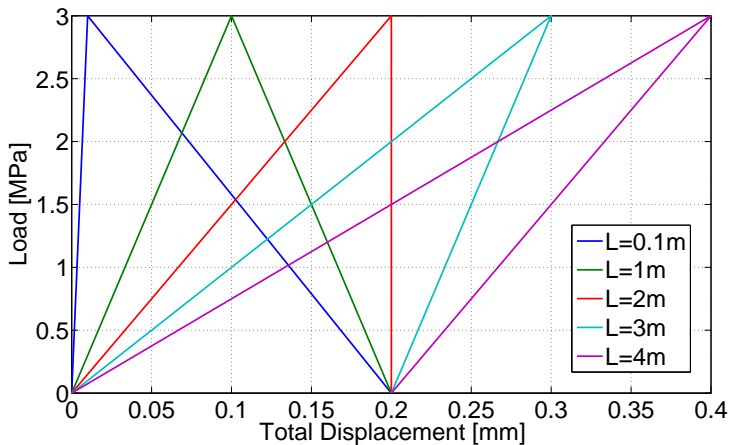
Note “similarity” with the **tangent modulus in plasticity**.

- From the figure, we note that depending on the number of element used (m), there is a wide range of possible responses.

- For $m = 1$ **Softening** curve reproduced
- For $m = n$ **brittle failure**.
- For $m = 2$ **half the bar localizes**
- For $m > n$ Strain decrease, i.e. **snap-back** behavior, impossible to achieve experimentally. Physically, that implies that the localization zone can not absorb the elastic energy released by the elastic part of the bar.
- If $m \rightarrow \infty$ **elastic unloading**. Physically, this is **impossible** as it would imply **failure occurred without dissipation of energy**. As a result we would have:
 - Loss of local material stability
 - Loss of structural stability
 - Loss of ellipticity
 - Mesh dependence

- Consider a softening material member subjected to **uniaxial displacement** with: $f'_t = 3\text{MPa}$; $E = 30\text{ GPa}$; $w_{max} = .02\text{ cm}$.
- **Fracture energy** $G_F = \frac{1}{2}(3 \times 10^6)(2 \times 10^{-4}) = 300\text{ N/m}$.
- **Peak elastic strain** is $\epsilon_0 = \frac{3 \times 10^6}{3 \times 10^{10}} = 10^{-4}$.
- **Maximum elastic displacement** is $10^{-4}L$.
- Consider the **load displacement curve** ($P - u$) of this member for various lengths L .
 - In all cases the **peak load will be** $P_{max} = 3A$ A is the cross sectional area (since results are independent of A we shall assume $A=1$).
 - **Corresponding displacement:** $u = \epsilon_0 \times L$.
 - In all cases **maximum displacement:** $u_{max} = w_{max} = .02\text{ cm}$ and the corresponding load will obviously be equal to zero.
 - **Displacement corresponding to peak load** will be equal to w_{max} if

$$L = \frac{w_{max}}{\epsilon_0} = \frac{2 \times 10^{-4}}{10^{-4}} = 2\text{ m}.$$



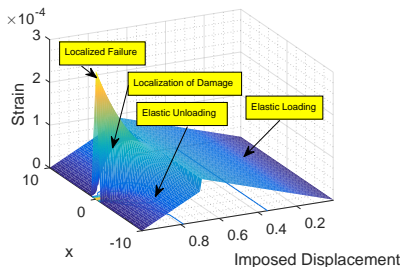
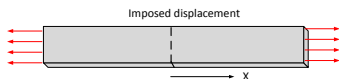
- This figure calls for the following observations:
 - ① Specimens **less than 2 m long: softening** branch which can be experimentally obtained only through displacement controlled tests.
 - ② For a **2 m specimen, perfectly brittle response**.
 - ③ For specimens **larger than 2 m, snapback**, which can only be hypothesized but not experimentally obtained.
 - ④ Large specimens could still be tested, however rather than using the entire specimen length as “gage length” (or displacement/stroke control test), we would have to **use a smaller gage length** (through strain control tests) across a potential crack. Thus a notched specimen should be used.
- Load displacement curve of this simple test is clearly **size dependent**. **The larger the specimen, the larger the stored strain energy which would be released to form surface energy.**
- An **energetic interpretation** of this figure would lead us to compare the elastic energy $U = \frac{1}{2} f'_t \epsilon_u AL = \frac{1}{2} (3 \times 10^6)(10^{-4})AL = 150AL$ at peak load with the fracture energy $G_F = 300 \text{ N/m}$, thus $300A = 150AL$ and $L = 2 \text{ m}$.

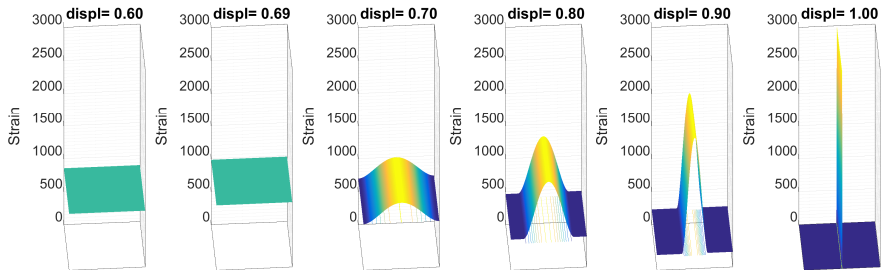
- As long as the strain energy is smaller than the fracture energy, then we do have structural softening
- if the two energies are equal, then we would have a **perfectly brittle response**.
- If the elastic energy exceeds the fracture energy, then we would have a sudden failure with **snap-back**.

L (m)	0.1	1.	2.	3.	4.
$\frac{U}{A}$	15.	150.	300.	450.	600.

- We observe that $\frac{U}{A} = G_F$ for $L = 2$ m. Thus, as long as the energy released can be transformed into fracture energy, we do have a stable configuration.
- However if the accumulated strain energy being released (including not only the one stored in the specimen, but also in the experimental set-up) is greater than the one which can be absorbed to create new surface energy (cracks), then we do have instability.

- For a successful post-peak experiment the **total strain energy** (of the specimen and of the testing frame) **should be less than the fracture energy**. Hence, to avoid snap-backs the testing frame should be as stiff as possible.





The remaining frames of this file have been imported from my book [Aging, Shaking and Cracking of Structures](#). Formatting is certainly “sub-optimal”.

This is a fascinating subject, one which seems to have been ignored by many researchers (who prefer a heuristic/observational approach), yet one that have multiple potential applications to better understand crack nucleation, coalescence, and ultimately failure or delamination.

Strength Griffith addressed the impact of imperfections to the strength of (perfect crystalline) solids by revisiting the work of Inglis.

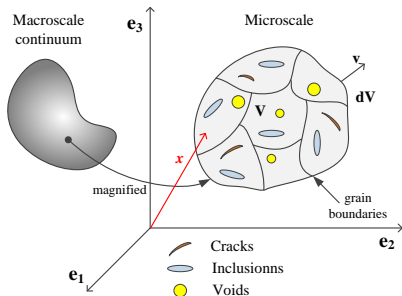
$$\sigma_{nominal} = \sigma_{the} \left(1 + 2\sqrt{\frac{a}{\rho}} \right) \quad (2)$$

where σ_{th} is the theoretical strength of solids estimated to be

$$\sigma_{th} \approx \frac{E}{10} \quad (3)$$

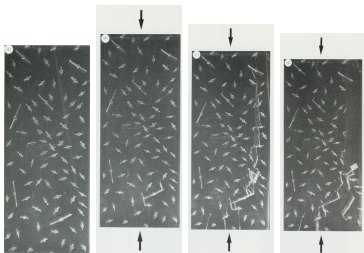
Which explains why smaller solids, in defiance to the theory of plasticity, have higher strength.

Compliance The impact of imperfections, on the formation, propagation and compliance in brittle material was experimentally and analytically investigated by the seminal book of Nemat-Nasser (1993)

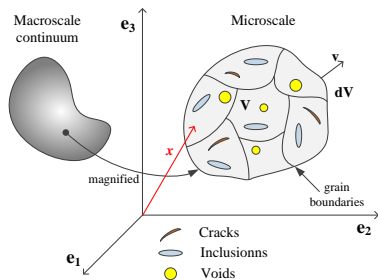


Experimental Evidence

- The attached figures are indeed an illustration of the response of flawed (inherently caused by “manufacturing”) solids to increasing compressive load.
- First crack will nucleate, then they coalesce and finally failure occurs and is driven by a predominantly coalesced crack.



- The impact of imperfections, on the formation, propagation and compliance in brittle material was experimentally and analytically investigated by the seminal book of Nemat-Nasser (1993)



Analytical Considerations

- In a comprehensive and detailed study, Nemat-Nasser (1993) derived analytical expressions for the impact of micro-cracks on the compliance (E) of a brittle solid by considering penny-shaped micro-cracks defined by their radius a_α and orientation given by the unit normal $\mathbf{n}_\alpha = \mathbf{n}$

$$n_1 = \sin \Psi \cos \theta; \quad n_2 = \sin \Psi \sin \theta; \quad n_3 = \cos \Psi \quad (4)$$

- When there are a very large number of microcracks with radii ranging from a_m to a_M , and with unit normals ranging over all orientations, a density function, $w = w(a, \theta, \Psi)$, may be introduced such that the number of cracks per unit volume with radii in the range of a to $a + da$, and orientations in the range of (θ, Ψ) to $(\theta + d\theta, \Psi + d\Psi)$ is given by $w(a, \theta, \Psi) \sin \Psi da d\theta d\Psi$, then the total number of cracks per unit volume, N , is

$$N = \frac{1}{4\pi} \int_{a_m}^{a_M} \int_0^{2\pi} \int_0^\pi w(a, \theta, \Psi) \sin \Psi da d\theta d\Psi \quad (5)$$

- $\sin \Psi d\theta d\Psi$ defines the elementary solid angle with orientation (θ, Ψ) . With θ ranging from 0 to 2π and Ψ ranging from 0 to π , the corresponding unit vector traces a unit sphere.

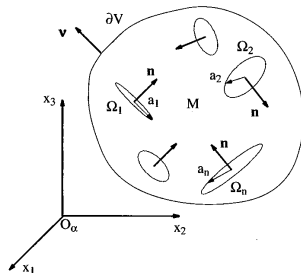
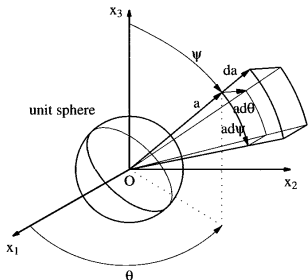
- When the crack size distribution is independent of the crack orientation, the density function may be expressed as

$$w(a, \theta, \Psi) = w_r(a) w_0(\theta, \Psi) \quad (6)$$

and

$$N = \int_{a_m}^{a_M} w_r(a) da \quad (7)$$

$$1 = \frac{1}{4\pi} \int_0^{2\pi} \int_0^\pi w_0(\theta, \Psi) \sin \Psi d\theta d\Psi \quad (8)$$



- Now, if we consider a simple case where: (1) the distribution of microcracks is dilute (which assumes that the inhomogeneities are small and far apart, so that their interaction may be neglected) and (2) the crack orientation distribution is random; and (3) the crack size distribution is independent of the crack orientation (right figure). Then, the crack orientation distribution function, $w_0(\theta, \Psi)$ given by Equation 6 becomes

$$w_0(\theta, \Psi) = \text{constant} = 1 \quad (9)$$

Then

$$\frac{\bar{E}}{E} = 1 - f \frac{16(1 - \nu^2)(10 - 3\nu)}{45(2 - \nu)} + O(f^2) \quad (10)$$

where

f is the crack density parameter

$$f \equiv \int_{a_n}^{a_M} a^3 w_r(a) da \quad (11)$$

- Since the microcracks distribution is dilute $f \ll 1$, for a uniform crack size distribution

$$w_r(a) = \frac{N}{a_M - a_m} \quad (12)$$

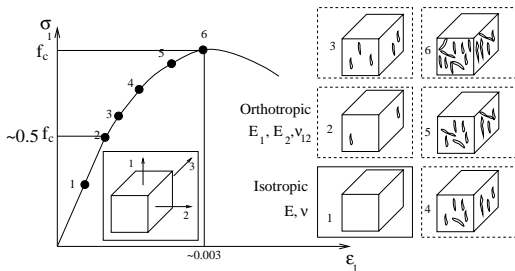
and the crack density parameter f becomes

$$f = \frac{N}{a_n - a_M} \int_{a_n}^{a_M} a^3 da = \frac{N}{4} (a_M^3 + a_M^2 a_m + a_M a_m^2 + a_m^3) \quad (13)$$

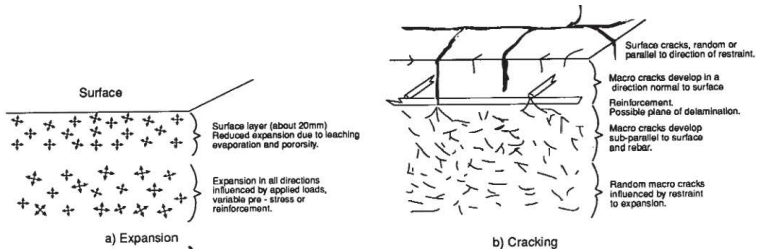
- if all the microcracks in the RVE have the same radius a then

$$f = Na^3 \quad (14)$$

- Micro-cracks are omnipresent in concrete. Under tension, we have a macro-crack, and in this context, the model of Hillerborg is by now universally accepted, and is characterized by a so-called fracture process zone composed of multiple micro-cracks.
- Under compression, micro cracks are most likely to initiate at Interface Transition Zones (ITZ) around (non-shrinking) aggregate, then we do have micro-cracks due to poor vibration.
- Micro-cracks will form and extend due to external strain or internal swelling. Hsu et al. (1963) were the first to connect the formation (and propagation) of micro-cracks to the nonlinear (compressive) stress strain curve of concrete,

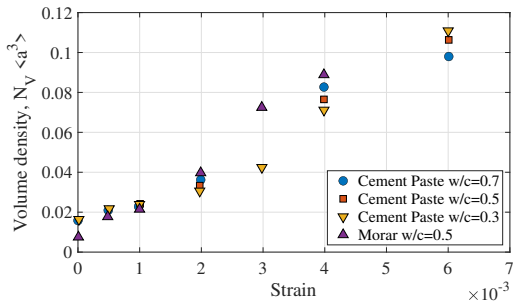


- ASR, by virtue of the (often constrained) expansion will induce the formation of micro cracks that will propagate as a result of additional swelling. Indeed, for ASR, the reduced elastic modulus due to ASR could conceivably be interpreted through the prisms of Nemat-Nasser's model.



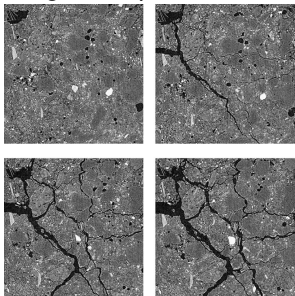
- Experimental quantification of the impact of micro-crack on the macro response of concrete is notoriously difficult to achieve.
- In a seminal paper, Atiogbe and Darwiin (1987) measured the submicroscopic cracking of cement paste and mortar under uniaxial compression and compared them to applied strain. They showed that
 - 1 Crack density in cement paste and mortar increases with increasing uniaxial compressive strain, starting at strains as low as 0.0005.
 - 2 The density of surface cracks in cement paste and mortar is an order of magnitude greater than the density of bond and mortar microcracks in concrete at the same values of compressive strain.
 - 3 Under uniaxial compressive loading, the mean size of submicroscopic cracks increases with increasing strain, while the number of cracks per unit volume decreases. This suggests that as compressive strain increases, small cracks *coalesce* to form larger cracks.
 - 4 Under increasing uniaxial compression, three-dimensional distributions of submicroscopic cracks become skewed towards the direction of applied stress.

- 5 On the average, three-dimensional crack distributions in cement paste show only small variations with water to cement (w/c) ratio. However, at high strains volumetric crack density increases more rapidly the lower the w/c.
- 6 Crack density is lower initially but increases more rapidly in mortar than in cement paste. Thus, sand particles appear to act as stress raisers that result in a greater degree of softening and a lower strain capacity for mortar than for cement paste.

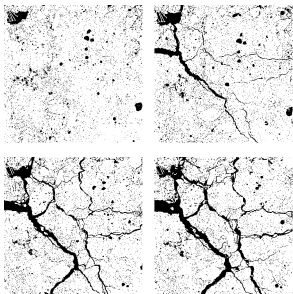


- Landis (2005) used three-dimensional measurements of internal cracking and simple relationships were made between the quantity of cracking and a corresponding scalar damage variable. A scalar damage variable was determined from the changes in stiffness measured in successive loading cycles. Results showed a nearly linear relationship between the damage variable and the fractal dimension of the internal crack system. In contrast, results showed a nonlinear relationship between the damage variable and the crack surface area.

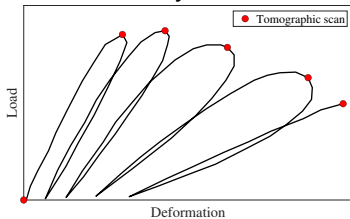
Images of specimen sections at different levels of damage:



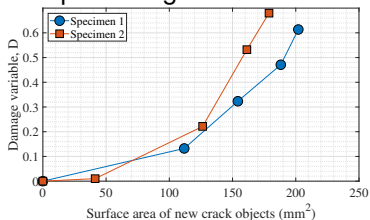
Binary images highlighting crack and void space in the same sections



Load-unload cycles and tomographic scans



Damage variable plotted against the cumulative increase in crack object



surface area

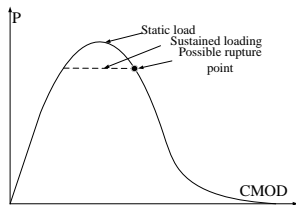
- Finally, those micro-crack may propagate as a result of creep, and may coalesce leading to failure (of a concrete cylinder or worst a delamination in the absence of reinforcement). This will be addressed next.

- The structures considered are likely to sustain large, sustained compressive stresses in the presence of internal damage (micro-cracks) possibly caused by ASR. Accordingly their long term response must be ascertained and possibly accounted for in some critical cases.
- The time dependence of fracture has two sources:
 - 1 Viscoelasticity of material behavior in the bulk of the structure
 - 2 the rate process of the breakage of bonds in the fracture process zone which causes the softening law for the crack opening to be rate-dependent Bazant 1997.

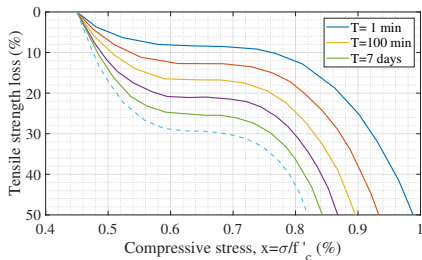
Load Carrying Capacity

- Zhou (1992) was the first to experimentally investigate creep fracture in his doctoral research Time-Dependent Crack Growth and Fracture of Concrete).

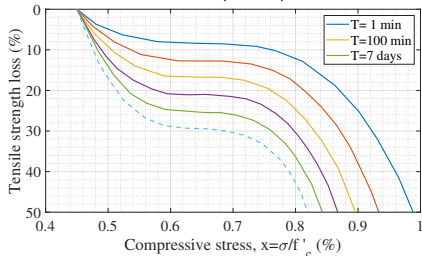
- His experimental work has been extensively referenced thereafter, and to the best of my knowledge, they have never since been replicated. The premises of the investigation is the observation that if we increase the rate of loading, there is an increase in “strength” (Malvars 1998), would there be a corollary, that is for very slow loading (such as effect of time, or simply creep), there would be a decrease in “strength”?
- Hence, fracture tests under sustained loading were performed, and an empirical relationship for the rate effect on the fracture energy was determined. It was found that if the stress is close to the tensile strength, then under sustained static loading, we may have a rupture point



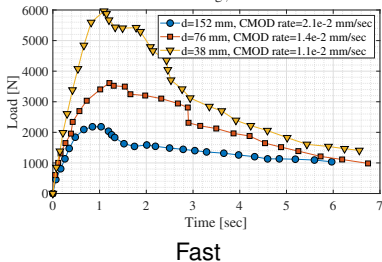
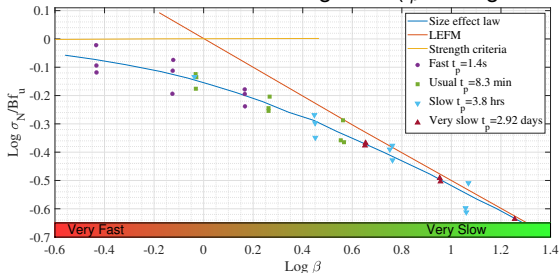
Possible Failure Under Sustained Load adapted from Zhou (1992)

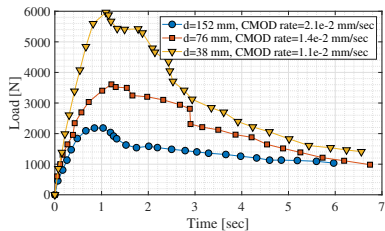


Tensile strength loss vs time and sustained compressive stress, adapted from Liniers (1987)

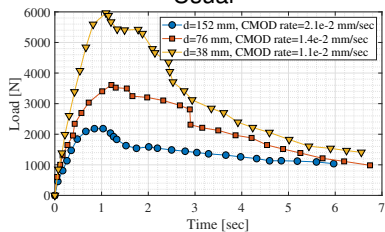


- Analogous results were obtained by Bazant & Gettu (1992) who followed a fracture mechanics interpretation, and showed that under sustained loading, behavior shifts from quasi-brittle material to brittle material.
- In other words whereas under normal load energy is smeared along the fracture process zone, under sustained load, the fracture process zone tends to shrink to almost zero, and we are now closer to the linear elastic fracture mechanics condition (with singularity at the tip).
- Likewise, it was found that the load he work of Zhou (1992) (with A. Hillerborg) has been widely referenced by modelers and seldom replicated by experimentalists. It provides ample experimental evidence that creep fracture is a phenomenon to be reckoned with.
- Carpinteri (1997) did carry out additional tests (with Zhou), and those results have been primarily used by the “Italian” school of fracture. They have shown that a slow rate of loading will reduce the peak load, and more importantly that the mode of failure is altered from one of a quasi-brittle to brittle (i.e approaching linear elastic fracture mechanics), Figure 36.
- Likewise, it was found that the load rate will have an influence on the peak load carrying capacity of concrete.

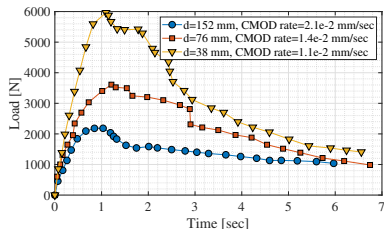
Change in Mode of Failure with Loading Rate (t_p average time to peak)



Usual



Slow



Very Slow

Effect of loading rate on peak load (adapted from Bazant & Gettu 1992)

- A theoretical framework for creep fracture was set by Bazant (1997a-b)
- Application to nuclear container was (indirectly) addressed by Masuero (1995), and most recently by Vanzij (2001) who analyzed the test results of Zhou (1992).
- Mihashi (1980) presented a power law for the tensile strength of concrete in terms of the load rate, which is actually analogous to the one of Zhou (1992).

- To the best of my knowledge, the only experimental work reporting on the decrease of tensile strength due to compression induced “damage” is the one of Liniers (1987) who first applied compressive loads on concrete specimens, and then determined the splitting tensile strength using a “Brazilian Tests”. It was determined that for compressive stresses over 40% of compressive strength there is a substantial (up to 50%) decrease in tensile strength reduction.
- This tensile strength reduction is further exacerbated by time as shown below,
- On a related issue, the role of pre-damage (micro-cracks) in tension of the compressive strength of concrete has also been studied by Katsarakis (2009).

Fracture Energy

- In the preceding section, we reported on the impact of creep on load carrying capacity (compression or tension). However, for applications relevant in this course, one seeks to quantify the decrease in G_F and f_t following creep fracture.

- Specifically, based on his tests, Zhou (1992) has shown that the fracture energy decreases as loading rate decreases. For the tested beams, the fracture energy was found to be related to deflection rate in a power law

$$\frac{G_F}{G_{F0}} = \left(\frac{\dot{u}}{\dot{u}_0} \right)^{0.04} \quad (15)$$

where \dot{u} is the displacement rate, and $\dot{u}_0 = 2 \mu\text{m/s}$.

- Alternatively, one can attempt to infer the decrease in G_F from the one of the elastic modulus E .
- Recalling that the characteristic length is given by

$$l_{ch} = \frac{EG_F}{f_t^2} \quad (16)$$

- Bazant (personal communication) estimates that it should drop about 10 times, the long term tensile strength being about 80% of the static one. If we use Equation ?? $E_{eff} = E/(1 + \Phi)$, then

$$\frac{G_F^\infty}{G_F^0} = \frac{\frac{(0.1)l_0(0.8)^2 f_t^2}{E}}{\frac{l_0 f_t^2}{E}}, \text{ or } G_F^\infty = 0.192 G_F^0 \quad (17)$$

Thus, we could have a decrease of about 80% in G_F as a result of creep fracture.

- Using a highly analytical approach, the interaction of adjacent cracks, (such as those in a fracture process zone, or possibly caused by ASR), were first investigated by Horii (1987) and explicit asymptotic expressions are obtained for the stress intensity factors of the macro-crack, as well as those of the micro-cracks.
- The mechanism of fracture coalescence in hard, porous material has been investigated experimentally and through numerical simulation Shen (1995)
- It was found that fracture coalescence can be generated by mode I failure, mode II failure, or mixed mode I and II failure. The mode II failure plays an important role in the coalescence between two non-overlapping cracks. The mechanism of coalescence observed in gypsum does not agree with previous experimental results where glass and polymer have been used.
- For those materials coalescence only occurs between overlapping cracks and is caused by mode I failure. The possible reason why mode II failure can occur in gypsum and other earth materials such as rock and concrete is the existence of voids and pores in these materials.

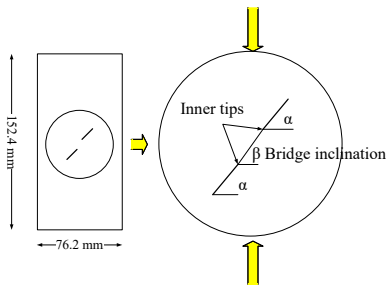
- Porous material can absorb the shear dilation in the fracture process zone and prevent the development of resistant stress due to shear dilation. The mode II fracture toughness of material with high porosity is known to be low (in concrete G_F'' is about 10 times smaller than G_F').
- A (mixed mode) crack propagation model was developed for the failures in compression Hussain and Pu. It is an extension of the classical maximum energy release rate G . However, the authors found that when applied to crack propagation under compressive load, the original G criterion can lead to wrong results, especially for the direction of wing crack initiation and it does not consider difference between mode I surface energy (G_{Icr}) and mode II surface energy (G_{IIcr}).
- Therefore, a modified G criterion, (called the F criterion, was proposed

$$F = \frac{G_I}{G_{Icr}} + \frac{G_{II}}{G_{IIcr}} \geq 1.0 \quad (18)$$

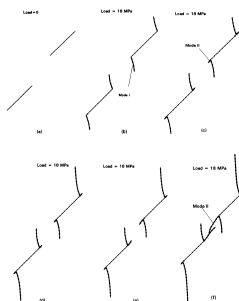
where G_I and G_{II} are the mode I and II energy release rates during crack growth.

- Extension occurs in the direction θ which maximizes F .

Geometry of gypsum samples and pre-existing cracks

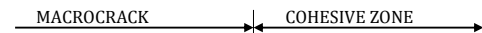
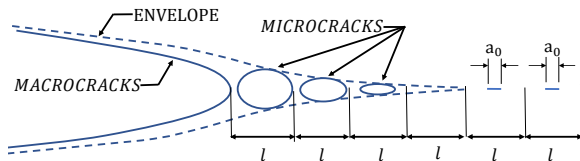


Simulated coalescence of two 45 /105 closed cracks



- Whereas the previous model was experimentally driven (or heuristic in nature), a mechanics based one was followed by Ortiz (1988) (albeit for mode I crack propagation only). In this model the author studied the analytical estimation of the effect of microcracking on crack growth initiation in brittle solids.
- Particular attention was given to the counteracting effects of toughness degradation and shielding (reduction of the stress intensity factors) by macrocracking, with a view to determining the range of dominance of each mechanism.

- Crack growth initiation by coalescence with microcracks was studied with the aid of a cohesive zone model. The extent of shielding of the crack tip by the intervening microcracks is estimated under isotropic damage conditions.
- A comparison of these effects reveals that, were the crack capable of growing within its plane, the toughness enhancement derived from shielding would be almost exactly counterbalanced by the reduction of toughness in the microcracked material.



Crack coalescence (adapted from Ortiz 1988)

Two excellent papers, not reviewed in the preparation of these notes, are:

- 1 Huq, F., Liu, J., Tonge, A.L. and Graham-Brady, L., 2019. A micromechanics based model to predict micro-crack coalescence in brittle materials under dynamic compression. *Engineering Fracture Mechanics*, 217, p.106515.
- 2 Li, X., Li, X., Yang, H. and Jiang, X., 2018. *Interaction between a Macrocrack and a Cluster of Microcracks by Muskhelishvili's Complex Potential Method*. *Mathematical Problems in Engineering*, 2018.

Size Effect

Victor E. Saouma
saouma@colorado.edu

University of Colorado, Boulder

Spring 2022

1 Introduction

2 Derivation

- Original: Bažant
- Derivation: Saouma

3 Implications of the SEL

Size Effect

- Recall that

$$\begin{aligned}
 -\frac{\partial \Pi}{\partial a} &= -\frac{\partial U^e}{\partial a} + \frac{\partial W}{\partial a} \\
 &= \frac{\partial U^p}{\partial a} + \frac{\partial \Gamma}{\partial a}
 \end{aligned}$$

- For quasi-static crack growth: **Rate of potential energy decrease during crack growth is equal to the rate of energy dissipated in plastic deformation and crack growth.**
- For brittle material ($U^p = 0$) potential energy released stored in \mathbb{R}^3 is released to create a surface energy (crack) in \mathbb{R}^2 . Thus we have a **Size Effect**.
- It has profound influence in assessing the strength of “large” structures.

- Examine the **Energy exchanged** during infinitesimal crack extension in a plate.
- Noting that: $\frac{y}{a_0 + c_f} = \frac{k}{1}$, the **Energy released under the shaded area** can be **approximated** by $b2k(a_0 + c_f)\Delta a\sigma_n^2/2E$, which must be equal to the **energy consumed** during crack growth: $bG_F\Delta a$, hence

$$b2k(a_0 + c_f)\Delta a\sigma_n^2/2E = bG_F\Delta a \quad (1)$$

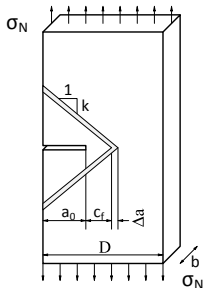
yielding

$$\sigma_n = \frac{Bf_t'}{\sqrt{1 + \frac{D}{D_0}}}$$

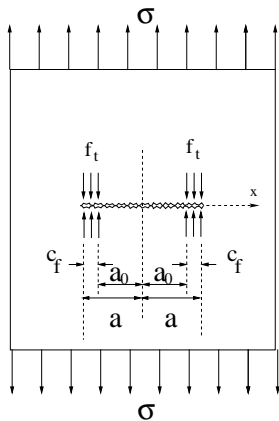
where

$$Bf_t' = \sqrt{\frac{G_F E}{k c_f}} \quad \text{and} \quad \frac{D}{D_0} = \frac{a_0}{c_f} = \beta$$

In his original paper, Bažant noted that analytical or numerical derivation of B and β is **too difficult**, and they are best obtained through statistical regression analysis of test data.



- Bažant's derivation **does not clearly establish the tie between LEFM and NLFM**
- Alternate derivation based on classical elasto-plastic fracture mechanics. As with Barenblatt and Dugdale, in its simplest form the **stress intensity factors caused by the cohesive stresses (in a plastic zone or process zone), are assumed to cancel the ones caused by the far field load.**
- The size effect law will be shown to have **explicit roots in plasticity and linear elastic fracture mechanics.**
- Not only quasi-brittle materials exhibit a size effect, but **elasto-plastic ones as well.**
- An infinite plate subjected to a far field uniform tensile stress σ and a crack of length $2a$, at the tip of which we have a uniform cohesive compressive stress (Dugdale type) equal to the tensile strength f'_t ,



- The stress intensity factors due to the far field and cohesive stresses are:

$$K_a = \sigma\sqrt{\pi a}$$

$$K_b = f'_t \sqrt{\pi a} \left(1 - \frac{2}{\pi} \arcsin \frac{a - c_f}{a} \right); \quad \arcsin \theta = \frac{1}{\sin \theta}$$

respectively,

- Equating those two stress intensity factors, we obtain the **nominal strength**

$$\sigma_n = f'_t \left[1 - \frac{2}{\pi} \arcsin \left(1 - \frac{c_f}{a} \right) \right]$$

- In the limit, for small sizes when $a \simeq c_f$, σ_n approaches asymptotically f'_t . On the other hand, for **large sizes**, $c_f \simeq 0$, σ_n will asymptotically approach zero.

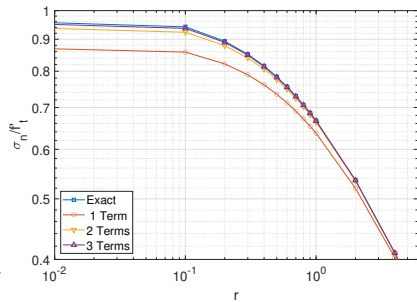
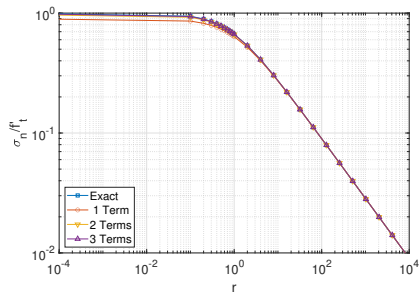
- Whereas the expression of σ_n appears to have the same limits as the Size Effect Law, it is not mathematically similar to it. This will only become apparent if one takes a **series expansion of the ArcSin function, and substituting c_f/a by s** :

$$\begin{aligned}\sigma_n &= \sigma_n = f'_t \left[1 - \frac{2}{\pi} \arcsin(1 - s) \right] \\ &\simeq \frac{2\sqrt{2}f'_t}{\pi} s^{1/2} + \frac{f'_t}{3\sqrt{2}\pi} s^{3/2} + \frac{3f'_t}{40\sqrt{2}\pi} s^{5/2} + O[s]^{7/2}\end{aligned}$$

- Neglecting the terms of power greater than 1 (since s is at most equal to 1), and substituting $s = 1/(1 + r)$ where $r = a_0/c_f$, we obtain

$$\sigma_n = \underbrace{\frac{2\sqrt{2}}{\pi}}_B f'_t \sqrt{1 + \underbrace{r}_\beta}$$

- We have thus recovered the size effect law as originally derived by Bažant as expressed by Eq. 1, with the additional benefit that B is quantified for this combination of geometry and cohesive stresses.

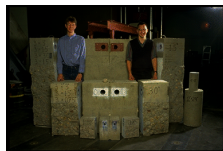
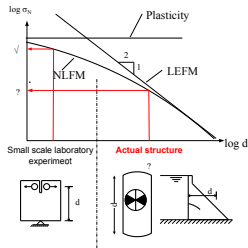


- We can rewrite Eq. 1 as

$$f_t^* = \frac{f_t'}{\sqrt{1 + \beta}} = \frac{\sigma_N}{B}, \quad (2)$$

where f_t^* is termed the **size-reduced-strength** and is a characteristic of the **entire structure and not only of the material**.

- Bazant has defined $\beta = \frac{\lambda}{\lambda_0} = \frac{D}{D_0}$ where D is a representative dimension of the structure and D_0 the average aggregate size.
- Undoubtedly the size effect law is a very elegant generalized model for concrete fracture. It attempts to provide a **unified mathematical model for concrete cracking by merging two different approaches**. Furthermore, it has been **experimentally validated** with numerous tests, many of which involved uncracked (initial) structures.
- The size effect law can be plotted on a log-log scale with σ_n versus size d .



Tests by Saouma, $1' < h < 5'$,
 $3/4" < d_a < 3"$

- For structures of a **small size relative to the size of aggregate**, i.e for small λ
 - The value of $\frac{\lambda}{\lambda_0}$ in Eq. 2 may be neglected in comparison to 1, yielding $f_t^* \simeq f_t'$, and the **classical strength criterion governs**.
 - $B = \frac{\sigma_N}{f_t'}$ and can be determined from plastic limit analysis.
- For structures with **very large size** compared to aggregate size, $\frac{\lambda}{\lambda_0} \gg 1$. Thus Eq. 2 reduces to $f_t^* \simeq f_t' \sqrt{\frac{\lambda_0}{\lambda}}$, and we see that “For very large concrete structures, such as dams (or large rock masses), Eq. 2 **asymptotically approaches the size effect of linear elastic fracture mechanics**”.
- In general, Eq. 2 represents a **gradual transition** from the strength criterion for small structures to linear elastic fracture mechanics for large structures.
- To **assess** the size effect law, **geometrically identical specimens, but with different sizes** must be tested. Then Eq. 2 can be cast in the form:

$$Y = a + b\lambda = \frac{1}{\sigma_N^2}, \quad (3)$$

where $a = \frac{1}{B^2}$ and $b = \frac{1}{B^2\lambda_0}$.

- From statistical regression analysis, the intercept a , and the slope b can be determined, and then $B = \frac{1}{\sqrt{a}}$ and $\lambda_0 = \frac{a}{b}$
- If $\frac{\lambda}{\lambda_0} = \beta$ is less than 0.1, then a strength criterion must be used, and if β is greater than 10, then a LEFM criterion is to be used. Note that **those are arbitrary guidelines**.
- The point of intersection of the two asymptotes corresponds to $\beta = 1$.
- It can be shown, that the **fracture energy G_F can be recovered from the Size Effect Law**
- There is a strong **analogy between the size effect and column buckling**

Column Buckling	Size Effect
Euler Equation	LEFM
Slenderness ratio	Size
Plastic failure	Plastic failure
Inelastic stresses	Cohesive stresses
Inelastic Buckling	NLFM
Column Equation (SSRC)	Size Effect law (Bažant)
$\sigma_{cr} = \sigma_y \left[1 - \frac{\sigma_y}{4\pi^2 E} \left(\frac{KL}{r_{min}} \right)^2 \right]$	$\sigma_n = \frac{Bf_t'}{\sqrt{1+\beta}}$

- Size Effect is most critical in **unreinforced concrete**, this is the case in many old structures with **no shear reinforcement**.
- Recently (and finally) implicitly accounted for in the latest ACI-318-19 design code.

Chapter 22: New Sectional Shear Strength Equations

ACI 318-19 introduces a new set of simplified equations for one-way shear strength, applicable to nonprestressed beams, slabs, and walls loaded out-of-plane. The equations include a size effect for sections that do not have minimum shear reinforcement. The size effect is also applicable to two-way shear and to strut capacity for strut-and-tie models without a minimum grid of reinforcement. The size effect factor is not applicable to isolated and combined footings.

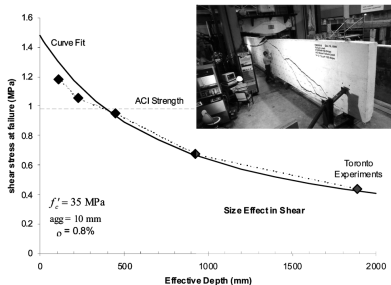


Fig. 1—Example of size effect in shear for reinforced concrete members without stirrups.¹

Fictitious and Interface Crack Models

Victor E. Saouma
saouma@colorado.edu

University of Colorado, Boulder

Spring 2022

1 Introduction

2 Fictitious Crack Model

- Approach
- Computational Algorithm
- Weak Form of Governing Equations
- Discretization of Governing Equations
- Penalty Method Solution
- Incremental-Iterative Solution Strategy

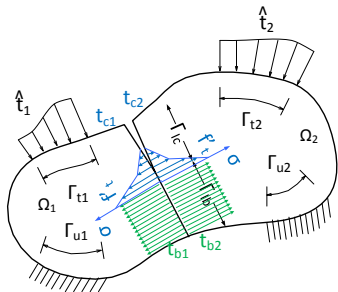
3 Interface Crack Model

- Premises
- Model
- Application: Gilboa Dam
- Application: Seismic Safety of Buttress Dam
- Application: Crystal River
- Polymers

- Finite element simulation of solids with cohesive materials (post-peak softening curve in tension) is addressed in this lecture.
- Two models (based on 2 PhD thesis of the author) will be presented:
 - 1 **Fictitious Crack Model** by Reich. Very efficient model, limited to Mode I, with load scale.
 - 2 **Interface crack model** a very comprehensive zero thickness element developed by Červenka.
- An extension of the interface crack model to account for surface degradation was developed by Puntel, but will not be presented.

- Treat the structure as a set of sub-domains bonded along assumed crack paths.
- Crack paths are defined by **fictitious interface elements** that initially act as constraints enforcing the bond between adjacent sub-domains.
- Change of state will function as standard interface elements as the crack propagates.
- Constraints are enforced on the global system of equations using a **penalty approach**.
- **Load scaling strategy**, which allows for load controlled analyses in the post-peak regime, is used to enforce stress continuity at the tip of the Fracture Process Zone (FPZ).

- Treatment of the structure as a set of bonded sub-domains results in a system of **mixed equations with the unknowns being displacements and surface tractions on the interface between the sub-domains.**
- The weak form of the system of mixed equations will be derived from the **Principle of Virtual Work.** The weak form equations will then be discretized for solution using the finite element method.
- The **penalty method solution** for the mixed system of equations will be used.
- An **incremental-iterative solution strategy** based on the modified-Newton algorithm that includes load scaling and allows for load control in the post-peak regime will be discussed.



- Body consisting of **two sub-domains**, Ω_1 and Ω_2 that intersect on a surface Γ_I without penetration. Each sub-domain may be subject to **body forces b_m** or to **prescribed surface tractions \hat{t}_m** on Γ_{tm} .
- Define the volume of the body as

$$\Omega = \Omega_1 \cup \Omega_2$$

and the surface of the body subject to prescribed surface tractions as

$$\Gamma_t = \Gamma_{t1} \cup \Gamma_{t2}, \quad (1)$$

- **Principle of Virtual Work** for the body is

$$\int_{\Omega} \delta \epsilon^T \sigma d\Omega - \int_{\Omega} \delta u^T b d\Omega - \int_{\Gamma_t} \delta u^T \hat{t} d\Gamma = 0 \quad (2)$$

where

$$\delta \epsilon = L \delta \mathbf{u} \quad (3)$$

$$\epsilon = L \mathbf{u} \quad (4)$$

$$\sigma = D \epsilon \quad (5)$$

- Within each sub-domain of the body Ω_m the Principle of Virtual Work must also hold, but **additional integrals** are required to account for the work performed by the **surface tractions $t_{I,m}$ on the interface Γ_I** .
- Surface tractions on the interface are due to bonding of the sub-domains t_{b_m} or to **cohesive stresses in the FPZ t_{c_m}** . In either case, **stress continuity on Γ_I** requires that

$$t_{b_2} = -t_{b_1} \quad (6)$$

$$t_{c_2} = -t_{c_1} \quad (7)$$

- Defining the interface surface as

$$\Gamma_I = \Gamma_{I_b} \cup \Gamma_{I_c},$$

where Γ_{I_b} is the bonded interface surface and Γ_{I_c} is the interface surface subject to cohesive stresses.

- External work on interface

$$\begin{aligned} \int_{\Gamma_I} \delta u_1^T t_{I_1} d\Gamma &= \int_{\Gamma_{I_b}} \delta u_1^T t_b d\Gamma + \int_{\Gamma_{I_c}} \delta u_1^T t_c d\Gamma \\ \int_{\Gamma_I} \delta u_2^T t_{I_2} d\Gamma &= - \int_{\Gamma_{I_b}} \delta u_2^T t_b d\Gamma - \int_{\Gamma_{I_c}} \delta u_2^T t_c d\Gamma \end{aligned}$$

Both t_b and t_c are unknown, but as t_b acts on the bonded, or constrained, interface it will be treated as a Lagrange multiplier

$$\lambda = t_b$$

- Substituting λ into Equations 2 and 3-5 and including the external work performed by the surface tractions on the interface surface, the **Principle of Virtual Work for sub-domains Ω_1 and Ω_2** is

$$\int_{\Omega_1} \delta e_1^T \sigma_1 d\Omega - \int_{\Omega_1} \delta u_1^T b_1 d\Omega - \int_{\Gamma_{t_1}} \delta u_1^T \hat{t}_1 d\Gamma - \int_{\Gamma_{l_b}} \delta u_1^T \lambda d\Gamma - \int_{\Gamma_{l_c}} \delta u_1^T t_c d\Gamma = 0 \quad (8)$$

$$\int_{\Omega_2} \delta e_2^T \sigma_2 d\Omega - \int_{\Omega_2} \delta u_2^T b_2 d\Omega - \int_{\Gamma_{t_2}} \delta u_2^T \hat{t}_2 d\Gamma + \int_{\Gamma_{l_b}} \delta u_2^T \lambda d\Gamma + \int_{\Gamma_{l_c}} \delta u_2^T t_c d\Gamma = 0 \quad (9)$$

- On Γ_{l_b} the displacements for the two sub-domains, $u_1|_{\Gamma_{l_b}}$ and $u_2|_{\Gamma_{l_b}}$, must be equal. This condition can be written as a **constraint in the strong form**

$$u_2|_{\Gamma_{l_b}} - u_1|_{\Gamma_{l_b}} = 0,$$

but a weak form is required to be compatible with Equation 6-7.

- The following **weak form**

$$\int_{\Gamma_j} \delta \lambda^T (u_2 - u_1) d\Gamma = 0 \quad (10)$$

was chosen for the constraint equation as it makes the **system of mixed equations symmetric**.

- **Discretization of Equations 8-9.** Each sub-domain Ω_m is discretized for displacements \mathbf{u}_m such that nodes on Γ_{t_m} and Γ_I are included in the vector of discrete displacements $\bar{\mathbf{u}}_m$.
- Number of nodes on Γ_I in Ω_1 is equal to the number of nodes on Γ_I in Ω_2 . For each node on Γ_I in Ω_1 there is a node on Γ_I in Ω_2 with the same coordinates.
- Displacements \mathbf{u}_m within the sub-domains Ω_m and the surface tractions λ on the **bonded interface Γ_{I_b}** :

$$\mathbf{u}_m = \mathbf{N}_{u_m} \bar{\mathbf{u}}_m \quad (11)$$

$$\lambda = \mathbf{N}_\lambda \bar{\lambda} \quad (12)$$

$$\delta \mathbf{u}_m = \mathbf{N}_{u_m} \delta \bar{\mathbf{u}}_m \quad (13)$$

$$\delta \lambda = \mathbf{N}_\lambda \delta \bar{\lambda} \quad (14)$$

\mathbf{N}_{u_m} and \mathbf{N}_λ are **standard shape functions**.

- To discretize the integral defining the virtual strain energy, the stresses and the virtual strains defined in Equation 3-5 must be expressed in terms of the discrete displacements and virtual displacements using Equations 11-12 and 13-14

$$\begin{aligned}\delta \epsilon_m &= \mathbf{L} \mathbf{N}_{u_m} \delta \bar{u}_m \\ \sigma_m &= \mathbf{D}_m \mathbf{L} \mathbf{N}_{u_m} \bar{u}_m\end{aligned}$$

- Defining the discrete strain-displacement operator \mathbf{B}_m as

$$\mathbf{B}_m = \mathbf{L} \mathbf{N}_{u_m},$$

the virtual strain energy can be written as

$$\int_{\Omega_m} \delta \epsilon_m^T \sigma_m d\Omega = \delta \bar{u}_m^T \int_{\Omega_m} \mathbf{B}_m^T \mathbf{D}_m \mathbf{B}_m d\Omega \bar{u}_m \quad (15)$$

- $\mathbf{K}_m = \int_{\Omega_m} \mathbf{B}_m^T \mathbf{D}_m \mathbf{B}_m d\Omega$ is the standard stiffness matrix for the finite element method, thus Equation 15 can be rewritten as

$$\int_{\Omega_m} \delta \epsilon_m^T \sigma_m d\Omega = \delta \bar{u}_m^T \mathbf{K}_m \bar{u}_m \quad (16)$$

- Discretization of the integrals for the **internal virtual work due to body forces** and the **external virtual work due to prescribed surface tractions** simply involves expressing the virtual displacements in terms of the discrete virtual displacements using Equation 13-14

$$\int_{\Omega_m} \delta \mathbf{u}_m^T \mathbf{b}_m d\Omega = \delta \bar{\mathbf{u}}_m^T \int_{\Omega_m} \mathbf{N}_{u_m}^T \mathbf{b}_m d\Omega$$

$$\int_{\Gamma_{t_m}} \delta \mathbf{u}_m^T \hat{\mathbf{t}}_m d\Gamma = \delta \bar{\mathbf{u}}_m^T \int_{\Gamma_{t_m}} \mathbf{N}_{u_m}^T \hat{\mathbf{t}}_m d\Gamma$$

- Recognizing that

$$\mathbf{f}_m = \int_{\Omega_m} \mathbf{N}_{u_m}^T \mathbf{b}_m d\Omega + \int_{\Gamma_{t_m}} \mathbf{N}_{u_m}^T \hat{\mathbf{t}}_m d\Gamma$$

is the standard applied load vector for the finite element method, the sum of the internal virtual work and the external virtual work is

$$\int_{\Omega_m} \delta \mathbf{u}_m^T \mathbf{b}_m d\Omega + \int_{\Gamma_{t_m}} \delta \mathbf{u}_m^T \hat{\mathbf{t}}_m d\Gamma = \delta \bar{\mathbf{u}}_m^T \mathbf{f}_m \quad (17)$$

- Discretization of the **external virtual work due to surface tractions on the interface**, requires that the surface tractions and the virtual displacements be expressed in terms of the discrete surface tractions and virtual displacements using Equations 11-12 and 13-14

$$\int_{\Gamma_{l_b}} \delta \mathbf{u}_m^T \boldsymbol{\lambda} d\Gamma = \delta \bar{\mathbf{u}}_m^T \int_{\Gamma_{l_b}} \mathbf{N}_{u_m}^T \mathbf{N}_\lambda d\Gamma \bar{\boldsymbol{\lambda}}$$

$$\int_{\Gamma_{t_c}} \delta \mathbf{u}_m^T \mathbf{t}_c d\Gamma = \delta \bar{\mathbf{u}}_m^T \int_{\Gamma_{t_c}} \mathbf{N}_{u_m}^T \mathbf{t}_c d\Gamma$$

- Define the **operator matrix** for the load vector due to surface tractions on the bonded interface as

$$\mathbf{Q}_m = \int_{\Gamma_{l_b}} \mathbf{N}_{u_m}^T \mathbf{N}_\lambda d\Gamma$$

and the **load vector** for the cohesive stresses as

$$\mathbf{f}_{c_m} = \int_{\Gamma_{t_c}} \mathbf{N}_{u_m}^T \mathbf{t}_c d\Gamma \quad (18)$$

the external work due to surface tractions on the interface is

$$\int_{\Gamma_{I_b}} \delta \mathbf{u}_m^T \boldsymbol{\lambda} d\Gamma + \int_{\Gamma_{I_c}} \delta \mathbf{u}_m^T \mathbf{t}_c d\Gamma = \delta \bar{\mathbf{u}}_m^T (\mathbf{Q}_m \bar{\boldsymbol{\lambda}} + \mathbf{f}_{c_m}) \quad (19)$$

- To discretize the **weak constraint equation**, the displacements and the virtual surface tractions must be expressed in terms of the discrete displacements and the discrete virtual surface tractions using Equations 11-12 and 13-14

$$\int_{\Gamma_{I_b}} \delta \boldsymbol{\lambda}^T \mathbf{u}_1 d\Gamma = \delta \bar{\boldsymbol{\lambda}}^T \int_{\Gamma_{I_b}} \mathbf{N}_\lambda^T \mathbf{N}_{u_1} d\Gamma \bar{\mathbf{u}}_1$$

$$\int_{\Gamma_{I_b}} \delta \boldsymbol{\lambda}^T \mathbf{u}_2 d\Gamma = \delta \bar{\boldsymbol{\lambda}}^T \int_{\Gamma_{I_b}} \mathbf{N}_\lambda^T \mathbf{N}_{u_2} d\Gamma \bar{\mathbf{u}}_2$$

- Recognizing that

$$Q_m^T = \int_{\Gamma_{lb}} N_\lambda^T N_{u_m} d\Gamma$$

is the **transpose of the operator matrix for the load vector due to surface tractions on the bonded interface** defined in Equation 18, the **weak constraint equation** can be rewritten as

$$\int_{\Gamma_{lb}} \delta \lambda^T (u_2 - u_1) d\Gamma = \delta \bar{\lambda}^T (Q_2^T \bar{u}_2 - Q_1^T \bar{u}_1) = 0 \quad (20)$$

- Define the discrete system of mixed equations. Substituting Equations 16, 17, and 19 into Equation 8-9 and rearranging terms, the discrete Principle of Virtual Work is written as

$$\delta \bar{u}_1^T (K_1 \bar{u}_1 - Q_1 \bar{\lambda}) = \delta \bar{u}_1^T (f_1 + f_{c_1}) \quad (21)$$

$$\delta \bar{u}_2^T (K_2 \bar{u}_2 + Q_2 \bar{\lambda}) = \delta \bar{u}_2^T (f_2 - f_{c_2}) \quad (22)$$

- As $\delta \bar{u}_m^T$ appears in both sides of Equation 21-22, it can be eliminated, leaving

$$K_1 \bar{u}_1 - Q_1 \bar{\lambda} = f_1 + f_{c_1} \quad (23)$$

$$K_2 \bar{u}_2 + Q_2 \bar{\lambda} = f_2 - f_{c_2} \quad (24)$$

- In a similar fashion, $\delta \bar{\lambda}^T$ can be eliminated from Equation 20, leaving

$$Q_2^T \bar{u}_2 - Q_1^T \bar{u}_1 = 0 \quad (25)$$

as the discrete constraint equation.

- Finally, the discrete system of mixed equations is defined by Equations 23-24 and 25, which can be written in matrix form as

$$\begin{bmatrix} K_1 & 0 & -Q_1 \\ 0 & K_2 & Q_2 \\ -Q_1^T & Q_2^T & 0 \end{bmatrix} \begin{Bmatrix} \bar{u}_1 \\ \bar{u}_2 \\ \bar{\lambda} \end{Bmatrix} = \begin{Bmatrix} f_1 + f_{c_1} \\ f_2 - f_{c_2} \\ 0 \end{Bmatrix} \quad (26)$$

- The **penalty method** is used to solve the discrete system of **mixed equations** as it **reduces the problem to that of a single-field**.
- Crack propagation is simulated by the release of constraints on the interface, the **total number of unknowns changes as the crack propagates**.
- Equation 26 is rewritten as

$$\begin{bmatrix} K_1 & 0 & -Q_1 \\ 0 & K_2 & Q_2 \\ -Q_1^T & Q_2^T & -\frac{1}{\alpha}I \end{bmatrix} \begin{Bmatrix} \bar{u}_1 \\ \bar{u}_2 \\ \bar{\lambda} \end{Bmatrix} = \begin{Bmatrix} f_1 + f_{c_1} \\ f_2 - f_{c_2} \\ 0 \end{Bmatrix} \quad (27)$$

where α is the **penalty number** and should be sufficiently large that $\frac{1}{\alpha}I$ is close to zero.

- Express $\bar{\lambda}$ in terms of \bar{u}_1 and \bar{u}_2

$$\bar{\lambda} = \alpha(Q_2\bar{u}_2 - Q_1\bar{u}_1) \quad (28)$$

- Substituting Equation 28 into Equation 27, a single-field penalized stiffness matrix equation is obtained

$$\begin{bmatrix} (K_1 + \alpha Q_1 Q_1^T) & -\alpha Q_1 Q_2^T \\ -\alpha Q_2 Q_1^T & (K_2 + \alpha Q_2 Q_2^T) \end{bmatrix} \begin{Bmatrix} \bar{u}_1 \\ \bar{u}_2 \end{Bmatrix} = \begin{Bmatrix} f_1 + f_{c_1} \\ f_2 - f_{c_2} \end{Bmatrix} \quad (29)$$

- Selection of a **good penalty number is a rather difficult task**. If too small substantial error in in the constraint equation

$$Q_2 \bar{u}_2 - Q_1 \bar{u}_1 = \epsilon \gg 0$$

If too large $\epsilon \rightarrow 0$, but impact of K_1 and K_2 is diminished: large errors in displacements not associated with the constraint equation (**round off errors**).

- Goal is to select a penalty number that **yields an acceptable error**. This may be **problem dependent**. Reich's experience is that a penalty number selected using

$$\alpha = \frac{\max(\text{diag}(K_m))}{\max(\text{diag}(Q_m Q_m^T))} \times 10^6 \quad (30)$$

yields very good results for the class of problems being considered (computed \bar{u}_1 and \bar{u}_2 on the interface tend to be identical for the **first five or six digits** when the penalized stiffness matrix is assembled in double precision.

- Incremental-iterative solution strategy is used.
- At zero load, the entire interface is constrained (i.e., fully bonded). As load is applied, surface tractions on the constrained interface violate a strength criteria and corresponding constraints are released.
- On that portion of the interface where constraints have been released, cohesive stresses act until the relative displacements of the unconstrained interface surfaces become large enough to dictate otherwise.
- In this solution strategy crack propagation occurs after every increment.
- The magnitude of the applied loads must be such that the surface tractions at a node on the constrained interface are precisely equal to the maximum allowable stress. Hence normal surface traction and the uniaxial tensile strength must be equal.
- However, magnitude of the applied loads that causes the strength criteria to be satisfied exactly is not known *a priori*, some form of automatic load scaling is used.

- Assuming that the applied loads are proportional, a **load factor β can be used to scale** an arbitrary set of applied load vector f of some arbitrary magnitude.
- At the beginning of each load increment i , the load factor is β_i and the applied load vector is

$$\beta_i f = \beta_i \left\{ \begin{array}{c} f_1 \\ f_2 \end{array} \right\}$$

β_i is zero at the beginning of the first increment. The incremental load factor for increment i is $\Delta\beta_i$ and the applied incremental load vector is

$$\Delta\beta_i f = \Delta\beta_i \left\{ \begin{array}{c} f_1 \\ f_2 \end{array} \right\}$$

The load factor at the end of increment i is

$$\beta_{i+1} = \beta_i + \Delta\beta_i$$

- **Modified-Newton algorithm** is used to solve for incremental displacements due to the applied incremental loads. The incremental displacements for a generic increment are defined as

$$\Delta \bar{\mathbf{u}}^{n+1} = \Delta \bar{\mathbf{u}}^n + \delta \bar{\mathbf{u}}^n$$

where

$$\bar{\mathbf{u}} = \left\{ \begin{array}{c} \bar{u}_1 \\ \bar{u}_2 \end{array} \right\}$$

and $\Delta \bar{\mathbf{u}}^n$ is the **incremental displacement vector at the beginning of iteration n** and $\delta \bar{\mathbf{u}}^n$ is the correction to the incremental displacement vector for iteration n .

- In a similar fashion, the incremental load factor is defined as

$$\Delta \beta^{n+1} = \Delta \beta^n + \delta \beta^n$$

where $\Delta \beta^n$ is the incremental load factor at the beginning of iteration n and $\delta \beta^n$ is the correction to the incremental load factor for iteration n . At the beginning of the first iteration both $\Delta \bar{\mathbf{u}}^n$ and $\Delta \beta^n$ are zero.

- **Displacement corrections** are computed by solving

$$K_{\alpha} d\bar{u}^n = (\beta f + \Delta\beta^n f + d\beta^n f + f_c^n - p^n) \quad (31)$$

where

$$K_{\alpha} = \begin{bmatrix} (K_1 + \alpha Q_1 Q_1^T) & -\alpha Q_1 Q_2^T \\ -\alpha Q_2 Q_1^T & (K_2 + \alpha Q_2 Q_2^T) \end{bmatrix}$$

is the penalized stiffness matrix;

$$f_c^n = \left\{ \begin{array}{c} f_{c_1}^n \\ -f_{c_2}^n \end{array} \right\}$$

is the **load vector due to cohesive stresses on the interface at the beginning of iteration n** ; and

$$p^n = \sum_{i=1}^{nelem} \int_{\Omega_{e_i}} B^T D(\epsilon + \Delta\epsilon^n) d\Omega$$

is the reaction vector for the state of stress at iteration n .

- Recognizing that

$$\mathbf{r}^n = \beta \mathbf{f} + \Delta \beta^n \mathbf{f} + \mathbf{f}_c^n - \mathbf{p}^n$$

is the residual force vector at the beginning of iteration n , Equation 31 can be written in a more compact fashion as

$$d\bar{\mathbf{u}}^n = \mathbf{K}_\alpha^{-1}(\delta\beta^n \mathbf{f} + \mathbf{r}^n)$$

- Since the $\mathbf{K}_\alpha^{-1} \mathbf{f}$ term does not change throughout the course of the iterative process it can be defined as a constant value for the increment

$$\delta\bar{\mathbf{u}}_T = \mathbf{K}_\alpha^{-1} \mathbf{f}$$

- The displacement vector $\delta\bar{\mathbf{u}}_T$ is commonly called the **tangent displacement vector**. At this point, the iterative displacement correction can be defined as

$$\delta\bar{\mathbf{u}}^n = \delta\beta^n \delta\bar{\mathbf{u}}_T + \mathbf{K}_\alpha^{-1} \mathbf{r}^n$$

- $\delta\beta^n$ must be computed such that **the strength criteria is exactly satisfied**. Since the surface tractions on the constrained interface are used to determine the magnitude of the applied load, the total surface tractions for iteration n must be expressed in terms of its various contributions

$$\bar{\lambda}^{n+1} = \bar{\lambda} + \Delta\bar{\lambda}^n + \delta\bar{\lambda}_r^n + \delta\beta^n\delta\bar{\lambda}_T$$

where

- $\bar{\lambda}$ is the surface traction vector at the beginning of the increment.
- $\Delta\bar{\lambda}^n$ is the incremental surface traction vector at the beginning of iteration n .
- $\delta\bar{\lambda}_r^n$ is correction to the incremental surface traction vector due to the residual load vector r^n for iteration n .
- $\delta\bar{\lambda}_T$ is the surface traction vector due to the tangent displacement vector $\delta\bar{u}_T$.

$\delta\bar{\lambda}_r^n$ and $\delta\bar{\lambda}_T$ are defined as

$$\delta\bar{\lambda}_r^n = \alpha(Q_2^T\delta\bar{u}_{r_2}^n - Q_1^T\delta\bar{u}_{r_1}^n)$$

$$\delta\bar{\lambda}_T = \alpha(Q_2^T\delta\bar{u}_T - Q_1^T\delta\bar{u}_T)$$

- The strength criteria is applied to $\bar{\lambda}^{n+1}$ on a **node-by-node basis** such that

$$\max((\bar{\lambda}^{n+1})_i(\mathbf{n})_i) = f_t$$

where $(\mathbf{n})_i$ is the normal vector at node i and f_t is the **uniaxial tensile strength**.

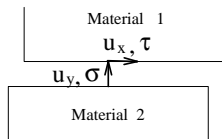
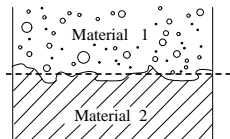
- Recognizing that $\bar{\lambda}$, $\Delta\bar{\lambda}^n$, and $\delta\bar{\lambda}_r^n$ are fixed for iteration n , the **iterative load factor correction** is defined as

$$\delta\beta^n = \min \left\{ \frac{f_t - [(\bar{\lambda})_i + (\Delta\bar{\lambda}^n)_i + (\delta\bar{\lambda}_r^n)_i] (\mathbf{n})_i}{(\delta\bar{\lambda}_r^n)_i (\mathbf{n})_i} \right\}$$

Provided that the **cohesive stresses on the interface are treated as forces and no stiffness matrix is assembled** for those interface elements, this solution strategy allows for **load control in the post peak regime**.

- The use of stiffness matrices for the interface elements subject to softening is avoided because their presence in the global stiffness matrix will eventually cause it to become **non-positive definite**.

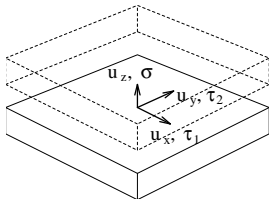
- Objective is to develop a **physically sound model**, yet **simple enough so that all its parameters can be easily derived from laboratory tests**
- Define relationships between normal and tangential stresses with opening and



sliding displacements.

Interface

Interface Model



- Major premises upon which the model is developed are:

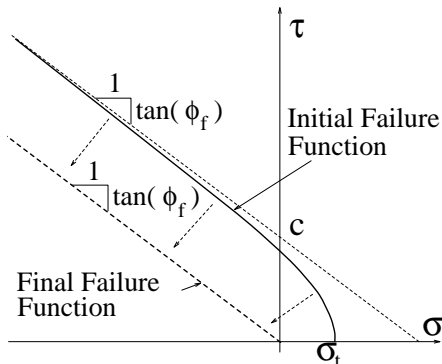
- 1 Softening is present both in shear and tension (Hillerborg extended)
- 2 Residual shear strength due to the friction along the interface, which depends on the compressive normal stress, (Coulomb).
- 3 Reduction in strength, i.e. softening, is caused by crack formation.
- 4 Zero normal and shear stiffness when the interface is totally destroyed.
- 5 Under compressive normal stresses neither the shear and nor the normal stiffnesses decrease to zero. In addition, should a compressive stress be introduced in the normal direction following a full crack opening, two faces of the interface come to contact, and both tangential and normal stiffnesses become nonzero. (contact problem).
- 6 Irreversible relative displacements are caused by broken segments of the interface material and by friction between the two crack surfaces, (permanent plastic damage)
- 7 Roughness of the interface causes opening displacements (i.e. dilatancy) when subjected to sliding displacements.
- 8 The dilatancy vanishes with increasing sliding or opening displacements.

- **Strength of the interface** is described by a hyperbolic failure function:

$$F = (\tau_1^2 + \tau_2^2) - 2c \tan(\phi_f)(\sigma_t - \sigma) - \tan^2(\phi_f)(\sigma^2 - \sigma_t^2) = 0 \quad (32)$$

where:

- c is the **cohesion**
 - ϕ_f is the **angle of friction**
 - σ_t is the **tensile strength of the interface**
 - τ_1 and τ_2 are the two **tangential components of the interface traction vector**
 - σ is the **normal traction component**
- Initially proposed by **Carol**
 - The general three-dimensional failure function is obtained by mere rotation around the σ -axis.



- The **evolution of the failure function** is based on a **softening parameter** u^{ieff} which is the norm of the **inelastic displacement vector** \mathbf{u}^i .
- The inelastic displacement vector is obtained by **decomposition of the displacement vector** \mathbf{u} into an elastic part \mathbf{u}^e and an inelastic part \mathbf{u}^i .
- The inelastic part can subsequently be **decomposed into plastic (i.e. irreversible) displacements** \mathbf{u}^p and **fracturing displacements** \mathbf{u}^f .
- The plastic displacements are assumed to be caused by friction between crack surfaces and the fracturing displacements by the formation of microcracks.

$$\begin{aligned}
 F &= F(c, \sigma_t, \phi_f), \quad c = c(u^{\text{ieff}}), \quad \sigma_t = \sigma_t(u^{\text{ieff}}) \\
 \mathbf{u} &= \mathbf{u}^e + \mathbf{u}^i, \quad \mathbf{u}^i = \mathbf{u}^p + \mathbf{u}^f \\
 u^{\text{ieff}} &= \|\mathbf{u}^i\| = (u_x^i{}^2 + u_y^i{}^2 + u_z^i{}^2)^{1/2}
 \end{aligned} \tag{33}$$

- Linear and bilinear relationship are used for $c(u^{\text{ieff}})$ and $\sigma_t(u^{\text{ieff}})$.

$$\left. \begin{aligned} c(u^{\text{ieff}}) &= c_0 \left(1 - \frac{u^{\text{ieff}}}{w_c}\right) & \forall u^{\text{ieff}} < w_c \\ c(u^{\text{ieff}}) &= 0 & \forall u^{\text{ieff}} \geq w_c \\ w_c &= \frac{2G_F^{la}}{c_0} \end{aligned} \right\} \text{linear for cohesion}$$

$$\left. \begin{aligned} c(u^{\text{ieff}}) &= c_0 + u^{\text{ieff}} \frac{s_{1c} - c_0}{w_{1c}} & \forall u^{\text{ieff}} < w_{1c} \\ c(u^{\text{ieff}}) &= s_c \left(1 - \frac{u^{\text{ieff}} - w_{1c}}{w_c - w_{1c}}\right) & \forall u^{\text{ieff}} \in \langle w_{1c}, w_c \rangle \\ c(u^{\text{ieff}}) &= 0 & \forall u^{\text{ieff}} > w_c \\ w_c &= \frac{2G_F^{la} - (s_{1c} + c_0)w_{1c}}{s_{1c}} \end{aligned} \right\} \text{bi-linear for cohesion}$$

(34)

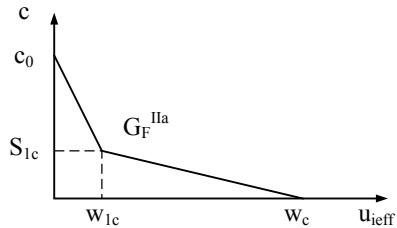
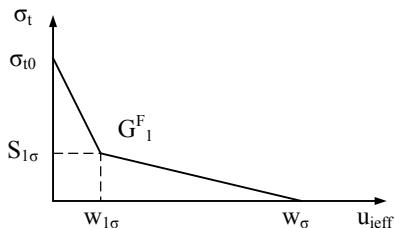
$$\left. \begin{aligned} \sigma_t(u^{\text{ieff}}) &= \sigma_{t0} \left(1 - \frac{u^{\text{ieff}}}{w_\sigma}\right) & \forall u^{\text{ieff}} < w_\sigma \\ \sigma_t(u^{\text{ieff}}) &= 0 & \forall u^{\text{ieff}} \geq w_{\sigma_t} \\ w_\sigma &= \frac{2G_F^I}{\sigma_{t0}} \end{aligned} \right\} \text{linear for tensile strength}$$

$$\left. \begin{aligned} \sigma_t(u^{\text{ieff}}) &= \sigma_{t0} + u^{\text{ieff}} \frac{s_{1\sigma} - \sigma_{t0}}{w_{1\sigma}} & \forall u^{\text{ieff}} < w_{1\sigma} \\ \sigma_t(u^{\text{ieff}}) &= s_{1\sigma} \left(1 - \frac{u^{\text{ieff}} - w_{1\sigma}}{w_{\sigma_t} - w_{1\sigma}}\right) & \forall u^{\text{ieff}} \in \langle w_{1\sigma}, w_\sigma \rangle \\ \sigma_t(u^{\text{ieff}}) &= 0 & \forall u^{\text{ieff}} > w_\sigma \\ w_\sigma &= \frac{2G_F^I - (s_{1\sigma} + \sigma_{t0})w_{1\sigma}}{s_{1\sigma}} \end{aligned} \right\} \text{bi-linear for tensile strength}$$

(35)

where G_F^I and G_F^{IIa} are mode I and II fracture energies. s_{1c} , w_{1c} and $s_{1\sigma}$, $w_{1\sigma}$ are the coordinates of the breakpoint in the bi-linear softening laws for cohesion and tensile strength respectively.

- The **critical opening and sliding corresponding** to zero cohesion and tensile strength are denoted by w_σ and w_c respectively, and they are determined from the condition that the area under the linear or bilinear softening law must be equal to G_F^I and G_F^{IIa} respectively.



- G_F^{IIa} is not the pure mode II fracture energy (i.e. the area under a $\tau-u_x$ curve), but rather is the **energy dissipated during a shear test with high confining normal stress** (Carol).

- Determination of G_F^{II} would require a **pure shear test without confinement**, which is extremely difficult to perform.
- G_F^{IIa} test requires a **large normal confinement**, and is therefore easier to accomplish.
- **Residual shear strength** is obtained from the failure function by setting both c and σ_t equal to 0, which corresponds to the final shape of the failure function and is given by:

$$\tau_1^2 + \tau_2^2 = \tan^2(\phi_f) \sigma^2 \quad (36)$$

- **Stiffness degradation** is modeled through a **damage parameter**, $D \in \langle 0, 1 \rangle$, which is a relative measure of the fractured surface. Thus, D is related to the secant of the normal stiffness K_{ns} in the uniaxial case:

$$D = \frac{A_f}{A_o} = 1 - \frac{K_{ns}}{K_{no}} \quad (37)$$

where K_{no} is the initial normal stiffness of the interface; A_o and A_f are the total interface area and the fractured area respectively.

- It is assumed, that the damage parameter D can be determined by converting the mixed mode problem into an equivalent uniaxial one. In the equivalent uniaxial problem the normal inelastic displacement is set equal to u^{ieff} . Then, the secant normal stiffness can be determined from:

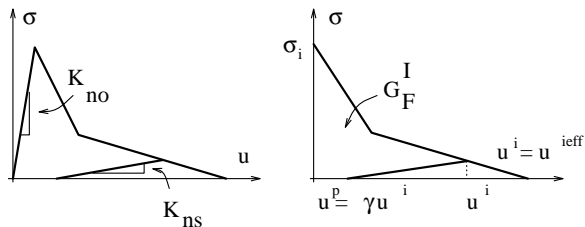
$$K_{ns} = \frac{\sigma}{u - u^p} = \frac{\sigma_t(u^{ieff})}{u^e + u^p + u^f - u^p} = \frac{\sigma_t(u^{ieff})}{\sigma_t(u^{ieff})/K_{no} + (1 - \gamma)u^{ieff}} \quad (38)$$

where γ is the ratio of irreversible inelastic normal displacement to the total value of inelastic displacement.

- Experimentally, γ can be determined from a pure mode I test through:

$$\gamma = \frac{u_p}{u_i} \quad (39)$$

where u^p is the residual displacement after unloading and u^i is the inelastic displacement before unloading.



- For concrete, γ is usually assumed equal to 0.2 or 0.3
- **Evolution of the damage parameter D** is defined by

$$D = 1 - \frac{\sigma_t(u^{ieff})}{\sigma_t(u^{ieff}) + (1 - \gamma)u^{ieff}K_{no}} \quad (40)$$

which is obtained by substituting Equation 38 into Eq. 37.

- The stress-displacement relationship of the interface is expressed as:

$$\boldsymbol{\sigma} = \alpha \mathbf{E}(\mathbf{u} - \mathbf{u}^p) \quad (41)$$

where:

- $\boldsymbol{\sigma}$ is the vector of **tangential and normal stress** at the interface.

$$\boldsymbol{\sigma} = \{\tau_1, \tau_2, \sigma\}^T \quad (42)$$

- α is the integrity parameter defining the **relative active area of the interface**, and it is related to the damage parameter D .

$$\alpha = 1 - \frac{|\sigma| + \sigma}{2|\sigma|} D \quad (43)$$

The activation of D is controlled through the fraction $\frac{|\sigma| + \sigma}{2|\sigma|}$, which is equal to one if σ is positive, and is zero otherwise.

- \mathbf{E} is the **elastic stiffness matrix** of the interface.

$$\mathbf{E} = \begin{bmatrix} K_{to} & 0 & 0 \\ 0 & K_{to} & 0 \\ 0 & 0 & K_{no} \end{bmatrix} \quad (44)$$

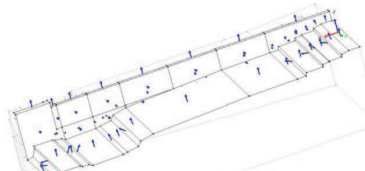
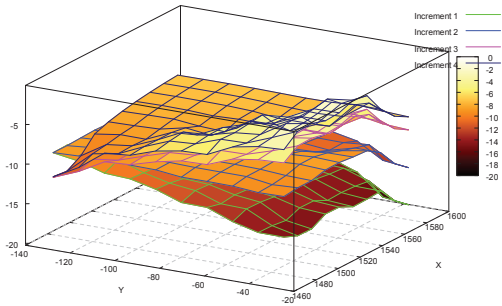
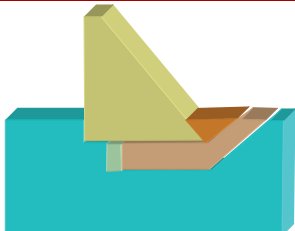
- It should be noted, that the off-diagonal terms in the elastic stiffness matrix \mathbb{E} of the interface are all equal to zero, which implies that **no dilatancy is considered in the elastic range**.
- The dilatancy of the interface is given by **dilatancy angle ϕ_d** , which is again assumed to be a function of u^{ieff} .

$$\begin{aligned}\phi_d(u^{\text{ieff}}) &= \phi_{d0} \left(1 - \frac{u^{\text{ieff}}}{u_{dil}}\right) & \forall u^{\text{ieff}} \leq u_{dil} \\ \phi_d(u^{\text{ieff}}) &= 0 & \forall u^{\text{ieff}} > u_{dil}\end{aligned} \quad (45)$$

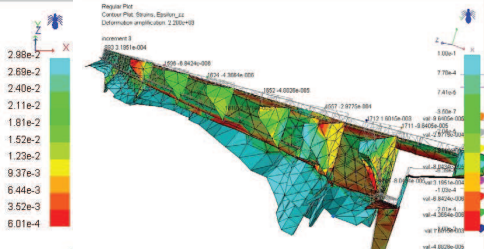
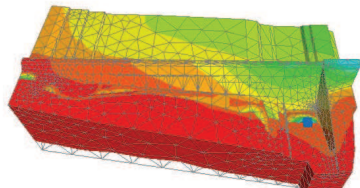
where u_{dil} is the **critical relative displacement after which, the interface does not exhibit the dilatancy effect any more**, and ϕ_{d0} is the initial value of the dilatancy angle.

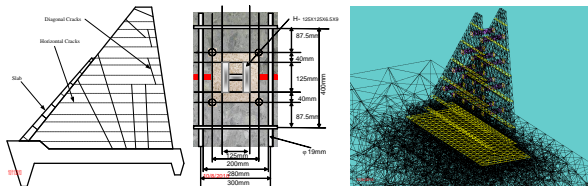
Identify potential failure modes, insert joint elements, load, and compute safety factor against sliding.



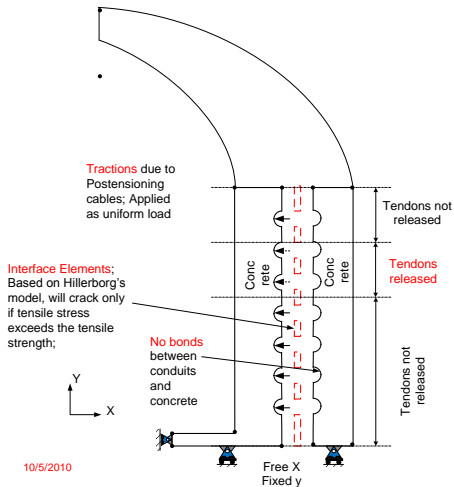


Regular Plot
Contour Plot Displacements vector length, Vector length
increment 3

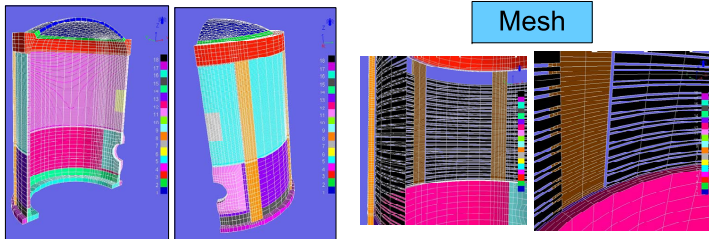




- Anticipated rehabilitation (multi-billion Yens)
- Performed nonlinear transient fracture mechanics based analysis (interface elements modified to model dowel effects)
- Analysis proved the dam to be safe, **no rehabilitation performed**.
- About \$ 150,000 saved multi-million dollars in unnecessary rehabilitation.



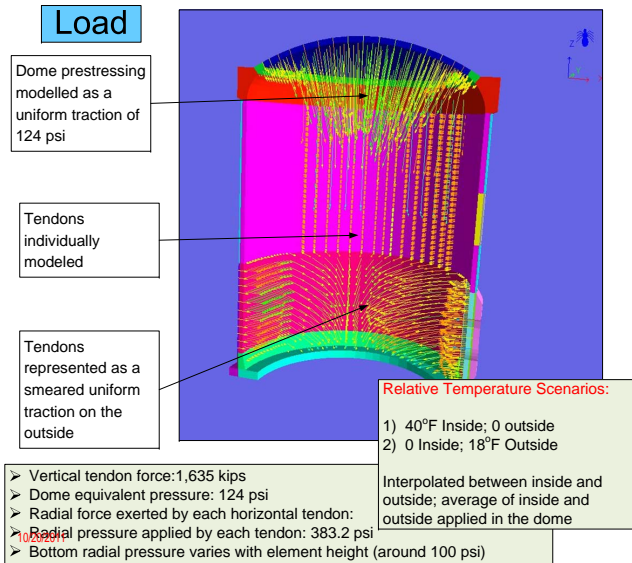
- Location of delamination known
- Insert zero-thickness discrete interface elements along the potential plane of delamination
- Concrete otherwise linear elastic
- Account for creep
item Carefully release tendons in the proper sequence, and observe potential cracking along the joints



- Used exclusively 3D solid elements with variable gradation.
- All the tendons above the hatch and up to 240' are individually modeled.
- Each one of those tendons can be individually released
- Vertical tendons in panel 45 plus four on each side) are individually modeled and can be individually released.
- Vertical tendons elsewhere are modeled by a uniform downward traction
- Post tensioning of the dome is modeled by a uniform pressure of 240 psi;
- An upward uniform load of 0.5 ksi is applied along the ring to negate the effect of the dome pressure on the shell (since dome post tensioning is self-equilibrated by the top ring)
- Cables below the hatch elevations are modeled as external pressure
- Mesh has about 60,000 nodes, or about 180k dof

10/20/2011

Close up of the interface elements' (shown in black), each one of them can separately delaminate. In between, we have the cables.



Increment		Final			Initial			Description				
1	0	0								Gravity	Initial	
2	3	1	2							Pretensioning		
4	5	3	4							Creep		
6	5									Temperature, Hot inside		
7	6									Restore temperature		
8	7									Temperature, Hot outside		
9	8									Restore temperature		
10	9	31	32	42	43							
11	10	31	V14	31	V15	31	V16	53	42	42		
12	11	31	V17	53	H28	42	H29	42	H30			
13	12	53	H29	42	H31	42	H32	42	H33			
14	13	53	H31	42	H32	53	H33	42	H34			
15	14	53	H33	53	H35							
16	15									Concrete Removal		
Increment		Final		Initial		Seq.		Release of				
17	17	V-1	V-1	61	V11	61	V14				Pass 1	
18	18	V-2	V-2	61	V33	61	V18					
19	19	V-3	V-3	61	V12	61	V13					
20	20	V-4	V-4	61	V10	61	V15					
21	21	V-5	V-5	61	V38	61	V17					
22	22	4	4	4	4	4	4	4	4	4		Pass 2
23	23	2	3	4	4	4	4	4	4	4		
24	24	3	4	4	4	4	4	4	4	4		
25	25	4	5	4	4	4	4	4	4	4		
26	26	5	6	4	4	4	4	4	4	4		
27	27	6	7	4	4	4	4	4	4	4		Pass 3
28	28	V-6	V-6	61	V17	61	V19	34	V20	34		
29	29	V-7	V-7	61	V25	61	V20	34	V25	34		
30	30	V-8	V-8	61	V33	61	V22	34	V23	34		
31	31	V-9	V-9	61	V21	61	V24	34	V24	34		
32	32	V-10	V-10	61	V23	61	V22	34	V23	34		
33	33	V-11	V-11	61	V22	61	V24	34	V23	34		
34	34	4	4	4	4	4	4	4	4	4		
35	35	7	9	4	H19	4	H21	4	H21	4		
36	36	8	10	4	H21	4	H21	4	H21	4		
37	37	9	11	4	H23	4	H23	4	H23	4		
38	38	10	12	4	H23	4	H23	4	H23	4		
39	39	11	13	4	H39	4	H41	4	H41	4		
40	40	12	14	4	H41	4	H41	4	H41	4		
		13	15	4	H43	4	H43	4	H43	4		
27	27	44	46	46	46	46	46				Pass 5	
		41	14	17	35	H15						
		43	15	19	35	H20	35	H21				
		43	16	19	35	H23	51	H23				
		44	17	20	35	H25	51	H25				
		45	18	21	35	H27	51	H27				
		46	19	22	35	H29	51	H29				
		47	20	23	35	H31	51	H31				
		48	21	24	35	H33	51	H33				
		49	22	25	35	H35	51	H35				
		50	23	26	35	H37	51	H37				
		51	24	27	35	H39	51	H39				
		52	25	28	35	H41	51	H41				
		53	26	29	35	H43	51	H43				
		54	30	30	35	H44						
		54	27	31	42	H20	64	H20				
		55	28	32	42	H22	64	H22				
		56	29	33	42	H24	64	H24				
		57	30	34	42	H26	64	H26				
		58	31	35	42	H28	64	H28				
		59	32	36	42	H30	64	H30				
		60	33	37	42	H32	64	H32				
		61	34	38	42	H34	64	H34				
		62	35	39	42	H36	64	H36				
		63	36	40	42	H38	64	H38				
		64	37	41	42	H40	64	H40				
		65	38	42	42	H42	64	H42				
		66	39	43	42	H44	64	H44				
		67	40	44	42	H46	64	H46				
		68	41	45	42	H48	64	H48				
		69	42	46	42	H50	64	H50				
		70	43	47	42	H52	64	H52				
		71	44	48	42	H54	64	H54				
		72	45	49	42	H56	64	H56				
		73	46	50	42	H58	64	H58				
		74	V-12	V-12	61	V19	34	V19	34	V19	Pass 6	
		75	V-13	V-13	61	V24	34	V24	34	V24		
		76	V-14	V-14	61	V23	34	V23	34	V23		
		77	V-15	V-15	61	V24	34	V24	34	V24		
		78	V-16	V-16	61	V22	34	V22	34	V22		
32	32	79	47	51	42	H54	64	H54	64	H54	Pass 10	
		80	48	52	42	H56	64	H56	64	H56		
		81	49	53	42	H58	64	H58	64	H58		
		82	50	54	42	H60	64	H60	64	H60		
		83	51	55	42	H62	64	H62	64	H62		
		84	52	56	42	H64	64	H64	64	H64		
		85	53	57	42	H66	64	H66	64	H66		
												Pass 11

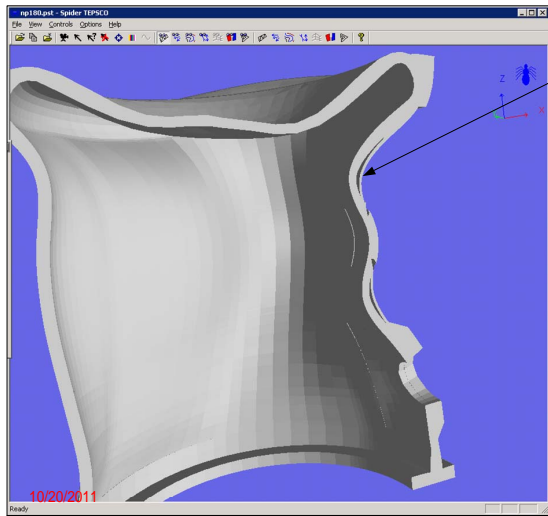
Load Increments

Notes:

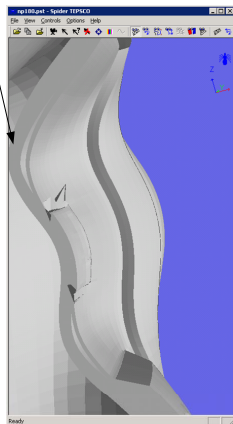
- We simulate gravity, pretensioning, creep, temperature, detensioning in SGR zone, and concrete removal in the first 16 increments.
- From increments 17 to 85 we simulate all the detensioning with exception to 4 because they entail cables which are lower than 19 (not explicitly modeled in Merlin).
- Those sequences are H1, H8, H16, and H18).

These cables are modeled as "inner" and can not be released

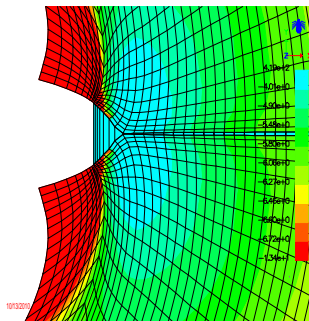
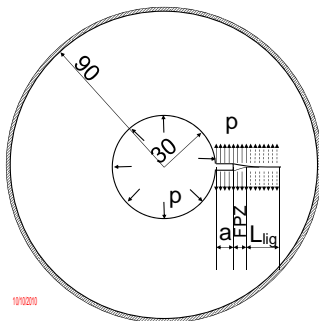
These cables are outside the zone modeled



Note delamination above and below SGR cut. This is increment 15 (concrete removal).



Cohesive crack growth in solid rocket propellants (may induce unsymmetrical comustion leading to explosion)



Corrosion Fracture

Victor E. Saouma
saouma@colorado.edu

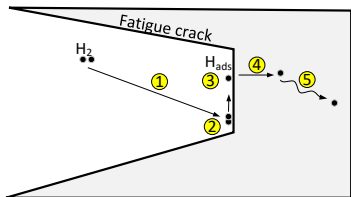
University of Colorado, Boulder

Spring 2022

- 1 Mechanism
- 2 Hydrogeneous gases
- 3 Aqueous Media gases
- 4 Growth of Corrosion-Fatigue Cracks
- 5 Models

- **Hydrogen embrittlement:** hydrogenous gases (H_2 , H_2S or **water vapor** hydrogen can be introduced into the metal. Under **cyclic load** the embrittling environment can accelerate the **initiation of surface cracks**
- **Liquid metal embrittlement:** embrittling medium is a liquid metal. Embrittlement of alloys resulting from **aqueous** solution is **stress corrosion cracking** (SCC).
- **Metal embrittlement:** weakening of higher melting point metal when in contact with certain lower melting point metals; for instance mercury will corrode metals.

All the above will result in **corrosion fatigue** commonly used to denote damage (and failure) of material under **combined actions of cyclic stresses and embrittling medium**.



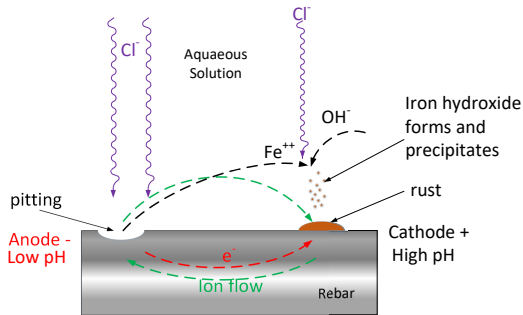
- 1 Transport of gaseous hydrogen
- 2 Surface adsorption
- 3 Dissociation into hydrogen atom
- 4 Hydrogen into the lattice
- 5 Transport in material of high tensile hydrostatic stresses

- No **single theory** can account for all phenomenon.
- **Decohesion** provide a partial explanation in high strength steel

$$C_b = C_0 \exp \left(\sigma_H \frac{\bar{v}}{R_0 T} \right) \quad (1)$$

C_0	Equilibrium concentration of hydrogen in unstressed region
\bar{v}	Partial molar volume of hydrogen in iron
σ_H	Tensile hydrostatic stress
R_0	Universal gas constant
T	Absolute temperature

- Fracture of metals in the presence of hydrogen generally occurs in any one of two ways:
 - ① Rate of failure is **accelerated** by the presence of hydrogen without a change in the microscopic mode of failure
 - ② Transition from normally ductile mode of failure to a brittle mode of failure in the presence of hydrogen (very common inside nuclear reactors).

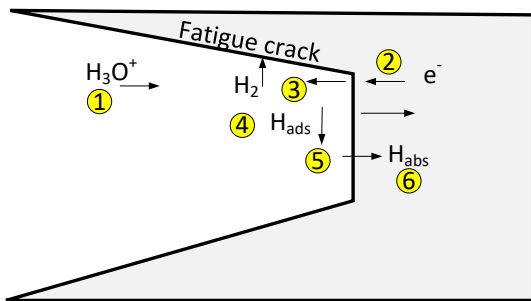


First analogy with concrete

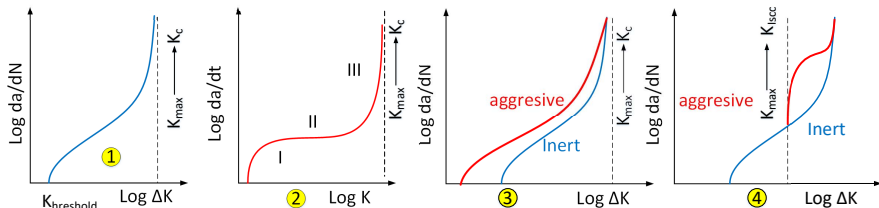
- Under high pH rebars are “passivated” and immune to corrosion.
- With ingress of chloride, pH decreases, and steel loses its protection.
- corrosion begins.

For ductile alloy/aqueous environment under both monotonic and cyclic loads: electrochemical reaction at freshly formed slip steps or at crack tips Can occur through either one of two mechanisms

- Anodic slip dissolution with an accompanying rupture of protective oxide film at a crack tip by strain concentration between the crack faces.
- Hydrogen embrittlement
 - Occurs in acidic solution



- ① **Liquid diffusion** of water molecules or hydrogen ions between the crack walls toward the crack tip.
- ② Discharge and reduction to create adsorbed hydrogen atoms at the crack tip. Adsorption on the surface is a process that prefaces absorption of gases in the bulk of solids
- ③ **Hydrogen adatom recombination**
- ④ Surface diffusion of an adatom (an atom that is on a crystal surface).
- ⑤ **Hydrogen absorption in metal**
- ⑥ **Diffusion of absorbed hydrogen**



- 1 Fatigue crack growth in **inert environment**
- 2 Stress corrosion crack growth under **sustained loading**. Typical variation of da/dt is a function of K . Environment has no effect on fracture behavior of material below the static SIF K_{ISCC} . Above K_{ISCC} , three region:
 - I Crack velocity increases with increased K
 - II Crack velocity independent of applied K .
 - III As K_{max} approaches K_{IC} , rapid increase in crack velocity

Hence, **subcritical** crack growth can occur for $K < K_{\text{IC}}$. For example 4340 steel has $K_{\text{IC}} = 56 \text{MPa}\sqrt{\text{m}}$, but in seawater $K_{\text{ISCC}} = 17 \text{MPa}\sqrt{\text{m}}$

- ③ True corrosion-fatigue arising from synergistic effects of cyclic loading and aggressive environment
- ④ Stress corrosion fatigue behavior obtained from a superposition of mechanical fatigue (1) and stress corrosion cracking (2)

- Corrosion fatigue is a process which is an outcome of **synergetic interactions** among
 - Environment
 - Material microstructure
 - Cyclic loads
- There is **not yet a single model** to account for all three.
- Simple models based on the principle of **superposition**

$$\left(\frac{da}{dN}\right)_C = \left(\frac{da}{dN}\right)_F + \int \frac{da}{dt} \cdot k(t) dt \quad (2)$$

where

- $(da/dN)_C$ Rate of fatigue crack growth in an aggressive environment
 $(da/dN)_F$ Rate of fatigue crack growth in an inert environment
 $\int \frac{da}{dt} \cdot k(t) dt$ Environmental component computed from sustained-load crack growth data obtained in the same aggressive environment

Note that below K_{ISCC} there is no environmental effect.

Dynamic Fracture

Victor E. Saouma

`saouma@colorado.edu`

University of Colorado, Boulder

Spring 2022

1 Disclaimer

2 Introduction

3 Linear Elastodynamics

- Introduction
- Helmholtz Decomposition
- P and S waves
- Displacement and Stress
- Surface Waves

4 Dynamic Crack Tip Fields

- Mode I
- Mode II

5 Dynamic Stress Intensity Factors

- Mode I; Stationary
- Non-Stationary

6 Energy Balance Equation and Fracture Criteria

7 Dynamic Toughnesses

- Crack Initiation
- Crack Growth
- Crack Arrest Toughness

8 Crack Branching

9 Conclusion

The following slides are adapted from the term projects of Rezgar Shakeri, (2018), and to a much lesser extent the project of Aldo Ghisi (2003)

- In **dynamic fracture mechanics** (DFM), there is an interaction between **stress waves and propagating cracks**. Hence, the dynamic stress intensity factors must be determined).
- DFM is relevant in impact load, seismology, and others.
- Inertial effects become relevant (thus DFM) when the **speed of the crack tip or edge is a significant fraction of the lowest characteristic wave speed** of the material.
- Derivation of DSIF is relatively simple to follow (if the introductory review of Mechanics is well understood), however there will be one notable exception (highlighted below).
- Need to first address **wave propagation** in solids.

- Strain-Displacement relation

$$\boldsymbol{\varepsilon}(\mathbf{x}, t) = \frac{1}{2}(\nabla \mathbf{u} + (\nabla \mathbf{u})^T) \quad (1)$$

- Constitutive equation for linear homogeneous elastic

$$\boldsymbol{\sigma}(\mathbf{x}, t) = \lambda \varepsilon_{kk} \mathbf{I} + 2\mu \boldsymbol{\varepsilon} \quad (2)$$

- The Balance of linear momentum

$$\nabla \cdot \boldsymbol{\sigma} + \mathbf{f} = \rho \ddot{\mathbf{u}} \quad (3)$$

- Substitute constitutive equation (in terms of Lamé's parameters) in (3), the above equation in terms of displacement will be **Navier's Equation**

$$\mu \nabla^2 \mathbf{u} + (\lambda + \mu) \nabla \nabla \cdot \mathbf{u} + \mathbf{f} = \rho \ddot{\mathbf{u}} \quad (4)$$

or

$$(\lambda + \mu) u_{i,jj} + \mu_{j,ii} + b_j = \rho \ddot{u}_j \quad (5)$$

where, λ and μ are Lamé constants, \mathbf{f} is body force and ρ is density.

- In mechanics we like to take an **alternative representation** (or “tricks”):
 - Coordinate system → **Galilean transformation**, and many others
 - Time series data → **Fast Fourier** transform.
 - Second order tensors
 - **Eigenvalues/Eigenmodes**
 - **Helmholtz** decomposition
 - Deformation gradient (strain) → **Polar Decomposition**
 - Stress → **Hydrostatic/volumetric**
- From vector calculus, Helmholtz has shown that any sufficiently smooth, rapidly decaying vector field in three dimensions (such as displacement \mathbf{u} can be decomposed into the sum of an irrotational (curl-free) vector field (i.e. a vector field that is the gradient of some function) and a solenoidal (where the divergence is zero at every point, $\nabla \cdot \mathbf{u} = 0$) vector field; this is known as the **Helmholtz decomposition**.
- The vector displacement \mathbf{u} will be decomposed into the gradient of a **scalar potential** ϕ and the curl of a **vector potential** ψ .
- Potentials exist to be ultimately **differentiated**.

- Note analogy with the ϕ potential of **Westergaard**, or the **Kolonov-Muskhelishvili complex potentials** $\psi(z)$ and $\chi(z)$ used by Inglis solution

$$\mathbf{u} = \nabla\phi + \nabla \times \boldsymbol{\psi}; \quad \& \quad \nabla \cdot \boldsymbol{\psi} = 0 \quad (6)$$

- Recalling the following identities:

$$\nabla \cdot (\nabla \times \mathbf{A}) = 0 \quad (7)$$

$$\nabla^2(\nabla\phi) = \nabla(\nabla^2\phi) \quad (8)$$

$$\nabla^2(\nabla \times \mathbf{A}) = \nabla \times \nabla^2\mathbf{A} \quad (9)$$

Equation (6) reduces to

$$(\lambda + \mu) \nabla (\nabla \cdot \nabla\phi + \nabla \cdot \nabla \times \boldsymbol{\psi}) + \mu \nabla^2 (\nabla\phi + \nabla \times \boldsymbol{\psi}) = \rho \frac{\partial^2 (\nabla\phi + \nabla \times \boldsymbol{\psi})}{\partial t^2} \quad (10)$$

- In the absence of body force, this reduces to

$$\underbrace{\nabla \left[(\lambda + 2\mu) \nabla^2 \phi - \rho \ddot{\phi} \right]}_0 + \nabla \times \underbrace{\left[\mu \nabla^2 \boldsymbol{\psi} - \rho \ddot{\boldsymbol{\psi}} \right]}_0 = 0 \quad (11)$$

or

$$\nabla^2 \phi = \frac{1}{C_p^2} \frac{\partial \phi}{\partial t^2} \quad (12)$$

$$\nabla^2 \boldsymbol{\psi} = \frac{1}{C_s^2} \ddot{\boldsymbol{\psi}} \quad (13)$$

where

$$C_p = \sqrt{\frac{\lambda + 2\mu}{\rho}} \quad \text{Pressure wave (P) velocity} \quad (14)$$

$$C_s = \sqrt{\frac{\mu}{\rho}} \quad \text{Shear wave (S) velocity} \quad (15)$$

in the elastic medium, respectively.

- Clearly $C_p > C_s$; and

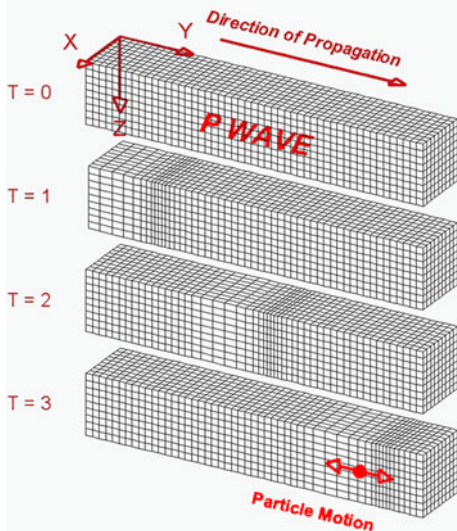
$$\frac{C_p}{C_s} = \sqrt{\frac{2-2\nu}{1-2\nu}} = \kappa \quad (16)$$

- Note that (12) is the classical (hyperbolic) **wave equation**, in 1D it reduces to

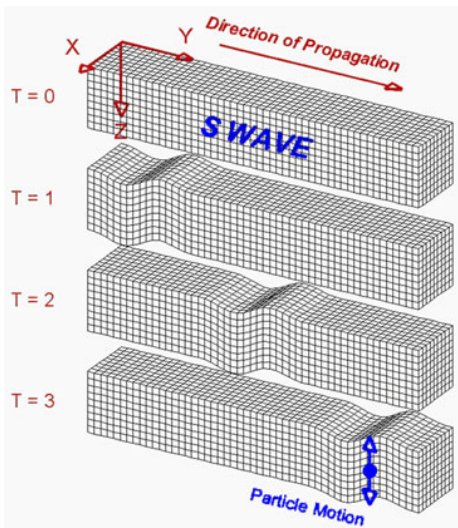
$$\frac{\partial^2 \phi}{\partial t^2} = C^2 \frac{\partial^2 \phi}{\partial x^2} \quad (17)$$

not to be confused with the (parabolic) heat (or transport) equation

$$\frac{\partial \phi}{\partial t} = C^2 \frac{\partial^2 \phi}{\partial x^2} \quad (18)$$



Propagation of P-waves in an elastic body, the particle motion is parallel to direction of propagation.



Propagation of S-waves in an elastic body, the particle motion is perpendicular to direction of propagation.

- **displacement and stress fields** are defined in terms of the potential function ϕ and ψ (Just like stresses were defined in terms of Airy stress functions).
- For 2D configuration, we have only ψ_3 component, for simplicity it is written ψ in following equations

$$\begin{aligned} u_1 &= \frac{\partial \phi}{\partial x_1} + \frac{\partial \psi}{\partial x_2} \\ u_2 &= \frac{\partial \phi}{\partial x_2} - \frac{\partial \psi}{\partial x_1} \end{aligned} \quad (19)$$

$$\begin{aligned} \sigma_{11} &= \lambda \nabla^2 \phi + 2\mu \left[\frac{\partial^2 \phi}{\partial x_1^2} + \frac{\partial^2 \psi}{\partial x_1 \partial x_2} \right] \\ \sigma_{22} &= \lambda \nabla^2 \phi + 2\mu \left[\frac{\partial^2 \phi}{\partial x_2^2} - \frac{\partial^2 \psi}{\partial x_1 \partial x_2} \right] \\ \sigma_{12} &= \mu \left[2 \frac{\partial^2 \phi}{\partial x_1 \partial x_2} + \frac{\partial^2 \psi}{\partial x_2^2} - \frac{\partial^2 \psi}{\partial x_1^2} \right] \end{aligned} \quad (20)$$

where ∇^2 is the two-dimensional Laplacian operator.

- In so far, we have focused on bulk waves **inside the medium**.
- When a surface is present, there is a special **wave that travels along the surface and decays into the medium**. It is the **Rayleigh wave**.
- Consider the region $x_2 > 0$, with a traction free boundary at $x_2 = 0$. A surface wave propagating along the x_1 direction with a **speed c** and decaying in the x_2 direction can be represented as

$$\begin{aligned}\phi &= f(x_2)\exp[ik(x_1 - ct)] \\ \psi &= g(x_2)\exp[ik(x_1 - ct)]\end{aligned}\tag{21}$$

where $i = \sqrt{-1}$, $k = \omega/c$ is the wave number and ω is the **frequency of a time harmonic disturbance**.

- Substituting in the wave equations (12) and (13) gives two ordinary differential equation for f and g

$$\begin{aligned}\frac{d^2 f}{dx_2^2} - k^2 \alpha_p^2 f &= 0 \\ \frac{d^2 g}{dx_2^2} - k^2 \alpha_s^2 g &= 0\end{aligned}\tag{22}$$

where

$$\alpha_p = \sqrt{1 - \frac{c^2}{C_p^2}}, \quad \text{and} \quad \alpha_s = \sqrt{1 - \frac{c^2}{C_s^2}}\tag{23}$$

- Solving these equation and retaining only the **solution that decays as $x_2 \rightarrow \infty$**

$$\begin{aligned}\phi &= A \exp(-\alpha_p k x_2) \exp[ik(x_1 - ct)] \\ \psi &= B \exp(-\alpha_s k x_2) \exp[ik(x_1 - ct)]\end{aligned}\tag{24}$$

where A and B are arbitrary constants.

- Substitute the above into relation of stresses (20) and satisfying the traction free condition ($\sigma_{12} = 0, \sigma_{22} = 0$) at $x_2 = 0$

$$\begin{aligned}(1 + \alpha_s^2)A + i2\alpha_s B &= 0 \\ -i2\alpha_p A + (1 + \alpha_s^2)B &= 0\end{aligned}\tag{25}$$

- For a nontrivial solution the determinant of coefficients must be zero

$$R(c) = 4\alpha_p\alpha_s - (1 + \alpha_s^2)^2 = 0,\tag{26}$$

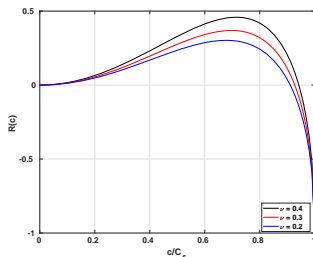
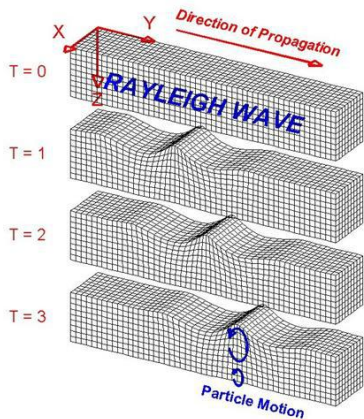
- Function $R(c)$ is called the **Rayleigh function** and its variation with c for different Poisson's ratio is shown below.
- Letting $c/C_s = \kappa_R$ and recalling from equation (16) that the ratio of the bulk wave speeds, κ , depends only on the Poisson's ratio, the above can be written as

$$R(c) = 4\sqrt{1 - \frac{\kappa_R^2}{\kappa^2}}\sqrt{1 - \kappa_R^2} - (2 - \kappa_R^2)^2 = 0\tag{27}$$

- The root of the preceding equation is the **Rayleigh wave speed, C_R** and it is clear that $C_R < C_s$.

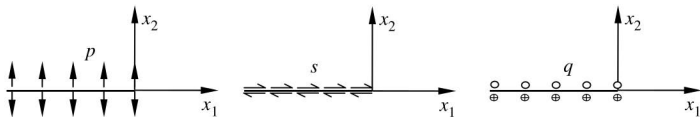
- Viktorov (1967) developed an approximate representation for the Rayleigh wave speed, C_R

$$k_R = \frac{C_R}{C_S} = \frac{0.862 + 1.14\nu}{1 + \nu}, \quad (28)$$



Variation of the Rayleigh function $R(c)$ with speed.

Propagation of Rayleigh-waves in the surface of elastic body, the particles move in elliptical path.



Mode I, II and III.

- As with Westergaard, assume a crack along $x_1 < 0$, $x_2 = 0$ and moving along $x_2 = 0$ at a **constant** speed $V < C_R$.
- The governing differential equations for the potentials $\phi = \phi(x_1, x_2, t)$ and $\psi = \psi(x_1, x_2, t)$ are the wave equations (12) and (13).
- Introducing the **Galilean transformation** (transformation between the coordinates of two reference frames which differ only by constant relative motion) $\xi_1 = x_1 - Vt$ and $\xi_2 = x_2$ the wave equations reduce to

$$\begin{aligned}
 \left(1 - \frac{V^2}{C_p^2}\right) \frac{\partial^2 \phi}{\partial \xi_1^2} + \frac{\partial^2 \phi}{\partial \xi_2^2} + \frac{\dot{V}}{C_p^2} \frac{\partial^2 \phi}{\partial \xi_1^2} + 2 \frac{V}{C_p^2} \frac{\partial^2 \phi}{\partial t \partial \xi_1} &= \frac{1}{C_p^2} \frac{\partial^2 \phi}{\partial t^2} \\
 \left(1 - \frac{V^2}{C_s^2}\right) \frac{\partial^2 \psi}{\partial \xi_1^2} + \frac{\partial^2 \psi}{\partial \xi_2^2} + \frac{\dot{V}}{C_s^2} \frac{\partial^2 \psi}{\partial \xi_1^2} + 2 \frac{V}{C_s^2} \frac{\partial^2 \psi}{\partial t \partial \xi_1} &= \frac{1}{C_s^2} \frac{\partial^2 \psi}{\partial t^2}
 \end{aligned} \tag{29}$$

- If we assumed that $\dot{V} = 0$, for the **stationary crack growth**, the wave equations become

$$\begin{aligned}\beta_p^2 \frac{\partial^2 \phi}{\partial \xi_1^2} + \frac{\partial^2 \phi}{\partial \xi_2^2} &= 0 \\ \beta_s^2 \frac{\partial^2 \psi}{\partial \xi_1^2} + \frac{\partial^2 \psi}{\partial \xi_2^2} &= 0\end{aligned}\tag{30}$$

where

$$\beta_p^2 = 1 - \frac{V^2}{C_p^2}, \quad \beta_s^2 = 1 - \frac{V^2}{C_s^2}$$

- Changing the coordinate $y_1 = \beta_p \xi_2$, $y_2 = \beta_s \xi_2$, $x = \xi_1$ (30) becomes

$$\begin{aligned}\frac{\partial^2 \phi}{\partial x^2} + \frac{\partial^2 \phi}{\partial y_1^2} &= 0 \\ \frac{\partial^2 \psi}{\partial x^2} + \frac{\partial^2 \psi}{\partial y_2^2} &= 0\end{aligned}\tag{31}$$

- Hence, clearly the potential functions ϕ and ψ **satisfy the Laplacian equation** and they can be real or imaginary part of analytic function in complex plane of the complex variable
- Recall **Williams' (1952)** solution to the crack stress field (alternative to Westergaard) based on **separation of variables**

$$\Phi(r, \theta) \equiv r^{\lambda+1} F(\theta, \lambda) \quad (32)$$

where $F(\theta, \lambda) = e^{m(\lambda)\theta}$ is a real function, and $m(\lambda)$ is yet to be determined, by satisfying the bi-harmonic equation.

- Likewise, for dynamic crack:

$$\begin{aligned} z_1 &= x + iy_1 = \xi_1 + \beta_p \xi_2 = r_1 e^{i\theta_1} \\ z_2 &= x + iy_2 = \xi_1 + \beta_s \xi_2 = r_2 e^{i\theta_2} \end{aligned} \quad (33)$$

where

$$\begin{aligned} r_1 &= \sqrt{\xi_1^2 + \beta_p^2 \xi_2^2} = \sqrt{(x_1 - Vt)^2 + \beta_p^2 x_2^2} & \theta_1 &= \arctan\left(\frac{\beta_p \xi_2}{\xi_1}\right) \\ r_2 &= \sqrt{\xi_1^2 + \beta_s^2 \xi_2^2} = \sqrt{(x_1 - Vt)^2 + \beta_s^2 x_2^2} & \theta_2 &= \arctan\left(\frac{\beta_s \xi_2}{\xi_1}\right) \end{aligned} \quad (34)$$

- **Introducing the complex function** for ϕ and ψ as

$$\begin{aligned}\phi(r_1, \theta_1) &= A \operatorname{Re}[z_1^m] = Ar_1^m \cos(m\theta_1) \\ \psi(r_2, \theta_2) &= B \operatorname{Im}[z_1^m] = Br_2^m \sin(m\theta_2)\end{aligned}\quad (35)$$

- satisfaction of boundary condition at $\theta_1 = \theta_2 = \pi$ gives

$$\begin{aligned}(1 + \beta_s^2)A \cos(m-1)\pi + 2\beta_s B \cos(m-1)\pi &= 0, \\ 2\beta_p A \sin(m-1)\pi + (1 + \beta_s^2)B \sin(m-1)\pi &= 0,\end{aligned}\quad (36)$$

- For nontrivial solutions, the determinant for the above system of equations must be zero;
- **Characteristic equation** is thus needed, giving

$$m = \frac{1}{2}n + 1, \quad n = 1, 2, 3, \dots, \quad (37)$$

- Negative values of n make (35) and therefore displacement singular at the crack tip and are rejected.

- From equation (36) it can be shown that for $n = 1$ the constant A and B are related by

$$B = -\frac{2\beta_p}{1 + \beta_s^2} A, \quad (38)$$

- Using equations (35), (37) and (38) in (19) and (20), the displacement components can be determined as

$$\begin{aligned} u_1(r, \theta) &= \frac{3}{2} A \left[r_1^{1/2} \cos\left(\frac{\theta_1}{2}\right) - \frac{2\beta_p\beta_s}{1 + \beta_s^2} r_2^{1/2} \cos\left(\frac{\theta_2}{2}\right) \right] \\ u_2(r, \theta) &= \frac{3}{2} \beta_p A \left[-r_1^{1/2} \sin\left(\frac{\theta_1}{2}\right) + \frac{2}{1 + \beta_s^2} r_2^{1/2} \sin\left(\frac{\theta_2}{2}\right) \right] \end{aligned} \quad (39)$$

- The corresponding stress components are

$$\begin{aligned}\sigma_{11}(r, \theta) &= \frac{3}{4} \frac{\mu A}{(1 + \beta_s^2)} \left[(1 + \beta_s^2)(1 + 2\beta_p^2 - \beta_s^2) \frac{\cos\left(\frac{\theta_1}{2}\right)}{r_1^{1/2}} - 4\beta_p\beta_s \frac{\cos\left(\frac{\theta_2}{2}\right)}{r_2^{1/2}} \right] \\ \sigma_{22}(r, \theta) &= \frac{3}{4} \frac{\mu A}{(1 + \beta_s^2)} \left[-(1 + \beta_s^2)^2 r_1^{-1/2} \cos\left(\frac{\theta_1}{2}\right) + 4\beta_p\beta_s r_2^{-1/2} \cos\left(\frac{\theta_2}{2}\right) \right] \\ \sigma_{12}(r, \theta) &= \frac{3}{4} \frac{\mu A}{(2\beta_s)} \left[4\beta_s\beta_p r_1^{-1/2} \sin\left(\frac{\theta_1}{2}\right) - 4\beta_p\beta_s r_2^{-1/2} \sin\left(\frac{\theta_2}{2}\right) \right]\end{aligned}\quad (40)$$

- These are the **dynamic counterpart of Westergaard (static)** solutions previously derived.
- Introducing the **dynamic stress intensity factor** for mode I

$$K_I = \lim_{\xi_1 \rightarrow 0} \sqrt{2\pi\xi_1} \sigma_{22}(r, 0^\pm) = \frac{3\sqrt{2\pi}\mu D(V)}{4(1 + \beta_s^2)} A \quad (41)$$

- Crack tip stress and displacement fields:

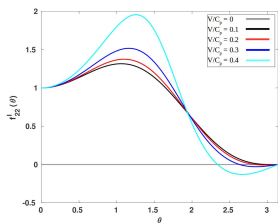
$$\begin{aligned}\sigma_{11}(r, \theta) &= \frac{K_I}{\sqrt{2\pi r}} f'_{11}(\theta) \\ \sigma_{22}(r, \theta) &= \frac{K_I}{\sqrt{2\pi r}} f'_{22}(\theta) \\ \sigma_{12}(r, \theta) &= \frac{K_I}{\sqrt{2\pi r}} f'_{12}(\theta) \\ u_1(r, \theta) &= \frac{K_I}{\mu\sqrt{2\pi}} g'_1(\theta) \\ u_2(r, \theta) &= \frac{K_I}{\mu\sqrt{2\pi}} g'_2(\theta)\end{aligned}\tag{42}$$

where the polar distribution is given by

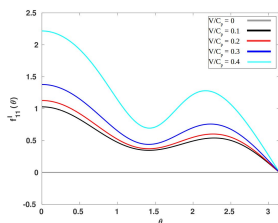
$$\begin{aligned}
 f'_{11}(\theta) &= \frac{1}{D(V)} [(1 + \beta_s^2)(1 + 2\beta_p^2 - \beta_s^2)\gamma_p^{-1/2} \cos\left(\frac{\theta_1}{2}\right) \\
 &\quad - 4\beta_p\beta_s\gamma_s^{-1/2} \cos\left(\frac{\theta_2}{2}\right)] \\
 f'_{22}(\theta) &= \frac{1}{D(V)} \left[-(1 + \beta_s^2)^2\gamma_p^{-1/2} \cos\left(\frac{\theta_1}{2}\right) + 4\beta_p\beta_s\gamma_s^{-1/2} \cos\left(\frac{\theta_2}{2}\right) \right] \\
 f'_{12}(\theta) &= \frac{2\beta_p(1 + \beta_s^2)}{D(V)} \left[\gamma_p^{-1/2} \sin\left(\frac{\theta_1}{2}\right) - \gamma_s^{-1/2} \sin\left(\frac{\theta_2}{2}\right) \right] \\
 g'_1(\theta) &= \frac{2}{D(V)} \left[(1 + \beta_s^2)r_1^{1/2} \cos\left(\frac{\theta_1}{2}\right) - 2\beta_p\beta_s r_2^{1/2} \cos\left(\frac{\theta_2}{2}\right) \right] \\
 g'_2(\theta) &= \frac{2\beta_p}{D(V)} \left[(1 + \beta_s^2)r_1^{1/2} \sin\left(\frac{\theta_1}{2}\right) - 2r_2^{1/2} \sin\left(\frac{\theta_2}{2}\right) \right]
 \end{aligned} \tag{43}$$

and

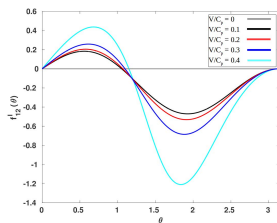
$$\begin{aligned}
 D(V) &= 4\beta_p\beta_s - (1 + \beta_s^2)^2 \\
 \gamma_p &= \sqrt{1 - (V \sin \theta / C_p)^2} \quad \text{and} \quad \gamma_s = \sqrt{1 - (V \sin \theta / C_s)^2} \\
 \tan \theta_1 &= \beta_p \tan \theta, \quad \tan \theta_2 = \beta_s \tan \theta = \frac{r_1}{\gamma_p} = \frac{r_2}{\gamma_s}
 \end{aligned} \tag{44}$$



Angular Variation of $f_{22}^I(\theta)$ for mode I.



Angular Variation of $f_{11}^I(\theta)$ for mode I.



Angular Variation of $f_{12}^I(\theta)$ for mode I.

- Following a procedure similar to mode I
- The stress and displacement field corresponding to a mode II crack growing at a constant speed V can be determined in a similar manner except the antisymmetric solutions of (31) will be used

$$\begin{aligned}\phi(r_1, \theta_1) &= A \operatorname{Im}[z_1^m] = Ar_1^m \sin(m\theta_1), \\ \psi(r_2, \theta_2) &= B \operatorname{Re}[z_1^m] = Br_2^m \cos(m\theta_2),\end{aligned}\tag{45}$$

- Following the same procedure as described in previous section, the displacement fields for mode II can be given as

$$\begin{aligned}u_1(r, \theta) &= \frac{3}{2}A \left[r_1^{1/2} \sin\left(\frac{\theta_1}{2}\right) - \frac{1 + \beta_s^2}{2} r_2^{1/2} \sin\left(\frac{\theta_2}{2}\right) \right], \\ u_2(r, \theta) &= \frac{3}{2}\beta_p A \left[r_1^{1/2} \sin\left(\frac{\theta_1}{2}\right) - \frac{1 + \beta_s^2}{2\beta_s\beta_p} r_2^{1/2} \sin\left(\frac{\theta_2}{2}\right) \right],\end{aligned}\tag{46}$$

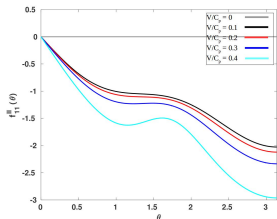
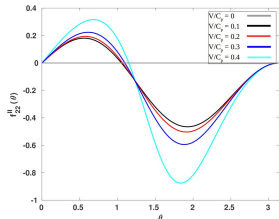
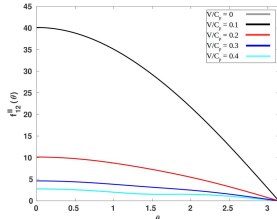
$$\begin{aligned} \sigma_{11}(r, \theta) &= \frac{3}{4} \frac{\mu A}{(1 + \beta_s^2)} \left[-(1 + \beta_s^2)(1 + 2\beta_p^2 - \beta_s^2) \frac{\sin\left(\frac{\theta_1}{2}\right)}{r_1^{1/2}} + \right. \\ &\quad \left. (1 + \beta_s^2)^2 \frac{\sin\left(\frac{\theta_2}{2}\right)}{r_2^{1/2}} \right], \\ \sigma_{22}(r, \theta) &= \frac{3}{4} \frac{\mu A}{(1 + \beta_s^2)} \left[(1 + \beta_s^2)^2 r_1^{-1/2} \sin\left(\frac{\theta_1}{2}\right) - (1 + \beta_s^2)^2 r_2^{-1/2} \sin\left(\frac{\theta_2}{2}\right) \right] \\ \sigma_{12}(r, \theta) &= \frac{3}{4} \frac{\mu A}{(2\beta_s)} \left[4\beta_s \beta_p r_1^{-1/2} \cos\left(\frac{\theta_1}{2}\right) - (1 + \beta_s^2)^2 r_2^{-1/2} \cos\left(\frac{\theta_2}{2}\right) \right], \end{aligned} \quad (47)$$

- Introducing the **dynamic stress intensity factor** for mode II

$$K_{II} = \lim_{\xi_1 \rightarrow 0} \sqrt{2\pi\xi_1} \sigma_{12}(r, 0^\pm) = \frac{3\sqrt{2\pi}\mu D(V)}{8\beta_s} A \quad (48)$$

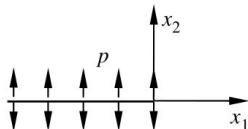
- The crack tip stress and displacement fields may be written as

$$\begin{aligned}\sigma_{11}(r, \theta) &= \frac{K_{II}}{\sqrt{2\pi r}} f_{11}''(\theta) \\ \sigma_{22}(r, \theta) &= \frac{K_{II}}{\sqrt{2\pi r}} f_{22}''(\theta) \\ \sigma_{12}(r, \theta) &= \frac{K_{II}}{\sqrt{2\pi r}} f_{12}''(\theta) \\ u_1(r, \theta) &= \frac{K_{II}}{\mu\sqrt{2\pi}} g_1''(\theta) \\ u_2(r, \theta) &= \frac{K_{II}}{\mu\sqrt{2\pi}} g_2''(\theta)\end{aligned}\quad (49)$$

Angular Variation of $f_{11}''(\theta)$ Angular Variation of $f_{22}''(\theta)$ Angular Variation of $f_{12}''(\theta)$

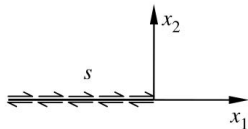
- If a **normal pressure** of magnitude p begins to act on the crack faces at time $t = 0$, then the stress intensity factor for mode I is given by

$$K_I(t) = \frac{2p}{1-\nu} \sqrt{\frac{C_p t(1-2\nu)}{\pi}} \quad (50)$$



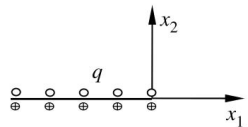
- If a shear **traction** of magnitude s begins to act on the crack faces at time $t = 0$, then the stress intensity factor for mode II is given by

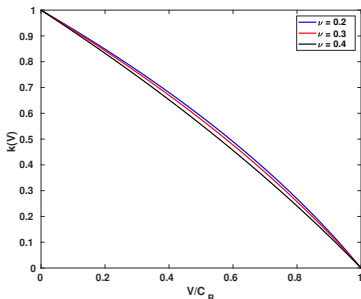
$$K_{II}(t) = 2s \sqrt{\frac{2C_s t}{\pi(1-\nu)}} \quad (51)$$



- If a **out of plane shear traction** of magnitude q begins to act on the crack faces at time $t = 0$, then the stress intensity factor for mode III is given by

$$K_{III}(t) = 2q \sqrt{\frac{2C_s t}{\pi}} \quad (52)$$





Universal Function

- For example for mode I

$$K_I(t, a, \dot{a}) = k(V)K_I(t, a, 0), \quad (53)$$

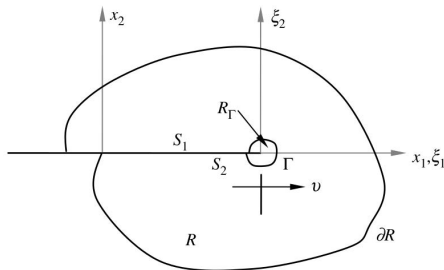
- So far, the crack speed was constant.
- For nonuniform crack growth Freund (1973) considered a crack growing at a nonuniform speed to be the limit of a sequence of piecewise constant velocity segments, and he showed the stress intensity factor for non-stationary case can be given by universal function $k(V)$ times the stress intensity factor for steady crack growth.

a is the length of crack and $\dot{a} = V$ is the speed of crack growth. The universal function $k(V)$ is

$$k(V) \approx \frac{1 - V/C_R}{\sqrt{1 - V/C_p}}, \quad (54)$$

- Failure criteria for dynamic fracture may be motivated by an **extension of Griffith's ideas postulated for equilibrium cracks**.

$$\dot{U} + \dot{K} = \frac{d}{dt} \int_R \frac{1}{2} [\sigma_{ij} \varepsilon_{ij} + \rho \dot{u}_i \dot{u}_i] dA, \quad (55)$$



Crack tip contour for evaluation of the energy flux integral

- Integral (55) could be applied on any closed contour within the body, and R is any region near the crack tip bounded by the curve ∂R .

- Assuming that crack propagates along the x_1 direction at a constant speed V . Due to the singularity of the stress and strain fields, we must exclude a small region near the crack tip. This region is enclosed by the contour labeled Γ and is indicated by R_Γ .
- Thus, the rate of change of the strain energy and kinetic energy can be written as

$$\dot{U} + \dot{K} = \frac{d}{dt} \int_{R-R_\Gamma} \frac{1}{2} [\sigma_{ij} \varepsilon_{ij} + \rho \dot{u}_i \dot{u}_i] dA, \quad (56)$$

- In evaluating the integrals above, the **limits of integration vary with time as well**; hence **Reynolds transport theorem** should be invoked in taking the time derivatives indicated in the terms on the right-hand side of (56) which gives

$$\dot{U} + \dot{K} = \lim_{\Gamma \rightarrow 0} \int_{R-R_\Gamma} [\sigma_{ij} \dot{u}_{i,j} + \rho \dot{u}_i \ddot{u}_i] dA + \lim_{\Gamma \rightarrow 0} \int_\Gamma \frac{1}{2} [\sigma_{ij} u_{i,j} + \rho \dot{u}_i \dot{u}_i] V n_1 ds, \quad (57)$$

where V is the speed of translation of the contour Γ and n_1 is the component of the outward normal to the contour in the direction of translation of the contour.

- The first integral in (57) can be simplified by replacing $\rho \ddot{u}_i = \sigma_{ij,j}$ and then applying the divergence theorem to yield

$$\lim_{\Gamma \rightarrow 0} \int_{R-R_\Gamma} [\sigma_{ij} \dot{u}_{i,j} + \rho \dot{u}_i \ddot{u}_i] dA = \int_{\partial R} \sigma_{ij} \dot{u}_i n_j ds + \lim_{\Gamma \rightarrow 0} \int_{\Gamma} \sigma_{ij} \dot{u}_i n_j ds, \quad (58)$$

- That the newly created crack surfaces are traction free has been used in writing the above equation. The first term on the right-hand side of (??) is the power of the external forces, P . Now, (57) can be rewritten as

$$P - (\dot{U} + \dot{K}) = - \lim_{\Gamma \rightarrow 0} \int_{\Gamma} \left[\sigma_{ij} \dot{u}_i n_j + \frac{1}{2} (\sigma_{ij} u_{i,j} + \rho \dot{u}_i \dot{u}_i) V n_1 \right] ds, \quad (59)$$

The integral represents the **amount of energy flowing out of the region R and into the crack tip region through the contour Γ** . The crack tip energy flux integral is then defined as follows

$$F = \int_{\Gamma} \left[\sigma_{ij} \dot{u}_i n_j + \frac{1}{2} (\sigma_{ij} u_{i,j} + \rho \dot{u}_i \dot{u}_i) V n_1 \right] ds, \quad (60)$$

- This **energy flux is dissipated in the crack tip process zone** as the crack propagates along the x_1 direction at a constant speed V . For steady-state crack growth assumed in the present analysis, it turns out to be independent of the path Γ .
- If D is the total dissipation in the fracture process, $dD/dt = VdD/da = V\gamma$ is the **rate of energy dissipation at the moving crack tip**, where γ is the fracture energy per unit extension of the crack and a is the crack length.
- In analogy with the quasi-static crack problems, it is possible to define a **dynamic energy release, G**

$$G = V^{-1}F = \gamma \quad (61)$$

- It corresponds to the energy released into the crack tip process zone per unit crack extension and must be equal to the dissipation per unit extension.

- Introducing the **elastodynamics singular stress field** from (42) in (61), G can be related to the dynamic stress intensity factor as

$$G = \frac{1 - \nu^2}{E} [A_I(V)K_I^2 + A_{II}(V)K_{II}^2] + \frac{1}{2\mu} A_{III}(V)K_{III}^2, \quad (62)$$

$$A_I(V) = \frac{V^2 \beta_p}{(1 - \nu) C_s^2 D(V)}, \quad A_{II}(V) = \frac{V^2 \beta_s}{(1 - \nu) C_s^2 D(V)}, \quad A_{III}(V) = \frac{1}{\beta_s}$$

- Clearly, if $V = 0$ we recover the static expression of G
- First, it has been assumed that the fracture energy is a material constant. Second, the functions $A_I(V)$ and $A_{II}(V)$ are singular as $V \rightarrow C_R$ and the function $A_{III}(V)$ is singular as $V \rightarrow C_s$.
- To satisfy the energy balance equation, the **dynamic stress intensity factors K_I and K_{II} must tend to zero as $V \rightarrow C_R$ and K_{III} must tend to zero as $V \rightarrow C_s$** . This implies that the **limiting crack speed in modes I and II is the Rayleigh wave speed and in mode III, the shear wave speed**.

- In dynamic formulations, due to practical complications in evaluating (62) the **fracture criterion is simply evaluated in terms of the stress intensity factors** rather than in terms of energy
- The **dynamic fracture criterion is traditionally separated into three parts:**
 - 1 Dynamic crack **initiation** criterion
 - 2 Dynamic crack **growth**
 - 3 Dynamic crack **arrest** criterion

all imposed independently on the growing crack, and each one having its own corresponding **toughness**

- Since the state of stress near the crack tip is described in terms of the dynamic stress intensity factor, K_I^{dyn} ; crack initiation can be identified with the **stress intensity factor reaching a critical value**, just as in the case of quasi-static fracture.
- Therefore, the crack initiation criterion can be **postulated as follows**

$$K_I^{dyn}(t_f) = K_{Id}(T, \dot{K}_I^{dyn}) \quad (63)$$

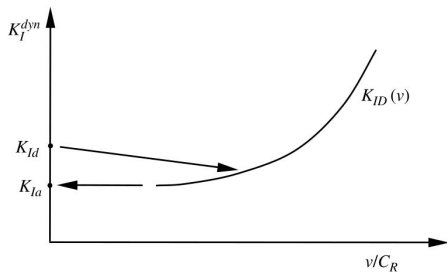
The right-hand side represents the **dynamic initiation toughness**.

- The dependence of the dynamic crack initiation toughness on the temperature and rate of loading is indicated through the arguments; this dependence must be determined through experiments covering the range of temperatures and rates of loading of interest.

- Once dynamic crack growth has been initiated as per the conditions of the dynamic initiation toughness, subsequent growth must be determined through a **separate criterion that characterizes the energy rate balance during growth.**
- The **dynamic stress field** near a growing crack is still characterized by the dynamic stress intensity factor, but now this **is a function of loading, time, crack position, and speed and is represented as $K_I^{dyn}(t, V)$.** the dynamic crack growth criterion is written as

$$K_I^{dyn}(t, V) = K_{ID}(V; \dot{K}_I^{dyn}, T), \quad (64)$$

- The upper case subscript **D** is used to indicate the **dynamic crack growth toughness instead of the lower case d** used to indicate the dynamic initiation toughness.
- Once again, the right-hand side represents the **material property to be characterized through experiments** and the left-hand side represents the dynamic stress intensity factor calculated from the solution of the boundary initial value problem in elastodynamics.



Dynamic crack growth criterion (Ravi. 2004)

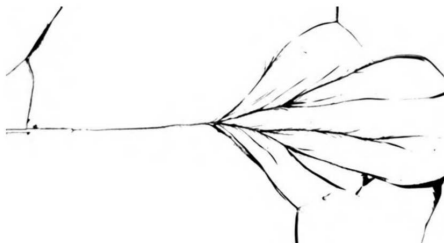
- In numerical simulations, the crack extension must be imposed in such a manner that (64) is satisfied at each increment in time.

- Dynamic crack arrest toughness is defined as the **smallest value of the dynamic stress intensity factor for which a growing crack cannot be maintained**; thus the crack arrests when

$$K_I^{dyn}(t) < K_{Ia}(T) \quad (65)$$

- In applications, the most conservative approach to design would utilize (??), thus assuring that the dynamic stress intensity factor for all possible loading conditions never exceeds the crack arrest toughness.

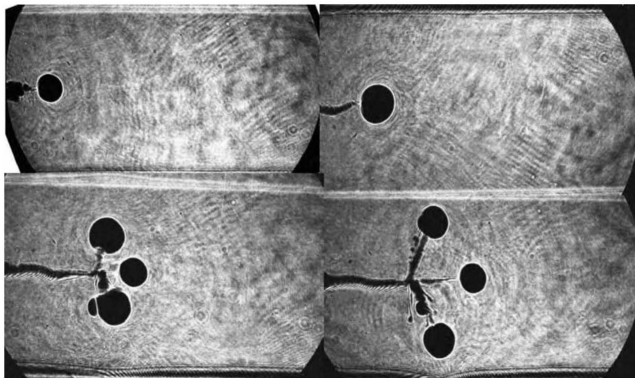
- Crack branching is a phenomenon that the main crack inside the material separated to two or more cracks.



Branching pattern in a Homalite-100 specimen

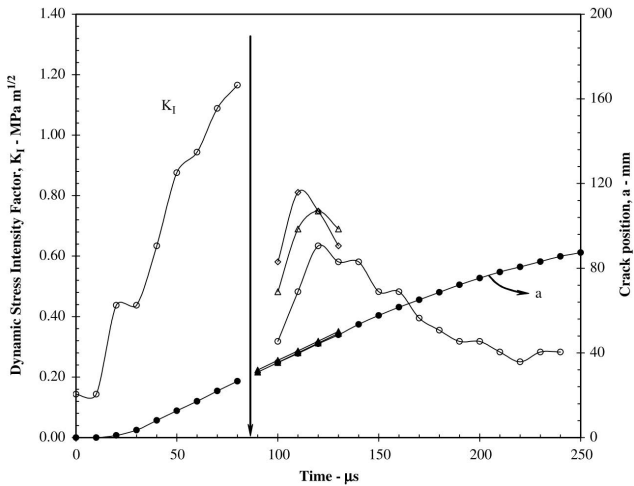
- Yoffe (1951) attempted to explain the branching of cracks from an analysis of the problem of a crack with a constant velocity in an unbounded medium. From this solution she found that the maximum of the hoop stress acted normal to lines that make an angle of 60° with the direction of crack propagation when the crack speed exceeded $0.60C_R$.

- Therefore, Yoffe suggested that this stress field rearrangement might lead to crack branching.
- A lot of experiments after Yoffe, showed that the velocity is not only significant parameters for branching, and it should be noted that in practical experiment crack cannot reach the $0.60C_R$.
- Measurements from different investigators indicate that branching occurs when the stress intensity factor reaches a critical value that is between two and three times the quasi-static fracture toughness of the material, but the crack speed at branching varied in different experiments.
- A narrow strip specimen, 500 mm long and 50 mm wide and 4.76 mm thick. The electromagnetic loading scheme was used to generate a uniform pressure loading over the crack surfaces.

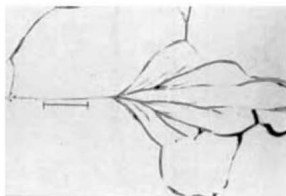
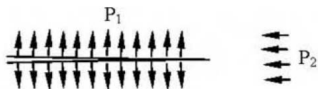


Selected frames from a high-speed sequence showing caustics at the tip of a branching crack. The vertical dimension is 25 mm (Ravi (2004)).

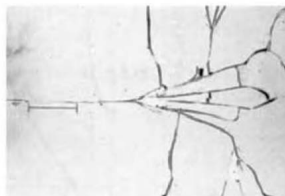
- Continued loading from the pressure loading on the parent crack and the **arrival of reflected stress waves in the narrow strip configuration cause additional increase in the stress intensity factor**



- Variations in the crack branching angle were also found different. Clearly, the macroscopic stress field also influences the angle and number of branches that appear. Ravi-Chandar and Knauss (1984d) explored this by altering the crack parallel compressive stress at the branch location; the following loading was generated with the electromagnetic loading device.

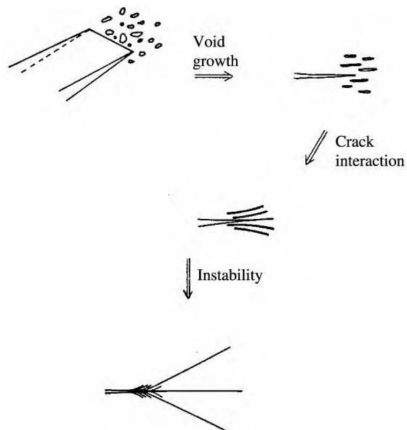


$P_1 = 10.35 \text{ MPa}; P_2 = 5.5 \text{ MPa}$



$P_1 = 10.35 \text{ MPa}; P_2 = 10.35 \text{ MPa}$

- The process of **branching is governed by the inner problem and not the outer problem that is treated by the continuum elastodynamics**. A mechanism for crack branching illustrated in below



- Linear elastodynamics, P, S and Rayleigh Waves
- Dynamic Fields for crack with constant speed derived in terms of DSIF (Stationary crack growth)
- In non-stationary case, the relation of DSIF in this case with DSIF in stationary case presented by using universal function $k(V)$
- Energy balance and fracture criteria, Dynamic Crack initiation, crack growth, and crack arrest discussed
- Crack branching discussed. First attempt in branching was based on crack speed.
- More measurement showed that we have branching when when the stress intensity factor reaches a critical value that is between two and three times the quasi-static fracture toughness
- Some specific experiment discussed to see the angle and length of branching

Part III

Homeworks

All homework, along with their solution

**CVEN 7161
FRACTURE MECHANICS**

SPRING 2020

HOME-WORK 1

Review Mechanics

Due: Feb. 6, 2020

You are strongly encouraged to use *Mathematica* for the following assignment (possible exception problem 1)

1. Show that

$$z^2 = (x^2 - y^2) + 2xyi \quad (1)$$

satisfies the Cauchy-Riemann equation.

2. The stress tensor at a point P is given by

$$T = \begin{bmatrix} 7 & 0 & -2 \\ 0 & 5 & 0 \\ -2 & 0 & 4 \end{bmatrix} \quad (2)$$

Determine the traction (stress vector) on the plane at P whose unit normal is $\vec{\mathbf{n}} = \frac{2}{3}\vec{\mathbf{e}}_1 - \frac{2}{3}\vec{\mathbf{e}}_2 + \frac{1}{3}\vec{\mathbf{e}}_3$.

3. The stress tensor throughout a continuum is given by

$$T = \begin{bmatrix} 3x_1x_2 & 5x_2^2 & 0 \\ 5x_2^2 & 0 & 2x_3 \\ 0 & 2x_3 & 0 \end{bmatrix} \quad (3)$$

Determine the stress vector acting at the point $P(2, 1, \sqrt{3})$ of the plane that is tangent to the cylindrical surface $x_2^2 + x_3^2 = 4$ at P

4. For the stress distribution given by the preceding problem, what should be the body force vector $\rho\mathbf{b}$ to ensure equilibrium
5. For the stress tensor

$$T = \begin{bmatrix} 6 & -3 & 0 \\ -3 & 6 & 0 \\ 0 & 0 & 8 \end{bmatrix} \quad (4)$$

- (a) Determine the three invariants $I_\sigma, II_\sigma, III_\sigma$.
- (b) Determine the principal stresses and the principal stress directions.
- (c) Show that the transformation tensor of direction cosines transforms the original stress tensor into the diagonal principal axes stress tensor.
- (d) Recompute the three invariants from the principal stresses.
- (e) Split the stress tensor into its spherical and deviator parts.
- (f) Show that the first invariant of the deviator is zero.

6. Determine the stress tensor at a point where the Lagrangian strain tensor is given by

$$T = \begin{bmatrix} 30 & 50 & 20 \\ 50 & 40 & 0 \\ 20 & 0 & 30 \end{bmatrix} 10^{-6} \quad (5)$$

and the material is steel: $\lambda = 119.2$ GPa, and $\mu = 79.2$ GPa.

7. Determine the strain tensor at a point where the Cauchy stress tensor is given by

$$T = \begin{bmatrix} 100 & 42 & 6 \\ 42 & -2 & 0 \\ 6 & 0 & 15 \end{bmatrix} \text{MPa} \quad (6)$$

and $E = 207$ GPa, $\mu=79.2$ GPa, and $\nu=0.30$

8. For the following proposed Airy stress function:

$$\Phi = \frac{3F}{4c} \left(x_1 x_2 - \frac{x_1 x_2^3}{3c^2} \right) + \frac{P}{4c} x_2^2 \quad (7)$$

- (a) Show that it is indeed suitable as an Airy stress function.
- (b) Determine the stress components in the region $x_1 > 0$, $-c < x_2 < c$.
- (c) Plot σ_{11} , σ_{12} and show that these stresses are those of a cantilever beam subjected to a transverse end load and axial pull (which one is P and which one is F ?).

Fracture Mechanics

Spring 2018

HW-1

(Rezgar Shakeri)

Note: To solve the following problems, you may need the following Mathematica functions: Chop[], Clear[], ClearAll["Global`*"], Det[], Div[], Eigenvalues[], Eigenvectors[], Grad[], Inverse[], MatrixForm[], N[], Normalize[], Orthogonalize[], Plot, Simplify[], Solve[], Sqrt[], Tr[], Transpose[], [[]],

```
ClearAll["Global`*"]
```

Stress

1. The stress tensor at P is given by
$$\begin{pmatrix} 7 & 0 & -2 \\ 0 & 5 & 0 \\ -2 & 0 & 4 \end{pmatrix}$$
 determine the traction (stress vector) on the plane at P whose unit normal is $n = \frac{2}{3} e_1 - \frac{2}{3} e_2 + \frac{1}{3} e_3$

Answer: We know that the traction vector on the surface can be found by dot product of unit normal vector and stress tensor.

the traction is

$$t_1 = 4 e_1 - 10/3 e_2$$

$$t_1 = \left\{ \left\{ \frac{2}{3}, -\frac{2}{3}, \frac{1}{3} \right\} \cdot \left\{ \{7, 0, -2\}, \{0, 5, 0\}, \{-2, 0, 4\} \right\} \right\}$$

$$\left\{ \left\{ 4, -\frac{10}{3}, 0 \right\} \right\}$$

2. The state of stress through a continuum is given with respect to the cartesian axes by
$$\begin{pmatrix} 3x_1x_2 & 5x_2^2 & 0 \\ 5x_2^2 & 0 & 2x_3 \\ 0 & 2x_3 & 0 \end{pmatrix}$$
 MPa; Determine the stress vector at point P(2,1,√3) of the plane that is normal to the tangent to the cylindrical surface $x_2^2 + x_3^2 = 4$ at P.

Answer: The gradient vector is along the normal vector to the surface at desired point. we can show that. For example point P is at the surface of the cylinder, if you look at this point in (x2,x3) plane the direction of the radius (line between center (0,0) and (1,√3)) which is normal to the surface of the cylinder is $n = 1e_2 + \sqrt{3} e_3$.

And the gradient of cylinder is $\text{gradient}(x^2+x^3-4)=2x_2 e_2+2x_3 e_3$ and at point P is gradient at P = $2 e_2+2\sqrt{3} e_3$, which is at the same direction of n.

We have to evaluate the given stress tensor at point P, and finding the unit normal vector by calculating the gradient of cylinder eq at point P, then dot product of unit vector and stress tensor gives the stress vector at point P.

$$s1 = \{ \{ 3 x1 x2, 5 x2^2, 0 \}, \{ 5 x2^2, 0, 2 x3 \}, \{ 0, 2 x3, 0 \} \}$$

$$\{ \{ 3 x1 x2, 5 x2^2, 0 \}, \{ 5 x2^2, 0, 2 x3 \}, \{ 0, 2 x3, 0 \} \}$$

$$Nq1 = \text{Grad}[x2^2 + x3^2 - 4, \{x1, x2, x3\}]$$

$$\{ 0, 2 x2, 2 x3 \}$$

$$x1 = 2;$$

$$x2 = 1;$$

$$x3 = \text{Sqrt}[3];$$

$$nq1 = \text{Normalize}[Nq1]$$

$$\left\{ 0, \frac{1}{2}, \frac{\sqrt{3}}{2} \right\}$$

$$t2 = nq1.s1$$

$$\left\{ \frac{5}{2}, 3, \sqrt{3} \right\}$$

3. For the stress distribution given by the preceding problem, what would be the the body force vector ρb to ensure equilibrium.

Answer: we have to find vector b such that the equilibrium be satisfied. We have to solve the following Divergence (stress) +B=0 or

$$B = -\text{Divergence}(\text{stress}).$$

So the the three components of $\rho b=B$ vector are

$$\text{Clear}[x1, x2, x3]$$

$$s11 = \{ \{ 3 x1 x2, 5 x2^2, 0 \} \};$$

$$s12 = \{ \{ 5 x2^2, 0, 2 x3 \} \};$$

$$s13 = \{ \{ 0, 2 x3, 0 \} \};$$

$$B1 = -\text{Div}[s11, \{x1, x2, x3\}]$$

$$\{-13 x2\}$$

$$B2 = -\text{Div}[s12, \{x1, x2, x3\}]$$

$$\{-2\}$$

$$B3 = -\text{Div}[s13, \{x1, x2, x3\}]$$

$$\{0\}$$

4. For the following stress tensor $\begin{pmatrix} 6 & -3 & 0 \\ -3 & 60 & 0 \\ 0 & 0 & 8 \end{pmatrix}$. a) Determine directly the three

invariants $I_\sigma, II_\sigma, III_\sigma$. b) Determine the principal stresses and the principal stress directions. c) Show that the transformation tensor of direction cosines transforms the original stress tensor into the diagonal principal axes stress tensor. d) Recompute the three invariants from the principal stresses. e) Split the stress tensor into its spherical and deviator parts. f) Show that the first invariant of the deviator is zero.

a) we have to find first trace of T, and trace of T² and determinant of T as follow

$$T = \{\{6, -3, 0\}, \{-3, 60, 0\}, \{0, 0, 8\}\}$$

$$\{\{6, -3, 0\}, \{-3, 60, 0\}, \{0, 0, 8\}\}$$

$$I1 = \text{Tr}[T]$$

$$I2 = ((\text{Tr}[T])^2 - \text{Tr}[T.T]) / 2$$

$$I3 = \text{Det}[T]$$

$$74$$

$$879$$

$$2808$$

b) The equation for Principal stress is “n.[T-λI]=0”, we are looking for nontrivial solution for “n” so the determinant of [T-λI]=0, gives the principal stress $\lambda_1, \lambda_2, \lambda_3$.

So we have to find the eigenvalues of the “T” which are our principal stresses, and corresponding eigenvector for each eigenvalue is principal stress direction

$$\lambda = \text{Simplify}[\text{Eigenvalues}[T]]$$

$$\{3 (11 + \sqrt{82}), 8, 33 - 3 \sqrt{82}\}$$

Nq4 = Eigenvectors[T]

$$\{\{9 - \sqrt{82}, 1, 0\}, \{0, 0, 1\}, \{9 + \sqrt{82}, 1, 0\}\}$$

we have to normalize eigenvectors which are our principal stress directions

n1q4 = Normalize[Nq4[[1]]]

$$\left\{ \frac{9 - \sqrt{82}}{\sqrt{1 + (-9 + \sqrt{82})^2}}, \frac{1}{\sqrt{1 + (-9 + \sqrt{82})^2}}, 0 \right\}$$

n2q4 = Normalize[Nq4[[2]]]

$$\{0, 0, 1\}$$

n3q4 = Normalize[Nq4[[3]]]

$$\left\{ \frac{9 + \sqrt{82}}{\sqrt{1 + (9 + \sqrt{82})^2}}, \frac{1}{\sqrt{1 + (9 + \sqrt{82})^2}}, 0 \right\}$$

c) The above unit eigenvectors, actually can be seen as the unit bases for “Principal frame”. We

Q = {n1q4, n2q4, n3q4}

$$\left\{ \left\{ \frac{9 - \sqrt{82}}{\sqrt{1 + (-9 + \sqrt{82})^2}}, \frac{1}{\sqrt{1 + (-9 + \sqrt{82})^2}}, 0 \right\}, \{0, 0, 1\}, \left\{ \frac{9 + \sqrt{82}}{\sqrt{1 + (9 + \sqrt{82})^2}}, \frac{1}{\sqrt{1 + (9 + \sqrt{82})^2}}, 0 \right\} \right\}$$

Simplify[Q.T.Transpose[Q]]

$$\{\{3(11 + \sqrt{82}), 0, 0\}, \{0, 8, 0\}, \{0, 0, 33 - 3\sqrt{82}\}\}$$

d) We have $\lambda^3 - I_1 \lambda^2 + I_2 \lambda - I_3 = 0$

$$I_1 = \lambda_1 + \lambda_2 + \lambda_3$$

$$I_2 = \lambda_1 \lambda_2 + \lambda_1 \lambda_3 + \lambda_2 \lambda_3$$

$$I_3 = \lambda_1 \lambda_2 \lambda_3$$

```

λ1 = 33 + 3 * Sqrt[82];
λ2 = 8;
λ3 = 33 - 3 * Sqrt[82];
I1 = λ1 + λ2 + λ3
I2 = Simplify[λ1 * λ2 + λ1 * λ3 + λ2 * λ3]
I3 = Simplify[λ1 * λ2 * λ3]

```

74

879

2808

e) We have to find mean stress for spherical or hydrostatics stress, and then subtract it from original stress tensor to find the deviator stress

$$T_m = \text{Tr}[T] / 3$$

$$\frac{74}{3}$$

$$T_d = \text{Simplify}[T - T_m * \text{IdentityMatrix}[3]]$$

$$\left\{ \left\{ -\frac{56}{3}, -3, 0 \right\}, \left\{ -3, \frac{106}{3}, 0 \right\}, \left\{ 0, 0, -\frac{50}{3} \right\} \right\}$$

f) The first invariant of deviator stress (T_d) is the trace of T_d .

$$\text{FirstInvariantofTd} = \text{Tr}[T_d]$$

0

Constitutive Relations

5. Determine the stress tensor at a point where the

Lagrangian strain tensor is given by $\begin{pmatrix} 30 & 50 & 20 \\ 50 & 40 & 0 \\ 20 & 0 & 30 \end{pmatrix} 10^{-6}$

and the material is steel: $\lambda = 119.2 \text{ GPa}$, and $\mu = 79.2 \text{ GPa}$

$$\text{Strain} = \left\{ \{30\}, \{40\}, \{30\}, \{50\}, \{0\}, \{20\} \right\} 10^{-6}$$

$$\left\{ \left\{ \frac{3}{100000} \right\}, \left\{ \frac{1}{25000} \right\}, \left\{ \frac{3}{100000} \right\}, \left\{ \frac{1}{20000} \right\}, \{0\}, \left\{ \frac{1}{50000} \right\} \right\}$$

The constitutive relation is $\sigma_{ij} = \lambda \text{trace}(\epsilon) \delta_{ij} + 2\mu \epsilon_{ij}$ where $\epsilon_{ij} = \frac{1}{2}(u_{ij} + u_{ji})$, u is the displacement. or in matrix form

$$\begin{pmatrix} \sigma_{11} \\ \sigma_{22} \\ \sigma_{33} \\ \sigma_{12} \\ \sigma_{23} \\ \sigma_{13} \end{pmatrix} = \begin{pmatrix} \lambda + 2\mu & \lambda & \lambda & 0 & 0 & 0 \\ \lambda & \lambda + 2\mu & \lambda & 0 & 0 & 0 \\ \lambda & \lambda & \lambda + 2\mu & 0 & 0 & 0 \\ 0 & 0 & 0 & 2\mu & 0 & 0 \\ 0 & 0 & 0 & 0 & 2\mu & 0 \\ 0 & 0 & 0 & 0 & 0 & 2\mu \end{pmatrix} \begin{pmatrix} \varepsilon_{11} \\ \varepsilon_{22} \\ \varepsilon_{33} \\ \varepsilon_{12} \\ \varepsilon_{23} \\ \varepsilon_{13} \end{pmatrix}$$

$$\lambda q5 = 119.2 * 10^9;$$

$$\mu q5 = 79.2 * 10^9;$$

$$\text{Cc} = \{ \{ \lambda q5 + 2 * \mu q5, \lambda q5, \lambda q5, 0, 0, 0 \},$$

$$\{ \lambda q5, \lambda q5 + 2 * \mu q5, \lambda q5, 0, 0, 0 \}, \{ \lambda q5, \lambda q5, \lambda q5 + 2 * \mu q5, 0, 0, 0 \},$$

$$\{ 0, 0, 0, 2 * \mu q5, 0, 0 \}, \{ 0, 0, 0, 0, 2 * \mu q5, 0 \}, \{ 0, 0, 0, 0, 0, 2 * \mu q5 \} \}$$

$$\{ \{ 2.776 \times 10^{11}, 1.192 \times 10^{11}, 1.192 \times 10^{11}, 0, 0, 0 \},$$

$$\{ 1.192 \times 10^{11}, 2.776 \times 10^{11}, 1.192 \times 10^{11}, 0, 0, 0 \},$$

$$\{ 1.192 \times 10^{11}, 1.192 \times 10^{11}, 2.776 \times 10^{11}, 0, 0, 0 \}, \{ 0, 0, 0, 1.584 \times 10^{11}, 0, 0 \},$$

$$\{ 0, 0, 0, 0, 1.584 \times 10^{11}, 0 \}, \{ 0, 0, 0, 0, 0, 1.584 \times 10^{11} \} \}$$

$$\sigma q5 = \text{Cc} \cdot \text{Strain}$$

$$\{ \{ 1.6672 \times 10^7 \}, \{ 1.8256 \times 10^7 \}, \{ 1.6672 \times 10^7 \}, \{ 7.92 \times 10^6 \}, \{ 0. \}, \{ 3.168 \times 10^6 \} \}$$

6. Determine the strain tensor at a point where the Cauchy

stress tensor is given by $\begin{pmatrix} 100 & 42 & 6 \\ 42 & -2 & 0 \\ 6 & 0 & 15 \end{pmatrix}$ MPa with E =

207 GPa, $\mu = 79.2$ GPa, and $\nu = 0.30$

The inverse Hooke's law is given as $\varepsilon_{ij} = \frac{1+\nu}{E} \sigma_{ij} - \frac{\nu}{E} \text{trace}(\sigma) \delta_{ij}$ or in matrix form, we know also $\mu = \frac{E}{2(1+\nu)}$

$$\begin{pmatrix} \varepsilon_{11} \\ \varepsilon_{22} \\ \varepsilon_{33} \\ \varepsilon_{12} \\ \varepsilon_{23} \\ \varepsilon_{13} \end{pmatrix} = \begin{pmatrix} \frac{1}{E} & \frac{-\nu}{E} & \frac{-\nu}{E} & 0 & 0 & 0 \\ \frac{-\nu}{E} & \frac{1}{E} & \frac{-\nu}{E} & 0 & 0 & 0 \\ \frac{-\nu}{E} & \frac{-\nu}{E} & \frac{1}{E} & 0 & 0 & 0 \\ 0 & 0 & 0 & \frac{1+\nu}{E} & 0 & 0 \\ 0 & 0 & 0 & 0 & \frac{1+\nu}{E} & 0 \\ 0 & 0 & 0 & 0 & 0 & \frac{1+\nu}{E} \end{pmatrix} \begin{pmatrix} \sigma_{11} \\ \sigma_{22} \\ \sigma_{33} \\ \sigma_{12} \\ \sigma_{23} \\ \sigma_{13} \end{pmatrix}$$

$$E_m = 207 \times 10^9; \mu = 79.2 \times 10^9; \nu = 0.3;$$

$$\text{Stress} = \{ \{ 100 \}, \{ -2 \}, \{ 15 \}, \{ 42 \}, \{ 0 \}, \{ 6 \} \} * 10^6;$$

$$\text{Ccc} = \{ \{ 1/E_m, -\nu/E_m, -\nu/E_m, 0, 0, 0 \}, \{ -\nu/E_m, 1/E_m, -\nu/E_m, 0, 0, 0 \},$$

$$\{ -\nu/E_m, -\nu/E_m, 1/E_m, 0, 0, 0 \}, \{ 0, 0, 0, 1/(2 * \mu), 0, 0 \},$$

$$\{ 0, 0, 0, 0, 1/(2 * \mu), 0 \}, \{ 0, 0, 0, 0, 0, 1/(2 * \mu) \} \};$$

$$\varepsilon = \text{Ccc} \cdot \text{Stress}$$

$$\{ \{ 0.000464251 \}, \{ -0.000176329 \},$$

$$\{ -0.0000695652 \}, \{ 0.000265152 \}, \{ 0. \}, \{ 0.0000378788 \} \}$$

Airy Stress Function

7. For the following proposed Airy stress function $\Phi =$

$$\frac{3F}{4c} \left(x_1 x_2 - \frac{x_1 x_2^3}{3c^2} \right) + \frac{P}{4c} x_2^2$$

a) The Airy stress function must satisfy biharmonic equation

$$\nabla^4 \Phi = 0, \quad \text{or} \quad \Phi_{,1111} + 2\Phi_{,2211} + \Phi_{,2222} = 0$$

$$\Phi_{,11} = 0, \quad \Rightarrow \Phi_{,1111} = 0 \quad \text{and} \quad \Phi_{,2211} = 0$$

$$\Phi_{,22} = -\frac{3F}{2c^3} x_1 x_2 + \frac{P}{2c} \Rightarrow \Phi_{,2222} = 0$$

So the given function satisfies biharmonic equation.

b) The stress components are given by

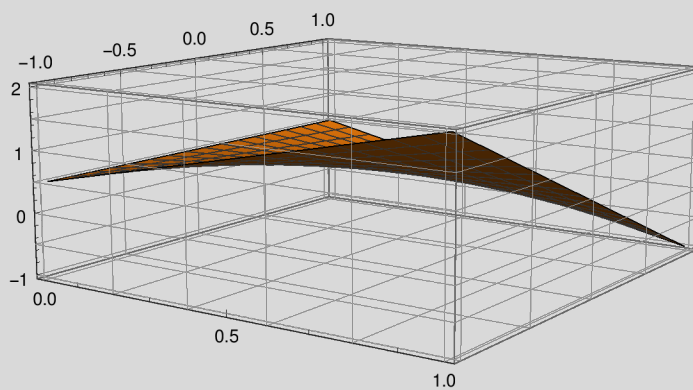
$$\sigma_{11} = \Phi_{,22} = -\frac{3F}{2c^3} x_1 x_2 + \frac{P}{2c}$$

$$\sigma_{22} = \Phi_{,11} = 0$$

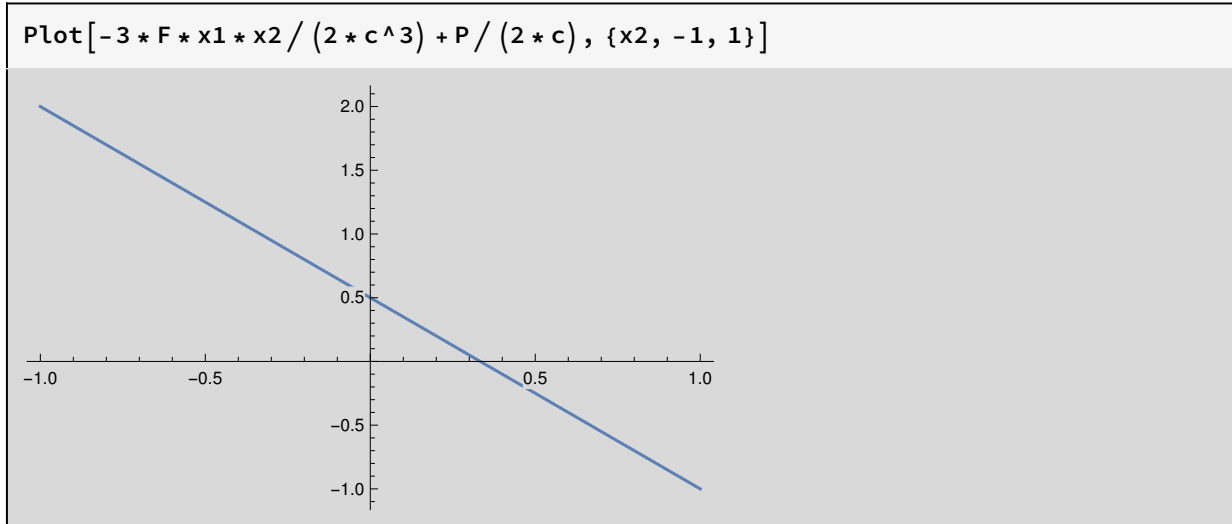
$$\sigma_{12} = -\Phi_{,12} = \frac{-3F}{4c} \left(1 - \frac{x_2}{c^2} \right)$$

c) plot of σ_{11}

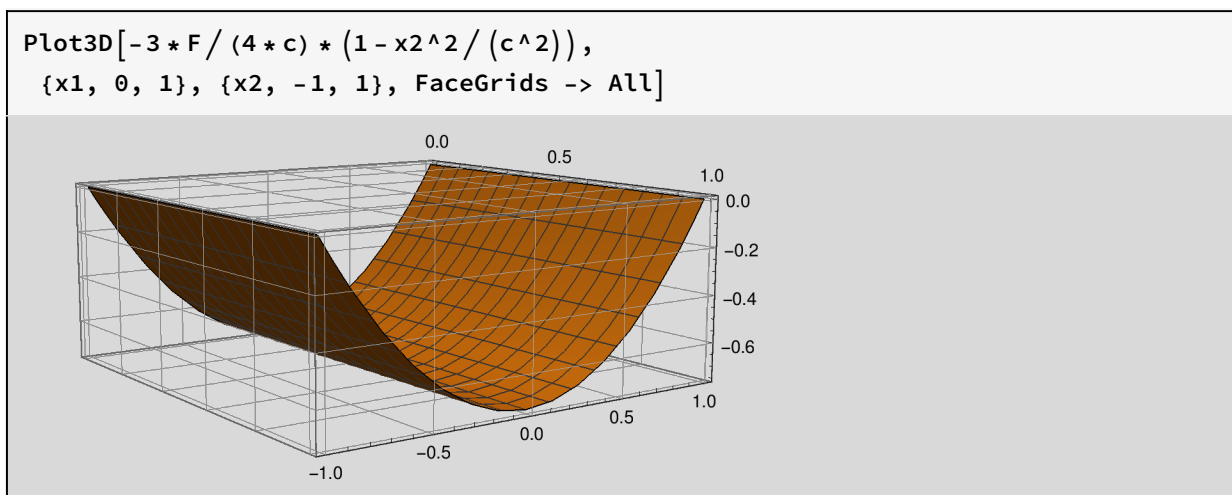
```
c = 1; P = 1; F = 1;
Plot3D[-3 * F * x1 * x2 / (2 * c^3) + P / (2 * c),
{x1, 0, 1}, {x2, -1, 1}, FaceGrids -> All]
```



```
x1 = 1;
```



plot of σ_{12}



If we consider the cantilever beam with length L (in x_1 -direction), height $2c$ (in x_2 -direction) and the width $b=1$ unit (x_3 -direction-normal to the surface), yields to cross section area, $A=2c$, and second moment of area about x_3 $I = \frac{b(2c)^3}{12} = \frac{2c^3}{3}$.

Now, look at the relation σ_{11}

$$\sigma_{11} = -\frac{3F}{2c^3} x_1 x_2 + \frac{P}{2c}$$

It is clear that second term is normal force P over cross section area which gives stress in x_1 direction. So, the axial pull is P .

Now look at the first term, we can say $F * x_1 = M$, the moment about x_3 direction, $\frac{3}{2c^3} = \frac{1}{I}$. So, F is transverse end load and we can rewrite the σ_{11} as

$$\sigma_{11} = \frac{P}{A} - \frac{Mx_2}{I},$$

which is exactly the relation for stress of the beam under bending moment and axial pull.

And it is linear function of x_2 , which the plot above shows that.

The relation for shear stress is given by $\sigma_{12} = -\frac{VQ}{Ib}$, where V is shear force (in x_2 -direction), Q is the first moment of area, $Q = \int y dA$, which $dA = b * dx_2$.

for rectangle cross section with $b=1$, $Q = \frac{1}{2}(c^2 - x_2^2)$, and I is given in above so shear stress is

$$\sigma_{12} = -\frac{VQ}{I} = -\frac{3V}{4c^3}(c^2 - x_2^2) = -\frac{3V}{4c}\left(1 - \frac{x_2^2}{c^2}\right)$$

If compare it with what is obtained from Airy stress function, we conclude again that the F is transverse end load (in x_2 -direction). And it is the function of x_2 square, which the plot above shows that.

$$\sigma_{12} = -\Phi_{,12} = \frac{-3F}{4c} \left(1 - \frac{x_{22}}{c^2}\right)$$

New Question in Revised HW

The Cauchy-Riemann equation for complex function $f(z)=u(x,y)+iv(x,y)$ is

$$u_{,x} = v_{,y}$$

$$u_{,y} = -v_{,x}$$

So we have $z^2 = (x^2 - y^2) + 2xyi \implies z^2 = (x + iy)^2 \implies z_1 = f(z) = x + iy$ and $z_2 = g(z) = -x - iy$

for the $f(z)$ the C-R is

$$1 = 1$$

$$0 = 0$$

and for $g(z)$

$$-1 = -1$$

$$0 = 0$$

which satisfy the C-R relations, and $f(z)$ and $g(z)$ are analytical functions.

Before we do that, it was obvious that the $f(z)$ and $g(z)$ are analytical functions, because with the definition $z=x+iy$

$$f(z)=z, g(z)=-z$$

we know that these functions are differentiable everywhere in z -plane.

**CVEN 7161
FRACTURE MECHANICS**

SPRING 2020

HOME-WORK 2

Derivation of SIF

Due: Thursday Feb. 20, 2020

1. Show that

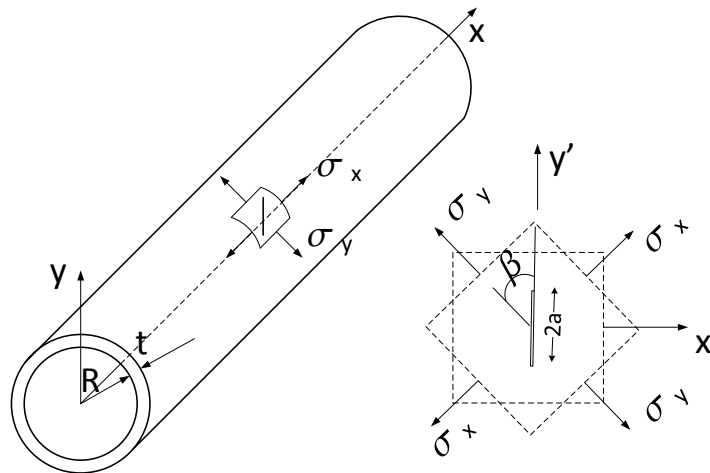
$$z^2 = (x^2 - y^2) + 2xyi \quad (1)$$

satisfies the Cauchy-Riemann equation.

2. For the following proposed Airy stress function:

$$\Phi = \frac{3F}{4c} \left(x_1 x_2 - \frac{x_1 x_2^3}{3c^2} \right) + \frac{P}{4c} x_2^2 \quad (2)$$

- (a) Show that it is indeed suitable as an Airy stress function.
 (b) Determine the stress components in the region $x_1 > 0$, $-c < x_2 < c$.
 (c) Plot σ_{11} , σ_{12} and show that these stresses are those of a cantilever beam subjected to a transverse end load and axial pull (which one is P and which one is F ?).
3. A cylindrical pressure vessel of radius R and thickness t contains a through crack of length $2a$ oriented at an angle β with the circumferential direction. When the vessel is subjected to an internal pressure p , determine the stress intensity factors at the crack tip.



Hint Show that $\sigma_{xx} = \frac{pR}{2t}$ (corresponding to the longitudinal stress), and that $\sigma_{yy} = \frac{pR}{t}$, (corresponding to the tangential stress) and then transform into $\sigma_{x'x'}$, $\sigma_{y'y'}$, and $\sigma_{x'y'}$

using

$$\begin{bmatrix} \sigma_{x'x'} & \sigma_{x'y'} \\ \sigma_{x'y'} & \sigma_{y'y'} \end{bmatrix} = \begin{bmatrix} \cos \theta & \sin \theta \\ -\sin \theta & \cos \theta \end{bmatrix} \begin{bmatrix} \sigma_{xx} & 0 \\ 0 & \sigma_{yy} \end{bmatrix} \begin{bmatrix} \cos \theta & \sin \theta \\ -\sin \theta & \cos \theta \end{bmatrix}^T \quad (3)$$

(4)

Those relationships may be helpful:

$$\sin 2\beta = 2 \sin \beta \cos \beta \quad (5)$$

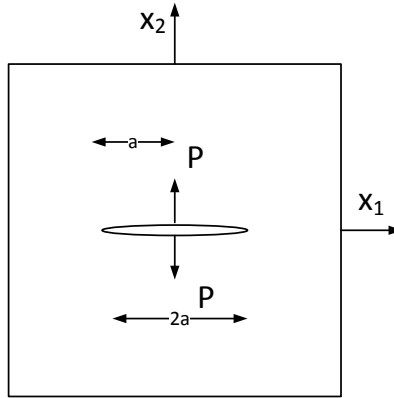
$$\cos 2\beta = 1 - 2 \sin^2 \beta \quad (6)$$

$$\sin^2 \beta = \frac{1 - \cos 2\beta}{2} \quad (7)$$

$$\cos^2 \beta = \frac{1 + \cos 2\beta}{2} \quad (8)$$

$$\sin \beta \cos \beta = \frac{\sin 2\beta}{2} \quad (9)$$

4. The stress function for a crack subjected to splitting forces P , as shown below



is given by:

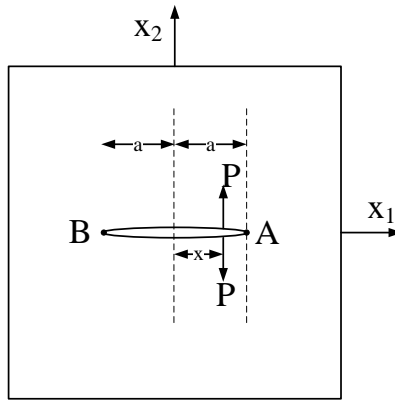
$$\phi = \frac{Pa}{\pi z \sqrt{z^2 - a^2}} \quad (10)$$

where $z = x_1 + ix_2$ and P is a load per unit thickness. Calculate the expressions of σ_{22} at $x_2 = 0$ and derive an expression for K_I . ($K_P = \frac{P}{\sqrt{\pi a}}$) Hint:

(a) At crack tip $\frac{\eta}{a} \ll 1$.

(b) $\eta = z - a = z = re^{i\theta}$

5. The stress intensity factor of the following problem:



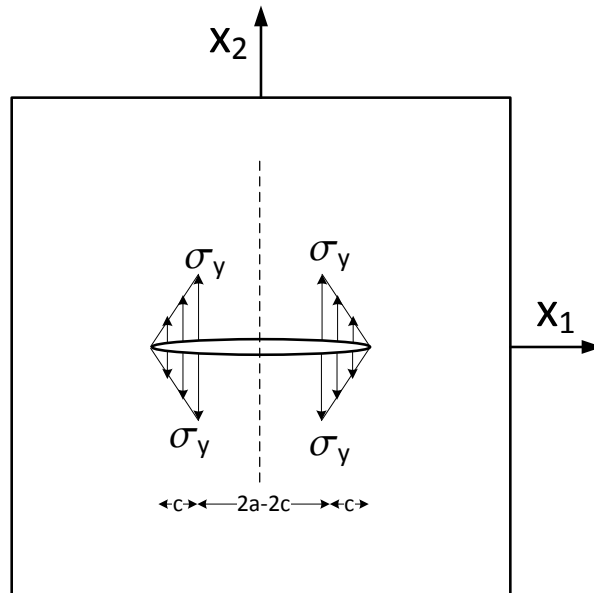
is given by:

$$K_A = \frac{P}{\sqrt{\pi a}} \sqrt{\frac{a+x}{a-x}} \quad (11)$$

$$K_B = \frac{P}{\sqrt{\pi a}} \sqrt{\frac{a-x}{a+x}} \quad (12)$$

Based on those expressions, and results from the previous problem, determine the stress function Φ .

6. Barenblatt's model assumes a linearly varying closing pressure at the tip of a crack,



Using Mathematica and the expressions of K_A and K_B from the previous problem, determine an expression for the stress intensity factors for this case.

SOLUTION

1 Problem 1

The Cauchy-Riemann equation for complex function $f(z) = u(x, y) + iv(x, y)$ is

$$u_{,x} = v_{,y} \quad (13)$$

$$u_{,y} = -v_{,x} \quad (14)$$

So we have

$$z^2 = (x^2 - y^2) + 2xyi \Rightarrow z^2 = (x + iy)^2 \Rightarrow z_1 = f(z) = x + iy \text{ and } z_2 = g(z) = -x - iy \quad (15)$$

for the $f(z)$ the Cauchy-Riemann is

$$1 = 1 \quad (16)$$

$$0 = 0 \quad (17)$$

and for $g(z)$

$$-1 = -1 \quad (18)$$

$$0 = 0 \quad (19)$$

which satisfy the C-R relations, and $f(z)$ and $g(z)$ are analytical functions.

However, it was obvious that the $f(z)$ and $g(z)$ were analytical functions, because given $z = x + iy$ $f(z) = z$, $g(z) = -z$ we know that these functions are differentiable everywhere in z -plane.

2 Problem 2

$$\Phi = \frac{(3F) \left(x_1 x_2 - \frac{x_1 x_2^3}{3c^2} \right)}{4c} + \frac{P x_2^2}{4c} \quad (20)$$

satisfies the Laplacian

$$\sigma_{11} = \frac{\partial^2 \Phi}{\partial (x_2)^2} \quad (21)$$

$$= \frac{P}{2c} - \frac{3F x_1 x_2}{2c^3} \quad (22)$$

$$\sigma_{22} = \frac{\partial^2 \Phi}{\partial (x_1)^2} \quad (23)$$

$$= 0 \quad (24)$$

$$\sigma_{12} = \left[-\frac{\partial}{\partial x_2} \frac{\partial \Phi}{\partial x_1} \right] \quad (25)$$

$$= -\frac{3F (c^2 - x_2^2)}{4c^3} \quad (26)$$

If we consider the cantilever beam with length L (in x_1 -direction), height $2c$ (in x_2 -direction) and the width $b = 1$ unit (x_3 -direction-normal to the surface), yields to cross section area, $A=2c$, and second moment of area about x_3 , $I = b(2c)^3/12 = (2c^3)/3$.

From σ_{11} It is clear that second term is normal force P over cross section area which gives stress in x_1 direction. So, the axial pull is P .

Now look at the first term , we can say $Fx_1 = M$, the moment about x_3 direction, $3/(2c^3) = 1/I$. So, F is transverse end load and we can rewrite the

3 Problem 3

$$\begin{bmatrix} \sigma_{x'x'} & \sigma_{x'y'} \\ \sigma_{x'y'} & \sigma_{y'y'} \end{bmatrix} = \begin{bmatrix} \cos \theta & \sin \theta \\ -\sin \theta & \cos \theta \end{bmatrix} \begin{bmatrix} \sigma_{xx} & 0 \\ 0 & \sigma_{yy} \end{bmatrix} \begin{bmatrix} \cos \theta & \sin \theta \\ -\sin \theta & \cos \theta \end{bmatrix}^T \quad (27)$$

$$(28)$$

But $\theta = \frac{\pi}{2} - \beta$, substituting, we obtain

$$\sigma_{x'x'} = \frac{1}{2}\sigma_{xx}(1 - \cos 2\beta) + \frac{1}{2}\sigma_{yy}(1 + \cos 2\beta) \quad (29)$$

$$\sigma_{y'y'} = \frac{1}{2}\sigma_{xx}(1 + \cos 2\beta) + \frac{1}{2}\sigma_{yy}(1 - \cos 2\beta) \quad (30)$$

$$\sigma_{x'y'} = -\frac{1}{2}(\sigma_{xx} - \sigma_{yy}) \sin 2\beta \quad (31)$$

for this problem

$$\sigma_{xx} = \frac{pR}{2t} \quad (32)$$

$$\sigma_{yy} = \frac{pR}{t} \quad (33)$$

$$K_I = \sqrt{\pi a} \sigma_{y'y'} \quad (34)$$

$$= \frac{pR}{2t} (1 + \sin^2 \beta) \sqrt{\pi a} \quad (35)$$

$$K_{II} = \sqrt{\pi a} \sigma_{x'y'} \quad (36)$$

$$= \frac{pR}{2t} \sin \beta \cos \beta \sqrt{\pi a} \quad (37)$$

Note that we have used various trigonometric relationships in order to solve this problem

$$\sin 2\beta = 2 \sin \beta \cos \beta \quad (38)$$

$$\cos 2\beta = 1 - 2 \sin^2 \beta \quad (39)$$

$$\sin^2 \beta = \frac{1 - \cos 2\beta}{2} \quad (40)$$

$$\cos^2 \beta = \frac{1 + \cos 2\beta}{2} \quad (41)$$

$$\sin \beta \cos \beta = \frac{\sin 2\beta}{2} \quad (42)$$

4 Problem 4

$$\phi = \frac{Pa}{\pi z} \frac{1}{\sqrt{z^2 - a^2}} \quad (43)$$

$$z = x_1 + ix_2 \quad (44)$$

$$\sigma_{22} = \operatorname{Re}\phi(z) + x_2\operatorname{Im}\phi'(z) \quad (45)$$

$$x_2 = 0 \Rightarrow \operatorname{Re}\phi(z) = \operatorname{Re}\left[\frac{Pa}{\pi z} \frac{1}{\sqrt{z^2 - a^2}}\right] \quad (46)$$

$$z = \eta + a \quad (47)$$

$$\sigma_{22} = \operatorname{Re}\left[\frac{Pa}{\pi\eta + a} \frac{1}{\sqrt{\eta^2 + 2a\eta + a^2 - a^2}}\right] \quad (48)$$

$$= \operatorname{Re}\left[\frac{P}{\pi} \sqrt{\frac{a^2}{(\eta + a)^2(\eta^2 + 2a\eta)}}\right] \quad (49)$$

$$= \operatorname{Re}\left[\frac{P}{\pi} \sqrt{\frac{a^2}{a^3\eta\left(\frac{\eta^3}{a^3} + 4\frac{\eta^2}{a^2} + 5\frac{\eta}{a} + 2\right)}}\right] \quad (50)$$

But $\frac{\eta}{a} \ll 1$, thus we can simplify

$$\sigma_{22} = \operatorname{Re}\left[\frac{P}{\pi a} \sqrt{\frac{a}{2\eta}}\right] \quad (51)$$

we now substitute $\eta = re^{i\theta}$

$$\sigma_{22} = \operatorname{Re}\left[\frac{P}{\pi a} \sqrt{\frac{a}{2r}} e^{-i\frac{\theta}{2}}\right] \quad (52)$$

but $e^{-i\theta} = \cos\theta - i\sin\theta$, thus

$$\sigma_{22} = \operatorname{Re}\left[\frac{P}{\pi a} \sqrt{\frac{a}{2r}} \left(\cos\frac{\theta}{2} - i\sin\frac{\theta}{2}\right)\right] \quad (53)$$

$$= \frac{P}{\pi a} \sqrt{\frac{a}{2r}} \cos\frac{\theta}{2} \quad (54)$$

Finally,

$$K_I = \lim_{r \rightarrow 0, \theta=0} \sqrt{2\pi r} \sigma_{22} \quad (55)$$

$$= \lim_{r \rightarrow 0, \theta=0} \sqrt{2\pi r} \frac{P}{\pi a} \sqrt{\frac{a}{2r}} \cos\frac{\theta}{2} \quad (56)$$

$$= \frac{P}{\sqrt{a\pi}} \quad (57)$$

5 Problem 5

$$K_A = \frac{P}{\sqrt{\pi a}} \sqrt{\frac{a+x}{a-x}} \quad (58)$$

$$K_B = \frac{P}{\sqrt{\pi a}} \sqrt{\frac{a-x}{a+x}} \quad (59)$$

$$\sigma_{22} = \operatorname{Re}\phi(z) + x_2\phi'(z) = \frac{K_I}{\sqrt{2\pi r}} \quad (60)$$

$$\sigma_{22}^A = \frac{K^A}{\sqrt{2\pi r}} = \frac{P}{\pi\sqrt{2ar}} \sqrt{\frac{a+x}{a-x}} \quad (61)$$

$$z = r(\cos\theta + i\sin\theta) \text{ and } \theta = 0 \quad (62)$$

Replace r by z

$$\boxed{\phi^A(z) = \frac{P}{\pi\sqrt{2az}} \sqrt{\frac{a+x}{a-x}}} \quad (63)$$

Similarly for point B

$$\boxed{\phi^B(z) = \frac{P}{\pi\sqrt{2az}} \sqrt{\frac{a-x}{a+x}}} \quad (64)$$

6 Problem 6

$$K = K^A = K^B \quad (65)$$

$$p(x) = \frac{P}{c}(a-x) \quad (66)$$

$$K = \int_{a-c}^a \frac{p(x)}{\sqrt{\pi a}} \sqrt{\frac{a+x}{a-x}} dx + \int_{a-c}^a \frac{p(x)}{\sqrt{\pi a}} \sqrt{\frac{a-x}{a+x}} dx \quad (67)$$

$$x' = a-x \Rightarrow p(x') = \frac{P}{c}x' \quad (68)$$

$$K = \int_0^c \frac{p(x')}{\sqrt{\pi a}} \sqrt{\frac{2a-x'}{x'}} dx' + \int_0^c \frac{p(x')}{\sqrt{\pi a}} \sqrt{\frac{x'}{2a-x'}} dx' \quad (69)$$

$$= \frac{P}{c\sqrt{\pi a}} \int_0^c \left[\sqrt{\frac{2a-x'}{x'}} + \sqrt{\frac{x'}{2a-x'}} \right] x' dx' \quad (70)$$

$$= \frac{P}{c\sqrt{\pi a}} \int_0^c \sqrt{\frac{2ax'}{2ax' - x'^2}} dx' \quad (71)$$

$$(72)$$

Using Mathematica, we obtain

$$\boxed{K = \frac{2aP}{c\sqrt{\pi a}} \left[\frac{\pi a}{2} - a \arcsin \frac{a-c}{a} - \sqrt{2ac - c^2} \right]} \quad (73)$$

7 Problem XX

The stress function is given by

$$\Phi_{II}(z) = -x_2 \operatorname{Re} \left[\int \phi_{II}(z) dz \right] \quad (74)$$

where ϕ_{II} is an arbitrary function which must satisfy

$$\frac{\partial \Phi_{II}(z)}{\partial x_1} = -x_2 \operatorname{Re}[\phi_{II}(z)] \quad (75)$$

$$\frac{\partial^2 \Phi_{II}(z)}{\partial x_1^2} = -x_2 \operatorname{Re}[\phi'_{II}(z)] \quad (76)$$

$$\frac{\partial \Phi_{II}(z)}{\partial x_2} = -\operatorname{Re}[\phi_{II}(z)] + x_2 \operatorname{Im}[\phi_{II}(z)] \quad (77)$$

$$\frac{\partial^2 \Phi_{II}(z)}{\partial x_2^2} = \text{Im}[\phi_{II}(z)] + \text{Im}[\phi_{II}(z)] + x_2 \text{Re}[\phi'_{II}(z)] \quad (78)$$

$$= 2\text{Im}[\phi_{II}(z)] + x_2 \text{Re}[\phi'_{II}(z)] \quad (79)$$

$$\frac{\partial^2 \Phi_{II}(z)}{\partial x_1 \partial x_2} = -\text{Re}[\phi_{II}(z)] + x_2 \text{Im}[\phi'_{II}(z)] \quad (80)$$

$$\frac{\partial^2 \Phi_{II}(z)}{\partial x_1^2} + \frac{\partial^2 \Phi_{II}(z)}{\partial x_2^2} = 2\text{Im}[\phi'_{II}(z)] \quad (81)$$

The compatibility equation is

$$\nabla^2(\nabla^2 \Phi) = \left(\frac{\partial^2}{\partial x_1^2} + \frac{\partial^2}{\partial x_2^2} \right) 2\text{Im}[\phi'_{II}(z)] \quad (82)$$

$$\frac{\partial^2}{\partial x_1^2} \text{Im}[\Phi_{II}(z)] = \text{Im}[\Phi''_{II}(z)] \quad (83)$$

$$\frac{\partial}{\partial x_2} \text{Im}[\Phi_{II}(z)] = \text{Re}[\Phi''_{II}(z)] \quad (84)$$

$$\frac{\partial^2}{\partial x_2^2} \text{Im}[\Phi_{II}(z)] = -\text{Im}[\Phi''_{II}(z)] \quad (85)$$

$$(86)$$

It is clear that substituting Eq. 83 and 85 into 82 then $\Phi_{II}(z)$ satisfies the compatibility equation

$$\nabla^2(\nabla^2 \Phi) = 0 \quad (87)$$

The stresses are then given by

$$\sigma_{11} = \frac{\partial^2 \Phi_{II}(z)}{\partial x_2^2} = \text{Im}[\phi_{II}(z)] + \text{Im}[\phi_{II}(z)] + x_2 \text{Re}[\phi'_{II}(z)] \quad (88)$$

$$\sigma_{22} = \frac{\partial^2}{\partial x_1^2} = -x_2 \text{Re}[\Phi''_{II}(z)] \quad (89)$$

$$\sigma_{12} = -\frac{\partial^2 \Phi_{II}(z)}{\partial x_1 \partial x_2} = \text{Re}[\phi_{II}(z)] - x_2 \text{Im}[\phi'_{II}(z)] \quad (90)$$

The boundary conditions are

$$x_1 = \pm\infty \quad \sigma_{12} = \tau \quad (91)$$

$$x_2 = \pm\infty \quad \sigma_{12} = \tau \quad (92)$$

$$x_2 = 0 - a < x_1 < a \quad \sigma_{22} = 0 \quad (93)$$

$$x_2 = 0 - a < x_1 < a \quad \sigma_{12} = 0 \quad (94)$$

$$|x_1 - a| < \epsilon \quad \sigma_{12} \gg 1 \quad (95)$$

To determine the function ϕ_{II} which satisfies those B.C. we follow a similar line of arguments as the one developed for mode I and select

$$\phi_{II} = \frac{\tau}{\sqrt{1 - \frac{a^2}{z^2}}} \quad (96)$$

To determine the stress distribution near the crack tip we introduce $\eta = z - a = r e^{i\theta}$, thus for $\eta \ll a$

$$\operatorname{Re}[\phi_{II}] = \operatorname{Re} \left[\frac{\tau}{\sqrt{1 - \frac{a^2}{z^2}}} \right] = \operatorname{Re} \left[\frac{\tau}{\sqrt{\frac{a\eta(2+\eta/a)}{a^2(1+2\eta/a+\eta^2/a^2)}}} \right] \quad (97)$$

$$\simeq \operatorname{Re} \left[\tau \frac{\sqrt{a}}{2\eta} \right] \simeq \operatorname{Re} \left[\tau \frac{\sqrt{a}}{2r e^{i\theta}} \right] \quad (98)$$

$$\simeq \operatorname{Re} \left[\tau \frac{\sqrt{a}}{r} e^{-\frac{1}{2}i\theta} \right] \simeq \tau \sqrt{\frac{a}{2r}} \cos \frac{\theta}{2} \quad (99)$$

$$\frac{d\phi_{II}}{dz} = -\frac{1}{2}\tau \left(1 - \frac{a^2}{z^2} \right)^{-\frac{3}{2}} \frac{2a^2}{z^3} = -\tau(z^2 - a^2)^{-\frac{3}{2}} a^2 \quad (100)$$

$$= -\tau(\eta^2 + 2a\eta)^{-\frac{3}{2}} a^2 = -\frac{\tau}{2} \sqrt{\frac{a^4}{2a^3\eta^3}} = -\frac{\tau}{2} \sqrt{\frac{a}{2r^3 e^{i3\theta}}} \quad (101)$$

$$= -\frac{\tau}{2r} \sqrt{\frac{a}{2r}} e^{-\frac{3}{2}\theta i} \quad (102)$$

$$x_2 \operatorname{Im}[\phi'(z)] = r \sin \theta \left(-\frac{\tau}{2r} \sqrt{\frac{a}{2r}} \right) \sin\left(-\frac{3}{2}\theta\right) \quad (103)$$

$$= \tau \sqrt{a} 2r \sin \frac{\theta}{2} \cos \frac{\theta}{2} \sin \frac{3}{2}\theta \quad (104)$$

Substituting to solve for the stresses

$$\sigma_{11} = 2\operatorname{Im}[\phi_{II}(z)] + x_2 \operatorname{Re}[\phi'_{II}(z)] \quad (105)$$

$$= 2\operatorname{Im} \left[\tau \sqrt{\frac{a}{2r}} e^{-\frac{1}{2}\theta i} \right] + r \sin \theta \operatorname{Re} \left[-\frac{\tau}{2r} \sqrt{\frac{a}{2r}} e^{-\frac{3}{2}\theta i} \right] \quad (106)$$

$$= -2\tau \sqrt{\frac{a}{2r}} \sin \frac{\theta}{2} - \tau \sqrt{\frac{a}{2r}} \sin \frac{\theta}{2} \cos \frac{\theta}{2} \cos \frac{3\theta}{2} \quad (107)$$

$$= -\tau \sqrt{\frac{a}{2r}} \sin \frac{\theta}{2} \left(2 + \cos \frac{\theta}{2} \cos \frac{3\theta}{2} \right) \quad (108)$$

$$\sigma_{22} = -x_2 \operatorname{Re}[\phi''_{II}(z)] = -r \sin \theta - \frac{\tau}{2r} \sqrt{\frac{a}{2r}} \cos -\frac{3\theta}{2} \quad (109)$$

$$= \tau \sqrt{a} 2r \sin \frac{\theta}{2} \cos \frac{\theta}{2} \cos \frac{3}{2}\theta \quad (110)$$

$$\sigma_{12} = \operatorname{Re}[\phi_{II}(z)] - x_2 \operatorname{Im}[\phi'_{II}(z)] \quad (111)$$

$$= \tau \sqrt{\frac{a}{2r}} \cos \frac{\theta}{2} \left(1 - \sin \frac{\theta}{2} \sin \frac{3\theta}{2} \right) \quad (112)$$

**CVEN 7161
FRACTURE MECHANICS**

SPRING 2020

HOME-WORK

Application of LEFM

Due: Mar 3, 2020

1 Assignment

1. A cylindrical pressure vessel of diameter 3 m and length 9 m, with closed ends, is to be constructed using butt-welded steel plates which are 0.03 m thick and approximately 1 m square. It must be designed to contain a pressure p without failure by yielding or by brittle fracture. Yield occurs when the equivalent tensile stress equals the yield stress, i.e., when:

$$(\sigma_1 - \sigma_2)^2 + (\sigma_2 - \sigma_3)^2 + (\sigma_3 - \sigma_1)^2 = 2\sigma_y^2 \quad (1)$$

The butt welds joining the plates are known to contain a thumbnail (semi-circular) cracks with a maximum depth of a . For such cracks $K_I = 1.128\sigma\sqrt{\pi a}$ where σ is the tensile stress across a crack, and brittle failure will occur when $K_I \geq K_{Ic}$. Three steels are available for constructing the pressure vessel. Their yield strength and fracture toughnesses are:

STEEL	σ_y (MPa)	$K_{Ic}(MNm^{-3/2})$
HY 140	965	280
T 1	690	180
HY 180	1240	180

Construct a plot of maximum pressure against crack depth a for each steel, showing the region of p and a which is safe against fracture and yielding. If non-destructive testing can detect cracks of depths $a_1 \geq 20$ mm (allowing welds with larger cracks than this to be repaired) which steel gives the greatest margin of safety? If a more refined technique will detect cracks of depth $a_1 \geq 2$ mm which steel offers the greatest margin of safety? *Discuss* your results.

2. Design (by selecting the most economical material and the thickness t) a high strength steel pressure vessel which must withstand 5,000 psi of internal pressure p , the nominal diameter d is 30 in., and the wall thickness t must be greater than 0.5 in.

The steels available for use are:

Steel	σ_{ys} (Ksi)	K_{Ic} Ksi $\sqrt{\text{in}}$	Cost \$/lb
A	260	80	1.40
B	220	110	1.40
C	180	140	1.00
D	180	220	1.20
E	140	260	0.50
F	110	170	0.15

Assume that inspection procedures dictate a surface (elliptical) flaw with a depth b of 0.5 inch and $b/2a=0.25$; Assume a factor of safety of two for both the design stress (*vs* yield stress) and the stress intensity factor (*vs* the fracture toughness). Make sure to check for fracture failure and yielding of the section.

- Repeat the beer barrel problem discussed in class, by determining the reliability index assuming that we have:

Variable	Mean	Standard Deviation
$2a$ (in)	3.5	0.2
b (in)	0.05	0.01
p (psi)	600	20
K_{Ic} ksi $\sqrt{\text{in}}$	40	5

Try to understand and implement the following sample code:

```

1 clear; clc; close all;
2 %% Initialization
3 %mean and standard deviation value (units kips and inches)
4 P=0.6;          sd_P=0.02;
5 a=3.5/2;       sd_a=0.2;
6 b=0.05;        sd_b=0.01;
7 theta=pi/2;
8 t=0.126;
9 Diam=15;
10 C=40;          sd_C=5; % Capacity Kic
11 % number of dice throwing
12 m=5; %try m=3,4,5; 6 is too slow.
13 n=10^m;
14 % number of failures
15 nf=0;
16 %% Create arrays with random normal distributions
17 fprintf('Generating arrays with normal distributions\n');
18 YP=normrnd(P,sd_P,1,n);
19 Ya=XX
20 Yb=XX
21 YC=XX
22 %% loop
23 waitbar(0,'Be patient ');
24 fprintf('Generating Demand data\n');
25 for i=1:n
26     h=waitbar(i/n);
27     % Hoop stress
28     Sigma=YP(i)*Diam/(2*t);
29     %some constants
30     bda=Yb(i)/Ya(i);
31     bdt=Yb(i)/t;
32     % compute
33     M1=1.13-0.09*bda;
34     M2=0.89*(0.2+bda)^-1-0.54;
35     M3=0.5-(0.65+bda)^-1+14*(1-bda)^24;
36     g1=(M1+M2*(bdt)^2+M3*bdt^4);
37     g2=(1+1.464*(bda^1.65))^-0.5;
38     g3=(bda^2*cos(theta)^2+sin(theta)^2)^0.25;
39     g4=1+(0.1+0.35*bdt^2)*(1-sin(theta))^2;
40     % Demand
41     YD(i)=Sigma*xx
42     lnD(i)=XX
43     lnC(i)=XX
44     CoD(i)=XX
45     if XXX
46         nf=nf+1;
47     end
48 end
49 delete(h);
50 %% Compute mean and standard deviation of demand
51 D=mean(YD);
52 sd_D=std(YD);
53 % Generate data for plotting
54 x1=min(YD); x2=max(YC); xr=(x2-x1)/100;
55 x=x1: xr: x2;
56 % Define arrays with normal distributions of capacity and demands
57 Cap=normpdf(x,C,sd_C);
58 Dem=xxx
59 %% Compute Beta
60 beta1=mean(CoD)/std(CoD);
61 beta2=(mean(lnC)-mean(lnD))/sqrt(std(lnC)^2+std(lnD)^2);
62 pf1=nf/n;
63 pf2=(1/2*(1+erf(-beta1/(sqrt(2)))));
64 fprintf('beta: %f; probability of failure: %e; %e\n',beta1,pf1,pf2);

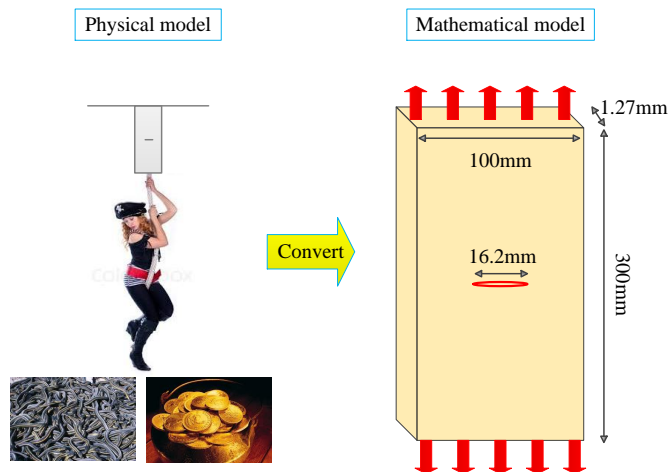
```

```

65 %% Graphics
66 % Graphics initialization
67 fs=12;
68 scrsz=get(0,'ScreenSize');
69 figpos=[2 2 scrsz(3)/2 scrsz(4)/2];
70 h = figure('Position',figpos); set(gca,'FontSize',fs);
71 % Plot 1; Based on analytical data
72 plot(x, Cap, x, Dem, 'LineWidth', 2)
73 grid
74 title('PDF of Cap and Dem (Analytical)')
75 xlabel('XXX')
76 ylabel('XXX')
77 legend('Capacity', 'Demand')
78 grid minor;
79 set(h,'PaperPositionMode','auto');
80 print(gcf, '-depsc2', 'Ca-Dem-Anal.eps')
81 %-----
82 h = figure('Position',figpos); set(gca,'FontSize',fs);
83 % Plot 2 based on raw data
84 plot(x, hist(YC,x)/n, x, hist(YD,x)/n, 'LineWidth', 2);
85 strg=['PDF of Cap and Dem (Raw data, n = ' num2str(n) ' )'];
86 title(strg);
87 xlabel('K-I and K-I.c (ksi-sqrt(in))')
88 ylabel('PDF')
89 legend('Capacity', 'Demand')
90 grid minor; set(gcf,'PaperPositionMode','auto');
91 print -depsc2 Cap-Dem-2.eps

```

4. Determine the residual strength diagram (crack size versus residual strength) in terms of a for longitudinal surface flaws for both embedded and surface cracks with $\frac{b}{a} = 1$ and $\frac{b}{a} = 0.3$ in a pressurized cylinder 10 inch diameter with a wall thickness of 0.5 inch; assume $K_{Ic} = 35 \text{ ksi}\sqrt{\text{in}}$, $\sigma_y = 70 \text{ ksi}$. Use Newman's equation
5. You are offered an opportunity to earn \$10 million by simply hanging from a rope for only one minute. The rope is attached to a glass sheet (300 cm long by 10 cm wide and 0.127 cm thick). Complicating the situation is the fact that the glass sheet contains a central crack with total length of 1.62 cm that is oriented parallel to the ground. The fracture toughness of the glass is $0.93 \text{ MPa}\sqrt{\text{m}}$.



The rope is suspended 3 m above a pit of poisonous snakes. Would you try for the pot of gold?

6. (Open-Ended) Using Newman's solution and Mathematica/Matlab, write a function which will give the stress intensity factor for an elliptical hole in terms of $\frac{b}{a}$, $\frac{b}{t}$, and the angle θ . Use this function to develop some relevant plots.

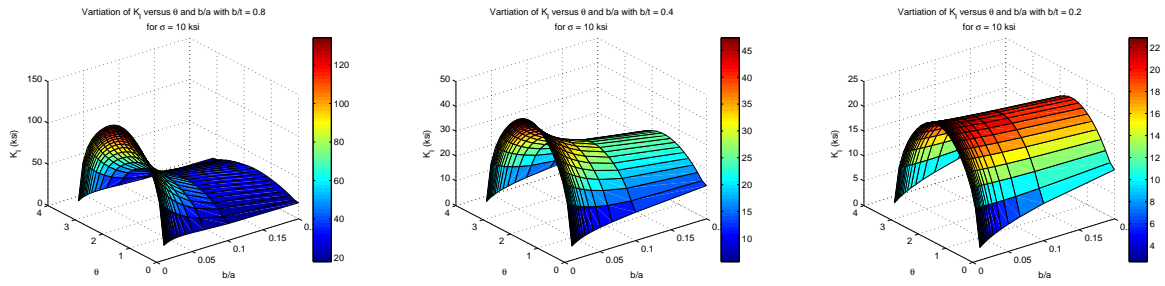


Figure 1: Plot of K_I versus θ and $\frac{b}{a}$

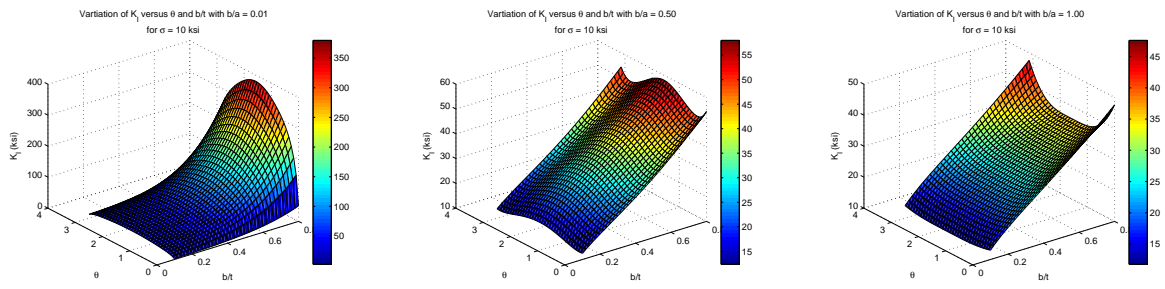


Figure 2: Plot of K_I versus θ and $\frac{b}{t}$

2 Solution

2.1 Problem 1

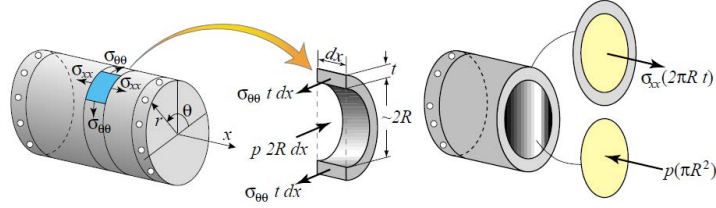


Figure 3: Schematic of longitudinal and tangential stresses calculation in cylindrical vessel [Felippa, C. 2013]

1. The diameter to thickness ratio is $3/0.03 = 100 > 20$,
2. We neglect flexural stresses, and use thin vessel analysis

$$\text{Longitudinal stress } \sigma_{zz} = \frac{pr}{2t} = \frac{1.5p}{2(0.03)} = 25p \quad (2)$$

$$\text{Tangential stress } \sigma_{\theta\theta} = \frac{pr}{t} = \frac{1.5p}{0.03} = 50p \quad (3)$$

$$\text{Radial stress } \sigma_{rr} = -\frac{p}{2} \quad (4)$$

3. Yield condition

$$2\sigma_y^2 = (\sigma_{\theta\theta} - \sigma_{rr})^2 + (\sigma_{rr} - \sigma_{zz})^2 + (\sigma_{zz} - \sigma_{\theta\theta})^2 \quad (5)$$

$$= p_y^2 [(50 - 0.5)^2 + (-0.5 - 25)^2 + (25 - 50)^2] \quad (6)$$

$$\sigma_y = 43.16p_y \quad (7)$$

Note if we neglected σ_r we obtain $\sigma_y = 43.3p_y$

4. Stress intensity factor

$$K_I = 1.128\sigma_\theta\sqrt{\pi a} = (1.128)(50p)(\pi a)^{1/2} = 99.97p_f\sqrt{a} \quad (8)$$

5. We now consider each of the three types of steel alloy

$$\text{HY140 } K_I = 99.97p_f\sqrt{a} = 280\text{MNm}^{-3/2} \quad (9)$$

$$\Rightarrow p_f = 2.8a^{-1/2} \text{ MPa} \quad (10)$$

$$p_y = \frac{\sigma_y}{43.3} = \frac{965}{43.3} = 22.29 \text{ MPa} \quad (11)$$

$$\text{HY180 } K_I = 99.97p_f\sqrt{a} = 180\text{MNm}^{-3/2} \quad (12)$$

$$\Rightarrow p_f = 1.8a^{-1/2} \text{ MPa} \quad (13)$$

$$p_y = \frac{\sigma_y}{43.3} = \frac{1240}{43.3} = 28.64 \text{ MPa} \quad (14)$$

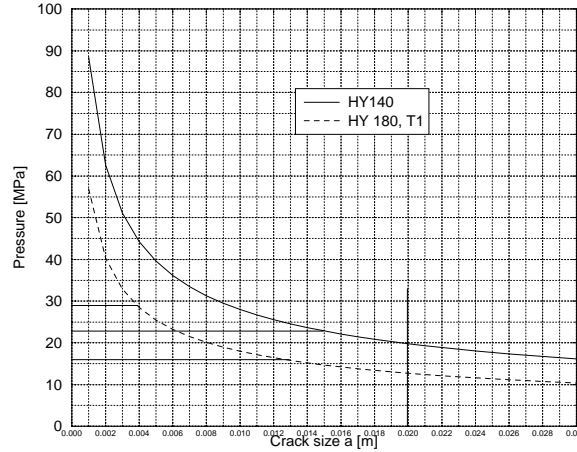
$$\text{T1 } K_I = 99.97p_f\sqrt{a} = 180\text{MNm}^{-3/2} \quad (15)$$

$$\Rightarrow p_f = 1.8a^{-1/2} \text{ MPa} \quad (16)$$

$$p_y = \frac{\sigma_y}{43.3} = \frac{690}{43.3} = 15.94 \text{ MPa} \quad (17)$$

$$(18)$$

6. Plotting the results



For $a = 20 \text{ mm}$, all are susceptible to brittle failure, HY140 is best

For leak before failure ($a=0.03 \text{ m}$) HY140 will provide $P_L=16.2 \text{ MPa}$, and HY180/T1 $P_L=10.4 \text{ MPa}$

7. Additional results¹: If we construct a plot of pressure (based on σ_y and K_{Ic}) against crack depth a for each steel, we could be able to find a safe region against fracture and yielding.

According to the Figures 4 and 5 the first type of steel (HY 140) gives the greatest margin of safety for $a_1 \geq 20\text{mm}$, because the area of intersection of $a_1 = 20\text{mm}$ line and the fracture curve is bigger for steel type one (HY 140). In both three cases for $a_1 \geq 20\text{mm}$ the collapse is dominated by fracture rather than yielding.

For $a_1 \geq 2\text{mm}$ in all curves both yielding and fracture should be considered. In steels type HY 140 and T 1 for $2 \leq a_1 < 15\text{mm}$ the collapse dominated by yielding rather than

¹Courtesy Hehrou/Hariri

fracture, however, for steel types HY 180 the collapse dominated by fracture rather than yielding. Generally steel type HY 140 offers the greatest margin of safety for $a_1 \geq 20mm$ because the area under the curves is bigger than others, Figure 6.

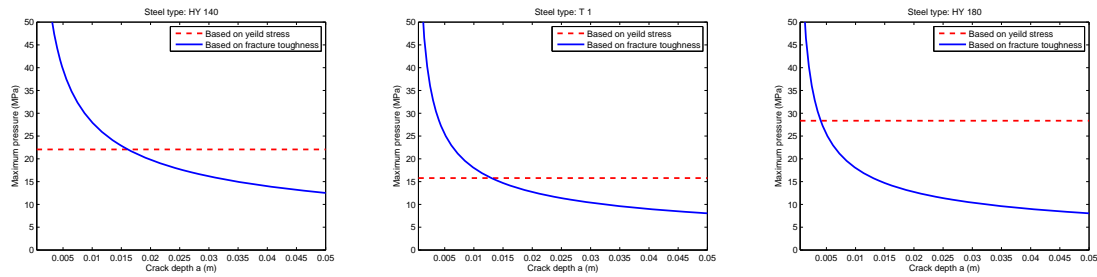


Figure 4: Maximum pressures versus crack depth a for different steel type

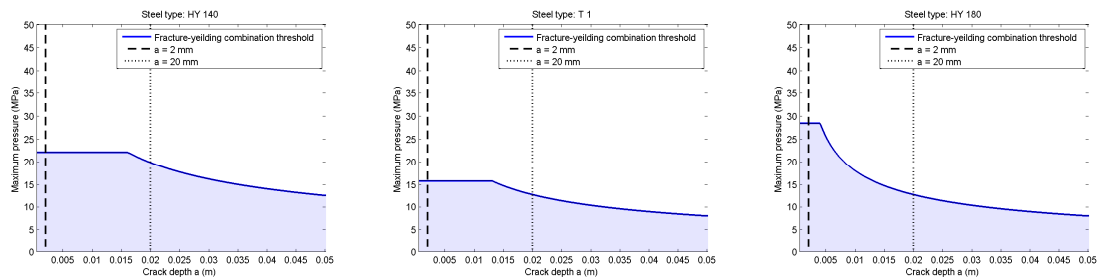


Figure 5: Maximum pressure versus crack depth a for the combination of fracture toughness and yield stress

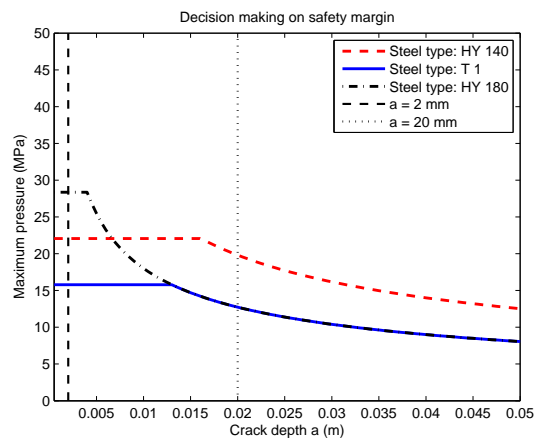


Figure 6: Summary of three threshold curves for three steel types

2.2 Problem 2

1. stresses

$$\text{Longitudinal stress } \sigma_{zz} = \frac{pr}{2t} = \frac{5 \times 15}{2(t)} = \frac{37.5}{t} \quad (19)$$

$$\text{Tangential stress } \sigma_{\theta\theta} = \frac{pr}{t} = \frac{5 \times 15}{t} = \frac{75}{t} \quad (20)$$

$$\text{Radial stress } \sigma_{rr} = -\frac{p}{2} = \frac{5}{2} = 2.5 \simeq 0. \quad (21)$$

2. Thickness must satisfy three requirements:

- (a) Plasticity (based on yield stress)
- (b) Fracture mechanics (fracture toughness)
- (c) $t > 0.5\text{in}$

3. Yield condition

$$2 \left(\frac{\sigma_y}{2} \right)^2 = (\sigma_{\theta\theta} - \sigma_{rr})^2 + (\sigma_{rr} - \sigma_{zz})^2 + (\sigma_{zz} - \sigma_{\theta\theta})^2 \quad (22)$$

$$= \frac{1}{t^2} [(75)^2 + (-37.5)^2 + (37.5 - 75)^2] = \frac{8,437.5}{t^2} \quad (23)$$

$$t = \frac{130}{\sigma_y} \quad (24)$$

4. Fracture mechanics

$$K_I = \frac{K_{Ic}}{2} = \sigma \sqrt{\pi b} \left[M_1 + M_2 \left(\frac{b}{t} \right)^2 + M_3 \left(\frac{b}{t} \right)^4 \right] \left[1 + 1.464 \left(\frac{b}{a} \right)^{1.65} \right]^{-\frac{1}{2}} \\ \left[\left(\frac{b}{a} \right)^2 \cos^2 \theta + \sin^2 \theta \right]^{\frac{1}{4}} \left\{ 1 + \left[0.1 + 0.35 \left(\frac{b}{t} \right)^2 \right] (1 - \sin^2 \theta)^2 \right\} \quad (25)$$

where

$$M_1 = 1.13 - 0.09 \left(\frac{b}{a} \right) \quad (26)$$

$$M_2 = 0.89 \left[0.2 + \left(\frac{b}{a} \right) \right]^{-1} - 0.54 \quad (27)$$

$$M_3 = 0.5 - \left[0.65 + \left(\frac{b}{a} \right) \right]^{-1} + 14 \left[1.0 - \left(\frac{b}{a} \right) \right]^{24} \quad (28)$$

5. Substituting we get

So, Steel type F is the most economical material.

Table 1: Design parameters for different steel type.

Steel	σ_{ys} Ksi	K_{Ic} Ksi \sqrt{in}	Cost \$/lb	t_{plas} in	t_{fm} in	t_{final} in.	Weight lb	Cost \$
A	260.00	80.00	1.40	0.50	2.18	2.18	697.19	976.07
B	220.00	110.00	1.40	0.59	1.62	1.62	519.91	727.87
C	180.00	140.00	1.00	0.72	1.31	1.31	420.00	420.00
D	180.00	220.00	1.20	0.72	0.90	0.90	288.08	345.70
E	140.00	260.00	0.50	0.93	0.79	0.93	296.98	148.49
F	110.00	170.00	0.15	1.18	1.11	1.18	377.98	56.70

```

1 clc;clear;close all;
2 fid=fopen('problem-2.out','w+');
3 b = 0.5; a = 1.0; th = pi/2; p = 5; D = 30;r=D/2;
4 sy = [260 220 180 180 140 110]';
5 KIc = [80 110 140 220 260 170]';
6 cost=[1.4 1.4 1.0 1.2 0.5 0.15];
7 density=0.283; % lbs/in^3
8 % initialize
9 t_sy = zeros(size(sy,1),1);
10 t_KI = zeros(size(sy,1),1);
11 ns = size(sy,1);
12 tsigzz=p*r/2;
13 tsighoop=p*r;
14 temp=tsigzz^2+tsighoop^2+(tsighoop-tsigzz)^2;
15 tsigy=sqrt(temp*2);
16 fprintf(fid,'t_plas t_fm t_final Weight Cost \n');
17
18 for i = 1:ns
19     t_plas = tsigy/sy(i);
20     kIc = KIc(i,1) / 2;
21     t0=5;
22     [t,fval]=fsolve(@(t)Kellep(t,tsighoop,a,b,th,kIc),t0);
23     t_fm=t;
24     t_final=max(t_fm,t_plas);
25     t_final=max(t_final,0.5);
26     weight=pi*D*t_final*12*density;
27     Cost_i=cost(i)*weight;
28     fprintf(fid,'%5.2f %5.2f %5.2f %5.2f %5.2f %5.2f %5.2f %5.2f \n',sy(i),KIc(i),cost(i),t_plas,t_fm,t_final,wei
29 end
30 fclose(fid);

```

```

1 function F=Kellep(t,tsighoop,a,b,th,kIc)
2 M1 = 1.13 - 0.09*(b/a);
3 M2 = 0.89 * (0.2 + b/a)^(-1) - 0.54;
4 M3 = 0.5 - (0.65 + b/a)^(-1) + 14*(1.0 - b/a)^(24);
5 % constant part of KI
6 C1 = sqrt(pi*b);
7 C2 = M1 + M2*(b/t)^(2) + M3*(b/t)^(4);
8 C3 = (1 + 1.464*(b/a)^1.65)^(-1/2);
9 C4 = (((b/a)^2) * (cos(th))^2 + (sin(th))^2);
10 C5 = 1 + (0.1 + 0.35*(b/t)^2) * (1 - sin(th))^2;
11 sigma=tsighoop/t;
12 Kin=sigma*(C1 * C2 * C3 * C4 * C5);
13 F=Kin-kIc;
14 end

```

2.3 Problem 3

1. Assuming normal distributions, generate arrays of random normal distributions for P , a , b and C (size n).
2. Loop from 1 to n
 - (a) Select P_i , a_i , b_i and C_i .
 - (b) Hoop stress $\sigma = \frac{P_i D}{2t}$
 - (c) Parameters M_i and g_i .
 - (d) Demand $D_i = K$.

(e) If $D_i > C_i$ failure occurs at i , increment $n_f = n_f + 1$.

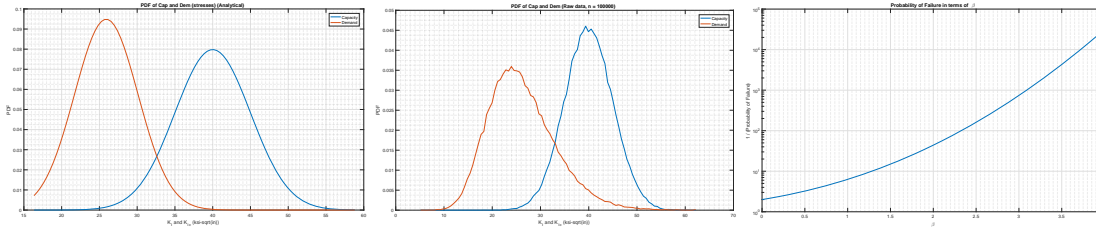
(f) Compute $CoD_i = C_i/D_i$

3. Determine mean and standard deviation of demand.

$$4. \beta = \frac{\mu(CoD)}{\sigma(CoD)}$$

5. Prob of failure = n_f/n .

$\beta = 3.3$ and probability of failure is 0.06.



```

1 clear; clc; close all;
2 %% Initialization
3 %mean and standard deviation value (units kips and inches)
4 P=0.6;      sd_P=0.02;
5 a=3.5/2 ;   sd_a=0.2;
6 b=0.05 ;    sd_b=0.01;
7 theta=pi/2;
8 t=0.126;
9 Diam=15;
10 C=40;      sd_C=5; % Capacity Kic
11 % number of dice throwing
12 m=5; %try m=3,4,5; 6 is too slow.
13 n=10^m;
14 % number of failures
15 nf=0;
16 %% Create arrays with random normal distributions
17 fprintf('Generating arrays with normal distributions\n');
18 YP=normrnd(P,sd_P,1,n);
19 Ya=normrnd(a,sd_a,1,n);
20 Yb=normrnd(b,sd_b,1,n);
21 YC=normrnd(C,sd_C,1,n);
22 %% loop
23 waitbar(0,'Be patient');
24 fprintf('Generating Demand data\n');
25 for i=1:n
26     h=waitbar(i/n);
27     % Hoop stress
28     Sigma=YP(i)*Diam/(2*t);
29     %some constants
30     bda=Yb(i)/Ya(i);
31     bdt=Yb(i)/t;
32     % compute
33     M1=1.13-0.09*bda;
34     M2=0.89*(0.2+bda)^-1-0.54;
35     M3=0.5-(0.65+bda)^-1+14*(1-bda)^24;
36     g1=(M1+M2*(bdt)^2+M3*bdt^4);
37     g2=(1+1.464*(bda^1.65))^-0.5;
38     g3=(bda^2*cos(theta)^2+sin(theta)^2)^0.25;
39     g4=1+(0.1+0.35*bdt^2)*(1-sin(theta))^2;
40     % Demand
41     YD(i)=Sigma*(sqrt(pi*Yb(i))*g1*g2*g3*g4);
42     lnD(i)=log(YD(i));
43     lnC(i)=log(YC(i));
44     CoD(i)=YC(i)/YD(i);
45     if CoD(i)<1
46         nf=nf+1;
47     end
48 end
49 delete(h);
50 %% Compute mean and standard deviation of demand
51 D=mean(YD);
52 sd_D=std(YD);
53 % Generate data for plotting
54 x1=min(YD); x2=max(YC); xr=(x2-x1)/100;
55 x=x1: xr : x2;
56 % Define arrays with normal distributions of capacity and demands
57 Cap=normpdf(x,C,sd_C);
58 Dem=normpdf(x,D,sd_D);
59 %% Compute Beta

```

```

60| beta1=mean(CoD)/std(CoD);
61| beta2=(mean(lnC)-mean(lnD))/sqrt(std(lnC)^2+std(lnD)^2);
62| pf1=nf/n;
63| pf2=(1/2*(1+erf(-beta1/(sqrt(2)))));
64| fprintf('beta: %f; probability of failure: %e; %e\n',beta1,pf1,pf2);
65| %% Graphics
66| %% Graphics initialization
67| fs=12;
68| scrsz=get(0,'ScreenSize');
69| figpos=[2 2 scrsz(3)/2 scrsz(4)/2];
70| h = figure('Position',figpos); set(gca,'FontSize',fs);
71| % Plot 1; Based on analytical data
72| plot(x,Cap,x,DEM,'LineWidth',2)
73| grid
74| title('PDF of Cap and Dem (Analytical)')
75| xlabel('K.I and K.I-c (ksi-sqrt(in))')
76| ylabel('PDF')
77| legend('Capacity','Demand')
78| grid minor;
79| set(h,'PaperPositionMode','auto');
80| print(gcf,'-depsc2','Ca-Dem-Anal.eps')
81| %====
82| h = figure('Position',figpos); set(gca,'FontSize',fs);
83| % Plot 2 based on raw data
84| plot(x,hist(YC,x)/n,x,hist(YD,x)/n,'LineWidth',2);
85| strg=['PDF of Cap and Dem (Raw data, n = ' num2str(n) ' )'];
86| title(strg);
87| xlabel('K.I and K.I-c (ksi-sqrt(in))')
88| ylabel('PDF')
89| legend('Capacity','Demand')
90| grid minor; set(gcf,'PaperPositionMode','auto');
91| print -depsc2 Cap-Dem-2.eps
92| %% Bonus
93| % Semi-log Plot of probability of failure given by Beta Vary Beta from 0
94| % to 4
95| beta = 0.0:0.1:4;
96| % Equation for Standard Normal Cumulative Probability
97| PhiOfX = (1 / 2 * (1 + erf(-beta / (sqrt(2)))));
98| % Define Prob. of Failure as 1 / Ix
99| pf = 1 ./ PhiOfX;
100| % Plot of beta vs. Prob. on with a y-axis in log scale
101| fs=20;
102| h = figure('Position',figpos); set(gca,'FontSize',fs);
103| semilogy(beta,pf,'LineWidth',2)
104| grid
105| title('Probability of Failure in terms of \beta')
106| xlabel('\beta')
107| ylabel('1 / (Probability of Failure)')
108| grid minor; set(gcf,'PaperPositionMode','auto');
109| print -depsc2 PlotBeta.eps

```

3 Problem 4

1. Assuming elliptical cracks, one can use the Newman's equation to compute the critical stress in terms of a .
2. Plots must be capped to the yield stress.
3. Below are the residual stresses for two set of values for $\frac{b}{a}$ and for θ equal to zero and $\frac{\pi}{2}$

```

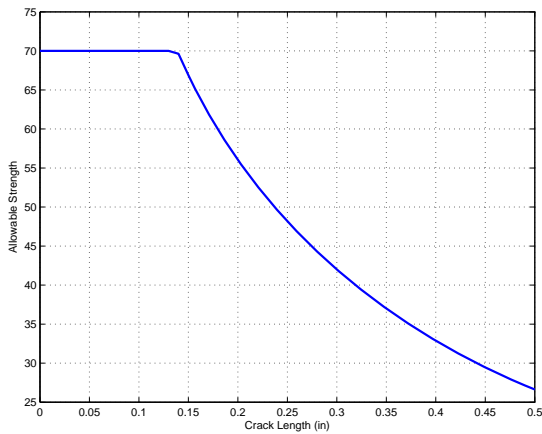
1| clear all; clc; close all;
2| for theta=0:pi/2:pi/2
3|     i=0; %theta=pi/2;
4|     for a =0:0.01:1
5|         i=i+1;
6|         b=a;
7|         if b>0.5
8|             break
9|         end
10|         bda=1;
11|         bdt=b/0.5;
12|         M1=1.13-0.09*bda;
13|         M2=0.89*(0.2+bda)^-1-0.54;
14|         M3=0.5-(0.65+bda)^-1+14*(1-bda)^24;
15|         g1=(M1+M2*(bdt)^2+M3*bdt^4);
16|         g2=(1+1.464*bda^1.65)^-0.5;
17|         g3=(bda^2*cos(theta)^2+sin(theta)^2)^0.25;
18|         g4=1+(0.1+0.35*bdt^2)*(1-sin(theta))^2;
19|         Sc(i)=35/(sqrt(pi*b)*g1*g2*g3*g4);
20|         if Sc(i)>70
21|             Sc(i)=70;

```

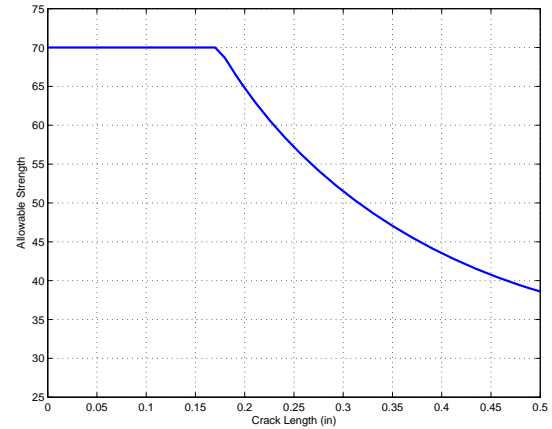
```

22|         end
23|         A(i)=a;
24|     end
25|     h=figure;
26|     plot(A,Sc,'LineWidth',2)
27|     axis([0 0.5 25 75])
28|     xlabel('Crack Length (in)')
29|     ylabel('Allowable Strength')
30|     grid
31|     fn=['theta=' num2str(theta) 'boa=' num2str(b/a) '.eps'];
32|     print(h,'-dpsc2',fn)
33|     A=0;
34|     Sc=0;
35|     i=0;
36|     for a =0:0.01:2
37|         i=i+1;
38|         b=0.3*a;
39|         if b>0.5
40|             break
41|         end
42|         bda=0.3;
43|         bdt=b/0.5;
44|         M1=1.13-0.09*bda;
45|         M2=0.89*(0.2+bda)^-1-0.54;
46|         M3=0.5-(0.65+bda)^-1+14*(1-bda)^24;
47|         g1=(M1+M2*(bdt)^2+M3*bdt^4);
48|         g2=(1+1.464*bda^1.65)^-0.5;
49|         g3=(bda^2*cos(theta)^2+sin(theta)^2)^0.25;
50|         g4=1+(0.1+0.35*bdt^2)*(1-sin(theta))^2;
51|         Sc(i)=35/(sqrt(pi*b)*g1*g2*g3*g4);
52|         if Sc(i)>70
53|             Sc(i)=70;
54|         end
55|         A(i)=a;
56|     end
57|     h=figure;
58|     plot(A,Sc,'LineWidth',2)
59|     axis([0 A(end) 10 75])
60|     xlabel('Crack Length (in)')
61|     ylabel('Allowable Strength')
62|     grid
63|     fn=['theta=' num2str(theta) 'boa=' num2str(b/a) '.eps'];
64|     print(h,'-dpsc2',fn)
65| end

```



(a) $\theta = 0$



(b) $\theta = \frac{\pi}{2}$

Figure 7: Residual Strength Diagram for $b/a = 1$

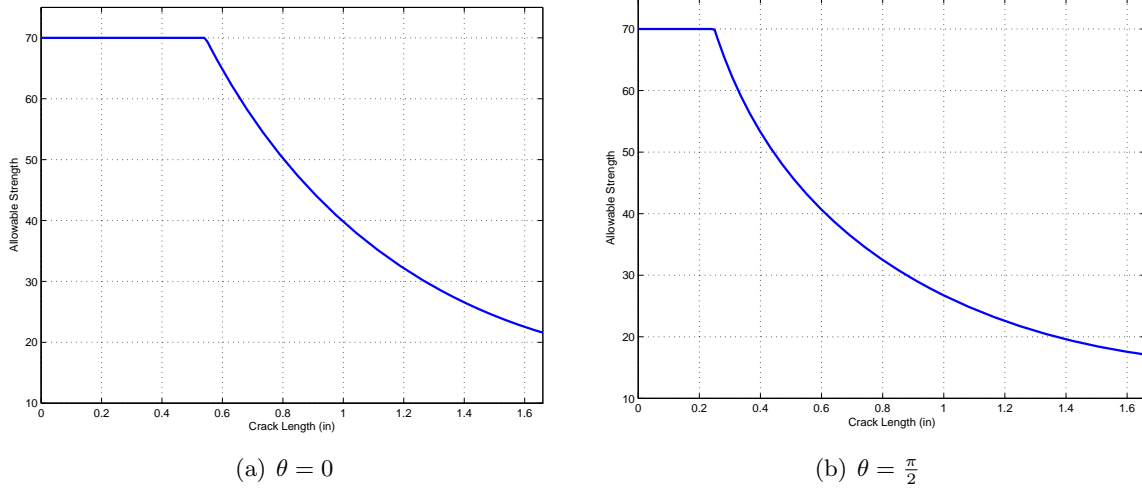


Figure 8: *Residual Strength Diagram with $b/a = 0.3$*

4 Problem 5

Courtesy Benet, Behru, Hariri

1. Assume that the mass of the person is uniformly distributed along the surface of the glass.
2. For $L/W = 30$ we determine the stress intensity factor from

$$K_I = \left[1 + 0.256 \left(\frac{a}{W} \right) - 1.152 \left(\frac{a}{W} \right)^2 + 12.2 \left(\frac{a}{W} \right)^3 \right] \sigma \sqrt{\pi a} \quad (29)$$

3. For a mass of 80 kg, the applied stress is

$$Mass = 80\text{kg} \Rightarrow \text{Weight} = 80 \cdot 9.81 = 784.8 \text{ N} \Rightarrow \sigma = \frac{784.8}{0.00127 \cdot 0.10 \cdot 1e6} = 6.1795 \text{ Mpa} \quad (30)$$

4. Substituting with $a = 0.81 \text{ cm}$, and $W = 10 \text{ cm}$

$$K_I = 1.0051 \text{ Mpa}\sqrt{\text{m}} > 0.93 \text{ Mpa}\sqrt{\text{m}} \quad (31)$$

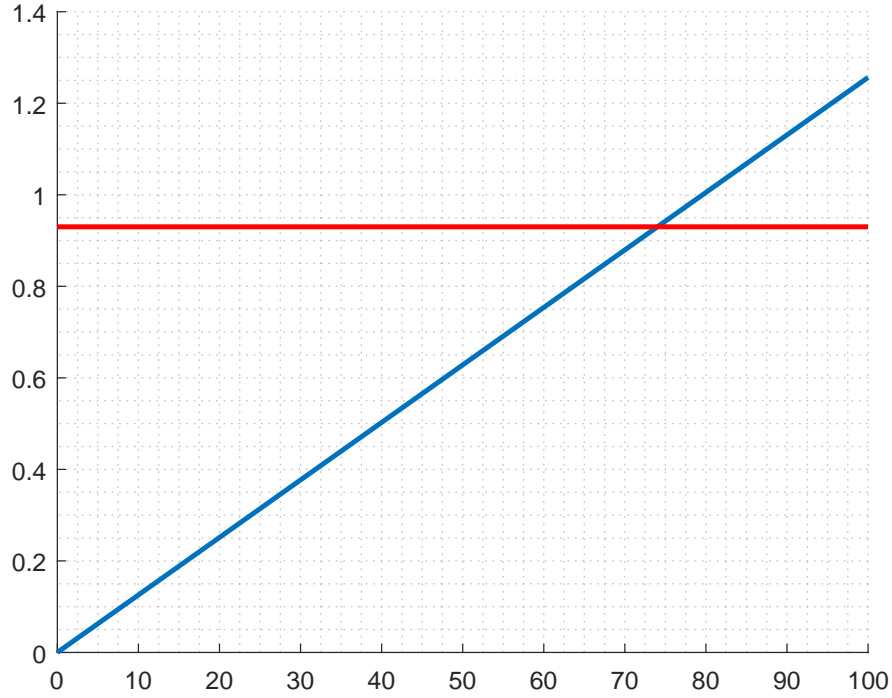
hence, no hanging.

5. The limit weight can be easily determined:

$$\sigma_c = \frac{K_{Ic}}{\left[1 + 0.256 \left(\frac{a}{W} \right) - 1.152 \left(\frac{a}{W} \right)^2 + 12.2 \left(\frac{a}{W} \right)^3 \right] \sqrt{\pi a}} \quad (32)$$

and for $K_{Ic} = 0.93$

$$\sigma_c = 5.7175 \text{ Mpa} \Rightarrow \text{Max Weight} = 74.0\text{kg} \quad (33)$$



5 Problem 6

Courtesy Behrou, Hariri

In this question we tried to demonstrate the effects of $\frac{b}{a}$, $\frac{b}{t}$, and θ on stress intensity factor. The results are presented in Figures 9 and 10 for different configuration.

$$K_{Ic} = \sigma_c \sqrt{\pi b} \left[M_1 + M_2 \left(\frac{b}{t} \right)^2 + M_3 \left(\frac{b}{t} \right)^4 \right] \left[1 + 1.464 \left(\frac{b}{a} \right)^{1.65} \right]^{-\frac{1}{2}} \left[\left(\frac{b}{a} \right)^2 \cos^2 \theta + \sin^2 \theta \right]^{\frac{1}{4}} \left\{ 1 + \left[0.1 + 0.35 \left(\frac{b}{t} \right)^2 \right] (1 - \sin \theta)^2 \right\} \quad (34)$$

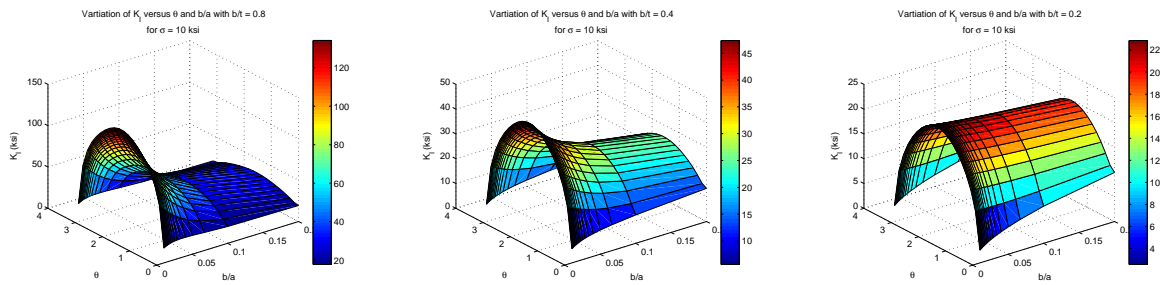


Figure 9: Plot of K_I versus θ and $\frac{b}{a}$

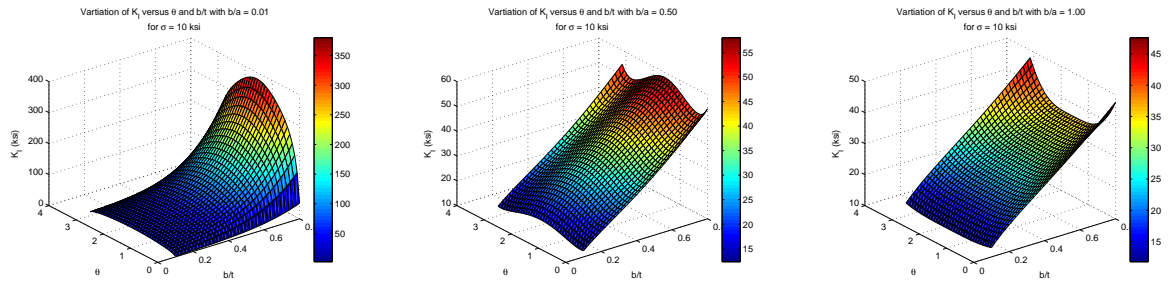


Figure 10: Plot of K_I versus θ and $\frac{b}{t}$

**CVEN 7161
FRACTURE MECHANICS**

SPRING 2020

HOME-WORK 4

LEFM; Energy

Due: March 12, 2020

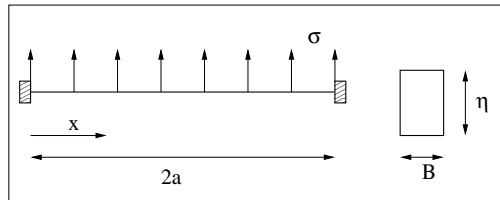
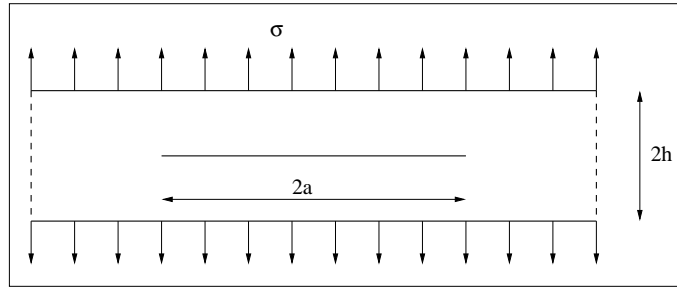
1. The following data were obtained from a series of tests conducted on precracked specimens with 1 mm thickness

Crack Length a (mm)	Critical Load P_{cr} (kN)	Critical Displacement u_{cr} (mm)
30.0	4.00	0.40
40.00	3.50	0.50
50.5	3.12	0.63
61.6	2.80	0.78
71.7	2.62	0.94
79.0	2.56	1.09

The load displacement curve for all cracks is linearly elastic up to the critical point.

Determine G_c from: 1) the load displacement records (based on the mean of the measurements in between two consecutive values), and b) from the compliance curve. Discuss your results.

2. Assume that the R curve of a certain material can be represented by $R = \frac{K_{Ic}^2}{E} + 0.4(\Delta a)^{0.25}$ (kip/in), and that $K_{Ic} = 30\text{Ksi}\sqrt{\text{in}}$, $E = 30,000$. Ksi, and $\sigma_{yld} = 100$ Ksi. For a center cracked panel of a thickness for which the above R curve is applicable and of width $W = 50$ in with a crack $2a = 2$ in, calculate a_c , σ_c , and Δa . the amount of stable growth, the final crack size and the fracture stress. Show graphically your results. Assume plane stress condition $E' = E$, and we can consider that for all practical purposes we have an infinite plate ($W \gg 2a$).
3. Using the data from the previous problem, repeat the calculation for a finite size panel with $W = 6$ in and $2a = 2$ in and $R = \frac{K_{Ic}^2}{E} + 0.4(\Delta a)^{0.25}$ (kip/in). Assume plane stress conditions.
4. Consider a long strip of height $2h$ and thickness B with a crack length $2a$ subjected to a uniform stress σ along its upper and lower faces. For $a \gg h$, determine the stress intensity factor.



Note that:

$$M = -\frac{qB}{6}(2a^2 - 6ax + 3x^2) \quad \text{for } 0 \leq x \leq a \quad (1)$$

$$U = 2 \int_0^a \frac{M^2}{2EI} dx \quad (2)$$

SOLUTION

Problem 1

```

B=1;
a=[30., 40., 50.5, 61.6, 71.7, 79.]; % mm
p=[4., 3.5, 3.12, 2.8, 2.62, 2.56]; % kN
u=[0.4, 0.5, 0.63, 0.78, 0.94, 1.09]; % mm
%
a=a/1000; % m
u=u/1000; % m
p=p*1000; % N
% From Load displacement curve
for i=1:5
    j=i+1;
    g_ld(i)=(p(i)*u(j)-p(j)*u(i))/(2*B*(a(j)-a(i))); %J/m^2
end
g_ld_mean=mean(g_ld)
% From the compliance
c=u./p;
for i=1:5
    j=i+1;
    dcda_rgt(i)=(c(j)-c(i))/(a(j)-a(i));
end
for i=2:6
    j=i-1;
    dcda_lft(i)=(c(i)-c(j))/(a(i)-a(j));
end
dcda(1)=dcda_rgt(1);
dcda(6)=dcda_lft(6);
for i=2:5
    dcda(i)=0.5*(dcda_lft(i)+dcda_rgt(i));
end
g_cmp=p.^2.*dcda./(2*B);
g_cmp_mean=mean(g_cmp)
%
fid = fopen('hw5-sol.out','wt');
fprintf(fid,'\n-----+-----+-----+-----+');
fprintf(fid,'\n a | G_ld || C | dC/da | G_cmp |');
fprintf(fid,'\n m | J/m^2 || 1/N | 1/Nm | J/m^2 |');
fprintf(fid,'\n-----+-----+-----+-----+');
for i=1:6
    fprintf(fid,'\n %4.3f | %4.2f || %3.2e | %3.2e | %4.2f |',a(i),g_ld(i),c(i),dcda(i),g_cmp(i));
end
fprintf(fid,'\n-----+-----+-----+-----+');
fprintf(fid,'\n mean | %4.2f %4.2f',g_ld_mean,g_cmp_mean);
fprintf(fid,'\n-----+-----+-----+-----+');
st=fclose('all');

```

```

-----+-----+-----+-----+
a | G_ld || C | dC/da | G_cmp |
m | J/m^2 || 1/N | 1/Nm | J/m^2 |
-----+-----+-----+-----+
0.030 | 30.00 || 1.00e-07 | 4.29e-06 | 34.29 |
0.040 | 30.71 || 1.43e-07 | 4.96e-06 | 30.35 |
0.051 | 30.16 || 2.02e-07 | 6.27e-06 | 30.49 |

```

0.062		29.13		2.79e-07		7.42e-06		29.10	
0.072		30.78		3.59e-07		8.56e-06		29.38	
0.079				4.26e-07		9.18e-06		30.08	
-----+-----+-----+-----+-----+									
mean		30.10						30.61	
-----+-----+-----+-----+-----+									

Problem 2

$R = \frac{K_{Ic}^2}{E} + 0.4(\Delta a)^{0.25}$, $K_{Ic} = 30\text{ksi}\sqrt{\text{in}}$, $E = 30,000$ ksi, $\sigma_{yld} = 100$ ksi, $W = 50$ in, $\beta = 1$,
 $a = 1$ in

$$G = \frac{K_I^2}{E} = \frac{\sigma^2 \pi a}{E} \quad (3)$$

$$R = \frac{30^2}{30,000} + 0.4(a_c - 1)^{0.25} \quad (4)$$

$$G = R \Rightarrow \frac{\sigma_c^2 \pi a_c}{E} = 0.03 + 0.4(a_c - 1)^{0.25} \quad (5)$$

$$\frac{\partial G}{\partial a} = \frac{\sigma_c^2 \pi}{E} \quad (6)$$

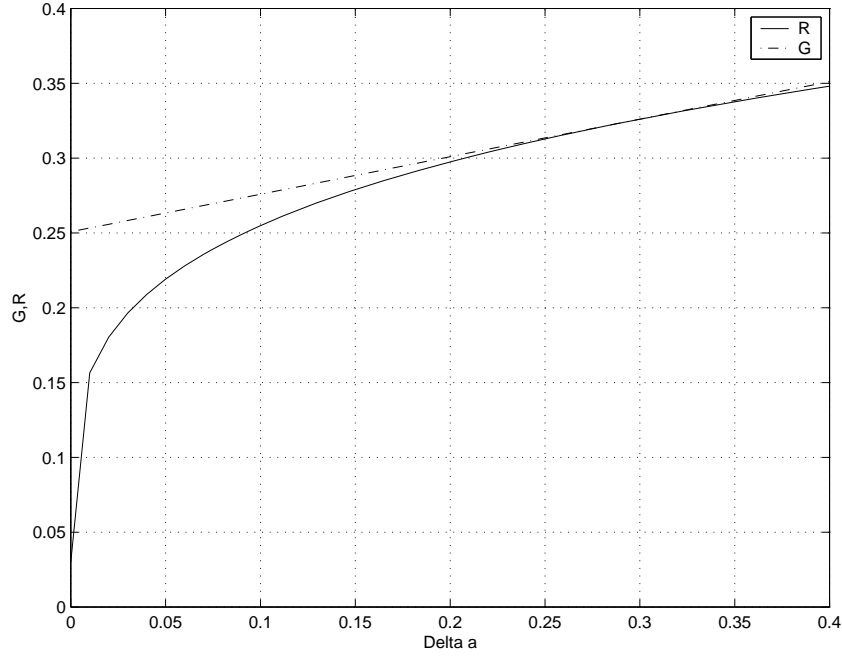
$$\frac{\partial R}{\partial a} = 0.1(a_c - 1)^{-3/4} \quad (7)$$

$$\frac{\partial G}{\partial a} = \frac{\partial R}{\partial a} \Rightarrow \frac{\sigma_c^2 \pi}{E} = 0.1(a_c - 1)^{-3/4} \quad (8)$$

$$\Rightarrow a_c(0.1)(a_c - 1)^{-3/4} - 0.03 - 0.4(a_c - 1)^{0.25} = 0 \quad (9)$$

Solving, we obtain: $a_c = 1.295$ in., $\Delta a = .295$ in., $\sigma_c = 48.9$ ksi.

```
% zoom on the curve to solve for x
x=[1.29:0.00001:1.295];
y=0.1*x.*(x-1).^(-0.75)-0.03-0.4*(x-1).^0.25;
%plot(x,y)
%grid
% x=a_c=1.2935
ac=1.2935;
E=30000;
sigma=sqrt((0.03+0.4*(ac-1)^(0.25))*E/(pi*ac));
sigma2=sqrt(0.1*E*(ac-1)^(-0.75)/pi)
%sigma=46.7
a=1;
delta_a=[0.:0.01:0.4];
a_c=a+delta_a;
g=sigma.^2*pi*a_c'./E;
r=30^2/E+0.4*(a_c-1).^0.25;
plot(delta_a,r,'k-',delta_a,g,'k-.');
grid
legend('R','G')
xlabel('Delta a')
ylabel('G,R')
```



Problem 3

For $W = 6$,

$$K_I = \sigma \sqrt{\pi a} \sqrt{\sec \frac{\pi a}{W}} \quad (10)$$

$$G = \frac{K_I^2}{E} = \frac{\sigma^2 \pi a}{E} \sec \frac{\pi a}{W} \quad (11)$$

$$R = \frac{K_{Ic}^2}{E} + 0.4(\Delta a)^{0.25} \quad (12)$$

$$= \frac{30^2}{30,000} + 0.4(a_c - 1)^{0.25} \quad (13)$$

$$G = R \Rightarrow \frac{\sigma^2 \pi a}{E} \sec \frac{\pi a}{W} = \frac{0.3^2}{30,000} + 0.4(a_c - 1)^{0.25} \quad (14)$$

$$\Rightarrow \sigma_c^2 = \left[0.03 + 0.4(a_c - 1)^{0.25} \right] \frac{E}{\pi a_c} \sec \frac{\pi a_c}{W} \quad (15)$$

$$\frac{\partial G}{\partial a} = \frac{\sigma_c^2 \pi}{E} \sec \frac{\pi a}{W} \left(1 + \frac{\pi a}{W} \tan \frac{\pi a}{W} \right) \quad (16)$$

$$\frac{\partial R}{\partial a} = 0.1(a_c - 1)^{-3/4} \quad (17)$$

$$\frac{\partial G}{\partial a} = \frac{\partial R}{\partial a} \Rightarrow \underbrace{\frac{\sigma_c^2 \pi}{E} \sec \frac{\pi a}{W}}_{G/a} \left(1 + \frac{\pi a}{W} \tan \frac{\pi a}{W} \right) = 0.1(a_c - 1)^{-3/4} \quad (18)$$

or

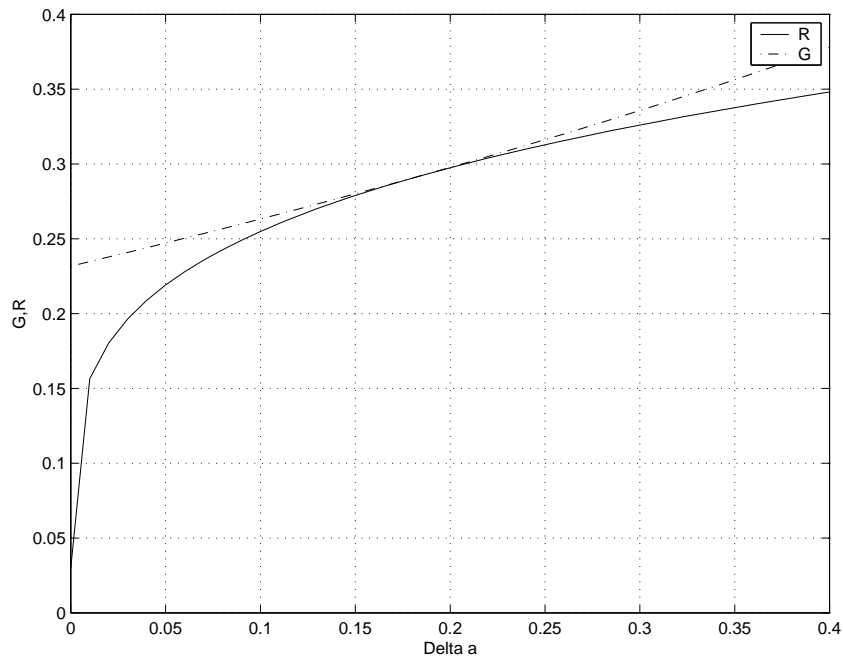
$$\left[0.03 + 0.4(a_c - 1)^{0.25} \right] \left(1 + \frac{\pi a}{W} \tan \frac{\pi a}{W} \right) - 0.1 a_c (a_c - 1)^{-3/4} = 0 \quad (19)$$

Solving, we obtain: $a_c = 1.184$ in., $\Delta a = .184$ in., $\sigma_c = 43.7$ ksi.

```

% zoom on the curve to solve for x
W=6
x=[1.18:0.00001:1.185];
y=(0.03+0.4*(x-1).^0.25).*(1+pi*x/W.*tan(pi*x./W))-0.1*x.*(x-1).^(-0.75);
%plot(x,y)
%grid
% x=a_c=1.184
ac=1.184;
E=30000;
sigma=sqrt((0.03+0.4*(ac-1)^0.25)*E/(pi*ac*sec(pi*ac/W)));
%sigma=43.78
a=1;
delta_a=[0.:0.01:0.4];
a_c=a+delta_a;
g=sigma^2*pi*a_c.*sec(pi*a_c/W)./E;
r=30^2/E+0.4*(a_c-1).^0.25;
plot(delta_a,r,'k-',delta_a,g,'k-');
grid
legend('R','G')
xlabel('Delta a')
ylabel('G,R')

```



Problem 4

courtesy Rezgar Shakeri

Thermodynamic law

$$\dot{W} = \dot{U}^e + \dot{U}^p + \dot{K} + \dot{\Gamma}, \quad (20)$$

For quasi static $K = 0$, and the variation of energy respect to time can be represent as

$$\frac{\partial}{\partial t} = \dot{A} \frac{\partial}{\partial A}, \quad (21)$$

where A is crack face, and rewriting Eq. 20

$$\frac{\partial W}{\partial A} - \frac{\partial U^e}{\partial A} = \frac{\partial U^p}{\partial A} + \frac{\partial \Gamma}{\partial A}, \quad (22)$$

the left hand side of above equation is called G . For fixed displacement external work is zero, so

$$G = -\frac{\partial U^e}{\partial A}, \quad (23)$$

and for constant load, based on Clapeyron's theorem

$$\frac{\partial W}{\partial A} = 2 \frac{\partial U^e}{\partial A}$$

then G is

$$G = \frac{\partial U^e}{\partial A}, \quad (24)$$

In this problem, load is fixed and we have to use Eq. 24.

The strain energy can be decomposed in two parts, far from the crack which is given by

$$U_1^e = \frac{1}{2E} \sigma^2 w B L, \quad (25)$$

where L is length, w is width and B is the thickness. And strain energy near the crack is obtained by using Eq. 24

$$G = \frac{\partial U_1^e}{\partial A} + \frac{\partial U_2^e}{\partial A}, \quad (26)$$

the first term of Eq. 26 is zero, then strain energy near the crack U_2^e with crack face $A = 2aB$ is

$$G = \frac{1}{2B} \frac{\partial U_2^e}{\partial a}, \quad (27)$$

and for plane stress condition and $w \gg a$, G is

$$G = \frac{K_I^2}{E} = \frac{\sigma^2 \pi a}{E}, \quad (28)$$

and from 27

$$\frac{\partial U_2^e}{\partial a} = 2B \frac{\sigma^2 \pi a}{E} \implies U_2^e = \frac{\sigma^2 \pi B a^2}{E}, \quad (29)$$

Thus, total strain energy is

$$U^e = \frac{\sigma^2}{2E} (w B L + 2B \pi a^2), \quad (30)$$

by equating external work and strain energy we have

$$(\sigma w B)v = \frac{\sigma^2}{2E}(wBL + 2B\pi a^2), \quad (31)$$

which gives the displacement v as

$$v = \frac{\sigma}{2E}\left(L + \frac{2\pi a^2}{w}\right), \quad (32)$$

and dv is

$$dv = \frac{dv}{da}da + \frac{dv}{d\sigma}d\sigma = \frac{\sigma}{2E} \frac{4\pi a}{w} da + \frac{1}{2E}\left(L + \frac{2\pi a^2}{w}\right)d\sigma, \quad (33)$$

solving for $dv = 0$

$$\frac{\sigma}{2E} \frac{4\pi a}{w} da = -\frac{1}{2E}\left(L + \frac{2\pi a^2}{w}\right)d\sigma \implies -\frac{d\sigma}{\sigma} = \frac{4\pi a}{Lw + 2\pi a^2} da, \quad (34)$$

integrating the above equation

$$-\ln(\sigma) = \ln(Lw + 2\pi a^2) + \ln(C), \quad (35)$$

$$\ln\left(\frac{1}{\sigma}\right) = \ln C(Lw + 2\pi a^2), \quad (36)$$

$$\sigma = \frac{C_1}{Lw + 2\pi a^2}, \quad (37)$$

where $C_1 = 1/C$ is constant of integration which is obtained by $\sigma|_{a_c} = \sigma_c$, then

$$\sigma = \sigma_c \left(\frac{Lw + 2\pi a_c^2}{Lw + 2\pi a^2} \right), \quad (38)$$

I am wondering can we say that for large w , $\sigma = \sigma_c$?! because we can rewrite (19) as

$$\sigma = \sigma_c \left(\frac{L + 2\pi a_c^2/w}{L + 2\pi a^2/w} \right), \quad (39)$$

and a/w is very small compare to L then

$$\sigma = \sigma_c$$

+++++

The **total** strain energy is composed of the one away from the crack in the plate, and the one close to the crack tip. Assuming $B=1$:

$$U = U_p + U_c \quad (40)$$

$$U_p = \frac{1}{2}\sigma\varepsilon Vol \quad (41)$$

$$= \frac{1}{2} \frac{\sigma^2}{E} WL \quad (42)$$

$$U_c = \int G da \quad (43)$$

$$G = \frac{K_I^2}{E} \quad (44)$$

$$K_I = \sigma\sqrt{\pi a} \quad (45)$$

$$G = \frac{\sigma^2 \pi a}{E} \quad (46)$$

$$U_c = \int \frac{\sigma^2 \pi a}{E} da \quad (47)$$

$$= \frac{1}{2} \frac{\sigma^2 \pi a^2}{E} \quad (48)$$

$$U = U_p + U_c \quad (49)$$

$$= \frac{1}{2} \frac{\sigma^2}{E} WL + \frac{1}{2} \frac{\sigma^2 \pi a^2}{E} \quad (50)$$

The total external work is

$$W = Pv \quad (51)$$

Equating external work to strain energy

$$Pv = \frac{1}{2} \frac{\sigma^2}{E} WL + \frac{1}{2} \frac{\sigma^2 \pi a^2}{E} \quad (52)$$

$$P = \sigma W \quad (53)$$

$$\sigma W v = \frac{1}{2} \frac{\sigma^2}{E} WL + \frac{1}{2} \frac{\sigma^2 \pi a^2}{E} \quad (54)$$

$$\Rightarrow v = \frac{\sigma}{2EW} (WL + \pi a^2) \quad (55)$$

But v is stationary, thus

$$dv = \frac{d\sigma}{2EW} (LW + \pi a^2) + \frac{\sigma \pi a}{EW} da = 0 \quad (56)$$

$$\Rightarrow \frac{d\sigma}{\sigma} = -\frac{2\pi a da}{LW + \pi a^2} \quad (57)$$

$$\ln |\sigma| = -\int \frac{2\pi a da}{LW + \pi a^2} \quad (58)$$

$$= -\ln |LW + \pi a^2| + \ln |C| \quad (59)$$

$$\Rightarrow \sigma = \frac{C}{LW + \pi a^2} \quad (60)$$

$$a = a_c; \sigma = \sigma_c \Rightarrow C = \sigma_c (LW + \pi a_c^2) \quad (61)$$

$$\sigma = \sigma_c \frac{LW + \pi a_c^2}{LW + \pi a^2} \quad (62)$$

Problem 5

For $L = 50''$, $W = 50''$, $a_c = 1.295''$, $\sigma_c = 48.9$ ksi, $\sigma = 48.9 \frac{50^2 + \pi(1.295)^2}{50^2 + \pi a^2}$ and $R = 0.03 + 0.4(\Delta a)^{0.25}$.

E=30000;

sigma=48.9;

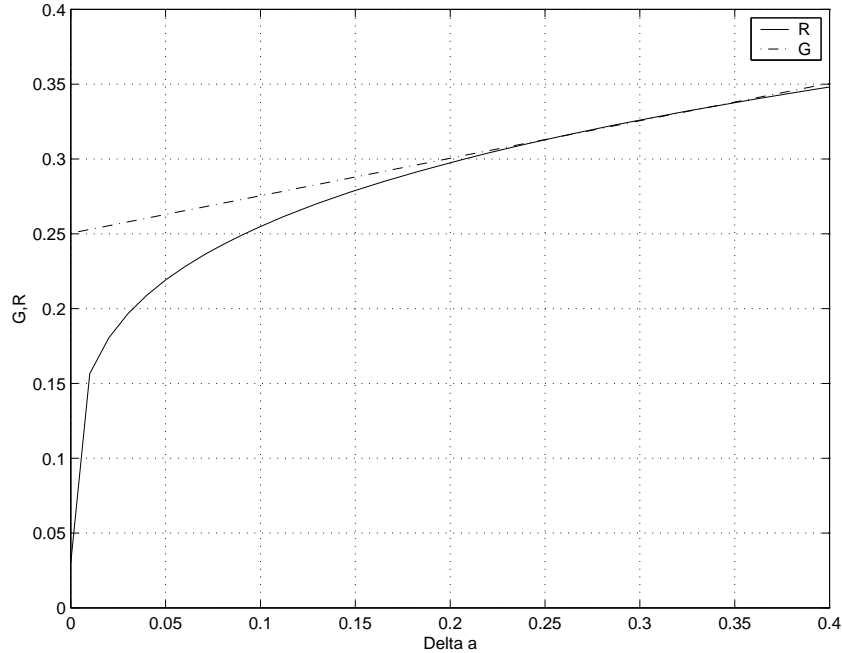
a=1;

delta_a=[0.:0.01:0.4];

```

a_c=a+delta_a;
g=sigma^2*pi*a_c./E;
r=30^2/E+0.4*(a_c-1).^0.25);
plot(delta_a,r,'k-',delta_a,g,'k-.');
grid
legend('R','G')
xlabel('Delta a')
ylabel('G,R')

```



Problem 6

From structural analysis, the fixed end moment is $qBL^2/12$, but $L = 2a$, thus the moment at the support will be $M = -\frac{qBa^2}{3}$, and

$$M = -\frac{qB}{6}(2a^2 - 6ax + 3x^2) \text{ for } 0 \leq x \leq a \quad (63)$$

$$U = 2 \int_0^a \frac{M^2}{2EI} dx \quad (64)$$

$$I = \frac{Bh^3}{12} \quad (65)$$

$$\Rightarrow U = \frac{24 q^2 a^5 B}{45 Eh^3} \quad (66)$$

$$G = \frac{\partial U}{\partial A} \quad (67)$$

$$= \frac{1}{2B} \frac{\partial U}{\partial a} \quad (68)$$

$$= \frac{4 q^2 a^4}{3 Eh^3} \quad (69)$$

$$K_I = \sqrt{EG} \quad (70)$$

$$= \frac{2}{\sqrt{3}} \frac{qa^2}{h^{3/2}} \quad (71)$$

**CVEN 7161
FRACTURE MECHANICS**

SPRING 2020

HOME-WORK 5

Mixed-Mode; FPZ

Due: March 27, 2020

1. A large thick plate containing a crack length of 4 mm oriented at an angle $\beta = 60^\circ$ with respect to the the direction of the applied uniaxial tensile stress σ fractures at a value of $\sigma_c = 1,000\text{MPa}$. Using the minimum strain energy density model, compute K_{Ic} with $E = 210\text{ GPa}$ and $\nu = 0.3$
2. For the preceding problem, plot the deviatoric and volumetric strain energy densities around the crack tip.
3. Repeat for pure Mode I and Mode II cases.
4. For the first problem, plot the plastic zone size for plane strain and for plane stress. Assume $\sigma_y = 2,000\text{ MPa}$

To facilitate the task, I am providing you with the following Matlab files:

`HW6_part_1.m` Which a short master file that should call the script `HW6_part_2.m`.

`HW6_part_2.m` The rest of the code; I have inserted a couple of XXX, you just have to type the correct Matlab code. (you may want to replace all the `-dpsc2` with `-dpng` to save the figures as `.png` files).

`HW6_part_2.p` which is the exact, correct file for part 2, however the content is obfuscated (i.e.e non readable).

What to submit?

A word file composed of two arts:

1. A table showing the line number of `HW6_part_2.m` and the correct complete line
2. A word file, with the figures, and a discussion

Note: The problem can be described as shown in figure 2.

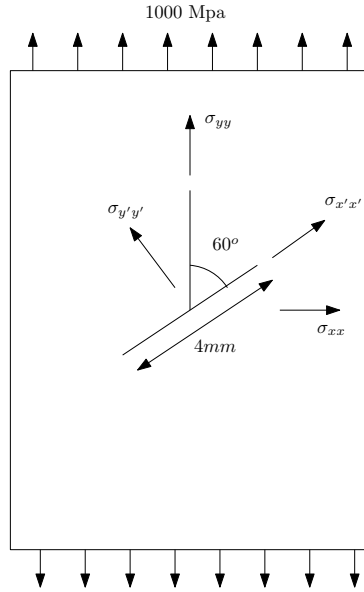


Figure 1: *Sketch of the problem*

Since we only have uniaxial tensile stress, the corresponding stress tensor is given by

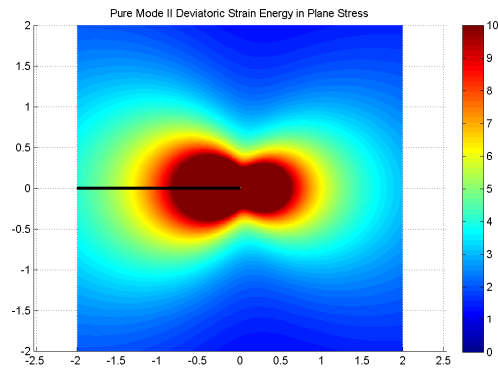
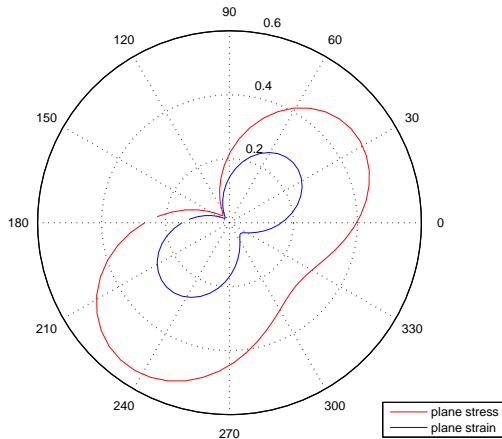
$$\sigma = \begin{pmatrix} 0 & 0 \\ 0 & \sigma_c \end{pmatrix} \quad (1)$$

We need to determine K_I and K_{II} we need the stresses in the axis x' and y' as shown in figure 2. Therefore we apply a rotation of 30° to the stress tensor obtaining:

$$\begin{pmatrix} \sigma_{x'x'} & \sigma_{x'y'} \\ \sigma_{x'y'} & \sigma_{y'y'} \end{pmatrix} = \begin{pmatrix} \cos(30) & \sin(30) \\ -\sin(30) & \cos(30) \end{pmatrix} \begin{pmatrix} 0 & 0 \\ 0 & \sigma_c \end{pmatrix} \begin{pmatrix} \cos(30) & -\sin(30) \\ \sin(30) & \cos(30) \end{pmatrix} = \quad (2)$$

Resulting:

$$\sigma' = \begin{pmatrix} 250 & 433 \\ 433 & 750 \end{pmatrix} \text{Mpa} \quad (3)$$



Solution

Courtesy Benet

1 PROBLEM 1

1. The problem can be described as shown in figure 2.

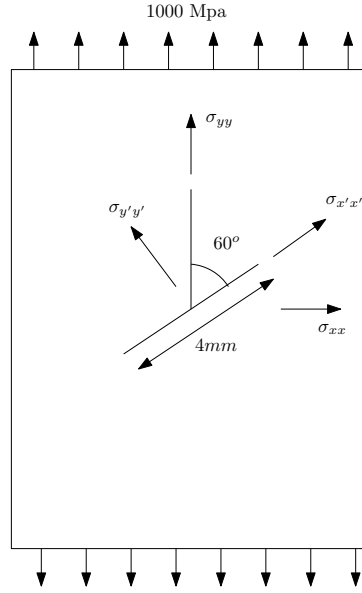


Figure 2: *Sketch of the problem*

2. Since we only have uniaxial tensile stress, the corresponding stress tensor is given by

$$\sigma = \begin{pmatrix} 0 & 0 \\ 0 & \sigma_c \end{pmatrix} \quad (4)$$

3. Since we need to determine K_I and K_{II} we need the stresses in the axis x' and y' as shown in figure 2. Therefore we apply a rotation of 30° to the stress tensor obtaining:

$$\begin{pmatrix} \sigma_{x'x'} & \sigma_{x'y'} \\ \sigma_{x'y'} & \sigma_{y'y'} \end{pmatrix} = \begin{pmatrix} \cos(30) & \sin(30) \\ -\sin(30) & \cos(30) \end{pmatrix} \begin{pmatrix} 0 & 0 \\ 0 & \sigma_c \end{pmatrix} \begin{pmatrix} \cos(30) & -\sin(30) \\ \sin(30) & \cos(30) \end{pmatrix} = \quad (5)$$

Resulting:

$$\sigma' = \begin{pmatrix} 250 & 433 \\ 433 & 750 \end{pmatrix} \text{Mpa} \quad (6)$$

4. Next, we compute the stress intensity factors:

$$K_I = \sigma_{y'y'}\sqrt{\pi a} = 750\sqrt{\pi 2} = 1880 \text{ Mpa}\sqrt{\text{mm}} \quad (7)$$

$$K_{II} = \sigma_{x'y'}\sqrt{\pi a} = 433\sqrt{\pi 2} = 1085 \text{ Mpa}\sqrt{\text{mm}} \quad (8)$$

5. The strain energy density per unit volume, S is determined next

$$S = (a_{11}K_I^2 + 2a_{12}K_IK_{II} + a_{22}K_{II}^2) \quad (9)$$

6. For plane stress problem

$$\kappa = 3 - 4\nu \quad \mu = \frac{E}{2(1 + \nu)} \quad (10)$$

7. According to the minimum strain energy density model, the direction of propagation occurs when the following two conditions are met:

$$\frac{\partial S}{\partial \theta} = 0 \quad \text{and} \quad \frac{\partial^2 S}{\partial \theta^2} > 0 \quad (11)$$

8. Derivatives are given by

$$\begin{aligned} \frac{\partial S}{\partial \theta} = & \frac{1}{16\mu} [2 \cos \theta - (\kappa - 1)] \sin \theta K_I^2 + \frac{2}{16\mu} [2 \cos 2\theta - (\kappa - 1) \cos \theta] K_I K_{II} \\ & + \frac{1}{16\mu} [(\kappa - 1 - 6 \cos \theta) \sin \theta] K_{II}^2 = 0 \end{aligned} \quad (12)$$

$$\begin{aligned} \frac{\partial^2 S}{\partial \theta^2} = & \frac{1}{16\mu} [2 \cos 2\theta - (\kappa - 1) \cos \theta] K_I^2 + \frac{2}{16\mu} [(\kappa - 1) \sin \theta - 4 \sin 2\theta] K_I K_{II} \\ & + \frac{1}{16\mu} [(\kappa - 1) \cos - 6 \cos 2\theta] K_{II}^2 > 0 \end{aligned} \quad (13)$$

9. We plot S and its derivatives (figure 3). By observation, crack propagation occurs around -40 degrees.

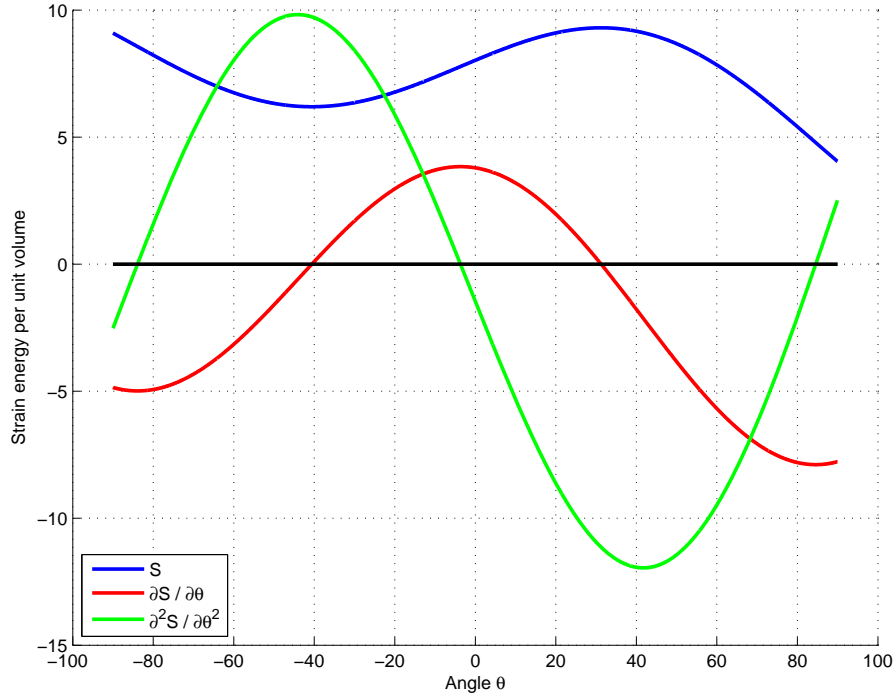


Figure 3: *Strain Energy against the angle in plain strain*

10. The exact solution can be determined solving equation 12 using a Newton-Raphson algorithm. This would give:

- $\theta_c = -40.5839$
- $S_{cr} = 7.3461$

11. Now that the minimum strain energy is known, we can determine the critical stress intensity factor K_{Ic} from

$$K_{Ic} = \sqrt{\frac{8\pi\mu S_{cr}}{\kappa - 1}} = 4317.5 \text{ Mpa}\sqrt{\text{mm}} \quad (14)$$

12. For plane stress, κ is given by

$$\kappa = \frac{3 - \nu}{1 + \nu} \quad (15)$$

and the strain energy density is shown in figure 4

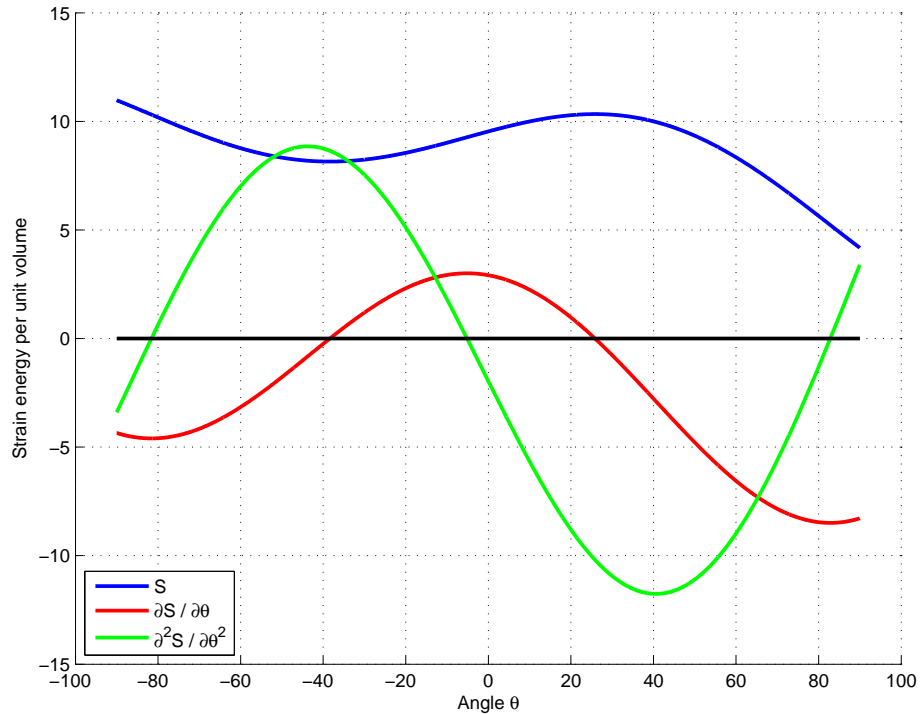


Figure 4: *Strain Energy against the angle in plain stress*

The corresponding values are now:

- $\theta_c = -38.3776$
- $S_{cr} = 8.1502$
- $K_{Ic} = 3919.6 \text{ Mpa}\sqrt{\text{mm}}$

2 PROBLEM 2

The deviatoric and volumetric parts of the strain energy are respectively given by:

$$S_D = \frac{1+\nu}{6E} [(\sigma_{xx} - \sigma_{yy})^2 + (\sigma_{yy} - \sigma_{zz})^2 + (\sigma_{zz} - \sigma_{xx})^2 + 6(\tau_{xy}^2 + \tau_{yz}^2 + \tau_{xz}^2)] \quad (16)$$

$$S_V = \frac{1-2\nu}{6E} (\sigma_{xx} + \sigma_{yy} + \sigma_{zz})^2 \quad (17)$$

And the values of σ_{xx} , σ_{yy} and τ_{xy} can be calculated from Westergaard as:

$$\sigma_{xx} = \frac{K_I}{\sqrt{2\pi r}} \cos \frac{\theta}{2} \left(1 - \sin \frac{\theta}{2} \sin \frac{3\theta}{2}\right) - \frac{K_{II}}{\sqrt{2\pi r}} \sin \frac{\theta}{2} \left(2 + \cos \frac{\theta}{2} \cos \frac{3\theta}{2}\right) \quad (18)$$

$$\sigma_{yy} = \frac{K_I}{\sqrt{2\pi r}} \cos \frac{\theta}{2} \left(1 + \sin \frac{\theta}{2} \sin \frac{3\theta}{2}\right) + \frac{K_{II}}{\sqrt{2\pi r}} \sin \frac{\theta}{2} \cos \frac{\theta}{2} \cos \frac{3\theta}{2} \quad (19)$$

$$\sigma_{xy} = \frac{K_I}{\sqrt{2\pi r}} \sin \frac{\theta}{2} \cos \frac{\theta}{2} \cos \frac{3\theta}{2} + \frac{K_{II}}{\sqrt{2\pi r}} \cos \frac{\theta}{2} \left(1 - \sin \frac{\theta}{2} \sin \frac{3\theta}{2}\right) \quad (20)$$

$$\sigma_{zz} = 0 \text{ in plane stress} \quad \sigma_{zz} = \nu(\sigma_{xx} + \sigma_{yy}) \text{ in plane strain} \quad (21)$$

$$\sigma_{xz} = \sigma_{yz} = 0 \quad (22)$$

Therefore, using the values of K_I and K_{II} from problem 1, we can calculate the volumetric and deviatoric energies at any point. The results obtained for PLANE STRESS are shown in figures 5 and 6. Note that the value of the strain goes to infinity at the crack tip because is inversely proportional to the radius, so the values inside the red zone keep growing up but for the sake of having a nice plot we limited them.

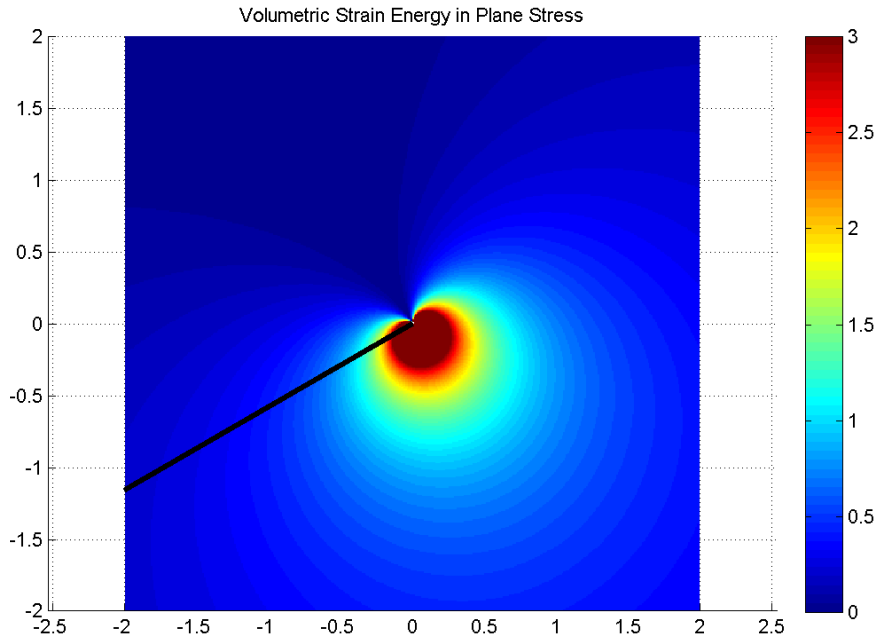


Figure 5: *Volumetric Strain Energy in PLANE STRESS*

Also, it is good to note that in the deviatoric strain energy, the minimum of the "kidney" shape is aligned with -40 degree, which is the direction of propagation.

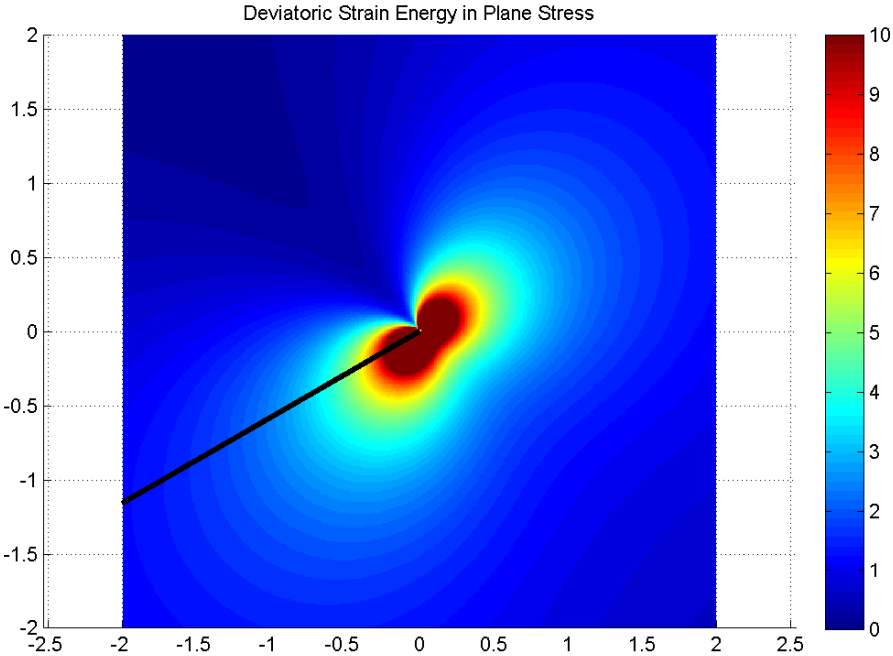


Figure 6: *Deviatoric Strain Energy in PLANE STRESS*

For PLANE STRAIN we can obtain similar plots by just considering different values of κ and σ_{zz} as shown in equations 15 and 21 obtaining:

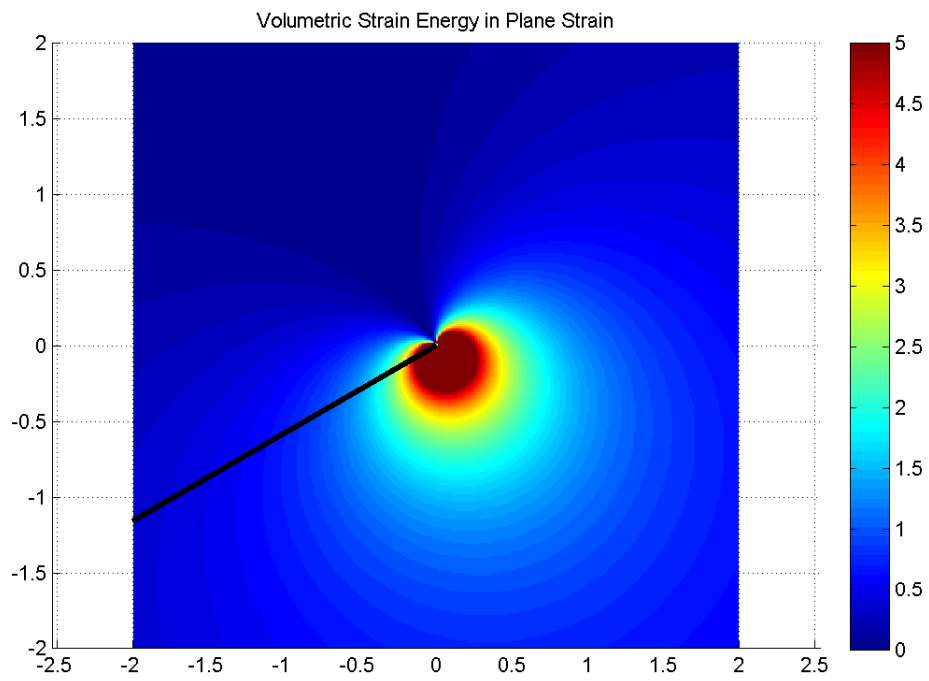


Figure 7: *Volumetric Strain Energy in PLANE STRAIN*

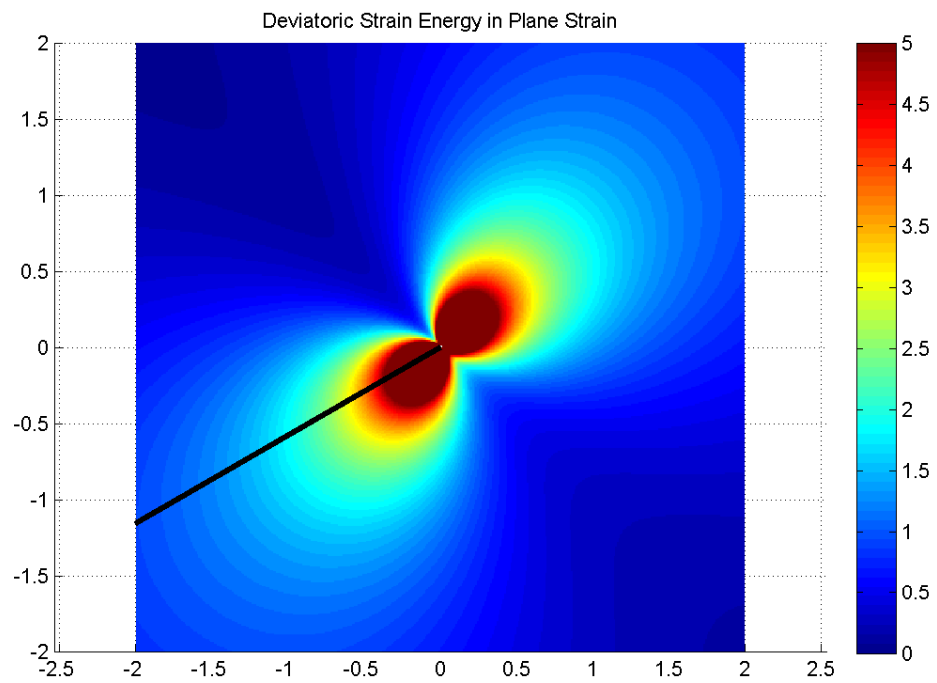


Figure 8: *Deviatoric Strain Energy in PLANE STRAIN*

3 PROBLEM 3

3.1 Mode I

For mode I we repeat the exact same problem that we did before with the difference that now the stress tensor is:

$$\sigma = \begin{pmatrix} 0 & 0 \\ 0 & \sigma_c \end{pmatrix} \quad (23)$$

For PLANE STRESS the strain energy density and its derivatives result:

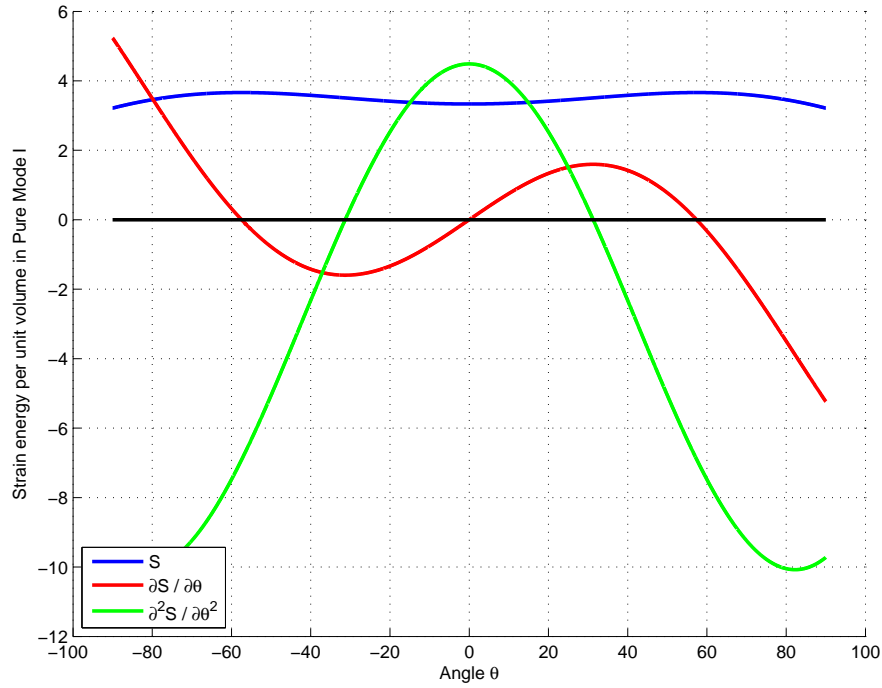


Figure 9: *Strain energy density and its derivatives for PLANE STRESS*

Note that now the propagation angle is set when $\theta = 0$, which means that the crack will propagate along its axis, or what is the same, perpendicular to the stress. In this case we obtain:

- $\theta_c = 0$
- $S_{cr} = 10.4720$
- $K_{Ic} = 4442.9 \text{ Mpa}\sqrt{\text{mm}}$

And doing the exact same problem in MODE I for PLANE STRAIN we get:

- $\theta_c = 0$
- $S_{cr} = 7.7792$
- $K_{Ic} = 4442.9 \text{ Mpa}\sqrt{\text{mm}}$

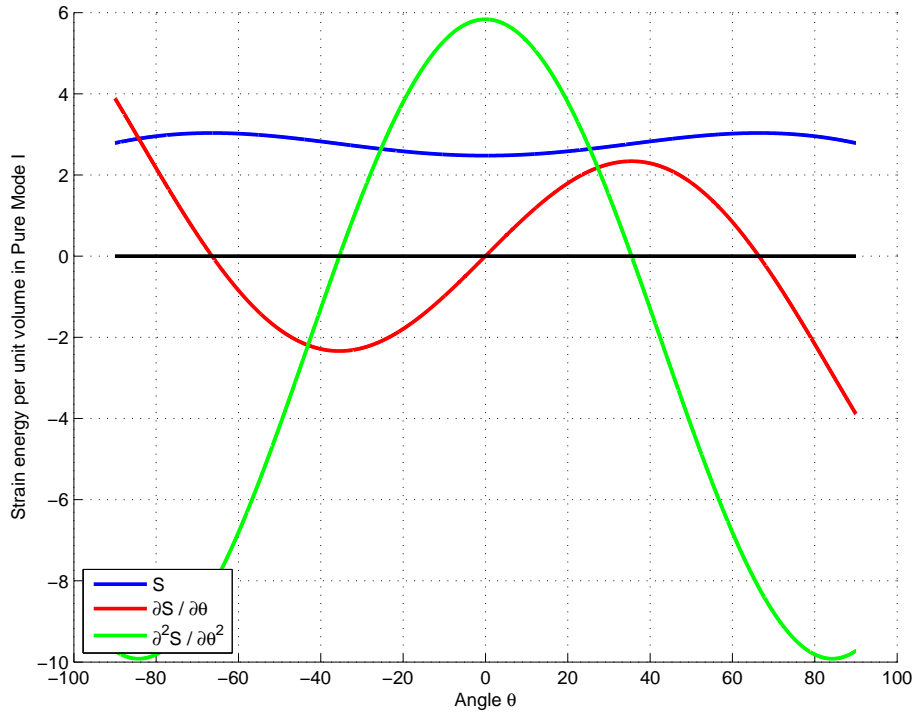


Figure 10: *Strain energy density and its derivatives for PLANE STRAIN*

Again we plot the results obtained for the volumetric and deviatoric energies in PLANE STRESS (figures 9 and 10). In this case we considered a horizontal crack to simplify the representation of mode I, so we didn't have to rotate the stresses. Note that now the minimum of the deviatoric strain energy is located in the same line of the crack which means that the crack will propagate horizontally.

Also, it is good to note that the shape of the deviatoric stress is similar to the plastic zone defined in class for mode I, which means that the results are reasonable.

Similar results could be obtained for plane strain by just changing the values of κ and σ_{zz} .

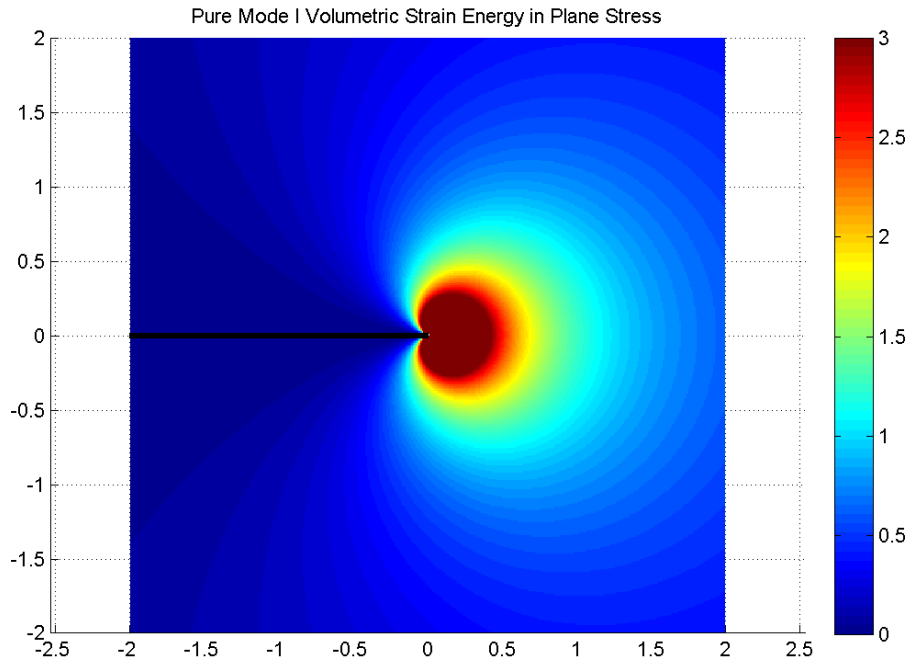


Figure 11: *Volumetric Strain Energy in Mode I for PLANE STRESS*

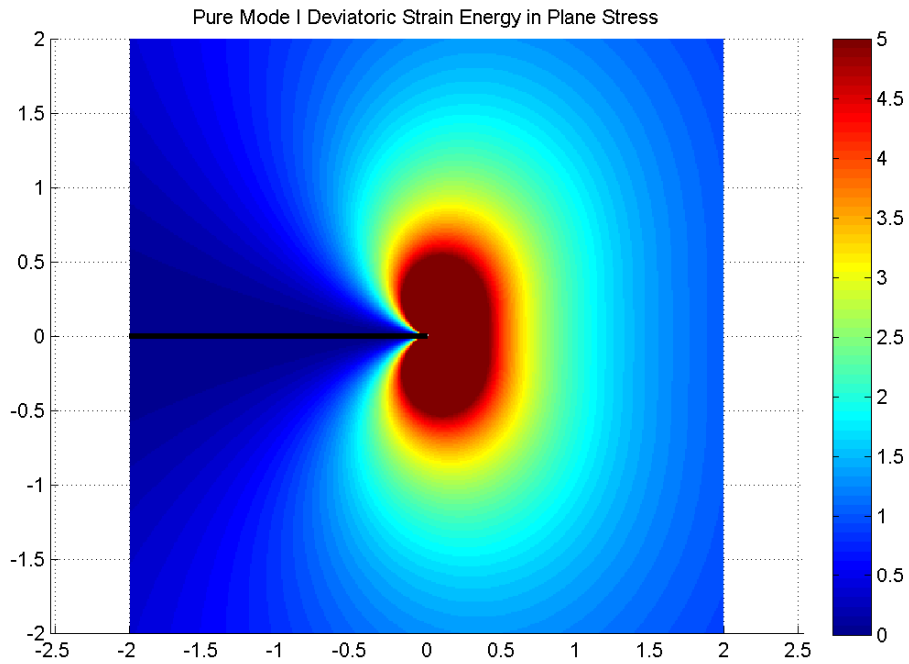


Figure 12: *Deviatoric Strain Energy in Mode I for PLANE STRESS*

3.2 Mode II

We repeat the problem for an horizontal crack with the following stress tensor:

$$\sigma = \begin{pmatrix} 0 & \sigma_c \\ \sigma_c & 0 \end{pmatrix} \quad (24)$$

For PLANE STRESS, the strain energy density and its derivatives result:

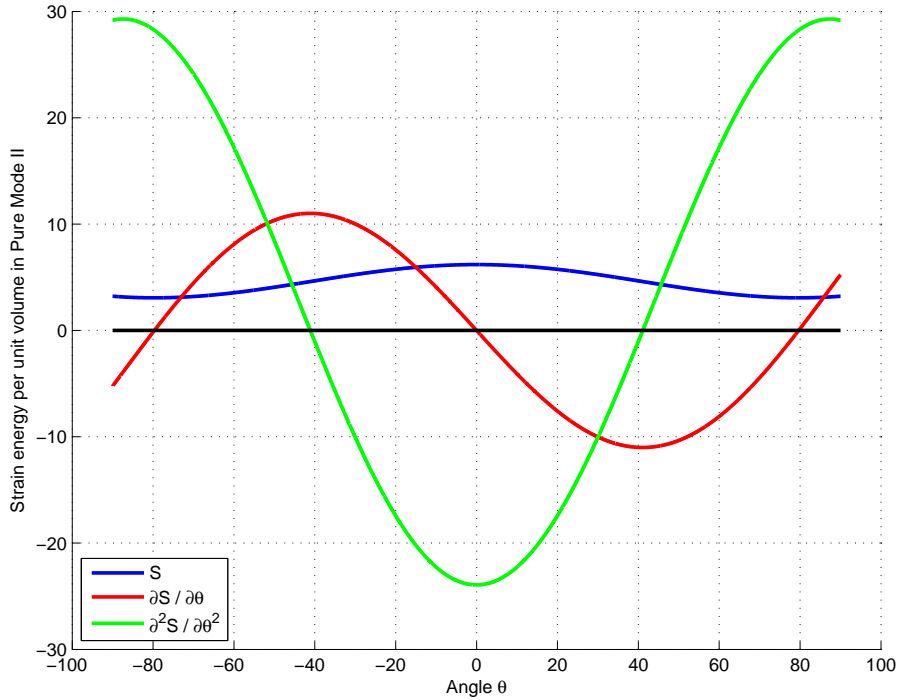


Figure 13: *Strain energy density and its derivatives in PLANE STRESS*

Note that in this case there are two possible solutions for the propagation angle approximately at -80 and 80 degrees, and there is no mathematical way to chose one or the other. However, because we considered a positive value of σ_{xy} , we know that the correct value is the negative one. Hence we obtained:

- $\theta_c = -79.6601$
- $S_{cr} = 15.1432$
- $K_{Ic} = 5342.7 \text{ Mpa}\sqrt{\text{mm}}$

And doing the same problem in PLANE STRAIN we obtain:

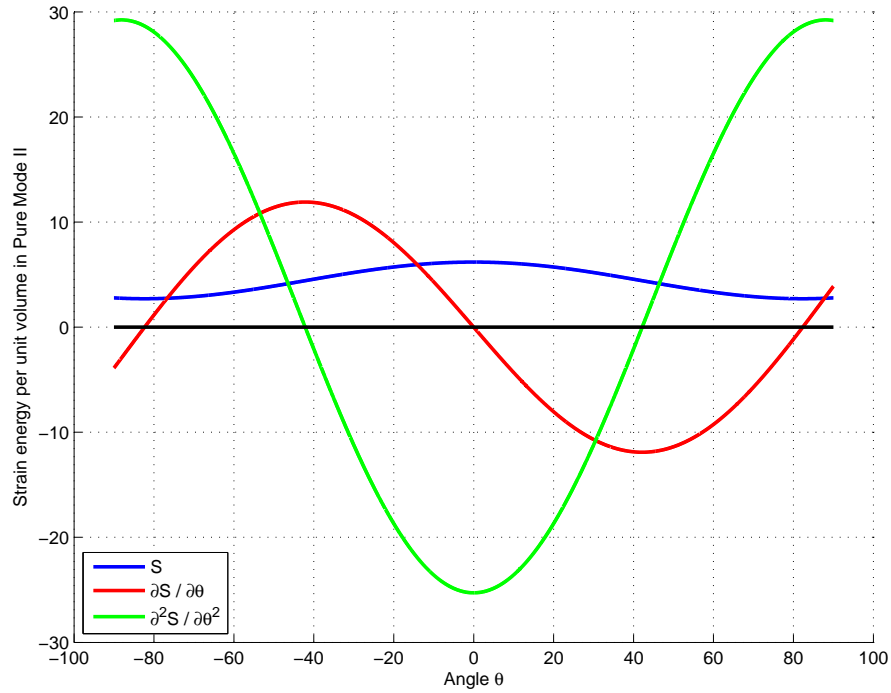


Figure 14: *Strain energy density and its derivatives in PLANE STRAIN*

And the exact values are:

- $\theta_c = -82.3377$
- $S_{cr} = 14.8248$
- $K_{Ic} = 6133.3 \text{ Mpa}\sqrt{\text{mm}}$

The critical angle for the plane strain case can be easily verified in the literature, so it assures that the code implemented is correct.

Next, for the PLANE STRESS CASE we plot the volumetric and deviatoric energy densities, obtaining:

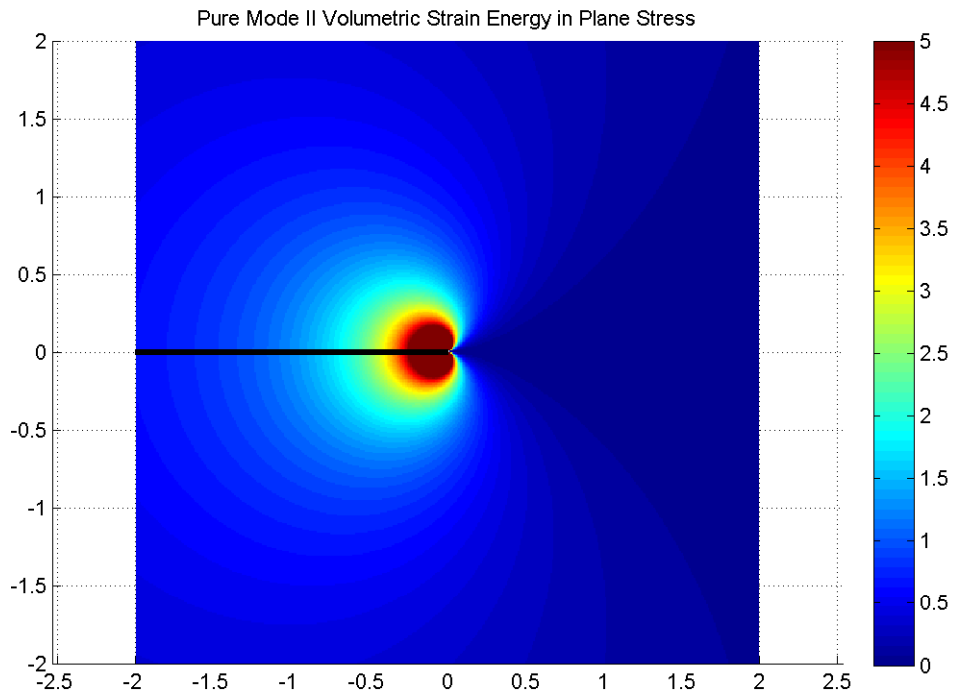


Figure 15: *Volumetric Strain Energy in PLANE STRESS*

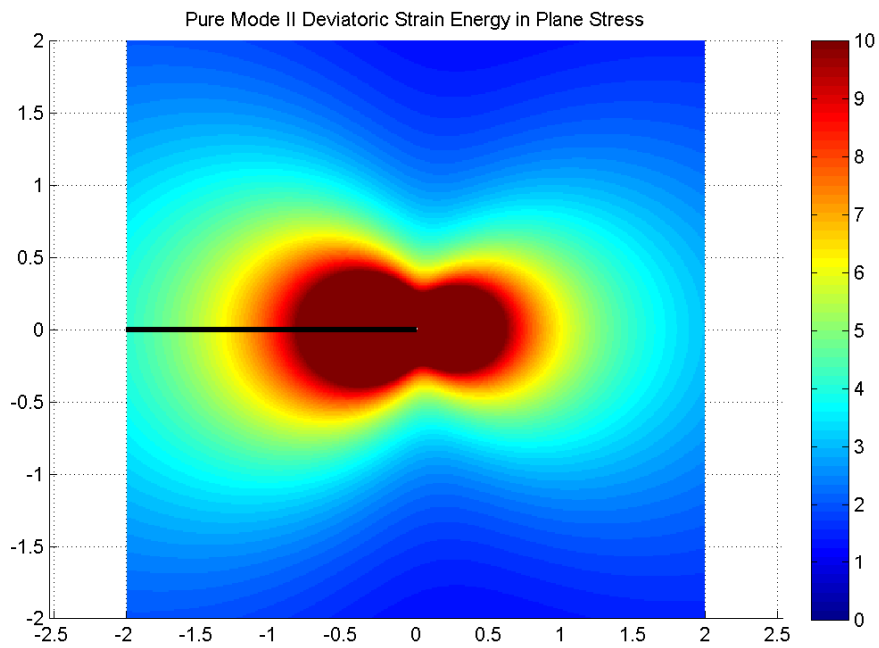


Figure 16: *Deviatoric Strain Energy in PLANE STRESS*

4 PROBLEM 4

To calculate the plastic zone we simply use the von Mises criteria. Since we know that yield occurs when $\sigma_e = \sigma_y$ we can write:

$$\sigma_y = \frac{1}{\sqrt{2}} [(\sigma_x - \sigma_y)^2 + (\sigma_y - \sigma_z)^2 + (\sigma_z - \sigma_x)^2 + 6\tau_{xy}^2]^{\frac{1}{2}} \tag{25}$$

The plastic zone is defined by the values of r that solve the previous equation. Therefore, substituting the stresses from Westergaard (equations 18,19,20,21,22) for the mixed mode case and solving the equation we will find the plastic zone.

The problem is done in both plane strain and plane stress using the MATLAB solver directly on equation 25 so we obtained:

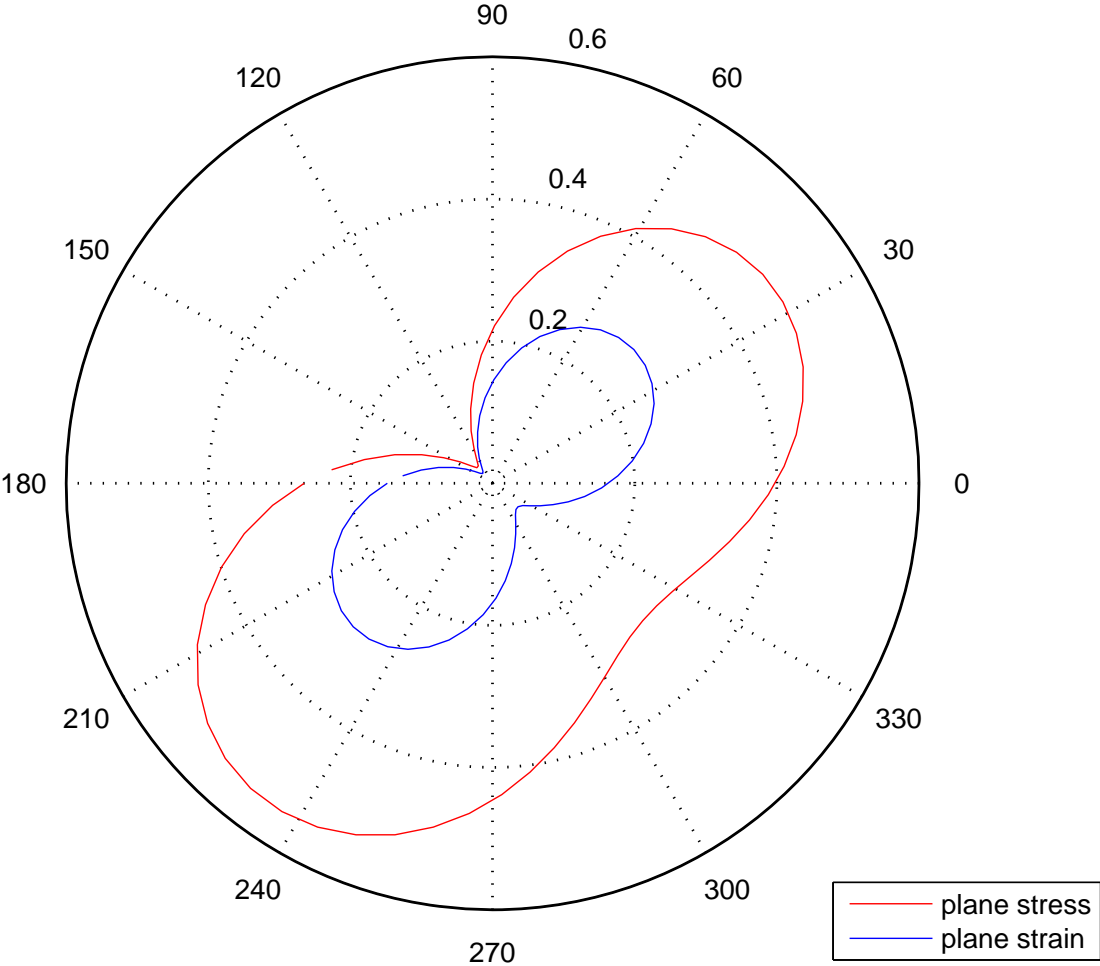


Figure 17: Plastic Zone in Plane Stress and Plane Strain

Note that the plastic zone has the same shape as the deviatoric strain energy density plot from PROBLEM 2, which means that the results are reasonable.

**CVEN 7161
FRACTURE MECHANICS**

SPRING 2018

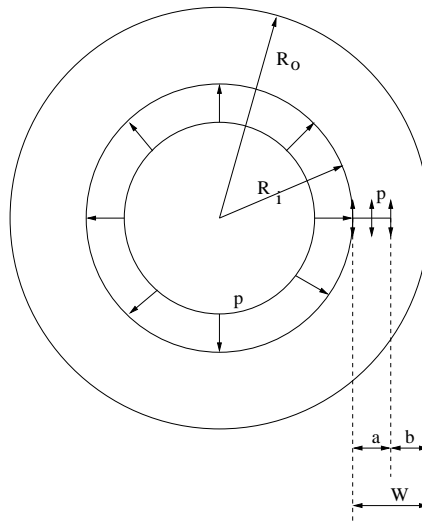
HOME-WORK 6

***J* Integral; Application**

Due: April 2, 2020

A pipe with 1.10 m outside diameter and 50 mm thick wall contains a long axial flaw 10 mm deep. The material flow properties have been fit to a Ramberg-Osgood equation: $\sigma_y = 450$ MPa; $\varepsilon_y = \sigma_y/E$; $\alpha = 1.25$; $n = 7$; $E = 207,000$ MPa.

1. Plot the applied J_{el} , J_{pl} , and J versus internal pressure.
2. If J_{Ic} is 300 kJ/m^2 , determine the pressure required to initiate ductile crack growth.
3. What would be the pressure to initiate brittle crack growth, assume $K_{Ic} = 110 \text{ MPa}\sqrt{\text{m}}$



Solution

$$R_o = \frac{1.10}{2} = 0.55 \text{ m} \quad (1)$$

$$R_i = 0.55 - t = 0.55 - 0.05 = 0.50 \text{ m} \quad (2)$$

$$\sigma_y = 450 \times \text{MPa} \quad (3)$$

$$E = 207,000 \text{ MPa} \quad (4)$$

$$\alpha = 1.25 \quad (5)$$

$$\varepsilon_y = \frac{\sigma_y}{E} = \frac{450 \times 10^6}{207 \times 10^9} = 2.17 \times 10^{-3} \quad (6)$$

$$n = 7 \quad (7)$$

$$a = 0.01 \text{ m} \quad (8)$$

$$W = 0.05 \text{ m} \quad (9)$$

$$b = W - a = 0.05 - 0.01 = 0.04 \text{ m} \quad (10)$$

$$R_c = R_i + a = 0.50 + 0.01 = 0.51 \text{ m} \quad (11)$$

$$p_0 = \frac{2b\sigma_y}{\sqrt{3}R_c} = \frac{2(0.04)(450)}{0.51\sqrt{3}} = 40.7 \text{ MPa} \quad (12)$$

$$g_1 = \frac{a}{W} = \frac{0.01}{0.05} = 0.2 \quad (13)$$

$$g_2 = 1 \quad (14)$$

$$\frac{W}{R_i} = \frac{0.05}{0.5} = 0.1 \quad (15)$$

$$(16)$$

From the table, and through interpolation

$$h_1 = 8.4 \text{ (by interpolation; Table 11.6)} \quad (17)$$

$$F = 1.34 \text{ (by interpolation; Table 11.7)} \quad (18)$$

$$K_I = \frac{2pR_0^2\sqrt{\pi a}}{R_0^2 - R_i^2} F \left(\frac{a}{W}, \frac{R_i}{R_0} \right) \quad (19)$$

$$= \frac{2p(0.55)^2\sqrt{0.01\pi}}{0.55^2 - 0.50^2} 1.33 = 2.745p \quad (20)$$

$$2.74p_{cr}^e = 110 \text{ MPa}\sqrt{\text{m}} \Rightarrow p_{cr}^e = 40.07 \text{ MPa} \quad (21)$$

$$J_{el} = \frac{K_I^2}{E} \quad (22)$$

$$= \frac{(2.745p)^2}{207,000} \quad (23)$$

$$= 3.64 \times 10^{-5} p^2 \text{ MJ/m}^2 \quad (24)$$

$$J_p = \alpha \varepsilon_y \sigma_y b g_1 (a/W) h_1 (a/W, n) \left(\frac{P}{P_0} \right)^{n+1} \quad (25)$$

$$= (1.25)(2.17 \times 10^{-3})(450)(0.04)(0.2)(8.31) \left(\frac{p}{40.7} \right)^{7+1} \quad (26)$$

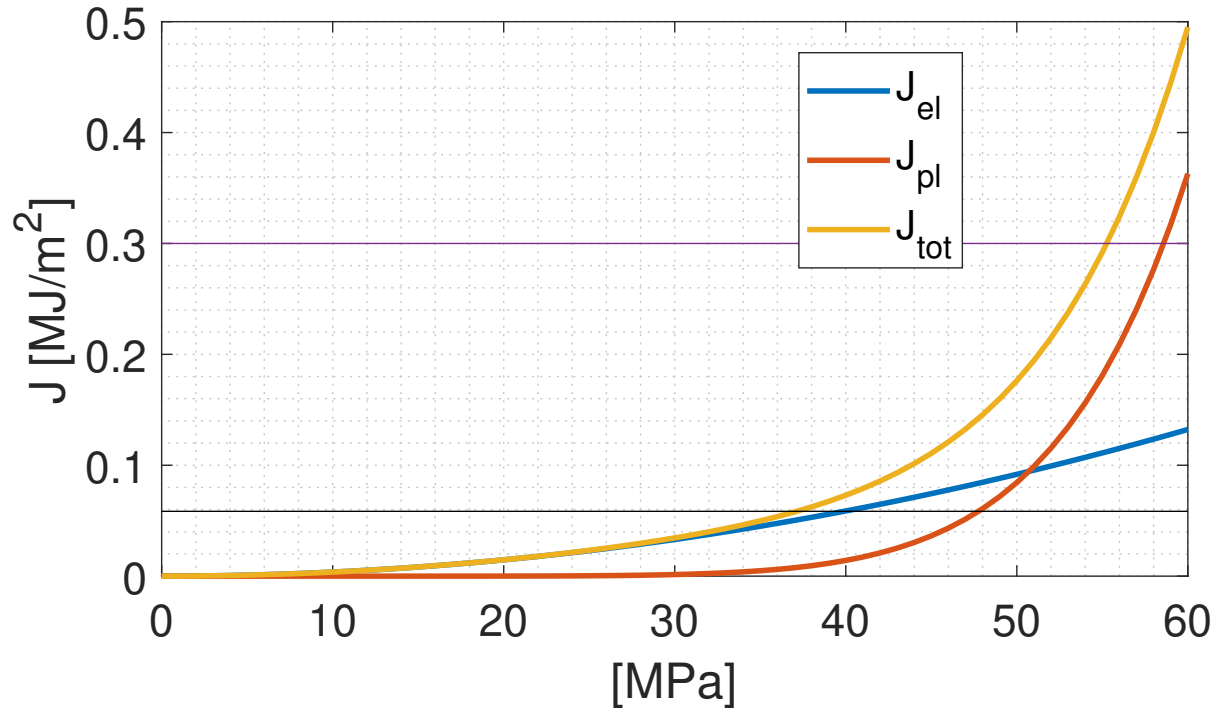
$$= 2.16 \times 10^{-15} p^8 \text{ MJ/m}^2 \quad (27)$$

$$J_{total} = J_{el} + J_{pl} = 3.64 \times 10^{-5} p^2 + 2.16 \times 10^{-15} p^8 \quad (28)$$

$$J_{cr} = J_{total} \quad (29)$$

$$300,000 = 3.64 \times 10^{-5} p^2 + 2.16 \times 10^{-15} p^8 \text{ MJ/m}^2 \quad (30)$$

$$p_{cr} \simeq 55.2 \text{ MPa} \quad (31)$$



**CVEN 7161
FRACTURE MECHANICS**

SPRING 2020

HOME-WORK 7

Fatigue

Due: April 15, 2020

Weight=2

Revised April 15, 2020

1. The crack growth properties of a certain material can be described by

$$\frac{da}{dN} = 1 \times 10^{-8} \Delta K^2 K_{max}^{1.5} \quad (1)$$

If the geometric factor β is equal to 1., what would be the rate of growth of a crack of length $a = 0.5$ in if $\sigma_{max} = 12$ Ksi, and $R = 0.2$. How many cycles does it take for this crack to grow to $a = 0.51$ in?

2. The following data was obtained from crack growth tests at constant amplitude for a center crack with $W = 20$ inches.

a (inches)	N (cycles)	
	$\Delta\sigma = 16$ Ksi; $R=0$	$\Delta\sigma = 10$ Ksi; $R=0.5$
0.1	0	0
0.105	1,100	2,000
1.5	i	k
1.55	$i + 100$	$k + 170$

- (a) Establish the rate diagram (i.e. compute $\Delta a/\Delta N$, ΔK for each of the two sets, and for both $R = 0$ and $R = 0.5$)
- (b) Determine the Paris Law constants C and n (Take the log of the Paris law, and you will have two linear equations in terms of C and n to determine).

Note:

3. Write a Matlab code to perform fatigue life prediction for constant and variable amplitude loading (using the Wheeler model). Use functions to define a) fatigue law (Paris or other); b) stress intensity factors; Output of the program: a plot crack lengths a in terms of cycles N , number of cycles for a to reach a_{cr} .

Test your code (convert to m first) by repeating the class example (aircraft), with the assumptions:

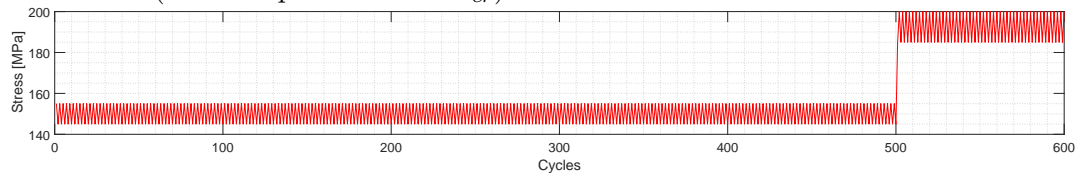
a_i 1 mm

a_{cr} 8 mm

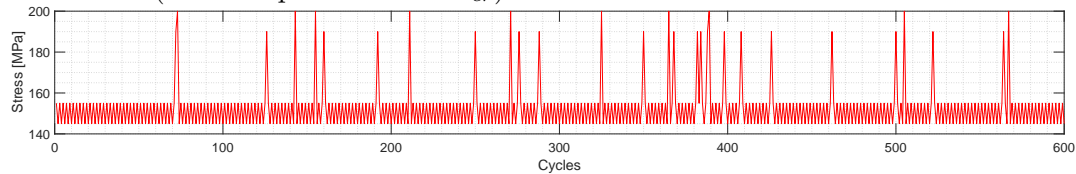
C 5×10^{-10} m/cycle/MPa \sqrt{m}
 n 3
 m 2; for retardation
 σ_y 100 MPa

under the following conditions:

- (a) Same loading as in the example, but replace analytical integration by step by step calculation.
- (b) Data set 1 (to be looped until $a = a_{cr}$).

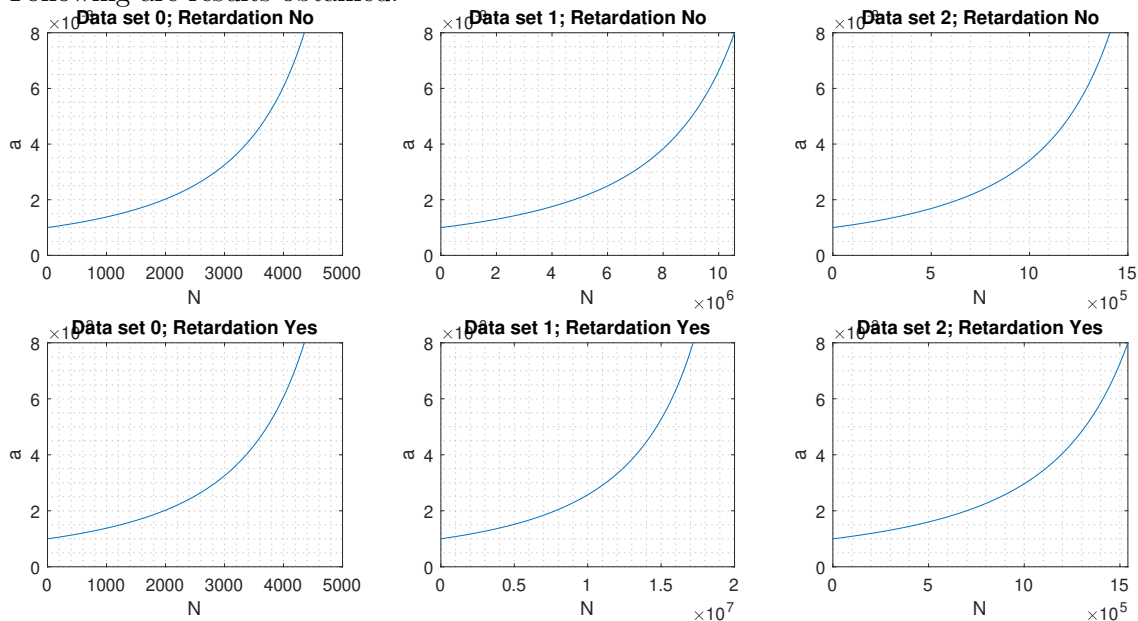


- (c) Data set 2 (to be looped until $a = a_{cr}$).



using two approaches: without and with retardation

Following are results obtained.



Matlab code that generated the data

```

1 close all;clc;clear all
2 %INPUT MATERIAL PROPERTIES DATA
3 a_initial=1; %mm
4 a_critical= 8.; %mm
5 %convert to meters
6 a_initial=a_initial*.001; %m
7 a_critical=a_critical*.001; %m
8 C=5*10^-10; %(m/cycle (cycle (MPasqrt(m)))
  
```

```

9 n=3;
10 m2=2; %for retardation
11 stress_y=100;
12 %=====
13 retars={'No' 'Yes'};
14 for retar=1:2
15     for dataset=1:3
16         switch dataset
17             case 1
18                 sigma_set=data_set_airplane;
19             case 2
20                 sigma_set=data_set_1;
21             case 3
22                 sigma_set=data_set_2;
23         end
24         %%%%%%%%%%%%%%%%%%%%%%%%%%%%%%%%%%%%%%%%%%%%%%%%%%%%%%%%%%%%%%%%%%%%%%%%%
25         %Step-by-step Paris law
26         N=0;
27         a=a_initial;
28         spike_xpz=0;
29         k=1;
30         j=0;
31         while a<a_critical
32             Sigma1=sigma_set(k+1);
33             Sigma2=sigma_set(k);
34             SigmaMin=XXX
35             SigmaMax=XXX
36             k=k+XXX;
37             Kmin=XXX
38             Kmax=XXX
39             delta_K=XXX
40             da_dN=XXX
41             %calculate plastic zone
42             Rp=XXX
43             %plastic zone max coordinate
44             xpz=XXX
45             if retar==2 %Check for retardation
46                 if xpz<spike_xpz
47                     Cp=XXX
48                     a=XXX
49                 elseif xpz>=spike_xpz
50                     spike_xpz=xpz;
51                     Rpspike=XXX
52                     aspik=XXX
53                     a=XXX
54                 end
55             else
56                 a=XXX
57             end
58             %Check for end of data block
59             if k==length(sigma_set)-1
60                 k=1;
61             end
62             %counts cycles
63             N=N+1;
64             %record values for plot
65             a_plot(N)=a;
66             N_plot(N)=N;
67         end
68         subplot(2,3,(retar-1)*3+dataset);
69         y0=a_plot; y=y0(y0~=0);
70         x0=N_plot; x=x0(x0~=0);
71         clear a_plot N_plot
72         plot(x,y);
73         strg=['Data set ', num2str(dataset-1) ', Retardation ', char(retars(retar))];
74         title(strg);
75         xlabel('N'); ylabel('a'); grid minor
76     end
77     clear sigma_set
78 end

```


SOLUTION

Problem 1

$$\begin{aligned} \frac{da}{dN} &= 1 \times 10^{-8} \Delta K^2 K_{max}^{1.5} \\ a &= 0.5 \text{ in}; \sigma_{max} = 12 \text{ ksi}; R = 0.2; \beta = 1 \\ R &= \frac{\sigma_{min}}{\sigma_{max}} \Rightarrow \sigma_{min} = (0.2)(12) = 2.4 \text{ ksi} \\ K &= \sigma \beta \sqrt{\pi a} \\ \Delta \sigma &= 12 - 2.4 = 9.6 \\ K_{max} &= 12 \sqrt{\pi(0.5)} = 15.0 \text{ ksi} \sqrt{\text{in}} \\ \Delta K &= 9.6 \sqrt{\pi(0.5)} = 12 \text{ ksi} \sqrt{\text{in}} \\ \frac{da}{dN} &= 1 \times 10^{-8} (12)^2 (15)^{1.5} = 8.4 \times 10^{-5} \text{ in/cycle} \\ N &\simeq \frac{0.01}{8.4 \times 10^{-5}} = \boxed{120 \text{ cycles}} \end{aligned}$$

Problem 2

$$K = \sigma \sqrt{\sec \frac{\pi a}{W}} \sqrt{\pi a}$$

$$\frac{da}{dN} = C(\Delta K)^n \quad \Rightarrow \quad \frac{\Delta a}{\Delta N} \simeq C(\Delta K)^n$$

$$\Delta K = \Delta \sigma \sqrt{\sec \frac{\pi a}{W}} \sqrt{\pi a}$$

$$a_e = \frac{0.1+0.105}{2} = 0.1025; \quad \Delta a = 0.005; \quad \Delta K = 16 \sqrt{\sec \frac{0.1025\pi}{20}} \sqrt{0.1025\pi} = 9.08$$

$$a_e = \frac{1.5+1.55}{2} = 1.525; \quad \Delta a = 0.05; \quad \Delta K = 16 \sqrt{\sec \frac{1.525\pi}{20}} \sqrt{1.525\pi} = 35.53$$

1.0146

For $R = 0$;

$$\frac{da}{dN} \simeq \frac{0.005}{1,100} = 4.55 \times 10^{-6}; \quad \Delta K = 9.08 \text{ ksi} \sqrt{\text{in}}$$

$$\frac{da}{dN} \simeq \frac{0.05}{100} = 5.00 \times 10^{-4}; \quad \Delta K = 35.52 \text{ ksi} \sqrt{\text{in}}$$

For $R = 0.5$; we just scale the stress by $\frac{10}{16}$

$$\frac{da}{dN} \simeq \frac{0.005}{2,000} = 2.50 \times 10^{-6}; \quad \Delta K = \frac{9.08}{16} 10 = 5.68 \text{ ksi} \sqrt{\text{in}}$$

$$\frac{da}{dN} \simeq \frac{0.05}{170} = 2.94 \times 10^{-4}; \quad \Delta K = \frac{35.52}{16} 10 = 22.2 \text{ ksi} \sqrt{\text{in}}$$

For $R = 0$, solve for the constants by taking the log

$$\log \left(\frac{da}{dN} \right) = \log C + n \log \Delta K$$

$$\log(4.55 \times 10^{-6}) = \log C + n \log 9.08 \Rightarrow -5.34 = \log C + 0.96n$$

$$\log(5.00 \times 10^{-4}) = \log C + n \log 35.52 \Rightarrow -3.30 = \log C + 1.55n$$

Solving we get $C = 2.27 \times 10^{-9}$ in/cycle, and $n = 3.44$.

Similarly, for $R = 0.5$

$$\log(2.5 \times 10^{-6}) = \log C + n \log 5.68 \Rightarrow -5.60 = \log C + 0.75n$$

$$\log(2.94 \times 10^{-4}) = \log C + n \log 22.2 \Rightarrow -3.53 = \log C + 1.35n$$

Solving we get $C = 5.8 \times 10^{-9}$ in/cycle, and $n = 3.49$.

Problem 3

```

1 retars={'No' 'Yes'};
2 for retar=1:2
3     for dataset=2:2 %%%%1:3
4         switch dataset
5             case 1
6                 sigma_set=data_set_airplane;
7             case 2
8                 sigma_set=data_set_1;
9             case 3
10                sigma_set=data_set_2;
11        end
12        %+++++
13        %Step-by-step Paris law
14        N=0;
15        a=a_initial;
16        %prev_sigma=sigma_set(1);
17        %prev_K=sigma_set(1)*sqrt(pi*a);
18        spike_xpz=0;
19        k=1;
20        j=0;
21        while a<a_critical
22            Sigma1=sigma_set(k+1);
23            Sigma2=sigma_set(k);
24            SigmaMin=min(Sigma1,Sigma2);
25            SigmaMax=max(Sigma1,Sigma2);
26            k=k+2;
27            Kmin=SigmaMin*sqrt(pi*a);
28            Kmax=SigmaMax*sqrt(pi*a);
29            delta_K=Kmax-Kmin;
30            j=j+1;
31            junk(j)=delta_K;
32            %determine if stress increased, apply paris law and retardation if
33            %relevant
34            %if sigma>prev_sigma
35
36            da_dN=C*(delta_K)^n;
37            %calculate plastic zone
38            Rp=a*(Kmax^2/stress_y);
39            %plastic zone max coordinate
40            xpz=a+Rp;
41            if retar==2 %Check for retardation
42                if xpz<spike_xpz
43                    Cp=(Rp/(aspoke+Rpspike-a))^m2;
44                    a=a+Cp*da_dN;
45                elseif xpz>=spike_xpz
46                    spike_xpz=xpz;
47                    Rpspike=Rp;
48                    aspoke=a;
49                    a=a+da_dN;
50                end
51            else
52                a=a+da_dN
53            end
54            %Check for end of data block
55            if k==length(sigma_set)-1
56                k=1;
57            end
58            %counts cycles
59            N=N+1;
60            %record values for plot
61            a_plot(N)=a;
62            N_plot(N)=N;
63        end
64        subplot(2,3,(retar-1)*3+dataset);
65        y0=a_plot;y=y0(y0~=0);
66        x0=N_plot;x=x0(x0~=0);
67        clear a_plot N_plot
68        plot(x,y);
69        strg=['Data set ' num2str(dataset-1) ' ; Retardation ' char(retars(retar))];
70        title(strg);
71        xlabel('N');ylabel('a');grid minor
72    end
73    clear sigma_set

```


Part IV

Exam

This is the single (closed notes/book) exam given around 3/4th of the course. It is meant to test students fundamental and practical understanding of fracture mechanics

CVEN 7161
FRACTURE MECHANICS
CLOSE NOTES EXAM

2.5 hrs

Note: 1) This exam is composed of two parts (theory and applications) with respective weights α and β ($\alpha + \beta = 100\%$). Please specify clearly what would you like α to be, ($\alpha \in [50, 70]\%$). 2) return this exam sheet with your name and α .

PART I $\alpha\%$

Answer 40 of the following 54 questions. Each question is 2pt.

1. For the Maximum energy release rate theory, it was assumed that $G = K_I^2(\theta) + K_{II}^2(\theta)$. Using an appropriate figure, explain what is $K_I(\theta)$ and $K_{II}(\theta)$
2. Using a figure explain why is J non-zero around a traction free crack.
3. Why do we have size effect?
4. Using an appropriate figure explain softening in concrete.
5. Draw the figure associated with the residual strength diagram of a structure.
6. Draw a figure explaining how often inspection of a potentially cracked structure is to be performed.
7. What is (or are) the criteria for stable and unstable crack propagation.
8. Write the definition of the three stress intensity factors in terms of the stresses.
9. Why was $\Phi = \frac{\sigma}{\sqrt{1-\frac{a}{z^2}}}$ a good choice for Westergaard's solution of a cracked infinite plate under uniform tensile stress σ , where $\sigma_{22} = Re(\Phi(z))$
10. Who developed the following solutions:
 - (a) Elliptical hole in infinite plate
 - (b) Crack in isotropic solid.
 - (c) Elliptical crack.
 - (d) Crack in anisotropic material.
11. What is the stress intensity factor for an infinite plate with central crack a subjected to uniform traction σ .
12. Using an appropriate diagram, describe the boundary conditions associated with William's solution for an interface crack between two dissimilar materials.
13. In not more than two lines, and one figure, show how Irwin derived an expression for the energy release rate G .
14. Show the figure summarizing Griffith's experimental study on the strength of solids, explain how his work related to Inglis equation.
15. What is the theoretical strength of crystalline solids? Explain the basics of the derivation using one or two (or n) figures.
16. Why is the actual measured strength of solids much lower than their theoretical values?
17. Would you expect an elliptical crack to grow along its major or minor axis, why?

18. Discuss the energy transfer occurring during crack growth under constant load.
19. Which inherent assumption is made in the following equation: $G = G_I + G_{II} + G_{III}$? is this correct? why?
20. Derive an expression for the energy transferred during an infinitesimal crack extension δa under fixed load P .
21. Using an appropriate figure discuss (stable and unstable) crack growth in plane stress problems (in terms of G and R).
22. Label the following figure:
23. What is the fundamental difference between the spatial stress distribution around (and close to) the crack tip for isotropic and anisotropic solids?
24. What is the order of strain singularity in cracked anisotropic solids?
25. Describe a criteria for mixed mode crack propagation.
26. What are the assumptions of the Maximum Energy Release Rate model?
27. Given K_I, K_{II} and K_{IC} outline the procedure to assess whether the crack will grow or not, and at which angle θ_0 .
28. Plot the strain energy density at a point close to the crack tip subjected to pure mode I loading, and show the directions of S_{max} and S_{min} .
29. For the above figure indicate where does the maximum distortional and dilational deformation take place.
30. On two separate figures, and using two simple equations, show the first and second order Irwin approximation for the plastic zone.
31. How can you approximate the plastic zone size in metals?
32. Why do you get an unsymmetric process zone in pure mode II using the Drucker-Prager yield criterion, while a symmetric one is obtained using the tresca criterion?
33. Under which circumstances would the size of the process zone under plane stress and plane strain be identical?
34. Show the variation of plastic zone size ahead of a crack front across the thickness of a steel plate.
35. What is the difference between K_{Ic} and K_{Ic} , which one is larger.
36. Briefly explain how we can determine the orientation of the crack growth under plane stress and plane strain conditions.
37. Write the expression of the J integral for a crack aligned with the x axis.
38. Show through an appropriate diagram why is J a path independent contour line integral.
39. What are the fundamental differences between G and J ?
40. What is HRR singularity?
41. How can we determine if crack propagation and possibly kinking occur in interface crack (Hutchinson model)?
42. Give two examples of subcritical crack growth.
43. What is meant by stage I in fatigue crack growth?
44. Write Paris law for fatigue.
45. Explain, using a figure, what causes retardation in fatigue crack growth.

46. Using a diagram, and appropriate equations, indicate how is retardation accounted for by Wheeler's model.
47. Show how you can distort a quadratic isoparametric element to achieve the 1/2 stress singularity (no equations, just one figure).
48. What is a transition element?
49. Outline a solution procedure to extract the mixed mode stress intensity factors K_I and K_{II} from a finite element analysis in which the stress singularity is not accounted for.
50. Outline a solution procedure to extract the mixed mode stress intensity factors K_I and K_{II} from a finite element analysis in which the stress singularity is modeled by the quarter point element (QPE).
51. What is a Process zone?
52. Label and draw the following three graphs.
53. In no more than 3 lines discuss wave propagation in softening material.
54. Outline Bazant's and Saouma's size effect laws.

PART II Theory $\beta\%$

Solve three of the following five problems:

1. A thick cylindrical pipe with inner radius $b = 10$ cm and outer radius $c = 20$ cm is internally stressed due to a temperature difference ΔT across the wall. Positive ΔT indicates that the outside wall temperature is higher than the inside. The pipe has an initial crack length of 2 mm ($a = 1$ mm) emanating from its inner radius. Yield stress is 1,000 MPa, Poisson's ratio is 0.3, modulus of elasticity $E = 210$ GPa, coefficient of thermal expansion $\alpha = 6.6 \times 10^{-6}$ °F, and a fracture toughness $K_{Ic} = 100 \text{MPa}\sqrt{\text{m}}$. For fatigue, it was found from separate tests on identical material that the crack growth per cycle is 1×10^{-12} m, and that the exponent n is proportional to the square of the size of the plastic zone.
 - (a) (50%) Determine the maximum temperature difference $(\Delta T)_c$ the pipe can withstand without failure with a factor of safety $S = 2$ against yielding and $S = 3$ against fracture.
 - (b) (25%) What is the corresponding size of the plastic zone (use the simplest approximation, and recall that we can write $K = \sigma\sqrt{2\pi r}$)
 - (c) (25%) If the cylinder is subjected to thermal cycles for ΔT ranging from 0 to 200°F, estimate the number of thermal cycles to double the crack size (do not account for the safety factors).

Note The maximum stress at the rim of the inner radius of a pipe is given by

$$\sigma_{max} = \frac{\alpha E \Delta T}{2(1 - \nu)} \left[\frac{2}{1 - (b/c)^2} - \frac{1}{\ln(c/b)} \right] \quad (1)$$

the stress intensity factor can be approximated by

$$K_I = 1.12 \sigma_{max} \sqrt{\pi a} \quad (2)$$

2. A 10 cm square, 20 cm long extruded bar of 7075-T6511 is hollowed out to form a thin walled cylinder (closed at one end), 20 cm long with an outer diameter of 9 cm. The cylinder is fitted with a 7 cm diameter piston designed to increase pressure within the cylinder to 55 MPa. On one occasion, a malfunction in the system caused an unanticipated pressure surge of unknown magnitude, and the cylinder burst. Examination of the fracture surface revealed a metallurgical defect in the form of an elliptical flaw of 0.45 cm long at the inner diameter wall and 0.15 cm deep. This flaw was oriented normal to the hoop stress of the cylinder.

- (a) Compute the magnitude of the pressure surge responsible for failure.
- (b) Assume that another cylinder had a similarly oriented surface flaw but with a semi-circular shape ($a=0.15$ cm). How many pressure cycles could the cylinder withstand before failure?

Assume the following:

- (a) Fatigue law: Assume the Paris Law to prevail.
 - i. The value of n was never computed but it was noted that the crack growth rate varied directly with the square of the plastic zone dimensions at the crack tip.
 - ii. Through microscopic measurement it was found that the spacing between adjacent striation is 5×10^{-39} m.
 - (b) $K_{Ic} = 20.9 MPa\sqrt{m}$
 - (c) Stress intensity factors are given by:
 - i. Part a: $K_I = 1.1\sigma\sqrt{\pi\frac{a}{Q}}\sqrt{\sec\frac{\pi a}{2t}}$ and $Q = 1.65$
 - ii. Part b: $K_I = (1.1)(1.1)\sigma(\frac{2}{\pi})\sqrt{\pi a}$
 - (d) Hoop stress is: $\sigma_{hoop} = \frac{PD}{2t}$, where P , D , and t are the internal pressure, internal diameter, and thickness respectively.
3. A material possessing a plane strain fracture toughness of $50 MPa(m)^{1/2}$ and a yield stress of 1000 MPa is to be made into a large panel.
- (a) If the panel is stressed to a level of 250 MPa, what is the maximum size flaw that can be tolerated before catastrophic failure occurs (assume a center notch configuration).
 - (b) At the point of fracture, what is the size of the plastic zone at the middle of the panel along the crack front?
 - (c) If the plate thickness is 2.5 cm, do we have a plane stress or plane strain condition?
 - (d) If the critical flaw size is to be at least equal to 5 cm., what could be the maximum applied stress?
4. Determine the fracture toughness using the compliance method from the following test results:

a	1	2
P	1	1
Δ	1	2

Assuming $P = 1$, $E = 1$, $B = 1$, and Plane Stress conditions. (Recall that $G = \frac{1}{2} \frac{P^2}{B} \frac{\partial C}{\partial a}$)

5. A steam engine develop 105 HP at 15 RPM with 2.5 meter stroke. A through-thickness crack of 2 cm is found in the crankshaft. Its crankshaft cross sectional area is $0.04m^2$ and is made of cast iron (Fracture toughness $18MNm^{-3/2}$, and C and n for cast iron are 4.3×10^{-8} and 4 respectively).
- (a) Will we be able to use this motor?
 - (b) If yes for how long (assuming the engine runs for 2 hrs/day)?

NOTE: Power = Force x Stroke x 2 x Speed. Where Force is the axial force in the crankshaft (Newtons), Speed is in radians/sec, Stroke is in meter, Power is in Joules/sec ($7.8 J/sec = 1 HP$)

Part V

Mathematica Solutions

Contains Mathematica based solutions (Courtesy of Thomas Allard) to all the homework (albeit at times there is a mismatch between problem numbers). Also included are Westergaard and William solutions (for both similar and dissimilar materials).

Homework 1

Thomas Allard
CVEN 7161

Problem 1

Show that $z^2 = (x^2 - y^2) + 2xyi$ satisfies the Cauchy-Riemann equation.

The Cauchy-Riemann equations require a function $f(z)$ to be of the form $f(z) = \alpha + i\beta$. Here,

In[1]:= `alpha[x_, y_] := x^2 - y^2;`

and

In[2]:= `beta[x_, y_] := 2 * x * y;`

Now in order to satisfy the Cauchy-Riemann equations, the following must be true:

$$\frac{\partial \alpha}{\partial x} = \frac{\partial \beta}{\partial y} \quad \text{and} \quad \frac{\partial \alpha}{\partial y} = -\frac{\partial \beta}{\partial x}$$

Compute each component:

In[3]:= `adx = D[alpha[x, y], x]`

Out[3]= 2 x

In[4]:= `bdy = D[beta[x, y], y]`

Out[4]= 2 x

Here we see the first Cauchy-Riemann equation, $\frac{\partial \alpha}{\partial x} = \frac{\partial \beta}{\partial y}$, is satisfied!

In[5]:= `ady = D[alpha[x, y], y]`

Out[5]= -2 y

In[6]:= `bdx = D[beta[x, y], x]`

Out[6]= 2 y

And here we see that the second Cauchy-Riemann equation, $\frac{\partial \alpha}{\partial y} = -\frac{\partial \beta}{\partial x}$, is satisfied!

Problem 2

The stress tensor at a point P is given by:

```
In[7]:= T = {{7, 0, -2}, {0, 5, 0}, {-2, 0, 4}};  
MatrixForm[T]
```

Out[8]/MatrixForm=

$$\begin{pmatrix} 7 & 0 & -2 \\ 0 & 5 & 0 \\ -2 & 0 & 4 \end{pmatrix}$$

Determine the traction (stress vector) on the plane at P whose unit normal is (in a rectangular coordinate system):

```
In[9]:= n = {2/3, -2/3, 1/3};  
MatrixForm[n]
```

Out[10]/MatrixForm=

$$\begin{pmatrix} \frac{2}{3} \\ -\frac{2}{3} \\ \frac{1}{3} \end{pmatrix}$$

The stress vector is simply the dot product of the stress T with the normal n.

```
In[11]:= tau = n.T;  
MatrixForm[tau]
```

Out[12]/MatrixForm=

$$\begin{pmatrix} 4 \\ -\frac{10}{3} \\ 0 \end{pmatrix}$$

This is the stress vector at point P!

Problem 3

A 3d cylinder is described by the following surface function:

$$x_2^2 + x_3^2 = 4$$

A point of interest P is given by coordinates $(2, 1, \sqrt{3})$, which can be defined explicitly as:

```
In[13]:=
x1 = 2;
x2 = 1;
x3 = Sqrt[3.];
```

The stress tensor throughout a continuum is described by:

```
In[16]:=
T = {{3 * x1 * x2, 5 * x2^2, 0}, {5 * x2^2, 0, 2 * x3}, {0, 2 * x3, 0}};
MatrixForm[T]
```

Out[17]//MatrixForm=

$$\begin{pmatrix} 6 & 5 & 0 \\ 5 & 0 & 3.4641 \\ 0 & 3.4641 & 0 \end{pmatrix}$$

Determine the stress vector acting at the point P of the plane tangent to the cylindrical surface.

By inspection of the surface function, it is clear that the cylinder's longitudinal axis is in the x_1 direction. The radius of the cylinder is $\sqrt{4} = 2$. This can be confirmed by taking the length of the vector joining the cylindrical axis with the point P.

```
In[18]:=
r = Sqrt[x2^2 + x3^2]
```

Out[18]=

2.

We need to find the normal vector at point P in the x_2 - x_3 plane at $x_1=2$. Since we are looking at a circle in the x_2 - x_3 plane, the normal will simply be the vector with components $n=\{0, x_2/r, x_3/r\}$

```
In[19]:=
n = {0., x2 / r, x3 / r}
```

Out[19]=

{0., 0.5, 0.866025}

Now that we have the normal vector and stress tensor defined at point P, the stress vector is simply the inner product of n and T .

```
In[20]:=
tau = n.T
```

Out[20]=

{2.5, 3., 1.73205}

This is our stress vector at point P!

Problem 4

For the stress distribution given by problem 3, what should be the body force $\rho\mathbf{b}$ vector to ensure equilibrium?

Static equilibrium is given as

$$\nabla T + \rho\mathbf{b} = 0 \rightarrow \nabla T = -\rho\mathbf{b}$$

So we must take the divergence of T and multiply by -1 to get $\rho\mathbf{b}$.

```
In[21]:= TTT[xx1_, xx2_, xx3_] =
  {{3 * xx1 * xx2, 5 * xx2^2, 0}, {5 * xx2^2, 0, 2 * xx3}, {0, 2 * xx3, 0}};
MatrixForm[TTT[xx1, xx2, xx3]]
```

Out[22]//MatrixForm=

$$\begin{pmatrix} 3 \, xx1 \, xx2 & 5 \, xx2^2 & 0 \\ 5 \, xx2^2 & 0 & 2 \, xx3 \\ 0 & 2 \, xx3 & 0 \end{pmatrix}$$

```
In[23]:= TTTdiv = Div[TTT[xx1, xx2, xx3], {xx1, xx2, xx3}]
```

Out[23]=

$$\{13 \, xx2, 2, 0\}$$

This expresses the divergence of the stress tensor in general. Here we see that the vector only depends on x_2 . Substitute the value of x_2 with 1 as was done for problem 3.

```
In[24]:= Tdiv = With[{xx2 = 1}, Evaluate[TTTdiv]]
```

Out[24]=

$$\{13, 2, 0\}$$

Finally the body force vector required for equilibrium at the point P $(2, 1, \sqrt{3})$ is the negative of the divergence of the stress tensor at P.

```
In[25]:= pb = -Tdiv;
MatrixForm[pb]
```

Out[26]//MatrixForm=

$$\begin{pmatrix} -13 \\ -2 \\ 0 \end{pmatrix}$$

Problem 5

For the stress tensor

```
In[27]:= TT = {{6, -3, 0}, {-3, 6, 0}, {0, 0, 8}};
MatrixForm[TT]
```

Out[28]/MatrixForm=

$$\begin{pmatrix} 6 & -3 & 0 \\ -3 & 6 & 0 \\ 0 & 0 & 8 \end{pmatrix}$$

(a) Determine the invariants

The first invariant is the trace of the tensor .

```
In[29]:= Invariant1 = Tr [TT]
```

Out[29]=

20

The second invariant is given by the following expression. (It is important to use the MatrixPower[] function for this operation, otherwise the calculation will be incorrect.)

```
In[30]:= TTs = MatrixPower [TT, 2];
Invariant2 = 0.5 * (Tr [TT]^2) - Tr [TTs]
```

Out[31]=

123.

The third invariant is the determinant of the tensor .

```
In[32]:= Invariant3 = Det [TT]
```

Out[32]=

216

(b) Determine principal stresses and stress directions

Find the eigenvalues by simply using the "Eigenvalues" function .

```
In[33]:= Eigenvalues [TT]
```

Out[33]=

{9, 8, 3}

Here we see that the first eigenvalue is 9, the second is 8, and the third is 3! Store these variables to be

used later.

```
In[34]:= sig1 = 9;
sig2 = 8;
sig3 = 3;
```

Similarly, the eigenvectors can be found using the "Eigenvectors" function .

```
In[37]:= MatrixForm[Eigenvectors[TT]]
```

Out[37]/MatrixForm=

$$\begin{pmatrix} -1 & 1 & 0 \\ 0 & 0 & 1 \\ 1 & 1 & 0 \end{pmatrix}$$

Here we see that the first eigenvector is $\{-1, 1, 0\}$, the second is $\{0, 0, 1\}$, and the third is $\{1, 1, 0\}$. Store these vectors after normalizing.

```
In[38]:= vec1 = Normalize[{-1, 1, 0}];
vec2 = Normalize[{0, 0, 1}];
vec3 = Normalize[{1, 1, 0}];
```

(c) Show that the transformation tensor of direction cosines transforms the original stress tensor into the diagonal principal axes stress tensor

```
In[41]:= Trec = sig1 * TensorProduct[vec1, vec1] +
sig2 * TensorProduct[vec2, vec2] + sig3 * TensorProduct[vec3, vec3]
```

Out[41]= $\{\{6, -3, 0\}, \{-3, 6, 0\}, \{0, 0, 8\}\}$

Define Cartesian Basis vectors

```
In[42]:= x1 = {1, 0, 0};
x2 = {0, 1, 0};
x3 = {0, 0, 1};
```

Create Direction Cosine Matrix (DCM)


```
In[45]:= DCM = {{x1.vec1, x2.vec1, x3.vec1},
           {x1.vec2, x2.vec2, x2.vec3}, {x1.vec3, x2.vec3, x3.vec3}};
MatrixForm[
  DCM]
```

Out[46]//MatrixForm=

$$\begin{pmatrix} -\frac{1}{\sqrt{2}} & \frac{1}{\sqrt{2}} & 0 \\ 0 & 0 & \frac{1}{\sqrt{2}} \\ \frac{1}{\sqrt{2}} & \frac{1}{\sqrt{2}} & 0 \end{pmatrix}$$

Calculate the diagonal principal axes stress tensor using the DCM as a rotation matrix .

```
In[47]:= New = DCM.TT.Transpose[DCM];
MatrixForm[N[New]]
```

Out[48]//MatrixForm=

$$\begin{pmatrix} 9. & 0. & 0. \\ 0. & 4. & 0. \\ 0. & 0. & 3. \end{pmatrix}$$

Unfortunately it looks like the middle entry is one half of the expected value of 8. By looking at our DCM, we see that there is a factor of $\frac{1}{\sqrt{2}}$ in the (2,3) location. When rotating TT by the DCM, this operation results in a factor of $(\frac{1}{\sqrt{2}} \times \frac{1}{\sqrt{2}}) = \frac{1}{2}$ which is why the (2,2) location of the “New” matrix is one half of 8. We may manually modify the DCM as follows:

```
In[49]:= DCM2 = {{x1.vec1, x2.vec1, x3.vec1},
              {x1.vec2, x2.vec2, (x2.vec3) * Sqrt[2]}, {x1.vec3, x2.vec3, x3.vec3}};
MatrixForm[
  DCM2]
```

Out[50]//MatrixForm=

$$\begin{pmatrix} -\frac{1}{\sqrt{2}} & \frac{1}{\sqrt{2}} & 0 \\ 0 & 0 & 1 \\ \frac{1}{\sqrt{2}} & \frac{1}{\sqrt{2}} & 0 \end{pmatrix}$$

```
In[51]:= New2 = DCM2.TT.Transpose[DCM2];
MatrixForm[N[New2]]
```

Out[52]//MatrixForm=

$$\begin{pmatrix} 9. & 0. & 0. \\ 0. & 8. & 0. \\ 0. & 0. & 3. \end{pmatrix}$$

We have recovered the diagonal principal axes stress tensor! There is a mistake somewhere that resulted in the the matrix “New” having its second diagonal entry one half of the expected value.

(d) Recombine the three invariants from the principal stresses

The first invariant can be calculated from the principal stresses as follows:

```
In[53]:= Invariant11 = sig1 + sig2 + sig3
```

```
Out[53]= 20
```

Clearly this matches the first invariant that was calculated previously. A simple check shows this to be true:

```
In[54]:= Invariant11 - Invariant1
```

```
Out[54]= 0
```

The second invariant can be calculated from the principal stresses as follows:

```
In[55]:= Invariant22 = -1 * ((sig1 * sig2) + (sig2 * sig3) + (sig3 * sig1))
```

```
Out[55]= -123
```

This second invariant was calculated according to the second equation given in equation 2.40 of the class notes. This value matches the second invariant that was calculated previously, but with a negative sign. The same check shows the difference to be non-zero.

```
In[56]:= Invariant22 - Invariant2
```

```
Out[56]= -246.
```

But if we take the absolute value, we can see these invariants have the same magnitude:

```
In[57]:= Abs[Invariant22] - Invariant2
```

```
Out[57]= 0.
```

The third invariant can be calculated from the principal stresses as follows:

```
In[58]:= Invariant33 = sig1 * sig2 * sig3
```

```
Out[58]= 216
```

Clearly this matches the third invariant that was calculated previously. A simple check shows this to be true:

In[59]:=

Invariant33 - Invariant3

Out[59]=

0

(e) Split the stress tensor into its spherical and deviator parts

The pressure (or mean stress) is computed as follows

In[60]:=

p = (1 / 3) * Tr[TT]

Out[60]=

$$\frac{20}{3}$$

Thus the hydrostatic stress tensor is simply a diagonal matrix in which each term on the diagonal is the pressure p.

In[61]:=

Sighyd = DiagonalMatrix[{p, p, p}];
MatrixForm[Sighyd]

Out[62]//MatrixForm=

$$\begin{pmatrix} \frac{20}{3} & 0 & 0 \\ 0 & \frac{20}{3} & 0 \\ 0 & 0 & \frac{20}{3} \end{pmatrix}$$

Finally, the deviatoric stress is the hydrostatic stress tensor subtracted from the original stress tensor.

In[63]:=

Sigdev = TT - Sighyd;
MatrixForm[Sigdev]

Out[64]//MatrixForm=

$$\begin{pmatrix} -\frac{2}{3} & -3 & 0 \\ -3 & -\frac{2}{3} & 0 \\ 0 & 0 & \frac{4}{3} \end{pmatrix}$$

(f) Show that the first invariant of the deviator is zero

Here, just take the trace of the deviatoric stress to find the first invariant.

In[65]:=

Tr [Sigdev]

Out[65]=

0

The first invariant of the deviatoric stress is zero as expected!

Problem 6

The Lagrangian Strain Tensor is given by:

```
In[66]:= T = (1.00*^-6) * {{30.0, 50.0, 20.0}, {50.0, 40.0, 0.0}, {20.0, 0.0, 30.0}};
ScientificForm[MatrixForm[T]]
```

Out[67]//ScientificForm=

$$\begin{pmatrix} 3. \times 10^{-5} & 5. \times 10^{-5} & 2. \times 10^{-5} \\ 5. \times 10^{-5} & 4. \times 10^{-5} & 0. \\ 2. \times 10^{-5} & 0. & 3. \times 10^{-5} \end{pmatrix}$$

The material is a steel with the following material parameters in Pascals:

```
In[68]:= lambda = 119.2 * (1.00*^9);
mu = 79.2 * (1.00*^9);
```

Determine the stress tensor.

The stress tensor is calculated using Hooke's Law in the following form where σ is the stress tensor and T is the strain tensor.

$$\sigma_{ij} = \lambda \delta_{ij} T_{kk} + 2 \mu T_{ij}$$

```
In[70]:= sig = lambda * IdentityMatrix[3] * Tr[T] + 2 * mu * T;
```

Thus the stress in Pascals is:

```
In[71]:= MatrixForm[sig]
```

Out[71]//MatrixForm=

$$\begin{pmatrix} 1.6672 \times 10^7 & 7.92 \times 10^6 & 3.168 \times 10^6 \\ 7.92 \times 10^6 & 1.8256 \times 10^7 & 0. \\ 3.168 \times 10^6 & 0. & 1.6672 \times 10^7 \end{pmatrix}$$

Or in Mega Pascals (MPa):

```
In[72]:= MatrixForm[Evaluate[sig / (1*^6)]]
```

Out[72]//MatrixForm=

$$\begin{pmatrix} 16.672 & 7.92 & 3.168 \\ 7.92 & 18.256 & 0. \\ 3.168 & 0. & 16.672 \end{pmatrix}$$

Problem 7

Determine the strain tensor at a point where the Cauchy stress tensor is given by T where the elastic modulus is 207 GPa, mu is 79.2 GPa, and Poisson's ratio is 0.3

The Cauchy stress tensor is given by T:

```
In[73]:= T = (1.0*^6) * {{100, 42, 6}, {42, -2, 0}, {6, 0, 15}};
MatrixForm[T]
```

Out[74]/MatrixForm=

$$\begin{pmatrix} 1. \times 10^8 & 4.2 \times 10^7 & 6. \times 10^6 \\ 4.2 \times 10^7 & -2. \times 10^6 & 0. \\ 6. \times 10^6 & 0. & 1.5 \times 10^7 \end{pmatrix}$$

The material properties are given as follows (elastic modulus and shear modulus are in Pascals):

```
In[75]:= Emod = 207 * (1.0*^9);
mu = 79.2 * (1.0*^9);
nu = 0.3;
```

Determine the strain tensor given T and material properties above.

First calculate Lamé parameter λ .

```
In[78]:= lambda = (nu * Emod) / ((1 + nu) * (1 - 2 * nu));
```

The strain tensor can be calculated using Hooke's Law using the following form where T is the stress tensor and E is the strain tensor:

$$E_{ij} = \frac{1}{2\mu} \left(T_{ij} - \frac{\lambda}{3\lambda + 2\mu} \delta_{ij} T_{kk} \right)$$

Finally, here is the strain tensor:

```
In[79]:= EE = (1 / (2 * mu)) * (T - (lambda / (3 * lambda + 2 * mu)) * IdentityMatrix[3] * Tr[T]);
ScientificForm[MatrixForm[EE]]
```

Out[80]/ScientificForm=

$$\begin{pmatrix} 4.66421 \times 10^{-4} & 2.65152 \times 10^{-4} & 3.78788 \times 10^{-5} \\ 2.65152 \times 10^{-4} & -1.77518 \times 10^{-4} & 0. \\ 3.78788 \times 10^{-5} & 0. & -7.01948 \times 10^{-5} \end{pmatrix}$$

Problem 8

For the following proposed Airy Stress function:

```
In[81]:= ClearAll[x1, x2, x3]
```

```
In[82]:= phi[x1_, x2_, F_, c_, P_] :=
  ((3 * F) / (4 * c)) * (x1 * x2 - ((x1 * x2^3) / (3 * c^2))) + (P / (4 * c)) * x2^2;
phi[
  x1,
  x2,
  F,
  c,
  P]
```

```
Out[83]= 
$$\frac{P x_2^2}{4 c} + \frac{3 F \left( x_1 x_2 - \frac{x_1 x_2^3}{3 c^2} \right)}{4 c}$$

```

(a) Show that it is indeed suitable as an Airy stress function

First, let's check equilibrium. Airy has shown that the stresses can be defined in terms of the function Φ as follows:

$$\sigma_{11} = \frac{\partial^2 \Phi}{\partial x_2^2}, \quad \sigma_{22} = \frac{\partial^2 \Phi}{\partial x_1^2}, \quad \sigma_{12} = \frac{\partial^2 \Phi}{\partial x_1 \partial x_2}$$

```
In[84]:= sig11 = D[phi[x1, x2, F, c, P], {x2, 2}]
```

```
Out[84]= 
$$\frac{P}{2 c} - \frac{3 F x_1 x_2}{2 c^3}$$

```

```
In[85]:= sig22 = D[phi[x1, x2, F, c, P], {x1, 2}]
```

```
Out[85]= 0
```

```
In[86]:= sig12 = D[phi[x1, x2, F, c, P], {x1, 1}, {x2, 1}]
```

```
Out[86]= 
$$\frac{3 F \left( 1 - \frac{x_2^2}{c^2} \right)}{4 c}$$

```

The 2d stress tensor is thus:

In[87]=

```
sig = {{sig11, sig12}, {sig12, sig22}};
MatrixForm[sig]
```

Out[88]//MatrixForm=

$$\begin{pmatrix} \frac{P}{2c} - \frac{3F x_1 x_2}{2c^3} & \frac{3F \left(1 - \frac{x_2^2}{c^2}\right)}{4c} \\ \frac{3F \left(1 - \frac{x_2^2}{c^2}\right)}{4c} & 0 \end{pmatrix}$$

To check that the proposed Airy Stress function satisfies equilibrium, make sure that the divergence of the stress is zero.

In[89]=

```
Div[sig, {x1, x2}]
```

Out[89]=

$$\left\{ -\frac{3F x_2}{c^3}, 0 \right\}$$

For some reason the divergence of the stress is not a vector of zeros... There must be a mistake somewhere! :(

Now, lets check the compatibility equations.

$$\frac{\partial^4 \Phi}{\partial x_1^4} + 2 \frac{\partial^4 \Phi}{\partial x_1^2 \partial x_2^2} + \frac{\partial^4 \Phi}{\partial x_2^4} = 0$$

In[90]=

```
term1 = D[phi[x1, x2, F, c, P], {x1, 4}];
term2 = 2 * D[phi[x1, x2, F, c, P], {x1, 2}, {x2, 2}];
term3 = D[phi[x1, x2, F, c, P], {x2, 4}];
term1 + term2 + term3
```

Out[93]=

```
0
```

Compatibility is satisfied!

(b) Determine the stress components in the region $x_1 > 0$, $-c < x_2 < c$

As shown before, the stresses are as follows:

In[94]=

```
sig11
```

Out[94]=

$$\frac{P}{2c} - \frac{3F x_1 x_2}{2c^3}$$

In[95]:=

sig22

Out[95]=

0

In[96]:=

sig12

Out[96]=

$$\frac{3 F \left(1 - \frac{x2^2}{c^2} \right)}{4 c}$$

(c) Plot sig_11, sig_12 and show that these stresses are those of a cantilever beam subjected to a transverse end load and axial pull (which one is P and which one is F?).

Let variable F=-10, c=5, and length=100. F is an end load. Using a negative value for F means there is a downward force acting on the left-end of the beam. P is an axial load. A positive value of P indicates a compressive force acting on the left-end of the beam. The parameter c is half of the depth of the beam. The locations x2=-c and x2=c correspond to the bottom fiber and top fiber of beam.

In[97]:=

```
vF = -10;
vc = 5;
L = 100;
```

Evaluate the expression for normal stresses.

In[100]:=

```
normal = With[{F = vF, c = vc}, Evaluate[sig11]]
```

Out[100]=

$$\frac{P}{10} + \frac{3 x1 x2}{25}$$

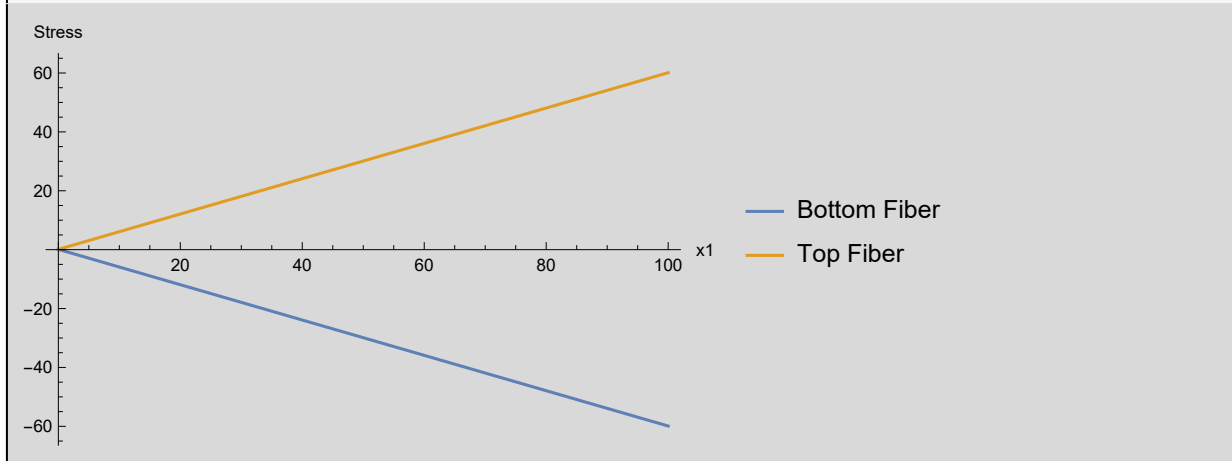
We see here that, for F = -10, the normal stresses depend on the axial load P, location along the length of the beam x1, and the location along them beam depth x2.

Plot of sig_11 for a modest axial load of P=1.

In[101]=

```
Plot[{With[{x2 = -vc, P = 1}, Evaluate[normal]],
      With[{x2 = vc, P = 1}, Evaluate[normal]]], {x1, 0, L},
      PlotLegends -> {"Bottom Fiber", "Top Fiber"}, AxesLabel -> {"x1", "Stress"}]
```

Out[101]=



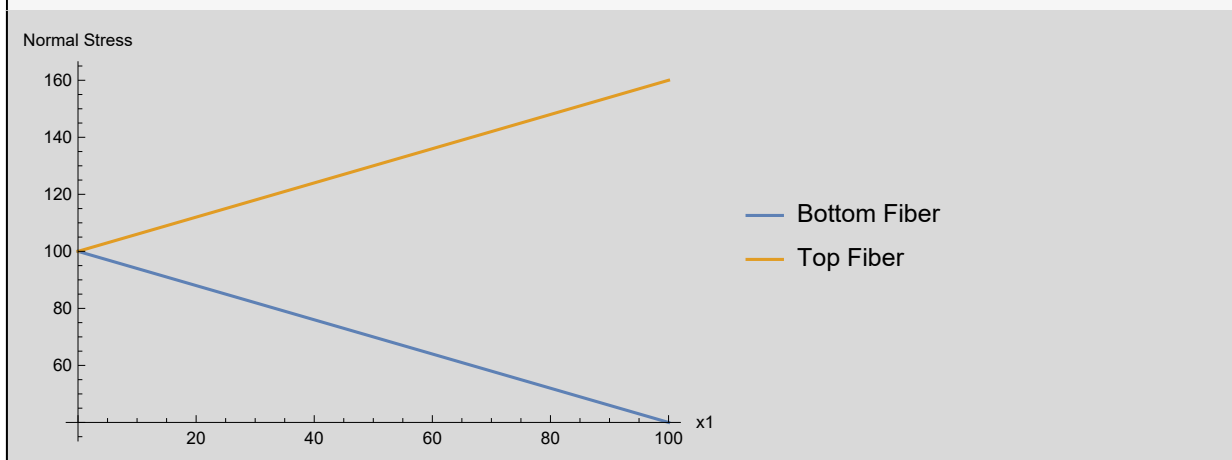
Here we see that the top fiber of the beam is in tension while the bottom fiber is in compression as expected.

Lets investigate what happens when we increase the axial load P to a value of 1000.

In[102]=

```
Plot[{With[{x2 = -vc, P = 1000}, Evaluate[normal]],
      With[{x2 = vc, P = 1000}, Evaluate[normal]]], {x1, 0, L},
      PlotLegends -> {"Bottom Fiber", "Top Fiber"}, AxesLabel -> {"x1", "Normal Stress"}]
```

Out[102]=



By applying a very large tensile load, the entire normal stress distribution throughout the beam is now tensile despite the bending moment imposed by the force F.

Evaluate the expression for shear stresses.

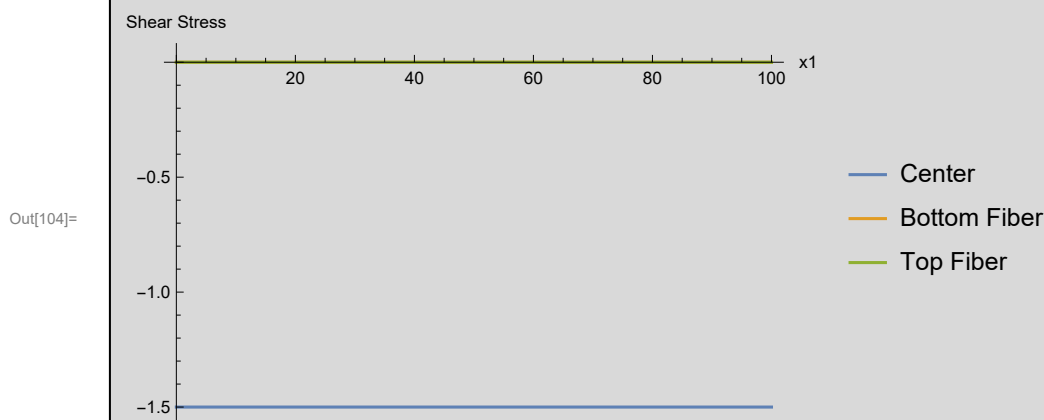
In[103]:= `shear = With[{F = vF, c = vc}, Evaluate[sig12]]`

Out[103]=
$$-\frac{3}{2} \times \left(1 - \frac{x_2^2}{25} \right)$$

We see here that, for $F = -10$, the shear stress depends on the location along the beam depth x_2 , but does not depend on the axial load P or location along the length of the beam x_1 .

This can be verified by plotting the shear stress along the length at the center, top, and bottom of the beam.

In[104]:= `Plot[{With[{x2 = 0}, Evaluate[shear]],
With[{x2 = -vc}, Evaluate[shear]], With[{x2 = vc}, Evaluate[shear]]},
{x1, 0, L}, PlotLegends -> {"Center", "Bottom Fiber", "Top Fiber"},
AxesLabel -> {"x1", "Shear Stress"}]`



Here we confirm that the shear stress in the beam does not depend on length. The shear stress appears to be zero at the top and bottom fibers which should be expected.

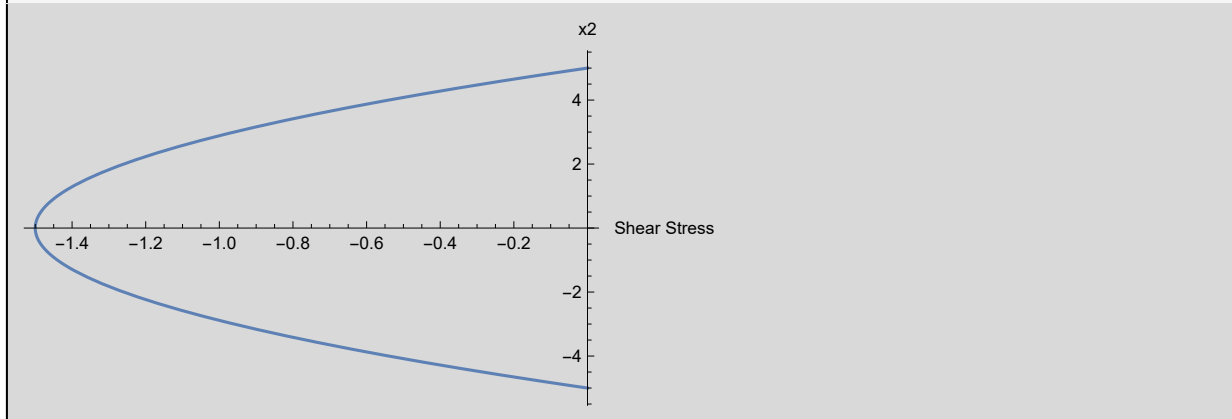
Lets look further at the distribution of shear stresses along the depth of the beam.

In[105]:= `axisFlip = # /. {x_Line | x_GraphicsComplex -> MapAt[#, Reverse ~ 2 &, x, 1],
x : (PlotRange -> _) -> x ~ Reverse ~ 2} &;`

In[106]:=

```
shearplot = Plot[With[{x1 = 0}, Evaluate[shear]],
  {x2, -5, 5}, AxesLabel -> {"Shear Stress", "x2"}];
shearplot // axisFlip
```

Out[107]=



Check that this is Airy Stress Function describes a cantilever beam

Finally, let's make sure these stresses do indeed describe a cantilever beam with both a transverse and axial point load.

Normal Stresses

We will exploit superposition to analyse the contribution from the (1) transverse load F and (2) axial load P . We will assume that the cantilever beam has a rectangular cross section given by a width of 1 and height $2c$.

(1) For a cantilever beam subjected to a transverse load F , the normal stress distribution is described using the following simple equation:

$$\sigma = \frac{My}{I} = \frac{-F * x * y}{I}$$

Assuming that the width of the beam (in the out-of-plane direction) is 1 and height is $2c$, the moment of inertia (second moment of area) is:

$$I = \frac{1}{12} (\text{width}) * (\text{height})^3 = \frac{1}{12} * (1) * (2 * c)^3 = \frac{2}{3} c^3$$

So the normal stress, using the variables $x=x_1$ and $y=x_2$, is given as:

$$\sigma = \frac{-3 * F * x_1 * x_2}{2 * c^3}$$

(2) For a beam subjected to an axial load P , the normal stress is uniform and simply given by the P divided by cross-sectional area A . The area A is the product of width 1 and height $2c$.

$$\sigma = \frac{P}{A} = \frac{P}{(1) * (2c)} = \frac{P}{2c}$$

Now we superimpose the two stresses giving:

$$\sigma = \frac{P}{A} + \frac{My}{I} = \frac{P}{2c} - \frac{3 * F * x1 * x2}{2 * c^3}$$

Comparing to sig11, they are identical!

In[108]:=

sig11

Out[108]=

$$\frac{P}{2c} - \frac{3F x1 x2}{2c^3}$$

Shear Stresses

For shear stresses, we do not need to superimpose the contribution of transverse force F and axial force P . This is because the axial force does not contribute to any shear stresses. For a cantilever beam, we know that the shear stress will be zero at the extreme fibers. A quadratic distribution describes the variation from the bottom fiber to the top. The maximum shear stress occurs at the neutral axis ($x_2 = 0$ for our rectangular beam) given by the following simple formula:

$$\tau = \frac{3V}{2A}$$

Here V indicates the shear force acting on the beam at a location along the length x_1 . We know that for a cantilever beam with an end load F , the shear force distribution is constant and equal to F . The area A is still simply $2c$.

$$\tau = \frac{3 * F}{2 * (2c)} = \frac{3 * F}{4 * c}$$

For our chosen $F = -10$ and $c = 5$,

$$\tau = \frac{3 * F}{2 * (2c)} = \frac{3 * (-10)}{4 * 5} = \frac{-30}{20} = -\frac{3}{2}$$

We can check that our shear stress formula equals tau max by substituting $x_2 = 0$.

In[109]:=

With[{x2 = 0}, Evaluate[shear]]

Out[109]=

$$-\frac{3}{2}$$

Everything checks out!

Homework 2

Thomas Allard

CVEN 7161

Answers are highlighted with a light blue background and are occasionally boxed.

Problem 1

Completed as problem 1 in Homework 1

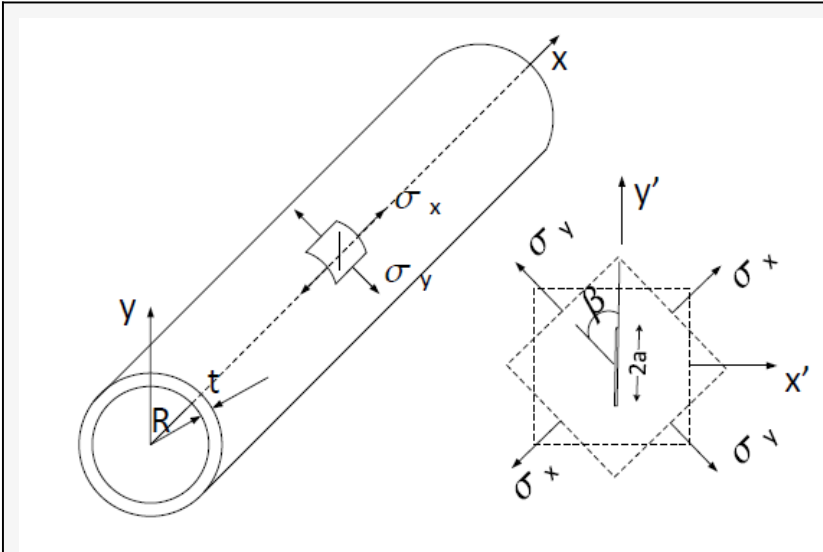
Problem 2

Completed as problem 8 in Homework 1

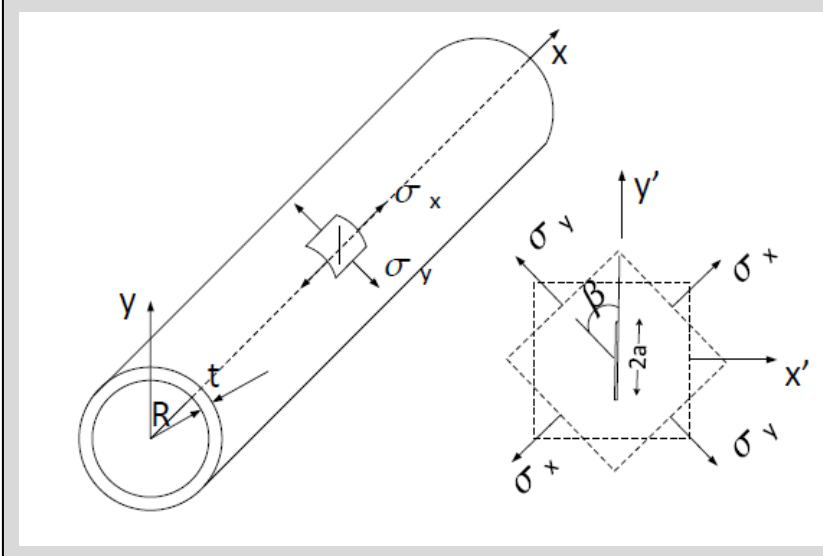
Problem 3

A cylindrical pressure vessel of Radius R and thickness t contains a through crack of length $2a$ oriented at an angle β with the circumferential direction. When the vessel is subjected to an internal pressure p , determine the stress intensity factors at the crack tip.

In[110]=



Out[110]=



Hint: Show that $\sigma_{xx} = \frac{pR}{2t}$ (corresponding to the longitudinal stress), and that $\sigma_{yy} = \frac{pR}{t}$ (corresponding to the tangential stress) and then transform into $\sigma_{x'x'}$, $\sigma_{y'y'}$, and $\sigma_{x'y'}$ using

$$\begin{pmatrix} \sigma_{x'x'} & \sigma_{x'y'} \\ \sigma_{x'y'} & \sigma_{y'y'} \end{pmatrix} = \begin{pmatrix} \cos\theta & \sin\theta \\ -\sin\theta & \cos\theta \end{pmatrix} \begin{pmatrix} \sigma_{xx} & 0 \\ 0 & \sigma_{yy} \end{pmatrix} \begin{pmatrix} \cos\theta & \sin\theta \\ -\sin\theta & \cos\theta \end{pmatrix}^T$$

These relations may be helpful:

$$\sin 2\beta = 2\sin\beta\cos\beta$$

$$\cos 2\beta = 1 - 2(\sin\beta)^2$$

$$(\sin\beta)^2 = \frac{1 - \cos 2\beta}{2}$$

$$(\cos\beta)^2 = \frac{1 + \cos 2\beta}{2}$$

$$\sin\beta\cos\beta = \frac{\sin 2\beta}{2}$$

Solution

For a thin-walled cylindrical pressure vessel, internal pressure p is balanced by hoop stresses ($\sigma_h = \sigma_y$) and longitudinal/axial stresses ($\sigma_l = \sigma_x$). These stresses may be determined by balancing forces. Observing a cross-section of the vessel along the longitudinal axis to analyze the hoop stress, the pressure acts upon an area of 2 times the radius times a differential length dx while the hoop stress acts on an area of 2 times the thickness of the vessel times a differential length dx .

```
In[111]:= (*2*σh*t*dx-p*2*r*dx=0;*)
σh[p_, R_, t_] :=  $\frac{p * R}{t}$ ;
```

Observing a circular cross-section of the vessel to analyze the longitudinal stress, the pressure acts upon an the circular area of πr^2 while the longitudinal stress acts on an area of the thickness of the vessel times the circumference $2\pi r$.

```
In[112]:= (*σl*t*2*π*r - p*π*r2=0;*)
σl[p_, R_, t_] :=  $\frac{p * R}{2 * t}$ ;
```

The stress transformation from coordinates x,y to x',y' (by the angle $-\beta$) can be calculated as:

```
In[113]:= rot[β_] := {{Cos[β], Sin[β]}, {-Sin[β], Cos[β]}};
T[p_, R_, t_, β_] := rot[-β].{{σl, 0}, {0, σh}}.Transpose[rot[-β]];
MatrixForm[Simplify[T[p, R, t, β]]]
```

SetDelayed: Tag List in $\{\{1. \times 10^8, 4.2 \times 10^7, 6. \times 10^6\}, \{4.2 \times 10^7, -2. \times 10^6, 0.\}, \{6. \times 10^6, 0., 1.5 \times 10^7\}\}$ [p_, R_, t_, β_] is Protected.

Out[115]//MatrixForm=

```
{ {1. × 108, 4.2 × 107, 6. × 106},
  {4.2 × 107, -2. × 106, 0.}, {6. × 106, 0., 1.5 × 107} } [  $\frac{2\theta}{3}$ , R, t, β ]
```

We know that the shear components are equal because of symmetry, so lets move to Voigt notation. Lets substitute in the values for hoop and longitudinal stress.

```
In[116]:= sigxx = Sin[β]2 σhh + Cos[β]2 σll;
sigxy = Cos[β] Sin[β] (σhh - σll);
sigyy = Cos[β]2 σhh + Sin[β]2 σll;
```

Substitute and simplify


```
In[119]:= Simplify[sigxx /. {σhh →  $\frac{p * R}{t}$ , σ11 →  $\frac{p * R}{2 * t}$ }]
Simplify[sigxy /. {σhh →  $\frac{p * R}{t}$ , σ11 →  $\frac{p * R}{2 * t}$ }]
Simplify[sigyy /. {σhh →  $\frac{p * R}{t}$ , σ11 →  $\frac{p * R}{2 * t}$ }]
```

```
Out[119]= 
$$-\frac{5 R (-3 + \text{Cos}[2 \beta])}{3 t}$$

```

```
Out[120]= 
$$\frac{5 R \text{Sin}[2 \beta]}{3 t}$$

```

```
Out[121]= 
$$\frac{5 R (3 + \text{Cos}[2 \beta])}{3 t}$$

```

Finally, we may express the stress intensity factors. Sigxx provides mode I loading and Sigxy provides mode II loading while Sigyy does not contribute. We must simply multiply by the factor $\sqrt{\pi a}$.

```
In[122]:= K1[p_, β_, t_, a_, R_] :=  $\sqrt{\pi * a} * \frac{-p * R * (-3 + \text{Cos}[2 * \beta])}{4 * t}$ ;
Framed[Simplify[K1[p, β, t, a, R]]]
K2[p_, β_, t_, a_, R_] :=  $\sqrt{\pi * a} * \frac{p * R * \text{Cos}[\beta] * \text{Sin}[\beta]}{2 * t}$ ;
Framed[Simplify[K2[p, β, t, a, R]]]
```

```
Out[122]= 
$$\frac{5 \sqrt{a} \sqrt{\pi} R (-3 + \text{Cos}[2 \beta])}{3 t}$$

```

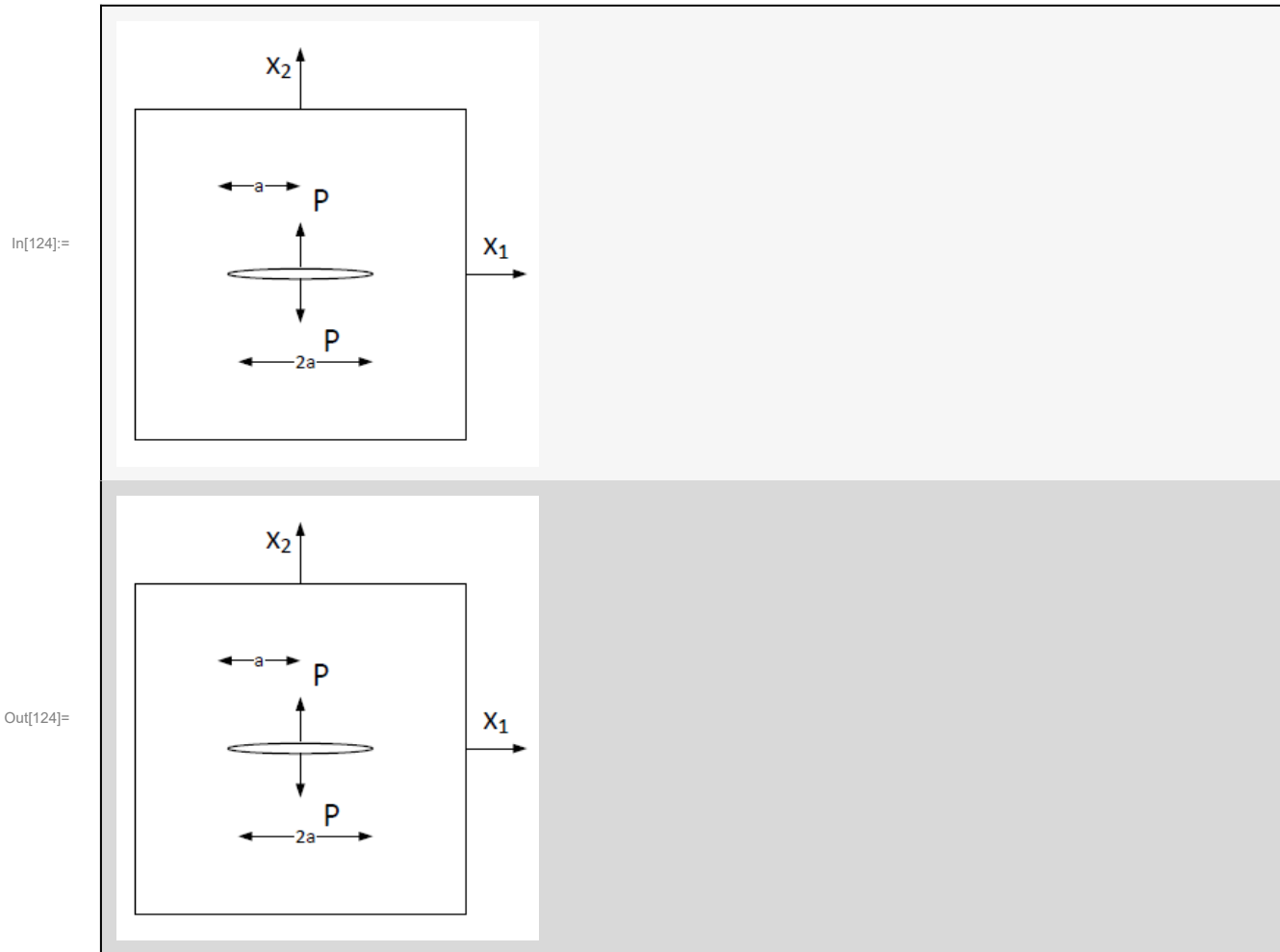
```
Out[123]= 
$$\frac{5 \sqrt{a} \sqrt{\pi} R \text{Sin}[2 \beta]}{3 t}$$

```

These are the stress intensity factors!

Problem 4

The stress function for a crack subjected to splitting forces P , as shown below:



Is given by:

$$\phi = \frac{Pa}{\pi z \sqrt{z^2 - a^2}}$$

where $z = x_1 + ix_2$ and P is a load per unit thickness.

Calculate the expressions of σ_{22} at $x_2 = 0$ and derive an expression for K_I . ($K_I = \frac{P}{\sqrt{\pi a}}$)

Hint:

(a) At crack tip $\frac{\eta}{a} \ll 1$

(b) $\eta = z - a = z = re^{i\theta}$

Solution

Find σ_{22}

In[125]:= `ClearAll[p, β, t, a, R, r, sigxx, sigxy, sigyy]`

In[126]:= `zz[x1_, x2_] := x1 + i * x2`

In[127]:= `φ[z_, P_, a_] := $\frac{P * a}{\pi * z \sqrt{z^2 - a^2}}$`

Apply the change of variables $z=\eta+a$.

In[128]:= `Simplify[With[{z = η + a}, Evaluate[$\frac{P * a}{\pi * z \sqrt{z^2 - a^2}}$]]]`

Out[128]=
$$\frac{a P}{\pi (a + \eta) \sqrt{\eta (2 a + \eta)}}$$

This can be expanded to:

$$\phi = \frac{a P}{\pi (a + \eta) \sqrt{2 a \eta + \eta^2}}$$

Since $\frac{\eta}{a} \ll 1$, we may drop the high order term η^2 . So now

$$\phi = \frac{a P}{\pi (a + \eta) \sqrt{2 a \eta}}$$

Lets make the substitution that $\eta = r e^{i\theta}$

In[129]:= `Simplify[With[{η = r * ei*θ}, Evaluate[$\frac{a P}{\pi (a + \eta) \sqrt{2 a * \eta}}$]]]`

Out[129]=
$$\frac{a P}{\sqrt{2} \pi \sqrt{a e^{i\theta} r} (a + e^{i\theta} r)}$$

This equation may be further simplified

$$\phi = \frac{a * P * e^{-i \frac{\theta}{2}}}{\pi (a + r * e^{i\theta}) \sqrt{2 a r}}$$

Now we may define the stress as follows:

In[130]:=
$$\text{stress}[r_ , \theta_ , P_ , a_] := \text{Re} \left[\frac{a * P * e^{-i \frac{\theta}{2}}}{\pi (a + r * e^{i \theta}) \sqrt{2 a r}} \right];$$

Simplify[stress[r, θ , P, a]]

Out[130]=
$$\frac{\text{Re} \left[\frac{a e^{-i \frac{\theta}{2}} P}{\sqrt{a r} (a + e^{i \theta} r)} \right]}{\sqrt{2} \pi}$$

Mathematica seems to need some help. Lets do some manual evaluation of terms.

In[131]:= **ComplexExpand**[Re[e^{-i $\frac{\theta}{2}$}]]

Out[131]=
$$\text{Cos} \left[\frac{\theta}{2} \right]$$

In[132]:= **ComplexExpand**[Re[r * e^{i θ}]]

Out[132]=
$$r \text{Cos}[\theta]$$

So now we can define stress as follows:

In[133]:=
$$\text{stress}[r_ , \theta_ , P_ , a_] := \frac{a * P * \text{Cos} \left[\frac{\theta}{2} \right]}{\pi (a + r * \text{Cos}[\theta]) \sqrt{2 a * r}};$$

Framed[**Simplify**[stress[r, θ , P, a]]]

Out[133]=
$$\frac{P \sqrt{a r} \text{Cos} \left[\frac{\theta}{2} \right]}{\sqrt{2} (a \pi r + \pi r^2 \text{Cos}[\theta])}$$

Find K_I

Now we can find the stress intensity factor! Let r and θ go to 0.

In[134]:=
$$K1[P_ , a_] := \text{Limit} \left[\sqrt{2 * \pi * r} \text{stress}[r, \theta, P, a], \{r \rightarrow 0\} \right];$$

Simplify[K1[P, a]]

Out[134]= Indeterminate

Lets take the 2 limits one at a time.

In[135]:= `Simplify[Limit[$\frac{\sqrt{2} * \pi * r * P \sqrt{a r} \text{Cos}[\frac{\theta}{2}]}{\sqrt{2} (a \pi r + \pi r^2 \text{Cos}[\theta])}$, $\theta \rightarrow \theta$]]]`

Out[135]=
$$\frac{P \sqrt{a r}}{\sqrt{\pi} \sqrt{r} (a + r)}$$

In[136]:= `Simplify[Limit[$\frac{P \sqrt{a r}}{\sqrt{\pi} \sqrt{r} (a + r)}$, $r \rightarrow \theta$]]]`

Out[136]= Indeterminate

Lets use L'Hopital's rule to simplify. Take the r derivative of the numerator and denominator.

In[137]:= `numer[P_, a_, r_] := D[P \sqrt{a * r}, {r, 1}]; Simplify[numer[P, a, r]]`

Out[137]=
$$\frac{a P}{2 \sqrt{a r}}$$

In[138]:= `denom[P_, a_, r_] := D[\sqrt{\pi} \sqrt{r} (a + r), {r, 1}]; Simplify[denom[P, a, r]]`

Out[138]=
$$\frac{\sqrt{\pi} (a + 3 r)}{2 \sqrt{r}}$$

In[139]:= `Simplify[$\frac{\text{numer}[P, a, r]}{\text{denom}[P, a, r]}$]`

Out[139]=
$$\frac{P \sqrt{a r}}{\sqrt{\pi} \sqrt{r} (a + 3 r)}$$

Alright, now lets cancel the \sqrt{r} in the numerator and denominator and take the limit:

In[140]:= `Framed[Simplify[Limit[$\frac{P \sqrt{a}}{(a + 3 * r) * \sqrt{\pi}}$, $r \rightarrow \theta$]]]`

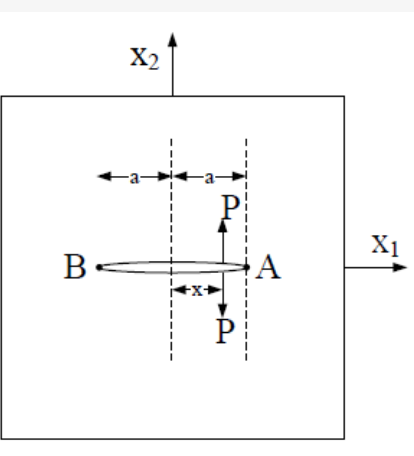
Out[140]=
$$\boxed{\frac{P}{\sqrt{a} \sqrt{\pi}}}$$

This is our stress intensity factor! It matches K_p

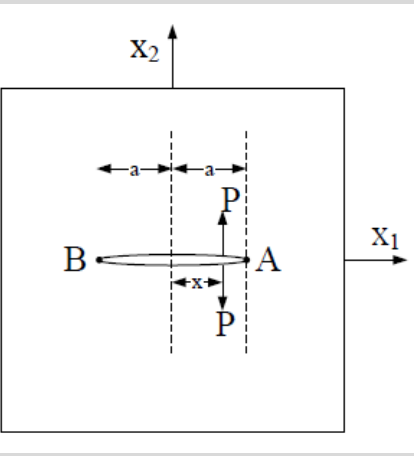
Problem 5

The stress intensity factor of the following problem:

In[141]:=



Out[141]=



is given by:

$$K_A = \frac{P}{\sqrt{\pi a}} \sqrt{\frac{a+x}{a-x}}$$

$$K_B = \frac{P}{\sqrt{\pi a}} \sqrt{\frac{a-x}{a+x}}$$

Based on those expressions, and results from the previous problem, determine the stress function Φ .

Solution

The stress intensity factors are related as follows:

$$K_I = K_A = K_B = \sqrt{2 \pi r} \sigma_{22}$$

The tensile stress may be related to the stress function as follows:

$$\sigma_{22} = \operatorname{Re}[\phi(z)] + x_2 \phi'(z) = \frac{K_I}{\sqrt{2\pi r}}$$

Using the right side of the crack, we may substitute $K_I = K_A$

$$\sigma_{22}^A = \frac{K_A}{\sqrt{2\pi r}} = \frac{P}{\sqrt{\pi a} \sqrt{2\pi r}} \sqrt{\frac{a+x}{a-x}} = \frac{P}{\pi \sqrt{2ar}} \sqrt{\frac{a+x}{a-x}}$$

And similarly for the left side where $K_I = K_B$

$$\sigma_{22}^B = \frac{K_B}{\sqrt{2\pi r}} = \frac{P}{\sqrt{\pi a} \sqrt{2\pi r}} \sqrt{\frac{a-x}{a+x}} = \frac{P}{\pi \sqrt{2ar}} \sqrt{\frac{a-x}{a+x}}$$

In this case, x_2 is zero. The tensile stress is also related to the stress intensity factors, so

$$\sigma_{22} = \operatorname{Re}[\phi(z)] = \frac{K_I}{\sqrt{2\pi r}}$$

For the relationship between stress and the stress function, x_2 is zero.

$$\sigma_{22} = \operatorname{Re}[\phi(z)]$$

And the complex function z may also be simplified because $\theta=0$.

$$z = r(\cos[\theta] + i\sin[\theta]) = r$$

Finally, upon simplification, the results are as follows.

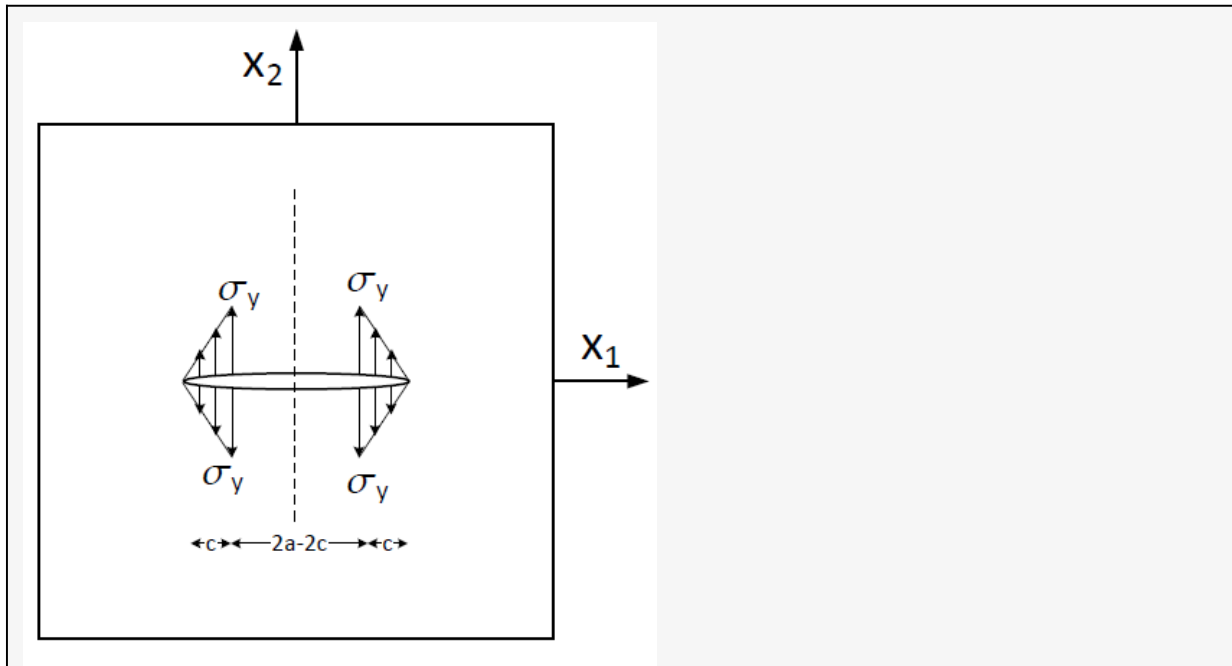
$$\phi^A(z) = \frac{P}{\pi \sqrt{2az}} \sqrt{\frac{a+x}{a-x}}$$

$$\phi^B(z) = \frac{P}{\pi \sqrt{2az}} \sqrt{\frac{a-x}{a+x}}$$

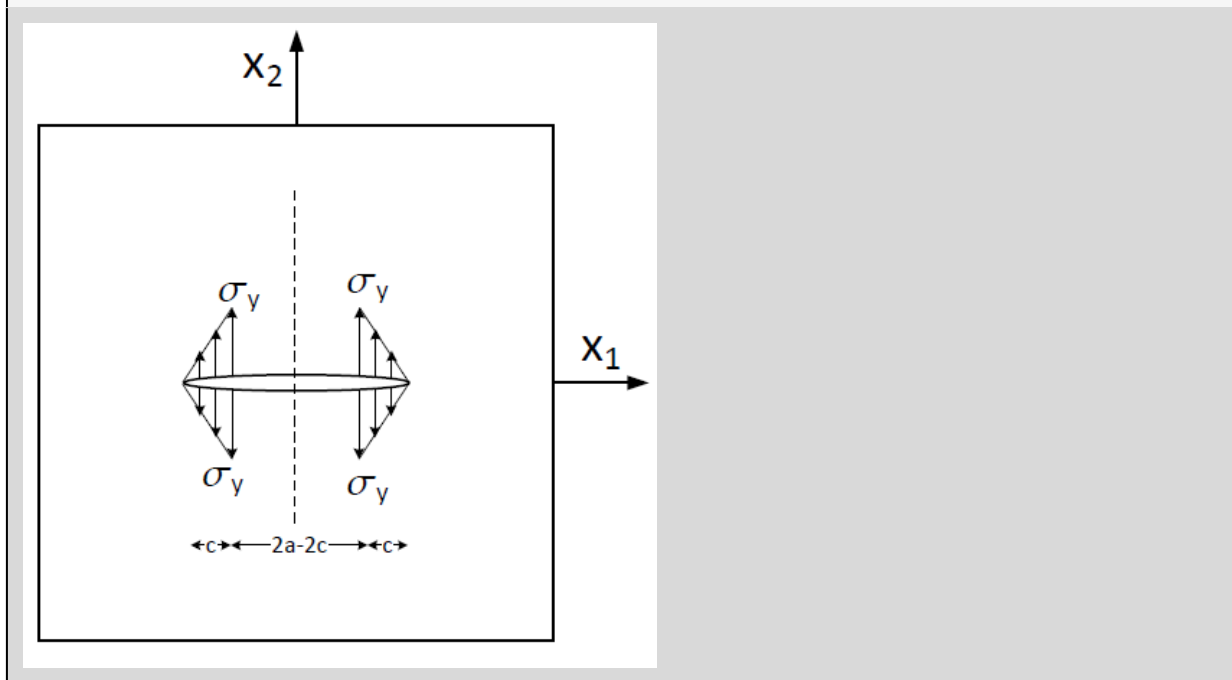
Problem 6

Barenblatt's model assumes a linearly varying closing pressure at the tip of a crack,

In[142]:=



Out[142]=



Using the expressions of K_A and K_B from the previous problem, determine an expression for the stress intensity factors for this case.

Solution

Before we only had the loads P acting on a single crack location. We can easily replace the stress distribution with the resultant load.

$$R = \frac{c * \sigma_y}{2}$$

These loads acts at the centroid of their respective distribution, which is $\frac{2}{3}c$ away from the crack tip. Replace P with R . Allow σ_y to equal y for convenience. We may replace the previous expressions of K_A and K_B as follows:

```
In[143]:= KA[a_, y_, c_] :=  $\frac{0.5 * y * c}{\sqrt{\pi * a}} \sqrt{\frac{a + (a - \frac{2}{3} c)}{a - (a - \frac{2}{3} c)}}$ ; Simplify[KA[a, y, c]]

KB[a_, y_, c_] :=  $\frac{0.5 * y * c}{\sqrt{\pi * a}} \sqrt{\frac{a - (-a + \frac{2}{3} c)}{a + (-a + \frac{2}{3} c)}}$ ;

Simplify[KB[a, y, c]]

Out[143]=  $\frac{0.282095 \sqrt{-1 + \frac{3a}{c}} c y}{\sqrt{a}}$ 

Out[144]=  $\frac{0.282095 \sqrt{-1 + \frac{3a}{c}} c y}{\sqrt{a}}$ 
```

We see here that the stress intensity factors are the same! We may clean this up, and the two factors together, and the final stress intensity factor is:

$$K_I = \frac{c * \sigma_y \sqrt{\frac{3a}{c} - 1}}{\sqrt{\pi * a}}$$

The stress intensity factors for both sides of the crack will be the same due to symmetry.

$$K = K_A = K_B$$

We may follow a similar approach to the method from the previous problem, except that the concentrated force P is replaced by a distribution. In order to determine the stress intensity factor we will need to integrate over the loaded crack length.

The distributed force can be defined as follows.

$$p(x) = \frac{P}{c} (a - x)$$

Replacing P with $p(x)$, we may integrate over the loaded crack lengths for K_A and K_B provided in the previous problem.

$$K = \int_{a-c}^a \frac{p(x)}{\sqrt{\pi a}} \sqrt{\frac{a+x}{a-x}} dx + \int_{a-c}^a \frac{p(x)}{\sqrt{\pi a}} \sqrt{\frac{a-x}{a+x}} dx$$

First, lets use a change of variables for $x^1 = a - x$. Now,

$$p(x^1) = \frac{Px^1}{c}$$

And the updated integral for K is

$$K = \int_{\theta}^c \frac{Px^1}{c \sqrt{\pi a}} \sqrt{\frac{2a-x^1}{x^1}} dx^1 + \int_{\theta}^c \frac{Px^1}{c \sqrt{\pi a}} \sqrt{\frac{x^1}{2a-x^1}} dx^1$$

$$K = \frac{P}{c \sqrt{\pi a}} \left[\int_{\theta}^c \left(\sqrt{\frac{2a-x^1}{x^1}} + \sqrt{\frac{x^1}{2a-x^1}} \right) x^1 dx^1 \right]$$

$$K = \frac{P}{c \sqrt{\pi a}} \int_{\theta}^c \sqrt{\frac{2 * a * x^1}{2 * a * x^1 - x^{12}}} dx^1$$

Finally, evaluate the integral. Lets just look at portion in the integral.

```
In[145]:= (*Kint[x_,c_,a_,P_] :=  $\frac{P}{c \sqrt{\pi a}}$  *Integrate[ $\sqrt{\frac{2 * a * x}{2 * a * x - x^2}}$ , {x,  $\theta$ , c}] *)
```

```
In[146]:= Int[x_, a_, c_] := Integrate[ $\sqrt{\frac{2 * a * x}{2 * a * x - x^2}}$ , x]; Simplify[Int[x, a, c]]
```

```
Out[146]=  $-\frac{2a}{\sqrt{\frac{a}{4a-2x}}}$ 
```

We may now evaluate the bounds of this integral and combine it with the other components of the expression for K to get

$$K = \frac{2aP}{c \sqrt{\pi a}} \left[2 - \left(\frac{a}{4a-2c} \right)^{\frac{1}{2}} \right]$$

There is likely further expansion and simplification to evaluate K in terms of inverse trigonometric functions, but we will stop here for now.

Homework 3

Thomas Allard
CVEN 7161

Answers are highlighted in a light blue background and are occasionally boxed.

Problem 1

A cylindrical pressure vessel of diameter 3 m and length 9 m, with closed ends, is to be constructed using butt-welded steel plates which are 0.03 m thick and approximately 1 m square. It must be designed to contain a pressure p without failure by yielding or by brittle fracture. Yield occurs when the equivalent tensile stress equals the yield stress, i.e., when:

$$(\sigma_1 - \sigma_2)^2 + (\sigma_2 - \sigma_3)^2 + (\sigma_3 - \sigma_1)^2 = 2 \sigma_y^2$$

The butt welds joining the plates are known to contain a thumbnail (semi-circular) cracks with a maximum depth of a . For such cracks $K_I = 1.128 \sigma \sqrt{\pi a}$ where σ is the tensile stress across a crack, and brittle failure will occur when $K_I \geq K_{Ic}$. Three steels are available for constructing the pressure vessel. Their yield strength and fracture toughnesses are:

In[1]:=

STEEL	σ_y (MPa)	$K_{Ic}(MNm^{-3/2})$
HY 140	965	280
T 1	690	180
HY 180	1240	180

Out[1]=

STEEL	σ_y (MPa)	$K_{Ic}(MNm^{-3/2})$
HY 140	965	280
T 1	690	180
HY 180	1240	180

Construct a plot of maximum pressure against crack depth a for each steel, showing the region of p and a which is safe against fracture and yielding. If non-destructive testing can detect cracks of depths $a_1 \geq 20$ mm (allowing welds with larger cracks than this to be repaired) which steel gives the greatest margin of safety? If a more refined technique will detect cracks of depth $a_1 \geq 2$ mm, which steel offers the greatest margin of safety? *Discuss* your results.

Solution

Yield criteria

```
In[2]:= ClearAll["Global'*"]
Clear[p, r, t, y]
```

For the state of biaxial stress induced by the hoop and longitudinal stresses, we need to find the pressure that causes yield. We will ignore radial stress as it is very small in comparison. Allow $\sigma_1 = \sigma_{\text{hoop}}$, $\sigma_2 = \sigma_{\text{long}}$, and $\sigma_3 = 0$.

```
In[4]:= 
$$\sigma_{\text{hoop}} = \frac{pr}{t}$$


$$\sigma_{\text{long}} = \frac{pr}{2t}$$

```

```
Out[4]= 
$$\frac{pr}{t}$$

```

```
Out[5]= 
$$\frac{pr}{2t}$$

```

Plugging $\sigma_1 = \sigma_{\text{hoop}}$, $\sigma_2 = \sigma_{\text{long}}$, and $\sigma_3 = 0$ into the provided yield criteria and solving for pressure p we get the following function which depends only on σ_y (here denoted “y”) since t and r are fixed.

```
In[6]:= yielding[p_, r_, t_, y_] := 
$$\left(\frac{p * r}{t} - \frac{p * r}{2 * t}\right)^2 + \left(\frac{p * r}{2 * t}\right)^2 + \left(-\frac{p * r}{t}\right)^2 - 2 y^2;$$

Simplify[yielding[p, r, t, y]]
```

```
Out[6]= 
$$\frac{3 p^2 r^2}{2 t^2} - 2 y^2$$

```

```
In[7]:= Solve[yielding[p, r, t, y] == 0, p]
```

```
Out[7]= 
$$\left\{ \left\{ p \rightarrow -\frac{2 t y}{\sqrt{3} r} \right\}, \left\{ p \rightarrow \frac{2 t y}{\sqrt{3} r} \right\} \right\}$$

```

Lets define the yield function as Pyield[y]

```
In[8]:= r = 1.500; (**)
t = .030; (**)
```

```
In[10]:= Pyield[y_] := 
$$\frac{2 * y * t}{r * \sqrt{3}};$$
 Simplify[Pyield[y]]
```

```
Out[10]= 0.023094 y
```

As expected, this results in only a linear dependence between a material's yield strength and the maximum pressure before yield.

Fracture Criteria

The expression for K_I can be solved for the applied tensile stress. In this case the tensile stress is the hoop stress. We may then solve for pressure p to come up with another max pressure criteria, but this one will also depend on the crack length a .

$$\sigma_{\text{hoop}} = \frac{K}{1.128 \sqrt{\pi a}} = \frac{pr}{t} \rightarrow p = \frac{K * t}{1.128 * r \sqrt{\pi a}}$$

```
In[11]:= Pfrac[K_, aa_] :=  $\frac{K * t}{1.128 * r * \sqrt{\pi * aa}}$ ; Simplify[Pfrac[K, aa]]
```

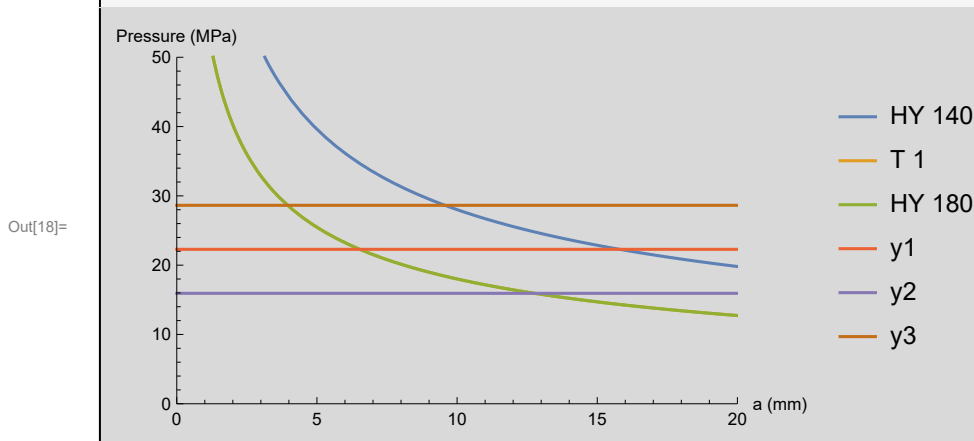
```
Out[11]=  $\frac{0.0100034 K}{\sqrt{aa}}$ 
```

Plots and analysis

We may now plot the pressure associated with crack growth against crack length a . We may also plot the pressure associated with yield.

```
In[12]:= y1 = 965 * 106; (*Pa*)
y2 = 690 * 106; (*Pa*)
y3 = 1240 * 106; (*Pa*)
k1 = 280 * 106; (*N*m-3/2*)
k2 = 180 * 106; (*N*m-3/2*)
k3 = 180 * 106; (*N*m-3/2*)
```

```
In[18]:= Plot[{Pfrac[k1, a / 1000] / 106, Pfrac[k2, a / 1000] / 106,
  Pfrac[k3, a / 1000] / 106, Pyield[y1] / 106, Pyield[y2] / 106, Pyield[y3] / 106},
  {a, 0.0, 20}, PlotLegends -> {"HY 140", "T 1", "HY 180", "y1", "y2", "y3"},
  AxesLabel -> {"a (mm)", "Pressure (MPa)"}, PlotRange -> {{0, 20}, {0, 50}}
```



For each material, we may create an envelope that gives the minimum allowable pressure depending on if yielding or fracture is more likely.

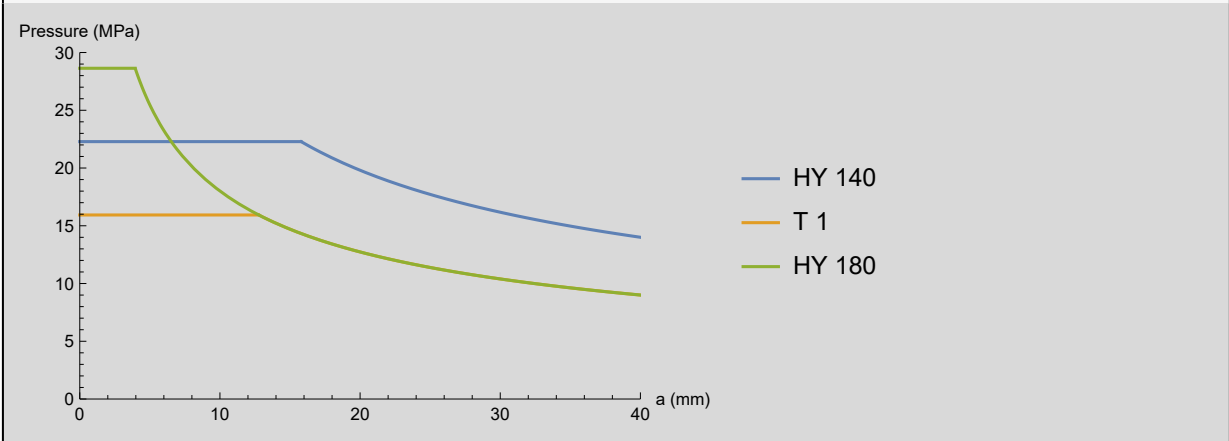
In[19]=

```

envelope1[aa_] := Min[Pfrac[k1, aa], Pyield[y1]]
envelope2[aa_] := Min[Pfrac[k2, aa], Pyield[y2]]
envelope3[aa_] := Min[Pfrac[k3, aa], Pyield[y3]]
Plot[{envelope1[a / 1000] / 106, envelope2[a / 1000] / 106, envelope3[a / 1000] / 106},
{a, 0, 40}, PlotRange -> {{0, 40}, {0, 30}}, AxesLabel -> {"a (mm)", "Pressure (MPa)"},
PlotLegends -> {"HY 140", "T 1", "HY 180"}]

```

Out[22]=



For each material, there are two stages of the maximum pressure curves corresponding to failure of the pressure vessel. The initial flat portion of these envelopes corresponds to yielding. The descending branch corresponds to fracture. As crack length “a” increases, the maximum allowable pressure dramatically decreases.

$a_1 \geq 20 \text{ mm}$

According to these results, the only difference between the materials T 1 and HY 180 is their yield limit for cracks smaller than about 12mm. They have the same fracture criteria. Considering that only cracks of 20mm and larger can be determined, we can find the maximum allowable pressure for each material.

In[23]=

```

Framed[envelope1[20 / 1000] / 106]
envelope2[20 / 1000] / 106
envelope3[20 / 1000] / 106

```

Out[23]=

19.8056

Out[24]=

12.7322

Out[25]=

12.7322

Clearly the first material, HY 140, has the greatest margin of safety since the maximum allowable pressure for cracks of 20mm is higher than that of the other materials.

$a_1 \geq 2 \text{ mm}$

The results of this analysis will be the same as the previous case where **HY 140** will be the best. This is

obvious by looking at the most recent plot. We may calculate the max pressures associated with cracks of 2mm.

In[26]=

```
envelope1[2 / 1000] / 106  
envelope2[2 / 1000] / 106  
Framed[envelope3[2 / 1000] / 106]
```

Out[26]=

22.2857

Out[27]=

15.9349

Out[28]=

28.6366

Now we see that the **HY 180** material has the greatest margin of safety!

Problem 2

Design (by selecting the most economical material and the thickness t) a high strength steel pressure vessel which must withstand 5,000 psi of internal pressure p , the nominal diameter d is 30 in., and the wall thickness t must be greater than 0.5 in.

The steels available for use are:

In[29]=

Steel	σ_{ys} (Ksi)	K_{Ic} Ksi $\sqrt{\text{in}}$	Cost \$/lb
A	260	80	1.40
B	220	110	1.40
C	180	140	1.00
D	180	220	1.20
E	140	260	0.50
F	110	170	0.15

Out[29]=

Steel	σ_{ys} (Ksi)	K_{Ic} Ksi $\sqrt{\text{in}}$	Cost \$/lb
A	260	80	1.40
B	220	110	1.40
C	180	140	1.00
D	180	220	1.20
E	140	260	0.50
F	110	170	0.15

Assume that inspection procedures dictate a surface (elliptical) flaw with a depth b of 0.5 inch and $b/2a=0.25$; Assume a factor of safety of two for both the design stress (vs yield stress) and the stress intensity factor (vs the fracture toughness). Make sure to check for fracture failure and yielding of the section.

Solution

We will check both the yielding and fracture criteria separately. We will calculate the minimum thickness required for each material for each criteria. Since the global dimensions of the vessel will only differ between different material designs by the thickness, the cost per pound can be multiplied by the plate thickness to come up with a value we want minimized, thus giving the most cost effective design.

In[30]=

```
Clear [p, r, t, y]
```

1. Stress

We may use the same yield criteria as the previous problem in which $\sigma_1 = \sigma_{\text{hoop}}$, $\sigma_2 = \sigma_{\text{long}}$, and $\sigma_3 = 0$. This time the thickness “ t ” is unknown. We will solve for the yield stress this time.


```
In[31]:= yielding[p_, r_, t_, y_] :=  $\left(\frac{p * r}{t} - \frac{p * r}{2 * t}\right)^2 + \left(\frac{p * r}{2 * t}\right)^2 + \left(-\frac{p * r}{t}\right)^2 - 2 y^2;$ 
Solve[yielding[p, r, t, y] == 0, y]
```

```
Out[31]:=  $\left\{\left\{y \rightarrow -\frac{\sqrt{3} p r}{2 t}\right\}, \left\{y \rightarrow \frac{\sqrt{3} p r}{2 t}\right\}\right\}$ 
```

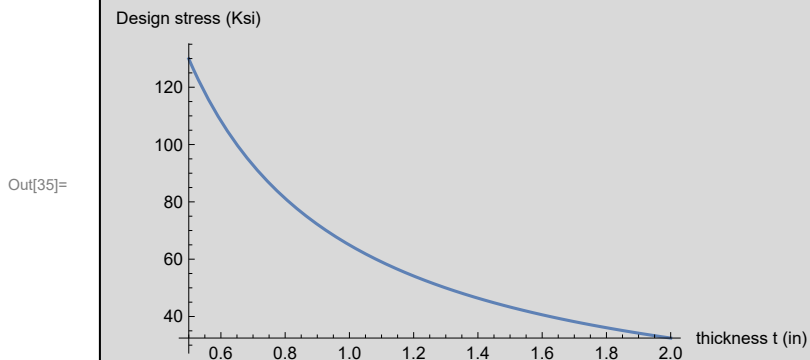
Now we will define the max design stress as:

```
In[32]:= p = 5000; (*psi*)
r = 15; (*inches*)
```

```
In[34]:=  $\sigma[t_] := \frac{p * r * \sqrt{3}}{2 * t};$  Simplify[ $\sigma[t]$ ]
```

```
Out[34]:=  $\frac{37500 \sqrt{3}}{t}$ 
```

```
In[35]:= Plot[{Evaluate[ $\sigma[t]$ ] / 1000}, {t, 0.5, 2},
AxesLabel -> {"thickness t (in)", "Design stress (Ksi)"}]
```



Define the yield stress for each material:

```
In[36]:= yA = 260 * 103; (*psi*)
yB = 220 * 103; (*psi*)
yC = 180 * 103; (*psi*)
yD = 180 * 103; (*psi*)
yE = 140 * 103; (*psi*)
yF = 110 * 103; (*psi*)
```

As can be seen in the figure above, comparing with yield strengths in the provided table, we see that some materials will be unable to be used for $t = 0.5$. We may calculate the minimum thickness required for each material by substituting the max allowable design stress ($0.5 * \sigma_{ys}$) and solving for thickness, t .

```
In[42]:=
tAS = NSolve[ $\sigma[t] - 0.5 * yA == 0, t]$ 
tBS = NSolve[ $\sigma[t] - 0.5 * yB == 0, t]$ 
tCS = NSolve[ $\sigma[t] - 0.5 * yC == 0, t]$ 
tDS = NSolve[ $\sigma[t] - 0.5 * yD == 0, t]$ 
tES = NSolve[ $\sigma[t] - 0.5 * yE == 0, t]$ 
tFS = NSolve[ $\sigma[t] - 0.5 * yF == 0, t]$ 
```

```
Out[42]=
{{t → 0.49963}}
```

```
Out[43]=
{{t → 0.590472}}
```

```
Out[44]=
{{t → 0.721688}}
```

```
Out[45]=
{{t → 0.721688}}
```

```
Out[46]=
{{t → 0.927884}}
```

```
Out[47]=
{{t → 1.18094}}
```

Lets define the cost per pound for each material

```
In[48]:=
costA = 1.4; (*$/lb*)
costB = 1.4; (*$/lb*)
costC = 1.0; (*$/lb*)
costD = 1.2; (*$/lb*)
costE = 0.5; (*$/lb*)
costF = 0.15; (*$/lb*)
```

Since all geometric parameters are fixed except for thickness, we do not need to calculate the weight of the proposed design for each material. We may simply calculate a cost metric for each material as follows.

In[54]:=

```

CA1 = t * costA / . tAS[[1]]
CB1 = t * costB / . tBS[[1]]
CC1 = t * costC / . tCS[[1]]
CD1 = t * costD / . tDS[[1]]
CE1 = t * costE / . tES[[1]]
CF1 = t * costF / . tFS[[1]]

```

Out[54]=

0.699482

Out[55]=

0.826661

Out[56]=

0.721688

Out[57]=

0.866025

Out[58]=

0.463942

Out[59]=

0.177142

We will wait to make a design decision until both yield and fracture criteria have been addressed.

2. Fracture

For this problem, we will use The Newman and Raju 1981 empirical SIF equation. For this case with $b/2a = 0.25$, we have a ratio $b/a = 0.5$. First, calculate the factors $M1$, $M2$, and $M3$ since they are the same regardless of material.

In[60]:=

```

ba = 0.5;
b = 0.5;
M1 = 1.13 - 0.09 * ba;
M2 = 0.89 * (0.2 + ba)-1 - 0.54;
M3 = 0.5 - (0.65 + ba)-1 + 14 * (1 - ba)24;

```

Now we may define the stress intensity factor as a function of the design thickness t and angle θ according to Newman & Raju.

In[65]=

```

part1[t_] :=  $\frac{p * r}{t} \sqrt{\pi * b}$ ;
part2[t_] :=  $\left( M1 + M2 \left( \frac{b}{t} \right)^2 + M3 \left( \frac{b}{t} \right)^4 \right) * (1 + 1.464 ba^{1.65})^{-0.5}$ ;
part3[t_,  $\theta$ ] :=  $(ba^2 \text{Cos}[\theta]^2 + \text{Sin}[\theta]^2)^{0.25}$ ;
part4[t_,  $\theta$ ] :=  $\left( 1 + \left( 0.1 + 0.35 \left( \frac{b}{t} \right)^2 \right) (1 - \text{Sin}[\theta])^2 \right)$ ;
K[t_,  $\theta$ ] := part1[t] * part2[t] * part3[t,  $\theta$ ] * part4[t,  $\theta$ ];
Simplify[K[t,  $\theta$ ]]

```

Out[70]=

$$\frac{1}{t} 77621.5 \times \left(1.085 - \frac{0.0230978}{t^4} + \frac{0.182857}{t^2} \right) \times \left(1 + \left(0.1 + \frac{0.0875}{t^2} \right) (-1 + \text{Sin}[\theta])^2 \right) (0.25 \text{Cos}[\theta]^2 + \text{Sin}[\theta]^2)^{0.25}$$

For the sake of comparison, we may investigate a reduced form of the Newman and Raju equation for $\frac{b}{a} \approx 0.25$. We shouldn't expect this relationship to hold for our case since $\frac{b}{a} = 0.5$.

In[71]=

```

Kk[t_] := 1.13 *  $\frac{p * r}{t} * \sqrt{\pi * b} * (1 - 0.08 * ba) * (1 + 1.464 * ba^{1.65})^{-0.5}$ 

```

The reduced relationship does not depend on θ , while the Newman & Raju form does. We are interested in the maximum stress intensity factors which will occur at $\theta = \frac{\pi}{2}$. Lets plot the two approaches.

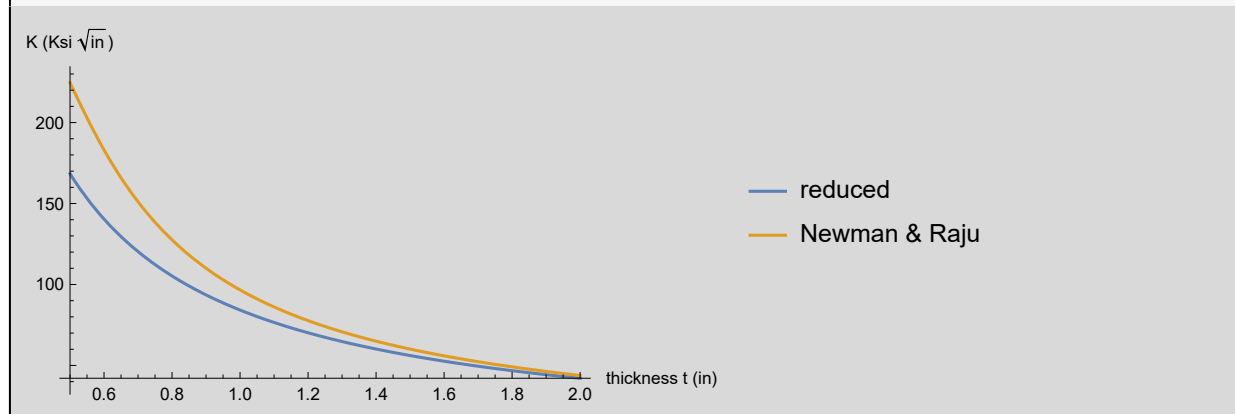
In[72]=

```

Plot[{{Evaluate[Kk[t]] / 1000, With[{ $\theta = \frac{\pi}{2}$ }, Evaluate[K[t,  $\theta$ ] / 1000]}},
{t, 0.5, 2}, AxesLabel -> {"thickness t (in)", "K (Ksi  $\sqrt{\text{in}}$ )"},
PlotLegends -> {"reduced", "Newman & Raju"}}]

```

Out[72]=



Here we see that the reduced form does not agree with the Newman & Raju equation and under estimates the stress intensity factor! We will use the Newman & Raju system. Now lets find the minimum thickness for each steel to meet fracture criteria.

```
In[73]:=
kA = 80 * 103; (*psi sqrt[in *]
kB = 110 * 103; (*psi sqrt[in *]
kC = 140 * 103; (*psi sqrt[in *]
kD = 220 * 103; (*psi sqrt[in *]
kE = 260 * 103; (*psi sqrt[in *]
kF = 170 * 103; (*psi sqrt[in *]
```

```
In[79]:=
tAK = NSolve[K[t,  $\frac{\pi}{2}$ ] - 0.5 * kA == 0, t]
tBK = NSolve[K[t,  $\frac{\pi}{2}$ ] - 0.5 * kB == 0, t]
tCK = NSolve[K[t,  $\frac{\pi}{2}$ ] - 0.5 * kC == 0, t]
tDK = NSolve[K[t,  $\frac{\pi}{2}$ ] - 0.5 * kD == 0, t]
tEK = NSolve[K[t,  $\frac{\pi}{2}$ ] - 0.5 * kE == 0, t]
tFK = NSolve[K[t,  $\frac{\pi}{2}$ ] - 0.5 * kF == 0, t]
```

```
Out[79]=
{{t → 2.17827}, {t → -0.0414279 - 0.492018 i},
 {t → -0.0414279 + 0.492018 i}, {t → 0.295594}, {t → -0.285531}}
```

```
Out[80]=
{{t → 1.62438}, {t → -0.0535194 - 0.484202 i},
 {t → -0.0535194 + 0.484202 i}, {t → 0.297837}, {t → -0.28392}}
```

```
Out[81]=
{{t → 1.31225}, {t → -0.0634828 - 0.475603 i},
 {t → -0.0634828 + 0.475603 i}, {t → 0.300229}, {t → -0.282377}}
```

```
Out[82]=
{{t → 0.900071}, {t → -0.0817002 - 0.452464 i},
 {t → -0.0817002 + 0.452464 i}, {t → 0.307516}, {t → -0.278556}}
```

```
Out[83]=
{{t → 0.787924}, {t → -0.0875518 - 0.441753 i},
 {t → -0.0875518 + 0.441753 i}, {t → 0.311807}, {t → -0.276787}}
```

```
Out[84]=
{{t → 1.11205}, {t → -0.0715652 - 0.466782 i},
 {t → -0.0715652 + 0.466782 i}, {t → 0.302791}, {t → -0.280896}}
```

Similar to what was done for stress based minimum thickness, we may define a cost metric based on the maximum allowable stress intensity factor as follows:

In[85]=

```

CA2 = t * costA / . tAK[[1]]
CB2 = t * costB / . tBK[[1]]
CC2 = t * costC / . tCK[[1]]
CD2 = t * costD / . tDK[[1]]
CE2 = t * costE / . tEK[[1]]
CF2 = t * costF / . tFK[[1]]

```

Out[85]=

3.04958

Out[86]=

2.27413

Out[87]=

1.31225

Out[88]=

1.08008

Out[89]=

0.393962

Out[90]=

0.166808

Select best material

The best material and design will be based on the material with the lowest cost metric. We must only look at the cost metric associated with a thickness that passes both criteria for a material.

In[91]=

```

Framed [Min [Max [CA1, CA2], Max [CB1, CB2],
  Max [CC1, CC2], Max [CD1, CD2], Max [CE1, CE2], Max [CF1, CF2] ] ]

```

Out[91]=

0.177142

The material that meets all of the criteria and has the lowest cost is **material F**. The wall thickness is limited by the yield strength and requires a thickness of at least 1.11 inches.

Problem 3

Repeat the beer barrel problem discussed in class, by determining the reliability index assuming that we have:

Variable	Mean	Standard Deviation
$2a$ (in)	3.5	0.2
b (in)	0.05	0.01
p (psi)	600	20
K_{Ic} ksi $\sqrt{\text{in}}$	40	5

In[92]=

Variable	Mean	Standard Deviation
$2a$ (in)	3.5	0.2
b (in)	0.05	0.01
p (psi)	600	20
K_{Ic} ksi $\sqrt{\text{in}}$	40	5

Out[92]=

A small beer barrel of diameter 15" and wall thickness of 0.126" made of aluminum alloy exploded when a pressure reduction valve malfunctioned and the barrel experienced the 610 psi full pressure of the CO2 cylinder supplying it with gas. Afterwards, cracks approximately 4.0 inch long by (probably) 0.07 inch deep were discovered on the inside of the salvaged pieces of the barrel. Independent tests gave 40 ksi $\sqrt{\text{in}}$ for K_{Ic} of the aluminum alloy.

The question is whether the cracks were critical for the 610 psi of pressure?

Hint: try to understand and implement the code given in the assignment.

Solution

This problem was solved using a matlab code which is [attached at the end of this assignment](#). The likelihood of failure is estimated by randomly sampling the crack length "a", the crack depth "b", the pressure "p," and the critical stress intensity factor " K_{Ic} " on normal distributions characterized by the mean and standard deviations given in the provided table. The capacity is compared to the demand and a reliability index "beta" and probability of failure is determined. This analysis was conducted for sample sizes of 10^n where n is {3,4,5}. A summary of these calculations is provided below.

n=3: **beta: 3.387822**; probability of failure; 5.800000e-02; 3.522503e-04

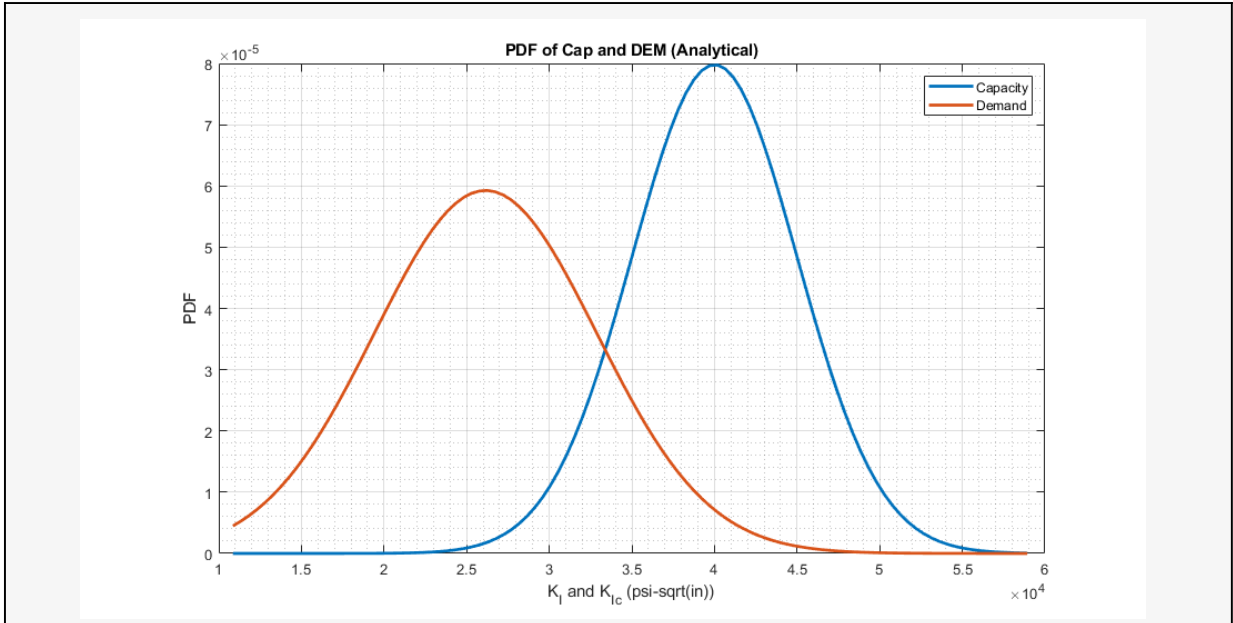
n=4: **beta: 3.364352**; probability of failure; 5.840000e-02; 3.836174e-04

n=5: **beta: 3.326491**; probability of failure; 5.843000e-02; 4.397344e-04

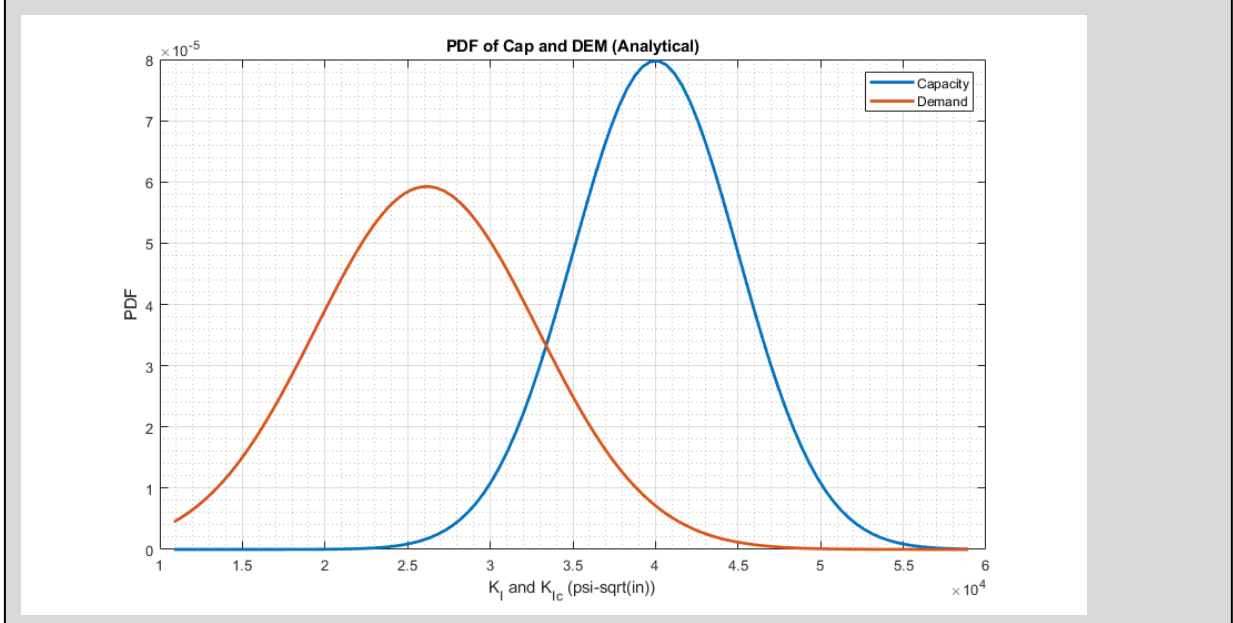
We see that the results are in good agreement for each case with a beta of 3.33 calculated for n=5 with a corresponding probability of failure of 5.843%. Here are the resulting probability density functions for an approximate normal distribution and the real data. The PDF for the fit data is pretty much identical for each case, so only the one for n=3 will be shown.

n=3

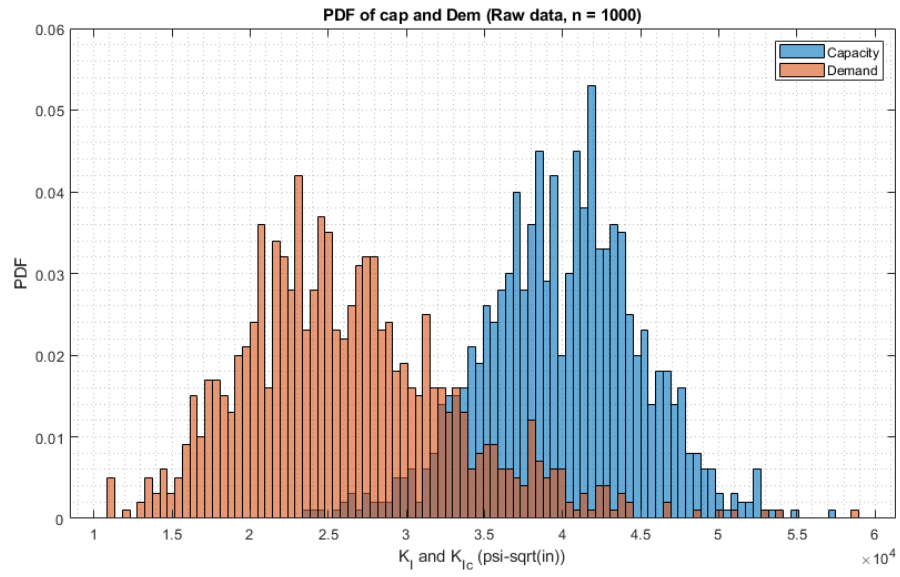
In[93]=



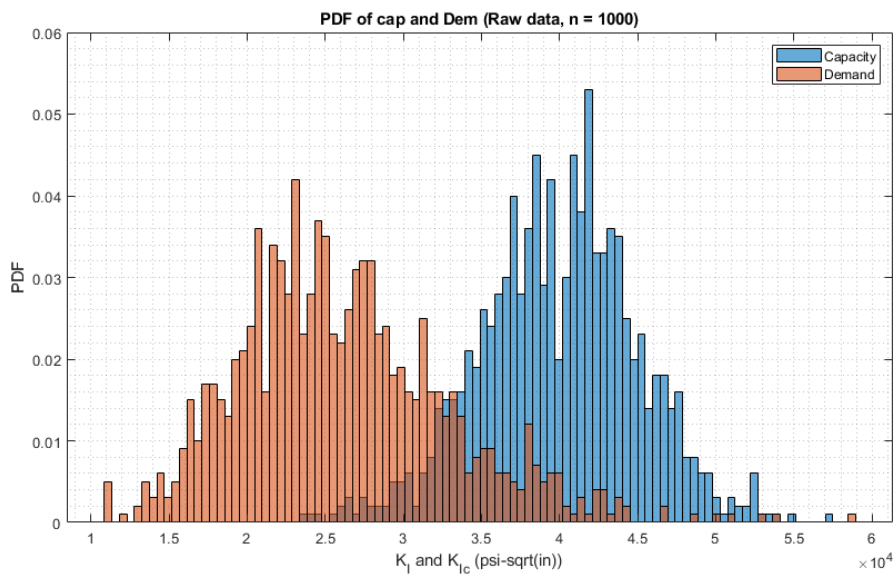
Out[93]=



In[94]:=

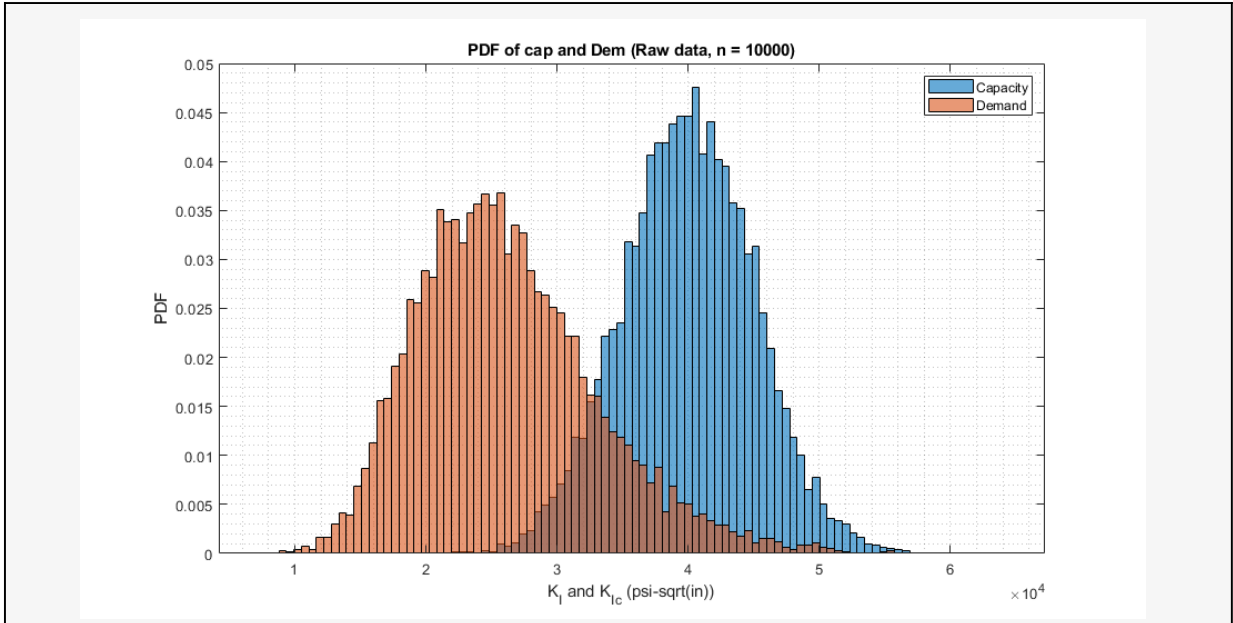


Out[94]=

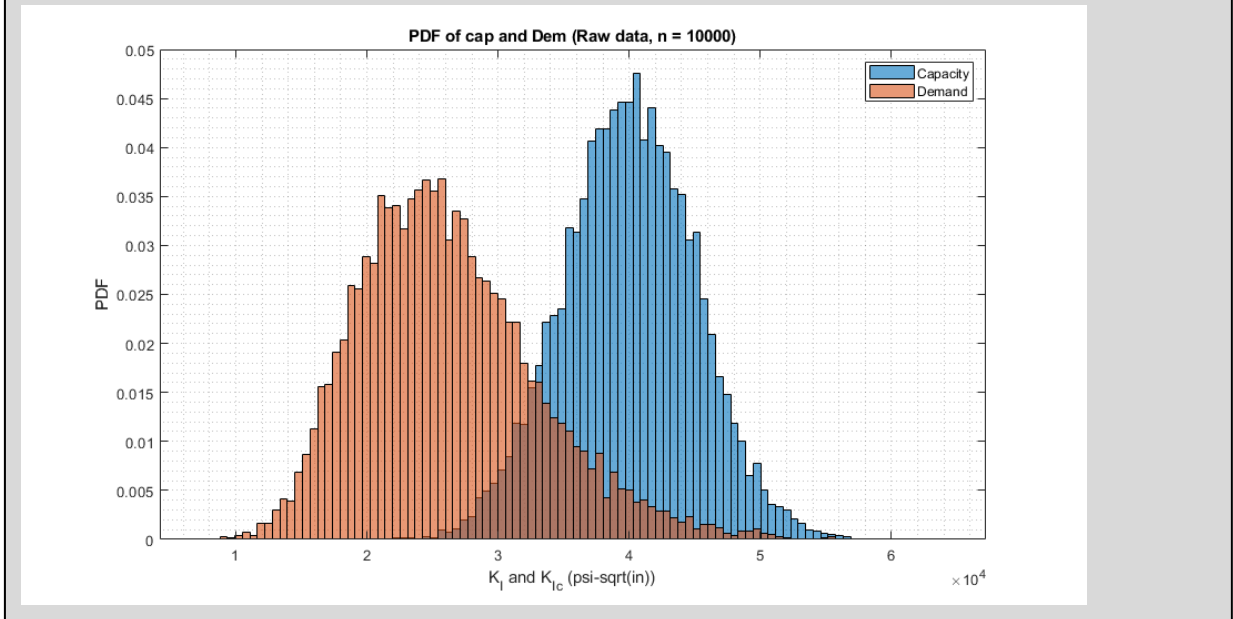


n = 4

In[95]=

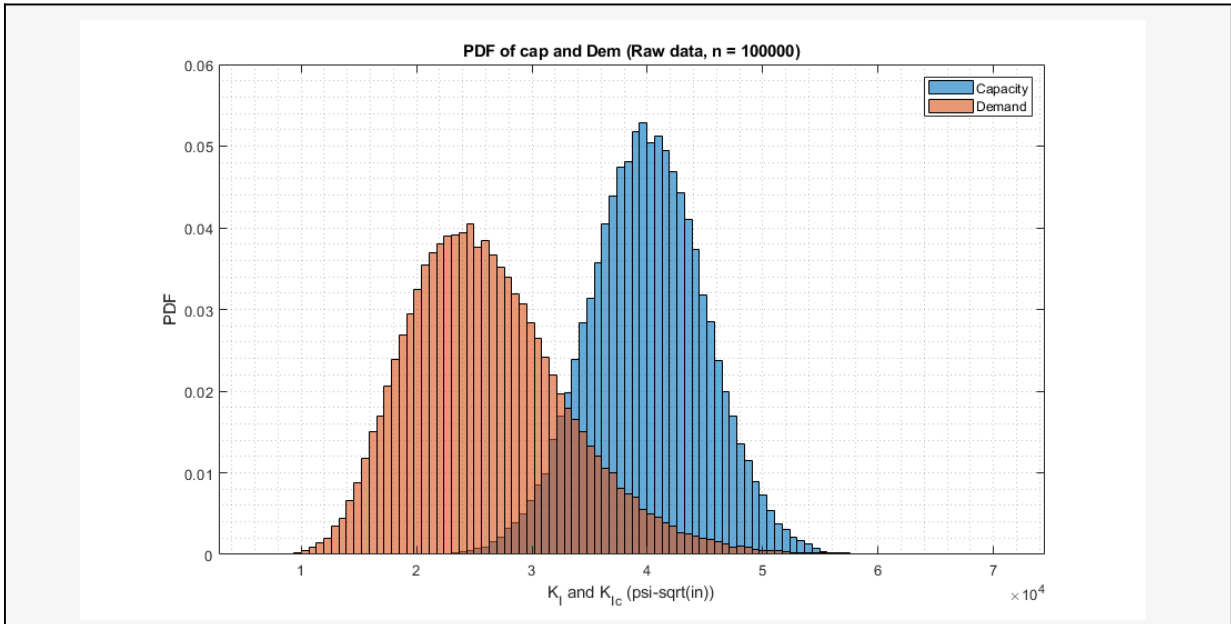


Out[95]=

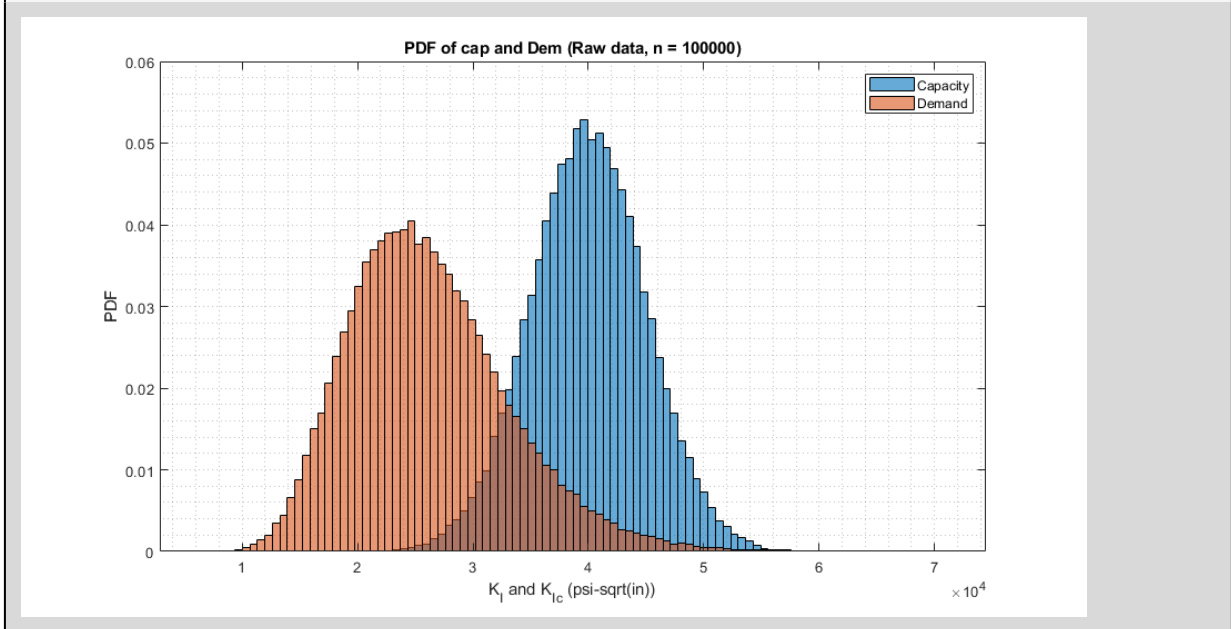


n=5

In[96]:=



Out[96]=



As can be seen, as the number of samples increase, the smoother the plots become.

Problem 4

Determine the residual strength diagram (crack size versus residual strength) in terms of a for longitudinal surface flaws for both embedded and surface cracks with $\frac{b}{a} = 1$ and $\frac{b}{a} = 0.3$ in a pressurized cylinder 10 inch diameter with a wall thickness of 0.5 inch; assume $K_{1c} = 35 \text{ ksi} \sqrt{\text{in}}$, $\sigma_y = 70 \text{ ksi}$. Use Newman's equation.

Solution - Surface Crack

```
In[97]:= Clear[p, r, t, y, b, ba, M1, M2, M3, σ]
```

```
In[98]:= (*ba = 0.5; MAKE THINGS A FUNCTION OF THIS*)
(*b = 0.5;*)
r = 5; (*in*)
t = 0.5; (*in*)
M1[ba_] := 1.13 - 0.09 * ba;
M2[ba_] := 0.89 * (0.2 + ba)^-1 - 0.54;
M3[ba_] := 0.5 - (0.65 + ba)^-1 + 14 * (1 - ba)^24;
```

```
In[103]:= part1[ba_, a_, p_] := (p * r / t) * Sqrt[π * ba * a];
part2[ba_, a_] :=
  (M1[ba] + M2[ba] * (ba * a / t)^2 + M3[ba] * (ba * a / t)^4) * (1 + 1.464 ba^1.65)^-0.5;
part3[ba_, θ_] := (ba^2 Cos[θ]^2 + Sin[θ]^2)^0.25;
part4[ba_, a_, θ_] := (1 + (0.1 + 0.35 (ba * a / t)^2) (1 - Sin[θ])^2);
K[ba_, a_, p_, θ_] := part1[ba, a, p] * part2[ba, a] * part3[ba, θ] * part4[ba, a, θ];
Simplify[K[ba, a, p, θ]]
```

```
Out[108]:= (1 / (1 + 1.464 ba^1.65)^0.5) 17.7245 Sqrt[a ba]
(1.13 - 0.09 ba + 4. a^2 ba^2 (-0.54 + (0.89 / (0.2 + ba))) + 16. a^4 ba^4 (0.5 + 14 (-1 + ba)^24 - (1. / (0.65 + ba))))
p (1 + 1.4 * (0.0714286 + 1. a^2 ba^2) (-1. + Sin[θ])^2) (ba^2 Cos[θ]^2 + Sin[θ]^2)^0.25
```

We will check for the maximum K at $\theta = 0$ and $\theta = \frac{\pi}{2}$. Lets look at $\theta = \frac{\pi}{2}$ first.

$$\theta = \frac{\pi}{2}$$

In[109]:=

Simplify[K[ba, a, p, $\frac{\pi}{2}$]]

Out[109]=

$$\frac{1}{(1 + 1.464 ba^{1.65})^{0.5}} 17.7245 \sqrt{a ba} \left(1.13 - 0.09 ba + 4. a^2 ba^2 \left(-0.54 + \frac{0.89}{0.2 + ba} \right) + 16. a^4 ba^4 \left(0.5 + 14 (-1 + ba)^{24} - \frac{1.}{0.65 + ba} \right) \right) p$$

Now divide the stress intensity factor by K_{Ic} to establish a residual strength and solve for p.

In[110]:=

KIc = 35 * 10³; (*psi sqrt(in *)

newK[ba_, a_, p_] := K[ba, a, p, $\frac{\pi}{2}$]/ KIc; Simplify[newK[ba, a, p]]

Out[111]=

$$\frac{1}{(1 + 1.464 ba^{1.65})^{0.5}} 0.000506415 \sqrt{a ba} \left(1.13 - 0.09 ba + 4. a^2 ba^2 \left(-0.54 + \frac{0.89}{0.2 + ba} \right) + 16. a^4 ba^4 \left(0.5 + 14 (-1 + ba)^{24} - \frac{1.}{0.65 + ba} \right) \right) p$$

Although this equation looks complicated, we must simply solve for p. Since we have divided K/K_{Ic}, we want to know p when this ratio equals 1.

In[112]:=

pK[ba_, a_] :=

$$\left((1 + 1.464 * ba^{1.65})^{0.5} \right) / \left(0.0005064153859730045 * \sqrt{a * ba} \left(1.13 - 0.09 * ba + 4. * a^2 * ba^2 \left(-0.54 + \frac{0.89}{0.2 + ba} \right) + 16. * a^4 * ba^4 \left(0.5 + 14 (-1 + ba)^{24} - \frac{1.}{0.65 + ba} \right) \right) \right);$$

Simplify[

**pK[
ba,
a]**

Out[113]=

$$\frac{1974.66 (1 + 1.464 ba^{1.65})^{0.5}}{\sqrt{a ba} \left(1.13 - 0.09 ba + 4. a^2 ba^2 \left(-0.54 + \frac{0.89}{0.2 + ba} \right) + 16. a^4 ba^4 \left(0.5 + 14 (-1 + ba)^{24} - \frac{1.}{0.65 + ba} \right) \right)}$$

The stress will be calculated using the same equation as for problem 2.

In[114]:=

$\sigma[p] := \frac{p * r * \sqrt{3}}{2 * t}$; Simplify[$\sigma[p]$]

Out[114]=

8.66025 p

We will plug in the expression for p into the previous equation to determine allowable strength versus crack size.

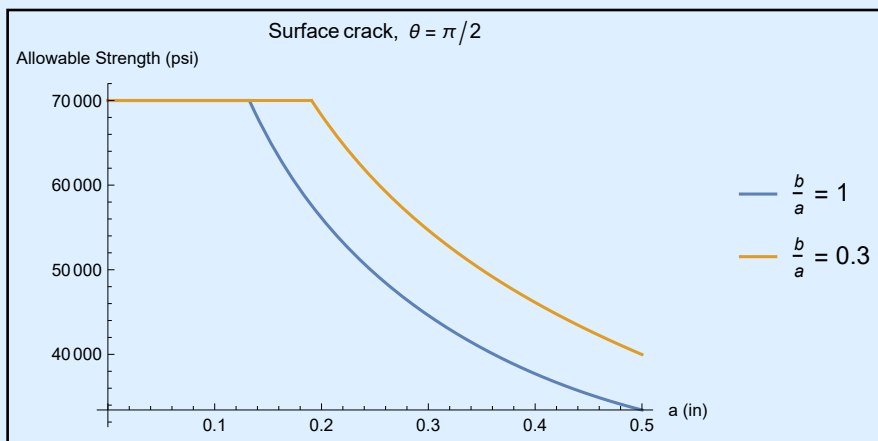
In[115]:= **sigy = 70 * 10³; (*psi*)**

Now establish envelopes for the two cases where $\frac{b}{a} = 1$ and $\frac{b}{a} = 0.3$.

In[116]:= **env1[a_] := Min[8.66025 * pK[1, a], sigy];**
env2[a_] := Min[8.66025 * pK[0.3, a], sigy];

In[118]:= **Framed[Plot[{env1[a], env2[a]}, {a, 0, 0.5},**
AxesLabel → {"a (in)", "Allowable Strength (psi)"},
PlotLegends → {" $\frac{b}{a} = 1$ ", " $\frac{b}{a} = 0.3$ "}, PlotLabel → "Surface crack, $\theta = \pi / 2$ "]]

Out[118]=



In[119]:= **$\theta = 0$**

Out[119]=

θ

In[120]:= **Simplify[K[ba, a, p, θ]]**

Out[120]=

$$\frac{1}{(1 + 1.464 ba^{1.65})^{0.5}} 17.7245 \sqrt{a ba} (ba^2)^{0.25} (1.1 + 1.4 a^2 ba^2) \times \left(1.13 - 0.09 ba + 4. a^2 ba^2 \left(-0.54 + \frac{0.89}{0.2 + ba} \right) + 16. a^4 ba^4 \left(0.5 + 14 (-1 + ba)^{24} - \frac{1.}{0.65 + ba} \right) \right) p$$

Now divide the stress intensity factor by K_{Ic} to establish a residual strength and solve for p.

In[121]:= **newK2[ba_, a_, p_] := K[ba, a, p, θ] / K1c; Simplify[newK2[ba, a, p]]**

Out[121]=

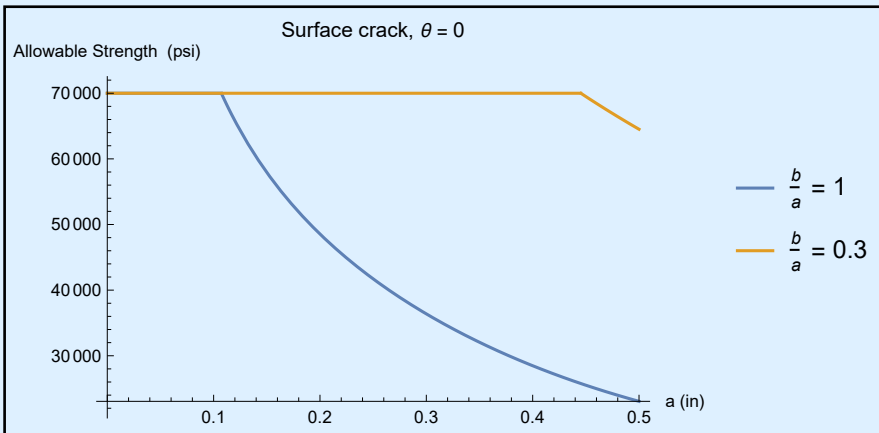
$$\frac{1}{(1 + 1.464 ba^{1.65})^{0.5}} 0.000506415 \sqrt{a ba} (ba^2)^{0.25} (1.1 + 1.4 a^2 ba^2) \times \left(1.13 - 0.09 ba + 4. a^2 ba^2 \left(-0.54 + \frac{0.89}{0.2 + ba} \right) + 16. a^4 ba^4 \left(0.5 + 14 (-1 + ba)^{24} - \frac{1.}{0.65 + ba} \right) \right) p$$

Solve for p as we did for $\theta = \frac{\pi}{2}$. Since we have divided K/K_{Ic}, we want to know p when this ratio equals 1.

```
In[122]:= pK2[ba_, a_] :=
  (1 + 1.464 * ba1.65)0.5 / (0.0005064153859730045 * sqrt(a * ba) (ba2)0.25 (1.1 + 1.4 * a2 * ba2) *
  (1.13 - 0.09 * ba + 4.0 * a2 * ba2 (-0.54 +  $\frac{0.89}{0.2 + ba}$ ) + 16.0 *
  a4 * ba4 (0.5 + 14 * (-1 + ba)24 -  $\frac{1.}{0.65 + ba}$ )));
Simplify[
  pK2[
    ba,
    a]]
Out[123]:= (1974.66 (1 + 1.464 ba1.65)0.5) / (sqrt(a ba) (ba2)0.25 (1.1 + 1.4 a2 ba2) *
  (1.13 - 0.09 ba + 4. a2 ba2 (-0.54 +  $\frac{0.89}{0.2 + ba}$ ) + 16. a4 ba4 (0.5 + 14 (-1 + ba)24 -  $\frac{1.}{0.65 + ba}$ )))
```

Just like before, establish envelopes for the two cases where $\frac{b}{a} = 1$ and $\frac{b}{a} = 0.3$.

```
In[124]:= env01[a_] := Min[8.66025 * pK2[1, a], sigy];
env02[a_] := Min[8.66025 * pK2[0.3, a], sigy];
In[126]:= Framed[Plot[{env01[a], env02[a]}, {a, 0, 0.5},
  AxesLabel -> {"a (in)", "Allowable Strength (psi)"},
  PlotLegends -> {" $\frac{b}{a} = 1$ ", " $\frac{b}{a} = 0.3$ "}, PlotLabel -> "Surface crack,  $\theta = 0$ "]]
Out[126]=
```



Note that for both values of theta, the solutions for $\frac{b}{a} = 0.3$ show that there is still some residual strength when the crack reaches 0.5". This indicates that the vessel would "leak before fail"!

Solution - Embedded crack

For an embedded crack, we will use the Cherepanov 1979 solution.

```
In[127]:= Clear [p, y, b, ba, M1, M2, M3, σ]
```

```
In[128]:= K[ba_, a_, p_, θ_] :=  $\frac{p * r}{t} \sqrt{\pi * ba * a} * ((\text{Sin}[\theta])^2 + (ba)^2 * (\text{Cos}[\theta])^2)^{\frac{1}{4}}$ ;
Simplify[K[ba, a, p, θ]]
```

```
Out[128]= 17.7245  $\sqrt{a ba} (ba^2)^{1/4} p$ 
```

As before, let $\theta = 0$ and $\theta = \frac{\pi}{2}$

For $\theta = 0$

```
In[129]:= Simplify[K[ba, a, p, 0]]
```

```
Out[129]= 17.7245  $\sqrt{a ba} (ba^2)^{1/4} p$ 
```

And for $\theta = \frac{\pi}{2}$

```
In[130]:= Simplify[K[ba, a, p,  $\frac{\pi}{2}$ ]]
```

```
Out[130]= 17.7245  $\sqrt{a ba} p$ 
```

Now lets define the function for the residual strength by dividing by K_{Ic} and solving for p.

For $\theta = 0$

```
In[131]:= ppK0[ba_, a_] :=  $K_{Ic} / (17.724538509055158 * \sqrt{a * ba} * (ba^2)^{1/4})$ ;
Simplify[ppK0[ba, a]]
```

```
Out[131]=  $\frac{1974.66}{\sqrt{a ba} (ba^2)^{1/4}}$ 
```

For $\theta = \frac{\pi}{2}$

```
In[132]:= ppK[ba_, a_] :=  $K_{Ic} / (\sqrt{a * ba})$ ; Simplify[ppK[ba, a]]
```

```
Out[132]=  $\frac{1974.66}{\sqrt{a ba}}$ 
```

We do not need to redefine the stress function. We may go ahead and define the envelope necessary to show our residual strength diagram.

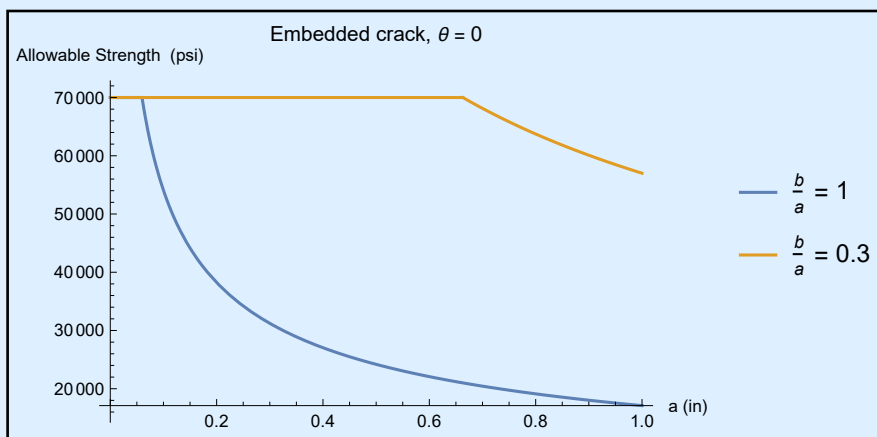
For $\theta = 0$

```
In[133]:= env210[a_] := Min[8.66025 * ppK0[1, a], sigy];
env220[a_] := Min[8.66025 * ppK0[0.3, a], sigy];
```

Extend the range for plotting to see the trends, but note that the wall thickness is 0.5", so a crack cannot extend further then that as the vessel will fail.

```
In[135]:= Framed[Plot[{env210[a], env220[a]}, {a, 0, 1.0},
  AxesLabel -> {"a (in)", "Allowable Strength (psi)"},
  PlotLegends -> {" $\frac{b}{a} = 1$ ", " $\frac{b}{a} = 0.3$ "}, PlotLabel -> "Embedded crack,  $\theta = 0$ "]]
```

Out[135]=



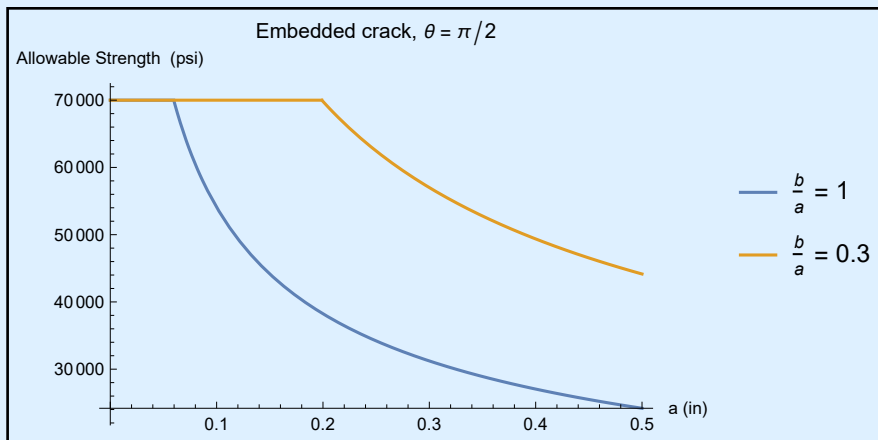
For $\theta = \frac{\pi}{2}$

```
In[136]:= env21[a_] := Min[8.66025 * ppK[1, a], sigy];
env22[a_] := Min[8.66025 * ppK[0.3, a], sigy];
```

In[138]:=

```
Framed[Plot[{env21[a], env22[a]}, {a, 0, 0.5},
  AxesLabel -> {"a (in)", "Allowable Strength (psi)"},
  PlotLegends -> {" $\frac{b}{a} = 1$ ", " $\frac{b}{a} = 0.3$ "}, PlotLabel -> "Embedded crack,  $\theta = \pi / 2$ "]]
```

Out[138]=

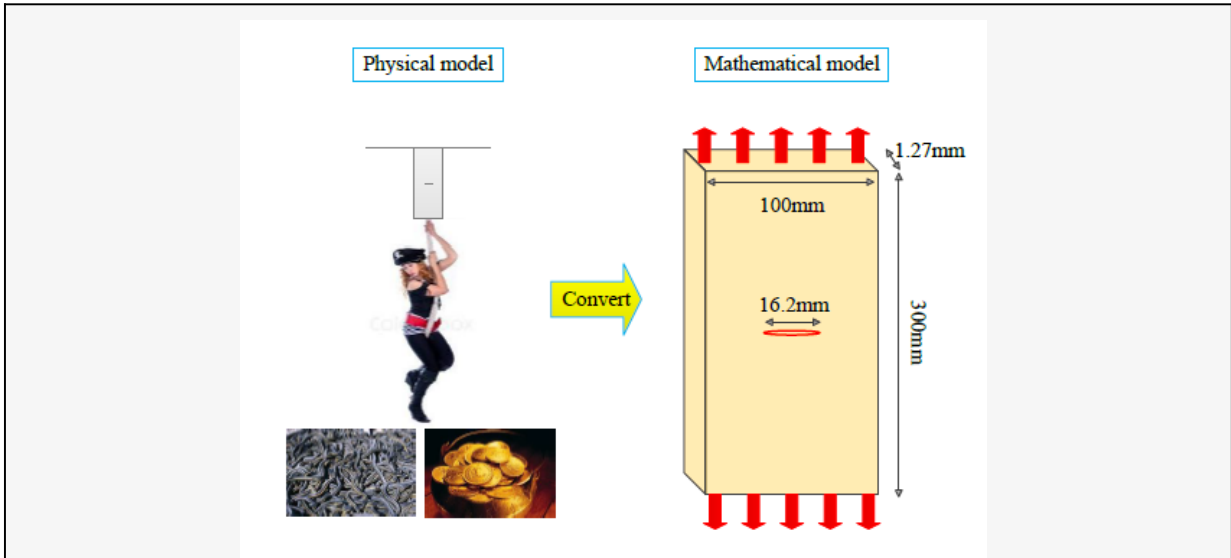


Notice that for $\frac{b}{a} = 0.3$ for both values of theta, there is still some residual strength even once the crack length equals the thickness (i.e. the crack “pierces” through the thickness of the vessel). This shows that for this situation, the pressure vessel would experience a “Leak Before Fail.”

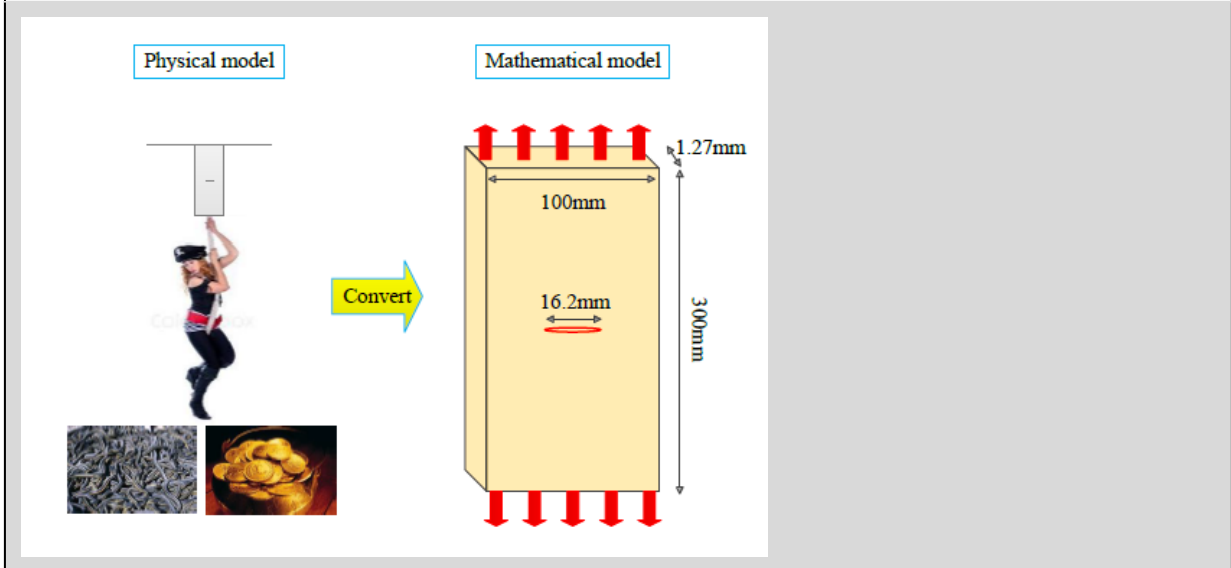
Problem 5

You are offered an opportunity to earn \$10 million by simply hanging from a rope for only one minute. The rope is attached to a glass sheet (300 cm long by 10 cm wide and 0.127 cm thick). Complicating the situation is the fact that the glass sheet contains a central crack with total length of 1.62 cm that is oriented parallel to the ground. The fracture toughness of the glass is $0.93 \text{ MPa} \sqrt{m}$.

In[139]:=



Out[139]=



The rope is suspended 3 m above a pit of poisonous snakes. Would you try for the pot of gold?

Solution

For the sake of this problem, let's assume that a dead weight of 890N (~200lb) is acting on the glass sheet. The uncracked cross-sectional area of the glass is $100 \times 1.27 = 127 \text{ mm}^2$. The nominal stress is thus:

```
In[140]:= sig =  $\frac{890.0}{127.0}$ ;
DecimalForm[sig, 0]
```

```
Out[141]/DecimalForm=
7.00787
```

So the far field stress is 7.01 MPa.

For Middle Tension Panel, we may use the following formula to calculate the stress intensity factor based on a polynomial expansion:

```
In[142]:= a = 16.2 / (2 * 1000); (*meters*)
W = 100.0 / 1000; (*meters*)
KI =  $\left(1 + 0.256 * \left(\frac{a}{W}\right) - 1.152 * \left(\frac{a}{W}\right)^2 + 12.2 * \left(\frac{a}{W}\right)^3\right) * sig * \sqrt{\pi * a}$ 
```

```
Out[144]=
1.13988
```

Just to make sure, calculate again using the original formula

```
In[145]:= KIb =  $\sqrt{\text{Sec}\left[\frac{\pi * a}{W}\right]} * sig * \sqrt{\pi * a}$ 
```

```
Out[145]=
1.13635
```

The calculated stress intensity factor is 1.14 MPa \sqrt{m} for both calculations which exceeds the fracture toughness of 0.93 MPa \sqrt{m} , so I would not try for the pot of gold.

Problem 6

(Open-ended) Using Newman's solution and Mathematica/Matlab, write a function which will give the stress intensity factor for an elliptical hole in terms of $\frac{b}{a}$, $\frac{b}{t}$, and the angle θ . Use this function to develop some relevant plots.

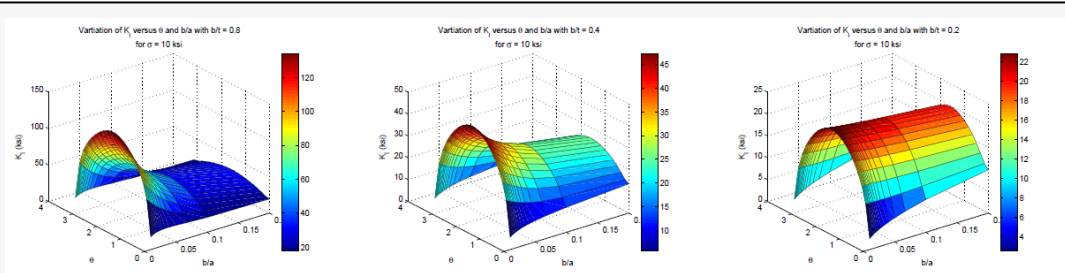


Figure 1: Plot of K_I versus θ and $\frac{b}{a}$

In[146]:=

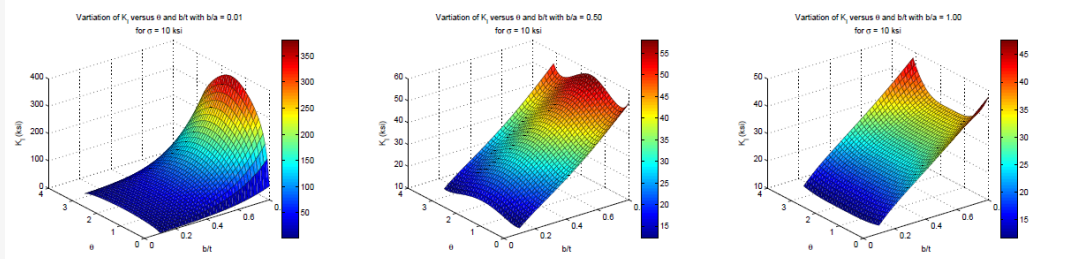


Figure 2: Plot of K_I versus θ and $\frac{b}{t}$

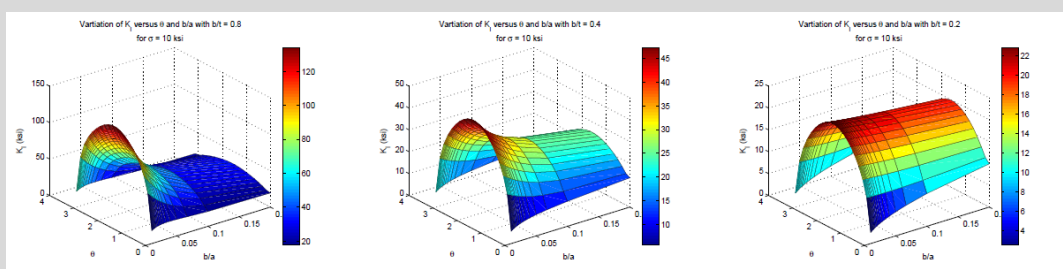


Figure 1: Plot of K_I versus θ and $\frac{b}{a}$

Out[146]=

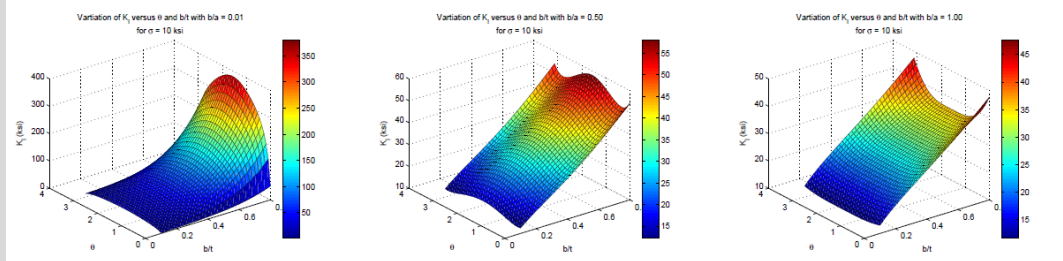


Figure 2: Plot of K_I versus θ and $\frac{b}{t}$

Solution

In[147]:=

```
Clear[p, r, t, y, b, ba, bt, M1, M2, M3,  $\sigma$ ]
```

```
In[148]:= (*ba = 0.5; MAKE THINGS A FUNCTION OF THIS*)
(*b = 0.5;*)
σ = 10; (*psi*)
M1[ba_] := 1.13 - 0.09 * ba;
M2[ba_] := 0.89 * (0.2 + ba)-1 - 0.54;
M3[ba_] := 0.5 - (0.65 + ba)-1 + 14 * (1 - ba)24;
a = 1.0;
```

```
In[153]:= part1[ba_] := σ √π * ba * a;
part2[ba_, bt_] := (M1[ba] + M2[ba] * (bt)2 + M3[ba] * (bt)4) * (1 + 1.464 ba1.65)-0.5;
part3[ba_, θ_] := (ba2 Cos[θ]2 + Sin[θ]2)0.25;
part4[bt_, θ_] := (1 + (0.1 + 0.35 (bt)2) (1 - Sin[θ])2);
K[ba_, bt_, θ_] := part1[ba] * part2[ba, bt] * part3[ba, θ] * part4[bt, θ];
Simplify[K[ba, bt, θ]]
```

```
Out[158]=
```

$$\frac{1}{(1 + 1.464 ba^{1.65})^{0.5}} 17.7245 \sqrt{ba} (ba^2)^{0.25} (1.1 + 0.35 bt^2) \times$$

$$\left(1.13 - 0.09 ba + \left(-0.54 + \frac{0.89}{0.2 + ba} \right) bt^2 + \left(0.5 + 14 (-1 + ba)^{24} - \frac{1.}{0.65 + ba} \right) bt^4 \right)$$

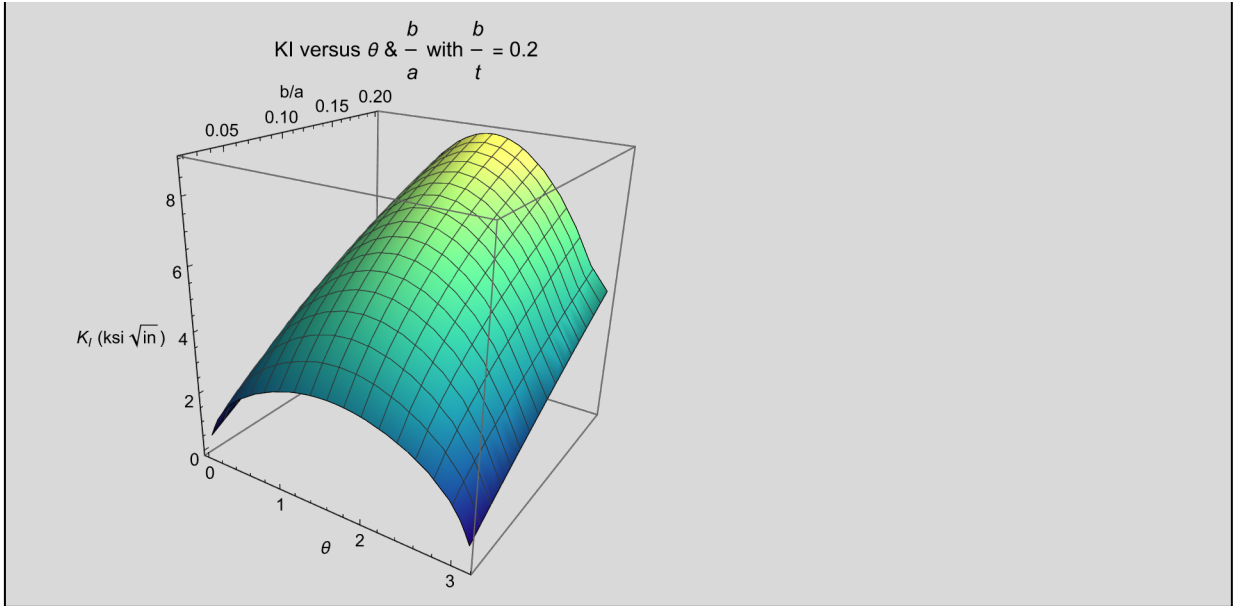
Fix b/t

```
In[159]:= Plot3D[{K[ba, 0.2, θ]}, {θ, 0, π},
{ba, 0.02, 0.2}, AxesLabel → {"θ", "b/a", "KI (ksi √in)"},
ColorFunction → "BlueGreenYellow", ViewPoint → {1.2, -2, 1},
BoxRatios → {1, 1, 1}, PlotLabel → "KI versus θ &  $\frac{b}{a}$  with  $\frac{b}{t} = 0.2$ "]

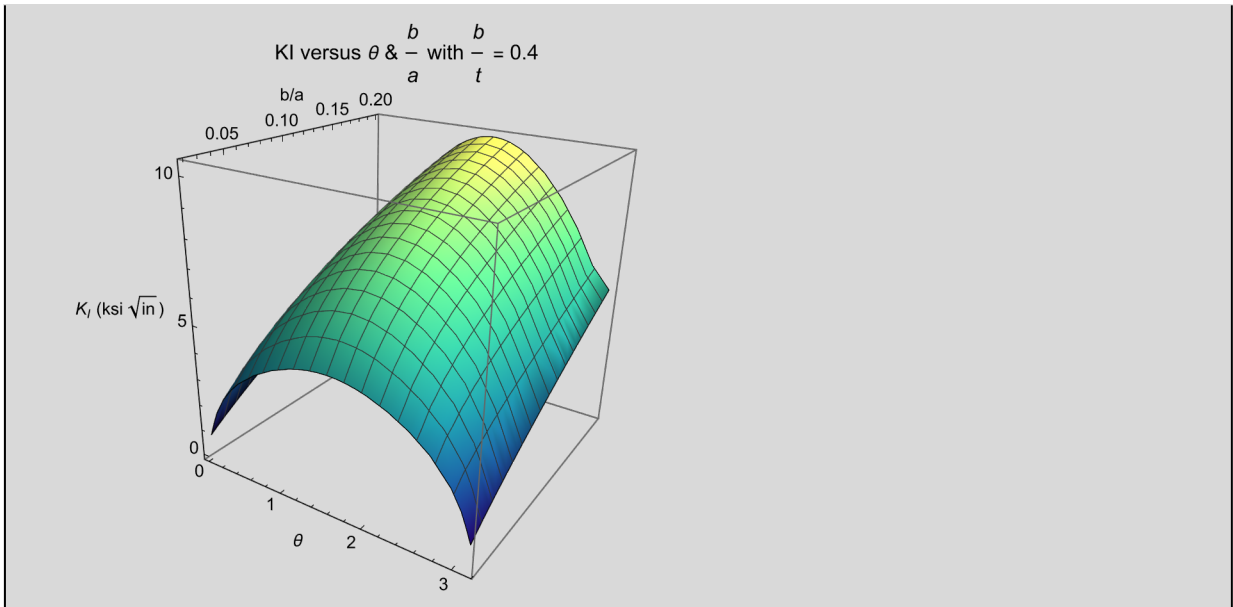
Plot3D[{K[ba, 0.4, θ]}, {θ, 0, π}, {ba, 0.02, 0.2},
AxesLabel → {"θ", "b/a", "KI (ksi √in)"},
ColorFunction → "BlueGreenYellow", ViewPoint → {1.2, -2, 1},
BoxRatios → {1, 1, 1}, PlotLabel → "KI versus θ &  $\frac{b}{a}$  with  $\frac{b}{t} = 0.4$ "]

Plot3D[{K[ba, 0.8, θ]}, {θ, 0, π}, {ba, 0.02, 0.2},
AxesLabel → {"θ", "b/a", "KI (ksi √in)"},
ColorFunction → "BlueGreenYellow", ViewPoint → {1.2, -2, 1},
BoxRatios → {1, 1, 1}, PlotLabel → "KI versus θ &  $\frac{b}{a}$  with  $\frac{b}{t} = 0.8$ "]
```

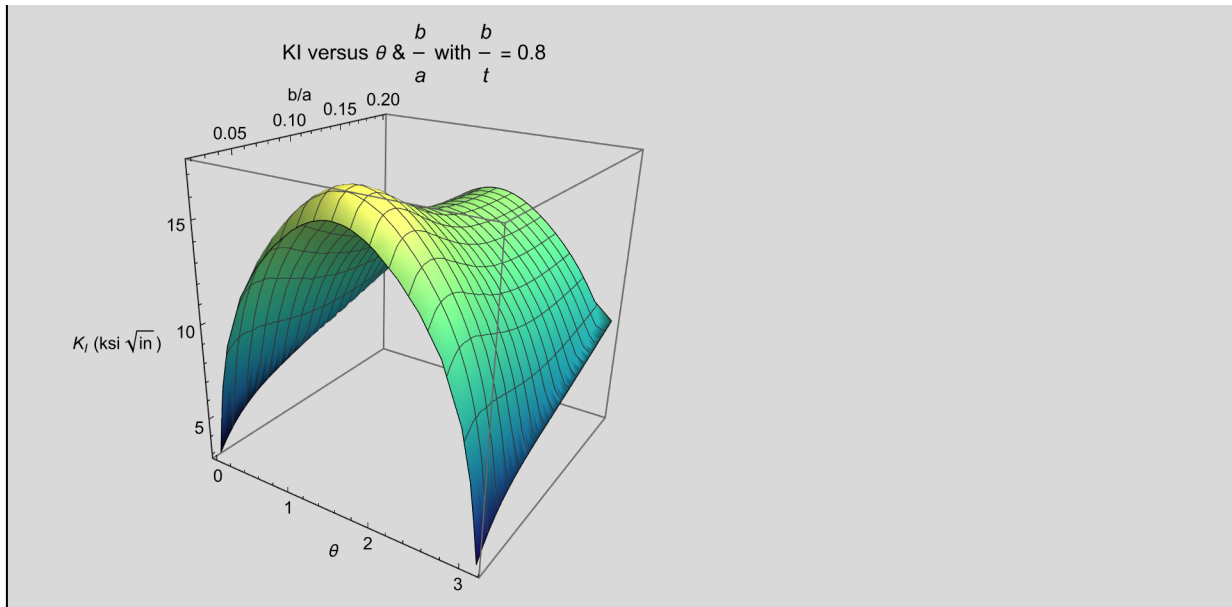

Out[159]=



Out[160]=



Out[161]=

**Fix b/a**

In[162]=

```

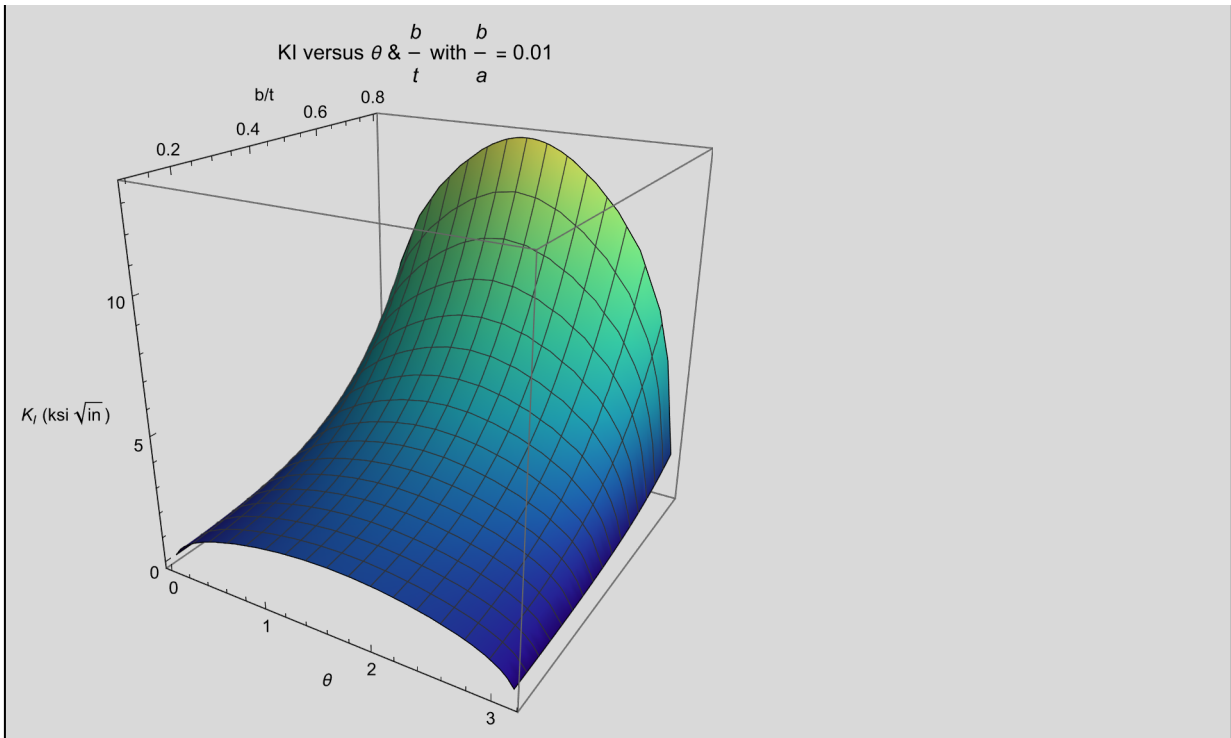
Plot3D[{K[0.01, bt, theta]}, {theta, 0, pi},
  {bt, 0.1, 0.8}, AxesLabel -> {"theta", "b/t", "K_I (ksi sqrt(in))"},
  ColorFunction -> "BlueGreenYellow", ViewPoint -> {1.2, -2, 1},
  BoxRatios -> {1, 1, 1}, PlotLabel -> "KI versus theta & b/t with b/a = 0.01"]

Plot3D[{K[0.5, bt, theta]}, {theta, 0, pi}, {bt, 0.1, 0.8},
  AxesLabel -> {"theta", "b/t", "K_I (ksi sqrt(in))"},
  ColorFunction -> "BlueGreenYellow", ViewPoint -> {1.2, -2, 1},
  BoxRatios -> {1, 1, 1}, PlotLabel -> "KI versus theta & b/t with b/a = 0.5"]

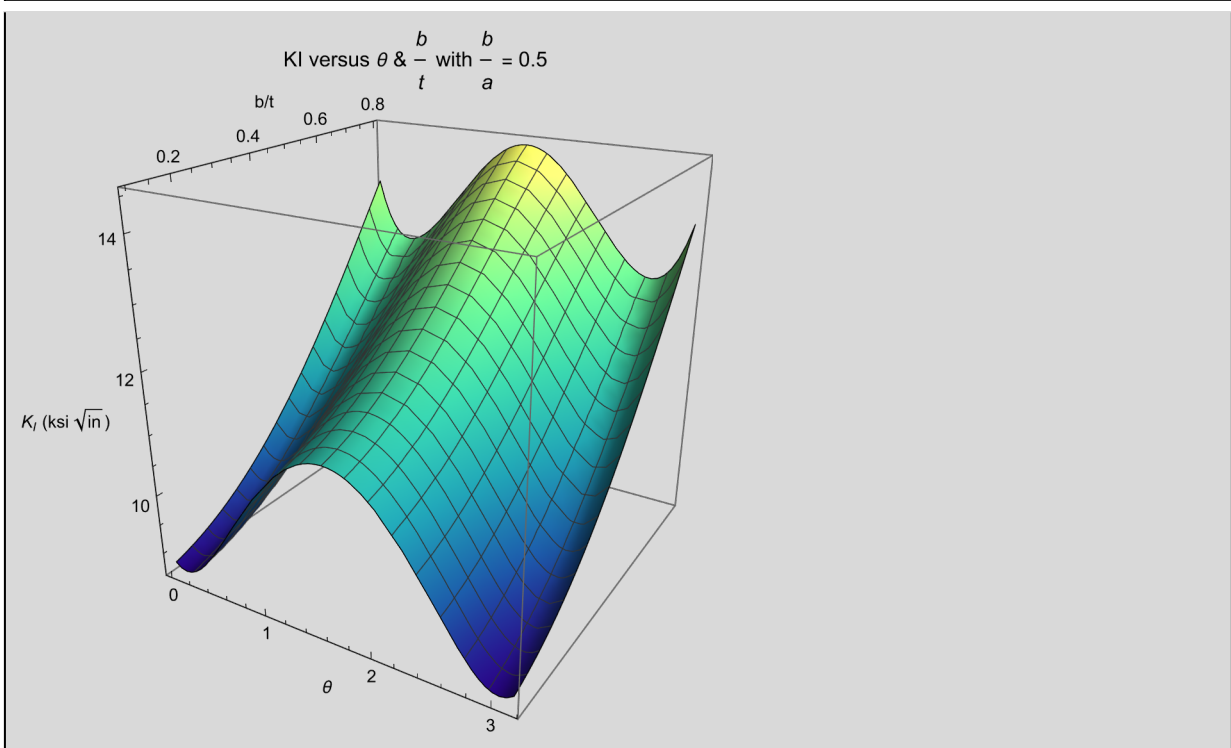
Plot3D[{K[1, bt, theta]}, {theta, 0, pi}, {bt, 0.1, 0.8},
  AxesLabel -> {"theta", "b/t", "K_I (ksi sqrt(in))"},
  ColorFunction -> "BlueGreenYellow", ViewPoint -> {1.2, -2, 1},
  BoxRatios -> {1, 1, 1}, PlotLabel -> "KI versus theta & b/t with b/a = 1"]

```

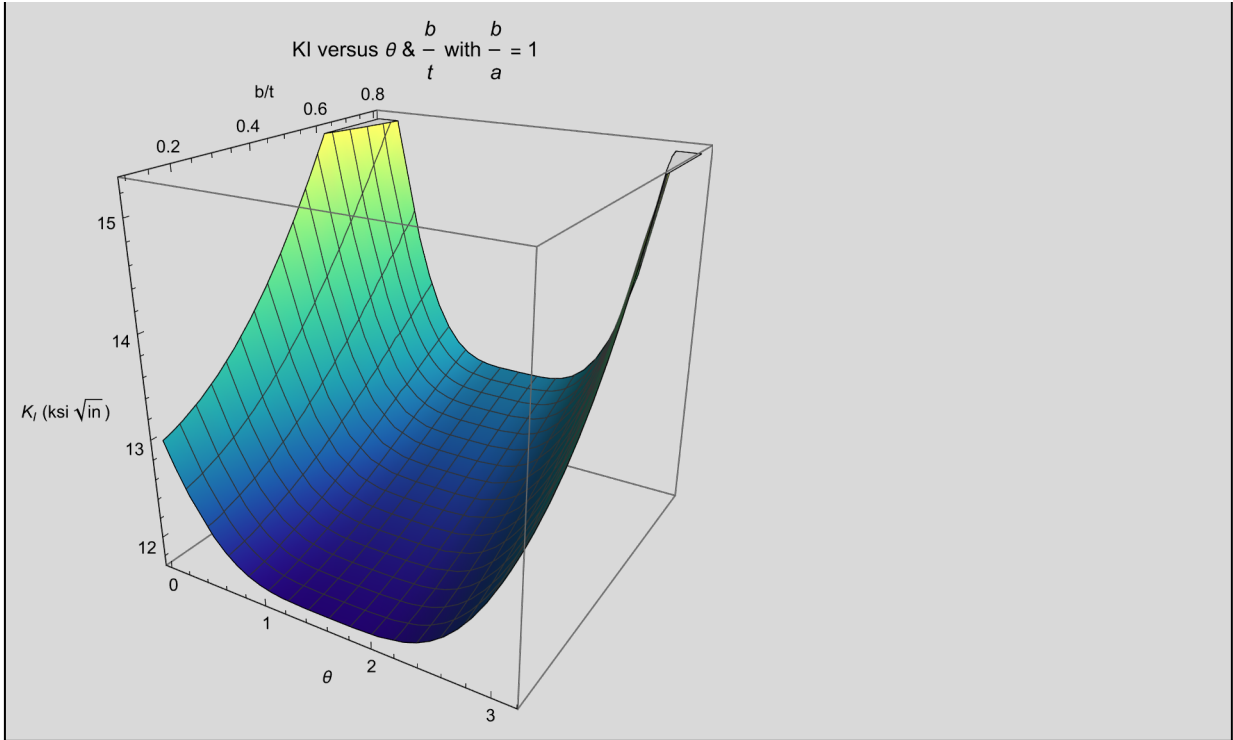
Out[162]=



Out[163]=



Out[164]=



Homework 4

Thomas Allard
CVEN 7161

Problem 1

The following data were obtained from a series of tests conducted on pre-cracked specimens with 1 mm thickness

In[1]:=

Crack Length a (mm)	Critical Load P_{cr} (kN)	Critical Displacement u_{cr} (mm)
30.0	4.00	0.40
40.00	3.50	0.50
50.5	3.12	0.63
61.6	2.80	0.78
71.7	2.62	0.94
79.0	2.56	1.09

Out[1]=

Crack Length a (mm)	Critical Load P_{cr} (kN)	Critical Displacement u_{cr} (mm)
30.0	4.00	0.40
40.00	3.50	0.50
50.5	3.12	0.63
61.6	2.80	0.78
71.7	2.62	0.94
79.0	2.56	1.09

The load displacement curve for all cracks is linearly elastic up to the critical point.

Determine G_c from:

- The load displacement records (based on the mean of the measurements in between two consecutive values, and
- from the compliance curve.

Discuss your results.

Solution

In[2]:=

```
ClearAll["Global'*"]
Clear[c1, c2, c3, cc1, cc2, cc3, d1, d2, d3, dd1, dd2, dd3]
```

Determining the critical energy release rate from experimental data can be done in several different

ways. We will explore the results of several methods.

(a) G_c from load displacement records

```
In[4]:= alist = {30.0, 40.0, 50.5, 61.6, 71.7, 79.0};
Plist = {4.0, 3.5, 3.12, 2.8, 2.62, 2.56};
ulist = {0.4, 0.5, 0.63, 0.78, 0.94, 1.09};
```

We may determine G_c using the following formula:

$$G = \sum_{i=1}^n \frac{0.5 A_i A_{i+1}}{a_{i+1} - a_i}$$

We have 6 data points, but we will set $n=5$ since there are only 5 consecutive steps between points. Lets calculate each area directly.

```
In[7]:= area1 = 0.5 * (Plist[[1]] * ulist[[2]] - Plist[[2]] * ulist[[1]]);
area2 = 0.5 * (Plist[[2]] * ulist[[3]] - Plist[[3]] * ulist[[2]]);
area3 = 0.5 * (Plist[[3]] * ulist[[4]] - Plist[[4]] * ulist[[3]]);
area4 = 0.5 * (Plist[[4]] * ulist[[5]] - Plist[[5]] * ulist[[4]]);
area5 = 0.5 * (Plist[[5]] * ulist[[6]] - Plist[[6]] * ulist[[5]]);
```

Now we'll calculate each contribution to the energy release rate

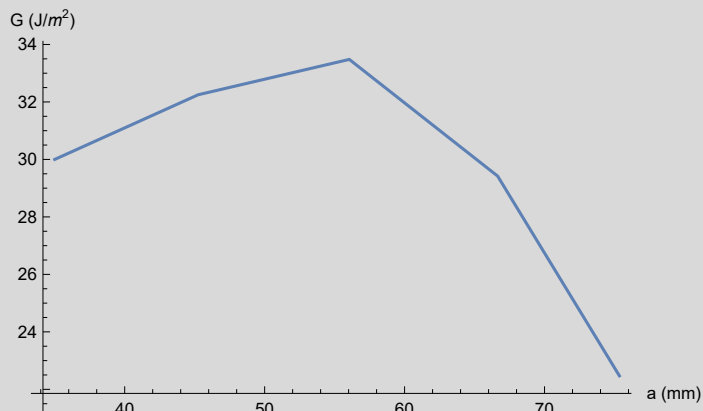
```
In[12]:= da1 = 0.5 * (alist[[2]] + alist[[1]]);
da2 = 0.5 * (alist[[3]] + alist[[2]]);
da3 = 0.5 * (alist[[4]] + alist[[3]]);
da4 = 0.5 * (alist[[5]] + alist[[4]]);
da5 = 0.5 * (alist[[6]] + alist[[5]]);
G1 = area1 / (alist[[2]] - alist[[1]]) * 1000;
G2 = area2 / (alist[[2]] - alist[[1]]) * 1000;
G3 = area3 / (alist[[2]] - alist[[1]]) * 1000;
G4 = area4 / (alist[[2]] - alist[[1]]) * 1000;
G5 = area5 / (alist[[2]] - alist[[1]]) * 1000;
```

Lets plot this.

In[22]=

```
gdata = Transpose[{{da1, da2, da3, da4, da5}, {G1, G2, G3, G4, G5}}];
ListLinePlot[{gdata}, AxesLabel → {"a (mm)", "G (J/m2)"}]
```

Out[23]=



In[24]=

```
gdata
```

Out[24]=

```
{{35., 30.}, {45.25, 32.25}, {56.05, 33.48}, {66.65, 29.42}, {75.35, 22.47}}
```

In[25]=

```
Mean[{G1, G2, G3, G4, G5}]
```

Out[25]=

```
29.524
```

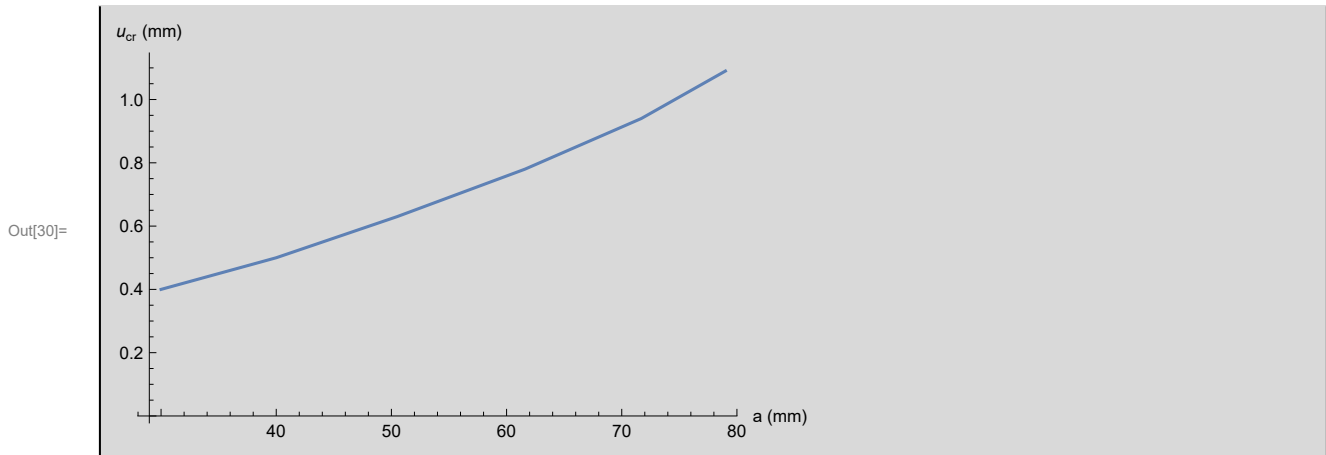
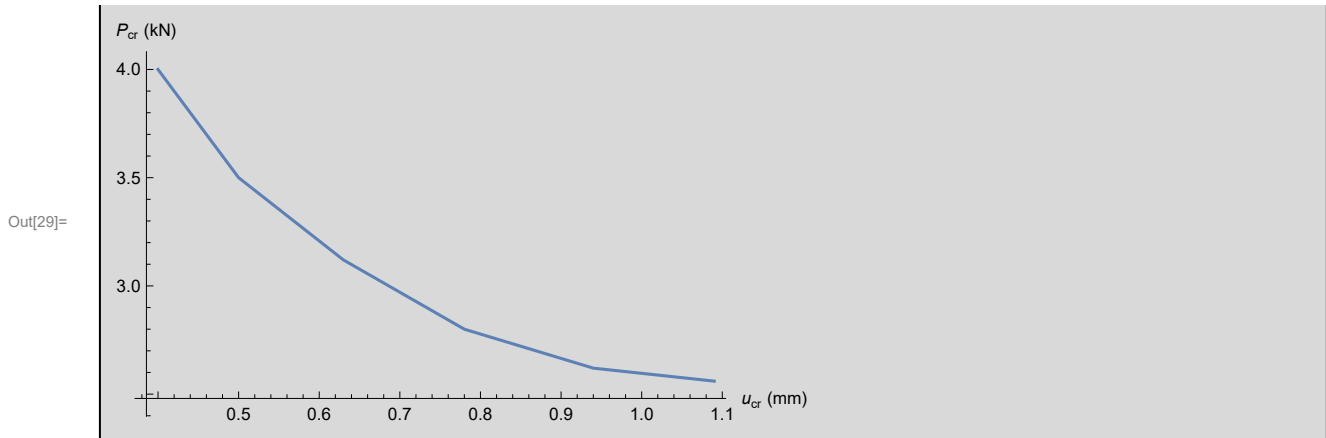
Using numerical derivatives, we calculate that the average energy release rate is **29.5 J/m²** while the maximum is **33.5 J/m²**!

(b) G_c from compliance curve

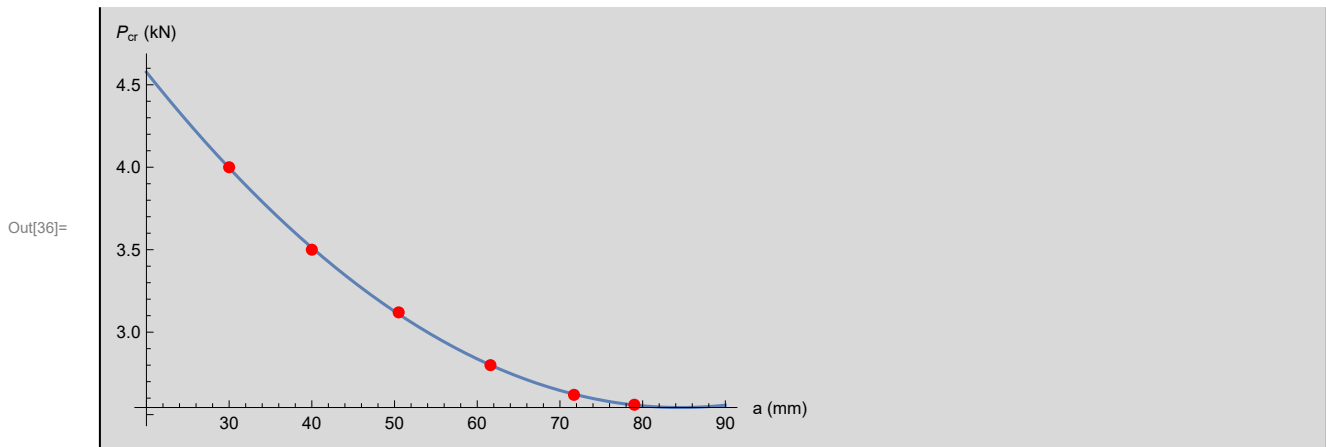
Lets start off by putting our data into lists and plotting. We'll fit a quadratic curve to P_{cr} vs. a for reasons that will be apparent later.

In[26]=

```
data1 = Transpose[{ulist, Plist}];
data2 = Transpose[{alist, ulist}];
data3 = Transpose[{alist, Plist}];
ListLinePlot[data1, AxesLabel → {"ucr (mm)", "Pcr (kN)"}]
ListLinePlot[data2, AxesLabel → {"a (mm)", "ucr (mm)"}]
Pcoeffs = FindFit[data3, (d1 * aa2) + (d2 * aa) + d3, {d1, d2, d3}, aa];
dd1 = d1 /. Pcoeffs[[1]];
dd2 = d2 /. Pcoeffs[[2]];
dd3 = d3 /. Pcoeffs[[3]];
Pcr[aa_] = (dd1 * aa2) + (dd2 * aa) + dd3; Simplify[Pcr[aa]]
Show[Plot[{Pcr[aa]}, {aa, 20, 90}, AxesLabel → {"a (mm)", "Pcr (kN)"}],
ListPlot[data3, PlotStyle → {Red, PointSize[0.02]}]]
```



Out[35]= $6.03197 - 0.0825085 aa + 0.000487821 aa^2$



Our trend-line for P_{cr} looks great.

We may compute the compliance by dividing each u_{cr} by P_{cr} .

In[37]:= **Clist = uelist / Plist**

Out[37]= {0.1, 0.142857, 0.201923, 0.278571, 0.358779, 0.425781}

Lets plot the compliance versus crack length a. Lets also fit a quadratic trend line to the data which will be convenient later.

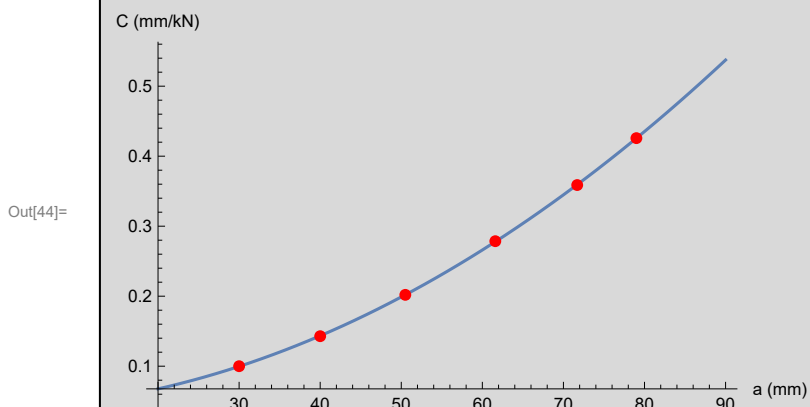
```
In[38]:= data4 = Transpose[{alist, Clist}];
coeffs = FindFit[data4, (c1 * aa2) + (c2 * aa) + c3, {c1, c2, c3}, aa]
```

```
Out[39]:= {c1 → 0.0000583911, c2 → 0.000287841, c3 → 0.0385099}
```

```
In[40]:= cc1 = c1 /. coeffs[[1]];
cc2 = c2 /. coeffs[[2]];
cc3 = c3 /. coeffs[[3]];
```

```
In[43]:= comp[aa_] := (cc1 * aa2) + (cc2 * aa) + cc3;
```

```
In[44]:= Show[Plot[{comp[aa]}, {aa, 20, 90}, AxesLabel → {"a (mm)", "C (mm/kN)"}],
ListPlot[data4, PlotStyle → {Red, PointSize[0.02]}]]
```



It looks like we have a perfect fit! To determine the energy release rate, we will use the following equation:

$$G = \frac{1}{2} \frac{P^2}{B} \left(\frac{dC}{da} \right)$$

Where B is the specimen width which is 1mm and P is the critical load P_{cr} .

Lets first try to determine G using numerical derivatives and plot.

```
In[45]:= Clist2 = Clist[[2 ;; 6]] - Clist[[1 ;; 5]];
alist2 = alist[[2 ;; 6]] - alist[[1 ;; 5]];
Plist2 = 0.5 * (Plist[[2 ;; 6]] + Plist[[1 ;; 5]])
dCda = Clist2 / alist2
```

```
Out[47]:= {3.75, 3.31, 2.96, 2.71, 2.59}
```

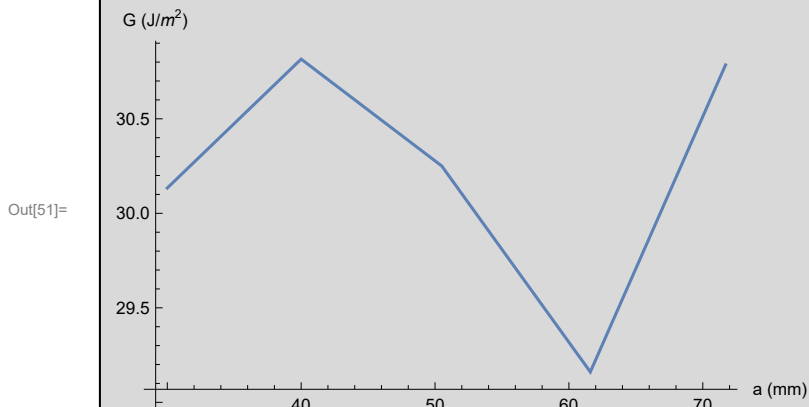
```
Out[48]:= {0.00428571, 0.00562533, 0.00690526, 0.00794131, 0.00917844}
```

```
In[49]:= Gg = 0.5 * (Plist2^2) * dCda
```

```
Out[49]:= {0.0301339, 0.0308158, 0.0302505, 0.0291609, 0.030785}
```

```
In[50]:= data5 = Transpose[{alist[[1 ;; 5]], Gg * 1000}];
```

```
In[51]:= ListLinePlot[data5, AxesLabel -> {"a (mm)", "G (J/m2)"}]
```



```
Out[51]=
```

```
In[52]:= Mean[Gg] * 1000
```

```
Out[52]:= 30.2292
```

Based on this plot, we can see that the energy release rate calculated for each crack length is close to each other. The average value is **30.2 J/m²** and the max is **30.8 J/m²**!

However, the plot above is very jagged. Lets use an approach with analytical derivatives using our the curve-fits.

```
In[53]:= dCda2[aa_] := D[comp[aa], {aa, 1}]; Simplify[dCda2[aa]]
```

```
Out[53]:= 0.000287841 + 0.000116782 aa
```

Now calculate energy release rate. We'll need to use our trend-line for P_{Cr} .

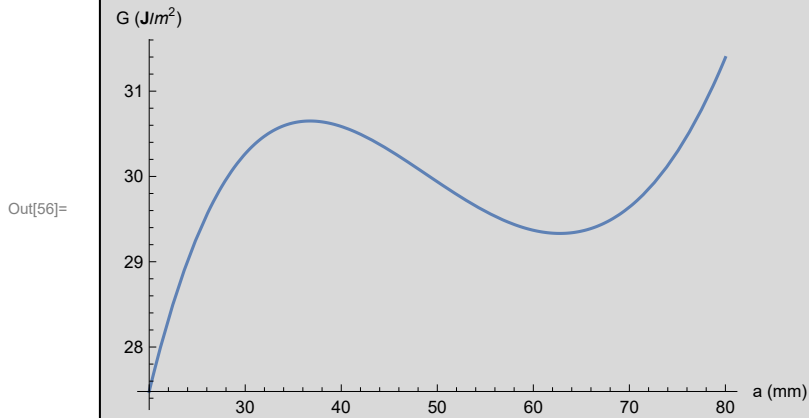
```
In[54]:= Gg2[aa_] := (Pcr[aa])^2 / 2 * dCda2[aa]; Simplify[Gg2[aa]]
```

```
Out[54]:= 1.38953 × 10-11 × (2.46477 + 1. aa) (12365.1 - 169.137 aa + 1. aa2)2
```

Mathematica seems to have a hard time plotting this function directly, so we'll redefine it.

```
In[55]:= release[aa_] := (1.3895272400576719*^-11 * (2.4647685549212377 + aa)
(12365.140727904993 - 169.13697736800404 aa + aa^2)^2) * 1000;
```

```
In[56]:= (*Plot[{Gg2[a]}, {a, 30, 80}]*)
Plot[{release[aa]}, {aa, 20, 80}, AxesLabel -> {"a (mm)", "G (J/m^2)"}]
```



Lets find the release rate corresponding to the top of the bump between crack lengths of 30 and 40 mm.

```
In[57]:= dGda[aa_] := D[release[aa], {aa, 1}];
acrit = NSolve[dGda[aa] == 0, aa]
```

```
Out[58]= {{aa -> 36.7435}, {aa -> 62.7669}, {aa -> 84.5685 - 72.2033 i}, {aa -> 84.5685 + 72.2033 i}}
```

The solution for G_c occurs at a crack length of 36.74mm and is thus:

```
In[59]:= Framed[Gcrit = release[aa] /. acrit[[1]]]
```

```
Out[59]= 30.65
```

Finally, lets calculate the average energy release rate by integrating and dividing by the interval length (between 20 and 80mm).

```
In[60]:= Framed[Integrate[release[aa], {aa, 20, 80}] / (80 - 20)]
```

```
Out[60]= 29.8992
```

Whether using numerical or analytical derivatives, the average energy release rate calculated for each method was **29.5, 30.2, and 29.9 J/m²**. The maximum value for each method are calculated as **33.5, 30.8, and 30.7 J/m²**. These methods all give roughly the same answer!

Problem 2

Assume that the R curve of a certain material can be represented by $R = \frac{K_{Ic}^2}{E} + 0.4 (\Delta a)^{0.25}$ (kip/in), and that $K_{Ic} = 30 \text{ Ksi } \sqrt{\text{in}}$, $E=30,000 \text{ Ksi}$, and $\sigma_y = 100 \text{ Ksi}$. For a center cracked panel of a thickness for which the above R curve is applicable and of width $W=50 \text{ in}$ with a crack $2a=2\text{in}$, calculate a_c (the final crack size), σ_c (the fracture stress), and Δa (the final amount of stable growth).

Show graphically your results. Assume plane stress condition $E'=E$, and we can consider that for all practical purposes we have an infinite plate ($W \gg 2a$).

Solution

In[61]:=

```
ClearAll["Global'*"]
Clear[c1, c2, c3, cc1, cc2, cc3, d1, d2, d3, dd1, dd2, dd3, a, aa, da, G, Gg, release]
```

First, plot the R curve versus Δa .

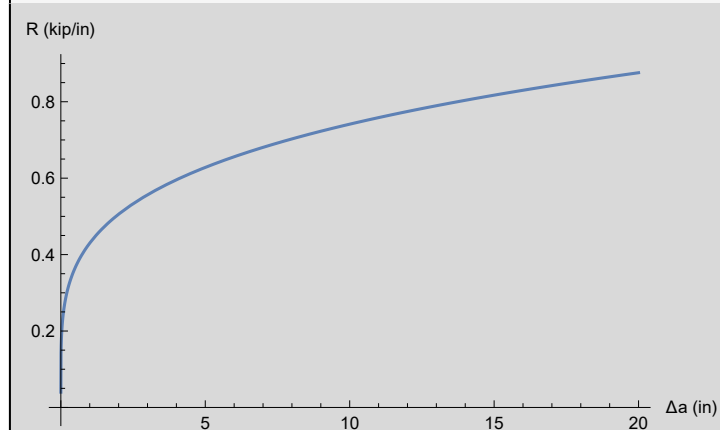
In[63]:=

```
KIc = 30; (*Ksi*(in)^0.5*)
Emod = 30000; (*Ksi*)
W = 50; (*in*)
sigy = 100; (*ksi*)

R[Δa_] := (KIc^2 / Emod) + 0.4 * (Δa)^0.25;

a0 = 1; (*inch*)
Plot[{R[Δa]}, {Δa, 0.0, 20}, AxesLabel -> {"Δa (in)", "R (kip/in)"}]
```

Out[69]=



For a centered crack panel, we may calculate the stress intensity factor as follows:

In[70]:=

$$K1[a_, s_] := \sqrt{\text{Sec}\left[\frac{\pi * a}{W}\right]} * s * \sqrt{\pi * a};$$

However, $W \gg 2a$, we may set $\sqrt{\text{Sec}\left[\frac{\pi * a}{W}\right]} = 1$, so

In[71]:= $KI[a_, s_] := s * \sqrt{\pi * a};$

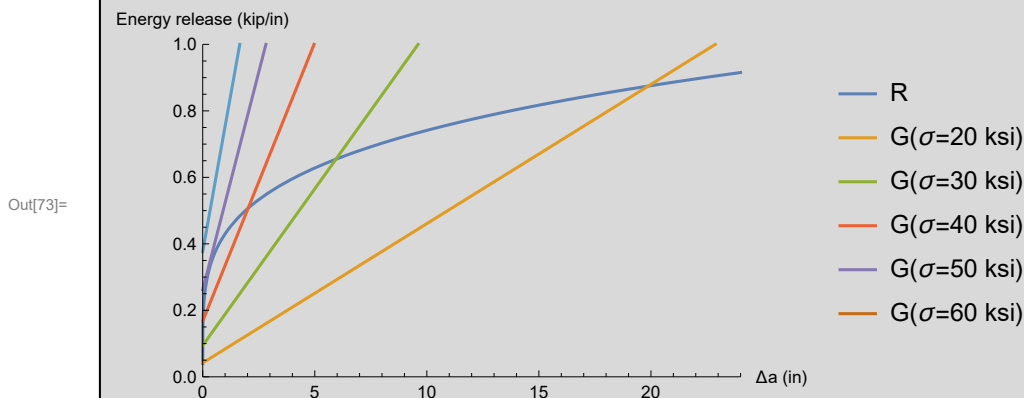
We may convert this to an energy release rate as follows:

In[72]:= $G[a_, s_] := \frac{(KI[a, s])^2}{E_{mod}}; \text{Simplify}[G[a, s]]$

Out[72]= $\frac{a \pi s^2}{30000}$

Lets look at several different energy release rates for varying applied stresses “s” versus the R curve

In[73]:= `Plot[{R[da], G[a0 + da, 20], G[a0 + da, 30], G[a0 + da, 40], G[a0 + da, 50], , G[a0 + da, 60]},
{da, 0.0, 24}, AxesLabel -> {"Δa (in)", "Energy release (kip/in)"},
PlotRange -> {{0, 24}, {0, 1}}, PlotLegends ->
{"R", "G(σ=20 ksi)", "G(σ=30 ksi)", "G(σ=40 ksi)", "G(σ=50 ksi)", "G(σ=60 ksi)"}]`

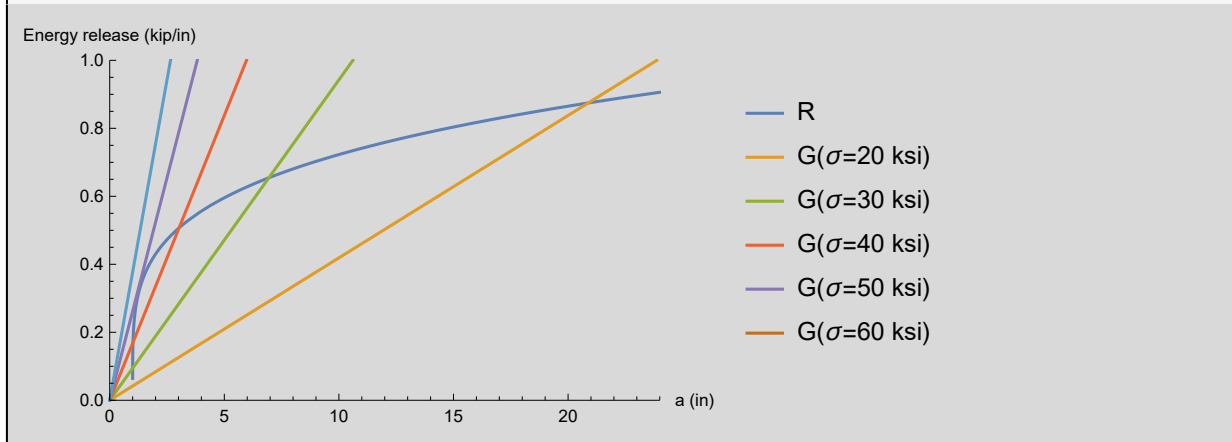


Or in terms of the crack length “a”.

In[74]=

```
Plot[{R[a - a0], G[a, 20], G[a, 30], G[a, 40], G[a, 50], , G[a, 60]},
{a, 0.0, 24}, AxesLabel -> {"a (in)", "Energy release (kip/in)"},
PlotRange -> {{0, 24}, {0, 1}}, PlotLegends ->
{"R", "G( $\sigma=20$  ksi)", "G( $\sigma=30$  ksi)", "G( $\sigma=40$  ksi)", "G( $\sigma=50$  ksi)", "G( $\sigma=60$  ksi)"}]
```

Out[74]=



Here we see that for applied stresses of 20, 30, and 40 ksi, a long regime of stable crack growth is possible because the energy release rate is less than the R-curve. We may determine how the critical crack length changes as a function of applied stress as follows:

In[75]=

```
ac10 = NSolve[G[a, 10] - R[a - a0] == 0, a]
ac15 = NSolve[G[a, 15] - R[a - a0] == 0, a]
ac20 = NSolve[G[a, 20] - R[a - a0] == 0, a]
ac25 = NSolve[G[a, 25] - R[a - a0] == 0, a]
ac30 = NSolve[G[a, 30] - R[a - a0] == 0, a]
ac35 = NSolve[G[a, 35] - R[a - a0] == 0, a]
ac40 = NSolve[G[a, 40] - R[a - a0] == 0, a]
ac45 = NSolve[G[a, 45] - R[a - a0] == 0, a]
```

Out[75]=

```
{{a -> 132.12}}
```

Out[76]=

```
{{a -> 44.9953}}
```

Out[77]=

```
{{a -> 20.8802}, {a -> 1.}}
```

Out[78]=

```
{{a -> 11.4455}, {a -> 1.00006}}
```

Out[79]=

```
{{a -> 6.94564}, {a -> 1.00067}}
```

Out[80]=

```
{{a -> 4.49827}, {a -> 1.00372}}
```

Out[81]=

```
{{a -> 3.02793}, {a -> 1.01504}}
```

Out[82]=

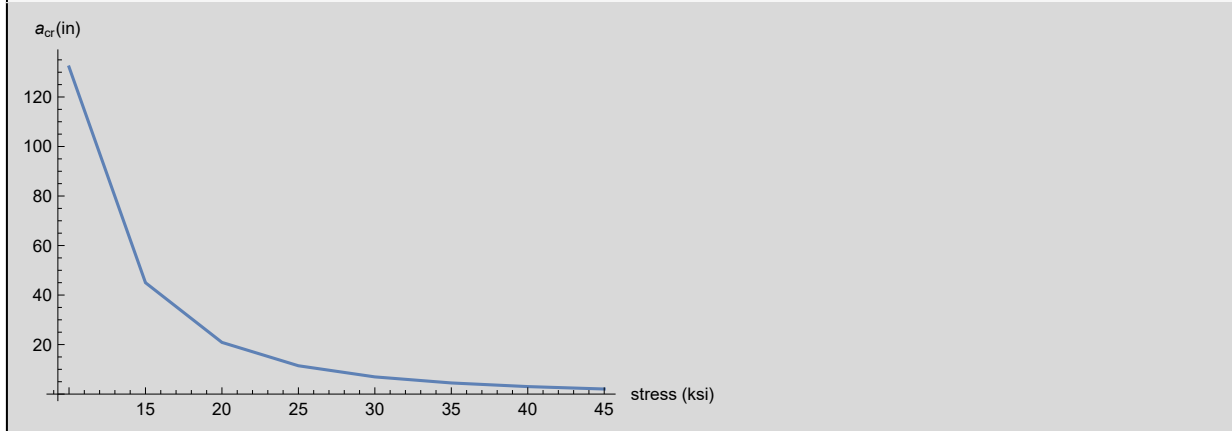
```
{{a -> 2.05165}, {a -> 1.05502}}
```

Lets put this in a table and plot.

In[83]=

```
acrList = {a /. ac10[[1]], a /. ac15[[1]], a /. ac20[[1]],
  a /. ac25[[1]], a /. ac30[[1]], a /. ac35[[1]], a /. ac40[[1]], a /. ac45[[1]]};
stresses = {10, 15, 20, 25, 30, 35, 40, 45};
ListLinePlot[Transpose[{stresses, acrList}], AxesLabel -> {"stress (ksi)", "acr (in)"}]
```

Out[85]=



Since the plate is 50 inches wide, only cracks of 25 in or lower are even possible. We see that for stresses greater than 30 ksi, the critical crack length rapidly approaches 0.

Lets investigate the unstable crack growth regime. We know that unstable crack growth occurs when:

$$G = R \quad \& \quad \frac{\partial G}{\partial a} > \frac{\partial R}{\partial a}$$

The critical point will be when the slopes of the G and R curves are equal AND G=R. Based on previously shown plots, this is likely to occur around 50ksi of applied stress.

A Matlab code was written to iteratively solve for this point of tangency. It is attached. The final answers are:

In[86]=

```
Framed [σc = 48.9389]
Framed [ac = 1.2930]
Framed [Δac = ac - a0]
```

Out[86]=

48.9389

Out[87]=

1.293

Out[88]=

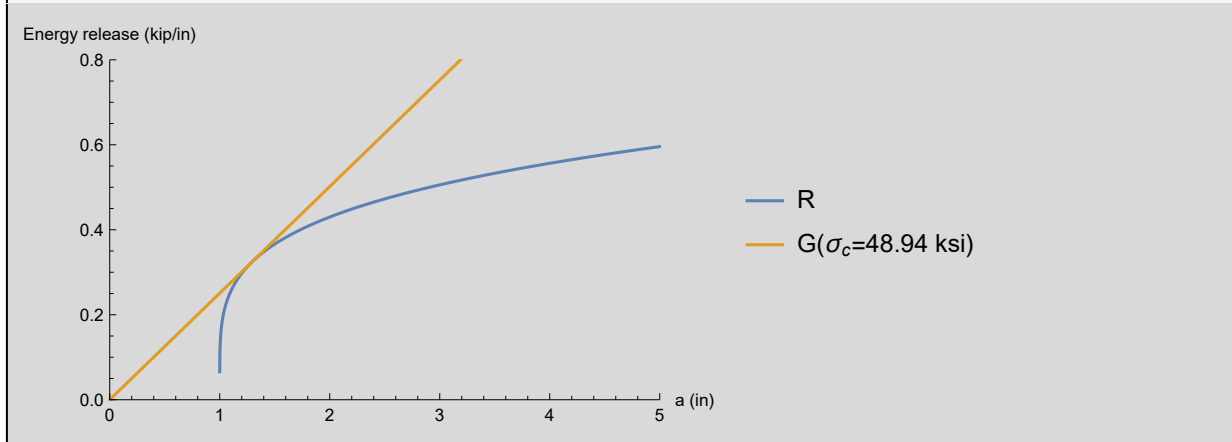
0.293

Lets plot these results

In[89]=

```
Plot[{R[a - a0], G[a,  $\sigma_c$ ]}, {a, 0.0, 5},
  AxesLabel -> {"a (in)", "Energy release (kip/in)"},
  PlotRange -> {{0, 5}, {0, 0.8}}, PlotLegends -> {"R", "G( $\sigma_c=48.94$  ksi)"}]
```

Out[89]=



For stresses below the **critical stress of 48.94 ksi**, stable crack growth occurs! Cracks do not grow until energy release rate equals the resistance curve. After the crack starts to grow, the energy release rate will decrease and no more energy can be released by the material without an increase in the applied stress. This stable crack growth will continue until the applied stress is 48.94 ksi. At this point, the energy release rate is tangent to the resistance curve. An increase in stress will result in a sudden release of energy that can not be arrested by the material. For this applied stress, the crack can only grow an additional 0.293 inches. While the yield stress is 100 ksi, fracture occurs long before any yielding is possible.

Problem 3

Using the data from the previous problem, repeat the calculation for a finite sized panel with $W=6$ in and $2a=2$ in and $R = \frac{K_{Ic}^2}{E} + 0.4 (\Delta a)^{0.25}$ (kip/in). Assume plane stress conditions.

Solution

```
In[90]:= ClearAll["Global' *"]
Clear[c1, c2, c3, cc1, cc2, cc3, d1, d2, d3,
      dd1, dd2, dd3, a, aa, da, G, Gg, release, R, K, K1, KI]
```

```
In[92]:= KIC = 30; (*ksi*(in)^0.5*)
Emod = 30000; (*ksi*)
W2 = 6; (*in*)
sigy = 100; (*ksi*)
R[Δa_] :=  $\frac{KIC^2}{Emod} + 0.4 * (\Delta a)^{0.25}$ ;
a0 = 1; (*inch*)
```

```
In[98]:= K1b[a_, s_] :=  $\sqrt{\text{Sec}\left[\frac{\pi * a}{W2}\right] * s * \sqrt{\pi * a}}$ ;
```

```
In[99]:= Gb[a_, s_] :=  $\frac{(K1b[a, s])^2}{Emod}$ ; Simplify[Gb[a, s]]
```

```
Out[99]=  $\frac{a \pi s^2 \text{Sec}\left[\frac{a \pi}{6}\right]}{30000}$ 
```

Similar to the previous problem, a Matlab code was used to solve this problem. The final results are shown below:

```
In[100]:= Framed[σc = 43.7798]
Framed[ac = 1.1841]
Framed[Δac = ac - a0]
```

```
Out[100]= 43.7798
```

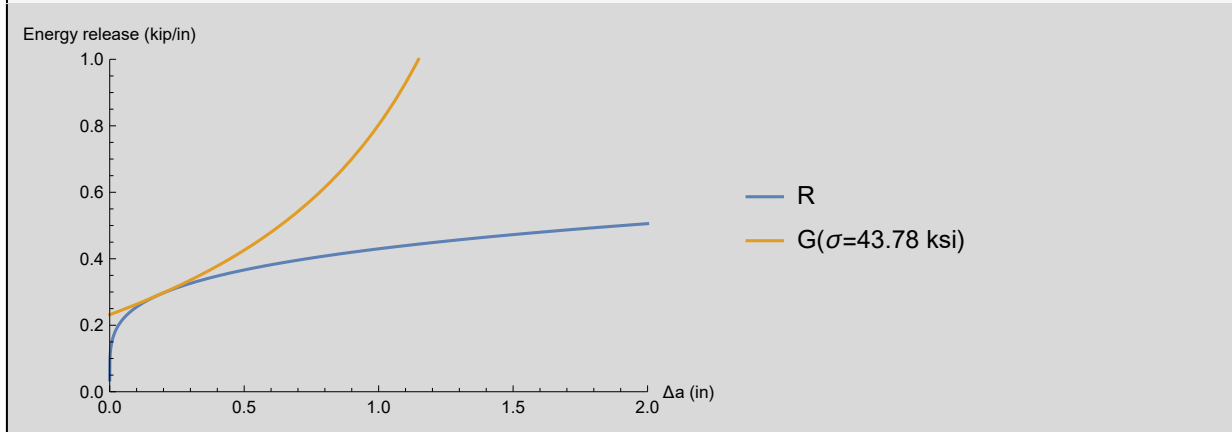
```
Out[101]= 1.1841
```

```
Out[102]= 0.1841
```

In[103]=

```
Plot[{R[da], Gb[a0 + da,  $\sigma_c$ ]}, {da, 0.0, 2},
  AxesLabel -> {" $\Delta a$  (in)", "Energy release (kip/in)"},
  PlotRange -> {{0, 2}, {0, 1}}, PlotLegends -> {"R", "G( $\sigma=43.78$  ksi)"}]
```

Out[103]=

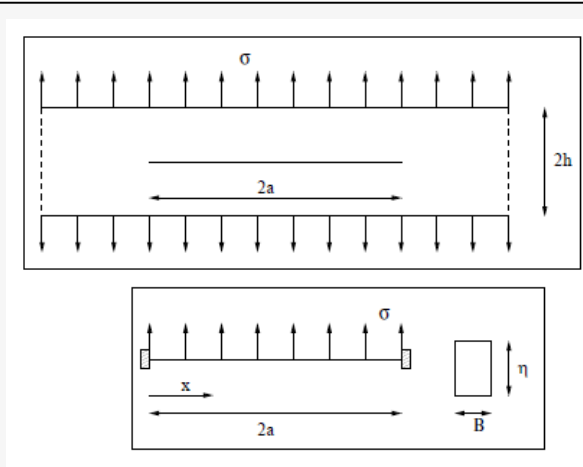


We can see that the energy release rate for the finite width plate is nonlinear compared to the previous problem. The critical energy release rate for this problem is slightly lower at 43.78 kip/in compared to 48.94 kip/in. The critical crack length also decreased from 1.293 inches to 1.1841.

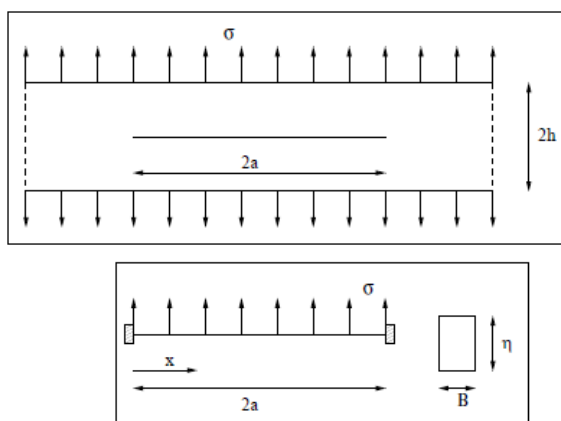
Problem 4

Consider a long strip of height $2h$ and thickness B with a crack length $2a$ subjected to a uniform stress σ along its upper and lower faces. For $a \gg h$, determine the stress intensity factor.

In[104]:=



Out[104]=



Note that:

In[105]:=

$$M = -\frac{qB}{6} (2a^2 - 6ax + 3x^2) \text{ for } 0 \leq x \leq a$$

$$U = \int_0^a \frac{M^2}{2EI} dx$$

Out[105]=

$$0 \leq x \leq a$$

Out[106]=

$$\int_0^a \frac{(0 \leq x \leq a)^2}{2EI} dx$$

Solution

We may treat this problem symmetrically like two double cantilever beams (DCB) that are joined in the middle. See the image of a DCM below borrowed from Zehnder 2012.

In[107]:=

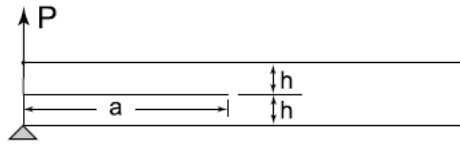


Fig. 3.4 DCB geometry, thickness B , load-point displacement q . This geometry is particularly useful for the study of delamination in composite materials

Out[107]=

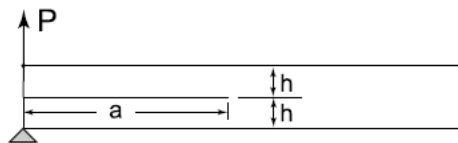


Fig. 3.4 DCB geometry, thickness B , load-point displacement q . This geometry is particularly useful for the study of delamination in composite materials

We will need to analyze a traction applied to the top and bottom surfaces instead of an applied point load.

The second moment of area (or moment of inertia) can be calculated simply as:

In[108]:=

```
ClearAll["Global' *"]
Clear[c1, c2, c3, cc1, cc2, cc3, d1, d2, d3,
      dd1, dd2, dd3, a, aa, da, G, Gg, release, R, K, K1, KI]
```

In[110]:=

```
Inert[B_, h_] :=  $\frac{1}{12} B * h^3$ ;
```

We'll define the moment "M" and the internal strain energy "U" as follows:

```
In[111]:= M[q_, B_, a_, x_] :=  $\frac{-q * B}{6} * (2 a^2 - 6 * a * x + 3 x^2)$ ;
U[q_, B_, a_, x_, h_, Em_] :=  $2 * \int_0^a \frac{(M(q, B, a, x))^2}{2 * Em * Inert(B, h)} dx$ ;
Simplify[U[q, B, a, x, h, Em]]
```

SetDelayed: Tag LessEqual in (0 ≤ x ≤ a)[q_, B_, a_, x_] is Protected.

SetDelayed: Tag Integrate in $\left(\int_0^a \frac{(0 \leq x \leq a)^2}{2 EI} dx\right)$ [q_, B_, a_, x_, h_, Em_] is Protected.

Out[112]= $\left(\int_0^a \frac{(0 \leq x \leq a)^2}{2 EI} dx\right) [q, B, a, x, h, Em]$

We want to take the potential energy (internal energy) and relate it to the energy release rate which will then be related to the stress intensity factor. Here is the expression we wish to determine:

$$G = \frac{\partial U}{\partial A} = \frac{1}{2 B} \frac{\partial U}{\partial a}$$

The energy release rate is then

```
In[113]:= G[q_, B_, a_, x_, h_, Em_] := D[U[q, B, a, x, h, Em], {a, 1}] / (2 * B);
Simplify[G[q, B, a, x, h, Em]]
```

Out[113]=
$$\frac{\left(\frac{(a \geq 0)^2}{2 EI} + \int_0^a \frac{\partial_a (0 \leq x \leq a) * (0 \leq x \leq a)}{EI} dx\right) [q, B, a, x, h, Em] + \left(\int_0^a \frac{(0 \leq x \leq a)^2}{2 EI} dx\right)^{(\theta, \theta, 1, \theta, \theta, \theta)} [q, B, a, x, h, Em]}{2 B}$$

Lastly, we can determine the energy release rate as

$$K_I = \sqrt{G * E}$$

So

```
In[114]:= KI[q_, B_, a_, x_, h_, Em_] :=  $\sqrt{G[q, B, a, x, h, Em] * Em}$ ;
Framed[Simplify[KI[q, B, a, x, h, Em]]]
```

Out[114]=
$$\sqrt{\frac{Em \left(\left(\frac{(a \geq 0)^2}{2 EI} + \int_0^a \frac{\partial_a (0 \leq x \leq a) * (0 \leq x \leq a)}{EI} dx\right) [q, B, a, x, h, Em] + \left(\int_0^a \frac{(0 \leq x \leq a)^2}{2 EI} dx\right)^{(\theta, \theta, 1, \theta, \theta, \theta)} [q, B, a, x, h, Em]\right)}{B}}$$

This is the stress intensity factor! Simplifying further:

$$K_I = \frac{\sqrt{2} qa^2}{\sqrt{3 h^3}}$$

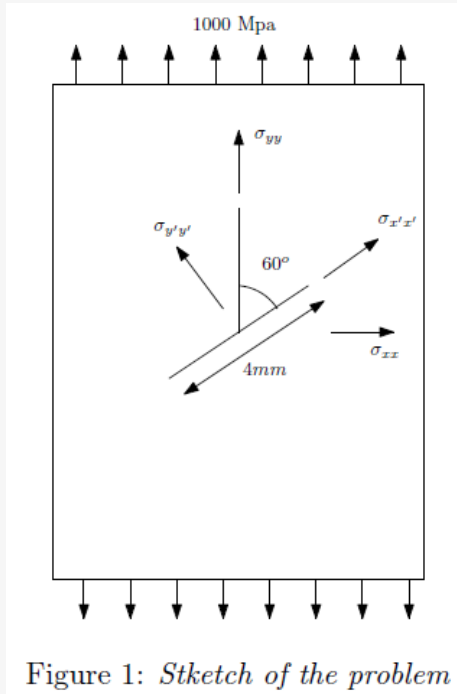
Homework 5

Thomas Allard
CVEN 7161

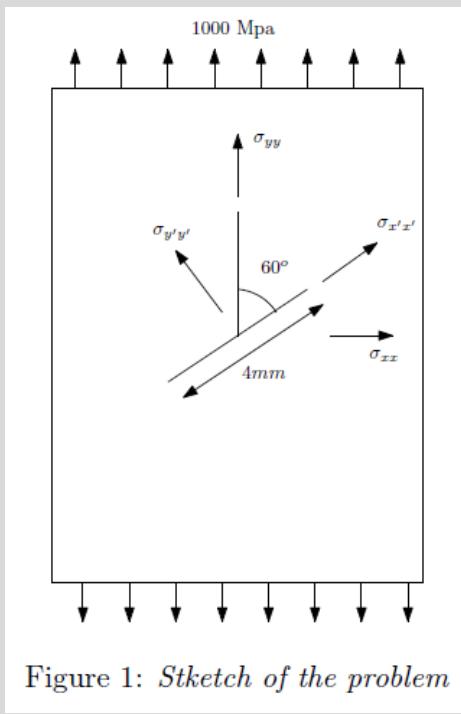
Problem 1

A large plate, containing a crack length of 4mm oriented at an angle $\beta = 60^\circ$ with respect to the direction of the applied uniaxial tensile stress σ , fractures at a value of $\sigma_c = 1,000$ MPa. Using the minimum strain energy density model, compute K_{Ic} with $E = 210$ GPa and $\nu = 0.3$.

In[1]:=



Out[1]=



Solution

In[2]:=

```
ClearAll["Global' *"]  
Clear[ $\theta$ ]
```


Background from Sih and Gdoutos

Sih formulated the Minimum Strain Energy Density Criteria in 1974. The strain energy density per unit volume can be calculated using the following formula.

$$\frac{dU}{dV} = \frac{1}{2E} (\sigma_{xx}^2 + \sigma_{yy}^2 + \sigma_{zz}^2) - \frac{\nu}{E} (\sigma_{xx} \sigma_{yy} + \sigma_{yy} \sigma_{zz} + \sigma_{zz} \sigma_{xx}) + \frac{1}{2\mu} (\sigma_{xy}^2 + \sigma_{yz}^2 + \sigma_{zx}^2)$$

Sih defines the following strain energy density factor S for 2D geometries as follows:

$$S = a_{11} K_I^2 + 2 a_{12} K_I K_{II} + a_{22} K_{II}^2$$

Where

$$a_{11} = \frac{1}{16 \pi \mu} ((\kappa - \cos[\theta]) (1 + \cos[\theta]))$$

$$a_{12} = \frac{1}{16 \pi \mu} \sin[\theta] (2 \cos[\theta] - (\kappa - 1))$$

$$a_{22} = \frac{1}{16 \pi \mu} ((\kappa + 1) (1 - \cos[\theta]) + (1 + \cos[\theta]) \times (3 \cos[\theta] - 1))$$

Calculations

First, we need to transform our stress vector (assuming $\sigma = \sigma_c$) to determine K_I and K_{II} in the x' and y' directions.

In[4]:=

```

σc = 1000.0; (*MPa*)
β = π / 3;
βrot = (π / 2) - β;
σ' = ( Cos[βrot] Sin[βrot] ) · ( 0 0 ) · ( Cos[βrot] -Sin[βrot] );
      ( -Sin[βrot] Cos[βrot] ) · ( 0 σc ) · ( Sin[βrot] Cos[βrot] );
MatrixForm[Simplify[σ']]

```

Out[7]/MatrixForm=

```

( 250. 433.013 )
( 433.013 750. )

```

The stress intensity factors are then calculated with the shape parameter equal to 1 for an infinitely wide plate.

In[8]:=

```

KI[a_] := σ'[[2, 2]] * √(π * a); Simplify[KI[2]]
KII[a_] := σ'[[1, 2]] * √(π * a);
Simplify[KII[2]]

```

Out[8]=

```
1879.97
```

Out[9]=

```
1085.4
```

We need to calculate the shear modulus.

```
In[10]:= Em = 210 000;
nu = 0.3;
mu = Em / (2 * (1 + nu))
```

```
Out[12]= 80 769.2
```

First, we will assume plane stress conditions. Therefore kappa:

```
In[13]:= kappa = (3 - nu) / (1 + nu)
```

```
Out[13]= 2.07692
```

The coefficients a11, a12, and a22 can be defined as follows:

```
In[14]:= (*theta=pi/3; (*60 degrees*) *)
a11[theta_] := (1 / (16 * mu)) * ((kappa - Cos[theta]) * (1 + Cos[theta]));
a12[theta_] := (Sin[theta] / (16 * mu)) * (2 * Cos[theta] - (kappa - 1));
a22[theta_] := (1 / (16 * mu)) * ((kappa + 1) * (1 - Cos[theta]) + (1 + Cos[theta]) * (3 * Cos[theta] - 1));
```

Now define a function for the strain energy density factor.

```
In[17]:= S[a_, theta_] := (a11[theta] * KI[a]^2) + (2 * a12[theta] * KI[a] * KII[a]) + (a22[theta] * KII[a]^2);
Simplify[S[a, theta]]
```

```
Out[17]= a (3.78674 + 6.66134 × 10-16 Cos[theta]2 - 1.70044 Sin[theta] + Cos[theta] (0.981748 + 3.15795 Sin[theta]))
```

The fundamental hypothesis of the strain energy density criterion are that (1) the crack will extend in the direction of minimum strain energy density and (2) crack extension occurs when the minimum strain energy density factor, $S = S_{\min}$, reaches a critical values, say S_{cr} . This results in two criterion for the strain energy density in which we will look for the critical crack propagation angle θ_c .

$$\frac{\partial S}{\partial \theta} = 0$$

$$\frac{\partial^2 S}{\partial \theta^2} > 0$$

Take the first and second derivatives of S with respect to θ .

```
In[18]:= dS[a_, θ_] := D[S[a, θ], {θ, 1}]; Simplify[dS[a, θ]]
ddS[a_, θ_] := D[S[a, θ], {θ, 2}];
Simplify[ddS[a, θ]]
```

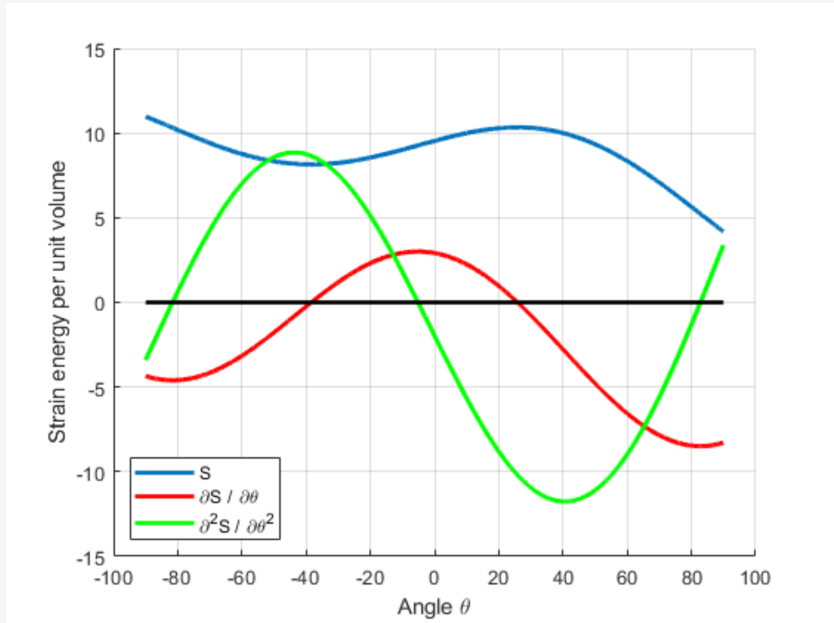
```
Out[18]= a (3.15795 Cos[θ]^2 +
Cos[θ] (-1.70044 - 1.33227 × 10-15 Sin[θ]) + (-0.981748 - 3.15795 Sin[θ]) Sin[θ])
```

```
Out[19]= a (-1.33227 × 10-15 Cos[θ]^2 +
Cos[θ] (-0.981748 - 12.6318 Sin[θ]) + (1.70044 + 1.33227 × 10-15 Sin[θ]) Sin[θ])
```

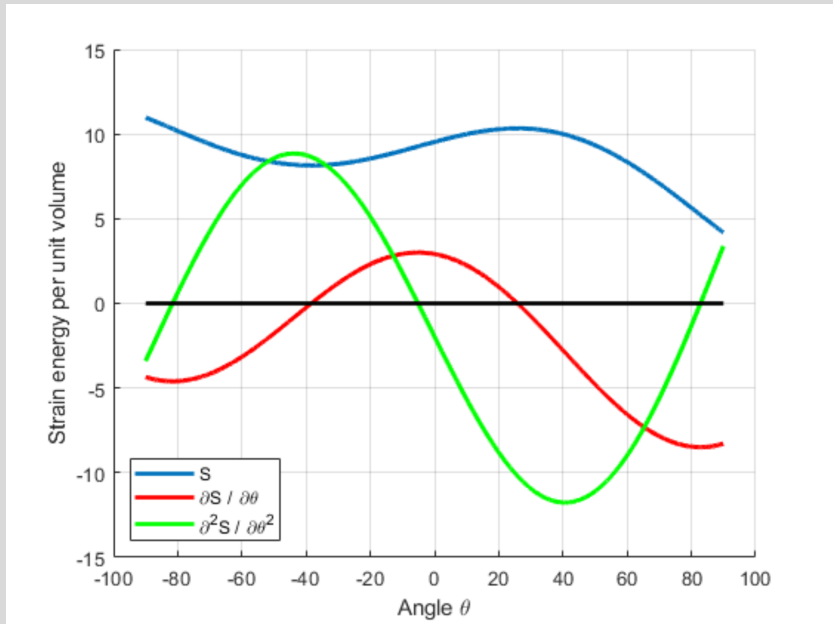
As outlined by Gdoutos 1989, for a particular problem under consideration with known values of K_I and K_{II} the value of crack extension angle θ_c can be determined by finding the roots of the preceding equations. By substituting θ_c into the stress energy density factor, the value of S_{\min} is determined and equated to the critical strain energy density factor S_{cr} to determine if crack propagation will occur.

A Matlab script (attached at the end of this assignment) was written that performs the calculation of θ_c . In the rotated coordinate frame, a value of for θ_c was determined as **-38.3776° or 8.3776°** with respect to the original Cartesian frame. The plot below shows the variation in the strain energy per unit volume with angle theta. We see the $\frac{\partial S}{\partial \theta}$ has two roots, but only one of which occurs when $\frac{\partial^2 S}{\partial \theta^2} > 0$. It should be noted that this will give an S_{cr} that isn't necessarily the minimum value of S.

In[20]:=



Out[20]=



In[21]:=

```

theta_c = -38.3776 * (pi / 180);
a11[theta_c]
a12[theta_c]
a22[theta_c]

```

Out[22]=

$$1.78487 \times 10^{-6}$$

Out[23]=

$$-2.35858 \times 10^{-7}$$

Out[24]=

$$2.38051 \times 10^{-6}$$

We may now calculate S_{cr} .

In[25]:=

```

S_cr = S[2, theta_c]

```

Out[25]=

$$8.15019$$

And finally the critical stress intensity factor is determined using the following formula:

In[26]:=

```

Framed[ K_Ic = sqrt( (S_cr * 8 * pi * mu) / (kappa - 1) ) ]

```

Out[26]=

$$3919.53$$

This is our stress intensity factor!! The same procedure could be repeated for plane strain conditions by simply changing the expression for kappa.

Problem 2

For the preceding problem, plot the deviatoric and volumetric strain energy densities around the crack tip.

Solution

The strain energy density (per unit volume) may be decomposed into deviatoric (D) and volumetric (V) components as follows:

$$\frac{dW}{dV} = \left(\frac{dW}{dV} \right)_D + \left(\frac{dW}{dV} \right)_V$$

$$\left(\frac{dW}{dV} \right)_D = \frac{1+\nu}{6E} [(\sigma_{xx} - \sigma_{yy})^2 + (\sigma_{yy} - \sigma_{zz})^2 + (\sigma_{zz} - \sigma_{xx})^2 + 6(\sigma_{xy}^2 + \sigma_{yz}^2 + \sigma_{zx}^2)]$$

$$\left(\frac{dW}{dV} \right)_V = \frac{1-2\nu}{6E} (\sigma_{xx} + \sigma_{yy} + \sigma_{zz})^2$$

In 2D plane stress, $\sigma_{yz} = \sigma_{xz} = 0$ and $\sigma_{zz} = 0$. Thus

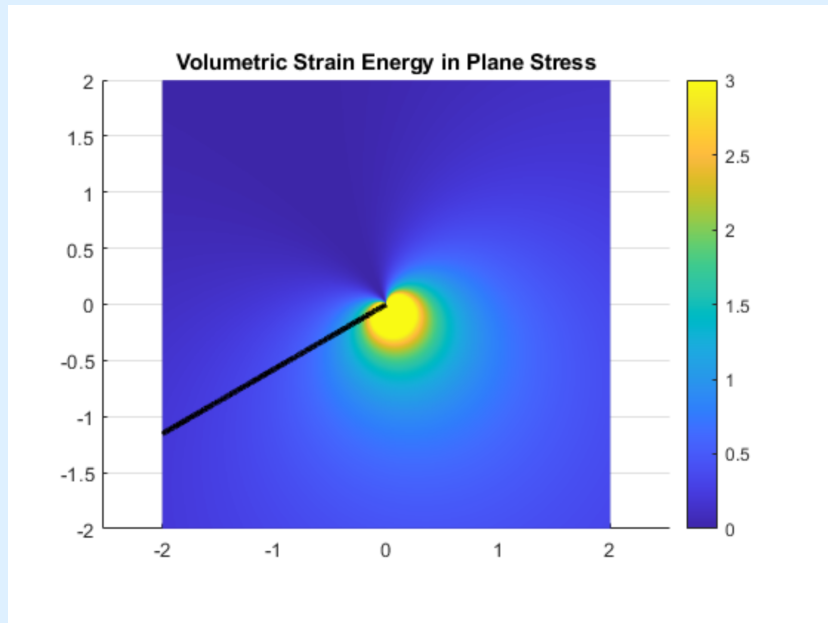
$$\left(\frac{dW}{dV} \right)_D = \frac{1+\nu}{6E} [(\sigma_{xx} - \sigma_{yy})^2 + (\sigma_{yy})^2 + (\sigma_{xx})^2 + 6\sigma_{xy}^2]$$

$$\left(\frac{dW}{dV} \right)_V = \frac{1-2\nu}{6E} (\sigma_{xx} + \sigma_{yy})^2$$

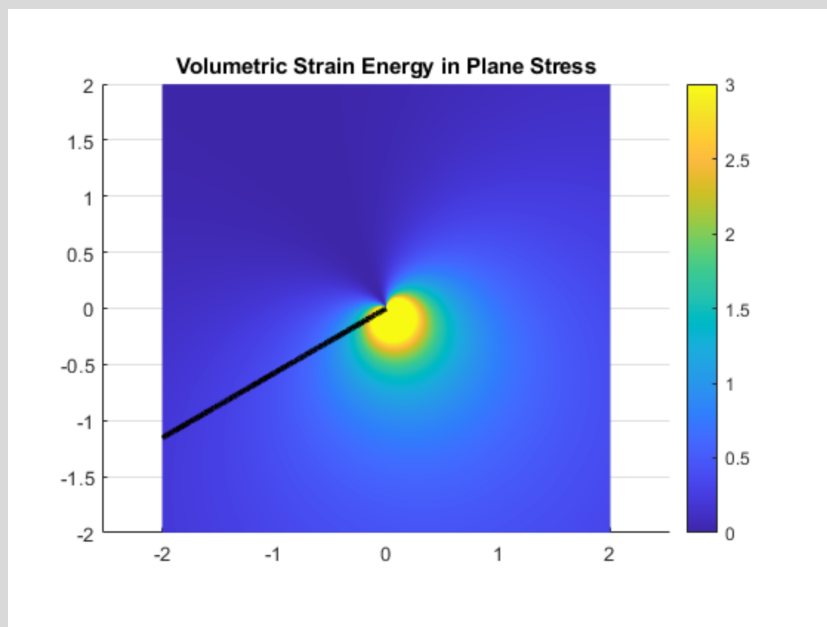
Plots were generated using the same Matlab code as for the previous problem.

Below is a plot of the **Volumetric strain energy**

In[27]:=

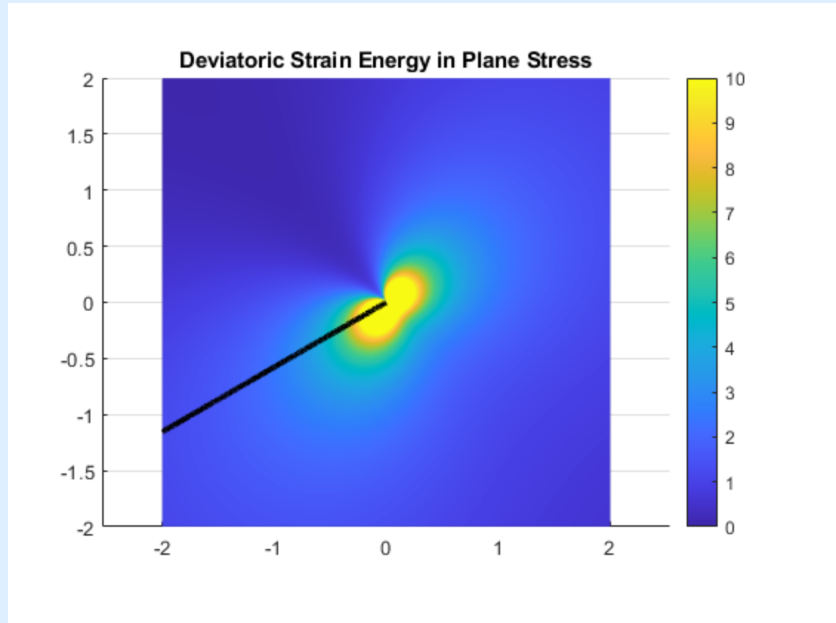


Out[27]=

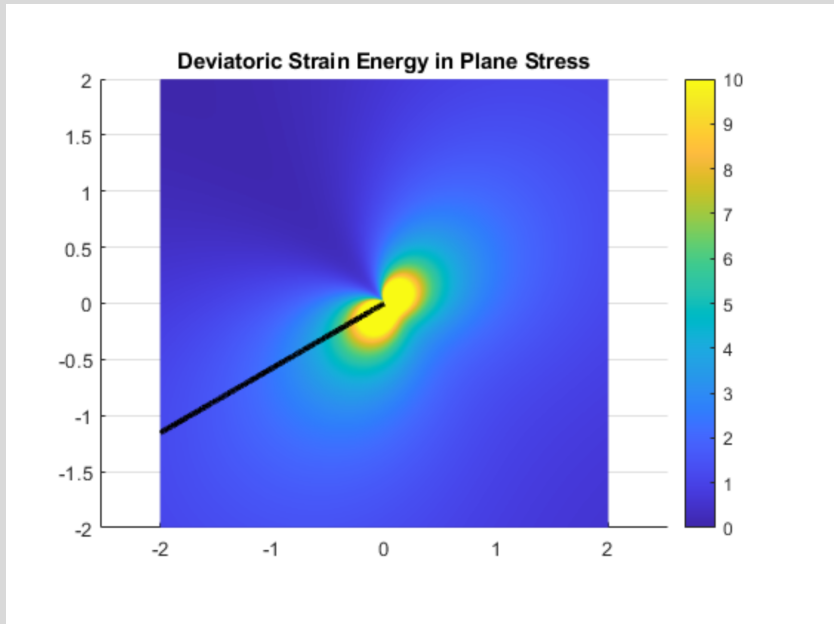


Below is a plot of the **Deviatoric strain energy**

In[28]:=



Out[28]=



The volumetric strain energy represents the strain energy associated with volume change and no shape change. The deviatoric strain energy represents the strain energy associated with distortional shape change and no volume change.

Problem 3

Repeat for pure Mode I and Mode II cases.

Solution

Mode I

The two stress intensity factors will now be defined as

```
In[29]:= KIa[a_] =  $\sigma_c * \sqrt{\pi * a}$  ;
          KIIa = 0;
```

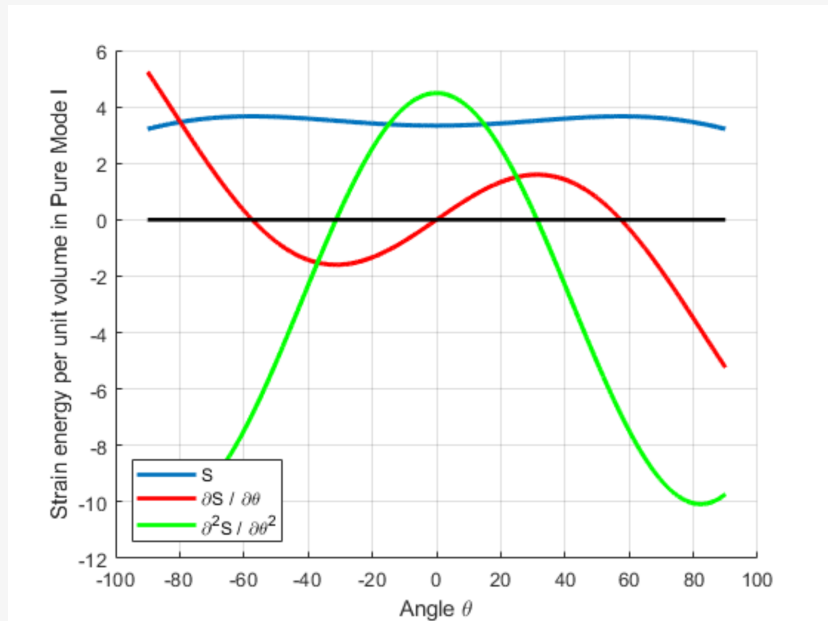
And the strain energy density factor is then

```
In[31]:= Sa[a_,  $\theta$ ] := (a11[ $\theta$ ] * KIa[a]^2) + (2 * a12[ $\theta$ ] * KIa[a] * KIIa) + (a22[ $\theta$ ] * KIIa^2);
          Simplify[Sa[a,  $\theta$ ]]
```

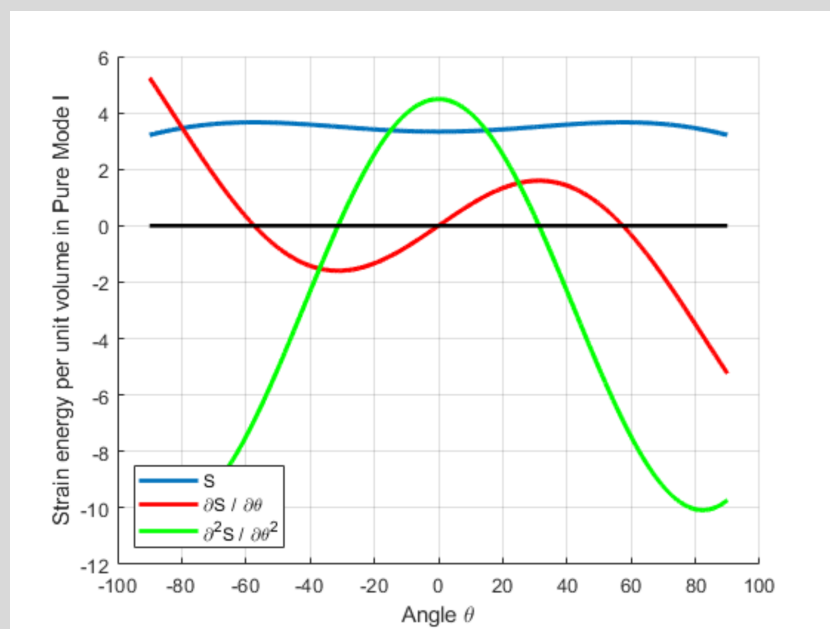
```
Out[31]= -2.43099 a (-2.07692 + Cos[ $\theta$ ]) * (1. + Cos[ $\theta$ ])
```

The same Matlab code is used again to determine θ_c which is calculated as 0° as expected. The plot below shows the variation in S and its derivatives with angle, clearly showing 0° to be the critical direction of strain energy factor.

In[32]=



Out[32]=



In[33]=

$\theta_{ca} = 0;$

The stain energy factor is thus

In[34]=

$Scra = Sa[2, \theta_{ca}]$

Out[34]=

10.472

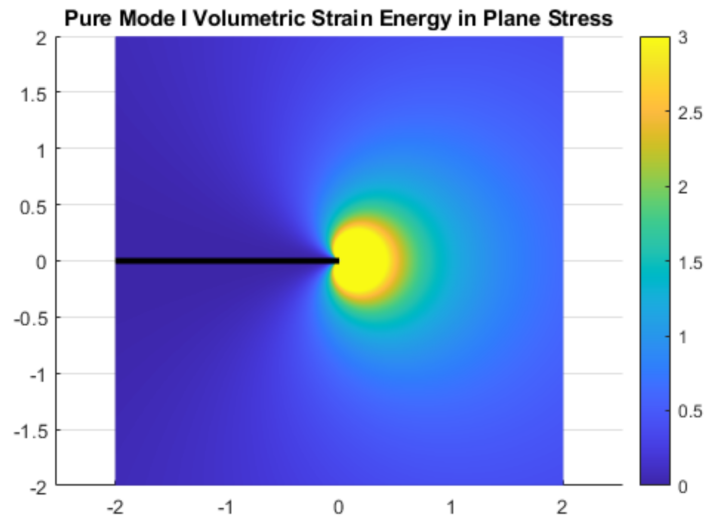
And the critical stress intensity factor

In[35]:= `Framed`
$$\left[K_{Ica} = \sqrt{\frac{S_{cra} * 8 * \pi * \mu}{(\kappa - 1)}} \right]$$

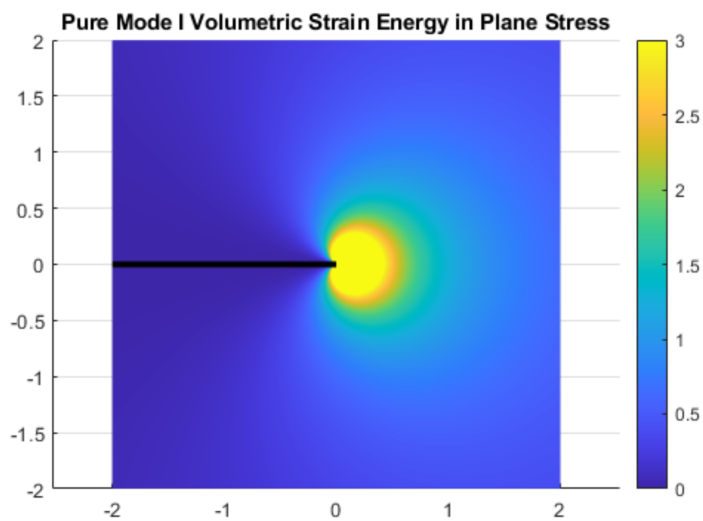
Out[35]= `4442.88`

We may plot the **Volumetric strain energy** using the same Matlab code as before.

In[36]:=

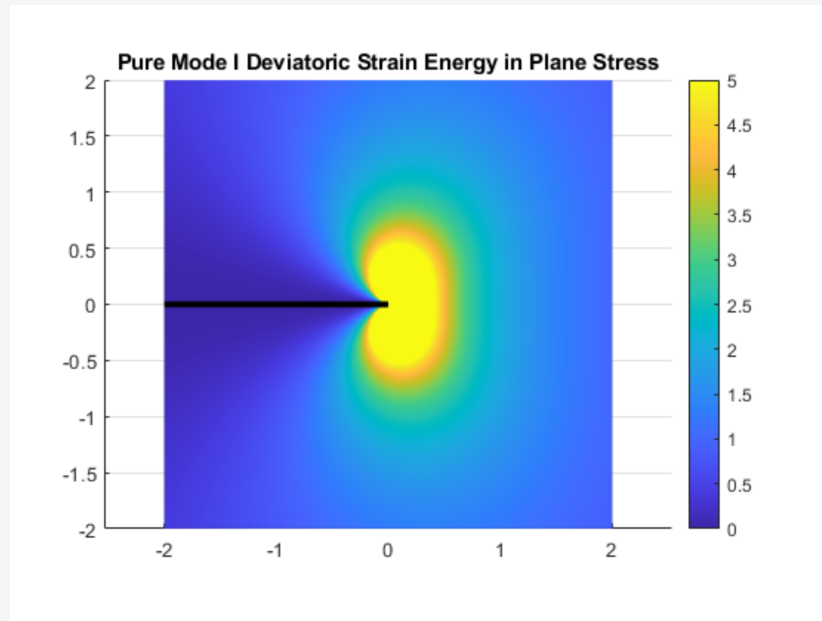


Out[36]=

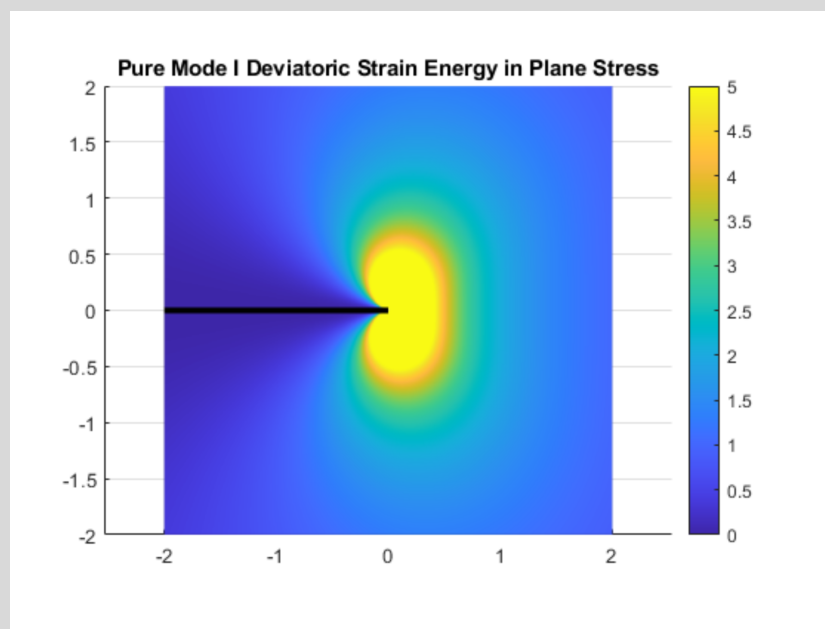


And the **Deviatoric strain energy**

In[37]:=



Out[37]=



These plots show that the strain energy is symmetric about a line parallel and coincident with the crack front as expected! The deviatoric strain energy is more intense and occupies a larger region than the volumetric strain energy.

Mode II

The two stress intensity factors will now be defined as

In[38]:=

$$\begin{aligned} \mathbf{KIb} &= \mathbf{0}; \\ \mathbf{KIIb}[a_] &= \sigma_c * \sqrt{\pi * a}; \end{aligned}$$

And the strain energy density factor is then

In[40]=

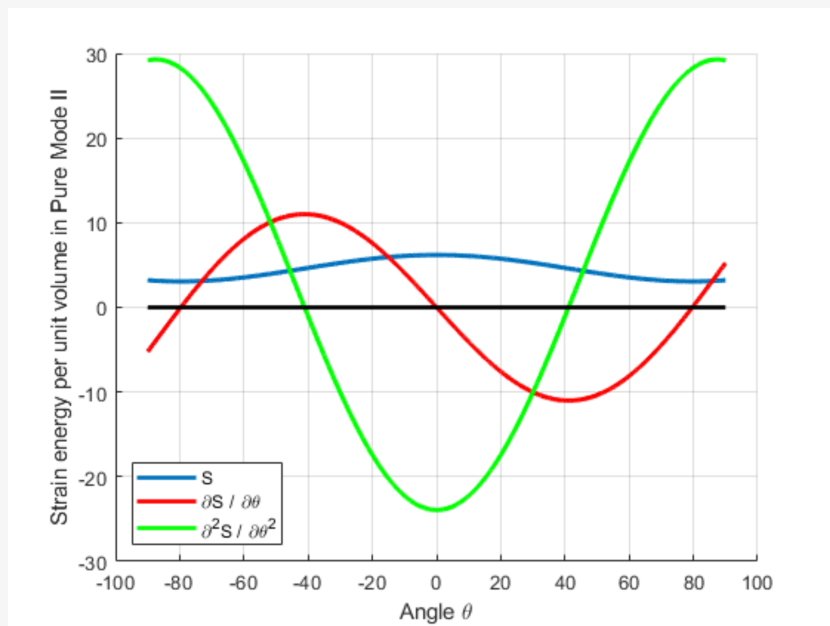
```
Sb[a_,  $\theta$ _] := (a11[ $\theta$ ] * KIb2) + (2 * a12[ $\theta$ ] * KIb * KIIb[a]) + (a22[ $\theta$ ] * KIIb[a]2);  
Simplify[Sb[a,  $\theta$ ]]
```

Out[40]=

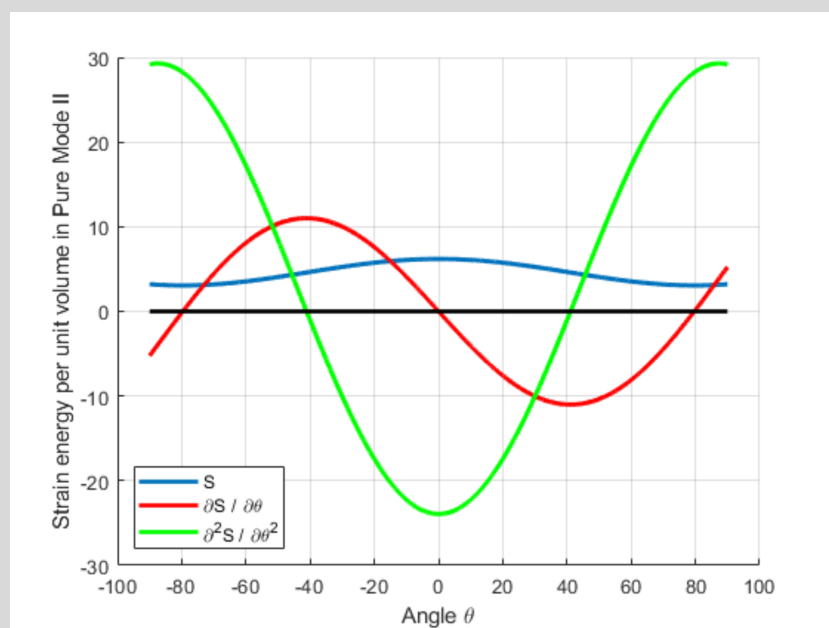
```
7.29298 a (0.692308 - 0.358974 Cos[ $\theta$ ] + Cos[ $\theta$ ]2)
```

The same Matlab code is used again to determine θ_c which is calculated as -79.6601° . The plot below shows the variation in S and its derivatives with angle. Notice that the negative of the calculated angle, 79.6601° is also a valid solution!

In[41]=



Out[41]=



In[42]:=

In[43]:=

$$\theta_{cb} = -79.6601 * \frac{\pi}{180};$$

The strain energy factor is thus

In[44]:=

$$S_{crb} = S_b[2, \theta_{cb}]$$

Out[44]:=

9.62808

The same strain energy factor is calculated for the negative of the angle!

In[45]:=

$$S_{crb} = S_b[2, -1 * \theta_{cb}]$$

Out[45]:=

9.62808

And the critical stress intensity factor

In[46]:=

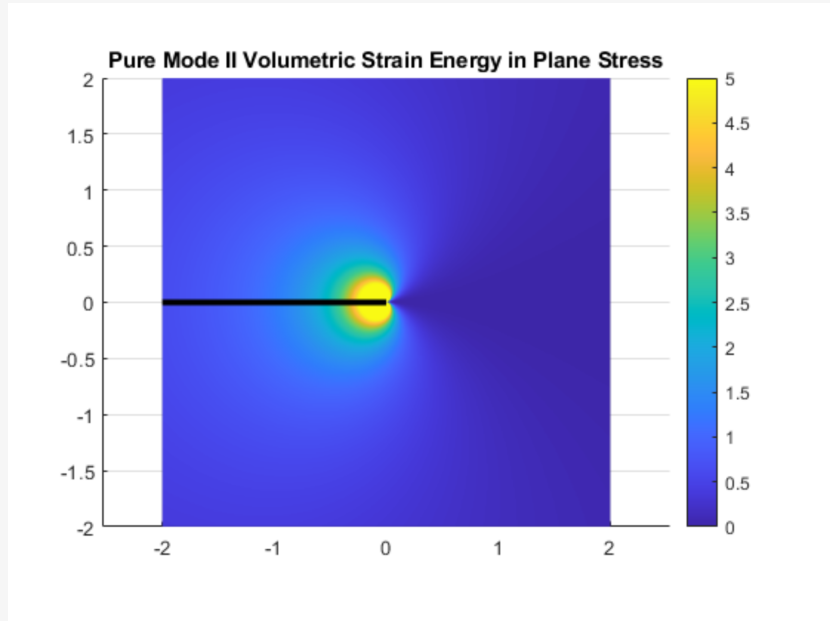
$$\text{Framed} \left[K_{Icb} = \sqrt{\frac{S_{crb} * 8 * \pi * \mu}{(\kappa - 1)}} \right]$$

Out[46]:=

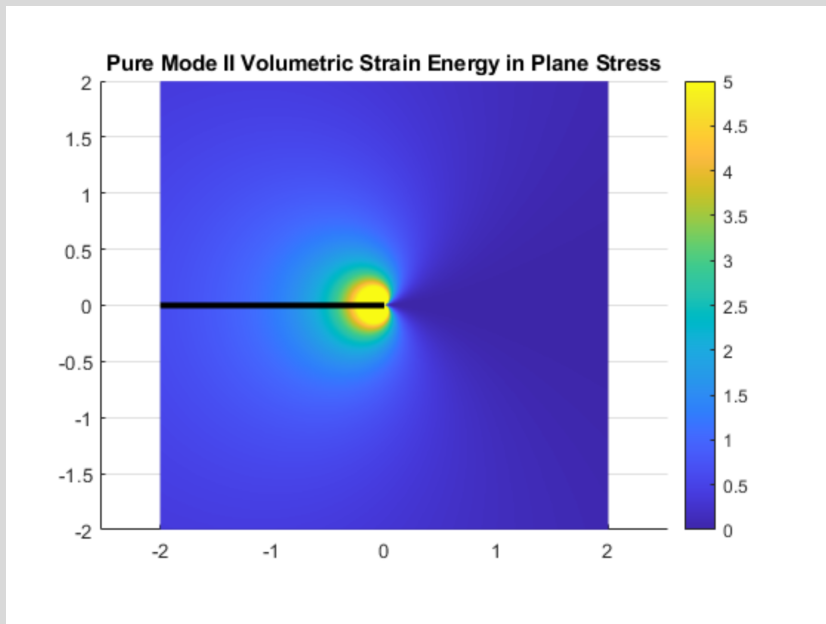
4260.11

We may plot the **Volumetric strain energy** using the same Matlab code as before.

In[47]:=

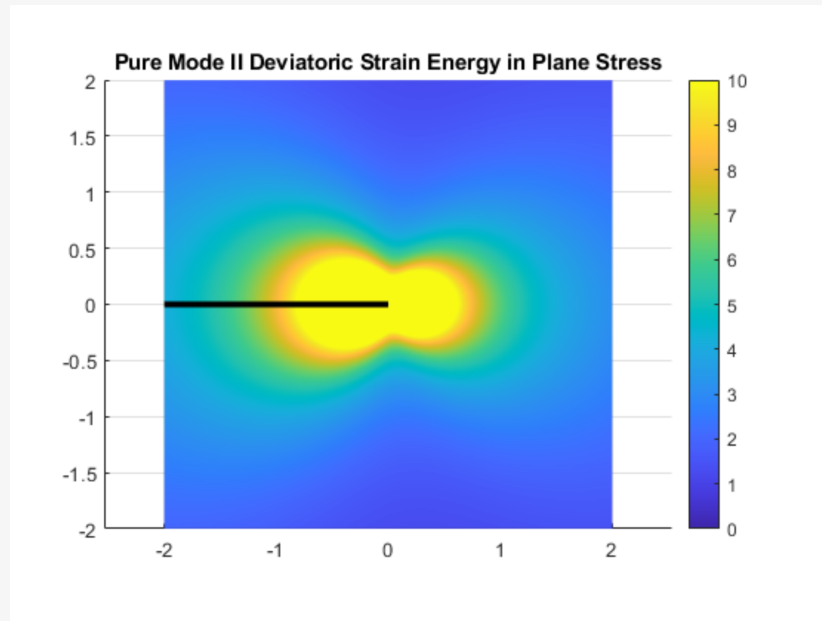


Out[47]=

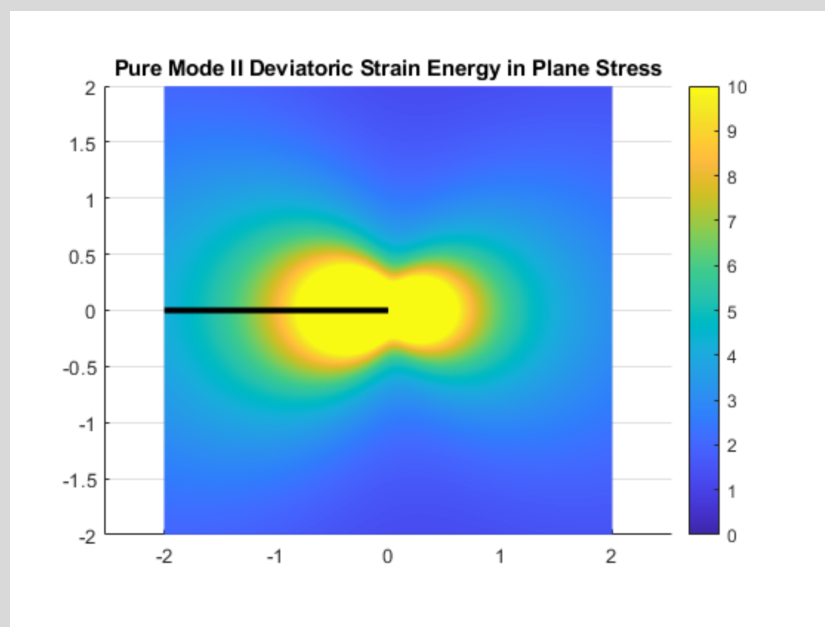


And the **Deviatoric strain energy**

In[48]:=



Out[48]=



These plots are also symmetric. It is interesting to see that there is a considerable amount of strain energy behind the crack tip for the the deviatoric component and the volumetric part is almost only behind the crack tip.

Considering the result that the new crack propagation angle could be -79.6601° or 79.6601° , this problem sheds light on the complexity of this system and a potentially non-unique solution under ideal circumstances. This point may be worth paying attention to in the context of crack branching. Or perhaps in a heterogeneous system, there may be an imperfection that results in a preferential crack growth in one of these two directions.

Problem 4

For the first problem, plot the plastic zone size for plane strain and for plane stress. Assume $\sigma_y = 2,000$ MPa.

Solution

First, we will discuss how the plastic zone will be calculated under plane stress and plane strain conditions. The plot for both cases will be shown at the end

Plane Stress

We may use the same system for stress and strain energy density as was used for problem 1.

We will determine the plastic zone size using the most straightforward model. We will equate the deviatoric stress (which is associated with distortion and therefore yielding) to the square of the yield stress of 2000 MPa and search for the radius of the plastic zone as a function of angle θ . Our criteria:

$$\sigma_y^2 - \frac{1}{\sqrt{2}} [(\sigma_{xx}[r, \theta] - \sigma_{yy}[r, \theta])^2 + (\sigma_{yy}[r, \theta] - \sigma_{zz}[r, \theta])^2 + (\sigma_{zz}[r, \theta] - \sigma_{xx}[r, \theta])^2 + 6 \sigma_{xy}[r, \theta]^2] = 0$$

For plane stress where $\sigma_{zz} = 0$, this reduces to

$$\sigma_y^2 - \frac{1}{\sqrt{2}} [(\sigma_{xx}[r, \theta] - \sigma_{yy}[r, \theta])^2 + (\sigma_{yy}[r, \theta])^2 + (\sigma_{xx}[r, \theta])^2 + 6 \sigma_{xy}[r, \theta]^2] = 0$$

The stresses of interest are calculated as follows

$$\begin{aligned} \sigma_{xx}[r, \theta] &= \frac{K_I}{\sqrt{2} \pi r} \cos\left[\frac{\theta}{2}\right] \left(1 - \sin\left[\frac{\theta}{2}\right] \times \sin\left[\frac{3\theta}{2}\right]\right) - \frac{K_{II}}{\sqrt{2} \pi r} \sin\left[\frac{\theta}{2}\right] \left(2 + \cos\left[\frac{\theta}{2}\right] \times \cos\left[\frac{3\theta}{2}\right]\right) \\ \sigma_{yy}[r, \theta] &= \frac{K_I}{\sqrt{2} \pi r} \cos\left[\frac{\theta}{2}\right] \left(1 + \sin\left[\frac{\theta}{2}\right] \times \sin\left[\frac{3\theta}{2}\right]\right) + \frac{K_{II}}{\sqrt{2} \pi r} \sin\left[\frac{\theta}{2}\right] \times \cos\left[\frac{\theta}{2}\right] \times \cos\left[\frac{3\theta}{2}\right] \\ \sigma_{xy}[r, \theta] &= \frac{K_I}{\sqrt{2} \pi r} \cos\left[\frac{\theta}{2}\right] \times \sin\left[\frac{\theta}{2}\right] \times \cos\left[\frac{3\theta}{2}\right] + \frac{K_{II}}{\sqrt{2} \pi r} \cos\left[\frac{\theta}{2}\right] \left(1 - \sin\left[\frac{\theta}{2}\right] \times \sin\left[\frac{3\theta}{2}\right]\right) \end{aligned}$$

The attached Matlab code then searches for the radius that meets this criteria for each angle of θ from 0 to 2π .

Plane Strain

For plane strain, the out-of-plane stress is no longer zero. This stress may be calculated as follows:

$$\sigma_{zz} = \nu (\sigma_{xx} + \sigma_{yy})$$

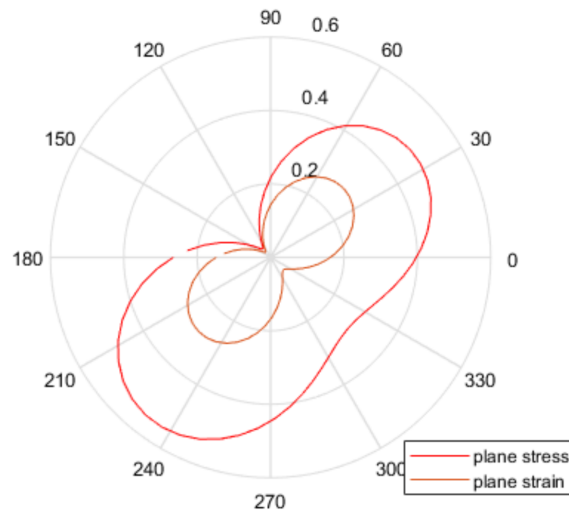
Our yield criteria for plane strain is then the same as the original one shown (before removing σ_{zz} for plane stress).

The attached Matlab code then searches for the radius that meets this criteria for each angle of θ from 0 to 2π .

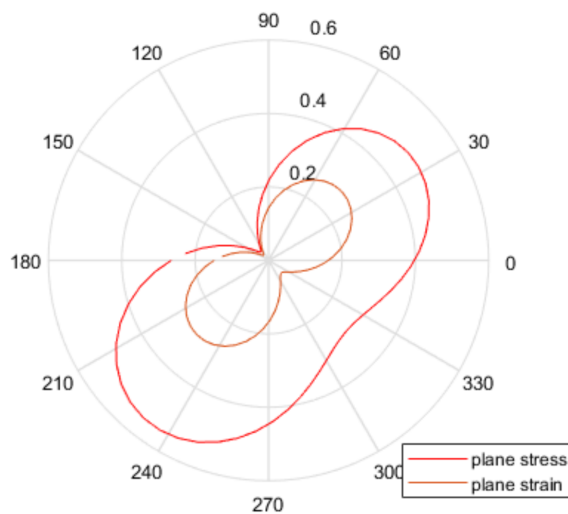
Final Plot

The final plot for the plastic zone sizes, using the same Matlab script, is shown below

In[49]=



Out[49]=



As expected, the plastic zone looks like a peanut for plane strain and a kidney for plane stress. Under plane strain conditions, the additional out-of-plane stress σ_{zz} significantly contributes to the “right-hand side” of the yield criteria thus reducing the plastic zone radius. With $\sigma_{zz} = 0$ for plane stress, this contribution changes the stress state for yield and the plastic zone is much larger in size.

Part: Part 1 of {} does not exist.

Part: Part 3 of {}[1] does not exist.

- ⋮ **Set:** Tag Part in {}[[1]][3][Source] is Protected.
- ⋮ **Lookup:** The argument {}[[1]][3] is not a valid Association or a list of rules.
- ⋮ **Set:** Part 3 of {}[[1]] does not exist.
- ⋮ **Part:** Part specification KeyAbsent is not applicable.
- ⋮ **Append:** Nonatomic expression expected at position 1 in Append[KeyAbsent, Switch[Missing[KeyAbsent, Source], _List, None, _After, -1, _Before, 1]].
- ⋮ **Part:** The expression Switch[Missing[KeyAbsent, Source], _List, None, _After, -1, _Before, 1] cannot be used as a part specification.
- ⋮ **Append:** Append called with 3 arguments; 1 or 2 arguments are expected.
- ⋮ **Part:** The expression Switch[Missing[KeyAbsent, Source], _List, None, _After, -1, _Before, 1] cannot be used as a part specification.
- ⋮ **Append:** Append called with 4 arguments; 1 or 2 arguments are expected.
- ⋮ **Part:** The expression Switch[Missing[KeyAbsent, Source], _List, None, _After, -1, _Before, 1] cannot be used as a part specification.
- ⋮ **General:** Further output of Part::pkspec1 will be suppressed during this calculation.
- ⋮ **Append:** Append called with 5 arguments; 1 or 2 arguments are expected.
- ⋮ **General:** Further output of Append::argt will be suppressed during this calculation.
- ⋮ **MapAt:** Position specification Append[KeyAbsent, Switch[Missing[KeyAbsent, Source], _List, None, _After, -1, _Before, 1], Switch[Missing[KeyAbsent, Source], _List, None, _After, -1, _Before, 1], <<6>>, Switch[Missing[KeyAbsent, Source], _List, None, _After, -1, _Before, 1], <<991>>] in MapAt[Function[CodeInspector`LinterUI`Private`token\$, CodeInspector`LinterUI`Private`varSet[{NotebookObject[

Homework-5_Thomas_Allard_corrected.nb

Input

InspectionObject[


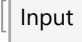

+ An internal Source: Mis

 inactive]; With[{CodeInspector`LinterUI`Private`markup\$ = DynamicModuleBox[{<<2>>}, Evaluate[<<1>>], RuleDelayed[<<2>>]], If[<<1>>]], , Append[<<1>>]] is not a machine-sized integer or a list of machine-sized integers.

 **MapAt:** Position specification Append[KeyAbsent, Switch[Missing[

KeyAbsent, Source], _List, None, _After, -1, _Before, 1], Switch[Missing[
 KeyAbsent, Source], _List, None, _After, -1, _Before, 1], <<6>>, Switch[Missing[
 KeyAbsent, Source], _List, None, _After, -1, _Before, 1], <<991>>] in

MapAt[Function[CodeInspector`LinterUI`Private`token\$, CodeInspector`LinterUI`Private`varSet[{NotebookObject[

 Homework-5_Thomas_Allard_corrected.nb], CellObject[ Input], InspectionObject[ An internal Source: Mis

inactive]; With[{CodeInspector`LinterUI`Private`markup\$ = DynamicModuleBox[{<<2>>}, Evaluate[<<1>>], RuleDelayed[<<2>>]], If[<<1>>]], , Append[<<1>>]] is not a machine-sized integer or a list of

machine-sized integers.

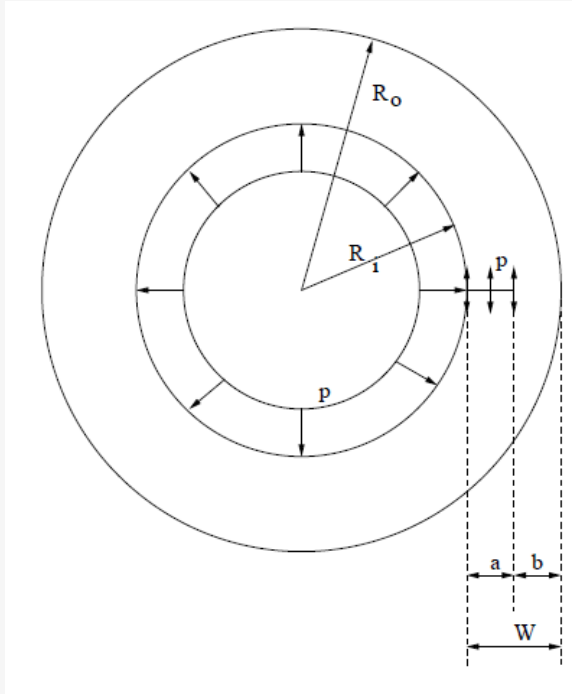
Homework 6

Thomas Allard
CVEN 7161

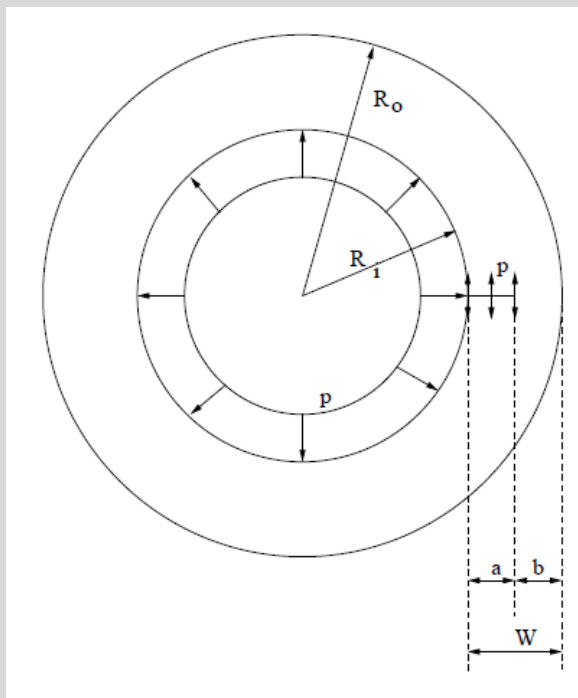
A pipe with 1.10m outside diameter and 50 mm thick wall contains a long axial flaw 10 mm deep. The material properties have been fit to a Ramberg-Osgood equation: $\sigma_y = 450$ MPa, $\epsilon_y = \frac{\sigma_y}{E}$, $\alpha = 1.25$, $n = 7$, and $E = 207,000$ MPa.

1. Plot the applied J_{el} , J_{pl} , and J versus internal pressure.
2. If J_{Ic} is 300 kJ/m^2 , determine the pressure required to initiate ductile crack growth.
3. What would be the pressure to initiate brittle crack growth? Assume $K_{Ic} = 110 \text{ MPa } \sqrt{m}$

In[1]:=



Out[1]=



Solution

In[2]:=

```
ClearAll["Global' *"]
```

As mentioned in the course notes, the solution of a plastic problem involves the determination of the J

integral. This usually involves a finite element analysis, but a first order approximation of J can be achieved. Following the simplified engineering approach for a Ramberg-Osgood material, we can write:

$$J = J_e (a_e) + J_p (a, n)$$

In[3]:=

```

r0 = 1.10 / 2; (*meters*)
t = 0.05; (*meters*)
ri = r0 - t;
a0 = 0.01; (*meters*)
b = t - a0;
σy = 450 * 106; (*Pa*)
Emod = 207000 * 106; (*Pa*)
α = 1.25;
n = 7;
εy = σy / Emod;
W = t;

```

(1) Determine J integrals

We will follow the solution outlined by Kumar et al. 1981 for an axially cracked cylinder (section 4.2).

Elastic

In the linear elastic range, the stress intensity factor can be written as:

$$K_{Ie} = \frac{2 p R_0^2 \sqrt{\pi a}}{R_0^2 - R_i^2} F \left(\frac{a}{b}, \frac{R_i}{R_0} \right)$$

The function for $F \left(\frac{a}{b}, \frac{R_i}{R_0} \right)$ is determined by interpolating values in the table provided by Kumar et al. 1981 which is shown below. For our case, $\frac{W}{R_i}$ is $\frac{1}{10}$. Also, $\frac{a}{W}$ is $\frac{a}{t} = \frac{1}{5}$. We will interpolate between $a/W = \frac{1}{8}$ and $a/W = \frac{1}{4}$ to determine the function F.

In[14]:=

```
W / ri
```

Out[14]=

```
0.1
```


In[15]:=

		$\frac{a}{W} = \frac{1}{8}$	$\frac{a}{W} = \frac{1}{4}$	$\frac{a}{W} = \frac{1}{2}$	$\frac{a}{W} = \frac{3}{4}$
$\frac{W}{R_I} = \frac{1}{5}$	F	1.19	1.38	2.10	3.30
	V ₁	1.51	1.83	3.44	7.50
$\frac{W}{R_I} = \frac{1}{10}$	F	1.20	1.44	2.36	4.23
	V ₁	1.54	1.91	3.96	10.40
$\frac{W}{R_I} = \frac{1}{20}$	F	1.20	1.45	2.51	5.25
	V ₁	1.54	1.92	4.23	13.50

Out[15]=

		$\frac{a}{W} = \frac{1}{8}$	$\frac{a}{W} = \frac{1}{4}$	$\frac{a}{W} = \frac{1}{2}$	$\frac{a}{W} = \frac{3}{4}$
$\frac{W}{R_I} = \frac{1}{5}$	F	1.19	1.38	2.10	3.30
	V ₁	1.51	1.83	3.44	7.50
$\frac{W}{R_I} = \frac{1}{10}$	F	1.20	1.44	2.36	4.23
	V ₁	1.54	1.91	3.96	10.40
$\frac{W}{R_I} = \frac{1}{20}$	F	1.20	1.45	2.51	5.25
	V ₁	1.54	1.92	4.23	13.50

In[16]:=

Fa = 1.20;
Fb = 1.44;

In[18]:=

$$F = Fa + \left(\frac{1}{5} - \frac{1}{8} \right) * \frac{Fb - Fa}{\frac{1}{4} - \frac{1}{8}}$$

Out[18]=

1.344

So, the elastic stress intensity factor as a function of pressure is given as:

In[19]:=

$$KIE[p_] := \frac{2 p r \theta^2 \sqrt{\pi * a \theta}}{r \theta^2 - r_i^2} F;$$

Simplify[KIE[p]]

Out[20]=

2.74518 p

The elastic J integral is then

In[21]:=

$$Jel[p_] := \frac{KIE[p]^2}{E_{mod}};$$

Simplify[Jel[p]]

Out[22]=

$3.64058 \times 10^{-11} p^2$

Plastic

We can write the fully plastic J solution as :

$$J_p = \alpha \epsilon_y \sigma_y b \frac{a}{W} h_1 \left(\frac{a}{W}, n \right) \left(\frac{P}{P_\theta} \right)^{n+1}$$

The limit load, P_0 , can be calculated as:

In[23]=

$$P_0 = \frac{2}{\sqrt{3}} \frac{b * \sigma_y}{r_i + a\theta}$$

Out[23]=

$$4.07541 \times 10^7$$

The table below shows the h - functions for an internally pressurized, axially cracked cylinder as investigated by Kumar et al. 1981.

In[24]=

		$n = 1$	$n = 2$	$n = 3$	$n = 5$	$n = 7$	$n = 10$
$\frac{W}{R_i} = \frac{1}{5}$							
$\frac{a}{W} = \frac{1}{8}$	h1	6.32	7.93	9.32	11.50	13.1	14.94
	h2	5.83	7.01	7.96	9.49	10.6	11.96
$\frac{a}{W} = \frac{1}{4}$	h1	7.00	9.34	9.03	9.59	9.71	9.45
	h2	5.92	8.72	7.07	7.26	7.14	6.71
$\frac{a}{W} = \frac{1}{2}$	h1	9.79	10.37	9.07	5.61	3.52	2.11
	h2	7.05	6.97	6.01	3.70	2.28	1.25
$\frac{a}{W} = \frac{3}{4}$	h1	11.00	5.54	2.84	1.24	0.83	0.493
	h2	7.35	3.86	1.86	0.56	0.26	0.129
$\frac{W}{R_i} = \frac{1}{10}$							
$\frac{a}{W} = \frac{1}{8}$	h1	5.22	6.64	7.59	8.76	9.34	9.55
	h2	5.31	6.25	6.88	7.65	8.02	8.09
$\frac{a}{W} = \frac{1}{4}$	h1	6.16	7.49	7.96	8.08	7.78	6.98
	h2	5.56	6.31	6.52	6.40	6.01	5.27
$\frac{a}{W} = \frac{1}{2}$	h1	10.5	11.6	10.7	6.47	3.95	2.27
	h2	7.48	7.72	7.01	4.29	2.58	1.37
$\frac{a}{W} = \frac{3}{4}$	h1	16.10	8.19	3.87	1.46	1.05	0.787
	h2	9.57	5.40	2.57	0.71	0.37	0.232
$\frac{W}{R_i} = \frac{1}{20}$							
$\frac{a}{W} = \frac{1}{8}$	h1	4.50	5.79	6.62	7.65	8.07	7.75
	h2	4.96	5.71	6.20	6.82	7.02	6.66
$\frac{a}{W} = \frac{1}{4}$	h1	5.57	6.91	7.37	7.47	7.21	6.53
	h2	5.29	5.98	6.16	6.01	5.63	4.93
$\frac{a}{W} = \frac{1}{2}$	h1	10.80	12.80	12.80	8.16	4.88	2.62
	h2	7.66	8.33	8.13	5.33	3.20	1.65
$\frac{a}{W} = \frac{3}{4}$	h1	23.10	13.10	5.87	1.90	1.23	0.883
	h2	12.10	7.88	3.84	1.01	0.45	0.24

Out[24]=

		$n = 1$	$n = 2$	$n = 3$	$n = 5$	$n = 7$	$n = 10$
$\frac{W}{R_i} = \frac{1}{5}$							
$\frac{a}{W} = \frac{1}{8}$	h1	6.32	7.93	9.32	11.50	13.1	14.94
	h2	5.83	7.01	7.96	9.49	10.6	11.96
$\frac{a}{W} = \frac{1}{4}$	h1	7.00	9.34	9.03	9.59	9.71	9.45
	h2	5.92	8.72	7.07	7.26	7.14	6.71
$\frac{a}{W} = \frac{1}{2}$	h1	9.79	10.37	9.07	5.61	3.52	2.11
	h2	7.05	6.97	6.01	3.70	2.28	1.25
$\frac{a}{W} = \frac{3}{4}$	h1	11.00	5.54	2.84	1.24	0.83	0.493
	h2	7.35	3.86	1.86	0.56	0.26	0.129
$\frac{W}{R_i} = \frac{1}{10}$							
$\frac{a}{W} = \frac{1}{8}$	h1	5.22	6.64	7.59	8.76	9.34	9.55
	h2	5.31	6.25	6.88	7.65	8.02	8.09
$\frac{a}{W} = \frac{1}{4}$	h1	6.16	7.49	7.96	8.08	7.78	6.98
	h2	5.56	6.31	6.52	6.40	6.01	5.27
$\frac{a}{W} = \frac{1}{2}$	h1	10.5	11.6	10.7	6.47	3.95	2.27
	h2	7.48	7.72	7.01	4.29	2.58	1.37
$\frac{a}{W} = \frac{3}{4}$	h1	16.10	8.19	3.87	1.46	1.05	0.787
	h2	9.57	5.40	2.57	0.71	0.37	0.232
$\frac{W}{R_i} = \frac{1}{20}$							
$\frac{a}{W} = \frac{1}{8}$	h1	4.50	5.79	6.62	7.65	8.07	7.75
	h2	4.96	5.71	6.20	6.82	7.02	6.66
$\frac{a}{W} = \frac{1}{4}$	h1	5.57	6.91	7.37	7.47	7.21	6.53
	h2	5.29	5.98	6.16	6.01	5.63	4.93
$\frac{a}{W} = \frac{1}{2}$	h1	10.80	12.80	12.80	8.16	4.88	2.62
	h2	7.66	8.33	8.13	5.33	3.20	1.65
$\frac{a}{W} = \frac{3}{4}$	h1	23.10	13.10	5.87	1.90	1.23	0.883
	h2	12.10	7.88	3.84	1.01	0.45	0.24

For our case, $\frac{W}{R_i}$ is $\frac{1}{10}$. In our case, $\frac{a}{W}$ is $\frac{a}{t} = \frac{1}{5}$. We will interpolate between $a/W = \frac{1}{8}$ and $a/W = \frac{1}{4}$ to determine h1 and h2 for n=7.

In[25]=

h1a = 9.34;
h1b = 7.78;
h2a = 8.02;
h2b = 6.01;

In[29]=

$$h1 = h1a + \left(\frac{1}{5} - \frac{1}{8} \right) * \frac{h1b - h1a}{\frac{1}{4} - \frac{1}{8}}$$

$$h2 = h2a + \left(\frac{1}{5} - \frac{1}{8} \right) * \frac{h2b - h2a}{\frac{1}{4} - \frac{1}{8}}$$

Out[29]=

8.404

Out[30]=

6.814

Finally, lets determine the plastic J integral.

```
In[31]:= Jpl[p_] :=  $\alpha * \epsilon_y * \sigma_y * b * \frac{a\theta}{W} * h1 * \left(\frac{p}{P_0}\right)^{n+1}$  ;
```

```
Simplify[Jpl[p]]
```

```
Out[32]=  $1.08036 \times 10^{-56} p^8$ 
```

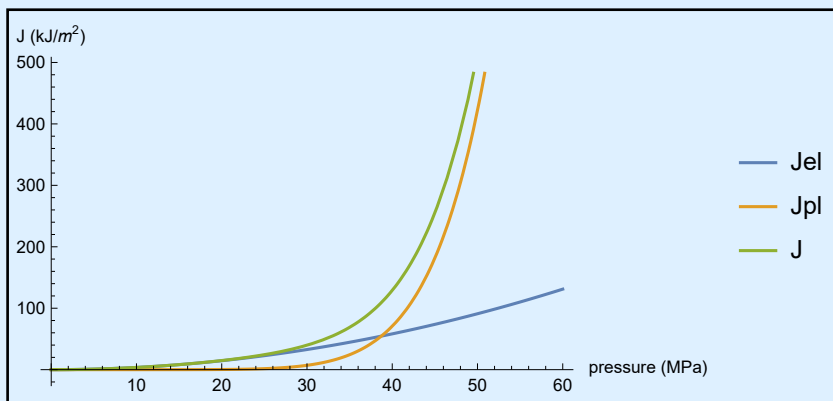
So the total integral is :

```
In[33]:= J[p_] := Jel[p] + Jpl[p];
Framed[Simplify[J[p]]]
```

```
Out[34]=  $3.64058 \times 10^{-11} p^2 + 1.08036 \times 10^{-56} p^8$ 
```

```
In[35]:= Framed[Plot[{Jel[p * 106] / 1000, Jpl[p * 106] / 1000, J[p * 106] / 1000}, {p, 0, 60},
  AxesLabel -> {"pressure (MPa)", "J (kJ/m2)"}, PlotLegends -> {"Jel", "Jpl", "J"}]]
```

```
Out[35]=
```



(2) Ductile crack growth

```
In[36]:= JIc = 300 * 1000; (*J/m^2*)
```

We simply need to find the pressure associated with J equaling the critical value.

```
In[37]:= Pcp1 = NSolve[J[p] - JIc == 0, p]
```

```
Out[37]= {{p ->  $-4.61539 \times 10^7$ }, {p ->  $-3.51182 \times 10^7 - 3.27632 \times 10^7 i$ },
  {p ->  $-3.51182 \times 10^7 + 3.27632 \times 10^7 i$ }, {p ->  $0. - 4.94965 \times 10^7 i$ },
  {p ->  $0. + 4.94965 \times 10^7 i$ }, {p ->  $3.51182 \times 10^7 - 3.27632 \times 10^7 i$ },
  {p ->  $3.51182 \times 10^7 + 3.27632 \times 10^7 i$ }, {p ->  $4.61539 \times 10^7$ }}
```

Here the solution of interest (ignoring negative or imaginary pressures) is when the pressure is equal to **46.15 MPa!**

In[38]:= Framed [(p / 10⁶) /. Pcp1[[8]]]

Out[38]= 46.1539

(3) Brittle Crack Growth

In[39]:= $K_{Ic} = 110 * 10^6; (*Pa \sqrt{m} *)$

We simply need to find the pressure associated with K_{Ie} equaling the critical value.

In[40]:= Pce1 = NSolve [KIE [p] - KIC == 0, p]

Out[40]= { {p → 4.00703 × 10⁷ } }

Here the solution of interest is is when the pressure is equal to **40.1 MPa!**

In[41]:= Framed [(p / 10⁶) /. Pce1[[1]]]

Out[41]= 40.0703

Alternatively, we can convert K_{Ic} to an equivalent energy release rate.

In[42]:= $Gc = \frac{K_{Ic}^2}{E_{mod}}; DecimalForm[Gc, 2]$

Out[42]//DecimalForm= $\frac{12100000}{207}$

In[43]:= Pce12 = NSolve [Jel [p] - Gc == 0, p]

Out[43]= { {p → -4.00703 × 10⁷ }, {p → 4.00703 × 10⁷ } }

In[44]:= Framed [(p / 10⁶) /. Pce12[[2]]]

Out[44]= 40.0703

Now we have the same answer as before. It looks like brittle crack growth is more likely than plastic!

Homework 7

Thomas Allard
CVEN 7161

Problem 1

The crack growth properties of a certain material can be described by

$$\frac{da}{dN} = 1 \cdot 10^{-8} \Delta K^2 K_{\max}^{1.5}$$

If the geometric factor β is equal to 1, what would be the rate of growth of a crack of length $a = 0.5$ in if $\sigma_{\max} = 12$ Ksi, and $R = 0.2$?

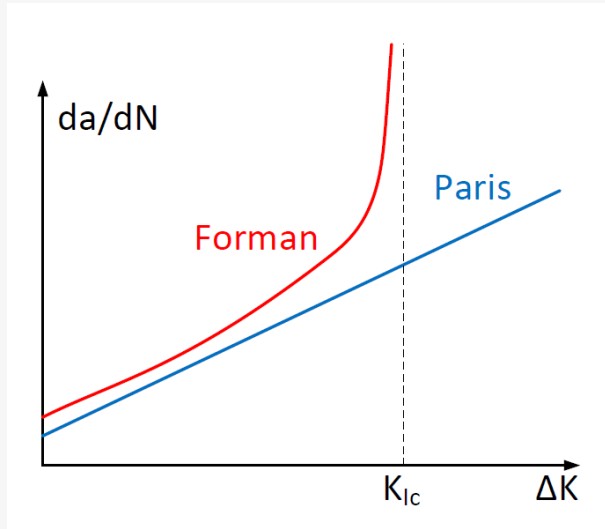
How many cycles does it take for this crack to grow to $a = 0.51$ in?

Solution

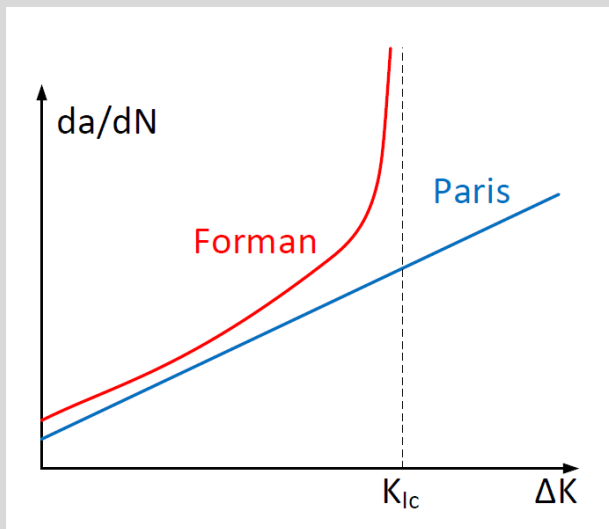
Crack Growth Rate

A shortcoming of Paris's law is its inability to account for an increase in crack growth rate as K_{\max} approaches K_{IC} . Several models have been proposed to address this issue. The following image (borrowed from the lecture slides) qualitatively compares Paris's law with a model proposed by Forman:

In[1]:=



Out[1]:=



Since we know the function (da/dN) for our material, the crack growth rate can be determined by differentiating with respect to ΔK . First, let's manipulate our equations.

$$\frac{da}{dN} = 1 * 10^{-8} \Delta K^2 K_{max}^{1.5}$$

$$R = 0.2 = \frac{K_{min}}{K_{max}} = \frac{\sigma_{min}}{\sigma_{max}} \rightarrow K_{min} = 0.2 K_{max}, \sigma_{min} = 0.2 \sigma_{max}$$

$$\Delta K = K_{max} - K_{min} = K_{max} - 0.2 K_{max} = 0.8 K_{max} \rightarrow K_{max} = \frac{\Delta K}{0.8} = 1.25 \Delta K$$

$$\frac{da}{dN} = 1 * 10^{-8} \Delta K^2 (1.25 \Delta K)^{1.5}$$

Do some algebra

In[2]:= `dadN[ΔK_] := 1 * 10-8 * ΔK2 * (1.25 * ΔK)1.5;
Simplify[dadN[ΔK]]`

Out[3]= $1.39754 \times 10^{-8} \Delta K^{3.5}$

In[4]:= `σmax = 12; (*KSi*)
a = 0.5; (*inches*)
rate = With[{ΔK = 0.8 σmax √(π * a)}, Evaluate[dadN[ΔK]]];
Framed[rate]`

Out[7]= 0.0000844353

This is the crack growth rate!

Cycles to reach a=0.51 inches

The number of cycles for the crack to grow from 0.50" to 0.51" can simply be evaluated as

In[8]:= `Nn = $\frac{0.01}{\text{rate}}$`

Out[8]= 118.434

So it will take ~118 cycles for the crack to grow from 0.5 to 0.51 inches!

Problem 2

The following data was obtained from crack growth tests at constant amplitude for a center crack with $W = 20$ inches.

	a (inches)	N (cycles)	
		$\Delta\sigma = 16$ Ksi; $R=0$	$\Delta\sigma = 10$ Ksi; $R=0.5$
In[9]:=	0.1	0	0
	0.105	1,100	2,000
	1.5	i	k
	1.55	$i + 100$	$k + 170$

	a (inches)	N (cycles)	
		$\Delta\sigma = 16$ Ksi; $R=0$	$\Delta\sigma = 10$ Ksi; $R=0.5$
Out[9]=	0.1	0	0
	0.105	1,100	2,000
	1.5	i	k
	1.55	$i + 100$	$k + 170$

- (a) Establish the rate diagram (i.e. compute $\Delta a / \Delta N$, ΔK for each of the two sets, and for both $R = 0$ and $R = 0.5$).
- (b) Determine the Paris Law constants C and n (take the log of the Paris law, and you will have two linear equations in terms of C and n).

Solution

(a) Rate diagram

Lets calculate Δa for both rows of data.

```
In[10]:=
 $\Delta a_1 = 0.105 - 0.1;$ 
 $\Delta a_2 = 1.55 - 1.5;$ 
```

ΔN for each set of data is determined simply.

```
In[12]:=
 $\Delta N_{11} = 1100;$ 
 $\Delta N_{12} = 100;$ 
 $\Delta N_{21} = 2000;$ 
 $\Delta N_{22} = 170;$ 
```

Lastly, we will need to calculate ΔK .

$$\Delta K = K_{\max} - K_{\min} = (\sigma_{\max} - \sigma_{\min}) \beta \sqrt{\pi a} = \Delta\sigma \beta \sqrt{\pi a}$$

For a center cracked panel:

$$\beta = \sqrt{\sec\left(\frac{\pi a}{W}\right)} \approx \left(1 + 0.256 * \left(\frac{a}{W}\right) - 1.152 * \left(\frac{a}{W}\right)^2 + 12.2 * \left(\frac{a}{W}\right)^3\right)$$

Lets assume that "a" refers to the initial crack length . Since we are using Mathematica, lets use the Secant form for β .

In[16]:=

```

W = 20; (*inches*)
ΔK11 = (16) * √Sec[π * (0.1) / W] * √π * (0.1)
ΔK12 = (16) * √Sec[π * (1.5) / W] * √π * (1.5)
ΔK21 = (10) * √Sec[π * (0.1) / W] * √π * (0.1)
ΔK22 = (10) * √Sec[π * (1.5) / W] * √π * (1.5)

```

Out[17]=

8.96854

Out[18]=

35.2229

Out[19]=

5.60534

Out[20]=

22.0143

Lets arrange our data and plot for the two cases (R=0 and R=0.5)

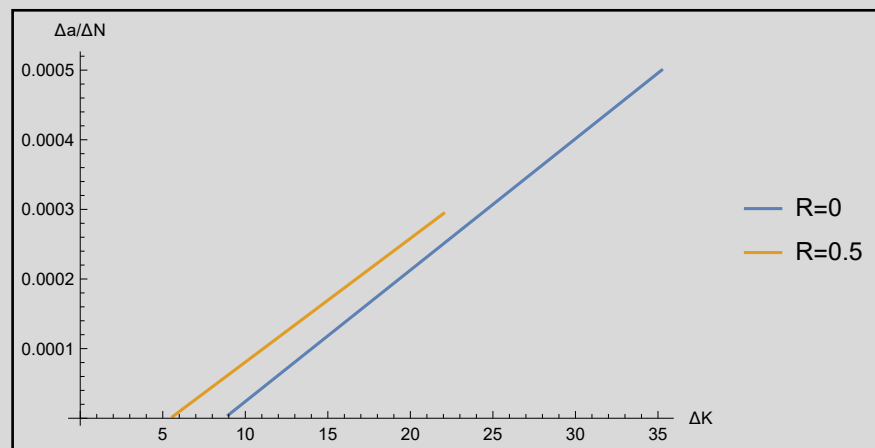
In[21]:=

```

series1 = {{ΔK11, Δa1 / ΔN11}, {ΔK12, Δa2 / ΔN12}};
series2 = {{ΔK21, Δa1 / ΔN21}, {ΔK22, Δa2 / ΔN22}};
Framed[ListLinePlot[{series1, series2},
  PlotLegends -> {"R=0", "R=0.5"}, AxesLabel -> {"ΔK", "Δa/ΔN"}]]

```

Out[23]=



(b) Paris Law Constants

We can determine the constants for Paris's law by “hand.” In general:

$$\frac{\Delta a}{\Delta N} = C (\Delta K)^n \rightarrow \log \left(\frac{\Delta a}{\Delta N} \right) = \log (C) + n * \log (\Delta K)$$

For both cases (R = 0 and R = 0.5) we have 2 equations and 2 unknowns .

For R = 0:

$$\log \left(\frac{\Delta a1}{\Delta N11} \right) = \log (C) + n * \log (\Delta K11)$$

$$\log \left(\frac{\Delta a2}{\Delta N12} \right) = \log (C) + n * \log (\Delta K12)$$

Subtract the equations:

$$\log \left(\frac{\Delta a1}{\Delta N11} \right) - \log \left(\frac{\Delta a2}{\Delta N12} \right) = n * (\log (\Delta K11) - \log (\Delta K12)) \rightarrow \log \left(\frac{\Delta a1 \Delta N12}{\Delta N11 \Delta a2} \right) = n * \log \left(\frac{\Delta K11}{\Delta K12} \right)$$

$$n = \log \left(\frac{\Delta a1 \Delta N12}{\Delta N11 \Delta a2} \right) / \log \left(\frac{\Delta K11}{\Delta K12} \right)$$

This gives us

In[24]:=

$$\text{Framed} \left[n1 = \text{Log} \left[\frac{\Delta a1 * \Delta N12}{\Delta N11 * \Delta a2} \right] / \text{Log} \left[\frac{\Delta K11}{\Delta K12} \right] \right]$$

Out[24]=

3.43609

Now lets find C

$$\frac{\Delta a}{\Delta N} = C (\Delta K)^n \rightarrow C = \frac{\Delta a}{\Delta N} / (\Delta K)^n$$

In[25]:=

$$\text{Framed} \left[C1 = \frac{\Delta a1}{\Delta N11} / \Delta K11^{n1} \right]$$

Out[25]=

2.42068×10^{-9}

So for R = 0, the Paris Law constants are $C = 2.42068 \times 10^{-9}$ and $n = 3.43609$.

For R = 0.5

We can use the same equations as before but with the data for R=0.5

In[26]:=

$$\text{Framed} \left[n2 = \text{Log} \left[\frac{\Delta a1 * \Delta N22}{\Delta N21 * \Delta a2} \right] / \text{Log} \left[\frac{\Delta K21}{\Delta K22} \right] \right]$$

Out[26]=

3.48522

In[27]:=

$$\text{Framed} \left[C2 = \frac{\Delta a1}{\Delta N21} / \Delta K21^{n2} \right]$$

Out[27]=

$$6.15031 \times 10^{-9}$$

So for R=0.5, the Paris Law constants are $C=6.15031 \times 10^{-9}$ and $n=3.48522$

Problem 3

Write a Matlab code to perform fatigue life prediction for constant and variable amplitude loading (using the Wheeler model).

Use functions to define:

- fatigue law (Paris or other),
- stress intensity factors,
- a plot of crack lengths a in terms of cycles N , and
- the number of cycles for a to reach a_{cr} .

Test Your code (convert to m first) by repeating the class example (aircraft), with the assumptions:

$$a_i = 1 \text{ mm}$$

$$a_{cr} = 8 \text{ mm}$$

$$C = 5 \cdot 10^{-10} \text{ m/cycle/MPa} \sqrt{m}$$

$$n = 3$$

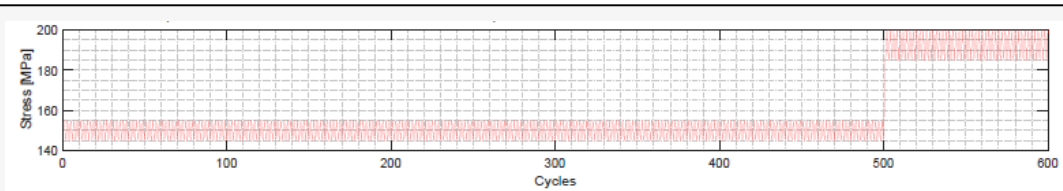
$$m = 2; \text{ for retardation}$$

$$\sigma_y = 100 \text{ MPa}$$

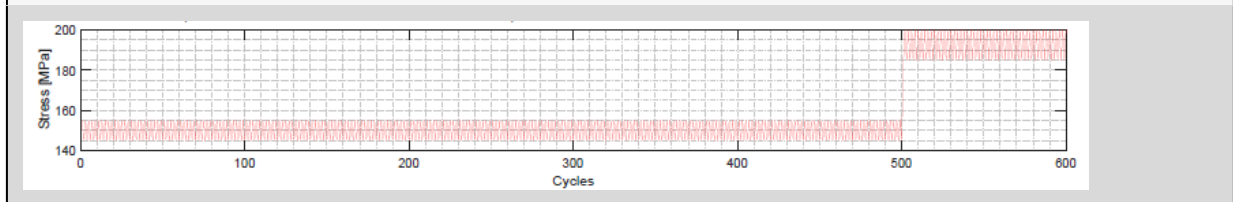
Under the following conditions:

- Same loading as in the example, but replace analytical integration by step-by-step calculation.
- Data set 1 (to be looped until $a = a_{cr}$).

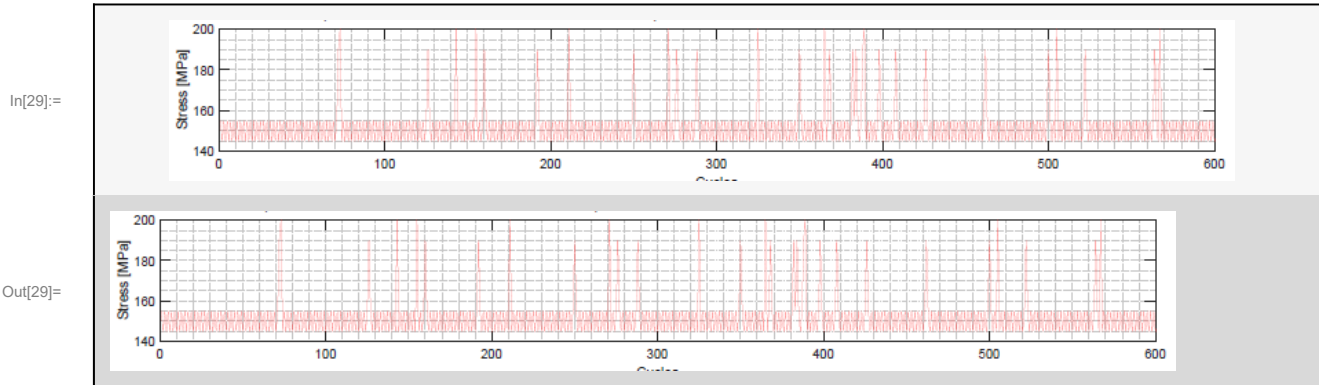
In[28]=



Out[28]=



- Data set 2 (to be looped until $a = a_{cr}$).

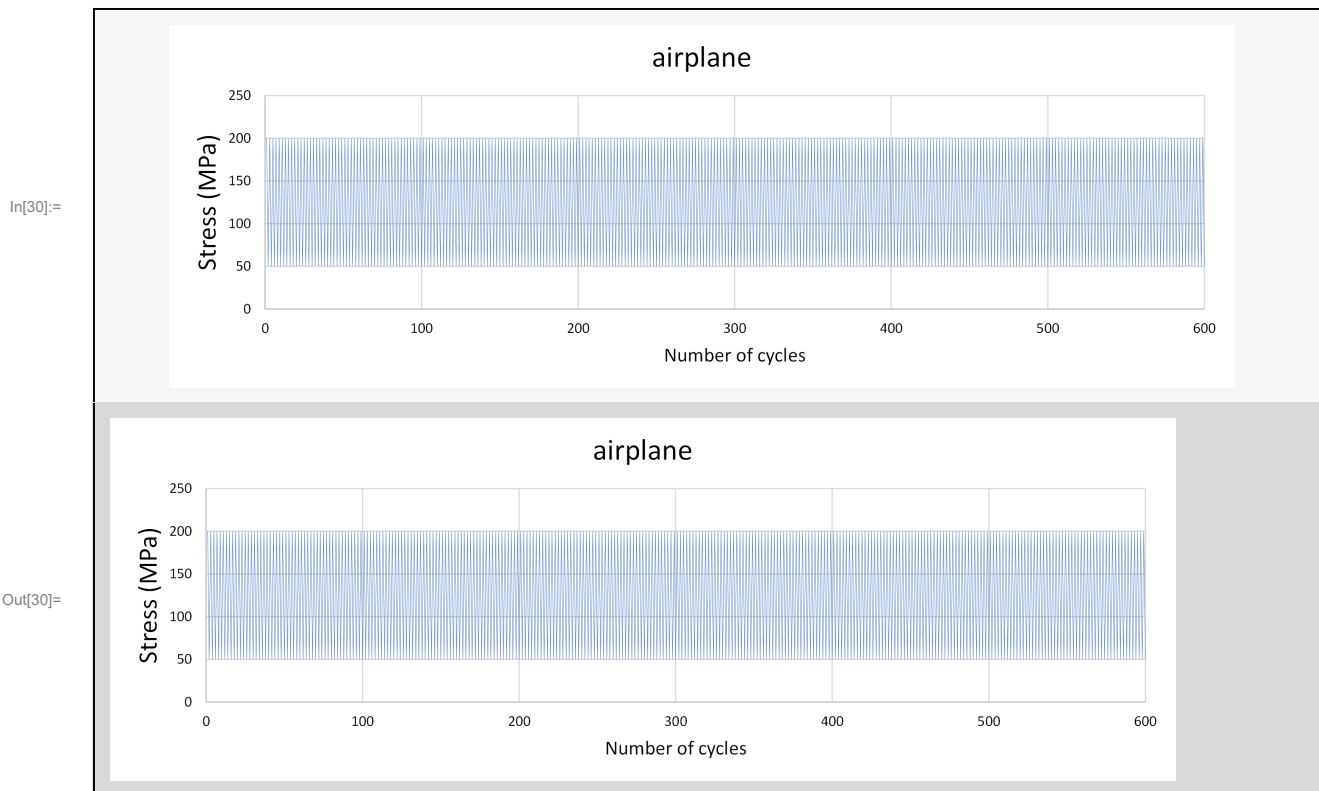


Solution

A Matlab script was modified to run fatigue life prediction for the three cases requested and is attached to the end of this assignment.

The stress history and the number of cycles to failure for each case with and without retardation are shown below:

(a) Airplane:

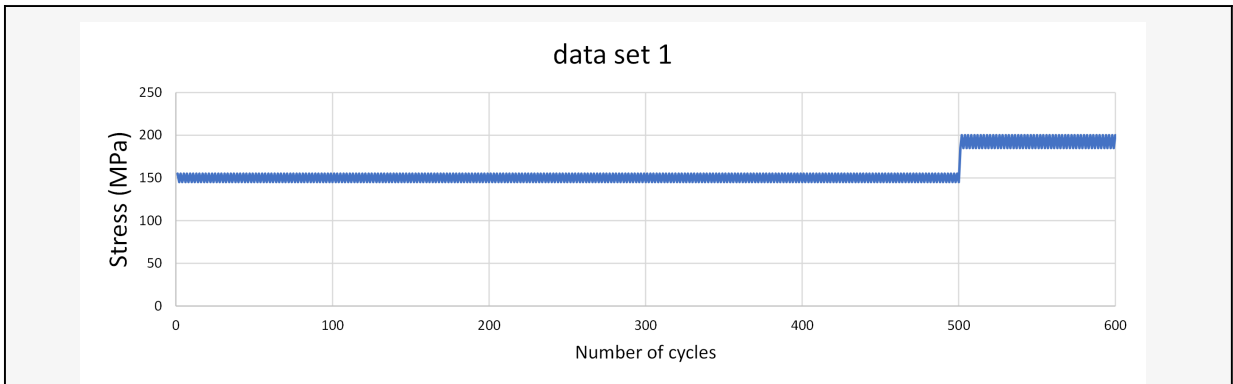


N = 4353 cycles without retardation

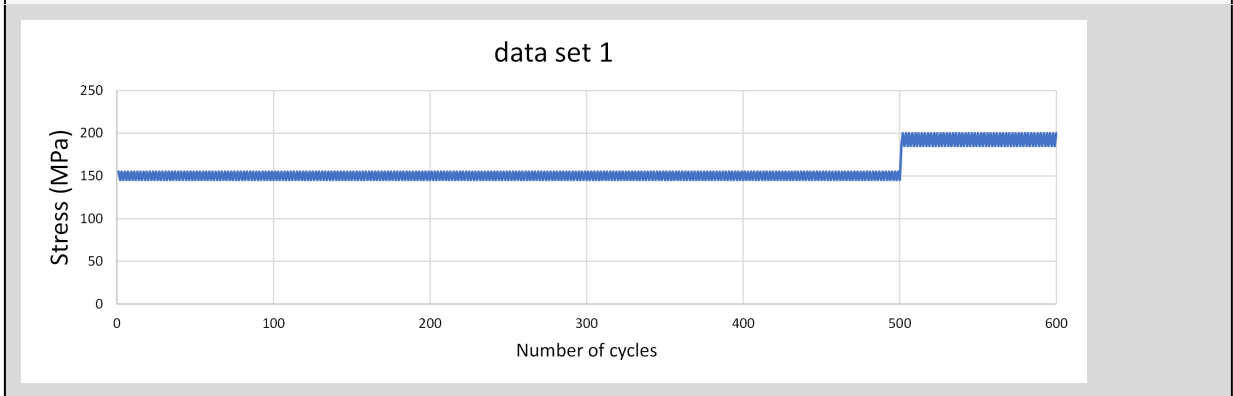
N = 4353 cycles with retardation

(b) Data set 1

In[31]:=



Out[31]=

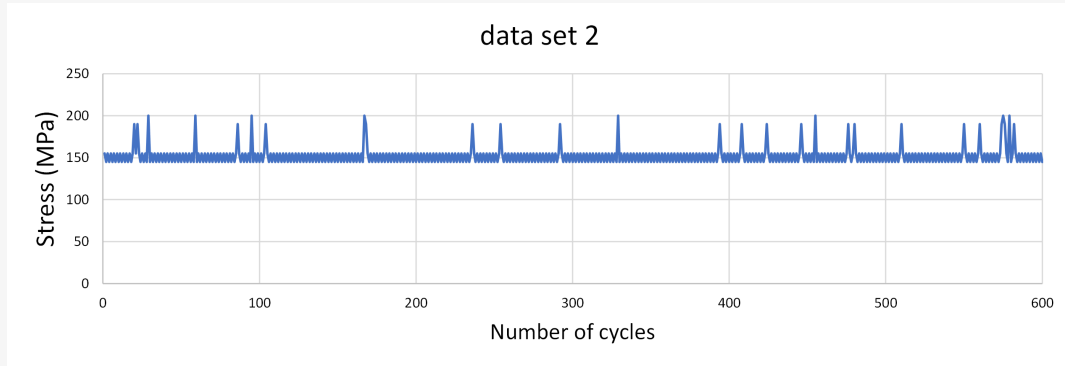


N = 10,570,592 cycles without retardation

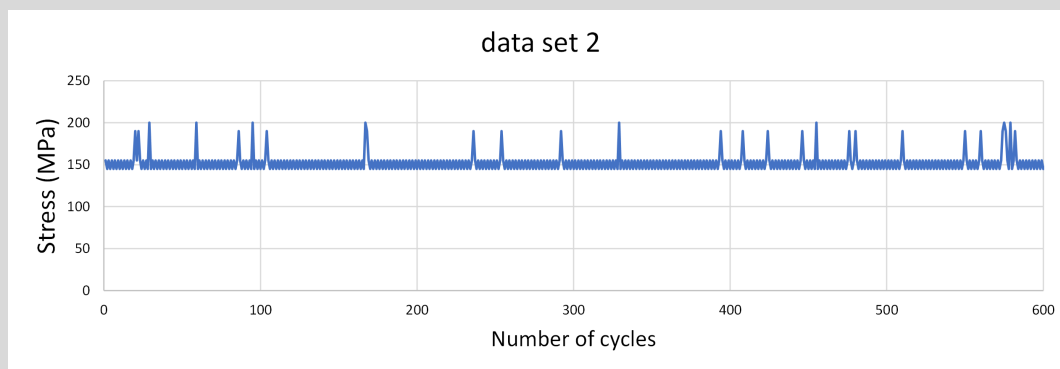
N = 17,180,495 cycles with retardation

(c) Data set 2

In[32]=



Out[32]=

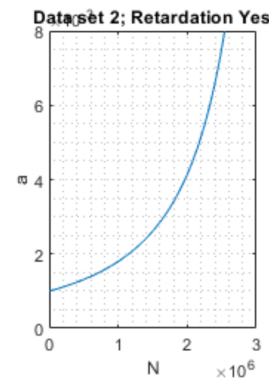
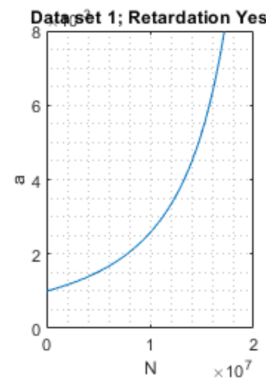
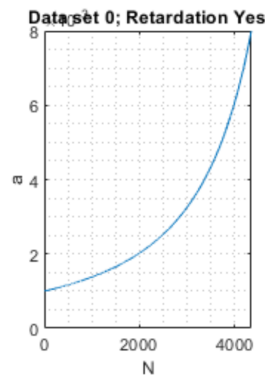
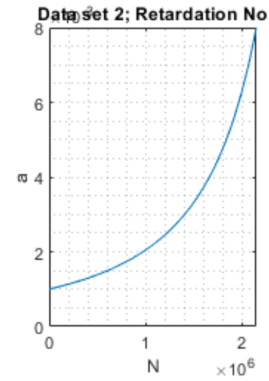
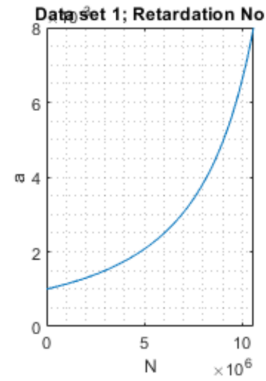
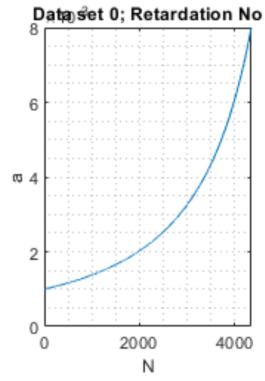


N = 2,147,110 cycles without retardation

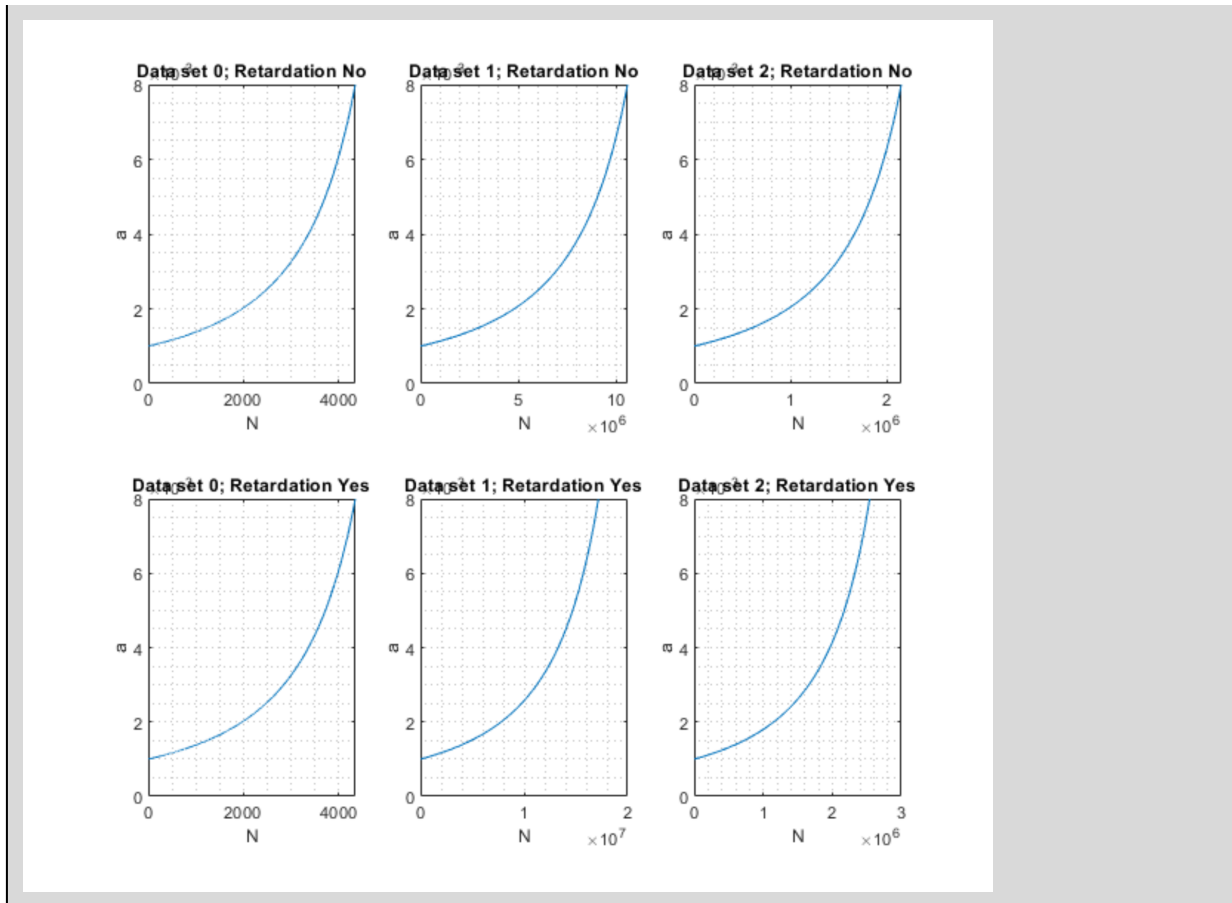
N = 2,541,814 cycles with retardation

Here is a plot showing the crack length “a” versus for each case with and without retardation.

In[33]:=



Out[33]=



For the airplane loading scenario, it takes the same number of cycles for the crack to grow to a_{cr} . Looking at the load history, we can see that the peak stress of 200 MPa is well above the yield stress of 100 MPa while the minimum stress is 50 MPa. This results in a consistent growth of the plastic zone every 2 cycles and there is no “overloading” effect that retardation has any influence on. The high mean stress also makes sense of why the number of cycles to failure is so low compared to the other 2 cases (3 to 4 order of magnitude lower).

For data set 1, the effect of retardation greatly increases the number of cycles to failure from around 11 million to 17 million! This data set was the most influenced by retardation as there is a very regular, periodic “overloading” that takes place on the for 1/6th of the time. This looks like the best scenario for the benefits of retardation!

Similar to data set 1, the effect of retardation increases the number cycles to failure from around 2.1 million cycles to 2.5 million cycles for data set 2. In this dataset, the applied number of cycles “randomly” increases as opposed to data set 2’s very periodic overloading. The effect of retardation is somewhat mild in this case, but certainly noticeable.

Isoparametric Singular Elements

Define Shape functions for 8 noded element

$$\text{In[1]: } \mathbf{N1}[\xi_ , \eta_] = \frac{1}{4} \times (1 + \xi \xi 1) \times (1 + \eta \eta 1) (\xi \xi 1 + \eta \eta 1 - 1);$$

$$\text{In[2]: } \mathbf{N3}[\xi_ , \eta_] := \frac{1}{4} \times (1 + \xi \xi 3) \times (1 + \eta \eta 3) (\xi \xi 3 + \eta \eta 3 - 1);$$

$$\text{In[3]: } \mathbf{N5}[\xi_ , \eta_] = \frac{1}{4} \times (1 + \xi \xi 5) \times (1 + \eta \eta 5) (\xi \xi 5 + \eta \eta 5 - 1);$$

$$\text{In[4]: } \mathbf{N7}[\xi_ , \eta_] := \frac{1}{4} \times (1 + \xi \xi 7) \times (1 + \eta \eta 7) (\xi \xi 7 + \eta \eta 7 - 1);$$

$$\text{In[5]: } \mathbf{N2}[\xi_ , \eta_] := \frac{1}{2} \times (1 - \xi^2) \times (1 + \eta \eta 2);$$

$$\text{In[6]: } \mathbf{N6}[\xi_ , \eta_] := \frac{1}{2} \times (1 - \xi^2) \times (1 + \eta \eta 6);$$

$$\text{In[7]: } \mathbf{N4}[\xi_ , \eta_] := \frac{1}{2} \times (1 + \xi \xi 4) \times (1 - \eta^2);$$

$$\text{In[8]: } \mathbf{N8}[\xi_ , \eta_] := \frac{1}{2} \times (1 + \xi \xi 8) \times (1 - \eta^2);$$

Set natural coordinates

$$\text{In[9]: } \xi 1 = -1; \xi 2 = 0; \xi 3 = 1; \xi 4 = 1; \xi 5 = 1; \xi 6 = 0; \xi 7 = -1; \xi 8 = -1;$$

$$\text{In[10]: } \eta 1 = -1; \eta 2 = -1; \eta 3 = -1; \eta 4 = 0; \eta 5 = 1; \eta 6 = 1; \eta 7 = 1; \eta 8 = 0;$$

Determine x in terms of shape functions

$$\text{In[11]: } \mathbf{Nmat} = \{\mathbf{N1}[\xi, \eta], \mathbf{N2}[\xi, \eta], \mathbf{N3}[\xi, \eta], \mathbf{N4}[\xi, \eta], \mathbf{N5}[\xi, \eta], \mathbf{N6}[\xi, \eta], \mathbf{N7}[\xi, \eta], \mathbf{N8}[\xi, \eta]\};$$

$$\text{In[12]: } \mathbf{xnodes} = \{0, x2, L, L, L, x2, 0, 0\};$$

In[13]=

xint = Nmat.xnodes

Out[13]=

$$\frac{1}{2} L (1 - \eta^2) \times (1 + \xi) + \frac{1}{4} L (1 - \eta) \times (1 + \xi) \times (-1 - \eta + \xi) +$$

$$\frac{1}{4} L (1 + \eta) \times (1 + \xi) \times (-1 + \eta + \xi) + \frac{1}{2} x2 (1 - \eta) \times (1 - \xi^2) + \frac{1}{2} x2 (1 + \eta) \times (1 - \xi^2)$$

In[14]=

 $\eta = -1;$

Take

$\frac{dx}{d\xi}$ and set it equal to zero to make $|j| = 0$, solve for x2

In[15]=

dxdξ = Simplify[D[xint, ξ]]

Out[15]=

$$-2 x2 \xi + L \left(\frac{1}{2} + \xi \right)$$

In[16]=

Solve[dxdξ == 0, x2] /. {ξ → -1}

Out[16]=

$$\left\{ \left\{ x2 \rightarrow \frac{L}{4} \right\} \right\}$$

In[17]=

x2 = L / 4;

Solve for ξ in terms of x

In[18]=

expr = x - xint

Out[18]=

$$x - \frac{1}{2} L \xi (1 + \xi) - \frac{1}{4} L (1 - \xi^2)$$

In[19]=

Simplify[Solve[expr == 0, ξ]]

Out[19]=

$$\left\{ \left\{ \xi \rightarrow -1 - \frac{2\sqrt{x}}{\sqrt{L}} \right\}, \left\{ \xi \rightarrow -1 + \frac{2\sqrt{x}}{\sqrt{L}} \right\} \right\}$$

In[20]=

unodes = {u1, u2, u3, u4, u5, u6, u7, u8};

Write displacement field in terms of x

In[21]:= $\mathbf{uint} = \mathbf{Nmat.unodes} /. \xi \rightarrow -1 + \frac{2 \sqrt{x}}{\sqrt{L}}$

Out[21]=
$$u_2 \left(1 - \left(-1 + \frac{2 \sqrt{x}}{\sqrt{L}} \right)^2 \right) - \frac{1}{2} u_1 \left(2 - \frac{2 \sqrt{x}}{\sqrt{L}} \right) \times \left(-1 + \frac{2 \sqrt{x}}{\sqrt{L}} \right) + \frac{u_3 \left(-1 + \frac{2 \sqrt{x}}{\sqrt{L}} \right) \sqrt{x}}{\sqrt{L}}$$

Determine the strain ϵ_{xx}

In[22]:= $\mathbf{Simplify[D[uint, x]]}$

Out[22]=
$$\frac{2 (u_1 - 2 u_2 + u_3)}{L} - \frac{3 u_1 - 4 u_2 + u_3}{2 \sqrt{L} \sqrt{x}}$$

Write the displacement field in terms of the 3 nodal displacements for the displacement correlation technique of SIF determination

In[23]:= $\mathbf{Expand[uint]}$

Out[23]=
$$u_1 - \frac{3 u_1 \sqrt{x}}{\sqrt{L}} + \frac{4 u_2 \sqrt{x}}{\sqrt{L}} - \frac{u_3 \sqrt{x}}{\sqrt{L}} + \frac{2 u_1 x}{L} - \frac{4 u_2 x}{L} + \frac{2 u_3 x}{L}$$

In[24]:= $\mathbf{Simplify[Coefficient[uint, \sqrt{x}] \sqrt{L}]}$

Out[24]= $-3 u_1 + 4 u_2 - u_3$

Westergaard Mode I

Complex Stress function for the Westergaard's solution:

In[1]:= $\Phi = \sigma\theta / \sqrt{1 - \frac{a^2}{z^2}}$

Out[1]= $\frac{\sigma\theta}{\sqrt{1 - \frac{a^2}{z^2}}}$

Modified Φ , $z = \eta + a = re^{i\theta}$; $\frac{\eta}{a} \ll 1$

In[2]:= `appPhi = Expand[Phi] /. {z -> (eta + a)}`

Out[2]= $\frac{\sigma\theta}{\sqrt{1 - \frac{a^2}{(a+\eta)^2}}}$

In[3]:= `intPhi = FunctionExpand[appPhi /. {eta -> r (E^(I * theta))}]`

Out[3]= $\frac{\sqrt{\frac{a e^{-i\theta}}{r}} \sigma\theta}{\sqrt{2}}$

Since $\sigma_{22} = \text{Re}(\Phi(z)) + x_2 \text{Im}(\Phi'(z))$,

therefore we require to find the real and imaginary parts of the complex stress function and that of its derivative

We first find the real part of function $\Phi(z)$:

In[4]:= `ComplexExpand[Re[ExpToTrig[E^(-I theta / 2)]], TargetFunctions -> {Re, Im}]`

Out[4]= $\text{Cos}\left[\frac{\theta}{2}\right]$

Therefore real part of $\Phi(z)$ is:

In[5]:=
$$\text{part1} = \sigma\theta \sqrt{\frac{a}{2}} r^{(-1/2)} \text{Cos}[\theta/2]$$

Out[5]=
$$\frac{\sqrt{a} \sigma\theta \text{Cos}\left[\frac{\theta}{2}\right]}{\sqrt{2} \sqrt{r}}$$

The first derivative of $\Phi(z)$ is:

In[6]:=
$$\text{dash} = (\sigma\theta/2) \sqrt{\frac{a}{2 (r E^{I+\theta})^3}}$$

Out[6]=
$$\frac{\sqrt{\frac{a e^{-3 I \theta}}{r^3}} \sigma\theta}{2 \sqrt{2}}$$

Imaginary part of this function derivative is the imaginary part of the exponential term since all other quantities are real. Therefore imaginary part of Φ' is :

In[7]:= `ComplexExpand[Im[ExpToTrig[E^(-3 I \theta / 2)]], TargetFunctions -> {Re, Im}]`

Out[7]=
$$-\text{Sin}\left[\frac{3\theta}{2}\right]$$

Therefore the second part of the stress expression is obtained as : $x_2 \text{Im}\Phi'$. Using $x_2 = r \text{Sin}\theta = 2 r \text{Sin}\frac{\theta}{2} \text{Cos}\frac{\theta}{2}$ we get : \rightarrow

In[8]:=
$$\text{part2} = \text{FullSimplify}\left[(\sigma\theta/2) r 2 \text{Sin}\left[\frac{\theta}{2}\right] \text{Cos}\left[\frac{\theta}{2}\right] \sqrt{\frac{a}{2}} r^{(-3/2)} \text{Sin}\left[\frac{3\theta}{2}\right]\right]$$

Out[8]=
$$\frac{\sqrt{a} \sigma\theta \text{Sin}[\theta] \text{Sin}\left[\frac{3\theta}{2}\right]}{2 \sqrt{2} \sqrt{r}}$$

In[9]:=

 $\sigma_{22} = \text{part1} + \text{part2}$

Out[9]=

$$\frac{\sqrt{a} \sigma \theta \cos\left[\frac{\theta}{2}\right]}{\sqrt{2} \sqrt{r}} + \frac{\sqrt{a} \sigma \theta \sin[\theta] \sin\left[\frac{3\theta}{2}\right]}{2 \sqrt{2} \sqrt{r}}$$

In[10]:=

 $\sigma_{11} = -\text{part2} + \text{part1}$

Out[10]=

$$\frac{\sqrt{a} \sigma \theta \cos\left[\frac{\theta}{2}\right]}{\sqrt{2} \sqrt{r}} - \frac{\sqrt{a} \sigma \theta \sin[\theta] \sin\left[\frac{3\theta}{2}\right]}{2 \sqrt{2} \sqrt{r}}$$

For the stress σ_{12} , we need to find the real part of Φ' :

In[11]:=

 $\text{ComplexExpand}[\text{Re}[\text{ExpToTrig}[E^{(-3 I \theta / 2)}]], \text{TargetFunctions} \rightarrow \{\text{Re}, \text{Im}\}]$

Out[11]=

$$\cos\left[\frac{3\theta}{2}\right]$$

Therefore $\sigma_{12} = \text{Re}(\Phi')$ is given by :

In[12]:=

$$\sigma_{12} = (\sigma \theta / 2) \sqrt{\frac{a}{2r}} 2 \sin\left[\frac{\theta}{2}\right] \cos\left[\frac{\theta}{2}\right] \cos[3\theta / 2]$$

Out[12]=

$$\frac{\sqrt{\frac{a}{r}} \sigma \theta \cos\left[\frac{\theta}{2}\right] \cos\left[\frac{3\theta}{2}\right] \sin\left[\frac{\theta}{2}\right]}{\sqrt{2}}$$

Westergaard Mode II

Given $\Phi_{II} = -x_2 \text{Re} \bar{\phi}_{II}$, where $\phi_{II} = \frac{\tau}{\sqrt{1 - \frac{a^2}{z^2}}}$

Where, $\bar{\phi} = \int \phi(z) dz$

We know that $\sigma_{11} = \frac{\partial^2 \Phi}{\partial x_2^2}$

$$\sigma_{22} = \frac{\partial^2 \Phi}{\partial x_1^2}$$

$$\sigma_{12} = \frac{\partial^2 \Phi}{\partial x_1 \partial x_2}$$

Using the Cauchy - Riemann equalities we can show that,

given a complex function $F(z) = \alpha + i\beta$, the following identities hold :

$$\operatorname{Re} \left(\frac{dF}{dz} \right) = \frac{\partial \operatorname{Re}(F)}{\partial x_1} = \frac{\partial \operatorname{Im}(F)}{\partial x_2}$$

$$\operatorname{Im} \left(\frac{dF}{dz} \right) = \frac{\partial \operatorname{Im}(F)}{\partial x_1} = -\frac{\partial \operatorname{Re}(F)}{\partial x_2}$$

Using these expressions we have :

$$\frac{\partial \Phi}{\partial x_1} = \frac{\partial (-x_2 \operatorname{Re} \bar{\phi}_{II})}{\partial x_1} = -x_2 \frac{\partial (\operatorname{Re} \bar{\phi}_{II})}{\partial x_1} = -x_2 \operatorname{Re} \frac{\partial (\bar{\phi}_{II})}{\partial z} = -x_2 \operatorname{Re} \phi'_{II}$$

$$\sigma_{22} = \frac{\partial^2 \Phi}{\partial x_1^2} = \frac{\partial (-x_2 \operatorname{Re} \phi'_{II})}{\partial x_1} = -x_2 \frac{\partial (\operatorname{Re} \phi'_{II})}{\partial x_1} = -x_2 \operatorname{Re} \frac{\partial (\phi'_{II})}{\partial z} = -x_2 \operatorname{Re} \phi''_{II}$$

$$\frac{\partial \Phi}{\partial x_2} = \frac{\partial (-x_2 \operatorname{Re} \bar{\phi}_{II})}{\partial x_2} =$$

$$-\operatorname{Re} \bar{\phi}_{II} - x_2 \frac{\partial (\operatorname{Re} \bar{\phi}_{II})}{\partial x_2} = -\operatorname{Re} \bar{\phi}_{II} + x_2 \operatorname{Im} \frac{\partial (\bar{\phi}_{II})}{\partial z} = -\operatorname{Re} \bar{\phi}_{II} + x_2 \operatorname{Im} \phi'_{II}$$

$$\sigma_{11} = \frac{\partial^2 \Phi}{\partial x_2^2} = \frac{\partial (-\operatorname{Re} \bar{\phi}_{II} + x_2 \operatorname{Im} \phi'_{II})}{\partial x_2} = \operatorname{Im} \frac{\partial (\bar{\phi}_{II})}{\partial z} + \operatorname{Im} \phi'_{II} + x_2 \operatorname{Re} \frac{\partial (\phi'_{II})}{\partial z} =$$

$$2 \operatorname{Im} \phi'_{II} + x_2 \operatorname{Re} \phi''_{II}$$

$$\sigma_{12} = \frac{\partial^2 \Phi}{\partial x_1 \partial x_2} = \frac{\partial (-\operatorname{Re} \bar{\phi}_{II} + x_2 \operatorname{Im} \phi'_{II})}{\partial x_1} = -\operatorname{Re} \frac{\partial (\bar{\phi}_{II})}{\partial z} + x_2 \operatorname{Im} \frac{\partial (\phi'_{II})}{\partial z} =$$

$$-\operatorname{Re} \phi'_{II} + x_2 \operatorname{Im} \phi''_{II}$$

Consider ϕ_{II} :

In[13]:=

$$\phi_{II} = \tau / (\operatorname{Sqrt}[1 - ((a^2) / (z^2))]) /. z \rightarrow (\eta + z)$$

Out[13]=

$$\frac{\tau}{\sqrt{1 - \frac{a^2}{(z+\eta)^2}}}$$

Using $\frac{\eta}{a} \ll 1$,

In[14]:=

$$\phi_{IIint} = \operatorname{FunctionExpand} \left[\sigma \theta \sqrt{\frac{a}{2\eta}} /. \eta \rightarrow r (E^{(i\theta)}) \right]$$

Out[14]=

$$\frac{\sqrt{\frac{a e^{-i\theta}}{r}} \sigma \theta}{\sqrt{2}}$$

In[15]=

Re ϕ II = Sqrt[a / (2 r)] $\sigma\theta$ ComplexExpand[Re[E^{-I θ / 2}], TargetFunctions \rightarrow {Re, Im}]

Out[15]=

$$\frac{\sqrt{\frac{a}{r}} \sigma\theta \cos\left[\frac{\theta}{2}\right]}{\sqrt{2}}$$

In[16]=

Im ϕ II = Sqrt[a / (2 r)] $\sigma\theta$ ComplexExpand[Im[E^{-I θ / 2}], TargetFunctions \rightarrow {Re, Im}]

Out[16]=

$$-\frac{\sqrt{\frac{a}{r}} \sigma\theta \sin\left[\frac{\theta}{2}\right]}{\sqrt{2}}$$

In[17]=

Im ϕ dash =

Sqrt[a / (2 r³)] ($\sigma\theta$ / 2) ComplexExpand[Im[E^{-3 I θ / 2}], TargetFunctions \rightarrow {Re, Im}]

Out[17]=

$$-\frac{\sqrt{\frac{a}{r^3}} \sigma\theta \sin\left[\frac{3\theta}{2}\right]}{2 \sqrt{2}}$$

In[18]=

Re ϕ dash =

Sqrt[a / (2 r³)] ($\sigma\theta$ / 2) ComplexExpand[Re[E^{-3 I θ / 2}], TargetFunctions \rightarrow {Re, Im}]

Out[18]=

$$\frac{\sqrt{\frac{a}{r^3}} \sigma\theta \cos\left[\frac{3\theta}{2}\right]}{2 \sqrt{2}}$$

In[19]=

$\sigma_{22} = -r^2 \sin[\theta / 2] \cos[\theta / 2] \text{Re}\phi\text{dash}$

Out[19]=

$$-\frac{\sqrt{\frac{a}{r^3}} r \sigma\theta \cos\left[\frac{\theta}{2}\right] \cos\left[\frac{3\theta}{2}\right] \sin\left[\frac{\theta}{2}\right]}{\sqrt{2}}$$

In[20]=

$\sigma_{11} = 2 \text{Im}\phi_{II} + 2 r \sin[\theta / 2] \cos[\theta / 2] \text{Re}\phi\text{dash}$

$$-\sqrt{2} \sqrt{\frac{a}{r}} \sigma\theta \sin\left[\frac{\theta}{2}\right] + \frac{\sqrt{\frac{a}{r^3}} r \sigma\theta \cos\left[\frac{\theta}{2}\right] \cos\left[\frac{3\theta}{2}\right] \sin\left[\frac{\theta}{2}\right]}{\sqrt{2}}$$

Simplifying: $\sigma_{11} = -\sigma\theta \sqrt{\frac{a}{2r}} \sin[\theta/2] (2 + \cos[\theta/2] \cos[3\theta/2])$

In[21]=

$$\sigma_{12} = -\text{Re}\phi_{II} + 2r \sin[\theta/2] \cos[\theta/2] \text{Im}\phi_{dash}$$

Out[21]=

$$-\frac{\sqrt{\frac{a}{r}} \sigma\theta \cos\left[\frac{\theta}{2}\right]}{\sqrt{2}} - \frac{\sqrt{\frac{a}{r^3}} r \sigma\theta \cos\left[\frac{\theta}{2}\right] \sin\left[\frac{\theta}{2}\right] \sin\left[\frac{3\theta}{2}\right]}{\sqrt{2}}$$

William's Solution

Dissimilar Material

Function Definition

```
In[1]:=  $\Phi_1[r_, \theta_] := r^{\lambda+1} F_1[\theta]$ 
```

```
In[2]:=  $\Phi_2[r_, \theta_] := r^{\lambda+1} F_2[\theta]$ 
```

Define the biharmonic Equation, test on Φ_1

```
In[3]:=  $g1[r_, \theta_] := D[\Phi_1[r, \theta], r, r] + D[\Phi_1[r, \theta], r] / r +$   
 $D[\Phi_1[r, \theta], \theta, \theta] / r^2$ 
```

```
In[4]:=  $g2[r_, \theta_] := D[g1[r, \theta], r, r] + D[g1[r, \theta], r] / r +$   
 $D[g1[r, \theta], \theta, \theta] / r^2$ 
```

Define the function F

```
In[5]:=  $F_1[\theta_] = \text{Exp}[m[\lambda] \theta]$ 
```

```
Out[5]=  $e^{\theta m[\lambda]}$ 
```

Solve the differential equation

In[6]:= `eqdiff = Simplify[Factor[g2[r, θ]] r3- λ]`

Out[6]:= $e^{\theta m[\lambda]} \left((-1 + \lambda)^2 + m[\lambda]^2 \right) \left((1 + \lambda)^2 + m[\lambda]^2 \right)$

In[7]:= `Solve[eqdiff Exp[-m[λ] θ] == 0, m[λ]]`

Out[7]:= $\left\{ \left\{ m[\lambda] \rightarrow -\sqrt{-1 - 2\lambda - \lambda^2} \right\}, \left\{ m[\lambda] \rightarrow \sqrt{-1 - 2\lambda - \lambda^2} \right\}, \right.$
 $\left. \left\{ m[\lambda] \rightarrow -\sqrt{-1 + 2\lambda - \lambda^2} \right\}, \left\{ m[\lambda] \rightarrow \sqrt{-1 + 2\lambda - \lambda^2} \right\} \right\}$

Define the general solution

In[8]:= `F1[$\theta_$] := a1 Cos[$\lambda \theta - \theta$] + b1 Cos[$\lambda \theta + \theta$] + c1 Sin[$\lambda \theta - \theta$] + d1 Sin[$\lambda \theta + \theta$]`

In[9]:= `F2[$\theta_$] := a2 Cos[$\lambda \theta - \theta$] + b2 Cos[$\lambda \theta + \theta$] + c2 Sin[$\lambda \theta - \theta$] + d2 Sin[$\lambda \theta + \theta$]`

In[10]:= `$\Phi_1[r_$, $\theta_$] := r $\lambda+1$ F1[θ]`

In[11]:= `$\Phi_2[r_$, $\theta_$] := r $\lambda+1$ F2[θ]`

Evaluate the stresses in polar coordinates

In[12]:= `temp1[r_, $\theta_$] = D[$\Phi_1[r$, θ], θ]`

Out[12]:= $r^{1+\lambda} \left(- \left((1 - \lambda) \text{Sin}[\theta - \theta \lambda] a_1 \right) - (1 + \lambda) \text{Sin}[\theta + \theta \lambda] b_1 - \right.$
 $\left. (1 - \lambda) \text{Cos}[\theta - \theta \lambda] c_1 + (1 + \lambda) \text{Cos}[\theta + \theta \lambda] d_1 \right)$

In[13]:= `$\sigma_{1r\theta}[r_$, $\theta_$] := -D[temp1[r, θ] / r, r]`

In[14]:= $\text{temp2}[r_ , \theta_] = D[\Phi_2[r, \theta], \theta]$

Out[14]:= $r^{1+\lambda} (- (1 - \lambda) \text{Sin}[\theta - \theta \lambda] a_2 - (1 + \lambda) \text{Sin}[\theta + \theta \lambda] b_2 - (1 - \lambda) \text{Cos}[\theta - \theta \lambda] c_2 + (1 + \lambda) \text{Cos}[\theta + \theta \lambda] d_2)$

In[15]:= $\sigma_{2r\theta}[r_ , \theta_] := -D[\text{temp2}[r, \theta] / r, r]$

In[16]:= $\sigma_{1\theta\theta}[r_ , \theta_] := \text{Factor}[D[\Phi_1[r, \theta], r, r]]$

In[17]:= $\sigma_{2\theta\theta}[r_ , \theta_] := \text{Factor}[D[\Phi_2[r, \theta], r, r]]$

In[18]:= $\sigma_{1rr}[r_ , \theta_] := \text{Factor}[D[\Phi_1[r, \theta], r] / r + D[\Phi_1[r, \theta], \theta, \theta] / r^2]$

In[19]:= $\sigma_{2rr}[r_ , \theta_] := \text{Factor}[D[\Phi_2[r, \theta], r] / r + D[\Phi_2[r, \theta], \theta, \theta] / r^2]$

Displacements

In[20]:= $u_{1r}[r_ , \theta_] := \frac{r^\lambda}{2 \mu_1} (- (\lambda + 1) F_1[\theta] + 4 \times (1 - \alpha_1) (c_1 \text{Sin}[(\lambda - 1) \theta] + a_1 \text{Cos}[(\lambda - 1) \theta]))$

In[21]:= $u_{2r}[r_ , \theta_] := \frac{r^\lambda}{2 \mu_2} (- (\lambda + 1) F_2[\theta] + 4 \times (1 - \alpha_2) (c_2 \text{Sin}[(\lambda - 1) \theta] + a_2 \text{Cos}[(\lambda - 1) \theta]))$

In[22]:=

$$u_{1\theta}[r_-, \theta_-] := \frac{r^\lambda}{2\mu_1} \left(-D[F_1[\theta], \theta] - 4 \times (1 - \alpha_1) (c_1 \cos[(\lambda - 1)\theta] - a_1 \sin[(\lambda - 1)\theta]) \right)$$

In[23]:=

$$u_{2\theta}[r_-, \theta_-] := \frac{r^\lambda}{2\mu_2} \left(-D[F_2[\theta], \theta] - 4 \times (1 - \alpha_2) (c_2 \cos[(\lambda - 1)\theta] - a_2 \sin[(\lambda - 1)\theta]) \right)$$

Apply the boundary conditions

In[24]:=

$$bc1 = -\sigma_{1\theta\theta}[r, \pi] \frac{r^{1-\lambda}}{\lambda(1+\lambda)}$$

Out[24]=

$$\cos[\pi\lambda] a_1 + \cos[\pi\lambda] b_1 + \sin[\pi\lambda] c_1 + \sin[\pi\lambda] d_1$$

In[25]:=

$$bc2 = -\sigma_{2\theta\theta}[r, -\pi] \frac{r^{1-\lambda}}{\lambda(1+\lambda)}$$

Out[25]=

$$\cos[\pi\lambda] a_2 + \cos[\pi\lambda] b_2 - \sin[\pi\lambda] c_2 - \sin[\pi\lambda] d_2$$

In[26]:=

$$bc3 = \sigma_{1r\theta}[r, \pi] \frac{r^{1-\lambda}}{\lambda}$$

Out[26]=

$$(1 - \lambda) \sin[\pi\lambda] a_1 - (1 + \lambda) \sin[\pi\lambda] b_1 - (1 - \lambda) \cos[\pi\lambda] c_1 + (1 + \lambda) \cos[\pi\lambda] d_1$$

In[27]:=
$$\mathbf{bc4} = \sigma_{2r\theta}[\mathbf{r}, -\pi] \frac{r^{1-\lambda}}{\lambda}$$

Out[27]=
$$-((1-\lambda) \sin[\pi\lambda] a_2) + (1+\lambda) \sin[\pi\lambda] b_2 - \\ (1-\lambda) \cos[\pi\lambda] c_2 + (1+\lambda) \cos[\pi\lambda] d_2$$

In[28]:=
$$\mathbf{bc5} = \text{Factor} \left[(\sigma_{1\theta\theta}[\mathbf{r}, \theta] - \sigma_{2\theta\theta}[\mathbf{r}, \theta]) \frac{r^{1-\lambda}}{\lambda(1+\lambda)} \right]$$

Out[28]=
$$a_1 - a_2 + b_1 - b_2$$

In[29]:=
$$\mathbf{bc6} = \text{Factor} \left[(\sigma_{1r\theta}[\mathbf{r}, \theta] - \sigma_{2r\theta}[\mathbf{r}, \theta]) \frac{r^{1-\lambda}}{\lambda} \right]$$

Out[29]=
$$c_1 - \lambda c_1 - c_2 + \lambda c_2 - d_1 - \lambda d_1 + d_2 + \lambda d_2$$

In[30]:=
$$\mathbf{bc7} = \text{Factor} \left[(u_{1r}[\mathbf{r}, \theta] - u_{2r}[\mathbf{r}, \theta]) r^{-\lambda} \right]$$

Out[30]=
$$-\frac{1}{2\mu_1\mu_2} (3a_2\mu_1 - \lambda a_2\mu_1 - b_2\mu_1 - \lambda b_2\mu_1 - \\ 4a_2\alpha_2\mu_1 - 3a_1\mu_2 + \lambda a_1\mu_2 + b_1\mu_2 + \lambda b_1\mu_2 + 4a_1\alpha_1\mu_2)$$

In[31]:=

```
bc8 = Factor [(u1_θ[r, zero] - u2_θ[r, zero]) r-λ]
```

Out[31]=

$$\begin{aligned}
 & -\frac{1}{2 \mu_1 \mu_2} (4 \sin[\text{zero}(-1 + \lambda)] a_2 \mu_1 + \sin[\text{zero} - \text{zero} \lambda] a_2 \mu_1 - \\
 & \quad \lambda \sin[\text{zero} - \text{zero} \lambda] a_2 \mu_1 + \sin[\text{zero} + \text{zero} \lambda] b_2 \mu_1 + \\
 & \quad \lambda \sin[\text{zero} + \text{zero} \lambda] b_2 \mu_1 - 4 \cos[\text{zero}(-1 + \lambda)] c_2 \mu_1 + \\
 & \quad \cos[\text{zero} - \text{zero} \lambda] c_2 \mu_1 - \lambda \cos[\text{zero} - \text{zero} \lambda] c_2 \mu_1 - \\
 & \quad \cos[\text{zero} + \text{zero} \lambda] d_2 \mu_1 - \lambda \cos[\text{zero} + \text{zero} \lambda] d_2 \mu_1 - \\
 & \quad 4 \sin[\text{zero}(-1 + \lambda)] a_2 \alpha_2 \mu_1 + 4 \cos[\text{zero}(-1 + \lambda)] c_2 \alpha_2 \mu_1 - \\
 & \quad 4 \sin[\text{zero}(-1 + \lambda)] a_1 \mu_2 - \sin[\text{zero} - \text{zero} \lambda] a_1 \mu_2 + \\
 & \quad \lambda \sin[\text{zero} - \text{zero} \lambda] a_1 \mu_2 - \sin[\text{zero} + \text{zero} \lambda] b_1 \mu_2 - \\
 & \quad \lambda \sin[\text{zero} + \text{zero} \lambda] b_1 \mu_2 + 4 \cos[\text{zero}(-1 + \lambda)] c_1 \mu_2 - \\
 & \quad \cos[\text{zero} - \text{zero} \lambda] c_1 \mu_2 + \lambda \cos[\text{zero} - \text{zero} \lambda] c_1 \mu_2 + \\
 & \quad \cos[\text{zero} + \text{zero} \lambda] d_1 \mu_2 + \lambda \cos[\text{zero} + \text{zero} \lambda] d_1 \mu_2 + \\
 & \quad 4 \sin[\text{zero}(-1 + \lambda)] a_1 \alpha_1 \mu_2 - 4 \cos[\text{zero}(-1 + \lambda)] c_1 \alpha_1 \mu_2)
 \end{aligned}$$

In[32]:=

```
zero = 0;
```

In[33]:=

```
Simplify[bc8]
```

Out[33]=

$$\begin{aligned}
 & \frac{1}{2 \mu_1 \mu_2} ((1 + \lambda) d_2 \mu_1 + c_2 (3 + \lambda - 4 \alpha_2) \mu_1 - \\
 & \quad ((1 + \lambda) d_1 + c_1 (3 + \lambda - 4 \alpha_1)) \mu_2)
 \end{aligned}$$

In[34]:=

```
μ1 = k μ2
```

Out[34]=

```
k μ2
```

Get the Matrix

In[35]:=

```
matrix =  
Factor[
```

```
{ {Coefficient[bc1, a1], Coefficient[bc1, b1],  
  Coefficient[bc1, c1], Coefficient[bc1, d1],  
  Coefficient[bc1, a2], Coefficient[bc1, b2],  
  Coefficient[bc1, c2], Coefficient[bc1, d2] },  
{Coefficient[bc2, a1], Coefficient[bc2, b1],  
  Coefficient[bc2, c1], Coefficient[bc2, d1],  
  Coefficient[bc2, a2], Coefficient[bc2, b2],  
  Coefficient[bc2, c2], Coefficient[bc2, d2] },  
{Coefficient[bc3, a1], Coefficient[bc3, b1],  
  Coefficient[bc3, c1], Coefficient[bc3, d1],  
  Coefficient[bc3, a2], Coefficient[bc3, b2],  
  Coefficient[bc3, c2], Coefficient[bc3, d2] },  
{Coefficient[bc4, a1], Coefficient[bc4, b1],  
  Coefficient[bc4, c1], Coefficient[bc4, d1],  
  Coefficient[bc4, a2], Coefficient[bc4, b2],  
  Coefficient[bc4, c2], Coefficient[bc4, d2] },  
{Coefficient[bc5, a1], Coefficient[bc5, b1],  
  Coefficient[bc5, c1], Coefficient[bc5, d1],  
  Coefficient[bc5, a2], Coefficient[bc5, b2],  
  Coefficient[bc5, c2], Coefficient[bc5, d2] },  
{Coefficient[bc6, a1], Coefficient[bc6, b1],  
  Coefficient[bc6, c1], Coefficient[bc6, d1],  
  Coefficient[bc6, a2], Coefficient[bc6, b2],  
  Coefficient[bc6, c2], Coefficient[bc6, d2] },  
{Coefficient[bc7, a1], Coefficient[bc7, b1],  
  Coefficient[bc7, c1], Coefficient[bc7, d1],  
  Coefficient[bc7, a2], Coefficient[bc7, b2],  
  Coefficient[bc7, c2], Coefficient[bc7, d2] },  
{Coefficient[bc8, a1], Coefficient[bc8, b1],  
  Coefficient[bc8, c1], Coefficient[bc8, d1],  
  Coefficient[bc8, a2], Coefficient[bc8, b2],  
  Coefficient[bc8, c2], Coefficient[bc8, d2] } } ]
```

Out[35]=

$$\begin{aligned}
& \{ \{ \text{Cos}[\pi \lambda], \text{Cos}[\pi \lambda], \text{Sin}[\pi \lambda], \text{Sin}[\pi \lambda], 0, 0, 0, 0] \}, \\
& \{ 0, 0, 0, 0, \text{Cos}[\pi \lambda], \text{Cos}[\pi \lambda], -\text{Sin}[\pi \lambda], -\text{Sin}[\pi \lambda] \} \}, \\
& \{ -((-1 + \lambda) \text{Sin}[\pi \lambda]), -(1 + \lambda) \text{Sin}[\pi \lambda] \}, \\
& \{ (-1 + \lambda) \text{Cos}[\pi \lambda], (1 + \lambda) \text{Cos}[\pi \lambda], 0, 0, 0, 0 \}, \\
& \{ 0, 0, 0, 0, (-1 + \lambda) \text{Sin}[\pi \lambda], (1 + \lambda) \text{Sin}[\pi \lambda] \}, \\
& \{ (-1 + \lambda) \text{Cos}[\pi \lambda], (1 + \lambda) \text{Cos}[\pi \lambda] \}, \\
& \{ 1, 1, 0, 0, -1, -1, 0, 0 \}, \\
& \{ 0, 0, 1 - \lambda, -1 - \lambda, 0, 0, -1 + \lambda, 1 + \lambda \}, \\
& \left\{ -\frac{-3 + \lambda + 4 \alpha_1}{2 k \mu_2}, -\frac{1 + \lambda}{2 k \mu_2}, 0, 0, \frac{-3 + \lambda + 4 \alpha_2}{2 \mu_2}, \frac{1 + \lambda}{2 \mu_2}, 0, 0 \right\}, \\
& \left\{ 0, 0, -\frac{3 + \lambda - 4 \alpha_1}{2 k \mu_2}, -\frac{1 + \lambda}{2 k \mu_2}, 0, 0, \frac{3 + \lambda - 4 \alpha_2}{2 \mu_2}, \frac{1 + \lambda}{2 \mu_2} \right\} \}
\end{aligned}$$

In[36]:=

MatrixForm[Factor[matrix]]

Out[36]//MatrixForm=

$$\begin{pmatrix}
\text{Cos}[\pi \lambda] & \text{Cos}[\pi \lambda] & \text{Sin}[\pi \lambda] \\
0 & 0 & 0 \\
-((-1 + \lambda) \text{Sin}[\pi \lambda]) & -(1 + \lambda) \text{Sin}[\pi \lambda] & (-1 + \lambda) \text{Cos}[\pi \lambda] \\
0 & 0 & 0 \\
1 & 1 & 0 \\
0 & 0 & 1 - \lambda \\
-\frac{-3 + \lambda + 4 \alpha_1}{2 k \mu_2} & -\frac{1 + \lambda}{2 k \mu_2} & 0 \\
0 & 0 & -\frac{3 + \lambda - 4 \alpha_1}{2 k \mu_2}
\end{pmatrix}$$

In[37]:=

```

det1 =
Factor [
FullSimplify [Det [matrix]  $\frac{k^2 \mu_2^2}{\text{Sin}[\pi \lambda]^2}$ 
 $\frac{1}{2 k (1 - \alpha_2) + 2 \times (1 - \alpha_1)}$  ] ]

```

Out[37]=

$$\begin{aligned}
& - \frac{1}{-1 - k + \alpha_1 + k \alpha_2} \\
& (1 + \lambda) \times \left(5 + 6 k + 5 k^2 + 3 \text{Cos} [2 \pi \lambda] + 10 k \text{Cos} [2 \pi \lambda] + \right. \\
& \quad 3 k^2 \text{Cos} [2 \pi \lambda] - 12 \alpha_1 - 4 k \alpha_1 - 4 \text{Cos} [2 \pi \lambda] \alpha_1 - 12 k \\
& \quad \text{Cos} [2 \pi \lambda] \alpha_1 + 8 \alpha_1^2 - 4 k \alpha_2 - 12 k^2 \alpha_2 - 12 k \text{Cos} [2 \pi \lambda] \alpha_2 - \\
& \quad \left. 4 k^2 \text{Cos} [2 \pi \lambda] \alpha_2 + 16 k \text{Cos} [2 \pi \lambda] \alpha_1 \alpha_2 + 8 k^2 \alpha_2^2 \right)
\end{aligned}$$

At this point, we should have obtained the following relations

In[38]:=

$$\beta = \frac{2 k (1 - \alpha_2) - 2 \times (1 - \alpha_1) - (k - 1)^2}{2 k (1 - \alpha_2) + 2 \times (1 - \alpha_1)}$$

Out[38]=

$$\frac{-(-1 + k)^2 - 2 \times (1 - \alpha_1) + 2 k (1 - \alpha_2)}{2 \times (1 - \alpha_1) + 2 k (1 - \alpha_2)}$$

This is the equation which must be solved for λ (eq1=0, or

$$\text{Cot} [\lambda \pi] = + - \mathbf{I} \beta^2$$

In[39]:=

$$\text{eq1} = \text{Cot} [\lambda \pi]^2 + \beta^2$$

Out[39]=

$$\text{Cot} [\pi \lambda]^2 + \frac{\left(-(-1 + k)^2 - 2 \times (1 - \alpha_1) + 2 k (1 - \alpha_2) \right)^2}{\left(2 \times (1 - \alpha_1) + 2 k (1 - \alpha_2) \right)^2}$$

In[40]:=

$$\lambda = \lambda r + I \lambda j$$

Out[40]=

$$i \lambda j + \lambda r$$

In[41]:=

$$u = \text{Tan}[\lambda r \pi]$$

Out[41]=

$$\text{Tan}[\pi \lambda r]$$

In[42]:=

$$v = \text{Tanh}[\lambda j \pi]$$

Out[42]=

$$\text{Tanh}[\pi \lambda j]$$

Exploit those trigonometric relations

In[43]:=

$$\sin 2\theta = \frac{2u}{1+u^2};$$

In[44]:=

$$\cos 2\theta = \frac{1-u^2}{1+u^2};$$

In[45]:=

$$\sinh 2\theta = \frac{2v}{1-v^2};$$

In[46]:=

$$\cosh 2\theta = \frac{1+v^2}{1-v^2};$$

In[47]:=

$$\text{myCot} = \frac{\text{Simplify}[\sin 2\theta - I \sinh 2\theta]}{\text{Simplify}[\cosh 2\theta - \cos 2\theta]}$$

Out[47]=

$$\frac{\text{Sin}[2 \pi \lambda r] - i \text{Sinh}[2 \pi \lambda j]}{-\text{Cos}[2 \pi \lambda r] + \text{Cosh}[2 \pi \lambda j]}$$

Since $\text{Re}[\text{Cot}[\lambda \pi]] = 0$, then $\text{Sin}[2 \lambda r \pi] = 0$, and

We must now solve for the Immaginary part

In[48]:=
$$\text{impart} = \frac{\text{Sinh}[2 \pi \lambda j]}{-\text{Cos}[2 \pi \lambda r] + \text{Cosh}[2 \pi \lambda j]}$$

Out[48]=
$$\frac{\text{Sinh}[2 \pi \lambda j]}{-\text{Cos}[2 \pi \lambda r] + \text{Cosh}[2 \pi \lambda j]}$$

In[49]:=
$$\lambda r = 1 / 2$$

Out[49]=
$$\frac{1}{2}$$

In[50]:=
$$\text{impart}$$

Out[50]=
$$\frac{\text{Sinh}[2 \pi \lambda j]}{1 + \text{Cosh}[2 \pi \lambda j]}$$

In[51]:=
$$\text{Simplify}[\text{Solve}[\text{impart} - c c == 0, \lambda j]]$$

Out[51]=
$$\left\{ \left\{ \lambda j \rightarrow i c_1 + \frac{\text{Log}\left[-\frac{1+c c}{-1+c c}\right]}{2 \pi} \text{ if } c_1 \in \mathbb{Z} \right\} \right\}$$

William's Solution

▼ Similar Material

▼ Function Definition

```
In[52]:=  $\Phi[r_, \theta_] := r^{\lambda+1} F[\theta, \lambda]$ 
```

▼ Define the biharmonic Equation (could use Laplacian)

```
In[53]:=  $g1[r_, \theta_] := D[\Phi[r, \theta], r, r] + D[\Phi[r, \theta], r] / r + D[\Phi[r, \theta], \theta, \theta] / r^2$ 
```

```
In[54]:=  $g2[r_, \theta_] := D[g1[r, \theta], r, r] + D[g1[r, \theta], r] / r + D[g1[r, \theta], \theta, \theta] / r^2$ 
```

▼ Define the function F

```
In[55]:=  $F[\theta, \lambda] = \text{Exp}[m[\lambda] \theta]$ 
```

```
Out[55]=  $e^{\theta m \left[ \frac{1}{2} + i \lambda j \right]}$ 
```

▼ Solve the differential equation

In[56]:=

```
eqdiff = Simplify[Factor[g2[r, θ]] r3-λ]
```

Out[56]:=

$$\frac{1}{16} e^{\theta m \left[\frac{1}{2} + i \lambda j \right]} \left(-i - 2 \lambda j + 2 m \left[\frac{1}{2} + i \lambda j \right] \right) \left(3 i - 2 \lambda j + 2 m \left[\frac{1}{2} + i \lambda j \right] \right) \left(i + 2 \lambda j + 2 m \left[\frac{1}{2} + i \lambda j \right] \right) \left(-3 i + 2 \lambda j + 2 m \left[\frac{1}{2} + i \lambda j \right] \right)$$

In[57]:=

```
Solve[eqdiff Exp[-m[λ] θ] == 0, m[λ]]
```

Out[57]:=

$$\left\{ \left\{ m \left[\frac{1}{2} + i \lambda j \right] \rightarrow \frac{1}{2} (-i - 2 \lambda j) \right\}, \left\{ m \left[\frac{1}{2} + i \lambda j \right] \rightarrow \frac{1}{2} \times (3 i - 2 \lambda j) \right\}, \left\{ m \left[\frac{1}{2} + i \lambda j \right] \rightarrow \frac{1}{2} (i + 2 \lambda j) \right\}, \left\{ m \left[\frac{1}{2} + i \lambda j \right] \rightarrow \frac{1}{2} \times (-3 i + 2 \lambda j) \right\} \right\}$$

▼ Define the general solution

In[58]:=

```
F[θ_] := a Cos[λ θ - θ] + b Cos[λ θ + θ] + c Sin[λ θ - θ] + d Sin[λ θ + θ]
```

In[59]:=

```
F[θ]
```

Out[59]:=

$$a \operatorname{Cos} \left[\theta - \theta \left(\frac{1}{2} + i \lambda j \right) \right] + b \operatorname{Cos} \left[\theta + \theta \left(\frac{1}{2} + i \lambda j \right) \right] - c \operatorname{Sin} \left[\theta - \theta \left(\frac{1}{2} + i \lambda j \right) \right] + d \operatorname{Sin} \left[\theta + \theta \left(\frac{1}{2} + i \lambda j \right) \right]$$

In[60]:= $\Phi[r_, \theta_] := r^{\lambda+1} F[\theta]$

▼ Evaluate the stresses in polar coordinates

In[61]:= $\text{temp}[r_, \theta_] = D[\Phi[r, \theta], \theta]$

Out[61]=
$$\begin{aligned} & r^{\frac{3}{2} + i \lambda j} \left(-c \left(\frac{1}{2} - i \lambda j \right) \text{Cos} \left[\theta - \theta \left(\frac{1}{2} + i \lambda j \right) \right] \right) + \\ & d \left(\frac{3}{2} + i \lambda j \right) \text{Cos} \left[\theta + \theta \left(\frac{1}{2} + i \lambda j \right) \right] - \\ & a \left(\frac{1}{2} - i \lambda j \right) \text{Sin} \left[\theta - \theta \left(\frac{1}{2} + i \lambda j \right) \right] - \\ & b \left(\frac{3}{2} + i \lambda j \right) \text{Sin} \left[\theta + \theta \left(\frac{1}{2} + i \lambda j \right) \right] \end{aligned}$$

In[62]:= $\sigma_{r\theta}[r_, \theta_] := -D[\text{temp}[r, \theta] / r, r]$

In[63]:= $\sigma_{r\theta}[r, \theta]$

Out[63]=
$$\begin{aligned} & -r^{-\frac{1}{2} + i \lambda j} \left(\frac{1}{2} + i \lambda j \right) \left(-c \left(\frac{1}{2} - i \lambda j \right) \text{Cos} \left[\theta - \theta \left(\frac{1}{2} + i \lambda j \right) \right] \right) + \\ & d \left(\frac{3}{2} + i \lambda j \right) \text{Cos} \left[\theta + \theta \left(\frac{1}{2} + i \lambda j \right) \right] - \\ & a \left(\frac{1}{2} - i \lambda j \right) \text{Sin} \left[\theta - \theta \left(\frac{1}{2} + i \lambda j \right) \right] - \\ & b \left(\frac{3}{2} + i \lambda j \right) \text{Sin} \left[\theta + \theta \left(\frac{1}{2} + i \lambda j \right) \right] \end{aligned}$$

In[64]:= $\sigma_{\theta\theta}[r_, \theta_] := \text{Factor}[D[\Phi[r, \theta], r, r]]$

In[65]:= $\sigma_{rr}[r_, \theta_] := \text{Factor}[D[\Phi[r, \theta], r] / r + D[\Phi[r, \theta], \theta, \theta] / r^2]$

▼ Apply the boundary conditions

In[66]:=

$$\mathbf{bc1} = \sigma_{\theta\theta}[\mathbf{r}, -\alpha]$$

Out[66]=

$$-\frac{1}{4} r^{-\frac{1}{2} + i \lambda j} (-i + 2 \lambda j) (-3 i + 2 \lambda j) \left(a \operatorname{Cos} \left[\alpha - \alpha \left(\frac{1}{2} + i \lambda j \right) \right] + b \operatorname{Cos} \left[\alpha + \alpha \left(\frac{1}{2} + i \lambda j \right) \right] + c \operatorname{Sin} \left[\alpha - \alpha \left(\frac{1}{2} + i \lambda j \right) \right] - d \operatorname{Sin} \left[\alpha + \alpha \left(\frac{1}{2} + i \lambda j \right) \right] \right)$$

In[67]:=

$$\mathbf{bc2} = \sigma_{\theta\theta}[\mathbf{r}, \alpha]$$

Out[67]=

$$-\frac{1}{4} r^{-\frac{1}{2} + i \lambda j} (-i + 2 \lambda j) (-3 i + 2 \lambda j) \left(a \operatorname{Cos} \left[\alpha - \alpha \left(\frac{1}{2} + i \lambda j \right) \right] + b \operatorname{Cos} \left[\alpha + \alpha \left(\frac{1}{2} + i \lambda j \right) \right] - c \operatorname{Sin} \left[\alpha - \alpha \left(\frac{1}{2} + i \lambda j \right) \right] + d \operatorname{Sin} \left[\alpha + \alpha \left(\frac{1}{2} + i \lambda j \right) \right] \right)$$

In[68]:=

$$\mathbf{bc3} = \sigma_{r\theta}[\mathbf{r}, -\alpha]$$

Out[68]=

$$-r^{-\frac{1}{2} + i \lambda j} \left(\frac{1}{2} + i \lambda j \right) \left(-c \left(\frac{1}{2} - i \lambda j \right) \operatorname{Cos} \left[\alpha - \alpha \left(\frac{1}{2} + i \lambda j \right) \right] + d \left(\frac{3}{2} + i \lambda j \right) \operatorname{Cos} \left[\alpha + \alpha \left(\frac{1}{2} + i \lambda j \right) \right] + a \left(\frac{1}{2} - i \lambda j \right) \operatorname{Sin} \left[\alpha - \alpha \left(\frac{1}{2} + i \lambda j \right) \right] + b \left(\frac{3}{2} + i \lambda j \right) \operatorname{Sin} \left[\alpha + \alpha \left(\frac{1}{2} + i \lambda j \right) \right] \right)$$

In[69]:=

$$\mathbf{bc4} = \sigma_{r\theta} [\mathbf{r}, \alpha]$$

Out[69]=

$$\begin{aligned} & -r^{-\frac{1}{2} + i\lambda j} \left(\frac{1}{2} + i\lambda j \right) \left(-c \left(\frac{1}{2} - i\lambda j \right) \cos \left[\alpha - \alpha \left(\frac{1}{2} + i\lambda j \right) \right] \right) + \\ & d \left(\frac{3}{2} + i\lambda j \right) \cos \left[\alpha + \alpha \left(\frac{1}{2} + i\lambda j \right) \right] - \\ & a \left(\frac{1}{2} - i\lambda j \right) \sin \left[\alpha - \alpha \left(\frac{1}{2} + i\lambda j \right) \right] - \\ & b \left(\frac{3}{2} + i\lambda j \right) \sin \left[\alpha + \alpha \left(\frac{1}{2} + i\lambda j \right) \right] \end{aligned}$$

▼ Rearrange Equations for BC

In[70]:=

$$\mathbf{c11} = -\mathbf{Factor} [\mathbf{bc1} + \mathbf{bc2}] r^{(1-\lambda)} / 2$$

Out[70]=

$$\begin{aligned} & \frac{1}{4} (-i + 2\lambda j) (-3i + 2\lambda j) \\ & \left(a \cos \left[\alpha - \alpha \left(\frac{1}{2} + i\lambda j \right) \right] + b \cos \left[\alpha + \alpha \left(\frac{1}{2} + i\lambda j \right) \right] \right) \end{aligned}$$

In[71]:=

$$\mathbf{c12} = \mathbf{Factor} [\mathbf{bc1} - \mathbf{bc2}] r^{1-\lambda} / 2$$

Out[71]=

$$\begin{aligned} & -\frac{1}{4} (-i + 2\lambda j) (-3i + 2\lambda j) \\ & \left(c \sin \left[\alpha - \alpha \left(\frac{1}{2} + i\lambda j \right) \right] - d \sin \left[\alpha + \alpha \left(\frac{1}{2} + i\lambda j \right) \right] \right) \end{aligned}$$

In[72]:=

c13 = Factor [bc3 + bc4] $r^{1-\lambda} / 2$

Out[72]=

$$\frac{1}{4} (-i + 2 \lambda j) \left(i c \operatorname{Cos} \left[\alpha - \alpha \left(\frac{1}{2} + i \lambda j \right) \right] + 2 c \lambda j \operatorname{Cos} \left[\alpha - \alpha \left(\frac{1}{2} + i \lambda j \right) \right] - 3 i d \operatorname{Cos} \left[\alpha + \alpha \left(\frac{1}{2} + i \lambda j \right) \right] + 2 d \lambda j \operatorname{Cos} \left[\alpha + \alpha \left(\frac{1}{2} + i \lambda j \right) \right] \right)$$

In[73]:=

c14 = -Factor [bc3 - bc4] $r^{1-\lambda} / 2$

Out[73]=

$$\frac{1}{4} (-i + 2 \lambda j) \left(i a \operatorname{Sin} \left[\alpha - \alpha \left(\frac{1}{2} + i \lambda j \right) \right] + 2 a \lambda j \operatorname{Sin} \left[\alpha - \alpha \left(\frac{1}{2} + i \lambda j \right) \right] + 3 i b \operatorname{Sin} \left[\alpha + \alpha \left(\frac{1}{2} + i \lambda j \right) \right] - 2 b \lambda j \operatorname{Sin} \left[\alpha + \alpha \left(\frac{1}{2} + i \lambda j \right) \right] \right)$$

▼ Solve for λ

In[74]:=

```
matrix =
Factor [
  {{Coefficient[c11, a], Coefficient[c11, b],
    Coefficient[c11, c], Coefficient[c11, d]},
  {Coefficient[c12, a], Coefficient[c12, b],
    Coefficient[c12, c], Coefficient[c12, d]},
  {Coefficient[c13, a], Coefficient[c13, b],
    Coefficient[c13, c], Coefficient[c13, d]},
  {Coefficient[c14, a], Coefficient[c14, b],
    Coefficient[c14, c], Coefficient[c14, d]}}
```

Out[74]=

$$\left\{ \left\{ \frac{1}{4} (-i + 2\lambda j) (-3i + 2\lambda j) \cos \left[\alpha - \alpha \left(\frac{1}{2} + i\lambda j \right) \right], \right. \right.$$

$$\frac{1}{4} (-i + 2\lambda j) (-3i + 2\lambda j) \cos \left[\alpha + \alpha \left(\frac{1}{2} + i\lambda j \right) \right],$$

$$\theta, \theta \left. \right\}, \left\{ \theta, \theta, \right.$$

$$-\frac{1}{4} (-i + 2\lambda j) (-3i + 2\lambda j) \sin \left[\alpha - \alpha \left(\frac{1}{2} + i\lambda j \right) \right],$$

$$\frac{1}{4} (-i + 2\lambda j) (-3i + 2\lambda j) \sin \left[\alpha + \alpha \left(\frac{1}{2} + i\lambda j \right) \right] \left. \right\},$$

$$\left\{ \theta, \theta, \frac{1}{4} (-i + 2\lambda j) (i + 2\lambda j) \cos \left[\alpha - \alpha \left(\frac{1}{2} + i\lambda j \right) \right], \right.$$

$$\frac{1}{4} (-i + 2\lambda j) (-3i + 2\lambda j) \cos \left[\alpha + \alpha \left(\frac{1}{2} + i\lambda j \right) \right] \left. \right\},$$

$$\left\{ \frac{1}{4} (-i + 2\lambda j) (i + 2\lambda j) \sin \left[\alpha - \alpha \left(\frac{1}{2} + i\lambda j \right) \right], -\frac{1}{4} \right.$$

$$\left. \left. (-i + 2\lambda j) (-3i + 2\lambda j) \sin \left[\alpha + \alpha \left(\frac{1}{2} + i\lambda j \right) \right], \theta, \theta \right\}$$

In[75]:=

MatrixForm[Simplify[%]]

Out[75]//MatrixForm=

$$\begin{pmatrix} \frac{1}{4} (-i + 2 \lambda j) (-3 i + 2 \lambda j) \cos\left[\frac{1}{2} \alpha (1 - 2 i \lambda j)\right] & \frac{1}{4} (-i + \\ & \emptyset \\ & \emptyset \\ \frac{1}{4} (-i + 2 \lambda j) (i + 2 \lambda j) \sin\left[\frac{1}{2} (\alpha - 2 i \alpha \lambda j)\right] & -\frac{1}{4} (-i - \end{pmatrix}$$

In[76]:=

 $\alpha = \pi$

Out[76]=

 π

In[77]:=

determinant = Factor[Det[matrix] / $(\lambda + \lambda^2)^2$]

Out[77]=

$$(-i + 2 \lambda j)^2 \cos\left[\pi \left(\frac{1}{2} + i \lambda j\right)\right]^2 \sin\left[\pi \left(\frac{1}{2} + i \lambda j\right)\right]^2$$

In[78]:=

Solve[determinant == 0, λ]

⋯ Solve: $\frac{1}{2} + i \lambda j$ is not a valid variable.

Out[78]=

$$\text{Solve}\left[\begin{aligned} & (-i + 2 \lambda j)^2 \cos\left[\pi \left(\frac{1}{2} + i \lambda j\right)\right]^2 \sin\left[\pi \left(\frac{1}{2} + i \lambda j\right)\right]^2 == 0, \\ & \frac{1}{2} + i \lambda j \end{aligned} \right]$$

In[79]:=

F[θ]

Out[79]=

$$a \operatorname{Cos}\left[\theta - \theta \left(\frac{1}{2} + i \lambda j\right)\right] + b \operatorname{Cos}\left[\theta + \theta \left(\frac{1}{2} + i \lambda j\right)\right] - \\ c \operatorname{Sin}\left[\theta - \theta \left(\frac{1}{2} + i \lambda j\right)\right] + d \operatorname{Sin}\left[\theta + \theta \left(\frac{1}{2} + i \lambda j\right)\right]$$

In[80]:=

$$\varpi = \frac{\lambda - 1}{\lambda + 1}$$

Out[80]=

$$\frac{-\frac{1}{2} + i \lambda j}{\frac{3}{2} + i \lambda j}$$

In[81]:=

$$\lambda = n / 2$$

Out[81]=

$$\frac{n}{2}$$

In[82]:=

F[θ]

Out[82]=

$$a \operatorname{Cos}\left[\theta - \frac{n \theta}{2}\right] + b \operatorname{Cos}\left[\theta + \frac{n \theta}{2}\right] - \\ c \operatorname{Sin}\left[\theta - \frac{n \theta}{2}\right] + d \operatorname{Sin}\left[\theta + \frac{n \theta}{2}\right]$$

In[83]:=

$$\mathbf{boa} = - \frac{\varpi \operatorname{Sin}[(\lambda - 1) \alpha]}{\operatorname{Sin}[(\lambda + 1) \alpha]}$$

Out[83]=

$$- \frac{\left(-\frac{1}{2} + i \lambda j\right) \operatorname{Csc}\left[\left(1 + \frac{n}{2}\right) \pi\right] \operatorname{Sin}\left[\left(-1 + \frac{n}{2}\right) \pi\right]}{\frac{3}{2} + i \lambda j}$$

In[84]:=

b = a boa

Out[84]=

$$-\frac{a \left(-\frac{1}{2} + i \lambda j\right) \operatorname{Csc}\left[\left(1 + \frac{n}{2}\right) \pi\right] \operatorname{Sin}\left[\left(-1 + \frac{n}{2}\right) \pi\right]}{\frac{3}{2} + i \lambda j}$$

In[85]:=

$$\mathbf{cod} = -\frac{\operatorname{Sin}\left[(\lambda - 1) \alpha\right]}{\operatorname{Sin}\left[(\lambda + 1) \alpha\right]}$$

Out[85]=

$$-\operatorname{Csc}\left[\left(1 + \frac{n}{2}\right) \pi\right] \operatorname{Sin}\left[\left(-1 + \frac{n}{2}\right) \pi\right]$$

In[86]:=

d = c / cod

Out[86]=

$$-c \operatorname{Csc}\left[\left(-1 + \frac{n}{2}\right) \pi\right] \operatorname{Sin}\left[\left(1 + \frac{n}{2}\right) \pi\right]$$

In[87]:=

n = 1

Out[87]=

1

In[88]:=

TrigReduce[F[θ]]

Out[88]=

$$\begin{aligned} & \frac{-\frac{3}{2} i a \operatorname{Cos}\left[\frac{\theta}{2}\right] - \frac{3}{2} a \operatorname{Sin}\left[\frac{\theta}{2}\right]}{-3 i + 2 \lambda j} + \\ & \frac{-\frac{3}{2} i a \operatorname{Cos}\left[\frac{\theta}{2}\right] + \frac{3}{2} a \operatorname{Sin}\left[\frac{\theta}{2}\right]}{-3 i + 2 \lambda j} + \\ & \frac{-\frac{3}{2} c \operatorname{Cos}\left[\frac{\theta}{2}\right] + \frac{3}{2} i c \operatorname{Sin}\left[\frac{\theta}{2}\right]}{-3 i + 2 \lambda j} + \\ & \frac{\frac{3}{2} c \operatorname{Cos}\left[\frac{\theta}{2}\right] + \frac{3}{2} i c \operatorname{Sin}\left[\frac{\theta}{2}\right]}{-3 i + 2 \lambda j} + \end{aligned}$$

$$\begin{aligned}
& \frac{a \lambda j \cos \left[\frac{\theta}{2} \right] - i a \lambda j \sin \left[\frac{\theta}{2} \right]}{-3 i + 2 \lambda j} + \\
& \frac{a \lambda j \cos \left[\frac{\theta}{2} \right] + i a \lambda j \sin \left[\frac{\theta}{2} \right]}{-3 i + 2 \lambda j} + \\
& \frac{-i c \lambda j \cos \left[\frac{\theta}{2} \right] - c \lambda j \sin \left[\frac{\theta}{2} \right]}{-3 i + 2 \lambda j} + \\
& \frac{i c \lambda j \cos \left[\frac{\theta}{2} \right] - c \lambda j \sin \left[\frac{\theta}{2} \right]}{-3 i + 2 \lambda j} + \\
& \frac{-\frac{1}{2} i a \cos \left[\frac{3\theta}{2} \right] - \frac{1}{2} a \sin \left[\frac{3\theta}{2} \right]}{-3 i + 2 \lambda j} + \\
& \frac{-\frac{1}{2} i a \cos \left[\frac{3\theta}{2} \right] + \frac{1}{2} a \sin \left[\frac{3\theta}{2} \right]}{-3 i + 2 \lambda j} + \\
& \frac{-\frac{3}{2} c \cos \left[\frac{3\theta}{2} \right] + \frac{3}{2} i c \sin \left[\frac{3\theta}{2} \right]}{-3 i + 2 \lambda j} + \\
& \frac{\frac{3}{2} c \cos \left[\frac{3\theta}{2} \right] + \frac{3}{2} i c \sin \left[\frac{3\theta}{2} \right]}{-3 i + 2 \lambda j} + \\
& \frac{-a \lambda j \cos \left[\frac{3\theta}{2} \right] - i a \lambda j \sin \left[\frac{3\theta}{2} \right]}{-3 i + 2 \lambda j} + \\
& \frac{-a \lambda j \cos \left[\frac{3\theta}{2} \right] + i a \lambda j \sin \left[\frac{3\theta}{2} \right]}{-3 i + 2 \lambda j} + \\
& \frac{-i c \lambda j \cos \left[\frac{3\theta}{2} \right] - c \lambda j \sin \left[\frac{3\theta}{2} \right]}{-3 i + 2 \lambda j} + \\
& \frac{i c \lambda j \cos \left[\frac{3\theta}{2} \right] - c \lambda j \sin \left[\frac{3\theta}{2} \right]}{-3 i + 2 \lambda j}
\end{aligned}$$

▼ Determine the polar stresses

In[89]:=

 $\sigma_{rr}[r, \theta]$

Out[89]=

$$\left(-15 i a \operatorname{Cos}\left[\frac{\theta}{2}\right] + 10 a \lambda j \operatorname{Cos}\left[\frac{\theta}{2}\right] + \right. \\ \left. 3 i a \operatorname{Cos}\left[\frac{3\theta}{2}\right] + 6 a \lambda j \operatorname{Cos}\left[\frac{3\theta}{2}\right] + 15 i c \operatorname{Sin}\left[\frac{\theta}{2}\right] - \right. \\ \left. 10 c \lambda j \operatorname{Sin}\left[\frac{\theta}{2}\right] - 9 i c \operatorname{Sin}\left[\frac{3\theta}{2}\right] + 6 c \lambda j \operatorname{Sin}\left[\frac{3\theta}{2}\right] \right) / \\ (4 \sqrt{r} (-3 i + 2 \lambda j))$$

In[90]:=

 $\text{Factor}[\sigma_{r\theta}[r, \theta]]$

Out[90]=

$$\frac{1}{4} r^{-\frac{1}{2} + i \lambda j} (-i + 2 \lambda j) \\ \left(i c \operatorname{Cos}\left[\theta - \theta \left(\frac{1}{2} + i \lambda j\right)\right] + 2 c \lambda j \operatorname{Cos}\left[\theta - \theta \left(\frac{1}{2} + i \lambda j\right)\right] + \right. \\ \left. 3 i c \operatorname{Cos}\left[\theta + \theta \left(\frac{1}{2} + i \lambda j\right)\right] - 2 c \lambda j \right. \\ \left. \operatorname{Cos}\left[\theta + \theta \left(\frac{1}{2} + i \lambda j\right)\right] + i a \operatorname{Sin}\left[\theta - \theta \left(\frac{1}{2} + i \lambda j\right)\right] + \right. \\ \left. 2 a \lambda j \operatorname{Sin}\left[\theta - \theta \left(\frac{1}{2} + i \lambda j\right)\right] + i a \right. \\ \left. \operatorname{Sin}\left[\theta + \theta \left(\frac{1}{2} + i \lambda j\right)\right] + 2 a \lambda j \operatorname{Sin}\left[\theta + \theta \left(\frac{1}{2} + i \lambda j\right)\right] \right)$$

In[91]:=

 $\sigma_{\theta\theta}[r, \theta]$

Out[91]=

$$\left(3 \times \left(-3 \, i \, a \, \text{Cos}\left[\frac{\theta}{2}\right] + 2 \, a \, \lambda j \, \text{Cos}\left[\frac{\theta}{2}\right] - i \, a \, \text{Cos}\left[\frac{3 \theta}{2}\right] - \right. \right. \\ \left. \left. 2 \, a \, \lambda j \, \text{Cos}\left[\frac{3 \theta}{2}\right] + 3 \, i \, c \, \text{Sin}\left[\frac{\theta}{2}\right] - 2 \, c \, \lambda j \, \text{Sin}\left[\frac{\theta}{2}\right] + \right. \right. \\ \left. \left. 3 \, i \, c \, \text{Sin}\left[\frac{3 \theta}{2}\right] - 2 \, c \, \lambda j \, \text{Sin}\left[\frac{3 \theta}{2}\right] \right) \right) / \\ (4 \sqrt{r} (-3 \, i + 2 \, \lambda j))$$

▼ Introduce SIF

In[92]:=

$$a = \frac{K_I}{\sqrt{2 \pi}}$$

Out[92]=

$$\frac{K_i}{\sqrt{2 \pi}}$$

In[93]:=

$$c = \frac{K_{II}}{\sqrt{2 \pi}}$$

Out[93]=

$$\frac{K_{II}}{\sqrt{2 \pi}}$$

In[94]:=

$$\sigma_{rr} = \sigma_{rr}[r, \theta]$$

Out[94]=

$$\frac{1}{4 \sqrt{2} \pi \sqrt{r} (-3 i + 2 \lambda j)} \left(-15 i \cos\left[\frac{\theta}{2}\right] K_i + 10 \lambda j \cos\left[\frac{\theta}{2}\right] K_i + 3 i \cos\left[\frac{3\theta}{2}\right] K_i + 6 \lambda j \cos\left[\frac{3\theta}{2}\right] K_i + 15 i \sin\left[\frac{\theta}{2}\right] K_{II} - 10 \lambda j \sin\left[\frac{\theta}{2}\right] K_{II} - 9 i \sin\left[\frac{3\theta}{2}\right] K_{II} + 6 \lambda j \sin\left[\frac{3\theta}{2}\right] K_{II} \right)$$

In[95]:=

$$\sigma_{\theta\theta} = \sigma_{\theta\theta}[r, \theta]$$

Out[95]=

$$\frac{1}{4 \sqrt{2} \pi \sqrt{r} (-3 i + 2 \lambda j)} \left(3 \times \left(-3 i \cos\left[\frac{\theta}{2}\right] K_i + 2 \lambda j \cos\left[\frac{\theta}{2}\right] K_i - i \cos\left[\frac{3\theta}{2}\right] K_i - 2 \lambda j \cos\left[\frac{3\theta}{2}\right] K_i + 3 i \sin\left[\frac{\theta}{2}\right] K_{II} - 2 \lambda j \sin\left[\frac{\theta}{2}\right] K_{II} + 3 i \sin\left[\frac{3\theta}{2}\right] K_{II} - 2 \lambda j \sin\left[\frac{3\theta}{2}\right] K_{II} \right) \right)$$

In[96]:=

 $\sigma_{r\theta} = \text{Factor}[\sigma_{r\theta}[r, \theta]]$

Out[96]=

$$\frac{1}{4 \sqrt{2} \pi} r^{-\frac{1}{2} + i \lambda j} (-i + 2 \lambda j) \left(i \sin\left[\theta - \theta \left(\frac{1}{2} + i \lambda j\right)\right] K_i + 2 \lambda j \sin\left[\theta - \theta \left(\frac{1}{2} + i \lambda j\right)\right] K_i + i \sin\left[\theta + \theta \left(\frac{1}{2} + i \lambda j\right)\right] K_i + 2 \lambda j \sin\left[\theta + \theta \left(\frac{1}{2} + i \lambda j\right)\right] K_i + i \cos\left[\theta - \theta \left(\frac{1}{2} + i \lambda j\right)\right] K_{II} + 2 \lambda j \cos\left[\theta - \theta \left(\frac{1}{2} + i \lambda j\right)\right] K_{II} + 3 i \cos\left[\theta + \theta \left(\frac{1}{2} + i \lambda j\right)\right] K_{II} - 2 \lambda j \cos\left[\theta + \theta \left(\frac{1}{2} + i \lambda j\right)\right] K_{II} \right)$$

▼ Stresses in Cartesian Coordinates

In[97]:=

$$\begin{pmatrix} \sigma_{xx} & \sigma_{xy} \\ \sigma_{xy} & \sigma_{yy} \end{pmatrix} = \text{Simplify}\left[\left(\begin{pmatrix} \cos[\theta] & \sin[\theta] \\ -\sin[\theta] & \cos[\theta] \end{pmatrix} \cdot \begin{pmatrix} \sigma_{rr} & \sigma_{r\theta} \\ \sigma_{r\theta} & \sigma_{\theta\theta} \end{pmatrix}\right) \cdot \text{Transpose}\left[\left(\begin{pmatrix} \cos[\theta] & \sin[\theta] \\ -\sin[\theta] & \cos[\theta] \end{pmatrix}\right)\right]\right]$$

Out[97]=

$$\left\{ \left\{ \frac{1}{4 \sqrt{2} \pi r (-3 i + 2 \lambda j)} \left(\left(\sqrt{r} (-3 i + 2 \lambda j) \cos\left[\frac{\theta}{2}\right] (4 + \cos[2 \theta]) + (i + 2 \lambda j) \left(3 \sqrt{r} \cos[\theta]^2 \cos\left[\frac{3 \theta}{2}\right] - \right) \right) \right\} \right\}$$

$$\begin{aligned}
& 3 \sqrt{r} \operatorname{Cos} \left[\frac{3\theta}{2} \right] \operatorname{Sin}[\theta]^2 + r^{\frac{1}{2}+i\lambda j} \left(-3 - 8 i \lambda j + \right. \\
& \quad \left. 4 \lambda j^2 \right) \operatorname{Sin}[2\theta] \left(\operatorname{Sin} \left[\frac{1}{2} \theta (1 - 2 i \lambda j) \right] + \right. \\
& \quad \left. \operatorname{Sin} \left[\frac{1}{2} \theta (3 + 2 i \lambda j) \right] \right) \Big) \Big) \mathbf{K}_i + \\
& (-3 i + 2 \lambda j) \times \left(-3 \sqrt{r} \operatorname{Sin} \left[\frac{\theta}{2} \right] \operatorname{Sin}[\theta]^2 - \right. \\
& \quad 3 \sqrt{r} \operatorname{Sin}[\theta]^2 \operatorname{Sin} \left[\frac{3\theta}{2} \right] + \\
& \quad \left. \sqrt{r} \operatorname{Cos}[\theta]^2 \left(-5 \operatorname{Sin} \left[\frac{\theta}{2} \right] + 3 \operatorname{Sin} \left[\frac{3\theta}{2} \right] \right) + \right. \\
& \quad r^{\frac{1}{2}+i\lambda j} \operatorname{Cos} \left[\frac{1}{2} \theta (1 - 2 i \lambda j) \right] \operatorname{Sin}[2\theta] + \\
& \quad 4 r^{\frac{1}{2}+i\lambda j} \lambda j^2 \operatorname{Cos} \left[\frac{1}{2} \theta (1 - 2 i \lambda j) \right] \operatorname{Sin}[2\theta] + \\
& \quad 3 r^{\frac{1}{2}+i\lambda j} \operatorname{Cos} \left[\frac{1}{2} \theta (3 + 2 i \lambda j) \right] \operatorname{Sin}[2\theta] + \\
& \quad 8 i r^{\frac{1}{2}+i\lambda j} \lambda j \operatorname{Cos} \left[\frac{1}{2} \theta (3 + 2 i \lambda j) \right] \operatorname{Sin}[2\theta] - \\
& \quad \left. 4 r^{\frac{1}{2}+i\lambda j} \lambda j^2 \operatorname{Cos} \left[\frac{1}{2} \theta (3 + 2 i \lambda j) \right] \operatorname{Sin}[2\theta] \right) \mathbf{K}_{II} \Big),
\end{aligned}$$

$$\begin{aligned}
& \frac{1}{4 \sqrt{2\pi} \sqrt{r} (3 i - 2 \lambda j)} \\
& \left(6 \operatorname{Cos} \left[\frac{\theta}{2} \right]^2 \right. \\
& \quad \left(-\operatorname{Sin} \left[\frac{\theta}{2} \right] + \operatorname{Sin} \left[\frac{3\theta}{2} \right] \right) \\
& \quad \left((i - 2 \lambda j + (i + 2 \lambda j) \operatorname{Cos}[\theta]) \mathbf{K}_i + \right. \\
& \quad \quad \left. (-3 i + 2 \lambda j) \operatorname{Sin}[\theta] \mathbf{K}_{II} \right) + \operatorname{Cos}[\theta] \operatorname{Sin}[\theta] \\
& \quad \left(2 \operatorname{Cos} \left[\frac{\theta}{2} \right] (-9 i + 2 \lambda j + (3 i + 6 \lambda j) \operatorname{Cos}[\theta]) \mathbf{K}_i + \right. \\
& \quad \quad \left. (-3 i + 2 \lambda j) \times \left(-5 \operatorname{Sin} \left[\frac{\theta}{2} \right] + 3 \operatorname{Sin} \left[\frac{3\theta}{2} \right] \right) \mathbf{K}_{II} \right) -
\end{aligned}$$

$$\begin{aligned}
& r^{i \lambda j} (-i + 2 \lambda j) (-3 i + 2 \lambda j) \text{Cos} [\theta]^2 \\
& \left(2 (i + 2 \lambda j) \text{Cos} \left[\theta \left(\frac{1}{2} + i \lambda j \right) \right] \text{Sin} [\theta] \mathbf{K}_i + \right. \\
& \quad 2 \times \left(2 i \text{Cos} [\theta] \text{Cos} \left[\theta \left(\frac{1}{2} + i \lambda j \right) \right] + \right. \\
& \quad \quad \left. \left. (-i + 2 \lambda j) \text{Sin} [\theta] \text{Sin} \left[\theta \left(\frac{1}{2} + i \lambda j \right) \right] \right) \mathbf{K}_{II} \right) + \\
& r^{i \lambda j} (-i + 2 \lambda j) (-3 i + 2 \lambda j) \text{Sin} [\theta]^2 \\
& \left(2 (i + 2 \lambda j) \text{Cos} \left[\theta \left(\frac{1}{2} + i \lambda j \right) \right] \text{Sin} [\theta] \mathbf{K}_i + \right. \\
& \quad 2 \times \left(2 i \text{Cos} [\theta] \text{Cos} \left[\theta \left(\frac{1}{2} + i \lambda j \right) \right] + \right. \\
& \quad \quad \left. \left. (-i + 2 \lambda j) \text{Sin} [\theta] \text{Sin} \left[\theta \left(\frac{1}{2} + i \lambda j \right) \right] \right) \mathbf{K}_{II} \right) \left. \right\}, \\
& \left\{ \frac{1}{4 \sqrt{2 \pi} \sqrt{r} (3 i - 2 \lambda j)} \left(\text{Cos} [\theta] \right. \right. \\
& \quad \left(\text{Sin} [\theta] \left(2 \text{Cos} \left[\frac{\theta}{2} \right] (-9 i + 2 \lambda j + \right. \right. \\
& \quad \quad \left. \left. (3 i + 6 \lambda j) \text{Cos} [\theta] \right) \mathbf{K}_i + (-3 i + 2 \lambda j) \times \right. \\
& \quad \quad \left. \left. \left(-5 \text{Sin} \left[\frac{\theta}{2} \right] + 3 \text{Sin} \left[\frac{3 \theta}{2} \right] \right) \mathbf{K}_{II} \right) - \right. \\
& \quad r^{i \lambda j} (-i + 2 \lambda j) (-3 i + 2 \lambda j) \text{Cos} [\theta] \\
& \quad \left(2 (i + 2 \lambda j) \text{Cos} \left[\theta \left(\frac{1}{2} + i \lambda j \right) \right] \text{Sin} [\theta] \mathbf{K}_i + 2 \times \right. \\
& \quad \quad \left(2 i \text{Cos} [\theta] \text{Cos} \left[\theta \left(\frac{1}{2} + i \lambda j \right) \right] + (-i + 2 \lambda j) \right. \\
& \quad \quad \quad \left. \left. \text{Sin} [\theta] \text{Sin} \left[\theta \left(\frac{1}{2} + i \lambda j \right) \right] \right) \mathbf{K}_{II} \right) \left. \right) + \\
& \quad \text{Sin} [\theta] \left(6 \text{Cos} \left[\frac{\theta}{2} \right] \text{Cos} [\theta] ((i - 2 \lambda j + (i + 2 \lambda j) \right. \right. \\
& \quad \quad \left. \left. \text{Cos} [\theta]) \mathbf{K}_i + (-3 i + 2 \lambda j) \text{Sin} [\theta] \mathbf{K}_{II} \right) + \right. \\
& \quad r^{i \lambda j} (-i + 2 \lambda j) (-3 i + 2 \lambda j) \text{Sin} [\theta] \\
& \quad \left. \left(2 (i + 2 \lambda j) \text{Cos} \left[\theta \left(\frac{1}{2} + i \lambda j \right) \right] \text{Sin} [\theta] \mathbf{K}_i + 2 \times \right. \right.
\end{aligned}$$

$$\begin{aligned}
& \left(2 \, \mathfrak{i} \, \text{Cos}[\theta] \, \text{Cos} \left[\theta \left(\frac{1}{2} + \mathfrak{i} \, \lambda \mathfrak{j} \right) \right] + (-\mathfrak{i} + 2 \, \lambda \mathfrak{j}) \right. \\
& \quad \left. \text{Sin}[\theta] \, \text{Sin} \left[\theta \left(\frac{1}{2} + \mathfrak{i} \, \lambda \mathfrak{j} \right) \right] \right) \mathbf{K}_{\text{II}} \Bigg) \Bigg), \\
& \frac{1}{4 \sqrt{2} \pi r (-3 \, \mathfrak{i} + 2 \, \lambda \mathfrak{j})} \left(\left(-3 \sqrt{r} (\mathfrak{i} + 2 \, \lambda \mathfrak{j}) \right. \right. \\
& \quad \text{Cos}[\theta]^2 \, \text{Cos} \left[\frac{3\theta}{2} \right] + \\
& \quad 3 \sqrt{r} \, \text{Cos} \left[\frac{\theta}{2} \right] (-4 \, \mathfrak{i} + \lambda \mathfrak{j} + (\mathfrak{i} + \lambda \mathfrak{j}) \, \text{Cos}[2\theta]) + \\
& \quad 3 \, \mathfrak{i} \sqrt{r} \, \text{Cos} \left[\frac{3\theta}{2} \right] \, \text{Sin}[\theta]^2 + 6 \sqrt{r} \, \lambda \mathfrak{j} \, \text{Cos} \left[\frac{3\theta}{2} \right] \\
& \quad \text{Sin}[\theta]^2 + 5 \sqrt{r} \, \lambda \mathfrak{j} \, \text{Csc} \left[\frac{\theta}{2} \right] \, \text{Sin}[\theta]^3 + \\
& \quad 3 \, \mathfrak{i} \, r^{\frac{1}{2} + \mathfrak{i} \, \lambda \mathfrak{j}} \, \text{Sin}[2\theta] \, \text{Sin} \left[\frac{1}{2} \theta (1 - 2 \, \mathfrak{i} \, \lambda \mathfrak{j}) \right] - \\
& \quad 2 \, r^{\frac{1}{2} + \mathfrak{i} \, \lambda \mathfrak{j}} \, \lambda \mathfrak{j} \, \text{Sin}[2\theta] \, \text{Sin} \left[\frac{1}{2} \theta (1 - 2 \, \mathfrak{i} \, \lambda \mathfrak{j}) \right] + \\
& \quad 12 \, \mathfrak{i} \, r^{\frac{1}{2} + \mathfrak{i} \, \lambda \mathfrak{j}} \, \lambda \mathfrak{j}^2 \, \text{Sin}[2\theta] \, \text{Sin} \left[\frac{1}{2} \theta (1 - 2 \, \mathfrak{i} \, \lambda \mathfrak{j}) \right] - \\
& \quad 8 \, r^{\frac{1}{2} + \mathfrak{i} \, \lambda \mathfrak{j}} \, \lambda \mathfrak{j}^3 \, \text{Sin}[2\theta] \, \text{Sin} \left[\frac{1}{2} \theta (1 - 2 \, \mathfrak{i} \, \lambda \mathfrak{j}) \right] + \\
& \quad 3 \, \mathfrak{i} \, r^{\frac{1}{2} + \mathfrak{i} \, \lambda \mathfrak{j}} \, \text{Sin}[2\theta] \, \text{Sin} \left[\frac{1}{2} \theta (3 + 2 \, \mathfrak{i} \, \lambda \mathfrak{j}) \right] - \\
& \quad 2 \, r^{\frac{1}{2} + \mathfrak{i} \, \lambda \mathfrak{j}} \, \lambda \mathfrak{j} \, \text{Sin}[2\theta] \, \text{Sin} \left[\frac{1}{2} \theta (3 + 2 \, \mathfrak{i} \, \lambda \mathfrak{j}) \right] + \\
& \quad 12 \, \mathfrak{i} \, r^{\frac{1}{2} + \mathfrak{i} \, \lambda \mathfrak{j}} \, \lambda \mathfrak{j}^2 \, \text{Sin}[2\theta] \, \text{Sin} \left[\frac{1}{2} \theta (3 + 2 \, \mathfrak{i} \, \lambda \mathfrak{j}) \right] - \\
& \quad \left. \left. 8 \, r^{\frac{1}{2} + \mathfrak{i} \, \lambda \mathfrak{j}} \, \lambda \mathfrak{j}^3 \, \text{Sin}[2\theta] \, \text{Sin} \left[\frac{1}{2} \theta (3 + 2 \, \mathfrak{i} \, \lambda \mathfrak{j}) \right] \right) \mathbf{K}_{\mathfrak{i}} - \right. \\
& \quad \left. (-3 \, \mathfrak{i} + 2 \, \lambda \mathfrak{j}) \, \text{Csc} \left[\frac{\theta}{2} \right] \left(3 \sqrt{r} \, \text{Cos}[\theta]^2 \, \text{Sin}[\theta]^2 + \right. \right. \\
& \quad \left. \left. \text{Sin} \left[\frac{\theta}{2} \right] \left(5 \sqrt{r} \, \text{Sin} \left[\frac{\theta}{2} \right] \, \text{Sin}[\theta]^2 - 3 \sqrt{r} \, \text{Sin}[\theta]^2 \right) \right) \right)
\end{aligned}$$

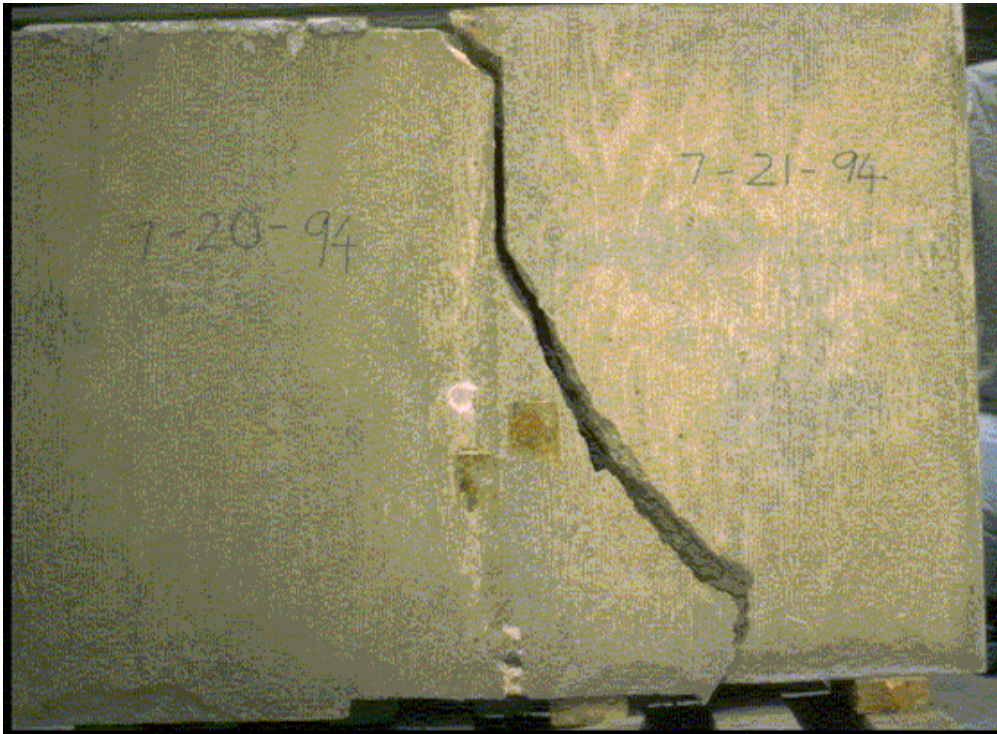
Part VI

Early (partially outdated) Manuscript

This an early version of an attempt to put the notes into a manuscript.

It is not as up to date as the lecture notes, however it will contain: a) more details in some cases; b) some topics not covered; and c) an extensive bibliography of referenced papers.

FRACTURE MECHANICS



Victor E. Saouma

Dept. of Civil Environmental and Architectural Engineering

University of Colorado, Boulder, CO 80309-0428

2012

Contents

1	INTRODUCTION	3
1.1	Modes of Failures	3
1.2	Examples of Structural Failures Caused by Fracture	3
1.3	Fracture Mechanics vs Strength of Materials	4
1.4	Major Historical Developments in Fracture Mechanics	7
1.5	Coverage	8
2	PRELIMINARY CONSIDERATIONS	9
2.1	Tensors	9
2.1.1	Indicial Notation	9
2.1.2	Tensor Operations	11
2.1.3	Rotation of Axes	11
2.1.4	Trace	12
2.1.5	Inverse Tensor	12
2.1.6	Principal Values and Directions of Symmetric Second Order Tensors	12
2.2	Kinetics	13
2.2.1	Force, Traction and Stress Vectors	13
2.2.2	Traction on an Arbitrary Plane; Cauchy's Stress Tensor	15
2.2.2.1	Stress Vectors	15
2.2.3	Invariants	16
2.2.4	Spherical and Deviatoric Stress Tensors	16
2.2.5	Stress Transformation	17
2.2.6	Polar Coordinates	17
2.3	Kinematic	17
2.3.1	Strain Tensors	17
2.3.2	Compatibility Equation	19
2.4	Fundamental Laws of Continuum Mechanics	19
2.4.1	Conservation Laws	20
2.4.2	Fluxes	20
2.4.3	Conservation of Mass; Continuity Equation	21
2.4.4	Linear Momentum Principle; Equation of Motion	21
2.4.5	Moment of Momentum Principle	22
2.4.6	Conservation of Energy; First Principle of Thermodynamics	22
2.5	Constitutive Equations	23
2.5.1	Transversely Isotropic Case	24
2.5.2	Special 2D Cases	24
2.5.2.1	Plane Strain	24
2.5.2.2	Axisymmetry	25
2.5.2.3	Plane Stress	25
2.6	Airy Stress Function	25
2.7	Complex Variables	26
2.7.1	Complex Airy Stress Functions	27
2.8	Curvilinear Coordinates	27
2.9	Basic Equations of Anisotropic Elasticity	28
2.9.1	Coordinate Transformations	30
2.9.2	Plane Stress-Strain Compliance Transformation	31
2.9.3	Stress Functions	31
2.9.4	Stresses and Displacements	33

2.10	Conclusion	33
3	ELASTICITY BASED SOLUTIONS FOR CRACK PROBLEMS	35
3.1	Introduction	35
3.2	Circular Hole, (Kirsch, 1898)	35
3.3	Elliptical hole in a Uniformly Stressed Plate (Inglis, 1913)	37
3.4	Crack, (Westergaard, 1939)	40
3.4.1	Stress Intensity Factors (Irwin)	43
3.4.2	Near Crack Tip Stresses and Displacements in Isotropic Cracked Solids	44
3.5	V Notch, (Williams, 1952)	46
3.6	Crack at an Interface between Two Dissimilar Materials (Williams, 1959)	49
3.6.1	General Function	49
3.6.2	Boundary Conditions	49
3.6.3	Homogeneous Equations	50
3.6.4	Solve for λ	52
3.6.5	Near Crack Tip Stresses	52
3.7	Homogeneous Anisotropic Material (Sih and Paris)	54
3.8	Assignment	56
4	LEFM DESIGN EXAMPLES	59
4.1	Design Philosophy Based on Linear Elastic Fracture Mechanics	59
4.2	Stress Intensity Factors	59
4.3	Fracture Properties of Materials	67
4.4	Examples	68
4.4.1	Example 1	68
4.4.2	Example 2	68
4.5	Additional Design Considerations	69
4.5.1	Leak Before Fail	69
4.5.2	Damage Tolerance Assessment	69
5	THEORETICAL STRENGTH of SOLIDS; (Griffith I)	71
5.1	Derivation	71
5.1.1	Tensile Strength	71
5.1.1.1	Ideal Strength in Terms of Physical Parameters	71
5.1.1.2	Ideal Strength in Terms of Engineering Parameter	73
5.1.2	Shear Strength	74
5.2	Griffith Theory	74
5.2.1	Derivation	75
6	ENERGY TRANSFER in CRACK GROWTH; (Griffith II)	77
6.1	Thermodynamics of Crack Growth	77
6.1.1	General Derivation	77
6.1.2	Brittle Material, Griffith's Model	78
6.2	Energy Release Rate; Global	80
6.2.1	From Load-Displacement	80
6.2.2	From Compliance	80
6.3	Energy Release Rate; Local	83
6.4	Theoretical Basis	85
6.4.1	R vs K_{Ic}	85
6.5	Crack Stability	86
6.5.1	Effect of Geometry; Π Curve	86
6.5.2	Effect of Material; R Curve	87
6.5.2.1	Plane Strain	87
6.5.2.2	Plane Stress	88
7	MIXED MODE CRACK PROPAGATION	91
7.1	Analytical Models for Isotropic Solids	91
7.1.1	Maximum Circumferential Tensile Stress.	92
7.1.2	Maximum Energy Release Rate	92
7.1.3	Minimum Strain Energy Density Criteria.	93

7.1.4	Observations	95
7.2	Empirical Models for Rocks	96
7.3	Extensions to Anisotropic Solids	96
7.4	Interface Cracks	99
7.4.1	Crack Tip Fields	102
7.4.2	Dimensions of Bimaterial Stress Intensity Factors	103
7.4.3	Interface Fracture Toughness	103
7.4.3.1	Interface Fracture Toughness when $\beta = 0$	105
7.4.3.2	Interface Fracture Toughness when $\beta \neq 0$	105
7.4.4	Crack Kinking Analysis	106
7.4.4.1	Numerical Results from He and Hutchinson	106
7.4.4.2	Numerical Results Using Merlin	107
7.4.5	Summary	110
8	PLASTIC ZONE SIZES	113
8.1	Uniaxial Stress Criteria	113
8.1.1	First-Order Approximation	113
8.1.2	Second-Order Approximation (Irwin)	114
8.1.2.1	Example	115
8.1.3	Dugdale's Model	116
8.2	Multiaxial Yield Criteria	118
8.3	Plane Strain vs. Plane Stress	118
9	FATIGUE CRACK PROPAGATION	121
9.1	Experimental Observation	121
9.2	Fatigue Laws Under Constant Amplitude Loading	122
9.2.1	Paris Model	122
9.2.2	Foreman's Model	123
9.2.3	Modified Walker's Model	123
9.2.4	Table Look-Up	123
9.2.5	Effective Stress Intensity Factor Range	124
9.2.6	Examples	124
9.2.6.1	Example 1	124
9.2.6.2	Example 2	124
9.2.6.3	Example 3	125
9.3	Variable Amplitude Loading	125
9.3.1	No Load Interaction	125
9.3.2	Load Interaction	125
9.3.2.1	Observation	125
9.3.2.2	Retardation Models	125
9.3.2.2.1	Wheeler's Model	126
9.3.2.2.2	Generalized Willenborg's Model	126
10	CRACK TIP OPENING DISPLACEMENTS	129
10.1	Derivation of CTOD	130
10.1.1	Irwin's Solution	130
10.1.2	Dugdale's Solution	131
10.2	G -CTOD Relations	131
11	J INTEGRAL	133
11.1	Genesis	133
11.2	Proof of Path Independence	133
11.3	Nonlinear Elastic Energy Release Rate	134
11.3.1	Virtual Line Crack Extension	135
11.3.2	†Virtual Volume Expansion	136
11.4	Nonlinear Energy Release Rate	139
11.5	J Testing	140
11.6	Crack Growth Resistance Curves	140
11.7	† Load Control versus Displacement Control	141
11.8	Plastic Crack Tip Fields	142

11.9	Engineering Approach to Fracture	146
11.9.1	Compilation of Fully Plastic Solutions	147
11.9.2	Numerical Example	157
11.10	J_1 and J_2 Generalization	158
11.11	Dynamic Energy Release Rate	159
11.12	Effect of Other Loading	161
11.12.1	Surface Traction on Crack Surfaces	161
11.12.2	Body Forces	162
11.12.3	Initial Strains Corresponding to Thermal Loading	162
11.12.4	Initial Stresses Corresponding to Pore Pressures	163
11.12.5	Combined Thermal Strains and Pore Pressures	165
11.13	Epilogue	165
12	FRACTURE DETERIORATION ANALYSIS OF CONCRETE	167
12.1	Introduction	167
12.2	Phenomenological Observations	167
12.2.1	Load, Displacement, and Strain Control Tests	167
12.2.2	Pre/Post-Peak Material Response of Steel and Concrete	168
12.3	Localisation of Deformation	169
12.3.1	Experimental Evidence	169
12.3.1.1	σ -COD Diagram, Hillerborg's Model	169
12.3.2	Theoretical Evidence	171
12.3.2.1	Static Loading	171
12.3.2.2	Dynamic Loading	173
12.3.2.2.1	Loss of Hyperbolicity	173
12.3.2.2.2	Wave Equation for Softening Materials	174
12.3.3	Conclusion	175
12.4	Griffith Criterion and FPZ	175
13	FRACTURE MECHANICS of CONCRETE	179
13.1	Fracture Toughness Testing of Concrete: a Historical Perspective	179
13.2	Nonlinear Fracture Models	180
13.2.1	Models	180
13.2.1.1	Cohesive Crack Model	180
13.2.1.2	Jenq and Shah Two Parameters Model	180
13.2.2	Characteristic Lengths	180
13.2.2.1	Hillerborg	180
13.2.2.2	Jenq and Shah	181
13.2.2.3	Carpinteri Brittleness Number	181
13.2.3	Comparison of the Fracture Models	181
13.2.3.1	Hillerborg Characteristic Length, l_{ch}	181
13.2.3.2	Bazant Brittleness Number, β	182
13.2.3.3	Carpinteri Brittleness Number, s	183
13.2.3.4	Jenq and Shah's Critical Material Length, Q	183
13.2.3.5	Discussion	183
13.2.4	Model Selection	184
13.3	Fracture Energies G_f and G_F	184
13.3.1	Maximum Load is Controlled by G_f , Postpeak by G_F	185
13.3.2	Statistical Scatter of G_f and G_F	185
13.3.3	Level I and Level II Testing	186
13.4	Proposed ACI/ASCE Test Methods	187
13.4.1	Test 1: Determination of Jenq & Shah Parameters ($K_{Ic(tp)}$ And $CTOD_{c(tp)}$)	187
13.4.1.1	Terminology	187
13.4.1.1.1	Definitions	187
13.4.1.1.2	Abbreviations	187
13.4.1.2	Summary of Test Method	187
13.4.1.3	Apparatus	188
13.4.1.4	Specimens	188
13.4.1.5	Procedure	189

13.4.1.6	Specimen Testing	189
13.4.1.7	Measured Values	189
13.4.1.8	Calculation	189
13.4.2	Test 2: Cohesive Crack Model Parameters; Level 1 (G_f)	190
13.4.2.1	Terminology	190
13.4.2.1.1	Definitions	190
13.4.2.1.2	Notation and Abbreviations	191
13.4.2.2	Summary of Test Method	191
13.4.2.3	Significance and Use	192
13.4.2.4	Specimens	192
13.4.2.5	Casting, Curing and Conservation	193
13.4.2.6	Procedure	193
13.4.2.7	Calculations	194
13.4.2.7.1	Tensile strength, f_t'	194
13.4.2.7.2	Elastic modulus, E	194
13.4.2.7.3	Net plastic flexural strength, f_p	194
13.4.2.7.4	Brittleness length, l_1 , and horizontal intercept, w_1	195
13.4.3	Test 3: Cohesive Crack Model Parameters; Level 2 (G_F)	195
13.4.3.1	Terminology	195
13.4.3.1.1	Definitions	195
13.4.3.1.2	Notation and Abbreviations	196
13.4.3.2	Summary of Test Method	197
13.4.3.3	Significance and Use	197
13.4.3.4	Specimens	198
13.4.3.5	Apparatus	198
13.4.3.6	Test Record	199
13.4.3.7	Procedure	199
13.4.3.8	Calculations	200
13.4.3.8.1	Tensile strength, f_t	200
13.4.3.8.2	Elastic modulus, E	200
13.4.3.8.3	Far tail constant, A	201
13.4.3.9	Net plastic flexural strength, f_p	201
13.4.3.10	Brittleness length, l_1 , and horizontal intercept, w_1	202
13.4.3.11	Fracture energy G_F	202
13.4.3.12	Center of gravity of the softening curve, w_G	203
13.4.3.13	Critical crack opening, w_c	203
13.4.3.14	Coordinates at the kink point (σ_k, w_k)	203
13.5	Wedge Splitting Test; Saouma <i>et. al.</i>	203
13.5.1	Apparatus	204
13.5.2	Test Specimens	204
13.5.3	Procedure	204
13.5.4	Measured Values	205
13.5.5	Calculation	205
13.5.5.1	Fracture Toughness	205
13.5.5.2	Fracture Energy	207
13.5.6	Report	207
13.5.7	Observations	208
14	SIZE EFFECT	209
14.0.1	Original Derivation	209
14.1	Analytical Derivation	210
14.1.1	Constant Cohesive Stresses	210
14.1.1.1	Central Crack	210
14.1.1.2	Edge Crack	212
14.1.2	Linear Cohesive Stresses	213
14.1.2.1	Edge Crack	213
14.1.2.2	Three-Point Bend Specimen	215
14.2	Discussion	216
14.2.1	Comparison with Experimental Data	216

14.2.2	Implications	217
14.2.3	LEFM vs NLFM Analyses	219
14.3	Conclusion	219
15	FRACTALS, FRACTURES and SIZE EFFECTS	221
15.1	Introduction	221
15.1.1	Fracture of Concrete	221
15.1.2	Fractal Geometry	221
15.1.3	Numerical Determination of Fractal Dimension	223
15.1.4	Correlation of Fractal Dimensions With Fracture Properties	223
15.2	Experimental Procedure	224
15.2.1	Fracture Testing	224
15.2.2	Profile Measurements	225
15.2.3	Computation of Fractal Dimension	225
15.3	Fractals and Fracture	227
15.3.1	Spatial Variation of the Fractal Dimension	230
15.3.2	Correlation Between Fracture Toughness and Fractal Dimensions	232
15.3.3	Macro-Scale Correlation Analysis	232
15.4	Fractals and Size Effects	235
15.5	Conclusions	237
16	On Fractals and Size Effects	239
16.1	Introduction	239
16.1.1	Fractals	239
16.1.1.1	Definition	239
16.1.1.2	Lacunar versus Invasive Fractals	239
16.1.1.3	Self-Similar and Self-Affine Fractals	240
16.1.1.4	Multifractals	240
16.1.1.5	Fractality of Cracks and Concrete	241
16.1.2	Size Effect	241
16.1.2.1	Bazant	241
16.1.2.2	Carpinteri	243
16.1.3	Historical Notes	244
16.2	Fractal Stress Intensity Factors	245
16.2.1	Far Field Stress	246
16.2.2	Cohesive Crack	246
16.3	Fractal Size Effect	248
16.4	Cellular Automata	248
16.5	Conclusion	250
17	FRACTURE MECHANICS PROPERTIES OF CONCRETE	251
17.1	Introduction	251
17.2	Experiments	251
17.2.1	Concrete Mix Design and Specimen Preparation	251
17.2.2	Loading Fixtures	253
17.2.3	Testing Procedure	253
17.2.4	Acoustic Emissions Monitoring	254
17.2.5	Evaluation of Fracture Toughness by the Compliance Method	255
17.3	Fracture Toughness Results	255
17.4	Specific Fracture Energy Results	257
17.5	Conclusions	258
17.6	Size Effect Law Assessment	259
17.7	Notation and Abbreviations	259
18	SINGULAR ELEMENT	261
18.1	Introduction	261
18.2	Displacement Extrapolation	261
18.3	Quarter Point Singular Elements	261
18.4	Review of Isoparametric Finite Elements	262
18.5	How to Distort the Element to Model the Singularity	264

18.6	Order of Singularity	265
18.7	Stress Intensity Factors Extraction	266
18.7.1	Isotropic Case	266
18.7.2	Anisotropic Case	267
18.8	Numerical Evaluation	267
18.9	Historical Overview	268
18.10	Other Singular Elements	269
19	ENERGY RELEASE BASED METHODS	271
19.1	Mode I Only	271
19.1.1	Energy Release Rate	271
19.1.2	Virtual Crack Extension	272
19.2	Mixed Mode Cases	272
19.2.1	Two Virtual Crack Extensions	272
19.2.2	Single Virtual Crack Extension, Displacement Decomposition	273
20	J INTEGRAL BASED METHODS	275
20.1	Numerical Evaluation	275
20.2	Mixed Mode SIF Evaluation	277
20.3	Equivalent Domain Integral (EDI) Method	278
20.3.1	Energy Release Rate J	278
20.3.1.1	2D case	278
20.3.1.2	3D Generalization	280
20.3.2	Extraction of SIF	282
20.3.2.1	J Components	282
20.3.2.2	σ and u Decomposition	283
21	RECIPROCAL WORK INTEGRALS	285
21.1	General Formulation	285
21.2	Volume Form of the Reciprocal Work Integral	288
21.3	Surface Traction on Crack Surfaces	289
21.4	Body Forces	290
21.5	Initial Strains Corresponding to Thermal Loading	290
21.6	Initial Stresses Corresponding to Pore Pressures	292
21.7	Combined Thermal Strains and Pore Pressures	292
21.8	Field Equations for Thermo- and Poro-Elasticity	293
22	FICTITIOUS CRACK MODEL	295
22.1	Introduction	295
22.2	Computational Algorithm	295
22.2.1	Weak Form of Governing Equations	295
22.2.2	Discretization of Governing Equations	297
22.2.3	Penalty Method Solution	299
22.2.4	Incremental-Iterative Solution Strategy	300
22.3	Validation	302
22.3.1	Load-CMOD	302
22.3.2	Real, Fictitious, and Effective Crack Lengths	303
22.3.3	Parametric Studies	303
22.4	Conclusions	305
22.5	Notation	305
23	INTERFACE CRACK MODEL	309
23.1	Introduction	309
23.2	Interface Crack Model	310
23.2.1	Relation to fictitious crack model	314
23.3	Finite Element Implementation	315
23.3.1	Interface element formulation	315
23.3.2	Constitutive driver	316
23.3.3	Non-linear solver	320
23.3.4	Secant-Newton method	321

23.3.5	Element secant stiffness.	322
23.3.6	Line search method.	323
23.4	Mixed Mode Crack Propagation	324
23.4.1	Griffith criterion and ICM.	324
23.4.2	Criterion for crack propagation.	325
23.5	Examples and validation	326
23.5.1	Direct shear test of mortar joints.	327
23.5.2	Biaxial interface test.	327
23.5.3	Modified Iosipescu's beam.	329
23.5.4	Anchor bolt pull-out test.	337
23.6	Conclusions	339
A	INTEGRAL THEOREMS	341
A.1	Integration by Parts	341
A.2	Green-Gradient Theorem	341
A.3	Gauss-Divergence Theorem	341
	Bibliography	343

DRAFT

List of Figures

1.1	Cracked Cantilevered Beam	4
1.2	Failure Envelope for a Cracked Cantilevered Beam	5
1.3	Generalized Failure Envelope	6
1.4	Column Curve	6
2.1	Stress Components on an Infinitesimal Element	14
2.2	Stresses as Tensor Components	14
2.3	Cauchy's Tetrahedron	15
2.4	Flux Through Area dS	20
2.5	Equilibrium of Stresses, Cartesian Coordinates	22
2.6	Curvilinear Coordinates	28
2.7	Transversely Isotropic Material	29
2.8	Coordinate Systems for Stress Transformations	31
3.1	Circular Hole in an Infinite Plate need to correct alignment of x	36
3.2	Elliptical Hole in an Infinite Plate	38
3.3	Crack in an Infinite Plate	40
3.4	Independent Modes of Crack Displacements	43
3.5	Plate with Angular Corners	46
3.6	Plate with Angular Corners	49
4.1	Middle Tension Panel	60
4.2	Single Edge Notch Tension Panel	60
4.3	Double Edge Notch Tension Panel	60
4.4	Three Point Bend Beam	61
4.5	Compact Tension Specimen	61
4.6	Approximate Solutions for Two Opposite Short Cracks Radiating from a Circular Hole in an Infinite Plate under Tension	62
4.7	Approximate Solutions for Long Cracks Radiating from a Circular Hole in an Infinite Plate under Tension	62
4.8	Radiating Cracks from a Circular Hole in an Infinite Plate under Biaxial Stress	63
4.9	Pressurized Hole with Radiating Cracks	64
4.10	Two Opposite Point Loads acting on the Surface of an Embedded Crack	64
4.11	Two Opposite Point Loads acting on the Surface of an Edge Crack	65
4.12	Embedded, Corner, and Surface Cracks	65
4.13	Elliptical Crack, and Newman's Solution	66
4.14	Growth of Semielliptical surface Flaw into Semicircular Configuration	69
5.1	Uniformly Stressed Layer of Atoms Separated by a_0	72
5.2	Energy and Force Binding Two Adjacent Atoms	72
5.3	Stress Strain Relation at the Atomic Level	72
5.4	Influence of Atomic Misfit on Ideal Shear Strength	74
6.1	Energy Transfer in a Cracked Plate	78
6.2	Determination of G_c From Load Displacement Curves	80
6.3	Experimental Determination of K_I from Compliance Curve	81
6.4	K_I for DCB using the Compliance Method	82
6.5	Variable Depth Double Cantilever Beam	83
6.6	Graphical Representation of the Energy Release Rate G	84
6.7	Effect of Geometry and Load on Crack Stability, (Gdoutos, 1993)	87

6.8	R Curve for Plane Strain	87
6.9	R Curve for Plane Stress	88
6.10	Plastic Zone Ahead of a Crack Tip Through the Thickness	89
7.1	Mixed Mode Crack Propagation and Biaxial Failure Modes	91
7.2	Crack with an Infinitesimal “kink” at Angle θ	93
7.3	S_θ Distribution ahead of a Crack Tip	95
7.4	Angle of Crack Propagation Under Mixed Mode Loading	95
7.5	Locus of Fracture Diagram Under Mixed Mode Loading	96
7.6	Fracture Toughnesses for Homogeneous Anisotropic Solids	97
7.7	Angles of Crack Propagation in Anisotropic Solids	100
7.8	Failure Surfaces for Cracked Anisotropic Solids	101
7.9	Geometry and conventions of an interface crack, (Hutchinson and Suo, 1992)	102
7.10	Geometry of kinked Crack, (Hutchinson and Suo, 1992)	103
7.11	Schematic variation of energy release rate with length of kinked segment of crack for $\beta \neq 0$, (Hutchinson and Suo, 1992)	104
7.12	Conventions for a Crack Kinking out of an Interface, (Hutchinson and Suo, 1992)	106
7.13	Geometry and Boundary Conditions of the Plate Analyzed	108
7.14	Finite Element Mesh of the Plate Analyzed	108
7.15	Variation of G/G_o with Kink Angle ω	110
8.1	First-Order Approximation of the Plastic Zone	114
8.2	Second-Order Approximation of the Plastic Zone	114
8.3	Dugdale’s Model	116
8.4	Point Load on a Crack	116
8.5	Effect of Plastic Zone Size on Dugdale’s Model	117
8.6	Barenblatt’s Model	117
8.7	Normalized Mode I Plastic Zone (von Myses)	119
8.8	Plastic Zone Size Across Plate Thickness	119
8.9	Plastic Zone Size in Comparison with Plate Thickness; Plane Stress and Plane Strain	120
8.10	Plate Thickness Effect on Fracture Toughness	120
9.1	S-N Curve and Endurance Limit	121
9.2	Repeated Load on a Plate	121
9.3	Stages of Fatigue Crack Growth	122
9.4	Forman’s Fatigue Model	123
9.5	Retardation Effects on Fatigue Life	126
9.6	Cause of Retardation in Fatigue Crack Growth	126
9.7	Yield Zone Due to Overload	127
10.1	Crack Tip Opening Displacement, (Anderson, 1995)	129
10.2	Estimate of the Crack Tip Opening Displacement, (Anderson, 1995)	130
11.1	J Integral Definition Around a Crack	133
11.2	Closed Contour for Proof of J Path Independence	135
11.3	Virtual Crack Extension Definition of J	136
11.4	Arbitrary Solid with Internal Inclusion	137
11.5	Elastic-Plastic versus Nonlinear Elastic Materials	139
11.6	Nonlinear Energy Release Rate, (Anderson, 1995)	139
11.7	Experimental Derivation of J	140
11.8	J Resistance Curve for Ductile Material, (Anderson, 1995)	141
11.9	J , J_R versus Crack Length, (Anderson, 1995)	142
11.10	J , Around a Circular Path	143
11.11	Normalize Ramberg-Osgood Stress-Strain Relation ($\alpha = .01$)	143
11.12	HRR Singularity, (Anderson, 1995)	145
11.13	Effect of Plasticity on the Crack Tip Stress Fields, (Anderson, 1995)	145
11.14	Compact tension Specimen	148
11.15	Center Cracked Panel	150
11.16	Single Edge Notched Specimen	150
11.17	Double Edge Notched Specimen	153

11.18	Axially Cracked Pressurized Cylinder	155
11.19	Circumferentially Cracked Cylinder	156
11.20	Dynamic Crack Propagation in a Plane Body, (Kanninen, 1984)	160
12.1	Test Controls	168
12.2	Stress-Strain Curves of Metals and Concrete	168
12.3	Caputring Experimentally Localization in Uniaxially Loaded Concrete Specimens	169
12.4	Hillerborg's Fictitious Crack Model	170
12.5	Concrete Strain Softening Models	171
12.6	Strain-Softening Bar Subjected to Uniaxial Load	171
12.7	Load Displacement Curve in terms of Element Size	173
12.8	Localization of Tensile Strain in Concrete	176
12.9	Griffith criterion in NLFM.	176
13.1	G_F vs G_f	185
13.2	G_F^{pred} Based on	186
13.3	Servo-Controlled Test Setup for Concrete K_{Ic} and G_F	188
13.4	Test Apparatus for Two Parameter Model	188
13.5	Typical response for a notched beam in CMOD control using the center-point loading method	189
13.6	Softening Curve and Initial Linear Portion	191
13.7	"Brazilian Test, (?)"	192
13.8	Specimen Geometry and Dimensions	193
13.9	Sketch of a Loading Apparatus	193
13.10	Softening Curve and Initial Linear Portion	195
13.11	Softening curve and bilinear approximation	196
13.12	Specimen Geometry and Dimensions	198
13.13	Plot of corrected load P_1 versus CMOD.	201
13.14	Plot of corrected load P_1 versus load-point displacement δ	202
13.15	Principle of the Wedge Splitting Test Set-up	204
13.16	Dimensions of the specimens for the Wedge Splitting Test (all dimensions in mm)	205
13.17	Representative Experimental Load-COD Curve	205
13.18	Test set-up and acting forces, for a prismatic specimen	206
13.19	Normalized Compliance and Stress Intensity Factors in Terms of Crack Length a	206
13.20	Compliance and Stress Intensity Factors in Terms of Crack Length a	207
13.21	Definition of the work of fracture and specific fracture energy	208
14.1	Energy Transfer During Infinitesimal Crack Extension	210
14.2	Central Crack With Constant Cohesive Stresses	211
14.3	Nominal Strength in Terms of Size for a Center Crack Plate with Constant Cohesive Stresses	212
14.4	Dugdale's Model	213
14.5	Size Effect Law for an Edge Crack with Constant Cohesive Stresses	214
14.6	Linear Cohesive Stress Model	214
14.7	Energy Transfer During Infinitesimal Crack Extension	215
14.8	Size Effect Law for an Edge Crack with Linear Softening and Various Orders of Approximation	216
14.9	Three Point Bend Specimen with Linear Cohesive Stresses	216
14.10	Size Effect Law	217
14.11	Inelastic Buckling	218
15.1	(A) Straight line initiator, fractal generator, and triadic Koch curve; (B) Quadratic Koch curve; (C) Modified Koch curve.	222
15.2	Frontal view of wedge-splitting-test specimen showing forces applied to specimen by lateral wedge loading (F_s) between two circular pins located near top of specimen on either side of the vertical starting notch. Crack Mouth Opening Displacement (CMOD) gage straddles the initial notch.	225
15.3	Orientations of measured profiles over the fractured surface, horizontally, vertically, and diagonally.	226
15.4	Typical grid overlying an object. Dashed lines indicate adjustable sidFixed grid boundaries; B, Flexible grid boundaries.	227
15.5	Plot of box counting method applied to the profile of a typical fractured concrete specimen. Number of occupied boxes (N) is plotted versus box size. Slope of line fit to data is the fractal dimension (D).	228

15.6	A-B) G_F and K_{Ic} versus D ; C) G_F versus D for concrete (this study), ceramics, and alumina (Mecholsky and Freiman, 1991); D) K_{Ic} versus D for concrete (this study); ceramics, and alumina (Mecholsky and Frieman, 1991); Flint (Mecholsky and Mackin, 1988); polystyrene (Chen and Runt, 1989); and silicon (Tsai and Mecholsky (1991))	233
15.7	G_F versus D for concrete (this study), ceramics, and alumina (Mecholsky and Freiman, 1991)	234
15.8	K_{Ic} versus D for concrete (this study); ceramics, and alumina (Mecholsky and Frieman, 1991); Flint (Mecholsky and Mackin, 1988); polystyrene (Chen and Runt, 1989); and silicon (Tsai and Mecholsky (1991))	234
15.9	Variation of $L(S)$ in terms of S	235
16.1	Triadic von-Koch Curve; Example of a Self Similar Invasive Fractal	239
16.2	Sierpinski Carpet; Example of a Self Similar Lacunar Fractal	239
16.3	Example of a Self-Affine Fractal	240
16.4	Example of an iteratively defined MultiFractal	241
16.5	Energy Transfer During Infinitesimal Crack Extension	242
16.6	Bazant's original size effect law	243
16.7	Multifractal Scaling Laws (Carpinteri)	243
16.8	The Scaling of Bones, ?	245
16.9	Cohesive Stress Distribution Along a Fractal Crack	247
16.10	Generalized Cohesive Stress Distribution	247
16.11	Fractal Size Effect Laws (Dugdale)	249
16.12	Slope of the Fractal Size Effect Law in terms of α as $r \rightarrow \infty$	249
16.13	Asymptotic Values of the Size Effect Law as $r \rightarrow 0$	249
16.14	Cellular Automata Definition of Rule 150 Along With Potential Crack Path	250
17.1	*Wedge-splitting specimen geometry.	252
17.2	*Wedge fixture and line support.	253
17.3	*Block diagram of the experimental system.	254
17.4	*Typical P_{SP} vs. CMOD curve for a "Large" specimen.	254
17.5	*Typical AE record for a "Large" WS specimen test.	254
17.6	*The three stages of the fracture toughness vs. effective crack length curve.	255
17.7	*Mean fracture toughness values obtained from the rounded MSA WS specimen tests.	256
17.8	*Mean specific fracture energy values obtained from the rounded MSA WS specimen tests.	257
17.9	Size effect for WS specimens for $d_a=38$ mm (1.5 in) (Brühwiler et al., 1991)	259
18.1	Stress Intensity Factor Using Extrapolation Technique	262
18.2	Isoparametric Quadratic Finite Element: Global and Parent Element	262
18.3	Singular Element (Quarter-Point Quadratic Isoparametric Element)	265
18.4	Finite Element Discretization of the Crack Tip Using Singular Elements	266
18.5	Displacement Correlation Method to Extract SIF from Quarter Point Singular Elements	266
18.6	Nodal Definition for FE 3D SIF Determination	268
19.1	Crack Extension Δa	271
19.2	Displacement Decomposition for SIF Determination	273
20.1	Numerical Extraction of the J Integral (Owen and Fawkes, 1983)	275
20.2	Simply connected Region A^* Enclosed by Contours Γ_1 , Γ_0 , Γ_+ , and Γ_- , (Anderson, 1995)	279
20.3	Surface Enclosing a Tube along a Three Dimensional Crack Front, (Anderson, 1995)	281
20.4	Interpretation of q in terms of a Virtual Crack Advance along ΔL , (Anderson, 1995)	281
20.5	Inner and Outer Surfaces Enclosing a Tube along a Three Dimensional Crack Front	282
21.1	Contour integral paths around crack tip for reciprocal work integral	286
22.1	Body Consisting of Two Sub-domains	296
22.2	Wedge Splitting Test, and FE Discretization	302
22.3	Numerical Predictions vs Experimental Results for Wedge Splitting Tests	303
22.4	Real, Fictitious, and Effective Crack Lengths for Wedge Splitting Tests	304
22.5	Effect of G_F on 50 ft Specimen	304
22.6	Effect of w_c on 50 ft Specimen	305
22.7	Effect of s_1 on 3 ft Specimen	306
23.1	Mixed mode crack propagation.	309

23.2	Wedge splitting tests for different materials, (Saouma et al., 1994)	310
23.3	Interface idealization and notations.	311
23.4	Interface fracture.	311
23.5	Failure function.	312
23.6	Bi-linear softening laws.	313
23.7	Stiffness degradation in the equivalent uniaxial case.	314
23.8	Interface element numbering.	316
23.9	Local coordinate system of the interface element.	316
23.10	Algorithm for interface constitutive model.	317
23.11	Definition of inelastic return direction.	318
23.12	Influence of increment size.	320
23.13	Shear-tension example.	320
23.14	Secant relationship.	322
23.15	Line search method.	324
23.16	Griffith criterion in NLFM.	325
23.17	Mixed mode crack propagation.	326
23.18	Schematics of the direct shear test setup.	327
23.19	Direct shear test on mortar joint.	328
23.20	Experimental set-up for the large scale mixed mode test.	328
23.21	Nonlinear analysis of the mixed mode test.	329
23.22	Crack propagation in Iosipescu's beam, (Steps 1 & 3).	331
23.23	Crack propagation in Iosipescu's beam, (Increment 11 & 39 in Step 6).	332
23.24	Multiple crack propagation in Iosipescu's beam (Steps 3,4).	333
23.25	Multiple crack propagation in Iosipescu's beam (Step 5).	334
23.26	Meshes for crack propagation in Iosipescu's beam (Steps 1,3,4,5).	335
23.27	Iosipescu's beam with ICM model.	336
23.28	Crack paths for Iosipescu's beam.	336
23.29	Large Iosipescu's beam, $h = 50 \times 100$ mm.	336
23.30	Crack propagation for anchor bolt pull out test I.	337
23.31	Crack propagation for anchor bolt pull out test II.	338
23.32	Crack patterns.	339
23.33	Load displacement curve for test I.	339
23.34	Load displacement curve for test II.	340

List of Tables

1.1	Column Instability Versus Fracture Instability	6
2.1	Number of Elastic Constants for Different Materials	29
3.1	Summary of Elasticity Based Problems Analysed	35
4.1	Newman’s Solution for Circular Hole in an Infinite Plate subjected to Biaxial Loading, and Internal Pressure	63
4.2	C Factors for Point Load on Edge Crack	65
4.3	Approximate Fracture Toughness of Common Engineering Materials	67
4.4	Fracture Toughness vs Yield Stress for .45C – N_i – C_r – M_o Steel	68
7.1	Material Properties and Loads for Different Cases	109
7.2	Analytical and Numerical Results	109
7.3	Numerical Results using S-integral without the bimaterial model	109
10.1	Comparison of Various Models in LEFM and EPFM	130
11.1	Effect of Plasticity on the Crack Tip Stress Field, (Anderson, 1995)	145
11.2	h -Functions for Standard ASTM Compact Tension Specimen, (Kumar et al., 1981)	149
11.3	Plane Stress h -Functions for a Center-Cracked Panel, (Kumar et al., 1981)	151
11.4	h -Functions for Single Edge Notched Specimen, (Kumar et al., 1981)	152
11.5	h -Functions for Double Edge Notched Specimen, (Kumar et al., 1981)	154
11.6	h -Functions for an Internally Pressurized, Axially Cracked Cylinder, (Kumar et al., 1981)	155
11.7	F and V_1 for Internally Pressurized, Axially Cracked Cylinder, (Kumar et al., 1981)	156
11.8	h -Functions for a Circumferentially Cracked Cylinder in Tension, (Kumar et al., 1981)	157
11.9	F , V_1 , and V_2 for a Circumferentially Cracked Cylinder in Tension, (Kumar et al., 1981)	158
12.1	Strain Energy versus Fracture Energy for uniaxial Concrete Specimen	173
13.1	Summary relations for the concrete fracture models.	183
13.2	When to Use LEFM or NLFM Fracture Models	184
14.1	Experimentally Determined Values of Bf_t' , (Bažant and Planas, 1998)	217
14.2	Size Effect Law vs Column Curve	218
15.1	Fractal dimension definition	221
15.2	Concrete mix design	224
15.3	Range and resolution of the profilometer (inches)	225
15.4	CHECK Mapped profile spacing, orientation, and resolution for the two specimen sizes investigated	226
15.5	Computed fractal dimensions of a straight line with various inclinations	227
15.6	Computed fractal dimensions for various synthetic curves	228
15.7	Fractal dimension D versus profile orientations	229
15.8	Fractal dimension for various profile segments and distances from centerline in specimen S33A	230
15.9	Comparison between D , K_{Ic} , and G_F for all specimens (MSA, Maximum size aggregate)	231
15.10	Linear regression coefficients between G_F and K_{Ic} with D	232
15.11	Amplification factors for fractal surface areas with $D = 1.1$	236
15.12	Comparison between “corrected” G_F^* and G_c values based on Swartz Tests (1992).	237
17.1	Concrete mix design.	252
17.2	Experimentally obtained material properties of the concrete mixes used.	252

17.3	Wedge-splitting specimen dimensions.	252
17.4	Test matrix.	253
17.5	Summary of fracture toughness data obtained from the WS tests.	256
17.6	Fracture toughness values obtained from the CJ-WS specimens.	256
17.7	Summary of specific fracture energy values obtained from the WS tests.	258
17.8	Fracture energy values obtained from the CJ-WS specimens.	258
17.9	Size Effect Law model assessment from the WS test program (average values)(Brühwiler et al, 1991)	259
18.1	Shape Functions, and Natural Derivatives for Q8 Element	263
23.1	Material properties for direct shear test.	327
23.2	Material properties for direct shear test.	329
23.3	Material properties for ICM for Iosipescu's test.	330

DRAFT

COVERAGE

	Mon.	Day	COVERAGE
	Jan.	14	Intro, Coverage
1		19 21	Overview, Elasticity Elasticity, Kirch, Hole
2		26 29	Crack, Griffith Notch, Williams
3	Feb.	2 4	LEFM LEFM, Examples
4		9 11	Bi-Material, Merlin Theoretical Strength
5		16 18	Theoretical Strength Energy
6		23 26	Energy MERLIN
7	Mar.	2 4	Mixed Mode Plastic Zone Size
8		9 11	CTOD, J J
9		16 18	Fatigue Fatigue
			Fatigue
10	Apr.	30 1	Concrete Fatigue
11		6 8	Concrete Concrete
12		13 15	EXAM Concrete
13		20 22	Num. Methods Num. Methods
14		27 29	Experiment Anisotropic

Chapter 1

INTRODUCTION

In this introductory chapter, we shall start by reviewing the various modes of structural failure and highlight the importance of fracture induced failure and contrast it with the limited coverage given to fracture mechanics in Engineering Education. In the next section we will discuss some examples of well known failures/accidents attributed to cracking. Then, using a simple example we shall compare the failure load predicted from linear elastic fracture mechanics with the one predicted by “classical” strength of materials. The next section will provide a brief panoramic overview of the major developments in fracture mechanics. Finally, the chapter will conclude with an outline of the lecture notes.

1.1 Modes of Failures

The fundamental requirement of any structure is that it should be designed to resist mechanical failure through any (or a combination of) the following modes:

1. Elastic instability (buckling)
2. Large elastic deformation (jamming)
3. Gross plastic deformation (yielding)
4. Tensile instability (necking)
5. Fracture

Most of these failure modes are relatively well understood, and proper design procedures have been developed to resist them. However, fractures occurring after earthquakes constitute the major source of structural damage (Duga et al., 1983), and are the least well understood.

In fact, fracture often has been overlooked as a potential mode of failure at the expense of an overemphasis on strength. Such a simplification is not new, and finds a very similar analogy in the critical load of a column. If column strength is based entirely on a strength criterion, an unsafe design may result as instability (or buckling) is overlooked for slender members. Thus failure curves for columns show a smooth transition in the failure mode from columns based on gross section yielding to columns based on instability.

By analogy, a cracked structure can be designed on the sole basis of strength as long as the crack size does not exceed a critical value. Should the crack size exceed this critical value, then a fracture-based failure results. Again, on the basis of those two theories (strength of materials and fracture mechanics), one could draw a failure curve that exhibits a smooth transition between those two modes.¹

1.2 Examples of Structural Failures Caused by Fracture

Some well-known, and classical, examples of fracture failures include:

- Mechanical, aeronautical, or marine
 1. Fracture of train wheels, axles, and rails
 2. Fracture of the Liberty ships during and after World War II
 3. Fracture of airplanes, such as the Comet airliners, which exploded in mid-air during the fifties, or more recently fatigue fracture of bulkhead in a Japan Air Line Boeing 747
 4. Fatigue fractures found in the Grumman buses in New York City, which resulted in the recall of 637 of them
 5. Fracture of the Glomar Java sea boat in 1984
 6. Fatigue crack that triggered the sudden loss of the upper cockpit in the Air Aloha plane in Hawaii in 1988
- Civil engineering
 1. Fractures of bridge girders (Silver bridge in Ohio)

¹When high strength rolled sections were first introduced, there was a rush to use them. However, after some spectacular bridge girder failures, it was found that strength was achieved at the expense of toughness (which is the material ability to resist crack growth).

2. Fracture of Statford A platform concrete off-shore structure
3. Cracks in nuclear reactor piping systems
4. Fractures found in dams (usually unpublicized)

Despite the usually well-known detrimental effects of fractures, in many cases fractures are man-made and induced for beneficial purposes Examples include:

1. Rock cutting in mining
2. hydrau-fracturing for oil, gas, and geothermal energy recovery
3. “Biting” of candies (!)

Costs associated with fracture in general are so exorbitant, that a recent NBS report (Duga et al., 1983) stated:

[The] cost of material fracture to the US [is] \$ 119 billion per year, about 4 percent of the gross national product. The costs could be reduced by an estimated missing 35 billion per year if technology transfer were employed to assure the use of best practice. Costs could be further reduced by as much as \$ 28 billion per year through fracture-related research.

In light of the variety, and complexity of problems associated with fracture mechanics, it has become a field of research interest to mathematicians, scientists, and engineers (metallurgical, mechanical, aerospace, and civil).

1.3 Fracture Mechanics vs Strength of Materials

In order to highlight the fundamental differences between strength of materials and fracture mechanics approaches, we consider a simple problem, a cantilevered beam of length L , width B , height H , and subjected to a point load P at its free end, Fig. 1.1 Maximum flexural stress is given by

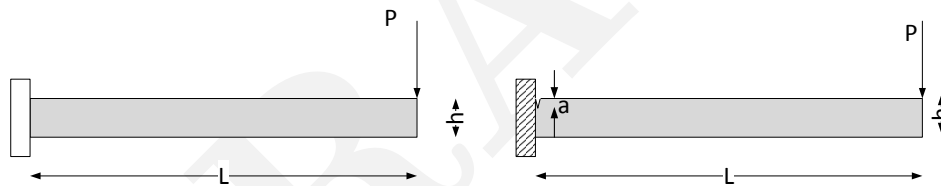


Figure 1.1: Cracked Cantilevered Beam

$$\sigma_{max} = \frac{6PL}{BH^2} \quad (1.1)$$

We will seek to determine its safe load-carrying capacity using the two approaches².

1. Based on classical strength of materials the maximum flexural stress should not exceed the yield stress σ_y , or

$$\sigma_{max} \leq \sigma_y \quad (1.2)$$

Thus, based on this first approach, the maximum load which can be safely carried is:

$$P_{max}^{SOM} = \frac{BH^2}{6L} \sigma_y \quad (1.3)$$

2. In applying a different approach, one based on fracture mechanics, the structure cannot be assumed to be defect free. Rather, an initial crack must be assumed. Eq. 1.2 governed failure; for the strength of materials approach in the linear elastic fracture mechanics approach (as discussed in the next chapter), failure is governed by:

$$K_I \leq K_{Ic} \quad (1.4)$$

²This example is adapted from (Kanninen and Popelar, 1985).

where K_I is a measure of the stress singularity at the tip of the crack and K_{Ic} is the critical value of K_I . K_I is related to σ_{max} through:

$$K_I = 1.12\sigma_{max}\sqrt{\pi a} \quad (1.5)$$

where a is the crack length. K_I is a *structural* parameter (analogous to σ_{max}), and K_{Ic} is a *material* parameter (analogous to σ_y). Fracture toughness is a measure of the material ability to resist crack growth (not to be confused with its tensile strength, which is associated with crack nucleation or formation). Thus, the maximum load that can be carried is given by:

$$P_{max}^{FM} = \frac{BH^2}{6L} \frac{K_{Ic}}{1.12\sqrt{\pi a}} \quad (1.6)$$

The two equations, Eq. 1.3 and 1.6 governing the load capacity of the beam according to two different approaches, call for the following remarks:

1. Both equations are in terms of $\frac{BH^2}{6L}$
 2. The strength of materials approach equation is a function of a material property that is not size dependent.
 3. The fracture mechanics approach is not only a function of an intrinsic material property,³ but also of crack size a .
- On the basis of the above, we can schematically represent the failure envelope of this beam in Fig. 1.2, where failure stress is

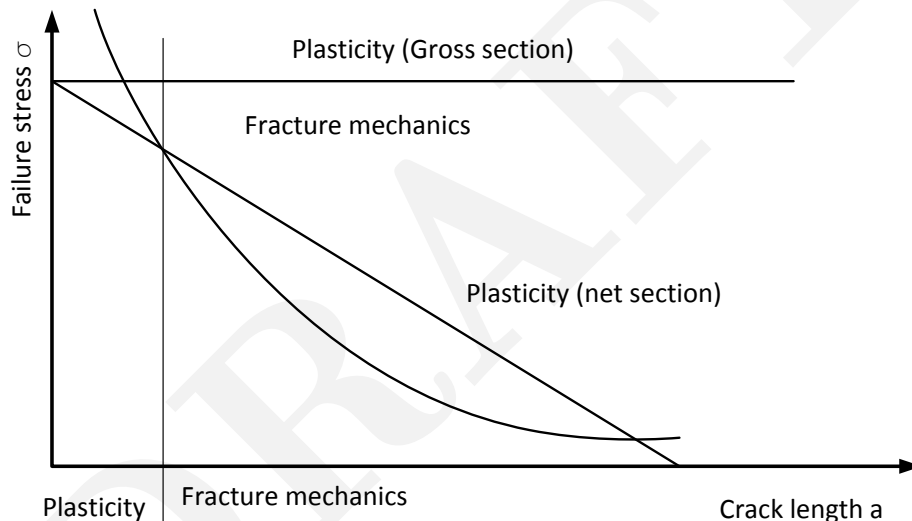


Figure 1.2: Failure Envelope for a Cracked Cantilevered Beam

clearly a function of the crack length.

On the basis of this simple example, we can generalize our preliminary finding by the curve shown in Fig. 1.3. We thus identify four corners: on the lower left we have our usual engineering design zone, where factors of safety are relatively high; on the bottom right we have failure governed by yielding, or plasticity; on the upper left failure is governed by linear elastic fracture mechanics; and on the upper right failure is triggered by a combination of fracture mechanics and plasticity. This last zone has been called elasto-plastic in metals, and nonlinear fracture in concrete.⁴

Finally, we should emphasize that size effect is not unique to fractures but also has been encountered by most engineers in the design of columns. In fact, depending upon its slenderness ratio, a column failure load is governed by either the Euler equation for long columns, or the strength of materials for short columns.

Column formulas have been developed, as seen in Fig. 1.4, which is similar to Fig. 1.2. Also note that column instability is caused by a not perfectly straight element, whereas fracture failure is caused by the presence of a crack. In all other cases, a perfect material is assumed, as shown in Table 1.1. As will be shown later, similar transition curves have also been developed by Bažant (Bažant, 1984) for the failure of small or large cracked structures on the basis of either strength of materials or linear elastic fracture mechanics.

³We will see later that K_{Ic} is often a function of crack length. Similarly compressive strength of concrete is known to be slightly affected by the cylinder size.

⁴This curve will be subsequently developed for concrete materials according to Bažant's size effect law.

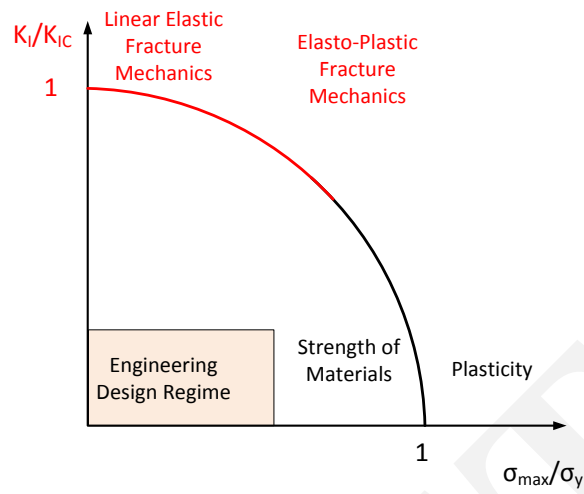


Figure 1.3: Generalized Failure Envelope

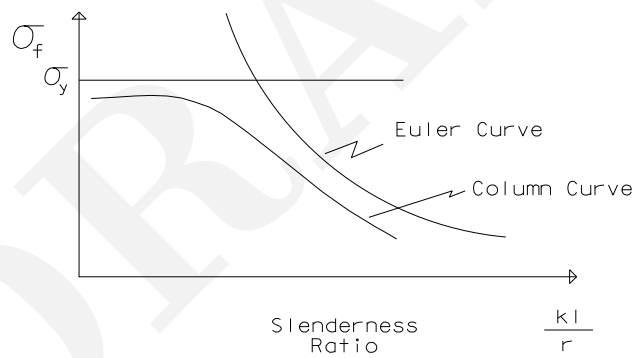


Figure 1.4: Column Curve

Approach	Governing Eq.	Theory		Imperfection
Strength of Material	$\sigma = \frac{F}{A}$	Plasticity	σ_y	Dislocation
Column Instability	$\sigma = \frac{\pi^2 E}{(\frac{KL}{r})^2}$	Euler	$\frac{KL}{r}$	Not Perfectly straight
Fracture	$\sigma = \frac{K_{Ic}}{\sqrt{\pi a}}$	Griffith	K_{Ic}	Micro-defects

Table 1.1: Column Instability Versus Fracture Instability

1.4 Major Historical Developments in Fracture Mechanics

As with any engineering discipline approached for the first time, it is helpful to put fracture mechanics into perspective by first listing its major developments:

1. In 1898, a German Engineer by the name of Kirsch showed that a stress concentration factor of 3 was found to exist around a circular hole in an infinite plate subjected to uniform tensile stresses (Timoshenko and Goodier, 1970).
2. While investigating the unexpected failure of naval ships in 1913, Inglis (Inglis, 1913) extended the solution for stresses around a circular hole in an infinite plate to the more general case of an ellipse. It should be noted that this problem was solved 3 years earlier by Kolosoff (who was the mentor of Muschelishvili) in St Petersburg, however history remembers only Inglis who showed that a stress concentration factor of

$$S.C.F. = 1 + 2 \left(\frac{a}{\rho} \right)^{1/2} \quad (1.7)$$

prevails around the ellipse (where a is the half length of the major axis, and ρ is the radius of curvature)⁵.

3. Inglis's early work was followed by the classical studies of Griffith, who was not originally interested in the strength of cracked structures (fracture mechanics was not yet a discipline), but rather in the tensile strength of crystalline solids and its relation to the theory based on their lattice properties, which is approximately equal to $E/10$ where E is the Young's Modulus (Kelly, 1974).

With his assistant Lockspeiser, Griffith was then working at the Royal Aircraft Establishment (RAE) at Farnborough, England (which had a tradition of tolerance for original and eccentric young researchers), and was testing the strength of glass rods of different diameters at different temperatures (Gordon, 1988). They found that the strength increased rapidly as the size decreased. Asymptotic values of 1,600 and 25 Ksi were found for infinitesimally small and bulk size specimens, respectively.

On the basis of those two observations, Griffith's first major contribution to fracture mechanics was to suggest that internal minute flaws acted as stress raisers in solids, thus strongly affecting their tensile strengths. Thus, in reviewing Inglis's early work, Griffith determined that the presence of minute elliptical flaws were responsible in dramatically reducing the glass strength from the theoretical value to the actually measured value.

4. The second major contribution made by Griffith was in deriving a thermodynamical criterion for fracture by considering the total change in energy taking place during cracking. During crack extension, potential energy (both external work and internal strain energy) is released and "transferred" to form surface energy.

Unfortunately, one night Lockspeiser forgot to turn off the gas torch used for glass melting, resulting in a fire. Following an investigation, (RAE) decided that Griffith should stop wasting his time, and he was transferred to the engine department.

5. After Griffith's work, the subject of fracture mechanics was relatively dormant for about 20 years until 1939 when Westergaard (Westergaard, 1939a) derived an expression for the stress field near a sharp crack tip.
6. Up to this point, fracture mechanics was still a relatively obscure and esoteric science. However, more than any other single factor, the large number of sudden and catastrophic fractures that occurred in ships during and following World War II gave the impetus for the development of fracture mechanics. Of approximately 5,000 welded ships constructed during the war, over 1,000 suffered structural damage, with 150 of these being seriously damaged, and 10 fractured into two parts. After the war, George Irwin, who was at the U.S. Naval Research Laboratory, made use of Griffith's idea, and thus set the foundations of fracture mechanics. He made three major contributions:
 - a) He (and independently Orowan) extended the Griffith's original theory to metals by accounting for yielding at the crack tip. This resulted in what is sometimes called the modified Griffith's theory.
 - b) He altered Westergaard's general solution by introducing the concept of the stress intensity factor (SIF).
 - c) He introduced the concept of energy release rate G
7. Subcritical crack growth was subsequently studied. This form of crack propagation is driven by either applying repeated loading (fatigue) to a crack, or surround it by a corrosive environment. In either case the original crack length, and loading condition, taken separately, are below their critical value. Paris in 1961 proposed the first empirical equation relating the range of the stress intensity factor to the rate of crack growth.

⁵Note that for a circle, a stress concentration of 3 is recovered.

8. Non-linear considerations were further addressed by Wells, who around 1963 utilized the crack opening displacement (COD) as the parameter to characterize the strength of a crack in an elasto-plastic solid, and by Rice, who introduced his J integral in 1968 in probably the second most referenced paper in the field (after Griffith); it introduced a path independent contour line integral that is the rate of change of the potential energy for an elastic non-linear solid during a unit crack extension.
9. Another major contribution was made by Erdogan and Sih in the mid '60s when they introduced the first model for mixed-mode crack propagation.
10. Other major advances have been made subsequently in a number of subdisciplines of fracture mechanics: (i) dynamic crack growth; (ii) fracture of laminates and composites; (iii) numerical techniques; (iv) design philosophies; and others.
11. In 1976, Hillerborg (Hillerborg et al., 1976a) introduced the fictitious crack model in which residual tensile stresses can be transmitted across a portion of the crack. Thus a new meaning was given to cracks in cementitious materials.
12. In 1979 Bažant and Cedolin (Bažant and Cedolin, 1979) showed that for the objective analysis of cracked concrete structure, fracture mechanics concepts must be used, and that classical strength of materials models would yield results that are mesh sensitive.

This brief overview is designed to make detailed coverage of subsequent topics better understood when put into global perspective.

1.5 Coverage

Following this brief overview, chapter two will provide the reader with a review of elasticity. In particular we shall revisit the major equations needed to analytically solve simple problems involving elliptical holes or sharp cracks.

Those solutions will be presented in detail in chapter three. This chapter, mathematically the most challenging, is an important one to understand the mathematical complexity of solutions of simple crack problem, and to appreciate the value of numerical based solutions which will be discussed later. First Inglis solution of a circular and elliptical hole will be presented, then the problem of a sharp crack in an infinite plate will be solved using the two classical methods. The first one is based on Westergaard's solution, and the second on Williams's classical paper. Through Westergaard's solution, we shall introduce the concept of stress intensity factors, and Williams's solution will be extended to cracks along an interface between two dissimilar materials. Also covered in this chapter will be the solutions of a crack in a homogeneous anisotropic solid based on the solution of Sih and Paris.

With the rigorous derivation of the stress field ahead of a crack tip performed, Chapter four will formalize the Linear Elastic Fracture Mechanics approach, and show how it can be used in some practical design cases.

A complementary approach to the stress based one, will be presented in chapter five which discusses Energy Methods in linear elastic fracture mechanics. First, we shall thoroughly examine the theoretical strength of crystalline materials and contrast it with the actual one, then we will define the energy release rate G , and discuss the duality between the stress based and the energy based approaches.

Chapter six will extend the simple mode I crack propagation criteria to mixed modes (where a crack is simultaneously subjected to opening and sliding) by discussing some of the major criterions.

Subcritical crack growth, and more specifically fatigue crack growth will be covered in chapter seven.

Elasto-Plastic fracture mechanics, and derivation of the J integral will then be covered in chapter eight. First we will derive expressions for the size of the plastic zone ahead of the crack tip, then criteria for crack growth presented.

In chapter nine, we shall examine some of the fracture testing techniques, with emphasize on both metallic and cementitious materials.

Fracture of cementitious material, such as concrete and rock, will be studied in chapter ten. In this extensive chapter, we shall review some of the major models currently investigated, and examine some applications.

Numerical techniques will then be discussed in chapter eleven. First techniques of modelling the stress singularity at the crack tip will be examined, followed by methods to extract the stress intensity factors from a finite element analysis and evaluation of J integral will be presented.

The last chapter, twelve, will focus on numerical techniques for cementitious materials.

For more detailed coverage, the reader is referred to the numerous excellent books available, such as Broek (Broek, 1986, 1989), Cherepanov (Cherepanov, 1979), Kanninen (Kanninen and Popelar, 1985), Knott (Knott, 1976), Barsom and Rolfe (Barsom and Rolfe, 1987), and Anderson's (Anderson, 1995). Finally, a recent book by Bažant (Bažant and Cedolin, 1991) covers (among other things) some of the issues related to fracture of concrete.

Chapter 2

PRELIMINARY CONSIDERATIONS

Needs some minor editing!

- ¹ Whereas, ideally, an introductory course in *Continuum Mechanics* should be taken prior to a fracture mechanics, this is seldom the case. Most often, students have had a graduate course in *Advanced Strength of Materials*, which can only provide limited background to a solid fracture mechanics course.
- ² Accordingly, this preliminary chapter (mostly extracted from the author's lecture notes in Continuum Mechanics) will partially remedy for occasional deficiencies and will be often referenced.
- ³ It should be noted that most, but not all, of the material in this chapter will be subsequently referenced.

2.1 Tensors

⁴ We now seek to generalize the concept of a vector by introducing the **tensor** (\mathbf{T}), which essentially *exists to operate on vectors \mathbf{v} to produce other vectors* (or on tensors to produce other tensors!). We designate this operation by $\mathbf{T}\cdot\mathbf{v}$ or simply $\mathbf{T}\mathbf{v}$.

⁵ We hereby adopt the **dyadic** and **indicial** notation for tensors as **linear vector operators**

$$\mathbf{u} = \mathbf{T}\cdot\mathbf{v} \text{ or } u_i = T_{ij}v_j \quad (2.1-a)$$

$$\mathbf{u} = \mathbf{v}\cdot\mathbf{S} \text{ where } \mathbf{S} = \mathbf{T}^T \quad (2.1-b)$$

- ⁶ Whereas a tensor is essentially an operator on vectors (or other tensors), it is also a physical quantity, independent of any particular coordinate system yet specified most conveniently by referring to an appropriate system of coordinates.
- ⁷ Tensors frequently arise as physical entities whose components are the coefficients of a linear relationship between vectors.
- ⁸ A tensor is classified by the rank or order. A Tensor of order zero is specified in any coordinate system by one coordinate and is a scalar (such as temperature). A tensor of order one has three coordinate components in space, hence it is a vector (such as force). In general 3-D space the number of components of a tensor is 3^n where n is the order of the tensor.
- ⁹ A force and a stress are tensors of order 1 and 2 respectively.

2.1.1 Indicial Notation

- ¹⁰ Whereas the Engineering notation may be the simplest and most intuitive one, it often leads to long and repetitive equations. Alternatively, the tensor and the dyadic form will lead to shorter and more compact forms.
- ¹¹ While working on general relativity, Einstein got tired of writing the summation symbol with its range of summation below and above (such as $\sum_{i=1}^{n=3} a_{ij}b_i$) and noted that most of the time the upper range (n) was equal to the dimension of space (3 for us, 4 for him), and that when the summation involved a product of two terms, the summation was over a repeated index (i in our example). Hence, he decided that there is no need to include the summation sign \sum if there was repeated indices (i), and thus any repeated index is a **dummy index** and is summed over the range 1 to 3. An index that is not repeated is called **free index** and assumed to take a value from 1 to 3.
- ¹² Hence, this so called **indicial notation** is also referred to **Einstein's notation**.
- ¹³ The following rules define indicial notation:

1. If there is one letter index, that index goes from i to n (range of the tensor). For instance:

$$a_i = a^i = [a_1 \quad a_2 \quad a_3] = \left\{ \begin{array}{c} a_1 \\ a_2 \\ a_3 \end{array} \right\} \quad i = 1, 3 \quad (2.2)$$

assuming that $n = 3$.

2. A repeated index will take on all the values of its range, and the resulting tensors summed. For instance:

$$a_{1i}x_i = a_{11}x_1 + a_{12}x_2 + a_{13}x_3 \quad (2.3)$$

3. Tensor's order:

- First order tensor (such as force) has only one free index:

$$a_i = a^i = [a_1 \quad a_2 \quad a_3] \quad (2.4)$$

other first order tensors $a_{ij}b_j = a_{i1}b_1 + a_{i2}b_2 + a_{i3}b_3$, F_{ikk} , $\varepsilon_{ijk}u_jv_k$

- Second order tensor (such as stress or strain) will have two free indices.

$$D_{ij} = \begin{bmatrix} D_{11} & D_{22} & D_{13} \\ D_{21} & D_{22} & D_{23} \\ D_{31} & D_{32} & D_{33} \end{bmatrix} \quad (2.5)$$

other examples A_{ijip} , $\delta_{ij}u_kv_k$.

- A fourth order tensor (such as Elastic constants) will have four free indices.

4. Derivatives of tensor with respect to x_i is written as $_{,i}$. For example:

$$\frac{\partial \Phi}{\partial x_i} = \Phi_{,i} \quad \frac{\partial v_i}{\partial x_i} = v_{i,i} \quad \frac{\partial v_i}{\partial x_j} = v_{i,j} \quad \frac{\partial T_{i,j}}{\partial x_k} = T_{i,j,k} \quad (2.6)$$

14 Usefulness of the indicial notation is in presenting systems of equations in compact form. For instance:

$$x_i = c_{ij}z_j \quad (2.7)$$

this simple compacted equation, when expanded would yield:

$$\begin{aligned} x_1 &= c_{11}z_1 + c_{12}z_2 + c_{13}z_3 \\ x_2 &= c_{21}z_1 + c_{22}z_2 + c_{23}z_3 \\ x_3 &= c_{31}z_1 + c_{32}z_2 + c_{33}z_3 \end{aligned} \quad (2.8)$$

Similarly:

$$A_{ij} = B_{ip}C_{jq}D_{pq} \quad (2.9)$$

$$\begin{aligned} A_{11} &= B_{11}C_{11}D_{11} + B_{11}C_{12}D_{12} + B_{12}C_{11}D_{21} + B_{12}C_{12}D_{22} \\ A_{12} &= B_{11}C_{11}D_{11} + B_{11}C_{12}D_{12} + B_{12}C_{11}D_{21} + B_{12}C_{12}D_{22} \\ A_{21} &= B_{21}C_{11}D_{11} + B_{21}C_{12}D_{12} + B_{22}C_{11}D_{21} + B_{22}C_{12}D_{22} \\ A_{22} &= B_{21}C_{21}D_{11} + B_{21}C_{22}D_{12} + B_{22}C_{21}D_{21} + B_{22}C_{22}D_{22} \end{aligned} \quad (2.10)$$

15 Using indicial notation, we may rewrite the definition of the dot product

$$\boxed{\mathbf{a} \cdot \mathbf{b} = a_i b_i} \quad (2.11)$$

and of the cross product

$$\boxed{\mathbf{a} \times \mathbf{b} = \varepsilon_{pqr} a_q b_r \mathbf{e}_p} \quad (2.12)$$

we note that in the second equation, there is one free index p thus there are three equations, there are two repeated (dummy) indices q and r , thus each equation has nine terms.

2.1.2 Tensor Operations

16 The **sum** of two (second order) tensors is simply defined as:

$$\mathbf{S}_{ij} = \mathbf{T}_{ij} + \mathbf{U}_{ij} \quad (2.13)$$

17 The **multiplication** of a (second order) tensor by a scalar is defined by:

$$\mathbf{S}_{ij} = \lambda \mathbf{T}_{ij} \quad (2.14)$$

18 The **inner product** is obtained from an outer product by contraction involving one index from each tensor. For example

$$a_i b_j \rightarrow a_i b_i \quad (2.15-a)$$

$$a_i E_{jk} \rightarrow a_i E_{ik} = f_k \quad (2.15-b)$$

$$E_{ij} F_{km} \rightarrow E_{ij} F_{jm} = G_{im} \quad (2.15-c)$$

$$A^i B_i{}^k \rightarrow A^i B_i{}^k = D^k \quad (2.15-d)$$

19 The **scalar product** of two tensors is defined as

$$\mathbf{T} : \mathbf{U} = T_{ij} U_{ij} \quad (2.16)$$

in any rectangular system.

20 The following **inner-product** axioms are satisfied:

$$\mathbf{T} : \mathbf{U} = \mathbf{U} : \mathbf{T} \quad (2.17-a)$$

$$\mathbf{T} : (\mathbf{U} + \mathbf{V}) = \mathbf{T} : \mathbf{U} + \mathbf{T} : \mathbf{V} \quad (2.17-b)$$

$$\alpha(\mathbf{T} : \mathbf{U}) = (\alpha\mathbf{T}) : \mathbf{U} = \mathbf{T} : (\alpha\mathbf{U}) \quad (2.17-c)$$

$$\mathbf{T} : \mathbf{T} > 0 \text{ unless } \mathbf{T} = \mathbf{0} \quad (2.17-d)$$

2.1.3 Rotation of Axes

21 The rule for changing second order tensor components under rotation of axes goes as follow:

$$\begin{aligned} \bar{u}_i &= a_i^j u_j && \text{From Eq. ??} \\ &= a_i^j T_{jq} v_q && \text{From Eq. 2.1-a} \\ &= a_i^j T_{jq} a_p^q \bar{v}_p && \text{From Eq. ??} \end{aligned}$$

But we also have $\bar{u}_i = \bar{T}_{ip} \bar{v}_p$ (again from Eq. 2.1-a) in the barred system, equating these two expressions we obtain

$$\bar{T}_{ip} - (a_i^j a_p^q T_{jq}) \bar{v}_p = 0 \quad (2.18)$$

hence

$$\begin{aligned} \bar{T}_{ip} &= a_i^j a_p^q T_{jq} && \text{in Matrix Form } [\bar{T}] = [A]^T [T] [A] \\ T_{jq} &= a_i^j a_p^q \bar{T}_{ip} && \text{in Matrix Form } [T] = [A] [\bar{T}] [A]^T \end{aligned} \quad (2.19)$$

By extension, higher order tensors can be similarly transformed from one coordinate system to another.

22 If we consider the 2D case, From Eq. ??

$$A = \begin{bmatrix} \cos \alpha & \sin \alpha & 0 \\ -\sin \alpha & \cos \alpha & 0 \\ 0 & 0 & 1 \end{bmatrix} \quad (2.20-a)$$

$$T = \begin{bmatrix} T_{xx} & T_{xy} & 0 \\ T_{xy} & T_{yy} & 0 \\ 0 & 0 & 0 \end{bmatrix} \quad (2.20-b)$$

$$\bar{T} = A^T T A = \begin{bmatrix} \bar{T}_{xx} & \bar{T}_{xy} & 0 \\ \bar{T}_{xy} & \bar{T}_{yy} & 0 \\ 0 & 0 & 0 \end{bmatrix} \quad (2.20-c)$$

$$= \begin{bmatrix} \cos^2 \alpha T_{xx} + \sin^2 \alpha T_{yy} + \sin 2\alpha T_{xy} & \frac{1}{2}(-\sin 2\alpha T_{xx} + \sin 2\alpha T_{yy} + 2 \cos 2\alpha T_{xy}) & 0 \\ \frac{1}{2}(-\sin 2\alpha T_{xx} + \sin 2\alpha T_{yy} + 2 \cos 2\alpha T_{xy}) & \sin^2 \alpha T_{xx} + \cos^2 \alpha T_{yy} - 2 \sin \alpha \cos \alpha T_{xy} & 0 \\ 0 & 0 & 0 \end{bmatrix} \quad (2.20-d)$$

alternatively, using $\sin 2\alpha = 2 \sin \alpha \cos \alpha$ and $\cos 2\alpha = \cos^2 \alpha - \sin^2 \alpha$, this last equation can be rewritten as

$$\begin{bmatrix} \bar{T}_{xx} \\ \bar{T}_{yy} \\ \bar{T}_{xy} \end{bmatrix} = \begin{bmatrix} \cos^2 \theta & \sin^2 \theta & 2 \sin \theta \cos \theta \\ \sin^2 \theta & \cos^2 \theta & -2 \sin \theta \cos \theta \\ -\sin \theta \cos \theta & \cos \theta \sin \theta & \cos^2 \theta - \sin^2 \theta \end{bmatrix} \begin{bmatrix} T_{xx} \\ T_{yy} \\ T_{xy} \end{bmatrix} \quad (2.21)$$

2.1.4 Trace

23 The **trace** of a second-order tensor, denoted $\text{tr } \mathbf{T}$ is a scalar invariant function of the tensor and is defined as

$$\boxed{\text{tr } \mathbf{T} \equiv T_{ii}} \quad (2.22)$$

Thus it is equal to the sum of the diagonal elements in a matrix.

2.1.5 Inverse Tensor

24 An inverse tensor is simply defined as follows

$$\boxed{\mathbf{T}^{-1}(\mathbf{T}\mathbf{v}) = \mathbf{v} \text{ and } \mathbf{T}(\mathbf{T}^{-1}\mathbf{v}) = \mathbf{v}} \quad (2.23)$$

alternatively $\mathbf{T}^{-1}\mathbf{T} = \mathbf{T}\mathbf{T}^{-1} = \mathbf{I}$, or $T_{ik}^{-1}T_{kj} = \delta_{ij}$ and $T_{ik}T_{kj}^{-1} = \delta_{ij}$

2.1.6 Principal Values and Directions of Symmetric Second Order Tensors

25 Since the two fundamental tensors in continuum mechanics are of the second order and symmetric (stress and strain), we examine some important properties of these tensors.

26 For every symmetric tensor T_{ij} defined at some point in space, there is associated with each direction (specified by unit normal n_j) at that point, a vector given by the inner product

$$v_i = T_{ij}n_j \quad (2.24)$$

If the direction is one for which v_i is **parallel** to n_i , the inner product may be expressed as

$$T_{ij}n_j = \lambda n_i \quad (2.25)$$

and the direction n_i is called **principal direction** of T_{ij} . Since $n_i = \delta_{ij}n_j$, this can be rewritten as

$$(T_{ij} - \lambda \delta_{ij})n_j = 0 \quad (2.26)$$

which represents a system of three equations for the four unknowns n_i and λ .

$$\begin{aligned} (T_{11} - \lambda)n_1 + T_{12}n_2 + T_{13}n_3 &= 0 \\ T_{21}n_1 + (T_{22} - \lambda)n_2 + T_{23}n_3 &= 0 \\ T_{31}n_1 + T_{32}n_2 + (T_{33} - \lambda)n_3 &= 0 \end{aligned} \quad (2.27\text{-a})$$

To have a non-trivial solution ($n_i \neq 0$) the determinant of the coefficients must be zero,

$$\boxed{|T_{ij} - \lambda\delta_{ij}| = 0} \quad (2.28)$$

²⁷ Expansion of this determinant leads to the following **characteristic equation**

$$\boxed{\lambda^3 - I_T\lambda^2 + II_T\lambda - III_T = 0} \quad (2.29)$$

the roots are called the **principal values** of T_{ij} and

$$\boxed{\begin{aligned} I_T &= T_{ij} = \text{tr } T_{ij} \\ II_T &= \frac{1}{2}(T_{ii}T_{jj} - T_{ij}T_{ji}) \\ III_T &= |T_{ij}| = \det T_{ij} \end{aligned}} \quad (2.30)$$

are called the first, second and third **invariants** respectively of T_{ij} .

²⁸ It is customary to order those roots as $\lambda_1 > \lambda_2 > \lambda_3$

²⁹ For a symmetric tensor with real components, the principal values are also real. If those values are distinct, the three principal directions are mutually orthogonal.

2.2 Kinetics

2.2.1 Force, Traction and Stress Vectors

³⁰ There are two kinds of **forces** in continuum mechanics

body forces: act on the elements of volume or mass inside the body, e.g. gravity, electromagnetic fields. $d\mathbf{F} = \rho \mathbf{b} dV ol.$

surface forces: are contact forces acting on the free body at its bounding surface. Those will be defined in terms of **force per unit area**.

³¹ The surface force per unit area acting on an element dS is called **traction** or more accurately **stress vector**.

$$\int_S \mathbf{t} dS = \mathbf{i} \int_S t_x dS + \mathbf{j} \int_S t_y dS + \mathbf{k} \int_S t_z dS \quad (2.31)$$

Most authors limit the term traction to an actual bounding surface of a body, and use the term **stress vector** for an imaginary interior surface (even though the state of stress is a tensor and not a vector).

³² The traction vectors on planes perpendicular to the coordinate axes are particularly useful. When the vectors acting at a point on three such mutually perpendicular planes is given, the **stress vector** at that point on any other arbitrarily inclined plane can be expressed in terms of the first set of tractions.

³³ A **stress**, Fig 2.1 is a second order cartesian tensor, σ_{ij} where the 1st subscript (i) refers to the direction of outward facing normal, and the second one (j) to the direction of component force.

$$\boldsymbol{\sigma} = \sigma_{ij} = \begin{bmatrix} \sigma_{11} & \sigma_{12} & \sigma_{13} \\ \sigma_{21} & \sigma_{22} & \sigma_{23} \\ \sigma_{31} & \sigma_{32} & \sigma_{33} \end{bmatrix} = \begin{Bmatrix} \mathbf{t}_1 \\ \mathbf{t}_2 \\ \mathbf{t}_3 \end{Bmatrix} \quad (2.32)$$

³⁴ In fact the nine rectangular components σ_{ij} of $\boldsymbol{\sigma}$ turn out to be the three sets of three vector components ($\sigma_{11}, \sigma_{12}, \sigma_{13}$), ($\sigma_{21}, \sigma_{22}, \sigma_{23}$), ($\sigma_{31}, \sigma_{32}, \sigma_{33}$) which correspond to the three tractions $\mathbf{t}_1, \mathbf{t}_2$ and \mathbf{t}_3 which are acting on the x_1, x_2 and x_3 faces

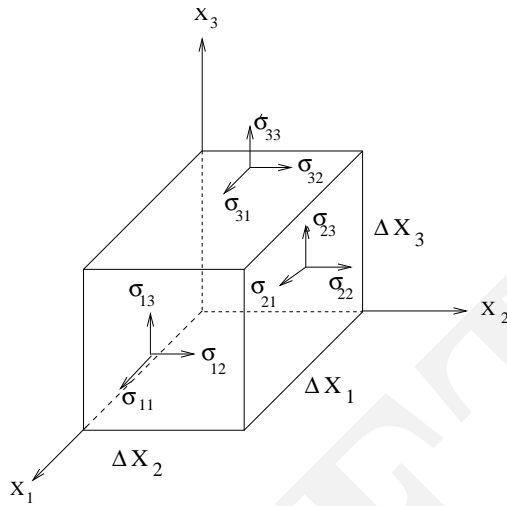


Figure 2.1: Stress Components on an Infinitesimal Element

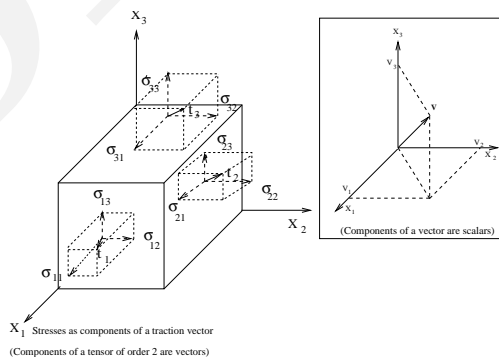


Figure 2.2: Stresses as Tensor Components

(It should be noted that those tractions are not necessarily normal to the faces, and they can be decomposed into a normal and shear traction if need be). In other words, stresses are nothing else than the components of tractions (stress vector), Fig. 2.2.

³⁵ The state of stress at a point cannot be specified entirely by a single vector with three components; it requires the second-order tensor with all nine components.

2.2.2 Traction on an Arbitrary Plane; Cauchy's Stress Tensor

³⁶ Let us now consider the problem of determining the traction acting on the surface of an oblique plane (characterized by its normal \mathbf{n}) in terms of the known tractions normal to the three principal axis, \mathbf{t}_1 , \mathbf{t}_2 and \mathbf{t}_3 . This will be done through the so-called Cauchy's tetrahedron shown in Fig. 2.3, and will be obtained without any assumption of equilibrium and it will apply in fluid

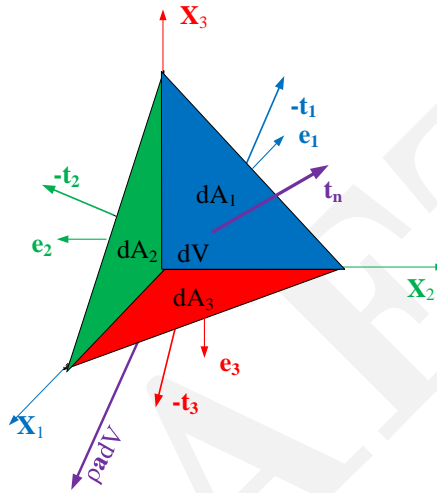


Figure 2.3: Cauchy's Tetrahedron

dynamics as well as in solid mechanics.

³⁷ This equation is a vector equation, and the corresponding algebraic equations for the components of \mathbf{t}_n are

t_{n_1}	$=$	$\sigma_{11}n_1 + \sigma_{21}n_2 + \sigma_{31}n_3$	(2.33)
t_{n_2}	$=$	$\sigma_{12}n_1 + \sigma_{22}n_2 + \sigma_{32}n_3$	
t_{n_3}	$=$	$\sigma_{13}n_1 + \sigma_{23}n_2 + \sigma_{33}n_3$	
Indicial notation t_{n_i}	$=$	$\sigma_{ji}n_j$	
dyadic notation \mathbf{t}_n	$=$	$\mathbf{n} \cdot \boldsymbol{\sigma} = \boldsymbol{\sigma}^T \cdot \mathbf{n}$	

³⁸ We have thus established that the nine components σ_{ij} are components of the second order tensor, **Cauchy's stress tensor**.

2.2.2.1 Stress Vectors

if the stress tensor at point P is given by

$$\boldsymbol{\sigma} = \begin{bmatrix} 7 & -5 & 0 \\ -5 & 3 & 1 \\ 0 & 1 & 2 \end{bmatrix} = \begin{Bmatrix} \mathbf{t}_1 \\ \mathbf{t}_2 \\ \mathbf{t}_3 \end{Bmatrix} \tag{2.34}$$

We seek to determine the traction (or stress vector) \mathbf{t} passing through P and parallel to the plane ABC where $A(4, 0, 0)$, $B(0, 2, 0)$ and $C(0, 0, 6)$.

The vector normal to the plane can be found by taking the cross products of vectors \mathbf{AB} and \mathbf{AC} :

$$\mathbf{N} = \mathbf{AB} \times \mathbf{AC} = \begin{vmatrix} \mathbf{e}_1 & \mathbf{e}_2 & \mathbf{e}_3 \\ -4 & 2 & 0 \\ -4 & 0 & 6 \end{vmatrix} \quad (2.35\text{-a})$$

$$= 12\mathbf{e}_1 + 24\mathbf{e}_2 + 8\mathbf{e}_3 \quad (2.35\text{-b})$$

The unit normal of N is given by

$$\mathbf{n} = \frac{3}{7}\mathbf{e}_1 + \frac{6}{7}\mathbf{e}_2 + \frac{2}{7}\mathbf{e}_3 \quad (2.36)$$

Hence the stress vector (traction) will be

$$\left[\frac{3}{7} \quad \frac{6}{7} \quad \frac{2}{7} \right] \begin{bmatrix} 7 & -5 & 0 \\ -5 & 3 & 1 \\ 0 & 1 & 2 \end{bmatrix} = \left[-\frac{9}{7} \quad \frac{5}{7} \quad \frac{10}{7} \right] \quad (2.37)$$

$$\text{and thus } \mathbf{t} = -\frac{9}{7}\mathbf{e}_1 + \frac{5}{7}\mathbf{e}_2 + \frac{10}{7}\mathbf{e}_3$$

2.2.3 Invariants

³⁹ The principal stresses are physical quantities, whose values do not depend on the coordinate system in which the components of the stress were initially given. They are therefore **invariants** of the stress state.

⁴⁰ When the determinant in the characteristic equation is expanded, the cubic equation takes the form

$$\lambda^3 - I_\sigma \lambda^2 - II_\sigma \lambda - III_\sigma = 0 \quad (2.38)$$

where the symbols I_σ , II_σ and III_σ denote the following scalar expressions in the stress components:

$$\begin{aligned} I_\sigma &= \sigma_{11} + \sigma_{22} + \sigma_{33} = \sigma_{ii} = \text{tr } \boldsymbol{\sigma} \\ II_\sigma &= -(\sigma_{11}\sigma_{22} + \sigma_{22}\sigma_{33} + \sigma_{33}\sigma_{11}) + \sigma_{23}^2 + \sigma_{31}^2 + \sigma_{12}^2 \\ &= \frac{1}{2}(\sigma_{ij}\sigma_{ij} - \sigma_{ii}\sigma_{jj}) = \frac{1}{2}\sigma_{ij}\sigma_{ij} - \frac{1}{2}I_\sigma^2 \\ &= \frac{1}{2}(\boldsymbol{\sigma} : \boldsymbol{\sigma} - I_\sigma^2) \\ III_\sigma &= \det \boldsymbol{\sigma} = \frac{1}{6}e_{ijk}e_{pqr}\sigma_{ip}\sigma_{jq}\sigma_{kr} \end{aligned} \quad (2.39)$$

⁴¹ In terms of the principal stresses, those invariants can be simplified into

$$\begin{aligned} I_\sigma &= \sigma_{(1)} + \sigma_{(2)} + \sigma_{(3)} \\ II_\sigma &= -(\sigma_{(1)}\sigma_{(2)} + \sigma_{(2)}\sigma_{(3)} + \sigma_{(3)}\sigma_{(1)}) \\ III_\sigma &= \sigma_{(1)}\sigma_{(2)}\sigma_{(3)} \end{aligned} \quad (2.40)$$

2.2.4 Spherical and Deviatoric Stress Tensors

⁴² If we let σ denote the mean normal stress p

$$\sigma = -p = \frac{1}{3}(\sigma_{11} + \sigma_{22} + \sigma_{33}) = \frac{1}{3}\sigma_{ii} = \frac{1}{3}\text{tr } \boldsymbol{\sigma} \quad (2.41)$$

then the stress tensor can be written as the sum of two tensors:

Hydrostatic stress in which each normal stress is equal to $-p$ and the shear stresses are zero. The hydrostatic stress produces volume change without change in shape in an isotropic medium.

$$\boldsymbol{\sigma}_{hyd} = -p\mathbf{I} = \begin{bmatrix} -p & 0 & 0 \\ 0 & -p & 0 \\ 0 & 0 & -p \end{bmatrix} \quad (2.42)$$

Deviatoric Stress: which causes the change in shape.

$$\boldsymbol{\sigma}_{dev} = \begin{bmatrix} \sigma_{11} - \sigma & \sigma_{12} & \sigma_{13} \\ \sigma_{21} & \sigma_{22} - \sigma & \sigma_{23} \\ \sigma_{31} & \sigma_{32} & \sigma_{33} - \sigma \end{bmatrix} \quad (2.43)$$

2.2.5 Stress Transformation

43 From Eq. 2.19 and 2.19, the stress transformation for the second order stress tensor is given by

$$\begin{cases} \bar{\sigma}_{ip} = a_i^j a_p^q \sigma_{jq} & \text{in Matrix Form } [\bar{\sigma}] = [A]^T [\sigma] [A] \\ \sigma_{jq} = a_i^j a_p^q \bar{\sigma}_{ip} & \text{in Matrix Form } [\sigma] = [A] [\bar{\sigma}] [A]^T \end{cases} \quad (2.44)$$

44 For the 2D plane stress case we rewrite Eq. 2.21

$$\begin{cases} \bar{\sigma}_{xx} \\ \bar{\sigma}_{yy} \\ \bar{\sigma}_{xy} \end{cases} = \begin{bmatrix} \cos^2 \alpha & \sin^2 \alpha & 2 \sin \alpha \cos \alpha \\ \sin^2 \alpha & \cos^2 \alpha & -2 \sin \alpha \cos \alpha \\ -\sin \alpha \cos \alpha & \cos \alpha \sin \alpha & \cos^2 \alpha - \sin^2 \alpha \end{bmatrix} \begin{cases} \sigma_{xx} \\ \sigma_{yy} \\ \sigma_{xy} \end{cases} \quad (2.45)$$

2.2.6 Polar Coordinates

It is often necessary to express cartesian stresses in terms of polar stresses and vice versa. This can be done through the following relationships

$$\sigma_{xx} = \sigma_{rr} \cos^2 \theta + \sigma_{\theta\theta} \sin^2 \theta - \sigma_{r\theta} \sin 2\theta \quad (2.46-a)$$

$$\sigma_{yy} = \sigma_{rr} \sin^2 \theta + \sigma_{\theta\theta} \cos^2 \theta + \sigma_{r\theta} \sin 2\theta \quad (2.46-b)$$

$$\sigma_{xy} = (\sigma_{rr} - \sigma_{\theta\theta}) \sin \theta \cos \theta + \sigma_{r\theta} (\cos^2 \theta - \sin^2 \theta) \quad (2.46-c)$$

and

$$\begin{aligned} \sigma_{rr} = & \left(\frac{\sigma_{xx} + \sigma_{yy}}{2} \right) \left(1 - \frac{a^2}{r^2} \right) + \left(\frac{\sigma_{xx} - \sigma_{yy}}{2} \right) \left(1 + \frac{3a^4}{r^4} - \frac{4a^2}{r^2} \right) \cos 2\theta \\ & + \sigma_{xy} \left(1 + \frac{3a^4}{r^4} - \frac{4a^2}{r^2} \right) \sin 2\theta \end{aligned} \quad (2.47-a)$$

$$\begin{aligned} \sigma_{\theta\theta} = & \left(\frac{\sigma_{xx} + \sigma_{yy}}{2} \right) \left(1 + \frac{a^2}{r^2} \right) - \left(\frac{\sigma_{xx} - \sigma_{yy}}{2} \right) \left(1 + \frac{3a^4}{r^4} \right) \cos 2\theta \\ & - \sigma_{xy} \left(1 + \frac{3a^4}{r^4} \right) \sin 2\theta \end{aligned} \quad (2.47-b)$$

$$\sigma_{r\theta} = - \left(\frac{\sigma_{xx} - \sigma_{yy}}{2} \right) \left(1 - \frac{3a^4}{r^4} + \frac{2a^2}{r^2} \right) \sin 2\theta + \sigma_{xy} \left(1 - \frac{3a^4}{r^4} + \frac{2a^2}{r^2} \right) \cos 2\theta \quad (2.47-c)$$

2.3 Kinematic

2.3.1 Strain Tensors

45 The Lagrangian finite strain tensor can be written as

$$E_{ij} = \frac{1}{2} \left(\frac{\partial u_i}{\partial X_j} + \frac{\partial u_j}{\partial X_i} + \frac{\partial u_k}{\partial X_i} \frac{\partial u_k}{\partial X_j} \right) \text{ or } \mathbf{E} = \frac{1}{2} \left(\underbrace{\mathbf{u} \nabla_{\mathbf{x}} + \nabla_{\mathbf{x}} \mathbf{u}}_{\mathbf{J} + \mathbf{J}_c} + \underbrace{\nabla_{\mathbf{x}} \mathbf{u} \cdot \mathbf{u} \nabla_{\mathbf{x}}}_{\mathbf{J}_c \cdot \mathbf{J}} \right) \quad (2.48)$$

or:

$$E_{11} = \frac{\partial u_1}{\partial X_1} + \frac{1}{2} \left[\left(\frac{\partial u_1}{\partial X_1} \right)^2 + \left(\frac{\partial u_2}{\partial X_1} \right)^2 + \left(\frac{\partial u_3}{\partial X_1} \right)^2 \right] \quad (2.49-a)$$

$$E_{12} = \frac{1}{2} \left(\frac{\partial u_1}{\partial X_2} + \frac{\partial u_2}{\partial X_1} \right) + \frac{1}{2} \left[\frac{\partial u_1}{\partial X_1} \frac{\partial u_1}{\partial X_2} + \frac{\partial u_2}{\partial X_1} \frac{\partial u_2}{\partial X_2} + \frac{\partial u_3}{\partial X_1} \frac{\partial u_3}{\partial X_2} \right] \quad (2.49-b)$$

$$\dots = \dots \quad (2.49-c)$$

46 The Eulerian finite strain tensor can be written as

$$E_{ij}^* = \frac{1}{2} \left(\frac{\partial u_i}{\partial x_j} + \frac{\partial u_j}{\partial x_i} - \frac{\partial u_k}{\partial x_i} \frac{\partial u_k}{\partial x_j} \right) \text{ or } \mathbf{E}^* = \frac{1}{2} \left(\underbrace{\mathbf{u} \nabla_{\mathbf{x}} + \nabla_{\mathbf{x}} \mathbf{u}}_{\mathbf{K} + \mathbf{K}_c} - \underbrace{\nabla_{\mathbf{x}} \mathbf{u} \cdot \mathbf{u} \nabla_{\mathbf{x}}}_{\mathbf{K}_c \cdot \mathbf{K}} \right) \quad (2.50)$$

47 Expanding

$$E_{11}^* = \frac{\partial u_1}{\partial x_1} - \frac{1}{2} \left[\left(\frac{\partial u_1}{\partial x_1} \right)^2 + \left(\frac{\partial u_2}{\partial x_1} \right)^2 + \left(\frac{\partial u_3}{\partial x_1} \right)^2 \right] \quad (2.51-a)$$

$$E_{12}^* = \frac{1}{2} \left(\frac{\partial u_1}{\partial x_2} + \frac{\partial u_2}{\partial x_1} \right) - \frac{1}{2} \left[\frac{\partial u_1}{\partial x_1} \frac{\partial u_1}{\partial x_2} + \frac{\partial u_2}{\partial x_1} \frac{\partial u_2}{\partial x_2} + \frac{\partial u_3}{\partial x_1} \frac{\partial u_3}{\partial x_2} \right] \quad (2.51-b)$$

$$\dots = \dots \quad (2.51-c)$$

48 Alternatively these equations may be expanded as

$$\begin{aligned} \varepsilon_{xx} &= \frac{\partial u}{\partial x} + \frac{1}{2} \left[\left(\frac{\partial u}{\partial x} \right)^2 + \left(\frac{\partial v}{\partial x} \right)^2 + \left(\frac{\partial w}{\partial x} \right)^2 \right] \\ \varepsilon_{yy} &= \frac{\partial v}{\partial y} + \frac{1}{2} \left[\left(\frac{\partial u}{\partial y} \right)^2 + \left(\frac{\partial v}{\partial y} \right)^2 + \left(\frac{\partial w}{\partial y} \right)^2 \right] \\ \varepsilon_{zz} &= \frac{\partial w}{\partial z} + \frac{1}{2} \left[\left(\frac{\partial u}{\partial z} \right)^2 + \left(\frac{\partial v}{\partial z} \right)^2 + \left(\frac{\partial w}{\partial z} \right)^2 \right] \\ \varepsilon_{xy} &= \frac{1}{2} \left(\frac{\partial v}{\partial x} + \frac{\partial u}{\partial y} + \frac{\partial u}{\partial x} \frac{\partial u}{\partial y} + \frac{\partial v}{\partial x} \frac{\partial v}{\partial y} + \frac{\partial w}{\partial x} \frac{\partial w}{\partial y} \right) \\ \varepsilon_{xz} &= \frac{1}{2} \left(\frac{\partial w}{\partial x} + \frac{\partial u}{\partial z} + \frac{\partial u}{\partial x} \frac{\partial u}{\partial z} + \frac{\partial v}{\partial x} \frac{\partial v}{\partial z} + \frac{\partial w}{\partial x} \frac{\partial w}{\partial z} \right) \\ \varepsilon_{yz} &= \frac{1}{2} \left(\frac{\partial w}{\partial y} + \frac{\partial v}{\partial z} + \frac{\partial u}{\partial y} \frac{\partial u}{\partial z} + \frac{\partial v}{\partial y} \frac{\partial v}{\partial z} + \frac{\partial w}{\partial y} \frac{\partial w}{\partial z} \right) \end{aligned} \quad (2.52)$$

or

$$\varepsilon_{ij} = \frac{1}{2} (u_{i,j} + u_{j,i} + u_{k,i} u_{k,j}) \quad (2.53)$$

From this equation, we note that:

1. We define the **engineering shear strain** as

$$\gamma_{ij} = 2\varepsilon_{ij} \quad (i \neq j) \quad (2.54)$$

2. If the strains are given, then these strain-displacements provide a system of (6) nonlinear partial differential equation in terms of the unknown displacements (3).
3. ε_{ik} is the **Green-Lagrange strain tensor**.
4. The strains have been expressed in terms of the coordinates x, y, z in the undeformed state, i.e. in the **Lagrangian coordinate** which is the preferred one in structural mechanics.
5. Alternatively we could have expressed $ds'^2 - dS^2$ in terms of coordinates in the deformed state, i.e. **Eulerian coordinates** x', y', z' , and the resulting strains are referred to as the **Almansi strain** which is the preferred one in fluid mechanics.
6. In most cases the deformations are small enough for the quadratic term to be dropped, the resulting equations reduce to

$$\begin{aligned} \varepsilon_{xx} &= \frac{\partial u}{\partial x} \\ \varepsilon_{yy} &= \frac{\partial v}{\partial y} \\ \varepsilon_{zz} &= \frac{\partial w}{\partial z} \\ \gamma_{xy} &= \frac{\partial v}{\partial x} + \frac{\partial u}{\partial y} \\ \gamma_{xz} &= \frac{\partial w}{\partial x} + \frac{\partial u}{\partial z} \\ \gamma_{yz} &= \frac{\partial w}{\partial y} + \frac{\partial v}{\partial z} \end{aligned} \quad (2.55)$$

or

$$\varepsilon_{ij} = \frac{1}{2} (u_{i,k} + u_{k,i}) \quad (2.56)$$

which is called the **Cauchy strain**

⁴⁹ In finite element, the strain is often expressed through the **linear operator L**

$$\boxed{\boldsymbol{\varepsilon} = \mathbf{L}\mathbf{u}} \tag{2.57}$$

or

$$\boxed{\begin{matrix} \left\{ \begin{matrix} \varepsilon_{xx} \\ \varepsilon_{yy} \\ \varepsilon_{zz} \\ \varepsilon_{xy} \\ \varepsilon_{xz} \\ \varepsilon_{yz} \end{matrix} \right\} \\ \boldsymbol{\varepsilon} \end{matrix} = \underbrace{\begin{bmatrix} \frac{\partial}{\partial x} & 0 & 0 \\ 0 & \frac{\partial}{\partial y} & 0 \\ 0 & 0 & \frac{\partial}{\partial z} \\ \frac{\partial}{\partial y} & \frac{\partial}{\partial x} & 0 \\ \frac{\partial}{\partial z} & 0 & \frac{\partial}{\partial x} \\ 0 & \frac{\partial}{\partial z} & \frac{\partial}{\partial y} \end{bmatrix}}_{\mathbf{L}} \underbrace{\left\{ \begin{matrix} u_x \\ u_y \\ u_z \end{matrix} \right\}}_{\mathbf{u}}} \tag{2.58}$$

2.3.2 Compatibility Equation

If $\varepsilon_{ij} = \frac{1}{2}(u_{i,j} + u_{j,i})$ then we have six differential equations (in 3D the strain tensor has a total of 9 terms, but due to symmetry, there are 6 independent ones) for determining (upon integration) three unknowns displacements u_i . Hence the system is overdetermined, and there must be some linear relations between the strains.

It can be shown (through appropriate successive differentiation of Eq. ??) that the compatibility relation for strain reduces to:

$$\boxed{\frac{\partial^2 \varepsilon_{ik}}{\partial x_j \partial x_j} + \frac{\partial^2 \varepsilon_{jj}}{\partial x_i \partial x_k} - \frac{\partial^2 \varepsilon_{jk}}{\partial x_i \partial x_j} - \frac{\partial^2 \varepsilon_{ij}}{\partial x_j \partial x_k} = 0.} \tag{2.59}$$

In 3D, this would yield 9 equations in total, however only six are distinct. In 2D, this results in (by setting $i = 2, j = 1$ and $l = 2$):

$$\boxed{\frac{\partial^2 \varepsilon_{11}}{\partial x_2^2} + \frac{\partial^2 \varepsilon_{22}}{\partial x_1^2} = \frac{\partial^2 \gamma_{12}}{\partial x_1 \partial x_2}} \tag{2.60}$$

(recall that $2\varepsilon_{12} = \gamma_{12}$).

When the compatibility equation is written in term of the stresses, it yields:

$$\frac{\partial^2 \sigma_{11}}{\partial x_2^2} - \nu \frac{\partial \sigma_{22}^2}{\partial x_2^2} + \frac{\partial^2 \sigma_{22}}{\partial x_1^2} - \nu \frac{\partial^2 \sigma_{11}}{\partial x_1^2} = 2(1 + \nu) \frac{\partial^2 \sigma_{21}}{\partial x_1 \partial x_2} \tag{2.61}$$

2.4 Fundamental Laws of Continuum Mechanics

⁵⁰ We have thus far studied the stress tensors (Cauchy, Piola Kirchoff), and several other tensors which describe strain at a point. In general, those tensors will vary from point to point and represent a **tensor field**.

⁵¹ We have also obtained only one differential equation, that was the compatibility equation.

⁵² In this section, we will derive additional differential equations governing the way stress and deformation vary at a point and with time. They will apply to any continuous medium, and yet we will not have enough equations to determine unknown tensor field. For that we need to wait for the next chapter where constitutive laws relating stress and strain will be introduced. Only with constitutive equations and boundary and initial conditions would we be able to obtain a well defined mathematical problem to solve for the stress and deformation distribution or the displacement or velocity fields.

⁵³ In this chapter we shall derive differential equations expressing locally the conservation of mass, momentum and energy. These differential equations of balance will be derived from integral forms of the equation of balance expressing the fundamental postulates of continuum mechanics.

2.4.1 Conservation Laws

54 Conservation laws constitute a fundamental component of classical physics. A conservation law establishes a balance of a scalar or tensorial quantity in volume V bounded by a surface S . In its most general form, such a law may be expressed as

$$\underbrace{\frac{d}{dt} \int_V \mathcal{A} dV}_{\text{Rate of variation}} + \underbrace{\int_S \alpha dS}_{\text{Exchange by Diffusion}} = \underbrace{\int_V \mathbf{A} dV}_{\text{Source}} \quad (2.62)$$

where \mathcal{A} is the volumetric density of the quantity of interest (mass, linear momentum, energy, ...) \mathbf{a} , \mathbf{A} is the rate of volumetric density of what is provided from the outside, and α is the rate of surface density of what is lost through the surface S of V and will be a function of the normal to the surface \mathbf{n} .

55 Hence, we read the previous equation as: The input quantity (provided by the right hand side) is equal to what is lost across the boundary, and to modify \mathcal{A} which is the quantity of interest. The dimensions of various quantities are given by

$$\dim(\mathbf{a}) = \dim(\mathcal{A}L^{-3}) \quad (2.63\text{-a})$$

$$\dim(\alpha) = \dim(\mathcal{A}L^{-2}t^{-1}) \quad (2.63\text{-b})$$

$$\dim(\mathbf{A}) = \dim(\mathcal{A}L^{-3}t^{-1}) \quad (2.63\text{-c})$$

56 Hence, this section will apply the previous conservation law to mass, momentum, and energy. the resulting differential equations will provide additional interesting relation with regard to the incompressibility of solids (important in classical hydrodynamics and plasticity theories), equilibrium and symmetry of the stress tensor, and the first law of thermodynamics.

57 The enunciation of the preceding three conservation laws plus the second law of thermodynamics, constitute what is commonly known as the **fundamental laws of continuum mechanics**.

2.4.2 Fluxes

58 Prior to the enunciation of the first conservation law, we need to define the concept of flux across a bounding surface.

59 The **flux** across a surface can be graphically defined through the consideration of an imaginary surface fixed in space with continuous “medium” flowing through it. If we assign a positive side to the surface, and take \mathbf{n} in the positive sense, then the volume of “material” flowing through the infinitesimal surface area dS in time dt is equal to the volume of the cylinder with base dS and slant height $v dt$ parallel to the velocity vector \mathbf{v} , Fig. 2.4 (If $\mathbf{v} \cdot \mathbf{n}$ is negative, then the flow is in the negative direction).

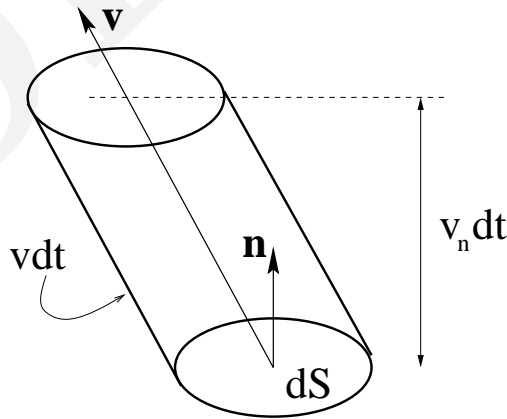


Figure 2.4: Flux Through Area dS

Hence, we define the volume flux as

$$\text{Volume Flux} = \int_S \mathbf{v} \cdot \mathbf{n} dS = \int_S v_j n_j dS \quad (2.64)$$

where the last form is for rectangular cartesian components.

⁶⁰ We can generalize this definition and define the following fluxes per unit area through dS :

Mass Flux	$= \int_S \rho \mathbf{v} \cdot \mathbf{n} dS = \int_S \rho v_j n_j dS$	(2.65)
Momentum Flux	$= \int_S \rho \mathbf{v} (\mathbf{v} \cdot \mathbf{n}) dS = \int_S \rho v_k v_j n_j dS$	
Kinetic Energy Flux	$= \int_S \frac{1}{2} \rho v^2 (\mathbf{v} \cdot \mathbf{n}) dS = \int_S \frac{1}{2} \rho v_i v_i v_j n_j dS$	
Heat flux	$= \int_S \mathbf{q} \cdot \mathbf{n} dS = \int_S q_j n_j dS$	
Electric flux	$= \int_S \mathbf{J} \cdot \mathbf{n} dS = \int_S J_j n_j dS$	

2.4.3 Conservation of Mass; Continuity Equation

$\frac{d\rho}{dt} + \rho \frac{\partial v_i}{\partial x_i} = 0$ or $\frac{d\rho}{dt} + \rho \nabla \cdot \mathbf{v} = 0$	(2.66)
--	--------

The vector form is independent of any choice of coordinates. This equation shows that the divergence of the velocity vector field equals $(-1/\rho)(d\rho/dt)$ and measures the rate of flow of material away from the particle and is equal to the unit rate of decrease of density ρ in the neighborhood of the particle.

⁶¹ If the material is incompressible, so that the density in the neighborhood of each material particle remains constant as it moves, then the continuity equation takes the simpler form

$\frac{\partial v_i}{\partial x_i} = 0$ or $\nabla \cdot \mathbf{v} = 0$	(2.67)
--	--------

this is the **condition of incompressibility**

2.4.4 Linear Momentum Principle; Equation of Motion

⁶² The momentum principle states that *the time rate of change of the total momentum of a given set of particles equals the vector sum of all external forces acting on the particles of the set, provided Newton's Third Law applies*. The continuum form of this principle is a basic **postulate** of continuum mechanics.

$$\int_S \mathbf{t} dS + \int_V \rho \mathbf{b} dV = \frac{d}{dt} \int_V \rho \mathbf{v} dV \quad (2.68)$$

Then we substitute $t_i = T_{ij} n_j$ and apply the divergence theorem to obtain

$$\int_V \left(\frac{\partial T_{ij}}{\partial x_j} + \rho b_i \right) dV = \int_V \rho \frac{dV_i}{dt} dV \quad (2.69-a)$$

$$\int_V \left[\frac{\partial T_{ij}}{\partial x_j} + \rho b_i - \rho \frac{dV_i}{dt} \right] dV = 0 \quad (2.69-b)$$

or for an arbitrary volume

$\frac{\partial T_{ij}}{\partial x_j} + \rho b_i = \rho \frac{dV_i}{dt}$ or $\nabla \cdot \mathbf{T} + \rho \mathbf{b} = \rho \frac{dV}{dt}$	(2.70)
--	--------

which is **Cauchy's (first) equation of motion**, or the **linear momentum principle**, or more simply **equilibrium equation**.

⁶³ When expanded in 3D, this equation yields:

$$\begin{aligned} \frac{\partial T_{11}}{\partial x_1} + \frac{\partial T_{12}}{\partial x_2} + \frac{\partial T_{13}}{\partial x_3} + \rho b_1 &= 0 \\ \frac{\partial T_{21}}{\partial x_1} + \frac{\partial T_{22}}{\partial x_2} + \frac{\partial T_{23}}{\partial x_3} + \rho b_2 &= 0 \\ \frac{\partial T_{31}}{\partial x_1} + \frac{\partial T_{32}}{\partial x_2} + \frac{\partial T_{33}}{\partial x_3} + \rho b_3 &= 0 \end{aligned} \quad (2.71)$$

⁶⁴ We note that these equations could also have been derived from the free body diagram shown in Fig. 2.5 with the assumption of **equilibrium** (via Newton's second law) considering an infinitesimal element of dimensions $dx_1 \times dx_2 \times dx_3$. Writing the summation of forces, will yield

$$\boxed{T_{ij,j} + \rho b_i = 0} \quad (2.72)$$

where ρ is the density, b_i is the body force (including inertia).

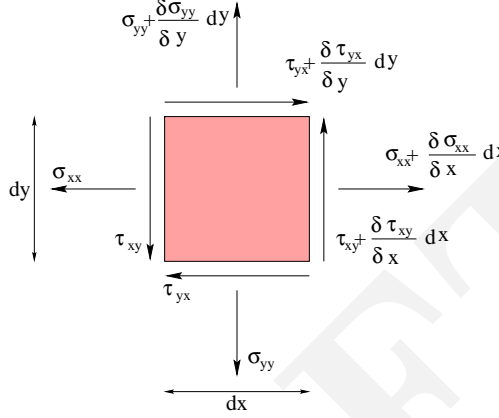


Figure 2.5: Equilibrium of Stresses, Cartesian Coordinates

2.4.5 Moment of Momentum Principle

⁶⁵ The moment of momentum principle states that *the time rate of change of the total moment of momentum of a given set of particles equals the vector sum of the moments of all external forces acting on the particles of the set.*

⁶⁶ Thus, in the absence of **distributed couples** (this theory of Cosserat will not be covered in this course) we postulate the same principle for a continuum as

$$\boxed{\int_S (\mathbf{r} \times \mathbf{t}) dS + \int_V (\mathbf{r} \times \rho \mathbf{b}) dV = \frac{d}{dt} \int_V (\mathbf{r} \times \rho \mathbf{v}) dV} \quad (2.73)$$

2.4.6 Conservation of Energy; First Principle of Thermodynamics

⁶⁷ The first principle of thermodynamics relates the work done on a (closed) system and the heat transfer into the system to the change in energy of the system. We shall assume that the only energy transfers to the system are by mechanical work done on the system by surface traction and body forces, by heat transfer through the boundary.

⁶⁸ If mechanical quantities only are considered, the **principle of conservation of energy** for the continuum may be derived directly from the equation of motion given by Eq. 2.70. This is accomplished by taking the integral over the volume V of the scalar product between Eq. 2.70 and the velocity v_i .

$$\int_V v_i T_{ji,j} dV + \int_V \rho b_i v_i dV = \int_V \rho v_i \frac{dV_i}{dt} dV \quad (2.74)$$

Applying the divergence theorem,

$$\boxed{\frac{dK}{dt} + \frac{dU}{dt} = \frac{dW}{dt} + Q} \quad (2.75)$$

this equation relates the time rate of change of total mechanical energy of the continuum on the left side to the rate of work done by the surface and body forces on the right hand side.

⁶⁹ If both mechanical and non mechanical energies are to be considered, the first principle states that *the time rate of change of the kinetic plus the internal energy is equal to the sum of the rate of work plus all other energies supplied to, or removed from the continuum per unit time (heat, chemical, electromagnetic, etc.)*.

⁷⁰ For a thermomechanical continuum, it is customary to express the time rate of change of internal energy by the integral expression

$$\frac{dU}{dt} = \frac{d}{dt} \int_V \rho u dV \quad (2.76)$$

where u is the internal energy per unit mass or **specific internal energy**. We note that U appears only as a differential in the first principle, hence if we really need to evaluate this quantity, we need to have a reference value for which U will be null. The dimension of U is one of energy $\dim U = ML^2T^{-2}$, and the SI unit is the Joule, similarly $\dim u = L^2T^{-2}$ with the SI unit of Joule/Kg.

2.5 Constitutive Equations

ceinosssttuu

Hooke, 1676

Ut tensio sic vis

Hooke, 1678

⁷¹ The Generalized Hooke's Law can be written as:

$$\sigma_{ij} = D_{ijkl} \varepsilon_{kl} \quad i, j, k, l = 1, 2, 3 \quad (2.77)$$

⁷² The (fourth order) tensor of elastic constants D_{ijkl} has 81 (3^4) components however, due to the symmetry of both σ and ε , there are at most 36 $\left(\frac{9(9-1)}{2}\right)$ distinct elastic terms.

⁷³ For the purpose of writing Hooke's Law, the double indexed system is often replaced by a simple indexed system with a range of six:

$$\sigma_k = \overbrace{D_{km}}^{6^2=36} \varepsilon_m \quad k, m = 1, 2, 3, 4, 5, 6 \quad (2.78)$$

⁷⁴ In terms of Lamé's constants, **Hooke's Law** for an isotropic body is written as

$$\begin{aligned} T_{ij} &= \lambda \delta_{ij} E_{kk} + 2\mu E_{ij} & \text{or} & \quad \mathbf{T} = \lambda \mathbf{I}_E + 2\mu \mathbf{E} \\ E_{ij} &= \frac{1}{2\mu} \left(T_{ij} - \frac{\lambda}{3\lambda+2\mu} \delta_{ij} T_{kk} \right) & \text{or} & \quad \mathbf{E} = \frac{-\lambda}{2\mu(3\lambda+2\mu)} \mathbf{I}_T + \frac{1}{2\mu} \mathbf{T} \end{aligned} \quad (2.79)$$

⁷⁵ In terms of engineering constants:

$$\begin{aligned} \frac{1}{E} &= \frac{\lambda+\mu}{\mu(3\lambda+2\mu)}; & \nu &= \frac{\lambda}{2(\lambda+\mu)} \\ \lambda &= \frac{\nu E}{(1+\nu)(1-2\nu)}; & \mu &= G = \frac{E}{2(1+\nu)} \end{aligned} \quad (2.80)$$

⁷⁶ Similarly in the case of pure shear in the x_1x_3 and x_2x_3 planes, we have

$$\sigma_{21} = \sigma_{12} = \tau \quad \text{all other } \sigma_{ij} = 0 \quad (2.81-a)$$

$$2\varepsilon_{12} = \frac{\tau}{G} \quad (2.81-b)$$

and the μ is equal to the **shear modulus** G .

⁷⁷ Hooke's law for isotropic material in terms of engineering constants becomes

$$\begin{aligned} \sigma_{ij} &= \frac{E}{1+\nu} \left(\varepsilon_{ij} + \frac{\nu}{1-2\nu} \delta_{ij} \varepsilon_{kk} \right) & \text{or} & \quad \boldsymbol{\sigma} = \frac{E}{1+\nu} \left(\boldsymbol{\varepsilon} + \frac{\nu}{1-2\nu} \mathbf{I}_\varepsilon \right) \\ \varepsilon_{ij} &= \frac{1+\nu}{E} \sigma_{ij} - \frac{\nu}{E} \delta_{ij} \sigma_{kk} & \text{or} & \quad \boldsymbol{\varepsilon} = \frac{1+\nu}{E} \boldsymbol{\sigma} - \frac{\nu}{E} \mathbf{I}_\sigma \end{aligned} \quad (2.82)$$

78 When the strain equation is expanded in 3D cartesian coordinates it would yield:

$$\begin{Bmatrix} \varepsilon_{xx} \\ \varepsilon_{yy} \\ \varepsilon_{zz} \\ \gamma_{xy}(2\varepsilon_{xy}) \\ \gamma_{yz}(2\varepsilon_{yz}) \\ \gamma_{zx}(2\varepsilon_{zx}) \end{Bmatrix} = \frac{1}{E} \begin{bmatrix} 1 & -\nu & -\nu & 0 & 0 & 0 \\ -\nu & 1 & -\nu & 0 & 0 & 0 \\ -\nu & -\nu & 1 & 0 & 0 & 0 \\ 0 & 0 & 0 & 1+\nu & 0 & 0 \\ 0 & 0 & 0 & 0 & 1+\nu & 0 \\ 0 & 0 & 0 & 0 & 0 & 1+\nu \end{bmatrix} \begin{Bmatrix} \sigma_{xx} \\ \sigma_{yy} \\ \sigma_{zz} \\ \tau_{xy} \\ \tau_{yz} \\ \tau_{zx} \end{Bmatrix} \quad (2.83)$$

79 If we invert this equation, we obtain

$$\begin{Bmatrix} \sigma_{xx} \\ \sigma_{yy} \\ \sigma_{zz} \\ \tau_{xy} \\ \tau_{yz} \\ \tau_{zx} \end{Bmatrix} = \frac{E}{(1+\nu)(1-2\nu)} \begin{bmatrix} 1-\nu & \nu & \nu \\ \nu & 1-\nu & \nu \\ \nu & \nu & 1-\nu \end{bmatrix} \begin{Bmatrix} \varepsilon_{xx} \\ \varepsilon_{yy} \\ \varepsilon_{zz} \\ \gamma_{xy}(2\varepsilon_{xy}) \\ \gamma_{yz}(2\varepsilon_{yz}) \\ \gamma_{zx}(2\varepsilon_{zx}) \end{Bmatrix} + \begin{matrix} 0 \\ 0 \\ 0 \end{matrix} + G \begin{bmatrix} 1 & 0 & 0 \\ 0 & 1 & 0 \\ 0 & 0 & 1 \end{bmatrix} \begin{Bmatrix} \tau_{xy} \\ \tau_{yz} \\ \tau_{zx} \end{Bmatrix} \quad (2.84)$$

2.5.1 Transversely Isotropic Case

80 For transversely isotropic, we can express the stress-strain relation in terms of

$$\begin{aligned} \varepsilon_{xx} &= a_{11}\sigma_{xx} + a_{12}\sigma_{yy} + a_{13}\sigma_{zz} \\ \varepsilon_{yy} &= a_{12}\sigma_{xx} + a_{11}\sigma_{yy} + a_{13}\sigma_{zz} \\ \varepsilon_{zz} &= a_{13}(\sigma_{xx} + \sigma_{yy}) + a_{33}\sigma_{zz} \\ \gamma_{xy} &= 2(a_{11} - a_{12})\tau_{xy} \\ \gamma_{yz} &= a_{44}\tau_{yz} \\ \gamma_{xz} &= a_{44}\tau_{xz} \end{aligned} \quad (2.85)$$

and

$$a_{11} = \frac{1}{E}; \quad a_{12} = -\frac{\nu}{E}; \quad a_{13} = -\frac{\nu'}{E'}; \quad a_{33} = -\frac{1}{E'}; \quad a_{44} = -\frac{1}{\mu'} \quad (2.86)$$

where E is the Young's modulus in the plane of isotropy and E' the one in the plane normal to it. ν corresponds to the transverse contraction in the plane of isotropy when tension is applied in the plane; ν' corresponding to the transverse contraction in the plane of isotropy when tension is applied normal to the plane; μ' corresponding to the shear moduli for the plane of isotropy and any plane normal to it, and μ is shear moduli for the plane of isotropy.

2.5.2 Special 2D Cases

81 Often times one can make simplifying assumptions to reduce a 3D problem into a 2D one.

2.5.2.1 Plane Strain

82 For problems involving a long body in the z direction with no variation in load or geometry, then $\varepsilon_{zz} = \gamma_{yz} = \gamma_{xz} = \tau_{xz} = \tau_{yz} = 0$. Thus, replacing into Eq. 2.84 we obtain

$$\begin{Bmatrix} \sigma_{xx} \\ \sigma_{yy} \\ \sigma_{zz} \\ \tau_{xy} \end{Bmatrix} = \frac{E}{(1+\nu)(1-2\nu)} \begin{bmatrix} (1-\nu) & \nu & 0 \\ \nu & (1-\nu) & 0 \\ \nu & \nu & 0 \\ 0 & 0 & \frac{1-2\nu}{2} \end{bmatrix} \begin{Bmatrix} \varepsilon_{xx} \\ \varepsilon_{yy} \\ \gamma_{xy} \end{Bmatrix} \quad (2.87)$$

2.5.2.2 Axisymmetry

⁸³ In solids of revolution, we can use a polar coordinate system and

$$\varepsilon_{rr} = \frac{\partial u}{\partial r} \quad (2.88-a)$$

$$\varepsilon_{\theta\theta} = \frac{u}{r} \quad (2.88-b)$$

$$\varepsilon_{zz} = \frac{\partial w}{\partial z} \quad (2.88-c)$$

$$\varepsilon_{rz} = \frac{\partial u}{\partial z} + \frac{\partial w}{\partial r} \quad (2.88-d)$$

⁸⁴ The constitutive relation is again analogous to 3D/plane strain

$$\begin{Bmatrix} \sigma_{rr} \\ \sigma_{zz} \\ \sigma_{\theta\theta} \\ \tau_{rz} \end{Bmatrix} = \frac{E}{(1+\nu)(1-2\nu)} \begin{bmatrix} 1-\nu & \nu & \nu & 0 \\ \nu & 1-\nu & \nu & 0 \\ \nu & \nu & 1-\nu & 0 \\ 0 & 0 & 0 & \frac{1-2\nu}{2} \end{bmatrix} \begin{Bmatrix} \varepsilon_{rr} \\ \varepsilon_{zz} \\ \varepsilon_{\theta\theta} \\ \gamma_{rz} \end{Bmatrix} \quad (2.89)$$

2.5.2.3 Plane Stress

⁸⁵ If the longitudinal dimension in z direction is much smaller than in the x and y directions, then $\tau_{yz} = \tau_{xz} = \sigma_{zz} = \gamma_{xz} = \gamma_{yz} = 0$ throughout the thickness. Again, substituting into Eq. 2.84 we obtain:

$$\begin{Bmatrix} \sigma_{xx} \\ \sigma_{yy} \\ \tau_{xy} \end{Bmatrix} = \frac{1}{1-\nu^2} \begin{bmatrix} 1 & \nu & 0 \\ \nu & 1 & 0 \\ 0 & 0 & \frac{1-\nu}{2} \end{bmatrix} \begin{Bmatrix} \varepsilon_{xx} \\ \varepsilon_{yy} \\ \gamma_{xy} \end{Bmatrix} \quad (2.90-a)$$

$$\varepsilon_{zz} = -\frac{1}{1-\nu} \nu (\varepsilon_{xx} + \varepsilon_{yy}) \quad (2.90-b)$$

2.6 Airy Stress Function

⁸⁶ In elasticity problems we seek a function in terms of the spatial coordinates which can satisfy both the equilibrium and the compatibility equations. Airy has shown that we can define such a function $\Phi(\mathbf{x})$ such that:

$$\sigma_{11} = \frac{\partial^2 \Phi}{\partial x_2^2}; \quad \sigma_{22} = \frac{\partial^2 \Phi}{\partial x_1^2}; \quad \sigma_{12} = -\frac{\partial^2 \Phi}{\partial x_1 \partial x_2}; \quad (2.91)$$

⁸⁷ In polar coordinates:

$$\sigma_{rr} = \frac{1}{r} \frac{\partial \Phi}{\partial r} + \frac{1}{r^2} \frac{\partial^2 \Phi}{\partial \theta^2}; \quad \sigma_{\theta\theta} = \frac{\partial^2 \Phi}{\partial r^2}; \quad \sigma_{r\theta} = -\frac{\partial}{\partial r} \left(\frac{1}{r} \frac{\partial \Phi}{\partial \theta} \right) \quad (2.92)$$

It can be shown (by direct substitution of these equations in Eq. 2.71) that the equilibrium equation is automatically satisfied.

⁸⁸ For linear elastic isotropic materials, the satisfaction of the compatibility equation (Eq. 2.61) further requires that Φ must be such that

$$\nabla^2 (\nabla^2 \Phi) \equiv \left(\frac{\partial^2}{\partial x_1^2} + \frac{\partial^2}{\partial x_2^2} \right) \left(\frac{\partial^2 \Phi}{\partial x_1^2} + \frac{\partial^2 \Phi}{\partial x_2^2} \right) = \frac{\partial^4 \Phi}{\partial x_1^4} + 2 \frac{\partial^4 \Phi}{\partial x_1^2 \partial x_2^2} + \frac{\partial^4 \Phi}{\partial x_2^4} = 0 \quad (2.93)$$

where ∇^2 is the **Laplacian operator**. A solution to Laplace's equation is referred to as a **harmonic function**.

⁸⁹ In polar coordinates

$$\nabla^2 (\nabla^2 \Phi) = \left(\frac{\partial^2}{\partial r^2} + \frac{1}{r} \frac{\partial}{\partial r} + \frac{1}{r^2} \frac{\partial^2}{\partial \theta^2} \right) \left(\frac{\partial^2 \Phi}{\partial r^2} + \frac{1}{r} \frac{\partial \Phi}{\partial r} + \frac{1}{r^2} \frac{\partial^2 \Phi}{\partial \theta^2} \right) \quad (2.94)$$

⁹⁰ Thus, the Airy stress function will enable us to solve elasticity problems provided we can come up with the right choice for Φ which satisfies the natural boundary conditions (stresses).

2.7 Complex Variables

⁹¹ As will be shown in the next chapter, we can use Airy stress function with real variables to determine the stress field around a circular hole, however we need to extend Airy stress functions to complex variables in order to analyze: 1) stresses around an elliptical hole (Inglis), and stresses at the tip of a crack (Westergaard).

⁹² First we define the complex number z as:

$$z = x_1 + ix_2 = re^{i\theta} \quad (2.95)$$

where $i = \sqrt{-1}$, x_1 and x_2 are the cartesian coordinates, and r and θ are the polar coordinates.

⁹³ We further define an **analytic function**, $f(z)$ one which derivatives depend only on z . Applying the chain rule

$$\frac{\partial}{\partial x_1} f(z) = \frac{\partial}{\partial z} f(z) \frac{\partial z}{\partial x_1} = f'(z) \frac{\partial z}{\partial x_1} = f'(z) \quad (2.96-a)$$

$$\frac{\partial}{\partial x_2} f(z) = \frac{\partial}{\partial z} f(z) \frac{\partial z}{\partial x_2} = f'(z) \frac{\partial z}{\partial x_2} = if'(z) \quad (2.96-b)$$

⁹⁴ If $f(z) = \alpha + i\beta$ where α and β are real functions of x_1 and x_2 , and $f(z)$ is analytic, then from Eq. 2.96-a and 2.96-b we have:

$$\left. \begin{aligned} \frac{\partial f(z)}{\partial x_1} &= \frac{\partial \alpha}{\partial x_1} + i \frac{\partial \beta}{\partial x_1} = f'(z) \\ \frac{\partial f(z)}{\partial x_2} &= \frac{\partial \alpha}{\partial x_2} + i \frac{\partial \beta}{\partial x_2} = if'(z) \end{aligned} \right\} i \underbrace{\left(\frac{\partial \alpha}{\partial x_1} + i \frac{\partial \beta}{\partial x_1} \right)}_{1^{st} \text{ Equation}} = \underbrace{\frac{\partial \alpha}{\partial x_2} + i \frac{\partial \beta}{\partial x_2}}_{2^{nd} \text{ Equation}} \quad (2.97)$$

⁹⁵ Equating the real and imaginary parts yields the **Cauchy-Riemann** equations:

$$\frac{\partial \alpha}{\partial x_1} = \frac{\partial \beta}{\partial x_2}; \quad \frac{\partial \alpha}{\partial x_2} = -\frac{\partial \beta}{\partial x_1} \quad (2.98)$$

⁹⁶ If we differentiate those two equation, first with respect to x_1 , then with respect to x_2 , and then add them up we obtain

$$\frac{\partial^2 \alpha}{\partial x_1^2} + \frac{\partial^2 \alpha}{\partial x_2^2} = 0 \quad \text{or} \quad \nabla^2 (\alpha) = 0 \quad (2.99)$$

which is Laplace's equation.

⁹⁷ Similarly we can have:

$$\nabla^2 (\beta) = 0 \quad (2.100)$$

Hence both the real (α) and the imaginary part (β) of an analytic function will separately provide solution to Laplace's equation, and α and β are **conjugate harmonic functions**.

2.7.1 Complex Airy Stress Functions

98 It can be shown that any stress function can be expressed as

$$\Phi = \text{Re}[(x_1 - ix_2)\psi(z) + \chi(z)] \quad (2.101)$$

provided that both $\psi(z)$ (psi) and $\chi(z)$ (chi) are harmonic (i.e. $\nabla^2(\psi) = \nabla^2(\chi) = 0$) analytic functions of x_1 and x_2 . ψ and χ are often referred to as the Kolonov-Muskhelishvili complex potentials.

99 If $f(z) = \alpha + i\beta$ and both α and β are real, then its conjugate function is defined as:

$$\bar{f}(\bar{z}) = \alpha - i\beta \quad (2.102)$$

100 Note that conjugate functions should not be confused with the conjugate harmonic functions. Hence we can rewrite Eq. 2.101 as:

$$\Phi = \text{Re}[\bar{z}\psi(z) + \chi(z)] \quad (2.103)$$

101 Substituting Eq. 2.103 into Eq. 2.91, we can determine the stresses

$$\begin{aligned} \sigma_{11} + \sigma_{22} &= 4\text{Re}\psi'(z) \\ \sigma_{22} - \sigma_{11} + 2i\sigma_{12} &= 2[\bar{z}\psi''(z) + \chi''(z)] \end{aligned} \quad (2.104)$$

and by separation of real and imaginary parts we can then solve for $\sigma_{22} - \sigma_{11}$ & σ_{12} .

102 Displacements can be similarly obtained.

2.8 Curvilinear Coordinates

103 A variable $z = x_1 + ix_2$ in the cartesian coordinate system can be expressed as $re^{i\theta}$ in polar coordinate systems, and as $p = \alpha + i\beta$ in **curvilinear system**.

104 Next, we seek to solve for x_1 and x_2 in terms of α and β . The relationship between z and p is given by

$$z = c \cosh p \quad (2.105)$$

where c is a constant.

105 Recalling that

$$\cosh \alpha = \frac{1}{2}(e^\alpha + e^{-\alpha}) \quad (2.106-a)$$

$$\sinh \alpha = \frac{1}{2}(e^\alpha - e^{-\alpha}) \quad (2.106-b)$$

$$e^{i\beta} = \cos \beta + i \sin \beta \quad (2.106-c)$$

we substitute those equations into Eq. 2.105

$$\begin{aligned} x_1 + ix_2 &= \frac{c}{2} (e^{\alpha+i\beta} + e^{-\alpha-i\beta}) \\ &= \frac{c}{2} \left(\underbrace{e^\alpha \cos \beta + ie^\alpha \sin \beta}_{2 \cosh \alpha} + \underbrace{e^{-\alpha} \cos \beta - ie^{-\alpha} \sin \beta}_{2 \sinh \alpha} \right) \\ &= \cos \beta \underbrace{(e^\alpha + e^{-\alpha})}_{2 \cosh \alpha} + i \sin \beta \underbrace{(e^\alpha - e^{-\alpha})}_{2 \sinh \alpha} \\ &= c(\cosh \alpha \cos \beta + i \sinh \alpha \sin \beta) \end{aligned} \quad (2.107-a)$$

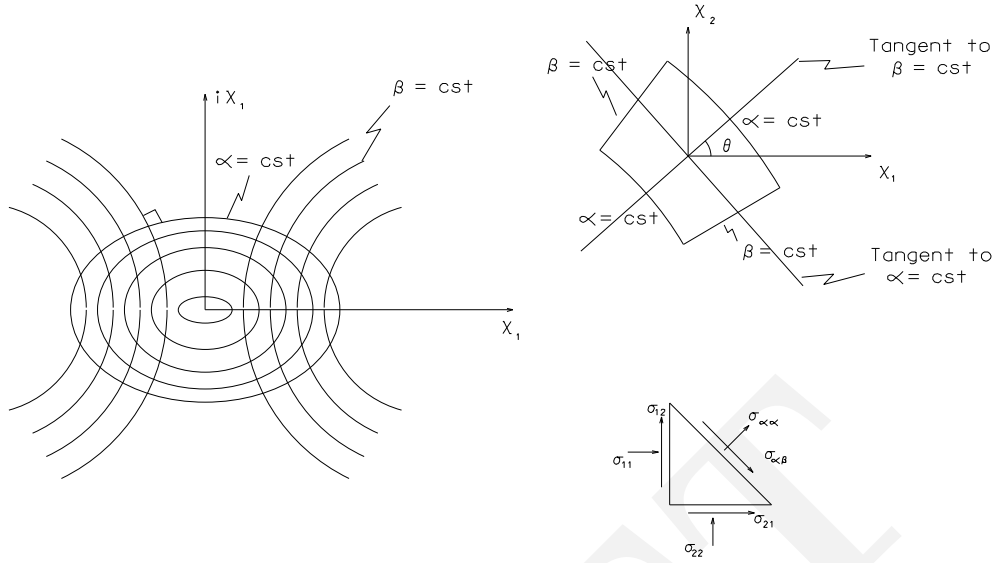


Figure 2.6: Curvilinear Coordinates

106 Separating reals from imaginary parts we obtain

$$\begin{aligned} x_1 &= c \cosh \alpha \cos \beta = \frac{c}{2} \cos \beta (e^\alpha + e^{-\alpha}) \\ x_2 &= c \sinh \alpha \sin \beta = \frac{c}{2} \sin \beta (e^\alpha - e^{-\alpha}) \end{aligned} \quad (2.108)$$

107 If we eliminate β from those equation, we obtain

$$\frac{x_1^2}{\cosh^2 \alpha} + \frac{x_2^2}{\sinh^2 \alpha} = c^2 \quad (2.109)$$

108 Thus for a constant value of α this represents the equation of an ellipse in the $x_1 - x_2$ plane. Similarly lines of constant β represent confocal hyperbolae which intersect the ellipse at right angle, Fig. 2.6.

109 In terms of complex potentials, it can be shown that the stresses are given in an analogous way as in Eq. 2.104:

$$\begin{aligned} \sigma_{\alpha\alpha} + \sigma_{\beta\beta} &= 2[\psi'(z) + \psi'(\bar{z})] = 4\text{Re}\psi'(z) \\ \sigma_{\beta\beta} - \sigma_{\alpha\alpha} + 2i\sigma_{\alpha\beta} &= 2e^{2i\theta}[\bar{z}\psi''(z) + \psi''(\bar{z})] \end{aligned} \quad (2.110)$$

Note that what we have here is a set of three equations in terms of three unknowns.

110 Individual stresses are obtained by separating the real from the imaginary components.

2.9 Basic Equations of Anisotropic Elasticity

111 An alternate form of Eq. 2.77 is

$$\varepsilon_i = a_{ij} \sigma_j \quad (2.111)$$

where the indices i and j go from 1 to 6.

112 In the most general case this would yield 36 independent constants a_{ij} , (Lekhnitskii, 1981), however by virtue of symmetry ($a_{ij} = a_{ji}$) this reduces to 21 $\binom{7+6}{2}$. If the material has one plane of elastic symmetry, then there would 13 independent constants; If it has three mutually orthogonal planes of elastic symmetry, then we would say that it is **orthogonally anisotropic**

or **orthotropic**, and we will have $a_{16} = a_{26} = a_{36} = a_{45} = 0$, thus there will be 9 independent constants.

$$\begin{Bmatrix} \varepsilon_1 \\ \varepsilon_2 \\ \varepsilon_3 \\ \varepsilon_4 \\ \varepsilon_5 \\ \varepsilon_6 \end{Bmatrix} = \begin{bmatrix} a_{11} & a_{12} & a_{13} & & & \\ & a_{22} & a_{23} & & & \\ & & a_{33} & & & \\ & & & a_{44} & & \\ & & & & a_{55} & \\ & & & & & a_{66} \end{bmatrix} \begin{Bmatrix} \sigma_1 \\ \sigma_2 \\ \sigma_3 \\ \sigma_4 \\ \sigma_5 \\ \sigma_6 \end{Bmatrix} \quad (2.112)$$

113 If the material is transversally isotropic then it will have 5 independent constants, Fig. 2.7,

$$\begin{Bmatrix} \varepsilon_1 \\ \varepsilon_2 \\ \varepsilon_3 \\ \varepsilon_4 \\ \varepsilon_5 \\ \varepsilon_6 \end{Bmatrix} = \begin{bmatrix} a_{11} & a_{12} & a_{13} & & & \\ & a_{11} & a_{13} & & & \\ & & a_{33} & & & \\ & & & 2(a_{11} - a_{12}) & & \\ & & & & a_{44} & \\ & & & & & a_{44} \end{bmatrix} \begin{Bmatrix} \sigma_1 \\ \sigma_2 \\ \sigma_3 \\ \sigma_4 \\ \sigma_5 \\ \sigma_6 \end{Bmatrix} \quad (2.113)$$

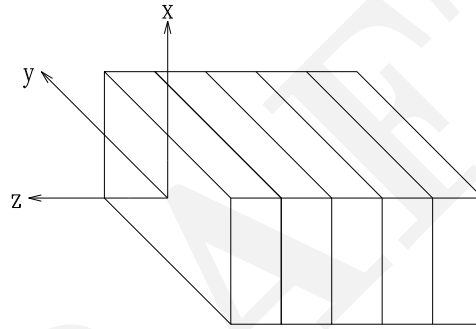


Figure 2.7: Transversely Isotropic Material

114 The total number of coefficients for different materials is summarized in Table 2.1.

Class of Material	Number of Non Zero Coeff.		Number of Indep. Coeff.	
	3D	2D	3D	2D
General Anisotropy	36	9	21	6
One plane of Symmetry	20	9	13	6
Orthotropic	12	5	9	4
Transversely Isotropic	12	5	5	4
Isotropic	12	5	2	2

Table 2.1: Number of Elastic Constants for Different Materials

115 In terms of engineering constants for an orthotropic solid we would have

$$\varepsilon_x = \frac{1}{E_1}\sigma_x - \frac{\nu_{21}}{E_2}\sigma_y - \frac{\nu_{31}}{E_3}\sigma_z \quad (2.114-a)$$

$$\varepsilon_y = -\frac{\nu_{12}}{E_1}\sigma_x + \frac{1}{E_2}\sigma_y - \frac{\nu_{32}}{E_3}\sigma_z \quad (2.114-b)$$

$$\varepsilon_z = -\frac{\nu_{13}}{E_1}\sigma_x - \frac{\nu_{23}}{E_2}\sigma_y + \frac{1}{E_3}\sigma_z \quad (2.114-c)$$

$$\gamma_{yz} = \frac{1}{\mu_{23}}\tau_{yz} \quad (2.114-d)$$

$$\gamma_{xz} = \frac{1}{\mu_{13}}\tau_{xz} \quad (2.114-e)$$

$$\gamma_{xy} = \frac{1}{\mu_{12}}\tau_{xy} \quad (2.114-f)$$

however, of the 12 elastic constants, only 9 are independent because the following relations

$$E_1\nu_{21} = E_2\nu_{12} \quad (2.115-a)$$

$$E_2\nu_{32} = E_3\nu_{23} \quad (2.115-b)$$

$$E_3\nu_{13} = E_1\nu_{31} \quad (2.115-c)$$

116 Note that the preceding equations are written for the principal directions of elasticity, x , y , and z in terms of the **principal elastic constants** (as opposed to constants in equations for an arbitrary system of coordinates).

117 Whereas very few natural or man-made materials are truly orthotropic (certain crystals as topaz are), a number of others are **transversely isotropic**. Transversely isotropic have through every point a plane in which all directions are equivalent with respect to elastic properties (such as in laminates, shist, quartz, roller compacted concrete, etc...). For transversely isotropic solids in 3D, we have

$$\varepsilon_x = a_{11}\sigma_x + a_{12}\sigma_y + a_{13}\sigma_z \quad (2.116-a)$$

$$\varepsilon_y = a_{12}\sigma_x + a_{11}\sigma_y + a_{13}\sigma_z \quad (2.116-b)$$

$$\varepsilon_z = a_{13}(\sigma_x + \sigma_y) + a_{33}\sigma_z \quad (2.116-c)$$

$$\gamma_{xy} = 2(a_{11} - a_{12})\tau_{xy} \quad (2.116-d)$$

$$\gamma_{yz} = a_{44}\tau_{yz} \quad (2.116-e)$$

$$\gamma_{xz} = a_{44}\tau_{xz} \quad (2.116-f)$$

and

$$a_{11} = \frac{1}{E}; \quad a_{12} = -\frac{\nu}{E}; \quad a_{13} = -\frac{\nu'}{E'}; \quad a_{33} = -\frac{1}{E'}; \quad a_{44} = -\frac{1}{\mu'} \quad (2.117)$$

118 Thus we have five elastic constants. Denoting by E the Young's modulus in the plane of isotropy and E' the one in the plane normal to it, we would have ν corresponds to the transverse contraction in the plane of isotropy when tension is applied in the plane; ν' corresponding to the transverse contraction in the plane of isotropy when tension is applied normal to the plane; μ' corresponding to the shear moduli for the plane of isotropy and any plane normal to it, and μ is shear moduli for the plane of isotropy.

2.9.1 Coordinate Transformations

119 If the elastic constants are to be determined for an arbitrary orientation 1-2, Fig. 2.8 then the compliance matrix is given by

$$[C'] = [\Gamma]^T [C] [\Gamma] \quad (2.118)$$

where $[\Gamma]$ is the usual second order tensor transformation for rotation in a plane.

$$[\Gamma] = \begin{bmatrix} \cos^2 \theta & \sin^2 \theta & 2 \sin \theta \cos \theta \\ \sin^2 \theta & \cos^2 \theta & -2 \sin \theta \cos \theta \\ -\sin \theta \cos \theta & \cos \theta \sin \theta & \cos^2 \theta - \sin^2 \theta \end{bmatrix} \quad (2.119)$$

120 Note that after transformation, a transversely isotropic material will not have anymore 5 nonzero coefficients, but 9 in (3-D).

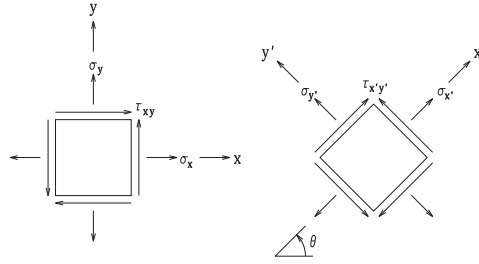


Figure 2.8: Coordinate Systems for Stress Transformations

2.9.2 Plane Stress-Strain Compliance Transformation

121 If we consider $\varepsilon_i = a_{ij}\sigma_j$ for plane strain and $\varepsilon_i = b_{ij}\sigma_j$ for plane stress then it can be shown that

$$b_{ij} = a_{ij} - \frac{a_{i3}a_{j3}}{a_{33}} \quad (2.120)$$

2.9.3 Stress Functions

122 The stress function $\Phi(x, y)$ can be written as

$$\Phi(x, y) = 2\text{Re}[\Phi_1(z_1) + \Phi_2(z_2)] \quad (2.121)$$

where $\Phi_1(z_1)$ is an arbitrary function of $z_1 = x + s_1y$ and $\Phi_2(z_2)$ is an arbitrary function of $z_2 = x + s_2y$

123 Note the analogy with $\phi = \text{Re}[(x_1 - ix_2)\psi(z) + \chi(z)]$ derived earlier for isotropic cases, Eq. 2.101, where ψ and χ were the Muskhelishvili complex potentials.

124 It can be shown that using the Airy stress function defined in Eq. 2.91 and combined with the compatibility Equation (Eq. 2.59) for anisotropic solids we obtain (neglecting body forces)

$$a_{22} \frac{\partial^4 \Phi}{\partial x^4} - 2a_{26} \frac{\partial^4 \Phi}{\partial x \partial y} + (2a_{12} + a_{66}) \frac{\partial^4 \Phi}{\partial x^2 \partial y^2} - 2a_{16} \frac{\partial^4 \Phi}{\partial x \partial y^3} + a_{11} \frac{\partial^4 \Phi}{\partial y^4} = 0 \quad (2.122)$$

125 For isotropic material this equation reduces to:

$$\frac{\partial^4 \Phi}{\partial x^4} + 2 \frac{\partial^4 \Phi}{\partial x^2 \partial y^2} + \frac{\partial^4 \Phi}{\partial y^4} = 0 \quad (2.123)$$

which is Eq. 2.93 as derived earlier.

126 The characteristic equation of this homogeneous partial differential equation is

$$a_{11}s^4 - 2a_{16}s^3 + (2a_{12} + a_{66})s^2 - 2a_{26}s + a_{22} = 0 \quad (2.124)$$

127 By energy considerations, Lekhnitskii, (Lekhnitskii, 1981) has shown that:

1. All roots are complex or purely imaginary for an ideally elastic body with $a_{11} \neq 0$, $2a_{12} + a_{66} \neq 0$, & $a_{22} \neq 0$
2. Only exceptions are:
 - a) $a_{22} = a_{26} = 0 \Rightarrow 2$ roots equal to zero
 - b) $a_{22} = a_{26} = 2a_{12} + a_{66} = a_{16} = 0 \Rightarrow$ all four roots are zero
 - c) $a_{11} = a_{16} = 0 \Rightarrow 2$ roots are infinite
 - d) $a_{11} = a_{16} = 2a_{12} + a_{66} = a_{26} = 0 \Rightarrow 4$ roots are infinite.

3. Two of the roots are conjugates of the two others: if we let

$$s_1 = \alpha_1 + i\beta_1 \quad s_2 = \alpha_2 + i\beta_2 \quad (2.125-a)$$

then

$$s_3 = \bar{s}_1 \quad s_4 = \bar{s}_2 \quad (2.126-a)$$

then β_1 & β_2 are both positive and $\beta_1 \neq \beta_2$

4. Two cases are possible:

- a) Roots are all different
- b) Roots are pairwise equal

5. For isotropic material

$$\alpha = 0 \quad (2.127-a)$$

$$\beta = 1 \quad (2.127-b)$$

$$s_1 = s_2 = i \quad (2.127-c)$$

$$\bar{s}_1 = \bar{s}_2 = -i \quad (2.127-d)$$

So s_1 and s_2 are complex parameters of first order of plane stress (or strain). They characterize the degree of anisotropy for plane problems. From it we can judge how much a body differs from isotropy.

6. If a material is orthotropic and x and y coincide with 1 and 2, then $a_{16} = a_{26} = 0$ and we have

$$s^4 + \left(\frac{E_1}{\mu} - 2\nu_1\right)s^2 + \frac{E_1}{E_2} = 0 \quad (2.128)$$

and

- a) $s_1 = \beta i$ & $s_2 = \delta i$; purely imaginary and unequal roots
- b) $s_1 = s_2 = \beta i$; complex and equal roots
- c) $s_1 = \alpha + \beta i$; $s_2 = -\alpha + \beta i$

7. In addition we have

$$s'_1 = \frac{s_2 \cos \psi - \sin \psi}{\cos \psi + s_1 \sin \psi} \quad (2.129-a)$$

$$s'_2 = \frac{s_1 \cos \psi - \sin \psi}{\cos \psi + s_2 \sin \psi} \quad (2.129-b)$$

8. Invariants for orthotropic bodies are

$$I_1 = a_{11} + a_{22} + 2a_{12} = \frac{1}{E_1} + \frac{1}{E_2} - \frac{2\nu_{12}}{E_1} \quad (2.130-a)$$

$$I_2 = a_{66} - 4a_{12} = \frac{1}{\mu_{12}} + \frac{4\nu_{12}}{E_1} \quad (2.130-b)$$

$$I_3 = a_{44} + a_{55} = \frac{1}{\mu_{13}} + \frac{1}{\mu_{23}} \quad (2.130-c)$$

$$I_4 = a_{13} + a_{23} = -\left(\frac{\nu_{13}}{E_1} + \frac{\nu_{23}}{E_2}\right) = -\frac{\nu_{31} + \nu_{32}}{E_2} \quad (2.130-d)$$

2.9.4 Stresses and Displacements

¹²⁸ If we define:

$$\phi_1(z_1) = \frac{d\Phi_1}{dz_1} \quad \text{and} \quad \phi_2(z_2) = \frac{d\Phi_2}{dz_2} \quad (2.131)$$

and using the definition of stress functions, the stresses are

$$\begin{cases} \sigma_x &= 2\text{Re}[s_1^2\phi_1'(z_1) + s_2^2\phi_2'(z_2)] \\ \sigma_y &= 2\text{Re}[\phi_1'(z_1) + \phi_2'(z_2)] \\ \tau_{xy} &= -2\text{Re}[s_1\phi_1'(z_1) + s_2\phi_2'(z_2)] \end{cases} \quad (2.132)$$

and the displacements are

$$\begin{cases} u &= 2\text{Re}[p_1\phi_1(z_1) + p_2\phi_2(z_2)] \\ v &= 2\text{Re}[q_1\phi_1(z_1) + q_2\phi_2(z_2)] \end{cases} \quad (2.133)$$

where

$$\begin{cases} p_i &= a_{11}s_i^2 + a_{12} - a_{16}s_i, \quad (i = 1, 2) \\ q_i &= a_{12}s_i + \frac{a_{22}}{s_i} - a_{26} \end{cases} \quad (2.134\text{-a})$$

2.10 Conclusion

¹²⁹ In summary, this chapter has provided the mathematical foundation required to develop the solutions of some “simple” problems which will be presented in the subsequent chapter.

Chapter 3

ELASTICITY BASED SOLUTIONS FOR CRACK PROBLEMS

3.1 Introduction

¹ This chapter will present mathematically rigorous derivations of some simple elasticity problems. All the theoretical basis required to follow those derivations have been covered in the previous chapter. A summary of problems to be investigated is shown in Table 3.1.

3.2 Circular Hole, (Kirsch, 1898)

² Analysing the infinite plate under uniform tension with a circular hole of diameter a , (Kirsch, 1898) and subjected to a uniform stress σ_0 , Fig. 3.1.

³ The peculiarity of this problem is that the far-field boundary conditions are better expressed in cartesian coordinates, whereas the ones around the hole should be written in polar coordinate system.

⁴ We will solve this problem by replacing the plate with a thick tube subjected to two different set of loads. The first one is a thick cylinder subjected to uniform radial pressure (solution of which is well known from *Strength of Materials*), the second one is a thick cylinder subjected to both radial and shear stresses which must be compatible with the traction applied on the rectangular plate.

⁵ First we select a stress function which satisfies the biharmonic Equation $\nabla^2 (\nabla^2 \Phi)$ (Eq. 2.93), and the far-field boundary conditions. From St Venant principle, away from the hole, the boundary conditions are given by:

$$\sigma_{xx} = \sigma_0; \quad \sigma_{yy} = \tau_{xy} = 0 \quad (3.1)$$

⁶ Recalling (Eq. 2.91) that $\sigma_{xx} = \frac{\partial^2 \Phi}{\partial y^2}$, this would suggest a stress function Φ of the form $\Phi = \sigma_0 y^2$. Alternatively, the presence of the circular hole would suggest a polar representation of Φ . Thus, substituting $y = r \sin \theta$ would result in $\Phi = \sigma_0 r^2 \sin^2 \theta$.

⁷ Since $\sin^2 \theta = \frac{1}{2}(1 - \cos 2\theta)$, we could simplify the stress function into

$$\Phi = f(r) \cos 2\theta \quad (3.2)$$

⁸ Substituting this function into the biharmonic equation (Eq. 2.94) yields

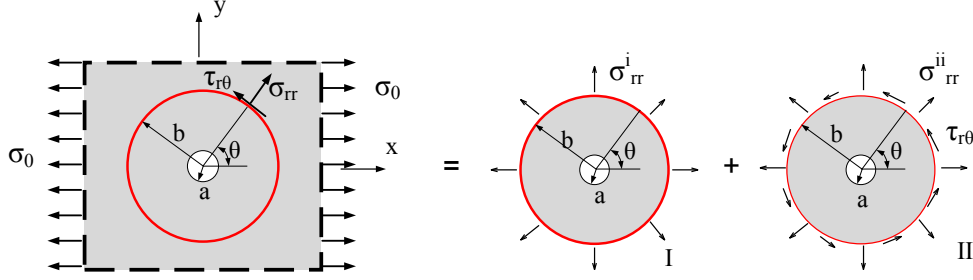
$$\left(\frac{\partial^2}{\partial r^2} + \frac{1}{r} \frac{\partial}{\partial r} + \frac{1}{r^2} \frac{\partial^2}{\partial \theta^2} \right) \left(\frac{\partial^2 \Phi}{\partial r^2} + \frac{1}{r} \frac{\partial \Phi}{\partial r} + \frac{1}{r^2} \frac{\partial^2 \Phi}{\partial \theta^2} \right) = 0 \quad (3.3-a)$$

$$\left(\frac{d^2}{dr^2} + \frac{1}{r} \frac{d}{dr} - \frac{4}{r^2} \right) \left(\frac{d^2 f}{dr^2} + \frac{1}{r} \frac{df}{dr} - \frac{4f}{r^2} \right) = 0 \quad (3.3-b)$$

(note that the $\cos 2\theta$ term is dropped)

Problem	Coordinate System	Real/Complex	Solution	Date
Circular Hole	Polar	Real	Kirsch	1898
Elliptical Hole	Curvilinear	Complex	Inglis	1913
Crack	Cartesian	Complex	Westergaard	1939
V Notch	Polar	Complex	Willimas	1952
Dissimilar Materials	Polar	Complex	Williams	1959
Anisotropic Materials	Cartesian	Complex	Sih	1965

Table 3.1: Summary of Elasticity Based Problems Analysed


 Figure 3.1: Circular Hole in an Infinite Plate **need to correct alignment of x**

9 The general solution of this ordinary linear fourth order differential equation is

$$f(r) = Ar^2 + Br^4 + C\frac{1}{r^2} + D \quad (3.4)$$

thus the stress function becomes

$$\Phi = \left(Ar^2 + Br^4 + C\frac{1}{r^2} + D \right) \cos 2\theta \quad (3.5)$$

10 Next, we must determine the four constants A , B , C , and D by applying four boundary conditions. Using Eq. 2.92, the stresses are given by

$$\begin{aligned} \sigma_{rr} &= \frac{1}{r} \frac{\partial \Phi}{\partial r} + \frac{1}{r^2} \frac{\partial^2 \Phi}{\partial \theta^2} = -\left(2A + \frac{6C}{r^4} + \frac{4D}{r^2} \right) \cos 2\theta \\ \sigma_{\theta\theta} &= \frac{\partial^2 \Phi}{\partial r^2} = \left(2A + 12Br^2 + \frac{6C}{r^4} \right) \cos 2\theta \\ \tau_{r\theta} &= -\frac{\partial}{\partial r} \left(\frac{1}{r} \frac{\partial \Phi}{\partial \theta} \right) = \left(2A + 6Br^2 - \frac{6C}{r^4} - \frac{2D}{r^2} \right) \sin 2\theta \end{aligned} \quad (3.6)$$

11 Next we seek to solve for the four constants of integration by applying the boundary conditions. We will identify two sets of boundary conditions:

1. Around outer boundaries: around an infinitely large circle of radius b inside a plate subjected to uniform stress σ_0 , the stresses in polar coordinates are obtained from *Strength of Materials*

$$\begin{bmatrix} \sigma_{rr} & \sigma_{r\theta} \\ \sigma_{r\theta} & \sigma_{\theta\theta} \end{bmatrix} = \begin{bmatrix} \cos \theta & -\sin \theta \\ \sin \theta & \cos \theta \end{bmatrix} \begin{bmatrix} \sigma_0 & 0 \\ 0 & 0 \end{bmatrix} \begin{bmatrix} \cos \theta & -\sin \theta \\ \sin \theta & \cos \theta \end{bmatrix}^T \quad (3.7)$$

yielding (recalling that $\sin^2 \theta = 1/2 \sin 2\theta$, and $\cos^2 \theta = 1/2(1 + \cos 2\theta)$).

$$(\sigma_{rr})_{r=b} = \sigma_0 \cos^2 \theta = \frac{1}{2} \sigma_0 (1 + \cos 2\theta) \quad (3.8-a)$$

$$(\sigma_{r\theta})_{r=b} = \frac{1}{2} \sigma_0 \sin 2\theta \quad (3.8-b)$$

$$(\sigma_{\theta\theta})_{r=b} = \frac{\sigma_0}{2} (1 - \cos 2\theta) \quad (3.8-c)$$

For reasons which will become apparent later, it is more convenient to decompose the state of stress given by Eq. 3.8-a and 3.8-b, into state I and II:

$$(\sigma_{rr})_{r=b}^I = \frac{1}{2} \sigma_0 \quad (3.9-a)$$

$$(\sigma_{r\theta})_{r=b}^I = 0 \quad (3.9-b)$$

$$(\sigma_{rr})_{r=b}^{II} = \frac{1}{2} \sigma_0 \cos 2\theta \quad \leftarrow \quad (3.9-c)$$

$$(\sigma_{r\theta})_{r=b}^{II} = \frac{1}{2} \sigma_0 \sin 2\theta \quad \leftarrow \quad (3.9-d)$$

Where state I corresponds to a thick cylinder with external pressure applied on $r = b$ and of magnitude $\sigma_0/2$. Hence, only the last two equations will provide us with boundary conditions.

2. Around the innerhole: the stresses should be equal to zero:

$$(\sigma_{rr})_{r=a} = 0 \quad \leftarrow \quad (3.10-a)$$

$$(\sigma_{r\theta})_{r=a} = 0 \quad \leftarrow \quad (3.10-b)$$

12 Upon substitution in Eq. 3.6 the four boundary conditions (Eq. 3.9-c, 3.9-d, 3.10-a, and 3.10-b) become

$$-\left(2A + \frac{6C}{b^4} + \frac{4D}{b^2}\right) = \frac{1}{2}\sigma_0 \quad (3.11-a)$$

$$\left(2A + 6Bb^2 - \frac{6C}{b^4} - \frac{2D}{b^2}\right) = \frac{1}{2}\sigma_0 \quad (3.11-b)$$

$$-\left(2A + \frac{6C}{a^4} + \frac{4D}{a^2}\right) = 0 \quad (3.11-c)$$

$$\left(2A + 6Ba^2 - \frac{6C}{a^4} - \frac{2D}{a^2}\right) = 0 \quad (3.11-d)$$

13 Solving for the four unknowns, and taking $\frac{a}{b} = 0$ (i.e. an infinite plate), we obtain:

$$A = -\frac{\sigma_0}{4}; \quad B = 0; \quad C = -\frac{a^4}{4}\sigma_0; \quad D = \frac{a^2}{2}\sigma_0 \quad (3.12)$$

14 To this solution, we must superimpose the one of a thick cylinder subjected to a uniform radial traction $\sigma_0/2$ on the outer surface (solution I), and with b much greater than a (Eq. 3.9-a and 3.9-b. These stresses are obtained from *Strength of Materials* yielding for this problem (careful about the sign)

$$\sigma_{rr} = \frac{\sigma_0}{2} \left(1 - \frac{a^2}{r^2}\right) \quad (3.13-a)$$

$$\sigma_{\theta\theta} = \frac{\sigma_0}{2} \left(1 + \frac{a^2}{r^2}\right) \quad (3.13-b)$$

15 Thus, substituting Eq. 3.11-a- into Eq. 3.6, we obtain

$$\sigma_{rr} = \frac{\sigma_0}{2} \left(1 - \frac{a^2}{r^2}\right) + \left(1 + 3\frac{a^4}{r^4} - \frac{4a^2}{r^2}\right) \frac{1}{2}\sigma_0 \cos 2\theta \quad (3.14-a)$$

$$\sigma_{\theta\theta} = \frac{\sigma_0}{2} \left(1 + \frac{a^2}{r^2}\right) - \left(1 + \frac{3a^4}{r^4}\right) \frac{1}{2}\sigma_0 \cos 2\theta \quad (3.14-b)$$

$$\sigma_{r\theta} = -\left(1 - \frac{3a^4}{r^4} + \frac{2a^2}{r^2}\right) \frac{1}{2}\sigma_0 \sin 2\theta \quad (3.14-c)$$

16 We observe that as $r \rightarrow \infty$, both σ_{rr} and $\sigma_{r\theta}$ are equal to the values given in Eq. 3.8-a and 3.8-b respectively.

17 Alternatively, at the edge of the hole when $r = a$ we obtain

$$\boxed{\begin{array}{l} \sigma_{rr} = 0 \\ \sigma_{r\theta} = 0 \\ \sigma_{\theta\theta}|_{r=a} = \sigma_0(1 - 2\cos 2\theta) \end{array}} \quad (3.15)$$

which for $\theta = \frac{\pi}{2}$ and $\frac{3\pi}{2}$ gives a stress concentration factor (SCF) of 3. For $\theta = 0$ and $\theta = \pi$, $\sigma_{\theta\theta} = -\sigma_0$.

3.3 Elliptical hole in a Uniformly Stressed Plate (Inglis, 1913)

18 Next we consider the problem of an elliptical hole in an infinite plate under uniform stress, Fig. 3.2. Adopting the curvilinear coordinate system described in sect. 2.8, we define a and b as the major and minor semi-axes respectively. The elliptical hole is itself defined along $\alpha = \alpha_0$, and as we go around the ellipse β varies from 0 to 2π .

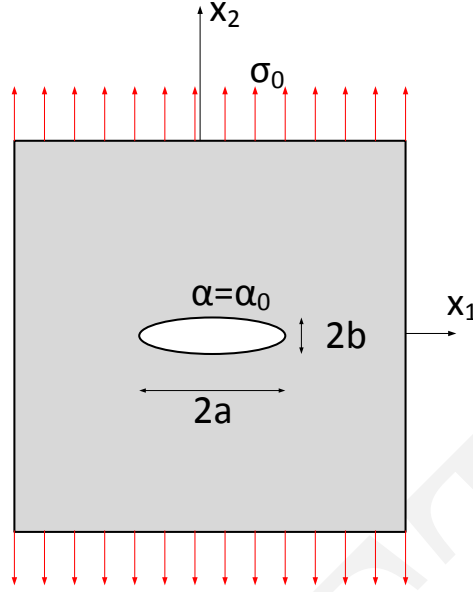


Figure 3.2: Elliptical Hole in an Infinite Plate

19 We need to relate a and b to α and β , thus we substitute $\beta = 0$ and $\beta = \frac{\pi}{2}$ in

$$x_1 = c \cosh \alpha \cos \beta = \frac{c}{2} \cos \beta (e^\alpha + e^{-\alpha}) \quad (3.16)$$

(Eq. 2.108) and we obtain

$$x_1|_{\beta=0; \alpha=\alpha_0} = a = c \cosh \alpha \cos \beta = c \cosh \alpha_0 \Rightarrow a = c \cosh \alpha_0 \quad (3.17-a)$$

$$x_2|_{\beta=\pi/2; \alpha=\alpha_0} = b = c \sinh \alpha \sin \beta = c \sinh \alpha_0 \Rightarrow b = c \sinh \alpha_0 \quad (3.17-b)$$

respectively.

20 We then seek to apply the boundary conditions in an analogous manner as we did for the circular hole problem:

1. At infinity we have $\sigma_{22} = \sigma_0$ and $\sigma_{11} = \sigma_{12} = 0$. Thus, substituting into Eq. 2.104 we obtain

$$\sigma_{11} + \sigma_{22} = 4\text{Re}\psi'(z) = \sigma_0 \quad (3.18-a)$$

$$\sigma_{22} - \sigma_{11} + 2i\sigma_{12} = 2[\bar{z}\psi''(z) + \chi''(z)] = \sigma_0 \quad (3.18-b)$$

2. Around the elliptical hole ($\alpha = \alpha_0$) we have $\sigma_{\alpha\alpha} = \sigma_{\alpha\beta} = 0$

21 Inglis found that the following complex potentials satisfy the boundary conditions, and are periodic in β (period of 2π)

$$4\psi(z) = \sigma_0 c [(1 + e^{2\alpha_0}) \sinh p - e^{2\alpha_0} \cosh p] \quad (3.19-a)$$

$$4\chi(z) = -\sigma_0 c^2 \left[(\cosh 2\alpha_0 - \cosh \pi) p + \frac{1}{2} e^{2\alpha_0} - \cosh 2 \left(p - \alpha_0 - i \frac{\pi}{2} \right) \right] \quad (3.19-b)$$

where $p = \alpha + i\beta$

22 Since $\sigma_{\alpha\alpha} = 0$ for $\alpha = \alpha_0$, we can solve for $\sigma_{\beta\beta}$ from Eq. 2.110

$$\underbrace{\sigma_{\alpha\alpha}}_0 + \sigma_{\beta\beta} = 2[\psi'(z) + \bar{\psi}'(\bar{z})] \quad (3.20)$$

thus differentiating

$$(\sigma_{\beta\beta})_{\alpha=\alpha_0} = \frac{\sinh 2\alpha_0 - 1 + e^{2\alpha_0} \cos 2\beta}{\cosh 2\alpha_0 - \cos 2\beta} \sigma_0 \quad (3.21)$$

²³ But we need to express $\sigma_{\beta\beta}$ in terms of a and b rather than α_0 . The maximum value of $\sigma_{\beta\beta}$ occurs at the end of the ellipse where $\beta = 0$ or π . For those points we have $\cos 2\beta = 1$, and since the tangent to the ellipse is now parallel to x_2 we have:

$$(\sigma_{\beta\beta})_{\alpha=\alpha_0}^{\beta=0,\pi} = \sigma_{22} = \frac{\sinh 2\alpha_0 - 1 + e^{2\alpha_0}}{\cosh 2\alpha_0 - 1} \sigma_0 \quad (3.22)$$

²⁴ We now have a solution for the stress at the tip of the ellipse. However it is expressed in curvilinear coordinates, and we shall rewrite this expression in terms of a and b . Combining Eq. 3.17-a and 3.17-b with

$$\cosh^2 \alpha - \sinh^2 \alpha = 1 \quad (3.23)$$

we obtain

$$c^2 = a^2 - b^2 \quad (3.24)$$

²⁵ The following relations

$$\cosh 2\alpha_0 = 2 \cosh^2 \alpha_0 - 1 \quad (3.25-a)$$

$$\sinh 2\alpha_0 = 2 \sinh \alpha_0 \cosh \alpha_0 \quad (3.25-b)$$

when combined with $\cosh \alpha_0 = \frac{a}{c}$ and $\sinh \alpha_0 = \frac{b}{c}$ yield

$$\sinh 2\alpha_0 = \frac{2ab}{c^2} \quad (3.26-a)$$

$$\cosh 2\alpha_0 = \frac{a^2 + b^2}{c^2} \quad (3.26-b)$$

²⁶ Finally, substituting those two equations into Eq. 3.22

$$\boxed{(\sigma_{\beta\beta})_{\alpha=\alpha_0}^{\beta=0,\pi} = \sigma_0 \left(1 + 2\frac{a}{b}\right)} \quad (3.27)$$

²⁷ We observe that for $a = b$, we recover the stress concentration factor of 3 of a circular hole, and that for a degenerated ellipse, i.e a crack there is an infinite stress.

²⁸ Alternatively, let ρ be the radius of curvature of a parametric curve. From analytical geometry,

$$\rho^2 = \frac{(dx_1^2 + dx_2^2)^3}{(dx_1 d^2 x_2 - dx_2 d^2 x_1)^2} \quad (3.28)$$

Using a parametric representation, we can define $x_1 = a \cos t$ and $x_2 = b \sin t$; substituting into the above equation gives:

$$\rho^2 = \frac{1}{a^2 b^2} (a^2 \sin^2 t + b^2 \cos^2 t)^3 \quad (3.29)$$

At the tip of the ellipse $x_2 = 0$ and $x_1 = \pm a$. Thus, $\sin t = 0$ and $\cos t = 1$, and ρ becomes equal to $\rho = \frac{b^2}{a}$. Substituting into Eq. 3.27

$$\boxed{(\sigma_{\beta\beta})_{\alpha=\alpha_0}^{\beta=0,\pi} = \sigma_0 \left(1 + 2\sqrt{\frac{a}{\rho}}\right)} \quad (3.30)$$

From this equation, we note that the stress concentration factor is inversely proportional to the radius of curvature of an opening.

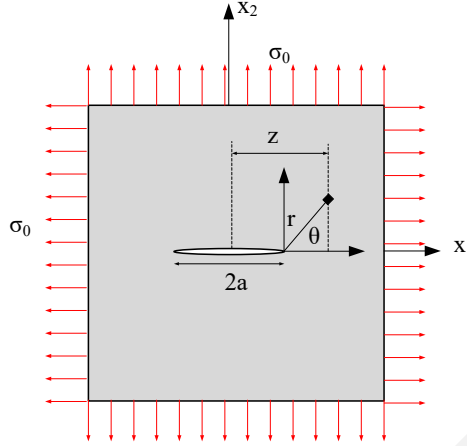


Figure 3.3: Crack in an Infinite Plate

3.4 Crack, (Westergaard, 1939)

²⁹ Just as both Kolosoff (1910) and Inglis (1913) independently solved the problem of an elliptical hole, there are two classical solutions for the crack problem. The first one was proposed by Westergaard, and the later by Williams. Whereas the first one is simpler to follow, the second has the advantage of being extended to cracks at the interface of two different homogeneous isotropic materials and be applicable for V notches.

³⁰ Let us consider an infinite plate subjected to uniform biaxial stress σ_0 with a central crack of length $2a$, Fig. 3.3. From Inglis solution, we know that there would be a theoretically infinite stress at the tip of the crack, however neither the nature of the singularity nor the stress field can be derived from it.

³¹ Westergaard's solution, (Westergaard, 1939b) starts by assuming $\Phi(z)$ as a harmonic function (thus satisfying Laplace's equation $\nabla^2(\Phi) = 0$). Denoting by $\phi'(z)$ and $\phi''(z)$ the first and second derivatives respectively, and $\bar{\phi}(z)$ and $\bar{\bar{\phi}}(z)$ its first and second integrals respectively of the function $\phi(z)$.

³² Westergaard has postulated that

$$\Phi = \text{Re}\bar{\bar{\phi}}(z) + x_2 \text{Im}\bar{\phi}(z) \quad (3.31)$$

is a solution to the crack problem¹. $\phi(z)$ is assumed to be analytic.

³³ Let us verify that Φ satisfies the biharmonic equation. Taking the first derivatives, and recalling from from Eq. 2.96-a that $\frac{\partial}{\partial x_1} f(z) = f'(z)$, we have

$$\frac{\partial \Phi}{\partial x_1} = \frac{\partial}{\partial x_1} \left(\text{Re} \bar{\bar{\phi}} \right) + \left[x_2 \frac{\partial}{\partial x_1} \text{Im} \bar{\phi}(z) + \text{Im} \bar{\phi}(z) \underbrace{\frac{\partial x_2}{\partial x_1}}_0 \right] \quad (3.32\text{-a})$$

$$= \text{Re} \bar{\phi}(z) + x_2 \text{Im} \phi(z) \quad (3.32\text{-b})$$

$$\sigma_{22} = \frac{\partial^2 \Phi}{\partial x_1^2} = \frac{\partial}{\partial x_1} \left(\text{Re} \bar{\phi}(z) \right) + \left[x_2 \frac{\partial}{\partial x_1} \text{Im} \phi(z) + \text{Im} \phi(z) \frac{\partial x_2}{\partial x_1} \right] \quad (3.32\text{-c})$$

$$= \text{Re} \phi'(z) + x_2 \text{Im} \phi'(z) \quad (3.32\text{-d})$$

¹Note that we should not confuse the Airy stress function Φ with the complex function $\phi(z)$.

Similarly, differentiating with respect to x_2 , and recalling from Eq. 2.96-b that $\frac{\partial}{\partial x_2} f(z) = if'(z)$, we obtain

$$\frac{\partial \Phi}{\partial x_2} = \frac{\partial}{\partial x_2} (\text{Re}\bar{\phi}(z) + [x_2 \frac{\partial}{\partial x_2} (\text{Im}\bar{\phi}(z)) + \frac{\partial x_2}{\partial x_2} \text{Im}\bar{\phi}(z)]) \quad (3.33-a)$$

$$= -\text{Im}\bar{\phi}(z) + x_2 \text{Re}\phi(z) + \text{Im}\bar{\phi}(z) \quad (3.33-b)$$

$$\sigma_{11} = \frac{\partial^2 \Phi}{\partial x_2^2} = x_2 \frac{\partial}{\partial x_2} \text{Re}\phi(z) + \text{Re}\phi(z) \frac{\partial x_2}{\partial x_2} \quad (3.33-c)$$

$$= -x_2 \text{Im}\phi'(z) + \text{Re}\phi(z) \quad (3.33-d)$$

Similarly, it can be shown that

$$\sigma_{12} = -\frac{\partial^2 \Phi}{\partial x_1 \partial x_2} = -x_2 \text{Re}\phi'(z) \quad (3.34)$$

Having derived expressions for the stresses and the second partial derivatives of Φ , substituting into Eq. 2.93, it can be shown that the biharmonic equation is satisfied, thus Φ is a valid solution.

³⁴ If we want to convince ourselves that the stresses indeed satisfy both the equilibrium and compatibility equations (which they do by virtue of Φ satisfying the bi-harmonic equation), we have from Eq. 2.71 in 2D:

1. Equilibrium:

$$\frac{\partial \sigma_{11}}{\partial x_1} + \frac{\partial \sigma_{12}}{\partial x_2} = 0 \quad (3.35-a)$$

$$\frac{\partial \sigma_{22}}{\partial x_2} + \frac{\partial \sigma_{12}}{\partial x_1} = 0 \quad (3.35-b)$$

Let us consider the first equation

$$\frac{\partial \sigma_{11}}{\partial x_1} = \frac{\partial}{\partial x_1} \left(\frac{\partial^2 \Phi}{\partial x_2^2} \right) = \frac{\partial}{\partial x_1} [\text{Re}\phi(z) - x_2 \text{Im}\phi'(z)] \quad (3.36-a)$$

$$= \text{Re}\phi'(z) - x_2 \text{Im}\phi''(z) \quad (3.36-b)$$

$$\frac{\partial \sigma_{12}}{\partial x_2} = \frac{\partial}{\partial x_2} \left(\frac{\partial^2 \Phi}{\partial x_1 \partial x_2} \right) = \frac{\partial}{\partial x_2} [-x_2 \text{Re}\phi'(z)] \quad (3.36-c)$$

$$= -\text{Re}\phi'(z) + x_2 \frac{\partial}{\partial x_1} \text{Im}\phi'(z) \quad (3.36-d)$$

$$= -\text{Re}\phi'(z) + x_2 \text{Im}\phi''(z) \quad (3.36-e)$$

If we substitute those two equations into Eq. 3.35-a then we do obtain zero. Similarly, it can be shown that Eq. 3.35-b is satisfied.

2. Compatibility: In plane strain, displacements are given by

$$2\mu u_1 = (1 - 2\nu) \text{Re}\bar{\phi}(z) - x_2 \text{Im}\phi(z) \quad (3.37-a)$$

$$2\mu u_2 = 2(1 - \nu) \text{Im}\bar{\phi}(z) - x_2 \text{Re}\phi(z) \quad (3.37-b)$$

and are obtained by integration of the strains, which in turn are obtained from the stresses. As a check we compute

$$2\mu \varepsilon_{11} = \frac{\partial u_1}{\partial x_1} \quad (3.38-a)$$

$$= (1 - 2\nu) \text{Re}\phi(z) - x_2 \text{Im}\phi'(z) \quad (3.38-b)$$

$$= (1 - \nu) \underbrace{[\text{Re}\phi(z) - x_2 \text{Im}\phi'(z)]}_{\sigma_{11}} - \nu \underbrace{[\text{Re}\phi(z) + x_2 \text{Im}\phi'(z)]}_{\sigma_{22}} \quad (3.38-c)$$

$$= (1 - \nu) \sigma_{11} - \nu \sigma_{22} \quad (3.38-d)$$

Recalling that

$$\mu = \frac{E}{2(1 + \nu)} \quad (3.39)$$

then

$$E\varepsilon_{11} = (1 - \nu^2)\sigma_{11} - \nu(1 + \nu)\sigma_{22} \quad (3.40)$$

this shows that $E\varepsilon_{11} = \sigma_{11} - \nu(\sigma_{22} - \sigma_{33})$, and for plane strain, $\varepsilon_{33} = 0 \Rightarrow \sigma_{33} = \nu(\sigma_{11} + \sigma_{22})$ and $E\varepsilon_{11} = (1 - \nu^2)\sigma_{11} - \nu(1 + \nu)\sigma_{22}$

³⁵ So far Φ was defined independently of the problem, and we simply determined the stresses in terms of it, and verified that the bi-harmonic equation was satisfied.

³⁶ Next, we must determine ϕ such that the boundary conditions are satisfied. For reasons which will become apparent later, we generalize our problem to one in which we have a biaxial state of stress applied on the plate. Hence:

1. Along the crack: at $x_2 = 0$ and $-a < x_1 < a$ we have $\sigma_{22} = 0$ (traction free crack).
2. At infinity: at $x_2 = \pm\infty$, $\sigma_{22} = \sigma_0$

We note from Eq. 3.32-d that at $x_2 = 0$, σ_{22} reduces to

$$(\sigma_{22})_{x_2=0} = \text{Re}\phi(z) \quad (3.41)$$

³⁷ Furthermore, we expect $\sigma_{22} \rightarrow \sigma_0$ as $x_1 \rightarrow \infty$, and σ_{22} to be greater than σ_0 when $|x_1 - a| > \epsilon$ (due to anticipated singularity predicted by Inglis), thus a possible choice for σ_{22} would be $\sigma_{22} = \frac{\sigma_0}{1 - \frac{a}{x_1}}$, for symmetry, this is extended to $\sigma_{22} = \frac{\sigma_0}{1 - \frac{a^2}{x_1^2}}$.

However, we also need to have $\sigma_{22} = 0$ when $x_2 = 0$ and $-a < x_1 < a$, thus the function $\phi(z)$ should become imaginary along the crack, and

$$\sigma_{22} = \text{Re} \left(\frac{\sigma_0}{\sqrt{1 - \frac{a^2}{x_1^2}}} \right) \quad (3.42)$$

³⁸ Thus from Eq. 3.41 we have (note the transition from x_1 to z).

$$\phi(z) = \frac{\sigma_0}{\sqrt{1 - \frac{a^2}{z^2}}} \quad (3.43)$$

³⁹ If we perform a change of variable and define $\eta = z - a = re^{i\theta}$ and assuming $\frac{\eta}{a} \ll 1$, and recalling that $e^{i\theta} = \cos \theta + i \sin \theta$, then the first term of Eq. 3.32-d can be rewritten as

$$\begin{aligned} \text{Re}\phi(z) &= \text{Re} \frac{\sigma_0}{\sqrt{\frac{\eta^2 + 2a\eta}{\eta^2 + a^2 + 2a\eta}}} \approx \text{Re} \frac{\sigma_0}{\sqrt{\frac{2a\eta}{a^2}}} \\ &\approx \text{Re}\sigma_0 \sqrt{\frac{a}{2\eta}} \approx \text{Re}\sigma_0 \sqrt{\frac{a}{2re^{i\theta}}} \approx \text{Re}\sigma_0 \sqrt{\frac{a}{2r}} e^{-i\frac{\theta}{2}} \approx \sigma_0 \sqrt{\frac{a}{2r}} \cos \frac{\theta}{2} \end{aligned} \quad (3.44-a)$$

⁴⁰ Recalling that $\sin 2\theta = 2 \sin \theta \cos \theta$ and that $e^{-i\theta} = \cos \theta - i \sin \theta$, we substitute $x_2 = r \sin \theta$ into the second term

$$x_2 \text{Im}\phi' = r \sin \theta \text{Im} \frac{\sigma_0}{2} \sqrt{\frac{a}{2(re^{i\theta})^3}} = \sigma_0 \sqrt{\frac{a}{2r}} \sin \frac{\theta}{2} \cos \frac{\theta}{2} \sin \frac{3\theta}{2} \quad (3.45)$$

⁴¹ Combining the above equations, with Eq. 3.32-d, 3.33-d, and 3.34 we obtain

$$\begin{cases} \sigma_{22} = \sigma_0 \sqrt{\frac{a}{2r}} \cos \frac{\theta}{2} \left(1 + \sin \frac{\theta}{2} \sin \frac{3\theta}{2} \right) + \dots \\ \sigma_{11} = \sigma_0 \sqrt{\frac{a}{2r}} \cos \frac{\theta}{2} \left(1 - \sin \frac{\theta}{2} \sin \frac{3\theta}{2} \right) + \dots \\ \sigma_{12} = \sigma_0 \sqrt{\frac{a}{2r}} \sin \frac{\theta}{2} \cos \frac{\theta}{2} \cos \frac{3\theta}{2} + \dots \end{cases} \quad (3.46)$$

⁴² Recall that this was the biaxial case, the uniaxial case may be reproduced by superimposing a pressure in the x_1 direction equal to $-\sigma_0$, however this should not affect the stress field close to the crack tip.

⁴³ Using a similar approach, we can derive expressions for the stress field around a crack tip in a plate subjected to far field shear stresses (mode II as defined later) using the following expression of ϕ

$$\Phi_{II}(z) = -x_2 \text{Re} \bar{\phi}_{II}(z) \Rightarrow \phi_{II} = \frac{\tau}{\sqrt{1 - \frac{a^2}{z^2}}} \quad (3.47)$$

and for the same crack but subjected to antiplane shear stresses (mode III)

$$\Phi'_{III}(z) = \frac{\sigma_{13}}{\sqrt{1 - \frac{a^2}{z^2}}} \quad (3.48)$$

3.4.1 Stress Intensity Factors (Irwin)

⁴⁴ Irwin² (Irwin, 1957) introduced the concept of *stress intensity factor* defined as:

$$\left\{ \begin{array}{l} K_I \\ K_{II} \\ K_{III} \end{array} \right\} = \lim_{r \rightarrow 0, \theta=0} \sqrt{2\pi r} \left\{ \begin{array}{l} \sigma_{22} \\ \sigma_{12} \\ \sigma_{23} \end{array} \right\} \quad (3.49)$$

where σ_{ij} are the near crack tip stresses, and K_i are associated with three independent kinematic movements of the upper and lower crack surfaces with respect to each other, as shown in Fig. 3.4:

- *Opening Mode, I:* The two crack surfaces are pulled apart in the y direction, but the deformations are symmetric about the $x - z$ and $x - y$ planes.
- *Shearing Mode, II:* The two crack surfaces slide over each other in the x -direction, but the deformations are symmetric about the $x - y$ plane and skew symmetric about the $x - z$ plane.
- *Tearing Mode, III:* The crack surfaces slide over each other in the z -direction, but the deformations are skew symmetric about the $x - y$ and $x - z$ planes.

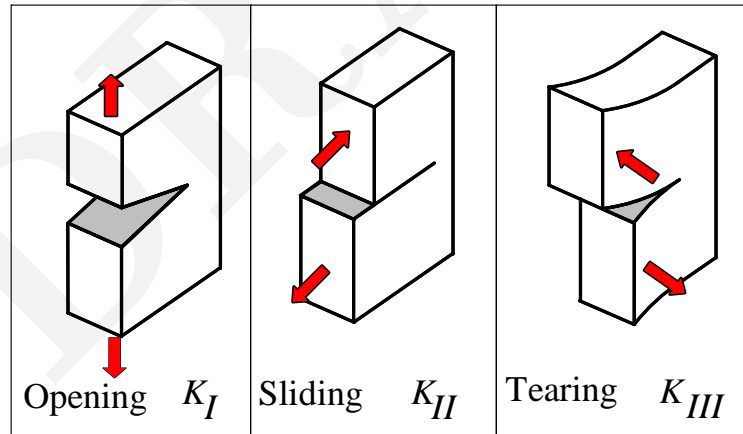


Figure 3.4: Independent Modes of Crack Displacements

⁴⁵ From Eq. 3.46, 3.46 and 3.46 with $\theta = 0$, we have

$$\begin{aligned} K_I &= \sqrt{2\pi r} \sigma_{22} \\ &= \sqrt{2\pi r} \sigma_0 \sqrt{\frac{a}{2r}} \\ &= \sigma_0 \sqrt{\pi a} \end{aligned} \quad (3.50-a)$$

²Irwin was asked by the Office of Naval Research (ONR) to investigate the Liberty ships failure during World War II, just as thirty years earlier Inglis was investigating the failure of British ships.

where r is the length of a small vector extending directly forward from the crack tip.

⁴⁶ Thus stresses and displacements can all be rewritten in terms of the SIF

$$\begin{Bmatrix} \sigma_{22} \\ \sigma_{12} \\ \sigma_{23} \end{Bmatrix} = \frac{1}{\sqrt{2\pi r}} \begin{bmatrix} f_{11}^I(\theta) & f_{11}^{II}(\theta) & f_{11}^{III}(\theta) \\ f_{22}^I(\theta) & f_{22}^{II}(\theta) & f_{22}^{III}(\theta) \\ f_{12}^I(\theta) & f_{12}^{II}(\theta) & f_{12}^{III}(\theta) \end{bmatrix} \begin{Bmatrix} K_I \\ K_{II} \\ K_{III} \end{Bmatrix} \quad (3.51-a)$$

i.e.

$$\sigma_{12} = \frac{K_{II}}{\sqrt{2\pi r}} \underbrace{\sin \frac{\theta}{2} \cos \frac{\theta}{2} \cos \frac{3\theta}{2}}_{f_{12}^{II}} \quad (3.52)$$

1. Since higher order terms in r were neglected, previous equations are exact in the limit as $r \rightarrow 0$
2. Distribution of elastic stress field at tip can be described by K_I , K_{II} and K_{III} . Note that this polar distribution is identical for all cases. As we shall see later, for anisotropic cases, the spatial distribution is a function of elastic constants.
3. SIF are additives, i.e.
4. The SIF is the measure of the strength of the singularity (analogous to SCF)
5. $K = f(g)\sigma\sqrt{\pi a}$ where $f(g)$ is a parameter³ that depends on the specimen, crack geometry, and loading.
6. Tada "Stress Analysis of Cracks", (Tada et al., 1973); and Cartwright & Rooke, "Compendium of Stress Intensity Factors" (Rooke and Cartwright, 1976).
7. One of the underlying principles of FM is that unstable fracture occurs when the SIF reaches a critical value K_{Ic} . K_{Ic} or fracture toughness represents the inherent ability of a material to withstand a given stress field intensity at the tip of a crack and to resist progressive tensile crack extensions.

3.4.2 Near Crack Tip Stresses and Displacements in Isotropic Cracked Solids

⁴⁷ Using Irwin's concept of the stress intensity factors, which characterize the strength of the singularity at a crack tip, the near crack tip ($r \ll a$) stresses and displacements are always expressed as:

Pure mode I loading:

$$\sigma_{xx} = \frac{K_I}{(2\pi r)^{\frac{1}{2}}} \cos \frac{\theta}{2} \left[1 - \sin \frac{\theta}{2} \sin \frac{3\theta}{2} \right] \quad (3.53-a)$$

$$\sigma_{yy} = \frac{K_I}{(2\pi r)^{\frac{1}{2}}} \cos \frac{\theta}{2} \left[1 + \sin \frac{\theta}{2} \sin \frac{3\theta}{2} \right] \quad (3.53-b)$$

$$\tau_{xy} = \frac{K_I}{(2\pi r)^{\frac{1}{2}}} \sin \frac{\theta}{2} \cos \frac{\theta}{2} \cos \frac{3\theta}{2} \quad (3.53-c)$$

$$\sigma_{zz} = \nu(\sigma_x + \sigma_y)\tau_{xz} = \tau_{yz} = 0 \quad (3.53-d)$$

$$u = \frac{K_I}{2\mu} \left[\frac{r}{2\pi} \right]^{\frac{1}{2}} \cos \frac{\theta}{2} \left[\kappa - 1 + 2 \sin^2 \frac{\theta}{2} \right] \quad (3.53-e)$$

$$v = \frac{K_I}{2\mu} \left[\frac{r}{2\pi} \right]^{\frac{1}{2}} \sin \frac{\theta}{2} \left[\kappa + 1 - 2 \cos^2 \frac{\theta}{2} \right] \quad (3.53-f)$$

$$w = 0 \quad (3.53-g)$$

³Note that in certain literature, (specially the one of Lehigh University), instead of $K = f(g)\sigma\sqrt{\pi a}$, $k = f(g)\sigma\sqrt{a}$ is used.

Pure mode II loading:

$$\sigma_{xx} = -\frac{K_{II}}{(2\pi r)^{\frac{1}{2}}} \sin \frac{\theta}{2} \left[2 + \cos \frac{\theta}{2} \cos \frac{3\theta}{2} \right] \quad (3.54-a)$$

$$\sigma_{yy} = \frac{K_{II}}{(2\pi r)^{\frac{1}{2}}} \sin \frac{\theta}{2} \cos \frac{\theta}{2} \cos \frac{3\theta}{2} \quad (3.54-b)$$

$$\tau_{xy} = \frac{K_{II}}{(2\pi r)^{\frac{1}{2}}} \cos \frac{\theta}{2} \left[1 - \sin \frac{\theta}{2} \sin \frac{3\theta}{2} \right] \quad (3.54-c)$$

$$\sigma_{zz} = \nu(\sigma_x + \sigma_y) \quad (3.54-d)$$

$$\tau_{xz} = \tau_{yz} = 0 \quad (3.54-e)$$

$$u = \frac{K_{II}}{2\mu} \left[\frac{r}{2\pi} \right]^{\frac{1}{2}} \sin \frac{\theta}{2} \left[\kappa + 1 + 2 \cos^2 \frac{\theta}{2} \right] \quad (3.54-f)$$

$$v = -\frac{K_{II}}{2\mu} \left[\frac{r}{2\pi} \right]^{\frac{1}{2}} \cos \frac{\theta}{2} \left[\kappa - 1 - 2 \sin^2 \frac{\theta}{2} \right] \quad (3.54-g)$$

$$w = 0 \quad (3.54-h)$$

Pure mode III loading:

$$\tau_{xz} = -\frac{K_{III}}{(2\pi r)^{\frac{1}{2}}} \sin \frac{\theta}{2} \quad (3.55-a)$$

$$\tau_{yz} = \frac{K_{III}}{(2\pi r)^{\frac{1}{2}}} \cos \frac{\theta}{2} \quad (3.55-b)$$

$$\sigma_{xx} = \sigma_y = \sigma_z = \tau_{xy} = 0 \quad (3.55-c)$$

$$w = \frac{K_{III}}{\mu} \left[\frac{2r}{\pi} \right]^{\frac{1}{2}} \sin \frac{\theta}{2} \quad (3.55-d)$$

$$u = v = 0 \quad (3.55-e)$$

where $\kappa = 3 - 4\nu$ for plane strain, and $\kappa = \frac{3-\nu}{1+\nu}$ for plane stress.

⁴⁸ Using Eq. 2.47-a, 2.47-b, and 2.47-c we can write the stresses in polar coordinates

Pure mode I loading:

$$\sigma_{rr} = \frac{K_I}{\sqrt{2\pi r}} \cos \frac{\theta}{2} \left(1 + \sin^2 \frac{\theta}{2} \right) \quad (3.56-a)$$

$$\sigma_{\theta\theta} = \frac{K_I}{\sqrt{2\pi r}} \cos \frac{\theta}{2} \left(1 - \sin^2 \frac{\theta}{2} \right) \quad (3.56-b)$$

$$\tau_{r\theta} = \frac{K_I}{\sqrt{2\pi r}} \sin \frac{\theta}{2} \cos^2 \frac{\theta}{2} \quad (3.56-c)$$

Pure mode II loading:

$$\sigma_{rr} = \frac{K_{II}}{\sqrt{2\pi r}} \left(-\frac{5}{4} \sin \frac{\theta}{2} + \frac{3}{4} \sin \frac{3\theta}{2} \right) \quad (3.57-a)$$

$$\sigma_{\theta\theta} = \frac{K_{II}}{\sqrt{2\pi r}} \left(-\frac{3}{4} \sin \frac{\theta}{2} - \frac{3}{4} \sin \frac{3\theta}{2} \right) \quad (3.57-b)$$

$$\tau_{r\theta} = \frac{K_{II}}{\sqrt{2\pi r}} \left(\frac{1}{4} \cos \frac{\theta}{2} + \frac{3}{4} \cos \frac{3\theta}{2} \right) \quad (3.57-c)$$

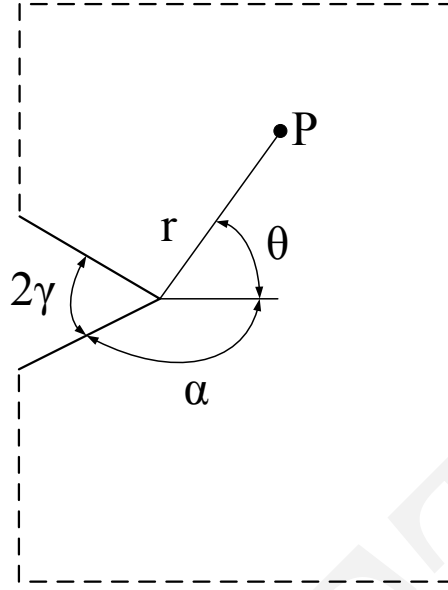


Figure 3.5: Plate with Angular Corners

3.5 V Notch, (Williams, 1952)

⁴⁹ Using the method of separation of variables in 1952, Williams (Williams, 1952, 1957) proposed the following solution

$$\Phi(r, \theta) \equiv r^{\lambda+1} F(\theta, \lambda) \quad (3.58)$$

where $F(\theta, \lambda) = e^{m(\lambda)\theta}$, and $m(\lambda)$ is yet to be determined, by satisfying the bi-harmonic equation, Eq. 2.94

$$\nabla^2 (\nabla^2 \Phi) = \left(\frac{\partial^2}{\partial r^2} + \frac{1}{r} \frac{\partial}{\partial r} + \frac{1}{r^2} \frac{\partial^2}{\partial \theta^2} \right) \left(\frac{\partial^2 \Phi}{\partial r^2} + \frac{1}{r} \frac{\partial \Phi}{\partial r} + \frac{1}{r^2} \frac{\partial^2 \Phi}{\partial \theta^2} \right) = 0 \quad (3.59)$$

⁵⁰ Note that the problem he originally considered was not a crack, but rather a plate under tension with angular corners, Fig. 3.5 making an angle 2γ . For $\gamma = 0$ we recover the crack problem of Westergaard.

⁵¹ Substituting Eq. 3.58 into the biharmonic equation (Eq. 3.59) gives

$$\frac{\partial^4 F(\theta, \lambda)}{\partial \theta^4} + 2(\lambda^2 + 1) \frac{\partial^2 F(\theta, \lambda)}{\partial \theta^2} + (\lambda^2 - 1)^2 F(\theta, \lambda) = 0 \quad (3.60)$$

⁵² Substituting $F(\theta, \lambda)$ with $e^{m(\lambda)\theta}$, this equation reduces to

$$e^{m(\lambda)\theta} [(\lambda - 1)^2 + m(\lambda)^2] [(1 + \lambda)^2 + m(\lambda)^2] = 0 \quad (3.61)$$

⁵³ The roots of this equation are

$$m(\lambda) = \pm i(\lambda - 1) \quad (3.62-a)$$

$$m(\lambda) = \pm i(\lambda + 1) \quad (3.62-b)$$

⁵⁴ Since $F(\theta, \lambda)$ is a real function then the solutions of the differential equation 3.59 are also real functions. Recalling that

$$e^{im(\lambda)\theta} = \cos m(\lambda)\theta + i \sin m(\lambda)\theta \quad (3.63)$$

we select as solution

$$\begin{aligned} F_1(\theta, \lambda) &= \cos(\lambda - 1)\theta \\ F_2(\theta, \lambda) &= \cos(\lambda + 1)\theta \\ F_3(\theta, \lambda) &= \sin(\lambda - 1)\theta \\ F_4(\theta, \lambda) &= \sin(\lambda + 1)\theta \end{aligned} \quad (3.64)$$

and finally $F(\theta, \lambda)$ will be a linear combination of F_1, F_2, F_3 and F_4 , thus

$$\Phi(r, \theta) = r^{\lambda+1} \underbrace{[A \cos(\lambda - 1)\theta + B \cos(\lambda + 1)\theta + C \sin(\lambda - 1)\theta + D \sin(\lambda + 1)\theta]}_{F(\theta, \lambda)} \quad (3.65)$$

⁵⁵ Next, we seek to determine the stresses in polar coordinates in order to apply the boundary conditions. Substituting Eq. 3.58 into Eq. 2.92

$$\sigma_{\theta\theta} = \frac{\partial^2 \Phi}{\partial r^2} \quad (3.66-a)$$

$$\sigma_{r\theta} = -\frac{\partial}{\partial r} \left(\frac{1}{r} \frac{\partial \Phi}{\partial \theta} \right) \quad (3.66-b)$$

we obtain:

$$\sigma_{\theta\theta} = r^{\lambda-1} \lambda(\lambda + 1) F(\theta) \quad (3.67-a)$$

$$\sigma_{r\theta} = r^{\lambda-1} [-\lambda F'(\theta)] \quad (3.67-b)$$

Substituting

$$\sigma_{\theta\theta} = r^{\lambda-1} \lambda(\lambda + 1) [A \cos(\lambda - 1)\theta + B \cos(\lambda + 1)\theta + C \sin(\lambda - 1)\theta + D \sin(\lambda + 1)\theta] \quad (3.68-a)$$

$$\sigma_{r\theta} = -\lambda r^{\lambda-1} [-A(\lambda - 1) \sin(\lambda - 1)\theta - B(\lambda + 1) \sin(\lambda + 1)\theta + C(\lambda - 1) \cos(\lambda - 1)\theta + D(\lambda + 1) \cos(\lambda + 1)\theta] \quad (3.68-b)$$

⁵⁶ The boundary conditions are next applied by considering a plate with a central crack, applying the following 4 boundary conditions along the crack edges

$$\sigma_{\theta\theta} |_{\theta=\pm\alpha} = 0 \quad (3.69-a)$$

$$\sigma_{r\theta} |_{\theta=\pm\alpha} = 0 \quad (3.69-b)$$

where $\alpha + \gamma = \pi$, which implies that

$$F(\alpha) = F(-\alpha) = F'(\alpha) = F'(-\alpha) = 0 \quad (3.70)$$

$$\begin{bmatrix} \cos(\lambda - 1)\alpha & \cos(\lambda + 1)\alpha & 0 & 0 \\ \omega \sin(\lambda - 1)\alpha & \sin(\lambda + 1)\alpha & 0 & 0 \\ 0 & 0 & \sin(\lambda - 1)\alpha & \sin(\lambda + 1)\alpha \\ 0 & 0 & \omega \cos(\lambda - 1)\alpha & \cos(\lambda + 1)\alpha \end{bmatrix} \begin{Bmatrix} A \\ B \\ C \\ D \end{Bmatrix} = 0 \quad (3.71)$$

where $\omega = \frac{\lambda-1}{\lambda+1}$.

⁵⁷ Note that whereas Eq. 3.67-a and 3.67-b are expressed in terms of the four constants (A, B, C , and D), the above equation is written in terms of the summation and the differences of the stress equations, thus yielding a block diagonal matrix.

⁵⁸ It can readily be seen that A and B are independent of C and D , and that for this homogeneous equation a nontrivial solution would exist if and only if the determinant of the system of linear equations vanishes to zero. This would lead (after some simplifications) to:

$$\sin 2\lambda\alpha \pm \lambda \sin 2\alpha = 0 \quad (3.72)$$

⁵⁹ We observe from Eq. 3.65 that the coefficients A and B correspond to symmetric loadings (mode I), and C and D to unsymmetric loading (mode II).

⁶⁰ Let us denote by λ_n the eigenvalues of λ which are solution of Eq. 3.72 for the symmetrical loading, and ξ_n solutions for the antisymmetric loading:

$$\sin 2\lambda_n \alpha + \lambda_n \sin 2\alpha = 0 \quad (3.73-a)$$

$$\sin 2\xi_n \alpha - \xi_n \sin 2\alpha = 0 \quad (3.73-b)$$

⁶¹ For the case of a crack, i.e $\alpha = \pi$ solution of the characteristic equation⁴ is

$$\sin(2\pi\lambda_n) = 0 \quad (3.74-a)$$

$$\sin(2\pi\xi_n) = 0 \quad (3.74-b)$$

which has solutions $\lambda_n = \frac{n}{2}$ with $n = 1, 3, 4, \dots$ (it can be shown that $n = 2$ gives rise to a rigid body motion contribution). Substituting into Eq. 3.65

$$\begin{aligned} F(\theta, \lambda) = & A_n \cos\left(\frac{n}{2} - 1\right)\theta + B_n \cos\left(\frac{n}{2} + 1\right)\theta \\ & + C_n \sin\left(\frac{n}{2} - 1\right)\theta + D_n \sin\left(\frac{n}{2} + 1\right)\theta \end{aligned} \quad (3.75-a)$$

⁶² We observe that the previous expression can be simplified by noting that for each eigenvalue λ_n and ξ_n there is a relationship between A and B , and between C and D in Eq. 3.71. For symmetrical loading we have

$$A_n \cos(\lambda_n - 1)\alpha + B_n \cos(\lambda_n + 1)\alpha = 0 \quad (3.76-a)$$

$$A_n \omega \sin(\lambda_n - 1)\alpha + B_n \sin(\lambda_n + 1)\alpha = 0 \quad (3.76-b)$$

and for antisymmetric loading we have

$$C_n \sin(\xi_n - 1)\alpha + D_n \sin(\xi_n + 1)\alpha = 0 \quad (3.77-a)$$

$$C_n \omega \cos(\xi_n - 1)\alpha + D_n \cos(\xi_n + 1)\alpha = 0 \quad (3.77-b)$$

⁶³ Thus we can define

$$a_n = \frac{A_n}{B_n} = -\frac{\cos(\lambda_n - 1)\alpha}{\cos(\lambda_n + 1)\alpha} = -\frac{\omega \sin(\lambda_n - 1)\alpha}{\sin(\lambda_n + 1)\alpha} \quad (3.78-a)$$

$$b_n = \frac{C_n}{D_n} = -\frac{\sin(\lambda_n - 1)\alpha}{\sin(\lambda_n + 1)\alpha} = -\frac{\omega \cos(\lambda_n - 1)\alpha}{\cos(\lambda_n + 1)\alpha} \quad (3.78-b)$$

these ratios are equal to $1/3$ and -1 respectively for $\alpha = \pi$ and $\lambda = 1/2$. and

$$F(\theta) = \sum \left[a_n \left(\sin \frac{3}{2}\theta + \sin \frac{1}{2}\theta \right) + b_n \left(\frac{1}{3} \cos \frac{3}{2}\theta + \cos \frac{1}{2}\theta \right) \right] \quad (3.79)$$

⁶⁴ The stresses are obtained by substituting

$$\sigma_{rr} = \sum \left[\frac{b_n}{\sqrt{r}} \left(\frac{5}{4} \cos \frac{\theta}{2} - \frac{1}{4} \cos \frac{3\theta}{2} \right) + \frac{a_n}{\sqrt{r}} \left(-\frac{5}{4} \sin \frac{\theta}{2} + \frac{3}{4} \sin \frac{3\theta}{2} \right) \right] \quad (3.80-a)$$

$$\sigma_{\theta\theta} = \sum \left[\frac{b_n}{\sqrt{r}} \left(\frac{3}{4} \cos \frac{\theta}{2} + \frac{1}{4} \cos \frac{3\theta}{2} \right) + \frac{a_n}{\sqrt{r}} \left(-\frac{3}{4} \sin \frac{\theta}{2} - \frac{3}{4} \sin \frac{3\theta}{2} \right) \right] \quad (3.80-b)$$

$$\sigma_{r\theta} = \sum \left[\frac{b_n}{\sqrt{r}} \left(\frac{1}{4} \sin \frac{\theta}{2} + \frac{1}{4} \sin \frac{3\theta}{2} \right) + \frac{a_n}{\sqrt{r}} \left(\frac{1}{4} \cos \frac{\theta}{2} + \frac{3}{4} \cos \frac{3\theta}{2} \right) \right] \quad (3.80-c)$$

⁶⁵ These equations can be further simplified into

$$\sigma_{rr} = \sum \left[\frac{b_n}{\sqrt{r}} \cos \frac{\theta}{2} \left(1 + \sin^2 \frac{\theta}{2} \right) + \frac{a_n}{\sqrt{r}} \left(-\frac{5}{4} \sin \frac{\theta}{2} + \frac{3}{4} \sin \frac{3\theta}{2} \right) \right] \quad (3.81-a)$$

$$\sigma_{\theta\theta} = \sum \left[\frac{b_n}{\sqrt{r}} \cos \frac{\theta}{2} \left(1 - \sin^2 \frac{\theta}{2} \right) + \frac{a_n}{\sqrt{r}} \left(-\frac{3}{4} \sin \frac{\theta}{2} - \frac{3}{4} \sin \frac{3\theta}{2} \right) \right] \quad (3.81-b)$$

$$\sigma_{r\theta} = \sum \left[\frac{b_n}{\sqrt{r}} \sin \frac{\theta}{2} \cos^2 \frac{\theta}{2} + \frac{a_n}{\sqrt{r}} \left(\frac{1}{4} \cos \frac{\theta}{2} + \frac{3}{4} \cos \frac{3\theta}{2} \right) \right] \quad (3.81-c)$$

⁴Note that the solution for λ_n and ξ_n for other angles can not be obtained algebraically, a numerical technique must be used.

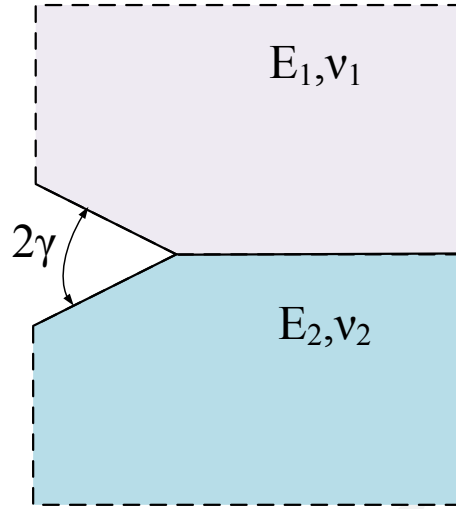


Figure 3.6: Plate with Angular Corners

⁶⁶ Finally, it can be shown that the displacements will be given by

$$u = \frac{1}{2\mu} \sum Re \left\{ a_n r^{\lambda_n} [(\kappa + \lambda_n \cos 2\alpha + \cos 2\lambda_n \alpha) \cos \lambda_n \theta - \lambda_n \cos(\lambda_n - 2)\theta] - b_n r^{\xi_n} [(\kappa + \xi_n \cos 2\alpha - \cos 2\xi_n \alpha) \sin \xi_n \theta - \xi_n \sin(\xi_n - 2)\theta] \right\} \quad (3.82-a)$$

$$v = \frac{1}{2\mu} \sum Re \left\{ a_n r^{\lambda_n} [(\kappa - \lambda_n \cos 2\alpha - \cos 2\lambda_n \alpha) \sin \lambda_n \theta + \lambda_n \sin(\lambda_n - 2)\theta] + b_n r^{\xi_n} [(\kappa - \xi_n \cos 2\alpha + \cos 2\xi_n \alpha) \cos \xi_n \theta + \xi_n \cos(\xi_n - 2)\theta] \right\} \quad (3.82-b)$$

⁶⁷ This solution can be compared with Westergaard's solution by comparing Equations 3.56-a and 3.57-a with Eq. 3.81-a; Eq. 3.56-b and 3.57-b with Eq. 3.81-b; and Eq. 3.56-c and 3.57-c with Eq. 3.81-c for $n = 1$. From this we observe that

$$\begin{cases} b_1 = \frac{K_I}{\sqrt{2\pi}} \\ a_1 = \frac{K_{II}}{\sqrt{2\pi}} \end{cases} \quad (3.83)$$

3.6 Crack at an Interface between Two Dissimilar Materials (Williams, 1959)

3.6.1 General Function

⁶⁸ We shall now consider the problem of a crack at the interface between two dissimilar isotropic materials, (Williams, 1959; Zak and Williams, 1963). Accordingly, we rewrite Eq. 3.58 as

$$\Phi_i(r, \theta) \equiv r^{\lambda+1} F_i(\theta, \lambda) \quad (3.84)$$

where the subscript i refers to material 1 and 2, Fig. 3.6

⁶⁹ Hence:

$$F_i(\theta, \lambda) = A_i \cos(\lambda - 1)\theta + B_i \cos(\lambda + 1)\theta + C_i \sin(\lambda - 1)\theta + D_i \sin(\lambda + 1)\theta \quad (3.85)$$

3.6.2 Boundary Conditions

⁷⁰ Boundary conditions for this problem are:

- zero stresses, $\sigma_{\theta\theta}$, on the free edges (at $\theta = \pm\pi$). Thus from Eq. 3.67-a

$$\sigma_{\theta\theta}|_{\theta=\pi} = r^{\lambda-1}\lambda(\lambda+1)[A_1 \cos(\lambda-1)\pi + B_1 \cos(\lambda+1)\pi + C_1 \sin(\lambda-1)\pi + D_1 \sin(\lambda+1)\pi] = 0 \quad (3.86-a)$$

$$\sigma_{\theta\theta}|_{\theta=-\pi} = r^{\lambda-1}\lambda(\lambda+1)[A_2 \cos(\lambda-1)\pi + B_2 \cos(\lambda+1)\pi - C_2 \sin(\lambda-1)\pi - D_2 \sin(\lambda+1)\pi] = 0 \quad (3.86-b)$$

$$\text{or } F_1(\pi) = F_2(-\pi) = 0$$

- zero stresses, $\sigma_{r\theta}$, on the free edges (at $\theta = \pm\pi$); From Eq. 3.67-b

$$\sigma_{r\theta}|_{\theta=\pi} = -\lambda r^{\lambda-1}[-A_1(\lambda-1)\sin(\lambda-1)\theta - B_1(\lambda+1)\sin(\lambda+1)\theta + C_1(\lambda-1)\cos(\lambda-1)\theta + D_1(\lambda+1)\cos(\lambda+1)\theta] = 0 \quad (3.87-a)$$

$$\sigma_{r\theta}|_{\theta=-\pi} = -\lambda r^{\lambda-1}F'(\theta) \quad (3.87-b)$$

$$= -\lambda r^{\lambda-1}[+A_2(\lambda-1)\sin(\lambda-1)\theta + B_2(\lambda+1)\sin(\lambda+1)\theta - C_2(\lambda-1)\cos(\lambda-1)\theta - D_2(\lambda+1)\cos(\lambda+1)\theta] = 0 \quad (3.87-c)$$

$$\text{or } F'_1(\pi) = F'_2(-\pi) = 0$$

- Continuity of $\sigma_{\theta\theta}$ at the interface, $\theta = 0$

$$A_1 + B_1 = A_2 + B_2 \quad (3.88)$$

- Continuity of $\sigma_{r\theta}$ at $\theta = 0$ along the interface

$$(\lambda-1)C_1 + (\lambda+1)D_1 = -(\lambda-1)C_2 - (\lambda+1)D_2 \quad (3.89)$$

- Continuity of displacements (u_r, u_θ) at the interface. Using the polar expression of the displacements

$$u_r^i = \frac{1}{2\mu_i} r^\lambda \{ -(\lambda+1)F_i(\theta) + 4(1-\alpha_i)[C_i \sin(\lambda-1)\theta + A_i \cos(\lambda-1)\theta] \} \quad (3.90-a)$$

$$u_\theta^i = \frac{1}{2\mu_i} r^\lambda \{ -F'_i(\theta) - 4(1-\alpha_i)[C_i \cos(\lambda-1)\theta - A_i \sin(\lambda-1)\theta] \} \quad (3.90-b)$$

where μ is the shear modulus, and $\alpha_i \equiv \frac{\nu_i}{1+\nu_i}$
we obtain

$$\frac{1}{2\mu_1} [-(\lambda+1)F_1(0) + 4A_1(1-\alpha_1)] = \frac{1}{2\mu_2} [-(\lambda+1)F_2(0) + 4A_2(1-\alpha_2)] \quad (3.91-a)$$

$$\frac{1}{2\mu_1} [-F'_1(0) - 4C_1(1-\alpha_1)] = \frac{1}{2\mu_2} [-F'_2(0) - 4C_2(1-\alpha_2)] \quad (3.91-b)$$

3.6.3 Homogeneous Equations

⁷¹ Applying those boundary conditions, will lead to 8 homogeneous linear equations (Eq. 3.86-a, 3.86-b, 3.87-b, 3.87-c, 3.88, 3.89, 3.91-a, 3.91-b) in terms of the 8 unknowns $A_1, B_1, C_1, D_1, A_2, B_2, C_2$ and D_2 .

⁷² A nontrivial solution exists if the determinant of the 8 equations is equal to zero. This determinant⁵ is equal to

$$\cot^2 \lambda\pi + \left[\frac{2k(1-\alpha_2) - 2(1-\alpha_1) - (k-1)}{2k(1-\alpha_2) + 2(1-\alpha_1)} \right]^2 = 0 \quad (3.92)$$

where $k = \frac{\mu_1}{\mu_2}$.

⁷³ For the homogeneous case $\alpha_1 = \alpha_2$ and $k = 1$, the previous equation reduces to $\cot^2 \lambda\pi = 0$ or $\sin^2 \lambda\pi = 0$ thus we recover the same solution as the one of Eq. 3.74-b for a crack in one material:

$$\lambda = \frac{n}{2} \quad n = 1, 2, 3, \dots \quad (3.93)$$

⁵The original paper states: ... After some algebraic simplification...

Note that we exclude negative values of n to ensure finite displacements as the origin is approached, and the lowest eigenvalue controls.

⁷⁴ Noting that there can not be a real solution to Eq. 3.92, we define

$$\beta = \frac{2k(1 - \alpha_2) - 2(1 - \alpha_1) - (k - 1)}{2k(1 - \alpha_2) + 2(1 - \alpha_1)} \quad (3.94)$$

and thus, Eq. 3.92 leads to $\cot^2 \lambda \pi = -\beta^2$, or

$$\cot \lambda \pi = \pm i\beta \quad (3.95)$$

⁷⁵ To solve this equation, we use the following trigonometric relations, (Abramowitz and Stegun, 1970)

$$\cot z = \frac{\sin 2x - i \sinh 2y}{\cosh 2y - \cos 2x} \quad (3.96-a)$$

$$\sin 2\theta\pi = \frac{2u}{1 + u^2} \quad (3.96-b)$$

$$\cos 2\theta\pi = \frac{1 - u^2}{1 + u^2} \quad (3.96-c)$$

$$\sinh 2\theta\pi = \frac{2v}{1 - v^2} \quad (3.96-d)$$

$$\cosh 2\theta\pi = \frac{1 + v^2}{1 - v^2} \quad (3.96-e)$$

where

$$u = \tan \lambda_r \pi \quad (3.97-a)$$

$$v = \tanh \lambda_j \pi \quad (3.97-b)$$

where we have assumed a complex value for λ

$$\lambda = \lambda_r + i\lambda_j \quad (3.98)$$

Then, we obtain

$$\sin 2\lambda_r \pi = \frac{2u}{1 + u^2} \quad (3.99-a)$$

$$\cos 2\lambda_r \pi = \frac{1 - u^2}{1 + u^2} \quad (3.99-b)$$

$$\sinh 2\lambda_j \pi = \frac{2v}{1 - v^2} \quad (3.99-c)$$

$$\cosh 2\lambda_j \pi = \frac{1 + v^2}{1 - v^2} \quad (3.99-d)$$

⁷⁶ Substituting in Eq. 3.96-a lead to

$$\cot \lambda \pi = \frac{u(1 - v^2) - iv(1 + u^2)}{u^2 + v^2} \quad (3.100-a)$$

$$= \underbrace{\frac{\tan \lambda_r \pi (1 - \tanh^2 \lambda_j \pi)}{\tan^2 \lambda_r \pi + \tanh^2 \lambda_j \pi}}_{\text{Re}(\cot \lambda \pi)=0} - i \underbrace{\frac{(\tan^2 \lambda_r \pi + 1) \tanh \lambda_j \pi}{\tan^2 \lambda_r \pi + \tanh^2 \lambda_j \pi}}_{\text{Im}(\cot \lambda \pi)=\pm\beta} \quad (3.100-b)$$

⁷⁷ Thus, Eq. 3.92 finally leads to

$$\text{Re}(\cot \lambda \pi) = 0 \quad (3.101-a)$$

$$\text{Im}(\cot \lambda \pi) = \pm\beta \quad (3.101-b)$$

we thus have two equations with two unknowns.

3.6.4 Solve for λ

78 Let us solve those two equations. Two sets of solutions are possible:

1. If from 3.100-b $\tan \lambda_r \pi = 0$ then

$$\lambda_r = n = 0, 1, 2, 3, \dots \quad (3.102)$$

and accordingly from Eq. 3.101-b

$$\lambda_j = \pm \frac{1}{\pi} \coth^{-1} \beta \quad (3.103)$$

2. Alternatively, from Eq. 3.101-a $\cot \lambda_r \pi = 0 \Rightarrow \tan \lambda_r \pi = \infty$ and⁶:

$$\lambda_r = \frac{2n+1}{2} \quad n = 0, 1, 2, 3, \dots \quad (3.104-a)$$

$$\lambda_j = \pm \frac{1}{\pi} \tanh^{-1} \beta \quad (3.104-b)$$

$$= \frac{1}{2\pi} \log \left[\frac{\beta+1}{\beta-1} \right] \quad (3.104-c)$$

We note that for this case, $\lambda_j \rightarrow 0$ as $\alpha_1 \rightarrow \alpha_2$ and $k \rightarrow 1$ in β .

3.6.5 Near Crack Tip Stresses

79 Now that we have solved for λ , we need to derive expressions for the near crack tip stress field. We rewrite Eq. 3.84 as

$$\Phi(r) = \underbrace{r^{\lambda+1}}_{G(r)} F(\theta, \lambda) \quad (3.105)$$

we note that we no longer have two sets of functions, as the effect of dissimilar materials has been accounted for and is embedded in λ .

80 The stresses will be given by Eq. 2.92

$$\sigma_{rr} = \frac{1}{r^2} \frac{\partial^2 \Phi}{\partial \theta^2} + \frac{1}{r} \frac{\partial \Phi}{\partial r} = r^{-2} G(r) F''(\theta) + r^{-1} G'(r) F'(\theta) \quad (3.106-a)$$

$$\sigma_{\theta\theta} = \frac{\partial^2 \Phi}{\partial r^2} = G''(r) F(\theta) \quad (3.106-b)$$

$$\sigma_{r\theta} = \frac{1}{r^2} \frac{\partial \Phi}{\partial \theta} - \frac{1}{r} \frac{\partial^2 \Phi}{\partial r \partial \theta} = r^{-2} G(r) F'(\theta) - r^{-1} G'(r) F'(\theta) \quad (3.106-c)$$

Therefore, we must solve for $F'(\theta)$, $F''(\theta)$, $G'(r)$ and $G''(r)$ in terms of $\lambda = \lambda_r + i\lambda_j$.

81 First we note that

$$G(r) = r^{\lambda+1} = r^{\lambda_r+1+i\lambda_j} \quad (3.107-a)$$

$$r^{i\lambda_j} = e^{i\lambda_j \log(r)} \quad (3.107-b)$$

recalling that $\log(z) = \log|z| + i \arg z$, and since $|z| = \sqrt{x^2 + y^2} = \sqrt{r^2 + 0} = r$, we have $\arg z = 2k\pi$, and $k = 0, \pm 1, \pm 2, \dots$. Hence,

$$\log(r) = \log|r| + i2k\pi \quad (3.108)$$

and Eq. 3.107-b becomes

$$r^{i\lambda_j} = e^{i\lambda_j \log(r)} \quad (3.109-a)$$

$$= e^{i\lambda_j [\log(r) + i2k\pi]} \quad (3.109-b)$$

$$= e^{i\lambda_j \log(r) - 2k\pi\lambda_j} \quad (3.109-c)$$

$$= e^{-2k\pi\lambda_j} e^{i\lambda_j \log(r)} \quad (3.109-d)$$

$$= e^{-2k\pi\lambda_j} [\cos(\lambda_j \log(r)) + i \sin(\lambda_j \log(r))] \quad (3.109-e)$$

⁶Recall that $\tanh^{-1} x = \frac{1}{2} \log \frac{1+x}{1-x}$

82 Now, for $k = 0$, $r^{i\lambda_j}$ becomes

$$r^{i\lambda_j} = \cos(\lambda_j \log(r)) + i \sin(\lambda_j \log(r)) \quad (3.110)$$

and accordingly, Eq. 3.107-a becomes

$$G(r) = r^{\lambda_r+1} = r^{\lambda_r+1} r^{i\lambda_j} \quad (3.111-a)$$

$$= r^{\lambda_r+1} [\cos(\lambda_j \log(r)) + i \sin(\lambda_j \log(r))] \quad (3.111-b)$$

and for $\lambda_r = 1/2$

$$G(r) = r^{\frac{3}{2}} [\cos(\lambda_j \log(r)) + i \sin(\lambda_j \log(r))] \quad (3.112-a)$$

$$\text{Re}G(r) = r^{\frac{3}{2}} \cos(\lambda_j \log(r)) \quad (3.112-b)$$

$$G'(r) = r^{\frac{1}{2}} \left[\frac{3}{2} \cos(\lambda_j \log(r)) + \lambda_j \sin(\lambda_j \log(r)) \right] \quad (3.112-c)$$

$$G''(r) = r^{-\frac{1}{2}} \left[\left(\frac{3}{4} - \lambda_j^2 \right) \cos(\lambda_j \log(r)) + \left(\frac{3}{2} + \frac{\lambda_j}{2} \right) \sin(\lambda_j \log(r)) \right] \quad (3.112-d)$$

83 Back to $F(\theta)$, which was defined in Eq. 3.85

$$F(\theta, \lambda) = A \cos(\lambda - 1)\theta + B \cos(\lambda + 1)\theta + C \sin(\lambda - 1)\theta + D \sin(\lambda + 1)\theta \quad (3.113)$$

we need to replace λ by $\lambda_r + i\lambda_j$. However, first we recall the following relations, (Abramowitz and Stegun, 1970)

$$\sin(x + iy) = \sin(x) \cosh(y) - i \cos(x) \sinh(y) \quad (3.114-a)$$

$$\cos(x + iy) = \cos(x) \cosh(y) + i \sin(x) \sinh(y) \quad (3.114-b)$$

thus,

$$\text{Re} \{ \sin [(\lambda_r \pm 1) + i\lambda_j] \theta \} = \sin(\lambda_r \pm 1) \cos(\theta) \cosh \lambda_j \theta \quad (3.115-a)$$

$$\text{Re} \{ \cos [(\lambda_r \pm 1) + i\lambda_j] \theta \} = \cos(\lambda_r \pm 1) \cos(\theta) \cosh \lambda_j \theta \quad (3.115-b)$$

84 Substituting those relations in Eq. 3.113

$$\text{Re} [F(\theta)] = \underbrace{\cosh \lambda_j \theta}_{f(\theta)} \quad (3.116-a)$$

$$\underbrace{[A \cos(\lambda_r - 1)\theta + B \cos(\lambda_r + 1)\theta + C \sin(\lambda_r - 1)\theta + D \sin(\lambda_r + 1)\theta]}_{g(\theta)} \quad (3.116-b)$$

$$\begin{aligned} \text{Re} [\Phi(r, \theta)] &= r^{\lambda_r+1} \cos(\lambda_j \log(r)) \cosh \lambda_j \theta \\ &\quad [A \cos(\lambda_r - 1)\theta + B \cos(\lambda_r + 1)\theta \\ &\quad + C \sin(\lambda_r - 1)\theta + D \sin(\lambda_r + 1)\theta] \end{aligned} \quad (3.116-c)$$

85 For $\lambda_r = \frac{1}{2}$

$$g(\theta) = A \cos \frac{\theta}{2} + B \cos \frac{3\theta}{2} - C \sin \frac{\theta}{2} + D \sin \frac{3\theta}{2} \quad (3.117)$$

86 Applying the boundary conditions at $\theta = \pm\pi$, $\sigma_{\theta\theta} = 0$, Eq. 3.106-b $F(\theta) = 0$, that is $g_1(-\pi) = g_2(\pi)$ or

$$C = -D = -a \quad (3.118)$$

87 Similarly at $\theta = \pm\pi$, $\sigma_{r\theta} = 0$. Thus, from Eq. 3.106-c $F'(\theta) = 0$, or $g'_1(-\pi) = g'_2(\pi)$ or

$$A = 3B = b \quad (3.119)$$

⁸⁸ From those two equations we rewrite Eq. 3.117

$$g(\theta) = a \left(\sin \frac{\theta}{2} + \sin \frac{3\theta}{2} \right) + b \left(3 \cos \frac{\theta}{2} + \cos \frac{3\theta}{2} \right) \quad (3.120)$$

⁸⁹ We now determine the derivatives

$$f'(\theta) = \lambda_j \sinh \lambda_j \theta \quad (3.121-a)$$

$$g'(\theta) = a \left(\frac{3}{2} \cos \frac{3\theta}{2} + \frac{1}{2} \cos \frac{\theta}{2} \right) + b \left(-\frac{3}{2} \sin \frac{3\theta}{2} - \frac{3}{2} \sin \frac{\theta}{2} \right) \quad (3.121-b)$$

⁹⁰ Thus, we now can determine

$$F'(\theta) = f'(\theta)g(\theta) + f(\theta)g'(\theta) \quad (3.122-a)$$

$$= a \left\{ \cosh \lambda_j \theta \left[\frac{3}{2} \cos \frac{3\theta}{2} + \frac{1}{2} \cos \frac{\theta}{2} \right] + \lambda_j \sinh \lambda_j \theta \left[\sin \frac{3\theta}{2} + \sin \frac{\theta}{2} \right] \right\} \\ + b \left\{ \cosh \lambda_j \theta \left[-\frac{3}{2} \sin \frac{3\theta}{2} - \frac{3}{2} \sin \frac{\theta}{2} \right] + \lambda_j \sinh \lambda_j \theta \left[\cos \frac{3\theta}{2} + 3 \cos \frac{\theta}{2} \right] \right\} \quad (3.122-b)$$

⁹¹ Similarly, the second derivative $F''(\theta)$ is determined

$$F''(\theta) = f''(\theta)g(\theta) + 2f'(\theta)g'(\theta) + f(\theta)g''(\theta) \quad (3.123-a)$$

$$= a \left\{ \cosh \lambda_j \theta \left[-\frac{9}{4} \sin \frac{3\theta}{2} - \frac{1}{4} \sin \frac{\theta}{2} \right] + 2\lambda_j \sinh \lambda_j \theta \left[\frac{3}{2} \cos \frac{3\theta}{2} + \frac{1}{2} \cos \frac{\theta}{2} \right] \right. \\ \left. + \lambda_j^2 \cosh^2 \lambda_j \theta \left[\sin \frac{3\theta}{2} + \sin \frac{\theta}{2} \right] \right\} + \\ b \left\{ \cosh \lambda_j \theta \left[-\frac{9}{4} \cos \frac{3\theta}{2} - \frac{3}{4} \cos \frac{\theta}{2} \right] + 2\lambda_j \sinh \lambda_j \theta \left[-\frac{3}{2} \sin \frac{3\theta}{2} - \frac{3}{2} \sin \frac{\theta}{2} \right] \right. \\ \left. + \lambda_j^2 \cosh^2 \lambda_j \theta \left[\cos \frac{3\theta}{2} + 3 \cos \frac{\theta}{2} \right] \right\} \quad (3.123-b)$$

⁹² We can now substitute in Eq. 3.106-b, 3.106-c and 3.106-a to determine the stresses

$$\sigma_{rr} = r^{-\frac{1}{2}} \cos(\lambda_j \log(r)) F''(\theta) + r^{-\frac{1}{2}} \left[\frac{3}{2} \cos(\lambda_j \log(r)) + \lambda_j \sin(\lambda_j \log(r)) \right] F(\theta) \quad (3.124-a)$$

$$\sigma_{\theta\theta} = r^{-\frac{1}{2}} \left[\left(\frac{3}{4} - \lambda_j^2 \right) \cos(\lambda_j \log(r)) + \left(\frac{3}{2} + \frac{\lambda_j}{2} \right) \sin(\lambda_j \log(r)) \right] F(\theta) \quad (3.124-b)$$

$$\sigma_{r\theta} = r^{-\frac{1}{2}} \left\{ \cos(\lambda_j \log(r)) F'(\theta) + \left[\frac{3}{2} \cos(\lambda_j \log(r)) + \lambda_j \sin(\lambda_j \log(r)) \right] F'(\theta) \right\} \quad (3.124-c)$$

3.7 Homogeneous Anisotropic Material (Sih and Paris)

⁹³ To analyze an anisotropic body with with a crack, we need to derive the two stress functions Φ_1 and Φ_2 in Eq. 2.121 such that they satisfy the boundary conditions of the problem under consideration.

⁹⁴ For an infinite plate with a central crack in an anisotropic body the derivation for the stress functions was undertaken by Sih,

Paris and Irwin, (Sih et al., 1965). This solution is the “counterpart” or generalization of Westergaard’s solutions.

$$u_1 = K_I \sqrt{\frac{2r}{\pi}} \operatorname{Re} \left\{ \frac{1}{s_1 - s_2} \left[s_1 p_2 (\cos \theta + s_2 \sin \theta)^{\frac{1}{2}} - s_2 p_1 (\cos \theta + s_1 \sin \theta)^{\frac{1}{2}} \right] \right\} \quad (3.125\text{-a})$$

$$v_1 = K_I \sqrt{\frac{2r}{\pi}} \operatorname{Re} \left\{ \frac{1}{s_1 - s_2} \left[s_1 q_2 (\cos \theta + s_2 \sin \theta)^{\frac{1}{2}} - s_2 q_1 (\cos \theta + s_1 \sin \theta)^{\frac{1}{2}} \right] \right\} \quad (3.125\text{-b})$$

$$w_1 = 0 \quad (3.125\text{-c})$$

$$u_2 = K_{II} \sqrt{\frac{2r}{\pi}} \operatorname{Re} \left\{ \frac{1}{s_1 - s_2} \left[p_2 (\cos \theta + s_2 \sin \theta)^{\frac{1}{2}} - p_1 (\cos \theta + s_1 \sin \theta)^{\frac{1}{2}} \right] \right\} \quad (3.125\text{-d})$$

$$v_2 = K_{II} \sqrt{\frac{2r}{\pi}} \operatorname{Re} \left\{ \frac{1}{s_1 - s_2} \left[q_2 (\cos \theta + s_2 \sin \theta)^{\frac{1}{2}} - q_1 (\cos \theta + s_1 \sin \theta)^{\frac{1}{2}} \right] \right\} \quad (3.125\text{-e})$$

$$w_2 = 0 \quad (3.125\text{-f})$$

$$u_3 = 0 \quad (3.125\text{-g})$$

$$v_3 = 0 \quad (3.125\text{-h})$$

$$w_3 = K_{III} \sqrt{\frac{2r}{\pi}} (c_{44}c_{55} - c_{45}^2)^{-\frac{1}{2}} \operatorname{Im} \left[(\cos \theta + s_3 \sin \theta)^{\frac{1}{2}} \right] \quad (3.125\text{-i})$$

⁹⁵ where s_1 and s_2 are roots, in general complex, of Eq. 2.124 where $s_j = \alpha_j + i\beta_j$ for $j = 1, 2$, and the roots of interests are taken such that $\beta_j > 0$, and

$$p_j = a_{11}s_j^2 + a_{12} - a_{16}s_j \quad (3.126)$$

$$q_j = a_{12}s_j + \frac{a_{22}}{s_j} - a_{26} \quad (3.127)$$

⁹⁶ After appropriate substitution, it can be shown that the cartesian stresses at the tip of the crack for symmetric loading are

$$\sigma_x = \frac{K_I}{\sqrt{2\pi r}} \operatorname{Re} \left[\frac{s_1 s_2}{s_1 - s_2} \left(\frac{s_2}{(\cos \theta + s_2 \sin \theta)^{\frac{1}{2}}} - \frac{s_1}{(\cos \theta + s_1 \sin \theta)^{\frac{1}{2}}} \right) \right] \quad (3.128\text{-a})$$

$$\sigma_y = \frac{K_I}{\sqrt{2\pi r}} \operatorname{Re} \left[\frac{1}{s_1 - s_2} \left(\frac{s_1}{(\cos \theta + s_2 \sin \theta)^{\frac{1}{2}}} - \frac{s_2}{(\cos \theta + s_1 \sin \theta)^{\frac{1}{2}}} \right) \right] \quad (3.128\text{-b})$$

$$\sigma_{xy} = \frac{K_I}{\sqrt{2\pi r}} \operatorname{Re} \left[\frac{s_1 s_2}{s_1 - s_2} \left(\frac{1}{(\cos \theta + s_1 \sin \theta)^{\frac{1}{2}}} - \frac{s_1}{(\cos \theta + s_2 \sin \theta)^{\frac{1}{2}}} \right) \right] \quad (3.128\text{-c})$$

⁹⁷ and, for plane skew-symmetric loading:

$$\sigma_x = \frac{K_{II}}{\sqrt{2\pi r}} \operatorname{Re} \left[\frac{1}{s_1 - s_2} \left(\frac{s_2^2}{(\cos \theta + s_2 \sin \theta)^{\frac{1}{2}}} - \frac{s_1^2}{(\cos \theta + s_1 \sin \theta)^{\frac{1}{2}}} \right) \right] \quad (3.129\text{-a})$$

$$\sigma_y = \frac{K_{II}}{\sqrt{2\pi r}} \operatorname{Re} \left[\frac{1}{s_1 - s_2} \left(\frac{1}{(\cos \theta + s_2 \sin \theta)^{\frac{1}{2}}} - \frac{1}{(\cos \theta + s_1 \sin \theta)^{\frac{1}{2}}} \right) \right] \quad (3.129\text{-b})$$

$$\sigma_{xy} = \frac{K_{II}}{\sqrt{2\pi r}} \operatorname{Re} \left[\frac{1}{s_1 - s_2} \left(\frac{s_1}{(\cos \theta + s_1 \sin \theta)^{\frac{1}{2}}} - \frac{s_2}{(\cos \theta + s_2 \sin \theta)^{\frac{1}{2}}} \right) \right] \quad (3.129\text{-c})$$

⁹⁸ For in-plane loadings, these stresses can be summed to give the stresses at a distance r and an angle θ from the crack tip.

⁹⁹ An important observation to be made is that the form of the stress singularity $r^{-1/2}$ is identical to the one found in isotropic solids.

¹⁰⁰ It should be noted that contrarily to the isotropic case where both the stress magnitude and its spatial distribution are controlled by the stress intensity factor only, in the anisotropic case they will also depend on the material elastic properties and the orientation of the crack with respect to the principal planes of elastic symmetry (through s_1 and s_2).

3.8 Assignment

CVEN-6831

FRACTURE MECHANICS

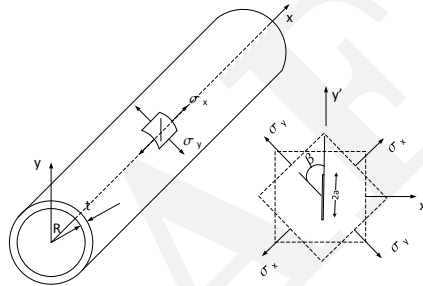
Spring 2000

Victor E. Saouma

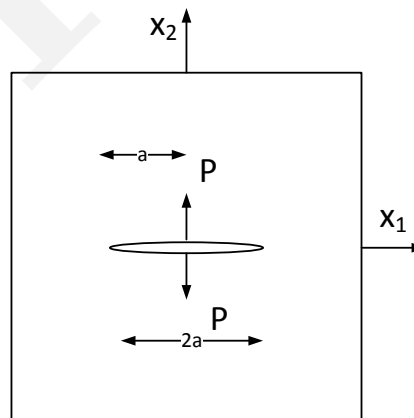
Home-Work No. 1
Derivation of SIF

Due Date: Feb. 15, 2000

1. A cylindrical pressure vessel of radius R and thickness t contains a through crack of length $2a$ oriented at an angle β with the circumferential direction. When the vessel is subjected to an internal pressure p , determine the stress intensity factors at the crack tip.



2. The stress function for a crack subjected to splitting forces P , as shown below



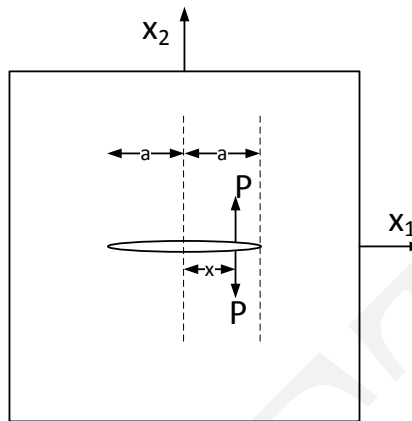
is given by:

$$\phi = \frac{Pa}{\pi z \sqrt{z^2 - a^2}} \quad (3.130)$$

where $z = x_1 + ix_2$ and P is a load per unit thickness. Calculate the expressions of σ_{22} at $x_2 = 0$ and derive an expression for K_I . ($K_P = \frac{P}{\sqrt{\pi a}}$)

Hint:

- a) At crack tip $\frac{\eta}{a} \ll 1$.
 b) $\eta = z - a = z = re^{i\theta}$
3. The stress intensity factor of the following problem:



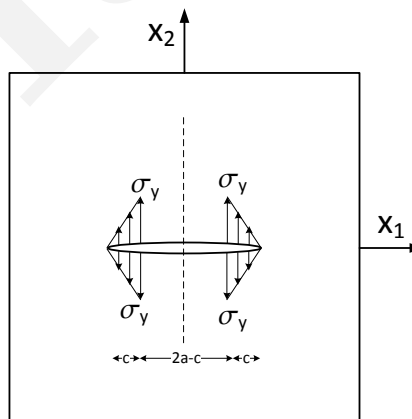
is given by:

$$K_A = \frac{P}{\sqrt{\pi a}} \sqrt{\frac{a+x}{a-x}} \quad (3.131)$$

$$K_b = \frac{P}{\sqrt{\pi a}} \sqrt{\frac{a-x}{a+x}} \quad (3.132)$$

Based on those expressions, and results from the previous problem, determine the stress function Φ .

4. Barenblatt's model assumes a linearly varying closing pressure at the tip of a crack,



Using Mathematica and the expressions of K_A and K_B from the previous problem, determine an expression for the stress intensity factors for this case.

5. Using Mathematica, program either:
- Westergaard's solution for a crack subjected to mode I and mode II loading.
 - Williams solution for a crack along dissimilar materials.

Chapter 4

LEFM DESIGN EXAMPLES

¹ Following the detailed coverage of the derivation of the linear elastic stress field around a crack tip, and the introduction of the concept of a stress intensity factor in the preceding chapter, we now seek to apply those equations to some (pure mode I) practical design problems.

² First we shall examine how is linear elastic fracture mechanics (LEFM) effectively used in design examples, then we shall give analytical solutions to some simple commonly used test geometries, followed by a tabulation of fracture toughness of commonly used engineering materials. Finally, this chapter will conclude with some simple design/analysis examples.

4.1 Design Philosophy Based on Linear Elastic Fracture Mechanics

³ One of the underlying principles of fracture mechanics is that *unstable* fracture occurs when the stress intensity factor (SIF) reaches a critical value K_{Ic} , also called *fracture toughness*. K_{Ic} represents the inherent ability of a material to withstand a given stress field intensity at the tip of a crack and to resist progressive tensile crack extension.

⁴ Thus a crack will propagate (under pure mode I), whenever the stress intensity factor K_I (which characterizes the strength of the singularity for a given problem) reaches a material constant K_{Ic} . Hence, under the assumptions of linear elastic fracture mechanics (LEFM), at the point of incipient crack growth:

$$K_{Ic} = \beta\sigma\sqrt{\pi a} \quad (4.1)$$

⁵ Thus for the design of a cracked, or potentially cracked, structure, the engineer would have to decide what design variables can be selected, as only, two of these variables can be fixed, and the third must be determined. The design variables are:

Material properties: (such as special steel to resist corrosive liquid) $\Rightarrow K_c$ is fixed.

Design stress level: (which may be governed by weight considerations) $\Rightarrow \sigma$ is fixed.

Flaw size: ¹, a .

⁶ In assessing the safety of a cracked body, it is essential that the crack length a be properly known. In most cases it is not. Thus assumptions must be made for its value, and those assumptions are dependent upon the crack detection methodology adopted. The presence of a crack, equal to the smallest one that can be detected, must be assumed.

⁷ Thus, a simpler inspection procedure would result in a larger minimum crack size than one detected by expensive non-destructive techniques. In return, simplified inspection would result in larger crack size assumptions.

Once two parameters are specified, the third one is fixed. Finally, it should be mentioned that whereas in most cases the geometry is fixed (hence β), occasionally, there is the possibility to alter it in such a way to reduce (or maximize) β .

4.2 Stress Intensity Factors

⁶ As shown in the preceding chapter, analytic derivation of the stress intensity factors of even the simplest problem can be quite challenging. This explain the interest developed by some mathematician in solving fracture related problems. Fortunately, a number of simple problems have been solved and their analytic solution is found in stress intensity factor handbooks. The most commonly referenced ones are Tada, Paris and Irwin's (Tada et al., 1973), and Rooke and Cartwright, (Rooke and Cartwright, 1976), and Murakami (Murakami, 1987)

⁷ In addition, increasingly computer software with pre-programmed analytical solutions are becoming available, specially in conjunction with fatigue life predictions.

⁸ Because of their importance, expressions of SIF of commonly encountered geometries will be listed below:

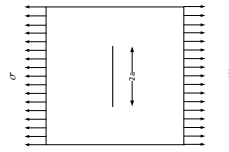


Figure 4.1: Middle Tension Panel

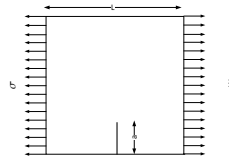


Figure 4.2: Single Edge Notch Tension Panel

Middle Tension Panel (MT), Fig. 4.1

$$K_I = \underbrace{\sqrt{\sec \frac{\pi a}{W}}}_{\beta} \sigma \sqrt{\pi a} \quad (4.2)$$

$$= \underbrace{\left[1 + 0.256 \left(\frac{a}{W} \right) - 1.152 \left(\frac{a}{W} \right)^2 + 12.2 \left(\frac{a}{W} \right)^3 \right]}_{\beta} \sigma \sqrt{\pi a} \quad (4.3)$$

We note that for W very large with respect to a , $\sqrt{\pi \sec \frac{\pi a}{W}} = 1$ as anticipated.

Single Edge Notch Tension Panel (SENT) for $\frac{L}{W} = 2$, Fig. 4.2

$$K_I = \underbrace{\left[1.12 - 0.23 \left(\frac{a}{W} \right) + 10.56 \left(\frac{a}{W} \right)^2 - 21.74 \left(\frac{a}{W} \right)^3 + 30.42 \left(\frac{a}{W} \right)^4 \right]}_{\beta} \sigma \sqrt{\pi a} \quad (4.4)$$

We observe that here the β factor for small crack ($\frac{a}{W} \ll 1$) is greater than one and is approximately 1.12.

Double Edge Notch Tension Panel (DENT), Fig. 4.3

$$K_I = \underbrace{\left[1.12 + 0.43 \left(\frac{a}{W} \right) - 4.79 \left(\frac{a}{W} \right)^2 + 15.46 \left(\frac{a}{W} \right)^3 \right]}_{\beta} \sigma \sqrt{\pi a} \quad (4.5)$$

Three Point Bend (TPB), Fig. 4.4

¹In most cases, a refers to half the total crack length.

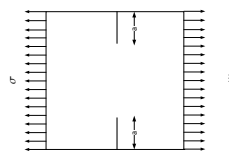


Figure 4.3: Double Edge Notch Tension Panel

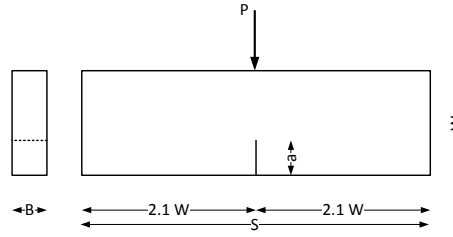


Figure 4.4: Three Point Bend Beam

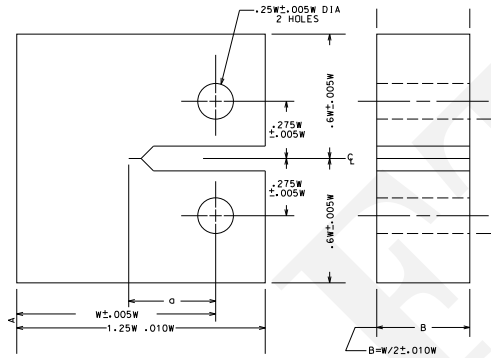


Figure 4.5: Compact Tension Specimen

$$K_I = \frac{3\sqrt{\frac{a}{W}} \left[1.99 - \left(\frac{a}{W}\right) \left(1 - \frac{a}{W}\right) \left(2.15 - 3.93\frac{a}{W} + 2.7\left(\frac{a}{W}\right)^2\right) \right]}{2 \left(1 + 2\frac{a}{W}\right) \left(1 - \frac{a}{W}\right)^{\frac{3}{2}}} \frac{PS}{BW^{\frac{3}{2}}} \quad (4.6)$$

Compact Tension Specimen (CTS), Fig. 4.5 used in ASTM E-399 (399) Standard Test Method for Plane-Strain Fracture Toughness of Metallic Materials

$$K_I = \underbrace{\left[16.7 - 104.6\left(\frac{a}{W}\right) + 370\left(\frac{a}{W}\right)^2 - 574\left(\frac{a}{W}\right)^3 + 361\left(\frac{a}{W}\right)^4 \right]}_{\beta} \underbrace{\frac{P}{BW}}_{\sigma} \sqrt{\pi a} \quad (4.7)$$

We note that this is not exactly the equation found in the ASTM standard, but rather an equivalent one written in the standard form.

Circular Holes: First let us consider the approximate solution of this problem, Fig. 4.6, then we will present the exact one:

Approximate: For a plate with a far field uniform stress σ , we know that there is a stress concentration factor of 3. for a crack radiating from this hole, we consider two cases

Short Crack: $\frac{a}{D} \rightarrow 0$, and thus we have an approximate far field stress of 3σ , and for an edge crack $\beta = 1.12$, Fig. 4.6 thus

$$\begin{aligned} K_I &= 1.12(3\sigma)\sqrt{\pi a} \\ &= 3.36\sigma\sqrt{\pi a} \end{aligned} \quad (4.8)$$

Long Crack $D \ll 2a + D$, in this case, we can for all practical purposes ignore the presence of the hole, and assume that we have a central crack with an effective length $a_{eff} = \frac{2a+D}{2}$, thus

$$\begin{aligned} K_I &= \sigma\sqrt{\pi\frac{2a+D}{2}} \\ &= \underbrace{\sqrt{1 + \frac{D}{2a}}}_{\beta} \sigma\sqrt{\pi a} \end{aligned} \quad (4.9)$$

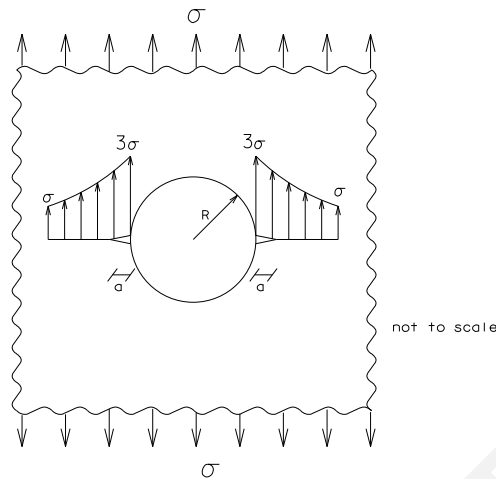


Figure 4.6: Approximate Solutions for Two Opposite Short Cracks Radiating from a Circular Hole in an Infinite Plate under Tension



Figure 4.7: Approximate Solutions for Long Cracks Radiating from a Circular Hole in an Infinite Plate under Tension

Similarly, if we had only one single crack radiating from a hole, for short crack, β remains equal to 3.36, whereas for long crack, Fig. 4.7 we obtain:

$$\begin{aligned}
 K_I &= \sigma \sqrt{\pi \frac{a+D}{2}} \\
 &= \underbrace{\sqrt{\frac{1}{2} + \frac{D}{2a}}}_{\beta} \sigma \sqrt{\pi a}
 \end{aligned}
 \tag{4.10}$$

Exact: Whereas the preceding equations give accurate results for both very short and very large cracks, in the intermediary stage an exact numerical solution was derived by Newman (Newman, 1971), Fig. 4.8

$$K_I = \beta \sigma \sqrt{\pi a}
 \tag{4.11}$$

where, using Newman's solution β is given in Table 4.1

Pressurized Hole with Radiating Cracks: Again we will use Newman's solution for this problem, and distinguish two cases:

Pressurized Hole Only: or $\lambda = 0$, Fig. 4.9

$$K_I = \beta \frac{2pR}{\sqrt{\pi a}}
 \tag{4.12}$$

Pressurized Hole and Crack: or $\lambda = 1$

$$K_I = \beta p \sqrt{\pi a}
 \tag{4.13}$$

For both cases, β is given in Table 4.1. We note that for the pressurized hole only, K_I decreases with crack length, hence we would have a stable crack growth. We also note that K_I would be the same for a pressurized crack and borehole, as it would have been for an unpressurized hole but an identical far field stress. (WHY?)

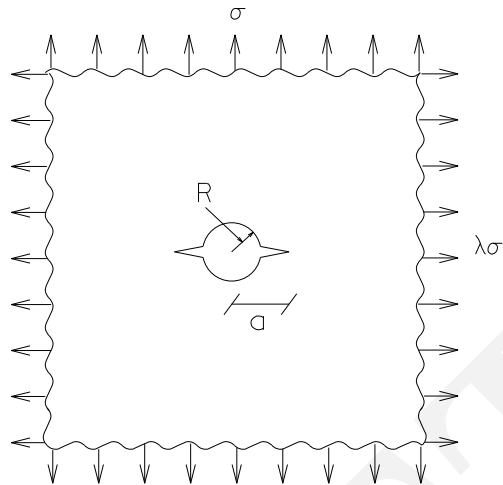


Figure 4.8: Radiating Cracks from a Circular Hole in an Infinite Plate under Biaxial Stress

$\frac{a}{R}$	β Biaxial Stress			β Pressurized Hole	
	$\lambda = -1$	$\lambda = 1$	$\lambda = 0$	$\lambda = 1$	$\lambda = 0$
1.01	0.4325	0.3256	0.2188	.2188	.1725
1.02	.5971	.4514	.3058	.3058	.2319
1.04	.7981	.6082	.4183	.4183	.3334
1.06	.9250	.7104	.4958	.4958	.3979
1.08	1.0135	.7843	.5551	.5551	.4485
1.10	1.0775	.8400	.6025	.6025	.4897
1.15	1.1746	.9322	.6898	.6898	.5688
1.20	1.2208	.9851	.7494	.7494	.6262
1.25	1.2405	1.0168	.7929	.7929	.6701
1.30	1.2457	1.0358	.8259	.8259	.7053
1.40	1.2350	1.0536	.8723	.8723	.7585
1.50	1.2134	1.0582	.9029	.9029	.7971
1.60	1.1899	1.0571	.9242	.9242	.8264
1.80	1.1476	1.0495	.9513	.9513	.8677
2.00	1.1149	1.0409	.9670	.9670	.8957
2.20	1.0904	1.0336	.9768	.9768	.9154
2.50	1.0649	1.0252	.9855	.9855	.9358
3.00	1.0395	1.0161	.99267	.99267	.9566
4.00	1.0178	1.0077	.9976	.9976	.9764

Table 4.1: Newman's Solution for Circular Hole in an Infinite Plate subjected to Biaxial Loading, and Internal Pressure

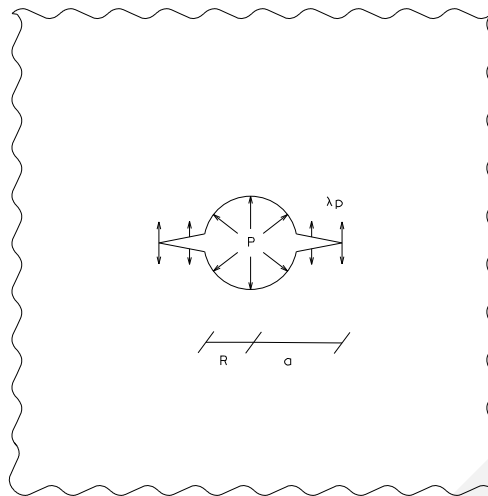


Figure 4.9: Pressurized Hole with Radiating Cracks

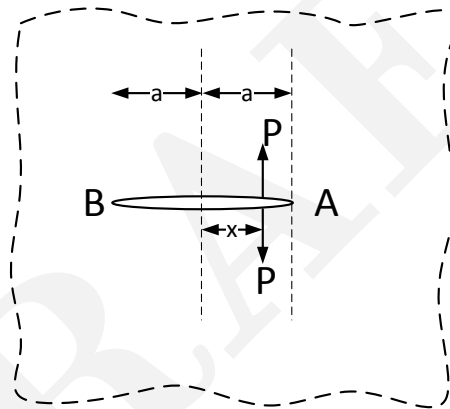


Figure 4.10: Two Opposite Point Loads acting on the Surface of an Embedded Crack

Point Load Acting on Crack Surfaces of an Embedded Crack: The solution of this problem, Fig. 4.10 and the subsequent one, is of great practical importance, as it provides the Green's function for numerous other ones.

$$K_I^A = \frac{P}{\pi a} \sqrt{\frac{a+x}{a-x}} \quad (4.14)$$

$$K_I^B = \frac{P}{\pi a} \sqrt{\frac{a-x}{a+x}} \quad (4.15)$$

Point Load Acting on Crack Surfaces of an Edge Crack: The solution of this problem, Fig. 4.11 is

$$K_I = \frac{2P}{\pi a} \frac{C}{\sqrt{1 + \left(\frac{x}{a}\right)^2}} \left[-0.4 \left(\frac{x}{a}\right)^2 + 1.3 \right] \quad (4.16)$$

where C is tabulated in Table 4.2

Embedded Elliptical Crack A large number of naturally occurring defects are present as embedded, surface or corner cracks (such as fillet welding) Irwin, (Irwin, 1962) proposed the following solution for the elliptical crack, with $x = a \cos \theta$ and

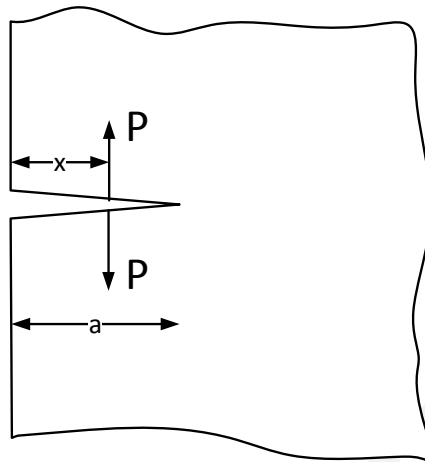


Figure 4.11: Two Opposite Point Loads acting on the Surface of an Edge Crack

$\frac{x}{a}$	C
< 0.6	1
0.6-0.7	1.01
0.7-0.8	1.03
0.8-0.9	1.07
> 0.9	1.11

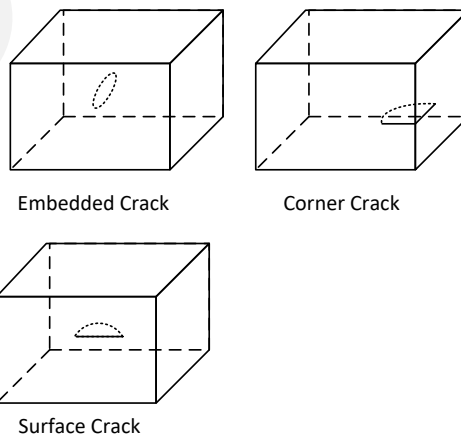
Table 4.2: C Factors for Point Load on Edge Crack

Figure 4.12: Embedded, Corner, and Surface Cracks

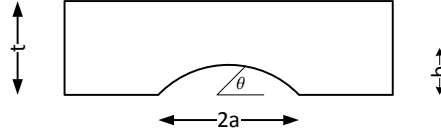


Figure 4.13: Elliptical Crack, and Newman's Solution

$$y = b \sin \theta:$$

$$K_I(\theta) = \frac{1}{\Phi_0} \left(\sin^2 \theta + \frac{b^2}{a^2} \cos^2 \theta \right)^{\frac{1}{4}} \sigma \sqrt{\pi b} \quad (4.17)$$

where Φ_0 is a complete elliptical integral of the second kind

$$\Phi_0 = \int_0^{\frac{\pi}{2}} \sqrt{1 - \frac{a^2 - b^2}{a^2} \sin^2 \theta} d\theta \quad (4.18)$$

$$= \sqrt{Q} \quad (4.19)$$

An approximation to Eq. 4.17 was given by Cherepanov (Cherepanov, 1979)

$$K_I = \left[\sin^2 \theta + \left(\frac{b}{a} \right)^2 \cos^2 \theta \right]^{\frac{1}{4}} \sigma \sqrt{\pi b} \quad (4.20)$$

for $0 \leq \frac{b}{a} \leq 1$.

This solution calls for the following observations:

1. If $a = b$ then we have a "penny-shape" circular crack and Eq. 4.17 reduces to

$$K_I = \frac{2}{\pi} \sigma \sqrt{\pi a} \quad (4.21)$$

2. If $a = \infty$ & $\theta = \frac{\pi}{2}$ then we retrieve the solution $K_I = \sigma \sqrt{\pi a}$ of a through crack.
3. At the end of the minor axes, $\theta = \frac{\pi}{2}$ the stress intensity factor is maximum:

$$(K_I)_{\theta=\frac{\pi}{2}} = \frac{\sigma \sqrt{\pi b}}{\Phi_0} = \sigma \sqrt{\frac{\pi b}{Q}} \quad (4.22)$$

4. At the end of the major axes, $\theta = 0$ the stress intensity factor is minimum

$$(K_I)_{\theta=0} = \frac{\sigma \sqrt{\pi \frac{b^2}{a}}}{\Phi_0} \quad (4.23)$$

Thus an embedded elliptical crack will propagate into a circular one "penny-shaped".

Surface Cracks Irwin's original solution has been extended to semi-elliptical surface flaws, quarter elliptical corner cracks, and to surface cracks emanating from circular holes. Using the results of three dimensional finite element analysis, Newman and Raju (Newman and Raju, 1981) developed an empirical SIF equation for semi-elliptical surface cracks, Fig. 4.13. The equation applies for cracks of arbitrary shape factor in finite size plates for both tension and bending loads. This is perhaps the most accurate solution and is almost universally used:

$$K = \sigma \sqrt{\pi b} \left[M_1 + M_2 \left(\frac{b}{t} \right)^2 + M_3 \left(\frac{b}{t} \right)^4 \right] \left[1 + 1.464 \left(\frac{b}{a} \right)^{1.65} \right]^{-\frac{1}{2}} \left[\left(\frac{b}{a} \right)^2 \cos^2 \theta + \sin^2 \theta \right]^{\frac{1}{4}} \left\{ 1 + \left[0.1 + 0.35 \left(\frac{b}{t} \right)^2 \right] (1 - \sin \theta)^2 \right\} \quad (4.24)$$

Material	K_{Ic} ksi $\sqrt{\text{in}}$
Steel, Medium Carbon	49
Steel, Pressure Vessel	190
Hardened Steel	20
Aluminum	20-30
Titanium	70
Copper	100
Lead	18
Glass	0.7
Westerly Granite	16
Cement Paste	0.5
Concrete	1
Nylon	3

Table 4.3: Approximate Fracture Toughness of Common Engineering Materials

$$M_1 = 1.13 - 0.09 \left(\frac{b}{a} \right) \quad (4.25)$$

$$M_2 = 0.89 \left[0.2 + \left(\frac{b}{a} \right) \right]^{-1} - 0.54 \quad (4.26)$$

$$M_3 = 0.5 - \left[0.65 + \left(\frac{b}{a} \right) \right]^{-1} + 14 \left[1 - \left(\frac{b}{a} \right) \right]^{24} \quad (4.27)$$

Newman and Raju report that this equation is accurate within ± 5 percent, provided $0 < \frac{b}{a} \leq 1.0$ and $\frac{b}{t} \leq 0.8$. For $\frac{b}{a}$ approximately equal to 0.25, K is roughly independent of θ . For shallow cracks $\frac{b}{t} \ll 1$, Equation 4.24 reduces to

$$K = 1.13\sigma\sqrt{\pi b} \left[1 - .08 \left(\frac{b}{a} \right) \right] \left[1 + 1.464 \left(\frac{b}{a} \right)^{1.65} \right]^{-\frac{1}{2}} \quad (4.28)$$

For very long cracks $\frac{b}{a} \ll 1$, Equation 4.24 reduces to

$$K = 1.13\sigma\sqrt{\pi b} \left[1 + 3.46 \left(\frac{b}{t} \right)^2 + 11.5 \left(\frac{b}{t} \right)^4 \right] \quad (4.29)$$

4.3 Fracture Properties of Materials

Whereas fracture toughness testing will be the object of a separate chapter, we shall briefly mention the appropriate references from where fracture toughness values can be determined.

Metallic Alloys: Testing procedures for fracture toughness of metallic alloys are standardized by various codes (see (399) and (BSI, 1977)). An exhaustive tabulation of fracture toughnesses of numerous alloys can be found in (Hudson and Seward, 1978) and (Hudson and Seward, 1982).

Concrete: Fracture mechanics evolved primarily from mechanical and metallurgical applications, but there has been much recent interest in its applicability to both concrete and rocks. Although there is not yet a standard for fracture toughness of concrete, Hillerborg (Anon., 1985) has proposed a standard procedure for determining G_F . Furthermore, a subcommittee of ASTM E399 is currently looking into a proposed testing procedure for concrete.

Rock: Ouchterlony has a comprehensive review of fracture toughnesses of numerous rocks in an appendix of (Ouchterlony, 1986), and a proposed fracture toughness testing procedure can be found in (Ouchterlony, 1982).

Table 4.3 provides an indication of the fracture toughness of common engineering materials. Note that stress intensity factors in metric units are commonly expressed in $\text{Mpa}\sqrt{\text{m}}$, and that

$$1\text{ksi}\sqrt{\text{in}} = 1.099\text{Mpa}\sqrt{\text{m}} \quad (4.30)$$

Yield Stress Ksi	K_{Ic} ksi $\sqrt{\text{in}}$
210	65
220	60
230	40
240	38
290	35
300	30

Table 4.4: Fracture Toughness vs Yield Stress for .45C – N_i – C_r – M_o Steel

4.4 Examples

4.4.1 Example 1

Assume that a component in the shape of a large sheet is to be fabricated from .45C – N_i – C_r – M_o steel, with a decreasing fracture toughness with increase in yield stress, Table 4.4. The smallest crack size ($2a$) which can be detected is approximately .12 in. The specified design stress is $\frac{\sigma_y}{2}$. To save weight, an increase of tensile strength from 220 ksi to 300 ksi is suggested. Is this reasonable?

At 220 ksi $K_{Ic} = 60$ ksi $\sqrt{\text{in}}$, and at 300 ksi $K_{Ic} = 30$ ksi $\sqrt{\text{in}}$. Thus, the design stress will be given by $\sigma_d = \frac{\sigma_y}{2}$ and from $K_{Ic} = \sigma_d \sqrt{\pi a_{cr}} \Rightarrow a_{cr} = \frac{1}{\pi} \left(\frac{K_{Ic}}{\frac{\sigma_y}{2}} \right)^2$

Thus,

Yield Stress σ_y	Design Stress σ_d	Fracture Toughness K_{Ic}	Critical Crack a_{cr}	Total Crack $2a_{cr}$
220	110	60	.0947	.189
300	150	30	.0127	.0255

We observe that for the first case, the total crack length is larger than the smallest one which can be detected (which is O.K.); Alternatively, for the second case the total critical crack size is approximately five times smaller than the minimum flaw size required and approximately eight times smaller than the flaw size tolerated at the 220 ksi level.

Hence, σ_y should not be raised to 300 ksi.

Finally, if we wanted to use the flaw size found with the 300 ksi alloy, we should have a decrease in design stress (since K_{Ic} and a_{cr} are now set) $K_{Ic} = \sigma_d \sqrt{\pi a_{vis}} \Rightarrow \sigma_d = \frac{K_{Ic}}{\sqrt{\pi a_{vis}}} = \frac{30 \text{ ksi} \sqrt{\text{in}}}{\sqrt{0.06\pi}} = 69$ ksi, with a potential factor of safety of one against cracking (we can not be sure 100% that there is no crack of that size or smaller as we can not detect it). We observe that since the design stress level is approximately half of that of the weaker alloy, there will be a two fold increase in weight.

4.4.2 Example 2

A small beer barrel of diameter 15" and wall thickness of .126" made of aluminum alloy exploded when a pressure reduction valve malfunctioned and the barrel experienced the 610 psi full pressure of the CO₂ cylinder supplying it with gas. Afterwards, cracks approximately 4.0 inch long by (probably) .07 inch deep were discovered on the inside of the salvaged pieces of the barrel (it was impossible to measure their depth). Independent tests gave 40. ksi $\sqrt{\text{in}}$ for K_{Ic} of the aluminum alloy. The question is whether the cracks were critical for the 610 psi pressure?

For a cylinder under internal pressure, the hoop stress is $\sigma = \frac{pD}{2t} = \frac{610 \text{ lb}}{\text{in}^2} \frac{15 \text{ in}}{2(.126) \text{ in}} = 36,310 \text{ psi} = 36.3 \text{ ksi}$. This can be used as the far field stress (neglecting curvature).

First we use the exact solution as given in Eq. 4.24, with $a = 2$ in, $b = .07$ in, and $t = .126$ in. upon substitution we obtain:

$$\begin{aligned}
 M_1 &= 1.13 - 0.09 \left(\frac{.07}{2} \right) \\
 &= 1.127 \\
 M_2 &= 0.89 \left[0.2 + \left(\frac{.07}{2} \right) \right]^{-1} - 0.54 \\
 &= 3.247 \\
 M_3 &= 0.5 - \left[0.65 + \left(\frac{.07}{2} \right) \right]^{-1} + 14 \left[1 - \left(\frac{.07}{2} \right) \right]^{24} \\
 &= 4.994
 \end{aligned}$$

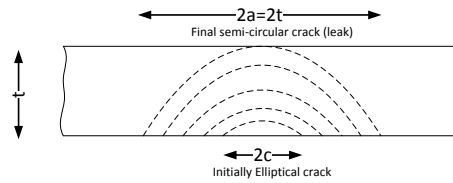


Figure 4.14: Growth of Semielliptical surface Flaw into Semicircular Configuration

Substituting

$$\begin{aligned}
 K &= 36.3\sqrt{\pi(.07)} \left[1.127 + 3.247 \left(\frac{.07}{.126} \right)^2 + 4.994 \left(\frac{.07}{.126} \right)^4 \right] \left[1 + 1.464 \left(\frac{.07}{2} \right)^{1.65} \right]^{-\frac{1}{2}} \\
 &\quad \left[\left(\frac{.07}{2} \right)^2 + 1 \right]^{\frac{1}{4}} \left\{ 1 + \left[0.1 + 0.35 \left(\frac{.07}{.126} \right)^2 \right] (1 - 1)^2 \right\} \\
 &= 44.2 \text{ksi}\sqrt{\text{in}}
 \end{aligned}$$

This is about equal to the fracture toughness.

Note that if we were to use the approximate equation, for long cracks we would have obtained:

$$\begin{aligned}
 K &= (1.13)(36.3)\sqrt{\pi(.07)} \left[1 + 3.46 \left(\frac{.07}{.126} \right)^2 + 11.5 \left(\frac{.07}{.126} \right)^4 \right] \\
 &= 60.85 \\
 &> K_{Ic}
 \end{aligned}$$

4.5 Additional Design Considerations

4.5.1 Leak Before Fail

¹⁰ As observed from the preceding example, many pressurized vessels are subject to crack growth if internal flaws are present. Two scenarios may happen, Fig. 4.14

Break-through: In this case critical crack configuration is reached before the crack has “daylighted”, and there is a sudden and unstable crack growth.

Leak Before Fail: In this case, crack growth occur, and the crack “pierces” through the thickness of the vessel before unstable crack growth occurs. This in turn will result in a sudden depressurization, and this will stop any further crack growth.

¹¹ Hence, pressurized vessels should be designed to ensure a *leak before fail* failure scenario, as this would usually be immediately noticed and corrected (assuming that there is no leak of flammable gas!).

¹² Finally, it should be noted that leak before break assessment should be made on the basis of a complete *residual strength diagram* for both the part through and the through crack. Various ratios should be considered

4.5.2 Damage Tolerance Assessment

¹³ Fracture mechanics is not limited to determining the critical crack size, load, or stress combination. It can also be applied to establish a fracture control plan, or damage tolerance analysis with the following objectives:

1. Determine the effect of cracks on strength. This will result in a plot of crack size versus residual strength, or *Residual Strength Diagram*
2. Determine crack growth with time, resulting in *Crack Growth Curve*.

Chapter 5

THEORETICAL STRENGTH of SOLIDS; (Griffith I)

¹ We recall that Griffith's involvement with fracture mechanics started as he was exploring the disparity in strength between glass rods of different sizes, (Griffith, 1921). As such, he had postulated that this can be explained by the presence of internal flaws (idealized as elliptical) and then used Inglis solution to explain this discrepancy.

² In this section, we shall develop an expression for the theoretical strength of perfect crystals (theoretically the strongest form of solid). This derivation, (Kelly, 1974) is fundamentally different than the one of Griffith as it starts at the atomic level.

5.1 Derivation

³ We start by exploring the energy of interaction between two adjacent atoms at equilibrium separated by a distance a_0 , Fig. 5.1. The total energy which must be supplied to separate atom C from C' is

$$U_0 = 2\gamma \quad (5.1)$$

where γ is the surface energy¹, and the factor of 2 is due to the fact that upon separation, we have two distinct surfaces.

5.1.1 Tensile Strength

5.1.1.1 Ideal Strength in Terms of Physical Parameters

⁴ We shall first derive an expression for the ideal strength in terms of physical parameters, and in the next section the strength will be expressed in terms of engineering ones.

Force being the derivative of energy, we have $F = \frac{dU}{da}$, thus $F = 0$ at $a = a_0$, Fig. 5.2, and is maximum at the inflection point of the $U_0 - a$ curve. Hence, the slope of the force displacement curve is the stiffness of the atomic spring and should be related to E . If we let $x = a - a_0$, then the strain would be equal to $\varepsilon = \frac{x}{a_0}$. Furthermore, if we define the stress as $\sigma = \frac{F}{a_0}$, then the $\sigma - \varepsilon$ curve will be as shown in Fig. 5.3. From this diagram, it would appear that the sine curve would be an adequate approximation to this relationship. Hence,

$$\sigma = \sigma_{max}^{theor} \sin 2\pi \frac{x}{\lambda} \quad (5.2)$$

and the maximum stress σ_{max}^{theor} would occur at $x = \frac{\lambda}{4}$. The energy required to separate two atoms is thus given by the area under the sine curve, and from Eq. 5.1, we would have

$$2\gamma = U_0 = \int_0^{\frac{\lambda}{2}} \sigma_{max}^{theor} \sin \left(2\pi \frac{x}{\lambda} \right) dx \quad (5.3)$$

$$= \frac{\lambda}{2\pi} \sigma_{max}^{theor} \left[-\cos \left(\frac{2\pi x}{\lambda} \right) \right] \Big|_0^{\frac{\lambda}{2}} \quad (5.4)$$

$$= \frac{\lambda}{2\pi} \sigma_{max}^{theor} \left[\overbrace{-\cos \left(\frac{2\pi \lambda}{2\lambda} \right)}^{-1} + \overbrace{\cos(0)}^1 \right] \quad (5.5)$$

$$\Rightarrow \lambda = \frac{2\gamma\pi}{\sigma_{max}^{theor}} \quad (5.6)$$

Also for very small displacements (small x) $\sin x \approx x$, thus Eq. 5.2 reduces to

$$\sigma \approx \sigma_{max}^{theor} \frac{2\pi x}{\lambda} \approx E \frac{x}{a_0} \quad (5.7)$$

¹From watching raindrops and bubbles it is obvious that liquid water has surface tension. When the surface of a liquid is extended (soap bubble, insect walking on liquid) work is done against this tension, and energy is stored in the new surface. When insects walk on water it sinks until the surface energy just balances the decrease in its potential energy. For solids, the chemical bonds are stronger than for liquids, hence the surface energy is stronger. The reason why we do not notice it is that solids are too rigid to be distorted by it. Surface energy γ is expressed in J/m^2 and the surface energies of water, most solids, and diamonds are approximately .077, 1.0, and 5.14 respectively.

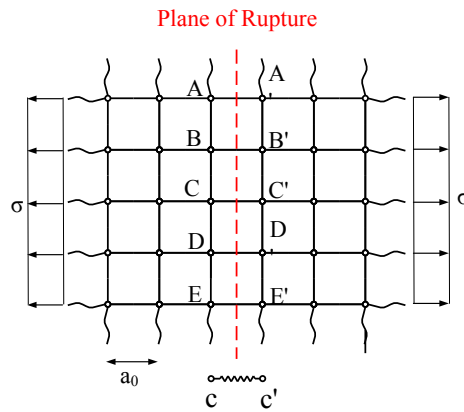
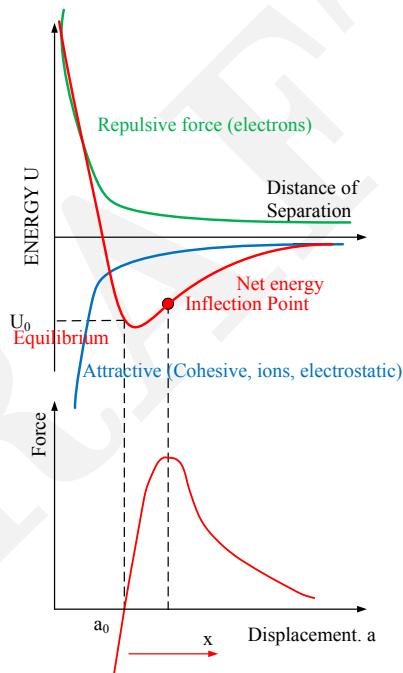


Figure 5.1: Uniformly Stressed Layer of Atoms Separated by a_0



Solution I:

Figure 5.2: Energy and Force Binding Two Adjacent Atoms

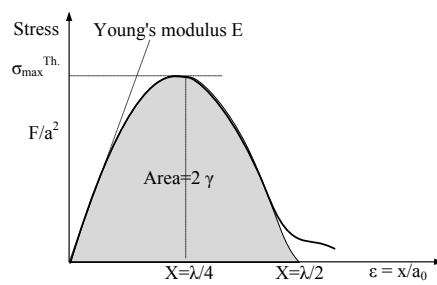


Figure 5.3: Stress Strain Relation at the Atomic Level

eliminating x ,

$$\sigma_{max}^{theor} \approx \frac{E}{a_0} \frac{\lambda}{2\pi} \quad (5.8)$$

Substituting for λ from Eq. 5.6, we get

$$\sigma_{max}^{theor} \approx \sqrt{\frac{E\gamma}{a_0}} \quad (5.9)$$

Solution II: For two layers of atoms a_0 apart, the strain energy per unit area due to σ (for linear elastic systems) is

$$\left. \begin{aligned} U &= \frac{1}{2} \sigma \varepsilon a_0 \\ \sigma &= E \varepsilon \end{aligned} \right\} U = \frac{\sigma^2 a_0}{2E} \quad (5.10)$$

If γ is the surface energy of the solid per unit area, then the total surface energy of two new fracture surfaces is 2γ .

For our theoretical strength, $U = 2\gamma \Rightarrow \frac{(\sigma_{max}^{theor})^2 a_0}{2E} = 2\gamma$ or $\sigma_{max}^{theor} = 2\sqrt{\frac{\gamma E}{a_0}}$

Note that here we have assumed that the material obeys Hooke's Law up to failure, since this is seldom the case, we can simplify this approximation to:

$$\sigma_{max}^{theor} = \sqrt{\frac{E\gamma}{a_0}} \quad (5.11)$$

which is the same as Equation 5.9

Example: As an example, let us consider steel which has the following properties: $\gamma = 1 \frac{J}{m^2}$; $E = 2 \times 10^{11} \frac{N}{m^2}$; and $a_0 \approx 2 \times 10^{-10} m$. Thus from Eq. 5.9 we would have:

$$\sigma_{max}^{theor} \approx \sqrt{\frac{(2 \times 10^{11})(1)}{2 \times 10^{-10}}} \quad (5.12)$$

$$\approx 3.16 \times 10^{10} \frac{N}{m^2} \quad (5.13)$$

$$\approx \frac{E}{6} \quad (5.14)$$

Thus this would be the ideal theoretical strength of steel.

5.1.1.2 Ideal Strength in Terms of Engineering Parameter

5 We note that the force to separate two atoms drops to zero when the distance between them is $a_0 + a$ where a_0 corresponds to the origin and a to $\frac{\lambda}{2}$. Thus, if we take $a = \frac{\lambda}{2}$ or $\lambda = 2a$, combined with Eq. 5.8 would yield

$$\sigma_{max}^{theor} \approx \frac{E}{a_0} \frac{a}{\pi} \quad (5.15)$$

6 Alternatively combining Eq. 5.6 with $\lambda = 2a$ gives

$$a \approx \frac{\gamma\pi}{\sigma_{max}^{theor}} \quad (5.16)$$

7 Combining those two equations

$$\gamma \approx \frac{E}{a_0} \left(\frac{a}{\pi}\right)^2 \quad (5.17)$$

8 However, since as a first order approximation $a \approx a_0$ then the surface energy will be

$$\gamma \approx \frac{E a_0}{10} \quad (5.18)$$

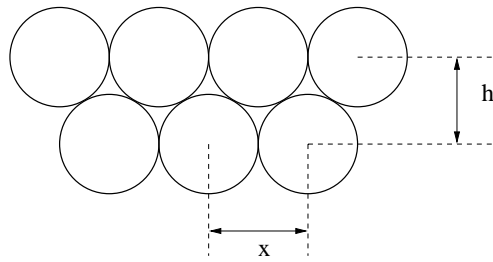


Figure 5.4: Influence of Atomic Misfit on Ideal Shear Strength

9 This equation, combined with Eq. 5.9 will finally give

$$\sigma_{max}^{theor} \approx \frac{E}{\sqrt{10}} \quad (5.19)$$

which is an approximate expression for the theoretical maximum strength in terms of E .

5.1.2 Shear Strength

10 Similar derivation can be done for shear. What happen if we slide the top row over the bottom one. Again, we can assume that the shear stress is

$$\tau = \tau_{max}^{theor} \sin 2\pi \frac{x}{\lambda} \quad (5.20)$$

and from basic elasticity

$$\tau = G\gamma_{xy} \quad (5.21)$$

and, Fig. 5.4 $\gamma_{xy} = x/h$.

11 Because we do have very small displacement, we can eliminate x from

$$\begin{aligned} \tau_{max}^{theor} \sin 2\pi \frac{x}{\lambda} &\simeq \frac{2\pi x}{\lambda} = \gamma G = \frac{x}{h} G \\ \Rightarrow \tau_{max}^{theor} &= \frac{G\lambda}{2\pi h} \end{aligned} \quad (5.22-a)$$

12 If we do also assume that $\lambda = h$, and $G = E/2(1 + \nu)$, then

$$\tau_{max}^{theor} \simeq \frac{E}{12(1 + \nu)} \simeq \frac{E}{18} \quad (5.23)$$

5.2 Griffith Theory

13 Around 1920, Griffith was exploring the theoretical strength of solids by performing a series of experiments on glass rods of various diameters. He observed that the tensile strength (σ_t) of glass decreased with an increase in diameter, and that for a diameter $\phi \approx \frac{1}{10,000}$ in., $\sigma_t = 500,000$ psi; furthermore, by extrapolation to “zero” diameter he obtained a theoretical maximum strength of approximately 1,600,000 psi, and on the other hand for very large diameters the asymptotic values was around 25,000 psi.

14 Griffith had thus demonstrated that the theoretical strength could be experimentally approached, he now needed to show why the great majority of solids fell so far below it.

5.2.1 Derivation

15 In his quest for an explanation, he came across Inglis's paper, and his "strike of genius" was to assume that strength is reduced due to the presence of internal flaws. Griffith postulated that the theoretical strength can only be reached at the point of highest stress concentration, and accordingly the far-field applied stress will be much smaller.

16 Hence, assuming an elliptical imperfection, and from equation 3.30

$$\sigma_{max}^{theor} = \sigma_{cr}^{act} \left(1 + 2\sqrt{\frac{a}{\rho}} \right) \quad (5.24)$$

σ is the stress at the tip of the ellipse which is caused by a (lower) far field stress σ_{cr}^{act} .

17 Assuming $\rho \approx a_0$ and since $2\sqrt{\frac{a}{a_0}} \gg 1$, for an ideal plate under tension with only one single elliptical flaw the strength may be obtained from

$$\underbrace{\sigma_{max}^{theor}}_{\text{micro}} = 2 \underbrace{\sigma_{cr}^{act}}_{\text{macro}} \sqrt{\frac{a}{a_0}} \quad (5.25)$$

hence, equating with Eq. 5.9, we obtain

$$\boxed{\sigma_{max}^{theor} = 2 \underbrace{\sigma_{cr}^{act}}_{\text{Macro}} \sqrt{\frac{a}{a_0}} = \underbrace{\sqrt{\frac{E\gamma}{a_0}}}_{\text{Micro}}} \quad (5.26)$$

18 From this very important equation, we observe that

1. The left hand side is based on a linear elastic solution of a macroscopic problem solved by Inglis.
2. The right hand side is based on the theoretical strength derived from the sinusoidal stress-strain assumption of the inter-atomic forces, and finds its roots in micro-physics.

19 Finally, this equation would give (at fracture)

$$\boxed{\sigma_{cr}^{act} = \sqrt{\frac{E\gamma}{4a}}} \quad (5.27)$$

20 As an example, let us consider a flaw with a size of $2a = 5,000a_0$

$$\left. \begin{aligned} \sigma_{cr}^{act} &= \sqrt{\frac{E\gamma}{4a}} \\ \gamma &= \frac{Ea_0}{10} \end{aligned} \right\} \left. \begin{aligned} \sigma_{cr}^{act} &= \sqrt{\frac{E^2 a_0}{40 a}} \\ \frac{a}{a_0} &= 2,500 \end{aligned} \right\} \sigma_{cr}^{act} = \sqrt{\frac{E^2}{100,000}} = \frac{E}{100\sqrt{10}} \quad (5.28)$$

21 Thus if we set a flaw size of $2a = 5,000a_0$ in $\gamma \approx \frac{Ea_0}{10}$ this is enough to lower the theoretical fracture strength from $\frac{E}{\sqrt{10}}$ to a critical value of magnitude $\frac{E}{100\sqrt{10}}$, or a factor of 100.

22 Also

$$\left. \begin{aligned} \sigma_{max}^{theor} &= 2\sigma_{cr}^{act} \sqrt{\frac{a}{a_0}} \\ a &= 10^{-6}m = 1\mu m \\ a_0 &= 1\text{\AA} = \rho = 10^{-10}m \end{aligned} \right\} \sigma_{max}^{theor} = 2\sigma_{cr}^{act} \sqrt{\frac{10^{-6}}{10^{-10}}} = 200\sigma_{cr}^{act} \quad (5.29)$$

23 Therefore at failure

$$\left. \begin{aligned} \sigma_{cr}^{act} &= \frac{\sigma_{max}^{theor}}{200} \\ \sigma_{max}^{theor} &= \frac{E}{10} \end{aligned} \right\} \sigma_{cr}^{act} \approx \frac{E}{2,000} \quad (5.30)$$

which can be attained. For instance for steel $\frac{E}{2,000} = \frac{30,000}{2,000} = 15$ ksi

Chapter 6

ENERGY TRANSFER in CRACK GROWTH; (Griffith II)

- ¹ In the preceding chapters, we have focused on the singular stress field around a crack tip. On this basis, a criteria for crack propagation, based on the strength of the singularity was first developed and then used in practical problems.
- ² An alternative to this approach, is one based on energy transfer (or release), which occurs during crack propagation. This dual approach will be developed in this chapter.
- ³ Griffith's main achievement, in providing a basis for the fracture strengths of bodies containing cracks, was his realization that it was possible to derive a thermodynamic criterion for fracture by considering the total change in energy of a cracked body as the crack length increases, (Griffith, 1921).
- ⁴ Hence, Griffith showed that material fail not because of a maximum stress, but rather because a certain energy criteria was met.
- ⁵ Thus, the Griffith model for elastic solids, and the subsequent one by Irwin and Orowan for elastic-plastic solids, show that crack propagation is caused by a transfer of energy transfer from external work and/or strain energy to surface energy.
- ⁶ It should be noted that this is a *global energy* approach, which was developed prior to the one of Westergaard which focused on the stress field surrounding a crack tip. It will be shown later that for linear elastic solids the two approaches are identical.

6.1 Thermodynamics of Crack Growth

6.1.1 General Derivation

- ⁷ If we consider a crack in a deformable continuum subjected to arbitrary loading, then the first law of thermodynamics gives: The change in energy is proportional to the amount of work performed. Since only the change of energy is involved, any datum can be used as a basis for measure of energy. Hence energy is neither created nor consumed.
- ⁸ The first law of thermodynamics states *The time-rate of change of the total energy (i.e., sum of the kinetic energy and the internal energy) is equal to the sum of the rate of work done by the external forces and the change of heat content per unit time:*

$$\frac{d}{dt}(K + U + \Gamma) = W + Q \quad (6.1)$$

where K is the kinetic energy, U the total internal strain energy (elastic plus plastic), Γ the surface energy, W the external work, and Q the heat input to the system.

- ⁹ Since all changes with respect to time are caused by changes in crack size, we can write

$$\frac{\partial}{\partial t} = \frac{\partial A}{\partial t} \frac{\partial}{\partial A} \quad (6.2)$$

and for an adiabatic system (no heat exchange) and if loads are applied in a quasi static manner (no kinetic energy), then Q and K are equal to zero, and for a unit thickness we can replace A by a , then we can rewrite the first law as

$$\underbrace{\frac{\partial W}{\partial a}}_{\text{External}} = \underbrace{\left(\frac{\partial U^e}{\partial a} + \frac{\partial U^p}{\partial a} \right)}_{\text{Internal}} + \frac{\partial \Gamma}{\partial a} \quad (6.3)$$

- ¹⁰ This equation represents the energy balance during crack growth. It indicates that the work rate supplied to the continuum by the applied external loads is equal to the rate of strain energy (elastic and plastic) dissipated during crack propagation.

- ¹¹ Thus

$$\begin{aligned}\Pi &\equiv U^e - W \\ \frac{\partial \Pi}{\partial a} &= \frac{\partial U^e}{\partial a} - \frac{\partial W}{\partial a} \\ &= \frac{\partial U^e}{\partial a} - \frac{\partial U^e}{\partial a} - \frac{\partial U^p}{\partial a} - \frac{\partial \Gamma}{\partial a}\end{aligned}\quad (6.4)$$

or

$$\boxed{-\frac{\partial \Pi}{\partial a} = \frac{\partial U^p}{\partial a} + \frac{\partial \Gamma}{\partial a}}\quad (6.5)$$

that is the rate of potential energy decrease during crack growth is equal to the rate of energy dissipated in plastic deformation and crack growth.

¹² It is very important to observe that the energy scales with a^2 , whereas surface energy scales with a . It will be shown later that this can have serious implication on the stability of cracks, and on size effects.

6.1.2 Brittle Material, Griffith's Model

¹³ For a perfectly brittle material, potential energy is released to create surface energy, hence we can rewrite Eq. 6.5 as

$$\boxed{G \stackrel{\text{def}}{=} -\frac{\partial \Pi}{\partial a} = \frac{\partial \Gamma}{\partial a} = 2\gamma}\quad (6.6)$$

the factor 2 appears because we have two material surfaces upon fracture. The left hand side represents the energy available for crack growth and is given the symbol G in honor of Griffith. Because G is derived from a potential function, it is often referred to as the crack driving force. The right hand side represents the resistance of the material that must be overcome for crack growth, and is a material constant (related to the toughness).

¹⁴ This equation represents the fracture criterion for crack growth, two limiting cases can be considered. They will be examined in conjunction with Fig. 6.1 in which we have a crack of length $2a$ located in an infinite plate subjected to load P . Griffith assumed

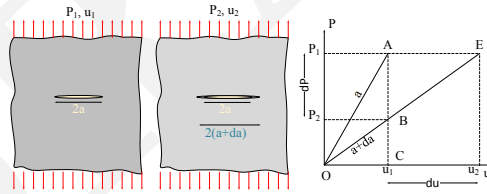


Figure 6.1: Energy Transfer in a Cracked Plate

that it was possible to produce a macroscopical load displacement ($P - u$) curve for two different crack lengths a and $a + da$.

Two different boundary conditions will be considered, and in each one the change in potential energy as the crack extends from a to $a + da$ will be determined:

Fixed Grip: ($u_2 = u_1$) loading, an increase in crack length from a to $a + da$ results in a decrease in stored elastic strain energy, ΔU ,

$$\Delta U = \frac{1}{2}P_2u_1 - \frac{1}{2}P_1u_1\quad (6.7)$$

$$= \frac{1}{2}(P_2 - P_1)u_1\quad (6.8)$$

$$< 0\quad (6.9)$$

Furthermore, under fixed grip there is no external work ($u_2 = u_1$), so the decrease in potential energy is the same as the decrease in stored internal strain energy, hence

$$\Pi_2 - \Pi_1 = \Delta W - \Delta U\quad (6.10)$$

$$= -\frac{1}{2}(P_2 - P_1)u_1 = \frac{1}{2}(P_1 - P_2)u_1\quad (6.11)$$

Fixed Load: $P_2 = P_1$ the situation is slightly more complicated. Here there is both external work

$$\Delta W = P_1(u_2 - u_1) \quad (6.12)$$

and a release of internal strain energy. Thus the net effect is a change in potential energy given by:

$$\Pi_2 - \Pi_1 = \Delta W - \Delta U \quad (6.13)$$

$$= P_1(u_2 - u_1) - \frac{1}{2}P_1(u_2 - u_1) \quad (6.14)$$

$$= \frac{1}{2}P_1(u_2 - u_1) \quad (6.15)$$

$$= \Gamma \quad (6.16)$$

¹⁵ Thus under fixed grip conditions there is a decrease in strain energy of magnitude $\frac{1}{2}u_1(P_1 - P_2)$ as the crack extends from a to $(a + \Delta a)$, whereas under constant load, there is a net decrease in potential energy of magnitude $\frac{1}{2}P_1(u_2 - u_1)$.

¹⁶ At the limit as $\Delta a \rightarrow da$, we define:

$$dP = P_1 - P_2 \quad (6.17)$$

$$du = u_2 - u_1 \quad (6.18)$$

then as $da \rightarrow 0$, the decrease in strain energy (and potential energy in this case) for the fixed grip would be

$$d\Pi = \frac{1}{2}udP \quad (6.19)$$

and for the constant load case

$$d\Pi = \frac{1}{2}Pdu \quad (6.20)$$

¹⁷ Furthermore, defining the compliance as

$$u = CP \quad (6.21)$$

$$du = CdP \quad (6.22)$$

¹⁸ Then the decrease in potential energy for both cases will be given by

$$\boxed{d\Pi = \frac{1}{2}CP dP} \quad (6.23)$$

¹⁹ In summary, **as the crack extends there is a release of excess energy**. Under fixed grip conditions, this energy is released from the strain energy. Under fixed load condition, external work is produced, half of it is consumed into strain energy, and the other half released. In either case, the energy released is consumed to form *surface energy*.

²⁰ Thus a criteria for crack propagation would be

$$\boxed{d\Pi \geq 2\gamma da} \quad (6.24)$$

The difference between the two sides of the inequality will appear as kinetic energy at a real crack propagation.

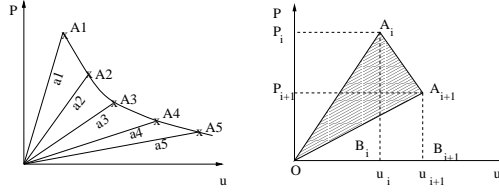
Energy Release Rate per unit crack extension = Surface energy

$$\frac{d\Pi}{da} = 2\gamma \quad (6.25)$$

²¹ Using Inglis solution, Griffith has shown that for plane stress infinite plates with a central crack of length $2a$ ¹

$$-\frac{d\Pi}{da} = \frac{\pi a \sigma_{cr}^2}{E} \quad (6.26)$$

¹This equation will be rederived in Sect. 6.5 using Westergaard's solution.


 Figure 6.2: Determination of G_c From Load Displacement Curves

note that the negative sign is due to the decrease in energy during crack growth. Combining with Eq. 6.25, and for incipient crack growth, this reduces to

$$\frac{\sigma_{cr}^2 \pi a da}{E'} = 2\gamma da \quad (6.27)$$

or

$$\sigma_{cr} = \sqrt{\frac{2E'\gamma}{\pi a}} \quad (6.28)$$

This equation derived on the basis of global fracture should be compared with Eq. 5.11 derived from local stress analysis.

6.2 Energy Release Rate; Global

6.2.1 From Load-Displacement

22 With reference to Fig. 6.2 The energy released, for unit crack surface, from increment i to increment $i + 1$ is given by

$$G = \sum_{i=1, n} \frac{OA_i A_{i+1}}{a_{i+1} - a_i} \quad (6.29)$$

where

$$OA_i A_{i+1} = (OA_i B_i) + (A_i B_i B_{i+1} A_{i+1}) - (OA_{i+1} B_{i+1}) \quad (6.30-a)$$

$$= \frac{1}{2} P_i u_i + \frac{1}{2} (P_i + P_{i+1})(u_{i+1} - u_i) - \frac{1}{2} P_{i+1} u_{i+1} \quad (6.30-b)$$

$$= \frac{1}{2} (P_i u_{i+1} - P_{i+1} u_i) \quad (6.30-c)$$

Thus, the total energy release rate will be given by

$$G = \sum_{i=1, n} \frac{1}{2B} \frac{P_i u_{i+1} - P_{i+1} u_i}{a_{i+1} - a_i} \quad (6.31)$$

where B is the thickness.

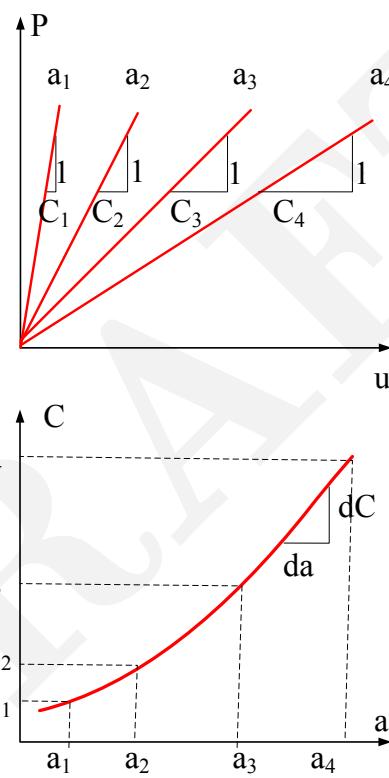
6.2.2 From Compliance

23 Under constant load we found the energy release needed to extend a crack by da was $\frac{1}{2} P du$. If G is the energy release rate, B is the thickness, and $u = CP$, (where u , C and P are the point load displacement, compliance and the load respectively), then

$$GBda = \frac{1}{2} Pd(CP) = \frac{1}{2} P^2 dC \quad (6.32)$$

at the limit as $da \rightarrow 0$, then we would have:

$$G = \frac{1}{2} \frac{P^2}{B} \left(\frac{dC}{da} \right) \quad (6.33)$$

Figure 6.3: Experimental Determination of K_I from Compliance Curve

24 Thus we can use an experimental technique to obtain G and from $G = \frac{K_I^2}{E'}$ (to be derived later) to get K_I , Fig. 6.3

25 With regard to accuracy since we are after K which does not depend on E , a low modulus plate material (i.e. high strength aluminum) can be used to increase observed displacement.

26 As an example, let us consider the double cantilever beam problem, Fig. 6.4. From strength of materials:

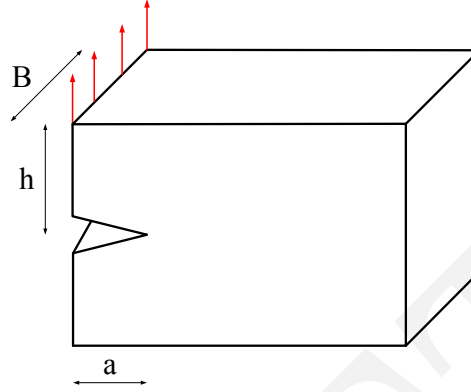


Figure 6.4: K_I for DCB using the Compliance Method

$$C = \underbrace{\frac{24}{EB} \int_0^a \frac{x^2}{h^3} dx}_{\text{flexural}} + \underbrace{\frac{6(1+\nu)}{EB} \int_0^a \frac{1}{h} dx}_{\text{shear}} \quad (6.34)$$

Taking $\nu = \frac{1}{3}$ we obtain

$$C = \frac{8}{EB} \int_0^a \left(\frac{3x^2}{h^3} + \frac{1}{h} \right) dx \quad (6.35)$$

$$\frac{dC}{da} = \frac{8}{EB} \left(\frac{3a^2}{h^3} + \frac{1}{h} \right) \quad (6.36)$$

Substituting in Eq. 6.33

$$G = \frac{1}{2} \frac{P^2}{B} \left(\frac{dc}{da} \right) \quad (6.37)$$

$$= \frac{1}{2} \frac{P^2 8}{EB^2} \left(\frac{3a^2}{h^3} + \frac{1}{h} \right) \quad (6.38)$$

$$= \frac{4P^2}{EB^2 h^3} (3a^2 + h^2) \quad (6.39)$$

Thus the stress intensity factor will be

$$K = \sqrt{GE} = \frac{2P}{B} \left(\frac{3a^2}{h^3} + \frac{1}{h} \right)^{\frac{1}{2}} \quad (6.40)$$

27 Had we kept G in terms of ν

$$G = \frac{4P^2}{EB^2 h^3} \left[3a^2 + \frac{3}{4} h^2 (1 + \nu) \right] \quad (6.41)$$

28 We observe that in this case K increases with a , hence we would have an unstable crack growth. Had we had a beam in which B increases with a , Fig. 6.5, such that

$$\frac{3a^2}{h^3} + \frac{1}{h} = m = \text{Cst} \quad (6.42)$$

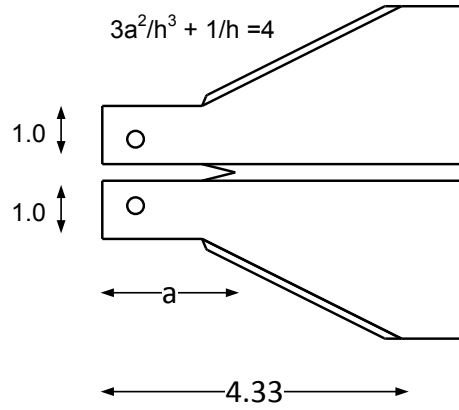


Figure 6.5: Variable Depth Double Cantilever Beam

then

$$K = \frac{2P}{B} m^{\frac{1}{2}} \quad (6.43)$$

Such a specimen, in which K remains constant as a increases was proposed by Mostovoy (Mostovoy, 1967) for fatigue testing.

6.3 Energy Release Rate; Local

²⁹ We showed in the previous section that a transfer of energy has to occur for crack propagation. Energy is needed to create new surfaces, and this energy is provided by either release of strain energy only, or a combination of strain energy and external work. It remains to quantify energy in terms of the stress intensity factors.

³⁰ In his original derivation, Eq. 6.26, Griffith used Inglis solution to determine the energy released. His original solution was erroneous, however he subsequently corrected it.

³¹ Our derivation instead will be based on Westergaard's solution. Thus, the energy released during a colinear unit crack extension can be determined by calculating the work done by the surface forces acting across the length da when the crack is closed from length $(a + da)$ to length a , Fig. 6.6.

³² This energy change is given by:

$$G = \frac{2}{\Delta a} \int_a^{a+\Delta a} \frac{1}{2} \sigma_{yy}(x) v(x - da) dx \quad (6.44)$$

³³ We note that the 2 in the numerator is caused by the two crack surfaces (upper and lower), whereas the 2 in the denominator is due to the linear elastic assumption.

³⁴ Upon substitution for σ_{yy} and v (with $\theta = \pi$) from the Westergaard equations (Eq. 3.53-b and 3.53-f)

$$\sigma_{yy} = \frac{K_I}{\sqrt{2\pi r}} \cos \frac{\theta}{2} \left[1 + \sin \frac{\theta}{2} \sin \frac{3\theta}{2} \right] \quad (6.45)$$

$$v = \frac{K_I}{2\mu} \sqrt{\frac{r}{2\pi}} \sin \frac{\theta}{2} \left[\kappa + 1 - 2 \cos^2 \frac{\theta}{2} \right] \quad (6.46)$$

(where μ is the shear modulus); Setting $\theta = \pi$, and after and simplifying, this results in:

$$G = \frac{K_I^2}{E'} \quad (6.47)$$

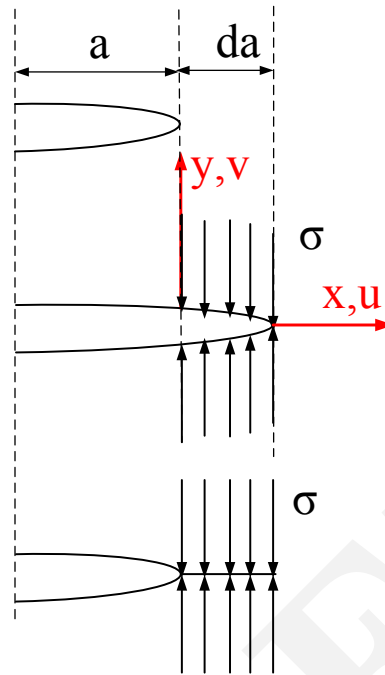


Figure 6.6: Graphical Representation of the Energy Release Rate G

where

$$E' = E \quad \text{plane stress} \quad (6.48)$$

and

$$E' = \frac{E}{1 - \nu^2} \quad \text{plane strain} \quad (6.49)$$

35 Substituting $K = \sigma\sqrt{\pi a}$ we obtain the energy release rate in terms of the far field stress

$$\boxed{G = \frac{\sigma^2 \pi a}{E'}} \quad (6.50)$$

we note that this is identical to Eq. 6.26 derived earlier by Griffith.

36 Finally, the total energy consumed over the crack extension will be:

$$d\Pi = \int_0^{da} G dx = \int_0^{da} \frac{\sigma^2 \pi a}{E'} dx = \frac{\sigma^2 \pi a da}{E'} \quad (6.51)$$

37 Sih, Paris and Irwin, (Sih et al., 1965), developed a counterpart to Equation 6.47 for anisotropic materials as

$$G = \sqrt{\left(\frac{a_{11}a_{22}}{2}\right) \left(\sqrt{\frac{a_{11}}{a_{22}}} + \frac{2a_{12} + a_{66}}{2a_{22}}\right)} K^2 \quad (6.52)$$

6.4 Theoretical Basis

³⁸ Revisiting Eq. 6.3

$$\frac{\partial W}{\partial a} = \left(\frac{\partial U^e}{\partial a} + \frac{\partial U^p}{\partial a} \right) + \frac{\partial \Gamma}{\partial a} \quad (6.53)$$

we can rewrite it as

$$\underbrace{\frac{\partial W}{\partial a} - \frac{\partial U^e}{\partial a}}_G = \underbrace{\frac{\partial U^p}{\partial a} + \frac{\partial \Gamma}{\partial a}}_R \quad (6.54)$$

where R represents the rate of energy dissipation during stable crack growth. The first part corresponds to plastic deformation, and the second to energy consumed during crack propagation.

6.4.1 R vs K_{Ic}

³⁹ Back to Eq. 6.51, crack instability will occur when for an infinitesimal crack extension da , the rate of energy released is just equal to surface energy absorbed.

$$\frac{\frac{\sigma_{cr}^2 \pi a da}{E'}}{d\pi} = 2\gamma da \quad (6.55)$$

or

$$\sigma_{cr} = \sqrt{\frac{2E'\gamma}{\pi a}} \quad (6.56)$$

Which is Eq. 6.28 as originally derived by Griffith (Griffith, 1921).

⁴⁰ This equation can be rewritten as

$$\underbrace{\frac{\sigma_{cr}^2 \pi a}{E'}}_{G_{cr}} \equiv \underbrace{R}_{2\gamma} \quad (6.57)$$

and as

$$\sigma_{cr} \sqrt{\pi a} = \sqrt{2E'\gamma} = K_{Ic} \quad (6.58)$$

thus

$$\boxed{G_{cr} = R = \frac{K_{Ic}^2}{E'}} \quad (6.59)$$

⁴¹ In general, the critical energy release rate is defined as R (for Resistance) and is only equal to a constant (G_{cr}) under plane strain conditions.

⁴² Critical energy release rate for plane stress is found not to be constant, thus K_{Ic} is not constant, and we will instead use K_{1c} and G_{1c} . Alternatively, K_{Ic} , and G_{Ic} correspond to plane strain in mode I which is constant. Hence, the shape of the R-curve depends on the plate thickness, where plane strain is approached for thick plates, and is constant; and for thin plates we do not have constant R due to plane stress conditions.

⁴³ Using this energetic approach, we observe that contrarily to the Westergaard/Irwin criteria where we zoomed on the crack tip, a global energy change can predict a local event (crack growth).

⁴⁴ The duality between energy and stress approach $G > G_{cr} = R$, or $K > K_{Ic}$, should also be noted.

⁴⁵ Whereas the Westergaard/Irwin criteria can be generalized to mixed mode loading (in chapter 7), the energy release rate for mixed mode loading (where crack extension is not necessarily collinear with the crack axis) was not derived until 1974 by Hussain *et al.* (Hussain *et al.*, 1974). However, should we assume a collinear crack extension under mixed mode loading, then

$$G = G_I + G_{II} + G_{III} = \frac{1-\nu^2}{E} (K_I^2 + K_{II}^2 + \frac{K_{III}^2}{1-\nu}) \quad (6.60)$$

46 From above, we have the energy release rate given by

$$G = \frac{\sigma^2 \pi a}{E'} \quad (6.61)$$

and the critical energy release rate is

$$R = G_{cr} = \frac{d\Pi}{da} = 2\gamma = \frac{K_{Ic}^2}{E'} \quad (6.62)$$

47 Criteria for crack growth can best be understood through a graphical representation of those curves under plane strain and plane stress conditions.

6.5 Crack Stability

48 Crack stability depends on both the geometry, and on the material resistance.

6.5.1 Effect of Geometry; Π Curve

49 From Eq. 6.6, crack growth is considered unstable when the energy at equilibrium is a maximum, and stable when it is a minimum. Hence, a sufficient condition for crack stability is, (Gdoutos, 1993)

$$\boxed{\frac{\partial^2(\Pi + \Gamma)}{\partial A^2} \begin{cases} < 0 & \text{unstable fracture} \\ > 0 & \text{stable fracture} \\ = 0 & \text{neutral equilibrium} \end{cases} \quad \&G > R} \quad (6.63)$$

and the potential energy is $\Pi = U - W$.

50 If we consider a line crack in an infinite plate subjected to uniform stress, Fig. 6.7, then the potential energy of the system is $\Pi = U^e$ where Eq. 6.6 yields

$$K_I = \sigma \sqrt{\pi a} \quad (6.64\text{-a})$$

$$G = \frac{K_I^2}{E'} \quad (6.64\text{-b})$$

$$= \frac{\sigma^2 \pi a}{E'} \quad (6.64\text{-c})$$

$$\Pi = U^e = \int G da \quad (6.64\text{-d})$$

$$= -\frac{1}{2} \frac{\sigma^2 \pi a^2}{E'} \quad (6.64\text{-e})$$

and $\Gamma = 4a$ (crack length is $2a$). Note that U^e is negative because there is a decrease in strain energy during crack propagation. If we plot Γ , Π and $\Gamma + \Pi$, Fig. 6.7, then we observe that the total potential energy of the system ($\Pi + \Gamma$) is maximum at the critical crack length which corresponds to unstable equilibrium.

51 If we now consider the cleavage of mica, a wedge of thickness h is inserted under a flake of mica which is detached from a mica block along a length a . The energy of the system is determined by considering the mica flake as a cantilever beam with depth d . From beam theory

$$U^e = \frac{Ed^3 h^2}{8a^3} \quad (6.65)$$

(note that U^e is positive because there is an increase in strain energy as a increases) and the surface energy is $\Gamma = 2\gamma a$. From Eq. 6.63, the equilibrium crack is

$$a_c = \left(\frac{3Ed^3 h^2}{16\gamma} \right)^{1/4} \quad (6.66)$$

Again, we observe from Fig. 6.7 that the total potential energy of the system at a_c is a minimum, which corresponds to stable equilibrium.

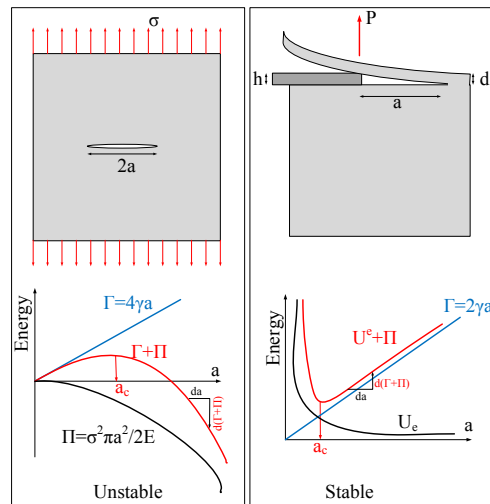


Figure 6.7: Effect of Geometry and Load on Crack Stability, (Gdoutos, 1993)

6.5.2 Effect of Material; R Curve

As shown earlier, a crack in a linear elastic flawed structure may be characterized by its:

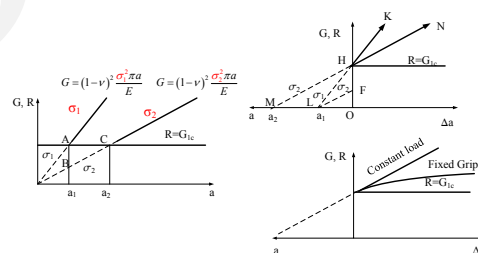
1. Stress intensity factor determined from the near crack tip stress field
2. Energy release rate determined from its global transfer of energy accompanying crack growth

Thus for a crack to extend, two criteria are possible:

1. Compare the stress intensity factor K with a material property called the critical stress intensity factor K_{Ic} , or fracture toughness.
2. Compare the energy release rate G with a material property called the critical energy release rate G_{Ic} .

6.5.2.1 Plane Strain

For plane strain conditions, the R curve is constant and is equal to G_{Ic} . Using Fig. 6.8 From Eq. 6.61, $G = \frac{\sigma^2 \pi a}{E'}$, G is always

Figure 6.8: R Curve for Plane Strain

a linear function of a , thus must be a straight line.

For plane strain problems, if the crack size is a_1 , the energy release rate at a stress σ_2 is represented by point B . If we increase the stress from σ_2 to σ_1 , we raise the G value from B to A . At A , the crack will extend. Had we had a longer crack a_2 , it would have extended at σ_2 .

⁵⁶ Alternatively, we can plot to the right Δa , and to the left the original crack length a_i . At a stress σ_2 , the G line is given by LF (really only point F). So by loading the crack from 0 to σ_2 , G increases from O to F, further increase of the stress to σ_1 raises G from F to H, and then fracture occurs, and the crack goes from H to K. On the other hand, had we had a crack of length a_2 loaded from 0 to σ_2 , its G value increases from O to H (note that LF and MH are parallel). At H crack extension occurs along HN.

⁵⁷ Finally, it should be noted that depending on the boundary conditions, G may increase linearly (constant load) or as a polynomial (fixed grips).

6.5.2.2 Plane Stress

⁵⁸ Under plane strain R was independent of the crack length. However, under plane stress R is found to be an increasing function of a , Fig. 6.9

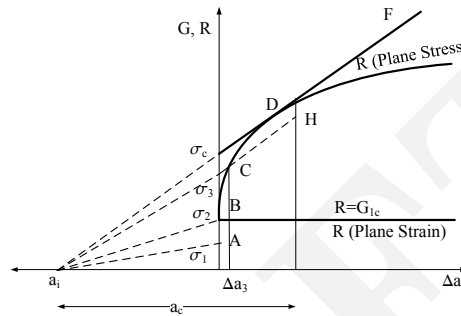


Figure 6.9: R Curve for Plane Stress

⁵⁹ If we examine an initial crack of length a_i :

1. under σ_1 at point A, $G < R$, thus there is no crack extension.
2. If we increase σ_1 to σ_2 , point B, then $G = R$ and the crack propagates by a small increment Δa and will immediately stop as G becomes smaller than R .
3. if we now increase σ_1 to σ_3 , (point C) then $G > R$ and the crack extends to $a + \Delta a$. G increases to H, however, this increase is at a lower rate than the increase in R

$$\frac{dG}{da} < \frac{dR}{da} \tag{6.67}$$

thus the crack will stabilize and we would have had a stable crack growth.

4. Finally, if we increase σ_1 to σ_c , then not only is G equal to R , but it grows faster than R thus we would have an unstable crack growth.

⁶⁰ From this simple illustrative example we conclude that

Stable Crack Growth: $G > R$ $\frac{dG}{da} < \frac{dR}{da}$	(6.68)
Unstable Crack Growth: $G > R$ $\frac{dG}{da} > \frac{dR}{da}$	

we also observe that for unstable crack growth, excess energy is transformed into kinetic energy.

⁶¹ Finally, we note that these equations are equivalent to Eq. 6.63 where the potential energy has been expressed in terms of G , and the surface energy expressed in terms of R .

⁶² Some materials exhibit a flat R curve, while other have an ascending one. The shape of the R curve is a material property. For ideally brittle material, R is flat since the surface energy γ is constant. Nonlinear material would have a small plastic zone at the tip of the crack. The driving force in this case must increase. If the plastic zone is small compared to the crack (as would be eventually the case for sufficiently long crack in a large body), then R would approach a constant value.

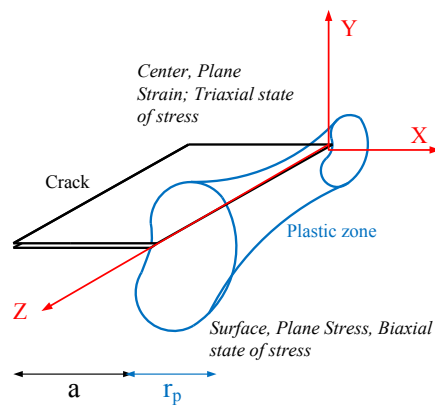


Figure 6.10: Plastic Zone Ahead of a Crack Tip Through the Thickness

⁶³ The thickness of the cracked body can also play an important role. For thin sheets, the load is predominantly plane stress, Fig. 6.10.

⁶⁴ Alternatively, for a thick plate it would be predominantly plane strain. Hence a plane stress configuration would have a steeper R curve.

Chapter 7

MIXED MODE CRACK PROPAGATION

¹ Practical engineering cracked structures are subjected to mixed mode loading, thus in general K_I and K_{II} are both nonzero, yet we usually measure only mode I fracture toughness K_{Ic} (K_{IIc} concept is seldom used). Thus, so far the only fracture propagation criterion we have is for mode I only (K_I vs K_{Ic} , and G_I vs R).

² Whereas under pure mode I in homogeneous isotropic material, crack propagation is collinear, in all other cases the propagation will be curvilinear and at an angle θ_0 with respect to the crack axis. Thus, for the general mixed mode case, we seek to formulate a criterion that will determine:

1. The angle of incipient propagation, θ_0 , with respect to the crack axis.
2. If the stress intensity factors are in such a critical combination as to render the crack locally unstable and force it to propagate.

³ Once again, for pure mode I problems, fracture initiation occurs if:

$$K_I \geq K_{Ic} \quad (7.1)$$

⁴ The determination of a fracture initiation criterion for an existing crack in mode I and II would require a relationship between K_I , K_{II} , and K_{Ic} of the form

$$F(K_I, K_{II}, K_{Ic}) = 0 \quad (7.2)$$

and would be analogous to the one between the two principal stresses and a yield stress, Fig. 7.1

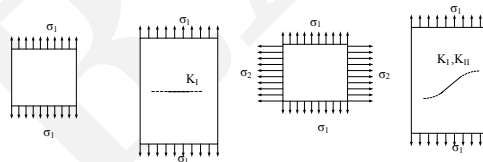


Figure 7.1: Mixed Mode Crack Propagation and Biaxial Failure Modes

$$F_{yld}(\sigma_1, \sigma_2, \sigma_y) = 0 \quad (7.3)$$

Such an equation may be the familiar von Mises criterion.

⁵ In the absence of a widely accepted criterion for mixed mode crack growth, three of the most widely used criterion are discussed below.

7.1 Analytical Models for Isotropic Solids

⁶ First four models for the mixed mode crack propagation will be presented, three for isotropic materials, and one for anisotropic ones. Subsequently the actual algorithmic implementation of those models will be presented.

7.1.1 Maximum Circumferential Tensile Stress.

⁷ Erdogan and Sih (1963) presented the first mixed-mode fracture initiation theory, the maximum circumferential tensile stress theory. It is based on the knowledge of the stress state near the tip of a crack, written in polar coordinates.

⁸ The maximum circumferential stress theory states that the crack extension starts:

1. At its tip in a radial direction
2. In the plane perpendicular to the direction of greatest tension, i.e at an angle θ_0 such that $\tau_{r\theta} = 0$
3. When $\overline{\sigma_{\theta_{max}}}$ reaches a critical material constant

⁹ It can be easily shown that σ_θ reaches its maximum value when $\tau_{r\theta} = 0$. Replacing $\tau_{r\theta}$ for mode I and II by their expressions given in Eq. 3.56-c and 3.57-c

$$\tau_{r\theta} = \frac{K_I}{\sqrt{2\pi r}} \sin \frac{\theta}{2} \cos^2 \frac{\theta}{2} + \frac{K_{II}}{\sqrt{2\pi r}} \left(\frac{1}{4} \cos \frac{\theta}{2} + \frac{3}{4} \cos \frac{3\theta}{2} \right) \quad (7.4)$$

$$\Rightarrow \cos \frac{\theta_0}{2} [K_I \sin \theta_0 + K_{II} (3 \cos \theta_0 - 1)] = 0 \quad (7.5)$$

this equation has two solutions:

$$\theta_0 = \pm\pi \quad \text{trivial} \quad (7.6)$$

$$K_I \sin \theta_0 + K_{II} (3 \cos \theta_0 - 1) = 0 \quad (7.7)$$

Solution of the second equation yields the angle of crack extension θ_0

$$\tan \frac{\theta_0}{2} = \frac{1}{4} \frac{K_I}{K_{II}} \pm \frac{1}{4} \sqrt{\left(\frac{K_I}{K_{II}} \right)^2 + 8} \quad (7.8)$$

¹⁰ For the crack to extend, the maximum circumferential tensile stress, σ_θ (from Eq. 3.56-b and 3.57-b)

$$\sigma_\theta = \frac{K_I}{\sqrt{2\pi r}} \cos \frac{\theta_0}{2} \left(1 - \sin^2 \frac{\theta_0}{2} \right) + \frac{K_{II}}{\sqrt{2\pi r}} \left(-\frac{3}{4} \sin \frac{\theta_0}{2} - \frac{3}{4} \sin \frac{3\theta_0}{2} \right) \quad (7.9)$$

must reach a critical value which is obtained by rearranging the previous equation

$$\sigma_{\theta_{max}} \sqrt{2\pi r} = K_{Ic} = \cos \frac{\theta_0}{2} \left[K_I \cos^2 \frac{\theta_0}{2} - \frac{3}{2} K_{II} \sin \theta_0 \right] \quad (7.10)$$

which can be normalized as

$$\frac{K_I}{K_{Ic}} \cos^3 \frac{\theta_0}{2} - \frac{3}{2} \frac{K_{II}}{K_{Ic}} \cos \frac{\theta_0}{2} \sin \theta_0 = 1 \quad (7.11)$$

¹¹ This equation can be used to define an equivalent stress intensity factor K_{eq} for mixed mode problems

$$K_{eq} = K_I \cos^3 \frac{\theta_0}{2} - \frac{3}{2} K_{II} \cos \frac{\theta_0}{2} \sin \theta_0 \quad (7.12)$$

7.1.2 Maximum Energy Release Rate

¹² In their original model, Erdogan and Sih (1963) noted that:

“If we accept Griffith (energy) theory as the valid criteria which explains crack growth, then the crack will grow in the direction along which the elastic energy release per unit crack extension will be maximum and the crack will start to grow when this energy reaches a critical value (or $G = G(\delta, \theta)$). Evaluation of $G(\delta, \theta)$ poses insurmountable mathematical difficulties.”

¹³ Finding $G(\delta, \theta)$ will establish for the general mixed mode case the duality which is the basis of fracture mechanics: the equivalence in viewing fracture initiation from either a global energy balance or a local stress intensity point of view.

¹⁴ This (insurmountable) problem was solved in 1974, by [Hussain et al. \(1974\)](#). Fundamentally, [Hussain et al. \(1974\)](#) have solved for the stress intensity factor of a major crack with an infinitesimal “kink” at an angle θ , $K_I(\theta)$ and $K_{II}(\theta)$ in terms of the stress intensity factors of the original crack K_I and K_{II} , Fig. 7.2:

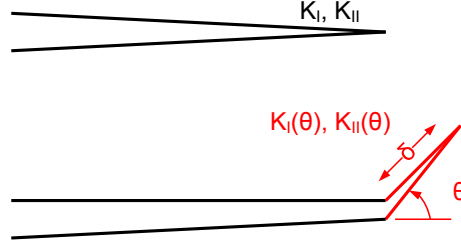


Figure 7.2: Crack with an Infinitesimal “kink” at Angle θ

$$\begin{Bmatrix} K_I(\theta) \\ K_{II}(\theta) \end{Bmatrix} = \left(\frac{4}{3 + \cos^2 \theta} \right) \left(\frac{1 - \frac{\theta}{\pi}}{1 + \frac{\theta}{\pi}} \right)^{\frac{\theta}{2\pi}} \begin{Bmatrix} K_I \cos \theta + \frac{3}{2} K_{II} \sin \theta \\ K_{II} \cos \theta - \frac{1}{2} K_I \sin \theta \end{Bmatrix} \quad (7.13)$$

¹⁵ Those expressions of $K_I(\theta)$ and $K_{II}(\theta)$ were then substituted into Irwin’s generalized expression for the energy release rate (assuming collinear crack growth), Eq. 6.60

$$G(\theta) = \frac{1}{E'} (K_I^2(\theta) + K_{II}^2(\theta)) \quad (7.14)$$

yielding

$$G(\theta) = \frac{4}{E'} \left(\frac{1}{3 + \cos^2 \theta} \right)^2 \left(\frac{1 - \frac{\theta}{\pi}}{1 + \frac{\theta}{\pi}} \right)^{\frac{\theta}{\pi}} [(1 + 3 \cos^2 \theta) K_I^2 + 8 \sin \theta \cos \theta K_I K_{II} + (9 - 5 \cos^2 \theta) K_{II}^2] \quad (7.15)$$

¹⁶ The angle of crack propagation θ_0 is found by maximizing $G(\theta)$;

$$\frac{\partial G(\theta)}{\partial \theta} = 0 \quad (7.16)$$

$$\frac{\partial^2 G(\theta)}{\partial \theta^2} < 0 \quad (7.17)$$

For pure mode II ($K_I = 0$), it is found that $\theta_0 = 75.2^\circ$

¹⁷ If crack extension occurs when G reaches a critical value which is the same scalar quantity for all cases, then this critical value can be determined by setting $K_{II} = 0$ and $G_{cr} = \frac{K_{Ic}^2}{E}$; thus, substituting in Eq. 7.15

$$\left[\left(\frac{1}{3 + \cos^2 \theta_0} \right)^2 \left(\frac{1 - \frac{\theta_0}{\pi}}{1 + \frac{\theta_0}{\pi}} \right)^{\frac{\theta_0}{\pi}} \left[(1 + 3 \cos^2 \theta_0) \left(\frac{K_I}{K_{Ic}} \right)^2 + 8 \sin \theta_0 \cos \theta_0 \left(\frac{K_I K_{II}}{K_{Ic}^2} \right) + (9 - 5 \cos^2 \theta_0) \left(\frac{K_{II}}{K_{Ic}} \right)^2 \right] \right] = 1$$

7.1.3 Minimum Strain Energy Density Criteria.

¹⁸ The minimum strain energy density theory, formulated by [Sih \(1974\)](#), postulates that a fracture initiates from the crack tip in a direction θ_0 , along which the strain energy density at a critical distance is a minimum (i.e. crack propagates along path of minimum resistance), when this minimum reaches a critical value.

¹⁹ The strain energy density dW per unit volume dV is

$$\frac{dW}{dV} = \frac{1}{2E} (\sigma_{xx}^2 + \sigma_{yy}^2 + \sigma_{zz}^2) - \frac{\nu}{E} (\sigma_{xx}\sigma_{yy} + \sigma_{yy}\sigma_{zz} + \sigma_{zz}\sigma_{xx}) + \frac{1}{2\mu} (\tau_{xy}^2 + \tau_{yz}^2 + \tau_{zx}^2) \quad (7.18)$$

where μ is the shear modulus (often referred to as G).

²⁰ In two dimensional problems, this equation reduces to:

$$\frac{dW}{dV} = \frac{1}{4\mu} \left[\frac{\kappa + 1}{4} (\sigma_{xx} + \sigma_{yy})^2 - 2(\sigma_{xx}\sigma_{yy} - \tau_{xy}^2) \right] \quad (7.19)$$

where $\kappa = 3 - 4\nu$ plane strain, and $\kappa = \frac{3-\nu}{1+\nu}$ for plane stress.

²¹ Using Westergaard's solution for a cracked infinite plate and substituting the stress into Eq. 7.29, $\frac{dW}{dV}$, we obtain

$$\frac{\partial W}{\partial V} = \frac{1}{r_0 \pi} (a_{11} K_I^2 + 2a_{12} K_I K_{II} + a_{22} K_{II}^2) = \frac{S(\theta)}{r_0} \quad (7.20)$$

where

$$a_{11} = \frac{1}{16\mu} [(1 + \cos \theta) (\kappa - \cos \theta)] \quad (7.21)$$

$$a_{12} = \frac{\sin \theta}{16\mu} [2 \cos \theta - (\kappa - 1)] \quad (7.22)$$

$$a_{22} = \frac{1}{16\mu} [(\kappa + 1) (1 - \cos \theta) + (1 + \cos \theta) (3 \cos \theta - 1)] \quad (7.23)$$

where

$$\kappa = \frac{3-\nu}{1+\nu} \quad (\text{plane stress}) \quad (7.24)$$

$$\kappa = 3 - 4\nu \quad (\text{plane strain}) \quad (7.25)$$

and μ is the shear modulus.

²² This model is based on the following assumptions:

1. Direction of fracture initiation (in 3-D) is toward the point of minimum strain energy density factor S_{min} as compared to other points on the same spherical surface surrounding that point

$$\frac{\partial S}{\partial \theta} = 0 \quad (7.26)$$

$$\frac{\partial^2 S}{\partial \theta^2} > 0 \quad (7.27)$$

2. Fracture initiation is assumed to occur when $S_{\theta_{min}}$ reaches the maximum critical value S_{cr} .

²³ We note that it is also possible to decompose the strain energy density into two components a volumetric one and a dilational one:

$$\frac{dU}{dV} = \left(\frac{dU}{dV} \right)_D + \left(\frac{dU}{dV} \right)_V \quad (7.28)$$

where the dilational part is given by

$$\left(\frac{dU}{dV} \right)_D = \frac{1 + \nu}{6E} [(\sigma_{xx} - \sigma_{yy})^2 + (\sigma_{yy} - \sigma_{zz})^2 + (\sigma_{zz} - \sigma_{xx})^2 + 6(\tau_{xy}^2 + \tau_{yz}^2 + \tau_{xz}^2)] \quad (7.29)$$

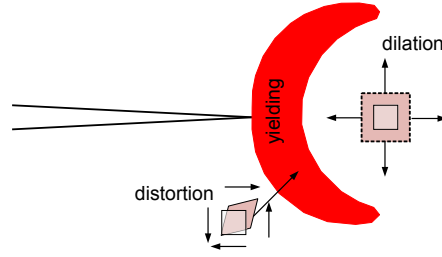
and the volumetric by

$$\left(\frac{dU}{dV} \right)_V = \frac{1 - 2\nu}{6E} (\sigma_{xx} + \sigma_{yy} + \sigma_{zz})^2 \quad (7.30)$$

²⁴ We note that S_{min} is associated with brittle fracture, and S_{max} is associated with yielding. Its direction coincides with the direction of maximum distortion while S_{min} coincides with maximum dilation, Fig. 7.3

²⁵ If we set $K_{II} = 0$, thus $\theta_0 = 0$ and $S_{cr} = (S(\theta))_{min} = S(\theta = 0) = a_{11} K_{Ic}$

$$\begin{aligned} S_{cr} &= \frac{2(\kappa - 1) K_{Ic}^2}{16\mu\pi} \\ &= \frac{(\kappa - 1)}{8\pi\mu} K_{Ic}^2 \end{aligned} \quad (7.31)$$

Figure 7.3: S_θ Distribution ahead of a Crack Tip

26 Thus, the fracture locus predicted by this theory is given by:

$$\frac{8\mu}{(\kappa - 1)} \left[a_{11} \left(\frac{K_I}{K_{Ic}} \right)^2 + 2a_{12} \left(\frac{K_I K_{II}}{K_{Ic}^2} \right) + a_{22} \left(\frac{K_{II}}{K_{Ic}} \right)^2 \right] = 1 \quad (7.32)$$

7.1.4 Observations

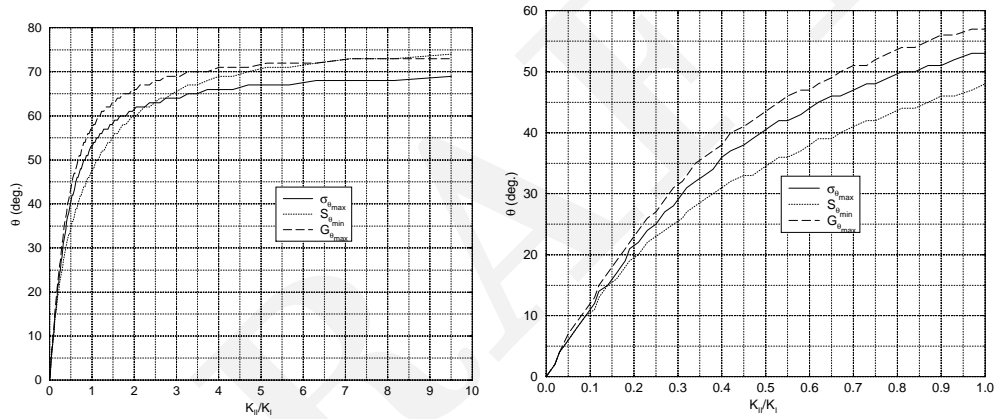


Figure 7.4: Angle of Crack Propagation Under Mixed Mode Loading

27 With reference to Fig. 7.4 and 7.5, we note the following

1. Algorithmically, the angle of crack propagation θ_0 is first obtained, and then the criteria are assessed for local fracture stability.
2. In applying $\sigma_{\theta_{max}}$, we need to define another material characteristic r_0 where to evaluate σ_θ . Whereas this may raise some fundamental questions with regard to the model, results are independent of the choice for r_0 .
3. $S_{\theta_{min}}$ theory depends on ν
4. $S_{\theta_{min}}$ & $\sigma_{\theta_{max}}$ depend both on a field variable that is singular at the crack tip thus we must arbitrarily specify r_o (which cancels out).
5. It can be argued whether all materials must propagate in directions of maximum energy release rate.
6. There is a scale effect in determining the tensile strength $\Rightarrow \sigma_{\theta_{max}}$
7. Near the crack tip we have a near state of biaxial stress
8. For each model we can obtain a K_{Ieq} in terms of K_I & K_{II} and compare it with K_{Ic}
9. All models can be represented by a normalized fracture locus.

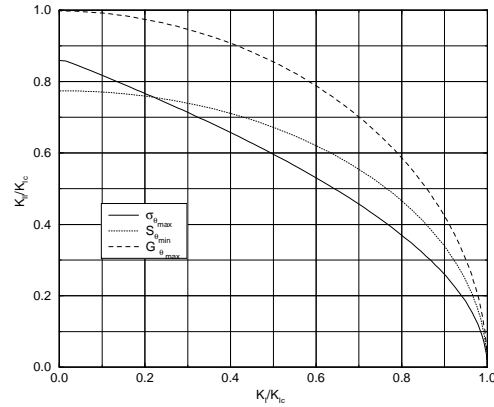


Figure 7.5: Locus of Fracture Diagram Under Mixed Mode Loading

10. For all practical purposes, all three theories give identical results for small ratios of $\frac{K_{II}}{K_I}$ and diverge slightly as this ratio increases.
11. A crack will always extend in the direction which minimizes $\frac{K_{II}}{K_I}$. That is, a crack under mixed-mode loading will tend to reorient itself so that K_{II} is minimized. Thus during its trajectory a crack will most often be in that portion of the normalized $\frac{K_I}{K_{Ic}} - \frac{K_{II}}{K_{IIc}}$ space where the three theories are in close agreement.
12. If the pair of SIF is inside the fracture loci, then that crack cannot propagate without sufficient increase in stress intensity factors. If outside, then the crack is locally unstable and will continue to propagate in either of the following ways:
 - a) With an increase in the SIF (and the energy release rate G), thus resulting in a global instability, failure of the structure (crack reaching a free surface) will occur.
 - b) With a decrease in the SIF (and the energy release rate G), due to a stress redistribution, the SIF pair will return to within the locus.

7.2 Empirical Models for Rocks

28 Many researchers have proposed empirical relations for the mixed mode crack propagation of cracks.

29 **Advani and Lee (1979)** proposed the following

$$\left(\frac{K_{II}}{2K_{Ic}}\right)^2 + \left(\frac{K_I}{K_{Ic}}\right) = 1 \quad (7.33)$$

30 **Awaji and Sato (1978)** proposed

$$\left(\frac{K_I}{K_{Ic}}\right)^u + \left(\frac{K_{II}}{K_{IIc}}\right)^u = 1 \quad (7.34)$$

where $u \approx 1.6$ is a material constant

31 Many other empirical relations have been derived, specially for composite materials.

7.3 Extensions to Anisotropic Solids

32 The maximum circumferential tensile stress theory, originally developed for isotropic solids, has been extended to the anisotropic case by **Saouma et al. (1987)**.

33 The fracture toughness, as the elastic modulus, is uniquely defined for an isotropic material. However, for a homogeneous transversely isotropic solid with elastic constants E_1, E_2, G_{12} , and μ_{12} , two values are needed to characterize the brittle behavior of the crack, K_{Ic}^1 and K_{Ic}^2 , as shown in Fig. 7.6 along the principal planes of elastic symmetry.

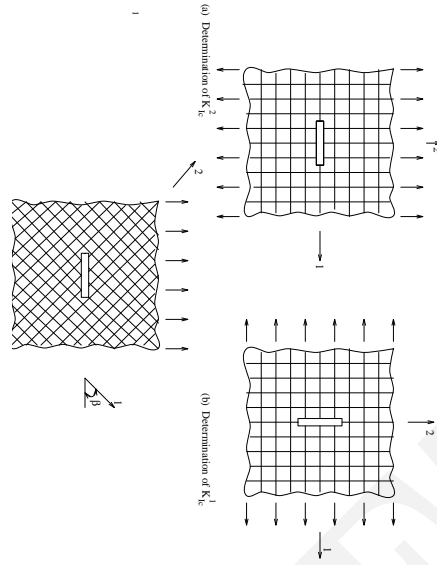


Figure 7.6: Fracture Toughnesses for Homogeneous Anisotropic Solids

³⁴ If the applied load and material properties are aligned symmetrically with reference to the crack, a pure mode I displacement occurs in isotropic materials, whereas a parasitic crack sliding displacement occurs in anisotropic materials. This can be readily seen from Eq. 3.128-c where a nonzero σ_{xy} may result from a pure mode I loading at $\theta = 0$.

³⁵ However, if the material is orthotropic and the crack is aligned with one of the principal planes of elastic-symmetry, then it can be shown (Lekhnitskii, 1981) that the roots of Eq. 2.124,

$$s_i = \alpha_i + i\beta_i \quad (7.35)$$

fall into one of three categories:

1. Case I:

$$\alpha_1 = \alpha_2 = 0 \quad (7.36)$$

$$\beta_1 \neq \beta_2 \quad (7.37)$$

2. Case II:

$$\alpha_1 = \alpha_2 = 0 \quad (7.38)$$

$$\beta_1 = \beta_2 \quad (7.39)$$

3. Case III:

$$\alpha_1 = -\alpha_2 = 0 \quad (7.40)$$

$$\beta_1 = \beta_2 \quad (7.41)$$

resulting in zero values of K_{II} .

³⁶ Finally, for a crack arbitrarily oriented with respect to direction 1, K_{Ic}^β would be a function of K_{Ic}^1 and K_{Ic}^2 . Recalling the stress intensity factor definition from Eq. 3.49, it can be readily seen that the spatial variation of K_{Ic}^β in terms of K_{Ic}^1 and K_{Ic}^2 will be the same as the one for a tensor of order two, thus:

$$K_{Ic}^\beta = K_{Ic}^1 \cos^2 \theta + K_{Ic}^2 \sin^2 \theta \quad (7.42)$$

³⁷ This is equivalent to a scalar and vectorial characterization of the fracture toughness for isotropic and anisotropic solids, respectively. It should be noted that a possible remedy to the need of performing two separate fracture toughness tests is to conduct only one for the determination of K_{Ic}^1 and then postulate that the ratio of the fracture toughness in both directions is equal to the ratio of the elastic moduli:

$$K_{Ic}^2 = K_{Ic}^1 \frac{E_1}{E_2} \quad (7.43)$$

³⁸ The maximum circumferential stress is expressed in terms of $\sigma_{\theta_{max}}$ where:

$$\sigma_{\theta} = \sigma_x \sin^2 \theta + \sigma_y \cos^2 \theta - 2\sigma_{xy} \sin \theta \cos \theta \quad (7.44)$$

and $\sigma_x, \sigma_y, \sigma_{xy}$ are the cartesian stresses at a point at which polar coordinates are r and θ with respect to the crack tip. This theory assumes that crack growth will start from the crack tip in the direction along which the tangential stress σ_{θ} is maximum and the shear stress is zero.

³⁹ This model could be readily extended to anisotropic bodies by first combining equations 3.129-c, and 7.44. After some algebraic manipulation this yields:

$$\sigma_{\theta} = \frac{K_I}{\sqrt{2\pi r}} \text{Re} [A (s_1 B - s_2 C)] + \frac{K_{II}}{\sqrt{2\pi r}} \text{Re} [A (B - C)] \quad (7.45)$$

where

$$A = \frac{1}{s_1 - s_2} \quad (7.46)$$

$$B = (s_2 \sin \theta + \cos \theta)^{\frac{3}{2}} \quad (7.47)$$

$$C = (s_1 \sin \theta + \cos \theta)^{\frac{3}{2}} \quad (7.48)$$

⁴⁰ For the isotropic case the angle of crack propagation θ_0 is obtained by simply maximizing $\sigma_{\theta_{max}}$ but a different approach should be followed for the anisotropic case where the angular variation of the fracture toughness (and thus critical tensile strength) is not constant. In this case one should maximize $\frac{\sigma_{\theta}}{\sigma_{\theta}^{max}}$ where σ_{θ}^{max} is obtained by setting $\theta = 0$ and equating K_I to K_{Ic}^{θ} in equation 7.45:

$$\frac{\sigma_{\theta}}{\sigma_{\theta}^{max}} = \frac{K_I \text{Re} [A (s_1 B - s_2 C)] + K_{II} \text{Re} [A (B - C)]}{K_{Ic}^1 \cos^2 \theta + K_{Ic}^2 \sin^2 \theta} = 1 \quad (7.49)$$

⁴¹ Thus, algorithmically the angle of crack propagation θ_0 is found by maximizing 7.49 or its normalized equivalent:

$$\text{Max} \frac{\text{Re} [A s_1 B - s_2 C] + \frac{K_{II}}{K_I} \text{Re} [A (B - C)]}{\cos^2 \theta + \frac{K_{Ic}^1}{K_{Ic}^2} \sin^2 \theta} \quad (7.50)$$

when θ_0 is determined from Eq. 7.50, it is then substituted for θ in equation 7.49 along with the proper values for K_I and K_{II} . If the left hand side of Eq. 7.49 is greater than 1, then the crack will propagate along the direction θ_0 .

⁴² Finally, note that an attempt to recover the isotropic case from this model would result in a singularity in evaluating A from Eq. 7.46. This singularity occurs because for the isotropic case the roots of the characteristic equation 2-a are known to be all identical and equal to i (Lekhnitskii, 1981). Appendix I of (Saouma et al., 1987) shows that by applying Hospital's rule, Erdogan and Sih's original formulation (Erdogan and Sih, 1963) can be recovered from this extension.

⁴³ In an attempt to evaluate and compare the above model for a wide range of E_1/E_2 a computer program was developed and a graphical representation of a parametric study was generated.

⁴⁴ In this study the following assumptions were made:

1. The crack is aligned with direction 1 assumed to correspond to one of the two major planes of elastic symmetry (corresponding to an orthotropic case).
2. The crack tip is subjected to a mixed mode loading.

45 Furthermore, to simplify the performance of a non-dimensionalized analysis, it was assumed:

$$\frac{K_{Ic}^1}{K_{Ic}^2} = \frac{E_2}{E_1} \quad (7.51)$$

46 Finally, in order to remove the dependency on μ_{12} , and in light of the potential application of these models to fracture of anisotropic rocks it was assumed:

$$G_{12} = \frac{E_1 E_2}{E_1 + E_2 + 2\mu_{12} E_2} \quad (7.52)$$

47 This approximation of G_{12} (which reduces the number of independent elastic properties to three) was observed by [Batugin and Nirenburg \(1972\)](#) in conjunction with their tabulation of elastic properties of 15 different anisotropic rocks.

48 In this parametric study, E_1/E_2 was varied from 0.25 to 4 and K_{II}/K_I from 0 to 10.

49 First the angles of crack propagations were determined. Those angles, Fig. 7.7, call for the following observations:

1. For E_1 less than E_2 , the angle of crack propagation is greater than the one predicted for the isotropic case.
2. Noncolinear crack propagation can take place under pure mode I if E_1/E_2 is less than 0.6.
3. For E_1 greater than E_2 , the angle of crack propagation is smaller than the one predicted for the isotropic case.
4. The angle of crack propagation predicted by the original isotropic theory is recovered by this generalization.
5. For predominantly mode II cases, and E_1 smaller than E_2 , the angle of crack propagation surface is nearly flat, and it approaches 85 degrees for the most extreme case.
6. For E_1 greater than E_2 , and almost pure mode II cases ($K_{II}/K_I = 10$), the angle of crack propagation is about 20 degrees, as opposed to 67 degrees for the isotropic case.

50 Then the normalized crack failure surface with respect to K_{Ic}^1 is plotted with respect to E_1/E_2 , Fig. 7.8 and we note that:

1. The isotropic case is recovered for $E_1 = E_2$.
2. For E_1 smaller than E_2 anisotropy accelerates the crack extension.
3. For E_1 greater than E_2 , anisotropy retards the crack extension.

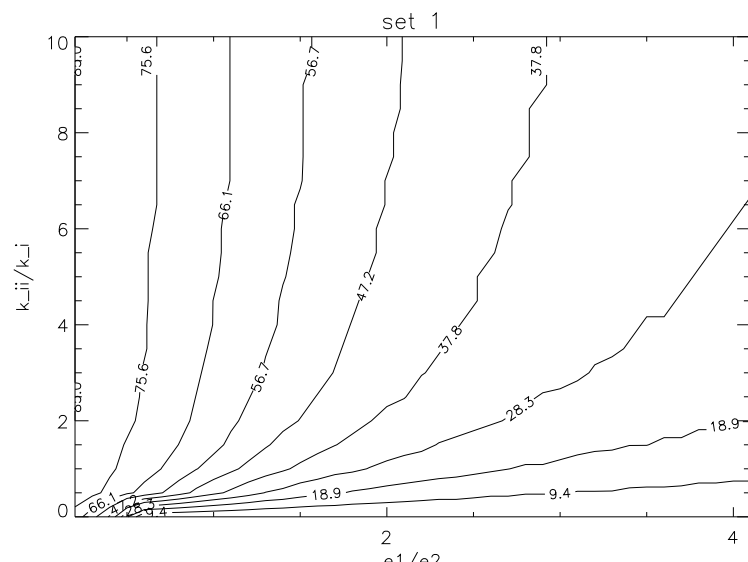
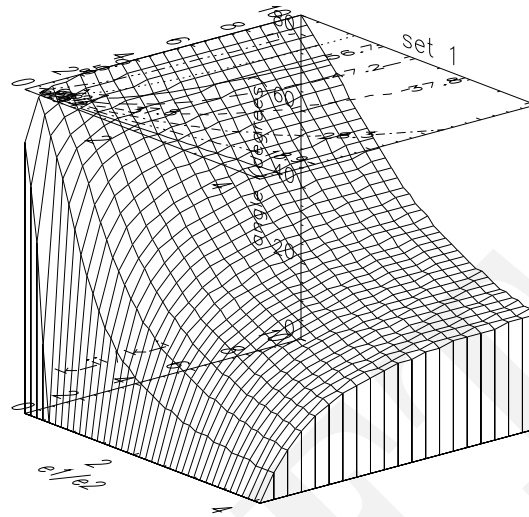
7.4 Interface Cracks

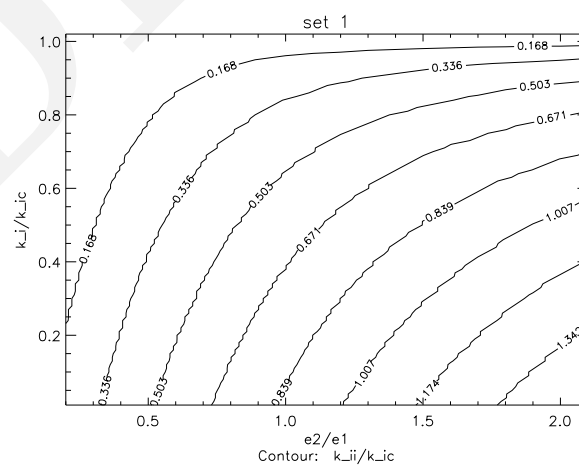
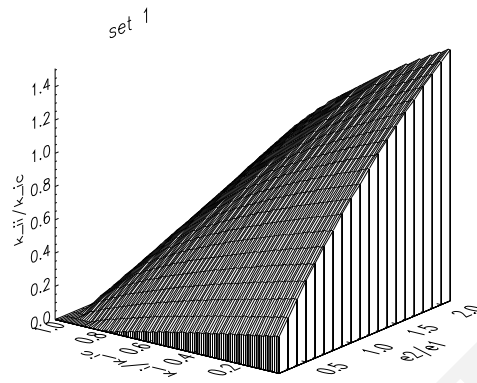
51 Interface crack propagation is rapidly gaining wide attention. Such crack growth is exceedingly important for composite materials, and can be extended to concrete/rock crack interfaces¹.

52 A crack once initiated within an interface can either be stable or propagate in an unstable manner. The unstable crack can propagate along the interface or kink into one of the materials. It can also branch out, that is, it can propagate along the interface and then kink. Whether a crack is forced to remain inside an interface or branch out, depends on the relative toughnesses of the interface and the ones of the adjacent materials. The criteria for an unstable crack to propagate or kink is described in this section. Also, if the crack has to kink, the angle of kink with respect to the interface will be considered.

53 The method presented is very similar to the one used for by the Maximum Energy Release rate. We determine the energy release rate G_0 if the crack were to propagate along the interface, the energy release rate G if the crack was to kink, and compare those two values with G_{0c} and G_c (material properties) respectively.

54 This section is introduced with the crack tip stresses at the bimaterial interface. As mentioned earlier, the stress intensity factor for a bimaterial interface is complex, its physical dimensions are briefly explained. These dimensions are used to obtain a relationship between the homogeneous and the bimaterial stress intensity factors. With these relations, an analytical expression for the energy release rate of the crack kinked into one of the materials is then derived in terms of the energy release rate of the crack advance in the interface.





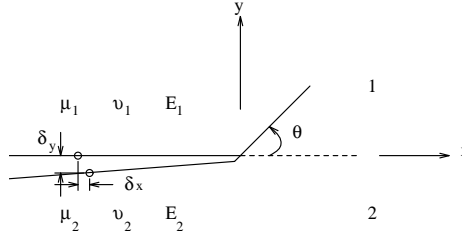


Figure 7.9: Geometry and conventions of an interface crack, (Hutchinson and Suo, 1992)

7.4.1 Crack Tip Fields

55 Considering the bimaterial interface crack in Fig. 7.9 for traction-free plane problems the near-tip normal and shear stresses σ_{yy} and τ_{xy} , may conveniently be expressed in complex form (Hutchinson and Suo, 1992)

$$\sigma_{yy} + i\tau_{xy} = \frac{(K_1 + iK_2)r^{i\varepsilon}}{\sqrt{(2\pi r)}} \quad (7.53)$$

where $i = \sqrt{-1}$, K_1 and K_2 are components of the complex stress intensity factor $K = K_1 + iK_2$ ², and ε is the oscillation index given by

$$\varepsilon = \frac{1}{2\pi} \ln \left[\frac{1 - \beta}{1 + \beta} \right] \quad (7.54)$$

where β is one of Dunders' elastic mismatch parameters (Dunders, 1969), which for plane strain is given by

$$\beta = \frac{\mu_1(1 - 2\nu_2) - \mu_2(1 - 2\nu_1)}{2[\mu_1(1 - \nu_2) + \mu_2(1 - \nu_1)]} \quad (7.55)$$

in which μ and ν are the shear modulus and Poisson's ratio, respectively, and subscripts 1 and 2 refer to the materials above and below the interface, respectively. Dunders defines an additional mismatch parameter α :

$$\alpha = \frac{\bar{E}_1 - \bar{E}_2}{\bar{E}_1 + \bar{E}_2} \quad (7.56)$$

where \bar{E} is the plane strain Young's modulus, $\bar{E} = E/(1 - \nu^2)$. We note that β , α and ε vanish when the materials above and below the interface are identical. When $\varepsilon \neq 0$, Equation 7.53 shows that the stresses oscillate³ heavily as the crack tip is approached ($r \rightarrow 0$). Furthermore, the relative proportion of interfacial normal and shear stresses varies slowly with distance from the crack tip because of the factor $r^{i\varepsilon}$. Thus K_1 and K_2 cannot be decoupled to represent the intensities of interfacial normal and shear stresses as in homogeneous fracture.

56 The crack flank displacements, for plane strain are given by (Hutchinson and Suo, 1992; Carlsson and Prasad, 1993)

$$\delta_y + i\delta_x = \frac{4}{\sqrt{2\pi}} \frac{(1/\bar{E}_1 + 1/\bar{E}_2)(K_1 + iK_2)}{(1 + 2i\varepsilon) \cosh(\pi\varepsilon)} \sqrt{r} r^{i\varepsilon} \quad (7.57)$$

where δ_y and δ_x are the opening and sliding displacements of two initially coincident points on the crack surfaces behind the crack tip, as shown in Fig. 7.9. It may be noted from Eqn. 7.57 that crack face interpenetration is implied when $\varepsilon \neq 0$, as ε is an oscillatory term as shown in Eqn. 7.54. The zone of contact, however, is generally exceedingly small compared to the crack tip plastic zone and may therefore be neglected (Hutchinson and Suo, 1992).

57 The energy release rate, G , for extension of the crack along the interface, for plane strain is given by (Carlsson and Prasad, 1993)

$$G = \frac{(1/\bar{E}_1 + 1/\bar{E}_2)(K_1^2 + K_2^2)}{2 \cosh^2(\pi\varepsilon)} \quad (7.58)$$

58 The complications associated with nonzero ε and β may be circumvented by the approach to bimaterial interface crack problems proposed by He and Hutchinson (1989). They have proposed to systematically take $\beta = 0$ in the analysis of fracture specimens and subsequent application of experimental data in failure predictions. Usually ε is very small and the effect of nonzero β is of secondary importance. This will be discussed later in more detail.

¹This section was written by Kishen Chandra.

²Note that for interface cracks, it is customary to replace K_I and K_{II} by K_1 and K_2 .

³Recall Eq. ?? $r^{i\lambda_j} = \cos(\lambda_j \log(r)) + i \sin(\lambda_j \log(r))$.

7.4.2 Dimensions of Bimaterial Stress Intensity Factors

⁵⁹ The tractions ahead of the crack tip, on the interface are given by Eqn. 7.53. Therefore K will necessarily have the dimensional form

$$K = K_1 + iK_2 = \frac{\sigma\sqrt{L}}{L^{i\varepsilon}} \quad (7.59)$$

where L is a length quantity such as crack length or ligament length, which would be discussed later.

⁶⁰ Alternatively for a homogeneous material, the dimensions of the stress intensity factor are

$$K = K_I + iK_{II} = \sigma\sqrt{L} \quad (7.60)$$

Thus it is clear that dimensionally, the homogeneous and bimaterial stress intensity factors differ by $L^{-i\varepsilon}$.

⁶¹ Considering the kinked crack of length a as shown in Fig. 7.10, the singular stress field at its tip is the classical field with the conventional stress intensity factors, K_I and K_{II} such that,

$$\sigma_{y'y'} + i\tau_{x'y'} = \frac{K_I + iK_{II}}{\sqrt{2\pi x'}} \quad (7.61)$$

ahead of the tip ($x' > 0, y' = 0$).

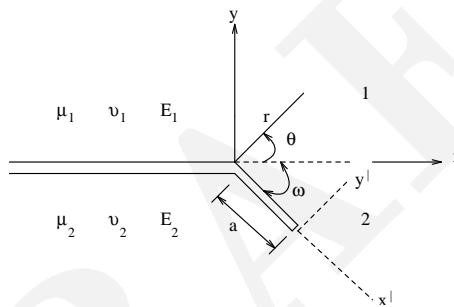


Figure 7.10: Geometry of kinked Crack, (Hutchinson and Suo, 1992)

⁶² From dimensional considerations, for the equality between K_I, K_{II} and K_1, K_2 , a length quantity must be used to relate those two sets of stress intensity factors (Hutchinson and Suo, 1992).

⁶³ A relation between the intensity factors of the kinked crack in the homogeneous material and the ones at the interface, was proposed by Hutchinson and Suo (1992), as⁴

$$K_I + iK_{II} = c(\omega, \alpha, \beta)Ka^{i\varepsilon} + d\bar{c}(\omega, \alpha, \beta)\bar{K}\bar{a}^{-i\varepsilon} \quad (7.62)$$

where $\bar{(\)}$ denotes complex conjugation for convenience, and c and d are complex valued functions of ω, α, β . The coefficients c and d values are tabulated in He and Hutchinson (1989). An approximations of these coefficients (He and Hutchinson, 1989), is

$$c = \frac{1}{2}(\exp^{-i\omega/2} + \exp^{-i3\omega/2}) \quad (7.63)$$

$$d = \frac{1}{4}(\exp^{-i\omega/2} - \exp^{i3\omega/2}) \quad (7.64)$$

7.4.3 Interface Fracture Toughness

⁶⁴ In plane strain, the energy release rate G_o of the interface crack advancing in the interface is related to K as shown in Eqn. 7.58, and may be rewritten in the form (Malyshev and Salganik, 1965)

$$G_o = \left[\frac{(1 - \nu_1)}{\mu_1} + \frac{(1 - \nu_2)}{\mu_2} \right] \frac{K\bar{K}}{4 \cosh^2(\pi\varepsilon)} \quad (7.65)$$

⁴Note the analogy between this expression and Eq. 7.13 for the SIF at the tip of a kinked crack as developed by Hussain et al. (1974) for the Maximum Energy Release Rate criterion.

where \bar{K} denotes the complex conjugate of K .

65 The energy release rate G of the kinked crack ($a > 0$) is given by,

$$G = \left[\frac{(1 - \nu_2)}{2\mu_2} \right] (K_I^2 + K_{II}^2) \quad (7.66)$$

66 Combining this equation with Eqn. 7.62 gives

$$G = \left[\frac{(1 - \nu_2)}{2\mu_2} \right] [(|c|^2 + |d|^2) K \bar{K} + 2\text{Re}(cdK^2 a^{2i\varepsilon})] \quad (7.67)$$

67 This expression can be reduced further by witting K as (He and Hutchinson, 1989),

$$K = K_1 + iK_2 = |K| e^{i\varepsilon} L^{-i\varepsilon} \quad (7.68)$$

where by 7.59, L is the in-plane length quantity characterizing the specific interface crack problem when $a = 0$. From Equations 7.65, 7.67 and 7.68 and using the real angular quantity γ as the measure of the loading combination,

$$G = q^{-2} G_o [|c|^2 + |d|^2 + 2\text{Re}(cd \exp^{2i\bar{\gamma}})] \quad (7.69)$$

where

$$q = \left[\frac{(1 - \beta^2)}{(1 + \alpha)} \right]^{1/2} \quad (7.70)$$

$$\bar{\gamma} = \gamma + \varepsilon \ln(a/L) \quad (7.71)$$

$$\gamma = \tan^{-1}(K_2/K_1) \quad (7.72)$$

68 When $\varepsilon = 0$, the stress intensity factors, K_I and K_{II} and G are independent of a . This is the case of similar moduli across the interface ($\alpha = \beta = 0$).

69 From Eqn. 7.54, ε is zero when $\beta = 0$ regardless the value of α . The oscillatory behavior of the interface crack fields and the a -dependence of G only appear when $\beta \neq 0$. According to He and Hutchinson (He and Hutchinson, 1989), a sensible approach to gaining insight into interfacial fracture behavior, while avoiding complications associated with the oscillatory singularity, would be to focus on material combinations with $\beta = 0$.

70 The interface crack with $a = 0$, suffers contact between the crack faces within some small distance from the tip, when $\beta \neq 0$, therefore $\varepsilon \neq 0$, as predicted by the elastic solutions of the crack fields (Comninou, 1977; Rice, 1988). Contact between crack faces is less likely for the kinked crack ($a > 0; \omega > 0$) loaded such that K_I and K_{II} are positive, since this will open up the crack at the kink. Nevertheless, contact will inevitably occur if $\varepsilon \neq 0$ when a is sufficiently small compared to L (He and Hutchinson, 1989).

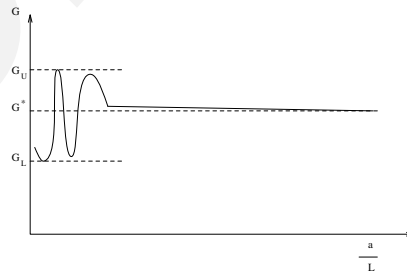


Figure 7.11: Schematic variation of energy release rate with length of kinked segment of crack for $\beta \neq 0$, (Hutchinson and Suo, 1992)

71 The dependence of G on a for a given kink angle is shown qualitatively in Fig. 7.11 as predicted by Eqn. 7.69 when $\varepsilon \neq 0$. (He and Hutchinson, 1989). When a/L becomes sufficiently small, G oscillates between a maximum G_U and a minimum G_L , which are found to be (He and Hutchinson, 1989)

$$G_U = q^{-2} G_o [|c| + |d|]^2 \quad (7.73)$$

$$G_L = q^{-2} G_o [|c| - |d|]^2 \quad (7.74)$$

and which depend on K_1 and K_2 only through G_o . For values of a/L outside the oscillatory range G approaches G^* , given by Eqn. 7.69, with $\bar{\gamma} = \gamma$, i.e.,

$$G^* = q^{-2} G_o [|c|^2 + |d|^2 + 2\text{Re}(cd \exp^{2i\gamma})] \quad (7.75)$$

G^* coincides with G given by Eqn. 7.69, when $\varepsilon = 0$. Contact between the crack faces will invalidate the prediction for G from Eqn. 7.69 when a/L is in the range where oscillatory behavior occurs.

⁷² From a physical standpoint, G^* should be relevant if there exists crack-like flaws emanating from the interface whose lengths are greater than the zone of contact. That is, G^* should be relevant in testing for kinking if the fracture process zone on the interface is large compared to the contact zone of the idealized elastic solution. If it is not, then more attention must be paid to the a -dependence of G and to the consideration of the contact. In any case G^* should play a prominent role in necessary conditions for a crack kinking out of an interface, because once nucleated, the kinked crack has an energy release rate which rapidly approaches G^* as it lengthens (He and Hutchinson, 1989).

7.4.3.1 Interface Fracture Toughness when $\beta = 0$

⁷³ When $\beta = 0$ (and thus $\varepsilon = 0$) Eqns. 7.53, 7.57 and 7.58, respectively become:

$$(\sigma_{yy}, \tau_{xy}) = \frac{(K_1, K_2)}{\sqrt{2\pi r}} \quad (7.76)$$

$$(\delta_y, \delta_x) = \frac{4}{\sqrt{2\pi}} \left[\frac{1}{E_1} + \frac{1}{E_2} \right] \sqrt{r} (K_1, K_2) \quad (7.77)$$

$$G = \frac{1}{2} \left[\frac{1}{E_1} + \frac{1}{E_2} \right] (K_1^2 + K_2^2) \quad (7.78)$$

⁷⁴ The interface stress intensity factors K_1 and K_2 play precisely the same role as their counterparts in elastic fracture mechanics for homogeneous, isotropic solids. The mode 1 component K_1 is the amplitude of the singularity of the normal stresses ahead of the tip and the associated normal separation of the crack flanks, while the mode 2 component, K_2 , governs the shear stress on the interface and the relative shearing displacement of the flanks.

⁷⁵ When $\beta = 0$, the measure of the relative amount of mode 2 to mode 1 at the crack tip is taken as (Hutchinson and Suo, 1992)

$$\gamma = \tan^{-1}(K_2/K_1) \quad (7.79)$$

⁷⁶ For the case of a finite crack in an infinite plane,

$$\gamma = \tan^{-1}(\tau_{xy}^\infty/\sigma_{yy}^\infty) \quad (7.80)$$

⁷⁷ The criteria for initiation of crack propagation along the interface when the crack tip is loaded in mixed mode by γ is

$$G = \Gamma(\gamma) \quad (7.81)$$

⁷⁸ Where $\Gamma(\gamma)$ is the toughness of the interface and can be thought of as an effective surface energy that depends on the mode of loading.

7.4.3.2 Interface Fracture Toughness when $\beta \neq 0$

⁷⁹ When $\beta \neq 0$, the decoupling of the normal and shear components of stress on the interface and associated displacements behind the crack tip within the zone dominated by the singularity, does not occur. When $\beta \neq 0$, the definitions of mode 1 and mode 2 require some modification. In addition, the traction-free line crack solution for the displacements implies that the crack faces interpenetrate at some point behind the tip. Both of these features have caused conceptual difficulties in the development of a mechanics of interfaces.

⁸⁰ As noted by Rice (1988), a generalized interpretation of the mode measure is the most important complication raised by the oscillatory singularity, and the approach explained here is along the lines of one of his proposals (Hutchinson and Suo, 1992). First, a definition of a measure of the combination of mode is made that generalizes Eqn. 7.79.

⁸¹ Let L be a reference length whose choice will be discussed later. Noting the stress distribution (7.53) on the interface from the K -field, define γ as

$$\gamma = \tan^{-1} \left[\frac{\text{Im}(KL^{i\varepsilon})}{\text{Re}(KL^{i\varepsilon})} \right] \quad (7.82)$$

where $K = K_1 + iK_2$ is the complex stress intensity factor.

⁸² For a choice of L within the zone of dominance of the K -field, Eqn. 7.82 is equivalent to

$$\gamma = \tan^{-1}\left[\left(\frac{\tau_{xy}}{\sigma_{yy}}\right)_{r=L}\right] \quad (7.83)$$

⁸³ Moreover, the definition reduces to Eqn. 7.79 when $\beta = 0$, since $L^{i\varepsilon} = 1$ when $\varepsilon = 0$. When $\varepsilon \neq 0$, a mode 1 crack is one with zero shear traction on the interface a distance L ahead of the tip, and a mode 2 crack has zero normal traction at that point. The measure of the proportion of "mode 2" to "mode 1" in the vicinity of the crack tip requires the specification of some length quantity since the ratio of the shear traction to normal traction varies (very slowly) with distance to the tip when $\beta \neq 0$.

⁸⁴ The choice of the reference length L is somewhat arbitrary, as explained by Hutchinson and Suo (1992). It is useful to distinguish between a choice based on an in-plane length L of the specimen geometry, such as crack length, and a choice based on a material length scale, such as the size of the fracture process zone or a plastic zone at fracture. The former is useful for discussing the mixed mode character of a bimaterial crack solution, independent of material fracture behavior, while the latter is advantageous in interpreting mixed mode fracture data.

7.4.4 Crack Kinking Analysis

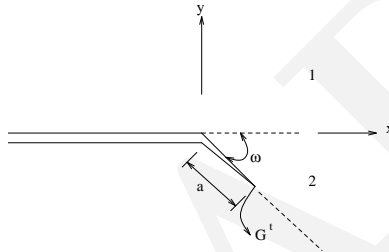


Figure 7.12: Conventions for a Crack Kinking out of an Interface, (Hutchinson and Suo, 1992)

⁸⁵ Fig. 7.12 shows a semi-infinite crack lying along the interface with its tip at the origin. Prior to kinking ($a = 0$), the parent crack is loaded with a complex interface stress intensity factor $K = K_1 + iK_2$ with mixity γ defined by Eqn. 7.82 relative to some reference length L . For definiteness, γ is taken to be positive with kinking down into material 2 as shown in Fig. 7.12. Negative γ -loadings with upward kinking can be analyzed by exchanging the materials, i.e., switching the signs on α and β . Roughly speaking, $\alpha > 0$ implies that material 1 is stiffer than material 2 and vice versa.

7.4.4.1 Numerical Results from He and Hutchinson

⁸⁶ In their paper (He and Hutchinson, 1989), the authors have carried out analysis of a crack kinking out of an interface with the aim of providing the crack mechanics needed to assess whether an interface crack will tend to propagate in the interface or whether it will advance by kinking out of the interface. The analysis provides the relationships among K_I and K_{II} for the kinked crack and K_1 and K_2 for the interface crack as dependent on the kink angle ω and the material moduli, as shown in Eqn. 7.62. The energy release rate of the kinked crack G is also related to the energy release rate of the interface crack, G_o , as shown in Eqn. 7.69. A parametric study is conducted using these relations and the qualitative features which emerge are listed below.

- Bimaterial Problem with $\beta = 0$

1. The more compliant is the material into which the crack kinks, i.e. the larger is α , the larger is the energy release rate, with all factors being equal. Conversely, if the lower material into which the crack kinks is relatively stiffer ($\alpha < 0$), then the energy release rate is reduced.
2. If the difference in the elastic moduli of the two materials are relatively large, the energy release rate for a crack kinking into the stiff material can be less than the interface release rate G_o , for all combinations of loading. This suggests that under conditions when the compliant material is tough and the stiff material and the interface are each relatively brittle with comparable toughnesses (as measured by a critical value of energy release rate), the crack will tend to be trapped in the interface for all loading combinations.

3. If the stiff material is even less tough than the interface, the crack may leave the interface, but not necessarily by kinking. For example, when $\alpha = -0.75$ (He and Hutchinson, 1989), the largest energy release rates occur when ω is small approaching zero, suggesting that the crack may smoothly curve out of the interface. Such a path, however, would not necessarily satisfy $K_{II} = 0$.
 4. From the plots (He and Hutchinson, 1989) showing the direction $\hat{\omega}$ corresponding to the maximum energy release rate (i.e. where $dG/d\omega = 0$ or at $\omega = 0$, whichever gives the larger G) as a function of the loading angle γ for various values of α , it is seen that for positive α i.e. for the crack kinking into the more compliant material, $\hat{\omega}$ increases smoothly as γ increases from 0 to 90 deg.
 5. When $\gamma = 0$, meaning $K_2 = 0$, the direction of maximum energy release rate is greater than zero for $\alpha > 0$. This shows that the crack kinks into more compliant material 2 with finite angle for $\gamma = 0$.
 6. When α is negative, i.e. when material 2 is more stiffer than material 1, there exists a range of γ in the vicinity of $\gamma = 0$ for which the maximum occurs at $\omega = 0$
 7. For sufficiently negative α , the maximum of G also occurs at $\omega = 0$ where γ is in the vicinity of 90 deg.
 8. For α , more negative than -0.67, the maximum occurs at $\omega = 0$ for all γ .
 9. The direction $\bar{\omega}$ corresponding to $K_{II} = 0$ is sometimes suggested as an alternative to $\hat{\omega}$ as the kink direction. A comparison between $\bar{\omega}$ and $\hat{\omega}$ is shown in He and Hutchinson (1989), for $\alpha = 0$ and $\alpha = \pm 0.5$. In the homogeneous case when $\alpha = 0$, the difference between $\bar{\omega}$ and $\hat{\omega}$ is less than 1 deg. for nearly all γ except near $\gamma = \pi/2$ where it becomes about 2 deg.
 10. The difference between the two directions is also very minor for $\alpha = \pm 0.5$.
 11. For more negative values of α than -0.5, the range of γ in which G_{max} occurs at $\hat{\omega} = 0$ becomes significant, while $K_{II} = 0$ at values of ω near the local maximum of G which occurs for ω between 45 deg. and 60 deg. depending on γ . In this range of γ , $\bar{\omega}$ and $\hat{\omega}$ are significantly different.
- Bimaterial Problems with $\beta \neq 0$

⁸⁷ As discussed in connection with Eqn. 7.69, G is not independent of a when $\varepsilon \neq 0$, but G approaches G^* for all but very small a . Plots of G^*/G_o as a function of ω are found in (He and Hutchinson, 1989) for ($\alpha = 0.5, \beta = 0.25$) and ($\alpha = -0.5, \beta = -0.25$). Although the β values in these examples are quite large, the curves are quite similar to three curves obtained with the same values of α and with $\beta = 0$. Curves of $\hat{\omega}$ associated with the maximum value of G^* versus γ are also shown in (He and Hutchinson, 1989), which indicate that the effect of β on $\hat{\omega}$ is relatively weak.

7.4.4.2 Numerical Results Using Merlin

⁸⁷ Merlin is a three dimensional finite element program having the capabilities of performing fracture mechanics based analysis. The Stern and Becker integral method has been implemented in it to determine the stress intensity factors for bimaterials. In order to check the accuracy of the numerical results with those of the analytical ones, the following analysis is performed.

⁸⁸ A square centre-cracked plate of dimensions 20 X 20 inches, consisting of two isotropic materials is analyzed. The plate is subjected to tensile stresses in all directions. The crack, of length 2 inches, is on the interface between the two materials. The geometry and the natural boundary conditions are shown in Fig. 7.13, and the finite element mesh is shown in Fig. 7.14. This mesh was generated using the pre-processor developed for Merlin. Since the analytical results for this problem were available for plane stress condition in (Lin and Mar, 1976), seven different cases with varying moduli ratios were considered in this analyses. The material in the upper portion of the plate is identified as material 1 and the material in the lower portion is identified as material 2. The elastic modulus E_2 for material 2 was kept fixed at 1 psi and the poisson's ratio of material 1 was fixed at 0.3. The tensile stress in the y-direction, σ_{yy} in all the cases was 1 psi and in the x-direction, the tensile stress σ_{xx} for material 1 was fixed at 1 psi. σ_{xx} for material 2 was varied for different cases as tabulated in Table 7.1. Symmetry of the plate about the centreline perpendicular to the crack and the material interface is considered in the finite element model.

⁸⁹ It is worth mentioning at this point that the modulus of elasticity of concrete is in the range $2 \times 10^6 - 4 \times 10^6 psi$ and for rock $5 \times 10^5 - 10 \times 10^6 psi$. Generally in the case of dams the ratio of the modulus of elasticity of concrete to that of rock is somewhere around 3.

⁹⁰ The stress intensity factors K_1 and K_2 ⁵ was obtained in (Lin and Mar, 1976) using the expressions derived by Rice and Sih

⁵ K_1 and K_2 as explained earlier are the real and imaginary parts of the complex stress intensity factor $K = K_1 + K_2$, used for bimaterial interfaces as compared to the conventional stress intensity factors K_I and K_{II} used in the case of homogeneous interface.

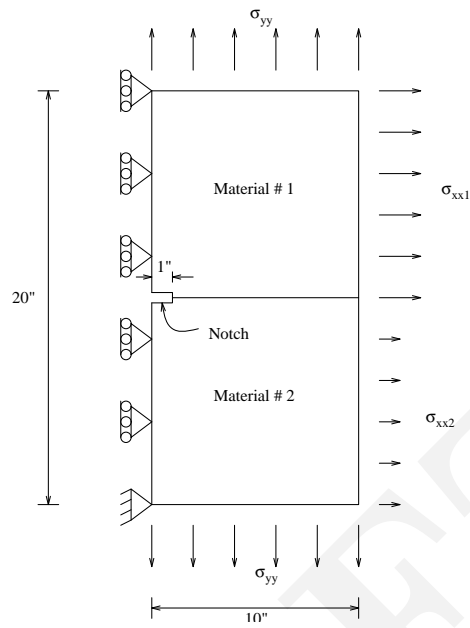


Figure 7.13: Geometry and Boundary Conditions of the Plate Analyzed

Figure 7.14: Finite Element Mesh of the Plate Analyzed

Case	E_1/E_2	ν_2	σ_{xx2}	α	β	ε
1	1.000	0.30	1.00	0.00	0.000	0.0
2	3.000	0.30	0.53	0.50	0.143	-4.579 E-02
3	10.000	0.30	0.37	0.82	0.234	-7.581 E-02
4	22.244	0.35	0.38	0.91	0.208	-6.711 E-02
5	100.000	0.30	0.31	0.98	0.280	-9.159 E-02
6	123.600	0.35	0.36	0.99	0.227	-7.352 E-02
7	1000.000	0.30	0.30	0.98	0.285	-9.335 E-02

Table 7.1: Material Properties and Loads for Different Cases

Case	Analytical		Numerical		% difference	
	K_1	K_2	K_1	K_2	K_1	K_2
1	1.773	0.00	1.841	0.15	4.01	—
2	1.770	0.13	1.872	0.16	5.76	20.77
3	1.765	0.21	1.872	0.22	5.76	0.0
4	1.750	0.22	1.869	0.23	6.80	0.0
5	1.760	0.27	1.875	0.26	6.82	0.0
6	1.747	0.24	1.871	0.24	6.86	0.0
7	1.761	0.26	1.873	0.26	6.25	0.0

Table 7.2: Analytical and Numerical Results

(1965), which are as follows:

$$K_1 = \frac{\sigma[\cos(\varepsilon \log 2a) + 2\varepsilon \sin(\varepsilon \log 2a)] + [\tau[\sin(\varepsilon \log 2a) - 2\varepsilon \cos(\varepsilon \log 2a)]]}{\cosh \pi \varepsilon} \sqrt{a} \quad (7.84)$$

$$K_2 = \frac{\tau[\cos(\varepsilon \log 2a) + 2\varepsilon \sin(\varepsilon \log 2a)] - [\sigma[\sin(\varepsilon \log 2a) - 2\varepsilon \cos(\varepsilon \log 2a)]]}{\cosh \pi \varepsilon} \sqrt{a} \quad (7.85)$$

⁹¹ To have a consistent definition of K_1 and K_2 as defined in earlier chapters, the above expressions have to be multiplied by the factor $\sqrt{\pi} \cosh \pi \varepsilon$. Using the modified values of K_1 and K_2 , the fracture energy G is calculated using Eqn. 7.58. These analytical results along with the numerical results obtained using Merlin is tabulated in Table 7.2. It is seen that the differences between the analytical and numerical results are very small.

⁹² The results of the stress intensity factors obtained by the S-integral method and without the use of the bimaterial model, which is used in the case of homogeneous interface is shown in Table 7.3. The stress intensity factors obtained in this case are the conventional ones K_I and K_{II} . It is seen that the percentage difference between these values and the theoretical stress intensity factors K_1 and K_2 are quite high. This implies that the use of the conventional S-integral to obtain the bimaterial stress intensity factors may lead to erroneous results.

⁹³ Plots showing the variation of G/G_o versus kink angle ω for the loading angle considered in the analyses are shown in Figs.

Case	Analytical		Numerical		% difference	
	K_1	K_2	K_I	K_{II}	K_1	K_2
1	1.773	0.00	1.386	0.2408	22.00	—
2	1.770	0.13	1.525	0.0047	13.70	96
3	1.765	0.21	1.352	0.0158	23.40	93
4	1.750	0.22	1.312	0.0083	25.02	96
5	1.760	0.27	1.275	0.0072	27.60	97
6	1.747	0.24	1.281	0.0041	26.70	98
7	1.761	0.26	1.265	0.0057	28.10	98

Table 7.3: Numerical Results using S-integral without the bimaterial model

7.15. These plots are obtained using Eqn. 7.69 along with the approximate expressions of c and d given by Eqns. 7.63 and 7.64. The loading parameter γ in the case of the analytical solution is obtained from Eqn. 7.79 and in the case of the numerical solution γ is obtained using the relation $\gamma = \tan^{-1}(\tau/\sigma_{yy})$, where τ and σ_{yy} are the shear and normal stresses at the crack tip, respectively.

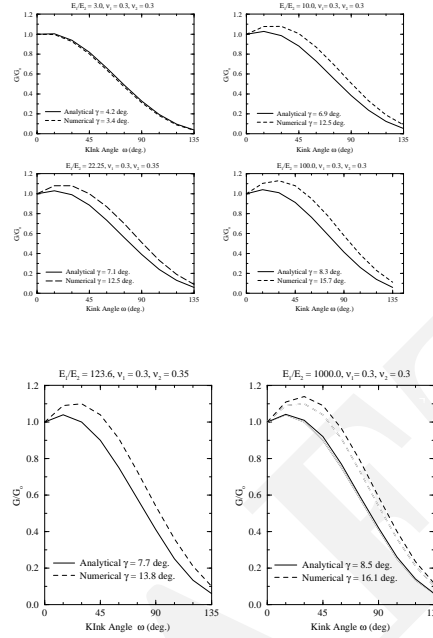


Figure 7.15: Variation of G/G_o with Kink Angle ω

7.4.5 Summary

94 The results for the kinked crack can be used to access whether an interface crack will propagate in the interface or whether it will kink out of the interface.

Let

G_{oc} = critical fracture energy of the interface,

G_{ic} = critical fracture energy of material i ,

G_{max} = maximum energy release rate in material i

1. The condition for propagation in the interface is $G_o = G_{oc}$ and that for propagating in any one of the two materials is $G = G_{ic}$.
2. Conditions for crack kinking and propagation:
 - $\left(\begin{array}{l} G_{max} < G_{ic} \\ G_o < G_{oc} \end{array} \right)$ no crack propagation.
 - $\left(\begin{array}{l} G_{max} \geq G_{ic} \\ G_o < G_{oc} \end{array} \right)$ crack kinks in material i .
 - $\left(\begin{array}{l} G_{max} < G_{ic} \\ G_o \geq G_{oc} \end{array} \right)$ crack propagates along the interface.
 - $\left(\begin{array}{l} G_{max} \geq G_{ic} \\ G_o \geq G_{oc} \end{array} \right)$ crack kinks and propagates i.e. the crack branches.
3. If G_{ic} is sufficiently large when compared to G_{oc} , the crack will never kink into material i .

4. When G_{ic} is comparable to G_{oc} , there will still be a loading range, i.e. $0 \leq \gamma \leq \gamma_{max}$, such that the crack stays in the interface, while for $\gamma > \gamma_{max}$, the interface crack will kink into material i .
5. When the fractured interface has some roughness, G_{oc} might depend on the loading parameter γ . Hence the level of G_{ic} required to prevent kinking out of the interface will depend on the interface toughness G_{oc} at the loading angle γ applied.
6. When there is no dissimilarity in the elastic properties of the materials across the interface, the direction of kinking associated with the maximum energy release rate and with $K_{II} = 0$ are virtually the same.
7. When the crack has penetrated well into material i , a criterion based on $K_{II} = 0$ is expected to hold.
8. Crack deflection analysis based on the crack kinking and maximum principal stress theories indicate that global mode I loading generally favors interfacial crack propagation. For global mode II loading, crack deflection into the core is a likely scenario because of favorable conditions and large crack driving force.
9. A choice of criterion for the initial kinking step will have to be guided by experiment.

DRAFT

Chapter 8

PLASTIC ZONE SIZES

¹ it was shown in chapter 3 that, under linear elastic fracture mechanics assumptions, the stress at the crack tip is theoretically infinite. Clearly, all materials have a finite strength, thus there will always be a small plastified zone around the crack tip.

² If this zone is small compared to the crack size, then our linear elastic assumptions are correct; if not, LEFM is not applicable (thus it would be incorrect to use a K or G criterion) and a nonlinear model must be used. This “damaged” zone is referred to as a *plastic zone* for metals, and a *fracture process zone* for cementitious materials and ceramics.

³ Thus there are two important issues associated with nonlinear fracture:

1. What is the size of the plastic or process zone?
2. What are the criteria for crack growth?

⁴ This chapter will answer the first question by focusing on metals¹, whereas the next chapter will develop criteria for crack growth.

⁵ The evaluation of the plastic zone for plastified materials can be determined through various levels of approximations:

1. Uniaxial stress criteria
 - a) first order approximation
 - b) second order approximation (Irwin)
 - c) Dugdale’s model
2. Multiaxial yield criteria

Each one of them will be separately reviewed.

8.1 Uniaxial Stress Criteria

⁶ First we shall examine criteria in which only the uniaxial stress state (σ_{yy} normal to the crack axis) and we shall consider three models of increasing complexities.

8.1.1 First-Order Approximation.

⁷ The simplest estimate of the size of a process zone is obtained by equating σ_y (Eq. 3.53-b)

$$\sigma_{yy} = \frac{K_I}{(2\pi r)^{\frac{1}{2}}} \cos \frac{\theta}{2} \left[1 + \sin \frac{\theta}{2} \sin \frac{3\theta}{2} \right] \quad (8.1)$$

to the yield stress σ_{yld} for $\theta = 0$, Fig. 8.1

$$\sigma_{yy} = \frac{K_I}{\sqrt{2\pi r_p^*}} = \sigma_{yld} \quad (8.2)$$

or

$$\boxed{r_p^* = \frac{1}{2\pi} \frac{K_I^2}{\sigma_{yld}^2} = \frac{a}{2} \left(\frac{\sigma}{\sigma_{yld}} \right)^2} \quad (8.3)$$

¹Due to the intrinsically different behavior of concrete compared to metals, estimates of the fracture process zone will be separately discussed.

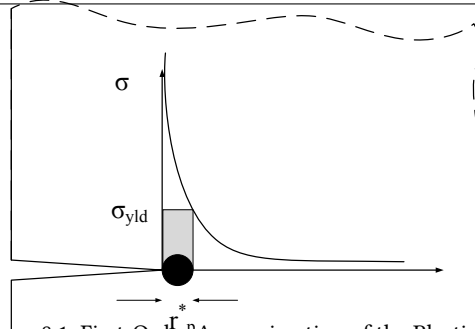


Figure 8.1: First-Order Approximation of the Plastic Zone

8.1.2 Second-Order Approximation (Irwin)

In 1960, Irwin (Irwin, 1960) developed a second-order approximation for the plastic zone based on the stress redistribution occurring at the crack tip. In the first model, we started with a stress distribution which satisfied equilibrium, and “cut down” all stresses exceeding σ_{yld} . As a result equilibrium was no longer satisfied. In this model the force (area under the stress curve) which was “eliminated” is simply redistributed to satisfy equilibrium requirements. Hence, with reference to Fig. 8.2, we have:

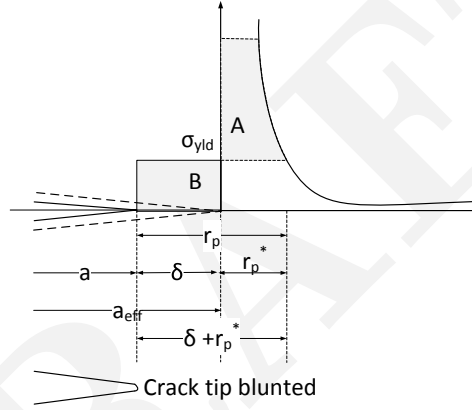


Figure 8.2: Second-Order Approximation of the Plastic Zone

$$B = \sigma_{yld} \delta \quad (8.4)$$

$$\begin{aligned}
 A &= \int_0^{r_p^*} \sigma dr - \sigma_{yld} r_p^* \\
 &= \int_0^{r_p^*} \frac{K}{\sqrt{2\pi r}} dr - \sigma_{yld} r_p^* \\
 &= \int_0^{r_p^*} \frac{\sigma \sqrt{\pi a}}{\sqrt{2\pi r}} dr - \sigma_{yld} r_p^* \\
 &= \int_0^{r_p^*} \sigma \sqrt{\frac{a}{2}} r^{-\frac{1}{2}} dr - \sigma_{yld} r_p^* \\
 &= \sigma \sqrt{\frac{a}{2}} 2r^{\frac{1}{2}} \Big|_0^{r_p^*} - \sigma_{yld} r_p^* \\
 &= \sigma \sqrt{2ar_p^*} - \sigma_{yld} r_p^* \quad (8.5)
 \end{aligned}$$

Equating A to B we obtain:

$$\begin{aligned}
 \sigma \sqrt{2ar_p^*} - \sigma_{yld} r_p^* &= \sigma_{yld} \delta \\
 \sigma_{yld} (\delta + r_p^*) &= \sigma \sqrt{2ar_p^*} \\
 (\delta + r_p^*)^2 &= \frac{2a\sigma^2}{\sigma_{yld}^2} r_p^* \quad (8.6)
 \end{aligned}$$

10 From Eq. 8.3, $r_p^* = \frac{a}{2} \left(\frac{\sigma}{\sigma_{\text{yld}}} \right)^2$, thus this simplifies into

$$\delta + r_p^* = 2r_p^* \Rightarrow \delta = r_p^* \quad (8.7)$$

$$r_p = 2r_p^* \quad (8.8)$$

$$\boxed{r_p = \frac{1}{\pi} \frac{K_I^2}{\sigma_{\text{yld}}^2} = \left(\frac{\sigma}{\sigma_{\text{yld}}} \right)^2 a} \quad (8.9)$$

11 Note that $r_p = 2r_p^*$ and that we can still use r_p^* but with $a_{\text{eff}} = a + r_p^*$; thus we can consider an effective crack length of $a + r_p^*$ which would result in:

$$\boxed{K_{\text{eff}} = f(g)\sigma\sqrt{\pi(a + r_p^*)} = f(g)\sigma\sqrt{\pi\left(a + \frac{K^2}{2\pi\sigma_{\text{yld}}^2}\right)}} \quad (8.10)$$

12 For linear elastic fracture mechanics to be applicable, we must have:

$$\boxed{\text{LEFM} \Leftrightarrow K \approx K_{\text{eff}}} \quad (8.11)$$

8.1.2.1 Example

13 Considering an infinite with central crack of size $2a = 16$ mm, a far field applied stress $\sigma_{\text{app}} = 350$ MPa, and the plate has a yield stress $\sigma_{\text{yld}} = 1,400$ MPa.

14 First we seek to determine the size of the plastic zone and the effective SIF.

Using the 1st order approximation:

$$r_p^* = \frac{\sigma^2 a}{2\sigma_{\text{yld}}^2} = \frac{(350)^2 (.008)}{2(1,400)^2} \approx .00025 \text{ m} = .25 \text{ mm} \quad (8.12)$$

Since $\frac{r_p}{a}$ is very small, $K_{\text{eff}} \approx K_{\text{applied}}$

$$K_{\text{eff}} = \sigma\sqrt{\pi(a + r_p^*)} = 350\sqrt{\pi(.008 + .00025)} = 56.4 \text{ MPa}\sqrt{\text{m}} \quad (8.13)$$

$$K_{\text{app}} = \sigma\sqrt{\pi a} = 350\sqrt{\pi(.008)} = 55.5 \text{ MPa}\sqrt{\text{m}} \quad (8.14)$$

15 We note that there is only 2 percent difference between those two solutions, hence LEFM is applicable.

16 If yield stress was decreased by heat treatment to 385 MPa, then

$$r_p^* = \frac{(350)^2 (.008)}{2(385)^2} = .0033 \text{ m} = 3.3 \text{ mm}. \quad (8.15)$$

and

$$K_{\text{eff}} = 350\sqrt{\pi(.008 + .0033)} = 66 \text{ MPa}\sqrt{\text{m}} \quad (8.16)$$

and in this case LEFM may no longer be applicable.

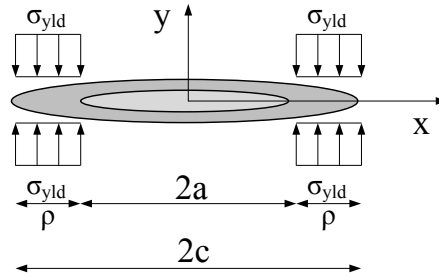


Figure 8.3: Dugdale's Model

8.1.3 Dugdale's Model.

¹⁷ Dugdale (Dugdale, 1960) assumed that the actual physical crack of length $2a$ is replaced by a total effective crack of length $2c$, where $c = a + \rho$, Fig. 8.3, such that:

1. A constant stress σ_{yld} is applied over ρ where $a < x < c$ causing (a negative) K_ρ .
2. c is selected in such a manner that $\sum K = 0$ or $K_{remote} = -K_\rho$.

¹⁸ The solution to this model is found by first considering a point load P applied at a distance x from the crack center, as in Fig. 8.4, where the stress intensity factors are given by:

$$\begin{aligned} K_A &= \frac{P}{\sqrt{\pi a}} \sqrt{\frac{a+x}{a-x}} \\ K_B &= \frac{P}{\sqrt{\pi a}} \sqrt{\frac{a-x}{a+x}} \end{aligned} \quad (8.17)$$

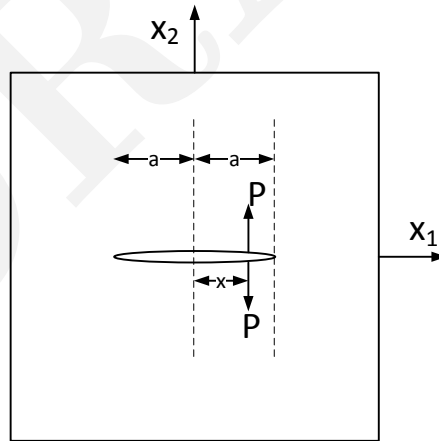


Figure 8.4: Point Load on a Crack

¹⁹ Assuming $dP = \sigma_{yld} dx$, and replacing in the above equations, we obtain:

$$K_\rho = \frac{\sigma_{yld}}{\sqrt{\pi a}} \int_a^c \left\{ \sqrt{\frac{a+x}{a-x}} + \sqrt{\frac{a-x}{a+x}} \right\} dx \quad (8.18)$$

²⁰ Integration of this equation results in

$$K_\rho = 2\sigma_y \sqrt{\frac{c}{\pi}} \arccos \frac{a}{c} \quad (8.19)$$

21 On the other hand, the stress intensity caused by the remote far field stress is given by:

$$K_{remote} = \sigma\sqrt{\pi c} \quad (8.20)$$

Equating Eq. 8.20 with Eq. 8.19 and solving, we obtain:

$$\frac{a}{c} = \cos\left(\frac{\pi}{2} \frac{\sigma}{\sigma_{yld}}\right) \quad (8.21)$$

22 From Eq. 8.21, we observe

1. As $\sigma \rightarrow \sigma_{yld}$, $\frac{a}{c} \rightarrow 0$, or $\rho \rightarrow \infty$, Fig 8.5

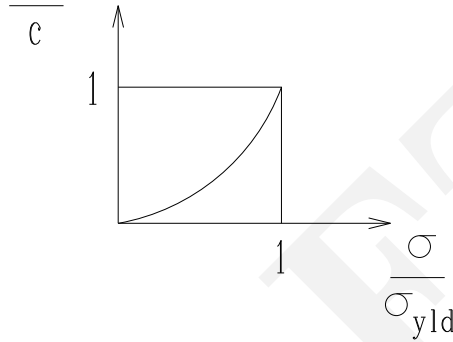


Figure 8.5: Effect of Plastic Zone Size on Dugdale's Model

2. Using the Cosine Taylor's expansion on Eq. 8.21, as $\frac{\sigma}{\sigma_{yld}} \rightarrow 0$, we can rewrite:

$$\frac{a}{c} = \frac{a}{a + \rho} = 1 - \frac{1}{2!} \left(\frac{\pi\sigma}{2\sigma_{yld}}\right)^2 + \frac{1}{4!} \left(\frac{\pi\sigma}{2\sigma_{yld}}\right)^4 - \frac{1}{6!} \left(\frac{\pi\sigma}{2\sigma_{yld}}\right)^6 \quad (8.22)$$

Neglecting all but the first two terms and solving for ρ

$$\rho = \frac{\pi^2}{8} \left(\frac{\sigma}{\sigma_{yld}}\right)^2 a = \frac{\pi}{8} \frac{K_I^2}{\sigma_{yld}^2} \quad (8.23)$$

Eq. 8.23 should be compared with Eq. 8.9 ($r_p = \left(\frac{\sigma}{\sigma_{yld}}\right)^2 a$) previously obtained.

23 Finally it should be mentioned that similar equations have been derived by Barenblatt (Barenblatt, 1962) on the basis of a linear stress distribution, see Fig. 8.6.

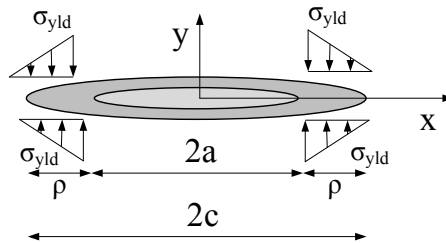


Figure 8.6: Barenblatt's Model

8.2 Multiaxial Yield Criteria

²⁴ All the previous models have restricted themselves to $\theta = 0$ and have used uniaxial yield criteria, but the size of the plastic zone can be similarly derived from a multi-axial yield criterion.

²⁵ The principal stresses at a point with respect to the crack tip are given by:

$$\sigma_{1,2} = \frac{\sigma_x + \sigma_y}{2} \pm \sqrt{\left(\frac{\sigma_x - \sigma_y}{2}\right)^2 + \tau_{xy}^2} \quad (8.24)$$

where the stresses were obtained in Eq. 3.53-a, 3.53-b, and 3.53-c

$$\sigma_1 = \frac{K_I}{\sqrt{2\pi r}} \cos \frac{\theta}{2} \left[1 + \sin \frac{\theta}{2} \right] \quad (8.25)$$

$$\sigma_2 = \frac{K_I}{\sqrt{2\pi r}} \cos \frac{\theta}{2} \left[1 - \sin \frac{\theta}{2} \right] \quad (8.26)$$

$$\sigma_3 = \nu(\sigma_1 + \sigma_2) \quad (8.27)$$

for plane strain, or

$$\sigma_3 = 0 \quad (8.28)$$

for plane stress.

²⁶ With those stress expressions, any yield criteria could be used. Using the von Mises criteria, we would obtain:

$$\sigma_e = \frac{1}{\sqrt{2}} [(\sigma_1 - \sigma_2)^2 + (\sigma_2 - \sigma_3)^2 + (\sigma_3 - \sigma_1)^2]^{\frac{1}{2}} \quad (8.29)$$

and yielding would occur when σ_e reaches σ_{yld} . Substituting the principal stresses (with $r = r_p$) into this equation and solving for r_p yields

• For plane strain:

$$r_p(\theta) = \frac{1}{4\pi} \frac{K_I}{\sigma_{yld}^2} \left[\frac{3}{2} \sin^2 \theta + (1 - 2\nu)^2 (1 + \cos \theta) \right] \quad (8.30)$$

• For plane stress:

$$r_p(\theta) = \frac{1}{4\pi} \frac{K_I}{\sigma_{yld}^2} \left[1 + \frac{3}{2} \sin^2 \theta + \cos \theta \right] \quad (8.31)$$

²⁷ For the Drucker-Prager model, and for different mixed mode ratios, the expected plastic (or more appropriately process) zones are shown in Fig. 8.7.

²⁸ In general, for the plastic zone sizes:

1. Different sizes would be obtained from alternative models (Tresca's would be larger than von Mises's).
2. The plastic zone for plane strain is much smaller than the one for plane stress (by a factor of $(1 - 2\nu)^2$).
3. Similar shapes could be derived if both K_I and K_{II} expressions were used.
4. This is only a first-order approximation, as no stress redistribution has been accounted for.

8.3 Plane Strain vs. Plane Stress

²⁹ Irrespective of a plate thickness, there is a gradual decrease in size of the plastic zone from the plate surface (plane stress) to the interior (plane strain), Fig. 8.8.

³⁰ The ratio of the plastic zone size to the plate thickness $\frac{r_p}{B}$ must be much smaller than unity for plane strain to prevail. It has been experimentally shown that this ratio should be less than 0.025.

Plane Strain	$K_{Ic} \Leftrightarrow r_p < .025B$	(8.32)
--------------	--------------------------------------	--------

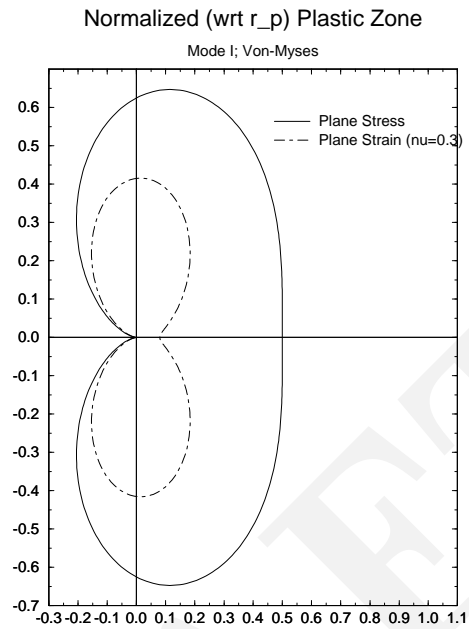


Figure 8.7: Normalized Mode I Plastic Zone (von Mises)

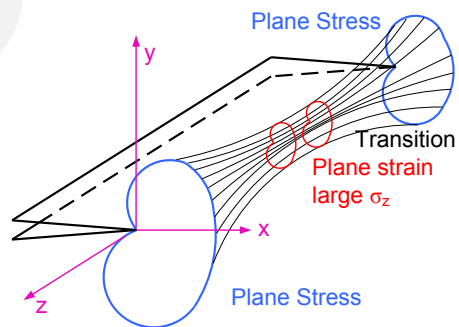


Figure 8.8: Plastic Zone Size Across Plate Thickness

31 We also observe that since r_p is proportional to $\left(\frac{K_I}{\sigma_{\text{yld}}}\right)^2$, the plate thickness should increase as either the SIF increase or the yield stress decrease.

32 Furthermore, the different stress fields present at the tip of the crack under plane stress and plane strain will result in different deformation patterns. This is best explained in terms of the orientation of the planes of maximum shear stress for both cases, Fig. 8.9.

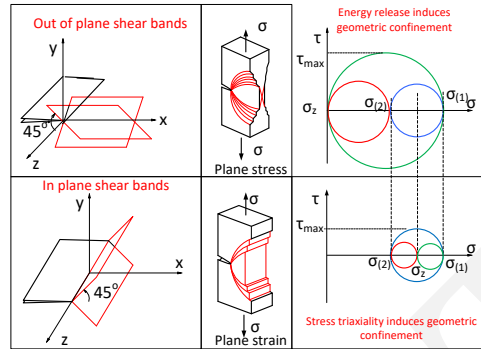


Figure 8.9: Plastic Zone Size in Comparison with Plate Thickness; Plane Stress and Plane Strain

Plane Stress: $\sigma_z = 0$, and the maximum shear stress τ_{max} is equal to $\frac{\sigma_x}{2}$. Slip is on planes through the X axis and at 45° to the plate surface in the 45° shear type of deformation typical of plane stress.

Plane Strain: In this case we have $\sigma_y < \sigma_z < \sigma_x$, and the maximum shear stress is equal to $\frac{\sigma_x - \sigma_y}{2}$ which is not only much smaller than $\frac{\sigma_x}{2}$ but occurs on different planes. The slip is on planes through the Z axis and gives rise to the hinge type of deformation typical of plane strain.

33 Finally, it should be noted, once again, that fracture toughness K_{Ic} can only be measured under plane strain conditions, Fig. 8.10

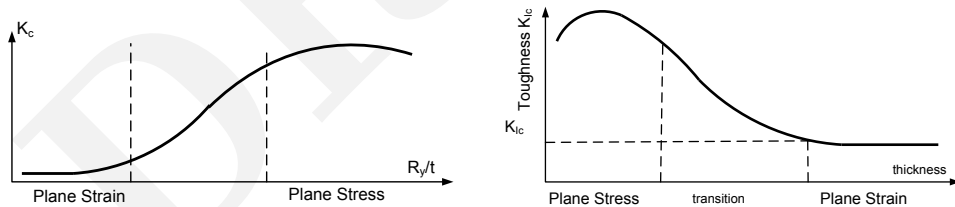


Figure 8.10: Plate Thickness Effect on Fracture Toughness

Chapter 9

FATIGUE CRACK PROPAGATION

1 When a subcritical crack (a crack whose stress intensity factor is below the critical value) is subjected to either repeated or fatigue load, or is subjected to a corrosive environment, crack propagation will occur.

2 As in many structures one has to assume the presence of minute flaws (as large as the smallest one which can be detected). The application of repeated loading will cause crack growth. The loading is usually caused by vibrations.

3 Thus an important question that arises is “how long would it be before this subcritical crack grows to reach a critical size that would trigger failure?” To predict the minimum fatigue life of metallic structures, and to establish safe inspection intervals, an understanding of the rate of fatigue crack propagation is required.

Historically, fatigue life prediction was based on $S - N$ curves, Fig. 9.1 (or Goodman’s Diagram) using a Strength of Material

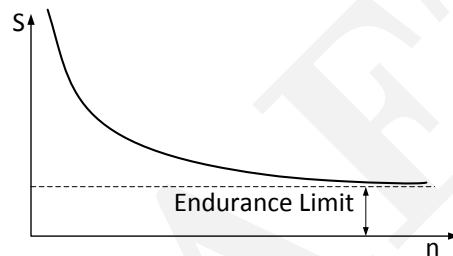


Figure 9.1: S-N Curve and Endurance Limit

Approach which did NOT assume the presence of a crack.

9.1 Experimental Observation

4 If we start with a plate that has no crack and subject it to a series of repeated loading, Fig. 9.2 between σ_{min} and σ_{max} , we

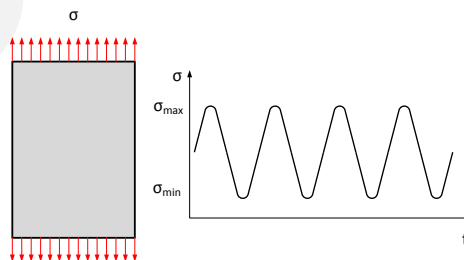


Figure 9.2: Repeated Load on a Plate

would observe three distinct stages, Fig. 9.3

1. Stage I : Micro coalescence of voids and formation of microcracks. This stage is difficult to capture and is most appropriately investigated by metallurgists or material scientists, and compared to stage II and III it is by far the longest.
2. Stage II : Now a micro crack of finite size was formed, its SIF well below K_{Ic} , ($K \ll K_{Ic}$), and crack growth occurs after each cycle of loading.

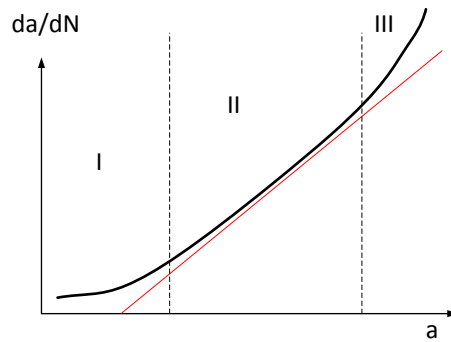


Figure 9.3: Stages of Fatigue Crack Growth

3. Stage III : Crack has reached a size a such that $a = a_c$, thus rapid unstable crack growth occurs.

5 Thus we shall primarily be concerned by stage II.

9.2 Fatigue Laws Under Constant Amplitude Loading

6 On the basis of the above it is evident that we shall be concerned with stage II only. Furthermore, fatigue crack growth can take place under:

1. Constant amplitude loading (good for testing)
2. Variable amplitude loading (in practice)

7 Empirical mathematical relationships which require the knowledge of the stress intensity factors (SIF), have been established to describe the crack growth rate. Models of increasing complexity have been proposed.

8 All of these relationships indicate that the number of cycles N required to extend a crack by a given length is proportional to the effective stress intensity factor range ΔK raised to a power n (typically varying between 2 and 9).

9.2.1 Paris Model

9 The first fracture mechanics-based model for fatigue crack growth was presented by Paris (Paris and Erdogan, 1963) in the early '60s. It is important to recognize that it is an empirical law based on experimental observations. Most other empirical fatigue laws can be considered as direct extensions, or refinements of this one, given by

$$\boxed{\frac{da}{dN} = C (\Delta K)^n} \quad (9.1)$$

which is a straight line on a log-log plot of $\frac{da}{dN}$ vs ΔK , and

$$\Delta K = K_{max} - K_{min} = (\sigma_{max} - \sigma_{min})f(g)\sqrt{\pi a} \quad (9.2)$$

a is the crack length; N the number of load cycles; C the intercept of line along $\frac{da}{dN}$ and is of the order of 10^{-6} and has units of m/cycle/(MPa \sqrt{m}) n ; and n is the slope of the line and ranges from 2 to 10. C and n are experimentally determined.

10 Equation 9.1 can be rewritten as :

$$\Delta N = \frac{\Delta a}{C [\Delta K(a)]^n} \quad (9.3)$$

or

$$N = \int dN = \int_{a_i}^{a_f} \frac{da}{C [\Delta K(a)]^n} \quad (9.4)$$

¹¹ Thus it is apparent that a small error in the SIF calculations would be magnified greatly as n ranges from 2 to 6. Because of the sensitivity of N upon ΔK , it is essential to properly determine the numerical values of the stress intensity factors.

¹² However, in most practical cases, the crack shape, boundary conditions, and load are in such a combination that an analytical solution for the SIF does not exist and large approximation errors have to be accepted. Unfortunately, analytical expressions for K are available for only few simple cases. Thus the stress analyst has to use handbook formulas for them (Tada et al., 1973). A remedy to this problem is the usage of numerical methods, of which the finite element method has achieved greatest success.

9.2.2 Foreman's Model

¹³ When compared with experimental data, it is evident that Paris law does not account for:

1. Increase in crack growth rate as K_{max} approaches K_{Ic}
2. Slow increase in crack growth at $K_{min} \approx K_{th}$

thus it was modified by Foreman (Foreman et al., 1967), Fig. 9.4

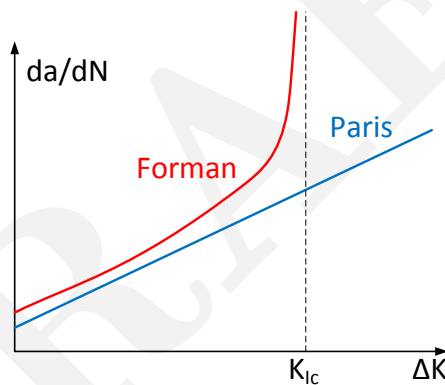


Figure 9.4: Forman's Fatigue Model

$$\frac{da}{dN} = \frac{C(\Delta K)^n}{(1-R)K_c - \Delta K} \quad (9.5)$$

9.2.3 Modified Walker's Model

¹⁴ Walker's (Walker, 1970) model is yet another variation of Paris Law which accounts for the stress ratio $R = \frac{K_{min}}{K_{max}} = \frac{\sigma_{min}}{\sigma_{max}}$

$$\frac{da}{dN} = C \left[\frac{\Delta K}{(1-R)^{(1-m)}} \right]^n \quad (9.6)$$

9.2.4 Table Look-Up

¹⁵ Whereas most methods attempt to obtain numerical coefficients for empirical models which best approximate experimental data, the table look-up method extracts directly from the experimental data base the appropriate coefficients. In a "round-robin" contest on fatigue life predictions, this model was found to be most satisfactory (Miller and Gallagher, 1981).

¹⁶ This method is based on the availability of the information in the following table:

$\frac{da}{dN}$	ΔK			
	R = -1	R = .1	R = .3	R = .4

17 For a given $\frac{da}{dN}$ and R , ΔK is directly read (or rather interpolated) for available data.

9.2.5 Effective Stress Intensity Factor Range

18 All the empirical fatigue laws are written in terms of ΔK_I ; however, in general a crack will be subjected to a mixed-mode loading resulting in both ΔK_I and ΔK_{II} . Thus to properly use a fatigue law, an effective stress intensity factor is sought.

19 One approach, consists in determining an effective stress intensity factor ΔK_{eff} in terms of ΔK_I and ΔK_{II} , and the angle of crack growth θ_0 . In principle each of the above discussed mixed-mode theories could yield a separate expression for the effective stress intensity factor.

20 For the case of maximum circumferential stress theory, an effective stress intensity factor is given by (Broek, 1986):

$$\Delta K_{Ieff} = \Delta K_I \cos^3 \frac{\theta_0}{2} - \frac{3}{2} \Delta K_{II} \cos \frac{\theta_0}{2} \sin \theta_0 \tag{9.7}$$

9.2.6 Examples

9.2.6.1 Example 1

An aircraft flight produces 10 gusts per flight (between take-off and landing). It has two flights per day. Each gust has a $\sigma_{max} = 200$ MPa and $\sigma_{min} = 50$ MPa. The aircraft is made up of aluminum which has $R = 15$ kJ/m² $E = 70$ GPa $C = 5 \times 10^{-11}$ m/cycle, and $n = 3$. The smallest detectable flaw is 4 mm. How long would it be before the crack will propagate to its critical length?

Assuming $K = \sigma\sqrt{\pi a}$ and $K_{Ic} = \sqrt{ER}$, then $a_c = \frac{K_{Ic}^2}{\sigma_{max}^2 \pi} = \frac{ER}{\sigma_{max}^2 \pi}$ or

$$a_c = \frac{(70 \times 10^9)(15 \times 10^3)}{(200 \times 10^6)^2 \pi} = 0.0084 \text{ m} = 8.4 \text{ mm} \tag{9.8}$$

$$\begin{aligned} \Rightarrow N &= \int_{a_i}^{a_f} \frac{da}{C[\Delta K(a)]^n} = \int_{a_i}^{a_f} \frac{da}{C \underbrace{(\sigma_{max} - \sigma_{min})^n}_{(\Delta\sigma)^n} ((\pi a)^{\frac{1}{2}})^n} \\ &= \int_{4 \times 10^{-3}}^{8.4 \times 10^{-3}} \frac{da}{\underbrace{(5 \times 10^{-11})^3}_C \underbrace{(200 - 50)^3}_{(\Delta\sigma)^3} \underbrace{(\pi a)^{1.5}}_{((\pi a)^{\cdot 5})^3}} = 1064 \int_{.004}^{.0084} a^{-1.5} da \\ &= -2128 a^{-.5} \Big|_{.004}^{.0084} = 2128 \left[-\frac{1}{\sqrt{.0084}} + \frac{1}{\sqrt{.004}} \right] \\ &= 10,428 \text{ cycles} \end{aligned} \tag{9.9}$$

thus the time t will be: $t = (10,428) \text{ cycles} \times \frac{1}{10} \frac{\text{flight}}{\text{cycle}} \times \frac{1}{2} \frac{\text{day}}{\text{flight}} \times \frac{1}{30} \frac{\text{month}}{\text{day}} \approx 17.38 \text{ month} \approx 1.5 \text{ years}$.

If a longer lifetime is desired, then we can:

1. Employ a different material with higher K_{Ic} , so as to increase the critical crack length a_c at instability.
2. Reduce the maximum value of the stress σ_{max} .
3. Reduce the stress range $\Delta\sigma$.
4. Improve the inspection so as to reduce the assumed initial crack length a_{min} .

9.2.6.2 Example 2

21 Repeat the previous problem except that more sophisticated (and expensive) NDT equipment is available with a resolution of .1 mm thus $a_i = .1\text{mm}$

$$t = 2128 \left[-\frac{1}{\sqrt{.0084}} + \frac{1}{\sqrt{.0001}} \right] = 184,583 \text{ cycles}$$

$$t = \frac{1738}{10,428} (189,583) = 316 \text{ months} \approx 26 \text{ years!}$$

9.2.6.3 Example 3

Rolfe and Barsoum p.261-263.

9.3 Variable Amplitude Loading

9.3.1 No Load Interaction

²² Most Engineering structures are subjected to variable amplitude repeated loading, however, most experimental data is based on constant amplitude load test. Thus, the following questions arise:

1. How do we put the two together?
2. Is there an interaction between high and low amplitude loading?

1. Root Mean Square Model (Barsoum)

$$\frac{da}{dN} = C(\Delta K_{rms})^n \quad (9.10)$$

$$\Delta K_{rms} = \sqrt{\frac{\sum_{i=1}^k \Delta K_i^2}{n}} \quad (9.11)$$

where ΔK_{rms} is the square root of the mean of the squares of the individual stress intensity factors cycles in a spectrum.

2. Accurate “block by block” numerical integration of the fatigue law

$$\Delta a = C(\Delta K)^n \Delta N \quad (9.12)$$

solve for a instead of N .

9.3.2 Load Interaction

9.3.2.1 Observation

²³ Under aircraft flight simulation involving random load spectrum:

- High wind related gust load, N_H
- Without high wind related gust load, N_L

$N_H > N_L$, thus “Aircraft that logged some bad weather flight time could be expected to possess a longer service life than a plane having a better flight weather history.”

²⁴ Is this correct? Why? Under which condition overload is damaging!

9.3.2.2 Retardation Models

²⁵ Baseline fatigue data are derived under constant amplitude loading conditions, but many structural components are subjected to variable amplitude loading. If interaction effects of high and low loads did not exist in the sequence, it would be relatively easy to establish a crack growth curve by means of a cycle-by-cycle integration. However crack growth under variable amplitude cycling is largely complicated by interaction effects of high and low loads.

²⁶ A high level load occurring in a sequence of low amplitude cycles significantly reduces the rate of crack growth during the cycles applied subsequent to the overload. This phenomena is called Retardation, Fig. 9.5.

²⁷ During loading, the material at the crack tip is plastically deformed and a tensile plastic zone is formed. Upon load release, the surrounding material is elastically unloaded and a part of the plastic zone experiences compressive stresses.

²⁸ The larger the load, the larger the zone of compressive stresses. If the load is repeated in a constant amplitude sense, there is no observable direct effect of the residual stresses on the crack growth behavior; in essence, the process of growth is steady state.

²⁹ Measurements have indicated, however, that the plastic deformations occurring at the crack tip remain as the crack propagates so that the crack surfaces open and close at non-zero (positive) levels.

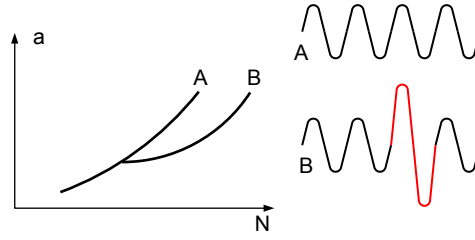


Figure 9.5: Retardation Effects on Fatigue Life

³⁰ When the load history contains a mix of constant amplitude loads and discretely applied higher level loads, the patterns of residual stress and plastic deformation are perturbed. As the crack propagates through this perturbed zone under the constant amplitude loading cycles, it grows slower (the crack is retarded) than it would have if the perturbation had not occurred. After the crack has propagated through the perturbed zone, the crack growth rate returns to its typical steady-state level, Fig. 9.6.

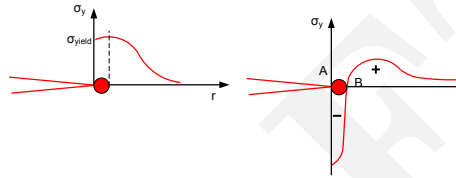


Figure 9.6: Cause of Retardation in Fatigue Crack Growth

9.3.2.2.1 Wheeler's Model

³¹ Wheeler (Wheeler, 1972) defined a crack-growth retardation factor C_p :

$$\frac{da}{dN}_{\text{retarded}} = C_p \left(\frac{da}{dN} \right)_{\text{linear}} \quad (9.13)$$

$$C_p = \left(\frac{r_{p_i}}{a_{oL} + r_{p_oL} - a_i} \right)^m \quad (9.14)$$

in which r_{p_i} is the current plastic zone size in the i^{th} cycle under consideration, a_i is the current crack size, r_{p_oL} is the plastic size generated by a previous higher load excursion, a_{oL} is the crack size at which the higher load excursion occurred, and m is an empirical constant, Fig. 9.7.

³² Thus there is retardation as long as the current plastic zone is contained within the previously generated one.

9.3.2.2.2 Generalized Willenborg's Model

³³ In the generalized Willenborg model (Willenborg et al., 1971), the stress intensity factor K_I is replaced by an effective one:

$$K_I^{\text{eff}} = K_I - K_R \quad (9.15)$$

in which K_R is equal to:

$$K_R = \phi K_R^w \quad (9.16)$$

$$\phi = \frac{1 - \frac{K_{\text{max},\text{th}}}{K_{\text{max},i}}}{s^{oL} - 1} \quad (9.17)$$

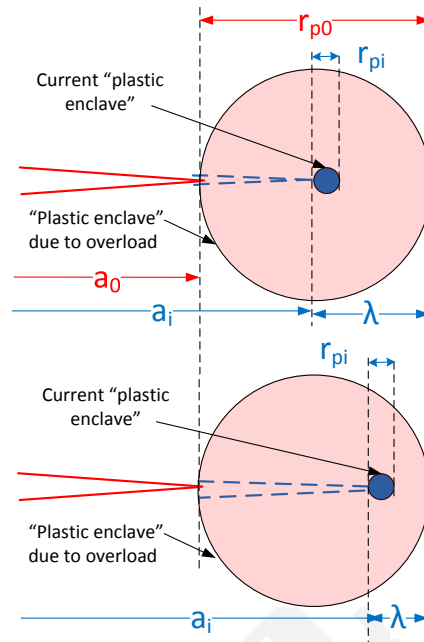


Figure 9.7: Yield Zone Due to Overload

$$K_R = K_R^w = K_{\max}^{oL} \sqrt{1 - \frac{a_i - a_{oL}}{r_{poL}}} - K_{\max,i} \quad (9.18)$$

and a_i is the current crack size, a_{oL} is the crack size at the occurrence of the overload, r_{poL} is the yield zone produced by the overload, K_{\max}^{oL} is the maximum stress intensity of the overload, and $K_{\max,i}$ is the maximum stress intensity for the current cycle.

³⁴ This equation shows that retardation will occur until the crack has generated a plastic zone size that reaches the boundary of the overload yield zone. At that time, $a_i - a_{oL} = r_{poL}$ and the reduction becomes zero.

³⁵ Equation 9.15 indicates that the complete stress-intensity factor cycle, and therefore its maximum and minimum levels ($K_{\max,i}$ and $K_{\min,i}$), are reduced by the same amount (K_R). Thus, the retardation effect is sensed by the change in the effective stress ratio calculated from:

$$R_{\text{eff}} = \frac{K_{\min,i}^{\text{eff}}}{K_{\max,i}^{\text{eff}}} = \frac{K_{\min,i} - K_R}{K_{\max,i} - K_R} \quad (9.19)$$

because the range in stress intensity factor is unchanged by the uniform reduction.

³⁶ Thus, for the i^{th} load cycle, the crack growth increment Δa_i is:

$$\Delta a_i = \frac{da}{dN} = f(\Delta K, R_{\text{eff}}) \quad (9.20)$$

³⁷ In this model there are two empirical constants: $K_{\max,th}$, which is the threshold stress intensity factor level associated with zero fatigue crack growth rate, and S^{oL} , which is the overload (shut-off) ratio required to cause crack arrest for the given material.

Chapter 10

CRACK TIP OPENING DISPLACEMENTS

¹ Within the assumptions and limitations of LEFM we have two valid (and equivalent) criteria for crack propagation: 1) K vs K_{Ic} which is a local criteria based on the strength of the stress singularity at the tip of the crack; and 2) G vs G_{Ic} (or R) which is a global criteria based on the amount of energy released (or consumed) during a unit surface crack's propagations.

² In many cases it is found that LEFM based criteria is either: too conservative and expensive as it does not account for plastification at the crack tip, and/or invalid based on calculations of r_p^* where LEFM assumptions are checked.

³ Thus, in those cases where LEFM is not applicable, an alternative criteria for crack growth in Elasto Plastic Fracture Mechanics (EPFM) is sought.

⁴ But first let us note the various stages of ductile fracture:

1. Blunting of an initially sharp crack. Under LEFM assumptions, the crack tip opening displacement (CTOD) is zero, however in elasto-plastic material due to blunting it is different from zero, Fig. 10.1.

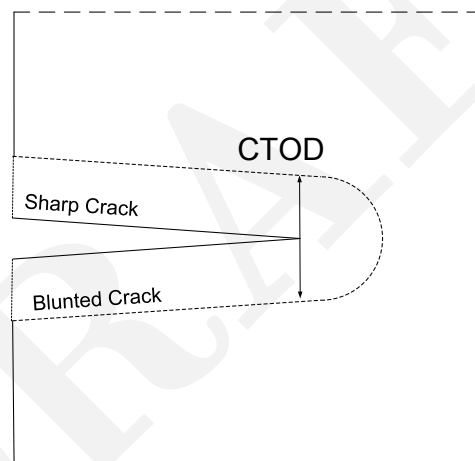


Figure 10.1: Crack Tip Opening Displacement, (Anderson, 1995)

2. Crack initiation
3. Slow (stable) crack growth
4. Unstable crack growth

⁵ Again two approaches are currently in use, Table 10.1

1. a local criterion based on the crack tip opening displacement (CTOD).
2. a global criterion based on the quasi-strain energy release rate (J integral), J_{Ic} .

⁶ Historically the CTOD was first proposed as a valid criteria for crack propagation on the basis of Cotterell and Wells work in the early 60's at the British Welding Institute. This has formed the basis of current "R-6" specifications for ductile failure in the U.K.

⁷ Under LEFM the crack tip opening displacement is clearly zero. However, when the material is allowed to yield, then the crack tip will blunt resulting in a non-zero crack tip opening displacement (CTOD).

	Local Vector	Global Scalar
LEFM	K	<i>G</i>
EPFM	CTOD	<i>J</i>

Table 10.1: Comparison of Various Models in LEFM and EPFM

8 References (Cottrell, 1963) and (Wells, 1963) have introduced the concept of the crack tip opening displacement to characterize elasto-plastic fracture. This criterion is still the one primarily used in the United Kingdom, whereas the J integral is more commonly used in the United States.

9 There are two approaches to determine the CTOD:

1. First-order approximation based on a fictitious crack.
2. Second-order approximation based on Dugdale's model.

10.1 Derivation of CTOD

10.1.1 Irwin's Solution

10 The vertical displacement of a point next to the crack tip due to mode I loading is given by Eq. 3.53-f, Fig. 10.2

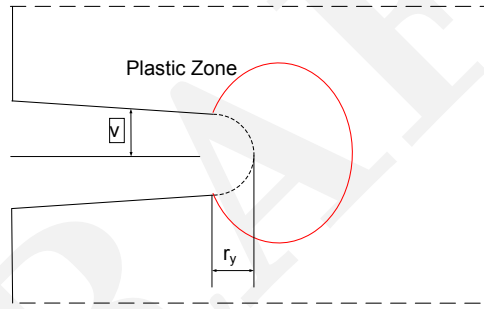


Figure 10.2: Estimate of the Crack Tip Opening Displacement, (Anderson, 1995)

$$v = \frac{K_I}{2\mu} \left[\frac{r}{2\pi} \right]^{\frac{1}{2}} \sin \frac{\theta}{2} \left[\kappa + 1 - 2 \cos^2 \frac{\theta}{2} \right] \quad (10.1)$$

11 If we substitute $\theta = \pm\pi$ we obtain the upper and lower displacements of the crack face, and due to symmetry their sum corresponds to the crack opening displacement. Hence the crack opening is given by

$$\text{COD} = 2v = \frac{\kappa + 1}{\mu} K_I \sqrt{\frac{r}{2\pi}} \quad (10.2)$$

12 If we substitute the crack tip opening displacement a distance r_p^* away from the crack tip using Irwin's plastic zone correction from Eq. 8.9

$$r_p^* = \frac{1}{2\pi} \frac{K_I^2}{\sigma_{\text{yld}}^2} \quad (10.3)$$

into Eq. 10.2 and using $\kappa = \frac{3-\nu}{1+\nu}$ for plane stress, and recall that $\mu = E/2(1 + \nu)$, we obtain

$$\boxed{\text{CTOD} = \frac{4}{\pi} \frac{K_I^2}{E\sigma_{\text{yld}}}} \quad (10.4)$$

10.1.2 Dugdale's Solution

¹³ Using Dugdale's solution, Kanninen (Kanninen, 1984) has shown that the crack opening along the crack is given by¹:

$$v(x) = \frac{2}{\pi} \frac{a\sigma_{\text{yld}}}{E} \left\{ \log \left| \frac{\sqrt{c^2 - a^2} + \sqrt{c^2 - x^2}}{\sqrt{c^2 - a^2} - \sqrt{c^2 - x^2}} \right| + \frac{x}{a} \log \left| \frac{x\sqrt{c^2 - a^2} + a\sqrt{c^2 - x^2}}{x\sqrt{c^2 - a^2} - a\sqrt{c^2 - x^2}} \right| \right\} \quad (10.5)$$

for $0 \leq x \leq c$. For $x = a$ this reduces to

$$v(a) = \frac{4}{\pi} \frac{a\sigma_{\text{yld}}}{E} \log \frac{c}{a} \quad (10.6)$$

¹⁴ Combining this equation with Dugdale's solution for c from Eq. 8.21,

$$\frac{a}{c} = \cos \frac{\pi}{2} \frac{\sigma}{\sigma_{\text{yld}}} \quad (10.7)$$

we would then obtain

$$CTOD = 2v = \frac{8}{\pi} \frac{a\sigma_{\text{yld}}}{E} \log \left[\sec \frac{\pi}{2} \frac{\sigma}{\sigma_{\text{yld}}} \right] \quad (10.8)$$

¹⁵ using the series expansion of log sec:

$$CTOD = \frac{8}{\pi} \frac{a\sigma_{\text{yld}}}{E} \left[\frac{1}{2} \left(\frac{\pi}{2} \frac{\sigma}{\sigma_{\text{yld}}} \right)^2 + \frac{1}{12} \left(\frac{\pi}{2} \frac{\sigma}{\sigma_{\text{yld}}} \right)^4 + \dots \right] \quad (10.9)$$

or

$$CTOD = \frac{K^2}{E\sigma_{\text{yld}}} \left[1 + \frac{\pi^2}{24} \frac{\sigma^2}{\sigma_{\text{yld}}^2} + \dots \right] \quad (10.10)$$

note that for small $\frac{\sigma}{\sigma_{\text{yld}}}$, the $CTOD$ can be approximated by $CTOD = \frac{K^2}{E\sigma_{\text{yld}}}$.

10.2 G-CTOD Relations

¹⁶ Recalling also that the energy release rate G is given by $G = \frac{K^2}{E'}$, we obtain the following approximate equation

$$CTOD = \frac{G}{\sigma_{\text{yld}}} \quad (10.11)$$

and its counterpart

$$CTOD_{cr} = \frac{R}{\sigma_{\text{yld}}} \quad (10.12)$$

¹Derivation of this equation can be found on p. 203 of (Anderson, 1995)

Chapter 11

J INTEGRAL

11.1 Genesis

¹ Eshelby (Eshelby, 1974) has defined a number of contour integrals that are path independent by virtue of the theorem of energy conservation. The two-dimensional form of one of these integrals can be written as:

$$J = \oint_{\Gamma} \left(w dy - \mathbf{t} \frac{\partial \mathbf{u}}{\partial x} d\Gamma \right) = 0 \quad (11.1)$$

with

$$w = \int_0^{\varepsilon} \sigma_{ij} d\varepsilon_{ij} \quad (11.2)$$

where w is the strain energy density; Γ is a closed contour followed counter-clockwise, as shown in Fig. 11.1; \mathbf{t} is the traction vector on a plane defined by the outward drawn normal \mathbf{n} and $\mathbf{t} = \boldsymbol{\sigma} \mathbf{n}$; \mathbf{u} the displacement vector, and $d\Gamma$ is the element of the arc along the path Γ .

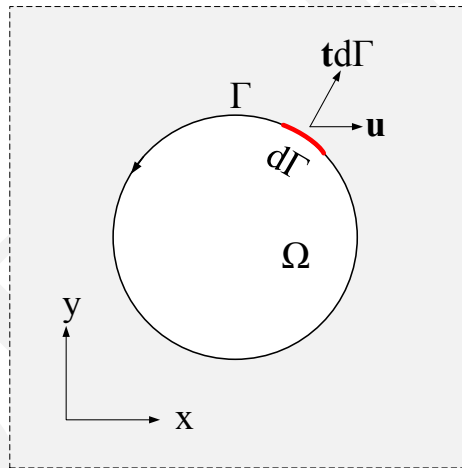


Figure 11.1: J Integral Definition Around a Crack

² Whereas Eshelby had defined a number of similar path independent contour integrals, he had not assigned them with a particular physical meaning.

11.2 Proof of Path Independence

³ Before we establish the connection between Eshelby's expression for J , and the energy release rate J , we need to show that the former is indeed equal to zero for a closed path.

$$J = \oint_{\Gamma} \left(w dy - t_i \frac{\partial u_i}{\partial x} d\Gamma \right) \quad (11.3)$$

and assuming Γ to be defined counterclockwise, then $dx = -n_y d\Gamma$, and $dy = n_x d\Gamma$ and $t_i = n_j \sigma_{ij}$ where n_x , n_y and n_j are direction cosines. Substituting

$$J = \oint_{\Gamma} \left(w n_x - n_j \sigma_{ij} \frac{\partial u_i}{\partial x} \right) d\Gamma \quad (11.4)$$

4 Invoking Green's theorem

$$\oint_{\Gamma} v_i n_i d\Gamma = \int_{\Omega} v_{i,i} d\Omega \quad (11.5)$$

we obtain

$$J = \int_{\Omega} \left[\frac{\partial w}{\partial x} - \frac{\partial}{\partial x_j} \left(\sigma_{ij} \frac{\partial u_i}{\partial x} \right) \right] dx dy \quad (11.6)$$

5 Applying the chain rule, the first term in the square bracket becomes

$$\frac{\partial w}{\partial x} = \frac{\partial w}{\partial \varepsilon_{ij}} \frac{\partial \varepsilon_{ij}}{\partial x} = \sigma_{ij} \frac{\partial \varepsilon_{ij}}{\partial x} \quad (11.7)$$

where the strain is given by Eq. ??

$$\varepsilon_{ij} = \frac{1}{2} (u_{i,j} + u_{j,i}) \quad (11.8)$$

6 Substituting for the first term

$$\frac{\partial w}{\partial x} = \frac{1}{2} \sigma_{ij} \left[\frac{\partial}{\partial x} \left(\frac{\partial u_i}{\partial x_j} \right) + \frac{\partial}{\partial x} \left(\frac{\partial u_j}{\partial x_i} \right) \right] \quad (11.9-a)$$

$$= \sigma_{ij} \frac{\partial}{\partial x_j} \left(\frac{\partial u_i}{\partial x} \right) \quad (11.9-b)$$

7 On the other hand, we have for the second term

$$\frac{\partial}{\partial x_j} \left(\sigma_{ij} \frac{\partial u_i}{\partial x} \right) = \sigma_{ij} \frac{\partial}{\partial x_j} \left(\frac{\partial u_i}{\partial x} \right) + \underbrace{\frac{\partial \sigma_{ij}}{\partial x_j}}_0 \frac{\partial u_i}{\partial x} \quad (11.10-a)$$

8 Hence,

$$\frac{\partial w}{\partial x} = \sigma_{ij} \frac{\partial}{\partial x_j} \left(\frac{\partial u_i}{\partial x} \right) \quad (11.11)$$

which is identical to the second term of Eq. 11.6.

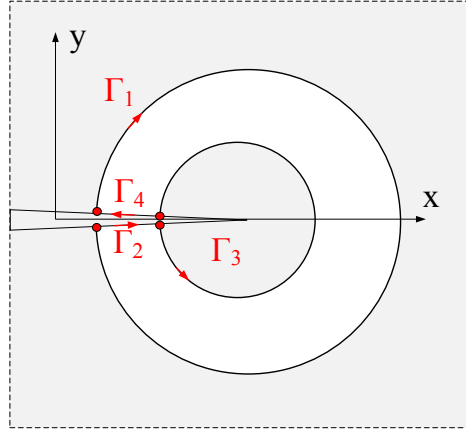
9 Thus the integrand of Eq. 11.3 vanishes and $J = 0$ for any closed contour.

10 Having shown that indeed $J = 0$, we will now exploit this to prove that around a crack, J is non-zero and is independent of the path.

11 With reference to Fig. 11.2 if we consider the closed path $\Gamma = \Gamma_1 + \Gamma_2 + \Gamma_3 + \Gamma_4$ in which Γ_1 and Γ_3 are arbitrarily chosen contours. Obviously $J = 0$ over Γ in order to satisfy compatibility conditions, provided that the stresses and displacement gradients are continuous. Along paths Γ_2 and Γ_4 , the traction vector $t_i = 0$ and also $dy = 0$. Consequently, the contributions to J from Γ_2 and Γ_4 vanish. Taking into account the difference sense of integration along paths Γ_1 and Γ_3 we arrive at the conclusion that the values of J integrated over paths Γ_1 and Γ_3 are identical. Because these two paths were arbitrarily chosen, the path independence of J is assured.

11.3 Nonlinear Elastic Energy Release Rate

12 Let us now establish the connection between the two previous interpretations of J , the one mathematically defined by Eshelby, and the one associated with the energy release rate (yet to be proven). We shall prove that when J is applied along a contour around a crack tip, it represents the change in potential energy for a virtual crack extension da . Two slightly different derivations are presented.


 Figure 11.2: Closed Contour for Proof of J Path Independence

11.3.1 Virtual Line Crack Extension

¹³ Considering a two-dimensional crack surrounded by a line Γ which encompasses an area Ω . Under quasi-static conditions, and in the absence of body forces, the potential energy is given by

$$\Pi = \underbrace{\int_{\Omega} w d\Omega}_U - \underbrace{\oint_{\Gamma} t_i u_i d\Gamma}_W \quad (11.12)$$

¹⁴ For a virtual crack extension, the change in potential energy is

$$\frac{d\Pi}{da} = \int_{\Omega} \frac{dw}{da} d\Omega - \oint_{\Gamma} \left[t_i \frac{du_i}{da} + u_i \frac{dt_i}{da} \right] d\Gamma \quad (11.13-a)$$

$$= \int_{\Omega} \frac{dw}{da} d\Omega - \underbrace{\oint_{\Gamma_u}}_0 \left[t_i \frac{du_i}{da} + u_i \frac{dt_i}{da} \right] d\Gamma - \oint_{\Gamma_t} \left[t_i \frac{du_i}{da} + \underbrace{u_i \frac{dt_i}{da}}_0 \right] d\Gamma \quad (11.13-b)$$

¹⁵ We have decomposed the contour path into two parts, the first one with prescribed displacement (Γ_u) and a second one with prescribed traction (Γ_t). Since Γ_u is zero along the path, we maintain a closed contour integral along Γ_t .

¹⁶ Furthermore, the second term inside the square bracket will be zero along Γ_t because the traction is constant during crack growth.

¹⁷ For a crack extension, the coordinate axis also moves, Fig. 11.3. Thus we can write

$$\frac{d}{da} = \frac{\partial}{\partial a} + \frac{\partial}{\partial x} \frac{\partial x}{\partial a} = \frac{\partial}{\partial a} - \frac{\partial}{\partial x} \quad (11.14)$$

for a crack extension along a ($\frac{\partial x}{\partial a} = -1$) with respect to the new coordinate system.

¹⁸ Substituting into Eq. 11.13-b

$$\frac{d\Pi}{da} = \int_{\Omega} \left[\frac{\partial w}{\partial a} - \frac{\partial w}{\partial x} \right] d\Omega - \oint_{\Gamma_t} t_i \left(\frac{\partial u_i}{\partial a} - \frac{\partial u_i}{\partial x} \right) d\Gamma \quad (11.15)$$

¹⁹ We can also rewrite:

$$\underbrace{\frac{\partial w}{\partial a} = \frac{\partial w}{\partial \varepsilon_{ij}} \frac{\partial \varepsilon_{ij}}{\partial a}}_{\text{Eq. 11.7}} = \underbrace{\sigma_{ij} \frac{\partial}{\partial x_j} \left(\frac{\partial u_i}{\partial a} \right)}_{\text{Eq. 11.9-b}} \quad (11.16)$$

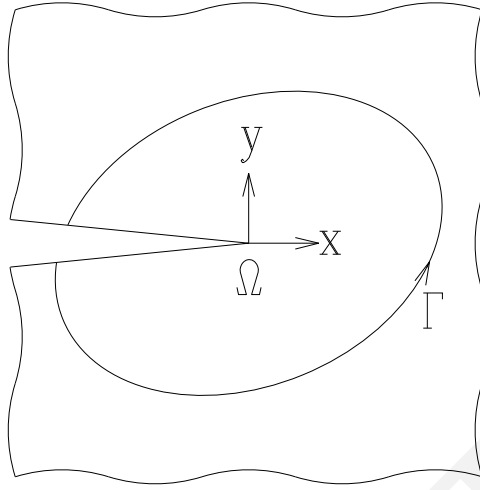


Figure 11.3: Virtual Crack Extension Definition of J

²⁰ But from the divergence theorem

$$\oint_{\Gamma_t} t_i \frac{\partial u_i}{\partial a} d\Gamma = \int_{\Omega} \sigma_{ij} \frac{\partial}{\partial x_j} \left(\frac{\partial u_i}{\partial a} \right) d\Omega \quad (11.17-a)$$

$$= \int_{\Omega} \frac{\partial w}{\partial a} d\Omega \quad (11.17-b)$$

Hence, from this Equation and Eq. 11.16, the first terms in each of the two integrals in Eq. 11.15 cancel out, and we are left with

$$\frac{d\Pi}{da} = \oint_{\Gamma_t} t_i \frac{\partial u_i}{\partial x} d\Gamma - \int_{\Omega} \frac{\partial w}{\partial x} d\Omega \quad (11.18)$$

²¹ We now apply the divergence theorem, multiply both sides by -1 and recalling that $n_x d\Gamma = dy$

$$\boxed{\begin{aligned} -\frac{d\Pi}{da} &= \oint_{\Gamma_t} \left(wn_x - t_i \frac{\partial u_i}{\partial x} \right) d\Gamma \\ &= \oint_{\Gamma_t} \left(wdy - t_i \frac{\partial u_i}{\partial x} d\Gamma \right) \end{aligned}} \quad (11.19)$$

which is the same as Eq. 11.1. Henceforth, the J integral is equal to the energy release rate for linear and nonlinear elastic material under quasi-static conditions.

11.3.2 †Virtual Volume Expansion

²² Following the brief preamble, let us thoroughly derive the expression for the J integral. We will derive an expression for the energy released during a unit surface crack extension based on the following assumptions:

1. Homogeneous body
2. Linear or non-linear elastic solid
3. No inertia, or body forces; no initial stresses
4. No thermal loading
5. 2-D stress and deformation field
6. Plane stress or plane strain
7. Mode I loading
8. Stress free crack

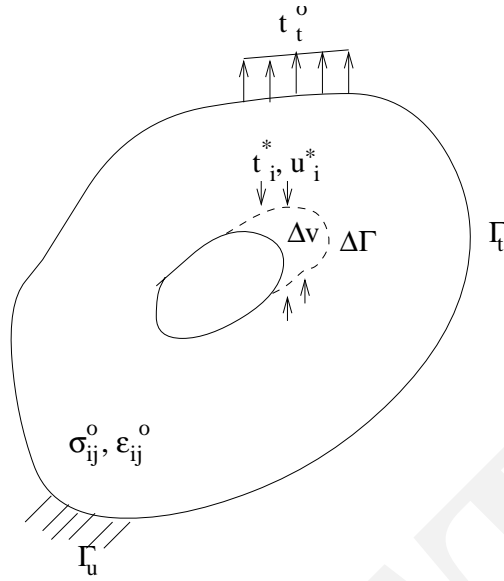


Figure 11.4: Arbitrary Solid with Internal Inclusion

23 Considering an arbitrary solid with both traction and displacement boundary conditions and an internal inclusion, Fig. 11.4

$$\Gamma = \Gamma_t + \Gamma_u \quad (11.20)$$

1. We define the initial boundary conditions as such

Surface initial boundary conditions:

- a) Displacements u_i^0 on Γ_u
- b) Tractions t_i^0 on Γ_t ;

Internal stress and strain: σ_{ij}^0 and ε_{ij}^0

2. Due to t_i and u_i , the hole will grow and will have a new boundary, $\Delta\Gamma$ and volume $\Delta\Omega$.

3. However to prevent growth we will apply $t_i^* = \sigma_{ij}^0 n_j$ on $\Delta\Gamma$ in order to maintain initial ε_{ij}^0 and σ_{ij}^0 (Recall Irwin's derivation of G).

4. Holding the loading on Γ_u and Γ_t constant, we reduce t_i^* on $\Delta\Gamma$ to zero. Thus we go from

$$\begin{cases} t_i^* \neq 0 \\ u_i^* = 0 \end{cases} \quad \text{to} \quad \begin{cases} t_i^* = 0 \\ u_i^* \neq 0 \end{cases} \quad (11.21)$$

This will result in a new internal state

$$\begin{cases} \sigma_{ij}^0 + \Delta\sigma_{ij} \\ \varepsilon_{ij}^0 + \Delta\varepsilon_{ij} \end{cases} \quad (11.22)$$

5. The total reduction in potential energy during this process was

$$-\Delta\Pi = \underbrace{\int_{\Delta\Omega} w(\varepsilon^0) d\Omega}_U - \underbrace{\int_{\Delta\Gamma} t_i^* du_i^* d\Gamma}_W \quad (11.23)$$

$$= \int_{\Delta\Omega} w(\varepsilon^0) d\Omega - \int_{\substack{t_i^*=0; u_i^*=u_i+\Delta u_i \\ t_i^*=t_i^0; u_i^*=u_i^0}} t_i^* du_i^* d\Gamma \quad (11.24)$$

$$= \frac{1}{2} \int_{\Delta\Omega} \sigma_{ij}^0 \varepsilon_{ij}^0 d\Omega - \frac{1}{2} \int_{\Delta\Gamma} t_i^0 du_i^* d\Gamma \quad (11.25)$$

for the case of linear elasticity

6. For a sharp crack and linear elastic systems during crack extension $\Delta\Omega = 0$ and during crack extension and $t_i^* = t_i^0$, thus

$$-\Delta\Pi = \int_{\Delta\Omega} \underbrace{\sigma_{ij}^0 \varepsilon_{ij}^0}_{0} d\Omega - \frac{1}{2} \int_{\Delta\Gamma} \underbrace{t_i^0 \Delta u_i}_{\text{Energy Release Rate } G} d\Gamma \quad (11.26)$$

7. For linear elastic systems, we can write

$$-\frac{d\Pi}{dA} = -\frac{d}{dA} \left(\int_{d\Omega} w d\Omega - \int_{d\Gamma} \mathbf{t}^* d\mathbf{u}^* d\Gamma \right) \quad (11.27)$$

For unit thickness $d\Omega = dx dy$ and $dA = dx$

$$\frac{d\Pi}{dA} = \int_{d\Gamma} w dy - \int_{d\Gamma} \mathbf{t} \frac{\partial \mathbf{u}}{\partial x} d\Gamma \quad (11.28)$$

8. Let us now define

$$J = \oint_{\Gamma} \left(w dy - \mathbf{t} \frac{\partial \mathbf{u}}{\partial x} d\Gamma \right) \quad (11.29)$$

It is identical to the previous expression but we do not restrict ourselves to go around $\Delta\Omega$, but around any closed path. This is indeed Eshelby's integral.

9. We can decompose $\Gamma = \Gamma_1 + \Gamma_2$ where Γ_1 is any external contour away from the crack tip and Γ_2 to be identified with $d\Gamma$ (increase in volume).

$$J = -\frac{\partial \Pi}{\partial a} = \oint_r \left(w dy - \mathbf{T} \frac{\partial \mathbf{u}}{\partial x} d\Gamma \right) \quad (11.30)$$

$$J = -\frac{\partial \Pi}{\partial a} \quad (11.31)$$

where Π is the potential energy. So for a linear elastic material $-\frac{\partial \Pi}{\partial a} = G$, which implies

$$J = G \quad (11.32)$$

²⁴ Allowing Γ_1 in Fig. 11.2 to shrink to an arbitrarily small contour Γ_c surrounding the crack tip, then the second term of Eq. 11.1 vanishes and

$$J = \int_{\Gamma_c} w dy \quad (11.33)$$

so that J is an averaged measure of the strain on the crack tip.

²⁵ An arbitrarily small curve Γ may then be chosen surrounding the tip, so the integral may be made to depend only on the crack tip singularity in the deformation field. The utility of the method rests in the fact that alternate choices of integration paths often permit a direct evaluation of J .

²⁶ In linear elastic analysis, and under pure mode I, Rice's J can be used for the computation of stress intensity factor K_I , as Eq. 11.1 yields

$$K_I = \sqrt{E J_1} \quad (\text{plane stress}) \quad (11.34)$$

$$= \sqrt{E J_1 / (1 - \nu^2)} \quad (\text{plane strain}) \quad (11.35)$$

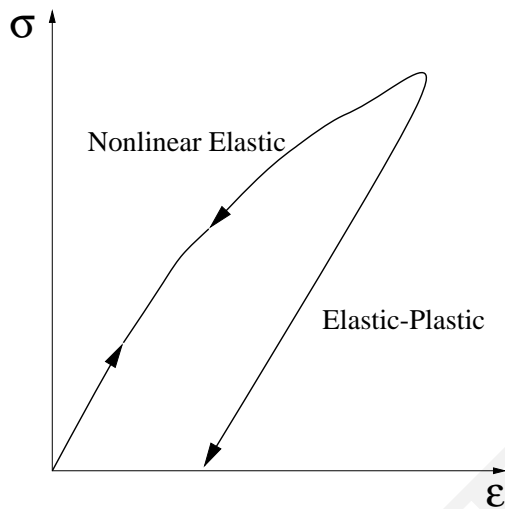


Figure 11.5: Elastic-Plastic versus Nonlinear Elastic Materials

11.4 Nonlinear Energy Release Rate

²⁷ Whereas LEFM is restricted to linear elastic materials, most metals have a nonlinear stress-strain curve. Fig. 11.5 illustrates the uniaxial stress-strain behavior of elastic-plastic and nonlinear elastic materials. Whereas the loading behavior of both materials is identical, they differ when they are unloaded. Thus, as long as there is no unloading, we can assume a nonlinear elastic behavior, and the deformation theory of plasticity, which relates the total strains to stresses, is applicable.

²⁸ For nonlinear elastic solids, we have already shown that J is the energy release rate in nonlinear elastic materials:

$$J = -\frac{d\Pi}{da} \quad (11.36)$$

for a unit thickness crack extension.

²⁹ Following a similar approach to the one of sect. 6.1.2, we consider the load displacement curves curve of a notched specimen made of nonlinear elastic material for two different conditions, Fig. 11.6 during crack extension from a to $a + da$:

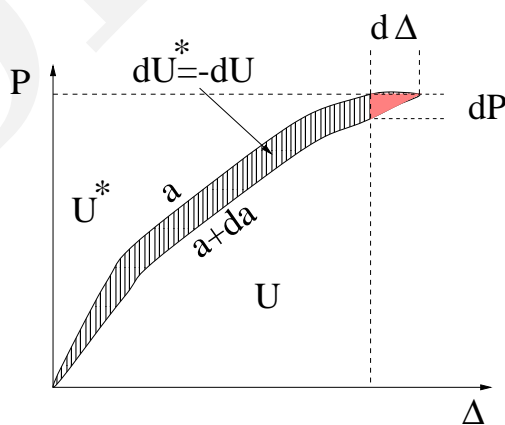


Figure 11.6: Nonlinear Energy Release Rate, (Anderson, 1995)

Load control we have $d\Delta = 0$ and

$$\Pi = U - W = U - P\Delta = -U^* \quad (11.37)$$

where

$$U^* \stackrel{\text{def}}{=} \int_0^P \Delta dP \tag{11.38}$$

is the complimentary strain energy. Thus for constant load

$$J_P = \left(\frac{dU^*}{da} \right)_P \tag{11.39}$$

Constant Displacement, $dP = 0$, and

$$J_\Delta = - \left(\frac{dU}{da} \right)_\Delta \tag{11.40}$$

From Fig. 11.6, the difference between J_P and J_Δ is $\frac{1}{2}dPd\Delta$ which is vanishingly small compared to dU .

³⁰ Therefore J for load control is equal to J for displacement control and for linear elastic materials $J = G = \frac{K^2}{E'}$.

11.5 J Testing

³¹ For linear elastic materials, the evaluation of J is straightforward since it is equal to G , which in turn is directly related to the stress intensity factor K . Hence, J could be obtained from a single test.

³² For nonlinear material, the principle of superposition does not apply, and hence we can not have a simple relation between J , the load, and the crack length. Whereas we could exploit the contour line integral definition of J to determine it from a single test by attaching an array of strain gages, this is usually impractical. Hence, we resort to the energy definition of J .

³³ This is accomplished by testing a number of identical specimens, but with slightly different crack lengths, Fig. 11.7. The area

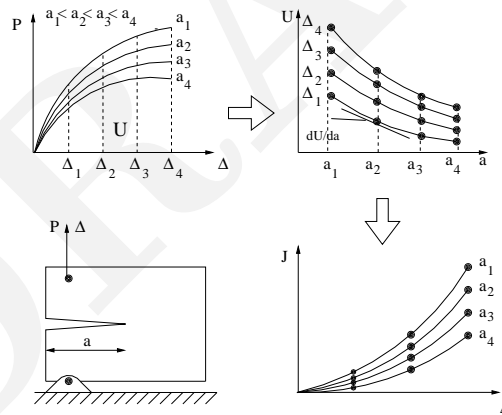


Figure 11.7: Experimental Derivation of J

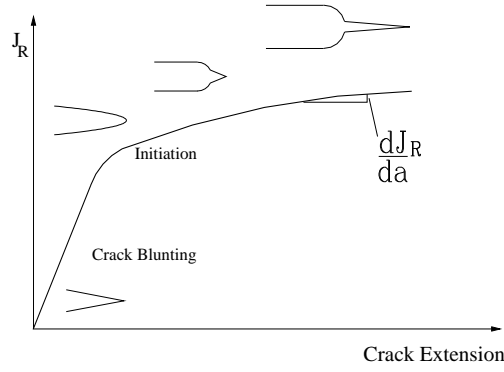
under each $P - \Delta$ curve is U , the energy absorbed by the specimen. We then plot U in terms of a , at various fixed displacements. Since $J = -\frac{1}{B} \frac{\partial U}{\partial A} \Big|_\Delta$, thus, J could be determined from the slope of the tangent to the curves.

11.6 Crack Growth Resistance Curves

³⁴ Just as the energy based criteria for crack propagation in LEFM was simply stated as $G > R$, a similar one applies to the J integral. However, many materials with high toughness do not necessarily fail catastrophically at a particular value of J . Instead, these materials display a rising R curve. Hence, in those cases, an LEFM would grossly overestimate the material resistance to crack growth.

³⁵ Rising R curve is associated with with growth and coalescence of microvoids.

³⁶ The rising R curve is illustrated in Fig. 11.8 where following blunting, crack initiation and propagation occurs. An arbitrary

Figure 11.8: J Resistance Curve for Ductile Material, (Anderson, 1995)

definition of a critical J , J_{Ic} can be specified at the onset of initiation.

37 We define, a tearing modulus as

$$T_R = \frac{E}{\sigma_{yld}^2} \frac{dJ_R}{da} \quad (11.41)$$

and the applied tearing modulus as

$$T_{app} = \frac{E}{\sigma_{yld}^2} \frac{dJ}{da} \quad (11.42)$$

38 Hence, crack growth would occur if

$\begin{aligned} J &= J_R \\ T_{app} &\leq T_R && \text{Stable crack growth} \\ T_{app} &> T_R && \text{Unstable crack growth} \end{aligned}$	(11.43)
---	---------

11.7 † Load Control versus Displacement Control

39 Crack propagation can occur under either load or displacement control. Whereas in both cases J (and G) is the same, the rate of change of J depends on the loading condition.

40 Unstable crack propagation will occur if the rate of change of J exceeds the rate of change of R .

41 The crack stability can be discussed within the context of the test stiffness (or its inverse the complinace). The total displacement is given by

$$\Delta_T = \Delta + C_m P \quad (11.44)$$

where C_m is the compliance of the system.

42 Differentiating this equation yields

$$d\Delta_t = \left(\frac{\partial \Delta}{\partial a} \right)_P da + \left(\frac{\partial \Delta}{\partial P} \right)_a dP + C_m dP = 0 \quad (11.45)$$

43 Similarly, we can take a similar derivative of $J(a, P)$

$$dJ = \left(\frac{\partial J}{\partial a} \right)_P da + \left(\frac{\partial J}{\partial P} \right)_a dP \quad (11.46)$$

dividing both sides by da , and keeping Δ_T constant

$$\left(\frac{dJ}{da} \right)_{\Delta_T} = \left(\frac{\partial J}{\partial a} \right)_P + \left(\frac{\partial J}{\partial P} \right)_a \left(\frac{dP}{da} \right)_{\Delta_T} \quad (11.47)$$

44 Substituting $\left(\frac{\partial P}{\partial a}\right)$ from Eq. 11.45 yields

$$\left(\frac{dJ}{da}\right)_{\Delta_T} = \left(\frac{\partial J}{\partial a}\right)_P - \left(\frac{\partial J}{\partial P}\right)_a \left(\frac{dP}{da}\right)_P \left[C_m + \left(\frac{\partial \Delta}{\partial P}\right)_a\right]^{-1} \quad (11.48)$$

45 For load control, $C_m = \infty$, and thus the second term vanishes, and $\frac{dJ}{da}$ is always positive and may thus lead to instability.

46 Alternatively, for displacement control, $C_m = 0$ corresponds to an infinitely stiff system, and $\frac{dJ}{da}$ is smaller than in the previous case, Fig. 11.9.

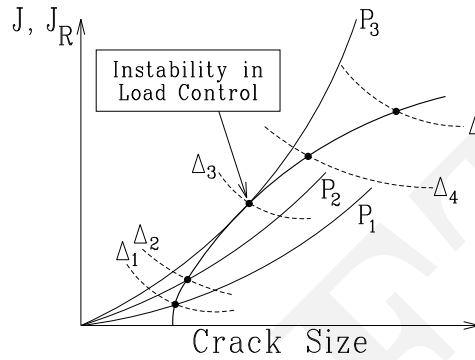


Figure 11.9: J, J_R versus Crack Length, (Anderson, 1995)

11.8 Plastic Crack Tip Fields

47 Whereas under LEFM assumptions, we had a $\frac{1}{\sqrt{r}}$ stress and strain singularity, we now seek to determine the corresponding ones, x and y respectively, for EPFM.

48 Starting with

$$J = \oint_{\Gamma} \left(w dy - \mathbf{t} \frac{\partial \mathbf{u}}{\partial x} d\Gamma \right) \quad (11.49)$$

49 Taking the contour around a circle of radius r , Fig. 11.10 we substitute $d\Gamma = r d\theta$; $y = r \sin \theta$; and $dy = r \cos \theta d\theta$

$$J = \oint_{-\pi}^{\pi} \left(w \cos \theta - \mathbf{t} \frac{\partial \mathbf{u}}{\partial x} \right) r d\theta \quad (11.50)$$

but J should be independent of r by virtue of path independence hence both $w \cos \theta$ and $\mathbf{t} \frac{\partial \mathbf{u}}{\partial x}$ should be proportional to $\frac{1}{r}$.

50 If we now consider a material with the following (uniaxial) power law hardening model (Ramberg-Osgood) which is often used to curve-fit stress-strain data:

$$\frac{\varepsilon}{\varepsilon_{yld}} = \frac{\sigma}{\sigma_{yld}} + \alpha \left(\frac{\sigma}{\sigma_{yld}} \right)^n \quad (11.51)$$

n is the strain hardening exponent, and for $n = 1$ we have a linear elastic response, and for $n = \infty$ we would have an elastic perfectly plastic one, Fig. 11.11. α is a dimensionless constant.

51 In the vicinity of the crack tip, the plastic strain is dominant (the elastic one is negligible) and

$$\frac{\varepsilon}{\varepsilon_{yld}} = \alpha \left(\frac{\sigma}{\sigma_{yld}} \right)^n \quad (11.52)$$

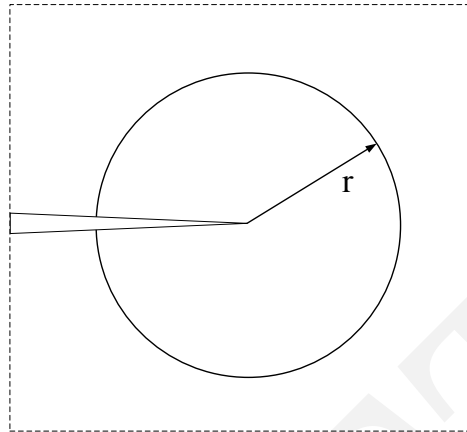


Figure 11.10: J , Around a Circular Path

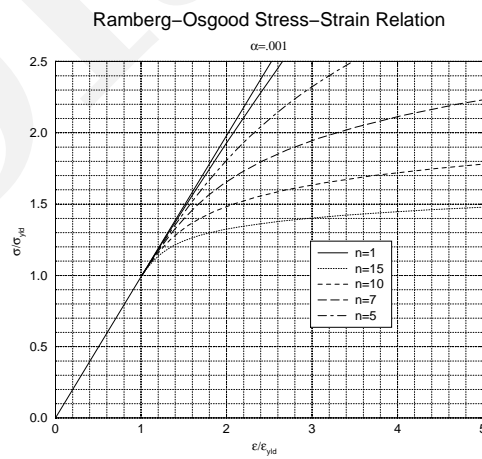


Figure 11.11: Normalize Ramberg-Osgood Stress-Strain Relation ($\alpha = .01$)

52 Denoting by x and y the order of the stress and strain singularities, we would have

$$\sigma = \frac{c_1}{r^x} \quad (11.53)$$

$$\varepsilon = \frac{c_2}{r^y} \quad (11.54)$$

53 From Eq. 11.50, we know that the energy w must be proportional to $\frac{1}{r}$

$$\sigma\varepsilon \propto \frac{1}{r} \Rightarrow x + y = 1 \quad (11.55)$$

54 Furthermore, from Eq. 11.51 and 11.52

$$\frac{c_2}{r^y \varepsilon_{yld}} = \alpha \left(\frac{c_1}{r^x \sigma_{yld}} \right)^n \Rightarrow \frac{c_3}{r^y} = c_4 \frac{1}{r^{nx}} \Rightarrow y = nx \quad (11.56)$$

55 Solving Eq. 11.55 and 11.56, we obtain

$$x = \frac{1}{1+n} \quad (11.57)$$

$$y = \frac{n}{1+n} \quad (11.58)$$

56 Thus in general we would have

$$\boxed{\begin{aligned} \varepsilon(r) &= \frac{C}{r^{\frac{n}{1+n}}} \\ \sigma(r) &= \frac{D}{r^{\frac{1}{1+n}}} \end{aligned}} \quad (11.59)$$

57 For linear elastic solids $n = 1$ and these equations reduce to the familiar

$$\varepsilon(r) = \frac{C}{r^{\frac{1}{2}}} \quad (11.60)$$

$$\sigma = \frac{D}{r^{\frac{1}{2}}} \quad (11.61)$$

58 For elastic perfectly plastic material $n = \infty$ and the stress field is non-singular a expected while the strain field has a singularity of the form r^{-1} .

59 Those singularities $\frac{n}{1+n}$ and $\frac{1}{1+n}$ are often referred to as the HRR singularities after Hutchinson, Rice, and Rosengren, (Hutchinson, 1968).

60 It can be shown that there is a relationship between J and the crack tip $\sigma - \varepsilon$ field:

$$\sigma_{ij} = \sigma_{yld} \left(\frac{EJ}{\alpha \sigma_{yld}^2 I_n r} \right)^{\frac{1}{1+n}} \tilde{\sigma}_{ij}(\theta, n) \quad (11.62)$$

$$\varepsilon_{ij} = \frac{\alpha \sigma_{yld}}{E} \left(\frac{EJ}{\alpha \sigma_{yld}^2 I_n r} \right)^{\frac{n}{1+n}} \tilde{\varepsilon}_{ij}(\theta, n) \quad (11.63)$$

where I_n is an integration constant which depends on the $\sigma - \varepsilon$ curve, and $\tilde{\sigma}$ & $\tilde{\varepsilon}$ are dimensionless functions of n and θ (analogous to f_{ij}^I in LEFM which also depend on the stress state (plane stress/strain))

61 Thus, J also characterizes the σ and ε singularities in EPFM just as K did in LEFM ($\sigma_{ij} = \frac{K}{\sqrt{2\pi r}}$).

62 Finally, we should note that at the crack tip we have two stress singularities, the first one $\frac{1}{\sqrt{r}}$ in the elastic region, and the later $\frac{1}{r^{\frac{1}{1+n}}}$. From Fig. 11.12, we observe that material behind a propagating crack unload elastically (as opposed to nonlinear elastic). The material directly in front of the crack also violates our assumption of of proportional loading, i.e. the stress components increase or decrease at different rates. For the crack to be J controlled, those two zones must be embedded within a zone of J dominance. If the crack grows outside it, then the measured R curve is no longer uniquely characterized by J .

63 Fig. 11.13, and table 11.1 schematically illustrate the effect of plasticity on crack tip stresses, where L represents a characteristic dimension of the structure.

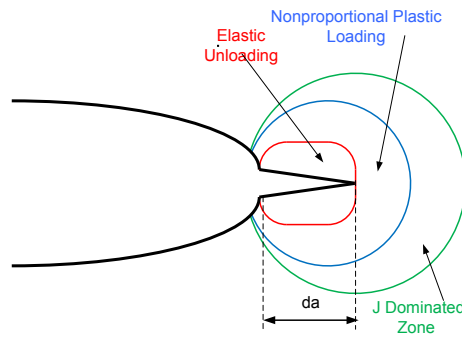


Figure 11.12: HRR Singularity, (Anderson, 1995)

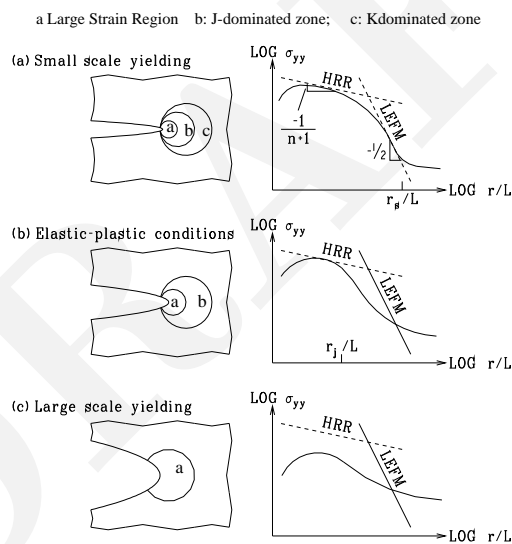


Figure 11.13: Effect of Plasticity on the Crack Tip Stress Fields, (Anderson, 1995)

	Large Strain	J Dominated	K Dominated
Small scale yielding	Y	Y	Y
Elastic Plastic Conditions	Y	Y	N
Large Scale Yielding	Y	N	N

Table 11.1: Effect of Plasticity on the Crack Tip Stress Field, (Anderson, 1995)

Small Scale Yielding: In this zone both K and J characterize this zone. At a short distance from the crack tip (relative to L), the stress is proportional to $\frac{1}{\sqrt{r}}$ and this area is called the K-dominated region. If we have monotonic loading, a J dominated region occurs in the plastic zone where the elastic singularity is no longer valid. Inside the plastic zone, the HRR is approximately valid. Finally, finite strain region occurs within approximately 2δ from the crack tip where the large deformation invalidates HRR.

Elastic-Plastic: J is still valid, but K no longer.

Large Scale Yielding: here the size of the finite strain zone becomes significant relative to L and there is no longer a region uniquely characterized by J . J becomes size and geometry dependent.

11.9 Engineering Approach to Fracture

⁶⁴ The solution of a plastic problem involves the determination of the J integral. This usually involves a finite element analysis.

⁶⁵ If such a capability is not available, and a first order approximation of J is required, then a simplified engineering approach can be followed, (Kumar et al., 1981).

General Solution: For Ramberg-Osgood material, we can write

$$J = J_e(a_e) + J_P(a, n) \quad (11.64-a)$$

$$\delta = \delta_e(a_e) + \delta_P(a, n) \quad (11.64-b)$$

$$\Delta_c = \Delta_{ec}(a_e) + \Delta_{Pc}(a, n) \quad (11.64-c)$$

where: J , δ , and Δ are the J integral, the crack tip opening displacement, and point load displacement respectively, and

$$a_e = a + \phi r_y \quad (11.65-a)$$

$$r_y = \frac{1}{\beta\pi} \frac{n-1}{n+1} \left(\frac{K_I}{\sigma_y} \right)^2 \quad (11.65-b)$$

$$\phi = \frac{1}{1 + (P/P_o)^2} \quad (11.65-c)$$

for plane stress $\beta = 2$ and for plane strain $\beta = 6$.

$J_p(a, n)$, $\delta_p(a, n)$, and $\Delta_{pc}(a, n)$ are the plastic contributions based on the material hardening exponent n .

We note that P is the generalized load per unit thickness, Δ is the load-point displacement, and that δ is the crack opening displacement.

Elastic Solution: The elastic solution can be written as

$$J_e = f_1 \left(\frac{a}{W} \right) \frac{P^2}{E'} = \frac{K_I^2}{E'} \quad (11.66-a)$$

$$\delta_e = f_2 \left(\frac{a}{W} \right) \frac{P}{E'} \quad (11.66-b)$$

$$\Delta_{ce} = f_3 \left(\frac{a}{W} \right) \frac{P}{E'} \quad (11.66-c)$$

We note that P is the generalized load per unit thickness, and that δ is the crack opening displacement.

Fully Plastic Solution: Considering a fully plastic incompressible cracked body, $\varepsilon^e \ll \varepsilon^p$. Consider a nonlinear or fully plastic incompressible body and with $\varepsilon^e \ll \varepsilon^p$, furthermore, if the plastic deformation can be described by J_2 , deformation plasticity theory with power law and isotropic hardening, then the small strain constitutive relation is given by

$$\frac{\varepsilon_{ij}}{\varepsilon_{yld}} = \frac{3}{2} \alpha \left(\frac{\bar{\sigma}}{\sigma_{yld}} \right)^{n-1} \frac{S_{ij}}{\sigma_{yld}} \quad (11.67)$$

where S_{ij} and $\sigma_e = \frac{3}{2} \sqrt{S_{ij}S_{ij}}$ are the stress deviator and the von-Mises effective stress, respectively.

For such a material Ilyushin (Ilyushin, 1946) has shown that the solution of the boundary value problems based on the above equation, and involving a single load or displacement parameter which is increasing monotonically has two important properties:

1. The field quantities increase in direct proportion to the load or displacement parameter raised to some power dependent on n . For example if the traction is $T_i = PT_i'$ and P is a loading parameter, then

$$\sigma_{ij} = P\sigma'_{ij}(x_i, n) \quad (11.68-a)$$

$$\varepsilon_{ij} = \alpha\varepsilon_y \left(\frac{P}{\sigma_y}\right)^n \varepsilon'_{ij}(x_i, n) \quad (11.68-b)$$

$$u_i = \alpha\varepsilon_y \left(\frac{P}{\sigma_y}\right)^n u'_i(x_i, n) \quad (11.68-c)$$

where $\sigma'_{ij}(x_i, n)$, $\varepsilon'_{ij}(x_i, n)$ and $u'_i(x_i, n)$ are functions of x_i and n and are independent of P .

2. Since σ and ε increase in the same proportion, fully plastic solution based on deformation plasticity is also the exact solution to the same problem posed for incremental or flow theory.

⁶⁶ Since the integrand of J involves the product of σ and u gradients, then the fully plastic J will be proportional to P^{n+1} and we can write:

$$J_p = \alpha\varepsilon_y\sigma_y b g_1(a/W) h_1(a/W, n) (P/P_0)^{n+1} \quad (11.69-a)$$

$$\delta_p = \alpha\varepsilon_y a g_2(a/W) h_2(a/W, n) (P/P_0)^n \quad (11.69-b)$$

$$\Delta_{cp} = \alpha\varepsilon_y a g_3(a/W) h_3(a/W, n) (P/P_0)^n \quad (11.69-c)$$

$$\delta_{tp} = \alpha\varepsilon_y b g_4(a/W) h_4(a/W, n) (P/P_0)^{n+1} \quad (11.69-d)$$

where P_0 corresponds to the limit load based on σ_y and b is the ligament length ($W - a$). α is from Eq. 11.52 $\varepsilon/\varepsilon_{yld} = \alpha(\sigma/\sigma_{yld})^n$.

⁶⁷ The dimensionless functions ($h_1 - h_4$) depend upon a/W and n and possibly other geometric parameters, but are independent of P . Those functions can be obtained from F.E. analysis and are tabulated ($\pm 5\%$) in (Kumar et al., 1981).

11.9.1 Compilation of Fully Plastic Solutions

Compact Tension Specimen: Table 11.2, Fig. 11.14.

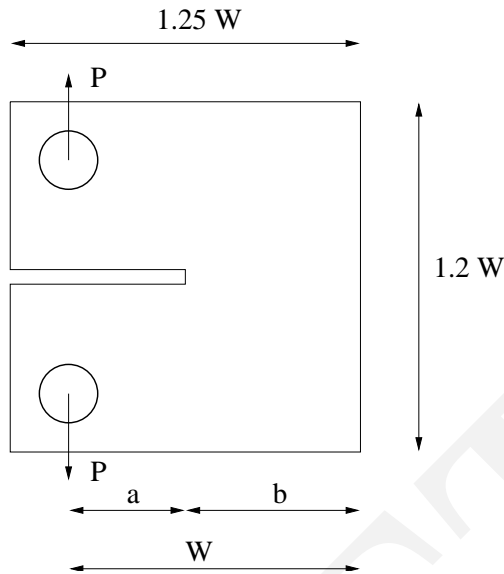


Figure 11.14: Compact tension Specimen

$$\text{Plane Strain } P_0 = 1.455\beta b\sigma_y \quad (11.70)$$

$$\text{Plane Stress } P_0 = 1.071\beta b\sigma_y \quad (11.71)$$

$$\beta = \sqrt{\left(2\frac{a}{b}\right)^2 + 4\frac{a}{b} + 2} - 2\frac{a}{b} - 1 \quad (11.72)$$

$$g_i = 1 \quad (11.73)$$

Δ corresponds to the crack opening displacement at the load line and δ is the crack mouth opening displacement.

Center Cracked Panel: Table 11.3, Fig. 11.15

$$\text{Plane Strain } P_0 = 4b\sigma_y/\sqrt{3} \quad (11.74)$$

$$\text{Plane Stress } P_0 = 2b\sigma_y \quad (11.75)$$

$$g_1 = g_4 = a/W \quad (11.76)$$

$$g_2 = g_3 = 1 \quad (11.77)$$

Δ corresponds to the average load-point displacement defined by

$$\Delta = \frac{1}{2W} \int_W^W [u_2(x_1, L) - u_2(x_1, L)] dx_1 \quad (11.78)$$

δ is the crack opening displacement at the center of the crack.

Single Edge Notched Specimen: Table 11.4, Fig. 11.16.

$$\text{Plane Strain } P_0 = 1.455\beta b\sigma_y \quad (11.79)$$

$$\text{Plane Stress } P_0 = 1.072\beta b\sigma_y \quad (11.80)$$

$$\beta = \sqrt{1 + \left(\frac{a}{b}\right)^2} - \frac{a}{b} \quad (11.81)$$

$$g_1 = g_4 = a/W \quad (11.82)$$

$$g_2 = g_3 = 1 \quad (11.83)$$

Δ is the load-point displacement at the centerline of the specimen, and δ is the crack mouth opening displacement.

		$n = 1$	$n = 2$	$n = 3$	$n = 5$	$n = 7$	$n = 10$	$n = 13$	$n = 16$	$n = 20$
Plane Strain										
$\frac{a}{W} = \frac{1}{4}$	h1	2.23	2.05	1.78	1.48	1.33	1.26	1.25	1.32	1.57
	h2	17.9	12.5	11.7	10.9	10.5	10.7	11.5	12.6	14.6
	h3	9.85	8.51	8.17	7.77	7.71	7.92	8.52	9.31	10.9
$\frac{a}{W} = \frac{3}{8}$	h1	2.15	1.72	1.39	0.97	0.69	0.443	0.28	0.176	0.098
	h2	12.60	8.18	6.52	4.32	2.97	1.79	1.10	0.686	0.370
	h3	7.94	5.76	4.64	3.10	2.14	1.29	0.793	0.494	0.266
$\frac{a}{W} = \frac{1}{2}$	h1	1.94	1.51	1.24	0.919	0.68	0.461	0.314	0.216	0.132
	h2	9.33	5.85	4.30	2.75	1.91	1.20	0.788	0.530	0.370
	h3	6.41	4.27	3.16	2.02	1.41	0.998	0.585	0.393	0.236
$\frac{a}{W} = \frac{5}{8}$	h1	1.76	1.45	1.24	0.97	0.75	0.602	0.459	0.347	0.248
	h2	7.61	4.57	3.42	2.36	1.51	1.32	0.983	0.749	0.485
	h3	5.52	3.43	2.58	1.79	1.37	1.00	0.746	0.568	0.368
$\frac{a}{W} = \frac{3}{4}$	h1	1.71	1.42	1.26	1.03	0.86	0.717	0.575	0.448	0.345
	h2	6.37	3.95	3.18	2.34	1.89	1.440	1.120	0.887	0.665
	h3	4.86	3.05	2.46	1.81	1.45	1.110	0.869	0.686	0.514
$\frac{a}{W} \approx 1$	h1	1.57	1.45	1.35	1.18	1.08	0.95	0.85	0.73	0.63
	h2	5.39	3.74	3.09	2.43	2.12	1.80	1.57	1.33	1.14
	h3	4.31	2.99	2.47	1.95	1.79	1.44	1.26	1.07	0.909
Plane Stress										
$\frac{a}{W} = \frac{1}{4}$	h1	1.61	1.460	1.28	1.06	0.90	0.729	0.601	0.511	0.395
	h2	17.60	12.00	10.70	8.74	7.32	5.74	4.63	3.75	2.92
	h3	9.67	8.00	7.21	5.94	5.00	3.95	3.19	2.59	2.023
$\frac{a}{W} = \frac{3}{8}$	h1	1.55	1.25	1.050	0.801	0.64	0.484	0.377	0.284	0.22
	h2	12.40	8.20	6.540	4.56	3.45	2.44	1.83	1.36	1.02
	h3	7.80	5.73	4.620	3.250	2.48	1.77	1.33	0.99	0.746
$\frac{a}{W} = \frac{1}{2}$	h1	1.40	1.08	0.901	0.686	0.55	0.436	0.356	0.298	0.238
	h2	9.16	5.67	4.21	2.80	2.12	1.57	1.25	1.03	0.814
	h3	6.29	4.15	3.11	2.09	1.59	1.18	0.938	0.774	0.614
$\frac{a}{W} = \frac{5}{8}$	h1	1.27	1.03	0.875	0.695	0.59	0.494	0.423	0.37	0.310
	h2	7.470	4.48	3.35	2.37	1.92	1.540	1.29	1.12	0.928
	h3	5.42	3.38	2.54	1.80	1.47	1.180	0.988	0.853	0.710
$\frac{a}{W} = \frac{3}{4}$	h1	1.23	0.977	0.833	0.683	0.59	0.506	0.431	0.373	0.314
	h2	6.25	3.78	2.89	2.14	1.78	1.440	1.20	1.03	0.857
	h3	4.77	2.92	2.24	1.66	1.38	1.120	0.936	0.80	0.666
$\frac{a}{W} \approx 1$	h1	1.130	1.01	0.775	0.68	0.65	0.620	0.490	0.47	0.42
	h2	5.29	3.54	2.41	1.91	1.73	1.59	1.23	1.17	1.03
	h3	4.23	2.83	1.93	1.52	1.39	1.270	0.985	0.933	0.824

Table 11.2: h -Functions for Standard ASTM Compact Tension Specimen, (Kumar et al., 1981)

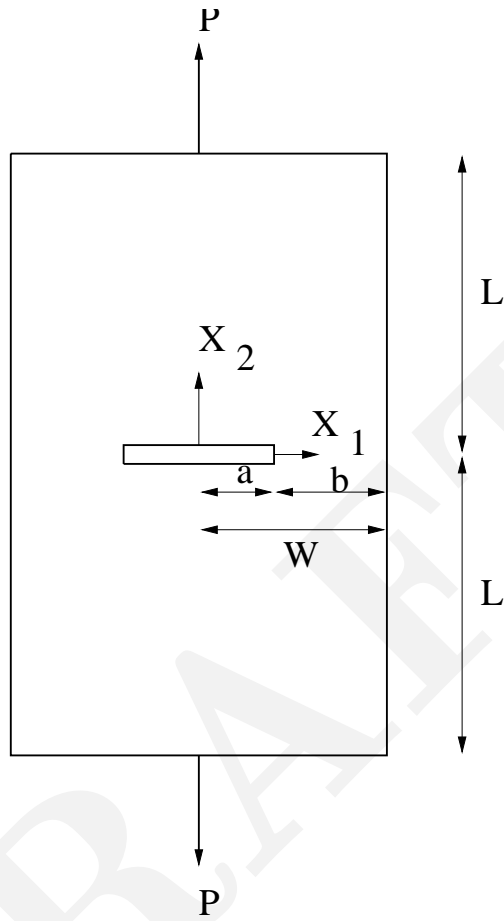


Figure 11.15: Center Cracked Panel

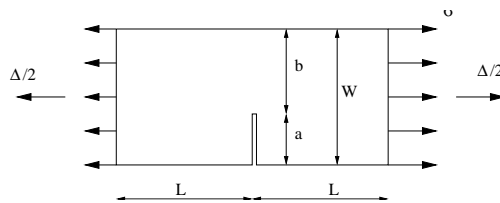


Figure 11.16: Single Edge Notched Specimen

		$n = 1$	$n = 2$	$n = 3$	$n = 5$	$n = 7$	$n = 10$	$n = 13$	$n = 16$	$n = 20$
Plane Strain										
$\frac{a}{W} = \frac{1}{8}$	h1	2.80	3.61	4.06	4.35	4.33	4.02	3.56	3.06	2.46
	h2	3.05	3.62	3.91	4.06	3.93	3.54	3.07	2.60	2.06
	h3	0.303	0.574	0.84	1.30	1.63	1.95	2.03	1.96	1.77
$\frac{a}{W} = \frac{1}{4}$	h1	2.54	3.01	3.21	3.29	3.18	2.92	2.63	2.34	2.03
	h2	2.68	2.99	3.01	2.85	2.61	2.30	1.00	1.71	1.45
	h3	0.536	0.911	1.22	1.64	1.84	1.85	1.80	1.64	1.43
$\frac{a}{W} = \frac{3}{8}$	h1	2.340	2.62	2.65	2.51	2.28	1.97	1.71	1.46	1.19
	h2	2.350	2.39	2.23	1.88	1.58	1.28	1.07	0.89	0.715
	h3	0.699	1.06	1.28	1.44	1.40	1.23	1.05	0.888	0.719
$\frac{a}{W} = \frac{1}{2}$	h1	2.21	2.29	2.20	1.97	1.76	1.52	1.32	1.16	0.978
	h2	2.030	1.860	1.60	1.23	1.00	0.799	0.664	0.564	0.466
	h3	0.803	1.07	1.16	1.10	0.96	0.796	0.665	0.565	0.469
$\frac{a}{W} = \frac{5}{8}$	h1	2.12	1.96	1.76	1.43	1.17	0.863	0.628	0.458	0.300
	h2	1.71	1.320	1.04	0.707	0.52	0.358	0.250	0.178	0.114
	h3	0.844	0.937	0.879	0.701	0.52	0.361	0.251	0.178	0.115
$\frac{a}{W} = \frac{3}{4}$	h1	2.070	1.73	1.47	1.11	0.89	0.642	0.461	0.337	0.216
	h2	1.350	0.857	0.596	0.361	0.25	0.167	0.114	0.081	0.0511
	h3	805	0.70	0.555	0.359	0.25	0.168	0.114	0.081	0.052
$\frac{a}{W} = \frac{7}{8}$	h1	2.08	1.64	1.40	1.14	0.98	0.814	0.688	0.573	0.461
	h2	0.889	0.428	0.287	0.181	0.13	0.105	0.084	0.068	0.0533
	h3	0.632	0.400	0.291	0.182	0.14	0.106	0.084	0.068	0.054
Plane Stress										
$\frac{a}{W} = \frac{1}{8}$	h1	2.80	3.57	4.01	4.47	4.65	4.62	4.41	4.13	3.72
	h2	3.530	4.09	4.43	4.74	4.79	4.63	4.33	4.00	3.55
	h3	0.350	0.661	1.00	1.55	2.05	2.56	2.83	2.95	2.92
$\frac{a}{W} = \frac{1}{4}$	h1	2.54	2.97	3.14	3.20	3.11	2.86	2.65	2.47	2.20
	h2	3.100	3.29	3.30	3.15	2.93	2.56	2.29	2.08	1.81
	h3	0.619	1.01	1.35	1.83	2.08	2.19	2.12	2.01	1.79
$\frac{a}{W} = \frac{3}{8}$	h1	2.340	2.53	2.52	2.35	2.17	1.95	1.77	1.61	1.43
	h2	2.710	2.62	2.41	2.03	1.75	1.47	1.28	1.13	0.988
	h3	0.807	1.20	1.43	1.59	1.57	1.43	1.27	1.13	0.994
$\frac{a}{W} = \frac{1}{2}$	h1	2.210	2.20	2.06	1.81	1.63	1.43	1.30	1.17	1.00
	h2	2.340	2.01	1.70	1.30	1.07	0.871	0.757	0.666	0.557
	h3	0.927	1.19	1.26	1.18	1.04	0.867	0.758	0.668	0.560
$\frac{a}{W} = \frac{5}{8}$	h1	2.12	1.91	1.69	1.41	1.22	1.01	0.853	0.712	0.573
	h2	1.970	1.46	1.13	0.785	0.61	0.474	0.383	0.313	0.256
	h3	0.975	1.05	0.97	0.763	0.62	0.478	0.386	0.318	0.273
$\frac{a}{W} = \frac{3}{4}$	h1	2.07	1.71	1.46	1.21	1.08	0.867	0.745	0.646	0.532
	h2	1.550	0.97	0.685	0.452	0.36	0.262	0.216	0.183	0.148
	h3	0.929	0.802	0.642	0.45	0.36	0.263	0.216	0.183	0.149
$\frac{a}{W} = \frac{7}{8}$	h1	2.08	1.57	1.31	1.08	0.97	0.862	0.778	0.715	0.630
	h2	1.030	0.485	0.31	0.196	0.15	0.127	0.109	0.0971	0.0842
	h3	0.730	0.452	0.313	0.198	0.15	0.127	0.109	0.0973	0.0842

Table 11.3: Plane Stress h -Functions for a Center-Cracked Panel, (Kumar et al., 1981)

		$n = 1$	$n = 2$	$n = 3$	$n = 5$	$n = 7$	$n = 10$	$n = 13$	$n = 16$	$n = 20$
Plane Strain										
$\frac{a}{W} = \frac{1}{8}$	h1	4.95	6.93	8.57	11.50	13.5	16.1	18.1	19.9	21.2
	h2	5.250	6.47	7.56	9.46	11.1	12.9	14.4	15.7	16.8
	h3	26.60	25.80	25.20	24.20	23.6	23.2	23.2	23.5	23.7
$\frac{a}{W} = \frac{1}{4}$	h1	4.34	4.77	4.64	3.82	3.06	2.170	1.55	1.11	0.712
	h2	4.760	4.56	4.28	3.39	2.64	1.910	1.25	0.875	0.552
	h3	10.30	7.64	5.87	3.70	2.48	1.500	0.97	0.654	0.404
$\frac{a}{W} = \frac{3}{8}$	h1	3.88	3.25	2.63	1.68	1.06	0.539	0.276	0.142	0.060
	h2	4.540	3.49	2.67	1.57	0.94	0.458	0.229	0.116	0.048
	h3	5.14	2.99	1.90	0.923	0.51	0.240	0.119	0.060	0.025
$\frac{a}{W} = \frac{1}{2}$	h1	3.40	2.30	1.69	0.928	0.51	0.213	0.090	0.039	0.012
	h2	4.450	2.77	1.89	0.954	0.50	0.204	0.085	0.036	0.011
	h3	3.15	1.54	0.91	0.417	0.21	0.085	0.036	0.015	0.004
$\frac{a}{W} = \frac{5}{8}$	h1	2.86	1.80	1.30	0.697	0.37	0.153	0.064	0.026	0.008
	h2	4.370	2.44	1.62	0.081	0.42	0.167	0.067	0.027	0.008
	h3	2.31	1.08	0.68	0.329	0.17	0.067	0.027	0.011	0.003
$\frac{a}{W} = \frac{3}{4}$	h1	2.34	1.61	1.25	0.769	0.47	0.233	0.116	0.059	0.022
	h2	4.320	2.52	1.79	1.03	0.69	0.296	0.146	0.074	0.027
	h3	2.02	1.10	0.765	0.435	0.26	0.125	0.062	0.031	0.011
$\frac{a}{W} = \frac{7}{8}$	h1	1.91	1.57	1.37	1.10	0.92	0.702			
	h2	4.29	2.75	2.14	1.55	1.23	0.921			
	h3	2.01	1.27	0.988	0.713	0.56	0.424			
Plane Stress										
$\frac{a}{W} = \frac{1}{8}$	h1	3.58	4.55	5.06	5.30	4.96	4.14	3.29	2.60	1.92
	h2	5.15	5.43	6.05	6.01	5.47	4.46	3.48	2.74	2.02
	h3	26.10	21.60	18.00	12.70	9.24	5.98	3.94	2.72	2.00
$\frac{a}{W} = \frac{1}{4}$	h1	3.14	3.26	2.920	2.120	1.53	0.96	0.615	0.40	0.23
	h2	4.67	4.30	3.700	2.530	1.76	1.05	0.656	0.419	0.237
	h3	10.10	6.49	4.360	2.190	1.24	0.63	0.362	0.224	0.123
$\frac{a}{W} = \frac{3}{8}$	h1	2.81	2.37	1.940	1.370	1.01	0.677	0.474	0.342	0.226
	h2	4.47	3.43	2.630	1.690	1.18	0.762	0.524	0.372	0.244
	h3	5.05	2.65	1.600	0.812	0.525	0.328	0.223	0.157	0.102
$\frac{a}{W} = \frac{1}{2}$	h1	2.46	1.67	1.250	0.776	0.510	0.286	0.164	0.0956	0.0469
	h2	4.37	2.73	1.91	1.09	0.694	0.380	0.216	0.124	0.0607
	h3	3.10	1.43	0.871	0.461	0.286	0.155	0.088	0.0506	0.0247
$\frac{a}{W} = \frac{5}{8}$	h1	2.07	1.41	1.105	0.755	0.551	0.363	0.248	0.172	0.107
	h2	4.30	2.55	1.840	1.160	0.816	0.523	0.353	0.242	0.150
	h3	2.27	1.13	0.771	0.478	0.336	0.215	0.146	0.100	0.062
$\frac{a}{W} = \frac{3}{4}$	h1	1.70	1.14	0.910	0.624	0.447	0.280	0.181	0.118	0.067
	h2	4.24	2.47	1.81	1.150	0.798	0.490	0.314	0.203	0.115
	h3	1.98	1.09	0.784	0.494	0.344	0.211	0.136	0.0581	0.0496
$\frac{a}{W} = \frac{7}{8}$	h1	1.38	1.11	0.962	0.792	0.677	0.574			
	h2	4.22	2.68	2.08	1.54	1.27	1.04			
	h3	1.97	1.25	0.969	0.716	0.592	0.483			

Table 11.4: h -Functions for Single Edge Notched Specimen, (Kumar et al., 1981)

Double Edge Notched Specimen: Table 11.5, Fig. 11.17.

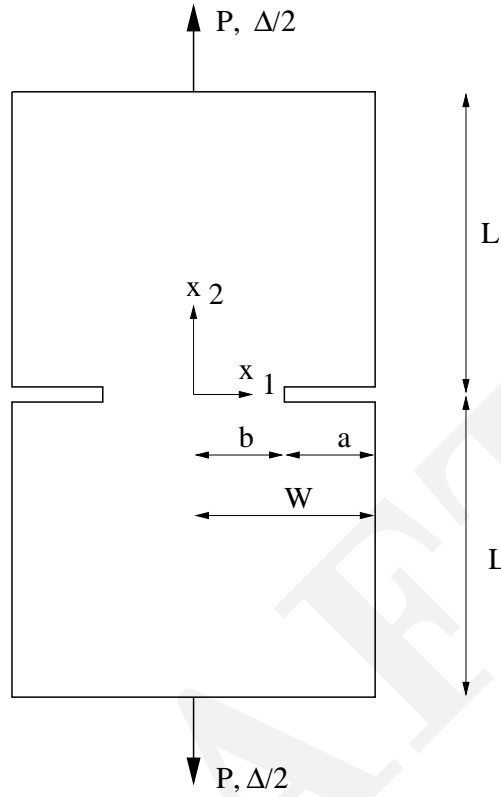


Figure 11.17: Double Edge Notched Specimen

$$\text{Plane Strain } P_0 = (0.72W + 1.82b)\sigma_y \quad (11.84)$$

$$\text{Plane Stress } P_0 = 4b\sigma_y/\sqrt{3} \quad (11.85)$$

$$\beta = \sqrt{1 + \left(\frac{a}{b}\right)^2} - \frac{a}{b} \quad (11.86)$$

$$g_1 = g_4 = 1 \quad (11.87)$$

$$g_2 = g_3 = W/a - 1 \quad (11.88)$$

Δ is the load-point displacement at the centerline of the specimen, and δ is the crack mouth opening displacement.

Axially Cracked Pressurized Cylinder: Table ??, Fig. 11.18.

$$p_0 = \frac{2b\sigma_y}{\sqrt{3}R_c} \quad (11.89)$$

$$R_c = R_i + a \quad (11.90)$$

$$g_1 = \frac{a}{W} \quad (11.91)$$

$$g_2 = 1 \quad (11.92)$$

δ is the crack mouth opening displacement. Note that in the elastic range:

$$K_I = \frac{2pR_0^2\sqrt{\pi a}}{R_0^2 - R_i^2} F\left(\frac{a}{W}, \frac{R_i}{R_0}\right) \quad (11.93)$$

$$\delta_e = \frac{8pR_0^2 a}{(R_0^2 - R_i^2)E'} V\left(\frac{a}{W}, \frac{R_i}{R_0}\right) \quad (11.94)$$

where the dimensionless functions F and V are tabulated in Table 11.7.

		$n = 1$	$n = 2$	$n = 3$	$n = 5$	$n = 7$	$n = 10$	$n = 13$	$n = 16$	$n = 20$
Plane Strain										
$\frac{a}{W} = \frac{1}{8}$	h1	0.572	0.772	0.922	1.13	1.35	1.61	1.86	2.09	2.44
	h2	0.732	0.852	0.961	1.14	1.29	1.50	1.70	1.94	2.17
	h3	0.063	0.126	0.200	0.372	0.57	0.911	1.30	1.74	2.29
$\frac{a}{W} = \frac{1}{4}$	h1	1.10	1.320	1.38	1.65	1.75	1.82	1.86	1.89	1.92
	h2	1.56	1.63	1.70	1.79	1.80	1.81	1.79	1.78	1.76
	h3	0.267	0.479	0.698	1.11	1.47	1.92	2.25	2.49	2.73
$\frac{a}{W} = \frac{3}{8}$	h1	1.61	1.83	1.92	1.92	1.84	1.68	1.49	1.32	1.12
	h2	2.51	2.41	2.35	2.15	1.94	1.68	1.44	1.25	1.05
	h3	0.637	1.05	1.40	1.87	2.11	2.20	2.09	1.92	1.67
$\frac{a}{W} = \frac{1}{2}$	h1	2.22	2.43	2.49	2.43	2.32	2.12	1.91	1.60	1.51
	h2	3.73	3.40	3.15	2.70	2.37	2.01	1.72	1.40	1.38
	h3	1.26	1.92	2.37	2.79	2.85	2.68	2.40	1.99	1.94
$\frac{a}{W} = \frac{5}{8}$	h1	3.16	3.38	3.45	3.42	3.28	3.00	2.54	2.36	2.27
	h2	5.57	4.76	4.23	3.46	2.97	2.48	2.02	1.82	1.66
	h3	2.36	3.29	3.74	3.90	3.68	3.23	2.66	2.40	2.19
$\frac{a}{W} = \frac{3}{4}$	h1	5.24	6.29	7.17	8.44	9.46	10.90	119.0	11.3	17.4
	h2	9.10	7.76	7.14	6.64	6.83	7.48	7.790	7.14	11.0
	h3	4.73	6.26	7.03	7.63	8.14	9.04	9.4	8.58	13.5
$\frac{a}{W} = \frac{7}{8}$	h1	14.2	24.8	39.0	78.4	140.	341.0	777.0	1570.0	3820.0
	h2	20.1	19.4	22.7	36.1	58.9	133.0	294.0	585.0	1400.0
	h3	12.7	18.2	24.1	40.4	65.9	149.0	327.0	650.0	1560.0
Plane Stress										
$\frac{a}{W} = \frac{1}{8}$	h1	0.583	0.825	1.02	1.37	1.71	2.24	2.84	3.54	4.62
	h2	0.853	1.050	1.23	1.55	1.87	2.38	2.96	3.65	4.70
	h3	0.0729	0.159	0.26	0.504	0.82	1.41	2.18	3.16	4.73
$\frac{a}{W} = \frac{1}{4}$	h1	1.01	1.23	1.36	1.48	1.54	1.58	1.59	1.59	1.59
	h2	1.73	1.82	1.89	1.92	1.91	1.85	1.80	1.75	1.70
	h3	0.296	0.537	0.77	1.17	1.49	1.82	2.02	2.12	2.20
$\frac{a}{W} = \frac{3}{8}$	h1	1.29	1.42	1.43	1.34	1.24	1.09	0.97	0.873	0.674
	h2	2.59	2.39	2.22	1.86	1.59	1.28	1.07	0.922	0.709
	h3	658	1.04	1.30	1.52	1.55	1.41	1.23	1.07	0.830
$\frac{a}{W} = \frac{1}{2}$	h1	1.48	1.47	1.38	1.17	1.01	0.845	0.732	0.625	0.208
	h2	3.51	2.82	2.34	1.67	1.28	0.944	0.762	0.630	0.232
	h3	1.18	1.58	1.69	1.56	1.32	1.01	0.809	0.662	0.266
$\frac{a}{W} = \frac{5}{8}$	h1	1.59	1.45	1.29	1.04	0.88	0.737	0.649	0.466	0.020
	h2	4.56	3.15	2.32	1.45	1.06	0.790	0.657	0.473	0.028
	h3	1.93	2.14	1.95	1.44	1.09	0.809	0.665	0.487	0.032
$\frac{a}{W} = \frac{3}{4}$	h1	1.65	1.43	1.22	0.979	0.83	0.701	0.630	0.297	
	h2	5.90	3.37	2.22	1.30	0.96	0.741	0.636	0.312	
	h3	3.06	2.67	2.06	1.31	0.97	0.747	0.638	0.318	
$\frac{a}{W} = \frac{7}{8}$	h1	1.69	1.43	1.22	0.979	0.84	0.738	0.664	0.614	0.562
	h2	8.02	3.51	2.14	1.27	0.97	0.775	0.663	0.596	0.535
	h3	5.07	3.180	2.16	1.30	0.98	0.779	0.665	0.597	0.538

Table 11.5: h -Functions for Double Edge Notched Specimen, (Kumar et al., 1981)

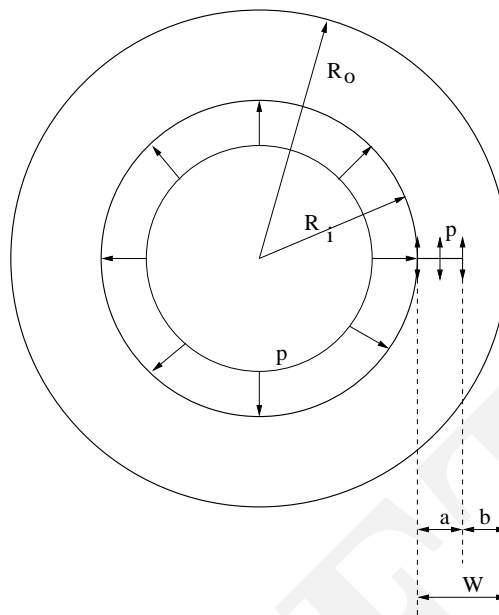


Figure 11.18: Axially Cracked Pressurized Cylinder

		$n = 1$	$n = 2$	$n = 3$	$n = 5$	$n = 7$	$n = 10$
		$\frac{W}{R_i} = \frac{1}{5}$					
$\frac{a}{W} = \frac{1}{8}$	h1	6.32	7.93	9.32	11.50	13.1	14.94
	h2	5.83	7.01	7.96	9.49	10.6	11.96
$\frac{a}{W} = \frac{1}{4}$	h1	7.00	9.34	9.03	9.59	9.71	9.45
	h2	5.92	8.72	7.07	7.26	7.14	6.71
$\frac{a}{W} = \frac{1}{2}$	h1	9.79	10.37	9.07	5.61	3.52	2.11
	h2	7.05	6.97	6.01	3.70	2.28	1.25
$\frac{a}{W} = \frac{3}{4}$	h1	11.00	5.54	2.84	1.24	0.83	0.493
	h2	7.35	3.86	1.86	0.56	0.26	0.129
		$\frac{W}{R_i} = \frac{1}{10}$					
$\frac{a}{W} = \frac{1}{8}$	h1	5.22	6.64	7.59	8.76	9.34	9.55
	h2	5.31	6.25	6.88	7.65	8.02	8.09
$\frac{a}{W} = \frac{1}{4}$	h1	6.16	7.49	7.96	8.08	7.78	6.98
	h2	5.56	6.31	6.52	6.40	6.01	5.27
$\frac{a}{W} = \frac{1}{2}$	h1	10.5	11.6	10.7	6.47	3.95	2.27
	h2	7.48	7.72	7.01	4.29	2.58	1.37
$\frac{a}{W} = \frac{3}{4}$	h1	16.10	8.19	3.87	1.46	1.05	0.787
	h2	9.57	5.40	2.57	0.71	0.37	0.232
		$\frac{W}{R_i} = \frac{1}{20}$					
$\frac{a}{W} = \frac{1}{8}$	h1	4.50	5.79	6.62	7.65	8.07	7.75
	h2	4.96	5.71	6.20	6.82	7.02	6.66
$\frac{a}{W} = \frac{1}{4}$	h1	5.57	6.91	7.37	7.47	7.21	6.53
	h2	5.29	5.98	6.16	6.01	5.63	4.93
$\frac{a}{W} = \frac{1}{2}$	h1	10.80	12.80	12.80	8.16	4.88	2.62
	h2	7.66	8.33	8.13	5.33	3.20	1.65
$\frac{a}{W} = \frac{3}{4}$	h1	23.10	13.10	5.87	1.90	1.23	0.883
	h2	12.10	7.88	3.84	1.01	0.45	0.24

Table 11.6: h -Functions for an Internally Pressurized, Axially Cracked Cylinder, (Kumar et al., 1981)

		$\frac{a}{W} = \frac{1}{8}$	$\frac{a}{W} = \frac{1}{4}$	$\frac{a}{W} = \frac{1}{2}$	$\frac{a}{W} = \frac{3}{4}$
$\frac{W}{R_I} = \frac{1}{5}$	F	1.19	1.38	2.10	3.30
	V_1	1.51	1.83	3.44	7.50
$\frac{W}{R_I} = \frac{1}{10}$	F	1.20	1.44	2.36	4.23
	V_1	1.54	1.91	3.96	10.40
$\frac{W}{R_I} = \frac{1}{20}$	F	1.20	1.45	2.51	5.25
	V_1	1.54	1.92	4.23	13.50

Table 11.7: F and V_1 for Internally Pressurized, Axially Cracked Cylinder, (Kumar et al., 1981)

Circumferentially Cracked Cylinder: Table 11.8, Fig. 11.19.

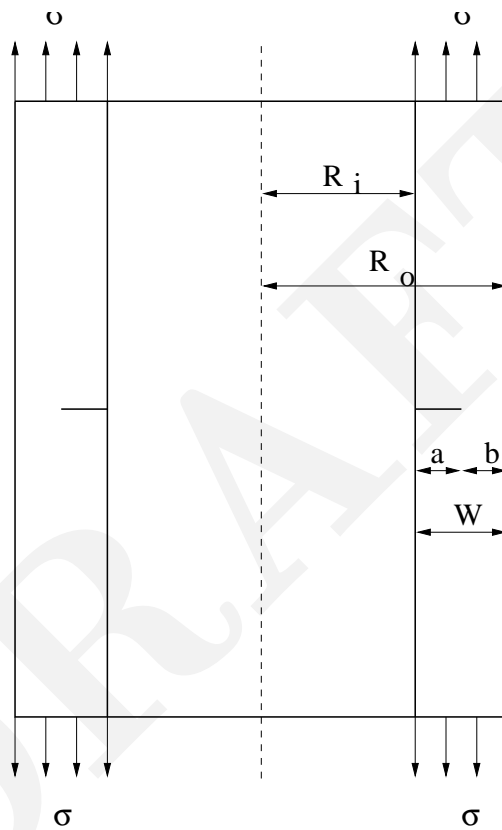


Figure 11.19: Circumferentially Cracked Cylinder

$$P_0 = \frac{2\pi\sigma_y(R_o^2 - R_i^2)}{\sqrt{3}} \tag{11.95}$$

$$R_c = R_i + a \tag{11.96}$$

$$g_1 = g_4 = \frac{a}{W} \tag{11.97}$$

$$g_2 = g_3 = 1 \tag{11.98}$$

δ is the crack mouth opening displacement.

In the elastic range

$$K_I = \sigma\sqrt{\pi a}F\left(\frac{a}{W}, \frac{R_i}{R_0}\right) \quad (11.99)$$

$$\delta_e = \frac{4\sigma a V_1\left(\frac{a}{W}, \frac{R_i}{R_0}\right)}{E'} \quad (11.100)$$

$$\Delta_{ce} = \frac{4\sigma a V_2\left(\frac{a}{W}, \frac{R_i}{R_0}\right)}{E'} \quad (11.101)$$

where the functions F , V_1 , and V_2 are tabulated in Table 11.9.

		$n = 1$	$n = 2$	$n = 3$	$n = 5$	$n = 7$	$n = 10$
		$\frac{W}{R_i} = \frac{1}{5}$					
$\frac{a}{W} = \frac{1}{8}$	h1	3.78	5.00	5.94	7.54	8.99	11.1
	h2	4.560	5.55	6.37	7.79	9.10	11.0
	h3	0.369	0.70	1.07	1.96	3.04	4.94
$\frac{a}{W} = \frac{1}{4}$	h1	3.88	4.95	5.64	6.49	6.94	7.22
	h2	4.40	5.12	5.57	6.07	6.28	6.30
	h3	0.673	1.25	1.79	2.79	3.61	4.52
$\frac{a}{W} = \frac{1}{2}$	h1	4.40	4.78	4.59	3.79	3.07	2.34
	h2	4.36	4.30	3.91	3.00	2.26	1.55
	h3	1.33	1.93	2.21	2.23	1.94	1.46
$\frac{a}{W} = \frac{3}{4}$	h1	4.12	3.03	2.23	1.546	1.30	1.110
	h2	3.46	2.19	1.36	0.638	0.43	0.325
	h3	1.54	1.39	1.04	0.686	0.50	0.366
		$\frac{W}{R_i} = \frac{1}{10}$					
$\frac{a}{W} = \frac{1}{8}$	h1	4.00	5.13	6.09	7.69	9.09	11.1
	h2	4.71	5.63	6.45	7.85	9.09	10.9
	h3	0.548	0.733	1.13	2.07	3.16	5.07
$\frac{a}{W} = \frac{1}{4}$	h1	4.17	5.35	6.09	6.93	7.30	7.41
	h2	4.58	5.36	5.84	6.31	6.44	6.31
	h3	757	1.35	1.93	2.96	3.78	4.60
$\frac{a}{W} = \frac{1}{2}$	h1	5.40	5.90	5.63	4.51	3.49	2.47
	h2	4.99	5.01	4.59	3.48	2.56	1.67
	h3	1.555	2.26	2.59	2.57	2.18	1.56
$\frac{a}{W} = \frac{3}{4}$	h1	5.18	3.78	2.57	1.59	1.31	1.10
	h2	4.22	2.79	1.67	0.725	0.48	0.30
	h3	1.86	1.73	1.26	0.775	0.56	0.36
		$\frac{W}{R_i} = \frac{1}{20}$					
$\frac{a}{W} = \frac{1}{8}$	h1	4.04	5.23	6.22	7.82	9.19	11.1
	h2	4.82	5.69	6.52	7.90	9.11	10.8
	h3	0.68	0.76	1.17	2.13	3.23	5.12
$\frac{a}{W} = \frac{1}{4}$	h1	4.39	5.68	6.45	7.29	7.62	7.65
	h2	4.71	5.56	6.05	6.51	6.59	6.39
	h3	0.82	1.43	2.03	3.10	3.91	4.69
$\frac{a}{W} = \frac{1}{2}$	h1	6.55	7.17	6.89	5.46	4.13	2.77
	h2	5.67	5.77	5.36	4.08	2.97	1.88
	h3	1.80	2.59	2.99	2.98	2.50	1.74
$\frac{a}{W} = \frac{3}{4}$	h1	6.64	4.87	3.08	1.68	1.30	1.07
	h2	5.18	3.57	2.07	0.808	0.47	0.316
	h3	2.36	2.18	1.53	0.772	0.49	0.330

Table 11.8: h -Functions for a Circumferentially Cracked Cylinder in Tension, (Kumar et al., 1981)

11.9.2 Numerical Example

From (Anderson, 1995), Consider a single edge notched panel with $W = 1$ m, $a = 125$ mm. Determine J in terms of the applied load assuming plane stress conditions, neglect plastic zone correction.

Assume: $\sigma_{yld} = 414$ MPa, $n = 10$, $\alpha = 1.0$, $E = 207,000$ MPa, $\varepsilon_{yld} = \sigma_{yld}/E = 0.002$.

$\frac{W}{R_I}$	F	$\frac{a}{W} = \frac{1}{8}$	$\frac{a}{W} = \frac{1}{4}$	$\frac{a}{W} = \frac{1}{2}$	$\frac{a}{W} = \frac{3}{4}$
		V_1	1.16	1.26	1.61
$\frac{1}{10}$	V_2	1.49	1.67	2.43	3.76
	F	0.117	0.255	0.743	1.67
$\frac{1}{20}$	V_1	1.19	1.32	1.82	2.49
	V_2	1.55	1.76	2.84	4.72
$\frac{1}{20}$	F	0.18	0.29	0.885	2.09
	V_1	1.22	1.36	2.03	2.89
$\frac{1}{20}$	V_2	1.59	1.81	3.26	5.99
	V_2	0.22	0.32	1.04	2.74

Table 11.9: F , V_1 , and V_2 for a Circumferentially Cracked Cylinder in Tension, (Kumar et al., 1981)

1. From Eq. 11.80

$$b = W - a = 1000 - 125 = 875 \text{ mm} \quad (11.102\text{-a})$$

$$\frac{a}{b} = \frac{125}{875} = 0.143 \quad (11.102\text{-b})$$

$$\beta = \sqrt{1 + \left(\frac{a}{b}\right)^2} - \frac{a}{b} \quad (11.102\text{-c})$$

$$= \sqrt{1 + (0.143)^2} - 0.143 = 0.867 \quad (11.102\text{-d})$$

$$P_0 = 1.072\beta b \sigma_y \quad (11.102\text{-e})$$

$$= (1.072)(0.867)(414 \text{ MPa})(875 \text{ mm})(25 \text{ mm}) = 8.42 \text{ MN} \quad (11.102\text{-f})$$

2. From Table 11.4, for $a/W = 0.125$, and $n = 10$, $h_1=4.14$. Thus the fully plastic J is given by Eq. 11.69-a

$$J_p = \alpha \varepsilon_y \sigma_y b g_1(a/W) h_1(a/W, n) (P/P_0)^{n+1} \quad (11.103\text{-a})$$

$$= (1.0)(0.002)(414,000 \text{ kPa})(0.875 \text{ m}) \frac{125}{1000} (4.14) \left(\frac{P}{8.42 \text{ MN}}\right)^{10+1} \quad (11.103\text{-b})$$

$$= 2.486 \times 10^{-8} P^{11} \quad (11.103\text{-c})$$

where P in in MN, and J_{pl} in in kJ/m^2 .

3. K_I is given by Eq. 4.4, and the Elastic J is given by

$$K_I = \left[1.12 - 0.23 \left(\frac{a}{W}\right) + 10.56 \left(\frac{a}{W}\right)^2 - 21.74 \left(\frac{a}{W}\right)^3 + 30.42 \left(\frac{a}{W}\right)^4 \right] \sigma \sqrt{\pi a} \quad (11.104\text{-a})$$

$$J_{el} = \frac{K_I^2}{E} = G \quad (11.104\text{-b})$$

$$= \frac{1,000 P^2 (0.770)^2}{(0.025)^2 \text{ m}^2 (1.0 \text{ m})(207,000 \text{ MPa})} = 4.584 P^2 \quad (11.104\text{-c})$$

where P in in MN, and J_{el} in in kJ/m^2 .

4. The total J is

$$J = J_{el} + J_{pl} \quad (11.105\text{-a})$$

$$= 4.584 P^2 + 2.486 \times 10^{-8} P^{11} \quad (11.105\text{-b})$$

11.10 J_1 and J_2 Generalization.

⁶⁶ Rice has shown that in linear elastic fracture, and in terms of the stress intensity factors, J can be written as:

$$(1 - \nu^2)(K_I^2 + K_{II}^2) + (1 + \nu)K_{III}^2 = E J_1 \quad (11.106)$$

where J_1 is expressed in indicial notation by:

$$J_1 = \int_{\Gamma} \left(w dy - \mathbf{t} \frac{\partial \mathbf{u}}{\partial x} d\Gamma \right) \quad (11.107)$$

$$= \int_{\Gamma} \left(w n_1 - t_i \frac{\partial u_i}{\partial x_1} d\Gamma \right) \quad (11.108)$$

where w is the strain energy density, n_i are the direction cosines of the normal to the contour, the T_i are the components of traction, and the contour of integration is around the tip.

⁶⁷ Knowles and Stenberg (1972) noted that this can be considered as the first component of a vector

$$J_k = \int \left\{ w n_k - t_i \frac{\partial u_i}{\partial x_k} \right\} d\Gamma \quad (11.109)$$

which is also path independent. When written in vector form, this gives

$$\begin{cases} J_1 = \int_{\Gamma} \left(w dy - \mathbf{t} \frac{\partial \mathbf{u}}{\partial x} d\Gamma \right) \\ J_2 = \int_{\Gamma} \left(w dx - \mathbf{t} \frac{\partial \mathbf{u}}{\partial y} d\Gamma \right) \end{cases} \quad (11.110)$$

⁶⁸ Hellen and Blackburn (1975a) showed that

$$J = J_1 - iJ_2 \quad (11.111)$$

$$= \frac{(1+\nu)(1+\kappa)}{4E} (K_I^2 + K_{II}^2 + 2iK_I K_{II}) \quad (11.112)$$

⁶⁹ Thus the values of energy release rates (J_1 and J_2) for crack extensions parallel and perpendicular to the crack, respectively, will be given by:

$$\begin{cases} J_1 = \frac{K_I^2 + K_{II}^2}{H} \\ J_2 = \frac{-2K_I K_{II}}{H} \end{cases} \quad (11.113)$$

where

$$H = \begin{cases} E & \text{plane strain} \\ \frac{E}{1-\nu^2} & \text{plane stress} \end{cases} \quad (11.114)$$

Note that solution of Eq. 11.113 and 11.113 is the intersection of a circle and a hyperbola. Hence, there exists more than one pair of stress intensity factors (or none).

11.11 Dynamic Energy Release Rate

⁷⁰ If we consider a body containing a propagating crack, (Kanninen, 1984), Fig. 11.20

⁷¹ We seek to determine the energy released to the crack tip and thus consider a vanishingly small loop Γ_0 surrounding the crack tip¹. Whereas the loop can have any shape, it must remain fixed relative to a coordinate system attached to the crack tip. We consider the area A bounded by the outer boundary Γ , the traction free crack faces, and the inner loop Γ_0 .

⁷² The rate of work P done by the tractions on Γ is equal to the rate of increase of the strain energy \dot{U} and kinetic energy \dot{T} in region A and the flux F of energy into the crack tip region:

$$P = \dot{U} + \dot{T} + F \quad (11.115)$$

where

$$P = \int_{\Gamma} t_i u_i d\Gamma \quad (11.116-a)$$

$$U = \lim_{\Gamma_0 \rightarrow 0} \int_A W(\varepsilon_{ij}) dA \quad (11.116-b)$$

$$T = \lim_{\Gamma_0 \rightarrow 0} \int_A \frac{1}{2} \rho \dot{u}_i \dot{u}_i dA \quad (11.116-c)$$

¹in contrast to the static case, the energy release rate can not be expressed by a path-independent contour integral because if a wave front intercepts one contour, but not the second one, then two different values would be represented by only the contour integral.

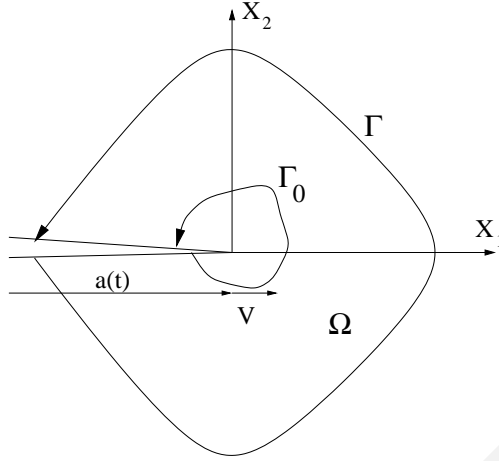


Figure 11.20: Dynamic Crack Propagation in a Plane Body, (Kanninen, 1984)

⁷³ Since the loop Γ_0 moves with the crack tip, region A is time dependent. Therefore, the time rate of change of the strain energy equals the integral over A of the time rate of change of the strain energy density $W(\varepsilon_{ij})$ less the flow of this density through the loop Γ_0 . Hence,

$$\dot{U} = \lim_{\Gamma_0 \rightarrow 0} \int_A \dot{W}(\varepsilon_{ij}) dA - \lim_{\Gamma_0 \rightarrow 0} \int_{\Gamma_0} W(\varepsilon_{ij}) V_n d\Gamma \quad (11.117)$$

where $V_n = V n_1 = V \cos \theta$ is the component of the crack-tip velocity normal to Γ_0 and θ is the angle that the outward unit normal to Γ_0 makes with the x_1 direction.

⁷⁴ Thus,

$$dw = \sigma_{ij} d\varepsilon_{ij} \quad (11.118-a)$$

$$\dot{W} = \sigma_{ij} \dot{\varepsilon}_{ij} = \sigma_{ij} \dot{u}_{i,j} \quad (11.118-b)$$

$$\dot{U} = \lim_{\Gamma_0 \rightarrow 0} \int_A \sigma_{ij} \dot{u}_{i,j} dA - \lim_{\Gamma_0 \rightarrow 0} \int_{\Gamma_0} W(\varepsilon_{ij}) V_n d\Gamma \quad (11.118-c)$$

$$\dot{T} = \lim_{\Gamma_0 \rightarrow 0} \int_A \rho \ddot{u}_i \dot{u}_i dA - \lim_{\Gamma_0 \rightarrow 0} \int_{\Gamma_0} \frac{1}{2} \rho \dot{u}_i \dot{u}_i V_n d\Gamma \quad (11.118-d)$$

⁷⁵ Substituting into Eq. 11.115 we obtain

$$F = \lim_{\Gamma_0 \rightarrow 0} \int_{\Gamma_0} \left(W + \frac{1}{2} \rho \dot{u}_i \dot{u}_i \right) V_n d\Gamma + \int_{\Gamma} t_i \dot{u}_i d\Gamma - \lim_{\Gamma_0 \rightarrow 0} \int_A (\sigma_{ij} \dot{u}_{i,j} + \rho \ddot{u}_i \dot{u}_i) dA \quad (11.119)$$

⁷⁶ We then use

$$\sigma_{ij} \dot{u}_{i,j} = (\sigma_{ij} \dot{u}_i)_{,j} - \sigma_{ij,j} \dot{u}_i \quad (11.120)$$

and the equation of motion

$$\sigma_{ij,j} = \rho \ddot{u}_i \quad (11.121)$$

and the divergence theorem, then Eq. 11.119 reduces to

$$F = \lim_{\Gamma_0 \rightarrow 0} \int_{\Gamma_0} \left[\left(W + \frac{1}{2} \rho \dot{u}_i \dot{u}_i \right) V_n + t_i \dot{u}_i \right] d\Gamma \quad (11.122)$$

⁷⁷ This is the rate at which energy is lost from the body due to flux through Γ_0 . This last equation can be rewritten in terms of the strain energy density w , and the kinetic energy density t (not to be confused with the traction),

$$F = \lim_{\Gamma_0 \rightarrow 0} \int_{\Gamma_0} [(w + t)V\delta_{1j} + \sigma_{ji}\dot{u}_i] n_j d\Gamma \quad (11.123)$$

⁷⁸ In an increment of time dt , the crack extends by $da = Vdt$ and the energy expended is Fdt . Thus the energy release rate is

$$J = \frac{F}{V} \quad (11.124)$$

⁷⁹ If we have a moving coordinate system $x - y$ attached to the crack tip where $x = X - a(t)$ and $y = Y$, then

$$\dot{u}_i = -V \frac{\partial u_i}{\partial x} + \frac{\partial u_i}{\partial t} \quad (11.125)$$

under steady condition, the second term is equal to zero. On the other hand, close to the crack tip the displacement changes rapidly with position (at a fixed time) and the first term dominates in all cases, ?? thus

$$J = \lim_{\Gamma_0 \rightarrow 0} \int_{\Gamma_0} \left[(w + t)\delta_{1j} - \sigma_{ji} \frac{\partial u_i}{\partial x} \right] n_j d\Gamma \quad (11.126)$$

or

$$J = \lim_{\Gamma_0 \rightarrow 0} \int_{\Gamma_0} \left[(w + t)dy - \sigma_{ji} n_j \frac{\partial u_i}{\partial x} d\Gamma \right] \quad (11.127)$$

This equation applies to all types of material.

11.12 Effect of Other Loading

This section is taken from (Reich, 1993)

11.12.1 Surface Traction on Crack Surfaces

⁸⁰ J integral was first extended by (Karlsson and Bäcklund, 1978) to account for the effect of surface tractions on the crack surfaces involves simply extending the definition of the contour path to include the crack surfaces. The resulting form of the J integral was then given as

$$J = \int_{\Gamma} (W dx_2 - t_j u_{j,1} d\Gamma) - \int_{\Gamma_t} \hat{t}_j u_{j,1} d\Gamma \quad (11.128)$$

where Γ_t is that portion of the upper and lower crack surfaces between the points where Γ ends and begins and \hat{t}_i is the applied surface traction vector.

⁸¹ The strain energy density W is absent from the integral over Γ_t since the crack surfaces are coincident with the negative x_1 -axis and there is no need to integrate in the x_2 -direction. Unfortunately, (Karlsson and Bäcklund, 1978) offered no proof showing that path independence was maintained and a significant portion of their discussion was devoted to the finite element implementation of this procedure.

⁸² Proof of path independence for this procedure was later provided by (Atluri, 1982) using the contour paths shown in Figure 21.1. The proof was given for the J_i integral, therefore, the strain energy density W is retained in the integrand of the integral accounting for the applied surface tractions \hat{t}_i

$$J_i = \int_{\Gamma} (W n_i - t_j u_{j,i}) d\Gamma + \int_{\Gamma_t} (W n_i - \hat{t}_j u_{j,i}) d\Gamma \quad (11.129)$$

where $\Gamma_t = \Gamma_t^+ \cup \Gamma_t^-$.

11.12.2 Body Forces

⁸³ The most straightforward method to account for body forces in the J integral is to add correction terms in the form of volume integrals such that path independence is maintained. When body forces are present $\sigma_{ij,j} = -b_i$ and $W_{,i} \neq (\sigma_{jk} u_{j,i})_{,k}$. Therefore, the integrand of volume form of the standard J_i integral (i.e. Equation ??) does not vanish, but instead is

$$J_i = \int_{\Omega} (b_j u_{j,i}) d\Omega \neq 0 \quad (11.130)$$

where b_j is the body force vector. This means that the strain energy density W is a function of position and that $(W_{,i})_{exp} \neq 0$, where $(W_{,i})_{exp}$ is the gradient of that portion of W that depends explicitly on x_i .

⁸⁴ For path independence to be maintained in the presence of body forces the volume integral shown above must be subtracted from the standard line integral form of the J_i integral

$$J_i = \int_{\Gamma} (W n_i - t_j u_{j,i}) d\Gamma - \int_{\Omega} (b_j u_{j,i}) d\Omega \quad (11.131)$$

which corresponds to the form proposed by (Atluri, 1982).

11.12.3 Initial Strains Corresponding to Thermal Loading

⁸⁵ In order to apply the J_i integral to problems in thermo-elasticity the strain energy density W must first be redefined. Looking forward to the presentation of the extension in which thermal strains and pore pressures will be considered in combination, W will be defined in terms of the net strains $\bar{\varepsilon}_{ij}$ and the net effective stresses $\bar{\sigma}'_{ij}$ as

$$W = \int_0^{\bar{\varepsilon}_{ij}} \bar{\sigma}'_{ij} d\bar{\varepsilon}_{ij} \quad (11.132)$$

and the net effective stresses $\bar{\sigma}'_{ij}$ being defined as

$$\bar{\sigma}'_{ij} = \frac{\partial W}{\partial \bar{\varepsilon}_{ij}} \quad (11.133)$$

⁸⁶ It must be noted that in the absence of initial stresses σ_{ij}^0 that $\sigma_{ij} = \bar{\sigma}'_{ij}$, where σ_{ij} are the total stresses. Therefore, $\bar{\sigma}'_{ij}$ can be replaced by σ_{ij} throughout this discussion. For a linear elastic material W is defined as

$$W = \frac{1}{2} C_{ijkl} \bar{\varepsilon}_{ij} \bar{\varepsilon}_{kl} \quad (11.134)$$

and the resulting constitutive law is

$$\bar{\sigma}'_{ij} = C_{ijkl} \bar{\varepsilon}_{kl} = C_{ijkl} (\varepsilon_{kl} - \alpha \mathcal{T} \delta_{kl}) \quad (11.135)$$

which is identical to Equation 21.53.

⁸⁷ Since the definition of the strain energy density W is now in terms of the net effective stresses $\bar{\sigma}'_{ij}$, the J_i integral must also be defined in terms of $\bar{\sigma}'_{ij}$ rather than the total stresses σ_{ij} . The appropriate form of the J_i integral is

$$J_i = \int_{\Gamma} (W n_i - \bar{t}'_j u_{j,i}) d\Gamma \quad (11.136)$$

where $\bar{t}'_i = \bar{\sigma}'_{ij} n_j$ are the net effective surface tractions. On application of Green's theorem to the line integral form of J_i the resulting volume integral form is

$$J_i = \int_{\Omega} [W_{,i} - (\bar{\sigma}'_{jk} u_{j,i})_{,k}] d\Omega \quad (11.137)$$

⁸⁸ Some changes are also required in the definition of $W_{,i}$ due to the change in the definition of W . The chain rule is still applied to obtain

$$W_{,i} = \frac{\partial W}{\partial \bar{\varepsilon}_{jk}} \frac{\partial \bar{\varepsilon}_{jk}}{\partial x_i} \quad (11.138)$$

but $\partial \bar{\varepsilon}_{jk} / \partial x_i$ is defined as

$$\frac{\partial \bar{\varepsilon}_{jk}}{\partial x_i} = \frac{\partial \varepsilon_{jk}}{\partial x_i} - \frac{\partial \varepsilon_{jk}^0}{\partial x_i} \quad (11.139)$$

reflecting the contributions of the total and thermal strains, ε_{jk} and ε_{jk}^0 , respectively. $\partial \varepsilon_{jk} / \partial x_i$ is defined as

$$\frac{\partial \varepsilon_{jk}}{\partial x_i} = \frac{1}{2} [(u_{j,k}),_i + (u_{k,j}),_i] = \frac{1}{2} [(u_{j,i}),_k + (u_{k,i}),_j] \quad (11.140)$$

and $\partial \varepsilon_{jk}^0 / \partial x_i$ is defined as

$$\frac{\partial \varepsilon_{jk}^0}{\partial x_i} = \alpha \mathcal{T}_{,i} \delta_{jk} \quad (11.141)$$

⁸⁹ Recalling that $\sigma_{jk} = \sigma_{kj}$ and substituting the above expressions for $\partial \varepsilon_{jk} / \partial x_i$ and $\partial \varepsilon_{jk}^0 / \partial x_i$ into Equation 11.138 the expression for $W_{,i}$ can be rewritten as

$$W_{,i} = \bar{\sigma}'_{jk} [(u_{j,i}),_k - \alpha \mathcal{T}_{,i} \delta_{jk}] \quad (11.142)$$

and inserted into Equation 11.137, the volume integral form of J_i . The expression for $W_{,i}$ clearly includes the $\bar{\sigma}'_{jk} (u_{j,i}),_k$ term that also results from $(\bar{\sigma}'_{jk} u_{j,i}),_k$. Therefore, in the absence of body forces $\bar{\sigma}'_{jk,k} = 0$ and $W_{,i} \neq (\bar{\sigma}'_{jk} u_{j,i}),_k$, leaving only a term involving $\mathcal{T}_{,i}$ in the integrand of the volume form of the J_i integral

$$J_i = - \int_{\Omega} (\alpha \bar{\sigma}'_{jj} \mathcal{T}_{,i}) d\Omega \neq 0 \quad (11.143)$$

where $\bar{\sigma}'_{jj}$ is the trace of the net effective stress tensor.

⁹⁰ This means that W is function of position due to the presence of the thermal strains ε_{jk}^0 and that $(W_{,i})_{exp} \neq 0$. To maintain path independence the volume integral shown above must be subtracted from the standard line integral form of J_i yielding

$$J_i = \int_{\Gamma} (W n_i - \bar{t}'_j u_{j,i}) d\Gamma + \int_{\Omega} (\alpha \bar{\sigma}'_{jj} \mathcal{T}_{,i}) d\Omega \quad (11.144)$$

which corresponds to the form proposed by (Shih et al., 1986) if the net effective stresses are replaced by the total stresses.

⁹¹ Including body forces along with the thermal strains at this point is actually quite simple. Recalling that $\bar{\sigma}'_{jk,k} = -b'_j$ in the presence of body forces the integrand of the volume form of the J_i integral will also include a term involving b'_j

$$J_i = - \int_{\Omega} (\alpha \bar{\sigma}'_{jj} \mathcal{T}_{,i} - b'_j u_{j,i}) d\Omega \neq 0 \quad (11.145)$$

⁹² To maintain path independence this volume integral must be subtracted from the standard line integral form of J_i to obtain

$$\boxed{J_i = \int_{\Gamma} (W n_i - \bar{t}'_j u_{j,i}) d\Gamma + \int_{\Omega} (\alpha \bar{\sigma}'_{jj} \mathcal{T}_{,i} - b'_j u_{j,i}) d\Omega} \quad (11.146)$$

which is quite clearly a simple combination of Equations 11.144 and 11.130.

11.12.4 Initial Stresses Corresponding to Pore Pressures

⁹³ As was the case when the J_i integral was applied to problems in thermo-elasticity, the strain energy density W must also be redefined for problems in poro-elasticity. However, in this case the redefinition is more cosmetic in nature, with W being defined in terms of the total strains ε_{ij} and the effective stresses σ'_{ij} as

$$W = \int_0^{\varepsilon_{ij}} \sigma'_{ij} d\varepsilon_{ij} \quad (11.147)$$

and the effective stresses σ'_{ij} are defined as

$$\sigma'_{ij} = \frac{\partial W}{\partial \varepsilon_{ij}} \quad (11.148)$$

⁹⁴ It must be noted that this definition of W is identical to the one given in Equation ??, where σ_{ij} was used in lieu of σ'_{ij} . However, since initial strains and stresses were not considered in Equation ??, $\sigma_{ij} = \sigma'_{ij}$ and this notation was valid, albeit slightly misleading. For a linear elastic material W is defined as

$$W = \frac{1}{2} C_{ijkl} \varepsilon_{ij} \varepsilon_{kl} \quad (11.149)$$

resulting in the following constitutive law

$$\sigma'_{ij} = C_{ijkl} \varepsilon_{kl} \quad (11.150)$$

⁹⁵ The stress-strain relationship defining the total stresses σ_{ij} is obtained by simply adding expressions for the initial stresses σ_{ij}^0 and the effective stresses σ'_{ij} , as is dictated by the principle of effective stress

$$\sigma_{ij} = C_{ijkl} \varepsilon_{kl} + \sigma_{ij}^0 = C_{ijkl} \varepsilon_{kl} - p \delta_{ij} \quad (11.151)$$

which is identical to Equation 21.62.

⁹⁶ Since the definition of the strain energy density W is now in terms of the effective stresses σ'_{ij} , the J_i integral must also be defined in terms of σ'_{ij} rather than the total stresses σ_{ij} . This would also seem to be in agreement with the classical interpretation of the effective stresses (Terzaghi and Peck, 1967), where σ'_{ij} are the only stresses acting on the skeleton of the porous material, which is in fact what is being fractured. The appropriate form of the J_i integral is

$$J_i = \int_{\Gamma} (W n_i - t'_j u_{j,i}) d\Gamma \quad (11.152)$$

where $t'_i = \sigma'_{ij} n_j$ are the effective surface tractions.

⁹⁷ This form of the J_i integral is valid so long as the only source of applied surface tractions \hat{t}_i on the crack surfaces is from fluid in the crack, since in this case $\sigma'_{ij} = 0$ and $\hat{t}'_i = 0$, where \hat{t}'_i are the applied effective surface tractions. On application of Green's theorem to the line integral form of J_i the resulting volume integral form is

$$J_i = \int_{\Omega} [W_{,i} - (\sigma'_{jk} u_{j,i})_{,k}] d\Omega \quad (11.153)$$

⁹⁸ Based on the expression for W given in Equation 11.147 and the previous proofs $W_{,i}$ can immediately be written as

$$W_{,i} = \frac{\partial W}{\partial \varepsilon_{ij}} \frac{\partial \varepsilon_{ij}}{\partial x_i} = \sigma'_{jk} (u_{j,i})_{,k} \quad (11.154)$$

and inserted in Equation 11.153, the volume integral form of J_i . In the absence of body forces $\sigma'_{jk,k} = p_{,k} \delta_{jk}$ and $W_{,i} \neq (\sigma'_{jk} u_{j,i})_{,k}$, leaving only the term involving $p_{,k}$ in the integrand of the volume form of J_i integral

$$J_i = - \int_{\Omega} p_{,k} \delta_{jk} u_{j,i} d\Omega = - \int_{\Omega} p_{,j} u_{j,i} d\Omega \neq 0 \quad (11.155)$$

where $p_{,j}$ is the gradient of the pore pressures. This means that W is a function of position due the presence of the pore pressures and that $(W_{,i})_{exp} = 0$.

⁹⁹ To maintain path independence the volume integral shown above must be subtracted from the standard line integral form of J_i yielding

$$J_i = \int_{\Gamma} (W n_i - t'_j u_{j,i}) d\Gamma + \int_{\Omega} p_{,j} u_{j,i} d\Omega \quad (11.156)$$

which is analogous to the form proposed by (Shih et al., 1986) for problems in thermo-elasticity.

¹⁰⁰ Including body forces along with the pore pressures, which is typically the case for problems in poro-elasticity, is actually quite simple at this point. Recalling that $\sigma'_{jk,k} = -b'_j$ in the presence of body forces, where the effective body forces b'_j are defined in Equation 21.64, the integrand of the volume form of the J_i integral can be written in one of two ways

$$J_i = - \int_{\Omega} b'_j u_{j,i} d\Omega = - \int_{\Omega} (b_j - p_{,j}) u_{j,i} d\Omega \neq 0 \quad (11.157)$$

with the latter form being somewhat more illuminating than the former.

¹⁰¹ To maintain path independence this volume integral must be subtracted from the standard line integral form of J_i to obtain

$$J_i = \int_{\Gamma} (W n_i - t'_j u_{j,i}) d\Gamma - \int_{\Omega} (b_j - p_{,j}) u_{j,i} d\Omega \quad (11.158)$$

which is quite clearly a simple combination of Equations 11.156 and 11.130.

11.12.5 Combined Thermal Strains and Pore Pressures

¹⁰² In the presence of both thermal strains and pore pressures the strain energy density W is defined in terms of the net strain tensor $\bar{\varepsilon}_{ij}$ and the net effective stress tensor $\bar{\sigma}'_{ij}$, just as it was in Equation 11.132 for problems in thermo-elasticity. The resulting constitutive law, as defined by Equation 11.135, is substituted into the principle of effective stress to obtain a stress-strain relationship defining the total stresses σ_{ij}

$$\sigma_{ij} = C_{ijkl} \bar{\varepsilon}_{kl} + \sigma_{ij}^0 = C_{ijkl} (\varepsilon_{kl} - \alpha \mathcal{T} \delta_{kl}) - p \delta_{ij} \quad (11.159)$$

which is identical to Equation 21.66. Of course, this stress-strain relationship is valid only so long as all initial stresses correspond to pore pressures.

¹⁰³ Since the definition of the strain energy density W corresponds to that given for problems in thermo-elasticity the form of the J_i integral and the gradient of the strain energy density $W_{,i}$ will also correspond to those for problems in thermo-elasticity. Therefore, when thermal strains and pore pressures are considered in combination the line integral form of J_i is given by Equation 11.136; the volume integral form of J_i is given by Equation 11.137; and the expression for $W_{,i}$ is given by Equation 11.138.

¹⁰⁴ However, in the absence of body forces $\bar{\sigma}'_{jk,k} = p_{,k} \delta_{jk}$ rather than $\bar{\sigma}'_{jk,k} = 0$, as it was in the same situation for problems in thermo-elasticity, and $W_{,i} \neq (\bar{\sigma}'_{jk} u_{j,i})_{,k}$, leaving terms involving both $\mathcal{T}_{,i}$ and $p_{,j}$ in the integrand of the volume form of J_i integral

$$J_i = - \int_{\Omega} (\alpha \bar{\sigma}'_{jj} \mathcal{T}_{,i} + p_{,j} u_{j,i}) d\Omega \neq 0 \quad (11.160)$$

where $\mathcal{T}_{,i}$ is the gradient of the temperatures and $p_{,j}$ is the gradient of the pore pressures. This means that W is a function of position due the presence of the pore pressures and that $(W_{,i})_{exp} = 0$. To maintain path independence the volume integral shown above must be subtracted from the standard line integral form of J_i yielding

$$J_i = \int_{\Gamma} (W n_i - \bar{t}'_j u_{j,i}) d\Gamma + \int_{\Omega} (\alpha \bar{\sigma}'_{jj} \mathcal{T}_{,i} + p_{,j} u_{j,i}) d\Omega \quad (11.161)$$

which is a simple combination of the extensions for thermal strains and pore pressures.

¹⁰⁵ Including body forces along with the thermal strains and pore pressures is again a simple procedure at this point. Recalling that $\bar{\sigma}'_{jk,k} = -b'_j$ in the presence of body forces, where the effective body forces b'_j are defined in Equation 21.64, the integrand of the volume form of the J_i integral can be written as

$$J_i = - \int_{\Omega} (\alpha \bar{\sigma}'_{jj} \mathcal{T}_{,i} - b'_j u_{j,i}) d\Omega = - \int_{\Omega} [\alpha \bar{\sigma}'_{jj} \mathcal{T}_{,i} - (b_j - p_{,j}) u_{j,i}] d\Omega \neq 0 \quad (11.162)$$

With the latter form again being the more illuminating of the two forms shown.

¹⁰⁶ To maintain path independence this volume integral must be subtracted from the standard line integral form of J_i to obtain

$$J_i = \int_{\Gamma} (W n_i - \bar{t}'_j u_{j,i}) d\Gamma + \int_{\Omega} [\alpha \bar{\sigma}_{jj} \mathcal{T}_{,i} - (b_j - p_{,j}) u_{j,i}] d\Omega \quad (11.163)$$

which is quite clearly a simple combination of Equations 11.161 and 11.130. If surface tractions are applied in the crack the contour path for J_i integral must be expanded to include the upper and lower crack surfaces, Γ_t^+ and Γ_t^- , respectively,

$$J_i = \int_{\Gamma} (W n_i - \bar{t}'_j u_{j,i}) d\Gamma + \int_{\Gamma_t} (W n_i - \hat{t}'_j u_{j,i}) d\Gamma + \int_{\Omega} [\alpha \bar{\sigma}_{jj} \mathcal{T}_{,i} - (b_j - p_{,j}) u_{j,i}] d\Omega \quad (11.164)$$

where $\Gamma_t = \Gamma_t^+ \cup \Gamma_t^-$ and \hat{t}'_j are the applied effective surface tractions, as defined in Equation 21.65.

11.13 Epilogue

¹⁰⁷ Finally, as an epilogue we note

1. When Rice derived the J integral in 1968 he did not propose it as a criteria for crack growth, this was done in 1971 by Brobery.

2. J is valid for non-linear elastic systems. Many problems in plasticity can be treated as such using deformation theory of plasticity (i.e. non-linear elastic systems). In general, however, if unloading occurs (during crack growth for instance), then incremental theory of plasticity should be used
3. Several attempts are continuously made to extend J while still retaining its essential features: a) Energy release rate; and b) contour integral; One of them, citepjextension:

$$\hat{J}_K = J_{Ke} + J_{Kd} + J_{Kt} + J_{Kp} + J_{Kb} \quad (11.165)$$

for elastic, dynamic, thermal, plastic, and body forces respectively. * An Elasto Plastic Finite Element Investigation of Crack Initiations Under Mined Mode Static and Dynamic Loading by Ahmad, Barnes, and Kanninen, in Elasto Plastic Fracture ASTM STP 803, 1983.

DRAFT

Chapter 12

FRACTURE DETERIORATION ANALYSIS OF CONCRETE

12.1 Introduction

¹ It is ironic that although the foundation for fracture mechanics was laid by Griffith in the early thirties for brittle materials (such as concrete) (Griffith, 1921), it has been mostly applied to metallic materials. Although there have been some pioneering efforts to apply fracture mechanics to concrete (Kaplan, 1961), it was not until the mid-seventies that a number of researchers from the academic community focused their attention on various aspects of this application.

² In applying fracture mechanics to concrete, much was initially borrowed from the wealth of information and research previously undertaken in conjunction with metals by metallurgists or mechanical engineers. However, it quickly became evident that by its very heterogeneous nature concrete has some unique fracture characteristics, which required the alteration of existing models.

³ By now fracture mechanics is universally acknowledged as a viable tool of analysis for investigation of concrete cracking. And after many years of development on numerous (plasticity based) constitutive models for concrete, tensile cracking remains its undisputed “Achille’s heel”. For the most part, even the simplest constitutive models appear to perform reasonably well under compressive regimes, however their capabilities are seriously challenged under tensile stresses. This apparent inability to properly model tensile cracking is of minor importance in reinforced concrete structures in which the steel “takes over” the tensile stresses.

⁴ However for unreinforced structures, such as dams, the apparent inability of the constitutive models to properly and efficiently model tensile cracking is a major handicap. As such for unreinforced concrete structures prone to tensile cracking, a fracture mechanics based model (rather than a plasticity based one) should be used.

⁵ Whereas an inappropriately large number of papers have been published on computational models for concrete (some of which will be discussed in a separate chapter), relatively few research has been undertaken to properly understand and characterize fracture models. Hence, this chapter will exclusively focus on the phenomenological aspects of concrete fracture from a material point of view.

⁶ For additional information, the reader is directed to the proceedings of the international conferences/workshops on Fracture of Concrete: Lausanne (Wittmann, 1983), Houston (Shah and Swartz, 1989), Evanston (Shah, 1984), Vienna (vie, 1988), Breckenridge (fra, 1992), Zurich (Whitman, 1993); to RILEM reports, (Carpinteri and Ingrassia, 1984), and (Sih and DiTommaso, 1984); special ACI publications (ACI 446.1R-91, 2002). More specialized coverage of dam fracture can be found in the proceedings of the Boulder (Saouma et al., 1991b) and Cahmberly (Bourdarot et al., 1994) conferences.

⁷ Finally, whereas we shall focus exclusively on concrete, most of the presentation in this chapter applies also to ceramics and fiber reinforced ceramic.

12.2 Phenomenological Observations

⁸ We start by discussing some of the general phenomenological aspects associated with fracture testing and response of concrete.

12.2.1 Load, Displacement, and Strain Control Tests

⁹ Before proceeding with the coverage of linear and non-linear fracture mechanics of concrete, it is essential that the reader understand the difference in material and structural response when a specimen is subjected to uniform tensile load, displacement or strain control during testing. Modern testing equipment can be programmed to apply a pre-determined rate of load (as measured by a load cell), of displacement (as measured by an internal displacement transducer), or of strain (measured by a strain/clip gage or other instruments), Fig. 12.1

Load Control: the cross-head applies an increasing load irrespective of the specimen deformation or response. For all materials, when the tensile strength is reached, there is a sudden and abrupt brittle failure. The strain energy accumulated in the specimen is suddenly released once the ultimate load of the specimen is reached, thus the sudden failure can be explosive.

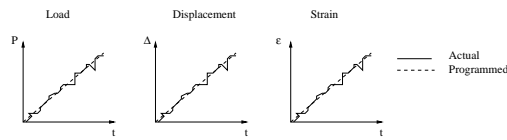


Figure 12.1: Test Controls

Displacement/Stroke Control: the cross-head applies an increasing displacement to the specimen. For softening material there will be a post-peak response with a gradual decrease in stress accompanying an increase in displacement. In this case, there is a gradual release of strain energy which is then transferred to surface energy during crack formation.

Strain Control: is analogous to displacement control, except that the feedback is provided by (“strategically positioned”) strain gage or a clip gage or an arbitrary specimen deformation (not necessarily corresponding to the loading direction). To accomplish this test a clip gage or a strain gage has to provide the feedback signal to the testing equipment in order to accordingly adjust the stroke.

¹⁰ Most concrete fracture tests are conducted under strain control with a gage located at the mouth of the crack providing the specimen response.

¹¹ Both stroke and strain controlled tests require a closed-loop experimental set up, which is usually expensive and was not widely available until very recently.

12.2.2 Pre/Post-Peak Material Response of Steel and Concrete

¹² As an introduction to concrete fracture, let us compare the pre- and post-peak response of metals and concrete, as illustrated in Fig.12.2, both obtained in a strain-controlled test of an uncracked or un-notched specimen.

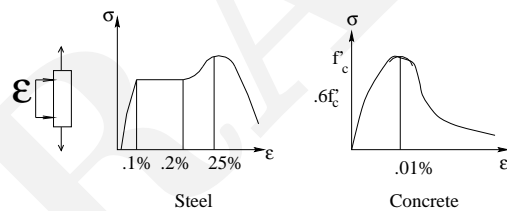


Figure 12.2: Stress-Strain Curves of Metals and Concrete

1. Pre-peak:

- Metal exhibits a linear elastic response up to the yield stress σ_{yld} , and an approximate strain of 0.1%. Subsequently, due to internal dislocation plastic deformation with strain up to 25% may result to be followed by strain hardening.
- Concrete exhibits a linear response up to approximately $0.6f'_c$. Subsequently, internal microcracking induces a non-linear response up to a peak stress f'_t and a corresponding strain of approximately 0.01%.

Under load control only the pre-peak response can be measured.

2. Post-peak:

- Metals response in the post-peak zone is not yet well understood. Not only is it not of practical usefulness, but also it is largely overshadowed by necking.
- Concrete response in the post-peak zone is most interesting, as it can exhibit additional strains. The descending branch of the concrete response in Fig. 12.2 is an idealization of the average material response. A more accurate description should account for the localization of the induced cracks. Thus away from the localized crack there is an elastic unloading, and at the crack, since a strain cannot be properly defined, a stress-crack opening displacement is a more appropriate model. This will be discussed in the subsequent section.

Post-peak responses can be obtained only under displacement or strain controlled tests.

¹³ In either case, the area under the stress-strain curve represents the energy that can be absorbed by a unit fracture surface and thus concrete will exhibit a more brittle response than metals.

¹⁴ Having experimentally observed that the *macroscopic* response of concrete exhibits a softening response, and having attributed the ductile response of metals to internal dislocation, we pose the next question, Why is concrete softening?

12.3 Localisation of Deformation

12.3.1 Experimental Evidence

¹⁵ If we consider a concrete specimen, loaded uniaxially by a tensile load F , we can record elongation by an LVDT (linearly variable displacement transducer) mounted as in configuration 1, 2 or 3, Fig. 12.3.

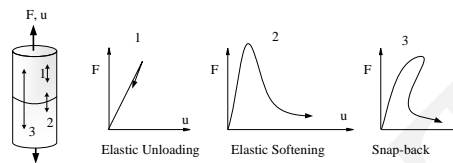


Figure 12.3: Capturing Experimentally Localization in Uniaxially Loaded Concrete Specimens

¹⁶ Once the peak load is reached, and cracking is initiated, transducer 1 will record elastic unloading, 2 strain softening, and 3 snap-back.

¹⁷ If we were to homogenize by taking $\sigma = F/A$, and $\varepsilon = u/L$, it is clear that we can not provide a unique definition of the strain across the crack. At this location, the strain can no longer be defined, and instead we should characterize the crack by its crack opening displacement COD which will then be plotted along with the stress (σ -COD).

¹⁸ This capability of transmitting stresses across a crack under controlled displacement is a characteristic of softening materials.

12.3.1.1 σ -COD Diagram, Hillerborg's Model

¹⁹ From the previous discussion, it is clear that concrete softening is characterized by a stress-crack opening width curve (and not stress-strain). The exact characterization of the softening response should ideally be obtained from a uniaxial test of an uncracked specimen. However, it has been found (Li and Liang, 1986; Hordijk et al., 1989) that not only are those tests extremely sensitive, but drastically different results can be obtained from different geometries, sizes, and testing machines. Hence, the softening curve is often indirectly determined by testing notched specimens.

²⁰ In what is probably the most referenced work in the nonlinear fracture of concrete literature, Hillerborg (Hillerborg et al., 1976a) presented in 1976 a very simple and elegant model which has been previously described qualitatively. In this model, the crack is composed of two parts, Fig. 12.4:

1. True or physical crack across which no stresses can be transmitted. Along this zone we have both displacement and stress discontinuities.
2. Fictitious crack, or Fracture Process Zone (FPZ) ahead of the previous one, characterized by:
 - a) peak stress at its tip equal to the tensile strength of concrete
 - b) decreasing stress distribution from f'_t at the tip of the fictitious crack to zero at the tip of the physical crack

It should be noted that along the FPZ, we have displacement discontinuity and stress continuity.

²¹ This model is among the most widely used in non-linear fracture mechanics finite element analysis, however due to the computational complexity, few "engineering" structures have been analyzed. In addition,

1. There is an inflection point in the descending branch.
 - a) The first part has been associated with (unconnected) microcracking ahead of the stress-free crack
 - b) The second part with bridging of the crack by aggregates

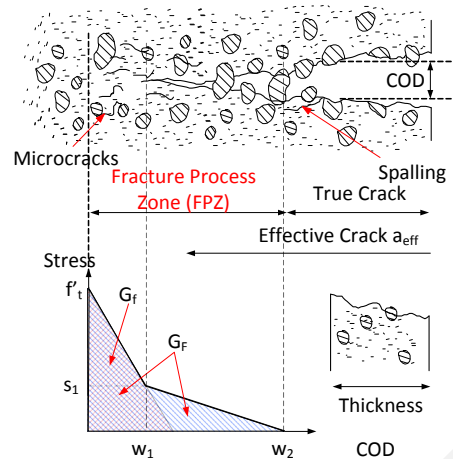


Figure 12.4: Hillerborg's Fictitious Crack Model

2. The area under the curve, termed the fracture energy G_F (not to be confused with G_c or critical energy release rate), is a measure of the energy that needs to be spent to generate a unit surface of crack.
3. By analyzing numerous test data, Bažant and Oh (Bažant, 1984) found that G_F may be predicted (with a coefficient of variation of about 16%) from the following empirical equation:

$$G_F = 0.0214(f'_t + 127)f_t'^2 \frac{d_a}{E_c} \quad (12.1)$$

where E_c and f'_t are in pounds per square inch, d_a is the aggregate size in inches.

4. G_F : or fracture energy. For gravity dams, a value of 1.35×10^{-3} kip/in. is recommended, (Saouma et al., 1991a). Note that for arch dams, this value could probably be increased on the basis of laboratory tests. Also, laboratory tests could be performed on recovered cores to obtain a better indication of G_F , (Brühwiler, E., 1988).
5. Shape of the softening diagram ($\sigma - COD$), and in general a bi-linear model for the strain softening should be used. With reference to Fig. 12.5, A topic of much research lately has been the experimental determination of the fracture energy G_F , and the resulting shape of the softening diagram (Cedolin et al., 1987; Petersson, 1981; Whitman et al., 1988; Jeang and Hawkins, 1985; Gopalaratnam and Shah, 1985; Duda, 1990; Giuriani and Rosati, 1986). In order to assess the relevance of the exact value of G_F and the softening curve shape on numerical simulations, three different set of fracture experiments are analysed using the average reported fracture energy. The shape of the softening diagram is assumed to be the bilinear one proposed in (Whitman et al., 1988), Fig. 12.5. This simple model can be uniquely defined in terms of the tensile strength f'_t , and the fracture energy G_F . In (Brühwiler and Whitman, 1990a), it was found that the optimal points for concrete with 1" maximum size aggregate are:

$$s_1 = 0.4f'_t \quad (12.2)$$

$$w_1 = 0.8 \frac{G_F}{f'_t} \quad (12.3)$$

$$w_2 = 3 \frac{G_F}{f'_t} \quad (12.4)$$

whereas for structural concrete, (Whitman et al., 1988), the corresponding values are:

$$s_1 = \frac{f'_t}{4} \quad (12.5)$$

$$w_1 = 0.75 \frac{G_F}{f'_t} \quad (12.6)$$

$$w_2 = 5 \frac{G_F}{f'_t} \quad (12.7)$$

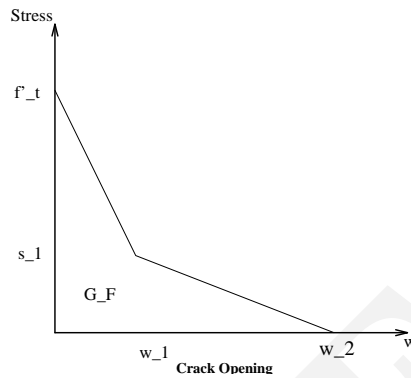


Figure 12.5: Concrete Strain Softening Models

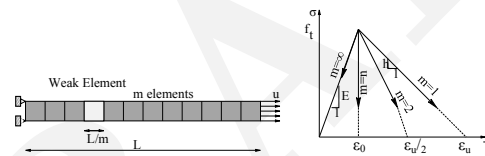


Figure 12.6: Strain-Softening Bar Subjected to Uniaxial Load

where f'_t is the uniaxial tensile strength. Within the context of a nonlinear fracture mechanics analysis, this tensile strength can not be taken as zero, otherwise there will be no fracture process zone. As f'_t is seldom determined experimentally, it is assumed to be 9% of f'_c , (Mindess and Young, 1981).

6. In lieu of a direct tension test, a flexural test can be performed under strain control, and the fracture energy G_F could still be determined from the area under the load and corresponding displacement curve.
7. For dynamic analysis, the fracture properties of dam concrete depend on both rate of loading and preloadings. Test results (Brühwiler and Whitman, 1990a) show that the fracture properties generally increase with increasing loading rate. However, dynamic compressive preloading leads to a reduction of the fracture properties at both quasi-static and high loading rates.

12.3.2 Theoretical Evidence

12.3.2.1 Static Loading

22 Let us consider a simple bar subjected to a uniform displacement (not load) and made up of m elements, Fig. 12.6.

23 Prior to reaching the peak stress f'_t , we have a linear stress strain relationship $\sigma = E\varepsilon$.

24 Once the peak load is reached, the concrete softens and the peak strain is ε_u . At that point the load carrying capacity of the bar is exhausted.

25 The post-peak stress is given by

$$\sigma = f'_t + h(\varepsilon - \varepsilon_0) \quad (12.8)$$

for degrading (softening) material h (softening modulus) is less than zero, and for linear softening

$$h = -\frac{f_t}{\varepsilon_u - \varepsilon_0} \quad (12.9)$$

where $\varepsilon_0 = f_t/E$.

²⁶ We next *assume* that one of the elements is weaker than the other $m - 1$ ones. Thus, when this element reaches its own tensile strength (lower than f_t), it fails. Upon failure of this element, the other ones will simply unload elastically. Thus, in the post-peak zone the displacement will be

$$u = \frac{L}{m}\varepsilon_f + (m-1)\frac{L}{m}\varepsilon_e \quad (12.10-a)$$

$$\varepsilon_f = \frac{f_t}{E} + \frac{\sigma - f_t}{h} \quad (12.10-b)$$

$$\varepsilon_e = \frac{\sigma}{E} \quad (12.10-c)$$

$$\bar{\varepsilon} = \frac{u}{L} \quad (12.10-d)$$

$$\Rightarrow \bar{\varepsilon} = \frac{\sigma}{E} + \frac{E-h}{Eh} \frac{\sigma - f_t}{m} \quad (12.10-e)$$

²⁷ If we define

$$n = \frac{\varepsilon_u}{\varepsilon_0} \quad (12.11)$$

then $h = -E/(n-1)$ and Eq. 12.10-e reduces to

$$\bar{\varepsilon} = \frac{\sigma}{E} + \frac{n(f_t - \sigma)}{mE} \quad (12.12)$$

and the post-peak slope is

$$\frac{\dot{\bar{\varepsilon}}}{\dot{\sigma}} = \frac{1}{E} - \frac{n}{mE} \quad (12.13)$$

²⁸ From Fig. 12.6, we note that depending on the number of element used (m), there is a wide range of possible responses. For $m = 1$ we have the softening curve reproduced, however for $m = n$ we do have a brittle failure. For $m = 2$ half the bar localizes, and for $m > n$ we would have a strain decrease, i.e. snap-back behavior. This is impossible to achieve experimentally. Physically, that implies that the localization zone can not absorb the elastic energy released by the elastic part of the bar.

²⁹ If we use an infinite number of elements ($m \rightarrow \infty$), then from Eq. 12.12 and 12.13 we note that we would have an elastic unloading. Physically, this is impossible as it would imply failure occurred without dissipation of energy. As a result we would have:

- Loss of local material stability
- Loss of structural stability
- Loss of ellipticity
- Mesh dependence

³⁰ To illustrate this, let us consider a concrete member subjected to uniaxial displacement with the following properties: $f_t' = 3$ MPa; $E = 30$ GPa; $w_{max} = .02$ cm; $G_F = \frac{1}{2}(3 \times 10^6)(2 \times 10^{-4}) = 300$ N/m. From these properties, the peak elastic strain is $\varepsilon_0 = \frac{3 \times 10^6}{3 \times 10^{10}} = 10^{-4}$. Hence, the maximum elastic displacement is $10^{-4}L$. Let us now consider the load displacement curve ($P - u$) of this member for various lengths L .

³¹ In all cases the peak load will be $P_{max} = 3A$ where A is the cross sectional area (since results are independent of A we shall assume $A=1$). The corresponding displacement will be given by $u = \varepsilon_0 \times L$.

³² Similarly, in all cases the maximum displacement will be $u_{max} = w_{max} = .02$ cm and the corresponding load will obviously be equal to zero.

³³ The displacement corresponding to the peak load will be equal to w_{max} if $L = \frac{w_{max}}{\varepsilon_0} = \frac{2 \times 10^{-4}}{10^{-4}} = 2$ m. Fig. 12.7 illustrates the load displacement curves in terms of the length L . This figure calls for the following observations:

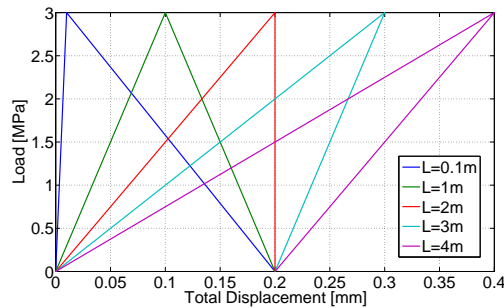


Figure 12.7: Load Displacement Curve in terms of Element Size

L (m)	0.1	1.	2.	3.	4.
$\frac{U}{A}$	15.	150.	300.	450.	600.

Table 12.1: Strain Energy versus Fracture Energy for uniaxial Concrete Specimen

1. Specimens less than 2 m long do exhibit a softening branch which can be experimentally obtained only through displacement controlled tests.
2. For a 2 m specimen, we do have a perfectly brittle response.
3. For specimens larger than 2 m, there is a snapback, which can only be hypothesized but not experimentally obtained.
4. Large specimens could still be tested, however rather than using the entire specimen length as “gage length” (or displacement/stroke control test), we would have to use a smaller gage length (through strain control tests) across a potential crack. Thus a notched specimen should be used.

³⁴ In summary, the load displacement curve of this simple test is clearly size dependent. The larger the specimen, the larger the stored strain energy which would be released to form surface energy.

³⁵ An energetic interpretation of this figure would lead us to compare the elastic energy $U = \frac{1}{2} f'_t \epsilon_u AL = \frac{1}{2} (3 \times 10^6)(10^{-4})AL = 150AL$ at peak load with the fracture energy $G_F = 300$ N/m. As long as the strain energy is smaller than the fracture energy, then we do have structural softening; if the two energies are equal, then we would have a perfectly brittle response; finally, if the elastic energy exceeds the fracture energy, then we would have a sudden failure with snap-back. Table 12.1 tabulates those energy values.

³⁶ Again we observe that $\frac{U}{A} = G_F$ for $L = 2$ m. Thus, as long as the energy released can be transformed into fracture energy, we do have a stable configuration. However if the accumulated strain energy being released (including not only the one stored in the specimen, but also in the experimental set-up) is greater than the one which can be absorbed to create new surface energy (cracks), then we do have instability.

³⁷ This simple exercise can be generalized to the analysis of simple tensile structures in which elements are either perfectly brittle and/or softening.

³⁸ Finally, and as a minor remark, for a successful post-peak experiment the total strain energy (of the specimen and of the testing frame) should be less than the fracture energy. Hence, to avoid snap-backs the testing frame should be as stiff as possible.

12.3.2.2 Dynamic Loading

Adapted from (Sluys, 1992)

12.3.2.2.1 Loss of Hyperbolicity

³⁹ We can write the dynamic equilibrium of a system along the x axis as

$$\rho \frac{\partial^2 u}{\partial t^2} = \frac{\partial \sigma_{xx}}{\partial x} + \frac{\partial \sigma_{xy}}{\partial y} + \frac{\partial \sigma_{xz}}{\partial z} \quad (12.14)$$

For a uniaxial state of stress, and with $\sigma_{xx} = f(\varepsilon_{xx})$, this equation reduces to

$$\boxed{c^2 \frac{\partial^2 u}{\partial x^2} = \frac{\partial^2 u}{\partial t^2}} \quad (12.15)$$

where $c^2 = 1/\rho \frac{\partial f}{\partial \varepsilon}$ and is the square of the speed of the wave propagation. Equation 12.15 is the classical wave equation of motion (hyperbolic equation). D'Alembert's solution of this equation is of the form

$$u = f(x + ct) + g(x - ct) \quad (12.16)$$

and a real solution exists as long as $\partial f/\partial \varepsilon \geq 0$. Thus, in a softening regime where $\partial f/\partial \varepsilon < 0$, the speed of wave propagation becomes complex and the problem is thus ill-posed. We thus have a **loss of hyperbolicity**.

12.3.2.2.2 Wave Equation for Softening Materials

40 Considering

$$\text{Equation of Motion: } \rho \frac{\partial^2 u}{\partial t^2} = \frac{\partial \dot{\sigma}}{\partial x} \quad (12.17\text{-a})$$

$$\text{Kinematic Equation: } \dot{\varepsilon} = \frac{\partial \dot{u}}{\partial x} \quad (12.17\text{-b})$$

$$\text{Constitutive Equation: } \sigma = f\varepsilon \quad (12.17\text{-c})$$

where \dot{u} is the velocity v , and the strain can be decomposed into an elastic and inelastic component.

$$\varepsilon = \varepsilon_e + \varepsilon_i \quad (12.18)$$

and thus

$$\dot{\sigma} = f' \dot{\varepsilon}_i \quad (12.19)$$

where f' denotes differentiation with respect to the inelastic strain,

41 Taking $\dot{\varepsilon}_e = \dot{\sigma}/E$, the x derivative of the preceding equation yields

$$\frac{\partial \dot{\sigma}}{\partial x} = f' \frac{\partial \dot{\varepsilon}_i}{\partial x} \quad (12.20\text{-a})$$

$$= f' \left[\frac{\partial \dot{\varepsilon}}{\partial x} - \frac{\partial \dot{\varepsilon}_e}{\partial x} \right] \quad (12.20\text{-b})$$

$$= f' \left[\frac{\partial^2 \dot{u}}{\partial x^2} - \frac{1}{E} \frac{\partial \dot{\sigma}}{\partial x} \right] \quad (12.20\text{-c})$$

$$\Rightarrow \frac{\partial \dot{\sigma}}{\partial x} = \frac{f' E}{E + f'} \frac{\partial^2 v}{\partial x^2} \quad (12.20\text{-d})$$

42 Substituting this equation into Eq. 12.17-a we obtain the wave equation for a one-dimensional strain-softening element

$$\boxed{\frac{f' + E}{c_e^2} \frac{\partial^2 v}{\partial t^2} - f' \frac{\partial^2 v}{\partial x^2} = 0} \quad (12.21)$$

where $c_e = \sqrt{E/\rho}$ is the linear elastic longitudinal wave velocity. This equation should be contrasted with Eq. 12.15 for the elastic solids.

43 One way to solve this second order partial differential equation (linear only if f' is constant) is to consider the variation of the first derivative of the velocity v with respect to both x and t

$$d \left(\frac{\partial v}{\partial t} \right) = \frac{\partial^2 v}{\partial t^2} dt + \frac{\partial^2 v}{\partial x \partial t} dx = 0 \quad (12.22\text{-a})$$

$$d \left(\frac{\partial v}{\partial x} \right) = \frac{\partial^2 v}{\partial x^2} dx + \frac{\partial^2 v}{\partial x \partial t} dt = 0 \quad (12.22\text{-b})$$

44 Combining the last three equations together yields a system of three second order differential equations

$$\begin{bmatrix} (E + f')/c_e^2 & 0 & -f' \\ dt & dx & 0 \\ 0 & dt & dx \end{bmatrix} \begin{Bmatrix} \frac{\partial^2 v}{\partial t^2} \\ \frac{\partial^2 v}{\partial x \partial t} \\ \frac{\partial^2 v}{\partial x^2} \end{Bmatrix} = 0 \quad (12.23)$$

45 The characteristic determinant is

$$\begin{vmatrix} (E + f')/c_e^2 & 0 & -f' \\ dt & dx & 0 \\ 0 & dt & dx \end{vmatrix} = \frac{E + f'}{c_e^2} dx^2 - f' dt^2 = 0 \quad (12.24)$$

If the determinant is equal to zero, then a solution for the curve in the $x - u - t$ plane should coincide with the characteristic direction.

$$\frac{dx}{dt} = \pm c_e \sqrt{\frac{f'}{E + f'}} \quad (12.25)$$

46 In a wave equation, the characteristic ($\pm dx/dt$) coincides with the wave speed ($\pm c$). In case of softening ($f' < 0$) and if we have snap-through ($f' > -E$), then the characteristics and therefore the wave speeds are imaginary. This results in a loss of hyperbolicity into ellipticity whenever softening occurs.

47 We thus have a domain governed by hyperbolicity, and another one by ellipticity where the wave can not propagate. Spatial interaction between the two is impossible, and we have an ill-posed problem.

48 A strain-softening material is thus non-dispersive. In a dispersive media, harmonic waves with different frequency propagate with different wave speeds.

49 Assuming that we have a single linear harmonic wave propagation

$$v(x, t) = A e^{i(kx - \omega t)} \quad (12.26)$$

where ω is the angular frequency, $k = 2\pi/\lambda$ the wave number. Substituting Eq. 12.26 into 12.21 we obtain

$$\omega = c_e \sqrt{\frac{f'}{E + f'}} k \quad (12.27)$$

The wave velocity being equal to

$$c_f = \frac{\omega}{k} \quad (12.28)$$

it is now apparent that in a softening material $c = c_f$ is independent of k and is therefore non-dissipative, thus all the waves would have the same imaginary speed.

50 For proper description of localisation, wave propagation must be dispersive.

12.3.3 Conclusion

In summary, Fig. 12.8 illustrates the localization of strain in a plate subjected to uniform tensile deformation.

12.4 Griffith Criterion and FPZ

51 Let us consider a cohesive crack with both normal and tangential tractions in a thin plate subjected to far field stresses, and let us assume the crack is to be under general mixed mode conditions, Figure 23.16.

52 To verify if the non-linear model satisfies Griffith criterion, it is necessary to compute the energy released by a unit crack propagation. The J-integral provides a method to evaluate the energy release rate. The J-integral is a path independent integral and in two-dimensional is given by:

$$J = \oint_{\Gamma} (W n_x - \hat{t} \frac{\partial u}{\partial x}) d\Gamma \quad (12.29)$$

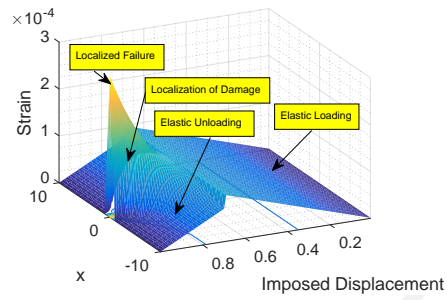


Figure 12.8: Localization of Tensile Strain in Concrete

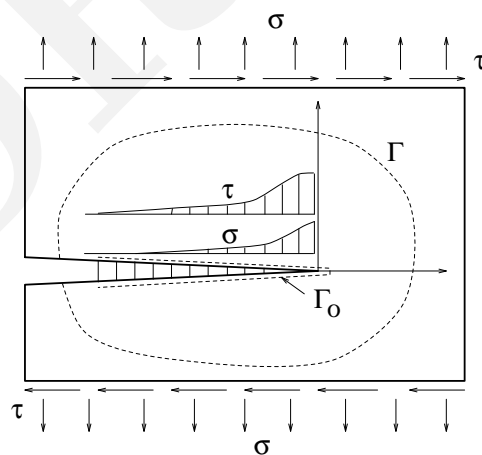


Figure 12.9: Griffith criterion in NLFM.

53 Due to its path independent character it is possible to evaluate the J-integral along the crack surfaces where $n_x = 0$.

$$J(\Gamma_o) = - \int_{\Gamma_o} \hat{\mathbf{t}} \frac{\partial \mathbf{u}}{\partial x} ds = \int_{FPZ} \left(\tau \frac{\partial u}{\partial x} + \sigma \frac{\partial v}{\partial x} \right) dx \quad (12.30)$$

54 Applying Leibnitz rule for the differentiation of definite integrals¹ the J-integral is equivalent to:

$$J(\Gamma_o) = \int_{FPZ} \left[\frac{d}{dx} \left(\int_0^u \tau du \right) \right] dx + \int_{FPZ} \left[\frac{d}{dx} \left(\int_0^v \sigma dv \right) \right] dx \quad (12.31)$$

55 The expressions in parentheses represent the surface energies dissipated in mode I and II at every point along the fracture process zone normalized with respect to crack surface.

56 Hence, we define:

$$\int_0^u \tau du = q^{II}(x), \quad \int_0^v \sigma dv = q^I(x) \quad (12.32)$$

$$J(\Gamma_o) = \int_{FPZ} \frac{dq^{II}(x)}{dx} dx + \int_{FPZ} \frac{dq^I(x)}{dx} dx = G_c^{II} + G_c^I = G_c \quad (12.33)$$

where G_c^{II} and G_c^I is the energy dissipated by a unit propagation of the cohesive crack in mode II and I respectively.

57 It should be noted that in general, G_c^{II} and G_c^I are not equivalent to G_F^{II} and G_F^I , but are rather functions of these and the stress state along the interface. However, it is possible to consider two special cases for pure mode I and II cracks.

58 In the case of pure mode I crack, the J-integral is equal to:

$$J(\Gamma_o) = \int_{FPZ} \left[\frac{d}{dx} \left(\int_0^{w_\sigma} \sigma dv \right) \right] dx = \int_0^{w_\sigma} \sigma(v) dv = G_F^I \quad (12.34)$$

59 Similarly, in the case of pure mode II crack, the J-integral is equal to:

$$J(\Gamma_o) = \int_{FPZ} \left[\frac{d}{dx} \left(\int_0^u \tau du \right) \right] dx = \int_0^{w_\tau} \tau(u) du = G_F^{II} \quad (12.35)$$

where w_σ and w_τ is the critical crack opening and sliding respectively for which normal and tangent stresses can no longer be transferred across the crack.

60 The following conclusion, can be drawn based on the basis of the previous discussion:

1. It was shown that a unit extension of a cohesive crack model dissipates energy whose amount depends on the softening laws used by the model. The amount of dissipated energy also depends on the loading conditions in FPZ. In pure mode I and mode II loading, specific fracture energies G_F^I and G_F^{II} are dissipated respectively. If the structural system cannot provide these energies, the crack would not propagate.
2. In the limiting case, when the dimensions of the analyzed problem increase, the cohesive crack gives identical results as LEFM.
3. In finite element implementation, errors are introduced due to discretization errors. In large structures, fine mesh would be necessary at the crack tip to model the fracture process zone. If the FPZ is not modeled adequately, the Griffith criterion for crack propagation is violated, and erroneous results will be obtained.

¹ $\frac{d}{dt} \int_a^b f(x, t) dx = \int_a^b \frac{\partial f}{\partial t}(x, t) dx$; In other words, differentiation and integration can be interchanged.

Chapter 13

FRACTURE MECHANICS of CONCRETE

13.1 Fracture Toughness Testing of Concrete: a Historical Perspective

Section adapted from **ACI Committee 446 (2009)**

- ¹ **ACI 446.1R-91 (2002)** describes various methods for fracture toughness testing of concrete, summarized and extended briefly here.
- ² **Kaplan (1961)**, assuming LEFM conditions prevail, was the first to attempt to determine the fracture toughness of concrete. Subsequent analysis in the 1970s and early 1980s showed that LEFM was not an appropriate model for fracture of concrete (**Walsh, 1972**), (**Walsh, 1976**), and (**Swartz et al., 1982**). In retrospect, now knowing that the fracture process zone may be very long, we understand why LEFM is inapplicable.
- ³ Many attempts have been made to measure the fracture toughness of concrete using beams, assuming the existence of an effective LEFM crack. These include various compliance calibration methods applied to beams (**Swartz et al., 1978**), (**Swartz and Go, 1984**), (**Swartz and Refai, 1989**) (**Jenq and Shah, 1985**).
- ⁴ Wedge splitting tests on various compact tension specimens have also been proposed (**Linsbauer and Tschegg, 1986**), (**Brühwiler, E., 1988**), (**Brühwiler and Whitman, 1990b**), (**Brühwiler et al., 1991**), (**Brühwiler, E. and Saouma, V.E., 1990**). The apparent fracture toughness, K_{Ic} , or more properly, K_Q , is obtained by the same method as described in for notched beam tests. The effective crack length, which accounts for the fracture process zone, is determined by the compliance method, based on finite element calibration. For that purpose, unload-reload cycles are performed during the test. Other methods such as the evaluation of fracture energy from the area under the load-displacement diagram and the size effect method are more applicable, as described next.
- ⁵ An effective LEFM crack method based on the work of **Nallathambi and Karihaloo (1986)** has been proposed to RILEM as a standard, (**Karihaloo and Nallathambi, 1987**).
- ⁶ The work of fracture method, originally developed for ceramics (**Nakayama, 1965**), (**Tattersall and Tappin, 1966**), is the first method of testing for fracture properties of concrete to be proposed as a standard (**RILEM Committee on Fracture Mechanics of Concrete - Test Methods, 1985**). The basis for applying this method to concrete was developed by Hillerborg and his co-workers, (**Hillerborg, 1985b**). Their method is based upon the cohesive crack model. The method can be applied to a variety of test specimen geometries but the proposed standard uses a beam specimen loaded in three-point bending with a central edge notch.
- ⁷ In summary, the RILEM work-of-fracture method is a practical approach, which is suitable for use in laboratories that do not have very elaborate equipment. The method incorporates a number of compromises in order to simplify testing while still obtaining useful results (**Hillerborg, 1985b**). The method is based on a theory that has gained wide acceptance, the cohesive crack model (**Hillerborg et al., 1976b**). The fracture energy method is conceptually simple, requiring no LEFM assumptions.
- ⁸ Round-robin tests from 14 laboratories incorporating about 700 beams were reported by **Hillerborg (1985a)**. With regard to variation of results within a given tests series, the coefficient of variation ranged from about 2.5% to 25% with most results around 10 to 15%.
- ⁹ There are, however, certain aspects in which the RILEM work-of-fracture method requires improvement. The size dependence of fracture energy G_{Rf} obtained according to the existing RILEM recommendation on the work of fracture method has been investigated by **Planas and Elices (1988b)** and **Planas and Elices (1988a)** on the basis of solution of an integral equation and by **Bažant and Kazemi (1990a)** on the basis of the size effect law.
- ¹⁰ The RILEM work-of-fracture method does not give results independent of the size of the cracked area for a given beam depth, and thus the value of G_{Rf} is only an approximation of the true energy parameter which characterizes the surface energy and the energy of process zone formation. Furthermore, the work-of-fracture method gives only one parameter, G_{Rf} , which is a lower bound on the true fracture energy of the concrete. Also, the true fracture energy, G_F , may not be the most important parameter in design; rather G_f (the area under the initial portion of the cohesive -COD curve may be more important).
- ¹¹ The size effect method has also been proposed as the basis for a fracture toughness test standard, (**Bažant and Kazemi, 1990b**), (**Bažant and Pfeiffer, 1987**), (**Karihaloo and Nallathambi, 1987**). This method is appealing in that only peak loads need be determined; no displacement measurements are required. However, after some testing and analysis, it has been determined that to

develop a fracture toughness test method based upon the size effect would (arguably) require an unreasonably wide range of specimen sizes, with required specimen sizes too large to be practical.

¹² A stiff direct tension test performed on a standard 6 inch diameter by 12 inch long cylinder to obtain the cohesive crack (-COD) relationship has been proposed by [Lenke and Gerstle \(2001\)](#), who have proposed a test standard based upon their work.

13.2 Nonlinear Fracture Models

13.2.1 Models

13.2.1.1 Cohesive Crack Model

¹³ The cohesive crack model of Hillerborg, is by far the most important and widely used model. It has already been discussed in Sect. ??sect:hillerborg-model.

13.2.1.2 Jenq and Shah Two Parameters Model

¹⁴ To circumvent the problems associated with nonlinear fracture, and combining the effective crack length proposed by Irwin (one which takes into account the plastic zone) with the CTOD criteria, [Jenq and Shah \(1985\)](#) have introduced a two-parameter-model. To introduce this model, let us first consider the load CMOD (crack mouth opening displacement) of a notched specimen. From this diagram the following three stages can be identified:

1. Linear elastic response up to a load corresponding approximately to $\frac{P_{cr}}{2}$. That is, the induced LFM K_I is less than $\frac{K_{Ic}}{2}$. During this stage the CTOD (crack tip opening displacement) is zero as predicted by LFM.
2. During the second stage, significant inelastic deformation takes place. This is caused by the formation of the process zone ahead of the crack tip (the existing crack being prenotched or precast, and not the result of some prior crack nucleation/extension, for which a process zone first has to be developed). This process zone formation has also been referred to as slow crack growth. As a result of this microcracking the crack tip starts to open in a fashion similar to the blunting of sharp cracks in metals due to yielding.
3. At the peak load, and for unstable geometries (i.e., increasing K_I with increasing crack length a), we have two conditions that are simultaneously satisfied:

$$K_I = K_{Ic}^S \quad (13.1)$$

$$CTOD = CTOD_c \quad (13.2)$$

where the right hand side values are now considered material properties, and the CTOD refers to the notch opening (and not crack) opening.

¹⁵ Thus in this simple, clear, and elegant model we implicitly account for softening by introducing a second parameter (CTOD), whereas in Hillerborg's approach the SIF concept is entirely discarded and replaced by a fictitious load, the distribution of which requires at least two parameters.

¹⁶ This model has been shown to yield results that are specimen size insensitive. A minor drawback of this model is that it requires an analytical expression of the COD and K_I along the crack for the geometry considered. In most cases this entails a finite element calibration.

¹⁷ This model requires an analytical expression for K_I and the $CTOD$ along the crack for each geometry considered, which in most cases can only be obtained through a finite element calibration. The model distinguishes between notch and crack length, and $CTOD_c$ is evaluated at the notch, thus the nonzero value for $CTOD_c$. Based on an extensive test program, the critical values, K_{Ic}^S and $CTOD_c$, were found to be size-independent material properties.

13.2.2 Characteristic Lengths

13.2.2.1 Hillerborg

¹⁸ Associated with this model is the characteristic length, l_{ch} , also proposed by [Hillerborg et al. \(1976a\)](#) in 1976 and which is a material property which gives an indication of the material brittleness, and is defined as:

$$l_{ch} = \frac{EG_F}{f_t'^2} \quad (13.3)$$

where, E is Young's Modulus, f'_t is the tensile strength, and G_F is the specific fracture energy. This equation should be compared with Irwin's plastic zone size Eq. 8.9

$$r_p = \frac{1}{\pi} \frac{K_I^2}{\sigma_{yld}^2} = \frac{GE}{\sigma_{yld}^2} \quad (13.4)$$

¹⁹ Hillerborg et al. (1976a) and Hillerborg, A. (1983) have shown that the ratio of structural dimension, d , to characteristic length, l_{ch} , is the dominant parameter for describing size effects using the Fictitious Crack Model (FCM). LEFM is considered to be applicable for large values of $\frac{d}{l_{ch}}$. Analysis of three point bending beams, where d is the beam depth, (Hillerborg, A., 1985) and of compact tension specimens, where d is the specimen height, (Brühwiler, E. and Roelfstra, P.E., 1989) showed that LEFM may not be valid for $d/l_{ch} < 25$, and that a ratio of $\frac{d}{l_{ch}} = 25$ would result in a 5% difference between the load carrying capacities predicted by LEFM and FCM.

13.2.2.2 Jenq and Shah

²⁰ Finally, when combined with Young's Modulus, E , a single fracture parameter describing the material, termed the critical material length, Q , was derived:

$$Q = \left(\frac{E \cdot CTOD_c}{K_{Ic}^S} \right)^2 \quad (13.5)$$

The Q -value is related to the brittleness of the specimen. For large Q -values the material exhibits a high brittleness.

13.2.2.3 Carpinteri Brittleness Number

²¹ In fracture testing, failure may be caused by different mechanisms: (1) ultimate strength collapse (SOM), and, (2) fracture collapse in terms of LEFM. The dimensionless brittleness number, s , was developed by Carpinteri to assess the existence of either one of the two failure mechanisms (Carpinteri, 1982a), (Carpinteri, 1982b), (Carpinteri, 1986). This parameter depends on the fracture toughness, K_{Ic} , the tensile strength, f'_t , and on a dimension d characteristic of the specimen (or structure) geometry being considered:

$$s = \frac{K_{Ic}}{f'_t \sqrt{d}} \quad (13.6)$$

²² For large brittleness numbers, i.e., small specimen dimension d , SOM governs, and the interpretation of tests through Fracture Mechanics (FM) is not valid. Conversely, for small brittleness numbers, fracture mechanics is applicable since the specimen is more brittle. The boundary between SOM and FM applicability, is defined by the critical brittleness number, s_0 , which is obtained from the nominal stress at failure.

13.2.3 Comparison of the Fracture Models

This section is taken from (Brühwiler et al., 1991)

²³ All models considered in this chapter are used to assess the brittleness and by consequence the applicability of LEFM. Because the models originate from different, but related, formulations describing identical physical phenomena, i.e., tensile softening of concrete and its size effects, this section will analytically show the similarity between them. Similar studies have been reported by Planas and Elices (Planas and Elices, 1988b).

²⁴ They showed in a numerical analysis that, over limited ranges, existing fracture models may be thought as approximations of one another in a mathematical sense and experimentally indistinguishable, based on size effect alone. First the relationship between Hillerborg's model and Griffith's LEFM model is rederived, and then all subsequent ones are found to be a variation of this model.

13.2.3.1 Hillerborg Characteristic Length, l_{ch}

²⁵ Hillerborg's characteristic length, l_{ch} , can be traced back to the fundamental equation governing linear elastic fracture mechanics (Hillerborg 1985a):

$$K_{Ic} = \beta \cdot \sigma_{cr} \sqrt{\pi a_{cr}} \quad (13.7)$$

where σ_{cr} and a_{cr} are critical stress and crack length, respectively, and β is a correction factor accounting for specimen geometry, boundary, and loading conditions. The fracture toughness K_{Ic} in turn can then be related to the critical energy release rate G_c as derived by Irwin (1957),

$$G_c = \frac{K_{Ic}^2}{E'} \quad (13.8)$$

where,

$$E' = \begin{cases} E & : \text{for plane stress} \\ \frac{E}{(1-\nu^2)} & : \text{for plane strain} \end{cases} \quad (13.9)$$

²⁶ Since concrete has a low Poisson's ratio ν , plane stress is primarily considered, and for "large" concrete structures in which LEFM is applicable, the strain energy release rate G_c becomes equal to G_F . Thus Eqs. 13.7 and 13.8 can be rewritten as:

$$EG_F = \beta^2 \sigma_{cr}^2 \pi a_{cr} \quad (13.10)$$

²⁷ Hillerborg's characteristic length is then obtained with $\sigma_{cr} = f'_t$, or:

$$\frac{EG_F}{f_t'^2} = \beta^2 \pi a_{cr} = l_{ch} \quad (13.11)$$

Eq. 13.11 shows that the critical crack size is of the same order of magnitude as the characteristic length l_{ch} , which, for a given specimen geometry, may be approximately proportional to the length of the fracture process zone.

13.2.3.2 Bažant Brittleness Number, β

²⁸ The intersection between the SOM and LEFM approaches in the size effect diagram (Fig. 14.10) where

$$\sigma_N^{LEFM} = \sigma_N^{SOM} \quad (13.12)$$

defines the point where the brittleness number, β is equal to 1, or $d = \lambda_0 d_a = d_0$. From

$$K_{Ic} = D \frac{P^{max}}{t \cdot d} \sqrt{d} \quad (13.13)$$

$$\frac{P^{max}}{td} = \frac{K_{Ic}}{D\sqrt{d_0}} \quad (13.14)$$

and combining with

$$\frac{P^{max}}{t \cdot d} = \frac{\sigma_N}{C} \quad (13.15)$$

we obtain

$$\frac{P^{max}}{td} = \frac{Bf'_t}{C} \quad (13.16)$$

Eqs. 13.14 and 13.16 are combined into one equation, yielding:

$$\frac{f_t'^2 d_0}{K_{Ic}^2} = \left(\frac{C}{BD} \right)^2 = \mathcal{K}^2 \quad (13.17)$$

²⁹ Because LEFM is assumed valid, substituting K_{Ic}^2 with $G_F \cdot E$ (Eq. 13.8), leads to:

$$\frac{f_t'^2 d_0}{G_F E} = \frac{d_0}{l_{ch}} = \mathcal{K}^2 \quad (13.18)$$

³⁰ Thus, the brittleness number β used to assess the applicability of LEFM in the Size Effect Law can be related to Hillerborg's characteristic length, l_{ch} . Eq. 13.18 indicates that d/l_{ch} has a similar significance to the ratio between structural dimension d and maximum aggregate size d_a in the Size Effect Law. Since l_{ch} is a comprehensive parameter to describe material fracture, the d/d_a ratio in the Size Effect Law may be replaced by d/l_{ch} (Brühwiler, E., 1988). Comparison between the Size Effect Law and the Fictitious Crack Model showed that both models yield good agreement in the prediction of the size effect (Hillerborg, A., 1985) and (?).

13.2.3.3 Carpinteri Brittleness Number, s

³¹ Squaring the expression s of the brittleness number (Eq. 13.6), and assuming that $K_{Ic}^2 = E \cdot G_F$, when LEFM is valid, the following expression is obtained:

$$s^2 = \frac{EG_F}{f_t'^2 d} = \frac{l_{ch}}{d} \quad (13.19)$$

or

$$s = \sqrt{\frac{l_{ch}}{d}} \quad (13.20)$$

13.2.3.4 Jenq and Shah's Critical Material Length, Q

³² In the Fictitious Crack Model, the area under the softening law, relating the tensile stress, σ , to fictitious crack width, w , is defined as the specific fracture energy, G_F , or:

$$G_F = \mathcal{C} f_t' \cdot w_c \quad (13.21)$$

where, \mathcal{C} is a constant characterizing the σ vs. w curve, and w_c is the crack width for which $\sigma = 0$. At the tip of the real crack (or notch) in the FCM, w_c can be interpreted as the critical crack tip opening displacement, $CTOD_c$, according to the Two-Parameter Model. Therefore, $CTOD_c$ is set equal to w_c , and Eq. 13.21 can be rewritten as:

$$CTOD_c = \frac{G_F}{\mathcal{C} f_t'} \quad (13.22)$$

Combining Q (Eq. 13.5) with Eq. 13.22:

$$Q = \frac{E^2 G_F^2}{K_{Ic}^2 \mathcal{C}^2 f_t'^2} \quad (13.23)$$

With $K_{Ic}^2 = G_F E$, Q is finally related to l_{ch} :

$$Q = \frac{EG_F}{\mathcal{C}^2 f_t'^2} = \frac{l_{ch}}{\mathcal{C}^2} \quad (13.24)$$

13.2.3.5 Discussion

³³ Table 13.1 summarizes the preceding analysis of models and indicates that all models are related to Hillerborg's characteristic

Table 13.1: Summary relations for the concrete fracture models.

Author	Hillerborg	Carpinteri	Jenq & Shah	Bažant
Year	1976	1982	1985	1984
Parameter	l_{ch}	s	Q	d_0
Relation	$l_{ch} = \frac{EG_F}{f_t'^2}$	$s = \sqrt{\frac{l_{ch}}{d}}$	$Q = \frac{l_{ch}}{\mathcal{C}^2}$	$d_0 = \mathcal{K}^2 l_{ch}$

length, and thus related to Griffith's model. Although relations among all the models have been demonstrated, differences in experimental results are due to the initial assumptions of very large concrete structures, where LEFM is valid, i.e., $G_c = \frac{K_{Ic}^2}{E'}$ and $G_c = G_F$. Yet, the results of the comparisons indicate a unified approach could possibly be postulated. Validation of such an approach in the laboratory would prove difficult due to specimen size considerations.

13.2.4 Model Selection

³⁴ In light of the diversity of models, Engineers should exercise great care in selecting an appropriate model. Model selection should account for:

1. Crack size: In a “large” crack, the effect of the process zone is smaller than for a “short” one. Thus LEFM is more applicable for the large ones.
2. Type of loading: If a structure is subjected to a load rather than imposed displacements (such as foundation settlements), than only a pre-peak response is of importance. Under those conditions non-linear effects may be negligible compared to the ones induced by LEFM.
3. Stability¹: In a structure subjected to imposed load rather than imposed displacement non-linear effects are not be as negligible in a stable structure as they are in an unstable one.

Thus Table 13.2 provides some guidance for model selection. Accordingly we should select:

1. An NLFM for an arch dam which cracking is caused by foundation settlement.
2. An LEFM model for a dam in which cracking is caused by flooding, no matter how small or large the crack is.

Loading	“Small” Crack	“Large” Crack
Load Control, Unstable	LEFM	LEFM
Load Control, Stable	NLFM	LEFM
Displacement Control	NLFM	LEFM

Table 13.2: When to Use LEFM or NLFM Fracture Models

³⁵ In all cases, it should be emphasized that ideally a non-linear analysis is to be undertaken, however in many (but not all) cases the complexity and expenses associated with such an analysis yield results very close to the ones obtained from a linear elastic ones. Thus ultimately the type of analysis to be undertaken hinges on both technical and economical considerations.

³⁶ Amongst the competing models for NLFM, the one recommended, and by far the most widely used, is the one based on the Cohesive Crack Model (CHM).

13.3 Fracture Energies G_f and G_F

Section adapted from (Bažant et al., 2002)

³⁷ One essential parameter of the cohesive (or fictitious) crack model is the tensile strength of the material, f_t' . The softening stress-separation curve of the cohesive crack model (Hillerborg et al. 1976, Petersson 1981, Hillerborg 1983, 1985a,b), is usually characterized by two parameters. They can be chosen as either

1. f_t' and fracture energy G_F , representing the area under the complete curve (Rice 1969, Hillerborg et al. 1976, Petersson 1991, Hillerborg 1983, 1985a,b), or
2. f_t' and fracture energy G_f , representing the area under the initial tangent of the softening curve, (Elices et al., 1992).

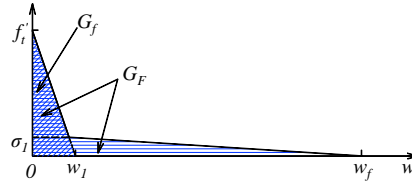
³⁸ The fracture energies G_f and G_F are two different material characteristics which are only partially correlated. G_F can be estimated from G_f and vice versa, but not accurately. Ideally, both G_f and G_F should be measured and used for calibrating the initial slope and the tail of the softening curve of the cohesive crack model (or crack band model), which are both needed for fracture analysis of structures.

³⁹ For concrete, as a rough approximation

$$G_F \approx 2.5G_f \tag{13.25}$$

as reported by Planas and Elices (1992) and further verified by Bažant and Becq-Giraudon (2001). Knowing this ratio, one can calibrate a bilinear softening curve, provided that the relative height of the knee (point of slope change, Fig. 13.1) is also known. The value $G_F = G_f = 2.5$, however, is doubtless a rather crude estimate. Properly, it should be regarded as a random quantity. The coefficient of variation of the ratio $G_F = G_f$ may be roughly guessed as perhaps $\omega_{G_F} \approx 40\%$.

¹ A stable structure is one in which K_I decreases with crack length, in an unstable one the stress intensity factor K_I increases with crack length.

Figure 13.1: G_F vs G_f

13.3.1 Maximum Load is Controlled by G_f , Postpeak by G_F

⁴⁰ The maximum loads of structures depend mainly on the initial tangent of the softening stress- separation curve, which is fully characterized by G_f . They are almost independent of the tail of this curve, which depends mainly of G_F .

⁴¹ The prediction of the entire postpeak softening load-deflection curve of a structure, which is often of secondary interest for design, depends mainly on the tail of the stress- separation curve of the cohesive crack model, and thus on G_F .

13.3.2 Statistical Scatter of G_f and G_F

⁴² An important consideration for the choice of fracture test is the statistical scatter of the measured quantity. As is well known, for estimating the mean, one can usually do with only about 6 tests. However, for a meaningful determination of the standard deviation, the number of tests must be of the order of 100. There is no test data set of that scale in the literature, for neither G_f nor G_F . Besides, even if such a data set were available, its usefulness would be limited because it would be difficult to infer from it the standard deviations for concretes of a different composition, curing, age and hygrothermal history.

⁴³ Thus, if any statistical information should be gained, it is inevitable to study the fracture test data for all concretes. Here the situation has become rosy: While a dozen years ago only about a dozen test series were available in the literature, **Bazant and Becq-Giraudon (2001)** collected from the literature 238 test series from different laboratories throughout the world, conducted on different concretes. Of these, 77 test series concerned G_f (or the related fracture toughness K_c), and 161 G_F . However, to be able to extract any statistics from these data, the basic deterministic trends must somehow be filtered out first, at least approximately.

⁴⁴ One must, therefore, first establish formulae that approximately describe the deterministic (mean) dependence of G_f and G_F on the basic characteristics of concrete. Using extensive nonlinear optimization studies based on the Levenberg-Marquardt algorithm, **Bazant and Becq-Giraudon (2001)** obtained two simple approximate formulae for the means of G_f and G_F as functions of the compressive strength f'_c , maximum aggregate size d_a , water-cement ratio w/c , and shape of aggregate (crushed or river);

$$\begin{aligned}
 G_f &= \alpha_0 \left(\frac{f'_c}{0.051} \right)^{0.46} \left(1 + \frac{d_a}{11.27} \right)^{0.22} \left(\frac{w}{c} \right)^{-0.30} & \omega_{G_f} &= 17.8\% \\
 G_F &= 2.5\alpha_0 \left(\frac{f'_c}{0.051} \right)^{0.46} \left(1 + \frac{d_a}{11.27} \right)^{0.22} \left(\frac{w}{c} \right)^{-0.30} & \omega_{G_F} &= 29.9\% \\
 c_f &= \exp \left[\gamma_0 \left(\frac{f'_c}{0.022} \right)^{-0.019} \left(1 + \frac{d_a}{15.05} \right)^{0.72} \left(\frac{w}{c} \right)^{0.2} \right] & \omega_{c_f} &= 47.6\%
 \end{aligned} \tag{13.26}$$

⁴⁵ Here $\alpha_0 = \gamma_0 = 1$ for rounded aggregates, while $\alpha_0 = 1.44$ and $\gamma_0 = 1.12$ for crushed or angular aggregates; ω_{G_f} and ω_{G_F} are the coefficients of variation of the ratios G_f^{test}/G_f and G_F^{test}/G_F , for which a normal distribution may be assumed, and ω_{c_f} is the coefficient of variation of c_f^{test}/c_f , for which a lognormal distribution should be assumed (ω_{c_f} is approximately equal to the standard deviation of $\ln c_f$).

⁴⁶ The fracture toughness and the mean critical crack tip opening displacement, used in the Jenq-Shah two-parameter method, are then predicted as

$$K_c = \sqrt{E'G_f} \quad \delta_{CTOD} = \sqrt{\frac{32 G_f c_f}{\pi E'}} \tag{13.27}$$

⁴⁷ In addition, they obtained a mean prediction formula for c_f , the effective length of the fracture process zone, from which δ_{CTOD} , the critical crack-tip opening displacement can be easily determined as well. The optimization studies confirmed that the optimum value of the ratio $G_F=G_f$ is about 2.5, and did not reveal any systematic dependence of this ratio on the basic parameters f'_c , d_a and w/c .

⁴⁸ Based on these mean predictions formulae, plots of the measured versus predicted values of G_f and G_F (as well as c_f) were constructed; see Fig. 13.2. The coefficients of variation of the vertical deviations of the data points from the the straight line of

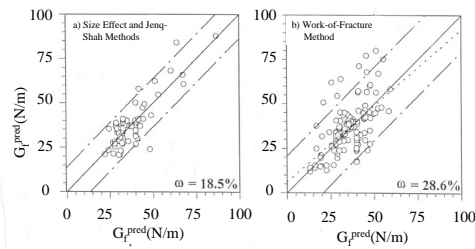


Figure 13.2: G_F^{pred} Based on

slope 1 (i.e., the line representing the case of perfect prediction by the deterministic formula), were found to be

$$\begin{aligned} \omega_{G_f} &= 18.5\% & \text{for } G_f \\ \omega_{G_F} &= 8.6\% & \text{for } G_F \end{aligned} \quad (13.28)$$

The large difference between these two values has significant implications for the choice of the testing standard, which we discuss next.

⁴⁹ It must, of course, be admitted that the errors of the prediction formulae for G_f and G_F , which are owed to limitations in the understanding of the effect of the differences in concrete composition, etc., make doubtless large contributions to the aforementioned coefficients of variations. However, there is no reason why these contributions to scatter should be biased in favor one or the other fracture energy. Eliminating the mean trend by an imperfect prediction formula is inevitable if any statistical comparisons at all should be made at the present level of experimental evidence. Therefore, we must accept that the difference between these two coefficients of variation characterizes the difference in the random scatter of either G_f and G_F , or their measurement methods, or (more likely) both.

⁵⁰ Why the data on G_F (Fig. 13.2 right) exhibit a much higher scatter than those on G_f ? The reasons appear to be: (1) An inherently higher randomness of the tail compared to the initial portion of the softening curve; (2) uncertainty in extrapolating the tail to zero stress; and (3) difficulties in eliminating energy dissipation not caused by fracture and in achieving independence of the results from the specimen size (Planas et al., 1992).

⁵¹ The fracture parameters measured by the size effect method have the advantage that they are, by definition, size and shape independent if the correct size effect law for the given size range is known.

13.3.3 Level I and Level II Testing

⁵² At the (pre-FraMCoS-2) workshop of European and American specialists in Cardiff in 1995, organized by B.I.G. Barr and S.E. Swartz, it was agreed that the testing standard should specify two levels of testing:

- At level I, acceptable for structures of not too high fracture sensitivity, one needs to measure only one of the two fracture energies, either G_F or G_f (a consensus at that workshop was to use measurements confined to the maximum load region and ignoring the tail).
- At level II, appropriate for structures of high sensitivity to fracture and size effect, both G_F and G_f (or K_c instead of G_f) should be directly measured.

⁵³ If the cohesive crack model is calibrated by a level I test, one must of course assume in advance the shape of the softening-stress separation curve, i.e., fix the ratios $G_F = G_f$ and σ_{knee}/f'_t based on prior knowledge. Therefore,

- If G_F is measured, one must estimate $G_f \approx 0.4G_F$, and from that determine the initial slope of the softening curve.
- If G_f is measured, and if the tail of the softening curve is needed, one must estimate $G_F \approx 2.5G_f$.

13.4 Proposed ACI/ASCE Test Methods

13.4.1 Test 1: Determination of Jenq & Shah Parameters ($K_{Ic(tp)}$ And $CTOD_{c(tp)}$)

Section adapted from ACI Committee 446 (2009)

⁵⁴ This test method determines indices of fracture toughness, $K_{Ic(tp)}$, critical crack tip opening displacement, $CTOD_{c(tp)}$ of hardened concrete with maximum aggregate size of 1.33" (3.39 cm) or less.

⁵⁵ The values of $K_{Ic(tp)}$, and $CTOD_{c(tp)}$ stated in SI units, are to be regarded as the standard.

⁵⁶ Supporting references: (Jenq and Shah, 1985) (RILEM Committee on Fracture Mechanics of Concrete-Test Methods, 1990) (Guinea et al., 1998).

13.4.1.1 Terminology

13.4.1.1.1 Definitions

linear elastic fracture mechanics (LEFM) : a theory of fracture mechanics crucial to the understanding of this test standard. LEFM assumes linear elastic material behavior together with a perfectly sharp crack with traction-free surfaces.

critical effective crack: a conceptual LEFM crack whose length, a_c , is selected to provide the same compliance as the observed unloading compliance at or above 95% of peak load.

critical stress intensity factor ($K_{Ic(tp)}$) the stress intensity factor of the critical effective crack, calculated using the measured maximum load, P_{max} , according to this test standard.

critical crack tip opening displacement ($CTOD_{c(tp)}$) the crack opening displacement calculated using LEFM at the original notch tip of the specimen, using the measured maximum load P_{max} and the critical effective crack length, a_c , according to this test standard.

13.4.1.1.2 Abbreviations

a_o	initial notch length
a_c	length of critical effective crack
b	width of specimen
C_i	initial compliance of specimen
C_u	unloading compliance of the specimen
$CMOD$	crack mouth opening displacement
$CTOD_{c(tp)}$	critical crack tip opening displacement, according to this test standard
d	depth of specimen
D_{max}	maximum size of coarse aggregate
g	acceleration of gravity
HO	thickness of clip gage
$K_{Ic(tp)}$	critical stress intensity factor, also called fracture toughness, according to this test standard
L	length of specimen
P	load on specimen
P_{max}	peak load on specimen
S	test span of the specimen
W_o	self-weight of specimen
W	weight of the specimen between supports = $W_o S/L$
TPFM	two-parameter fracture model

13.4.1.2 Summary of Test Method

⁵⁷ This test method uses center-point loading of notched-beam specimens of fixed size to determine three standard fracture parameters of concrete.

⁵⁸ The test employs a closed-loop-testing machine to simultaneously measure applied load, and crack mouth opening displacement, under crack mouth opening displacement control, Fig. ??.

⁵⁹ The method provides for computation of two fracture parameters: the critical stress intensity factor $K_{Ic(tp)}$, and the critical crack tip opening displacement $CTOD_{c(tp)}$.

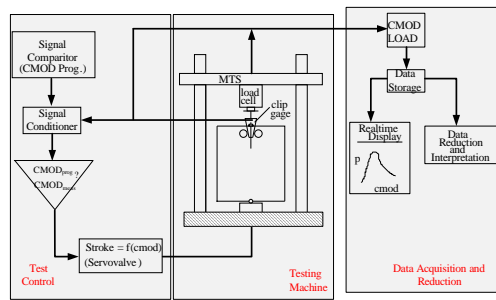


Figure 13.3: Servo-Controlled Test Setup for Concrete K_{Ic} and G_F

13.4.1.3 Apparatus

60 The loading apparatus shall conform to the requirements of the section on Loading Apparatus in C 293.

61 The loading fixture shall be designed to minimize the unwanted force contributions. A diagram of an apparatus that accomplishes this purpose is shown in Fig. 13.4.

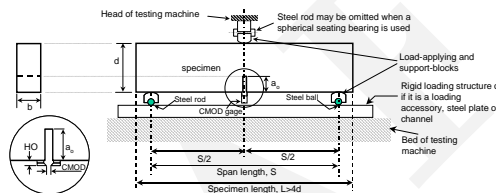


Figure 13.4: Test Apparatus for Two Parameter Model

62 The testing machine shall provide closed-loop control, with the crack mouth opening displacement (CMOD) as the feedback signal. The testing machine shall be of a type having sufficient load capacity and stiffness. In addition, the testing machine shall conform to the requirements of the section on Basis of Verification, Corrections, and Time Interval Between Verifications, of Practices for Verification of Testing Machines, E4.

63 A displacement-measuring gage shall be used to measure the opening of the mouth of the notch during testing. A clip gage, LVDT, or strain gage based extensometer is recommended to measure the CMOD. If a clip gage is used it shall be attached by using holders, as shown in Figure 1. The holders should be firmly attached to the lower concrete surface, within 0.5 in (1.29 cm) of the axial vertical center plane of the beam, using glue or epoxy to ensure that they do not move during the test. If an extensometer is used, it shall be attached to the surface of concrete either directly or by using holders. If the extensometer is attached directly to the concrete surface care must be taken to ensure that the extensometer does not move relative to the concrete surface.

64 The displacement gage output shall indicate relative displacement of two accurately located gage positions spanning the notch mouth. Accurate positioning of the gage is essential.

65 Working range of the gage used for measuring CMOD shall not exceed +0.02in (+0.508mm).

66 The clip gage or extensometer shall be checked for linearity, preferably using an extensometer calibrator or other suitable device. The gage shall be calibrated to within 1% of the working range.

67 The percentage of error for the loads within the proposed range of use of the testing machine shall not exceed +1% of the indicated load.

13.4.1.4 Specimens

68 The specimens shall conform to all requirements of Practice C 31, Practice C 192, and Test Method C 293 applicable to beam and prism specimens with the following exceptions. The span, S , shall be within 0.2 in. (0.508 cm) of 18 in. (45.72 cm). The width,

b , and depth, d , shall both be within 0.1 in. (0.254 cm) of 6 in. (15.24 cm). The beam length, L , shall be within 0.5 in. (1.27 cm) of 21 in. (53.34 cm).

⁶⁹ The top and the bottom faces of the specimen shall be within 2 degrees of parallel. The side faces of the specimen shall be within 2 degrees of perpendicular with the bottom face. All surfaces within $d/2$ of the beam centerline shall be smooth and free of indentations or holes.

13.4.1.5 Procedure

⁷⁰ Fracture tests of moist cured specimens shall be made as soon as practical after removal from moist storage. A notch shall be introduced within 0.25 in. (6.35 mm) of the mid-length of the beam using a band saw or diamond tipped saw such that the width of the cut is no wider than 3 mm. The notch shall be introduced as soon as possible prior to testing. The specimen shall be kept moist at all times and shall be protected from moisture loss by wrapping it in a plastic or wet burlap sheet at the time of test.

⁷¹ The notch shall be cut within one degree of perpendicular to the longitudinal axis of the specimen. The notch depth, a_o , shall satisfy the inequality $0.25d < a_o < 0.33d$.

⁷² The length of the notch, a_o , shall be measured from the bottom of the beam, on both faces, using a ruler with an accuracy of 0.5 mm. Each measurement shall be made three times on each face. The measured notch depth on each side shall not differ by more than 5 percent. The notch length shall equal the average of the six measurements.

13.4.1.6 Specimen Testing

⁷³ The specimen shall be placed in a testing machine in a center-point loading configuration as shown in Fig. 13.4. Use a closed-loop test machine with CMOD as the feedback. Continuously monitor both CMOD and the applied load, P , during the test.

⁷⁴ Apply load using a constant rate of increment of CMOD such that the peak load, P_{max} , is reached in between 1 and 10 minutes.

⁷⁵ When the load has passed the maximum load and decreased to no more than 95% of the peak load, reduce the applied load to between 1% and 5% of the peak load. Unloading can be performed in CMOD or load control, and shall be accomplished in no less than 1 minute and no more than 10 minutes. Reload using the same loading rate until the load has passed the maximum load. A typical loading and unloading curve for concrete is shown in Fig. 13.5.

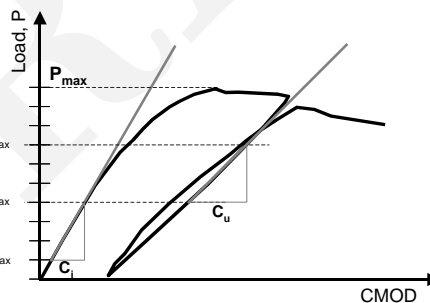


Figure 13.5: Typical response for a notched beam in CMOD control using the center-point loading method

13.4.1.7 Measured Values

⁷⁶ The following measured values shall be reported for each test: the dimensions L , S , b , and d ; the mass, m_0 ; and the initial notch length, a_0 . Report also the P-CMOD response of the specimen, including the one cycle of loading and unloading in the post-peak.

13.4.1.8 Calculation

⁷⁷ Calculation of fracture parameters, $K_{Ic(tp)}$ and $CTOD_{c(tp)}$, using the two-parameter fracture method (TPFM).

⁷⁸ The TPFM is used to determine $K_{Ic(tp)}$ and $CTOD_{c(tp)}$ from the measured compliance change in the load-CMOD response of a beam with a given initial notch length.

79 Estimate modulus of elasticity, E :

$$E = \frac{6S a_0 V(\alpha_0)}{C_i b d^2} \quad (13.29-a)$$

$$V(\alpha) = 0.8 - 1.7\alpha + 2.4\alpha^2 + \frac{0.66}{(1-\alpha)^2} + \frac{4}{S/d} (-0.04 - 0.58\alpha + 1.47\alpha^2 - 2.04\alpha^3) \quad (13.29-b)$$

where C_i is the loading compliance (the inverse of the initial slope of the load-CMOD curve), $\alpha_0 = (a_0 + HO)/(d + HO)$, d is the depth of the beam, S is the specimen loading spa.

80 To determine C_i a straight line shall be fit to the P-CMOD response between 10% and 40% of the peak load. Inverse of the slope of this line is C_i .

81 Determine the critical effective crack length, a_c (a_o + stable crack growth at peak load) from the following equation:

$$E = \frac{6s a_c V(\alpha_c)}{C_u b d^2} \quad (13.30)$$

where C_u is the inverse of the slope of the load-CMOD unloading curve, $\alpha_c = (a_c + HO)/(d + HO)$, and E is obtained from Eq. 13.29-a. C_u shall be determined from the P-CMOD curve obtained when unloading the specimen as described above. A straight line shall be fit to the unloading P-CMOD curve between 70% and 40% of the maximum load, P_{max} . Inverse of the slope of this line is C_u .

82 Calculate the critical stress intensity factor index, $K_{Ic(tp)}$:

$$K_{Ic(tp)} = 3(P_{max} + 0.5W) \frac{S\sqrt{\pi a_c} F(\alpha)}{2bd^2} \quad (13.31-a)$$

$$F(\alpha) = \frac{f_1(\alpha) + \frac{4}{S/d}(f_2(\alpha) - f_1(\alpha))}{\sqrt{\pi}(1+3\alpha)(1-\alpha)^{3/2}} \quad (13.31-b)$$

$$f_1(\alpha) = 1.99 + 0.83\alpha - 0.31\alpha^2 + 0.14\alpha^3 \quad (13.31-c)$$

$$f_2(\alpha) = 1.9 + 0.41\alpha + 0.51\alpha^2 - 0.17\alpha^3 \quad (13.31-d)$$

where P_{max} is the maximum load, $\alpha = a_c/d$.

83 Calculate the critical crack tip opening displacement index, $CTOD_{c(tp)}$:

$$CTOD_{c(tp)} = \frac{6P_{max} S a_c V(\alpha)}{E b d^2} [(1-\beta)^2 + (1.081 - 1.149\alpha)(\beta - \beta^2)]^{1/2} \quad (13.32-a)$$

$$V(\alpha) = 0.76 - 2.28\alpha + 3.87\alpha^2 - 2.04\alpha^3 + \frac{0.66}{(1-\alpha)^2} \quad (13.32-b)$$

where $\alpha = a_c/d$, and $\beta = a_o/a_c$.

13.4.2 Test 2: Cohesive Crack Model Parameters; Level 1 (G_f)

84 This standard provides a quantitative test method for determining fracture parameters of hardened concrete. It assumes that the essential aspects of fracture of concrete can be described by a cohesive or fictitious crack model, which is completely described by the cohesive stress versus crack opening curve, (Hillerborg, A., 1985). This method covers the determination of the initial linear portion of this curve for concrete using a combination of simple tests which require measuring peak loads only. The determination of a bilinear approximation of the full cohesive stress versus crack opening curve will be covered in a different standard.

85 This standard covers only mortars and concrete with maximum aggregate size of up to 25 mm.

86 The values stated in SI units are to be regarded as the standard.

13.4.2.1 Terminology

13.4.2.1.1 Definitions

Stress versus crack opening curve or softening curve the relationship between the stress (σ) transferred between the faces of a cohesive crack and the crack opening (w), Fig. 13.6.

Tensile strength (f'_t), the maximum cohesive stress or stress at zero crack opening.

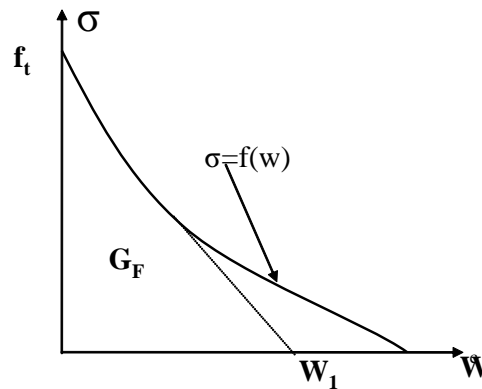


Figure 13.6: Softening Curve and Initial Linear Portion

Linear initial portion of the softening curve the linear approximation to the initial part of the softening curve as shown by the dashed line in Fig. 1. It is defined by the tensile strength (f_t) and the horizontal intercept (w_1) (Planas et al., 1999).

Brittleness length (l_1) defined as (Refer to Eq. 13.11)

$$l_1 = \frac{Ew_1}{2f_t'} \quad (13.33)$$

Net plastic flexural strength (f_p) the tensile strength of an ideal material rigid-perfectly plastic in tension and rigid in compression that would give the same peak load as the actual specimen for a beam of identical dimensions.

13.4.2.1.2 Notation and Abbreviations

a_0	notch length (initial crack length)
b	ligament length = $D - a_0$
B	thickness of specimen
d_a	maximum aggregate size
D	depth of specimen
E	elastic modulus
E_m	mean elastic modulus
f_t'	tensile strength
f_p	net plastic flexural strength
g	specific gravity = 9.81 m s^{-2}
l_1	brittleness length
L	length of specimen
m	mass of the specimen
N	notch width
$P_{m.a.x}$	corrected peak load of a specimen
$P'_{m.a.x}$	measured peak load of a specimen
S	test span of the specimen
T	splitting tensile strength
T_m	mean splitting tensile strength
w	cohesive crack opening
w_1	horizontal intercept of the linear initial portion of the softening curve
α_0	relative notch length

13.4.2.2 Summary of Test Method

⁸⁷ In this test method, notched beams and cylindrical concrete specimens are tested to determine fracture parameters of concrete.

⁸⁸ The cohesive tensile strength (f_t') is approximated by the splitting tensile strength of cylindrical concrete specimens tested according to 496 (2000) (so-called Brazilian Test, as illustrated in Fig. 13.7), with minor modifications.

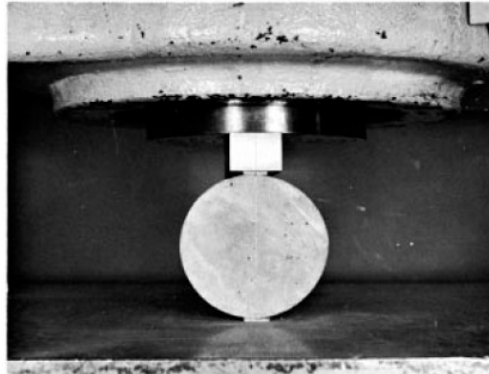


Figure 13.7: “Brazilian Test, (?)”

⁸⁹ Center-point loading tests are run up to peak load on notched concrete beams and the net plastic flexural strength (f_p) is determined from the peak load.

⁹⁰ From the results of tensile strength (f_t) and net plastic flexural strength (f_p), the brittleness length (l_1) is determined.

⁹¹ The elastic modulus (E) is determined according to ASTM C 469 test method.

⁹² The horizontal intercept (w_1) is determined from the brittleness length (l_1), the elastic modulus (E) and the tensile strength (f_t') solving from Eq. 13.33.

13.4.2.3 Significance and Use

⁹³ This test method is used to determine the initial linear portion of the softening curve for the cohesive crack model.

⁹⁴ The cohesive crack model describes in a simplified manner the cracking of concrete keeping a good balance between accuracy and complexity.

⁹⁵ Knowledge of only the linear initial portion of the softening curve is enough to solve some practical problems such as the determination of structural peak loads (Planas et al., 1999) or the description of the initial stages of cracking.

⁹⁶ Care must be exercised in the interpretation and use of the material properties obtained by this test method, because they are sensitive to any of the factors affecting concrete behavior such as batching and mixing procedures, the methods of sampling, molding and fabrication and the age, and temperature and moisture conditions during curing.

13.4.2.4 Specimens

⁹⁷ Cylindrical specimens shall be used to determine the splitting tensile strength and the static elastic modulus. The geometry and manufacture of these specimens shall conform to the general provisions of Practices C 31 (field specimens) or C 192 (laboratory specimens).

⁹⁸ Cylindrical specimens for splitting tensile strength shall further conform to any special provisions in Test Method C 496.

⁹⁹ Cylindrical specimens for static elastic modulus shall further conform to any special provisions in Test Method C 469.

¹⁰⁰ Beam specimens shall be used to determine the net plastic flexural strength. The geometry and manufacture of these specimens shall conform to the general provisions of Practices C 31 (field specimens) or C 192 (laboratory specimens) applicable to beam and prism specimens.

¹⁰¹ A minimum of six cylindrical specimens and three beam specimens shall be cast. Whenever practical, all the specimens must be cast from the same concrete batch. If this is not possible, a number of cylinder specimens twice the number of beam specimens must be obtained from each batch. A minimum of three split cylinders, three cylinders for elastic modulus and three beams must be tested.

¹⁰² The beam specimens shall be prismatic beams of rectangular cross section with a sawn central notch Fig. 13.8. The beams

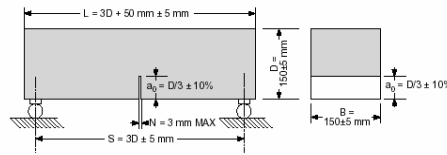


Figure 13.8: Specimen Geometry and Dimensions

defined in this standard are not to be used for materials with a maximum aggregate size d_a larger than 25 mm.

1. The beam thickness (B) must be 150 ± 5 mm.
2. The beam depth (D) must be 150 ± 5 mm.
3. The loading span (S) must be equal to three times the beam depth ($3D$), within ± 5 mm.
4. The total length (L) of the specimen shall be 50 mm longer than three times the beam depth ($3D + 50$ mm) within ± 5 mm.
5. The nominal notch depth (a_0) shall be equal $D/3$. Deviations up to 10% of the nominal value may be accepted for a whole test series ($0.30 \leq a_0/D \leq 0.37$). But, within a series, notch depths of individual specimens must not deviate from the mean more than 2%.
6. The notch width (N) must be no larger than 3 mm.

13.4.2.5 Casting, Curing and Conservation

103 After demolding, cure and conserve the specimens in a lime saturated bath at $23 \pm 2^\circ$ C until testing time.

104 After the removal of the specimen from the bath, and until the end of the test, drying of the surface of the specimen must be prevented.

13.4.2.6 Procedure

105 The procedure for splitting tensile tests shall be as described in the Test Method C 496, except that the loading rate shall be within the range 500 to 1000 kPa/min all the way up to the peak load. Provisions shall be taken for measuring and recording the loading rate up to the peak.

106 The procedure for static elastic modulus tests shall be as described in the Test Method C 469.

107 Beam Specimen Preparation: The preparation of the beam specimens for testing may include grinding of the load bearing areas, and notching.

108 Gently place the specimen on the loading device. At this stage the rolling supports may be clamped to ease the placement. Carefully center the specimen so that the notch is at mid position between the supports within 1 mm, and the mid-vertical-longitudinal plane of the specimen coincides with the loading plane defined by the shafts b and h in Fig. 13.9 (within 1 mm). An external frame with centering screws may prove useful to facilitate this task.

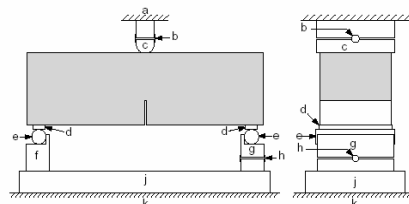


Figure 13.9: Sketch of a Loading Apparatus

109 Verify that the load channel is zeroed, and slowly pre-load the specimen up to a load of between 5 and 10 % of the estimated maximum load. After the test, this pre-load must be checked not to have exceeded 15% of the actual peak load. If this limit had been exceeded, the test must be considered invalid. During the pre-load, the spherical or cylindrical seatings must be free (and even helped) to accommodate any initial geometrical misfit.

110 Unclamp the rollers and run the test at constant crosshead rate. The rate must be selected so that the peak load is reached within 3 to 5 min.

111 The test can be stopped after peak load is reached.

13.4.2.7 Calculations

13.4.2.7.1 Tensile strength, f'_t 112 Calculate the splitting tensile strength (T) of each cylinder specimen according to ASTM C 496, in SI units (kPa).

113 Determine the mean splitting tensile strength (T_m) by averaging over all the specimens.

114 Determine the tensile strength of concrete (for the cohesive crack model) as

$$f_t = \frac{T_m}{1000} \quad (13.34)$$

where T_m = mean splitting tensile strength, kPa, f'_t = tensile strength, MPa.

13.4.2.7.2 Elastic modulus, E 115 Calculate the modulus of elasticity (E) of each cylinder specimen according to ASTM C 469, in SI units (MPa).

116 Determine the mean elastic modulus (E_m) by averaging over all the specimens.

13.4.2.7.3 Net plastic flexural strength, f_p 117 Calculate the net plastic flexural strength of each notched beam according to the following procedure:

1. From the test record or machine memory, determine the maximum load P'_{max} measured by the load cell.
2. Determine the self-weight equivalent load P_0 as

$$P_0 = mg \left(1 - \frac{L}{2S} \right) \quad (13.35)$$

where P_0 = self-weight equivalent load, N. m = specimen mass, kg. g = specific gravity = 9.80 m s^{-2} , L = specimen length, mm. S = loading span, mm.

3. Determine the maximum load corrected to take into account the weight of the specimen as

$$P_{max} = P'_{max} + P_0 \quad (13.36)$$

where P_{max} = corrected peak load, N; P'_{max} = measured peak load, N; P_0 = self-weight equivalent load, N.

4. Determine the net plastic flexural strength of the beam as:

$$f_p = \frac{P_{max}S}{2Bb^2} \quad (13.37)$$

where f_p = net plastic flexural strength, MPa; P_{max} = corrected peak load, N; B = beam thickness, mm; $b = D - a_0$ = beam ligament, mm; D = depth of specimen, mm; a_0 = notch length, mm; S = loading span, mm.

13.4.2.7.4 Brittleness length, l_1 , and horizontal intercept, w_1 118 For each specimen, determine the brittleness length l_1

$$l_1 = \kappa D \left[\frac{11.2}{(x^2 - 1)^2} + \frac{2.365}{x^2} \right] \quad (13.38)$$

where l_1 = brittleness length, mm; $\kappa = 1 - \alpha_0^{1.7}$; $\alpha_0 = a_0/D$ = notch-to-depth ratio; D = beam depth, mm; a_0 = notch length, mm; $x = f_t/f_p$; f_p = net plastic flexural strength, MPa; f_t = tensile strength, MPa.

119 Determine the average brittleness length l_{1m} as the mean of the determinations for individual specimens.

120 Determine the horizontal intercept of the softening curve (w_1) as

$$w_1 = 1000 \frac{2f_t}{E_m} l_{1m} \quad (13.39)$$

where w_1 = horizontal intercept, μm (microns); f_t = tensile strength, MPa; E_m = mean elastic modulus, MPa; l_{1m} = brittleness length, mm.

121 Finally we obtain the fracture energy from $G_f = \frac{f_t w_1}{2}$.

13.4.3 Test 3: Cohesive Crack Model Parameters; Level 2 (G_F)

122 This standard provides a quantitative test method for determining fracture parameters of hardened concrete. It assumes that the essential aspects of fracture of concrete can be described by a cohesive or fictitious crack model, which is completely described by the cohesive stress versus crack opening curve (Hillerborg, A., 1985).

123 This method covers the determination of a bilinear approximation of this curve for concrete using a combination of split cylinder tests and bending tests on notched beams.

124 This standard covers only mortars and concrete with maximum aggregate size of up to 25 mm.

125 The values stated in SI units are to be regarded as the standard.

13.4.3.1 Terminology

13.4.3.1.1 Definitions

Stress versus crack opening curve or softening curve: the relationship between the stress (σ) transferred between the faces of a cohesive crack and the crack opening (w), Fig. 13.10.

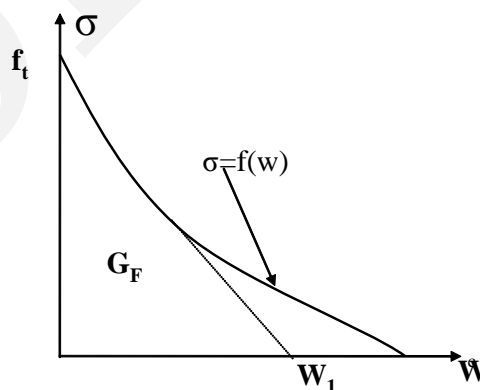


Figure 13.10: Softening Curve and Initial Linear Portion

Tensile strength (f_t), the maximum cohesive stress or stress at zero crack opening

Linear initial portion of the softening curve the linear approximation to the initial part of the softening curve as shown by the dashed line in Fig. 1. It is defined by the tensile strength (f_t) and the horizontal intercept (w_1).

Brittleness length (l_1) , defined as

$$l_1 = \frac{Ew_1}{2f_t} \quad (13.40)$$

Bilinear approximation of the softening curve a bilinear function that approximates the actual softening curve of concrete by a bilinear curve as shown in Fig. 13.11. The bilinear curve is defined by 4 parameters, usually taken to be the tensile

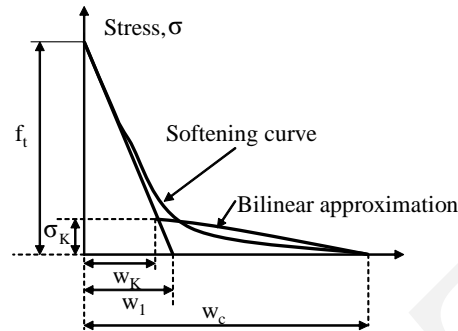


Figure 13.11: Softening curve and bilinear approximation

strength (f_t), the critical crack opening (w_c), and the crack opening and cohesive stress at the kink point (w_k, σ_k).

Net plastic flexural strength (f_p), the tensile strength of an ideal material rigid-perfectly plastic in tension and rigid in compression that would give the same peak load as the actual specimen for a beam of identical dimensions.

13.4.3.1.2 Notation and Abbreviations

a_0	notch length (initial crack length)
A	far tail constant
b	ligament length = $D - a_0$
B	thickness of specimen
C_i	initial compliance of beam specimen
CMOD	crack mouth opening displacement
d_a	maximum aggregate size
D	depth of specimen
E	elastic modulus
E_m	mean elastic modulus
f_t	tensile strength
f_p	net plastic flexural strength
g	specific gravity = 9.81 ms^{-2}
G_F	mean fracture energy
G_{Fm}	fracture energy, area below the softening curve
h	distance from the CMOD measuring line to the specimen surface
K	tail fitting parameter
l_1	brittleness length
l_{1m}	mean brittleness length
L	length of specimen
m	mass of the specimen
N	notch width
P	total load on specimen
P_1	corrected load on specimen = $P' - P'_R$
P'_R	residual measured load at the end of test
P_{max}	effective peak load of a specimen
P_{1max}	corrected peak load of a specimen = $P'_{max} - P'_R$
P'_{max}	effective peak load of a specimen
r	distance from the measuring line of the displacement extensometers to the center plane of the specimen

S	test span of the specimen
T	splitting tensile strength
T_m	mean splitting tensile strength
w	cohesive crack opening
w_1	horizontal intercept of the linear initial portion of the softening curve
w_c	critical crack opening (crack opening at which the cohesive stress vanishes)
w_{ch}	characteristic crack opening
w_G	center of gravity of the softening curve
w_{Gm}	mean center of gravity of the softening curve
w_k	crack opening at the kink point of the bilinear approximation
w_{MA}	CMOD at zero P_1
w_{MR}	CMOD at the end of the test
W_F	total work of fracture
W_{Fm}	measured work of fracture
X	auxiliary variable for far tail fitting
x	inverse relative plastic strength = f_t/f_p
Y	auxiliary variable for far tail fitting
α_0	relative notch length = a_0/D
δ	load point displacement
δ_A	load point displacement at zero P_1
δ_R	load point displacement at the end of test
δ_k	cohesive stress at the kink point of the bilinear approximation

13.4.3.2 Summary of Test Method

¹²⁶ In this test method, notched beams and cylindrical concrete specimens are tested to determine fracture parameters of concrete. The bilinear approximation is derived by forcing it 1) to give same peak loads as the actual softening curve for both the splitting cylinders and the notched beams, 2) to have same fracture energy as the actual softening curve, and 3) to have same center of gravity position as the actual softening curve.

¹²⁷ The cohesive tensile strength (f_t) is approximated by the splitting tensile strength of cylindrical concrete specimens tested according ASTM C496 standard, with minor modifications.

¹²⁸ Center-point loading tests are run under closed loop CMOD control on notched concrete beams (with compensation for the self-weight), and the curves of load versus load-point displacement and of load versus CMOD are recorded.

¹²⁹ The net plastic flexural strength (f_p) is determined from the peak load.

¹³⁰ From the results of tensile strength (f_t) and net plastic flexural strength (f_p), the brittleness length (l_1) is determined.

¹³¹ The elastic modulus (E) is determined from the initial slope of the load-CMOD curve.

¹³² The horizontal intercept (w_1) is determined from the mean brittleness length (l_{1m}), the mean elastic modulus (E_m) and the tensile strength (f_t) solving from Eq. 13.40.

¹³³ The fracture energy (G_F) is determined from the area under the load versus load-point displacement curve.

¹³⁴ The center of gravity of the area below the softening curve (w_G) is computed by curve fitting of the far end of the load vs. CMOD curve.

¹³⁵ The critical crack opening (w_c) and the coordinates of the kink point (w_k, σ_k) are finally computed from simple geometrical relations from the set of values (f_t, w_1, G_F, w_g).

13.4.3.3 Significance and Use

¹³⁶ This test method is used to determine a bilinear approximation of the softening curve for the cohesive crack model.

¹³⁷ The cohesive crack model describes in a simplified manner the cracking of concrete keeping a good balance between accuracy and complexity.

138 The actual softening curve of concrete can be approximated by a bilinear softening curve to get reasonable prediction of the overall cracking behavior, including peak load estimates, post-peak load-displacement response and energy dissipation.

139 Care must be exercised in the interpretation and use of the material properties obtained by this test method, because they are sensitive to any of the factors affecting concrete behavior such as batching and mixing procedures, the methods of sampling, molding and fabrication and the age, temperature and moisture conditions during curing.

13.4.3.4 Specimens

140 Cylindrical specimens shall be used to determine the splitting tensile strength. The geometry and manufacture of these specimens shall conform to the general provisions of Practices C 31 (field specimens) or C 192 (laboratory specimens).

141 Cylindrical specimens for splitting tensile strength shall further conform to any special provisions in Test Method C 496.

142 Beam specimens shall be used to determine the load vs. load-point displacement curve and the load vs. CMOD curve. The geometry and manufacture of these specimens shall conform to the general provisions of Practices C 31 (field specimens) or C 192 (laboratory specimens) applicable to beam and prism specimens.

143 A minimum of three cylindrical specimens and three beam specimens shall be cast. Whenever practical, all the specimens must be cast from the same concrete batch. If this is not possible, a number of cylinder specimens twice the number of beam specimens must be obtained from each batch. A minimum of three split cylinders and three beams must be tested.

144 The beam specimens shall be prismatic beams of rectangular cross section with a sawn central notch, Fig. 13.12. The beams

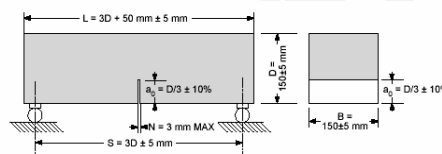


Figure 13.12: Specimen Geometry and Dimensions

defined in this standard are not to be used for materials with a maximum aggregate size d_a larger than 25 mm. The beam thickness (B) must be 150 ± 5 mm. The beam depth (D) must be 150 ± 5 mm. The loading span (S) must be equal to three times the beam depth ($3D$), within ± 5 mm. The total length (L) of the specimen shall be 50 mm longer than three times the beam depth ($3D + 50$ mm) within ± 5 mm. The nominal notch depth (a_0) shall be equal $D/3$. Deviations up to 10% of the nominal value may be accepted for a whole test series ($0.30 \leq a_0/D \leq 0.37$). But, within a series, notch depths of individual specimens must not deviate from the mean more than 2%. The notch width (N) must be no larger than 3 mm.

145 After demolding, cure and conserve the specimens in a lime saturated bath at $23 \pm 2^\circ\text{C}$ until testing time.

146 After the removal of the specimen from the bath, and until the end of the test, drying of the surface of the specimen must be prevented.

13.4.3.5 Apparatus

147 Apparatus for splitting tensile strength shall conform to the provisions of Test Method C 496, except that the bearing strips shall be 10 mm wide.

148 Servohydraulic or electromechanical testing machines, Fig. 13.3 shall be used that provide closed-loop control with the crack mouth opening displacement (CMOD) as the feedback signal. High machine stiffness is recommended. In addition, the testing machine shall conform to the requirements of the Sections on Basis of Verification, Corrections, and Time Interval Between Verifications of Practices E 4.

149 The load cell installed on the machine for these specific tests must give load readings accurate within 1% of the recorded peak load.

150 The CMOD must be measured with a clip-on gage or similar extensometer giving readings accurate within $5 \mu\text{m}$ (five micron) over a range of 2 mm.

- 151 The gage length of the extensometer must be centered on the notch; The gage length must be less than $0.2D$.
- 152 To avoid measuring the inelastic deformation originated at the supports, the displacement must be determined relative to the points directly above and below the loading points by means of a reference frame.
- 153 For this method to give accurate results, the frame for measuring the displacement shall be stiff enough. At the worse situation, a maximum frame deflection of $2\ \mu\text{m}$ (two microns) is allowed. The frame must stay on two ground hardened steel plates at the vertical of the lateral supports.
- 154 Two extensometers shall be symmetrically placed at both sides of the notch, at the bottom face of the specimen. The distance (r) from the measuring line to the center plane of the specimen shall be as small as possible. The load point displacement signal (δ) shall be computed as the average of the measuring signal of both extensometers.
- 155 The extensometers shall give readings accurate within $10\ \mu\text{m}$ (ten microns) over a range of 5 mm.
- 156 The loading apparatus for the bending tests will provide two supports and a central loading block suitably mounted to minimize eccentricities (torsion), to keep the loading span within the specified tolerances, and to minimize friction at the supports.
- 157 Weight compensation by using specimens longer than twice the loading span ($L = 2S + 50\ \text{mm}$) is very effective, although the weight of the specimen is very much increased and handling more difficult.

13.4.3.6 Test Record

- 158 Record of the load-CMOD curve must be performed so that there is no loss of resolution.
- 159 The time-delay between readings must be selected in such a way as to comply the following conditions: (1) a minimum of 20 well spaced readings must be performed in the load interval spanning from 0.15 to 0.55 of the final peak load; (2) the reading interval in the peak zone of the test must be low enough for the three load readings immediately before and after the peak be within 1% of the peak; (3) at least 20 well spaced readings must be recorded in the post peak region when the load decreases from the peak to 0.15 of the peak, (4) a minimum of 150 well spaced readings must be recorded in the post peak region up to the end of the test (conventionally considered to occur when the CMOD reaches 2 mm).

13.4.3.7 Procedure

- 160 The procedure for splitting tensile tests shall be as described in the Test Method C 496, except that the loading rate shall be within the range 500 to 1000 kPa/min all the way up to the peak load. Provisions shall be taken for measuring and recording the loading rate up to the peak.
- 161 The preparation of the specimen for testing may include grinding of the load bearing areas, preparation of attachment for clip-on gage, and notching.
1. Immediately after removing the specimen from the bath, mark the central section and the loading lines of the lateral supports (use pencil, not scaring instruments). Protect the surface to avoid drying, by coatings, wet clothes and water-spraying so that drying is completely avoided.
 2. Verify that the load-bearing areas and the contact zones with the vertical extensometers are plane using a ground steel rod and leaf-type feeler gages of 0.1 mm. If any gaps larger than 0.1 mm are detected, grind the surface of the specimen to eliminate the gap.
 3. Drill any hole that may be required to fasten the knife edges for the clip gage. Gluing of knife edges on the moist surface is not recommended.
 4. Cut the notch so that the notch front is perpendicular to planes that were horizontal during casting. Use a diamond saw with water refrigeration and keep the load as small as possible to avoid damaging the concrete.
 5. Handling of the specimen after notching must be very gentle to avoid damage. Lifting of the specimen must be performed by means of two attachments located at 1/4 from the ends of the specimens. Shocks must be avoided at all times.
 6. Attach the elements to hold the clip-on gage.
 7. Attach the hardened steel plates at the locations of the rolling supports.

162 Beam Test:

1. Gently place the specimen on the loading device. At this stage the rolling supports may be clamped to ease the placement. Attach the clip-on gage and set its output to zero (or record the initial reading). Carefully center the specimen so that the notch is at mid position between the supports within 1 mm or 0.25% of the span (whichever is the less), and the mid-vertical-longitudinal plane of the specimen coincides with the loading plane defined by the shafts b and h (within 0.5 mm or 0.5 % of the beam thickness). An external frame with centering screws may prove useful to facilitate this task.

¹⁶³ Place the hardened steel plates at the vertical of the lateral supports and the reference frame and the transducers for measuring the load point displacement, and set its output to zero (or record the initial reading). The supports of the frame must be placed on the vertical of the lateral supports of the specimen within 1 mm or 0.25% of the span (whichever is the less).

2. Verify that the load channel is zeroed, and slowly pre-load the specimen up to a load of between 5 and 10% of the estimated maximum load. After the test, this pre-load must be checked not to have exceeded 15% of the actual peak load. If this limit was exceeded, the test must be considered invalid. During the pre-load, the spherical or cylindrical seatings must be free (and even helped) to accommodate any initial geometrical misfit.
3. Unclamp the rollers and run the test under at constant CMOD rate. The rate must be selected so that the peak load is reached within 3 to 5 min. 8.4. Specimen Dimensions:
4. Measure the dimensions of the cross section to the nearest 0.1 mm. Measure the beam depth (D) at the central cross section at the two surfaces of each half of the specimen, and take the mean of the four measurements. Measure the notch depth (a_0) at the central cross section at the two surfaces of each half of the specimen and take the mean of the four measurements. Measure the beam thickness (B) at the front of the notch and at the top of the beam for the two halves of the specimen and take the mean of the four measurements.

13.4.3.8 Calculations

13.4.3.8.1 Tensile strength, f_t ¹⁶³ Calculate the splitting tensile strength (T) of each cylinder specimen according to point 7.1 of ASTM C 496, in SI units (kPa).

¹⁶⁴ Determine the mean splitting tensile strength (T_m) by averaging over all the specimens.

¹⁶⁵ Determine the tensile strength of concrete (for the cohesive crack model) as

$$f_t = \frac{T_m}{1000} \quad (13.41)$$

where T_m = mean splitting tensile strength, kPa; f_t = tensile strength, MPa.

13.4.3.8.2 Elastic modulus, E ¹⁶⁶ Calculate the elastic modulus of each notched beam according the following procedure:

1. From the load-CMOD record, select a linear segment with measured loads between 15% and 55% of the peak load ($0.15P'_{max} \leq P' \leq 0.55P'_{max}$).
2. Fit a straight line to this segment with all the data available. Use linear regression of CMOD vs. P . to determine the slope of the segment, which is taken to coincide with the initial compliance of the specimen:

$$C_i = \frac{\Delta(CMOD)}{\Delta P'} \quad (13.42)$$

where C_i = initial compliance, $\mu\text{m N}^{-1}$; $\Delta(CMOD)$ = variation of CMOD, μm ; P' = variation of measured load, N;

3. Determine the elastic modulus as

$$E = \frac{24}{C_i B D} [a_0 V_1(\alpha_0) + h W_1(\alpha_0)] \quad (13.43)$$

where E = elastic modulus, GPa; C_i = initial compliance, $\mu\text{m N}^{-1}$; B = beam thickness, mm; D = beam depth, mm; a_0 = notch length, mm; α_0 = relative notch length = a_0/D ; h = Distance of the knife edges to specimen surface, mm; and

$$V_1(\alpha) = 0.76 - 2.28\alpha + 3.87\alpha^2 - 2.04\alpha^3 + \frac{0.66}{(1-\alpha)^2} \quad (13.44-a)$$

$$W_1(\alpha) = 20.184 - 82.790\alpha + 121.64\alpha^2 \quad (13.44-b)$$

4. Determine the mean elastic modulus (E_m) by averaging over all the specimens.

13.4.3.8.3 Far tail constant, A 167 Determine the residual load P'_R measured by the load cell at the end of the test, for CMOD = 2 mm or nearest point on the record. Determine the corresponding CMOD (w_{MR}). Delete the recorded points with CMOD larger than w_{MR} .

168 Compute, for all the record points, the corrected load P_1 by subtracting from the measured load the residual load: $P_1 = P' - P'_R$

169 Plot the curve of corrected load P_1 versus CMOD. Determine the value w_{MA} of the intersection of the rising part of the curve with the CMOD axis (Fig. 13.13).

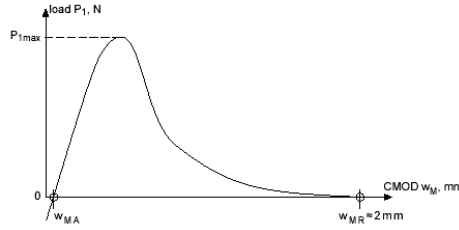


Figure 13.13: Plot of corrected load P_1 versus CMOD.

170 For the points in the record past the peak for which the corrected load is less than or equal to 5% of the corrected peak load, compute the quantity X defined as

$$X = \frac{1}{(w_M - w_{MA})^2} - \frac{1}{(w_{MR} - w_{MA})^2} \quad (13.45)$$

where w_M = recorded CMOD, mm; w_{MR} = CMOD at the end of test, mm; w_{MA} = CMOD at zero P_1 for the rising part of curve, mm.

171 Plot P_1 versus x and perform a least-squares fit of the quadratic equation

$$P_1 = X(A + KX) \quad (13.46)$$

Find A and K by least-squares fitting and give A in N mm^2 with three significant digits (K is not needed).

NOTE. Most computer packages for curve plotting will be able to perform the foregoing nonlinear fit. However, if such a program is not available, a linear regression of $Y = P_1/X$ versus X will solve the problem.

13.4.3.9 Net plastic flexural strength, f_p

172 Calculate the net plastic flexural strength of each notched beam according to the following procedure:

1. Determine the effective peak load taking into account the finite length of the tail of the record as

$$P_{max} = P_{1max} + \frac{A}{(w_{MR} - w_{MA})^2} \quad (13.47)$$

where P_{max} = effective peak load, N; P_{1max} = corrected peak load, N. A = far tail constant, Nmm^2 ; w_{MR} = CMOD at the end of test, mm; w_{MA} = CMOD at zero P_1 for the raising part of curve, mm;

2. Determine the net plastic flexural strength of the beam as:

$$f_p = \frac{P_{max}S}{2Bd^2} \quad (13.48)$$

where f_p = net plastic flexural strength, MPa; P_{max} = effective peak load, N; B = beam thickness, mm; $b = D - a_0$ = ligament length, mm; D = depth of specimen, mm; a_0 = notch length, mm; S = test span of the specimen, mm.

13.4.3.10 Brittleness length, l_1 , and horizontal intercept, w_1

173 For each specimen, determine the brittleness length l_1

$$l_1 = \kappa D \left[\frac{11.2}{(x^2 - 1)^2} + \frac{2.365}{x^2} \right] \quad (13.49)$$

where l_1 = brittleness length, mm; $\kappa = 1 - \alpha_0^{1.7}$; $\alpha_0 = a_0/D$ = notch-to-depth ratio; D = beam depth, mm; a_0 = notch length, mm; $x = f_t/f_p$ = inverse relative plastic strength; f_p = net plastic flexural strength, MPa; f_t = tensile strength, MPa.

174 Determine the mean brittleness length l_{1m} as the average of the determinations for individual specimens.

175 Determine the horizontal intercept of the softening curve (w_1) as

$$w_1 = 1000 \frac{2f_t}{E_m} l_{1m} \quad (13.50)$$

where w_1 = horizontal intercept, μm (microns); f_t = tensile strength, MPa; E_m = mean elastic modulus, MPa; l_{1m} = mean brittleness length, mm.

13.4.3.11 Fracture energy G_F

176 For each specimen, plot the curve of corrected load P_1 versus load-point displacement δ . Determine the value δ_A of the intersection of the raising part of the curve with the δ -axis, Fig. 13.14.

177 For each specimen, determine the load-point displacement δ_R of the last point of the test record

For each specimen, compute the measured work of fracture W_{Fm} as the area enclosed between the positive part of the P_1 vs. δ curve and the δ axis. Express it in N mm (mJ) to the nearest 5 N mm.

178 For each specimen, compute the total work of fracture W_F as

$$W_F = W_{Fm} + \frac{2A}{\delta_R - \delta_A} \quad (13.51)$$

where W_F = total work of fracture, N mm (mJ); W_{Fm} = measured work of fracture, N mm (mJ); A = far tail constant N mm²; δ_R = load-point at the end of test, mm; δ_A = CMOD at zero P_1 for the raising part of curve, mm.

179 For each specimen, compute the fracture energy G_F as

$$G_F = 1000 \frac{W_F}{Bb} \quad (13.52)$$

where G_F = fracture energy, N/m (J/m²); W_F = total work of fracture, N mm (mJ); B = beam thickness, mm; $b = D - a_0$ = ligament length, mm.

180 Determine the mean fracture energy G_{Fm} as the average of the determinations for individual specimens.

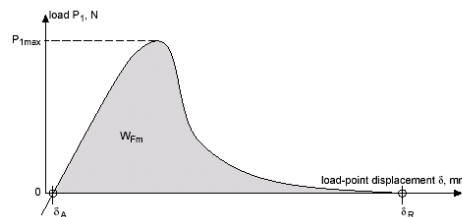


Figure 13.14: Plot of corrected load P_1 versus load-point displacement δ

13.4.3.12 Center of gravity of the softening curve, w_G

181 For each specimen, compute the abscissa of the center of gravity of the area under the softening curve as

$$w_G = \frac{4A}{BSG_F} \times 10^{-6} \quad (13.53)$$

where w_G = center of gravity of the area under the softening curve, μm (microns); A = far tail constant, N mm^2 ; B = beam thickness, mm; S = loading span, mm; G_F = fracture energy of the specimen, N/m .

182 Determine the mean center of gravity w_{Gm} as the average of the determinations for individual specimens.

13.4.3.13 Critical crack opening, w_c

183 Compute the characteristic crack opening defined as

$$w_{ch} = \frac{G_{Fm}}{f_t} \quad (13.54)$$

where w_{ch} = characteristic crack opening, μm (microns); G_{Fm} = mean fracture energy, N/m ; f_t = tensile strength, MPa .

184 Compute the critical crack opening of the bilinear approximation as

$$w_c = w_{ch} \frac{3w_{Gm} - w_1}{2w_{ch} - w_1} \left[1 + \sqrt{1 - \frac{2w_1(3w_{Gm} - 2w_{ch})(2w_{ch} - w_1)}{w_{ch}(3w_{Gm} - w_1)^2}} \right] \quad (13.55)$$

where w_c = critical crack opening, μm (microns); w_{ch} = characteristic crack opening, μm (microns); w_{Gm} = mean center of gravity of the area under the stress versus crack opening curve, μm (microns) w_1 = horizontal intercept, μm (microns).

13.4.3.14 Coordinates at the kink point (σ_k, w_k)

185 Compute the stress at the kink point of the bilinear approximation as

$$\sigma_k = f_t \frac{2w_{ch} - w_1}{w_c - w_1} \quad (13.56)$$

where σ_k = stress at the kink point, MPa ; f_t = tensile strength, MPa ; w_{ch} = characteristic crack opening, μm (microns); w_1 = horizontal intercept, μm (microns); w_c = critical crack opening, μm (microns).

186 Compute the crack opening at the kink point of the bilinear approximation as

$$w_k = w_1 \frac{w_c - 2w_{ch}}{w_c - w_1} \quad (13.57)$$

where w_k = crack opening at the kink point, μm (microns); w_c = critical crack opening, μm (microns); w_{ch} = characteristic crack opening, μm (microns); w_1 = horizontal intercept, μm (microns).

13.5 Wedge Splitting Test; Saouma et. al.

This paper proposes consideration of the wedge splitting test configuration to determine both the fracture toughness and the fracture energy of rock.

The test method introduces, through a wedge, a controlled lateral opening displacement to induce stable crack growth in a prismatic or cylindrical specimen, Fig. 13.15. From the splitting force - average crack opening displacement response of the specimen, the specific fracture energy is determined. For fracture toughness evaluation, a series of unload-reload is necessary.

This test method provides a means of measuring rock's resistance to crack propagation through linear elastic fracture mechanics (K_{Ic}) or nonlinear fracture mechanics (G_F). Results of this method may be used in numerical simulations as well as in comparative studies of the fracture properties of different rocks.

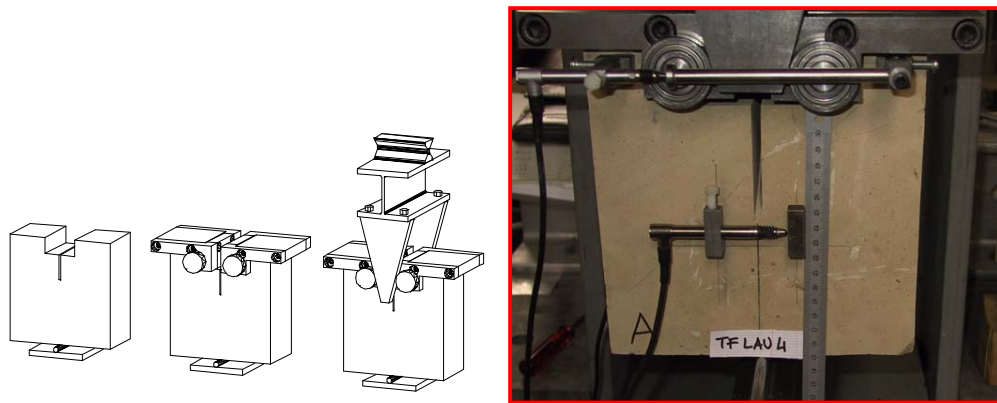


Figure 13.15: Principle of the Wedge Splitting Test Set-up

13.5.1 Apparatus

Testing System - The testing system consists of frame, actuator, force cell, controller, and data acquisition equipment as a minimum. Whereas it is preferable to have a closed-loop servo-controlled machine, this is not essential if the testing machine is rigid enough.

1. *Force Cell* - The force-measuring device shall have sufficient capacity and shall be accurate to within 1.0 % of the peak force measured in the test.
2. *Displacement Measurement Devices* - Two displacement measuring devices shall be used for measuring the displacements in the axis of the horizontal splitting force, one on each side of the specimen (COD_1 on side 1, COD_2 on side 2). The displacement measurement devices shall be of a type having sufficient capacity to enable the complete splitting of the specimen in two halves, and shall be accurate to within 1.0 % of the displacement measured while the specimen is at peak force.

Test Set-up - The principle of the wedge splitting test set-up, Fig. 13.15, with the successive steps, from 1 to 3, of mounting of the test for a prismatic specimen. The test set-up between the actuator or force cell and the specimen consists of a beam with wedges (A), plates equipped with roller bearings (B), and a rounded support (C).

13.5.2 Test Specimens

Specimen Configuration and Dimensions - The wedge splitting test specimen can be either prismatic or cylindrical, cast in moulds or taken as cores from the structure. Dimensions are shown below on Fig. 13.16 (all dimensions in mm). The following ligament lengths are recommended to obtain a stable crack propagation and to avoid unintentional mixed mode crack propagation:

Closed-loop control of COD: $h_1 = 130$ mm.

Stroke control: $h_1 = 85$ mm.

It should be noted that these are recommended values for “stiff” rock. For “soft” rock (defined by a relatively low fracture energy G_F), it is recommended to use a ligament length of 85 mm in conjunction with a closed-loop COD control.

Specimen Preparation - The groove and notch shall be cut into the specimen. In order to force a straight path of the crack propagation, a 5 mm deep groove can be cut on both sides of the specimen, on the surface following the plane of the ligament.

13.5.3 Procedure

1. Place displacement measuring systems on both sides of the specimen.
2. Place specimen on a suitable rounded support.
3. Carefully insert the wedge between the roller bearings.
4. Bring the wedges in contact with the roller bearings and perform the test, in either one of two test control modes:
 - a) Under COD control in a closed loop, servo-controlled test system, at a COD rate of 0.005 to 0.01 mm/min.
 - b) Under stroke control, at a stroke (cross-head) displacement rate of of =0.01 to 0.02 mm/min.

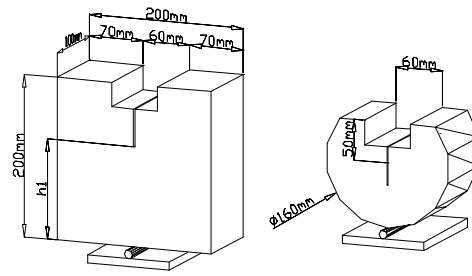


Figure 13.16: Dimensions of the specimens for the Wedge Splitting Test (all dimensions in mm)

The actual speed of the test should be commensurate with the ultimate application. Fracture energy determination for blast loading will undoubtedly require a much faster load rate than the one for long term “creep” cracking, and the values can be quite different as shown by Bažant and Xi (1993).

- For fracture toughness test, perform an unload/reload at the same rate as loading, Fig. 13.17:

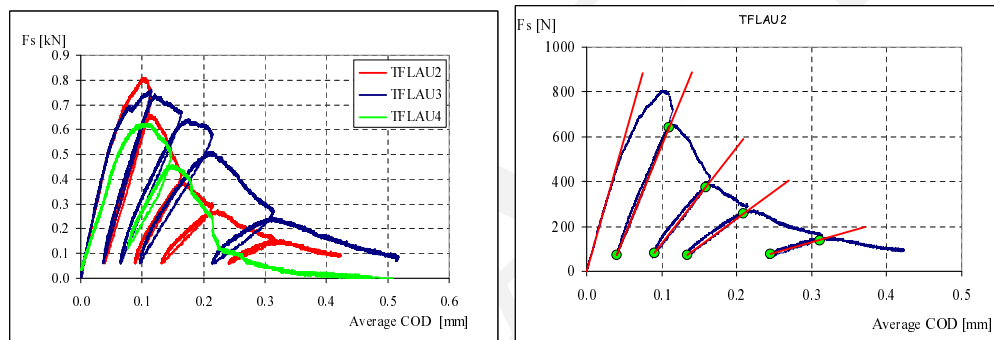


Figure 13.17: Representative Experimental Load-COD Curve

- Close to the peak load.
- At least 4 times in the post-peak zone.

Fig. 13.18 illustrates the test set-up with a (prismatic) specimen with the forces induced by the imposed COD or crosshead displacement. The resultant splitting force acts at 10 mm below the top side of the specimen.

13.5.4 Measured Values

Measured values are: 1) Vertical force F_V as a function of time; and 2) Crack Opening Displacements COD_1 and COD_2 on both sides of the specimen, as a function of time.

13.5.5 Calculation

13.5.5.1 Fracture Toughness

The determination of the fracture toughness requires not only the maximum load but also the corresponding crack size. However, in rock, as in concrete, the tip of the crack may not be easily identifiable due to the heterogeneity introduced by the fine grains. Hence, the concept of an elastic equivalent crack length has to be used to determine the fracture toughness. This is determined through the compliance method which combines finite element calibration with analysis of experimental data.

This Finite (or boundary) element analysis of the geometry, with $E = 1$, is conducted in two parts. First a unit horizontal load is applied at the location of the wedges, and the initial normalized compliance is determined. In this case C_n^0 is simply equal to the COD_{F_S} measured along a unit splitting force F_S .

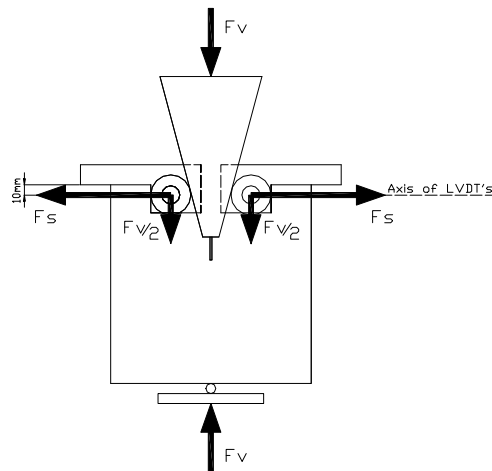
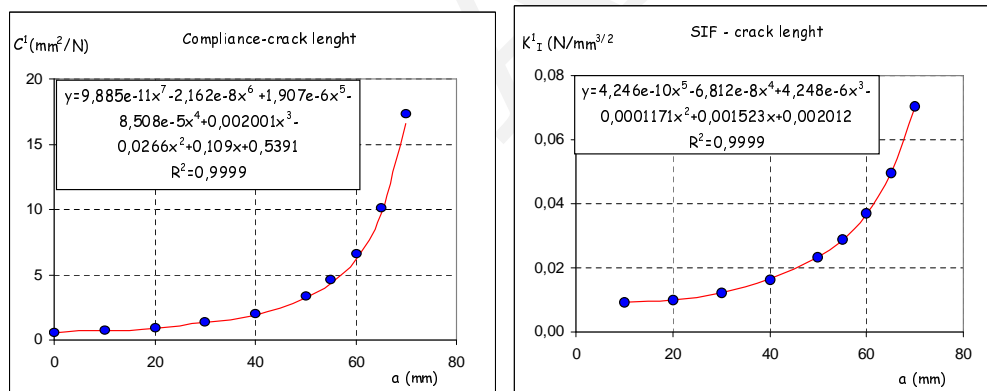


Figure 13.18: Test set-up and acting forces, for a prismatic specimen

187 Subsequently, geometries with increasing crack lengths (again with $E = 1$) are also subjected to a unit F_S and analyzed. For each analysis (crack length, a) we compute: the fracture toughness, and the compliance. These analyses results are then tabulated, and a least square best fit is performed to determine $a_{eff} = a_{eff}(C_n)$, and $K_{Ic} = K_{Ic}(a_{eff})$, where a_{eff} is the effective crack length.

188 Fig. 13.19, and 13.20 show representative normalized and actual compliance and stress intensity factor curves.


 Figure 13.19: Normalized Compliance and Stress Intensity Factors in Terms of Crack Length a

At this point, test interpretation proceeds as follows:

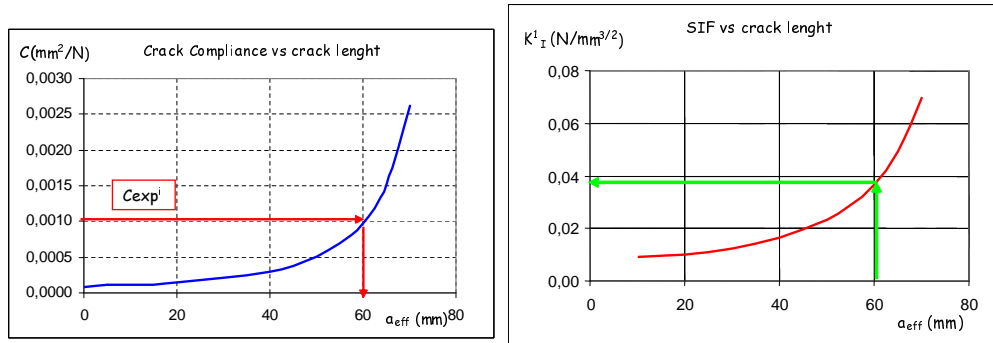
1. From the first unload-reload cycle, determine the effective elastic modulus from

$$E_{eff} = \frac{C_n^0}{C_{exp}^0} \quad (13.58)$$

Where C_n^0 is the normalized compliance (obtained from the pre-test calibration) and C_{exp}^0 is the initial experimental compliance given by

$$C_{exp}^0 = \frac{COD_{F_S}}{F_S} \quad (13.59)$$

where COD_{F_S} is the crack mouth opening displacement measured along the splitting force F_S .

Figure 13.20: Compliance and Stress Intensity Factors in Terms of Crack Length a

2. Having determined the effective elastic modulus, the normalized compliance is determined from $C_n = E_{eff} C_{exp}$.

3. For each of the subsequent post-peak response determine:

- The experimental compliance, C_{exp} .
- The corresponding elastic equivalent (or effective) crack length from

$$a_{eff} = a_{eff}(C_n) \quad (13.60)$$

- The fracture toughness for this particular crack length

$$K_{Ic} = K_{Ic}(a_{eff}) \quad (13.61)$$

4. Plot the determine fracture toughnesses in terms of effective crack length, and determine the average value. It should be noted that as a_{eff} approaches the ligament length (distance from tip of the notch to the bottom of the specimen), there will be a small decrease in K_{Ic} .

13.5.5.2 Fracture Energy

1. Determine the (horizontal) splitting force acting on the roller bearing, F_S from:

$$F_S = \frac{1}{2 \tan \alpha} F_V = \frac{1}{2 \tan 15^\circ} F_V = 1.866 F_V \quad (13.62)$$

2. Determine the average of the two displacements measured:

$$COD = \frac{COD_1 + COD_2}{2} \quad (13.63)$$

3. Plot F_S in terms of average COD and, if necessary, extrapolate curve to zero F_S .

4. Determine the ligament area A_{Lig} corresponding to the projected area of the crack on the ligament.

5. Determine the work of fracture W_F as the area under the $F_S - COD$ curve (Fig. 13.21).

6. Determine the specific fracture energy G_F :

$$G_F = \frac{W_F}{A_{Lig}} \quad (13.64)$$

13.5.6 Report

Report the following information:

- Specimen dimensions
- Test control method (stroke displacement or COD control, and displacement rate).
- Description of the fracture surface, especially any unusual appearance or significant deviation from a vertical plane centered on the pre-notch tip.
- Splitting force - average COD curve.
- Work of Fracture W_F and Specific Fracture Energy G_F .

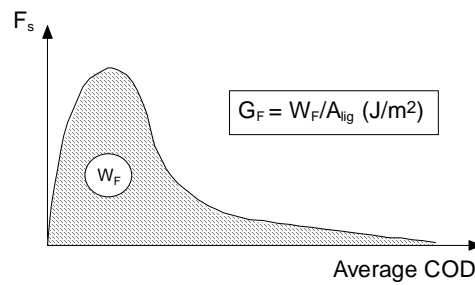


Figure 13.21: Definition of the work of fracture and specific fracture energy

13.5.7 Observations

Major advantages of the proposed test include:

1. Can be run on usual mechanical testing machines in compression mode (albeit with a longer relative notch length), or on a servo-controlled one.
2. Can be performed on specimens, prismatic or cylindrical cores extracted from the rock.
3. Has a substantially longer ligament length per unit weight of concrete as compared to other tests (and in particular compared to the Three-Point-Bending-Beam Test), and a smaller amount of elastic strain energy is stored in the specimen during cracking. This is a particularly important characteristic which facilitates stable tests without risks of snap-backs.
4. Self-weight effect can be neglected for usual sizes (20 x 20 x 10 cm prismatic specimen) (Denarié, E. and Saouma, V.E. and Iocco, A. and Varelas, D., 1999).
5. Test set-up and specimen geometry can be easily adapted for bigger or smaller specimen sizes, (Trunk, 2000).
6. Has been for now 15 years extensively used by researchers, and practitioners in the US, Europe and Japan with specimens ranging from 5 cm up to 3.2 m in size, on various types of concretes, mortars, advanced cementitious materials and rock.

Moreover, the interpretation of the tests results for the determination of G_F as well as the tensile softening diagram is straightforward and requires only very simple calculations. In a first approximation, the derivation of the tensile softening diagram can be based on the regressions performed on extensive data sets, for different types of concretes, at quasi-static imposed displacement rates, (Brühwiler, E., 1992). The uniaxial tensile strength f_t should be preferably determined experimentally by means of a uniaxial tensile test. If adequate software modules are available, f_t and the tensile softening diagram can also be indirectly determined by means of an inverse analysis using a FEM simulation of the experimental specimen response, (Bolzon et al., 2002).

Finally, this test has been used by one of the author to test limestone, (Brühwiler, E. and Saouma, V.E., 1990) and limestone concrete interfaces, (Chandra and Saouma, 2004).

Chapter 14

SIZE EFFECT

Paper in print

¹ Crack bridging occurs when cohesive stresses join the opposite faces of a crack, shielding the tip from the full effect of the applied load and thus giving rise to increased fracture resistance. Cohesive stresses are present both in elasto-plastic materials such as metals (through crack tip yielding), (Dugdale, 1960), (Barenblatt, 1962) and in quasi-brittle ones. In the later, they are present not only in cementitious materials, but also in ceramics, (Saouma et al., 2002) and are caused by reinforcing fibers, particles (such as aggregates or inclusions), or simply regions of microscopically irregular crack surfaces causing topological interference.

² Cohesive stress models were first suggested by Dugdale (1960) using a constant stress, then Barenblatt (1962) generalized this concept to a more general stress distribution, one which causes the crack faces to close smoothly. It should be noted that those two pioneering studies attributed different causes to the cohesive stresses. For Dugdale it was caused by macroscopic plasticity (and can be of any size) while for Barenblatt it was caused by molecular cohesion (and must be restricted to a relatively very small zone), (Kanninen and Popelar, 1985). Finally, most recently Hillerborg et al. (1976a) assumed a nonlinear model where the stress is a function of the crack opening. The first two models are most appropriate for metals to account for the presence of a plastic zone, whereas Hillerborg's model is more suited for cementitious material with a fracture process zone.

³ In both Dugdale and Barenblatt solution, the stress intensity factors caused by the far field load, and the cohesive stresses are assumed to cancel each other. Hence, implicit in this assumption is a zero material fracture toughness.

⁴ Finally, Hillerborg does not consider any singularity at the tip of the crack. Implicit in his approach is that there can not be a stress singularity at the crack tip since the criterion for crack propagation is based on the crack tip stress. This assumption was recently challenged by Xu and Reinhardt (1998) who developed the double- K criterion where $K_R(\Delta a) = K_{Ic}^{ini} + K^C(\Delta a)$ and $K^C(\Delta a) = F(f_t, f(\sigma), \Delta a)$. In this model, developed for concrete, the resistance to crack growth (right hand side) is first set to the inherent toughness, and then to a cohesive term. Hence, contrarily to Hillerborg's model, a cohesive stress does not necessarily eliminate the stress singularity, and as such crack propagation is no longer governed by a stress criteria, but rather by a modified linear elastic fracture mechanics one. This model enables us to distinguish between initial crack growth (in the absence of a fracture process zone) governed by K_{Ic}^{ini} and subsequent unstable crack growth in terms of $K_{Ic}^{ini} + K^C(\Delta a)$. Despite its appeal, this model has not yet been widely embraced by the concrete research community which continues to use (for the most part) Hillerborg's model.

⁵ In this chapter, we shall closely examine the role played by the cohesive stresses in inducing a size effect. This has already been suggested by Karihaloo (1996) "... the origin of the size effect is in the non-singular stress distribution ahead of the notch/crack".

⁶ Hence, keeping with the original spirit of the derivations of Dugdale, Barenblatt and Hillerborg we will assume the (net) fracture toughness to be zero.

14.0.1 Original Derivation

⁷ Bažant and Planas (1998) presented a *unified* model for the nominal strength of quasi-brittle material. This simple and elegant equation is asymptotic to plasticity and linear elastic fracture mechanics, while capturing the intermediary quasi-brittle response.

⁸ Considering the energy exchanged during an infinitesimal crack extension in a plate of width D , Fig. 14.1, the energy released can be approximated by $b2k(a_0 + c_f)\Delta a\sigma_n^2/2E$, which must be equal to the energy consumed during crack growth: $bG_F\Delta a$, hence

$$b2k(a_0 + c_f)\Delta a\sigma_n^2/2E = bG_F\Delta a \quad (14.1)$$

yielding

$$\sigma_n = \frac{Bf'_t}{\sqrt{1 + \frac{D}{D_0}}} \quad (14.2)$$

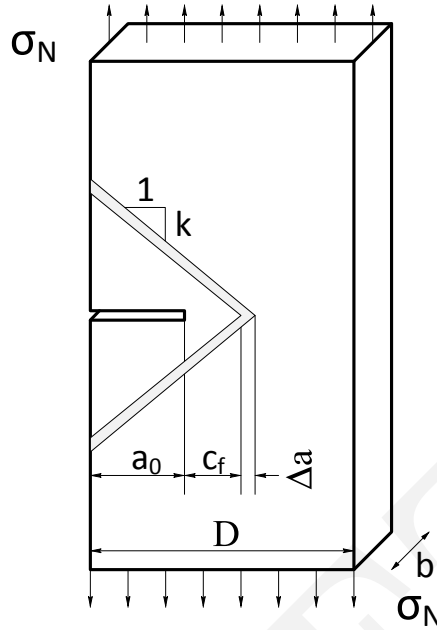


Figure 14.1: Energy Transfer During Infinitesimal Crack Extension

where

$$Bf'_t = \sqrt{\frac{G_F E}{kc_f}} \quad \text{and} \quad \frac{D}{D_0} = \frac{a_0}{c_f} = \beta \quad (14.3)$$

⁹ In his original paper, Bažant (1984) noted that the analytical or numerical derivation of B and β is too difficult, and they are best obtained through statistical regression analysis of test data.

¹⁰ This derivation would be characterized as semi-analytical, since it combines an analytical derivation (albeit with some simplifying assumptions), and experimental derivation of constants too complicated to be derived analytically. Finally, this derivation does not explicitly reference a plasticity and/or a linear elastic fracture mechanics solution. Yet, those two solutions are ultimately asymptotic to the derived size effect law.

14.1 Analytical Derivation

¹¹ In this section, an alternate derivation of the size effect law is presented. Whereas it hinges (for simplifying reasons) on Dugdale's or Barenblatt's model for the cohesive stresses (in lieu of Hillerborg's fracture energy), it will be shown that a purely analytical expression could be derived, hence problem specific numerical values of B can be obtained.

¹² This approach is based on classical elasto-plastic fracture mechanics, (Broek, 1986), where in its simplest form the stress intensity factors caused by the cohesive stresses (in a plastic zone or process zone), are assumed to cancel the ones caused by the far field load. Hence, contrarily to the original derivation by Bažant, the size effect law will be shown to have explicit roots in plasticity and linear elastic fracture mechanics theories. As a result, it will be shown that not only quasi-brittle materials exhibit a size effect, but elasto-plastic ones as well.

14.1.1 Constant Cohesive Stresses

14.1.1.1 Central Crack

¹³ Starting with a general case, we consider an infinite plate subjected to a far field uniform tensile stress σ and a crack of length $2a$, at the tip of which we have a uniform cohesive compressive stress (Dugdale type) equal to the tensile strength f'_t , Fig. 14.2.

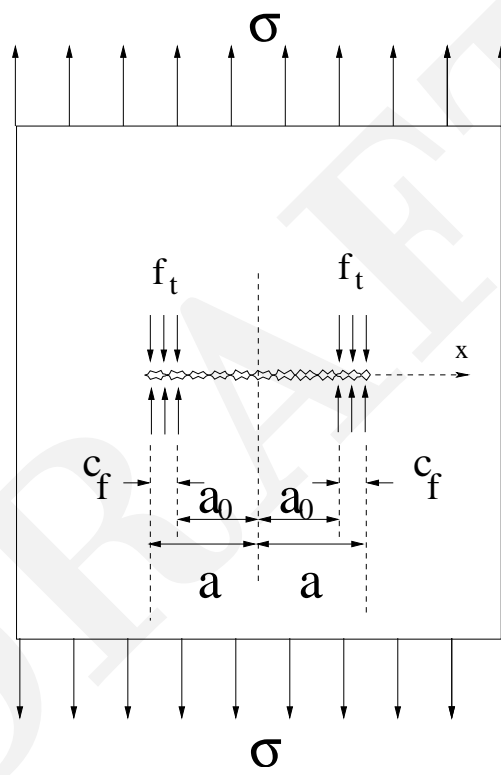


Figure 14.2: Central Crack With Constant Cohesive Stresses

14 The stress intensity factors due to the far field and cohesive stresses are:

$$K_a = \sigma\sqrt{\pi a} \quad (14.4)$$

$$K_b = f'_t\sqrt{\pi a} \left(1 - \frac{2}{\pi} \arcsin \frac{a - c_f}{a} \right) \quad (14.5)$$

respectively, (Cherepanov, 1979).

15 Equating those two stress intensity factors, we obtain the nominal strength

$$\sigma_n = f'_t \left[1 - \frac{2}{\pi} \arcsin \left(1 - \frac{c_f}{a} \right) \right] \quad (14.6)$$

16 In the limit, for small sizes when $a \simeq c_f$, σ_n approaches asymptotically f'_t . On the other hand, for large sizes, $c_f \simeq 0$, σ_n will asymptotically approach zero.

17 Whereas the expression of σ_n appears to have the same limits as the Size Effect Law, it is not mathematically similar to it. This will only become apparent if one takes a series expansion of the ArcSin function, and substituting c_f/a by s :

$$\sigma_n = \sigma_n = f'_t \left[1 - \frac{2}{\pi} \arcsin(1 - s) \right] \quad (14.7)$$

$$\simeq \frac{2\sqrt{2}f'_t}{\pi} s^{1/2} + \frac{f'_t}{3\sqrt{2}\pi} s^{3/2} + \frac{3f'_t}{40\sqrt{2}\pi} s^{5/2} + O[s]^{7/2} \quad (14.8)$$

Neglecting the terms of power greater than 1 (since s is at most equal to 1), and substituting $s = 1/(1 + r)$ where $r = a_0/c_f$, we obtain

$$\sigma_n = \underbrace{\frac{2\sqrt{2}}{\pi}}_B f'_t \sqrt{\frac{1}{1 + \underbrace{r}_\beta}} \quad (14.9)$$

18 We have thus recovered the size effect law as originally derived by Bažant as expressed by Eq. 14.2, with the additional benefit that B is quantified for this combination of geometry and cohesive stresses, Fig. 14.3.

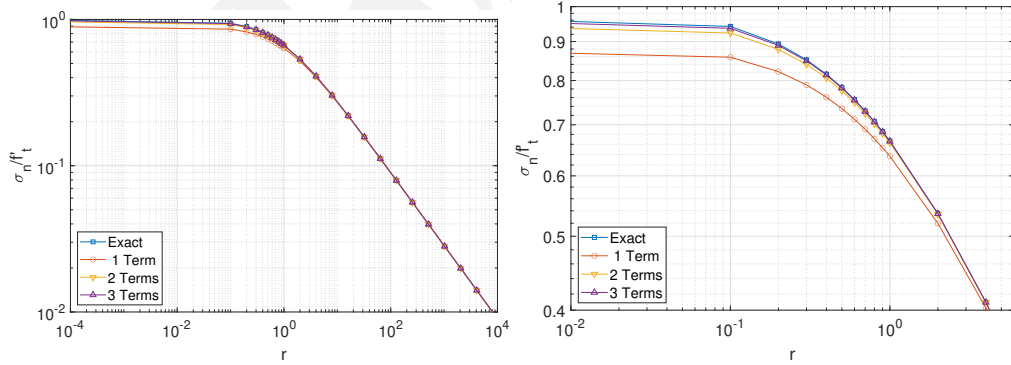


Figure 14.3: Nominal Strength in Terms of Size for a Center Crack Plate with Constant Cohesive Stresses

14.1.1.2 Edge Crack

19 We next consider an arbitrary geometry of a cracked structure whose stress intensity factor due to the far field stress can be expressed as

$$K_a = \alpha\sigma\sqrt{\pi a} \quad (14.10)$$

where α is a coefficient which accounts for geometry, boundary conditions, and load.

20 On the other hand, the stress intensity factor corresponding to a constant stress, Fig. 14.4 is given by Stevens and Guiu (1994) as

$$K_b = -f'_t \sqrt{\pi a} f_b \quad (14.11)$$

where

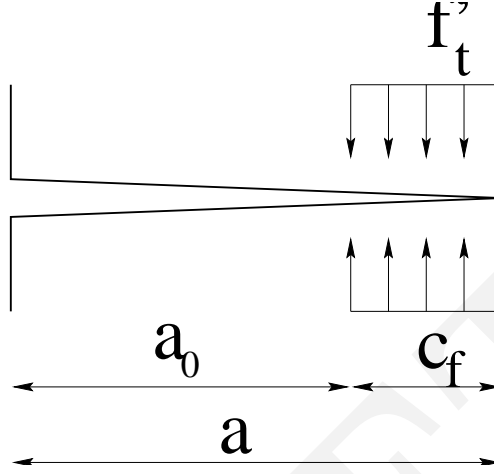


Figure 14.4: Dugdale's Model

$$f_b = 0.903s^{1/2} + \frac{1}{3}0.4406s^{3/2} + \frac{1}{5}0.4997s^{5/2} - \frac{1}{7}0.1438s^{7/2} - \frac{1}{9}0.04578s^{9/2} \quad (14.12)$$

and $s = c_f/a$. Since at most $s = 1$, we keep only the first term which has an exponent lower than one.

21 Equating K_a to K_b , we solve for the far field nominal stress σ_n which would result in a zero net stress intensity factor at the tip of the crack. For this problem, we obtain

$$\sigma_n = \frac{0.903}{\alpha} f'_t \sqrt{s} \quad (14.13)$$

Expressed in terms of $r = a_0/c_f$, $s = 1/(1+r)$, the far field nominal stress will be

$$\sigma_n = \underbrace{\frac{0.903}{\alpha}}_B f'_t \sqrt{\frac{1}{1 + \underbrace{r}_{\beta}}} \quad (14.14)$$

22 For an infinite plate with an edge crack, $\alpha = 1.1215$ (Tada et al., 1973), and the resulting nominal stress will be

$$\sigma_n = \underbrace{0.805}_B f'_t \sqrt{\frac{1}{1 + \underbrace{r}_{\beta}}} \quad (14.15)$$

This equation is shown in Fig. 14.5.

14.1.2 Linear Cohesive Stresses

14.1.2.1 Edge Crack

23 The stress intensity factor for an edge crack subjected to a pair of point forces on opposite faces at a distance x from the crack mouth, Fig. 14.6 is given by Gdoutos (1993) as

$$K_b^P = \frac{2}{\sqrt{\pi}} \frac{1 + F(x/a)}{\sqrt{a^2 - x^2}} P \sqrt{a} \quad \text{or} \quad dK_b^P = \frac{2}{\sqrt{\pi}} \frac{1 + F(x/a)}{\sqrt{a^2 - x^2}} dP \sqrt{a} \quad (14.16)$$

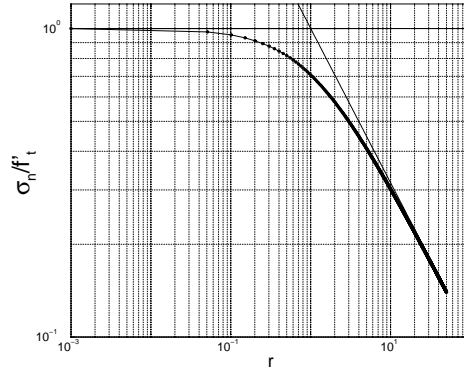


Figure 14.5: Size Effect Law for an Edge Crack with Constant Cohesive Stresses

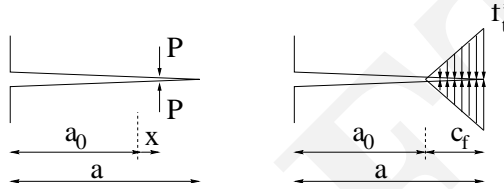


Figure 14.6: Linear Cohesive Stress Model

where

$$F(x/a) = [1 - (x/a)^2][0.2945 - 0.3912(x/a)^2 + 0.7685(x/a)^4 - 0.9942(x/a)^6 + 0.5094(x/a)^8] \quad (14.17)$$

²⁴ The stress intensity factor for a linearly varying stress distribution (analogous to, but not exactly, Barenblatt's model) is simply obtained by replacing dP by $\frac{dx}{c_f} f'_t$ in Eq. 14.16 and integrating

$$K_b = \int_{a_0}^a K_b^P dx = \frac{2}{\sqrt{\pi}} \int_{a_0}^a \frac{1 + F(x/a)}{\sqrt{a^2 - x^2}} \frac{x}{c_f} f'_t \sqrt{a} dx \quad (14.18)$$

²⁵ Equating this stress intensity factor caused by local plastification, to the far field stress intensity factor given by Eq. 14.10 (with $\alpha = 1.1215$) we solve for the nominal stress σ_n which would cause the net stress intensity factor to be equal to zero. Using $s = (a - a_0)/a$, and expanding in terms of s about $s = 0$, we obtain

$$\begin{aligned} \frac{\sigma_n}{f'_t} = & \frac{0.000124102}{s} - \frac{0.0000668046}{\sqrt{s}} - 0.000124102 + 0.535096\sqrt{s} \\ & + 0.0675175s^{3/2} - 0.388195s^{5/2} + 0.19108s^{7/2} - 0.411846s^{9/2} \\ & + O[s]^5 \end{aligned} \quad (14.19)$$

²⁶ Even though s is very small, we can drop the first three terms which are negligibly small compared to the others. This is first confirmed by replacing s with $1/(1+r)$, and plotting Eq. 14.19 with all the terms up to $s^{3/2}$, and the very same equation with the first three terms omitted, Fig. 14.7. We observe that those two graphs (plotted on a linear scale to enhance the potential discrepancies) are practically identical, with a small deviation in the high range of r .

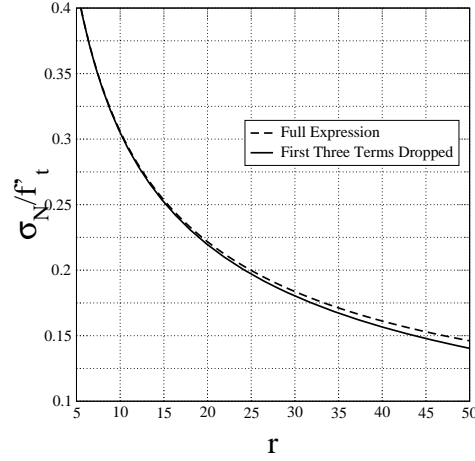


Figure 14.7: Energy Transfer During Infinitesimal Crack Extension

Hence, we may now justifiably drop the first three terms in Eq. 14.19, and rewrite this equation as:

$$\sigma_n = \frac{0.5351 f_t'}{\sqrt{1+r}} \left(1 + \frac{0.126182}{1+r} \right) + O[s]^2 \quad (14.20)$$

$$= \frac{0.5351 f_t'}{\sqrt{1+r}} \left[-0.0728836 \left(-4.66957 + \frac{1}{1+r} \right) \left(2.93828 + \frac{1}{1+r} \right) \right] + O[s]^3 \quad (14.21)$$

$$= \frac{0.5351 f_t'}{\sqrt{1+r}} \left[0.357092 \left(2.21298 + \frac{1}{(1+r)^2} - \frac{1.46954}{1+r} \right) \left(1.26544 + \frac{1}{1+r} \right) \right] + O[s]^4 \quad (14.22)$$

$$= \frac{0.5351 f_t'}{\sqrt{1+r}} \left[-0.769662 \left(1.16279 + \frac{1}{(1+r)^2} - \frac{0.164699}{1+r} \right) \left(-1.21723 + \frac{1}{1+r} \right) \left(0.917969 + \frac{1}{1+r} \right) \right] + O[s]^5 \quad (14.23)$$

²⁷ We note that the derived size effect law contains higher order terms than those originally derived by Bažant through Eq. 14.2.

²⁸ Bažant size effect law is recovered through Eq. 14.20 by dropping the second term in the parenthesis. As to Eq. 14.21-14.23 they definitely contain even higher order terms, Fig. 14.8.

14.1.2.2 Three-Point Bend Specimen

²⁹ We then turn our attention to a slightly more complex geometry, a three point bend specimen, Fig. 14.9, for which the stress intensity factor is now given by Gdoutos (1993) as:

$$K_a = \frac{PS}{BW^{3/2}} \left[2.9(a/W)^{1/2} - 4.6(a/W)^{3/2} + 21.8(a/W)^{5/2} - 37.6(a/W)^{7/2} + 38.7(a/W)^{9/2} \right] \quad (14.24)$$

³⁰ The stress intensity factor for an edge crack subjected to a linearly varying cohesive stress (Barenblatt's type) K_b , Fig. 14.6 was given by Equation 14.18.

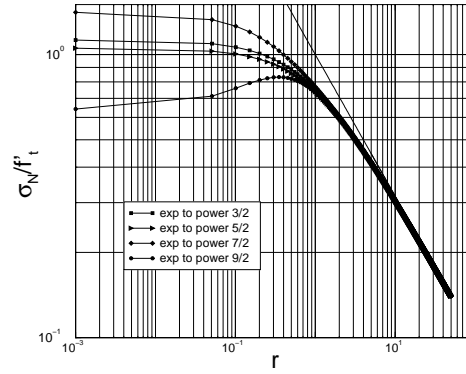


Figure 14.8: Size Effect Law for an Edge Crack with Linear Softening and Various Orders of Approximation

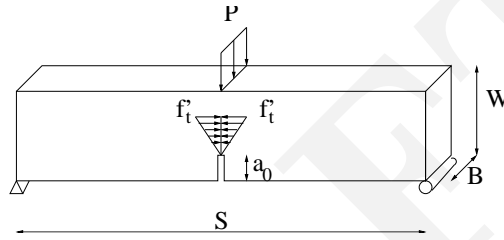


Figure 14.9: Three Point Bend Specimen with Linear Cohesive Stresses

As before, equating the two stress intensity factors, solving for σ , substituting $s = (a - a_0)/a$, and expanding in terms of s about $s = 0$, we obtain

$$\frac{\sigma}{f'_t} = -\frac{0.000067298}{s} + \frac{0.0000597828}{\sqrt{s}} + 0.000067298 + 1.06378\sqrt{s} + 8.32667 \times 10^{-17}s + 0.132783s^{3/2} + O[s]^2 \quad (14.25)$$

As for Eq. 14.19, it can be shown that we can retain the terms in $s^{1/2}$ and $s^{3/2}$ without loss of accuracy, and thus obtain

$$\sigma_n = \frac{1.06738f'_t}{\sqrt{1+r}} \left(1 + \frac{0.124401}{1+r} \right) + O[s]^2 \quad (14.26)$$

³¹ Again, this newly derived size effect law for a three point bend beam with a linearly varying cohesive stress along the fracture process zone is to be contrasted with Eq. 14.2. Should we drop the second term within the parenthesis, then and only then we will recover an equation analogous to Eq. 14.2.

14.2 Discussion

14.2.1 Comparison with Experimental Data

³² In order to assess the results, we closely examine experimental size effects tests on three point bending concrete specimens as reported in Table 1.5.2 of [Bažant and Planas \(1998\)](#).

Table 14.1 gives the compressive strength and Bf'_t . For the sake of simplification, we assume $f'_t = 0.1f'_c$, and thus determine the experimental value of the B coefficient.

The average experimentally determined value is 1.39 (with a standard deviation of 0.61), and compares relatively well (given the assumption of a Barenblatt cohesive stress model) with the analytically derived value of 1.07 in Eq. 14.26. Interestingly enough, we note that the experimentally determined B value is clearly inversely proportional to the nominal specimen size D_0 .

Series	f'_c MPa	Bf'_t MPa	B	D_0 mm	Reference
A5	46.8	2.9	0.62	212.	(Walsh, 1972)
A2	35.4	2.8	0.79	157.	(Walsh, 1972)
A4	15.6	1.7	1.09	126.	(Walsh, 1972)
B1	34.1	6.0	1.76	60.	(Bažant and Pfeiffer, 1987)
A6	32.7	4.1	1.25	55.	(Walsh, 1972)
A1	23.1	4.5	1.95	36.	(Walsh, 1972)
A3	14.3	3.2	2.24	34.	(Walsh, 1972)

Table 14.1: Experimentally Determined Values of Bf'_t , (Bažant and Planas, 1998)

14.2.2 Implications

33 We can rewrite Eq. 14.2 as

$$f_t^* = \frac{f'_t}{\sqrt{1 + \beta}} = \frac{\sigma_N}{B}, \quad (14.27)$$

where f_t^* is termed the size-reduced-strength and is a characteristic of the entire structure and not only of the material.

34 Undoubtedly the size effect law is a very elegant generalized model for concrete fracture. It attempts to provide a unified mathematical model for concrete cracking by merging two different approaches. Furthermore, it has been experimentally validated with numerous tests, many of which involved uncracked (initial) structures.

35 Despite its general appeal, this model calls for the following comments:

1. The size effect law can be plotted on a log-log scale, as shown in Fig. 14.10, with σ_n versus size d .

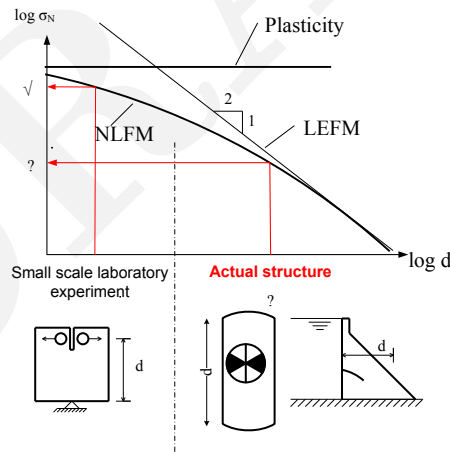


Figure 14.10: Size Effect Law

2. For structures of a small size relative to the size of aggregate, i.e for small λ , the value of $\frac{\lambda}{\lambda_0}$ in Eq. 14.27 may be neglected in comparison to 1, yielding $f_t^* \simeq f'_t$, and the classical strength criterion governs.
3. Again for small structures (small β), $B = \frac{\sigma_N}{f'_t}$ and can be determined from plastic limit analysis.
4. For structures with very large size compared to aggregate size, $\frac{\lambda}{\lambda_0} \gg 1$. Thus Eq. 14.27 reduces to $f_t^* \simeq f'_t \sqrt{\frac{\lambda_0}{\lambda}}$, and we see that “For very large concrete structures, such as dams (or large rock masses), Eq. 14.27 asymptotically approaches the size effect of linear elastic fracture mechanics”.

Column Buckling	Size Effect
Euler Equation	LEFM
Slenderness ratio	Size
Plastic failure	Plastic failure
Inelastic stresses	Cohesive stresses
Inelastic Buckling	NLFM
Column Equation (SSRC)	Size Effect law (Bažant)
$\sigma_{cr} = \sigma_y \left[1 - \frac{\sigma_y}{4\pi^2 E} \left(\frac{KL}{r_{min}} \right)^2 \right]$	$\sigma_n = \frac{B f'_t}{\sqrt{1+\beta}}$

Table 14.2: Size Effect Law vs Column Curve

5. In general, Eq. 14.27 represents a gradual transition from the strength criterion for small structures to linear elastic fracture mechanics for large structures.

6. To assess the size effect law, geometrically identical specimens, but with different sizes must be tested. Then Eq. 14.27 can be cast in the form:

$$Y = a + b\lambda = \frac{1}{\sigma_N^2}, \tag{14.28}$$

where $a = \frac{1}{B^2}$ and $b = \frac{1}{B^2 \lambda_0}$. From statistical regression analysis, the intercept a , and the slope b can be determined, and then $B = \frac{1}{\sqrt{a}}$ and $\lambda_0 = \frac{a}{b}$

7. If $\frac{\lambda}{\lambda_0} = \beta$ is less than 0.1, then a strength criterion must be used, and if β is greater than 10, then a LEFM criterion is to be used. Note that those are arbitrary guidelines.

8. The point of intersection of the two asymptotes corresponds to $\beta = 1$.

9. At no stage did we have to introduce (explicitly or implicitly) any LEFM equation (in the sense of a stress singularity at the crack tip).

10. The square root relationship between f'_t and d (through λ) comes from:

- an appropriate choice of the normalizing parameter for the crack length a in defining α_1 and α_2 .
- expression for G_F in terms of the square of f'_t in Eq. ???. Although it is correct to directly relate G_F to the area under the uniaxial stress strain curve (a measure of the energy required to produce a unit surface), the square component is again not linked to LEFM.

11. It can be shown, (Bažant and Cedolin, 1991) that the fracture energy G_F can be recovered from the Size Effect Law

12. There is a strong analogy between the size effect and column buckling, Fig. 14.11, Table 14.2.

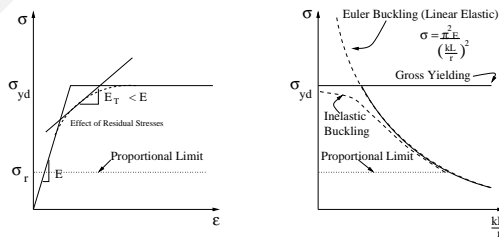


Figure 14.11: Inelastic Buckling

14.2.3 LEFM vs NLFM Analyses

³⁶ Ideally, we should extend the analytical solution to encompass Hillerborg's model as applied to a three point bending concrete specimen. To the best of the author's knowledge only two researchers addressed this complex nonlinear problem. **Xu and Reinhardt (2000)** developed a closed form solution, albeit an empirical one (as termed by its authors). Another solution was presented by **Karihaloo (1999)** who again indirectly solved this problem, but with some rather restricting assumptions by enforcing a zero net stress intensity factor at the tip of the FPZ. Because of the restrictions imposed to those two solutions, the authors have not considered them in this study.

³⁷ In a nonlinear fracture mechanics analysis the crack growth criteria is stress based, i.e the crack tip maximum tensile stress can not exceed the (non-zero) concrete tensile strength. Alternatively, in an LEFM analysis, we can set as a criteria a zero fracture toughness.

³⁸ Whereas both criteria are readily accepted by the research community, practicing engineers have difficulties in accepting a non-zero tensile strength (hence rendering a NLFM analysis impossible), but can accept a small (preferably zero) fracture toughness, (**FERC, 2016**) (in this context, the double-K method might be more acceptable to practicing engineers than solutions based on G_F and a non-zero f'_t). By the same token, a NLFM analysis should extend the fracture process zone to the point where the stress singularity no longer exists.

³⁹ In order to highlight the duality between a zero fracture toughness criteria in an LEFM analysis, and a non-zero tensile strength criteria in a NLFM analysis a series of numerical analysis were performed. Considering a three point bend specimen, with $G_F=100$ N/m, $f'_t=2$ MPa, $S/W = 8$, $a/W = 0.6$, $s_0=100$ mm, beams with s_0 , $10s_0$, $50s_0$ and $100s_0$ were analyzed using the code Merlin (**Saouma et al., 2010**). Through those analyses, the two stress intensity factors K_a (caused by the external load) and K_b (caused by the cohesive Hillerborg's stress) were determined. Whereas contour integral techniques should be favored, one should be careful to leave a small zone at the tip of the crack traction free, otherwise the J integral will be equal to zero. Hence, in the context of this analysis (with surface traction on the crack faces) we used singular elements.

⁴⁰ In each analysis, P_{max} corresponded to the onset of unstable crack growth (based on tensile stress at the crack tip), and the corresponding stress intensity factor K_{a+b} were determined. It should be noted that in our implementation of the interface element (based on the extended Hillerborg's model) pre-peak crack opening can occur. This results in a nonlinear pre-peak load-cod curve.

⁴¹ Whereas the variation of P_{max} with respect to s was indeed according to Bažant's size effect law, the net stress intensity factors at P_{max} ranged between 0.05 and 1.5 MPa $\sqrt{\text{mm}}$. Given that a representative value for the fracture toughness of concrete is about 1 MPa $\sqrt{\text{m}}$ or 31 MPa $\sqrt{\text{mm}}$, the net stress intensity factor can be considered as essentially zero. These values should be independent of the tensile strength, as a higher f'_t would result in a larger external load, and a higher K_a , but also in a higher (negative) K_b caused by the cohesive stresses. Indeed, when the tensile strength was increased from 2 MPa to 4 MPa, P_{max} was about twice the original values, however there was no discernable variation in K_{a+b} .

⁴² Thus, we conclude that for all practical purposes a NLFM analysis yields a very small non-zero stress intensity factor in comparison with fracture toughness. Hence, practicing engineers who accept a zero fracture toughness LEFM analysis should be reassured that a non-zero tensile strength in the context of a NLFM is, for all practical purposes, identical.

14.3 Conclusion

⁴³ The size effect law is rederived through a balancing of far-field induced stress intensity factors with those caused by the cohesive stresses. Hence, a direct relationship between plasticity and LEFM to the size effect law is presented. It is shown that the shape of the cohesive stresses is irrelevant, that the B coefficient can, albeit with some restriction, be analytically derived. Furthermore, in the context of the reported derivation, it is shown that not only quasi-brittle materials exhibit a size effect, but elasto-plastic ones (such as metals) too.

⁴⁴ Finally, it was also shown that a NLFM analysis with a non-zero tensile strength is practically identical to a LEFM analysis with zero fracture toughness.

Chapter 15

FRACTALS, FRACTURES and SIZE EFFECTS

Adapted from (?)

15.1 Introduction

15.1.1 Fracture of Concrete

There is not yet a standard for concrete fracture testing although several have been proposed Anon. (1985) Concrete fracture properties include fracture toughness K_{Ic} , characteristic length l_{ch} , brittleness number β , fracture energy G_F , crack-tip opening displacement $CTOD$, and at least three additional parameters that characterize the concrete strain softening curve.

This chapter addresses a technique that uses fractal geometry to determine whether there is any surface indication of the direction of crack propagation in concrete and whether there is a correlation between fracture properties (K_{Ic} and G_F , which characterize the material resistance to cracking) and the roughness of the fracture surface as characterized by the fractal dimension D . The implications of the fractal nature of the cracked surface on the “true” fracture or surface energy are then discussed.

15.1.2 Fractal Geometry

Although most manmade objects have linear or smoothly curvilinear shapes, natural objects (such as rivers, mountains, clouds, and fractures) are commonly rough, fragmented, or discontinuous. The apparent randomness of these irregularities, coupled with our bias toward Euclidian geometry, handicapped us in studying and properly modeling such objects until the advent of fractal geometry (Mandelbrot, 1983).

By definition, an inherent property of fractal objects is the statistical replication of patterns at different scales; a magnified part of a fractal object is statistically identical to the whole. Hence, Fig. 15.1-A illustrates the generation of a self-similar synthetic fractal curve, the triadic Koch curve.. First, an *initiator*, which represents an initial geometric form, is defined, then a *generator*, which describes a transformation on the initiator, is applied. As the transformation operation is repeatedly applied to the figure, a fractal curve is generated. For the triadic Koch curve, we note that at each step the number of line segments is increased by a factor of 4 and that the length of each new line segment generated is one third the length of line segments in the previous generation. This increases the total length of the fractal curve by four thirds at each step. Thus, as the number of iterations increases, the number of subdivisions N will vary from 1, 4, 16; $s = \frac{1}{3}$ where S is the scaling factor from 1, 3, 9; and the corresponding lengths will be 1, $\frac{4}{3}$, and $\frac{16}{9}$. The total length will eventually tend to infinity. The results of this operation are tabulated in Table 15.1. The fractal dimension D is defined as

$$D = \frac{\ln N}{\ln s}, \quad (15.1)$$

An alternative form of this equation is

$$N = s^D. \quad (15.2)$$

Note that the Euclidian definition of dimension, that is the topological dimension, is recovered if a line is subdivided into equal parts without changing its length. Since $N = S$ in this case, $D = 1$.

In our previous example, we subdivided line segments into four parts, thus $N = 4$ and we used $S = 1/3$ or $s = 3$. This gives a fractal dimension of $D = \frac{\ln 4}{\ln 3} = 1.2619$ for the curve shown in Fig. 15.1-A.

Mandelbrot (1983) offered the following tentative definition of a fractal. A fractal is a set for which the Hausdorf-Besicovitch dimension (D) strictly exceeds the topological dimension (D_T). For the curve shown in Fig. 15.1-A the topological dimension is 1, whereas the Hausdorf-Besicovitch dimension is 1.2619.

Step	N	S	s	Length
1	1	1	1	1
2	4	$\frac{1}{3}$	3	$\frac{4}{3}$
3	16	$\frac{1}{9}$	9	$\frac{16}{9}$

Table 15.1: Fractal dimension definition

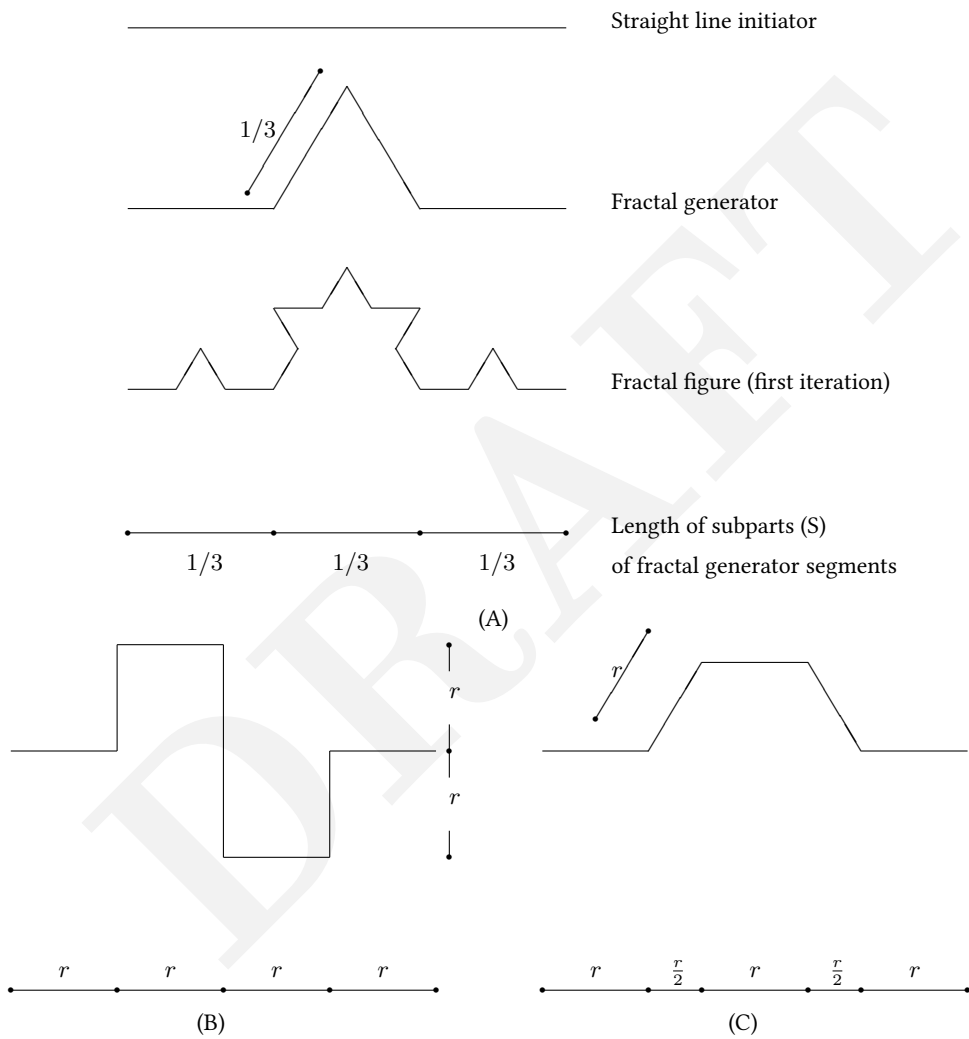


Figure 15.1: (A) Straight line initiator, fractal generator, and triadic Koch curve; (B) Quadratic Koch curve; (C) Modified Koch curve.

Hence, fractal surfaces have $D_T = 2$ and fractal dimensions $D > 2$. Mandelbrot (1983) showed that, as a *rule of thumb*, for a set S that is the product of two independent fractal sets S_1 and S_2 the fractal dimension of S equals the sum of the fractal dimensions of S_1 and S_2 . Hence, if the triadic Koch surface is uniformly extruded along the z direction, the fractal dimension of the surface is $S = S_1 + S_2 = 1.2619 + 1 = 2.2619$ (Feder, 1988) provided that we have two independent fractal sets. Alternatively, if the extrusion is fractal, then D is greater than 2.2619.

15.1.3 Numerical Determination of Fractal Dimension

Although the fractal dimension D of synthetic curves can be readily determined analytically, the dimension of arbitrary curves requires the use of numerical methods. Three of the most commonly used methods for measuring the fractal dimension of surface roughness are reviewed here.

Ruler Method: In the ruler method, (Aviles and Scholz, 1987; Mandelbrot, 1983) a divider (that is ruler) of given length S is used to determine the total length of the curve. Note that no fractional lengths can be taken. Thus, for a given ruler length, the curve length L is given by SN where N is an integer. This operation is repeated for a ruler of smaller and smaller length S , and the fractal dimension is given by

$$\begin{aligned} N &= \left(\frac{1}{S}\right)^D \\ &= s^D, \\ \underbrace{S \cdot N}_L &= \underbrace{S \cdot \left(\frac{1}{S}\right)^D}_{s^{1-D}} \end{aligned} \tag{15.3}$$

$$\ln L = (1 - D) \ln S. \tag{15.4}$$

Box Method: The box method is used in this study to measure the fractal dimension of the fracture roughness profiles. In principal, the method is simple; a sequence of grids, each having a different cell size, is placed over maps of the fracture traces and the number of cells intersected by fracture traces counted, (Barton et al., 1989). The number of grid cells intersected by the profile N is then plotted on a log-log scale with respect to the inverse of the grid cell size $s = \frac{1}{S}$. If a linear relationship is found, then the object is said to be *fractal* within the specified range of cell sizes and the fractal dimension is the slope of the line.

The box method, as well as the ruler method, is strictly applicable to self-similar data sets. Fracture roughness profiles in rock have been shown to be self-affine (Brown, 1987, 1988). Brown's analysis shows that application of the ruler method to self-affine data sets yields the correct fractal dimension only when the maximum ruler length used is less than the crossover length, which is defined as the ruler length beyond which the ruler method will always yield a fractal dimension of approximately one. Brown (1987) and Brown (1988) showed that the crossover is the length where the standard deviation of amplitude is equal to the wavelength, which for our profiles is approximately 8×10^{-2} meters. We expect the box method to exhibit a crossover length when applied to self-affine data sets such as our fracture surface profiles. Therefore, in this study we limited the largest box size to 8×10^{-2} m.

Slit Island Method: Whereas the preceding two methods measure the fractal dimension of fracture profiles ($1 < D < 2$), the Slit Island method is applicable to fractal surfaces ($2 < D < 3$). For each contour line of different elevation over the fracture surface, the perimeter \mathcal{L} and the area \mathcal{A} are determined and then plotted on a log-log scale. The fractal dimension is then be obtained from (Feder, 1988)

$$A = L^{\frac{2}{D-1}}. \tag{15.5}$$

15.1.4 Correlation of Fractal Dimensions With Fracture Properties

Fractal analysis is a simple and powerful tool for quantifying complex physical quantities. It has been used in numerous fields, ranging from clustering of co-citations in scientific papers (Van Raan, 1990) to earthquake prediction (Levi, 1990).

The roughness and irregularities of fractured surfaces make them ideal candidates for a fractal analysis. Indeed, as pointed out by Cahn (1989) fracture and fraction (fractals have fractional dimensions) have the same latin root *fractus*, which means to break and to create irregular fragments. This potential correlation has been the subject of numerous studies, which have yielded conflicting conclusions.

In the first study of fracture surfaces, Mandelbrot et al. (1984) showed that not only are cracked metallic surfaces (300-grade maraging steel) fractal but their fractal dimension is inversely proportional to the impact energy determined by the Charpy impact test (itself proportional to fracture toughness). Through simulation of a numerical model for fracture based failure of a polymeric, Termonia and Meakin (1986) showed that the synthetic fracture surfaces are also fractal and that the fractal dimension has a universal value of $D = 1.27 \pm 0.02$. More recently Peng and D. (1990) showed through a simple theoretical kinetic model which

Contents	Maximum size aggregate	
	1.5 in.	3.0 in.
Water (lbs/yd ³)	280	208
Cement (lbs/yd ³)	424	315
Water/Cement ratio	0.66	0.66
Sand (lbs/yd ³)	1,318	1,171
Gravel (lbs/yd ³)	2,054	2,481

Table 15.2: Concrete mix design

simulates crack propagation, that the resulting fracture surface is fractal and that its dimension depends on the material's elastic constants.

Although most researchers have found that fractured surfaces are fractal, [Underwood and Banerji \(1986\)](#) using AISI4340 steel specimens, did not detect a linear fractal curve and constant D but rather a reverse sigmoidal curve and variable D .

[Mecholsky et al. \(1989\)](#) concluded that the toughness increases with the roughness for six different alumina materials and five glass-ceramics having different microstructures and that the fracture toughness is directly related to the fractal dimension $K_{Ic} = E a_0^{\frac{1}{2}} D^{*\frac{1}{2}}$, where D^* is the fractional part of D , E is the elastic modulus, and a_0 a parameter having the units of length. Similar results were subsequently obtained for single crystal silicon ([Tsai and Mecholsky, 1991](#)) and for polystyrene fracture surfaces ([Chen and Runt, 1989](#)). More recently, [Mecholsky and Freiman \(1991\)](#) showed that there is a spatial variation of D along the length of the crack reflecting crack initiation and, later on, microbranching.

Discrepancy between results was recently pointed out by [Cahn \(1989\)](#) who noted that the relationship between fracture roughness as quantified by fractal dimension and fracture toughness is diametrically opposite for ductile fracture (maraging steel) and for brittle fracture (chert, and polycrystalline ceramics).

Recently, a fractal approach was applied to the fracture of rocks and soil. [Heping \(1987\)](#) postulated that the surface area of a crack for which the critical energy release rate $G_c = \frac{dU}{dA}$ is determined, should be adjusted to reflect the rough nature of the surface rather than the flat nominal surface. This would then systematically result in fracture toughness values ($K_{Ic} = \sqrt{G_c E'}$) that would increase with fractal dimension. Similarly, [Mosolov \(1991\)](#) has shown that for fractal cracks, the J integral ceases to be an invariant. [Mecholsky and Mackin \(1988\)](#) correlated the fracture toughness of Ocala chert (flint) with the fractal dimension and determined that one increased with the other. [Chelidze and Gueguen \(1990\)](#) showed that the fractal dimension increases with the surface energy (and hence the fracture toughness) of rocks. For fractures in soils, [Young and Crawford \(1992\)](#) determined that fracture profiles are fractal, with fractal dimensions very close to one.

[Winslow \(1985\)](#) showed through X-ray scattering techniques that, on the microscopic level, hydrated cement paste is fractal and has a fractal dimension of about 3.

All of the reported studies concern themselves with metals, polymers, rocks, or cement pastes, and only limited research has been reported in the fractal analyses of cracked concrete surfaces. [Saouma et al. \(1990\)](#) showed that cracked concrete surfaces are fractal. [Issa et al. \(1993\)](#) based on two-dimensional surface studies, found that the fractal dimension D varies from 2.1 to 2.22 and increases with aggregate sizes. Most recently, [Lange et al. \(1993\)](#) investigated the correlation between fracture roughness and fracture toughness, fractal dimensions and other physical properties. They report a fractal dimension of 2.087 for cement paste and 2.117 for fine mortar, and an increase between fractal dimension and fracture toughness.

Finally, it should be pointed out that it has been recently hypothesized that there is a universal value ($2.1 < D < 2.3$) for the fractal dimension of fractured surfaces ([Bouchaud et al., 1990](#)). This hypothesis was more recently strengthened by the finding of [Måløy et al. \(1992\)](#), ([Måløy et al., 1992](#)) who tested both ductile and brittle materials and reported a universal fractal dimension of $D = 2.11 \pm 0.006$.

15.2 Experimental Procedure

15.2.1 Fracture Testing

As part of a study on the applicability of fracture mechanics to the failure analysis of concrete dams by [Saouma et al. \(1991a\)](#), a series of wedge splitting (WS) tests was performed on specimens 3 and 5 ft long (Fig. 15.2), 16 in. thick and with maximum aggregate sizes up to three inches¹, as given in Table 15.2.

The effects of both aggregate size and the type of aggregate (crushed subangular as opposed to river rounded) were studied, as well as the effect of cold-joints.

In the WS experiments, the primary deformation measured was the crack-mouth opening displacement (CMOD), which also provided the feedback control to achieve a constant rate of 1.0- μ m/sec for the CMOD. Through this configuration, stable crack

¹Since all experiments and data reduction were performed using U.S. customary units, the following conversions factors should be considered: 1 in.=2.54 cm; 1ft=30.48 cm; 1 psi=689.48 Pa; 1 ksi= $\sqrt{\text{in}}$ =0.910 Mpa $\sqrt{\text{m}}$; 1 lb/in.=175.44 N/m.

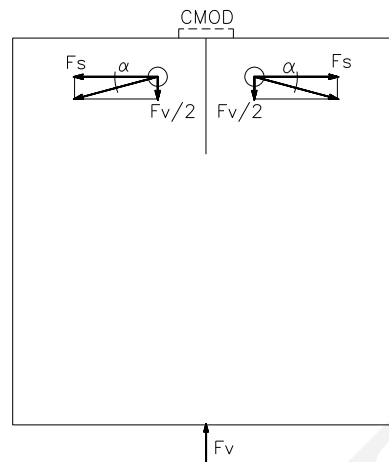


Figure 15.2: Frontal view of wedge-splitting-test specimen showing forces applied to specimen by lateral wedge loading (F_S) between two circular pins located near top of specimen on either side of the vertical starting notch. Crack Mouth Opening Displacement (CMOD) gage straddles the initial notch.

	Range	Precision
X	24	.0021
Y	60	.0013
Z	5	.005

Table 15.3: Range and resolution of the profilometer (inches)

growth with structural post-peak response was achieved. During the test both vertical load and CMOD were monitored and recorded. Finally, unload/reload cycles were performed to monitor change in specimen compliance from which the effective crack length a_{eff} was then calculated.

15.2.2 Profile Measurements

A fully automated profilometer [Saouma et al. \(1990\)](#), which scans the surface by means of a motorized computer-controlled placement of a linear variable differential transformer (LVDT), was used to determine crack profile with an average resolution of 0.001 in. the precision shown in [Table 15.4](#). The LVDT is seated on a composite bushing that slides along two parallel, ground-steel rods which are rigidly attached to a second bushing. The second bushing traverses a second pair of rods, which, in turn, are mounted at right angles with respect to the first set of rods. The entire system is placed on a rigid steel base over the specimen. Movements of the two bushing sets are controlled by two-worm gear and stepped-motor assemblies such that the LVDT can travel along any preprogrammed path in the $X - Y$ plane. Two separate computers are used, the first to control positioning of the LVDT, the second to record and store its reading (following reception of a signal from the first one). Finally, for each specimen profile, measurements along the four principal orientations (at 45° increments) were recorded in order to assess potential geometric anisotropy in fractal dimensions as shown in [Fig. 15.3](#).

15.2.3 Computation of Fractal Dimension

Following preliminary tests, it was determined that the box method yielded more consistent results than the ruler method, and hence it was adopted. The box method can be applied to both self-affine and self-similar profiles with the limitations stated above.

Although the implementation of the box method may *a priori* appear to be quite simple, that is a count of the number of cells intersected by the profile, three factors influence its reliability: (1) orientation of the grid with respect to the profile; (2) distribution

SPECIMEN SIZE		3 ft	5 ft
Profile length	0°	16.0 in.	26.67 in.
	90°	15.0 in.	15.0 in.
	±45°	17.0 in.	20.0 in.
Resolution of readings	0°	160 /in.	160/in.
	90°	192/ in.	192/in.
	±45°	175/ in.	175/in.
Spacing between profiles	0°	4.0 in.	4.0 in.
	90°	4.0 in.	4.0 in.
	±45°	2.0 in.	4.0 in.

Table 15.4: CHECK Mapped profile spacing, orientation, and resolution for the two specimen sizes investigated

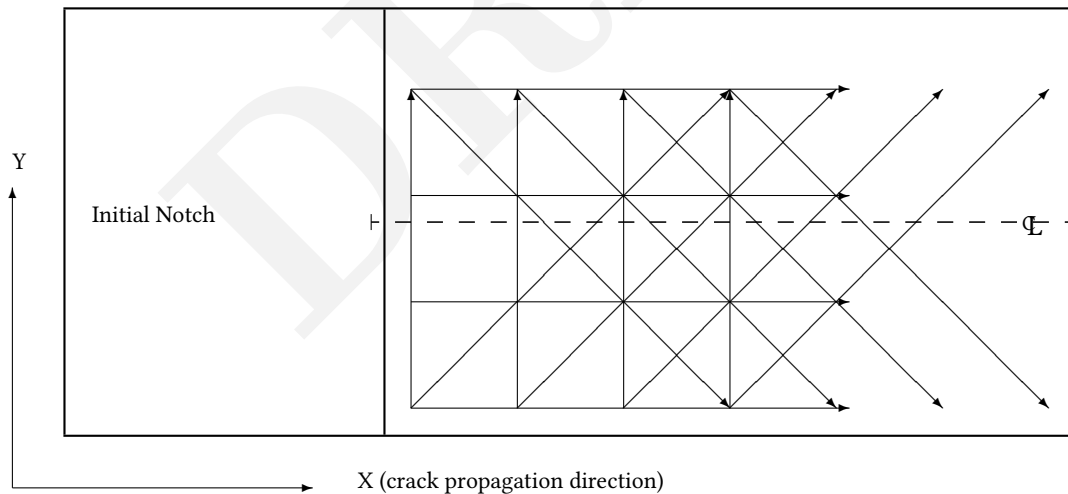


Figure 15.3: Orientations of measured profiles over the fractured surface, horizontally, vertically, and diagonally.

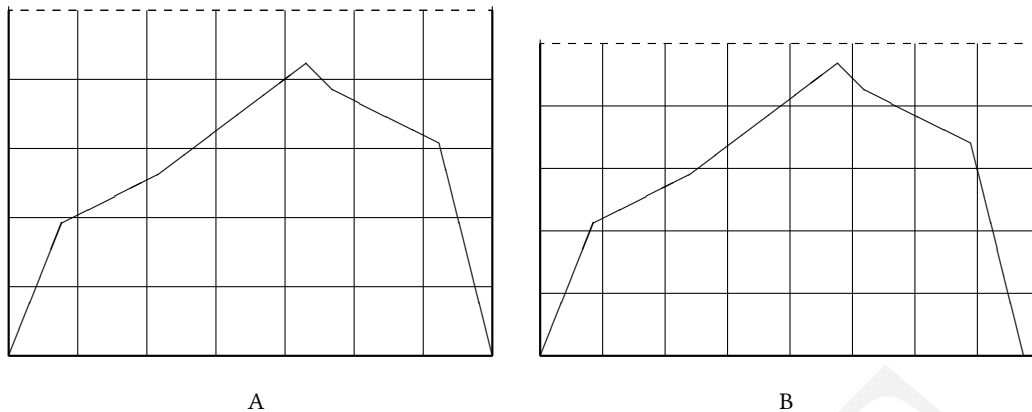


Figure 15.4: Typical grid overlying an object. Dashed lines indicate adjustable fixed grid boundaries; B, Flexible grid boundaries.

Angle of inclination	Grid size		
	40 points	300 points	1000 points
0°	1.000	1.000	1.000
5.0°	1.030	1.013	1.006
10.0°	1.048	1.017	1.008
15.0°	1.057	1.017	1.008
20.0°	1.062	1.017	1.008
25.0°	1.078	1.020	1.009
30.0°	1.062	1.017	1.007
35.0°	1.068	1.017	1.007
40.0°	1.080	1.019	1.008
45.0°	1.000	1.000	1.000

Table 15.5: Computed fractal dimensions of a straight line with various inclinations

and number of grid sizes; and (3) tolerance used in determining the number of intersected cells.

In our implementation, a reference base line was first defined by simply connecting the first and last profile points, then grids with a logarithmic size distribution ranging from 2×10^{-4} to 10^{-1} (from four times the profile precision to the profile length divided by four) were defined.

With regard to the initial grid definition, two strategies were considered -fixed and flexible grid boundaries, (Fig 15.4). In the method of fixed grid boundaries the two end points are fixed, whereas in the flexible grid method only the first one is fixed.

The resolution of the two algorithms was determined by testing against synthetic fractal curves. The curves included straight lines at different orientations to the box grid; 5th, 6th, and 8th generation triadic Koch curves (Fig. 15.1-A), 4th and 5th generations of the quadratic Koch curves (Fig. 15.1-B, and 5th and 6th generation modified Koch curves (Fig. 15.1-B-C).

Based on the results shown in Tables 15.5 and 15.6, it was concluded that fractal dimensions can at best be determined with an accuracy of ± 0.025 .

These test problems underscore the complexities in determining fractal dimensions of stochastic curves.

15.3 Fractals and Fracture

The fracture surfaces of our specimens are fractal for grid sizes ranging from $2 \times 10^{-3.2}$ to $10^{-2.1}$ m (Fig. 15.5). The average fractal dimension of approximately 1.1 compares exactly with the one determined experimentally for concrete by Issa *et al.*, (1992), ($D = \frac{2.2}{2} = 1.1$, assuming that we do have two independent and orthogonal fractal sets as partially supported by Table 15.7 and by Long *et al.* (1991)) and with the universal value of 2.11 proposed for fracture surfaces by Måløy *et al.* (1992). The division by two to obtain the profile fractal dimension from a surface fractal dimension was discussed previously, and is justified by the fractal nature of orthogonal profiles having almost identical fractal dimensions (as will be discussed following).

Having confirmed the fractal nature of the cracked surfaces, three important questions arise: (1) what is the spatial variation

Koch curve type	Generation	Fixed grids		Flexible grids		Theoretical Value
		D	Grid size	D	Grid size	
Triadic	5 th	1.377	15	1.305	500	1.262
Triadic	6 th	1.313	64	1.307	500	
Triadic	8 th	1.285	647	1.296	500	
Quadratic	4 th	1.410	17	1.477	500	1.500
Quadratic	5 th	1.477	93	1.486	500	
Modified	5 th	1.188	93	1.190	500	1.161
Modified	6 th	1.177	401	1.186	500	

Table 15.6: Computed fractal dimensions for various synthetic curves

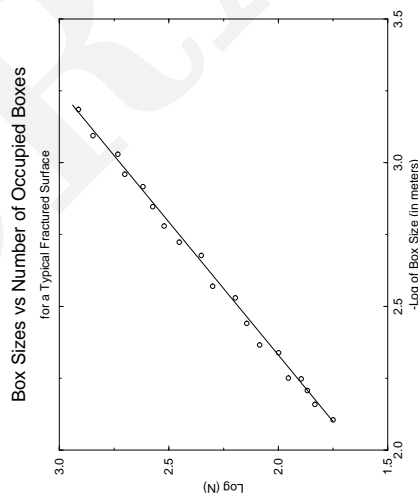


Figure 15.5: Plot of box counting method applied to the profile of a typical fractured concrete specimen. Number of occupied boxes (N) is plotted versus box size. Slope of line fit to data is the fractal dimension (D).

Specimen	Profile direction	Profile Distance from Centerline				Average	$\sigma_D\%$
		1 in.	3 in.	5 in.	7 in.		
3-ft specimens of 1.5-in. MSA							
A	0°	1.096	1.118	1.098	1.113	1.106	1.1
	90°	1.087	1.115	1.101	1.088	1.098	1.1
	+45°	1.096	1.100	1.104	1.123	1.106	1.1
	-45°	1.073	1.109	1.090	1.097	1.092	1.1
B	0°	1.096	1.118	1.064	1.112	1.097	2.2
	90°	1.109	1.100	1.088	1.133	1.107	1.7
	+45°	1.112	1.111	1.073	1.125	1.105	2.0
	-45°	1.094	1.085	1.096	1.085	1.090	0.5
C	0°	1.130	1.128	1.094	1.115	1.117	1.5
	90°	1.092	1.098	1.126	1.106	1.105	1.3
	+45°	1.108	1.087	1.122	1.105	1.105	1.3
	-45°	1.113	1.127	1.101	1.102	1.111	1.1
3-ft specimens of 3.0-in. MSA							
A	0°	1.099	1.107	1.084	1.097	1.097	0.9
	90°	1.123	1.107	1.087	1.129	1.111	1.7
	+45°	1.084	1.071	1.089	1.114	1.089	1.7
	-45°	1.148	1.115	1.094	1.123	1.120	2.0
B	0°	1.147	1.096	1.123	1.069	1.109	3.0
	90°	1.116	1.127	1.100	1.165	1.127	2.5
	+45°	1.104	1.111	1.083	1.110	1.102	1.2
	-45°	1.094	1.087	1.107	1.115	1.101	1.1
C	0°	1.118	1.098	1.113	1.106	1.109	0.8
	90°	1.115	1.101	1.088	1.098	1.100	1.0
	+45°	1.100	1.104	1.123	1.106	1.108	0.9
	-45°	1.109	1.090	1.097	1.092	1.097	0.8

Table 15.7: Fractal dimension D versus profile orientations

Distance from specimen centerline	Zone of analysis					
	First quarter	Second quarter	Third quarter	Fourth quarter	First half	Second half
1 in.	1.118	1.120	1.073	1.083	1.126	1.093
3 in.	1.128	1.106	1.111	1.150	1.121	1.119
5 in.	1.118	1.080	1.082	1.082	1.084	1.075
7 in.	1.110	1.099	1.113	1.119	1.100	1.124

Table 15.8: Fractal dimension for various profile segments and distances from centerline in specimen S33A

of the fractal dimension; (2) is there a correlation between fractal dimension and fracture properties for concrete; and (3) how do the results for concrete compare with other materials?

15.3.1 Spatial Variation of the Fractal Dimension

The spatial variation of the fractal dimension was investigated with particular attention to the (1) location and length of the profile within the width of the crack front; (2) the orientation of the profile with respect to the direction of crack propagation; and (3) specimen and aggregate sizes and aggregate angularity.

***D* versus Profile Location and Length:** Variation in fractal dimension as a function of profile location and profile length was studied for a series of profiles oriented parallel to the direction of fracture propagation on a single fracture specimen because it was postulated that:

1. Different D values across the thickness might be obtained due to the near plane stress condition on the edge of the specimen and the near plane strain condition at the center.
2. Different D values along the length may be obtained due to the lack of a fully developed process zone in the early part of the crack surface.

Assuming a linear relationship between fractal dimension D and the profile's distance x from the centerline,

$$D = a + bx \quad (15.6)$$

it was observed that in most cases b is negative, implying a reduction in fractal dimension D as the profile moves from the centerline to the edge. This was confirmed by visual inspection of the cracked surfaces, which showed that the center of the cracked surface appears to be rougher than the edge.

When the fractal dimensions of the same specimen were determined over different parts of the length (Table 15.8), it was observed that in most cases D is greater over the first half than over the second half. In most cases D is greater in the first quarter than in the fourth one. Even though the difference is quite small (more supporting experimental data is needed to fully address this point), it may be caused by the presence of a fully developed process zone in the first half as opposed to the second one.

***D* versus Orientation of Profile:** It has been speculated that the direction of crack propagation might affect the value of D . If this is correct, then it should be possible through *postmortem* investigation of a cracked surface to determine the direction of fracture propagation.

We concluded by examination of the results (Table 15.7), that there is no apparent correlation between the fractal dimension and the profile orientation. It should be noted that Long et al. (1991) found that there is such a correlation for metals.

***D* versus Specimen Size, Aggregate Size, and Aggregate Type:** Comparing the fractal dimension D obtained from 3- and 5-ft-long specimens (Table 15.9), there is a clear indication that the longer the specimen size, the lower the fractal dimension everywhere on the fracture surface. This may result from the correlation between D and K_{Ic} (discussed in the next section), that shows bigger specimens yield slightly higher fracture toughness and smaller D values than smaller specimens.

We find no correlation between D and the aggregate size. This confirms two earlier findings: (1) fracture toughness values are independent from aggregate sizes (Saouma et al., 1991a) and (2) the size-effect law (Bažant, 1984) is not dependent on aggregate sizes as reported in Saouma et al. (1991).

Table 15.9 shows that for 3-ft-long specimens having 1.5-in. maximum size aggregate (MSA), subangular aggregates yielded smaller D values than rounded ones. This correlates with our observation that during fracture, the crack circumvented rounded aggregates while breaking subangular ones. The former would yield rougher surfaces whereas the latter would yield tougher ones.

Specimen	Distance from centerline				Fractal dimension		G_F , [lb/in]	K_{Ic} [psi \sqrt{in}]	
	1 in.	3 in.	5 in.	7 in.	Average	σ_D %		Average	σ_K %
3-ft specimens of rounded 1.5-in. MSA									
S32A	1.096	1.094	1.096	1.112	1.100	0.8	1.28	812.	10.0
S32B	1.096	1.118	1.064	1.112	1.098	2.2	1.17	909.	5.5
S32C	1.130	1.128	1.094	1.115	1.117	1.5	1.36	1,004.	11.3
Average	1.107	1.113	1.085	1.113	1.105		1.27	908	
3-ft specimens of rounded 3.0-in. MSA									
S33A	1.099	1.107	1.084	1.097	1.097	0.9	1.21	901.	6.3
S33B	1.147	1.096	1.123	1.069	1.109	3.0	1.26	862.	6.4
S33C	1.118	1.098	1.113	1.081	1.103	1.5	1.40	1,166.	7.7
Average	1.121	1.100	1.107	1.082	1.103		1.29	976	
3-ft specimens of 1.5-in. MSA (subangular basalt aggregate)									
SS32A	1.084	1.089	1.096	1.052	1.080	1.8	1.73	1,274.	9.6
SS32B	1.090	1.077	1.096	1.076	1.085	0.9	1.42	1,137.	12.3
Average	1.087	1.083	1.096	1.064	1.083		1.57	1,206.	
5-ft specimens of rounded 1.5-in. MSA									
S52A	1.085	1.074	1.064	1.069	1.073	0.8	1.17	1,058.	6.9
S52B	1.066	1.070	1.072	1.050	1.065	0.9	1.63	1,164.	6.1
S52C	1.082	1.067	1.082	1.059	1.073	1.1	1.64	1,138.	3.5
Average	1.078	1.070	1.073	1.059	1.070		1.48	1,120.	
5-ft specimens of rounded 3.0-in. MSA									
S53A	1.091	1.077	1.088	1.073	1.082	0.8	1.35	893.	13.7
S53B	1.037	1.049	1.060	1.048	1.049	0.9	Not applicable		
Average	1.064	1.063	1.074	1.061	1.065				
5-ft cold joint specimens									
CJ52B	1.050	1.045	1.051	1.027	1.043	1.1	0.46	457.	3.3
CJ53A	1.051	1.064	1.056	1.050	1.055	0.6	0.76	643.	3.9
CJ53C	1.073	1.087	1.070	1.062	1.073	1.0	0.56	567.	2.6
Average	1.058	1.065	1.059	1.046	1.057		0.59	494	

Table 15.9: Comparison between D , K_{Ic} , and G_F for all specimens (MSA, Maximum size aggregate)

Profile distance from centerline	a	b	χ^2	$S_{x,y}\%$
$G_F = a + bD$				
1.0 in.	5.34	-3.605	0.183	12.4
3.0 in.	6.31	-4.511	0.212	12.2
5.0 in.	0.26	1.029	0.009	13.7
7.0 in.	7.26	-5.440	0.447	10.2
Average	7.87	-5.953	0.258	11.8
$K_{Ic} = a + bD$				
1.0 in.	4066	-2766	0.174	13.2
3.0 in.	4396	-3087	0.160	13.4
5.0 in.	1510	-444	0.003	14.6
7.0 in.	5507	-4147	0.419	11.1
Average	6220	-4766	0.267	12.5

 Table 15.10: Linear regression coefficients between G_F and K_{Ic} with D

15.3.2 Correlation Between Fracture Toughness and Fractal Dimensions

We now turn our attention to the possible correlation between fractal dimension D and fracture properties (Table 15.9). This analysis is possible because the specimens were originally tested for both fracture toughness K_{Ic} and fracture energy G_F as part of a different research study of Saouma *et al.* (1991).

If a correlation could be found, one could determine *post mortem* important fracture properties, K_{Ic} and G_F , by measuring roughness of the fracture surface in a forensic study. Table 15.9 summarizes fractal and fracture analyses for all specimens, as well as their respective averages and standard deviations, and Figs. 15.6-A and 15.6-B illustrate the variations of G_F and K_{Ic} versus D , respectively.

It should be noted that D , G_F , and K_{Ic} tested higher for concrete than for the cold-jointed specimens (Table 15.9). This is because of the weak bond between the two layers of concrete that results in relatively smooth surfaces.

Specimens prepared with subangular basalt aggregate had generally higher G_F and K_{Ic} and lower D . This can be explained by the nature of the fracture surfaces. The fracture plane went through this subangular strong aggregate leaving a relatively smooth surface. The fracture plane went around rounded aggregate, debonding the aggregate from the mortar and yielding a rougher surface obtained through less energy. If cold-joint specimens are excluded, D increases with a decrease in fracture toughness and energy.

Linear regression between D and both the specific fracture energy G_F and the fracture toughness K_{Ic} resulted in the following expressions:

$$G_F = 7.87 - 5.95D \quad \text{lb/in}; \quad \chi^2 = 0.258 \quad (15.7)$$

$$K_{Ic} = 6,220 - 4,766D \quad \text{psi}\sqrt{\text{in}}; \quad \chi^2 = 0.267 \quad (15.8)$$

Because of the low goodness of fit, great care should be exercised in using the above equations. Table 15.10 summarizes this correlation between fracture properties and fractal dimensions. Excluded are the results obtained from cold joints because these yield both lower fractal dimensions and lower fracture toughness due to the poor interface bond in those specimens. Alternatively, in regular specimens, a lower fractal dimension is synonymous with a higher fracture toughness because there is mostly aggregate rather than bond failure.

15.3.3 Macro-Scale Correlation Analysis

Noting that the range of variation for both D and K_{Ic} is indeed small, a comparison with ceramics and alumina was performed. Mecholsky and Freiman (1991) reported a much wider range of values, and those values are plotted along with the ones obtained from the present investigation (Fig. 15.6-).

There is no sharp discontinuity between the concrete and ceramic results; overall, D increases with K_{Ic} . This observation on the mesoscale clearly contradicts our earlier finding on the microscale, and may be explained by the different nature of the fracturing process in concrete aggregate.

A comparison of the fractal dimension and the fracture toughness in concrete determined in our investigation, as well as the same characteristics in other materials reported in the literature, is plotted in Fig. 15.6-D. From this figure, we note that only concrete has a negative slope (decrease in fracture toughness with increase in fractal dimension); all others have a positive slope. As indicated earlier, we conclude that this is caused by the heterogeneous nature of concrete and, more specifically, by the nature of the aggregate cement bond.

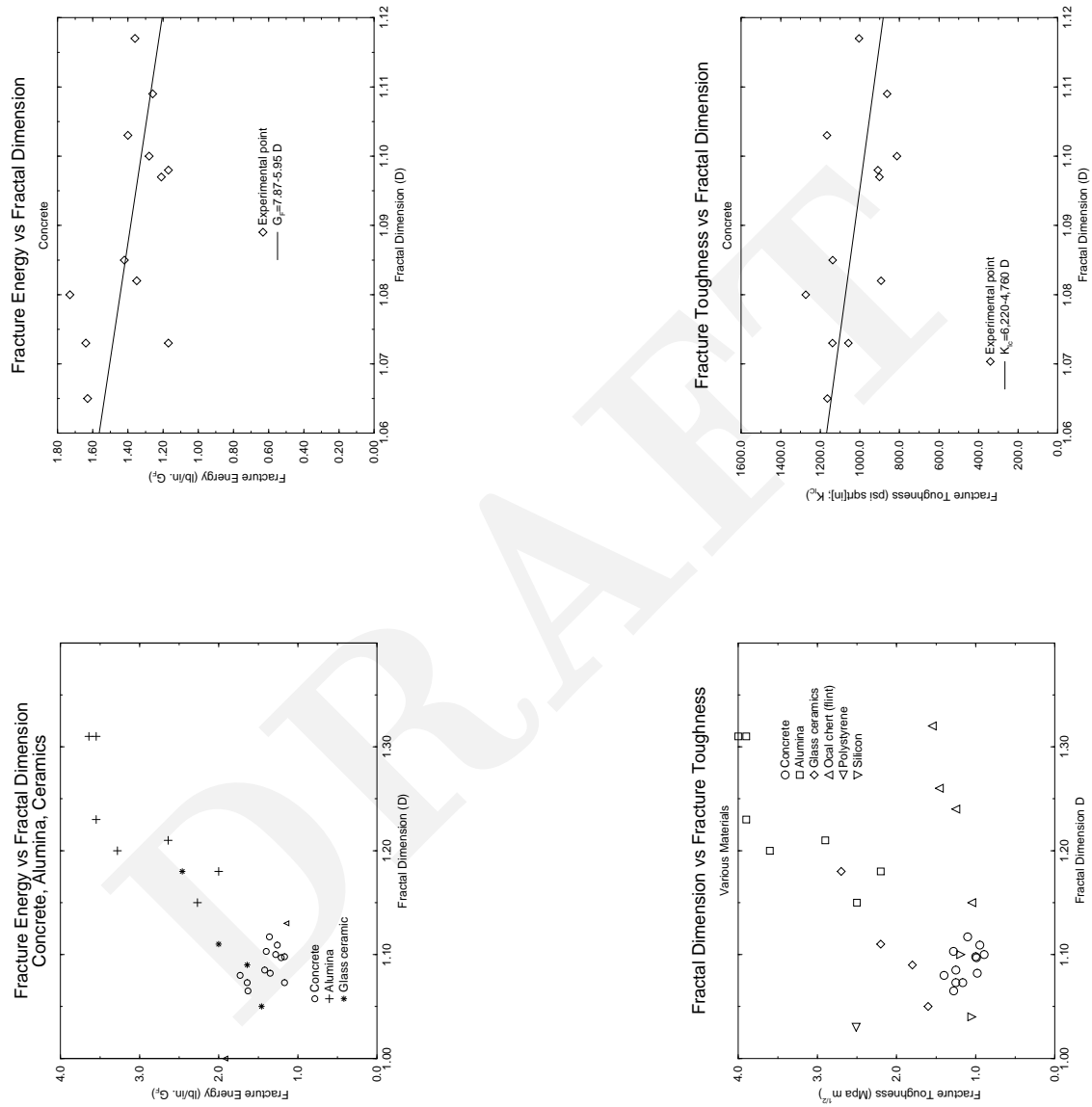


Figure 15.6: A-B) G_F and K_{Ic} versus D ; C) G_F versus D for concrete (this study), ceramics, and alumina (Mecholsky and Freiman, 1991); D) K_{Ic} versus D for concrete (this study); ceramics, and alumina (Mecholsky and Frieman, 1991); Flint (Mecholsky and Mackin, 1988); polystyrene (Chen and Runt, 1989); and silicon (Tsai and Mecholsky (1991)

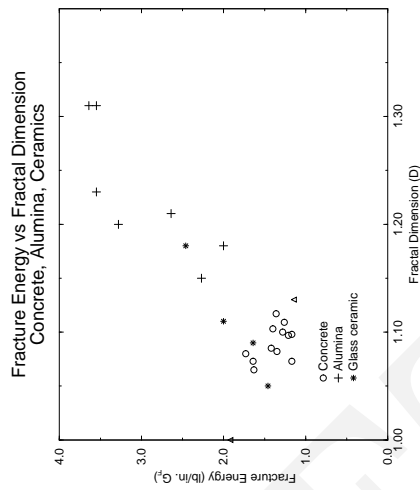


Figure 15.7: G_F versus D for concrete (this study), ceramics, and alumina (Mecholsky and Freiman, 1991)

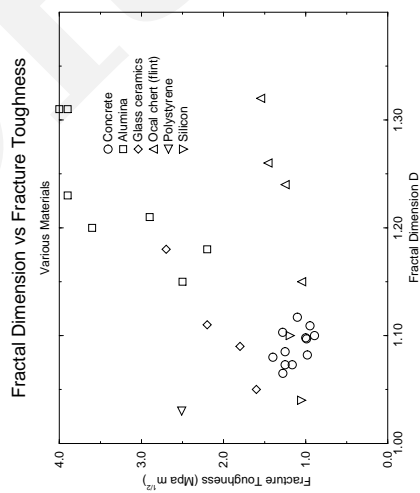


Figure 15.8: K_{Ic} versus D for concrete (this study); ceramics, and alumina (Mecholsky and Frieman, 1991); Flint (Mecholsky and Mackin, 1988); polystyrene (Chen and Runt, 1989); and silicon (Tsai and Mecholsky (1991)

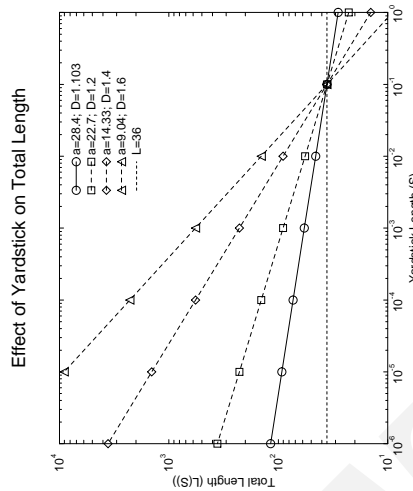


Figure 15.9: Variation of $L(S)$ in terms of S

15.4 Fractals and Size Effects

The size effect law (Bažant, 1984) and a fractal analysis bear many similarities:

Log-Log plot: In both cases the experimental investigation must be carried over at least two orders of magnitude of size (even though this is rarely done in size effect studies).

Size/Scale dependency: Neither a fractal investigation nor a size effect study yield a unique value for length/area or strength; however, these quantities depend on either the size of the specimen or of the ruler used.

Singularity of results is achieved for very small ruler or very large specimen sizes. In a fractal analysis, an infinitesimally small ruler should yield an infinite profile length, and the order of the singularity is $1 - D$. Alternatively, for very large specimens the order of singularity of stress is $-\frac{1}{2}$. As an example, consider the synthetic fractal curve of Fig. 15.1-A; the total length of the profile goes from 1, to $\frac{4}{3}$, to $\frac{16}{9}$ as the ruler length decreases from 1, to $\frac{1}{3}$, to $\frac{1}{9}$. Rewriting Eq. 15.4 we obtain the following relationship between the ruler length S and the total length $L(S)$ in terms of the fractal dimension D ,

$$L(S) = aS^{1-D}. \tag{15.9}$$

For the 3-ft-long specimens where L was measured with a ruler of length (S) approximately equal to 0.1 in., a fractal dimension (D) of 1.103 was determined. Hence, $a = \frac{L}{S^{1-D}} = \frac{36}{.11-1.103} = 28.40$ and the variation of $L(S)$ is shown in Fig. 15.9. Also shown are $L(S)$ for various hypothetical fractal dimensions of 1.2, 1.4, and 1.6. From this figure it is apparent that practically any profile length (hence surface area) can be obtained by choosing the appropriate ruler length². This figure also illustrates how a small variation in fractal dimension D results in substantially larger $L(S)$.

In determining the correct surface area, reference is made to the surface area obtained through measurements with a ruler of size S_0 . From Eq. 15.9, the correct profile length L^D is given by

$$L^* = \left(\frac{S^*}{S_0}\right)^{(1-D)} L_0, \tag{15.10}$$

where L_0 is the length measured with S_0 .

We hypothesize that

$$\lim_{d \rightarrow \infty} \mathcal{P}^{\text{SEL}} = \lim_{S \rightarrow 0} \mathcal{P}^{\text{F}}, \tag{15.11}$$

²Ironically, this singularity is reminiscent of the one associated with the recovery of (singular) crack tip stresses in terms of the finite element mesh size used; the smaller the crack tip element size, the larger the computed stress.

S_0	S^*			
	"Macro": sand		"Micro": C-S-H	
	#100 .0059 in.	# 200 .0029 in.	20 μ m .0008 in.	10 μ m .0004 in.
1.	2.79	3.22	4.18	4.78
.25	2.12	2.44	3.16	3.62
.1	1.76	2.03	2.63	3.02

 Table 15.11: Amplification factors for fractal surface areas with $D = 1.1$

where \mathcal{P}^{SEL} and \mathcal{P}^{F} are selected properties obtained from the size effect law and from a fractal analysis, respectively. In the former, this entails testing of various similar specimens with subsequent extrapolation to infinity through the size effect law; in the latter it entails careful analysis of just one specimen using various rulers lengths.

In order to validate the former hypothesis we consider the fracture energy G_F for which the following relation holds

$$\lim_{d \rightarrow \infty} G_F = G_c = \frac{K_{Ic}^2}{E}. \quad (15.12)$$

For 1.5-in. maximum size aggregates in 3-ft-long specimens, the following overall average values were determined (Saouma *et al.* 1991): $G_F = 1.37$ lb/in., $K_{Ic} = .929$ Ksi $\sqrt{\text{in}}$ and $E = 2,460$ Ksi. Using Eq. 15.12 we determine $G_c = \frac{.929^2}{2,460} 1,000 = 0.35$ lb/in. which is much lower than G_F .

To explain this discrepancy through fractal interpretation, recall that G_F is defined as the energy required to create a unit surface area. The total energy experimentally consumed is determined from the area under the load-displacement curve, but how do we define the cracked surface area?

Traditionally, the nominal surface area has been used (RILEM 1985), and this approach, although justified within the context of a finite element analysis where the roughness of the cracked surface is not accounted for, however may not yield the correct material G_F . As pointed out by Heping (1987) the roughness of the surface should be accounted for, which would increase the surface area and thus reduce G_F . For a surface area, Eq. 15.10 becomes

$$\begin{aligned} A^* &= \left(\frac{S^* \times S^*}{S_0 \times S_0} \right)^{(1-D)} A_0 \\ &= \left(\frac{S^*}{S_0} \right)^{2(1-D)} A_0. \end{aligned} \quad (15.13)$$

Recall that S_0 is the size of the ruler with which L_0 was determined (in our case 0.1 in.) and that S^* is a threshold or characteristic smallest length scale such as the size of an atom, molecule, or crystal. This quantity is referred to as a *monomers* by Feder (1988) and is associated with the physical structure of the surface.

For concrete S^* can be determined either "macroscopically" as the size of #100 or #200 ASTM sieves, with respective sizes of 0.0059 and 0.0029 in. Alternatively, S^* can be determined on the basis of a "microscopic" scale associated with the approximate size of the calcium silicate hydrate (C-S-H), which is approximately 10-20 μ m (0.0004-0.0008 in). Table 15.11 illustrates the amplification factor for a surface area on the basis of Eq. 15.13. Hence, fracture energy G_F should be decreased such that

$$\begin{aligned} G_F^* &= \left(\frac{S_0}{S^*} \right)^{2(1-D)} G_F \\ &= \left(\frac{.1}{.0004} \right)^{2(1-1.1)} 1.37 = 0.45 \quad \text{lb/in} \end{aligned} \quad (15.14)$$

Note that G_F^* is closer to G_c than G_F is.

As an additional evaluation of this approach, we re-examine tests results of Swartz and Kan (1992) who investigated the influence of aggregate/paste bonding on the mode I fracture strength. Using the same correction factor as the one employed above $\left(\left(\frac{.1}{.0004} \right)^{2(1-1.1)} = 0.331 \right)$, we obtained the results shown in Table 15.12.

Finally, it should be mentioned that whereas G_F^* is quite sensitive to the assumed S^* values, the choices of this later parameter is entirely justified from a purely material point of view.

Using the proposed approach in which the cross sectional area is adjusted by the fractal dimension, a fracture parameter was approximated from a single specimen size through fractal analysis. This approach is to be contrasted with the Euclidian analysis of multiple specimen sizes through the size effect law.

Specimen	Aggregate type	Water/cement	E_c	K_{Ic}	G_F	G_c	G_F^*
			psi $\times 10^6$	psi $\sqrt{\text{in}}$	lb/in.	lb/in.	lb/in.
NC-.64	Crushed Limestone	0.64	4.5	922	0.565	0.19	0.187
HC-.64	Crushed Quartzite	0.64	5.08	1,206	0.824	0.286	0.273
NP-.64	Crushed & Polished Limestone	0.64	4.74	980	0.570	0.203	0.189
NP-.30	Crushed & Polished Limestone	0.30	5.46	1,266	0.727	0.293	0.241
HC-.30	Crushed Quartzite	0.30	5.54	1,523	0.952	0.419	0.315
NC-.30	Crushed Limestone	0.30	6.03	1,308	0.679	0.280	0.225

Table 15.12: Comparison between “corrected” G_F^* and G_c values based on Swartz Tests (1992).

15.5 Conclusions

Wedge splitting tests on 3- and 5-ft-long specimens having a maximum size aggregate of 3 in. were first tested for fracture toughness K_{Ic} and fracture energy G_F . Subsequently, profile measurements along the cracked surfaces (with different lengths and orientations) were performed and their respective fractal dimensions D determined.

From this investigation, it was concluded that

1. Fractal dimensions numerically determined by the box method have a resolution of ± 0.025 .
2. Fracture surface profiles in concrete are fractal.
3. The fractal dimension of the monotonically cast specimens is in the narrow range of 1.06 to 1.12. These values are close to one independently measured by Issa *et al.* (1992), who used a different fractal analysis technique.
4. The fractal dimension of cracked concrete is insensitive to the orientation of the roughness profile.
5. Fractal dimensions near the center of the fracture surface are slightly larger than those computed on the sides of the same surface.
6. For the concrete studied here, fracture toughness increases with a decrease in fractal dimension in concrete; however, great care should be exercised in generalizing this finding, and the physical nature of the fracturing process should be closely examined.
7. There appears to be a linear relationship between fracture surface roughness as defined by fractal dimension and fracture energy for concrete and ceramics.
8. There are strong analogies between the fractal analysis and the size effect law.
9. Some fracture mechanics parameters can potentially be recovered from a fractal analysis of a single small specimen without resorting to increasingly large specimen sizes as is required by the size effect law.

Chapter 16

On Fractals and Size Effects

16.1 Introduction

In recent years, two opposing theories have emerged, the Size Effect Law (SEL) of Bažant, and the Multi-Fractal Size Law (MFSL) of Carpinteri. By now the debate on those two models has spilled out of the ivory towers of universities and there are strong indications that this duality of contradictory models is becoming an impediment to modernization of the ACI code.

Henceforth, this paper will re-examine scaling laws, size effects, and fractal theories in both historical and scientific context and with sufficient details to subsequently: 1) assess the MFSL; and 2) extend Bažant's SEL to cohesive fractal cracks.

16.1.1 Fractals

16.1.1.1 Definition

A fractal object of fractal dimension D , embedded in a Euclidian space of dimension E is defined first by an initiator of Euclidian dimension E and linear size L which can be divided into n equal smaller replicates of linear size rL covering the whole object so that $n(rL)^E = L^E$. The similarity ratio is enforced by $nr^E = 1$. Then, a generator which replaces the n small replicates of the initiator by N identical parts which are then replaced by the generator scaled by a factor r . This process is repeated in a recursive manner *ad infinitum*. The fractal dimension D (also known as the Hausdorff dimension) is then defined by

$$D = \frac{\log N}{\log \frac{1}{r}} \quad (16.1)$$

or equivalently by $Nr^D = 1$.

The quintessential fractal is the von von koch curve, (Koch, 1904), shown in Fig. 16.1. Per our definition, $N = 4$, $r = 3$, and



Figure 16.1: Triadic von-Koch Curve; Example of a Self Similar Invasive Fractal

thus the fractal dimension is $D = \ln 4 / \ln 1/3 = 1.2619$.

Another well known example is the Sierpinsky carpet, (Sierpinski, 1912), Fig. 16.2. Here, $N = 8$, $r = 3$, $E = 2$ and thus the



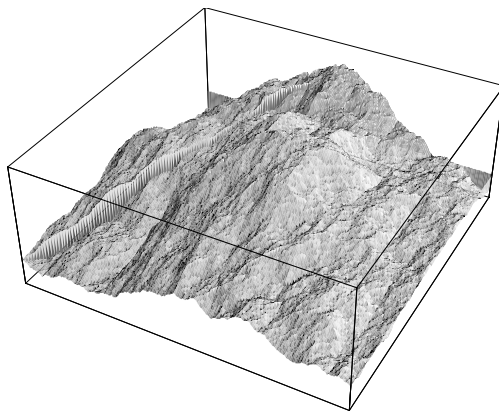
Figure 16.2: Sierpinski Carpet; Example of a Self Similar Lacunar Fractal

fractal dimension is $D = \ln 8 / \ln 1/3 = 1.8927$.

Indeed in both examples we do have fractal objects as the Hausdorff-Besicovitch dimension D strictly exceeds the topological dimension $D_T = 1$, (Mandelbrot, 1983).

16.1.1.2 Lacunar versus Invasive Fractals

Fractals can be characterized as lacunar or invasive. Lacunar fractals are obtained by creating at each stage a number N of replicates which is smaller than n . Hence, $N \leq n$ and thus $D \leq E$. Otherwise, the fractal is invasive. The area of lacunar fractal tends to zero, whereas the one of the invasive fractal surface tends to infinity. With reference to the previous two examples, the Sierpinski Carpet is lacunar since $1.8927 < 2$, whereas the von-Koch curve is invasive ($1.2618 > 1$).



<http://library.wolfram.com/infocenter/MathSource/4197/>

Figure 16.3: Example of a Self-Affine Fractal

16.1.1.3 Self-Similar and Self-Affine Fractals

In general scaling transformations can be expressed as $f(\lambda_x x, \lambda_y y) \sim f(x, y)$, or $x \rightarrow \lambda_x x$ and $y \rightarrow \lambda_y y$. If $\lambda_x = \lambda_y$, then we have a statistically isotropic fractal known as self-similar.

On the other hand, if we have rescaling by different factors in the $x - y$ plane, $\lambda_x \neq \lambda_y$, then we would have a self-affine transformation. **Turcotte (1992)** defines a self affine fractal in two-dimensional $x - y$ space if $f(\lambda_x x, \lambda_y y)$ is statistically self-similar to $f(x, y)$.

$H = \frac{\ln \lambda_y}{\ln \lambda_x}$ is called the Hurst exponent, (**Hurst, 1951**)¹. There is an ongoing debate (**Balankin, 1997**) as to whether H has a universal value ~ 0.8 , or whether it is material dependant.

Both Earth topology and crack surfaces are perfect examples of self-affine fractal. The “elevation” perpendicular to the average crack plane, and the one which defines the “roughness” of the fracture surface, are statistically related to the crack plane coordinates but have a consistently smaller magnitude, (**Weiss, 2001**). Fig. 16.3 illustrates a self-affine fractal surface which could be a landscape or a crack surface.

16.1.1.4 Multifractals

Many physical quantities are better modeled by multiple scaling schemes rather than by a single fractal. The term multifractal is applied when many fractal subsets with different scaling properties coexist simultaneously. In general, a multifractal field corresponds to an infinite hierarchy of fractal sets which are obtained by a cascade process described by an infinite number of parameters. Nevertheless, in some theories - as the Universal Multifractal theory by **Schertzer and Lovejoy (1997)** - the number of parameters can be reduced to three due to the simplifying assumption that the multifractal measure is the result of a special type of multiplicative process.

Multifractal processes are generally represented as multiplicative cascades. Fig. 16.4 illustrates the construction of a multiplicative cascade in a one-dimensional space. In this example, the field ϕ_0 is uniformly distributed over the length L at step 0. L is first partitioned into several parts and positive random weights i are generated for each part. In the simplest case, the scale ratio $\lambda = L/l$ (where L is the external scale of the cascade and l the scale of observation) takes discrete values: $\lambda = \lambda_1^n$ (λ_1 , usually equals 2, is the scale ratio for a discrete elementary step of the cascade). Each field in a corresponding sub-segment is multiplied by a random weight. At each cascade level the weights are selected such that their average is equal to 1. If the cascade preserves the measure of the initial set, it is called a deterministic cascade. Iterating the process indefinitely, the resulting field is a statistical multifractal.

$$\phi_{\lambda=2^n}(x) = \prod_{i=1}^n \mu_i \tag{16.2}$$

which corresponds to the multiplication of independently distributed random densities μ_i , and the cusps indicate the times where singularities occur.

¹Hurst was a “Nilologist” who studied the variation of the river Nile discharge and was seeking the design of an ideal reservoir (one which would release a volume each year equal to the mean influx for the period τ), (**Feder, 1988**). He defined $X(t, \tau)$ as the accumulated departure of the influx from the mean, $R(\tau)$ as the difference between the maximum and minimum amount of storage water, and $S(t, \tau)$ as the standard deviation of the influx. Hurst found that the observed rescaled range for many records in time is very well described by the empirical relation $R/S = (\tau/2)^H$.

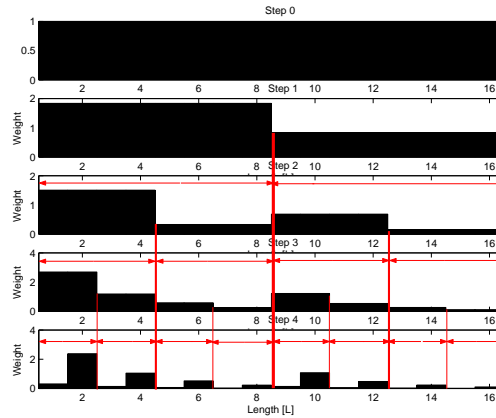


Figure 16.4: Example of an iteratively defined MultiFractal

16.1.1.5 Fractality of Cracks and Concrete

Inspired by the earlier work of [Mandelbrot et al. \(1984\)](#), [Saouma et al. \(1990\)](#) were among the first to conclusively show that cracked concrete surfaces are indeed fractal (within the range of measurements), that the fractal dimension varied between 2.1 and 2.22 and that it tended to increase with aggregate sizes. Subsequently, [Saouma and Barton \(1994\)](#) have attempted to correlate the fractal dimension with fracture energy and direction of crack propagation. It was found that there was no such correlation. In addition, a fractal fracture energy was defined as

$$G_F^* = \left(\frac{L_0}{L^*} \right)^{2(1-D)} G_F \quad (16.3)$$

where L_0 is the size of the “ruler” used to determine the crack surface and corresponding fracture energy G_F , and L^* is a macroscopic length associated with the physical properties of the constituent. It was shown that the statistical variation of G_F^* was indeed much smaller than the one of G_F , and approached the critical energy release rate G_c (which would be the case for G_F only for very large specimen sizes).

16.1.2 Size Effect

Every now and then, even Engineers are confronted with fundamental questions which may not (yet) have immediate practical applications to their professions, but which are nevertheless of basic essential and fundamental nature. The question, first (indirectly) posed by Galileo, is why is strength of some solids size dependant? Whereas historical notes are discussed later, one is compelled to note that at present there are two contradicting (and opposing) major theories. The size effect law of [Bažant \(1976\)](#), and the Multifractal model of [Carpinteri and Chiaia \(1994\)](#). Because of their importance, each will be reviewed separately.

16.1.2.1 Bažant

[Bažant \(1976\)](#) presented a model for the nominal strength of quasi-brittle material. It postulated that for quasi-brittle materials² and small sizes strength is driven by Plasticity and is thus size insensitive. On the other hand, for large sizes strength is driven by linear elastic fracture mechanics and thus has a $d^{-1/2}$ size dependency. Hence, the Size Effect Law, provides us with a simple and elegant equation for the strength-size relation which is asymptotic to plasticity for small size, and to linear elastic fracture mechanics for large ones.

Derivation of the size effect law is quite simple and elegant, ([Bažant, 1984](#)). If one considers the energy exchanged during an infinitesimal crack extension in a plate of width D , Fig. 16.5, the energy released can be approximated by $b2k(a_0 + c_f)\Delta a\sigma_n^2/2E$, which must be equal to the energy consumed during crack growth: $bG_F\Delta a$, hence

$$b2k(a_0 + c_f)\Delta a\sigma_n^2/2E = bG_F\Delta a \quad (16.4)$$

yielding

$$\sigma_n = \frac{Bf'_t}{\sqrt{1 + \frac{D}{D_0}}} \quad (16.5)$$

²Quasi-brittle materials are characterized by cohesive stresses in cementitious materials in the spirit of [Hillerborg et al. \(1976a\)](#), or by plastic zones around the crack tip in the spirit of [Dugdale \(1960\)](#).

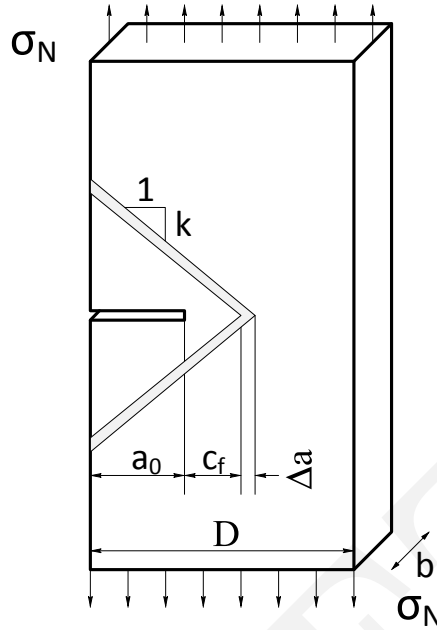


Figure 16.5: Energy Transfer During Infinitesimal Crack Extension

where

$$Bf'_t = \sqrt{\frac{G_F E}{kc_f}} \quad \text{and} \quad \frac{D}{D_0} = \frac{a_0}{c_f} = \beta \quad (16.6)$$

This original derivation has been followed by numerous refinements and generalizations. The simplicity and the power of this law are by now universally recognized, and was indeed the subject of Prof. Bažant inaugural article at the National Academy of Sciences, (Bažant, 2005).

Saouma et al. (2003) proposed an alternative derivation of only Bažant's original size effect law. Contrarily to the original Lagrangian derivation based in energy transfer, a Newtonian one based on local stress intensity factors was proposed. The stress intensity factors due to the far field (constant traction on an infinite plate) and cohesive stresses are:

$$K_a = \sigma\sqrt{\pi a} \quad (16.7)$$

$$K_b = f'_t\sqrt{\pi a} \left(1 - \frac{2}{\pi} \arcsin \frac{a - c_f}{a} \right) \quad (16.8)$$

respectively, (Cherepanov, 1979). Equating those two stress intensity factors, we obtain the nominal strength

$$\sigma_n = f'_t \left[1 - \frac{2}{\pi} \arcsin \left(1 - \frac{c_f}{a} \right) \right] \quad (16.9)$$

In the limit, for small sizes when $a \simeq c_f$, σ_n approaches asymptotically f'_t . On the other hand, for large sizes, $c_f \simeq 0$, σ_n will asymptotically approach zero. Whereas the expression of σ_n appears to have the same limits as the Size Effect Law, it is not mathematically similar to it. This will only become apparent if one takes a series expansion of the ArcSin function, and substituting c_f/a by s :

$$\sigma_n = \sigma_n = f'_t \left[1 - \frac{2}{\pi} \arcsin(1 - s) \right] \quad (16.10)$$

$$\simeq \frac{2\sqrt{2}f'_t}{\pi} s^{1/2} + \frac{f'_t}{3\sqrt{2}\pi} s^{3/2} + \frac{3f'_t}{40\sqrt{2}\pi} s^{5/2} + O[s]^{7/2} \quad (16.11)$$

Neglecting the terms of power greater than 1 (since s is at most equal to 1), and substituting $s = 1/(1 + r)$ where $r = a_0/c_f$, we obtain

$$\sigma_n = \underbrace{\frac{2\sqrt{2}}{\pi}}_B f'_t \sqrt{\frac{1}{1 + \underbrace{r}_\beta}} \quad (16.12)$$

Interestingly, this equation, Fig. 16.6 was derived on the basis of a simplified fixed cohesive stress profile, and not through the generally accepted fixed stress-displacement law of Hillerborg (similar analytical derivation was given in Sec. 9.4.1 of (Bažant, 2002)). Furthermore, this derivation has the advantage of establishing a direct relationship between fracture mechanics and size effect (though an earlier link, albeit through a radically different approach, was established by Bažant and Kazemi (1990a)). Finally, constants B and β are explicitly derived.

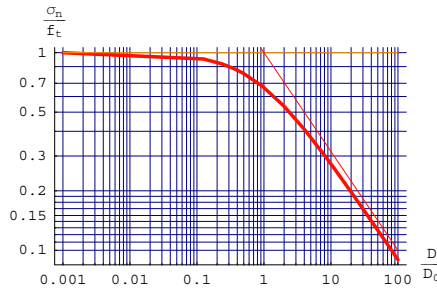


Figure 16.6: Bažant's original size effect law

16.1.2.2 Carpinteri

In one of his earliest publications, Carpinteri et al. (1995) presented a radically different model for the scale variation of strength. It was assumed that “the effect of microstructural disorder on mechanical behavior becomes progressively less important for larger scales, whereas it represents the fundamental feature for smaller scales”. The disorder being expressed through a fractality, it is postulated that the fractal dimension approaches the topological one asymptotically with increased observation scale length. At the other extreme, for very small dimensions, it is postulated that linear elastic fracture mechanics is supposed to govern the collapse mechanism of an unnotched material (“the Griffith's mode of collapse governed by 0.5 stress singularity becomes the main failure mechanism”). This purely speculative and qualitative model is called multifractal scaling law (MFSL) and is expressed as, Fig. 16.7.

$$\sigma_u(b) = f_t \left[1 + \frac{l_{ch}}{b} \right]^{1/2} \tag{16.13}$$

Indeed for “large” dimensions, a constant stress, unburdened by fractals or disorder, is reached. Whereas, for “small” sizes, the

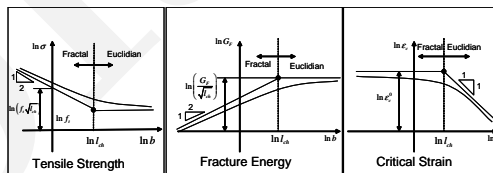


Figure 16.7: Multifractal Scaling Laws (Carpinteri)

bilogarithmic diagram tends to -0.5.

This model calls for the following observations:

1. Conceptually it is hard to refer to a stress singularity when there is no crack (for very small sizes), and should there be one, we are at a scale where it is well established that (in either elasto-plastic metals, or in cementitious material) there are cohesive stresses which defeat the applicability of LEFM as was well established by Irwin (1960) (elasto-plastic fracture mechanics), and Hillerborg et al. (1976a) (cohesive crack model). Furthermore, and most surprisingly, this model makes absolutely no reference to the geometry of the structure where the fractal crack is embedded. Surely, this should have to be accounted for somewhat.
2. Whereas Bažant's asymptotic analysis, (Bažant, 1997) yields a non zero strength for large sizes Carpinteri's model can be criticized for not having an upper bound to the strength as size is reduced. It is well known that the theoretical strength, based on inter-atomic forces, will have to be an upper bound as size is reduced (such as in nano-tubes), (Kelly, 1974).

$$\sigma_{max}^{theor} = \sqrt{\frac{E\gamma}{a_0}} \tag{16.14}$$

where E , γ and a_0 are the elastic modulus, surface energy, and distance separating two atoms respectively.

3. This model, first based on speculative assumptions (multifractal) is mathematically defined by an empirical relationship which happens to satisfactory fit reported experimental data (just as the empirical fatigue model of ? and contrarily to the analytically derived size effect law of Bažant).
4. There are no indications that this model is restricted to cementitious materials, and there is no explicit reference to cohesive stresses.

Hence, the mere fact that it adequately fits some experimental data, is of no scientific relevance.

The most recent formal derivation of the multifractal model was presented in a recent (survey) paper, by [Carpinteri et al. \(2003\)](#). Hence transforming a previously presented empirical law into a semi-analytical one. This derivation was itself a restatement of an earlier one by [Carpinteri \(1994\)](#) which was recently shown in the Appendix of ([Bažant and Yavari, 2005](#)) to be mathematically flawed.

Without going through the details, we note that the fracture energy G_F is now shown to be also size dependant, or more specifically multifractal. Furthermore, the $-1/2$ exponent, previously attributed to LEFM for small size, is now attributed/justified by Brownian disorder which (according to the authors) should correspond to fractal scaling of $+1/2$ and $-1/2$ for invasive (strength) and lacunar (fracture energy) morphologies.

Starting from³

$$W = G_F A_0 = G_F^* A_o \quad (16.15)$$

where G_F^* is a true scale invariant material parameter, whereas G_F is subjected to a scale effect described by a positive power law, the authors go on in defining:

$$G_F(b) \sim G_F^* b^{D_G} \quad (16.16)$$

$$\sigma_u(b) \sim \sigma_u^* b^{-D_\sigma} \quad (16.17)$$

$$\epsilon_c(b) \sim \epsilon_c^* b^{1-D_\epsilon} \quad (16.18)$$

$$1 = D_G + D_\sigma + D_\epsilon \quad (16.19)$$

which ultimately yields:

$$G_F(b) = G_F^\infty \left[1 + \frac{l_{ch}}{b} \right]^{-1/2} \quad (16.20)$$

$$w_c(b) = w_c^\infty \left[1 + \frac{l_{ch}}{b} \right]^{-1} \quad (16.21)$$

where l_{ch} is a characteristic length, b a representative dimension. Again, it should be noted that whereas in his original publication [Carpinteri](#) associates the $+1/2$ exponent to LEFM, in this more recent ones, the fractal scaling of $+1/2$ and $-1/2$ now correspond to the highest possible (Brownian) disorder. This is at best a convenient (and yet unproven) conjecture as it is not clear what exactly is meant by Brownian movement⁴. Einstein's work on Brownian movement (in liquid and gas, and not in solids) is at a scale much smaller than the one of Engineering interest. At this scale Newtonian physics is certainly no longer applicable, and should be replaced by Quantum Physics. Hence, it is at best difficult to reconcile physical models at such different scales without a rigorous explicit justification. To the best of the authors knowledge, no model spanning those two realms has even been proposed by theoretical physicists.

16.1.3 Historical Notes

It is commonly stated that size effect phenomenon was first highlighted by ?, on the basis of his famous etchings of different sizes of animal bones, Fig. 16.8. Galileo was indeed the first to notice that smaller objects in nature are not just scaled replicas of similar big objects. In the *Dialogues concerning two new sciences*, Proposition IX (on the second day), [Salviati](#) states:

...I once drew the shape of a bone, lengthened three times, and then thickened in such proportion that it could function in its large animal relatively as the smaller bone serves the smaller animal: here are the pictures; You see how disproportionate the shape becomes in the enlarged bone. From this it is manifest that if one wished to maintain in an enormous giant those proportions of members that exist in an ordinary man, it would be necessary to either find much harder and more resistant material to form his bones, or else to allow his robustness to be proportionately weaker than in men of average stature; otherwise growing to unreasonable height, he would be seen crushed by his own weight and fallen.

³Incidentally, this equation is identical to Eq. 16.3.

⁴Brownian motion was discovered in the 19th century by R. Brown who observed through a microscope the random swarming motion of pollen grains in water (now understood to be due to molecular bombardment). The theory of Brownian motion was later developed by [Einstein \(1905\)](#) to estimate the size of molecules.

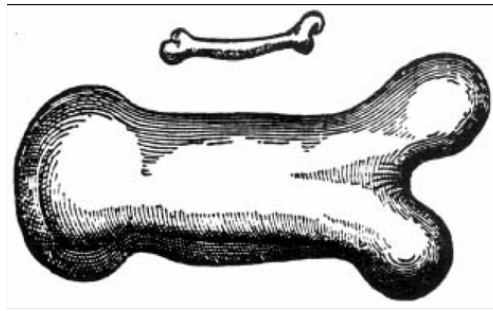


Figure 16.8: The Scaling of Bones, ?

Evidently, Galileo lacked the algebraic notation to do dimensional analysis in the way [Vashy \(1892\)](#) later on introduced it through the fundamental length parameter L . Hence, cast in the current context, Galileo's statement would simply read as follows: the weight a bone carries is proportional to the animal volume (L^3) whereas the strength of this same bone is proportional to its cross section area L^2 . A simple dimensional analysis shows that if an animal is, for example, three times larger, its bone would be three times longer but should be $3^{3/2} \cong 5$ times wider in order to carry the weight. This explains why a giant animal cannot have the same proportions as its smaller model. Hence, again Galileo's "paternalism" of the Size effect law can not be attributed to this observation, which again has more to do with mere dimensional analysis.

Hence, for a superficial observer (or a modern day *Simplicio*), Galileo would be the father of scaling (or dimensional) theory, and not of size effect theory. However, if we can (with all due respects) paraphrase Galileo we would simply say that weight increases with L^3 and load carrying capacity (constant strength, variable cross-section) increases with L^2 . This is exactly what the Size Effect law is all about: energy is released from a volume $\propto L^3$ and absorbed by a surface crack $\propto L^2$. As is well known by now, there are many experimental evidences supporting both Galileo and Bažant, ([RILEM TC QFS, 2004](#)).

To that far-reaching statement, the incredulous *Simplicio* states:

But the immense bulks that we encounter among fishes give me grave reason to doubt whether this is so. From what I hear, a whale is as large as ten elephants; yet whales hold together.

This questioning by *Simplicio* is not different than the incredulity of many skeptical modern time engineers, regarding the Size Effect law. But again, *Salviati* wisely replies:

Your doubt, Simplicio, enables me to deduce something that I did not mention before, a condition capable of making giants and other vast animals hold together and move around as well as smaller ones. That would follow if, but not only if, strength was added to the bones and other parts whose function is to sustain their own weight and that which rests on them.

Now, Galileo is implying that nominal strength (and not anymore mere load carrying capacity) can increase at times and that strength does not necessarily diminishes with size. In modern days terminology, Galileo is stating that strength does not necessarily drop to zero, which is a common feature of both Carpinteri's multi-fractal model, and Bažant's revised size effect law, ([Bažant and Novák, 2000](#)).

In more recent times, Weibull size effect was early on examined by [Griffith \(1921\)](#) who was seeking for an explanation of the increased strength with the reduction in glass filament diameter. His genius was to explain the strength reduction through the stress concentration around an elliptical crack as derived by [Inglis \(1913\)](#), and in postulating the energy transfer from strain to surface. However, it should be kept in mind that this model is applicable only for perfectly brittle solids, and not for quasi-brittle ones.

Finally, the size effect law provides us with a unified model for small scale plasticity to large scale fracture (linear elastic). In that context, it can be viewed as an analogy to the column curve which provides for a unified model of strength across a wide spectrum of slenderness ratios. At one end, failure is through yielding, and at the other through instability (Euler buckling). The first semiempirical column formula was developed by the second theory of elastic-plastic buckling of [Engesser \(1895\)](#) as cited in [Bažant and Cedolin \(1991\)](#).

16.2 Fractal Stress Intensity Factors

[Yavari et al. \(2002\)](#) investigated the stress and strain singularity at the tip of a fractal crack. It was shown that for modes I, the fractal crack stresses have the following asymptotic distribution

$$\sigma_{ij}^F(r, \theta) = K_I^F r^{-\alpha}(\theta, D|H) + \text{higher-order terms} \quad (16.22)$$

For self similar cracks,

$$\alpha = \frac{2 - D_F}{2} \quad 1 \leq D_F \leq 2 \quad (16.23)$$

where D_f varies from 1 to 2, the lower bound corresponds to the case of a smooth crack, while the upper limit represents an infinitely irregular fractal curve that “fills the plane”, and can be envisioned as a void contained within the plane. For self-affine cracks,

$$\alpha = \begin{cases} \frac{2H-1}{2H} & 1/2 \leq H \leq 1 \\ 0 & 0 \leq H \leq 1/2 \end{cases} \quad \text{Self-affine} \quad (16.24)$$

where H is the Hurst exponent and varies from 0 to 1; however stresses and strains are singular at the crack tip only if $1/2 \leq H \leq 1$, for very rough cracks ($H \leq 1/2$), there is no singularity. Hence a fractal crack has a weaker singularity than an Euclidian one.

16.2.1 Far Field Stress

The stress intensity factor for a fractal crack of length $2a$ and characterized by a fractal singularity α (or roughness H) in an infinite plate subjected to a uniform far field stress σ was derived by **Wnuk and Yavari (2003)**(Eq. A14 in which $s = x/a$) as

$$K_\sigma^F = \frac{\sigma}{\pi^\alpha a^{\alpha-1}} \underbrace{\int_0^1 \frac{(1+s)^{2\alpha} + (1-s)^{2\alpha}}{(1-s^2)^\alpha} ds}_{\chi(\alpha)} \quad (16.25)$$

For the Euclidian crack, $\alpha = 1/2$, $\chi(1/2) = \pi$, and $K_\sigma = \sigma\sqrt{\pi a}$.

16.2.2 Cohesive Crack

The cohesive crack model is illustrated by Fig. 16.2.2 where a crack of length $2a$ has cohesive stresses, applied over c_f at the crack tip. Introducing the nondimensional distance

$$\lambda = \frac{x - a_0}{a - a_0} = \frac{s - m}{1 - m} \quad (16.26)$$

Where $m = a_0/a$, **Wnuk and Legat (2002)** defined a generalized cohesive stress distribution

$$G(\lambda, \omega, n) = \lambda^n \exp[\omega(1 - \lambda)] \quad (16.27)$$

For $\omega = n = 0$, we would have a constant cohesive stress as defined by **Dugdale (1960)**, and for $\omega = 0, n = 1$ we recover the linear cohesive stress distribution of **Barenblatt (1962)**, Fig. 16.10. Using this representation of the cohesive stress, **Wnuk and Yavari (2003)** gave an expression of the non-fractal cohesive stress intensity factor (Eq. 16) which can be rewritten as

$$K_{coh} = \frac{2f'_t}{\pi} \sqrt{\pi a} \int_0^1 \frac{G(\lambda, \omega, n)(1 - m)}{\sqrt{1 - [(1 - m)\lambda - m]^2}} d\lambda \quad (16.28)$$

Following an approach similar to the authors, it can be shown that the fractal counterpart of this equation is

$$K_{coh}^F = \frac{2f'_t}{\pi} (\pi a)^{1-\alpha} (1 - m)^{1-\alpha} \underbrace{\int_0^1 \frac{G(\lambda, \omega, n)}{\{(1 - \lambda)[1 + (1 - m)\lambda + m]\}^\alpha} d\lambda}_{\Gamma(\omega, n, \alpha, m)} \quad (16.29)$$

For small scale yielding, $m \rightarrow 1$, then the preceding equation simplifies to the one given in Eq. 25 by **Wnuk and Yavari (2003)**

$$K_{coh}^F = \left[\frac{2f'_t}{\pi} (\pi a)^{1-\alpha} \right] \frac{(1 - m)^{1-\alpha}}{2^\alpha} \underbrace{\int_0^1 \frac{G(\lambda, \omega, n)}{(1 - \lambda)^\alpha} d\lambda}_{\Gamma(\omega, n, \alpha)} \quad (16.30)$$

which, for an Euclidian crack ($\alpha = 1/2$), is further simplified to

$$K_{coh} = \left[\frac{\sqrt{2}f'_t}{\pi} \sqrt{\pi a} \right] \sqrt{1 - m} \cdot \Gamma(\omega, n, \frac{1}{2}) \quad (16.31)$$

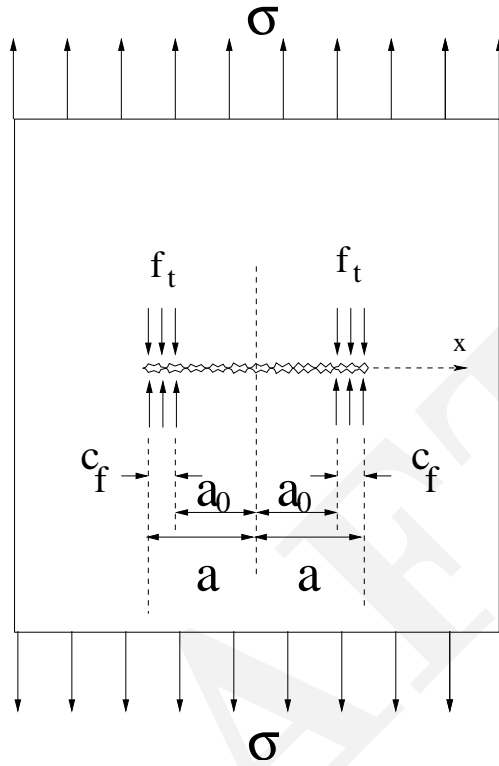


Figure 16.9: Cohesive Stress Distribution Along a Fractal Crack

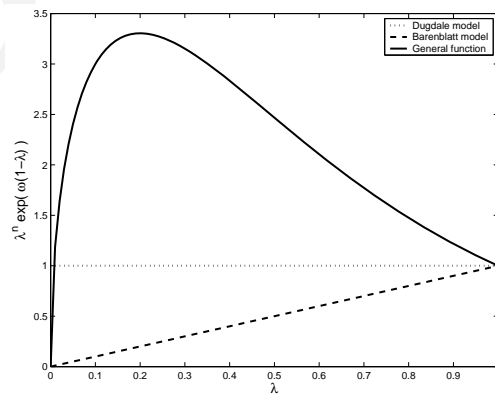


Figure 16.10: Generalized Cohesive Stress Distribution

16.3 Fractal Size Effect

Following the same approach developed by (Saouma et al., 2003) to rederive (all operations were performed with the help of Mathematica) the size effect law, we seek to remove the stress singularity by setting

$$K_{\sigma}^F + K_{coh}^F = 0 \quad (16.32)$$

and solving for σ .

First we attempt to obtain the generalized fractal size effect law by considering the general expression of K_{coh}^F (Eq. 16.29) and K_{σ}^F (Eq. 16.25), this yields

$$\frac{\sigma}{f_t'} = -2 \left(\frac{1}{1+r} \right)^{1-\alpha} \frac{\Gamma(\omega, n, \alpha, m)}{\chi(\alpha)} \quad (16.33)$$

We note that we recover Bažant's original size effect law for $\alpha = 1/2$, and that the size effect law is clearly independent of the cohesive stress distribution $\Gamma(\omega, n, \alpha, m)$.

On the other hand, if we make the assumption of small scale yielding $m \rightarrow 1$ we obtain

$$\frac{\sigma}{f_t'} = -2^{1-\alpha} \left(\frac{1}{1+r} \right)^{1-\alpha} \frac{\Gamma(\omega, n, \alpha)}{\chi(\alpha)} \quad (16.34)$$

Because of its complex form, $\chi(\alpha)$ can not be explicitly evaluated, hence, we take a series expansion with respect to $s = 0$, i.e. for $c_f \ll a$

$$\chi(\alpha) = 2 + O[s]^2 \quad (16.35)$$

Substituting the first series expansion of $\chi(\alpha)$ and the general expression of $\Gamma(\omega, n, \alpha, m)$ from Eq. 16.29 (with $G(\lambda, 0, 0) = 1$ for Dugdale's cohesive stress distribution) into Eq. 16.33 we obtain

$$\frac{\sigma}{f_t'} = - \frac{2^{-2\alpha} (-1-r) \left(\frac{1}{1+r} \right)^{2\alpha} \left[2^{2\alpha} \sqrt{\pi} \Gamma(1-\alpha) - 2B_{\frac{2r+1}{2(r+1)}}(1-\alpha, 1-\alpha) \Gamma(3/2-\alpha) \right]}{\Gamma(3/2-\alpha)} \quad (16.36)$$

where

$$\Gamma(z) = \int_0^{\infty} t^{z-1} e^{-t} dt \quad (16.37)$$

$$B_r(z, w) = \int_0^r t^{z-1} (1-t)^{w-1} dt \quad (16.38)$$

are the Gamma and Beta functions. Fig. 16.11 shows the size effect law for fractal cracks. We note that the strength of a fractal crack is always larger than the one of an Euclidian one. This is consistent with Eq. 16.22 derived by Yavari et al. (2002).

The analytical expression of the slope as $r \rightarrow \infty$ in terms of α , was derived but was exceedingly complex and could not be reduced to a simpler expression. However, when this expression is plotted, Fig. 16.12 it is exceedingly simple, and it would appear that the slope is simply equal to α . Indeed the $-1/2$ asymptotic slope of Bažant's original size effect law is recovered, and the strength of the size effect law is reduced for fractal cracks.

Similarly, if we one examine the asymptotic value of σ/f_t' as $r \rightarrow 0$, we obtain, Fig. 16.13

$$\frac{\sigma}{f_t'} \Big|_{r \rightarrow 0} = \frac{\sqrt{\pi} \Gamma(1-\alpha)}{2\Gamma\left[\frac{3}{2}-\alpha\right]} \quad (16.39)$$

which for $\alpha = 1/2$ is equal to $\frac{\pi}{2}$. Evidently, this limit value is problematic, as one would have expected to retrieve the value of 1. This discrepancy may be attributed to the approximation of $\chi(\alpha)$ in Eq. 16.35; nevertheless this discrepancy requires further investigation.

16.4 Cellular Automata

When Fractals were first introduced in the early 80's it rapidly spread in multiple disciplines of science and engineering. To the best of the author's knowledge, one of the first application in engineering was in fracture mechanics, when Mandelbrot et al. (1984) showed that metallic fracture surfaces are fractals. This was one key paper which subsequently inspired many others, including this one. Similarly, we recently witnessed the development of a "New Kind of Science" by Wolfram (2002). Again, just as Mandelbrot did in 1984, Wolfram asserts that his Cellular Automata can model the roughness of cracks. Given the inherent similarity between cellular automata and fractals, the authors conclude by examining what may become yet another fracture representation and its role in fracture mechanics.

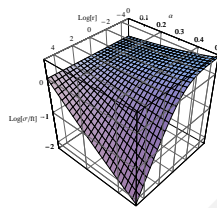
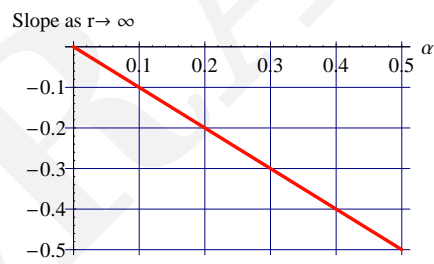
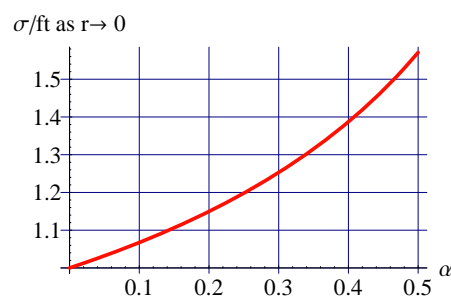


Figure 16.11: Fractal Size Effect Laws (Dugdale)

Figure 16.12: Slope of the Fractal Size Effect Law in terms of α as $r \rightarrow \infty$ Figure 16.13: Asymptotic Values of the Size Effect Law as $r \rightarrow 0$

Crack models need not only be based on continuum (even if fractal) models, but can be based on discontinuous ones too. Whereas the lattice model is by now making great strides toward its acceptability, (Cusatis et al., 2003), a new model based on cellular automata was recently proposed by Wolfram (2002) (*A New Kind of Science* (NKS)). This model is worth mentioning for two reasons. First it provides a simple algorithm to define complex objects, which at time are exact replicas of fractals. Secondly, the author claims that his rules 150 (shown below), 22, and 122 can be used to model a random crack, which in the context of this paper does indeed appear to be fractal.

Hence, using simple rules, Wolfram’s cellular automata operations can indeed generate fractal objects. In particular, Rule 150 generates a Sierpinski’s like surface, Fig. 16.14 which bears great resemblance to Fig. 16.2. Rule 150 (Weisstein, 2004) is identified

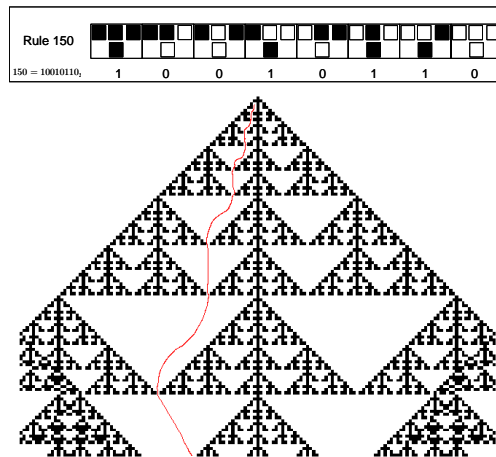


Figure 16.14: Cellular Automata Definition of Rule 150 Along With Potential Crack Path

by Wolfram (2002) (pg. 375) as a possible fracture and “at each step, the color of each cell, which roughly represents the displacement of an element of the solid, is updated according to the cellular automation rule. (The line), representing the location of a crack, moves from one cell to another based on the displacements of the neighboring cells, at each step setting the cell it reaches to be white.”

Hence, whereas fractals constitute a static way to mathematically catalog the points that make up the object, cellular automata are a dynamic way to create the object via a growth process.

Yet, despite the ability to replicate a fractal surface, which can greatly reassemble a cracked fractal surface, the NKS fails to provide any mathematical or physical parameters which can be exploited to further investigate the problem beyond a mere graphical representation. Nevertheless, it is somehow the intuition of the authors that this model could be further investigated through the prism of the size effect law, and may very well lead to some interesting (albeit qualitative) results.

16.5 Conclusion

Both Bažant’s size effect law (SEL) and Carpinteri’s multifractal scaling law (MFSL) are thoroughly reviewed. Serious reservations on the second model are cast, while the first one is extended to include fractal cracks. Historical notes pertaining to these models are also discussed. Finally, speculative remarks on the applicability of cellular automata on size effects and fractals are made.

The derived fractal size effect law does account for the geometry of the structure, is consistent with Bažant’s original derivation. However, it should be noted that there is still a discrepancy in the plastic asymptote, and this model does not extend Bažant’s subsequent refinements of his model. It is shown that as the fractal dimension increases (i.e. α decreasing from 1/2), the nominal strength does also increase. In the limiting case of $\alpha = 0$ (essentially a plate with a hole), then no longer is the strength dependant on the size, i.e plasticity reigns.

Accepting the cohesive crack model, the proposed Fractal Size Effect Law (FSEL) in no ways resembles MFSL (which still lacks a rigorous mathematical derivation).

Based on the comprehensive, historical and rigorous discussion presented in this paper, it is hoped that the controversy surrounding the discrepancy between SEL and MFSL is laid to rest, and that code writers should have no qualm in embracing Bažant’s Size Effect Law. Paraphrasing (Izquierdo-Encarnación, 2003), we can definitely conclude that *Effectus amplitudinis fractae rimae satisfaciendus est*. (Fractal cracks must obey Size Effects).

Chapter 17

FRACTURE MECHANICS PROPERTIES OF CONCRETE

Adapted from (Saouma et al., 1991a)

17.1 Introduction

Concrete dams are often referenced as a potential application of Fracture Mechanics, yet, little work has been performed to evaluate fracture properties of dam concrete. Most of the research undertaken on the fracture of concrete has concentrated on laboratory testing of small specimens constructed of structural concrete. Based on these test results, a basic understanding of the fracture processes occurring in concrete has been developed. However, since the fracture parameters often appear to be size and aggregate dependent, the experimentally determined values cannot be reasonably extrapolated to mass concrete structures such as dams.

The fracture properties obtained from small concrete specimens may be size and geometry dependent because the fracture ligament of the specimens is too short to achieve a steady crack propagation regime. Several experimental investigations have been performed on large concrete members to determine both “objective” fracture properties and minimum dimensions for test specimens. Large scale double cantilever beams with a length of 350-cm (138-in.) have been used at the “Laboratoire Central des Ponts et Chaussées” in Paris since 1976 (Chhuy *et al.* 1979, Rossi *et al.* 1984) for fracture testing of concrete. An investigation using four different specimen geometries ranging in size from 100-cm (39.4-in.) to 144-cm (56.7-in.) is presented in Wittmann & Metzener-Gheorghita (1985). Other large concrete fracture specimens include three-point bend (TPB) beams with a depth of 80-cm (31.5-in.) (Hilsdorf & Brameshuber 1985), compact tension (CT) specimens with heights ranging from 30-cm (12-in.) to 150-cm (59-in.) (Wittmann *et al.* 1988), and tapered double cantilever beams with a height of 210-cm (83-in.) (Rossi *et al.* 1990).

In this chapter, testing and data evaluation procedures developed for relatively small specimens are extended to a series of large concrete Wedge Splitting (WS) specimens with heights of 31-cm (12-in.), 91-cm (36-in.) and 152-cm (60-in.). Three different concretes with maximum aggregate sizes, 19-mm (0.75-in.), 38-mm (1.5-in.) and 76-mm (3.0-in.), representative of mass concrete used in dams are examined. A test series of WS specimens used to study the fracture behavior of the cold-joint between lifts in a dam is also presented. From each set of experiments, values for fracture toughness, K_{Ic} , and specific fracture energy, G_F , are determined and discussed. The influence of aggregate shape and geological origin on the fracture properties are also considered.

17.2 Experiments

17.2.1 Concrete Mix Design and Specimen Preparation

Unlike structural concrete, in which the maximum size aggregate (MSA) typically does not exceed 38-mm (1.5-in.) in diameter, in dam concrete mixes the MSA is, in general, equal to or larger than 76-mm (3.0-in.) in diameter. Based on the presence of such large aggregates in a dam concrete mix, three MSAs were selected for testing: 19-mm (0.75-in.), 38-mm (1.5-in.), and 76-mm (3.0-in.). For each aggregate size, a concrete mix similar to those used in actual gravity dams was obtained from the U.S. Bureau of Reclamation, which is the agency responsible for the design, construction, and maintenance of many federally owned dams in the western United States. The majority of the mixes were batched with rounded river aggregates, except for a batch of the 38-mm (1.5-in.) MSA mix, which consisted of quarried subangular aggregates. Details of the mix designs used for the construction of all specimens are shown in Table 17.1.

Ten standard 15-cm (6.0-in.) \times 30-cm (12.0-in.) cylinders for the 19-mm and 38-mm MSA mixes, and ten 30-cm (12.0-in.) \times 60-cm (24.0-in.) cylinders for the 76-mm mix were used for the determination of the concrete material properties. The compressive strength, f'_c , and tensile splitting strength, $f'_{t,sp}$, of each concrete mix were obtained prior to performing each wedge-splitting (WS) specimen test. The mean values obtained from unconfined compression tests, performed according to ASTM C39 (Anon. 1983), and the splitting tension test (Brazilian) described in ASTM C496-85 (Anon. 1985), are summarized in Table 17.2.

The test specimen shape used for the experimental program was the wedge-splitting geometry, shown in Fig. 17.1, which had been previously used in research programs for the testing of small concrete specimens (Hillemeier & Hilsdorf 1976, Linsbauer & Tschegg 1986, Brühwiler 1988, Brühwiler & Wittmann 1990). The WS specimen has a large fracture area compared to the concrete volume, approximately 4.6 times greater than a commonly used three-point bend (TPB) beam geometry (RILEM 1985) of equal volume. The large fracture area compared to the aggregate size and specimen volume makes the WS geometry well suited for testing large MSA and specimens under laboratory conditions.

The dimensions of the WS specimens tested in the experimental program are summarized in Table 17.3. The specimen dimensions and aggregate sizes were selected to enable a comparison with results previously obtained by other researchers in

Table 17.1: Concrete mix design.

CONCRETE MIX DESIGN (no entrained air, w/c ratio= 0.55)			
	MAXIMUM AGGREGATE SIZE MIX		
	19-mm (0.75-in.)	38-mm (1.5-in.)	76-mm (3.0-in.)
	Weight kg/m ³ (lb/yd ³)	Weight kg/m ³ (lb/yd ³)	Weight kg/m ³ (lb/yd ³)
WATER	163 (275)	139 (233)	102 (174)
CEMENT	297 (500)	252 (424)	187 (315)
SAND	918 (1,550)	782 (1,320)	695 (1,170)
19-mm MSA (0.75-in.)	978 (1,650)	609 (1,030)	491 (827)
38-mm MSA (1.5-in.)	0	609 (1,030)	491 (827)
76-mm MSA (3.0-in.)	0	0	491 (827)
TOTAL	2,390 (4,030)	2,420 (4,080)	2,480 (4,180)

Table 17.2: Experimentally obtained material properties of the concrete mixes used.

MSA	f'_c , MPa (psi)	$f'_{t,sp}$, MPa (psi)	E_{eff} , MPa (ksi)
19-mm (0.75-in.)	25.6 (3,710)	2.81 (407)	18,000 (2,610)
38-mm (1.5-in.)	24.8 (3,600)	2.67 (388)	16,900 (2,460)
38-mm (1.5-in.) sub-angular	36.6 (5,317)	3.96 (574)	23,200 (3,360)
76-mm (3.0-in.)	18.9 (2,740)	2.41 (349)	16,500 (2,400)

Figure 17.1: *Wedge-splitting specimen geometry.

Table 17.3: Wedge-splitting specimen dimensions.

Specimen Dimensions, cm (in.)							
Specimen Type	H	w	t	s	D	a_0	h
"Small"	31 (12.0)	31 (12.0)	23 (9.0)	6 (2.25)	3 (1.0)	4.5(1.75)	20 (8.0)
"Medium"	91 (36.0)	91 (36.0)	41 (16.0)	15 (6.0)	8 (3)	15.2 (6.0)	61 (24.0)
"Large"	152 (60.0)	152 (60.0)	41 (16.0)	15 (6.0)	8 (3)	30.5 (12.0)	107 (42.0)

the academic community, and to predict fracture properties of dam concrete with intermediary values to ensure a continuity of results.

Specimen construction consisted of wooden formwork built for the placing of the concrete, a sharpened 3.2-mm (0.125-in.) thick steel plate mounted inside each form to obtain the vertical notch normal to the load line, and two hollow steel sleeves flanking the plate. Two different ready-mix suppliers delivered the concrete. The first provided the 19-mm and 38-mm MSA mixes and the other the 76-mm MSA concrete mix. In all specimens, with the exception of the cold-joint (CJ) specimens, the concrete was placed with the notch in the vertical direction, and cured at room temperature in the laboratory for at least 28 days prior to testing.

For the CJ specimens, the concrete was placed in two separate lifts, with the notch plate initially in a horizontal orientation. The tendency of the crack to propagate into the cold-joint, which is a region of inherent weakness, was studied through a slight offset between the initial notch and the level of the concrete in the first lift. Three days after the first lift was placed, the surface was sand-blasted to remove surface laitance and ensure a good bond along the joint. Grade 16 silica sand, driven by an air pressure of 100 psi, was used in the blasting process. After sandblasting, the surface was continuously water cured but was saturated surface dry (SSD) when the second lift was placed. The sand-blasting operation and the placing of the second lift were performed on the same day. The 38-mm and 76-mm MSA concrete mixes used for the CJ specimens were identical to the mix designs used during the standard WS testing program. After curing for 28 days, the specimens were turned upright, such that the notch was in a vertical orientation, and tested using a procedure identical to the standard WS specimens experiments without the cold-joint. The concrete mixes associated with each specimen size and the number of specimens in each series are presented in the test matrix of Table 17.4.

Table 17.4: Test matrix.

		Number of Tests		
Specimen Type	Aggregate Shape	MAXIMUM AGGREGATE SIZE MIX		
		19-mm (0.75-in.)	38-mm (1.5-in.)	76-mm (3.0-in.)
"Small"	rounded	3	3	-
"Medium"	rounded	3	3	3
"Large"	rounded	-	3	3
"Medium"	subangular	-	3	-
"Large" (cold-joint)	rounded	-	3	3

17.2.2 Loading Fixtures

For testing, the WS specimens were centered on a steel rod, shown in Fig. 17.2, which acts as a line support along the bottom face

Figure 17.2: *Wedge fixture and line support.

of the specimen. The line support fixture was mounted to the actuator of a closed-loop servo-hydraulic materials testing system. Two steel rods were inserted through steel sleeves in the specimen, and needle bearing rings were mounted on the protruding ends. The wedge-loading apparatus, also shown in Fig. 17.2, was then fixed and the WS specimen was raised by the actuator such that the wedges were forced between the bearing rings on each side, imposing a horizontal displacement on the specimen at the point of contact. A flexible connection between the wedge-loading fixture and the testing machine load cell was used to account for any small misalignments and evenly distribute the induced load. As a result of the horizontal displacement imposed by the wedges, the specimen was subjected to a pure Mode I loading condition.

17.2.3 Testing Procedure

The experimental setup of the electronic controller, the data acquisition system, and the testing machine for the WS specimen tests are shown in a simplified block diagram in Fig. 17.3. In the WS specimen experiments, the primary deformation monitored was the crack-mouth opening displacement (CMOD). The CMOD was measured on the top surface of the specimen by a clip gage mounted over the mouth of the initial notch. The closed-loop servo-hydraulic test machine used a programmed constant rate of CMOD

Figure 17.3: *Block diagram of the experimental system.

(1.0- $\mu\text{m}/\text{sec}$, or 40- $\mu\text{in}/\text{sec}$) as the feedback control to obtain stable crack growth with structural post-peak response. During the test, the vertical load and the CMOD were monitored and recorded using a standard data acquisition system. Unload/reload cycles, which were used to monitor the change in the specimen compliance, or flexibility, were performed. The experiment was performed until the specimen was split into two halves.

The vertical force induced by the wedge fixture, P_V , was directly obtained from the load cell of the testing machine. The wedge fixture is a statically determinate beam, and therefore, the splitting force is given by $P_{SP} = \frac{P_V}{2 \cdot \tan \alpha}$, where the wedge angle, α , is equal to 15° . (Frictional forces were neglected; they were reduced by using hardened steel inserts along the inclined wedge surface and needle bearings with a low coefficient of friction.) A typical P_{SP} vs. CMOD curve representative of the WS specimens is presented in Fig. 17.4. In the P_{SP} vs. CMOD curve, both linear and nonlinear responses in the ascending prepeak branch and

Figure 17.4: *Typical P_{SP} vs. CMOD curve for a “Large” specimen.

a descending postpeak branch can be observed.

17.2.4 Acoustic Emissions Monitoring

In several WS tests, the microcracking associated with fracture process zone (FPZ) formation and with transient releases of elastic energy due to localized aggregate fracture and bond failure were monitored with an acoustic emission (AE) sensor mounted on the surface of the specimen. Inside the sensor, a piezoelectric crystal is stimulated by the stress waves and produces electrical signals. The signals are then amplified, filtered, processed, and related to the behavior of the material throughout the experiment.

The AE sensor was mounted on the face of the specimen in a direction such that the sensor was normal to the predicted fracture plane. The sensor used during testing was sensitive in the 30 kHz range, and the signal was filtered by a bandpass filter with a bandwidth of 45–135 kHz. The electrical signal was then amplified, converted into a DC voltage by the processing unit, and fed into a true-RMS (root-mean-square) voltmeter to eliminate the effects of constant background noise. With each AE burst, a rise in the RMS signal was recorded with an X-Y plotter. Based on the observed readings, the material response was evaluated as (1) large AE bursts or continuous activity, interpreted as crack extension or aggregate/matrix/bond failure, and (2) little or low AE activity, indicating microcracking associated with the formation of the process zone. The AE monitoring and evaluation techniques were used only as a qualitative aid to the test.

A typical record of the AE-RMS voltage signal for each corresponding load step vs. testing time is shown in Fig 17.5. The data

Figure 17.5: *Typical AE record for a “Large” WS specimen test.

shown in the curve can be divided essentially into three sections:

Section I: The specimen is in the ascending branch of the P_{SP} vs. CMOD curve, the observed low AE activity and lift-off of the RMS signal from a baseline value indicates microcracking and the formation of the process zone at the notch tip.

Section II: The peak load is reached and large AE spikes resulting from crack extension can be observed.

Section III: The AE bursts increase in amplitude and number, indicating continuous crack formation and growth during the descending branch.

The Kaiser Effect which is characterized by the absence of detectable acoustic emissions until previously applied stress levels are exceeded, is observed in AE testing of composite materials. This effect occurs primarily in the low CMOD regime, and is not visible in Section III. The lack of the Kaiser Effect in Section III during the unload/reload cycles may have been caused by crushed small concrete particles, and improper fit of the specimen halves. Further applications of this nondestructive evaluation method were performed in the field testing program as presented in Saouma *et al.* (1990).

17.2.5 Evaluation of Fracture Toughness by the Compliance Method

The fracture toughness, K_{Ic} , was determined using the compliance method. A finite element calibration analysis was first performed to determine a relationship between crack length and compliance, $a = a(C)$, and for the stress intensity factor, K_I in terms of crack length:

$$K_I = \frac{P_{SP}}{H \cdot t} \sqrt{\pi a_{eff}} \cdot f(\beta) \quad (17.1)$$

where $\beta = \frac{a_{eff}}{H}$ and $f(\beta)$ is the geometry function for the WS specimens (Saouma *et al.* 1989a, Broz 1989). In the analysis, both the splitting load and Young's Modulus E were taken as unity, vertical load components induced by the wedge fixture on the specimen were included, and singular elements were used for SIF determination.

The following general procedure was then followed to interpret the experimental data:

1. From the initial ascending branch of the P_{SP} vs. CMOD record, determine the experimental initial specimen compliance C_{exp}^i , and compare with the normalized (numerical) compliance C_n corresponding to a_0 . From those two values, determine the effective Young's Modulus $E_{eff} = \frac{C_n}{C_{exp}^i}$ (Fig. 17.4).
2. For each successive post-peak unload/reload cycle:
 - a) Determine the experimental compliance, C_{exp}^i , as the slope of the line obtained by connecting the initial unloading point to the final reloading point of each cycle (Fig. 17.4).
 - b) Normalize C_{exp}^i with respect to E_{eff} and then determine a_{eff} .
 - c) From a_{eff} and the P_{cr} corresponding to the unload point, determine the fracture toughness, K_{Ic} , from Eq. 17.1.

17.3 Fracture Toughness Results

Reduction of the experimental data resulted in a K_{Ic} vs. a_{eff} curve that typically exhibited three stages (Fig. 17.6). In Stage I, pre-

Figure 17.6: *The three stages of the fracture toughness vs. effective crack length curve.

peak unload/reload cycles are performed, and the section of the curve is included for reference only. Since this stage corresponds to the formation of the FPZ, the stress intensity factor, K_I , values increase monotonically up to a plateau. Stage II is obtained from the post peak data falling within a plateau. The plateau is synonymous with steady crack propagation and was also observed by Rossi *et al.* (1990). Stage III demonstrates a sudden decrease in the K_{Ic} values. A possible explanation for this phenomena is based on the inherent assumptions of the data reduction method. A perfectly linear elastic system was assumed in the finite element calibration (resulting in zero residual CMOD upon unloading), but the assumption was increasingly violated as the test progressed. As the effective crack length increased, larger residual CMOD (caused by the inability of the crack to perfectly close) was observed. This effect, at first negligible, eventually becomes predominant as the crack grew down the ligament.

Only the fracture toughness values associated with Stage II were considered in the statistical analysis. The mean values with the respective relative standard deviations are plotted in Fig. 17.7 and summarized in Tables 17.5 and 17.6. From the analysis of the experimental data the following observations are made:

Figure 17.7: *Mean fracture toughness values obtained from the rounded MSA WS specimen tests.

Table 17.5: Summary of fracture toughness data obtained from the WS tests.

Fracture Toughness, K_{Ic} , $MN/m^{3/2}$ ($psi\sqrt{in}$)					
Type		19-mm (0.75-in.)	38-mm (1.5-in.)	76-mm (3.0-in.)	Summary
"Small"	Mean	1.05 (953)	0.86 (783)	-	0.93 (843)
	rel. σ (%)	5.9	13.4	-	13.9
"Medium"	Mean	1.01 (923)	0.99 (909)	1.09 (991)	1.03 (941)
	rel. σ (%)	20.3	12.7	15.1	16.0
"Large"	Mean	-	1.23 (1,120)	0.98 (893)	1.16 (1,060)
	rel. σ (%)	-	6.3	12.7	12.8
Summary	Mean	1.03 (941)	1.02 (929)	1.05 (957)	1.03 (941)
	rel. σ (%)	13.5	16.9	15.3	15.2
"Medium" (subangular)	Mean	-	1.34 (1,220)	-	-
	rel. σ (%)	-	12.3	-	-

Table 17.6: Fracture toughness values obtained from the CJ-WS specimens.

Fracture Toughness, K_{Ic} , $MN/m^{3/2}$ ($psi\sqrt{in}$)				
MSA		SPECIMEN NO.		
		A	B	C
38-mm (1.5-in.)	Mean	0.64 (582)	0.50 (457)	0.72 (656)
	rel. σ (%)	9.8	3.3	12.1
76-mm (3.0-in.)	Mean	0.71 (643)	0.52 (476)	0.62 (567)
	rel. σ (%)	4.0	2.2	2.7

1. Since the relative standard deviations in the vertical columns of Table 17.5 are all within 20%, “objective” values, i.e. independent of specimen size, for the fracture toughness were determined.
2. Based on the relative standard deviation of the horizontal rows, the fracture toughness values also appear to be independent of aggregate sizes.
3. The previous observation was further evaluated through a test series of medium-size specimens constructed with subangular andesite aggregates (as opposed to the rounded aggregates used in all previous specimens). The trends in the results of the test series can be summarized as follows:
 - a) The experiments yielded a fracture toughness value of $1.34 \text{ MN/m}^{3/2}$ ($1,220 \text{ psi}\sqrt{\text{in}}$), which is 30% higher than the value obtained from the rounded aggregate specimens.
 - b) Aggregate debonding was prevalent in fracture surface of the rounded specimens, however, aggregate failures were more predominant in the subangular specimens.
 - c) At peak load, the effective crack length of the subangular MSA specimens was found to be smaller than the a_{eff} of the rounded MSA specimens, indicating the presence of a smaller process zone.
4. The CJ specimens, which were used to quantify the response of lift-joints found in dams, had:
 - a) Peak loads 50% lower than comparable specimens constructed with no “lift” joint.
 - b) Fracture toughness values approximately 30-60% lower than for specimens without lift joints.
 - c) Smaller residual crack opening displacements following each cycle of unload/reload, and no descending portions of the fracture toughness curve (as illustrated in Fig. 17.6).
5. A fractal analysis (Gamal-El-Din *et al.* 1990) of the concrete surfaces yielded a constant fractal dimension for all the rounded aggregate specimens. In the analysis of CJ fracture surfaces, a relationship between the fractal dimension and fracture toughness was observed.
6. The experiments reported here were conducted in the laboratory environment under unconfined conditions, the effects of confining stresses on the apparent fracture toughness are presented in Saouma *et al.* (1990).

17.4 Specific Fracture Energy Results

The specific fracture energy, G_F , is defined as the total energy required to break a specimen into halves, normalized by the projected fracture area. G_F is ideally obtained from the area underneath the load-deformation curve in a direct tension test. Alternatively, specific fracture energy can also be obtained directly from flexural-based specimen geometries, such as the WS specimen. In the WS specimens, G_F was calculated as the area under the curve of P_{SP} vs. corresponding CMOD, divided by the ligament area (Brühwiler 1988, Brühwiler & Wittmann 1990). Thus, each test specimen yields one single value of G_F . The G_F values determined from the experiments are shown Tables 17.7 and 17.8 and plotted in Fig. 17.8. Based on the analysis of the

Figure 17.8: *Mean specific fracture energy values obtained from the rounded MSA WS specimen tests.

experimental results the following comments can be made:

1. The 38-mm and 76-mm rounded MSA specimens yielded approximately equal values of G_F , which are 10-20 % higher than the values obtained for the 19-mm MSA concrete mix.
2. A similar size dependency for G_F for relatively small specimens with ligament lengths of less than 20-cm was observed by Rossi *et al.* (1990).
3. The experiments performed on the specimens constructed with the subangular aggregate mix indicated:
 - a) G_F values were 25% higher than the values obtained from the specimens constructed from the rounded aggregate mixes.

Table 17.7: Summary of specific fracture energy values obtained from the WS tests.

Specific Fracture Energy, G_F , N/m (kip/in)					
Type		19-mm (0.75-in.)	38-mm (1.5-in.)	76-mm (3.0-in.)	Summary
"Small"	Mean	206 (1.18×10^{-3})	238 (1.36×10^{-3})	-	226 (1.29×10^{-3})
	rel. σ (%)	9.0	11.2	-	12.2
"Medium"	Mean	173 (9.88×10^{-4})	223 (1.27×10^{-3})	226 (1.29×10^{-3})	211 (1.21×10^{-3})
	rel. σ (%)	29.1	7.5	15.1	15.5
"Large"	Mean	-	259 (1.48×10^{-3})	237 (1.35×10^{-3})	254 (1.45×10^{-3})
	rel. σ (%)	-	18.1	-	15.7
Summary	Mean	189 (1.08×10^{-3})	240 (1.37×10^{-3})	230 (1.31×10^{-3})	226 (1.29×10^{-3})
	rel. σ (%)	19.1	13.5	6.5	15.7
"Medium" (subangular)	Mean	-	277 (1.58×10^{-3})	-	-
	rel. σ (%)	-	13.8	-	-

Table 17.8: Fracture energy values obtained from the CJ-WS specimens.

Specific Fracture Energy, G_F , N/m (kip/in)				
MSA	SPECIMEN NO.			
	A	B	C	
38-mm (1.5-in.)	99.7 (5.70×10^{-4})	80.6 (4.55×10^{-4})	138.4 (7.85×10^{-4})	
76-mm (3.0-in.)	133.0 (7.59×10^{-4})	85.8 (4.90×10^{-4})	98.1 (5.60×10^{-4})	

- b) The subangular aggregate shape inhibited debonding, and more energy was required to break the sub-angular aggregate than to debond rounded aggregate.
- 4. For the cold-joint specimens:
 - a) The G_F values were approximately 40-70 % lower than the standard WS specimens. The lower fracture energy values were attributed to the inherent weakness of the cold-joint between specimen halves.
 - b) The higher G_F values were correlated to visibly rougher surfaces at the cold-joint.

17.5 Conclusions

1. Based on the concrete mixes tested, which were obtained from two separate local ready-mix suppliers, and using the compliance method for fracture toughness evaluation, the unconfined K_{Ic} of concrete is a material constant, equal to $1.04 \text{ MN}/\text{m}^{3/2}$ ($941 \text{ psi}\sqrt{\text{in}}$).
2. The evaluated fracture parameters, K_{Ic} and G_F , are independent of specimen size and are "objective" only if certain minimum dimensions are exceeded.
3. The fracture parameters, K_{Ic} and G_F , are practically independent of aggregate size and depend on the angularity, or shape, as well as, the aggregate's strength.
4. For the two types of aggregates used in this experimental program, more energy was required to fracture the subangular aggregates than to debond the rounded ones.
5. Debonding of rounded aggregates may result in a FPZ which is larger than the process zone caused by the fracture of subangular aggregates.
6. The fracture properties for CJ-WS specimens exhibited higher variations in results, and were lower than for specimens without cold-joints.

Table 17.9: Size Effect Law model assessment from the WS test program (average values)(Brühwiler et al., 1991)

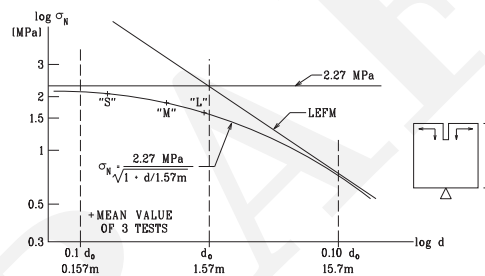
Specimen	Size d mm (in.)	d_a mm (in.)	a_0 mm (in.)	a_0/d	F_{sp}^{max} kN (kip)	σ_N MPa (psi)
"Small"	248	19	44.45	0.18	24.1	3.05
"Small"	248	38			17.5	2.21
"Medium"	762	19	152.4	0.20	64.0	1.68
"Medium"	762	38			69.1	1.81
"Medium"	762	76			63.1	1.65
"Large"	1,372	38	304.8	0.22	123.9	1.68
"Large"	1,372	76			113.5	1.54

17.6 Size Effect Law Assessment

More specifically, an assessment of the size effect law in terms of: 1) testing three concrete mixes (with different aggregate sizes) in identical specimen sizes; 2) The same concrete mix on three different specimen sizes; and finally 3) determination of the fracture toughness through an extrapolation of the size effect law, (Brühwiler et al., 1991).

In its original formulation, the Size Effect Law assumes a variation of the nominal strength in terms of the maximum aggregate size. To assess this dependency, the test data for specimens of "Medium" size, but different d_a , were analyzed. From Table 17.9 it appeared that aggregate size does not play a dominant role in assessing the nominal strength of a concrete structure. However, we determined that the shape and geological composition of the aggregates are far more important parameters.

Alternatively, when geometrically similar specimens with identical concrete mix were considered then indeed the size effect law proved to be a valid tool to determine structure's nominal strength, Fig. 17.9.

Figure 17.9: Size effect for WS specimens for $d_a=38$ mm (1.5 in) (Brühwiler et al., 1991)

Finally, the Size Effect Law can be re-arranged in a formulation to predict the fracture toughness K_{Ic}^{SEL} , from "small" laboratory test values of a geometrically identical "infinitely large" one. It can be shown, (Brühwiler et al., 1991) that as $d \rightarrow \infty$ $K_{Ic}^{SEL} = Y B f'_t \sqrt{d_0}$

Using this equation, the fracture toughness for the WS specimens for $d_0 = 1570$ mm is found to be $K_{Ic}^{SEL} = 1.54$ MN/m^{3/2} (1.40 ksi√in), which is 51% higher than the value of $K_{Ic}^{CM} = 1.02$ MN/m^{3/2} (0.93 ksi√in) obtained using the compliance method (CM) (Saouma et al., 1991a). The difference between K_{Ic}^{SEL} and K_{Ic}^{CM} appears to be large *a priori* however it can be explained by the two different approaches used to evaluate fracture toughness from experimental data. Also, the SEL covers a range of sizes of about 1:20, and therefore, extrapolation to infinite size may not be valid.

17.7 Notation and Abbreviations

a	Crack Length
a_0	Initial Notch Length
a_{eff}	Effective Crack Length
C_{exp_i}	Initial Experimental Compliance
C_{exp}	Experimental Compliance
C_n	Normalized Compliance
D	Diameter of Loading Rods
E	Young's Modulus
E_{eff}	Effective Young's Modulus
f'_c	Concrete Compressive Strength
f'_t	Concrete Uniaxial Tensile Strength
$f'_{t,sp}$	Concrete Splitting Tensile Strength
G_F	Specific Fracture Energy

H	Specimen Height
h	Specimen Ligament Length
K_I	Stress Intensity Factor
K_{Ic}	Fracture Toughness (Critical Stress Intensity Factor)
K_{Ic}^{APP}	Apparent Fracture Toughness
P_V	Vertical Force
P_{CR}	Splitting Force Corresponding to Unload/reload Cycle
P_{SP}	Splitting Force
s	Distance from Top of Specimen to Point of Load Application
t	Specimen Thickness
w	Specimen Width
AE	Acoustic Emission
ASTM	American Society of Materials Testing
CJ	Cold-Joint
CMOD	Crack Mouth Opening Displacement
CT	Compact Tension
FPZ	Fracture Process Zone
LEFM	Linear Elastic Fracture Mechanics
LVDT	Linear Variable Differential Transformer
MSA	Maximum Aggregate Size
NLFM	Non-Linear Fracture Mechanics
RMS	Root Mean Square
SOM	Strength of Materials
SSD	Saturated Surface Dry
TPB	Three Point Bending
WS	Wedge Splitting

Chapter 18

SINGULAR ELEMENT

18.1 Introduction

¹ For most practical problems, either there is no analytical solution, or the handbook ((Tada et al., 1973)) ones are only crude approximation. Hence numerical techniques should be used. Whereas Boundary Element Methods are increasingly being used, (Aliabadi and Rooke, 1991), they are far behind in sophistication the Finite Element Methods which will be exclusively covered in this chapter. For an overview of early finite element techniques in finite elements the reader should consult (Owen and Fawkes, 1983), some of the more recent methods are partially covered in (Anderson, 1995). Finally, the Ph.D. thesis of Reich (1993) and of ? contain some of the major extensions of modern techniques to include thermal load, body forces, surface tractions in 2D and 3D respectively.

² Numerical methods for fracture mechanics can be categorized in many different ways, in this chapter we shall use three criteria:

1. Those in which the singularity is modelled, that is the $r^{-\frac{1}{2}}$ stress field at the tip of the crack is properly represented.
2. Techniques in which the SIF are directly evaluated as part of the augmented global stiffness matrix.
3. Techniques through which the SIF can be computed *a post priori* following a standard finite element analysis via a special purpose post-processor.

18.2 Displacement Extrapolation

³ This technique was the predominant one prior to the serendipitous discovery of the quarter point singular element.

⁴ In early finite element studies of LEFM, it was recognized that unless singular elements could be used, it would necessitate to have a very fine mesh at the crack tip to approximate the stress singularity with non-singular elements.

⁵ Following a liner elastic analysis, the stress intensity factors were determined by equating the numerically obtained displacements with their analytical expression in terms of the SIF. Such a correlation will be performed along a radial line emanating from the crack tip, and then the following equations would be used:

$$4G\sqrt{\frac{2\pi}{r}} \begin{Bmatrix} \bar{u} \\ \bar{v} \end{Bmatrix} = K_I \begin{Bmatrix} (2\kappa - 1) \cos \frac{\theta}{2} - \cos \frac{3\theta}{2} \\ (2\kappa + 1) \sin \frac{\theta}{2} + \sin \frac{3\theta}{2} \end{Bmatrix} \quad (18.1)$$

$$4G\sqrt{\frac{2\pi}{r}} \begin{Bmatrix} \bar{u} \\ \bar{v} \end{Bmatrix} = K_{II} \begin{Bmatrix} -(2\kappa + 3) \sin \frac{\theta}{2} - \sin \frac{3\theta}{2} \\ (2\kappa - 3) \cos \frac{\theta}{2} + \cos \frac{3\theta}{2} \end{Bmatrix} \quad (18.2)$$

⁶ After the SIF would have been determined for each point, they would be plotted with respect to their distance from the crack tip, and the predicted SIF values should be the one extrapolated from the crack tip, Fig. 18.1

⁷ Usually, θ is taken to be equal to π . A similar approach could be used using stresses rather than displacements. However this is likely to yield less accurate predictions.

18.3 Quarter Point Singular Elements

⁸ This section discusses the easiest and most powerful technique used in finite elements to model a stress singularity.

⁹ Barsoum (1974) and Henshell and Shaw (1975) independently demonstrated that the inverse square root singularity characteristic of linear elastic fracture mechanics can be obtained in the 2D 8-noded isoparametric element (Q8) when the mid-side nodes near the crack tip are placed at the quarter point.

¹⁰ Thus, in order to model a stress singularity without altering the finite element code, the mid-side nodes adjacent to the crack tip must be shifted to their quarter-point position. Since then this element became known as the quarter-point element.

¹¹ In light of the simplicity and accuracy achieved by this element, this section will:

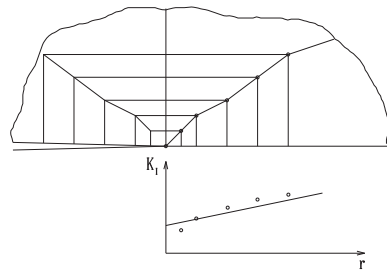


Figure 18.1: Stress Intensity Factor Using Extrapolation Technique

1. cover a brief review of the isoparametric element formulation
2. show how the element can be distorted in order to achieve a stress singularity
3. determine the order of the stress singularity
4. provide a brief review of all the historical developments surrounding this element
5. discuss the effect on numerical accuracy of element size, order of integration, and local meshing around the crack tip
6. briefly mention references to other singular elements

18.4 Review of Isoparametric Finite Elements

¹² In the isoparametric finite element representation, both the internal displacement and coordinates are related to their nodal values through the shape functions:

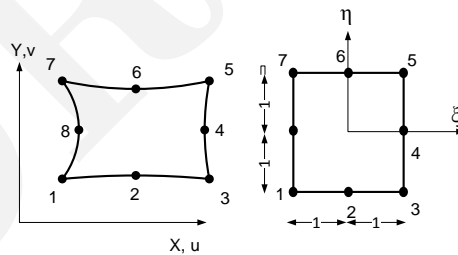


Figure 18.2: Isoparametric Quadratic Finite Element: Global and Parent Element

$$\begin{Bmatrix} x \\ y \end{Bmatrix} = \sum_{i=1}^8 \begin{bmatrix} N_i & 0 \\ 0 & N_i \end{bmatrix} \begin{Bmatrix} \bar{x}_i \\ \bar{y}_i \end{Bmatrix} \quad (18.3)$$

$$\{d\} = \begin{Bmatrix} u \\ v \end{Bmatrix} = \sum_{i=1}^8 \begin{bmatrix} N_i & 0 \\ 0 & N_i \end{bmatrix} \begin{Bmatrix} \bar{u}_i \\ \bar{v}_i \end{Bmatrix} \quad (18.4)$$

where the N_i are the assumed shape functions.

¹³ The shape functions are obtained by mere inspection (i.e. **serendipitiously**),

$$\begin{aligned} N_i &= \frac{1}{4} (1 + \xi\xi_i) (1 + \eta\eta_i) (\xi\xi_i + \eta\eta_i - 1) & i &= 1, 2, 3, 4 \\ N_i &= \frac{1}{2} (1 - \xi^2) (1 + \eta\eta_i) & i &= 5, 7 \\ N_i &= \frac{1}{2} (1 + \xi\xi_i) (1 + \eta^2) & i &= 6, 8 \end{aligned} \quad (18.5)$$

i	N_i	$N_{i,\xi}$	$N_{i,\eta}$
1	$\frac{1}{4}(1-\xi)(1-\eta)(-\xi-\eta-1)$	$\frac{1}{4}(2\xi+\eta)(1-\eta)$	$\frac{1}{4}(1-\xi)(2\eta+\xi)$
2	$\frac{1}{4}(1+\xi)(1-\eta)(\xi-\eta-1)$	$\frac{1}{4}(2\xi-\eta)(1-\eta)$	$\frac{1}{4}(1+\xi)(2\eta-\xi)$
3	$\frac{1}{4}(1+\xi)(1+\eta)(\xi+\eta-1)$	$\frac{1}{4}(2\xi+\eta)(1+\eta)$	$\frac{1}{4}(1+\xi)(2\eta+\xi)$
4	$\frac{1}{4}(1-\xi)(1+\eta)(-\xi-\eta-1)$	$\frac{1}{4}(2\xi-\eta)(1+\eta)$	$\frac{1}{4}(1-\xi)(2\eta-\xi)$
5	$\frac{1}{2}(1-\xi^2)(1-\eta)$	$-\xi(1-\eta)$	$-\frac{1}{2}(1-\xi^2)$
6	$\frac{1}{2}(1+\xi)(1-\eta^2)$	$\frac{1}{2}(1-\eta^2)$	$-(1+\xi)\eta$
7	$\frac{1}{2}(1-\xi^2)(1+\eta)$	$-\xi(1+\eta)$	$\frac{1}{2}(1-\xi^2)$
8	$\frac{1}{2}(1-\xi)(1-\eta^2)$	$-\frac{1}{2}(1-\eta^2)$	$-(1-\xi)\eta$

Table 18.1: Shape Functions, and Natural Derivatives for Q8 Element

and are tabulated in Table 18.1.

14 As the strain is the derivative of the displacement, we will need later to define $\frac{\partial N}{\partial x}$ and $\frac{\partial N}{\partial y}$. N has been defined in Eq. 18.5 in terms of the natural coordinates ξ and η . Thus the chain rule will have to be invoked and the inverse of the jacobian will be needed.

15 In this case, the jacobian matrix is:

$$[J] = \begin{bmatrix} \frac{\partial x}{\partial \xi} & \frac{\partial y}{\partial \xi} \\ \frac{\partial x}{\partial \eta} & \frac{\partial y}{\partial \eta} \end{bmatrix} \quad (18.6)$$

$$= \begin{bmatrix} \sum_{i=1}^8 \frac{\partial N_i}{\partial \xi} x_i & \sum_{i=1}^8 \frac{\partial N_i}{\partial \xi} y_i \\ \sum_{i=1}^8 \frac{\partial N_i}{\partial \eta} x_i & \sum_{i=1}^8 \frac{\partial N_i}{\partial \eta} y_i \end{bmatrix} \quad (18.7)$$

16 The inverse jacobian is then evaluated from:

$$[J]^{-1} = \begin{bmatrix} \frac{\partial \xi}{\partial x} & \frac{\partial \eta}{\partial x} \\ \frac{\partial \xi}{\partial y} & \frac{\partial \eta}{\partial y} \end{bmatrix} \quad (18.8)$$

$$= \frac{1}{Det J} \begin{bmatrix} \frac{\partial y}{\partial \eta} & -\frac{\partial y}{\partial \xi} \\ -\frac{\partial x}{\partial \eta} & \frac{\partial x}{\partial \xi} \end{bmatrix} \quad (18.9)$$

17 The strain displacement relationship is:

$$\{\epsilon\} = \sum_{i=1}^8 [B_i] [d_i] \quad (18.10)$$

where $[B_i]$ is the strain matrix given by:

$$[B_i] = \begin{bmatrix} \frac{\partial N_i}{\partial x} & 0 \\ 0 & \frac{\partial N_i}{\partial y} \\ \frac{\partial N_i}{\partial y} & \frac{\partial N_i}{\partial x} \end{bmatrix} \quad (18.11)$$

where the following chain rule is invoked to determine the coefficients of $[B]$:

$$\left\{ \begin{array}{c} \frac{\partial N}{\partial x} \\ \frac{\partial N}{\partial y} \end{array} \right\} = [J]^{-1} \left\{ \begin{array}{c} \frac{\partial N}{\partial \xi} \\ \frac{\partial N}{\partial \eta} \end{array} \right\} \quad (18.12)$$

18 Finally, it can be shown that the element stiffness matrix of an element is given by (Gallagher, 1975), (Zienkiewicz, 1967):

$$[K] = \int_{-1}^1 \int_{-1}^1 [B(\xi, \eta)] [D] [B(\xi, \eta)] det J d\xi d\eta \quad (18.13)$$

where the natural coordinates ξ and η are shown in Fig. 18.2 and $[D]$ is the stress-strain or constitutive matrix.

¹⁹ The stress is given by:

$$\{\sigma\} = [D][B] \begin{Bmatrix} \bar{u}_i \\ \bar{v}_i \end{Bmatrix} \quad (18.14)$$

18.5 How to Distort the Element to Model the Singularity

²⁰ In Eq. 18.14, if the stresses are to be singular, then $[B]$ has to be singular as the two other components are constants. Consequently, if $[B]$ is to be singular then the determinant of J must vanish to zero (Eq. 18.6) at the crack tip.

²¹ Now considering a rectangular element of length L along its first side (1-5-2, in Fig. 18.2), we can readily see that both off-diagonal terms ($\frac{\partial y}{\partial \xi}$ and $\frac{\partial x}{\partial \eta}$) in J (Eq. 18.6) are zero. Thus, for the determinant of the jacobian to be zero we must have either one of the diagonal terms equal to zero.

²² It will suffice to force $\frac{\partial x}{\partial \xi}$ to be zero. Making the proper substitution for $\frac{\partial x}{\partial \xi}$ at $\eta = -1$ we have:

$$\begin{aligned} \left. \frac{\partial x}{\partial \xi} \right|_{\eta=-1} &= \sum_{i=1}^8 \frac{\partial N_i}{\partial \xi} \bar{x}_i \\ &= \frac{1}{4} [-1 + 2\xi + 2\xi - 1] (0) \\ &\quad + \frac{1}{4} [1 + 2\xi + 2\xi + 1] (L) \\ &\quad + \frac{1}{4} [-1 + 2\xi - 2\xi + 1] (L) \\ &\quad + \frac{1}{4} [1 - 2\xi + 2\xi - 1] (0) \\ &\quad - 2\xi (x_5) \\ &\quad + \frac{1}{2} (1 - 1)L \\ &\quad + \frac{1}{2} (1 - 1) (L) \\ &\quad + \frac{1}{2} (1 - 1) \left(\frac{L}{2} \right) \\ &= \frac{1}{4} (2 + 4\xi) L - 2\xi x_5 \end{aligned} \quad (18.15)$$

²³ After simplification, and considering the first corner node (where $\eta = \xi = -1$), we would have:

$$\left. \frac{\partial x}{\partial \xi} \right|_{\substack{\xi=-1 \\ \eta=-1}} = 0 \Leftrightarrow (1 - 2) \frac{L}{2} + 2x_5 = 0 \quad (18.16)$$

$$\boxed{x_5 = \frac{L}{4}} \quad (18.17)$$

²⁴ Thus all the terms in the jacobian vanish if and only if the second node is located at $\frac{L}{4}$ instead of $\frac{L}{2}$, and subsequently both the stresses and strains at the first node will become singular.

²⁵ Thus singularity at the crack tip is achieved by shifting the mid-side node to its quarter-point position, see Fig. 18.3.

²⁶ We should observe that instead of enforcing $\frac{\partial x}{\partial \xi}$ along edge 1-2 to vanish at the crack tip, we could have enforced $\frac{\partial y}{\partial \eta}$ along edge 1-7 to be zero at the crack tip.

²⁷ A similar approach will show that if node 8 is shifted to its quarter-point position the same radial strain variation would be obtained along sides 1-4. However, along rays within the element emanating from node 1 the strain variation is not singular. The next section will discuss this issue and other variation of this distorted element in more detail.

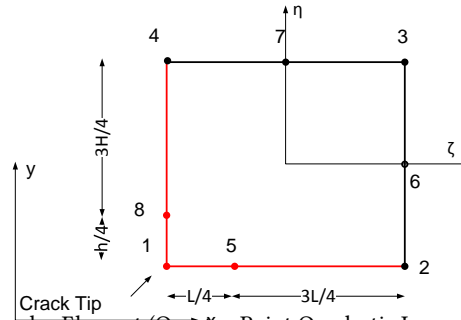


Figure 18.3: Singular Element (Quarter-Point Quadratic Isoparametric Element)

18.6 Order of Singularity

28 Having shown that the stresses at the first node are singular, the obvious question is what is the degree of singularity.

29 First let us solve for ξ in terms of x and L at $\eta = -1$ (that is, alongside 1-5-2):

$$\begin{aligned} x &= \sum_{i=1}^8 N_i \bar{x}_i \\ &= \frac{1}{2} (1 - \xi^2) (1 + 1) \frac{L}{4} + \frac{1}{4} (1 + \xi) (1 + 1) (\xi) L \\ &= \frac{1}{2} \xi (1 + \xi) L + (1 - \xi^2) \frac{L}{4} \end{aligned} \quad (18.18)$$

$$\Rightarrow \xi = -1 + 2\sqrt{\frac{x}{L}} \quad (18.19)$$

30 Recalling that in isoparametric elements the displacement field along $\eta = -1$ is given by:

$$u = -\frac{1}{2} \xi (1 - \xi) \bar{u}_1 + \frac{1}{2} \xi (1 + \xi) \bar{u}_5 + (1 - \xi^2) \bar{u}_2 \quad (18.20)$$

31 we can rewrite Eq. 18.20 by replacing ξ with the previously derived expression, Eq. 18.19):

$$\begin{aligned} u &= -\frac{1}{2} \left(-1 + 2\sqrt{\frac{x}{L}} \right) \left(2 - 2\sqrt{\frac{x}{L}} \right) \bar{u}_1 \\ &+ \frac{1}{2} \left(-1 + 2\sqrt{\frac{x}{L}} \right) \left(2\sqrt{\frac{x}{L}} \right) \bar{u}_5 \\ &+ \left(4\sqrt{\frac{x}{L}} - 4\frac{x}{L} \right) \bar{u}_2 \end{aligned} \quad (18.21)$$

32 This complex equation can be rewritten in the form:

$$\boxed{u = A + Bx + C\sqrt{\frac{x}{L}}} \quad (18.22)$$

33 We thus note that the displacement field has had its quadratic term replaced by $x^{\frac{1}{2}}$, which means that when the derivative of the displacement is taken, the strain (and stresses) are of the form:

$$\epsilon_x = -\frac{1}{2} \left(\frac{3}{\sqrt{xL}} - \frac{4}{L} \right) \bar{u}_1 + \frac{1}{2} \left(\frac{-1}{\sqrt{xL}} + \frac{4}{L} \right) \bar{u}_5 + \left(\frac{2}{\sqrt{xL}} - \frac{4}{L} \right) \bar{u}_2 \quad (18.23)$$

34 Thus the strength of the singularity is of order $\frac{1}{2}$, just as we wanted it to be for linear elastic fracture mechanics !

18.7 Stress Intensity Factors Extraction

³⁵ A number of techniques (including the ones discussed in the subsequent section) can be used to determine the SIF when quarter-point elements are used, Fig. 18.4 but by far the simplest one to use and implement is the one based on the nodal displacement

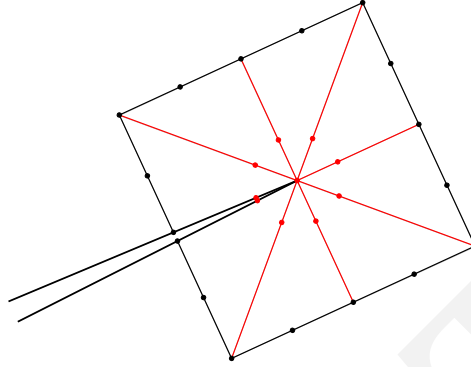


Figure 18.4: Finite Element Discretization of the Crack Tip Using Singular Elements

correlation technique.

³⁶ This technique, first introduced by [Shih et al. \(1976\)](#), equates the displacement field in the quarter-point singular element with the theoretical one. This method was subsequently refined by [Lynn and Ingraffea \(1977\)](#) who introduced the transition elements, and extended [Ingraffea and Manu \(1980\)](#) to three-dimensional isotropic problems.

³⁷ This method was finally extended to full three-dimensional anisotropic cases by [Saouma and Sikiotis \(1986\)](#).

18.7.1 Isotropic Case

³⁸ For the quarter-point singular element, in two dimensions, and with reference to Fig. 18.5, the displacement field is given by,

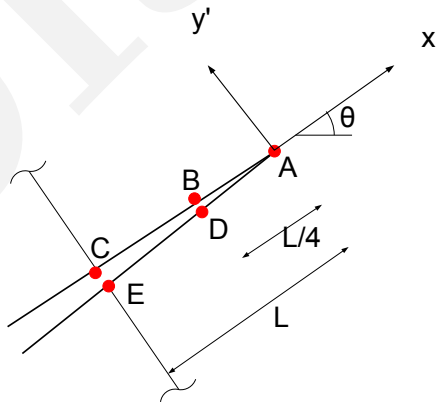


Figure 18.5: Displacement Correlation Method to Extract SIF from Quarter Point Singular Elements

Eq. 18.23:

$$u' = \bar{u}'_A + (-3\bar{u}'_A + 4\bar{u}'_B - \bar{u}'_C) \sqrt{\frac{r}{L}} + (2\bar{u}'_A + 2\bar{u}'_C - 4\bar{u}'_B) \frac{r}{L} \quad (18.24)$$

$$v' = \bar{v}'_A + (-3\bar{v}'_A + 4\bar{v}'_B - \bar{v}'_C) \sqrt{\frac{r}{L}} + (2\bar{v}'_A + 2\bar{v}'_C - 4\bar{v}'_B) \frac{r}{L} \quad (18.25)$$

where \bar{u}' and \bar{v}' are the local displacements (with x' aligned with the crack axis) of the nodes along the crack in the singular elements.

³⁹ On the other hand, the analytical expression for v is given by Eq. 3.53-f with $\theta = 180$, yielding:

$$v = K_I \frac{\kappa + 1}{2G} \sqrt{\frac{r}{2\pi}} \quad (18.26)$$

⁴⁰ Equating the terms of equal power ($\frac{1}{2}$) in the preceding two equations, the \sqrt{r} term vanishes, and we obtain:

$$K_I = \frac{2G}{\kappa + 1} \sqrt{\frac{2\pi}{L}} \left(-3\bar{v}'_A + 4\bar{v}'_B - \bar{v}'_C \right) \quad (18.27)$$

⁴¹ If this approach is generalized to mixed mode problems, then the two stress intensity factors are given by:

$$\begin{bmatrix} K_I \\ K_{II} \end{bmatrix} = \frac{1}{2} \frac{2G}{\kappa + 1} \sqrt{\frac{2\pi}{L}} \begin{bmatrix} 0 & 1 \\ 1 & 0 \end{bmatrix} \begin{bmatrix} -3\bar{u}'_A + 4 \left(\bar{u}'_B - \bar{u}'_D \right) - \left(\bar{u}'_C - \bar{u}'_E \right) \\ -3\bar{v}'_A + 4 \left(\bar{v}'_B - \bar{v}'_D \right) - \left(\bar{v}'_C - \bar{v}'_E \right) \end{bmatrix} \quad (18.28)$$

⁴² Thus it can be readily seen that the extraction of the SIF can be accomplished through a “post-processing” routine following a conventional finite element analysis in which the quarter-point elements have been used.

18.7.2 Anisotropic Case

⁴³ Following a similar procedure to the one previously described, for the anisotropic case,¹ Saouma and Sikiotis (1986) have shown that the three stress intensity factors can be evaluated from:

$$\begin{bmatrix} K_I \\ K_{II} \\ K_{III} \end{bmatrix} = [B]^{-1} [A] \sqrt{\frac{2\pi}{L}} \quad (18.29)$$

where $[A]$ is obtained from the displacements of those nodes along the crack in the singular quarter-point wedge element, as shown in Fig. 18.6:

$$[A] = \begin{bmatrix} 2\bar{u}_B - \bar{u}_C + 2\bar{u}_E - \bar{u}_F + \bar{u}_D + \frac{1}{2}\eta(-4\bar{u}_B + \bar{u}_C + 4\bar{u}_E - \bar{u}_F) + \frac{1}{2}\eta^2(\bar{u}_F + \bar{u}_C - 2\bar{u}_D) \\ 2\bar{v}_B - \bar{v}_C + 2\bar{v}_E - \bar{v}_F + \bar{v}_D + \frac{1}{2}\eta(-4\bar{v}_B + \bar{v}_C + 4\bar{v}_E - \bar{v}_F) + \frac{1}{2}\eta^2(\bar{v}_F + \bar{v}_C - 2\bar{v}_D) \\ 2\bar{w}_B - \bar{w}_C + 2\bar{w}_E - \bar{w}_F + \bar{w}_D + \frac{1}{2}\eta(-4\bar{w}_B + \bar{w}_C + 4\bar{w}_E - \bar{w}_F) + \frac{1}{2}\eta^2(\bar{w}_F + \bar{w}_C - 2\bar{w}_D) \end{bmatrix} \quad (18.30)$$

and $[B]$ is obtained from the analytical solution to the displacements around the crack tip in homogeneous anisotropic solids:

$$[B]^{-1} = \begin{bmatrix} \operatorname{Re} \left[\frac{i}{s_1 - s_2} (q_2 - q_1) \right] \frac{1}{D} & \operatorname{Re} \left[\frac{-i}{s_1 - s_2} (p_2 - p_1) \right] \frac{1}{D} & 0 \\ \operatorname{Re} \left[\frac{-i}{s_1 - s_2} (s_1 q_2 - s_2 q_1) \right] \frac{1}{D} & \operatorname{Re} \left[\frac{i}{s_1 - s_2} (s_1 p_2 - s_2 p_1) \right] \frac{1}{D} & 0 \\ 0 & 0 & \frac{1}{(c_{44} c_{55} - c_{45}^2)} \end{bmatrix} \quad (18.31)$$

18.8 Numerical Evaluation

⁴⁴ Based on an extensive parametric study, Saouma and Schwemmer (1984), have formulated the following recommendations for the use of the singular quarter point element:

1. Use a 2×2 (reduced) integration scheme.
2. Use at least four (in pure mode I problems), or eight (in mixed mode problems) singular elements around a crack tip.
3. Have the internal angles of all the singular elements around the crack tip approximately equal to 45 degrees.

¹Anisotropic modelling is important for either roller compacted concrete dams or layered rock foundations.

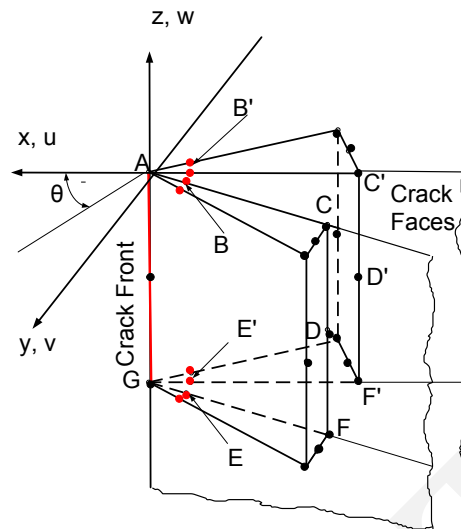


Figure 18.6: Nodal Definition for FE 3D SIF Determination

4. Unless an excessively small l/a ratio is used, little improvement is achieved by using transition elements.
5. For problems with uniform non-singular stress distribution, little improvement is achieved by using a small l/a .
6. For problems where a non-singular, stress gradient is expected, l/a should be less than 0.5.

⁴⁵ Note that the above recommendations remain valid in mixed mode crack propagation studies. Although initially they cannot be directly extended to cases with high $\frac{K_{II}}{K_I}$, it is well known that the crack tends to propagate in a direction that minimizes (but not completely eliminates) K_{II} where the above recommendations would be valid.

18.9 Historical Overview

⁴⁶ Because quarter point have been so popular (and still are) in light of their simplicity, this section will provide an overview of the major extensions to this simple method to determine SIF.

⁴⁷ Barsoum (1974) and Henshell and Shaw (1975) independently demonstrated that the inverse square root singularity characteristic of linear elastic fracture mechanics can be obtained in the 2D 8-noded isoparametric element (Q8) when the mid-side nodes near the crack tip are placed at the quarter point. This concept was subsequently extended to plate bending and shell fractures by Barsoum (1975) and Barsoum (1976a).

⁴⁸ Barsoum (1976b) then showed that the triangular element formed by collapsing one side of the Q8 led to far better results than the rectangular element. Freese and Tracy (1976) showed that the natural isoparametric triangle (NIT) and the collapsed quadrilateral perform equally well. If the side opposite to the crack tip is curved, then there is a substantial deterioration in the SIF calculation from the collapsed quadrilateral, and no change in the NIT. Such a discrepancy is caused by the fact that a collapsed 8-node quadrilateral does not actually degenerate into an NIT (Newton, 1973).

⁴⁹ The extension of the quadratic isoparametric quarter-point element to cubic isoparametric was proposed by Pu et al. (1977). Yamada et al. (1979) extended the concept of the 8-node isoparametric element to the variable numbering element.

⁵⁰ Hibbitt (1977) proved that the singular rectangular element has a singular stiffness whereas the triangular one does not, and that in the collapsed quadrilateral element the singularity prevails along the two sides only, whereas it is omnipresent inside the triangular element. He attributed this difference to the better results achieved by the triangular element as reported by Barsoum. He also demonstrated that a variety of stress singularities ($1/n$) can be achieved by isoparametric elements with a polynomial approximation of order n . In a recent paper, Ying (1982) showed that in his investigation Hibbitt erroneously concluded that the strain energy of a rectangular quarter-point element is singular, but that, as previously known, the singularity is along the edges and diagonal only. Also discussed by Ying is the error associated with the location of the quarter-point of a singular element. This was further elaborated on by Barsoum's discussion of the previous work (Barsoum, 1982), in which he has shown that the error

in estimating the SIF is one order of magnitude smaller than the discretization error in locating the quarter-point. Hence the exact location of the mid-side node is not crucial as long as the discretization error is small. Also by having multiple independent nodes (of a collapsed Q8), Barsoum (1977) showed that small-scale yielding (characterized by $1/r$ stress singularity) could be modelled.

⁵¹ Lynn and Ingraffea (1977) generalized the concept of the quarter-point singular element and showed that by varying the placement of the side node, between quarter- and mid-point, one can control the point where singularity is to occur (between the corner node and infinity, respectively). This led to the introduction of the transition element, which, when inserted around the singular elements, resulted in improved SIF calculations as the l/a (element length over total crack length) ratio decreased. Again Hussain et al. (1981) extended the concept of quadratic transition elements to cubic transition elements.

⁵² In his dissertation, Ingraffea (1977) investigated both the effect of the l/a and aspect ratio of the singular elements. An optimum ratio of $l/a=0.25$ was reported, and it was found that the aspect ratio effect was relatively unimportant. This dependency of the SIF on the l/a ratio was subsequently further described by Lynn and Ingraffea. Another detailed investigation of the optimum quarter point-element size was carried out by Ingraffea and Manu (1980), where l/a was varied from 0.2 to 0.03 in both two- and three-dimensional analyses. The errors in the two-dimensional results varied from -8 percent for $l/a = 0.20$ to -1 percent for $l/a = 0.03$.

⁵³ An assessment of the quarter-point elements (in pressure vessel fracture analysis) was offered by Barsoum (1981) for both two- and three-dimensional analysis. Three sources of modelling errors associated with the quarter-point elements were discussed: (a) those associated with the type of quarter-point element, triangular or rectangular; (b) those associated with the configuration of the element boundary, straight or curved; and (c) those associated with the location of the quarter-point node. Barsoum indicated that (a) triangular elements are to be preferred over the quadrilateral ones (whether collapsed or not); (b) the sides of the element should not be curved; and (c) perturbation of the quarter-point node by e leads to an error in calculating the stress intensity factor of ge^2 where g is the ratio of the crack tip element to crack length.

⁵⁴ In a recent paper, Harrop (1982) qualitatively discussed the optimum size of quarter-point crack tip elements. He indicated that the singular element can represent the stress singularity and a constant finite stress term only. Thus any singular element that is too large cannot represent a structure non-linear (and non-singular) stress variation. On the other hand, by using a singular element that is too small, the error in representing the finite stress term decreases, but the region of the mesh representing the stress singularity also decreases. This source of error would still hold even if transition elements were used. He thus pointed out that some crack tip element size has to be optimum, and concluded that "it is clearly impossible to recommend a particular crack tip element size suitable for all situations."

⁵⁵ An assessment of various crack tip singular elements for use with isoparametric elements was discussed by Fawkes et al. (1979). In this study, elements based on the use of distorted shape functions, standard shape functions, analytical solutions, superposition process, and hybrid techniques were evaluated using a test problem of both single and combined mode fracture. This study revealed that the best results were achieved by the analytic element, and the next best group was the one using the distorted shape function.

⁵⁶ Few of the above papers discussed the numerical accuracy achieved by the quarter-point element in any detail or attempted to provide recommendations for its best usage. At best there have been conflicting indications, usually based on few analyses, on the appropriate l/a ratio to be used. Also one of the major arguments expressed against the use of this element is the SIF dependency on l/a . Furthermore, in light of a new generation of computer programs (Saouma and Zatz, 1984), which simulates the discrete crack propagation inside a finite element mesh with automatic remeshing, it is important to quantify the discretization error associated with the quarter-point singular element.

⁵⁷ It is clear that such a numerical evaluation of this increasingly popular element is long overdue. It should provide the stress analyst (who could be using a general purpose finite element program) with guidelines for the mesh preparation around the crack tip and some idea about the level of accuracy to be expected from the analysis.

⁵⁸ In the present study, two problems with known analytical stress intensity factors are considered. A number of parameters will be varied during the executions, and numerical values of the stress intensity factors will be compared to the exact ones. From the numerous analyses, a data base will be created and graphically represented. It is anticipated that, through appropriate and careful interpretation of those results, guidelines for the mesh preparation around the crack tip could be achieved along with an approximate evaluation of the resulting accuracy.

18.10 Other Singular Elements

⁵⁹ For the most part this section discussed only the quarter point element, but one should be aware of the following alternative formulations:

1. exact field modelling (Rao et al., 1971), (Apostal, 1974)

2. hybrid elements by [Atluri et al. \(1979\)](#)

3. enriched elements by [Benzley \(1974\)](#), in which the shape functions are enriched with additional terms, which account for the singular terms:

$$u_i = \sum_{k=1}^4 f_k \bar{u}_{ik} + K_{\text{I}} \left(Q_{1i} \sum_{k=1}^4 f_k \bar{Q}_{1ik} \right) + K_{\text{II}} \left(Q_{2i} \sum_{k=1}^4 f_k \bar{Q}_{2ik} \right) \quad (18.32)$$

$$Q_{ij} = \frac{u_{ij}}{k_i} \quad (18.33)$$

$$u' = \left(1 + \frac{2x}{L} - 3\sqrt{\frac{x}{L}} \right) u'_1 + \left(4\sqrt{\frac{x}{L}} - 4\frac{x}{L} \right) u'_2 + \left(\frac{2x}{L} - \sqrt{\frac{x}{L}} \right) u'_3 \quad (18.34)$$

⁶⁰ In this method the stress intensity factors are treated as primary unknowns, and are thus obtained during the global stiffness matrix decomposition. Although this method has yielded some very good results, its main drawback is that the finite element program has to be altered in order to implement it. This method was first proposed by Benzley when the quarter-point element (discussed in the next chapter) was not yet known.

Chapter 19

ENERGY RELEASE BASED METHODS

¹ In this class of solutions, we will exploit the definition of the energy release rate G to derive a simple method of determining the stress intensity factors. We shall distinguish between mode I and mixed mode cases. The former one, although of academic relevance only, is a simple introduction to the second.

19.1 Mode I Only

19.1.1 Energy Release Rate

² Recalling that the strain energy release rate G is given by:

$$G = -\frac{\partial \Pi}{\partial a} = \frac{K_I^2}{E'} \approx \frac{\Delta U}{\Delta a} \quad (19.1)$$

a simple algorithm for the SIF calculation emerges:

1. For an initial crack length a , determine the total strain energy from either one of the following approaches:
 - a) $U = \mathbf{u}^t \mathbf{K} \mathbf{u}$ where \mathbf{u} is nodal displacement, and \mathbf{K} is the global structural stiffness matrix.
 - b) $U = \mathbf{u}^t \mathbf{P}$ where \mathbf{P} and \mathbf{u} are the externally applied nodal load and displacement, respectively.
2. Increase the crack length from a to $a + \Delta a$, Fig. 19.1, and reanalyze.

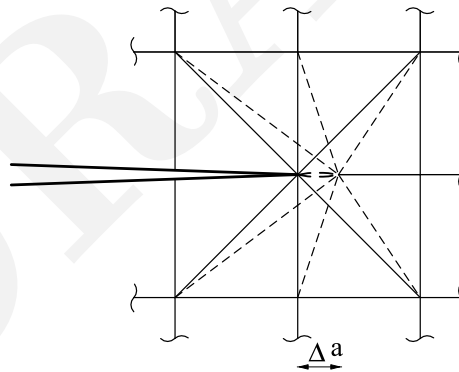


Figure 19.1: Crack Extension Δa

$$3. \text{ Determine } G \text{ from } G \simeq \frac{(U + \Delta U) - U}{(a + \Delta a) - a} = \frac{\Delta U}{\Delta a} = \frac{K_I^2}{E'}$$

³ Note that:

1. This procedure requires two complete separate analyses.
2. The stress singularity need not be modelled.¹
3. This technique is restricted to mode I only.
4. Usage of an over-relaxation solver (such as the Gauss-Seidel) can reduce computational time for the second analysis in which the global stiffness matrix is only slightly altered.

¹It has nevertheless been shown that slightly improved results can be obtained if quarter-point elements are used.

19.1.2 Virtual Crack Extension.

⁴ As previously noted, the stiffness matrix is only slightly perturbed in the second analysis (associated with $a + \Delta a$); thus both Parks (1974) and Hellen (1975) have independently proposed a modification of the preceding approach².

⁵ The potential energy Π is given by:

$$\Pi = \frac{1}{2} [u] [K] \{u\} - [u] \{p\} \quad (19.2)$$

and

$$\begin{aligned} -G &= \frac{\partial \Pi}{\partial a} = \frac{\partial [u]}{\partial a} [K] \{u\} + \frac{1}{2} [u] \frac{\partial [K]}{\partial a} \{u\} - \frac{\partial [u]}{\partial a} \{P\} - [u] \frac{\partial \{P\}}{\partial a} \\ &= -\frac{\partial [u]}{\partial a} \underbrace{([K] \{u\} - \{P\})}_0 + \frac{1}{2} [u] \frac{\partial [K]}{\partial a} \{u\} - [u] \frac{\partial \{P\}}{\partial a} \end{aligned} \quad (19.3)$$

⁶ Noting that the first term in the last equation is zero, we obtain:

$$G = -\frac{1}{2} [u] \frac{\partial [K]}{\partial a} \{u\} + [u] \frac{\partial \{P\}}{\partial a} \quad (19.4)$$

⁷ Thus if the load is unaltered during the crack extension, than the energy release rate is directly related to the derivative of the stiffness.

⁸ Finally, we note that:

1. Only the portion of the stiffness matrix associated with the elements surrounding the crack tip needs to be perturbed.
2. Better results are obtained if singular elements are used.
3. The method can easily be generalized to three-dimensional problems.
4. It can be shown (Parks, 1974) that this technique is equivalent to the determination of the J integral.
5. This method is restricted to mode I loading only.

19.2 Mixed Mode Cases

⁹ Having presented two simple techniques for the SIF extraction for pure mode I cases, we now generalize them to mixed mode loading.

19.2.1 Two Virtual Crack Extensions.

¹⁰ A major limitation of the preceding methods is that in its present form it does not distinguish the mode I from the mode II components in the energy release rate. Such a "discrimination" is possible if we take into account the expressions of the energy release rate obtained by Hellen and Blackburn (1975b) in which:

$$J_1 = G_1 = \frac{K_I^2 + K_{II}^2}{E'} + \frac{K_{III}^2}{2\mu} \quad (19.5)$$

$$J_2 = G_2 = \frac{-2K_I K_{II}}{E'} \quad (19.6)$$

where $E' = E$ for plane stress, and $E' = \frac{E}{1-\nu^2}$ for plane strain. G_1 and G_2 are associated with virtual crack extensions at $\theta = 0$ and $\theta = \frac{\pi}{2}$ respectively.

¹¹ Based on this decomposition of G , the algorithm for SIF extractions in mixed mode problems using virtual crack extensions is as follows:

1. For an initial crack length a , determine the total strain energy U .

²This same technique is now given two different names: stiffness derivative (Park) and virtual crack extension (Hellen).

2. Extend the crack length from a to $a + \Delta a$:

- a) Along $\theta = 0$, and determine G_1 .
- b) Along $\theta = \frac{\pi}{2}$, and determine G_2 .

3. Solve for the two SIF from:

$$\begin{cases} K_I = \frac{s \pm \sqrt{s^2 + \frac{8G_2}{\alpha}}}{2} \\ K_{II} = \frac{s \mp \sqrt{s^2 + \frac{8G_2}{\alpha}}}{2} \end{cases} \quad (19.7)$$

$$\text{where } s = 2\sqrt{\frac{G_1 - G_2}{\alpha}} \text{ and } \alpha = \frac{(1+\nu)(1+\kappa)}{E}$$

¹² An alternative to this technique is to use $G(\theta) = G_1 \cos(\theta) + G_2 \sin(\theta)$, and use two distinct values of θ , which are not necessarily 0 or $\frac{\pi}{2}$.

19.2.2 Single Virtual Crack Extension, Displacement Decomposition

¹³ A major disadvantage of the preceding techniques is that at least one complete finite element analysis is required, followed by either two separate ones or two virtual crack extensions. In the single solution displacement decomposition method of [Sha \(1984\)](#) and [Ishikawa \(1980\)](#), we have a technique in which only one analysis is required.

¹⁴ With reference to Fig. 19.2, we can decompose the nodal displacements into two local components:

$$\Delta = \Delta^1 + \Delta^2 \quad (19.8)$$

where

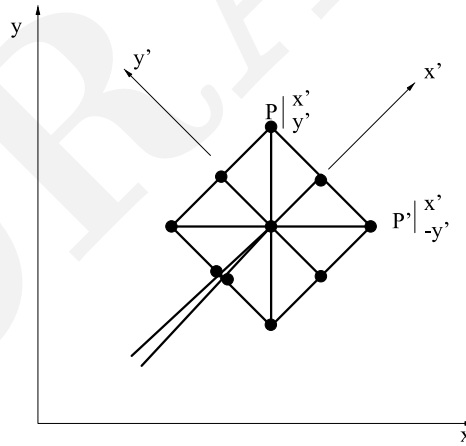


Figure 19.2: Displacement Decomposition for SIF Determination

$$\begin{cases} \{\Delta^1\} = \begin{Bmatrix} u^1 \\ v^1 \end{Bmatrix} = \frac{1}{2} \begin{Bmatrix} u + u' \\ v - v' \end{Bmatrix} \\ \{\Delta^2\} = \begin{Bmatrix} u^2 \\ v^2 \end{Bmatrix} = \frac{1}{2} \begin{Bmatrix} u - u' \\ v + v' \end{Bmatrix} \end{cases} \quad (19.9)$$

¹⁵ Noting that better results are achieved if singular elements are used around the crack tip, we can determine (following one single analysis):

$$G_1 = -\frac{1}{2}[\Delta^1] \frac{\partial[K]}{\partial a} \{\Delta^1\} + [\Delta^1] \frac{\partial\{P^1\}}{\partial a} \quad (19.10)$$

$$G_2 = -\frac{1}{2}[\Delta^2] \frac{\partial[K]}{\partial a} \{\Delta^2\} + [\Delta^2] \frac{\partial\{P^2\}}{\partial a} \quad (19.11)$$

¹⁶ Because propagation is now assumed to be colinear, we can determine the two stress intensity factors from

$$K_I = \sqrt{E'G_1} \quad (19.12)$$

$$K_{II} = \sqrt{E'G_{II}} \quad (19.13)$$

¹⁷ We emphasize that the saving of one analysis (or virtual crack extension) is made possible through the constraint of having a symmetrical local mesh around the crack tip.

Chapter 20

J INTEGRAL BASED METHODS

20.1 Numerical Evaluation

1 Within linear elastic fracture mechanics, the J integral is equivalent to G and we have:

$$G = J = -\frac{\partial \Pi}{\partial a} = \int_{\Gamma} (w dy - \mathbf{t} \cdot \frac{\partial \mathbf{d}}{\partial x} ds) \quad (20.1)$$

2 Thus it is evident that we do have two methods of evaluating J : the first one stems from its equivalence to the energy released rate, and the second one from its definition as an integral along a closed contour. Evaluation of J according to the first approach is identical to the one of G and has been previously presented.

3 In this chapter we shall present the algorithm to evaluate J on the basis of its contour line integral definition. Whereas derivation will be for J integral only, its extension to J_i is quite straightforward.

4 If the stresses were to be determined at the nodes, than the numerical evaluation of J will be relatively simple. However, most standard finite element codes only provide Gauss point stresses, and hence care must be exercised in properly determining the J integral along a path passing through them.

5 The algorithm for the J calculation closely follows the method presented in (Owen and Fawkes, 1983), and is as follows:

1. First let us restrict ourselves to the more general case in which isoparametric elements are used. Because the stresses are most accurately evaluated at the gauss points, the path can be conveniently chosen to coincide with $\xi = \xi_{cst}$ and/or $\eta = \eta_{cst}$. For the sake of discussion, let us assume that the element connectivity is such that the path is along $\xi = \xi_{cst}$, as in Fig. 20.1. We note that for corner elements the integration will have to be performed twice along the two directions.

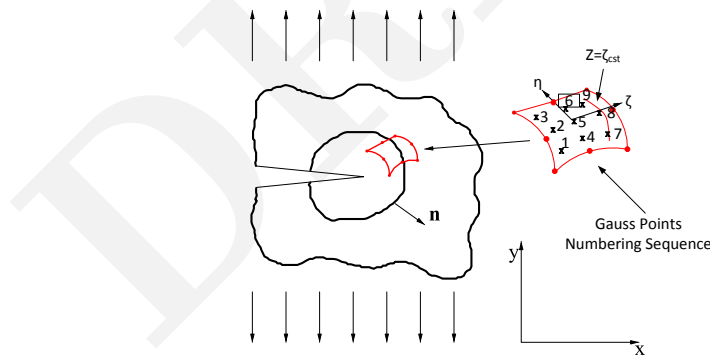


Figure 20.1: Numerical Extraction of the J Integral (Owen and Fawkes, 1983)

2. Now let us start from the basic definition of J :

$$J = \int_{\Gamma} w dy - \mathbf{t} \cdot \frac{\partial \mathbf{d}}{\partial x} ds \quad (20.2)$$

where \mathbf{t} is the traction vector along \mathbf{n} , which is normal to the path; \mathbf{d} is the displacement vector; ds is the element of arc along path Γ ; and w is the strain energy density. We note that the crack is assumed to be along the x axis. If it is not, stresses and displacements would first have to be rotated. Let us now determine each term of Eq. 20.2.

3. The traction vector is given by:

$$t_i = \sigma_{ij}n_j \Rightarrow \mathbf{t} = \begin{Bmatrix} \sigma_{xx}n_1 + \tau_{xy}n_2 \\ \tau_{xy}n_1 + \sigma_{yy}n_2 \end{Bmatrix} \quad (20.3)$$

4. The displacement vector is:

$$\mathbf{d} = \begin{Bmatrix} u \\ v \end{Bmatrix} \quad (20.4)$$

5. The strain energy density w is:

$$\begin{aligned} w &= \frac{1}{2}(\sigma_{xx}\varepsilon_{xx} + 2\tau_{xy}\gamma_{xy} + \sigma_{yy}\varepsilon_{yy}) \\ &= \frac{1}{2}\left[\sigma_{xx}\frac{\partial u}{\partial x} + \tau_{xy}\left(\frac{\partial u}{\partial y} + \frac{\partial v}{\partial x}\right) + \sigma_{yy}\frac{\partial v}{\partial y}\right] \end{aligned} \quad (20.5)$$

6. The arc length ds and dy are given by:

$$ds = \sqrt{dx^2 + dy^2} = \sqrt{\left(\frac{\partial x}{\partial \eta}\right)^2 + \left(\frac{\partial y}{\partial \eta}\right)^2} d\eta \quad (20.6)$$

$$= \frac{\partial y}{\partial \eta} d\eta \quad (20.7)$$

7. Next we can evaluate part of the second term of J :

$$\mathbf{t} \cdot \frac{\partial \mathbf{d}}{\partial x} = (\sigma_x n_1 + \tau_{xy} n_2) \frac{\partial u}{\partial x} + (\tau_{xy} n_1 + \sigma_y n_2) \frac{\partial v}{\partial x} \quad (20.8)$$

where n_1 and n_2 are the components of \mathbf{n} , which is a unit vector normal to the contour line at the Gauss point under consideration.

8. Having defined all the terms of J , we substitute in Eq. 20.2 to obtain the contribution to J from a particular Gauss point within an element.

$$\begin{aligned} J^e &= \int_{-1}^1 \left\{ \underbrace{\frac{1}{2} \left[\sigma_x \frac{\partial u}{\partial x} + \tau_{xy} \left(\frac{\partial u}{\partial y} + \frac{\partial v}{\partial x} \right) + \sigma_y \frac{\partial v}{\partial y} \right]}_w \underbrace{\frac{\partial y}{\partial \eta}}_{dy} \right. \\ &\quad \left. - \underbrace{\left[(\sigma_x n_1 + \tau_{xy} n_2) \frac{\partial u}{\partial x} + (\tau_{xy} n_1 + \sigma_y n_2) \frac{\partial v}{\partial x} \right]}_{\mathbf{t} \cdot \frac{\partial \mathbf{d}}{\partial x}} \right\} \underbrace{\sqrt{\left(\frac{\partial x}{\partial \eta}\right)^2 + \left(\frac{\partial y}{\partial \eta}\right)^2}}_{ds} d\eta \\ &= \int_{-1}^1 I d\eta \end{aligned} \quad (20.9)$$

9. Since the integration is to be carried out numerically along the path (using the same integration points used for the element stiffness matrix), we have:

$$J^e = \sum_{q=1}^{NGAUS} I(\xi_p, \eta_q) W_q \quad (20.10)$$

where W_q is the weighting factor corresponding to η_q and $NGAUS$ is the order of integration (2 or 3).

10. Stresses σ_x , σ_y , τ_{xy} are readily available at the Gauss points.

11. $\frac{\partial u}{\partial x}$, $\frac{\partial u}{\partial y}$, $\frac{\partial v}{\partial x}$, and $\frac{\partial v}{\partial y}$ are obtained through the shape function. For instance $\frac{\partial u}{\partial x} = \left[\frac{\partial N_i}{\partial x} \right] \{u_i\}$ where the u_i are the nodal displacements and $\frac{\partial N_i}{\partial x}$ is the cartesian derivative of the shape function stored in the $[B]$ matrix:

$$[B] = \begin{bmatrix} \frac{\partial N_i}{\partial x} & 0 \\ 0 & \frac{\partial N_i}{\partial y} \\ \frac{\partial N_i}{\partial y} & \frac{\partial N_i}{\partial x} \end{bmatrix} \quad (20.11)$$

where i ranges from 1 to 8 for quadrilateral elements.

12. Another term not yet defined in Eq. 20.9 is $\frac{\partial y}{\partial \eta}$. This term is actually stored already in the Gauss point Jacobian matrix:

$$[J] = \begin{bmatrix} \frac{\partial x}{\partial \xi} & \frac{\partial y}{\partial \xi} \\ \frac{\partial x}{\partial \eta} & \frac{\partial y}{\partial \eta} \end{bmatrix} \quad (20.12)$$

13. Finally we are left to determine n_1 and n_2 (components of \mathbf{n}). Since there is an infinite number of vectors normal to ξ , and we want the one which is in the $\xi - \eta$ plane. It should be noted that if we had a rectangular element, then η is orthogonal to ξ in the physical space, but in general we have a distorted element, and thus η and ξ are not necessarily orthogonal to each others in the physical space. Hence, we determine the normal is determined as follows:

a) Define two arbitrary vectors: \mathbf{A} along $\xi = \xi_{cst}$ and \mathbf{B} along $\eta = \eta_{cst}$ such that:

$$\mathbf{A}^t = \left[\frac{\partial x}{\partial \eta}, \frac{\partial y}{\partial \eta}, 0 \right] \quad (20.13)$$

$$\mathbf{B}^t = \left[\frac{\partial x}{\partial \xi}, \frac{\partial y}{\partial \xi}, 0 \right] \quad (20.14)$$

Note that we have defined the three-dimensional components of those two vectors.

b) Now we define a third vector, which is normal to the plane defined by the preceding two: $\mathbf{C} = \mathbf{A} \times \mathbf{B}$, or:

$$\begin{bmatrix} \mathbf{i} & \mathbf{j} & \mathbf{k} \\ \frac{\partial x}{\partial \eta} & \frac{\partial y}{\partial \eta} & 0 \\ \frac{\partial x}{\partial \xi} & \frac{\partial y}{\partial \xi} & 0 \end{bmatrix} \quad (20.15)$$

This leads to:

$$\mathbf{C} = \left[0, 0, \frac{\partial x}{\partial \eta} \frac{\partial y}{\partial \xi} - \frac{\partial y}{\partial \eta} \frac{\partial x}{\partial \xi} \right] \quad (20.16)$$

c) With \mathbf{C} defined, we can now return to the original plane and define

$$\mathbf{D} = \mathbf{C} \times \mathbf{A} \Rightarrow \mathbf{D} = \left[\underbrace{\frac{\partial y}{\partial \eta} \left(\frac{\partial y}{\partial \eta} \frac{\partial x}{\partial \xi} - \frac{\partial x}{\partial \eta} \frac{\partial y}{\partial \xi} \right)}_{D_1}, \underbrace{\frac{\partial x}{\partial \eta} \left(\frac{\partial x}{\partial \eta} \frac{\partial y}{\partial \xi} - \frac{\partial y}{\partial \eta} \frac{\partial x}{\partial \xi} \right)}_{D_2}, 0 \right] \quad (20.17)$$

d) The unit normal vector is now given by:

$$\mathbf{n} = \begin{Bmatrix} n_1 \\ n_2 \\ 0 \end{Bmatrix} = \begin{Bmatrix} \frac{D_1}{N} \\ \frac{D_2}{N} \\ 0 \end{Bmatrix} \quad (20.18)$$

where $N = \sqrt{D_1^2 + D_2^2}$ and all terms are taken from the Jacobian matrix.

20.2 Mixed Mode SIF Evaluation

⁶ In subsection 20.1 we have outlined two procedures to extract the J integral from a finite element analysis. Based on this technique, at best only K_I may be determined. In this section, we shall generalize the algorithm to extract both J_1 and J_2 through a postprocessing for our finite element analysis, and subsequently determine K_I and K_{II} from Eq. 19.7. Once again the outlined procedure is based on the method outlined in (Owen and Fawkes, 1983).

⁷ First let us redefine the two contour integrals according to (Knowles and Sternberg, 1972) as:

$$J_k = \int \left\{ w n_k - \mathbf{t} \cdot \frac{\partial \mathbf{d}}{\partial x_k} \right\} ds \quad (20.19)$$

combining with Eq. 11.113 and 11.113 we obtain

$$J_1 = \int \left\{ w dy - \mathbf{t} \cdot \frac{\partial \mathbf{d}}{\partial x} \right\} ds = \frac{K_I^2 + K_{II}^2}{H} + \frac{K_{III}^2}{\mu} \quad (20.20)$$

$$J_2 = \int \left\{ w dx - \mathbf{t} \cdot \frac{\partial \mathbf{d}}{\partial y} \right\} ds = \frac{-2K_I K_{II}}{H} \quad (20.21)$$

where

$$H = \begin{cases} E & \text{plane strain} \\ \frac{E}{1-\nu^2} & \text{plane stress} \end{cases} \quad (20.22)$$

⁸ We note that the original definition of *J* is recovered from *J*₁.

⁹ The procedure to determine *J*₁ and *J*₂ will be identical to the one outlined in 20.1 and previously presented with the addition of the following equations:

$$dx = -n_2 ds \quad (20.23)$$

$$dx = -\frac{\partial x}{\partial \eta} d\eta \quad (20.24)$$

20.3 Equivalent Domain Integral (EDI) Method

¹⁰ In this section, we shall derive an alternative expression for the energy release rate. Contrarily to the virtual crack extension method where two analyses (or a stiffness derivative) had to be evaluated, in this method, we have to perform only one analysis. The method is really based on Rice's *J* integral. However, it is recognized that evaluation of *J* in 2D involves a line integral only and a line integral plus a volume integral if body forces are present, (deLorenzi, H.G., 1985). For 3D problems, the line integral is replaced by a surface integral (and a volume integral for body forces).

¹¹ Recognizing that surface integrals may not be easily evaluated in 3D, Green's theorem is invoked, and *J* will be evaluated through a volume integral in 3D and a surface integral in 2D. Thus computationally, this method is quite attractive.

¹² Again as for the previous case, we will start by evaluating the energy release rate, and only subsequently we shall derive expressions for the SIF.

¹³ The essence of the method consists in replacing the contour integral, by a closed integral (outer and inner) while multiplying the expression of *J* by a function *q* equal to zero on the outer surface and unity on the inner one. We adopt the expression of *J* derived for a propagating crack (thus determined around a path close to the crack tip). Having defined a closed path, we then apply Green's theorem, and replace a contour integral by a surface integral.

20.3.1 Energy Release Rate *J*

20.3.1.1 2D case

¹⁴ Recalling the expression for the energy release rate of a propagating crack, Eq. 11.127

$$J = \lim_{\Gamma_0 \rightarrow 0} \int_{\Gamma_0} \left[(w + T) \delta_{1i} - \sigma_{ij} \frac{\partial u_j}{\partial x_1} \right] n_i d\Gamma \quad (20.25)$$

where *w* is the strain energy density, *T* is the kinetic energy

$$T = \frac{1}{2} \rho \frac{\partial u_i}{\partial t} \frac{\partial u_i}{\partial t} \quad (20.26)$$

and δ the Kronecker delta.

¹⁵ An alternative form of this equation (Anderson, 1995) is

$$J = \lim_{\Gamma_0 \rightarrow 0} \int_{\Gamma_0} \left[(w + T) dy - \sigma_{ij} n_i \frac{\partial u_j}{\partial x} d\Gamma \right] \quad (20.27)$$

Unlike the conventional *J* integral, the contour path for this equation can not be arbitrarily selected.

¹⁶ This equation is derived from an energy balance approach, and is thus applicable to all types of material models. However, this J integral is path independent only if Γ is within an elastic zone; if it is taken within the plastic zone than it will be path dependent.

¹⁷ This equation is not well suited for numerical evaluation as the path would have to be along a vanishingly small one where the stresses and strains could not be determined. As such, (Li et al., 1985), we will be rewriting an alternative form of this equation, by considering the contour shown in Fig. 20.2 where Γ_1 , is the outer finite contour, Γ_0 is the inner vanishingly small contour,

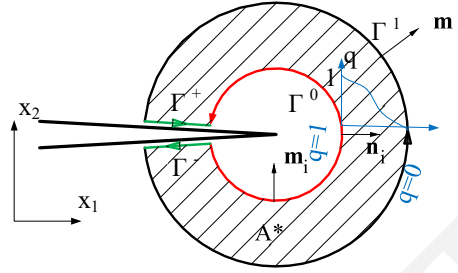


Figure 20.2: Simply connected Region A^* Enclosed by Contours Γ_1 , Γ_0 , Γ_+ , and Γ_- , (Anderson, 1995)

and Γ_+ , and Γ_- are respectively the upper and lower crack surfaces along the contour.

¹⁸ For quasi-static cases ($\dot{T} = 0$), let us construct a closed contour by connecting inner and outer ones. The outer one Γ_1 is finite, while the inner one Γ_0 is vanishingly small. For linear (or nonlinear) elastic material J can be evaluated along either one of those two contours, but only the inner one gives the exact solution in the general case. Thus, we can rewrite Eq. 20.25 around the following closed contour

$$\Gamma^* = \Gamma_1 + \Gamma_+ + \Gamma_- - \Gamma_0 \quad (20.28)$$

yielding (and assuming that the crack faces are traction free)

$$J = \int_{\Gamma^*} \left[\sigma_{ij} \frac{\partial u_j}{\partial x_1} - w \delta_{1i} \right] q m_i d\Gamma - \int_{\Gamma_+ \cup \Gamma_-} \sigma_{2j} \frac{\partial u_j}{\partial x_1} q d\Gamma \quad (20.29)$$

where m_i is the outward normal to Γ^* (thus $m_i = n_i$ on Γ_1 , and $m_i = -n_i$ on Γ_0 , $m_1 = 0$ and $m_2 = \pm 1$ on Γ_+ and Γ_-), and q is an arbitrary but smooth function which is equal to unity on Γ_0 and zero on Γ_1 .

¹⁹ Note that since the integral is taken along the contours, by explicitly specifying $q = 0$ on the outer one, and $q = 1$ on the inner one, Eq. 20.25 and 20.29 are identical. Furthermore, in the absence of crack surface tractions, the second term is equal to zero.

²⁰ Applying the divergence theorem to Eq. 20.29

$$\oint_{\Gamma} \mathbf{v} \cdot \mathbf{n} = \int_A \left(\frac{\partial v_x}{\partial x} + \frac{\partial v_y}{\partial y} \right) dx dy \quad (20.30)$$

we obtain

$$J = \int_{A^*} \frac{\partial}{\partial x_i} \left\{ \left[\sigma_{ij} \frac{\partial u_j}{\partial x_1} - w \delta_{1i} \right] q \right\} dA \quad (20.31)$$

$$= \int_{A^*} \left[\left(\sigma_{ij} \frac{\partial u_j}{\partial x_1} - w \delta_{1i} \right) \frac{\partial q}{\partial x_i} + \left(\frac{\partial}{\partial x_i} \left(\sigma_{ij} \frac{\partial u_j}{\partial x_1} \right) - \frac{\partial w}{\partial x_1} \right) q \right] dA \quad (20.32)$$

where A^* is the area enclosed by Γ^* .

²¹ Let us show that the second term is equal to zero:

$$\frac{\partial}{\partial x_i} \left(\sigma_{ij} \frac{\partial u_j}{\partial x_1} \right) = \underbrace{\sigma_{ij} \frac{\partial}{\partial x_i} \left(\frac{\partial u_j}{\partial x_1} \right)}_{\frac{\partial w}{\partial x}} + \underbrace{\frac{\partial \sigma_{ij}}{\partial x_i}}_0 \frac{\partial u_j}{\partial x_1} \quad (20.33)$$

however from equilibrium we have

$$\frac{\partial \sigma_{ij}}{\partial x_i} = 0 \quad (20.34)$$

22 Furthermore, the derivative of the strain energy density is

$$\frac{\partial w}{\partial x} = \frac{\partial w}{\partial \varepsilon_{ij}} \frac{\partial \varepsilon_{ij}}{\partial x} = \sigma_{ij} \frac{\partial \varepsilon_{ij}}{\partial x} \quad (20.35)$$

substituting

$$\varepsilon_{ij} = \frac{1}{2} \left(\frac{\partial u_i}{\partial x_j} + \frac{\partial u_j}{\partial x_i} \right) \quad (20.36)$$

we obtain

$$\frac{\partial w}{\partial x} = \frac{1}{2} \sigma_{ij} \left[\frac{\partial}{\partial x} \left(\frac{\partial u_i}{\partial x_j} \right) + \frac{\partial}{\partial x} \left(\frac{\partial u_j}{\partial x_i} \right) \right] = \sigma_{ij} \frac{\partial}{\partial x_j} \left(\frac{\partial u_i}{\partial x} \right) \quad (20.37)$$

23 Hence, it is evident that the second term of Eq. 20.32 vanishes and that we are left with

$$J = \int_{A^*} \left[\sigma_{ij} \frac{\partial u_i}{\partial x_1} - w \delta_{1i} \right] \frac{\partial q}{\partial x_i} dA \quad (20.38)$$

This expression, is analogous to the one proposed by Babuska for a surface integral based method to evaluate stress intensity factors, (Babuska and Miller, 1984).

24 We note that deLorenzi (deLorenzi, H.G., 1985) has shown that the energy release rate is given by

$$G = \frac{1}{\Delta A} \int \left(\sigma_{ij} \frac{\partial u_j}{\partial x_1} - w \delta_{i1} \right) \frac{\partial \Delta x_1}{\partial x_i} dA \quad (20.39)$$

for a unit crack growth extension along x_1 . Thus comparing Eq. 20.38 with 20.39, we observe that the two expressions are identical for $q = \frac{\Delta x_1}{\Delta a}$, and thus q can be interpreted as a normalized virtual displacement. In this context it was merely a mathematical device.

25 In summary, we have replace a contour integral by an equivalent area integral to determine J .

20.3.1.2 3D Generalization

26 In this section, we shall generalize to 3D our previous derivation, (Anderson, 1995). From Fig. 20.3 we define a local coordinate system such that x_1 is normal to the crack front, x_2 normal to the crack plane, and x_3 tangent to the crack front.

27 For an arbitrary point, the J integral is given by Eq. 20.25. We now consider a tube of length ΔL and radius r_0 that surrounds the segment of the crack front under consideration. We now define a weighted average J over the crack front segment of length ΔL as

$$\bar{J} \Delta L = \int_{\Delta L} J(\eta) q d\eta \quad (20.40)$$

$$= \lim_{r_0 \rightarrow 0} \int_{S_0} \left[w \delta_{1i} - \sigma_{ij} \frac{\partial u_j}{\partial x_1} \right] q n_i ds \quad (20.41)$$

where $J(\eta)$ is the point-wise value of J , S_0 is the vanishingly small surface area of the tube, q is the weight function previously introduced. q can be again interpreted as a virtual crack advance and Fig. 20.4 illustrates an incremental crack advance over ΔL where q is defined as

$$\Delta a(\eta) = q(\eta) \Delta a_{max} \quad (20.42)$$

and the corresponding incremental area of the virtual crack is

$$\Delta A_c = \Delta a_{max} \int_{\Delta L} q(\eta) d\eta \quad (20.43)$$

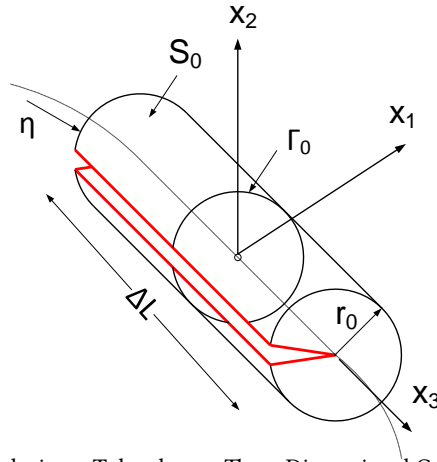
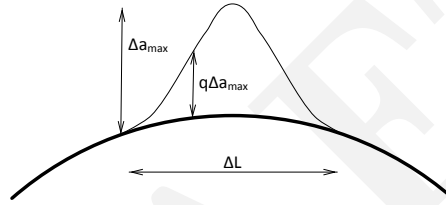


Figure 20.3: Surface Enclosing a Tube along a Three Dimensional Crack Front, (Anderson, 1995)


 Figure 20.4: Interpretation of q in terms of a Virtual Crack Advance along ΔL , (Anderson, 1995)

²⁸ As in the previous case, this expression of J can not be numerically determined for a vanishingly small radius r_0 , as such and as in the previous 2D case, we define a second tube of radius r_1 around the crack front, Fig. 20.5.

$$\bar{J}\Delta L = \oint_{S^*} \left[\sigma_{ij} \frac{\partial u_i}{\partial x_1} - w\delta_{1i} \right] q m_i dS - \oint_{S_- \cup S_+} \sigma_{2j} \frac{\partial u_j}{\partial x_1} q ds \quad (20.44)$$

where

$$S^* = S_1 + S_+ + S_- - S_0 \quad (20.45)$$

and S_+ and S_- are the upper and lower crack surfaces respectively, S_0 and S_1 the inner and outer tube surfaces. Note that this equation is the 3D counterpart of Eq. 20.29 which was written in 2D.

²⁹ Applying the divergence theorem, this equation reduces to a volume integral

$$\bar{J}\Delta L = \int_{V^*} \left\{ \left[\sigma_{ij} \frac{\partial u_j}{\partial x_1} - w\delta_{1i} \right] \frac{\partial q}{\partial x_i} + \left[-\frac{\partial w}{\partial x_1} + \frac{\partial}{\partial x_j} \left(\sigma_{ij} \frac{\partial u_i}{\partial x_1} \right) \right] q \right\} dV + \int_{A_1 \cup A_2} \left(w\delta_{1i} - \sigma_{ij} \frac{\partial u_i}{\partial x_1} \delta_{1i} \right) q dA \quad (20.46)$$

and q must be equal to zero at either end of ΔL that is on A_1 and A_2 . In (Nikishkov and Atluri, 1987) it is shown that in the absence of non-elastic (thermal and plastic) deformations the second term would be equal to zero. The third term will also be equal to zero because q is arbitrarily selected to be zero at each end.

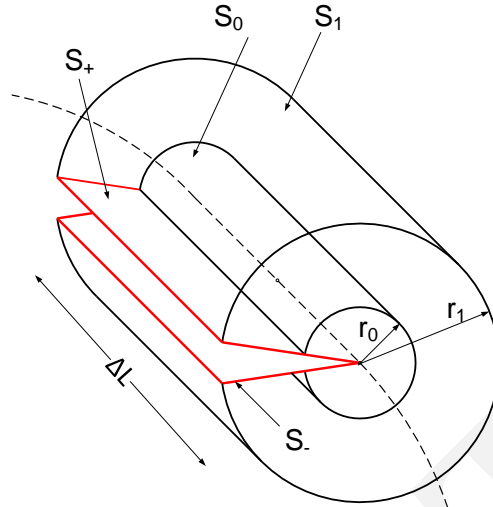


Figure 20.5: Inner and Outer Surfaces Enclosing a Tube along a Three Dimensional Crack Front

20.3.2 Extraction of SIF

³⁰ From Eq. 20.46 it is impossible to extract the 3 distinct stress intensity factors. Hence we shall generalize this equation and write it as (Nikishkov and Atluri, 1987) (ignoring the second and third terms)

$$\bar{J}_k \Delta L = \int_{V^*} \left(\sigma_{ij} \frac{\partial u_i}{\partial x_k} \frac{\partial q}{\partial x_j} - w \frac{\partial q}{\partial x_k} \right) dV \quad (20.47)$$

³¹ Note that $k = 1, 2$ only thus defining $G_1 = J_1$ and $G_2 = J_2$. However, (Nikishkov and Atluri, 1987) have shown that G_3 has a similar form and is equal to

$$G_{III} = \int_{V^*} \left(\sigma_{3j} \frac{\partial u_3}{\partial x_1} \frac{\partial q}{\partial x_j} - w^{III} \frac{\partial q}{\partial x_1} \right) dV \quad (20.48)$$

³² With G_1 , G_2 and G_3 known we need to extract the three stress intensity factors K_I , K_{II} and K_{III} . Again there are two approaches.

20.3.2.1 J Components

³³ Based on the solution by Nikishkov, (Nikishkov and Vainshtok, 1980)

$$\begin{aligned} K_I &= \frac{1}{2} \sqrt{E^*} \left(\sqrt{(J_1 - J_2 - G_3)} + \sqrt{(J_1 + J_2 - G_3)} \right) \\ K_{II} &= \frac{1}{2} \sqrt{E^*} \left(\sqrt{(J_1 - J_2 - G_3)} - \sqrt{(J_1 + J_2 - G_3)} \right) \\ K_{III} &= \sqrt{2\mu G_3} \end{aligned} \quad (20.49)$$

where, (Nikishkov and Atluri, 1987)

$$E^* = E \left[\frac{1}{1 - \nu^2} + \left(\frac{\nu}{1 + \nu} \right) \frac{\varepsilon_{33}}{\varepsilon_{11} + \varepsilon_{22}} \right] \quad (20.50)$$

which is a weighted value of E such that we retrieve $E^* = \frac{E}{1 - \nu^2}$ for plane strain and $E^* = E$ for plane stress.

20.3.2.2 σ and u Decomposition

³⁴ As for the solution by Shah, we can decompose the displacement field as

$$\begin{aligned} \{u\} &= \{u^I\} + \{u^{II}\} + \{u^{III}\} \\ &= \frac{1}{2} \begin{Bmatrix} u_1 + u'_1 \\ u_2 - u'_2 \\ u_3 + u'_3 \end{Bmatrix} + \frac{1}{2} \begin{Bmatrix} u_1 - u'_1 \\ u_2 + u'_2 \\ 0 \end{Bmatrix} + \frac{1}{2} \begin{Bmatrix} 0 \\ 0 \\ u_3 - u'_3 \end{Bmatrix} \end{aligned} \quad (20.51)$$

similarly the stresses are decomposed as

$$\begin{aligned} \{\sigma\} &= \{\sigma^I\} + \{\sigma^{II}\} + \{\sigma^{III}\} \\ &= \frac{1}{2} \begin{Bmatrix} \sigma_{11} + \sigma'_{11} \\ \sigma_{22} + \sigma'_{22} \\ \sigma_{33} + \sigma'_{33} \\ \sigma_{12} - \sigma'_{12} \\ \sigma_{23} - \sigma'_{23} \\ \sigma_{31} - \sigma'_{31} \end{Bmatrix} + \frac{1}{2} \begin{Bmatrix} \sigma_{11} - \sigma'_{11} \\ \sigma_{22} - \sigma'_{22} \\ 0 \\ \sigma_{12} + \sigma'_{12} \\ 0 \\ 0 \end{Bmatrix} + \frac{1}{2} \begin{Bmatrix} 0 \\ 0 \\ \sigma_{33} - \sigma'_{33} \\ 0 \\ \sigma_{23} + \sigma'_{23} \\ \sigma_{31} + \sigma'_{31} \end{Bmatrix} \end{aligned} \quad (20.52)$$

where

$$u'_i(x_1, x_2, x_3) = u_i(x_1, -x_2, x_3) \quad (20.53)$$

$$\sigma'_{ij}(x_1, x_2, x_3) = \sigma_{ij}(x_1, -x_2, x_3) \quad (20.54)$$

and the stress intensity factors are then determined from

$$K_I = \sqrt{E'G_I} \quad K_{II} = \sqrt{E'G_{II}} \quad K_{III} = \sqrt{2\mu G_{III}} \quad (20.55)$$

where

$$G_k = \int_{V^*} \left(\sigma_{kj} \frac{\partial u_k}{\partial x_1} \frac{\partial q}{\partial x_j} - w^k \frac{\partial q}{\partial x_1} \right) dV \quad (20.56)$$

³⁵ Whereas this method may be difficult to use in conjunction with a 3D finite element mesh generated by triangularization (due to the lack of symmetry around the crack front), it has been successfully used by Cervenka (1994) in conjunction with a unit volume integration in the FE code MERLIN (Saouma et al., 2010).

Chapter 21

RECIPROCAL WORK INTEGRALS

Chapter adapted from (Reich, 1993)

21.1 General Formulation

1 In addition to conservation laws, a form of Betti's reciprocal work theorem (Sokolnikoff, 1956) can also be exploited to directly compute stress intensity factors (Stern, 1973). The reciprocal work theorem defines the relationship between two equilibrium states for a solid.

2 For a solid free of body forces and initial strains and stresses the reciprocal work theorem is defined as

$$\oint_{\Gamma} t_i \tilde{u}_i d\Gamma = \oint_{\Gamma} \tilde{t}_i u_i d\Gamma \quad (21.1)$$

where Ω is any simply connected region within the solid and Γ is the contour of that region; u_i and t_i are the displacements and surface tractions, respectively, associated with one equilibrium state and \tilde{u}_i ; and \tilde{t}_i are the displacements and surface tractions, respectively, associated with another equilibrium state.

3 The equilibrium state defined by u_i and t_i is called the primary state and the equilibrium state defined by \tilde{u}_i and \tilde{t}_i is called the complementary or auxiliary state.

4 To apply the reciprocal work theorem to a cracked solid the simply connected region Ω must be defined such that the singularity at the crack tip is avoided. This is accomplished by defining a pair of surfaces, Γ and Γ_ϵ , that begin on one crack surface and end on the other.

5 Γ is an arbitrary surface defined in the counter-clockwise direction around the crack tip but far away from it.

6 Γ_ϵ is a circle of radius ϵ centered on the crack tip that is defined in the clockwise direction around the crack tip completely inside Γ .

7 Another pair of surfaces, Γ_t^+ and Γ_t^- , corresponding to the crack surfaces complete the definition of Γ , as is shown in Figure 21.1. Γ_t^+ is defined on the upper crack surface between Γ and Γ_ϵ and Γ_t^- is defined on the lower crack surface between Γ_ϵ and Γ .

8 Naturally, Ω is the region inside this closed path through the solid. Since the material inside Γ_ϵ is not included in the definition of Ω the singularity at the crack tip has been excluded.

9 Assuming that Γ_t^+ and Γ_t^- are traction free the definition of the reciprocal work theorem can be rewritten as

$$\oint_{\Gamma} t_i \tilde{u}_i d\Gamma = \int_{\Gamma} t_i \tilde{u}_i d\Gamma + \int_{\Gamma_\epsilon} t_i \tilde{u}_i d\Gamma = \int_{\Gamma} \tilde{t}_i u_i d\Gamma + \int_{\Gamma_\epsilon} \tilde{t}_i u_i d\Gamma \quad (21.2)$$

in which the contributions from Γ and Γ_ϵ are clearly separated.

10 This expanded expression is then rewritten in the form of Somigliana's identity to obtain

$$\int_{\Gamma} (t_i \tilde{u}_i - \tilde{t}_i u_i) d\Gamma + \int_{\Gamma_\epsilon} (t_i \tilde{u}_i - \tilde{t}_i u_i) d\Gamma = 0 \quad (21.3)$$

11 The displacements u_i and the stresses σ_{ij} for the primary state can be decomposed into

$$\begin{aligned} u_i &= u_i^s + u_i^\epsilon + u_i^0 \\ \sigma_{ij} &= \sigma_{ij}^s + \sigma_{ij}^\epsilon \end{aligned} \quad (21.4)$$

where u_i^s and σ_{ij}^s are the displacements and stresses, respectively, for the singular elastic state at the crack tip; u_i^ϵ and σ_{ij}^ϵ are the displacements and stresses, respectively, for the elastic state required to insure that boundary conditions on u_i and σ_{ij} are satisfied; and u_i^0 are the displacements of the crack tip.

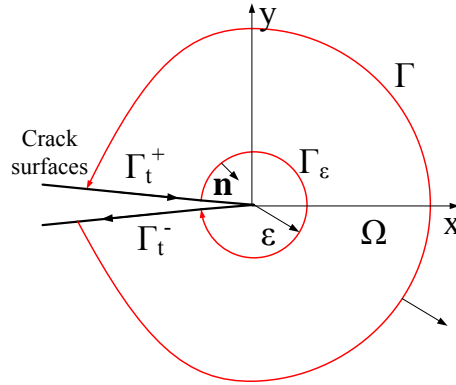


Figure 21.1: Contour integral paths around crack tip for reciprocal work integral

¹² Recognizing that the product $u_i^0 \tilde{t}_i$ has no contribution to the integral since the tractions \tilde{t}_i are self equilibrating due to the lack of body forces and taking into account the orders of the displacements and stresses in the various elastic states, (Stern, 1973) determined that

$$\int_{\Gamma_\epsilon} (t_i \tilde{u}_i - \tilde{t}_i u_i) d\Gamma = - \int_{\Gamma_\epsilon} (t_i^s \tilde{u}_i - \tilde{t}_i u_i^s) d\Gamma + o(1) \quad (21.5)$$

¹³ As ϵ is decreased the elastic singular state u_i^s and t_i^s becomes more dominant and the $o(1)$ terms can be ignored allowing the integrals over Γ_ϵ and Γ to be related in the following manner

$$I_\epsilon = \lim_{\epsilon \rightarrow 0} \int_{\Gamma_\epsilon} (t_i^s \tilde{u}_i - \tilde{t}_i u_i^s) d\Gamma = - \int_{\Gamma} (t_i \tilde{u}_i - \tilde{t}_i u_i) d\Gamma \quad (21.6)$$

¹⁴ Based on this relationship a singular elastic state u_i^s and t_i^s can be assumed; an auxiliary singular state \tilde{u}_i and \tilde{t}_i can be constructed from the assumed singular elastic state; and the value I_ϵ can be determined from the auxiliary singular state and far field displacements and tractions, u_i and t_i , computed using a suitable numerical method.

¹⁵ Perhaps the most attractive feature of this approach is that the singularity at the crack tip need not be rigorously modeled in the numerical method used to obtain u_i and t_i .

¹⁶ Auxiliary singular states have been constructed for a crack in a homogeneous isotropic medium (Stern et al., 1976), a crack in a homogeneous orthotropic medium (Stern and M.L., 1975), and a crack on the interface between dissimilar isotropic media (Hong and Stern, 1978).

¹⁷ The procedure for constructing an auxiliary singular state will be outlined here using the homogeneous isotropic medium for this discussion. Once the singular elastic state has been assumed, the auxiliary singular state is constructed by taking λ as the negative of the value used in the singular elastic state, $\lambda = -\frac{1}{2}$ in this case. This of course means that the strain energy for the auxiliary singular state is unbounded at the crack tip, but since the integral is evaluated well away from the crack tip this is of no concern (Stern, 1973).

¹⁸ The value of the complex constant A for the auxiliary singular state is determined to be

$$A = \frac{2\mu}{(2\pi)^{\frac{1}{2}}(1+\kappa)} (c_1 + i c_2) \quad (21.7)$$

where c_1 and c_2 are arbitrary constants.

¹⁹ This choice for A normalizes the integrand for Γ_ϵ involving the singular elastic state and the auxiliary singular state (Stern et al., 1976).

²⁰ Having determined A , the product of this integral is

$$I_\epsilon = c_1 K_I + c_2 K_{II} + o(1) \quad (21.8)$$

with the $o(1)$ term going to zero as ϵ is decreased.

²¹ The stress intensity factors, K_I and K_{II} , can therefore be directly related to the integral over Γ

$$c_1 K_I + c_2 K_{II} = \int_{\Gamma} [(u_i - u_i^0) \tilde{t}_i + \tilde{u}_i t_i] d\Gamma \quad (21.9)$$

as was shown in Equation 21.6. When the integral is evaluated using u_i and t_i obtained from the numerical method the constants associated with the coefficients c_1 and c_2 are the stress intensity factors.

²² For the isotropic case, in the neighborhood of the crack tip, the displacements and the stresses, in polar coordinate system, are given by Westergaard as:

$$u_r - u_r^0 = \frac{1}{4\mu} \left(\frac{r}{2\pi} \right)^{\frac{1}{2}} \left\{ \left[(2\kappa - 1) \cos \frac{\theta}{2} - \cos \frac{3\theta}{2} \right] K_I - \left[(2\kappa - 1) \sin \frac{\theta}{2} - 3 \sin \frac{3\theta}{2} \right] K_{II} \right\} + O\left(r^{\frac{1}{2}}\right) \quad (21.10)$$

$$u_{\theta} - u_{\theta}^0 = \frac{1}{4\mu} \left(\frac{r}{2\pi} \right)^{\frac{1}{2}} \left\{ \left[-(2\kappa + 1) \sin \frac{\theta}{2} + \sin \frac{3\theta}{2} \right] K_I - \left[(2\kappa + 1) \cos \frac{\theta}{2} - 3 \cos \frac{3\theta}{2} \right] K_{II} \right\} + O\left(r^{\frac{1}{2}}\right) \quad (21.11)$$

$$\sigma_r = \frac{1}{4(2\pi r)^{\frac{1}{2}}} \left\{ \left(5 \cos \frac{\theta}{2} - \cos \frac{3\theta}{2} \right) K_I - \left(5 \sin \frac{\theta}{2} - 3 \sin \frac{3\theta}{2} \right) K_{II} \right\} + O\left(r^{-\frac{1}{2}}\right) \quad (21.12)$$

$$\sigma_{\theta} = \frac{1}{4(2\pi r)^{\frac{1}{2}}} \left\{ \left(3 \cos \frac{\theta}{2} + \cos \frac{3\theta}{2} \right) K_I - \left(3 \sin \frac{\theta}{2} + 3 \sin \frac{3\theta}{2} \right) K_{II} \right\} + O\left(r^{-\frac{1}{2}}\right) \quad (21.13)$$

$$\sigma_{r\theta} = \frac{1}{4(2\pi r)^{\frac{1}{2}}} \left\{ \left(\sin \frac{\theta}{2} + \sin \frac{3\theta}{2} \right) K_I + \left(\cos \frac{\theta}{2} + 3 \cos \frac{3\theta}{2} \right) K_{II} \right\} + O\left(r^{-\frac{1}{2}}\right) \quad (21.14)$$

where u_r^0 and u_{θ}^0 are the radial and tangential components, respectively, of the displacements u^0 of the crack tip, and

$$K_I = \lim_{r \rightarrow 0} (2\pi r)^{\frac{1}{2}} \sigma_{\theta}|_{\theta=0} \quad (21.15)$$

$$K_{II} = \lim_{r \rightarrow 0} (2\pi r)^{\frac{1}{2}} \sigma_{r\theta}|_{\theta=0} \quad (21.16)$$

are the usual stress intensity factors.

The auxiliary solution to be used in the reciprocal work relation is based on Williams solution (Stern et al., 1976):

$$\tilde{u}_r = \frac{1}{2(2\pi r)^{\frac{1}{2}}(1+\kappa)} \left\{ \left[(2\kappa + 1) \cos \frac{3\theta}{2} - 3 \cos \frac{\theta}{2} \right] c_1 + \left[(2\kappa + 1) \sin \frac{3\theta}{2} - \sin \frac{\theta}{2} \right] c_2 \right\} \quad (21.17)$$

$$\tilde{u}_{\theta} = \frac{1}{2(2\pi r)^{\frac{1}{2}}(1+\kappa)} \left\{ \left[-(2\kappa - 1) \sin \frac{3\theta}{2} + 3 \sin \frac{\theta}{2} \right] c_1 + \left[(2\kappa - 1) \cos \frac{3\theta}{2} - \cos \frac{\theta}{2} \right] c_2 \right\} \quad (21.18)$$

$$\tilde{\sigma}_r = -\frac{\mu}{2(2\pi r^3)^{\frac{1}{2}}(1+\kappa)} \left\{ \left[7 \cos \frac{3\theta}{2} - 3 \cos \frac{\theta}{2} \right] c_1 + \left[7 \sin \frac{3\theta}{2} - \sin \frac{\theta}{2} \right] c_2 \right\} \quad (21.19)$$

$$\tilde{\sigma}_{\theta} = -\frac{\mu}{2(2\pi r^3)^{\frac{1}{2}}(1+\kappa)} \left\{ \left[\cos \frac{3\theta}{2} + 3 \cos \frac{\theta}{2} \right] c_1 + \left[\sin \frac{3\theta}{2} + \sin \frac{\theta}{2} \right] c_2 \right\} \quad (21.20)$$

$$\tilde{\sigma}_{r\theta} = -\frac{\mu}{2(2\pi r^3)^{\frac{1}{2}}(1+\kappa)} \left\{ 3 \left[\sin \frac{3\theta}{2} + \sin \frac{\theta}{2} \right] c_1 - \left[3 \cos \frac{3\theta}{2} - \cos \frac{\theta}{2} \right] c_2 \right\} \quad (21.21)$$

where c_1 and c_2 are arbitrary constants.

²³ Now, on the inner circular boundary, the evaluation of the contour integral in terms of traction and displacement takes the form:

$$\begin{aligned} I_\epsilon &= - \int_{C_\epsilon} ((\mathbf{u} - \mathbf{u}^0) \cdot \tilde{\mathbf{t}}) - \tilde{\mathbf{u}} \cdot \mathbf{t} ds \\ &= \int_{-\pi}^{\pi} [\tilde{\sigma}_r(u_r - u_r^0) \tilde{\sigma}_{r\theta}(u_\theta - u_\theta^0) - \sigma_r \tilde{u}_r + \sigma_{r\theta} \tilde{u}_\theta] r d\theta \end{aligned} \quad (21.22)$$

²⁴ When the two solutions are substituted into the preceding equation, we obtain:

$$I_\epsilon = c_1 K_I - c_2 K_{II} \quad (21.23)$$

²⁵ Thus, it can be readily seen that Eq. ?? now reduces to:

$$\boxed{c_1 K_I - c_2 K_{II} = \int_C [(\mathbf{u} - \mathbf{u}^0) \cdot \tilde{\mathbf{t}} - \tilde{\mathbf{u}} \cdot \mathbf{t}] ds} \quad (21.24)$$

²⁶ From this equation an algorithm for the SIF determination emerges:

1. Perform a linear elastic finite element analysis.
2. Extract \mathbf{u} and \mathbf{t} (displacements and traction) from the analysis.
3. Substitute into Eq. 21.24 along with the auxiliary solution.
4. The components of c_1 in Eq. 21.24 yield K_I .
5. The components of c_2 in Eq. 21.24 yield K_{II} .

²⁷ In addition to demonstrating the reciprocal work integral for cracks in homogeneous isotropic (Stern et al., 1976), homogeneous orthotropic (Stern and M.L., 1975), and on the interface between dissimilar isotropic materials (Hong and Stern, 1978), Stern also proposed extensions for treating body forces (Stern et al., 1976) and thermal strains (Stern, 1979). Unfortunately, the description of the extension for body forces was rather superficial, being limited to a footnote, and no example problems were presented for either of these extensions. However, for the case of thermal strains it was clearly shown that there is no need to consider thermal loading in the auxiliary state, meaning that the reciprocal work integral can also be extended include initial stresses without modifying the auxiliary solution. More recent developments include the treatment of dynamic crack propagation (Atkinson et al., 1986; Bastero et al., 1989), sharp notches (Atkinson et al., 1988; Atkinson and Bastero, 1991), and cracks in coupled poro-elastic media (Atkinson and Craster, 1992).

21.2 Volume Form of the Reciprocal Work Integral

²⁸ The first step to be taken when formulating extensions to the reciprocal work integral is the definition of the reciprocal work theorem accounting for the applied loads in the two equilibrium states. Unfortunately, it is not always obvious how the reciprocal work theorem should be defined to account for the applied loads, particularly when they are the result of initial strains or stresses.

²⁹ It will be shown here that the line integrals in the reciprocal work theorem can be converted to volume integrals using Green's theorem and that the form of the integrand for the volume integrals is such that the appropriate form of the reciprocal work theorem can be determined quite simply.

³⁰ (Sokolnikoff, 1956) defined the reciprocal work theorem relating two separate equilibrium states for a solid, both including body forces, as

$$\int_\Gamma t_i \tilde{u}_i d\Gamma + \int_\Omega b_i \tilde{u}_i d\Omega = \int_\Gamma \tilde{t}_i u_i d\Gamma + \int_\Omega \tilde{b}_i u_i d\Omega \quad (21.25)$$

where u_i , t_i , and b_i are the displacements, surface tractions, and body forces, respectively, for one equilibrium state; \tilde{u}_i , \tilde{t}_i , and \tilde{b}_i are the displacements, surface tractions, and body forces, respectively, for the other equilibrium state; Ω corresponds to the volume of the solid; and Γ corresponds to the entire surface of the solid.

³¹ The equilibrium state defined by u_i , t_i , and b_i is referred to as the primary state and the equilibrium state defined by \tilde{u}_i , \tilde{t}_i , and \tilde{b}_i is referred to as the auxiliary state. Recalling from the equilibrium equation that $b_i = -\sigma_{ij,j}$ and $\tilde{b}_i = -\tilde{\sigma}_{ij,j}$ the reciprocal work theorem can be rewritten as

$$\int_{\Gamma} t_i \tilde{u}_i \, d\Gamma - \int_{\Omega} \sigma_{ij,j} \tilde{u}_i \, d\Omega = \int_{\Gamma} \tilde{t}_i u_i \, d\Gamma - \int_{\Omega} \tilde{\sigma}_{ij,j} u_i \, d\Omega \quad (21.26)$$

where σ_{ij} and $\tilde{\sigma}_{ij}$ are the stress tensors for the two equilibrium states.

³² Adopting a counter-clockwise path around Γ the expressions relating $d\Gamma$ to dx_1 and dx_2 given in Equation ?? are still valid, allowing the line integrals to be written in a form compatible with Green's theorem

$$\begin{aligned} \int_{\Gamma} t_i \tilde{u}_i \, d\Gamma &= \int_{\Gamma} (-\sigma_{i2} \tilde{u}_i \, dx_1 + \sigma_{i1} \tilde{u}_i \, dx_2) \\ \int_{\Gamma} \tilde{t}_i u_i \, d\Gamma &= \int_{\Gamma} (-\tilde{\sigma}_{i2} u_i \, dx_1 + \tilde{\sigma}_{i1} u_i \, dx_2) \end{aligned} \quad (21.27)$$

by expanding t_i and \tilde{t}_i in terms of σ_{ij} , $\tilde{\sigma}_{ij}$, and n_i and collecting terms.

³³ Applying Green's theorem (Kreyszig, 1979) to convert the line integrals to volume integrals yields

$$\begin{aligned} \int_{\Gamma} t_i \tilde{u}_i \, d\Gamma &= \int_{\Omega} \sigma_{ij,j} \tilde{u}_i \, d\Omega + \int_{\Omega} \sigma_{ij} \tilde{u}_{i,j} \, d\Omega \\ \int_{\Gamma} \tilde{t}_i u_i \, d\Gamma &= \int_{\Omega} \tilde{\sigma}_{ij,j} u_i \, d\Omega + \int_{\Omega} \tilde{\sigma}_{ij} u_{i,j} \, d\Omega \end{aligned} \quad (21.28)$$

and the reciprocal work theorem clearly simplifies to

$$\int_{\Omega} \sigma_{ij} \tilde{u}_{i,j} \, d\Omega = \int_{\Omega} \tilde{\sigma}_{ij} u_{i,j} \, d\Omega \quad (21.29)$$

³⁴ In the absence of body forces the volume integrals are not included in the definition of the reciprocal work theorem and the expression shown above is still valid since $\sigma_{ij,j} = 0$ and $\tilde{\sigma}_{ij,j} = 0$. Knowing that the line integral form of the reciprocal work theorem can be rewritten in the volume integral form shown in Equation 21.29, the appropriate definition of the reciprocal work theorem to account for initial strains and stresses in the primary state can be obtained quite easily. This is accomplished by simply writing the volume form of the reciprocal work theorem such that there is a direct relationship between the stresses and displacements in the primary state.

21.3 Surface Traction on Crack Surfaces

³⁵ The extension to the reciprocal work integral to include the effect of surface tractions on the crack surfaces in the primary state parallels the approach proposed by (Karlsson and Bäcklund, 1978) for the J integral.

³⁶ For a primary state free of body forces with surface tractions on the crack surfaces the reciprocal work theorem is defined as

$$\int_{\Gamma} t_i \tilde{u}_i \, d\Gamma = \int_{\Gamma} \tilde{t}_i u_i \, d\Gamma \quad (21.30)$$

³⁷ This expression can be rewritten such that a separate integral is given for each portion of the contour path

$$\int_{\Gamma} t_i \tilde{u}_i \, d\Gamma + \int_{\Gamma_{\epsilon}} t_i \tilde{u}_i \, d\Gamma + \int_{\Gamma_t} \hat{t}_i \tilde{u}_i \, d\Gamma = \int_{\Gamma} \tilde{t}_i u_i \, d\Gamma + \int_{\Gamma_{\epsilon}} \tilde{t}_i u_i \, d\Gamma \quad (21.31)$$

where $\Gamma_t = \Gamma_t^+ \cup \Gamma_t^-$ and \hat{t}_i is the applied surface traction vector on the crack surfaces in the primary state.

³⁸ This expression for the reciprocal work theorem can be rewritten in the form of Somigliana's identity as

$$\int_{\Gamma} (t_i \tilde{u}_i - \tilde{t}_i u_i) \, d\Gamma + \int_{\Gamma_t} \hat{t}_i \tilde{u}_i \, d\Gamma + \int_{\Gamma_{\epsilon}} (t_i \tilde{u}_i - \tilde{t}_i u_i) \, d\Gamma = 0 \quad (21.32)$$

³⁹ Clearly, the integrand of the integral over Γ_{ϵ} is identical to that for the case of a primary state free of surface tractions on the crack surfaces, which means that Equation 21.5 still holds and the solution for the auxiliary singular state is still valid.

40 The value I_ϵ is then defined as

$$I_\epsilon = - \int_{\Gamma} (t_i \tilde{u}_i - \tilde{t}_i u_i) d\Gamma - \lim_{\epsilon \rightarrow 0} \int_{\Gamma_t} \hat{t}_i \tilde{u}_i d\Gamma \quad (21.33)$$

41 Provided that \hat{t}_i is not expressed in powers of r less than $-\frac{1}{2}$, the limit exists and the stress intensity factors are defined as

$$c_1 K_I + c_2 K_{II} = \int_{\Gamma} [\tilde{t}_i (u_i - u_i^0) - t_i \tilde{u}_i] d\Gamma - \int_{\Gamma_t} \hat{t}_i \tilde{u}_i d\Gamma \quad (21.34)$$

where u_i^0 are the displacements of the crack tip. However, when the integral over Γ_t is evaluated using numerical integration techniques, quadratures based on sampling points that coincide with the nodal locations should be avoided since \tilde{u}_i is singular at the crack tip.

21.4 Body Forces

42 For a primary state with body forces but free surface tractions on the crack surfaces and initial strains and stresses the reciprocal work theorem is defined as

$$\int_{\Gamma} t_i \tilde{u}_i d\Gamma + \int_{\Omega} b_i \tilde{u}_i d\Omega = \int_{\Gamma} \tilde{t}_i u_i d\Gamma \quad (21.35)$$

where b_i is the body force vector. It should be noted that since the line integrals are defined over Γ this form of the reciprocal work integral could also account for surface tractions on the crack surfaces.

43 The expression for the reciprocal work theorem can be rewritten such that a separate integral is given for each portion of the contour path

$$\int_{\Gamma} t_i \tilde{u}_i d\Gamma + \int_{\Gamma_\epsilon} t_i \tilde{u}_i d\Gamma + \int_{\Omega} b_i \tilde{u}_i d\Omega = \int_{\Gamma} \tilde{t}_i u_i d\Gamma + \int_{\Gamma_\epsilon} \tilde{t}_i u_i d\Gamma \quad (21.36)$$

44 This expression can be rewritten in the form of Somigliana's identity as

$$\int_{\Gamma} (t_i \tilde{u}_i - \tilde{t}_i u_i) d\Gamma + \int_{\Omega} b_i \tilde{u}_i d\Omega + \int_{\Gamma_\epsilon} (t_i \tilde{u}_i - \tilde{t}_i u_i) d\Gamma = 0 \quad (21.37)$$

45 Clearly, the integrand of the integral over Γ_ϵ is identical to that for the case of a primary state free of body forces, which means that Equation 21.5 still holds and the solution for the auxiliary singular state described is still valid.

46 The value I_ϵ is then defined as

$$I_\epsilon = - \int_{\Gamma} (t_i \tilde{u}_i - \tilde{t}_i u_i) d\Gamma - \lim_{\epsilon \rightarrow 0} \int_{\Omega} b_i \tilde{u}_i d\Omega \quad (21.38)$$

Provided that b_i is not expressed in powers of r less than $-\frac{1}{2}$, the limit exists and the stress intensity factors are defined as

$$c_1 K_I + c_2 K_{II} = \int_{\Gamma} [\tilde{t}_i (u_i - u_i^0) - t_i \tilde{u}_i] d\Gamma - \int_{\Omega} b_i \tilde{u}_i d\Omega \quad (21.39)$$

where u_i^0 are the displacements of the crack tip. However, when the integral over Ω is evaluated using numerical integration techniques, quadratures based on sampling points that coincide with the nodal locations should be avoided since \tilde{u}_i is singular at the crack tip.

21.5 Initial Strains Corresponding to Thermal Loading

47 For problems in thermo-elasticity the constitutive law defines net effective stresses $\bar{\sigma}'_{ij}$ in terms of the total strains ε_{ij} and the thermal strains ε^0_{ij} , as is shown in Equation 21.53.

48 $\bar{\sigma}'_{ij}$ can be decomposed into effective stresses σ'_{ij} and thermal stresses σ''_{ij} . σ'_{ij} are the result of ε_{ij} , which are, in turn, is defined by the displacements u_i . Therefore, the effective stresses σ'_{ij} are then directly related to the displacements u_i and should be used in the definition of the reciprocal work theorem rather than the net effective stresses $\bar{\sigma}'_{ij}$.

49 The volume form of the reciprocal work theorem for a primary state that includes thermal strains is

$$\int_{\Omega} \sigma'_{ij} \tilde{u}_{i,j} \, d\Omega = \int_{\Omega} \tilde{\sigma}_{ij} u_{i,j} \, d\Omega \quad (21.40)$$

50 The relationship between the line and volume integral forms of the reciprocal work theorem can be readily obtained by applying Green's theorem to the volume integral with σ'_{ij} in the integrand

$$\int_{\Gamma} t'_i \tilde{u}_i \, d\Gamma = \int_{\Omega} \sigma'_{ij,j} \tilde{u}_i \, d\Omega + \int_{\Omega} \sigma'_{ij} \tilde{u}_{i,j} \, d\Omega \quad (21.41)$$

where $t'_i = \sigma'_{ij} n_j$ is the effective surface traction vector.

51 Recalling from the equilibrium equation that $\sigma'_{ij,j} = \alpha C_{ijkl} \mathcal{T}_{,j} \delta_{kl}$ in the absence of body forces, it is clearly evident that a volume integral is required to complete the definition of the reciprocal work theorem.

52 Therefore, the appropriate form of the reciprocal work theorem for a primary state with thermal strains but no body forces is

$$\int_{\Gamma} t'_i \tilde{u}_i \, d\Gamma - \int_{\Omega} \alpha (C_{ijkl} \mathcal{T}_{,i} \delta_{kl}) \tilde{u}_i \, d\Omega = \int_{\Gamma} \tilde{t}_i u_i \, d\Gamma \quad (21.42)$$

where $\mathcal{T}_{,i}$ is the gradient of the temperatures.

53 A more general form of the reciprocal work theorem would be

$$\int_{\Gamma} t'_i \tilde{u}_i \, d\Gamma + \int_{\Omega} b'_i \tilde{u}_i \, d\Omega = \int_{\Gamma} \tilde{t}_i u_i \, d\Gamma \quad (21.43)$$

where b'_i is the effective body force vector, as defined in Equation 21.58, which in this particular case does not include a true body force vector b_i .

54 Recalling that the natural boundary conditions are defined in terms of the total stresses, $t'_i \neq 0$ on the crack surfaces. Therefore, the form of the reciprocal work theorem in which the line integrals on Γ have been separated is

$$\int_{\Gamma} t'_i \tilde{u}_i \, d\Gamma + \int_{\Gamma_{\epsilon}} t'_i \tilde{u}_i \, d\Gamma + \int_{\Gamma_t} \tilde{t}'_i \tilde{u}_i \, d\Gamma + \int_{\Omega} b'_i \tilde{u}_i \, d\Omega = \int_{\Gamma} \tilde{t}_i u_i \, d\Gamma + \int_{\Gamma_{\epsilon}} \tilde{t}_i u_i \, d\Gamma \quad (21.44)$$

where \tilde{t}'_i is the applied effective surface traction vector, as defined in Equation 21.60, which, much like the effective body force vector b'_i , does not include a true applied surface traction vector in this case.

55 This expression for the reciprocal work theorem can be rewritten in the form of Somigliana's identity as

$$\int_{\Gamma} (t'_i \tilde{u}_i - \tilde{t}_i u_i) \, d\Gamma + \int_{\Gamma_t} \tilde{t}'_i \tilde{u}_i \, d\Gamma + \int_{\Omega} b'_i \tilde{u}_i \, d\Omega + \int_{\Gamma_{\epsilon}} (t'_i \tilde{u}_i - \tilde{t}_i u_i) \, d\Gamma = 0 \quad (21.45)$$

56 Clearly, the integrand of the integral over Γ_{ϵ} is identical to that for the case of a primary state free of initial strains, which means that Equation 21.5 still holds and the solution for the auxiliary singular state described in Section ?? is still valid.

57 The value I_{ϵ} is then defined as

$$I_{\epsilon} = - \int_{\Gamma} (t'_i \tilde{u}_i - \tilde{t}_i u_i) \, d\Gamma - \lim_{\epsilon \rightarrow 0} \int_{\Gamma_t} \tilde{t}'_i \tilde{u}_i \, d\Gamma - \lim_{\epsilon \rightarrow 0} \int_{\Omega} b'_i \tilde{u}_i \, d\Omega \quad (21.46)$$

Provided that the temperature \mathcal{T} is not expressed in powers of r less than $\frac{1}{2}$, the limit exists and the stress intensity factors are defined as

$$c_1 K_I + c_2 K_{II} = \int_{\Gamma} [\tilde{t}'_i (u_i - u_i^0) - t'_i \tilde{u}_i] \, d\Gamma - \int_{\Gamma_t} \tilde{t}'_i \tilde{u}_i \, d\Gamma - \int_{\Omega} b'_i \tilde{u}_i \, d\Omega \quad (21.47)$$

where u_i^0 are the displacements of the crack tip.

58 However, when the integrals over Γ_t and Ω are evaluated using numerical integration techniques, quadratures based on sampling points that coincide with the nodal locations should be avoided since \tilde{u}_i is singular at the crack tip.

21.6 Initial Stresses Corresponding to Pore Pressures

⁵⁹ The stress-strain relationship for poro-elasticity, which is obtained by substituting the constitutive law defining the effective stresses σ'_{ij} into the principle of effective stress, defines the total stresses σ_{ij} in terms of the total strains ε_{ij} and the pore pressures p , as was shown in Equation 21.62.

⁶⁰ As was the case for problems in thermo-elasticity, σ_{ij} can again be decomposed, but in this instance the constituent stresses are σ'_{ij} and the initial stresses σ_{ij}^0 corresponding to the pore pressures. Since ε_{ij} is defined in terms of the displacements u_i , the effective stresses σ'_{ij} are then directly related to the displacements u_i and the reciprocal work theorem is again defined in terms of the effective stresses in the primary state.

⁶¹ Therefore, Equations 21.40 and 21.41 also apply when the primary state includes initial stresses. Recalling from the equilibrium equation that $\sigma'_{ij,j} = p_{,j}\delta_{ij}$ in the absence of body forces, it is clearly evident that a volume integral is required to complete the definition of the reciprocal work theorem.

⁶² Therefore, the appropriate form of the reciprocal work theorem for a primary state with pore pressures but no body forces is

$$\int_{\Gamma} t'_i \tilde{u}_i \, d\Gamma - \int_{\Omega} p_{,i} \tilde{u}_i \, d\Omega = \int_{\Gamma} \tilde{t}_i u_i \, d\Gamma \quad (21.48)$$

where $p_{,i}$ is the gradient of the pore pressures.

⁶³ A more general form of the reciprocal work integral is

$$\int_{\Gamma} t'_i \tilde{u}_i \, d\Gamma + \int_{\Omega} b'_i \tilde{u}_i \, d\Omega = \int_{\Gamma} \tilde{t}_i u_i \, d\Gamma \quad (21.49)$$

where b'_i is the effective body force vector, as defined in Equation 21.64, which does not include a true body force vector b_i in this case.

⁶⁴ Recognizing that the general form of the reciprocal work theorem accounting for initial stresses is identical to that accounting for initial strains (i.e. Equation 21.43), Equations 21.44 through 21.47 apply for initial stresses as well. However, the applied effective surface traction vector is defined by Equation 21.65 and the pore pressure p rather than the temperature \mathcal{T} must be expressed in a power of r greater than $\frac{1}{2}$ in order for the limits in Equation 21.46 to exist. Naturally, the restrictions on the choice of numerical integration techniques are also still in effect.

21.7 Combined Thermal Strains and Pore Pressures

⁶⁵ Recalling that in the absence of initial strains and stresses that the total stresses σ_{ij} and the effective stresses σ'_{ij} are equivalent, it is quite clear that Equation 21.43 also defines the reciprocal work theorem for solids that are free of initial strains and stresses.

⁶⁶ Due to the general definitions of the applied effective surface traction vector \hat{t}'_i and the effective body force vector b'_i , the cases of a primary state with true surface tractions \hat{t}_i on the crack surfaces and true body forces b_i are also addressed by Equation 21.43.

⁶⁷ Therefore, the stress intensity factors for a primary state which includes any combination of surface tractions on the crack surfaces, body forces, and initial strains and stresses are defined by Equation 21.47. The relationship between the stress intensity factors and the reciprocal work theorem is obtained by substituting the expressions for \hat{t}'_i and b'_i defined by Equation 21.69 into Equation 21.47

$$\begin{aligned} c_1 K_I + c_2 K_{II} &= \int_{\Gamma} [\tilde{t}_i (u_i - u_i^0) - (t_i + p n_i + \alpha \mathcal{T} C_{ijkl} n_i \delta_{kl}) \tilde{u}_i] \, d\Gamma \\ &- \int_{\Gamma_t} (\hat{t}_i + p n_i + \alpha \mathcal{T} C_{ijkl} n_i \delta_{kl}) \tilde{u}_i \, d\Gamma \\ &- \int_{\Omega} (b_i - p_{,i} - \alpha C_{ijkl} \mathcal{T}_i \delta_{kl}) \tilde{u}_i \, d\Omega \end{aligned} \quad (21.50)$$

⁶⁸ Naturally, the restrictions imposed on the power of r for \hat{t}_i , b_i , \mathcal{T} , and p are still in effect, as are the restrictions on the choice of numerical integration techniques.

21.8 Field Equations for Thermo- and Poro-Elasticity

⁶⁹ In thermo or poro-elasticity the thermal strains and pore pressures are usually treated as initial strains and initial stresses, respectively.

⁷⁰ The general stress-strain relationship obtained by substituting the constitutive law into the effective stress principle is

$$\sigma_{ij} = C_{ijkl} (\varepsilon_{kl} - \varepsilon_{kl}^0) + \sigma_{ij}^0 \quad (21.51)$$

⁷¹ Clearly, in the absence of initial stresses $\sigma_{ij} = \bar{\sigma}'_{ij}$ and in the absence of both initial strains and stresses $\sigma_{ij} = \sigma'_{ij}$.

⁷² The thermal strains for an isotropic material are defined in terms of the temperature \mathcal{T} and the coefficient of thermal expansion α as

$$\varepsilon_{ij}^0 = \alpha \mathcal{T} \delta_{ij} \quad (21.52)$$

where δ_{ij} is the Kronecker delta. Substituting this expression for the thermal strains into Equation 21.51, the resulting constitutive law for thermo-elasticity is

$$\bar{\sigma}'_{ij} = C_{ijkl} (\varepsilon_{kl} - \alpha \mathcal{T} \delta_{kl}) \quad (21.53)$$

⁷³ The thermal stresses σ''_{ij} are defined as

$$\sigma''_{ij} = \alpha \mathcal{T} C_{ijkl} \delta_{kl} \quad (21.54)$$

and the net strains \bar{E}_{ij} are defined as

$$\bar{E}_{ij} = \varepsilon_{kl} - \alpha \mathcal{T} \delta_{kl} \quad (21.55)$$

⁷⁴ Adopting the standard form of the effective stress principle the equilibrium equation and natural boundary conditions, respectively, can be rewritten in terms of the effective stresses

$$\begin{aligned} \sigma'_{ij,j} + b'_i &= 0 \\ \sigma'_{ij} n_j - \hat{t}'_i &= 0 \end{aligned} \quad (21.56)$$

where b'_i is the effective body force vector and \hat{t}'_i is the applied effective surface traction vector.

⁷⁵ The effective body force vector b'_i is defined as

$$b'_i = b_i - \sigma''_{ij,j} \quad (21.57)$$

and may be rewritten in terms of the temperature gradient vector $\mathcal{T}_{,i}$

$$b'_i = b_i - \alpha C_{ijkl} \mathcal{T}_{,i} \delta_{kl} \quad (21.58)$$

based on the definition of the thermal stresses given in Equation 21.54 and the assumption of a homogeneous material.

⁷⁶ The applied effective surface traction vector \hat{t}'_i is defined as

$$\hat{t}'_i = \hat{t}_i + \sigma''_{ij} n_j \quad (21.59)$$

and may be rewritten in terms of the temperature \mathcal{T}

$$\hat{t}'_i = \hat{t}_i + \alpha \mathcal{T} C_{ijkl} n_i \delta_{kl} \quad (21.60)$$

based on the definition of the thermal stresses given in Equation 21.54.

⁷⁷ Pore pressures are typically defined using the sign convention for soil mechanics in which compression is positive, but in the sign convention for standard solid mechanics tension is considered to be positive. Therefore, the initial stresses corresponding to a pore pressure are defined as

$$\sigma_{ij}^0 = -p \delta_{ij} \quad (21.61)$$

where p is the pore pressure defined using the compression positive sign convention; the minus sign corrects the discrepancy in the sign conventions; and δ_{ij} is the Kronecker delta. In the classical interpretation of the behavior of a porous material (Terzaghi

and Peck, 1967), the pore pressures p act only in the voids of the material and the effective stresses act only on the skeleton of the material.

⁷⁸ It must be noted that the pore pressures p being considered in this discussion and throughout the remainder of this chapter are the steady state pore pressures; excess pore pressures resulting from dilatant behavior in the skeleton of the material are not considered.

⁷⁹ The stress-strain relationship for poro-elasticity

$$\sigma_{ij} = C_{ijkl} \varepsilon_{kl} - p \delta_{ij} \quad (21.62)$$

is obtained by substituting the expression for the initial stresses into Equation 21.51.

⁸⁰ Adopting the standard form of the principle of effective stress the equilibrium equation and the natural boundary conditions, respectively, can be rewritten in terms of the effective stresses

$$\begin{aligned} \sigma'_{ij,j} + b'_i &= 0 \\ \sigma'_{ij} n_j - \hat{t}'_i &= 0 \end{aligned} \quad (21.63)$$

where b'_i is the effective body force vector and \hat{t}'_i is the applied effective surface traction vector.

⁸¹ The effective body force vector b'_i is defined as

$$b'_i = b_i - p_{,i} \quad (21.64)$$

where $p_{,i}$ is the pore pressure gradient vector. The applied effective surface traction vector \hat{t}'_i is defined as

$$\hat{t}'_i = \hat{t}_i + p n_i \quad (21.65)$$

⁸² Since $\sigma'_{ij} = 0$ on surfaces exposed to hydrostatic pressures but no other surface tractions, $\hat{t}'_i = -p n_i$ on these surfaces.

⁸³ When thermal strains and pore pressures are considered in combination the constitutive law is defined as a simple combination of Equations 21.53 and 21.62

$$\sigma_{ij} = C_{ijkl} (\varepsilon_{kl} - \alpha \mathcal{T} \delta_{kl}) - p \delta_{ij} \quad (21.66)$$

⁸⁴ The equilibrium equation and natural boundary conditions, respectively, can be rewritten in terms of either the effective stresses σ'_{ij}

$$\begin{aligned} \sigma'_{ij,j} + b'_i &= 0 \\ \sigma'_{ij} n_j - \hat{t}'_i &= 0 \end{aligned} \quad (21.67)$$

or the net effective stresses $\bar{\sigma}'_{ij}$

$$\begin{aligned} \bar{\sigma}'_{ij,j} + b'_i &= 0 \\ \bar{\sigma}'_{ij} n_j - \hat{t}'_i &= 0 \end{aligned} \quad (21.68)$$

⁸⁵ The field equations defined in terms of σ'_{ij} are obtained by adopting the standard form of the principle effective stress and the field equations defined in terms of $\bar{\sigma}'_{ij}$ are obtained by adopting the alternate form of the principle effective stress.

⁸⁶ When the equilibrium equation and natural boundary conditions are written in terms of σ'_{ij} the effective body forces b'_i and applied effective surface tractions \hat{t}'_i are defined as

$$\begin{aligned} b'_i &= b_i - p_{,i} - \alpha C_{ijkl} \mathcal{T}_{,i} \delta_{kl} \\ \hat{t}'_i &= \hat{t}_i + p n_i + \alpha \mathcal{T} C_{ijkl} n_i \delta_{kl} \end{aligned} \quad (21.69)$$

⁸⁷ However, when the equilibrium equation and natural boundary conditions are written in terms of $\bar{\sigma}'_{ij}$ the effective body forces b'_i and applied effective surface tractions \hat{t}'_i are identical to those for poro-elasticity (i.e. Equations 21.64 and 21.65, respectively).

Chapter 22

FICTITIOUS CRACK MODEL

Originally published as:

Implementation and Validation of a nonlinear fracture model in a 2D/3D finite element code by Reich, Plizzari, Cervenka and Saouma; in *Numerical Models in Fracture of Concrete*; Wittman Ed., Balkema (1993).

- ¹ An incremental formulation for the Fictitious Crack Model (FCM) will be presented. The computational algorithm treats the structure as a set of sub-domains bonded along assumed crack paths. The crack paths are defined by interface elements that initially act as constraints enforcing the bond between adjacent sub-domains, but change state to function as standard interface elements as the crack propagates. Constraints are enforced on the global system of equations using a penalty approach.
- ² A load scaling strategy, which allows for load controlled analyses in the post-peak regime, is used to enforce stress continuity at the tip of the Fracture Process Zone (FPZ).
- ³ To demonstrate the accuracy of the computational algorithm, a series of three wedge-splitting (WS) test specimens are analyzed. Specimen sizes are 31, 91, and 152 cm (1, 3, and 5 ft). Material properties for the concrete are taken as the mean values of the observed experimental results for all specimen sizes. The computed results are compared to the envelopes of the experimental response for each specimen size.

22.1 Introduction

- ⁴ The most commonly implemented nonlinear fracture model for concrete using the discrete crack approach is the FCM (Hillerborg et al., 1976a). In the FCM the zone of micro-cracking and debonding ahead of the crack front is modeled as a cohesive stress that acts to close the crack. The magnitude of the cohesive stresses on the crack surface are determined by a softening law that relates the stress to the relative displacement of the crack surfaces through the fracture energy.
- ⁵ Many implementations of the FCM have been reported (Ingraffea and Gerstle, 1984; Roelfstra and Sadouki, 1986; Dahlblom and Ottosen, 1990; Bocca et al., 1990; Gopalaratnam and Ye, 1991; Gerstle and Xie, 1992), but none of the implementations based on a discrete crack approach claim to be based on the standard incremental formulation normally associated with nonlinear analyses. Only the implementation by Dahlblom and Ottosen (Dahlblom and Ottosen, 1990), which is based on a smeared crack approach, uses an incremental formulation.
- ⁶ In this chapter, an incremental solution algorithm for the FCM based in the discrete crack approach will be presented and its performance evaluated by comparing the computed response of WS test specimens against known experimental results.

22.2 Computational Algorithm

- ⁷ Treatment of the structure as a set of bonded sub-domains results in a system of mixed equations with the unknowns being displacements and surface tractions on the interface between the sub-domains. The weak form of the system of mixed equations will be derived from the Principle of Virtual Work. The weak form equations will then be discretized for solution using the finite element method. The penalty method solution for the mixed system of equations will be discussed; particularly the automatic selection of the penalty number. Finally, an incremental-iterative solution strategy based on the modified-Newton algorithm that includes load scaling and allows for load control in the post-peak regime will be discussed.

22.2.1 Weak Form of Governing Equations

- ⁸ Figure 22.1 shows a body consisting of two sub-domains, Ω_1 and Ω_2 that intersect on a surface Γ_I without penetration. Each sub-domain may be subject to body forces \mathbf{b}_m or to prescribed surface tractions $\hat{\mathbf{t}}_m$ on Γ_{t_m} . Defining the volume of the body as

$$\Omega = \Omega_1 \cup \Omega_2 \quad (22.1)$$

and the surface of the body subject to prescribed surface tractions as

$$\Gamma_t = \Gamma_{t_1} \cup \Gamma_{t_2}, \quad (22.2)$$

the Principle of Virtual Work for the body is

$$\int_{\Omega} \delta \boldsymbol{\epsilon}^T \boldsymbol{\sigma} d\Omega - \int_{\Omega} \delta \mathbf{u}^T \mathbf{b} d\Omega - \int_{\Gamma_t} \delta \mathbf{u}^T \hat{\mathbf{t}} d\Gamma = 0 \quad (22.3)$$

where

$$\delta \boldsymbol{\epsilon} = \mathbf{L} \delta \mathbf{u} \quad (22.4-a)$$

$$\boldsymbol{\epsilon} = \mathbf{L} \mathbf{u} \quad (22.4-b)$$

$$\boldsymbol{\sigma} = \mathbf{D} \boldsymbol{\epsilon} \quad (22.4-c)$$

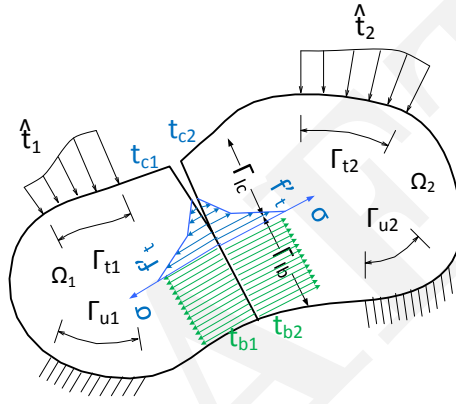


Figure 22.1: Body Consisting of Two Sub-domains

9 Within each sub-domain of the body Ω_m the Principle of Virtual Work must also hold, but additional integrals are required to account for the work performed by the surface tractions \mathbf{t}_{I_m} on the interface Γ_I . Surface tractions on the interface are due to bonding of the sub-domains \mathbf{t}_{b_m} or to cohesive stresses in the FPZ \mathbf{t}_{c_m} . In either case, stress continuity on Γ_I requires that

$$\mathbf{t}_{b_2} = -\mathbf{t}_{b_1} \quad (22.5-a)$$

$$\mathbf{t}_{c_2} = -\mathbf{t}_{c_1} \quad (22.5-b)$$

10 Defining the interface surface as

$$\Gamma_I = \Gamma_{I_b} \cup \Gamma_{I_c}, \quad (22.6)$$

where Γ_{I_b} is the bonded interface surface and Γ_{I_c} is the interface surface subject to cohesive stresses, the external work on the interface is written as

$$\int_{\Gamma_I} \delta \mathbf{u}_1^T \mathbf{t}_{I_1} d\Gamma = \int_{\Gamma_{I_b}} \delta \mathbf{u}_1^T \mathbf{t}_b d\Gamma + \int_{\Gamma_{I_c}} \delta \mathbf{u}_1^T \mathbf{t}_c d\Gamma \quad (22.7-a)$$

$$\int_{\Gamma_I} \delta \mathbf{u}_2^T \mathbf{t}_{I_2} d\Gamma = -\int_{\Gamma_{I_b}} \delta \mathbf{u}_2^T \mathbf{t}_b d\Gamma - \int_{\Gamma_{I_c}} \delta \mathbf{u}_2^T \mathbf{t}_c d\Gamma \quad (22.7-b)$$

Both \mathbf{t}_b and \mathbf{t}_c are unknown, but as \mathbf{t}_b acts on the bonded, or constrained, interface it will be treated as a Lagrange multiplier

$$\boldsymbol{\lambda} = \mathbf{t}_b \quad (22.8)$$

¹¹ Substituting λ into Equations 22.3 and 22.4-a-22.4-c and including the external work performed by the surface tractions on the interface surface, the Principle of Virtual Work for sub-domains Ω_1 and Ω_2 is written as

$$\begin{cases} \int_{\Omega_1} \delta \epsilon_1^T \sigma_1 d\Omega - \int_{\Omega_1} \delta \mathbf{u}_1^T \mathbf{b}_1 d\Omega - \int_{\Gamma_{t_1}} \delta \mathbf{u}_1^T \hat{\mathbf{t}}_1 d\Gamma - \int_{\Gamma_{I_b}} \delta \mathbf{u}_1^T \lambda d\Gamma - \int_{\Gamma_{I_c}} \delta \mathbf{u}_1^T \mathbf{t}_c d\Gamma = 0 \\ \int_{\Omega_2} \delta \epsilon_2^T \sigma_2 d\Omega - \int_{\Omega_2} \delta \mathbf{u}_2^T \mathbf{b}_2 d\Omega - \int_{\Gamma_{t_2}} \delta \mathbf{u}_2^T \hat{\mathbf{t}}_2 d\Gamma + \int_{\Gamma_{I_b}} \delta \mathbf{u}_2^T \lambda d\Gamma + \int_{\Gamma_{I_c}} \delta \mathbf{u}_2^T \mathbf{t}_c d\Gamma = 0 \end{cases} \quad (22.9)$$

¹² On Γ_{I_b} the displacements for the two sub-domains, $\mathbf{u}_1|_{\Gamma_{I_b}}$ and $\mathbf{u}_2|_{\Gamma_{I_b}}$, must be equal. This condition can be written as a constraint in the strong form

$$\mathbf{u}_2|_{\Gamma_{I_b}} - \mathbf{u}_1|_{\Gamma_{I_b}} = \mathbf{0}, \quad (22.10)$$

but a weak form is required to be compatible with Equation 22.5-a-22.5-b. The following weak form

$$\int_{\Gamma_i} \delta \lambda^T (\mathbf{u}_2 - \mathbf{u}_1) d\Gamma = 0 \quad (22.11)$$

was chosen for the constraint equation as it makes the system of mixed equations symmetric.

22.2.2 Discretization of Governing Equations

¹³ Discretization of Equations 22.9-22.9 and 22.11 will be presented as if each sub-domain were an element (?); the extension to multi-element sub-domains is straightforward and will be omitted from this discussion. Each sub-domain Ω_m is discretized for displacements \mathbf{u}_m such that nodes on Γ_{t_m} and Γ_I are included in the vector of discrete displacements $\bar{\mathbf{u}}_m$. The number of nodes on Γ_I in Ω_1 is equal to the number of nodes on Γ_I in Ω_2 . For each node on Γ_I in Ω_1 there is a node on Γ_I in Ω_2 with the same coordinates. The nodes at which the surface tractions due to bonding λ on Γ_{I_b} are discretized are at the same locations as those for the displacements.

¹⁴ Displacements \mathbf{u}_m within the sub-domains Ω_m and the surface tractions λ on the bonded interface Γ_{I_b} are defined in terms of their discretized counterparts using shape functions

$$\mathbf{u}_m = \mathbf{N}_{u_m} \bar{\mathbf{u}}_m \quad (22.12-a)$$

$$\lambda = \mathbf{N}_\lambda \bar{\lambda} \quad (22.12-b)$$

$$\delta \mathbf{u}_m = \mathbf{N}_{u_m} \delta \bar{\mathbf{u}}_m \quad (22.12-c)$$

$$\delta \lambda = \mathbf{N}_\lambda \delta \bar{\lambda} \quad (22.12-d)$$

\mathbf{N}_{u_m} and \mathbf{N}_λ are standard shape functions in that for each node there is a corresponding shape function whose value is one at that node and zero at all other nodes.

¹⁵ To discretize the integral defining the virtual strain energy, the stresses and the virtual strains defined in Equation 22.4-a-22.4-c must be expressed in terms of the discrete displacements and virtual displacements using Equations 22.12-a-22.12-b and 22.12-c-22.12-d

$$\delta \epsilon_m = \mathbf{L} \mathbf{N}_{u_m} \delta \bar{\mathbf{u}}_m \quad (22.13-a)$$

$$\sigma_m = \mathbf{D}_m \mathbf{L} \mathbf{N}_{u_m} \bar{\mathbf{u}}_m \quad (22.13-b)$$

¹⁶ Defining the discrete strain-displacement operator \mathbf{B}_m as

$$\mathbf{B}_m = \mathbf{L} \mathbf{N}_{u_m}, \quad (22.14)$$

the virtual strain energy can be written as

$$\int_{\Omega_m} \delta \epsilon_m^T \sigma_m d\Omega = \delta \bar{\mathbf{u}}_m^T \int_{\Omega_m} \mathbf{B}_m^T \mathbf{D}_m \mathbf{B}_m d\Omega \bar{\mathbf{u}}_m \quad (22.15)$$

¹⁷ Recognizing that

$$\mathbf{K}_m = \int_{\Omega_m} \mathbf{B}_m^T \mathbf{D}_m \mathbf{B}_m d\Omega \quad (22.16)$$

is the standard stiffness matrix for the finite element method, Equation 22.15 can be rewritten as

$$\int_{\Omega_m} \delta \boldsymbol{\epsilon}_m^T \boldsymbol{\sigma}_m d\Omega = \delta \bar{\mathbf{u}}_m^T \mathbf{K}_m \bar{\mathbf{u}}_m \quad (22.17)$$

¹⁸ Discretization of the integrals for the internal virtual work due to body forces and the external virtual work due to prescribed surface tractions simply involves expressing the virtual displacements in terms of the discrete virtual displacements using Equation 22.12-c-22.12-d

$$\int_{\Omega_m} \delta \mathbf{u}_m^T \mathbf{b}_m d\Omega = \delta \bar{\mathbf{u}}_m^T \int_{\Omega_m} \mathbf{N}_{u_m}^T \mathbf{b}_m d\Omega \quad (22.18-a)$$

$$\int_{\Gamma_{t_m}} \delta \mathbf{u}_m^T \hat{\mathbf{t}}_m d\Gamma = \delta \bar{\mathbf{u}}_m^T \int_{\Gamma_{t_m}} \mathbf{N}_{u_m}^T \hat{\mathbf{t}}_m d\Gamma \quad (22.18-b)$$

¹⁹ Recognizing that

$$\mathbf{f}_m = \int_{\Omega_m} \mathbf{N}_{u_m}^T \mathbf{b}_m d\Omega + \int_{\Gamma_{t_m}} \mathbf{N}_{u_m}^T \hat{\mathbf{t}}_m d\Gamma \quad (22.19)$$

is the standard applied load vector for the finite element method, the sum of the internal virtual work and the external virtual work is

$$\int_{\Omega_m} \delta \mathbf{u}_m^T \mathbf{b}_m d\Omega + \int_{\Gamma_{t_m}} \delta \mathbf{u}_m^T \hat{\mathbf{t}}_m d\Gamma = \delta \bar{\mathbf{u}}_m^T \mathbf{f}_m \quad (22.20)$$

²⁰ To discretize the external virtual work due to surface tractions on the interface, the surface tractions and the virtual displacements must be expressed in terms of the discrete surface tractions and virtual displacements using Equations 22.12-a-22.12-b and 22.12-c-22.12-d

$$\int_{\Gamma_{I_b}} \delta \mathbf{u}_m^T \boldsymbol{\lambda} d\Gamma = \delta \bar{\mathbf{u}}_m^T \int_{\Gamma_{I_b}} \mathbf{N}_{u_m}^T \mathbf{N}_\lambda d\Gamma \bar{\boldsymbol{\lambda}} \quad (22.21-a)$$

$$\int_{\Gamma_{t_c}} \delta \mathbf{u}_m^T \mathbf{t}_c d\Gamma = \delta \bar{\mathbf{u}}_m^T \int_{\Gamma_{t_c}} \mathbf{N}_{u_m}^T \mathbf{t}_c d\Gamma \quad (22.21-b)$$

²¹ Defining the operator matrix for the load vector due to surface tractions on the bonded interface as

$$\mathbf{Q}_m = \int_{\Gamma_{I_b}} \mathbf{N}_{u_m}^T \mathbf{N}_\lambda d\Gamma \quad (22.22)$$

and the load vector for the cohesive stresses as

$$\mathbf{f}_{c_m} = \int_{\Gamma_{t_c}} \mathbf{N}_{u_m}^T \mathbf{t}_c d\Gamma \quad (22.23)$$

the external work due to surface tractions on the interface is

$$\int_{\Gamma_{I_b}} \delta \mathbf{u}_m^T \boldsymbol{\lambda} d\Gamma + \int_{\Gamma_{t_c}} \delta \mathbf{u}_m^T \mathbf{t}_c d\Gamma = \delta \bar{\mathbf{u}}_m^T (\mathbf{Q}_m \bar{\boldsymbol{\lambda}} + \mathbf{f}_{c_m}) \quad (22.24)$$

²² To discretize the weak constraint equation, the displacements and the virtual surface tractions must be expressed in terms of the discrete displacements and the discrete virtual surface tractions using Equations 22.12-a-22.12-b and 22.12-c-22.12-d

$$\int_{\Gamma_{I_b}} \delta \boldsymbol{\lambda}^T \mathbf{u}_1 d\Gamma = \delta \bar{\boldsymbol{\lambda}}^T \int_{\Gamma_{I_b}} \mathbf{N}_\lambda^T \mathbf{N}_{u_1} d\Gamma \bar{\mathbf{u}}_1 \quad (22.25-a)$$

$$\int_{\Gamma_{I_b}} \delta \boldsymbol{\lambda}^T \mathbf{u}_2 d\Gamma = \delta \bar{\boldsymbol{\lambda}}^T \int_{\Gamma_{I_b}} \mathbf{N}_\lambda^T \mathbf{N}_{u_2} d\Gamma \bar{\mathbf{u}}_2 \quad (22.25-b)$$

²³ Recognizing that

$$\mathbf{Q}_m^T = \int_{\Gamma_{I_b}} \mathbf{N}_\lambda^T \mathbf{N}_{u_m} d\Gamma \quad (22.26)$$

is the transpose of the operator matrix for the load vector due to surface tractions on the bonded interface defined in Equation 22.23, the weak constraint equation can be rewritten as

$$\int_{\Gamma_{I_b}} \delta \lambda^T (\mathbf{u}_2 - \mathbf{u}_1) d\Gamma = \delta \bar{\lambda}^T (\mathbf{Q}_2^T \bar{\mathbf{u}}_2 - \mathbf{Q}_1^T \bar{\mathbf{u}}_1) = 0 \quad (22.27)$$

24 Having defined the discretized form of all integrals in the governing equations, it is now possible to define the discrete system of mixed equations. Substituting Equations 22.17, 22.20, and 22.24 into Equation 22.9-22.9 and rearranging terms, the discrete Principle of Virtual Work is written as

$$\delta \bar{\mathbf{u}}_1^T (\mathbf{K}_1 \bar{\mathbf{u}}_1 - \mathbf{Q}_1 \bar{\lambda}) = \delta \bar{\mathbf{u}}_1^T (\mathbf{f}_1 + \mathbf{f}_{c_1}) \quad (22.28-a)$$

$$\delta \bar{\mathbf{u}}_2^T (\mathbf{K}_2 \bar{\mathbf{u}}_2 + \mathbf{Q}_2 \bar{\lambda}) = \delta \bar{\mathbf{u}}_2^T (\mathbf{f}_2 - \mathbf{f}_{c_2}) \quad (22.28-b)$$

25 As $\delta \bar{\mathbf{u}}_m^T$ appears in both sides of Equation 22.28-a-22.28-b, it can be eliminated, leaving

$$\mathbf{K}_1 \bar{\mathbf{u}}_1 - \mathbf{Q}_1 \bar{\lambda} = \mathbf{f}_1 + \mathbf{f}_{c_1} \quad (22.29-a)$$

$$\mathbf{K}_2 \bar{\mathbf{u}}_2 + \mathbf{Q}_2 \bar{\lambda} = \mathbf{f}_2 - \mathbf{f}_{c_2} \quad (22.29-b)$$

26 In a similar fashion, $\delta \bar{\lambda}^T$ can be eliminated from Equation 22.27, leaving

$$\mathbf{Q}_2^T \bar{\mathbf{u}}_2 - \mathbf{Q}_1^T \bar{\mathbf{u}}_1 = \mathbf{0} \quad (22.30)$$

as the discrete constraint equation. The discrete system of mixed equations is defined by Equations 22.29-a-22.29-b and 22.30, which can be written in matrix form as

$$\begin{bmatrix} \mathbf{K}_1 & \mathbf{0} & -\mathbf{Q}_1 \\ \mathbf{0} & \mathbf{K}_2 & \mathbf{Q}_2 \\ -\mathbf{Q}_1^T & \mathbf{Q}_2^T & \mathbf{0} \end{bmatrix} \begin{Bmatrix} \bar{\mathbf{u}}_1 \\ \bar{\mathbf{u}}_2 \\ \bar{\lambda} \end{Bmatrix} = \begin{Bmatrix} \mathbf{f}_1 + \mathbf{f}_{c_1} \\ \mathbf{f}_2 - \mathbf{f}_{c_2} \\ \mathbf{0} \end{Bmatrix} \quad (22.31)$$

22.2.3 Penalty Method Solution

27 The penalty method (?) was chosen for the solution of the discrete system of mixed equations because it reduces the problem to that of a single-field. Reducing the system of mixed equations to a single-field equation decreases the number of unknowns that must be solved for and simplifies the use of direct solution methods.

28 Direct solution methods can be used with the system of mixed equations, but interlacing of the equations is required to avoid singularities (Wiberg, 1974). Another troublesome aspect related to the use of direct solution methods with the system of mixed equations is that since crack propagation is simulated by the release of constraints on the interface, the total number of unknowns would change as the crack propagates. Interlacing a system of mixed equations with an ever changing number of unknowns would certainly create major bookkeeping problems in a finite element code.

29 To obtain the penalty form of the system of mixed equations, Equation 22.31 is rewritten as

$$\begin{bmatrix} \mathbf{K}_1 & \mathbf{0} & -\mathbf{Q}_1 \\ \mathbf{0} & \mathbf{K}_2 & \mathbf{Q}_2 \\ -\mathbf{Q}_1^T & \mathbf{Q}_2^T & -\frac{1}{\alpha} \mathbf{I} \end{bmatrix} \begin{Bmatrix} \bar{\mathbf{u}}_1 \\ \bar{\mathbf{u}}_2 \\ \bar{\lambda} \end{Bmatrix} = \begin{Bmatrix} \mathbf{f}_1 + \mathbf{f}_{c_1} \\ \mathbf{f}_2 - \mathbf{f}_{c_2} \\ \mathbf{0} \end{Bmatrix} \quad (22.32)$$

where α is the penalty number. α should be sufficiently large that $\frac{1}{\alpha} \mathbf{I}$ is close to zero. It is now possible to express $\bar{\lambda}$ in terms of $\bar{\mathbf{u}}_1$ and $\bar{\mathbf{u}}_2$

$$\bar{\lambda} = \alpha (\mathbf{Q}_2 \bar{\mathbf{u}}_2 - \mathbf{Q}_1 \bar{\mathbf{u}}_1) \quad (22.33)$$

30 Substituting Equation 22.33 into Equation 22.32, a single-field penalized stiffness matrix equation is obtained

$$\begin{bmatrix} (\mathbf{K}_1 + \alpha \mathbf{Q}_1 \mathbf{Q}_1^T) & -\alpha \mathbf{Q}_1 \mathbf{Q}_2^T \\ -\alpha \mathbf{Q}_2 \mathbf{Q}_1^T & (\mathbf{K}_2 + \alpha \mathbf{Q}_2 \mathbf{Q}_2^T) \end{bmatrix} \begin{Bmatrix} \bar{\mathbf{u}}_1 \\ \bar{\mathbf{u}}_2 \end{Bmatrix} = \begin{Bmatrix} \mathbf{f}_1 + \mathbf{f}_{c_1} \\ \mathbf{f}_2 - \mathbf{f}_{c_2} \end{Bmatrix} \quad (22.34)$$

³¹ The selection of a good penalty number is a rather difficult task. If the penalty number is too small the computed displacements will yield a substantial error when inserted into the constraint equation

$$\mathbf{Q}_2 \bar{\mathbf{u}}_2 - \mathbf{Q}_1 \bar{\mathbf{u}}_1 = \epsilon \gg 0 \quad (22.35)$$

³² As the penalty number is increased the error ϵ approaches zero, but the character of the system of equations changes as the effect of \mathbf{K}_1 and \mathbf{K}_2 is diminished. When the effect of \mathbf{K}_1 and \mathbf{K}_2 is significantly diminished the computed displacements away from the interface, which are not included in the constraint equation, will lose accuracy due to round off errors. The goal is to select a penalty number that yields an acceptable error when the computed displacements are inserted in the constraint equation without sacrificing the accuracy of the displacements away from the interface. The author's experience is that a penalty number selected using

$$\alpha = \frac{\max(\text{diag}(\mathbf{K}_m))}{\max(\text{diag}(\mathbf{Q}_m \mathbf{Q}_m^T))} \times 10^6 \quad (22.36)$$

yields very good results for the class of problems being considered.

³³ Penalty numbers selected in this fashion result in computed values of $\bar{\mathbf{u}}_1$ and $\bar{\mathbf{u}}_2$ on the interface that tend to be identical for the first five or six digits when the penalized stiffness matrix is assembled in double precision.

22.2.4 Incremental-Iterative Solution Strategy

³⁴ An incremental-iterative solution strategy is used to obtain the equilibrium configuration for each crack length. At zero load, the entire interface is constrained (i.e., fully bonded). As load is applied, surface tractions on the constrained interface violate a strength criteria and the corresponding constraints are released. On that portion of the interface where constraints have been released, cohesive stresses act until the relative displacements of the unconstrained interface surfaces become large enough to dictate otherwise.

³⁵ In this solution strategy crack propagation occurs after every increment.

³⁶ The use of a strength criteria to detect the onset of crack propagation requires that the magnitude of the applied loads be such that the surface tractions at a node on the constrained interface are precisely equal to the maximum allowable stress. In this case, equality is required between the normal surface traction and the uniaxial tensile strength. However, as the magnitude of the applied loads that causes the strength criteria to be satisfied exactly is not known *a priori*, some form of automatic load scaling must be included in the solution strategy.

³⁷ Assuming that the applied loads are proportional, a load factor β can be used to scale an arbitrary set of applied load vector \mathbf{f} of some arbitrary magnitude. At the beginning of each load increment i , the load factor is β_i and the applied load vector is

$$\beta_i \mathbf{f} = \beta_i \begin{Bmatrix} \mathbf{f}_1 \\ \mathbf{f}_2 \end{Bmatrix} \quad (22.37)$$

The value of β_i is zero at the beginning of the first increment. The incremental load factor for increment i is $\Delta\beta_i$ and the applied incremental load vector is

$$\Delta\beta_i \mathbf{f} = \Delta\beta_i \begin{Bmatrix} \mathbf{f}_1 \\ \mathbf{f}_2 \end{Bmatrix} \quad (22.38)$$

The load factor at the end of increment i is

$$\beta_{i+1} = \beta_i + \Delta\beta_i \quad (22.39)$$

³⁸ The modified-Newton algorithm (Zienkiewicz et al., 2005) is used to solve for incremental displacements due to the applied incremental loads. The incremental displacements for a generic increment are defined as

$$\Delta\bar{\mathbf{u}}^{n+1} = \Delta\bar{\mathbf{u}}^n + \delta\bar{\mathbf{u}}^n \quad (22.40)$$

where

$$\bar{\mathbf{u}} = \begin{Bmatrix} \bar{\mathbf{u}}_1 \\ \bar{\mathbf{u}}_2 \end{Bmatrix} \quad (22.41)$$

and $\Delta\bar{\mathbf{u}}^n$ is the incremental displacement vector at the beginning of iteration n and $\delta\bar{\mathbf{u}}^n$ is the correction to the incremental displacement vector for iteration n .

³⁹ In a similar fashion, the incremental load factor is defined as

$$\Delta\beta^{n+1} = \Delta\beta^n + \delta\beta^n \quad (22.42)$$

where $\Delta\beta^n$ is the incremental load factor at the beginning of iteration n and $\delta\beta^n$ is the correction to the incremental load factor for iteration n . At the beginning of the first iteration both $\Delta\bar{\mathbf{u}}^n$ and $\Delta\beta^n$ are zero.

⁴⁰ Displacement corrections are computed by solving

$$\mathbf{K}_\alpha d\bar{\mathbf{u}}^n = (\beta\mathbf{f} + \Delta\beta^n\mathbf{f} + d\beta^n\mathbf{f} + \mathbf{f}_c^n - \mathbf{p}^n) \quad (22.43)$$

where

$$\mathbf{K}_\alpha = \begin{bmatrix} (\mathbf{K}_1 + \alpha\mathbf{Q}_1\mathbf{Q}_1^T) & -\alpha\mathbf{Q}_1\mathbf{Q}_2^T \\ -\alpha\mathbf{Q}_2\mathbf{Q}_1^T & (\mathbf{K}_2 + \alpha\mathbf{Q}_2\mathbf{Q}_2^T) \end{bmatrix} \quad (22.44)$$

is the penalized stiffness matrix;

$$\mathbf{f}_c^n = \begin{Bmatrix} \mathbf{f}_{c_1}^n \\ -\mathbf{f}_{c_2}^n \end{Bmatrix} \quad (22.45)$$

is the load vector due to cohesive stresses on the interface at the beginning of iteration n ; and

$$\mathbf{p}^n = \sum_{i=1}^{nelem} \int_{\Omega_{e_i}} \mathbf{B}^T \mathbf{D} (\boldsymbol{\epsilon} + \Delta\boldsymbol{\epsilon}^n) d\Omega \quad (22.46)$$

is the reaction vector for the state of stress at iteration n .

⁴¹ Recognizing that

$$\mathbf{r}^n = \beta\mathbf{f} + \Delta\beta^n\mathbf{f} + \mathbf{f}_c^n - \mathbf{p}^n \quad (22.47)$$

is the residual force vector at the beginning of iteration n , Equation 22.43 can be written in a more compact fashion as

$$d\bar{\mathbf{u}}^n = \mathbf{K}_\alpha^{-1} (\delta\beta^n\mathbf{f} + \mathbf{r}^n) \quad (22.48)$$

⁴² Since the $\mathbf{K}_\alpha^{-1}\mathbf{f}$ term does not change throughout the course of the iterative process it can be defined as a constant value for the increment

$$\delta\bar{\mathbf{u}}_T = \mathbf{K}_\alpha^{-1}\mathbf{f} \quad (22.49)$$

⁴³ The displacement vector $\delta\bar{\mathbf{u}}_T$ is commonly called the tangent displacement vector (Crisfield, M.A., 1981). At this point, the iterative displacement correction can be defined as

$$\delta\bar{\mathbf{u}}^n = \delta\beta^n \delta\bar{\mathbf{u}}_T + \mathbf{K}_\alpha^{-1}\mathbf{r}^n \quad (22.50)$$

⁴⁴ Having shown how the load factor is implemented within the incremental-iterative solution strategy, the last detail left to explain is the procedure for computing $\delta\beta^n$ such that the strength criteria is exactly satisfied. Since the surface tractions on the constrained interface are used to determine the magnitude of the applied load, the total surface tractions for iteration n must be expressed in terms of its various contributions

$$\bar{\boldsymbol{\lambda}}^{n+1} = \bar{\boldsymbol{\lambda}} + \Delta\bar{\boldsymbol{\lambda}}^n + \delta\bar{\boldsymbol{\lambda}}_r^n + \delta\beta^n \delta\bar{\boldsymbol{\lambda}}_T \quad (22.51)$$

where $\bar{\boldsymbol{\lambda}}$ is the surface traction vector at the beginning of the increment; $\Delta\bar{\boldsymbol{\lambda}}^n$ is the incremental surface traction vector at the beginning of iteration n ; $\delta\bar{\boldsymbol{\lambda}}_r^n$ is correction to the incremental surface traction vector due to the residual load vector \mathbf{r}^n for iteration n ; and $\delta\bar{\boldsymbol{\lambda}}_T$ is the surface traction vector due to the tangent displacement vector $\delta\bar{\mathbf{u}}_T$. $\delta\bar{\boldsymbol{\lambda}}_r^n$ and $\delta\bar{\boldsymbol{\lambda}}_T$ are defined as

$$\delta\bar{\boldsymbol{\lambda}}_r^n = \alpha(\mathbf{Q}_2^T \delta\bar{\mathbf{u}}_{r_2}^n - \mathbf{Q}_1^T \delta\bar{\mathbf{u}}_{r_1}^n) \quad (22.52-a)$$

$$\delta\bar{\boldsymbol{\lambda}}_T = \alpha(\mathbf{Q}_2^T \delta\bar{\mathbf{u}}_T - \mathbf{Q}_1^T \delta\bar{\mathbf{u}}_T) \quad (22.52-b)$$

45 The strength criteria is applied to $\bar{\lambda}^{n+1}$ on a node-by-node basis such that

$$\boxed{\max((\bar{\lambda}^{n+1})_i(\mathbf{n})_i) = f_t} \quad (22.53)$$

where $(\mathbf{n})_i$ is the normal vector at node i and f_t is the uniaxial tensile strength.

46 Recognizing that $\bar{\lambda}$, $\Delta\bar{\lambda}^n$, and $\delta\bar{\lambda}_r^n$ are fixed for iteration n , the iterative load factor correction is defined as

$$\boxed{\delta\beta^n = \min \left\{ \frac{f_t - [(\bar{\lambda})_i + (\Delta\bar{\lambda}^n)_i + (\delta\bar{\lambda}_r^n)_i](\mathbf{n})_i}{(\delta\bar{\lambda}_T)_i(\mathbf{n})_i} \right\}} \quad (22.54)$$

Provided that the cohesive stresses on the interface are treated as forces and no stiffness matrix is assembled for those interface elements, this solution strategy allows for load control in the post peak regime.

47 The use of stiffness matrices for the interface elements subject to softening is avoided because their presence in the global stiffness matrix will eventually cause it to become non-positive definite.

22.3 Validation

48 In order to assess the algorithm just presented, analysis of previously tested wedge-splitting test specimens was undertaken, Fig. 22.2. In those tests, described in (Saouma et al., 1991a), wedge-splitting specimens of 31, 91, and 152 cm (1, 3, and 5 ft) with

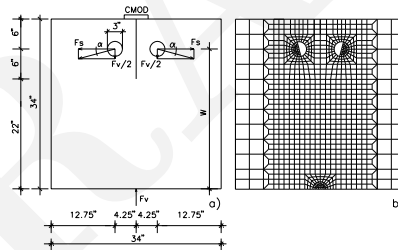


Figure 22.2: Wedge Splitting Test, and FE Discretization

maximum aggregate sizes ranging from 19, 38, and 76 mm (0.75, 1.5, and 3 in) were tested under crack mouth opening displacement control.

22.3.1 Load-CMOD

49 The selected material properties were the average values reported in (Saouma et al., 1991a) for the three specimen sizes with the 38 mm maximum aggregate size concrete. In order to facilitate the use of *Merlin* (Saouma et al., 2010) by practicing engineers, input

parameters were intentionally kept to a minimum, and included: 1) Young's modulus E , 2) Poisson's ratio ν , 3) tensile strength f'_t ; and 3) fracture energy G_F . The tensile strength f'_t was taken as $0.9f'_c$, and a bilinear curve for the softening behavior was systematically used with the inflection point defined by $s_1 = \frac{f'_t}{4}$, $w_1 = 0.75 \frac{G_F}{f'_t}$, and $w_2 = 5 \frac{G_F}{f'_t}$ as recommended in (Whitman et al., 1988).

50 For each analysis, numerical predictions are shown in comparison with the range of experimental results, Figure 22.3.

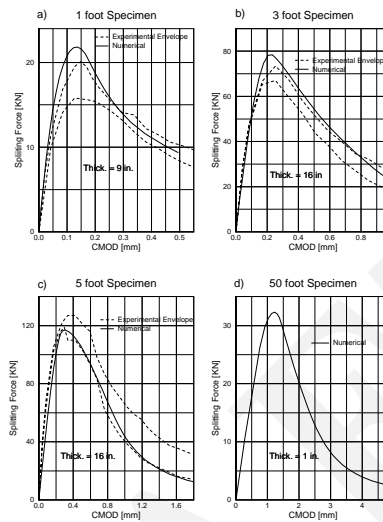


Figure 22.3: Numerical Predictions vs Experimental Results for Wedge Splitting Tests

51 From these figures, it can be readily observed that very good engineering comparison is achieved between numerical predictions and experimental results.

52 Also shown are the results of an analysis of a hypothetical 50 ft specimen, which is a scaled up version of the 5 ft specimen. Material properties are the same as used for the preceding analyses.

22.3.2 Real, Fictitious, and Effective Crack Lengths

53 For each of the preceding analysis, the lengths of the real, fictitious and effective cracks were determined. Whereas the first two are directly obtained from the nonlinear finite element analysis, the third one was obtained by a separate procedure. Following the nonlinear analysis, a series of linear elastic analyses with increasing crack lengths were performed using a unit load. For each crack length, the normalized stress intensity factor and the compliance ($\frac{CMOD}{P}$) were recorded. Finally, using the two analyses, the effective crack length was determined as the crack length in the linear elastic analysis which would yield the same compliance as the one obtained from the nonlinear analysis.

54 Observing those three diagrams, Figure 22.4 we observe that as the specimen size increases the relative size of the fracture process zone (difference between the total crack and the true crack length) decreases as anticipated. From the 5 ft and 50 ft specimens, it may be inferred that the size of the process zone tends to remain constant. Finally, we note that the effective length approximation appears to be a valid engineering assumption for the larger specimen sizes.

22.3.3 Parametric Studies

55 Finally, some basic parametric studies were undertaken to assess the effect of certain parameters.

Effect of G_F : First the effect of G_F on the response of the 50 ft specimen was investigated. This size was selected as it best approximates what may be perceived as “large” structures such as dams. From Figure 22.5 we observe that despite the

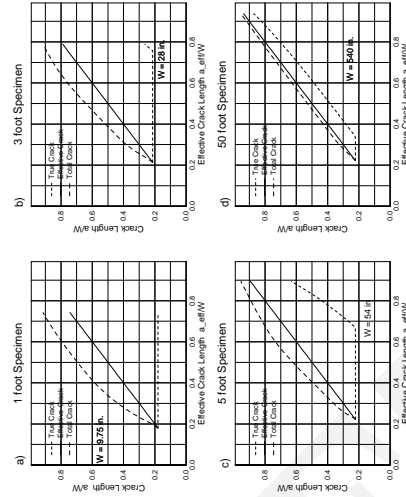


Figure 22.4: Real, Fictitious, and Effective Crack Lengths for Wedge Splitting Tests

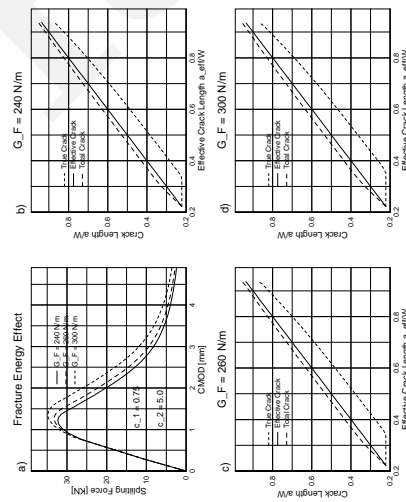


Figure 22.5: Effect of G_F on 50 ft Specimen

range of G_F , the load-cmod curves, as well as crack lengths are practically identical. Hence, this confirms what has long been known that is the relative importance of f'_t is much greater than that of G_F .

Softening Law: Whereas G_F for dam concrete was found not to exceed 300 N/m, it was speculated that the large aggregate sizes may result in larger w_c or critical crack opening displacement beyond which no tensile stresses can be transmitted across the crack. Hence a series of analyses in which w_c was varied from 0.54 to 1.6 mm, while w_1 and G_F were kept constant, were undertaken. The results of these analyses are shown in Figure 22.6. Interestingly we note that the peak load decreased

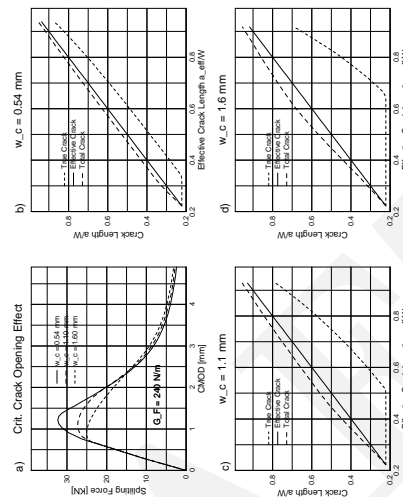


Figure 22.6: Effect of w_c on 50 ft Specimen

with the increase in w_c . These results may be attributed to the substantial drop of s_1 (from $\frac{f'_t}{4}$) required to maintain a constant G_F or area under the softening curve. Furthermore, as w_c increases, there is a slight increase in both total crack and true crack. However, we note that for large w_c values, the effective crack length becomes smaller than even the true crack. We currently have no explanation for these results.

Effect of s_1 : Whereas in the original analysis s_1 was taken as $\frac{f'_t}{4}$, the effect of its variation was investigated through Figure 22.7, which indicates that this parameter has practically no effect on the peak load, and a very limited one on the post-peak response. Similarly, it was found that it also has limited effect on the crack length.

22.4 Conclusions

⁵⁶ In summary, a new framework for linear/nonlinear fracture mechanics analysis of concrete was presented. Robustness of the algorithm was, to some extent, validated by the numerical duplication of experimental results with standard material properties and no parametric optimization.

⁵⁷ This model is currently being extended to include the effect of a pressurized true crack and FPZ and to perform mixed mode analysis and 3D analyses. Future analyses will focus on its application for the nonlinear analysis of cracked concrete dams.

22.5 Notation

- m = Sub-domain index; either 1 or 2
- Ω_m = Sub-domain m
- Ω = Domain of body
- \mathbf{b} = Body force vector
- \mathbf{b}_m = Body force vector for sub-domain m

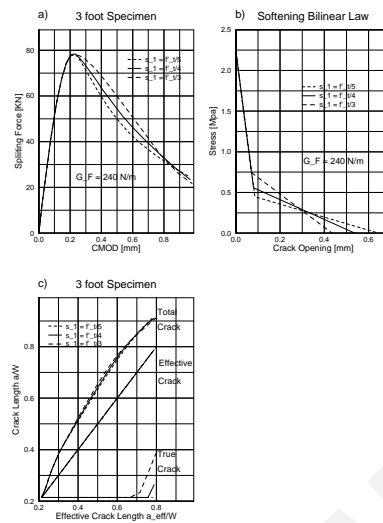


Figure 22.7: Effect of s_1 on 3 ft Specimen

- Γ_{t_m} = Surface of sub-domain m subject to prescribed surface tractions
- Γ_t = Surface of body subject to prescribed surface tractions
- $\hat{\mathbf{t}}$ = Prescribed surface traction vector
- $\hat{\mathbf{t}}_m$ = Prescribed surface traction vector for sub-domain m
- \mathbf{u} = Displacement vector
- \mathbf{u}_m = Displacement vector for sub-domain m
- $\delta\mathbf{u}$ = Virtual displacement vector
- $\delta\mathbf{u}_m$ = Virtual displacement vector for sub-domain m
- \mathbf{L} = Differential operator to obtain strain vector from displacement vector
- $\boldsymbol{\epsilon}$ = Strain vector
- $\boldsymbol{\epsilon}_m$ = Strain vector for sub-domain m
- $\delta\boldsymbol{\epsilon}$ = Virtual strain vector
- $\delta\boldsymbol{\epsilon}_m$ = Virtual strain vector for sub-domain m
- \mathbf{D} = Elastic stress strain matrix
- $\boldsymbol{\sigma}$ = Stress vector
- $\boldsymbol{\sigma}_m$ = Stress vector for sub-domain m
- Γ_I = Interface surface
- Γ_{I_b} = Bonded interface surface
- Γ_{I_c} = Interface surface subject to cohesive stresses
- \mathbf{t}_{I_m} = Surface tractions on interface surface
- \mathbf{t}_{b_m} = Surface tractions due to bonding on interface surface of sub-domain m
- \mathbf{t}_{c_m} = Surface tractions due to cohesive stresses on interface surface of sub-domain m
- \mathbf{t}_b = Surface tractions due to bonding on interface surface
- \mathbf{t}_c = Surface tractions due to cohesive stresses on interface surface
- $\boldsymbol{\lambda}$ = Lagrange multiplier vector
- \mathbf{N}_{u_m} = Shape functions for displacements in sub-domain m
- $\bar{\mathbf{u}}_m$ = Nodal displacement vector for sub-domain m
- \mathbf{N}_λ = Shape functions for Lagrange multipliers on bonded interface
- $\bar{\boldsymbol{\lambda}}$ = Nodal Lagrange multiplier vector; total nodal Lagrange multiplier vector at beginning of increment
- \mathbf{B}_m = Strain-displacement matrix for sub-domain m
- \mathbf{K}_m = Stiffness matrix for sub-domain m

- \mathbf{f}_m = Applied load vector for sub-domain m
 \mathbf{Q}_m = Operator matrix for load vector due to Lagrange multipliers on bonded interface surface of sub-domain m
 \mathbf{f}_{c_m} = Load vector due to cohesive stresses on interface surface of sub-domain m
 \mathbf{I} = Identity matrix
 α = Penalty number
 \mathbf{f} = Arbitrary applied load vector
 i = Increment number, element number, or node number
 β_i = Total load factor at beginning of increment i
 $\Delta\beta_i$ = Incremental load factor for increment i
 n = Iteration number
 $\Delta\bar{\mathbf{u}}^n$ = Incremental nodal displacement vector at beginning of iteration n
 $\delta\bar{\mathbf{u}}^n$ = Correction to incremental nodal displacement vector for iteration n
 $\Delta\bar{\mathbf{u}}^{n+\frac{1}{2}}$ = Incremental nodal displacement vector at end of iteration n
 $\Delta\beta^n$ = Incremental load factor at beginning of iteration n
 $\delta\beta^n$ = Correction to incremental load factor for iteration n
 $\Delta\beta^{n+\frac{1}{2}}$ = Incremental load factor at end of iteration n
 $\bar{\mathbf{u}}$ = Nodal displacement vector at beginning of increment
 \mathbf{K}_α = Penalized stiffness matrix
 β = Load factor at beginning of iteration n
 \mathbf{f}_c^n = Load vector due to cohesive stresses on interface at beginning of iteration n
 \mathbf{p}^n = Reaction vector at beginning of iteration n
 \mathbf{r}^n = Residual load vector at beginning of iteration n
 $\delta\bar{\mathbf{u}}_T$ = Nodal tangent displacement vector for increment
 $\delta\bar{\mathbf{u}}_r^n$ = Correction to incremental nodal displacement vector due to residual loads for iteration n
 $\Delta\bar{\lambda}^n$ = Incremental nodal Lagrange multiplier vector at beginning of iteration n
 $\delta\bar{\lambda}_r^n$ = Correction to incremental nodal Lagrange multiplier vector due to residual loads for iteration n
 $\delta\bar{\lambda}_T$ = Nodal Lagrange multiplier vector due to tangent displacement for increment
 $\Delta\bar{\lambda}^{n+\frac{1}{2}}$ = Incremental nodal Lagrange multiplier vector at end of iteration n
 \mathbf{n} = Normal vector
 f_t = Uniaxial tensile strength

Chapter 23

INTERFACE CRACK MODEL

This chapter was chapter 6 of the PhD thesis of Cervenka

¹ This chapter discusses the nonlinear modeling of concrete using a discrete crack fracture mechanics based model. It addresses two important issues: mixed mode fracture in homogeneous materials and interface fracture. A new three-dimensional interface crack model is derived. The model is a generalization of classical Hillerborg's fictitious crack model, which can be recovered if shear displacements are set to zero. Several examples are used to validate the applicability of the proposed interface crack model. First, direct shear tests on mortar joints are used to test the model performance in the shear-compression regime. The more complicated combination of shear-tension is investigated using large biaxial tests of concrete-rock interfaces. The applicability to mixed mode cracking in homogeneous concrete is tested using experiments on modified Iosipescu's shear beam and anchor bolt pull-out tests.

23.1 Introduction

² The assumption of singular stresses at the crack tip is mathematically correct only within the framework of linear elastic fracture mechanics, but physically unrealistic.

³ In concrete materials, a fracture process zone (Section ??) exists ahead of the crack tip. The most popular model simulating this behavior is Hillerborg's fictitious crack model (FCM) described in Section ?? and Figure ?. In a previous work, the classical FCM model was implemented by (Reich, 1993) for mode I crack propagation, and extended to account for the influence of water pressure inside the crack.

⁴ The classical FCM model, Chapter 22, defines a relationship between normal crack opening and normal cohesive stresses, and assumes that there are no sliding displacements nor shear stresses along the process zone. This assumption is only partially valid for concrete materials. Based on experimental observations, it is indeed correct that a crack is usually initiated in pure mode I (i.e. opening mode) in concrete, even for mixed mode loading. However, during crack propagation, the crack may curve due to stress redistribution or non-proportional loading, and significant sliding displacements develop along the crack as schematically shown in Figure 23.1. Therefore, it is desirable to incorporate these shear effects into the proposed crack model.

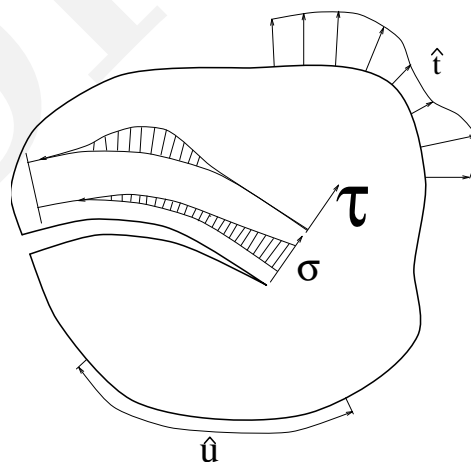


Figure 23.1: Mixed mode crack propagation.

⁵ Finally for concrete dams, it is well accepted that the weakest part of the structure is the dam-foundation interface, which is also the location of highest tensile stresses and lowest tensile strength. Given the scope of this work, as described in Chapter ??, it is necessary to address this problem.

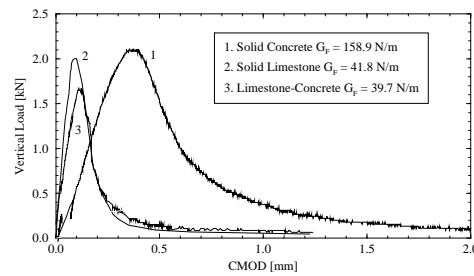


Figure 23.2: Wedge splitting tests for different materials, (Saouma et al., 1994)

6 Hence, the two major objectives of this chapter are:

- (1) Modification of the FCM model to account for shear effects along both the fracture process zone and the true crack.
- (2) Development of an interface model based on fracture mechanics to simulate cracking along rock-concrete interfaces.

7 The FCM model, within the framework of a discrete crack implementation, can be visualized as an interface between two identical materials. Therefore, we can develop a general model which addresses both objectives.

8 Interface elements were first proposed by (Goodman et al., 1968) to model non-linear behavior of rock joints. Since then, numerous interface constitutive models have been proposed for a wide range of applications such as rock-joints (Goodman et al., 1968) masonry structures (Lotfi, 1992) and concrete fracture (Stankowski, 1990) (Feenstra et al., 1991) and (Carol et al., 1992).

9 In the following section an interface crack model will first be proposed, and then it will be used to simulate cracking both in homogeneous concrete and along a rock-concrete interface. The presented model is a modification of the one first proposed by (Carol et al., 1992).

23.2 Interface Crack Model

10 The objective is to develop a physically sound model, yet simple enough so that all its parameters can be easily derived from laboratory tests. The model should be capable of simulating the behavior of rock-concrete and concrete-concrete interfaces.

11 Experimental data (Saouma et al., 1994) on rock-concrete interfaces show (Figure 23.2) that the decrease in tensile strength is not abrupt, but is rather gradual. This is caused by the presence of the fracture process zone, along which the energy of the system is gradually dissipated.

12 In the present model, the rock-concrete contact is idealized as an interface between two dissimilar materials with zero thickness. Thus, the objective is to define relationships between normal and tangential stresses with opening and sliding displacements. The notation used in the interface model is illustrated in Figure 23.2.

13 The major premises upon which the model is developed are:

- (1) Shear strength depends on the normal stress.
- (2) Softening is present both in shear and tension.
- (3) There is a residual shear strength due to the friction along the interface, which depends on the compressive normal stress.
- (4) Reduction in strength, i.e. softening, is caused by crack formation.
- (5) There is a zero normal and shear stiffness when the interface is totally destroyed.
- (6) Under compressive normal stresses neither the shear and nor the normal stiffnesses decrease to zero. In addition, should a compressive stress be introduced in the normal direction following a full crack opening, two faces of the interface come to contact, and both tangential and normal stiffnesses become nonzero.
- (7) Irreversible relative displacements are caused by broken segments of the interface material and by friction between the two crack surfaces.
- (8) Roughness of the interface causes opening displacements (i.e. dilatancy) when subjected to sliding displacements.
- (9) The dilatancy vanishes with increasing sliding or opening displacements.

14 Figure 23.4 illustrates the probable character of the fracturing process along an interface.

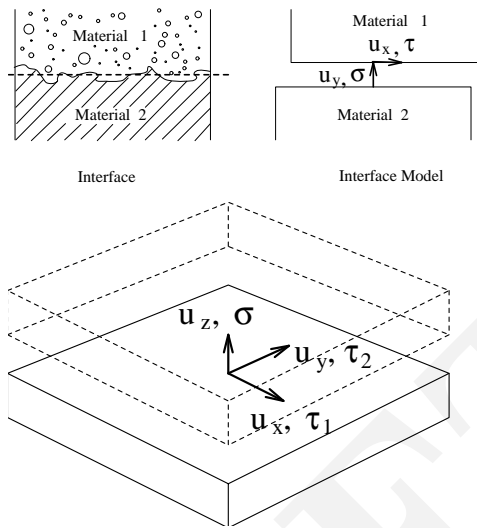


Figure 23.3: Interface idealization and notations.

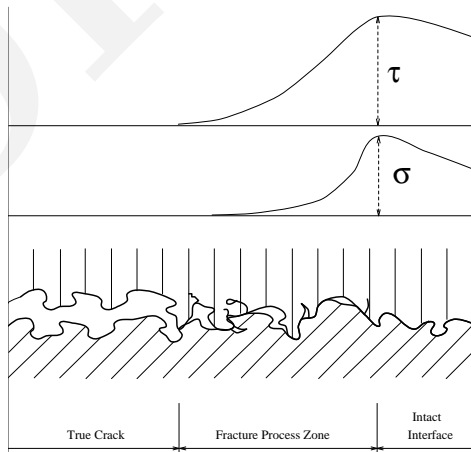


Figure 23.4: Interface fracture.

15 In the proposed model the strength of an interface is described by a hyperbolic failure function:

$$F = (\tau_1^2 + \tau_2^2) - 2c \tan(\phi_f)(\sigma_t - \sigma) - \tan^2(\phi_f)(\sigma^2 - \sigma_t^2) = 0 \quad (23.1)$$

where:

- c is the cohesion.
- ϕ_f is the angle of friction.
- σ_t is the tensile strength of the interface.
- τ_1 and τ_2 are the two tangential components of the interface traction vector.
- σ is the normal traction component.

16 The shape of the failure function in two-dimensional case is shown in Figure 23.5, and it corresponds to the failure criteria first proposed by (Carol et al., 1992). The general three-dimensional failure function is obtained by mere rotation around the σ -axis.

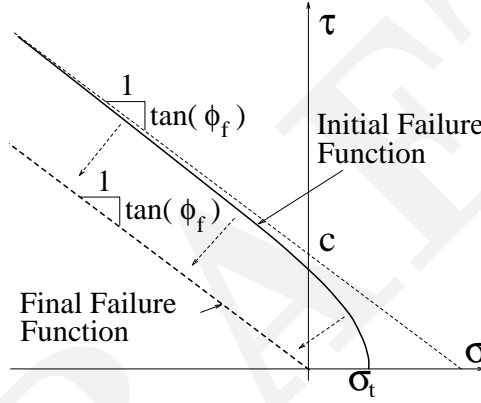


Figure 23.5: Failure function.

17 The evolution of the failure function is based on a softening parameter u^{ieff} which is the norm of the inelastic displacement vector \mathbf{u}^i . The inelastic displacement vector is obtained by decomposition of the displacement vector \mathbf{u} into an elastic part \mathbf{u}^e and an inelastic part \mathbf{u}^i . The inelastic part can subsequently be decomposed into plastic (i.e. irreversible) displacements \mathbf{u}^p and fracturing displacements \mathbf{u}^f . The plastic displacements are assumed to be caused by friction between crack surfaces and the fracturing displacements by the formation of microcracks.

$$\begin{aligned} F &= F(c, \sigma_t, \phi_f), & c &= c(u^{\text{ieff}}), & \sigma_t &= \sigma_t(u^{\text{ieff}}) \\ \mathbf{u} &= \mathbf{u}^e + \mathbf{u}^i, & \mathbf{u}^i &= \mathbf{u}^p + \mathbf{u}^f \\ u^{\text{ieff}} &= \|\mathbf{u}^i\| = (u_x^i{}^2 + u_y^i{}^2 + u_z^i{}^2)^{1/2} \end{aligned} \quad (23.2)$$

18 In this work both linear and bilinear relationship are used for $c(u^{\text{ieff}})$ and $\sigma_t(u^{\text{ieff}})$.

$$\left. \begin{aligned} c(u^{\text{ieff}}) &= c_0 \left(1 - \frac{u^{\text{ieff}}}{w_c}\right) & \forall u^{\text{ieff}} < w_c \\ c(u^{\text{ieff}}) &= 0 & \forall u^{\text{ieff}} \geq w_c \\ w_c &= \frac{2G_F^{IIa}}{c_0} \end{aligned} \right\} \text{linear for cohesion}$$

$$\left. \begin{aligned} c(u^{\text{ieff}}) &= c_0 + u^{\text{ieff}} \frac{s_{1c} - c_0}{w_{1c}} & \forall u^{\text{ieff}} < w_{1c} \\ c(u^{\text{ieff}}) &= s_c \left(1 - \frac{u^{\text{ieff}} - w_{1c}}{w_c - w_{1c}}\right) & \forall u^{\text{ieff}} \in (w_{1c}, w_c) \\ c(u^{\text{ieff}}) &= 0 & \forall u^{\text{ieff}} > w_c \\ w_c &= \frac{2G_F^{IIa} - (s_{1c} + c_0)w_{1c}}{s_{1c}} \end{aligned} \right\} \text{bi-linear for cohesion} \quad (23.3)$$

$$\left. \begin{aligned}
\sigma_t(u^{\text{ieff}}) &= \sigma_{t0} \left(1 - \frac{u^{\text{ieff}}}{w_\sigma}\right) & \forall u^{\text{ieff}} < w_\sigma \\
\sigma_t(u^{\text{ieff}}) &= 0 & \forall u^{\text{ieff}} \geq w_\sigma \\
w_\sigma &= \frac{2G_F^I}{\sigma_{t0}}
\end{aligned} \right\} \text{linear for tensile strength}$$

$$\left. \begin{aligned}
\sigma_t(u^{\text{ieff}}) &= \sigma_{t0} + u^{\text{ieff}} \frac{s_{1\sigma} - \sigma_{t0}}{w_{1\sigma}} & \forall u^{\text{ieff}} < w_{1\sigma} \\
\sigma_t(u^{\text{ieff}}) &= s_{1\sigma} \left(1 - \frac{u^{\text{ieff}} - w_{1\sigma}}{w_{\sigma t} - w_{1\sigma}}\right) & \forall u^{\text{ieff}} \in (w_{1\sigma}, w_\sigma) \\
\sigma_t(u^{\text{ieff}}) &= 0 & \forall u^{\text{ieff}} > w_\sigma \\
w_\sigma &= \frac{2G_F^I - (s_{1\sigma} + \sigma_{t0})w_{1\sigma}}{s_{1\sigma}}
\end{aligned} \right\} \text{bi-linear for tensile strength} \quad (23.4)$$

where G_F^I and G_F^{IIa} are mode I and II fracture energies. s_{1c} , w_{1c} and $s_{1\sigma}$, $w_{1\sigma}$ are the coordinates of the breakpoint in the bi-linear softening laws for cohesion and tensile strength respectively.

¹⁹ The critical opening and sliding corresponding to zero cohesion and tensile strength are denoted by w_σ and w_c respectively, and they are determined from the condition that the area under the linear or bilinear softening law must be equal to G_F^I and G_F^{IIa} respectively. The significance of these symbols can be best explained through Figure 23.6.

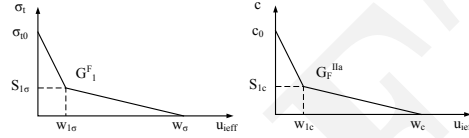


Figure 23.6: Bi-linear softening laws.

²⁰ It should be noted that G_F^{IIa} is not the pure mode II fracture energy (i.e. the area under a τ - u_x curve), but rather is the energy dissipated during a shear test with high confining normal stress. This parameter was first introduced by (Carol et al., 1992) in their microplane model. This representation seems to be more favorable to the pure mode II fracture energy G_F^{II} . The determination of G_F^{II} would require a pure shear test without confinement, which is extremely difficult to perform. Alternatively, a G_F^{IIa} test requires a large normal confinement, and is therefore easier to accomplish. Furthermore, if G_F^{II} is used, the whole shear-compression region of the interface model would be an extrapolation from the observed behavior, whereas the second approach represents an interpolation between the upper bound G_F^{IIa} and the lower bound G_F^I .

²¹ The residual shear strength is obtained from the failure function by setting both c and σ_t equal to 0, which corresponds to the final shape of the failure function in Figure 23.5 and is given by:

$$\tau_1^2 + \tau_2^2 = \tan^2(\phi_f) \sigma^2 \quad (23.5)$$

²² Stiffness degradation is modeled through a damage parameter, $D \in \langle 0, 1 \rangle$, which is a relative measure of the fractured surface. Thus, D is related to the secant of the normal stiffness K_{ns} in the uniaxial case:

$$D = \frac{A_f}{A_o} = 1 - \frac{K_{ns}}{K_{no}} \quad (23.6)$$

where K_{no} is the initial normal stiffness of the interface; A_o and A_f are the total interface area and the fractured area respectively.

²³ It is assumed, that the damage parameter D can be determined by converting the mixed mode problem into an equivalent uniaxial one (Figure 23.7). In the equivalent uniaxial problem the normal inelastic displacement is set equal to u^{ieff} . Then, the secant normal stiffness can be determined from:

$$K_{ns} = \frac{\sigma}{u - u^p} = \frac{\sigma_t(u^{\text{ieff}})}{u^e + u^p + u^f - u^p} = \frac{\sigma_t(u^{\text{ieff}})}{\sigma_t(u^{\text{ieff}})/K_{no} + (1 - \gamma)u^{\text{ieff}}} \quad (23.7)$$

where γ is the ratio of irreversible inelastic normal displacement to the total value of inelastic displacement.

²⁴ Experimentally, γ can be determined from a pure mode I test through:

$$\gamma = \frac{u_p}{u_i} \quad (23.8)$$

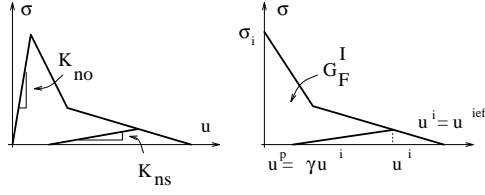


Figure 23.7: Stiffness degradation in the equivalent uniaxial case.

where u^p is the residual displacement after unloading and u^i is the inelastic displacement before unloading. (Figure 23.7).

²⁵ For concrete, γ is usually assumed equal to 0.2 (Dahlblom and Ottosen, 1990) or 0.3 (Alvaredo and Whitman, 1992). Then, the evolution of the damage parameter D is defined by formula:

$$D = 1 - \frac{\sigma_t(u^{ieff})}{\sigma_t(u^{ieff}) + (1 - \gamma)u^{ieff}K_{no}} \quad (23.9)$$

which is obtained by substituting Equation 23.7 into Eq. 23.6.

²⁶ The stress-displacement relationship of the interface is expressed as:

$$\boldsymbol{\sigma} = \alpha \mathbf{E}(\mathbf{u} - \mathbf{u}^p) \quad (23.10)$$

where: (a) $\boldsymbol{\sigma}$ is the vector of tangential and normal stress at the interface.

$$\boldsymbol{\sigma} = \{\tau_1, \tau_2, \sigma\}^T \quad (23.11)$$

(b) α is the integrity parameter defining the relative active area of the interface, and it is related to the damage parameter D .

$$\alpha = 1 - \frac{|\sigma| + \sigma}{2|\sigma|} D \quad (23.12)$$

It should be noted that α can be different from 1 only if the normal stress σ is positive (i.e. the interface is in tension). In other words, the damage parameter D is activated only if the interface is in tension. In compression, the crack is assumed to be closed, and there is full contact between the two crack surface. The activation of D is controlled through the fraction $\frac{|\sigma| + \sigma}{2|\sigma|}$, which is equal to one if σ is positive, and is zero otherwise.

(c) \mathbf{E} is the elastic stiffness matrix of the interface.

$$\mathbf{E} = \begin{bmatrix} K_{to} & 0 & 0 \\ 0 & K_{to} & 0 \\ 0 & 0 & K_{no} \end{bmatrix} \quad (23.13)$$

²⁷ It should be noted, that the off-diagonal terms in the elastic stiffness matrix \mathbf{E} of the interface are all equal to zero, which implies that no dilatancy is considered in the elastic range. The dilatancy is introduced later after the failure limit has been reached through the iterative solution process. The dilatancy of the interface is given by dilatancy angle ϕ_d , which is again assumed to be a function of u^{ieff} . In the proposed model, a linear relationship is assumed:

$$\begin{aligned} \phi_d(u^{ieff}) &= \phi_{d0} \left(1 - \frac{u^{ieff}}{u_{dil}}\right) & \forall u^{ieff} \leq u_{dil} \\ \phi_d(u^{ieff}) &= 0 & \forall u^{ieff} > u_{dil} \end{aligned} \quad (23.14)$$

where u_{dil} is the critical relative displacement after which, the interface does not exhibit the dilatancy effect any more, and ϕ_{d0} is the initial value of the dilatancy angle.

23.2.1 Relation to fictitious crack model.

²⁸ It is possible to prove that the proposed interface crack model (ICM) reduces to Hillerborg's fictitious crack model in the case of zero sliding displacements.

FCM a special case of ICM. We assume that all shear displacements are zero. Then, the interface stresses develop only along the σ -axis in the $\sigma \times \tau_1 \times \tau_2$ space (Figure 23.5). After the tensile strength σ_t is reached, softening starts, and the stress in the interface is given by:

$$\sigma = \sigma(u_z^i) \quad (23.15)$$

Normal traction σ is now a function of the normal inelastic displacement u_z^i only, since for zero sliding displacements, u^{eff} is equivalent to u_z^i . The total opening u_z of the interface is given by:

$$u_z = \frac{\sigma(u_z^i)}{K_{no}} + u_z^i$$

If the limiting case of K_{no} equal to infinity is considered, then u_z^i becomes equivalent to u_z , and the normal stress in Equation 23.15 becomes a function of the interface opening only:

$$\lim_{K_{no} \rightarrow \infty} \sigma = \sigma(u_z^i) = \sigma(u_z) = \sigma(COD) \quad (23.16)$$

which is precisely the definition of Hillerborg's fictitious crack model.

23.3 Finite Element Implementation

²⁹ The finite element implementation of the interface crack model previously presented will be discussed in this section. The implementation of a nonlinear model into a finite element code consists of three major subtasks:

1. Interface element formulation.
2. Constitutive driver for the computation of internal forces.
3. Non-linear solution algorithm on the structural level.

23.3.1 Interface element formulation.

³⁰ Standard interface elements are used in this work. The element stiffness matrix is computed using the well known relation:

$$\mathbf{K}^e = \int_{A_e} \mathbf{B}^T \mathbf{E} \mathbf{B} dA \quad (23.17)$$

where \mathbf{E} is the interface material stiffness matrix, given by Equation 23.13, and \mathbf{B} is the matrix relating element nodal displacements \mathbf{u}_e to slidings and openings along the interface:

$$\mathbf{u} = \sum_i^{1/2N_{en}} N_i(\bar{\mathbf{u}}_i^+ - \bar{\mathbf{u}}_i^-) = \mathbf{B} \mathbf{u}_e \quad (23.18)$$

where $\bar{\mathbf{u}}_i^+$ and $\bar{\mathbf{u}}_i^-$ denote the element nodal displacements in the local coordinate system of the interface on the upper and lower interface surface respectively. Given this definition, matrix \mathbf{B} is equal to:

$$\mathbf{B} = [-\mathbf{B}_1 \mathbf{T}, \quad \dots, \quad -\mathbf{B}_{p+1} \mathbf{T}, \quad +\mathbf{B}_1 \mathbf{T}, \quad \dots, \quad +\mathbf{B}_{p+1} \mathbf{T}] \quad (23.19)$$

where submatrix \mathbf{B}_i is a diagonal matrix of shape functions $N_i(\zeta, \eta)$ corresponding to node i . In three-dimensional case it has the form:

$$\mathbf{B}_i = \begin{bmatrix} N_i(\zeta, \eta) & 0 & 0 \\ 0 & N_i(\zeta, \eta) & 0 \\ 0 & 0 & N_i(\zeta, \eta) \end{bmatrix} \quad (23.20)$$

and in two-dimensional case it is given by:

$$\mathbf{B}_i = \begin{bmatrix} N_i(\zeta) & 0 \\ 0 & N_i(\zeta) \end{bmatrix} \quad (23.21)$$

Subscript i is a node numbering index on one element surface ranging from 1 to $\frac{N_{en}}{2}$, where N_{en} is the total number of element nodes, p is the order of the interface element, and is equal to $(\frac{N_{en}}{2} - 1)$. Finally, ζ and η are the natural coordinates of the interface element.

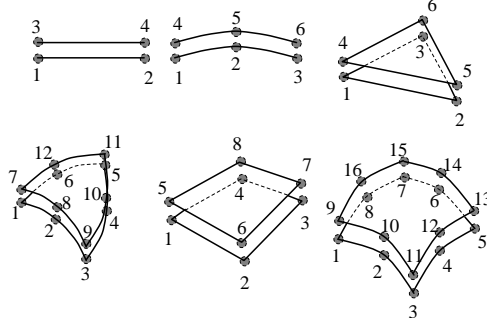


Figure 23.8: Interface element numbering.

³¹ This definition of matrix \mathbf{B} corresponds to the element numbering shown in Figure 23.8 for several two- and three-dimensional interface elements.

³² The transformation from global to local coordinate system of the interface element is accomplished through the transformation matrix \mathbf{T} , which in general three-dimensional case is:

$$\mathbf{T} = \begin{bmatrix} \mathbf{v}_1^T \\ \mathbf{v}_2^T \\ \mathbf{v}_3^T \end{bmatrix} \quad (23.22)$$

The rows of the transformation matrix \mathbf{T} are formed by vectors \mathbf{v}_i defined by following formulas:

$$\mathbf{v}_1 = \frac{\frac{\partial \mathbf{x}}{\partial \zeta}}{\left\| \frac{\partial \mathbf{x}}{\partial \zeta} \right\|}, \quad \mathbf{v}_3 = \frac{\frac{\partial \mathbf{x}}{\partial \zeta} \times \frac{\partial \mathbf{x}}{\partial \eta}}{\left\| \frac{\partial \mathbf{x}}{\partial \zeta} \times \frac{\partial \mathbf{x}}{\partial \eta} \right\|}, \quad \mathbf{v}_2 = \mathbf{v}_3 \times \mathbf{v}_1, \quad (23.23)$$

³³ The two-dimensional case can be recovered from the two preceding formulas by deleting the last row in matrix \mathbf{T} and considering the following definition of vectors \mathbf{v}_i .

$$\mathbf{v}_1 = \frac{\frac{\partial \mathbf{x}}{\partial \zeta}}{\left\| \frac{\partial \mathbf{x}}{\partial \zeta} \right\|}, \quad \mathbf{v}_2 = \{-v_{1y}, v_{1x}\} \quad (23.24)$$

Local coordinate systems defined by these transformations are shown in Figure 23.9.

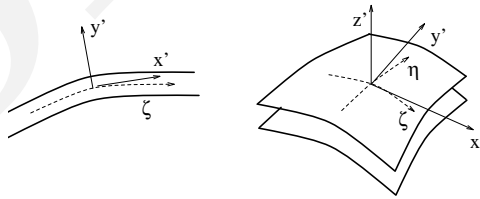


Figure 23.9: Local coordinate system of the interface element.

23.3.2 Constitutive driver.

³⁴ The mathematical theory of plasticity is used in the development of the constitutive driver for the interface crack model. On the constitutive level in the sense of finite element implementation, the problem can be stated as follows:

³⁵ For a given stress state $\boldsymbol{\sigma}_n$, softening parameter u_n^{ieff} and displacement increment $\Delta \mathbf{u}_n$, determine a new stress state $\boldsymbol{\sigma}_{n+1}$ and corresponding value of softening parameter u_{n+1}^{ieff} . In both states n and $n+1$, the failure criterion must be satisfied:

$$F_n(\boldsymbol{\sigma}_n, u_n^{\text{ieff}}) = 0 \quad \wedge \quad F_{n+1}(\boldsymbol{\sigma}_{n+1}, u_{n+1}^{\text{ieff}}) = 0 \quad (23.25)$$

These two conditions are equivalent to an incremental form of the consistency condition (Equation ??):

$$\Delta F = F_{n+1} - F_n = 0 \quad (23.26)$$

³⁶ Because the failure function is assumed to be satisfied for state n , it is necessary to also ensure the satisfaction of the failure function at state $n + 1$.

³⁷ In this work, plasticity theory is used to describe the evolution of the failure function based on the softening parameter u^{ieff} , which is the euclidean norm of the inelastic displacement vector. The inelastic displacements are subsequently decomposed according to Equation 23.8. Thus, plastic and fracturing effects can be separated.

³⁸ The elastic predictor is given by:

$$\boldsymbol{\sigma}_e = \boldsymbol{\sigma}_n + \mathbf{E}\Delta\mathbf{u}_n \quad (23.27)$$

where $\boldsymbol{\sigma}_e$ are the trial tractions outside the failure surface if a totally elastic behavior is considered. The inelastic corrector returns the trial stress state back to the failure surface:

$$\boldsymbol{\sigma}_{n+1} = \boldsymbol{\sigma}_e - \Delta\lambda \mathbf{E} \mathbf{m} \quad (23.28)$$

where $\Delta\lambda$ is the inelastic multiplier and \mathbf{m} is the direction of the inelastic displacements. Inelastic multiplier $\Delta\lambda$ is determined from the failure condition at state $n + 1$.

$$F_{n+1}(\boldsymbol{\sigma}_e - \Delta\lambda \mathbf{E} \mathbf{m}, u_{n+1}^{\text{ieff}}) = 0 \quad (23.29)$$

³⁹ In the three dimensional space $\sigma \times \tau_1 \times \tau_2$, the geometrical interpretation of this condition is the determination of an intersection of a line emanating from point $\boldsymbol{\sigma}_e$ in the direction $\mathbf{E} \mathbf{m}$ with the moving failure surface (Figure 23.10).

⁴⁰ The failure surface, $F = 0$, expands or shrinks depending on the softening introduced through u^{ieff} . This is schematically shown in Figure 23.10 for a two-dimensional case.

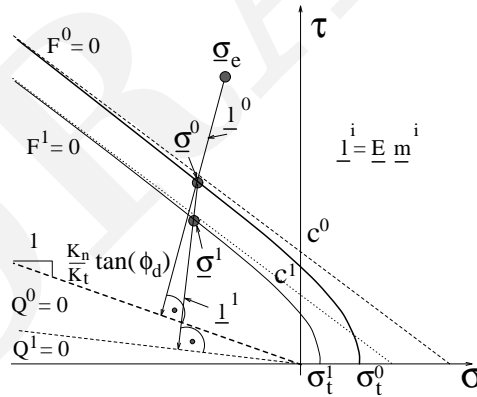


Figure 23.10: Algorithm for interface constitutive model.

⁴¹ The increment of the plastic multiplier $\Delta\lambda$ is computed by solving a quadratic equation obtained by considering the particular form of the failure function 23.1 in Equation 23.29.

⁴² For this case, the failure function is equal to:

$$F = (\tau_{1n+1}^2 + \tau_{2n+1}^2) - 2c \tan(\phi_f)(\sigma_t - \sigma_{n+1}) - \tan^2(\phi_f)(\sigma_{n+1}^2 - \sigma_t^2) = 0 \quad (23.30)$$

⁴³ To this equation, we substitute the expression for the new stress state $\boldsymbol{\sigma}_{n+1}$, which are equal to (Equation 23.28):

$$\begin{aligned} \tau_{1n+1} &= \tau_{1e} - \Delta\lambda K_{to} m_1 = \tau_{1e} - \Delta\lambda l_1 \\ \tau_{2n+1} &= \tau_{2e} - \Delta\lambda K_{to} m_2 = \tau_{2e} - \Delta\lambda l_2 \\ \sigma_{n+1} &= \sigma_e - \Delta\lambda K_{no} m_3 = \sigma_e - \Delta\lambda l_3 \end{aligned} \quad (23.31)$$

44 The result of this substitution is a quadratic equation with roots:

$$\Delta\lambda_{1,2} = \frac{-B \pm \sqrt{B^2 - 4AC}}{2A} \quad (23.32)$$

where

$$\begin{aligned} A &= l_1^2 + l_2^2 - \mu^2 l_3^2 \\ B &= 2\mu^2 \sigma_e l_3 - 2l_1 \tau_{1e} - 2l_2 \tau_{2e} - 2c\mu l_3 \\ C &= \tau_{1e}^2 + \tau_{2e}^2 - 2c\mu \sigma_t + \mu^2 \sigma_e^2 + \mu^2 \sigma_t^2 \end{aligned}$$

45 The required solution must satisfy the following conditions.

$$\Delta\lambda > 0 \quad \wedge \quad \Delta\lambda = \min(\Delta\lambda_1, \Delta\lambda_2) \quad (23.33)$$

46 In the previous equations, l_1 , l_2 and l_3 are components of vector l indicating the direction of inelastic return in the stress space, and they are related to the direction of inelastic displacements m through the stiffness matrix E .

$$l = Em \quad (23.34)$$

47 The direction of inelastic displacements m is defined as the normal vector to the plastic potential Q (Figure 23.10), which is defined using the dilatancy angle $\phi_d(u^{\text{eff}})$ as:

$$Q = \tau_1^2 + \tau_2^2 - \left(\frac{K_n}{K_t} \tan \phi_d\right)^2 \sigma^2 = 0 \quad (23.35)$$

48 For the definition of m , we must distinguish between the case, when the return direction m can be determined on the basis of Q , and the pathological case of the apex of Q , when the normal m cannot be constructed. For this case, m is defined by connecting the trial tractions σ_e with the origin of the $\sigma \times \tau_1 \times \tau_2$ space (Figure 23.11):

$$\begin{aligned} m &= \begin{cases} \begin{pmatrix} \tau_1/K_{to} \\ \tau_2/K_{to} \\ \sigma/K_{no} \end{pmatrix} & \text{if } \frac{\|\tau\|}{\sigma} \leq \frac{1}{\tan \phi_d} \frac{K_{to}}{K_{no}} \wedge \sigma > 0 \\ \begin{pmatrix} \tau_1 \\ \tau_2 \\ \sqrt{\tau_1^2 + \tau_2^2} \tan \phi_d \end{pmatrix} & \text{otherwise} \end{cases} \end{aligned} \quad (23.36)$$

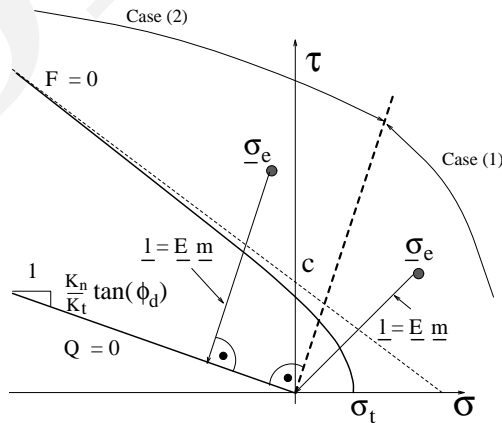


Figure 23.11: Definition of inelastic return direction.

49 At this stage, we can identify three major steps to the proposed algorithm:

1. Elastic predictor:

$$\boldsymbol{\sigma}_e = \boldsymbol{\sigma}_n + \mathbf{E}\Delta\mathbf{u}_n \quad (23.37)$$

2. Inelastic corrector simultaneously satisfying the following two equations:

$$\begin{aligned} F_{n+1}(\boldsymbol{\sigma}_e - \Delta\lambda\mathbf{E}\mathbf{m}, u_{n+1}^{\text{ieff}}) &= 0 \\ u_{n+1}^{\text{ieff}} &= u_n^{\text{ieff}} + \|\Delta\lambda\mathbf{m}\| \end{aligned} \quad (23.38)$$

3. Fracturing corrector:

$$\begin{aligned} \mathbf{E}_s &= \alpha\mathbf{E} \\ \mathbf{u}^p &= \mathbf{u} - \mathbf{E}_s^{-1}\boldsymbol{\sigma}_{n+1} \end{aligned} \quad (23.39)$$

⁵⁰ In the fracturing corrector, the inelastic displacements due to friction and microcracks development are separated. This separation is controlled by the damage parameter D defined by Equation 23.9. The evolution of damage parameter D is defined by converting the mixed mode problem into an equivalent uniaxial case as described in Section 23.2.

⁵¹ The complete algorithm of the interface constitutive driver is described in Algorithm 23.3.2 and is shown schematically on Figure 23.10.

ICM constitutive driver.

- Input: $\boldsymbol{\sigma}_n, u_n^{\text{ieff}}$ and $\Delta\mathbf{u}_n$
- $\boldsymbol{\sigma}_{n+1} = \boldsymbol{\sigma}_n + \alpha\mathbf{E}\Delta\mathbf{u}_n$
- if $F(\boldsymbol{\sigma}_{n+1}, u_n^{\text{ieff}}) > 0$
 - Update $\boldsymbol{\sigma}_n$, and $\Delta\mathbf{u}_n$ such that $F(\boldsymbol{\sigma}_n, u_n^{\text{ieff}}) = 0$.
 - Elastic predictor: $\boldsymbol{\sigma}_{n+1} = \boldsymbol{\sigma}_n + \mathbf{E}\Delta\mathbf{u}_n$
 - Inelastic corrector:
 - * $u_{n+1}^{\text{ieff}} = u_n^{\text{ieff}}$
 - * Do
 - Evaluate return direction \mathbf{m}
 - Determine $d\lambda$ such that $F(\boldsymbol{\sigma}_{n+1} - d\lambda\mathbf{E}\mathbf{m}, u_{n+1}^{\text{ieff}}) = 0$
 - $u_{n+1}^{\text{ieff}} = u_{n+1}^{\text{ieff}} + \|d\lambda\mathbf{m}\|$
 - $\boldsymbol{\sigma}_{n+1} = \boldsymbol{\sigma}_{n+1} - d\lambda\mathbf{E}\mathbf{m}$
 - * While $d\lambda < \varepsilon$
 - Fracturing corrector:
 - $\alpha = 1 - \frac{|\sigma| + \sigma}{2|\sigma|} D(u_{n+1}^{\text{ieff}})$
 - $\mathbf{E}_s = \alpha\mathbf{E}$
 - $\mathbf{u}^p = \mathbf{u} - \mathbf{E}_s^{-1}\boldsymbol{\sigma}_{n+1}$
- Output: $\boldsymbol{\sigma}_{n+1}, u_{n+1}^{\text{ieff}}$

⁵² Figure 23.12 illustrates a simple example of direct tension test with the proposed interface crack model. It demonstrates the accuracy of the proposed algorithm as the normal stresses are always correctly evaluated for the given displacements, and there is no loss of accuracy when larger increment steps are used. This is a direct consequence of the geometrical approach during the inelastic corrector phase of the algorithm and the displacement based softening. This example also illustrates the ability of the proposed model to simulate Hillerborg's fictitious crack model.

⁵³ The robustness of the interface constitutive driver can also be tested by analyzing an example of shear under fixed tension in the normal direction. This is clearly an unstable problem on the structural level, since following certain sliding displacement the tensile strength is lower than the originally applied normal stress, and the specimen fails in an unstable manner. This implies

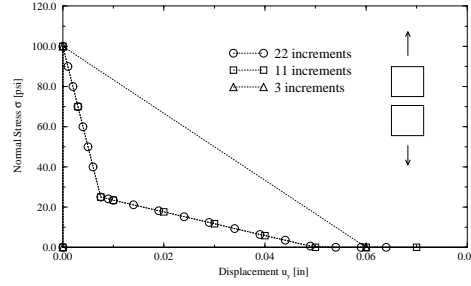


Figure 23.12: Influence of increment size.

that on the structural level the solution cannot converge. However, the algorithm should not fail on the constitutive level, which could occur in some plasticity based models in which the consistency condition is used to determine the increment of the plastic multiplier $d\lambda$. In these formulations, due to the snap-back on the constitutive level, a negative value of $d\lambda$ is obtained, and the second Kuhn-Tucker condition (Equation ??) is not satisfied causing the model to fail on the constitutive level. This is clearly an undesirable feature since a snap-back on the constitutive level could occur even in otherwise stable problems. To investigate the behavior of the proposed interface model in the shear-tension regime, a simple example of two quadrilateral elements connected by an interface element is analyzed. In the first increment tensile tractions are applied on the upper element, and in the subsequent increments horizontal displacements are prescribed for the upper element. The resulting load-displacement curve is shown in Figure 23.13.

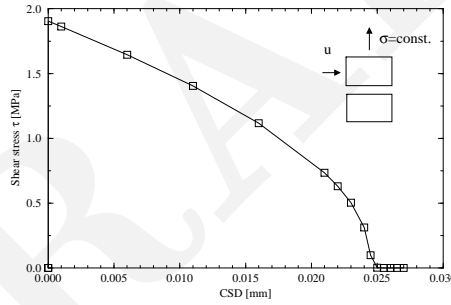


Figure 23.13: Shear-tension example.

⁵⁴ We observe the tendency for snap-back behavior when $CSD \approx 0.0245$ mm. After this point, due to the unstable nature of the problem, convergence on the structural level could no longer be achieved, however no problems on the constitutive level are observed.

23.3.3 Non-linear solver.

⁵⁵ The proposed interface crack model is clearly a nonlinear material formulation, and therefore, a finite analysis including this material formulation involves a system of nonlinear equations. Such system can be solved, for instance, by the Newton-Raphson method. To exploit the full Newton-Raphson method a tangent stiffness matrix would have to be computed at each iteration. The incremental tangent stiffness matrix for the proposed material formulation can be computed from the incremental stress-displacement relationship:

$$\Delta\sigma_n = \mathbf{E} \Delta\mathbf{u}_n - \Delta\lambda \mathbf{E} \mathbf{m} \quad (23.40)$$

when multiply the last term by a fraction which is equal to unity:

$$\Delta\sigma_n = \mathbf{E} \Delta\mathbf{u}_n - \Delta\lambda \mathbf{E} \mathbf{m} \frac{\mathbf{n}^T \mathbf{E} \Delta\mathbf{u}_n}{\mathbf{n}^T \mathbf{E} \Delta\mathbf{u}_n} \quad (23.41)$$

where \mathbf{n} is the normal vector to the failure surface passing through the trial stress state $\boldsymbol{\sigma}_e$ (Equation 23.27).

56 From this equation it is possible to derive a formula for an incremental tangent material stiffness matrix \mathbf{E}_T :

$$\Delta\boldsymbol{\sigma}_n = \mathbf{E}_T \Delta\mathbf{u}_n \quad (23.42)$$

where:

$$\mathbf{E}_T = \mathbf{E} \left(\mathbf{I} - \Delta\lambda \frac{\mathbf{E} \mathbf{m} \mathbf{n}^T \mathbf{E}}{\mathbf{n}^T \mathbf{E} \Delta\mathbf{u}_n} \right) \quad (23.43)$$

57 In this particular case, the new stress state is computed using the iterative process described in Algorithm 23.3.2. Therefore, the incremental stress-displacement is given by a sum:

$$\Delta\boldsymbol{\sigma}_n = \mathbf{E} \Delta\mathbf{u}_n - \sum_{i=1}^{N_{iter}} (\Delta\lambda_i \mathbf{E} \mathbf{m}_i) \quad (23.44)$$

where N_{iter} is the number of iterations in the inelastic corrector part of Algorithm 23.3.2. Following similar arguments leading to equation 23.43, the incremental tangent stiffness is computed by the following expression:

$$\mathbf{E}_T = \mathbf{E} \left[\mathbf{I} - \sum_{i=1}^{N_{iter}} \left(\Delta\lambda_i \frac{\mathbf{E} \mathbf{m}_i \mathbf{n}_i^T \mathbf{E}}{\mathbf{n}_i^T \mathbf{E} \Delta\mathbf{u}_n} \right) \right] \quad (23.45)$$

58 During softening, the tangent matrix \mathbf{E}_T becomes negative. In addition, the matrix becomes also unsymmetric due to the dilatancy, which is introduced in the softening regime of the interface model. This would imply the need to store the full stiffness matrix on the structural level, and a method for solving unsymmetric and non-positive system of equations would have to be adopted. This is clearly not an efficient approach, since only few elements will be affected by the non-linear behavior (i.e. interface elements), and therefore, only small portions of the structural stiffness matrix will be unsymmetric.

59 On the other hand, it can be expected that the initial stiffnesses of the interface elements are very large, and in some cases, they represent penalty numbers modeling a rigid contact. This means that it is not possible to use the initial structural stiffness throughout the whole iterative process, as it would result in an excessive number of iterations.

60 In this work two approaches are suggested to mitigate this problem:

- (1) Use of secant-Newton method to accelerate the convergence on the structural level.
 - (2) Use of secant interface stiffness on the element level while preserving its positiveness and symmetry.
- Both methods are supplemented with the line-search technique of (Crisfield, 1991).

23.3.4 Secant-Newton method.

61 The secant-Newton method is described in detail in (Crisfield, 1991). In this method, it is not necessary to recompute the structural stiffness matrix at each iteration, but rather the vector of iterative displacement corrections is updated to satisfy the secant relationship.

$$\frac{d\mathbf{u}_i^*}{r_i} = \frac{d\mathbf{u}_{i-1}^*}{r_i - r_{i-1}} \quad (23.46)$$

62 For one-dimensional case, the meaning of this formula is illustrated by Figure 23.14.

63 In this work, (Davidon, W.C., 1968) rank-one quasi-Newton update is used, and the corrected iterative update of the displacement vector in iteration i is equal to:

$$d\mathbf{u}_i^* = A d\mathbf{u}_i + B d\mathbf{u}_{i-1}^* + C d\mathbf{u}_{i-1} \quad (23.47)$$

where $d\mathbf{u}_i$ is the iterative update of the displacement vector computed in iteration i by solving:

$$d\mathbf{u}_i = \mathbf{K}^{-1} \mathbf{r}_i \quad (23.48)$$

where \mathbf{K} is the structural stiffness matrix, and \mathbf{r}_i are residual forces at iteration i . The starred symbols, \mathbf{u}_i^* and \mathbf{u}_{i-1}^* , represent the displacement vector updates based on the secant-Newton corrections (Equation 23.47), and coefficients A , B and C are given by (Davidon, W.C., 1968):

$$C = \frac{(d\mathbf{u}_{i-1}^* + d\mathbf{u}_i - d\mathbf{u}_{i-1})^T \mathbf{r}_i}{(d\mathbf{u}_{i-1}^* + d\mathbf{u}_i - d\mathbf{u}_{i-1})^T (\mathbf{r}_i - \mathbf{r}_{i-1})} \quad (23.49)$$

$$A = 1 - C, \quad B = -C$$

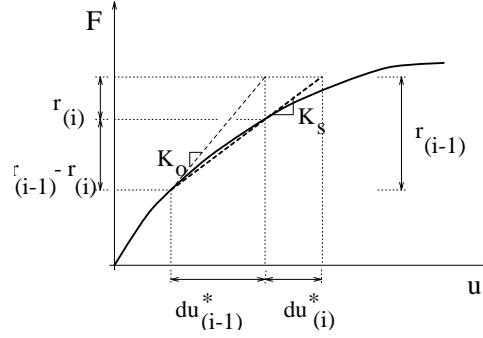


Figure 23.14: Secant relationship.

23.3.5 Element secant stiffness.

⁶⁴ It is also possible to employ the secant formula (Eq. 23.46) on the element level. Considering the diagonal form of the material stiffness matrix \mathbf{E} , it is possible to determine its secant form from the stress and displacement corrections in each iteration.

$$\begin{aligned} K_{t1}^i &= \frac{\tau_{n+1}^i - \tau_{n+1}^{i-1}}{\Delta u_{n+1}^i - \Delta u_{n+1}^{i-1}} \\ K_{t2}^i &= \frac{\tau_{n+1}^i - \tau_{n+1}^{i-1}}{\Delta u_{n+1}^i - \Delta u_{n+1}^{i-1}} \\ K_n^i &= \frac{\sigma_{n+1}^i - \sigma_{n+1}^{i-1}}{\Delta u_{n+1}^i - \Delta u_{n+1}^{i-1}} \end{aligned} \quad (23.50)$$

⁶⁵ To preserve the positiveness of the material stiffness matrix a minimal value for shear and normal stiffnesses must be specified. In this work the shear and normal stiffnesses cannot be less than 10^{-8} times their original value. This number is based on the assumption that the ratio of the lowest elastic modulus to the largest interface stiffness is below 10^{-4} . This ratio should be sufficient in most practical problems, since the interface stiffness can be estimated from:

$$K_n = \frac{E}{t} \quad (23.51)$$

where t is the interface thickness. Thus, the ratio $\frac{E}{K^{interface}} \approx 10^{-4}$ corresponds to the assumption of interface thickness being equal to 10^{-4} times a unit length of the problem. This should be adequate for the types of problems under consideration in this work. Alternatively, we consider an extreme case of $K^{interface}$ of the same order as E (i.e. $t \approx$ problem unit). Then after cracking, the interface stiffness will be reduced to 10^{-8} times its original value, and it is possible to estimate the condition number of the system using the elastic modulus, maximal and minimal element sizes.

$$\kappa \approx \frac{K_{max}^{elem}}{K_{min}^{interface}} \approx \frac{Eh_{max}}{(Eh_{min}^2)/t \times 10^{-8}} \approx 10^{14} \quad (23.52)$$

In the formula, the element sizes were assumed to be in the range of the order $\langle 10^{-2}, 10^2 \rangle$.

⁶⁶ The loss of accuracy due to finite precision arithmetic is given by:

$$s = p - \log(\kappa) \quad (23.53)$$

where p is the number of significant digits in the computer representation of real numbers and s is the accuracy of the solution. The system will become ill-conditioned when:

$$s \leq 0 \quad (23.54)$$

⁶⁷ A real number f is internally represented in a computer memory by three integers m , β and e .

$$f = .m \times \beta^e \quad (23.55)$$

The mantissa m gives the number of significant digits. For double precision data type, m is usually stored in 52 bits, which corresponds to approximately 16 significant digits. Therefore, the accuracy after decomposition is in the worst possible scenario equal to 2 (Equation 23.53), which is of course an unacceptable level of accuracy. However, it should be kept in mind that this is a worst case scenario, and it would be unrealistic to have a ratio of largest to smallest element of the order of 10^4 , as was assumed in Equation 23.52.

23.3.6 Line search method.

⁶⁸ Numerical experiments showed, that often the diagonal approximation of the secant stiffness underestimates the true stiffness of the interface and allows for excessive interface sliding. The excessive sliding in turn introduces large dilatancy effects and high compressive stresses in the normal direction in the subsequent iteration. These high compressive stresses and the frictional properties of the interface combined with the excessive slidings will cause large shear stresses, which may not be in equilibrium with the rest of the finite element mesh. Due to this, the resulting high residual forces attempt to slide the interface backwards, but since the stiffness of the interface is underestimated, the backward sliding is too large, and the iteration process diverges. This problem can be solved by combining the previously discussed secant-methods with line searches.

⁶⁹ The fundamental principle behind the line search method (Crisfield, 1991) is to determine a scaling factor ω , for the current iterative displacement correction, such that the functional of total potential energy is stationary.

$$\Pi(\omega) = \Pi(\mathbf{u}_{i-1} + \omega d\mathbf{u}_i) = \Pi(\omega) + \frac{\partial \Pi(\omega)}{\partial \mathbf{u}(\omega)} \frac{\partial \mathbf{u}(\omega)}{\partial \omega} \delta\omega \quad (23.56)$$

The functional $\Pi(\omega)$ would be stationary if the last term is equal to zero. It can be shown, (Crisfield, 1991), that the partial derivative of total potential energy $\Pi(\omega)$ with respect to displacements $\mathbf{u}(\omega)$ is equal to the vector of residual forces $\mathbf{r}(\mathbf{u})$. Thus, the last term of Equation 23.56 is equivalent to:

$$\frac{\partial \Pi(\omega)}{\partial \mathbf{u}(\omega)} \frac{\partial \mathbf{u}(\omega)}{\partial \omega} \delta\omega = \mathbf{r}(\omega) d\mathbf{u}_i \delta\omega = 0 \quad (23.57)$$

⁷⁰ If we introduce a new symbol $s(\omega)$ representing the scalar product of vectors $\mathbf{r}(\omega)$ and $d\mathbf{u}_i$, then the objective is to find a scalar multiplier ω such that $s(\omega)$ is equal to zero. Such ω can be approximately computed from $s(\omega)$ for ω equal to zero and one.

$$s(0) = \mathbf{r}(\mathbf{u}_{i-1}) d\mathbf{u}_i, \quad s(1) = \mathbf{r}(\mathbf{u}_{i-1} + d\mathbf{u}_i) d\mathbf{u}_i \quad (23.58)$$

⁷¹ Then an approximation of ω can be evaluated using the following formulas based on the linear interpolation between $s(0)$ and $s(1)$.

$$\omega = \frac{-s(0)}{s(1) - s(0)} \quad (23.59)$$

A more accurate value of ω can be determined through recursive applications of this formula.

$$\omega_{i+1} = \omega_i \frac{-s(0)}{s(\omega_i) - s(0)} \quad (23.60)$$

⁷² Graphically, the line search is illustrated in Figure 23.15.

⁷³ We observe that it corresponds exactly to the divergence problem previously described. Originally, the residual forces acted along the same direction as the iterative displacement correction, and their scalar product $s(0)$ was positive. However, after the iterative correction is considered, the residuals have opposite orientation with respect to the iterative displacement update $d\mathbf{u}_i$, and $s(1)$ is negative. This indicates that the displacements should be smaller, and this is exactly, what the line search method is able to recognize and correct.

⁷⁴ The line search method can be implemented in the context of various load control techniques. The implementation of line searches in the context of the arc-length method is discussed in (Crisfield, 1991). (Reich, 1993) implemented the line search method with an indirect displacement control technique, which is based on crack step control mechanism, and can be therefore easily used for non-linear fracture mechanics analyzes using the FCM model.

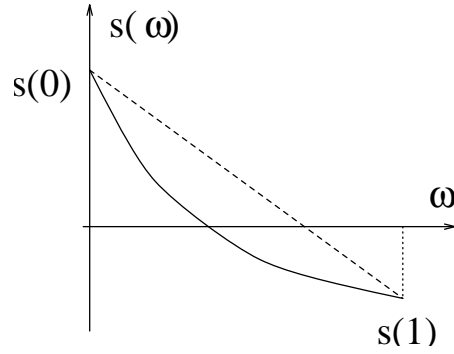


Figure 23.15: Line search method.

23.4 Mixed Mode Crack Propagation

⁷⁵ In most engineering problems, the crack path is not known a priori, and therefore, must be determined during an analysis. In the context of discrete crack analysis, this is accomplished by modifications of the initial mesh. It is, therefore, necessary to establish appropriate criteria for crack initiation and propagation. The criteria for LEFM analysis were discussed in Section ?? of Chapter ?. In the non-linear fracture mechanics analysis, a crack initiation criterion can be based on tensile stresses, and energy control is conducted through an appropriate softening diagram. This is to be contrasted with LEFM, where the stress based criteria are not applicable, as they are infinite at the crack tip. It can be readily verified that the Griffith energy based criterion is also satisfied in the non-linear fracture mechanics through an appropriate softening law.

23.4.1 Griffith criterion and ICM.

⁷⁶ Let us consider a cohesive crack with both normal and tangential tractions in a thin plate subjected to far field stresses, and let us assume the crack is to be under general mixed mode conditions, Figure 23.16. To verify if the non-linear model satisfies Griffith criterion, it is necessary to compute the energy released by a unit crack propagation.

⁷⁷ The J-integral provides a method to evaluate the energy release rate. The J-integral is a path independent integral and in two-dimensional is given by:

$$J = \oint_{\Gamma} (W n_x - \hat{\mathbf{t}} \frac{\partial \mathbf{u}}{\partial x}) d\Gamma \quad (23.61)$$

⁷⁸ Due to its path independent character it is possible to evaluate the J-integral along the crack surfaces.

$$J(\Gamma_o) = - \int_{\Gamma_o} \hat{\mathbf{t}} \frac{\partial \mathbf{u}}{\partial x} ds = \int_{FPZ} \left(\tau \frac{\partial \Delta_x}{\partial x} + \sigma \frac{\partial \Delta_y}{\partial x} \right) dx \quad (23.62)$$

⁷⁹ Applying Leibnitz rule for the differentiation of definite integrals the J-integral is equivalent to:

$$J(\Gamma_o) = \int_{FPZ} \left[\frac{d}{dx} \left(\int_0^{\Delta_x} \tau d\Delta_x \right) \right] dx + \int_{FPZ} \left[\frac{d}{dx} \left(\int_0^{\Delta_y} \sigma d\Delta_x \right) \right] dx \quad (23.63)$$

⁸⁰ The expressions in parentheses represent the surface energies dissipated in mode I and II at every point along the fracture process zone normalized with respect to crack surface. Hence, we define:

$$\int_0^{\Delta_x} \tau d\Delta_x = q^{II}(x), \quad \int_0^{\Delta_x} \sigma d\Delta_y = q^I(x) \quad (23.64)$$

$$J(\Gamma_o) = \int_{FPZ} \frac{dq^{II}(x)}{dx} dx + \int_{FPZ} \frac{dq^I(x)}{dx} dx = G_c^{II} + G_c^I = G_c \quad (23.65)$$

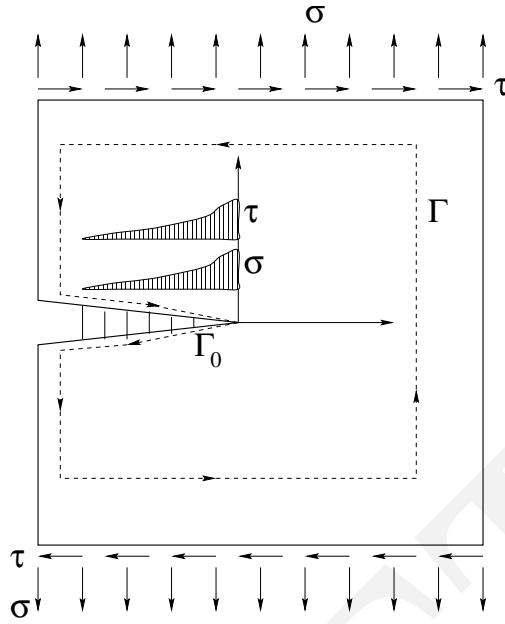


Figure 23.16: Griffith criterion in NLFM.

where G_c^{II} and G_c^I is the energy dissipated by a unit propagation of the cohesive crack in mode II and I respectively. It should be noted that in general, G_c^{II} and G_c^I are not equivalent to G_F^{II} and G_F^I , but are rather functions of these and the stress state along the interface. However, it is possible to consider two special cases for pure mode I and II cracks.

⁸¹ In the case of pure mode I crack, the J-integral is equal to:

$$J(\Gamma_o) = \int_{FPZ} \left[\frac{d}{dx} \left(\int_0^{\Delta_y} \sigma d\Delta_y \right) \right] dx = \int_0^{w_\sigma} \sigma(\Delta_y) d\Delta_y = G_F^I \quad (23.66)$$

⁸² Similarly, in the case of pure mode II crack, the J-integral is equal to:

$$J(\Gamma_o) = \int_{FPZ} \left[\frac{d}{dx} \left(\int_0^{\Delta_x} \tau d\Delta_x \right) \right] dx = \int_0^{w_\tau} \tau(\Delta_x) d\Delta_x = G_F^{II} \quad (23.67)$$

where w_σ and w_τ is the critical crack opening and sliding respectively for which normal and tangent stresses can no longer be transferred across the crack.

⁸³ The following conclusion can be drawn based on the basis of the previous discussion:

(1) It was shown that a unit extension of a cohesive crack model dissipates energy whose amount depends on the softening laws used by the model. The amount of dissipated energy also depends on the loading conditions in FPZ. In pure mode I and mode II loading, specific fracture energies G_F^I and G_F^{II} are dissipated respectively. If the structural system cannot provide these energies, the crack would not propagate.

(2) In the limiting case, when the dimensions of the analyzed problem increase, the cohesive crack gives identical results as LEFM.

(3) In finite element implementation, errors are introduced due to discretization errors. In large structures, fine mesh would be necessary at the crack tip to model the fracture process zone. If the FPZ is not modeled adequately, the Griffith criterion for crack propagation is violated, and erroneous results will be obtained.

23.4.2 Criterion for crack propagation.

⁸⁴ In this work a stress based criterion is used for crack initiation and propagation. A crack is initiated when a maximal principal stress σ_1 exceeds the tensile strength of the material. A crack of certain length Δa is inserted into the boundary representation of the model in the direction perpendicular to the direction of the maximal principal stress, and the length of the new crack Δa

is arbitrarily selected by the user. The exact solution is approached as this length tends to zero, this is however not feasible, and from author's experience, the crack step size should be:

$$\Delta a \leq \frac{L}{10} \tag{23.68}$$

where L is maximal dimension of the problem. From the updated boundary representation, a new mesh is generated, in which interface elements are placed along the crack.

⁸⁵ Then, a non-linear analysis is performed, and the maximal principal stresses at crack tips are monitored. When they are found to exceed the tensile strength of the material, the analysis is interrupted, and new crack surfaces are inserted into the boundary representation of the problem. Then, a new mesh is again generated and the problem is reanalyzed from the beginning. In this manner the finite element model is adaptively modified until the structure is fully cracked or the prescribed loading level is reached. This process is described by Algorithm 23.4.2, and is shown graphically in Figure 23.17.

Mixed mode crack propagation.

- (1) Input: Boundary representation.
- (2) Generate finite element model.
- (3) Do
 - (3.1) Non-linear finite element analysis.
- (4) While: maximal principal stresses $< f'_t$.
- (5) If maximal principal stress exceed f'_t .
 - (4.1) Add new crack surfaces of length Δa to the boundary representation in the direction perpendicular to σ_1 .
 - (4.2) Goto Step 2.
- (6) Output: Boundary representation, Finite element model.

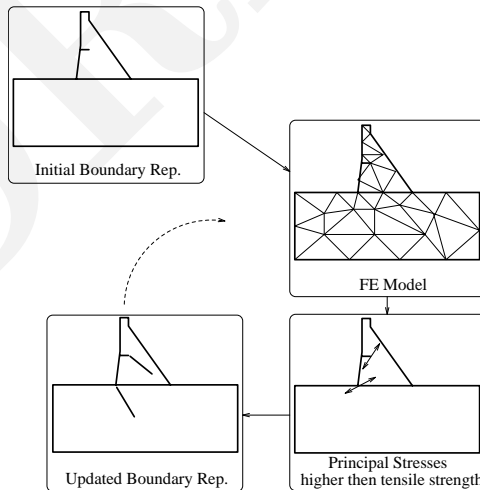


Figure 23.17: Mixed mode crack propagation.

23.5 Examples and validation

⁸⁶ Number of problems with known experimental or analytical results are analyzed in this section to validate the proposed interface mode for simulating discrete fracturing along interfaces and in homogeneous concrete.

23.5.1 Direct shear test of mortar joints.

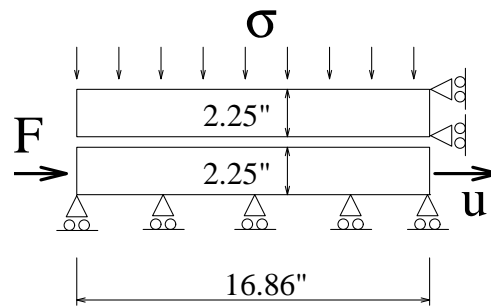


Figure 23.18: Schematics of the direct shear test setup.

⁸⁷ In this section, a nonlinear analyzes of a direct shear test with various levels of normal confinement are presented. The experiments were performed at the University of Colorado in Boulder (Shing et al., 1994). In these experiments, a mortar interface between two brick was tested at three different levels of compressive confinement (150, 100 and 50 psi). Analyses are performed for these confinement values and also for zero value, which corresponds to a pure shear test.

⁸⁸ Table 23.1 summarizes the selected material properties. Interface stiffnesses K_t and K_n were determined by data fitting in the elastic region. The remaining interface parameters were obtained from the experimental load-displacement curves.

⁸⁹ Figure 23.19 shows a good correlation between the experimental and analytical load-displacement curves.

Table 23.1: Material properties for direct shear test.

Material Parameter	Values
Brick	
Modulus of elasticity E	800 ksi
Poisson's ratio ν	0.2
Mortar Interface	
Shear stiffness K_t	600 ksi/in
Normal stiffness K_n	200 ksi/in
Tensile strength f'_t	50 psi
Cohesion c	80 psi
Friction angle ϕ_f	45.0 deg
Dilatancy angle ϕ_D	20.0 deg
Specific mode I fracture energy G_F^I	0.3 lbf/in
Specific mode II fracture energy G_F^{IIa}	3.0 lbf/in
Stress at break point of bilinear softening law s_1	12.5 psi
Crack opening at break point of bilinear softening law sw_1	0.0045 in
Cohesion at break point of bilinear softening law c_1	40.0 psi
Crack sliding at break point of bilinear softening law cw_1	0.025 in
Maximal dilatant displacement u_{dil}	0.2 in

23.5.2 Biaxial interface test.

⁹⁰ The interface constitutive model described above is used to analyze the biaxial test specimen in Figure 23.20. These specimens were tested at the University of Colorado by (Saouma et al., 1994).

⁹¹ In this first study, the material properties were optimized to yield comparable results with the experimental ones ($\sigma_t = 0.68$ [MPa], $c = 0.68$ [MPa], $\phi_f = 30$ [deg], $\phi_d = 40$ [deg], $G_F^I = 61$ [N/m], $G_F^{II} = 400$ [N/m]).

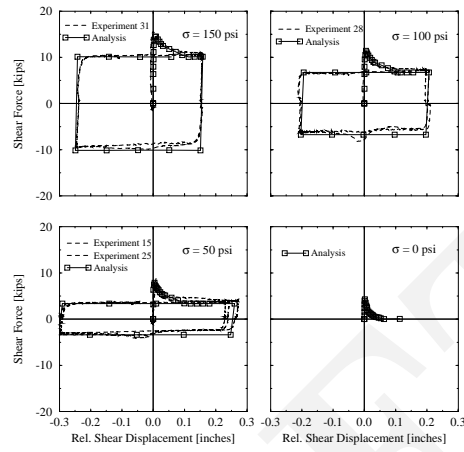


Figure 23.19: Direct shear test on mortar joint.

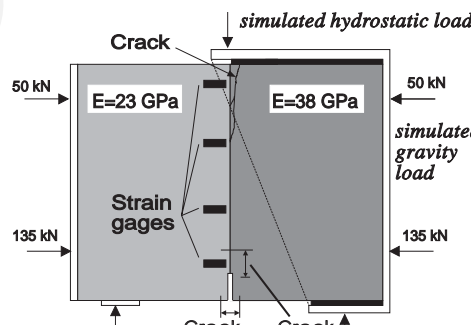


Figure 23.20: Experimental set-up for the large scale mixed mode test.

⁹² We observe that G_F^I is comparable with the G_F measured in wedge splitting tests on concrete, limestone and concrete-limestone in Figure 23.2. The comparison of the numerical results with experimental observations are shown in Figure 23.21. The numerical results show a good agreement with the experimental ones in the peak and post-peak region.

⁹³ In the pre-peak region, however, the initial stiffness of the specimen is overestimated. More analysis and experiments are necessary to determine the reason for this discrepancy.

Table 23.2: Material properties for direct shear test.

Material Parameter	Values
Concrete 1	
Modulus of elasticity E	$5.55 \cdot 10^6$ [Psi]
Poisson's ratio ν	0.18
Concrete 2	
Modulus of elasticity E	$3.36 \cdot 10^6$ [Psi]
Poisson's ratio ν	0.18
Interface	
Shear stiffness K_t	$1.887 \cdot 10^6$ [Psi/in]
Normal stiffness K_n	$4.453 \cdot 10^6$ [Psi/in]
Tensile strength f'_t	120 psi
Cohesion c	220 psi
Friction angle ϕ_f	60.0 deg
Dilatancy angle ϕ_D	45.0 deg
Specific mode I fracture energy G_F^I	0.35 lbf/in
Specific mode II fracture energy G_F^{IIa}	1.05 lbf/in
Ratio of irreversible displacement γ	0.15
Maximal dilatant displacement u_{dil}	0.5 in
Softening law for tensile strength	linear
Softening law for cohesion	linear

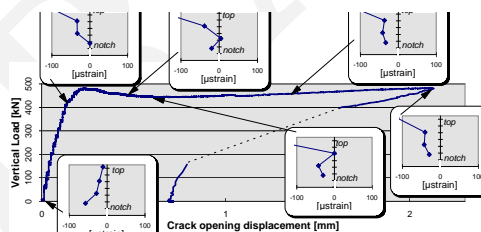


Figure 23.21: Nonlinear analysis of the mixed mode test.

23.5.3 Modified Iosipescu's beam.

⁹⁴ The presented interface crack model (ICM) can also be used to model discrete cracks in homogeneous material. This is documented on an analysis of the modified Iosipescu's beam from Section ???. The geometry, boundary conditions and material properties of the problem were discussed in detail in Section ??, and hence only the aspects of the analysis directly related to the use of interface crack model are discussed in this section. The material properties are listed in Table 23.3.

⁹⁵ The label ICM indicates the material properties for the interface crack model, which is used to simulate the fracture process zone.

⁹⁶ The model is supported at the two top plates and tractions are applied on the two bottom plates. The magnitude of the tractions is such that the total force on the left bottom steel plate is equal to $1/11 F$ and on the right bottom plate is $10/11 F$, where F is the total force applied in the vertical direction. The analysis is controlled by the relative sliding at the notch mouth. This means, that at each increment a unit vertical force F is applied. The applied forces are scaled to satisfy a prescribed value of the relative sliding. This displacement control scheme is described in detail in (Reich, 1993).

Table 23.3: Material properties for ICM for Iosipescu's test.

Material Parameter	Values
Concrete	
Young's modulus E	35 GPa
Poisson's ratio ν	0.15
Steel plates	
Young's modulus E	200 GPa
Poisson's ratio ν	0.22
ICM	
Shear stiffness K_t	15.2 GPa/m
Normal stiffness K_n	20.0 GPa/m
Tensile strength f'_t	2.8 MPa
Cohesion c	5.0 MPa
Friction angle ϕ_f	50.0 deg.
Dilatancy angle ϕ_D	45.0 deg.
Specific mode I fracture energy G_F^I	70.0 N/m
Specific mode II fracture energy G_F^{IIa}	700.0 N/m
Ratio of irreversible displacement γ	0.3
Maximal dilatant displacement u_{dil}	0.01 m
Softening law for tensile strength	bilinear (Wittmann & Brühwiler)
Softening law for cohesion	linear

⁹⁷ Two analysis were performed. In the first one, a single crack was propagated starting at the notch. However, during this analysis, tensile principal stresses were observed along the bottom edge between the two bottom supports that were higher than the tensile strength. Therefore, a second analysis was performed, in which totally five cracks were considered.

Single crack analysis:

Initially, there are no interface elements in the finite element mesh. They are inserted into the model after the maximal principal stresses at the notch reach the tensile strength. Then new crack faces are inserted into the boundary representation of the problem in the direction perpendicular to the direction of the maximal principal stress. A new finite element mesh is generated, and the analysis is restarted from the beginning. The analysis is stopped when the maximal principal stress at the crack tip is larger than the tensile strength. Then, again new crack faces are inserted into the boundary representation, and a new mesh is generated. This process is repeated until the whole beam is cracked. Six different finite element meshes were necessary in this analysis, and three of them are shown in Figures 23.22 and 23.23: the initial one, the mesh corresponding to the third step (i.e. third mesh regeneration) and the final mesh when the crack reached the bottom edge. The crack was initiated at the notch at an angle equal to -37.3 degrees with respect to the horizontal axis. Later it curved down, and reached the bottom edge of the beam exactly at the right corner of the right bottom plate. Figures 23.22 and 23.23 also show the positions on the load-displacement curve corresponding to each step and the normal and shear stresses along the crack.

Multiple cracks analysis:

This analysis was performed in an analogous way to the single crack one, but in the second step (i.e. after second remeshing), tensile stresses larger than tensile stress were observed along the bottom edge of the beam, therefore four additional cracks were inserted into the boundary representation at each node where the stress criterion was violated. In the subsequent step (i.e. step 4), two cracks were found to violate the stress criterion: the notch crack and the right bottom crack. In the following non-linear analysis, however, due to the stress redistribution, the bottom cracks were unloaded, and only the notch crack propagated. Altogether, five remeshing steps were necessary in this analysis, and some of them are shown in Figures 23.24 and 23.25. This figures show the shaded contour areas of maximal principal stresses on the deformed shapes at steps 3,4 and 5. The finite element meshes that were used at steps 1,3,4 and 5 are illustrated in Figure 23.26.

⁹⁸ The final load-displacement curves from both analyzes are shown in Figure 23.27, and can be compared to experimental data and classical fictitious crack analysis.

⁹⁹ In this figure, the label ICM indicates the results from this analysis, when the interface crack model was used, and the crack path was determined automatically during the analysis. The FCM label means that the classical Hillerborg fictitious model, as it was implemented by (Reich, 1993) was used. In this case, the crack patch must be known or assumed, therefore, the crack path, which was determined previously by the linear elastic fracture mechanics analysis was used. In other words, for the case of ICM the crack path was determined automatically during the nonlinear analysis, but for FCM the crack path was determined by a previous LEFM analysis (Section ??).

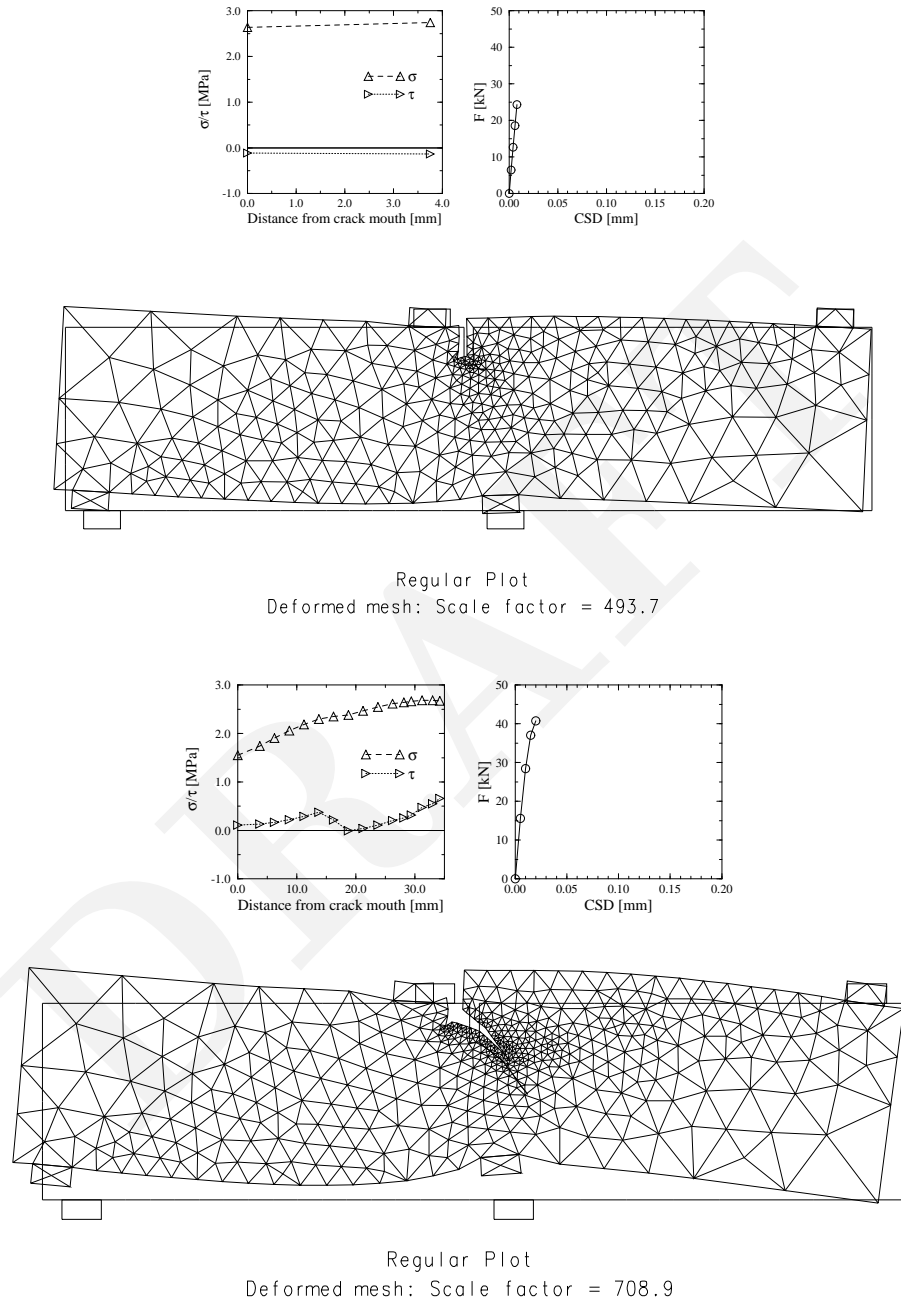


Figure 23.22: Crack propagation in Iosipescu's beam, (Steps 1 & 3).

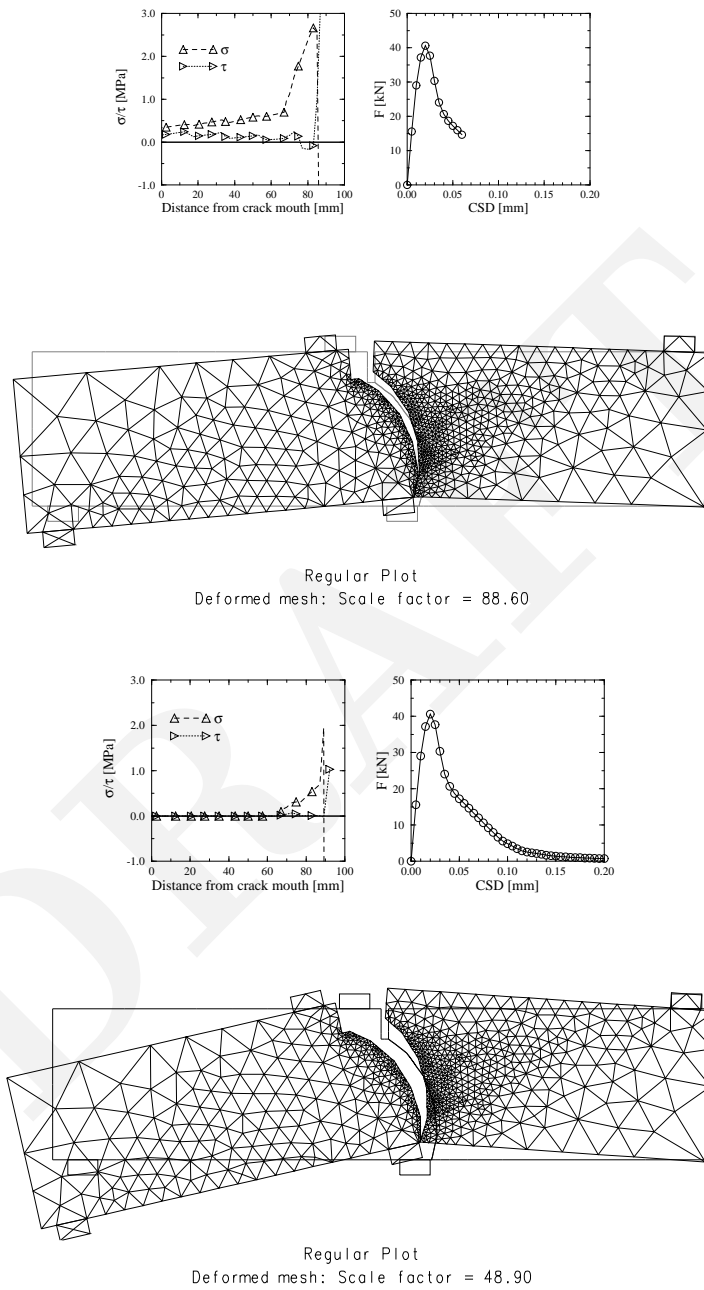
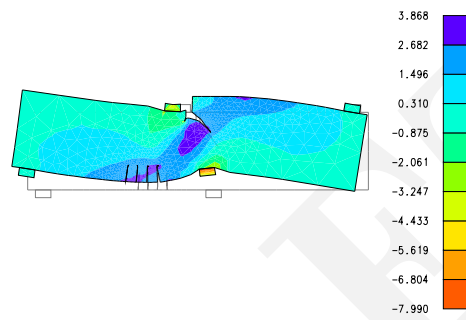
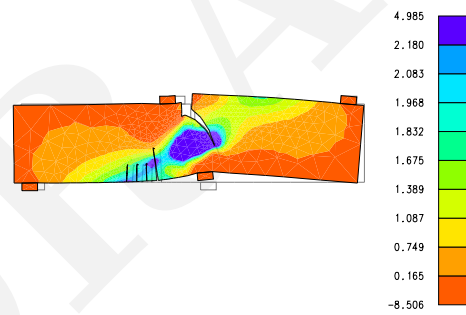


Figure 23.23: Crack propagation in Iosipescu's beam, (Increment 11 & 39 in Step 6).

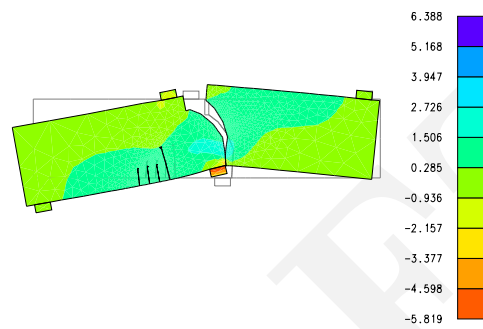


Contour plot: Principal Stresses, Maximum
Deformed mesh: Scale factor = 886.1

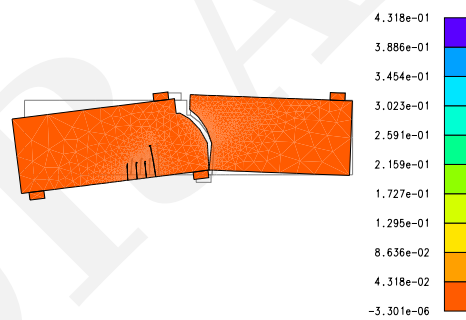


Contour plot: Principal Stresses, Maximum
Deformed mesh: Scale factor = 379.7

Figure 23.24: Multiple crack propagation in Iosipescu's beam (Steps 3,4).



Contour plot: Principal Stresses, Maximum
Deformed mesh: Scale factor = 320.7



Contour plot: Principal Strains, Maximum
Deformed mesh: Scale factor = 27.00

Figure 23.25: Multiple crack propagation in Iosipescu's beam (Step 5).

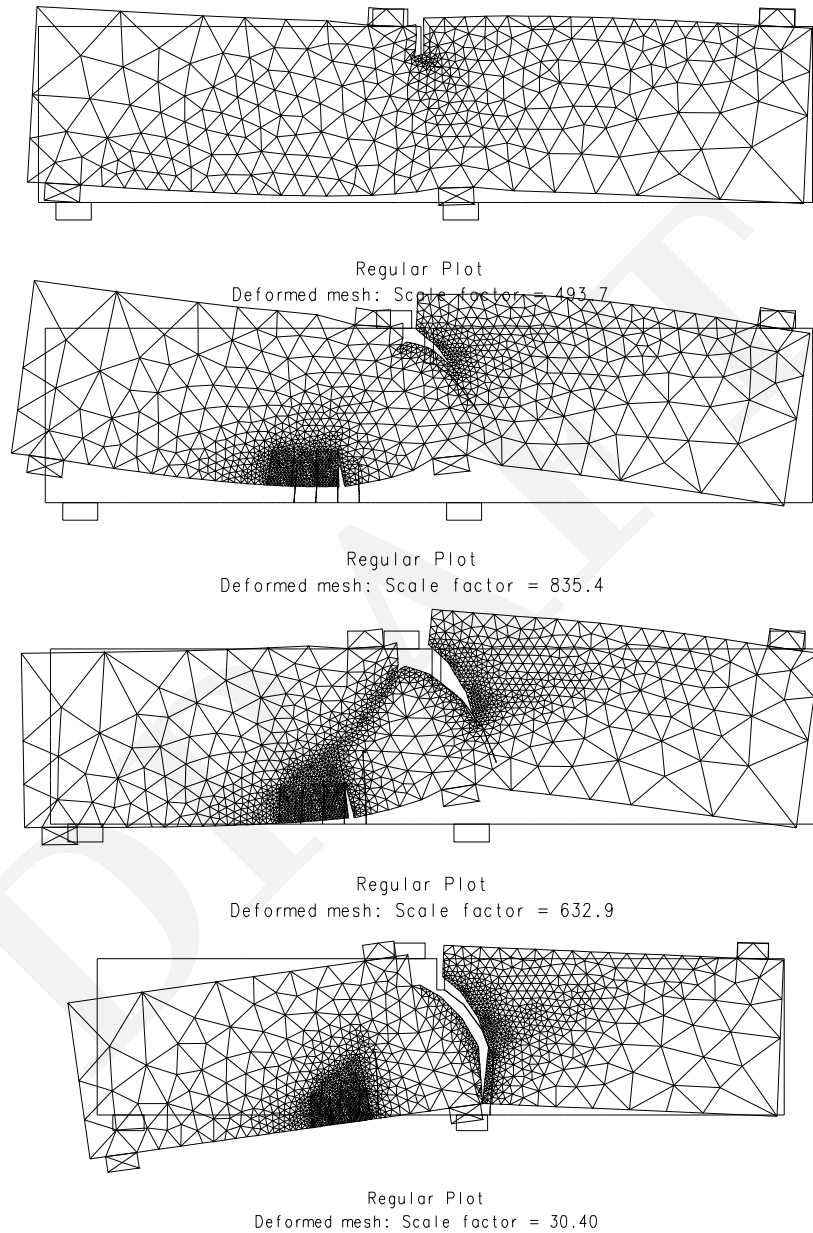


Figure 23.26: Meshes for crack propagation in Iosipescu's beam (Steps 1,3,4,5).

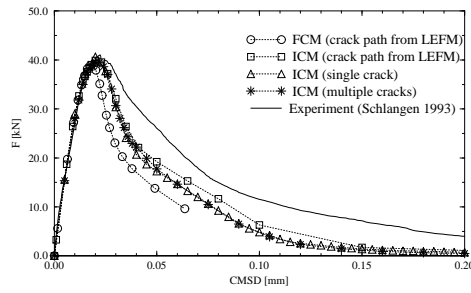


Figure 23.27: Iosipescu's beam with ICM model.

100 The crack paths determined by LEFM and ICM analyzes are compared in Figure 23.28. Clearly, there is almost no difference between the different crack paths, which implies that although LEFM is not applicable for this problem size, it can still be used

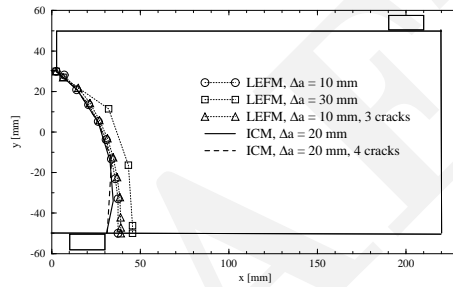


Figure 23.28: Crack paths for Iosipescu's beam.

for crack pattern prediction. The unsuitability of LEFM for this problem size is clearly demonstrated by the load-displacement curves in Figure ??, where the maximal peak load of about 40 kN is overestimated by almost 100 %.

101 Theoretically, as the problem size increases, the two approaches (i.e. LEFM and ICM) should become equivalent. This is demonstrated in Figure 23.29, which shows the load displacement curves for a specimen fifty times larger than the original one. Clearly, the two load-displacement curves are almost identical. This example can also be considered as a proof that the ICM model ap-

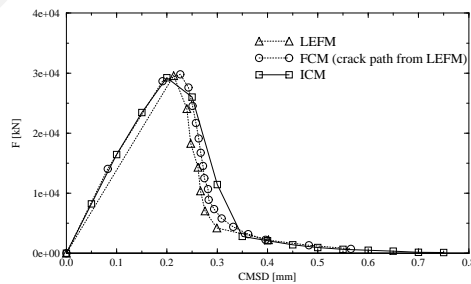


Figure 23.29: Large Iosipescu's beam, $h = 50 \times 100$ mm.

proaches LEFM as the structural size increases.

23.5.4 Anchor bolt pull-out test.

¹⁰² In Section ?? the anchor bolt pull-out experiments were analyzed using the linear elastic fracture mechanics (LEFM). LEFM is not applicable for this problem size as is documented on the resulting load-displacement curves (Figure ??). For both geometries the loads were overestimated if LEFM was used. In this section, same problem is reanalyzed, but nonlinear fracture mechanics is used. The fracture process zone is modeled using the interface crack model developed in this chapter.

¹⁰³ The problem geometry is shown in Figure ??, and material properties are listed in Table ??.

¹⁰⁴ The finite element meshes and crack patterns for specimen type I are illustrated in Figure 23.30.

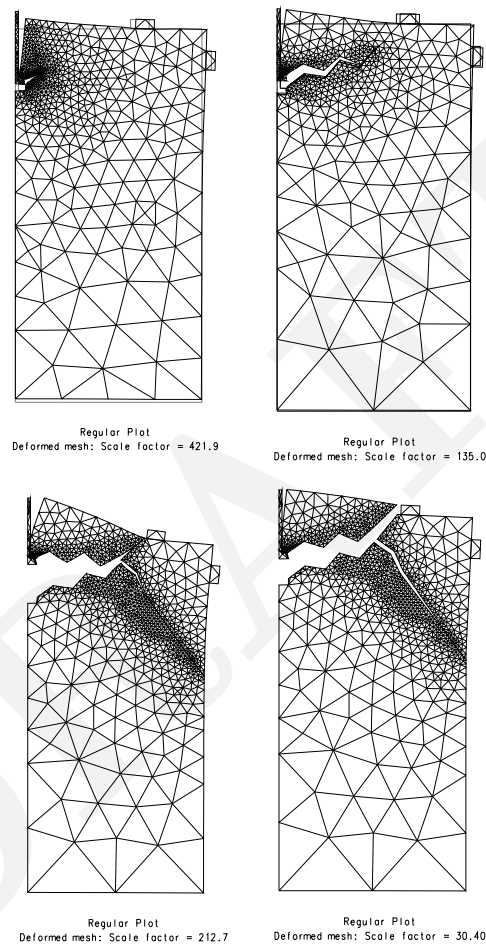


Figure 23.30: Crack propagation for anchor bolt pull out test I.

¹⁰⁵ This analysis exhibits a “zig-zag” crack pattern, which indicates that the selected crack increment Δa of 50 mm was too large, and the crack tip “oscillates” around the correct path. Originally the crack propagated at an angle of about 20 degrees, but when the crack approached the support, it sharply curved down, and continued at about -55 degrees. Subsequently a secondary vertical crack developed below the vertical support causing the final failure. Eight remeshing steps were necessary in this analysis.

¹⁰⁶ The results for specimen type II are shown in Figure 23.31, which shows the crack patterns and shaded areas of maximal principal stresses at remeshing steps 2,6,9 and 10. Altogether, ten different finite element meshes were used.

¹⁰⁷ Two cracks were considered in this analysis. One started at the top edge of the anchor head, and second at the bottom edge. The first crack proved to be the dominant one, and as for specimen I, it first propagated in an almost horizontal direction (10-20 deg.), but below the support, the crack again sharply turned downward, and continued at the angle of approximately -45 degrees. Again, a secondary vertical crack eventually developed under the support.

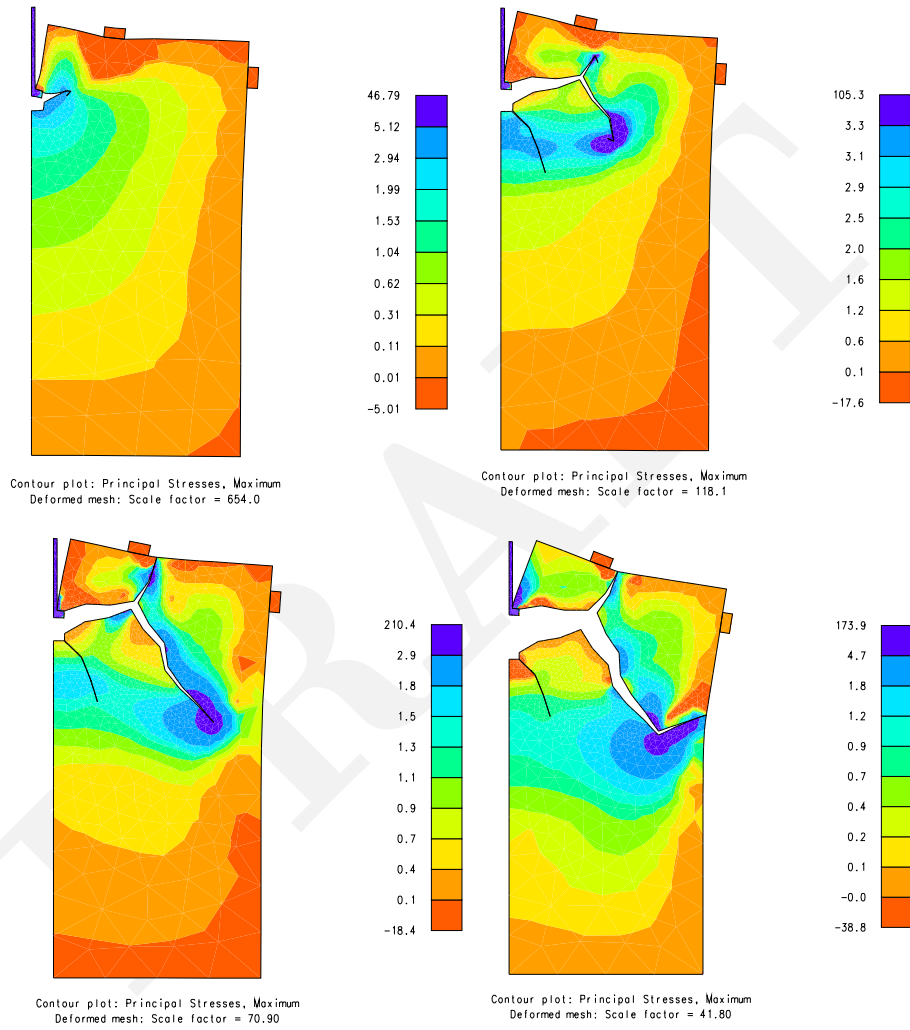


Figure 23.31: Crack propagation for anchor bolt pull out test II.

108 The crack paths for both specimens are plotted in Figure 23.32, and they show a good agreement with the experimentally observed ones. It should be noted however that the experimental crack patterns in this figure are only approximate, since no quantitative data about the exact crack patterns are reported in the literature.

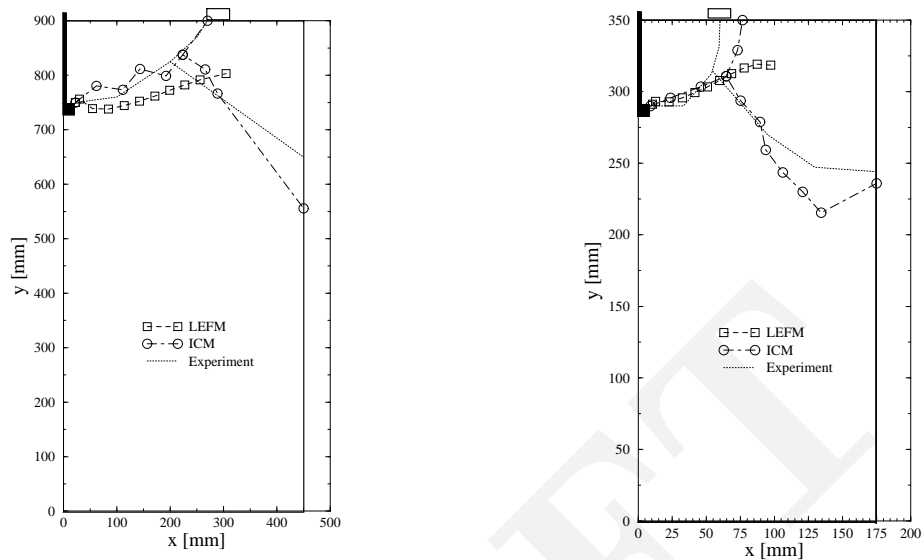


Figure 23.32: Crack patterns.

109 The load-displacement curves are shown in Figure 23.33 and 23.34 for specimen I and II respectively. These figures show comparison of this analysis with experiments and numerical simulations by other researchers. The experimental curves are adopted from (Shirai, 1993) and (Slowik, 1993) and the numerical curves correspond to the best results reported by (Shirai, 1993).

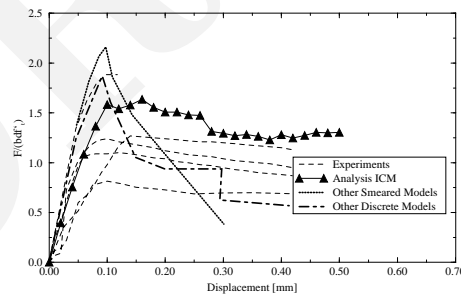


Figure 23.33: Load displacement curve for test I.

23.6 Conclusions

110 In this chapter, an interface crack model was developed and applied to modeling of discrete fracture of concrete, rock-concrete interfaces and masonry joints.

111 The proposed model is an extension of Hillerborg's fictitious crack model into a more general case of mixed mode fracture, when shear effects must be considered.

112 The robustness of the interface constitutive algorithm is ensured by fully exploiting the geometrical meaning of the predictor-corrector algorithm.

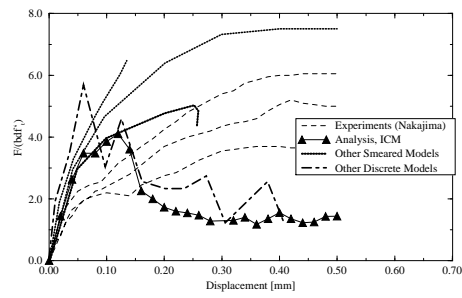


Figure 23.34: Load displacement curve for test II.

113 Due to the generality of the proposed model, it can be used for nonlinear fracture mechanics of both homogeneous materials and interfaces.

114 To model mixed mode crack propagation, the model was combined with the automated mesh generation to adaptively modify the finite element mesh to capture curve crack trajectories.

115 It was showed, that for large structures, the model approaches the linear elastic fracture mechanics solution, which implies the satisfaction of Griffith's criterion for crack propagation, and the capability to capture size effect.

Appendix A

INTEGRAL THEOREMS

¹ Some useful integral theorems are presented here without proofs. Schey's textbook *div grad curl and all that* provides an excellent informal presentation of related material.

A.1 Integration by Parts

The integration by part formula is

$$\int_a^b u(x)v'(x)dx = u(x)v(x)|_a^b - \int_a^b v(x)u'(x)dx \quad (\text{A.1})$$

or

$$\int_a^b u dv = uv|_a^b - \int_a^b v du \quad (\text{A.2})$$

A.2 Green-Gradient Theorem

Green's theorem is

$$\oint (Rdx + Sdy) = \int_{\Gamma} \left(\frac{\partial S}{\partial x} - \frac{\partial R}{\partial y} \right) dx dy \quad (\text{A.3})$$

A.3 Gauss-Divergence Theorem

² The general form of the Gauss' integral theorem is

$$\int_{\Gamma} \mathbf{v} \cdot \mathbf{n} d\Gamma = \int_{\Omega} \text{div} \mathbf{v} d\Omega \quad (\text{A.4})$$

or

$$\int_{\Gamma} v_i n_i d\Gamma = \int_{\Omega} v_{i,i} d\Omega \quad (\text{A.5})$$

³ In 2D-3D Gauss' integral theorem is

$$\int \int \int_V \text{div} \mathbf{q} dV = \int \int_S \mathbf{q}^T \cdot \mathbf{n} dS \quad (\text{A.6})$$

or

$$\int \int \int_V v_{i,i} dV = \int \int_S v_i n_i dS \quad (\text{A.7})$$

4 Alternatively

$$\int \int \int_V \phi \operatorname{div} \mathbf{q} dV = \int \int_S \phi \mathbf{q}^T \cdot \mathbf{n} dS - \int \int \int_V (\nabla \phi)^T \mathbf{q} dV \quad (\text{A.8})$$

5 For 2D-1D transformations, we have

$$\int \int_A \operatorname{div} \mathbf{q} dA = \oint_s \mathbf{q}^T \mathbf{n} ds \quad (\text{A.9})$$

or

$$\int \int_A \phi \operatorname{div} \mathbf{q} dA = \oint_s \phi \mathbf{q}^T \mathbf{n} ds - \int \int_A (\nabla \phi)^T \mathbf{q} dA \quad (\text{A.10})$$

Bibliography

- (1977). British standards institution, bs 5447, london.
- (1988). *International Conference on Fracture and Damage of Concrete and Rock*, Vienna. To be Published in Engineering Fracture Mechanics.
- (1992). Proceedings of the first international conference on fracture mechanics for concrete and concrete structures. Breckenridge, CO. Elsevier.
- 399, A. *Standard Test Method for Plane Strain Fracture Toughness of Metallic Materials, E399–74*. Annual Book of ASTM Standards.
- 496, A. (2000). *The Standard Test Method for Splitting Tensile Strength of Cylindrical Concrete Specimens*. Annual Book of ASTM Standards.
- Abramowitz, M. and Stegun, I. (1970). Handbook of mathematical functions. Technical report, National Bureau of Standard. Applied Mathematics Series, No. 55.
- ACI 446.1R-91 (2002). Fracture mechanics of concrete: Concepts, models and deformation of material properties (reapproved 1999). Technical Report ACI 446.1R-91, American Concrete Institute, Detroit, MI.
- ACI Committee 446 (2009). Fracture toughness testing of concrete. Technical Report ACI 446, American Concrete Institute, Detroit, MI.
- Advani, S. and Lee, K. (1979). Thermo-mechanical failure criteria for rock media. pages 19–25.
- Aliabadi, M. and Rooke, D. (1991). *Numerical Fracture Mechanics*. Kluwer Academic Publishers.
- Alvaredo, A. and Whitman, F. (1992). Crack formation due to hygral gradients. In *Third International Workshop on Behaviour of Concrete Elements Under Thermal and Hygral Gradients*. Weimar, Germany.
- Anderson, T. (1995). *Fracture Mechanics, Fundamentals and Applications*. CRC Press.
- Anon. (1985). RILEM Draft Recommendation (50–FCM): Determination of the Fracture Energy of Mortar and Concrete by Means of Three-Point Bend Tests on Notched Beams. *Materials and Structures*, 18:287–290.
- Apostal, M. (1974). *Development of an Anisotropic Singularity Finite Element Utilizing the Hybrid Displacement Method*. PhD thesis, State University of New York.
- Atkinson, C. and Bastero, J. (1991). On the use of betti's reciprocal theorem for computing the coefficients of stress singularities in anisotropic media. *International Journal of Engineering Science*, 29(6):727–741.
- Atkinson, C., Bastero, J., and Martinez-Esnaola, J. (1988). Stress analysis in sharp angular notches using auxiliary fields. *Engineering Fracture Mechanics*, 31(4):637–646.
- Atkinson, C., Bastero, J., and Miranda, I. (1986). Path-independent integrals in fracture dynamics using auxiliary fields. *Engineering Fracture Mechanics*, 25(1):53–62.
- Atkinson, C. and Craster, R. (1992). The application of invariant integrals in diffusive elastic solids. *Philosophical Transactions of the Royal Society of London, Series A*, 399(1653):231–263.
- Atluri, S. (1982). Path-independent integrals in finite elasticity and inelasticity, with body forces, inertia, and arbitrary crack-face conditions. *Engineering Fracture Mechanics*, 16(3):341–364.
- Atluri, S., Kobayachi, A., and Nakagaki, M. (1979). Application of an assumed displacement hybrid finite element procedure to two dimensional problems in fracture mechanics. In *AIAA/ASME/SAE 15th Structures, Structural Dynamics and Materials Conference, Las Vegas, Nevada*.
- Aviles, C. and Scholz, C. (1987). Fractal analysis applied to characteristic segments of the san andreas fault. *Jour. Geoph. Res.*, 92(B1):331–344.
- Awaji, H. and Sato, S. (1978). Combined mode fracture toughness measurement by the disc test. *J. of Engrg. Mat. Tech.*, 100:175–182.

- Babuska, I. and Miller, A. (1984). The post-processing approach to finite element method- part ii. *Int. J. Num. Meth. Engrg.*, 20:1111-1129.
- Balankin, A. (1997). Physics of fracture and mechanics of self-affine cracks. *Engineering Fracture Mechanics*, 57(2/3):135-203.
- Barenblatt, G. (1962). The mathematical theory of equilibrium crack in the brittle fracture. *Advances in Applied Mechanics*, 7:55-125.
- Barsom, J. and Rolfe, S. (1987). *Fracture & Fatigue Control in Structures, Applications of Fracture Mechanics, second Ed.* Prentice-Hall.
- Barsoum, R. (1974). Application of quadratic isoparametric finite elements in linear fracture mechanics. *Int. J. Fract.*, 10:603-605.
- Barsoum, R. (1975). Further application of quadratic isoparametric finite elements to linear fracture mechanics of plate bending and general shells. *Int. J. Fract.*, 11:167-169.
- Barsoum, R. (1976a). A degenerate solid element for linear fracture analysis of plate bending and general shells. *Int. J. num. Meth. Engrg.*, 10:551-564.
- Barsoum, R. (1976b). On the use of isoparametric finite elements in linear fracture mechanics. *Int. J. num. Meth. Engrg.*, 10:25-37.
- Barsoum, R. (1977). Triangular quarter point elements as elastic and perfectly plastic crack tip elements. *Int. J. num. Meth. Engrg.*, 11:85-98.
- Barsoum, R. (1981). An assessment of the quarter-point elements in pressure vessel fracture analysis. In *Structural Mechanics in Reactor Technology Conference*, Paris.
- Barsoum, R. (1982). Letter to the editor. *Int. J. num. Meth. Engrg.*, 18:1420-1422.
- Barton, C., Schutter, T., and Samuel, J. (1989). Dimension- a computer program that computes the fractal dimension of lines or points in a plane using the box, box-rotate, box-flex, box-density, and perimeter-area methods. Technical report, United States Geological Survey, Denver, CO. Unpublished.
- Bastero, J., Atkinson, C., and Martinez-Esnaola, J. (1989). Use of path-independent integral a for mixed-mode fast crack propagation in uncoupled thermoelastic media. *Engineering Fracture Mechanics*, 34(2):325-335.
- Batugin, S. and Nirenburg, R. (1972). Approximate relationship among the elastic constants of anisotropic rocks and anisotropy parameters. *Fiz-Tekhn. Probl. Razrabotki Polezn. Iskopaemykh*, 7(1):7-11.
- Bažant, Ž. (1976). Instability, ductility and size effect in strain softening concrete. *Journal of Engng. Mech., ASCE*, 102(2):331-344.
- Bažant, Ž. (1984). Size effect in blunt fracture: Concrete, rock, metal. *J. of Engineering Mechanics, ASCE*, 110(4):518-535.
- Bažant, Ž. (1997). Scaling of quasibrittle fracture: Asymptotic analysis. *Int. J. of Fracture Mechanics*, 83(1):19-40.
- Bažant, Ž. (2002). *Scaling of Structural Strength*. Hermes Penton Science, London.
- Bažant, Ž. (2005). Scaling theory for quasibrittle structural failure. *Proceedings National Academy of Sciences*, 101(37):13397-13399.
- Bažant, Ž. and Becq-Giraudon, E. (2001). Estimation of fracture energy from basic characteristics of concrete. In de Borst, R., Mazars, J., Pijaudier-Cabot, G., and van Mier, J., editors, *Fracture Mechanics of Concrete Structures (Proc., FraMCoS-4 Int. Conf., Paris)*, pages 491-495. Balkema.
- Bažant, Ž. and Cedolin, L. (1979). Blunt crack propagation in finite element analysis. *J. of the Engineering Mechanics Division, ASCE*, 105:297-315.
- Bažant, Ž. and Cedolin, L. (1991). *Stability of Structures*. Oxford University Press.
- Bažant, Ž. and Kazemi, M. (1990a). Determination of fracture energy, process zone length and brittleness number from size effect, with application to rock and concrete. *International Journal of Fracture*, 44:111-131.
- Bažant, Ž. and Kazemi, M. (1990b). Determination of fracture energy, process zone length and brittleness number from size effect, with application to rock and concrete. *Int. J. of Fract.*, 44:111-131.
- Bažant, Ž. and Novák, D. (2000). Energetic-statistical size effect in quasibrittle failure at crack initiation. *ACI Materials Journal*, 97(5):381-392.

- Bažant, Ž. and Pfeiffer, P. (1987). Determination of fracture energy properties from size effect and brittleness number. *ACI Material Journal*, 84(6):463–480.
- Bažant, Ž. and Planas, J. (1998). *Fracture and Size Effect in Concrete and Other Quasibrittle Materials*. CRC Press.
- Bažant, Ž. and Xi, Y. (1993). Stochastic drying and creep effects in concrete structures. *J. of Struc. Engrg.*, ASCE, 119(1):301–322.
- Bažant, Ž. and Yavari, A. (2005). Is the cause of size effect on structural strength fractal or energetic-statistical? *Engineering Fracture Mechanics*, 72:1–31.
- Bažant, Ž., Yu, Q., and Zi, G. (2002). Choice of standard fracture test for concrete and its statistical evaluation. *International Journal of Fracture*, 118(4):303–337.
- Benzeley, S. (1974). Representation of singularities with isoparametric finite elements. *Int. J. Num. Meth. Engng.*, 8:537.
- Bocca, P., Carpinteri, A., and Valente, S. (1990). Size effects in the mixed mode crack propagation: Softening and snap-back analysis. *Engineering Fracture Mechanics*, 35(1–3):159–170.
- Bolzon, G., Fedele, R., and Maier, G. (2002). Parameter identification of a cohesive crack model by kalman filter. *Computer Methods in Appl. Mech. Eng.*, 191:2847–2871.
- Bouchaud, E., Lapasset, G., and Planès, J. (1990). Fractal dimension of fractured surfaces: a universal value? *Europhysics Letters*, 13(1):73–79.
- Bourdarot, E., Mazars, J., and Saouma, V., editors (1994). *Proceedings of the International Workshop on Dam Fracture and Damage*. Balkema.
- Broek, D. (1986). *Elementary Engineering Fracture Mechanics, 4th Edition*. Martinus Nijhoff Publishers.
- Broek, D. (1989). *The Practical Use of Fracture Mechanics*. Kluwer Academic Publishers.
- Brown, S. (1987). A note on the description of surface roughness using fractal dimension. *Geophysical Research Letters*, 14(11):1095–1098.
- Brown, S. (1988). Correction to: A note on the description of surface roughness using fractal dimension. *Geophysical Research Letters*, 15(11):286.
- Brühwiler, E., Broz, J., and Saouma, V. (1991). Fracture model evaluation of dam concrete. *ASCE, Journal of Civil Engineering Materials*, 4:235–251.
- Brühwiler, E. and Whitman, F. (1990a). Failure of Dam Concrete Subjected to Seismic Loading Conditions. *Engineering Fracture Mechanics*, 35(3):565–572.
- Brühwiler, E. and Whitman, F. (1990b). The Wedge Splitting Test, a Method of Performing Stable Fracture Mechanics Tests. *Engineering Fracture Mechanics*, 35:117–126.
- Brühwiler, E. (1988). *Fracture Mechanics of Dam Concrete Subjected to Quasi-Static and Seismic Loading Conditions*. Doctoral Thesis No 739, Swiss Federal Institute of Technology, Lausanne. (in German).
- Brühwiler, E. (1992). The wedge splitting test for the determination of fracture properties. In Whitman, F., editor, *Numerical Models in Fracture Mechanics of Concrete, Proceedings of the 1st Bolomey Workshop on Numerical Models in Fracture Mechanics of Concrete*, pages 19–27, Zurich, Switzerland. Balkema.
- Brühwiler, E. and Roelfstra, P.E. (1989). Tensile Softening Properties and Structural Response of a Concrete Member. In *Proceedings, Int. Conf. on Recent Developments in the Fracture of Concrete and Rock*, University of Wales, Cardiff.
- Brühwiler, E. and Saouma, V.E. (1990). Fracture testing of rock by the wedge splitting test. In Hustrulid, W. and Johnson, G., editors, *Proceedings of the 31st US Symposium on Rock Mechanics*, pages 287–294, Golden, CO. Balkema.
- Cahn, R. (1989). Fractal dimension and fracture. *Nature*, 338:201–202.
- Carlsson, L. A. and Prasad, S. (1993). Interfacial fracture of sandwich beams. *Engineering Fracture Mechanics*, 44:581–590.
- Carol, I., Bažant, Ž., and Prat, P. (1992). Microplane type constitutive models for distributed damage and localized cracking in concrete structures. In *Proc. Fracture Mechanics of Concrete Structures*, pages 299–304, Breckenridge, CO. Elsevier.

- Carpinteri, A. (1982a). Application of fracture mechanics to concrete structures. *Journal of Structural Division, ASCE*, 108:833–848.
- Carpinteri, A. (1982b). Notch sensitivity in fracture testing of aggregative materials. *Engineering Fracture Mechanics*, 16:467–481.
- Carpinteri, A. (1986). *Mechanical Damage and Crack Growth in Concrete*. Martinus Nijhoff Publishers.
- Carpinteri, A. (1994). Scaling laws and renormalization groups for strength and toughness disordered materials. *Int. J. of Solids and Structures*, 31(3):291–302.
- Carpinteri, A. and Chiaia, B. (1994). Multifractal scaling law for the fracture energy variation of concrete structures. In F.H., W., editor, *Proceedings of Second International Conference on Fracture Mechanics of Concrete Structures FraMCoS2*, pages 581–596, Zurich, Switzerland. Aedificato.
- Carpinteri, A., Chiaia, B., and Cornetti, P. (2003). On the mechanics of quasi-brittle materials with a fractal microstructure. *Engineering Fracture Mechanics*, 70:2321–2349.
- Carpinteri, A., Chiaia, B., and Ferro, G. (1995). Size effects on nominal tensile strength of concrete structures: Multifractality of material ligaments and dimensional transition from order to disorder. *Materials and Structures*, 28:311–317.
- Carpinteri, A. and Ingrassia, A., editors (1984). *Fracture Mechanics of Concrete: Material Characterization and Testing*. Martinus Nijhoff Publishers.
- Cedolin, L., Dei Poli, S., and Iori, I. (1987). Tensile behavior of concrete. *J. of Engineering Mechanics, ASCE*, 113(3).
- Chandra, K. and Saouma, V. (2004). Fracture of rock-concrete interfaces: Laboratory tests and applications. *ACI Structural Journal*, 101(3).
- Chelidze, T. and Gueguen, Y. (1990). Evidence of fractal fracture. *Int. J. Rock Mech. Min. Sci. & Geomech. Abstr.*, 27(3):223–225.
- Chen, C. and Runt, J. (1989). Fractal analysis of polystyrene fracture surfaces. *Polymer Communications*, 30:334–335.
- Cherepanov, G. (1979). *Mechanics of Brittle Fracture*. McGraw-Hill.
- Comninou, M. (1977). The interface crack. *ASME, Journal of Applied Mechanics*, pages 631–636.
- Cottrell, A. (1963).
- Crisfield, M. (1991). *Non-linear Finite Element Analysis of Solids and Structures, Vol 1*. John Willey & Sons.
- Crisfield, M.A. (1981). A fast incremental/iterative solution procedure that handles ‘snap through’. *Computers and Structures*, 13(1-3):55–62.
- Cusatis, G., Bažant, Ž., and Cedolin, L. (2003). Confinement-shear lattice model for concrete damage in tension and compression: I. theory. *ASCE Journal of Engineering Mechanics*, 129(12):1439–1448.
- Dahlblom, O. and Ottosen, N. S. (1990). Smearred crack analysis using a generalized fictitious crack model. *Journal of Engineering Mechanics*, 116(1):55–76.
- Davidon, W.C. (1968). Variance algorithm for minimisation. *Computer J.*, 10:406–410.
- deLorenzi, H.G. (1985). Energy release rate calculations by the finite element method. *Engineering Fracture Mechanics*, 21:103–110.
- Denarié, E. and Saouma, V.E. and Iocco, A. and Varelas, D. (1999). Concrete fracture process zone characterization; part i experimentally with internal fiber bragg grating sensors. *Journal of Engineering Mechanics*, 127(5):494–502.
- Duda, H. (1990). Stress-crack-opening relation and size effect in high-strength concrete. *Darmstad Concrete*, 5:35–46.
- Duga, J., Fisher, W., Buxbam, R., Rosenfield, A., Buhr, A., Honton, E., and McMillan, S. (1983). The economic effects of fracture in the united states. Technical Report SP647-2, National Bureau of Standards.
- Dugdale, D. (1960). Yielding of steel sheets containing slits. *J. Mech. Phys. Sol.*, 8:100–108.
- Dunders, J. (1969). Edge - bonded dissimilar orthogonal elastic wedges under normal and shear loading. *Journal of Applied Mechanics*, 36:650–652.
- Einstein, A. (1905). On the movement of small particles suspended in stationary liquids required by the molecular-kinetic theory of heat. *Annalen der Physik*, 17:549–560.

- Elices, M., Guinea, G. V., and Planas, J. (1992). Measurement of the fracture energy using three-point bend tests: Part 3, influence of cutting the $p - \delta$ tail. *Materials and Structures*, 25:327–334.
- Engesser, F. (1895). Über Knickfragen. *Schweizerische Bauzeitung*, 26:24–26. (Sect. 8.1).
- Erdogan, F. and Sih, G. (1963). On the crack extension in plates under plane loading and transverse shear. *Journal of Basic Engineering*, 85:519–527.
- Eshelby, J. (1974). Calculation of energy release rate. *Prospect of Fracture Mechanics Nordhoff*, pages 69–84.
- Fawkes, A., Owen, D., and Luxmoore, A. (1979). An assessment of crack tip singularity models for use with isoparametric elements. *Eng. Fract. Mech.*, 11:143–159.
- Feder, J. (1988). *Fractals*. Plenum Press.
- Feenstra, P., de Borst, R., and Rots, J. (1991). Numerical study on crack dilatancy. i: Models and stability analysis. ii: Applications. *J. Eng. Mech.*, 117(4):733–769.
- FERC (2016). [Engineering Guidelines for the Evaluation of Hydropower Projects](#). Technical report, Federal Energy Regulatory Commission, Office of Energy Projects.
- Foreman, R., Kearney, V., and Engle, R. (1967). Numerical analysis of crack propagation in cyclic-loaded structures. *J. of Basic Engineering*, 89:459–464.
- Freese, C. and Tracy, D. (1976). The natural isoparametric triangle versus collapsed quadrilateral for elastic crack analysis. *Int. J. Fract.*, 12:768–770.
- Gallagher, R. (1975). *Finite Element Analysis Fundamentals*. Prentice Hall, Englewood Cliffs, N.J.
- Gdoutos, E. (1993). *Fracture Mechanics; An Introduction*. Kluwer Academic Press.
- Gerstle, W. and Xie, M. (1992). Fem modeling of fictitious propagation in concrete. *Journal of Engineering Mechanics*, 118(2):416–434.
- Giuriani, E. and Rosati, G. P. (1986). Behaviour of concrete elements under tension after cracking. *Studi e Ricerche, Corso di Perfezionamento per le Costruzioni in Cemento Armato*, 8:65–82. (in Italian).
- Goodman, R., Taylor, R., and Brekke, T. (1968). A Model for the Mechanics of Jointed Rocks. *J. of the Soil Mechanics and Foundations Division ASCE*, 94:637–659.
- Gopalaratnam, V. S. and Shah, S. (1985). Softening response of plain concrete in direct tension. *ACI Journal*, 82:310–323.
- Gopalaratnam, V. S. and Ye, B. S. (1991). Numerical characterization of the nonlinear fracture process in concrete. *Engineering Fracture Mechanics*, 40(6):991–1006.
- Gordon, J. (1988). *The Science of Structures and Materials*. Scientific American Library.
- Griffith, A. (1921). The phenomena of rupture and flow in solids. *Phil. Trans. Roy. Soc. London*, A221:163–197.
- Guinea, G., Pastor, J., Planas, J., and Elices, M. (1998). Stress intensity factor, compliance and cm₀d for general three-point-bend-beam. *International Journal of Fracture*, 89:103–116.
- Harrop, L. (1982). The optimum size of quarter-point crack tip element. *Int. J. num. Meth. Engng.*, 17:1101–1103.
- He, M. Y. and Hutchinson, J. W. (1989). Kinking of a crack out of an interface. *Journal of Applied Mechanics*, 56:270–278.
- Hellen, T. (1975). On the method of virtual crack extension. *Int. J. Num. Methods in Eng.*, 9(1).
- Hellen, T. and Blackburn, W. (1975a). The calculation of stress intensity factor for combined tensile and shear loading. *Int. J. Fract.*, 11:605–617.
- Hellen, T. K. and Blackburn, W. S. (1975b). The calculation of stress intensity factors for combined tensile and shear loading. *International Journal of Fracture*, 11(4):605–617.
- Henshell, R. D. and Shaw, K. G. (1975). Crack tip elements are unnecessary. *International Journal of Numerical Methods in Engineering*, 9(3):495–509.

- Heping, X. (1987). The fractal effect of irregularity of crack branching on the fracture toughness of brittle materials. *International Journal of Fracture*, 41:267–274.
- Hibbitt, H. (1977). Some properties of singular isoparametric elements. *Int. J. num. Meth. Engng.*, 11:180–184.
- Hillerborg, A. (1985a). Results of three comparative test series for determining the fracture energy g_f of concrete. *Mater. and Struct.*, 18(107).
- Hillerborg, A. (1985b). The theoretical basis of method to determine the fracture energy g_f of concrete. *Materials and Structures*, 18(106):291–296.
- Hillerborg, A., Mod er, M., and Petersson, P. (1976a). Analysis of crack formation and crack growth in concrete by means of fracture mechanics and finite elements. *Cement and Concrete Research*, 6(6):773–782.
- Hillerborg, A., Mod er, M., and Petersson, P. (1976b). Analysis of crack formation and crack growth in concrete by means of fracture mechanics and finite elements. *Cement and Concrete Research*, 6(6):773–782.
- Hillerborg, A. (1983). Analysis of One Single Crack. In Whittman, F., editor, *Fracture Mechanics of Concrete*, F.H. Wittmann (editor), pages 223–249. Elsevier, Amsterdam, The Netherlands.
- Hillerborg, A. (1985). The Theoretical Basis of a Method to Determine the Fracture energy G_F of Concrete. *RILEM Materials and Structures*, 18(106):291–296.
- Hong, C.-C. and Stern, M. (1978). The computation of stress intensity factors in dissimilar materials. *Journal of Elasticity*, 8(1):21–34.
- Hordijk, D., Reinhardt, H., and Cornelissen, H. (1989). Fracture mechanics parameters of concrete from uniaxial tensile tests as influenced by specimen length. In Shah, S. and Swartz, S., editors, *RILEM-SEM Int. Conference on Fracture Mechanics of Rock and Concrete*, New-York: Springer-Verlag.
- Hudson, C. and Seward, S. (1978). *A Compendium of Sources of Fracture Toughness and Fatigue Crack Growth Data for Metallic alloys*, volume 14. *Int. J. of Fracture*.
- Hudson, C. and Seward, S. (1982). A compendium of sources of fracture toughness and fatigue crack growth data for metallic alloys. *Int. J. of Fracture, Part II*, 20:R59–R117.
- Hurst, H. (1951). Long-term storage capacity of reservoirs. *Trans. Am. Soc. Civ. Eng.*, 116:770–808.
- Hussain, M., Pu, S., and Underwood, J. (1974). Strain energy release rate for a crack under combined mode i and mode ii. *ASTM, STP 560*, pages 2–28.
- Hussain, M., Vasilakis, J., and Pu, L. (1981). Quadratic and cubic transition elements. *Int. J. Num. Meth. Engng.*, 16:1397–1406.
- Hutchinson, J. (1968). Singular behavior at the end of a tensile crack tip in a power-law hardening material. *Journal of Mechanics and Physics of Solids*, 16:13–31.
- Hutchinson, J. W. and Suo, Z. (1992). Mixed mode cracking in layered materials. *Advances in Applied Mechanics*, 29:63–191.
- Il'yushin, A. (1946). The theory of small elastic-plastic deformations. *Prikladnaia Matematika i Mekhanika, PMM*, 10:347–356.
- Inglis, C. (1913). Stresses in a plate due to the presence of cracks and sharp corners. *Trans. Inst. Naval Architects*, 55:219–241.
- Ingraffea, A. (1977). *Discrete Fracture Propagation in Rocks: Laboratory Tests and Finite Element Analysis*. PhD thesis, University of Colorado.
- Ingraffea, A. and Gerstle, W. (1984). Non-linear fracture models for discrete crack propagation. In Shah, S., editor, *Proceedings of the NATO Advanced Workshop on Application of Fracture Mechanics to Cementitious Composites*, pages 171–209, Hingham, Mass. Martinus Nijhoff.
- Ingraffea, A. and Manu, C. (1980). Stress intensity factor computation in three dimension with quarter-point elements. *Int. J. num. Meth. Engng.*, 15(10):1427–1445.
- Irwin, G. (1957). Analysis of stresses and strains near the end of a crack traversing a plate. *Transactions ASME, J. Appl. Mech.*, 24.
- Irwin, G. (1960). Plastic zone near a crack and fracture toughness. In *Proc. 7th Sagamore Conf.*, page 63.

- Irwin, G. (1962). The crack extension force for a part through crack in a plate. *Transactions ASME, J. Appl. Mech.*, 29.
- Ishikawa, H. (1980). A finite element analysis of stress intensity factors for combined tensile and shear loading by only a virtual crack extension. *Int. J. Fracture*, 16:243.
- Issa, M., Hammad, A., and Chudnovsky, A. (1993). Correlation between crack tortuosity and fracture toughness in cementitious materials. *International Journal of Fracture*, 60:97–105.
- Izquierdo-Encarnación, J. (2003). Ars sine scientia nihil est. *Concrete International*, 25(5):7.
- Jeang, F. L. and Hawkins, N. M. (1985). Nonlinear analysis of concrete fracture. Structures and mechanics report, Department of Civil Engineering, University of Washington, Seattle, WA.
- Jenq, Y. and Shah, S. P. (1985). A two parameter fracture model for concrete. *Journal of Engineering Mechanics Division, ASCE*, 111(4):1227–1241.
- Kanninen, M. (1984). Applications of fracture mechanics to fiber composite materials and adhesive joint, a review. In *3rd Int. Conf. on Numerical Methods in Fracture Mechanics*, Swansea.
- Kanninen, M. and Popelar, C. (1985). *Advanced Fracture Mechanics*. Oxford University Press.
- Kaplan, M. (1961). Crack propagation and the fracture of concrete. *Journal of the American Concrete Institute*, 58(5):591–610.
- Karihaloo, B. (1996). Physical causes for size effect in concrete structures. In Carpinteri, A., editor, *Size-Scale Effects in the Failure Mechanisms of Materials and Structures*, pages 325–339, London. E. & FN Spon.
- Karihaloo, B. (1999). Size effect in shallow and deep notched quasi-brittle structures. *International Journal of Fracture*, 95:379–390. Special issue on Fracture Scaling ed. by Ž. Bažant and Y.D.S. Rajakapase.
- Karihaloo, B. L. and Nallathambi, P. (1987). Notched beam test: Mode I fracture toughness. Technical report, draft report to RILEM Committee 89-FMT, Fract. Mech. of Concrete: Test Method.
- Karlsson, A. and Bäcklund, J. (1978). J-integral at loaded crack surfaces. *International Journal of Fracture*, 14(6):R311–R314.
- Kelly, A. (1974). *Strong Solids*. Oxford University Press, second edition.
- Kirsch, C. (1898). Die theorie der elastizität und die bedürfnisse der festigkeitslehre. *Zeitschrift des Vereines Deutscher Ingenieure*, 42:797–807.
- Knott, J. (1976). *Fundamentals of Fracture Mechanics*. Butterworths, fourth edition.
- Knowles, J. and Stenberg, E. (1972). On a class of conservation laws in linearized and finite elastostatics. *Arch. Rat. Mech. Anal.*, 44:187–211.
- Knowles, J. and Stenberg, E. (1972). On a class of conservation laws in linearised and finite elastostatics. *Arch. Rat. Mech. Anal.*, 44:187–211.
- Koch, H. v. (1904). Sur une Courbe Continue sans Tangente, Obtenue par une Construction Géométrique Élémentaire. *Archiv für Matemat. and Astron. och Fys*, 1:681–702.
- Kreyszig, E. (1979). *Advanced Engineering Mathematics, 4th Edition*. John Wiley and Sons.
- Kumar, V., German, M., and Shih, C. (1981). *An Engineering Approach for Elastic-Plastic Fracture Analysis*. Electric Power Research Institute. EPRI-NP1931.
- Lange, D., Jennings, H., and Shah, S. (1993). Relationship between fracture surface roughness and fracture behavior of cement paste and mortar. *Journal of the American Ceramic Society*, 76(3).
- Lekhnitskii, S. (1981). *Theory of Elasticity of an Anisotropic Body*. Mir, Moscow (English Translation).
- Lenke, L. and Gerstle, W. (2001). Tension test of stress versus crack opening displacement using cylindrical concrete specimens. In Vipulanandan, C. and Gerstle, W., editors, *Fracture Mechanics for Concrete Materials: Testing and Applications*, pages 189–206. SP-201, American Concrete Institute, Farmington Hills, Michigan.
- Levi, B. (1990). Are fractures fractal or quakes chaotic. *Physics Today*, pages 17–19.

- Li, F., Shih, C., and Needleman, A. (1985). A comparison of methods for calculating energy release rates. *Engineering Fracture Mechanics*, 21(2):405–421.
- Li, V. C. and Liang, E. (1986). Fracture processes in concrete and fiber reinforced cementitious composites. *Journal of Engineering Mechanics, ASCE*, 112(6):566–586.
- Lin, K. Y. and Mar, J. W. (1976). Finite element analysis of stress intensity factors for cracks at a bi-material interface. *Int. Journal of Fracture*, 12:521–531.
- Linsbauer, H. and Tschegg, E. (1986). Test Method for the Determination of Fracture Mechanics Properties. Austrian Patent No. A-233/86 (in German).
- Long, Q., Suqin, L., and Lung, C. (1991). Studies on the fractal dimension of a fracture surface formed by slow stable crack propagation. *Journal of Physics, D*, 24(4).
- Lotfi, H. (1992). *Finite Element Analysis of Fracture of Concrete and Masonry Structures*. PhD thesis, University of Colorado, Boulder.
- Lynn, P. and Ingraffea, A. (1977). Transition elements to be used with quarter-point crack-tip elements. *Int. J. num. Meth. Engng.*, 11:1031–1036.
- Malyshev, B. M. and Salganik, R. L. (1965). The strength of adhesive joints using the theory of cracks. *Int. Journal of Fracture*, 1:114–118.
- Mandelbrot, B. (1983). *The Fractal Geometry of Nature*. W.H. Freeman, San Francisco.
- Mandelbrot, B., Passoja, D., and Paullay, A. (1984). Fractal character of fracture surfaces of metals. *Nature*, 308:721–722.
- Mecholsky, J. and Freiman, S. (1991). Relationship between fractal geometry and fractography. *Journal of the American Ceramic Society*, 74(12):3136–3138.
- Mecholsky, J. and Mackin, T. (1988). Fractal analysis of fracture in ocala chert. *Journal of Materials Science Letters*, 7:1145–1147.
- Mecholsky, J., Passoja, D., and Feinberg-Ringle, K. (1989). Quantitative analysis of brittle fracture surfaces using fractal geometry. *Jour. Amer. Ceram. Soc.*, 72(1):60–65.
- Miller, M. and Gallagher, J. (1981). An analysis of several fatigue crack growth rate (fcgr) descriptions. In S.J., H. and Bucci, R., editors, *Fatigue Crack Growth Measurements and Data Analysis, ASTM STP 738*, pages 205–251. ASTM, Philadelphia.
- Mindess, S. and Young, F. (1981). *Concrete*. Prentice-Hall, Inc.
- Måløy, K., Hansen, A., Hinrichsen, E., and Roux, S. (1992). Experimental measurements of the roughness of brittle cracks. *Physical Review Letters*, 68(2):213–215.
- Mosolov, A. (1991). Fractal j integral in fracture. *Soviet Technical Physics Letters*, 17(10):698–700.
- Mostovoy, e. a. (1967). Use of crack-line loaded specimens for measuring plane strain fracture toughness. *J. of Materials*, 2(3):661–681.
- Murakami, Y. (1987). *Stress Intensity Factors Handbook*. Pergamon Press. (2 Vols).
- Nakayama, J. (1965). Direct measurement of fracture energies of brittle heterogeneous material. *J. of the Amer. Ceram. Soc.*, 48(11).
- Nallathambi, P. and Karihaloo, B. (1986). Stress intensity factor and energy release rate for three-point bend specimens. *Magazine of Concrete Research*, 38(135):67–76.
- Newman, J. (1971). An improved method of collocation for the stress analysis of cracked plates with various shaped boundaries. Technical Report NASA TN D-6376, National Aeronautics and Space Administration, Langley Research Center, Hampton, VA.
- Newman, J. and Raju, I. (1981). An empirical stress intensity factor equation for surface cracks. *Engineering Fracture Mechanics*, 15:185–192.
- Newton, R. (1973). Degeneration of brick-type isoparametric elements. *Int. J. num. Meth. Engng.*, 7:579–581.
- Nikishkov, G. and Atluri, S. (1987). Calculation of fracture mechanics parameters for an arbitrary three-dimensional crack, by the 'equivalent domain integral' method. *International Journal of Numerical Methods in Engineering*, 24(9):1801–1821.

- Nikishkov, G. and Vainshtok, V. (1980). Method of virtual crack growth for determining stress intensity factors k_i and k_{II} . *Strength of Materials*, 12:696–701.
- Ouchterlony, F. (1982). Fracture toughness testing of rock. Technical report, SveDeFo, Swedish Detonic Research Foundation, Stockholm, Sweden.
- Ouchterlony, F. (1986). Suggested methods for determining fracture toughness of rock material. Technical report, International Society for Rock Mechanics, Commission on Testing Methods.
- Owen, D. and Fawkes, A. (1983). *Engineering Fracture Mechanics*. Pineridge Press, Swansea, U.K.
- Paris, P. and Erdogan, F. (1963). A critical analysis of crack propagation laws. *ASME J. of Basic Engineering*, 85(3):528–534.
- Parks, D. (1974). A stiffness derivative finite element technique for determination of crack tip stress intensity factors. *Int. J. Fracture*, 10:487–502.
- Peng, G. and D., T. (1990). The fractal nature of a fracture surface. *Journal of Physics A: Mathematical and General*, 23:3257–3261.
- Petersson, P. (1981). Crack growth and development of fracture zones in plain concrete and similar materials. Technical Report TVBM 1006, Lund Institute of Technology, Lund, Sweden.
- Planas, J. and Elices, M. (1988a). Conceptual and experimental problems in the determination of the fracture energy of concrete. In *Workshop on Fracture Toughness and Fracture Energy, Test Methods for Concrete and Rock*, pages 203–212, Tohoku Univ., Sendai, Japan.
- Planas, J. and Elices, M. (1988b). Size-effect in concrete structures: mathematical approximations and experimental validation. In Mazars, J. and Bažant, Ž., editors, *Cracking and Damage, Strain Localization and Size Effect*, pages 462–476, Cachan (F).
- Planas, J. and Elices, M. (1992). Asymptotic analysis of a cohesive crack: 1. theoretical background. *International Journal of Fracture*, 55:153–177.
- Planas, J., Guinea, G. V., and Elices, M. (1999). Size effect and inverse analysis in concrete fracture. *International Journal of Fracture*, 95:367–378.
- Pu, S., Hussain, M., and Lorensen, W. (1977). Collapsed 12 node triangular elements as crack tip elements for elastic fracture. Technical report, Technical Report ARLCB-TR-77047.
- Rao, A. K., Raju, I., and Krishna Murty, A. (1971). A powerful hybrid method in finite element analysis. *Int. J. Num. Meth. Engng.*, 3.
- Reich, R. (1993). *On the Marriage of Mixed Finite Element Methods and Fracture Mechanics: An Application to Concrete Dams*. PhD thesis, University of Colorado, Boulder.
- Rice, J. and Sih, G. (1965). Plane problems of cracks in dissimilar media. *J. Applied Mechanics*, pages 418–423.
- Rice, J. R. (1988). Elastic fracture mechanics concepts for interfacial cracks. *ASME, Journal of Applied Mechanics*, 55:98–103.
- RILEM Committee on Fracture Mechanics of Concrete - Test Methods (1985). Determination of the fracture energy of mortar and concrete by means of three-point bend tests on notched beams. *Materials and Structures*, 18(106):285–290.
- RILEM Committee on Fracture Mechanics of Concrete-Test Methods (1990). Determination of fracture parameters (k_{Ic} and $ctod_c$) of plain concrete using three point bend tests. *Materials and Structures*, 23:457–460.
- RILEM TC QFS (2004). Quasibrittle fracture scaling and size effect. *Materials and Structures*, 37(272):547–568.
- Roelfstra, P. and Sadouki, H. (1986). Fracture/1: Theory and applications. *Laboratory for Building Materials (LMC), EPF Lausanne*.
- Rooke, D. and Cartwright, D. (1976). *Compendium of Stress Intensity Factors*. HMSO, London.
- Saouma, V., Ayari, M., and Leavell, D. (1987). Mixed mode crack propagation in homogeneous anisotropic solids. *Engineering Fracture Mechanics*, 27(2):171–184.
- Saouma, V. and Barton, C. (1994). Fractals, fractures and size effects in concrete. *Journal of Engineering Mechanics of the American Society of Civil Engineers*, 120(4):835–854.
- Saouma, V., Barton, C., and Gamal-El-Din, N. (1990). Fractal Characterization of Cracked Concrete Surfaces. *Engineering Fracture Mechanics Journal*, 35(1):47–53.

- Saouma, V., Broz, J., Brühwiler, E., and Boggs, H. (1991a). Effect of aggregate and specimen size on fracture properties of dam concrete. *ASCE, Journal of Materials in Civil Engineering*, 3(3):204–218.
- Saouma, V., Červenka, J., Slowik, V., and Chandra, J. (1994). Mixed mode fracture of rock-concrete interfaces. In Bažant, Ž., editor, *US-Europe Workshop on Fracture and Damage of Quasi-Brittle Materials: Experiment, Modeling and Computer Analysis*, Prague, Czech Republic.
- Saouma, V., Dugar, R., and Morris, D., editors (1991b). *Proceedings Dam Fracture*, Boulder. Electric Power Research Institute (EPRI), Palo Alto, CA.
- Saouma, V., Natekar, D., and Hansen, E. (2003). Cohesive stresses and size effects in elasto-plastic and quasi-brittle materials. *International Journal of Fracture*, 119:287–298.
- Saouma, V., Natekar, D., and Sbaizero, O. (2002). Nonlinear finite element analysis and size effect study of a metal-reinforced ceramics-composite. *Materials Science and Engineering A*, 323:129–137.
- Saouma, V. and Schwemmer, D. (1984). Numerical evaluation of the quarter point singular element. *International Journal of Numerical Methods in Engineering*, 20:1629–1641.
- Saouma, V. and Sikiotis, E. (1986). Stress intensity factors in anisotropic bodies using singular isoparametric elements. *Engineering Fracture Mechanics*, 25(1):115–121.
- Saouma, V., Červenka, J., and Reich, R. (2010). [Merlin Finite Element User's Manual](#).
- Saouma, V. and Zatz, I. (1984). An automated finite element procedure for fatigue crack propagation analyses. *Engineering Fracture Mechanics Journal*, 20(2):321–333.
- Schertzer, D. and Lovejoy, S. (1997). Universal multifractals do exist!: Comments on “a statistical analysis of mesoscale rainfall as a random cascade. *Journal of Applied Meteorology*, 36:1296–1303.
- Sha, G. (1984). On the virtual crack extension technique for stress intensity factors and energy release rate calculation for mixed fracture modes. *Int. J. Fracture*, 25.
- Shah, S., editor (1984). *Application of Fracture Mechanics to Cementitious Composites*, Northwestern University. NATO Workshop.
- Shah, S. and Swartz, S., editors (1989). *RILEM-SEM Int. Conference on Fracture Mechanics of Rock and Concrete*, New-York. Springer-Verlag.
- Shih, C., de Lorenzi, H., and German, M. (1976). Crack extension modelling with singular quadratic isoparametric elements. *Int. J. Fract.*, 12:647–651.
- Shih, C., Moran, B., and Nakamura, T. (1986). Energy release rate along a 3-d crack front in a thermally stressed body. *Int. J. Fracture*, 30:79–102.
- Shing, P., Manzouri, T., Atkinson, R., Schuller, M., and Amadei, B. (1994). Evaluation of grout injection techniques for unreinforced masonry structures. In *Proc. of the Fifth U.S. National Conference on Earthquake Engineering, Vol. III*, pages 851–860, Chicago.
- Shirai, N. (1993). Jci round robin analysis in size effect in concrete structures. In *US-Japan Workshop on Fracture and Size Effect in Concrete*, Japan.
- Sierpinski, W. (1912). Sur une nouvelle courbe continue qui remplit toute une aire plane. *Bull. l'Acad. des Sciences Cracovie A*, pages 462–478.
- Sih, G. (1974). Strain energy factors applied to mixed mode crack problems. *Int. J. Fracture*, 10:305.
- Sih, G. and DiTommaso, A., editors (1984). *Fracture Mechanics of Concrete: Structural Application and Numerical Calculation*. Martinus Nijhoff Publishers.
- Sih, G., Paris, P., and Irwin, G. (1965). On cracks in rectilinearly anisotropic bodies. *International Journal of Fracture Mechanics*, 1.
- Slowik, W. (1993). Beiträge zur Experimentellen Bestimmung Bruchmechanischer Materialparameter von Betonen. Technical report, Institut für Baustoffe, ETH, Zürich, Switzerland. Research Report No. 3.
- Sluys, L. (1992). *Wave Propagation, Localisation and Dispersion of Softening Solids*. PhD thesis, Delft University of Technology.
- Sokolnikoff, I. (1956). *Mathematical Theory of Elasticity*. McGraw-Hill, New York, NY.

- Stankowski, T. (1990). *Numerical Simulation of Progressive Failure in Particle Composites*. PhD thesis, University of Colorado, Boulder.
- Stern, M. (1973). A boundary integral representation for stress intensity factors. In Chang, T. S., editor, *Recent Advances in Engineering Science*, pages 125–132. Scientific Publishers, Boston, MA. Volume 7.
- Stern, M. (1979). The numerical calculation of thermally induced stress intensity factors. *Journal of Elasticity*, 9(1):91–95.
- Stern, M., Becker, E., and Dunham, R. (1976). A contour integral computation of mixed mode stress intensity factors. *International Journal of Fracture*, 12(3):359–368.
- Stern, M. and M.L., S. (1975). The calculation of stress intensity factors in anisotropic materials by a contour integral method. In E.F., R. and Benzley, S., editors, *Computational Fracture Mechanics*, pages 161–171, New York, NY. ASME.
- Stevens, R. and Guiu, F. (1994). The application of the j integral to problems of crack bridging. *Acta Metall. Mater.*, 42(6):1805–1810.
- Swartz, S. and Kan, Y. (1992). The influence of aggregate/paste bonding and strength on mode I fracture mechanics properties of concrete. In Bažant, Ž., editor, *Fracture Mechanics of Concrete Structures*, pages 437–442. Elsevier Applied Science.
- Swartz, S. and Refai, T. (1989). Cracked surface revealed by dye and its utility in determining fracture parameters. In *et al.*, H. M., editor, *Fracture Toughness and Fracture Energy: Test Methods for Concrete and Rock*, pages 509–520. Balkema, Rotterdam.
- Swartz, S. E. and Go, C. G. (1984). Validity of compliance calibration to cracked concrete beams in bending. *Exp. Mech.*, 24(2):129–134.
- Swartz, S. E., Hu, K. K., Fartash, M., and Huang, C. (1982). Stress intensity factors for plain concrete in bending - prenotched versus precracked beams. *Exp. Mech.*, 22(11):412–417.
- Swartz, S. E., Hu, K. K., and Jones, G. L. (1978). Compliance monitoring of crack growth in concrete. *J. of the Engng. Mech. Div., ASCE*, 104(EM4):789–800.
- Tada, H., Paris, P., and Irwin, G. (1973). *The Stress Analysis of Cracks Handbook*. Del Research Corporation, Hellertown, PA.
- Tattersall, H. G. and Tappin, G. (1966). The work of fracture and its measurement in metals, ceramics and other materials. *J. of Mater. Sci.*, 1(3):296–301.
- Termonia, Y. and Meakin, P. (1986). Formation of fractal cracks in a kinetic fracture model. *Nature*, 320:429–431.
- Terzaghi, K. and Peck, R. (1967). *Soil Mechanics in Engineering Practice, 2nd edition*. John Wiley & Sons, New York, NY.
- Timoshenko, S. and Goodier, J. (1970). *Theory of Elasticity*. McGraw Hill.
- Trunk, B. (2000). Einfluss der bauteilgröße auf die bruchenergie von beton (effect of specimen size on the fracture energy of concrete). Technical report, Building Materials Report N 11, Aedificatio Verlag, Freiburg, Germany. In German.
- Tsai, Y. and Mecholsky, J. (1991). Fractal fracture of single crystal silicon. *Journal of Material Research*, 6(6):1240.
- Turcotte, D. (1992). *Fractals and Chaos in Geology and Geophysics*. Cambridge Press, Cambridge.
- Underwood, E. and Banerji, K. (1986). Fractals in fractography, (invited review). *Materials Science and Engineering*, 80:1–15.
- Van Raan, A. (1990). Fractal dimension of co-citation. *Nature*, 347:626.
- Vashy, A. (1892). Sur les lois de similitude en physique. *Annales Télégraphiques*, 19:25–28.
- Walker, E. (1970). The effect of stress ratio during crack propagation and fatigue for 2024-t3 and 7075-t6 aluminum. In Rosenfeld, M., editor, *Effects of Environment and Complex Load History on Fatigue Life*. ASTM STP 462.
- Walsh, P. (1972). Fracture of plain concrete. *Indian Concrete J.*, 46(11):469–470 and 476.
- Walsh, P. F. (1976). Crack initiation in plain concrete. *Mag. of Concr. Res.*, 28:37–41.
- Weiss, J. (2001). Self-affinity of fracture surfaces and implications on a possible size effect on fracture geometry. *International Journal of Fracture*, 109:365–381.
- Weisstein, E. (2004). Rule 150. from mathworld—a wolfram web resource.

- Wells, A. (1963). *Application of Fracture Mechanics at and Beyond General Yielding*. British Welding Research Ass., Report M13.
- Westergaard, H. (1939a). Bearing pressures and cracks. *J. Appl. Mech.*, 61.
- Westergaard, H. (1939b). Bearing pressures and cracks. *J. Appl. Mech.*, 61.
- Wheeler, O. (1972). Spectrum loading and crack growth. *J. of Basic Engineering*, 94:181–186.
- Whitman, F., editor (1993). *Numerical Models in Fracture Mechanics of Concrete*. Balkema. Proceedings of the first Bolomey Workshop, Zurich, 1992.
- Whitman, F., Rokugo, K., Brühwiler, E., Mihashi, H., and Simonin, P. (1988). Fracture Energy and Strain Softening of Concrete as Determined by Means of Compact Tension Specimens. *Materials and Structures*, 21:21–32.
- Wiberg, N.-E. (1974). Matrix structural analysis with mixed variables. *International Journal of Numerical Methods in Engineering*, 8(2):167–194.
- Willenborg, J., Engle, R., and Wood, R. (1971). A crack growth retardation model using an effective stress concept. Technical report, Air Force Flight Dynamics Laboratory Report, AFFDL-TM-71-1-FBR.
- Williams, M. (1952). Stress singularities from various boundary conditions in angular corners of plates in extension. *Jour. of Applied Mechanics, ASME*, 19(4):526–528.
- Williams, M. (1957). On the stress distribution at the base of a stationary crack. *Jour. of Applied Mechanics, ASME*, 24(1):109–114.
- Williams, M. L. (1959). The stresses around a fault or crack in dissimilar media. *Bulletin of the Seismological Society of America*, 49(2):199–204.
- Winslow, D. (1985). The fractal nature of the surface of cement paste. *Cement and Concrete Research*, 15:817–824.
- Wittmann, F. H., editor (1983). *Fracture Mechanics of Concrete*. Elsevier Science Publishers Company Inc. Proceedings of a Conference in Lausanne.
- Wnuk, M. and Legat, J. (2002). Work of fracture and cohesive stress distribution resulting from triaxiality dependent cohesive zone model. *International Journal of Fracture*, 114:29–46.
- Wnuk, M. and Yavari, A. (2003). On estimating stress intensity factors and modulus of cohesion for fractal cracks. *Engineering Fracture Mechanics*, 70:1659–1674.
- Wolfram, S. (2002). *A New Kind of Science*. Wolfram Media, Champaign, Ill. (1197 pp.).
- Xu, S. and Reinhardt, H. (1998). Crack extension resistance and fracture properties of quasi-brittle softening materials like concrete based on the complete process of fracture. *International Journal of Fracture*, 92:71–99.
- Xu, S. and Reinhardt, H. (2000). A simplified method for determining double-k fracture parameters for three-point bending tests. *International Journal of Fracture*, 104:181–209.
- Yamada, Y., Ezawa, Y., and Nishiguchi, I. (1979). Reconsiderations on singularity or crack tip elements. *Int. J. num. Meth. Engng.*, 14:1525–1544.
- Yavari, A., Sarkani, S., and Moyer, E. (2002). The mechanics of self-similar and self-affine fractal cracks. *Int. J. of Fracture*, 114:1–27.
- Ying, L. (1982). A note on the singularity and the strain energy of singular elements. *Int. J. num. Meth. Engng.*, 18:31–39.
- Young, I. and Crawford, J. (1992). The analysis of fracture profiles of soil using fractal geometry. *Australian Journal of Soil Research*, 30:291–295.
- Zak, A. and Williams, M. (1963). Crack point stress singularities at a bi-material interface. *Jour. of Applied Mechanics, ASME*, 30(1).
- Zienkiewicz, O. (1967). *The Finite Element in Structural and Continuum Mechanics*. McGraw-Hill, London, first edition.
- Zienkiewicz, O., Taylor, R. L., and Nithiarasu, P. (2005). *The Finite Element Method for Fluid Dynamics*. Elsevier Butterworth-Heinemann, 6th edition.